

REPORT SERIES IN AEROSOL SCIENCE

N:o 226 (2019)

**Proceedings of The Center of Excellence in Atmospheric Science
(CoE ATM)
Annual Seminar 2019**

Editors: Tiia Laurila, Anna Lintunen, Markku Kulmala

Helsinki 2019

ISBN 978-952-7276-34-1 (PDF)

ISSN 0784-3496

Helsinki 2019

Aerosolitutkimusseura ry - Finnish Association for Aerosol Research (FAAR)

<http://www.atm.helsinki.fi/FAAR/>

CONTENTS

OVERVIEW

Kulmala, M., A. Lintunen, Y. Viisanen, J. Bäck, A. Virtanen, M.-L. Riekkola, T. Vesala, E. Asmi, A. Asmi, F. Bianchi, M. Boy, M. Dal Maso, M. Ehn, H. Hakola, J. Heinonsalo, P. Hari, K. Hartonen, A.-P. Hyvriinen, K. Hmeri, T. Hltt, L. Jrvi, H. Jrvinen, J. Kangasluoma, H. Kokkola, J. Kontkanen, J. Kujansuu, A. Laaksonen, A. Lauri, T. Laurila, K. Lehtipalo, H. Lihavainen, H. K. Lappalainen, G. De Leeuw, K. Lehtinen, A. Lohila, R. Makkonen, I. Mammarella, A. Mkel, D. Moiseev, T. Nieminen, A. Ojala, P. Paasonen, T. Petj, M. Pihlatie, A. Porcar-Castell, J. Pumpanen, J. Puliainen, A. Pursula, L. Riuttanen, S. Romakkaniemi, T. Ruuskanen, S. Schobesberger, V. Singlair, M. Sipilä, H. Vehkamäki, D. R. Worsnop, T. Yli-Juuti, V.-M. Kerminen and COE ATM Team

THE CENTER OF EXCELLENCE IN ATMOSPHERIC SCIENCE - FROM MOLECULAR AND BIOLOGICAL PROCESSES TO THE GLOBAL CLIMATE; OVERVIEW FOR YEAR 2019

1

TEAM AND INFRASTRUCTURE OVERVIEWS

Boy, M., P. Zhou, M. Baykara, L. Pichelstorfer, C. Xavier, D. Chen, P. Clusius and P. Roldin

ACTIVITIES OF THE ATMOSPHERE MODELLING GROUP IN 2019

14

Bäck, J., T. Höltt, A. Porcar-Castell, M. Pihlatie, J. Heinonsalo, A. Mäkel, T. Vesala, J. Aalto, B. Adamczyk, A. Ahi, J. Anttila, Atherton, J., Berninger, F., Chan, T., Dominguez, M., Kalliokoski, T., Kohl, L., Kolari, P., J. F. J. Korhonen, M. Koskinen, L. Kulmala, A. Kumpu, A. Lintunen, L. Lindfors, I. Martikainen, L. Matkala, A. Mauranen, F. Minunno, M. Mäki, P. Mnd, T. Paljakka, M. Patama, J. Pumpanen, A. Putkinen, P. Rajewicz, K. Rissanen, Y. Salmon, M. Santalahti, P. Schiestl-Aalto, O.-M. Sieti, D. Taipale, S. Tenhoviirta, E. Vainio, A. Vanhatalo and P. Hari, et al.

ECOSYSTEM PROCESSES - ACTIVITIES IN 2018-19

19

Ehn, M., Y. Zhang, L. Qulver, O. Peräkyl, L. Heikkinen, O. Garmash, M. Riva and M. Äijälä

ATMOSPHERIC PHYSICAL CHEMISTRY (COALA) GROUP HIGHLIGHTS

34

Haapanala, P., M. Paramonov, E. Juurola, M. Kulmala, K. Lehtinen, H. Korhonen, J. Keskinen, T. Petäjä, H. Hakola, A. Virtanen, M. Dal Maso and S. Sorvari Sundet
ACTRIS - SHAPING THE FUTURE OF ATMOSPHERIC RESEARCH

36

Hakola, H., A. Helin, M. Hemmilä, K. Kyllnen, A. Liikanen, U. Makkonen, A. P. Praplan, S. Schallhart, A. Virkkula and H. Helln
MAIN RESEARCH TOPICS OF THE FMI AIR QUALITY GROUP IN 2019

41

Hemmilä, M., M. Juustila and M. Kulmala
FUTURE EARTH FINLAND (FES)

46

Hyvärinen, A.-P., E. Asmi, M. Aurela, J. Backman, D. Brus, K. Doulgeris, R. K. Hooda, J. Kesti, N. Kivekäs, A. Korpinen, J. Kuula, O. Meinander, E. O'Connor, A. Piedihierro, S. Saarikoski, H. Servomaa, J. Svensson, K. Teinilä, H. Timonen, S. Tuukiainen, V. Vakkari and A. Welti
ACTIVITIES OF THE ATMOSPHERIC AEROSOLS GROUP OF THE FMI

48

Kangasluoma, J., L. Ahonen, R. Baablaki, R. Cai, T. Chan, L. Dada, J. Enroth, S., Haataja, S. Holm, E. Häkkinen, F. Keshavarz, M. Lampimäki, T. Laurila, A. Skyttä, D. Stolzenburg, A. Toropainen, Y. Wu, P. Aalto, M. Passanati, H. Vehkamäki and T. Petäjä
AEROSOL SCIENCE AND TECHNOLOGY GROUP ABSTRACT

53

Kokkola, H., E. Holopainen, I. Kudzotsa, T. Kühn, A. Laakso, T. Mielonen, J. Tonttila and A. Ruuskanen
RESEARCH ACTIVITIES OF THE ATMOSPHERIC MODELING GROUP AT THE ATMOSPHERIC RESEARCH CENTRE OF EASTERN FINLAND

56

Kontkanen, J., P. Aalto, R. Baablaki, Z. Brasseur, J. Duplissy, T. Jokinen, L. Lampilahti, M. Lampimäki, K. Leino, K. Luoma, M. Okuljar, B. Rörup, J. Sulo, D. Wimmer, Y. Wu and K. Lehtipalo
SUMMARY ON THE ACTIVITIES OF THE ATMOSPHERIC AEROSOLS AND IONS GROUP DURING YEAR 2018-2019

60

Kujansuu, J., T. Petäjä, H. K. Lappalainen, F. Bianchi, J. Kangasluoma, C. Yao and M. Kulmala

PRESENT ACTIVITIES OF INAR IN ASIA

63

Kulmala, L., A. Lohila, T. Aalto, T. Laurila, J. Heinonsalo, T. Viskari, I. Fer, O. Nevalainen, L. Heimsch, H. Vekuri, J. Mäkelä, M. Aurela, and J. Liski

VERIFYING THE POTENTIAL OF CLIMATIC-FRIENDLY AGRICULTURE IN FINLAND

66

Lappalainen, H. K., J. Kujansuu, H. Junninen, A. Rusanen, N. Altimir, A. Mahura, L. Järvi, F. Bianchi, J. Kangasluoma, S. Noe, T. Vihma, P. Uotila, J. Bäck, T. Vesala, T. Petäjä, and M. Kulmala

STATION FOR MEASURING EARTH SURFACE ATMOSPHERE RELATIONS
CONCEPT GlobalSMEAR INITIATIVE

68

Lappalainen, H. K., T. Petäjä, V.-M. Kerminen, A. Mahura, N. Altimir, E. Ezhova, R. Makkonen, I. Bashmakova, J. Kujansuu, A. Lauri, S. Mazon, A. Borisova, F. Bianchi, T. Laurila, J. Bäck, T. Vihma, P. Uotila, L. Sogacheva, G. De Leeuw, L. Heininen, S. Chalov, P. Konstantinov, N. Chubarova, O. Popochova, M. Arshinov, B. Belan, V. Gennadinik, Y. Qiu, I. Ezau, V. Melnikov, G. Matvienko, A. Ding, A. Baklanov, Y. Viisanen, N. Kasimov, H. Guo, V. Bondur, S. Zilitinkevich, and M. Kulmala

PAN-EURASIAN EXPERIMENT (PEEX) PROGRAMME ACTIVITIES IN 2019
AND FUTURE PROSPECTS

72

Lauri, A., T. Ruuskanen, L. Riuttanen, M. Äijälä, and M. Santala

INAR EDUCATION RESEARCH AND DEVELOPMENT

81

Makkonen, R., A. Mahura, J.-P. Keskinen, P. Zhou, J. Bian, M. Santala, J. Lento, A. Rusanen, C. Xavier, and J. Hautala

EARTH SYSTEM MODELING: OVERVIEW OF ACTIVITIES

84

Neitola, K., J. Mukkala, A.-P. Hyvärinen, J. Bäck, and T. Petäjä

VÄRI-PROJECT AND DEVELOPMENT OF VRRI STATION

88

Nieminen, T., E. Ezhova, A. Demakova, E.-M. Duplissy, J. Heiskanen, V. Lheureux, S. B. Mazon, M. Rätty, K. Tabakova, D. Taipale, H. Uusitalo, I. Ylivinkka, M. Zaidan, V.-K. Kerminen, and M. Kulmala

OVERVIEW OF THE ACTIVITIES WITHIN GLOBAL ATMOSPHEREEARTH SURFACE FEEDBACKS GROUP

91

Paasonen, P., T. Hussein, J. Cai, L. Dada, W. Du, K. Dllenbach, B. Foreback, P.-L. Fung, S. Hakala, J. Kontkanen, M. Li, A. Shahiryer, S. Tuovinen, L. Wang, and L. Xinyang

AIR QUALITY RESEARCH GROUP AT INAR/PHYSICS

94

Pumpanen, J., H. Aaltonen, F. Berninger, H. R. Bhattaraj, C. Biasi, K. Köster, E. Köster, M. Marushchak, M. Maljanen, M. Palviainen, H. Nykänen, S. Siljanen, N. Shurpali, C. Voigt, H. Shang-Turpeinen, and X. Zhou

BIOGEOCHEMISTRY RESEARCH GROUP / FCoE TEAM ABSTRACT

97

Rasilo, T., M. Kaukolehto, M. Mirtl, and J. Bäck

ELTER RI DRIVES ECOSYSTEM RESEARCH FORWARD IN EUROPE

102

Riekkola, M.-L., K. Hartonen, J. Ruiz-Jimenez, H. Lan, M. Jussila, N. Zanca, S. Barua, G. Demaria, E. Zagatti, T. Liangsupree, Y. Leleev, Y., M. Salkinoja-Salonen, and H. M. M. Siren

RECENT DEVELOPMENTS IN THE ANALYSIS OF OUTDOOR AND INDOOR AIR

106

Ruuskanen, T., A. Kallinen, A. Lauri, L. Riuttanen, and H. Vehkamäki

INTEGRATION OF ART AND SCIENCE, FACING CLIMATE CHANGE TOGETHER

110

Sinclair, V. A., M. Bister, M. Ekblom, J. Hautala, H. Järvinen, J. Lento, J. Mikkola, M. Rantanen, J. Räisänen, I. Statnaia, L. Tuppi, and M. Virman

DYNAMIC METEOROLOGY: AN OVERVIEW

112

Sipilä, M. and F. Bianchi

ARCTIC, POLAR AND HIGH ALTITUDE ATMOSPHERIC RESEARCH AT INAR
IN 2019

118

Vehkamäki, H., V. B. Alfaouri, R. Halonen, F. Keshavarz, J. Kubecka, T. Kurtn, O. Pakarinen, M. Passananti, B. Reischl, G. Roudsari, A. Shcherbacheva, V. Tikkanen, T. Zanca, and E. Zapadinsky

AN OVERVIEW OF UNIVERSITY OF HELSINKI COMPUTATIONAL AEROSOL
PHYSICS GROUP ACTIVITIES IN 2019

121

Vesala, T., E. Vainio, H. Aaltonen, M. Aurela, J. Hatakka, L. Järvi, P. Keronen, P. Kolari, H. Korhonen, M. Korhikoski, L. Laakso, T. Laurila, K. Lehtinen, A. Leskinen, A. Lohila, I. Mammarella, A. Ojala, and E.-S. Tuittila

INTEGRATED CARBON OBSERVATION SYSTEM (ICOS) FINLAND

124

Vesala, T., L. Järvi, A. Lohila, I. Mammarella, T. Aslan, R. Dewa, T. Grönholm, M. Havu, P. Hietala, P. Keronen, K.-M. Kohonen, T. V. Kokkonen, P. Kolari, M. Kurppa, S. Karttunen, A. Leppänen, X. Li, A. Marchionn, O. Peltola, M. Raivonen, Ü Rannik, P. Rantala, G. Sahoo, Y. Salmon, J. Strömberg, R. Taipale, H. Zhang, A. Vähä, T. Laurila, J. Pulliainen, A. Ojala, E.-S. Tuittila, T. Höltt, M. Pihlatie, and J. Bäck

MICROMETEOROLOGY, GREENHOUSE GASES, BIOGEOCHEMICAL CYCLES
AND URBAN METEOROLOGY RESEARCH TEAM: OVERVIEW OF SCIENTI-
FIC ACTIVITIES

129

Virtanen, A., T. Yli-Juuti, S. Schobesberger, K. Lehtinen, and S. Mikkonen

FOCUS OF THE RESEARCH OF UEF TEAM, YEAR 2019

135

Äijälä, M. and L. Riuttanen

CO-CREATING NEW CLIMATE EDUCATION IN THE FINNISH UNIVERSITIES

138

RESEARCH ABSTRACTS

Aalto, J, T. Salminen, T. Matilainen, H. Laakso, M. Mäki, T. Petäjä, J. Bäck, and

M. Kulmala

NEW ALL-INCLUSIVE VOC SAMPLER FOR MANUAL ADSORBENT TUBE
SAMPLINGS

142

Aaltonen, H., M. Palviainen, X. Zhou, E. Köster, F. Berninger, J. Pumpanen, and K. Köster

FIRE-INDUCED CHANGES IN QUALITY OF SOIL ORGANIC MATTER IN BOREAL PERMAFROST REGION OF CANADA

145

Ahi, A., J. Bäck, and J. Aalto

IMPACTS OF SUB-CANOPY REMOVAL ON STAND LEVEL VOLATILE ORGANIC COMPOUNDS (VOC) EXCHANGE.

147

Ahonen L. R. , R. Baalbaki, F. Korhonen, J. Vanhanen, J. Kangasluoma, and T. Petäjä
NOVEL AEROSOL DILUTER MINIMIZING SIZE DEPENDENT LOSSES DOWN TO 1 NM PARTICLE SIZE

150

Alfaouri, D., N. Myllys, J. Kubeka, T. Zanca, E. Zapadinsky, L. Ahonen, J. Kangasluoma, M. Passananti, and H. Vehkamäki

SULFURIC ACID - DIMETHYLAMINE CLUSTERS FRAGMENTATION INSIDE AN ATMOSPHERIC PRESSURE INTERFACE TIME OF FLIGHT MASS SPECTROMETER

153

Aliaga, D., V. Sinclair, Z. Qiaozhi, M. Andrade, C. Mohr, and F. Bianchi

THE SOUTHERN HEMISPHERE HIGH ALTITUDE EXPERIMENT ON PARTICLE NUCLEATION AND GROWTH (SALTENA) CAMPAIGN AT MOUNT CHACALTAYA: TRANSPORT SIMULATIONS AND FOOTPRINT CLUSTERING

156

Piedehierro, A. A., A. Welti, A. Virtanen, A. Buchholtz, K. Korhonen, I. Pullinen, I. Summanen, and A. Laaksonen

ICE NUCLEATION ACTIVITY OF SOA PARTICLES FROM BOREAL FOREST

158

Anttila, J. V., T. Hlitt, M. Koskinen, A. Leppänen, M. Raivonen, A. Lohila, T. Vesala, and M. Pihlatie

MODELLING METHANE FLOWS BETWEEN SOIL, TREES, AND ATMOSPHERE

161

Aslan, T., K. Haahti, A.J. Kieloaho, A. Lehtonen, T. Grönholm, O. Peltola, I. Mammarella, and S. Launiaine

BIOPHYSICAL AND BIOGEOCHEMICAL RESPONSES OF BOREAL FOREST TO THINNING: A MODEL-ASSISTED REVIEW

163

Asmi, E., J. Backman, H., Servomaa, A.-P. Hyvärinen, M. Gini, K. Eleftheriadis, T. Müller, Y. Kondo, and P. Quincey

THE PALLAS SUMMER 2019 AEROSOL BLACK CARBON CAMPAIGN

165

Atherton, J., S. Xu, and A. Porcar-Castell

HEURISTIC METHODS TO CORRECT FOR WAVELENGTH OFFSET EFFECTS IN DUAL FIELD OF VIEW SPECTROMETER SYSTEMS

169

Baalbaki, R., M. Pikridas, T. Jokinen, T. Laurila, L. Dada, A. Maisser, K. Neitola, A. Christodoulou, F. Unga, K. Lehtipalo, J. Kangasluoma, G. Biskos, T. Petäjä, J. Sciare and M. Kulmala

TOWARDS UNDERSTANDING THE MECHANISMS OF NEW PARTICLE FORMATION IN THE EASTERN MEDITERRANEAN

172

Backman, J., A. Virkkula, T. Raatikainen, P.P. Aalto, A. Lupi, P. Cristofanelli L. Caiazzo, and R. Traversi

FIRST REFRACTORY BLACK CARBON MEASUREMENTS ON THE EAST ANTARCTIC PLATEAU

176

Beck, L. and M. Sipilä

BLOWING SNOW PRODUCING HALOGEN ION CLUSTERS IN ANTARCTICA

180

Besel, V., J. Kubeka, T. Kurtzn, and H. Vehkamäki

BLOWING SNOW PRODUCING HALOGEN ION CLUSTERS IN ANTARCTIC COMPUTATIONAL STUDIES ON NEW PARTICLE FORMATION INVOLVING CHARGED SULFURIC ACID - AMMONIA CLUSTERS

182

Bianco, A., P. A. Alpert, P. Corral Arroyo, J. Dou, F. Sordello, K. Witte, B. Watts, U. K. Krieger, M. Ammann, D. V. Vione, and M. Passananti
DEGRADATION OF NANOPLASTICS IN WATER: IMPACT ON GASEOUS AND AQUEOUS PHASE ORGANIC CARBON.

184

Brasseur, Z., J. Schneider, J. Lampilahti, P. Poutanen, M. Peltola, A. Franck, M. Lampimäki, A. Manninen, P. Hietala, F. Korhonen, K. Höhler, O. Möhler, B. Bertozzi, T. Schorr, N. Umo, F. Vogel, M. Kulmala, T. Petäjä, and J. Duplissy
VERTICAL PROFILE OF ICE NUCLEATING PARTICLE CONCENTRATIONS IN A BOREAL ENVIRONMENT

186

Buchholz, A., A. Ylisirniö, W. Huang, C. Mohr, M. Canagaratna, D. R. Worsnop, S. Schobesberger, and A. Virtanen
DECONVOLUTING FIGAERO-CIMS THERMAL DESORPTION PROFILES WITH POSITIVE MATRIX FACTORISATION (PMF)

188

Cai, J., B. Chu, L. Yao, C. Yan, L. M. Heikkinen, F. Zheng, C. Li, X. Fan, Y. Wang, T. V. Kokkonen, T. Chan, Y. Zhou, L. Dada, Y. Liu, H. He, S. Zhang, P. Paasonen, J. T. Kujansuu, T. Petäjä, J. Kangasluoma, F. Bianchi, Y. Sun, P. L. Croteau, D. R. Worsnop, V.-M. Kerminen, W. Du, M. Kulmala, and K. R. Daellenbach
Source apportionment of fine particulate matters by physical and chemical markers during the non-heating season in Beijing, China

191

Cai, R., J. Kangasluoma, and J. Jiang
TRANSMISSION OF CHARGED NANOPARTICLES THROUGH AN ADVERSE AXIAL ELECTRIC FIELD AND ITS IMPROVEMENT

193

Chan, T., J. Kangasluoma, R. Cai, L. Yiliang, Y. Zhou, L. Ahonen, J. Sulo, L. Wang, and M. Kulmala
UNDERSTANDING THE INVERSION METHODS FROM SUB-3 NM PARTICLE NUMBER CONCENTRATION DATA IN BEIJING, CHINA

196

Chen, D., P. Zhou, P. Roldin, T. Nieminen, M. Baykara, and M. Boy
TREND OF ATMOSPHERIC COMPOSITION AT SMEAR II, FINLAND OVER 2007-2018 HOW DID OXIDANTS CHANGE

198

Chu, B., L. Dada, J. Kangasluoma, T. Petäjä, V.-M. Kerminen, and M. Kulmala
A PROPOSED AEROSOL INDEX (AI) BASED ON 1-YEAR OBSERVATION OF
AEROSOL SIZE DISTRIBUTION IN BEIJING

200

Clusius, P., T. Olenius, J. Elm, P. Roldin, H. Vehkamäki, and M. Boy
The role of NH₃ and DMA in new particle formation in a boreal forest environment

205

Demakova, A., E. Ezhova, O. Garmash, M. Arshinov, B. Belan, T. Petäjä, and M.
Kulmala
EXPERIMENTAL RESEARCH AND ANALYSIS OF ATMOSPHERIC AEROSOL
AND ITS PRECURSORS IN SIBERIAN BOREAL FOREST

208

Dominguez-Carrasco, M. R., L. Kulmala, P. Schieslt-Aalto, P. Kolari, E. Juuorla, T.
Hölttä, J. Heinonsalo, and J. Bäck
CONNECTIONS OF NON-STRUCTURAL CARBON COMPOUNDS AND PHO-
TOSYNTHESIS IN BOREAL WOODY PLANTS FOREST

210

Doulgeris, K. M., K. Neitola, A. Hirsikko, C. Keleshi, P. Vouterakos, G. Schaufelber-
ger, M. Weiss, J. Sciare, and D. Brus
GROUND BASED AND AIRBORNE MEASUREMENTS OF AEROSOL AND
CLOUD PROPERTIES DURING PALLAS CLOUD EXPERIMENT 2017

213

Du, W., L. Dada, K. Dällenbach, C. Yan, J. Cai, B. Chu, L. Yao, F. Zheng, C. Li, X.
Fan, Y. Wang, Y. Zhou, T. Chan, Y. Liu, P. Paasonen, J. Kangasluoma, F. Bianchi,
D. R. Worsnop, Y. Sun, V.-M. Kerminen, and M. Kulmala
UNDERSTANDING NEW PARTICLE FORMATION EVENTS UNDER HIGH
CONDENSATION SINK CONDITIONS

217

Duplissy, E.-M., T. Nygrd, S. Hakala, R. Väänänen, V. Sinclair, V.-M. Kerminen, T.
Petäjä, and M. Kulmala
CHANGES IN AEROSOL LOADING RELATED TO AIRMASSES PASSING OVER
DECREASING SEA ICE ARE EVIDENT IN NORTHERN SCANDINAVIA

219

Daellenbach, K. R., J. Cai, F. Zheng, C. Yan, Y. Wang, B. Chu, L. Heikkinen, T. Chan, S. Hakala, J. Kangasluoma, H. Li, Y. Zhou, J. Kujansuu, T. Petäjä, V.-M. Kerminen, F. Bianchi, D. R. Worsnop, Y. Liu, and M. Kulmala

Sources and processes contributing to PM_{2.5} in Beijing

221

Ekblom, M., L. Tuppi, V. Shemyakin, M. Laine, P. Ollinaho, H. Haario, and H. Järvinen
ALGORITHMIC TUNING OF SPREAD-SKILL RELATIONSHIPS IN ENSEMBLE
FORECASTING SYSTEMS

225

Ezhova, E. D. Orlov, E. Suhonen, S. Malkhazova, V. Gennadinik, D. Drozdov, D. Kaverin, I. Kukkonen, H. Lappalainen, T. Petäjä, V.-M. Kerminen, S. Zilitinkevich, T. Christensen, and M. Kulmala

THE ROLE OF PRECIPITATION FOR THE RECENT OUTBREAK OF ANTHRAX IN SIBERIA

227

Fer, I., M. C. Dietze, T. Viskari, J. Mäkelä, L. Kulmala, J. Liski, M. Viikinkoski, M. Kaasalainen, and T. Aalto

COMPARISON OF MODEL PREDICTIVE PERFORMANCES FOR NORDIC GRASSLANDS

229

Freistetter, N. C., L. Kohl, T. Polvinen, M. Koskinen, and M. Pihlatie
IDENTIFICATION OF INTERFERING CH₄ AND VOCs EMISSIONS FROM CH₄
FLUX MEASUREMENT SET-UP MATERIALS

231

Fung P. L., M. A. Zaidan, S. Sillanpää, and T. Hussein
MISSING DATA IMPUTATION AS SIMPLE PROXY OF URBAN BLACK CARBON IN HELSINKI, FINLAND

234

Garmash, O., M. P. Rissanen, M. Riva, O. Peräkylä, P. Rantala, and M. Ehn
EFFECT OF OZONE ON HOM FORMATION IN OXIDATION OF TOLUENE

237

Hakala, S., P. Paasonen, V. Vakkari, C. Deng, Y. Fu, J. Jiang, J. Kangasluoma, T. Petäjä, J. Kujansuu, C. Yan, F. Bianchi, K. Dllenbach, Y Liu, L. Dada, and M. Kulmala

EFFECT OF AIR MASS HISTORY ON THE OBSERVED PARTICLE NUMBER SIZE DISTRIBUTION IN BEIJING

240

Halonen, R., E. Zapadinsky, T. Kurtn, H. Vehkamäki, and B. Reischl

RATE ENHANCEMENT IN COLLISIONS OF SULFURIC ACID MOLECULES DUE TO LONG-RANGE INTERMOLECULAR FORCES

245

Hao, L. Q., E. Kari, J. Jokiniemi , D. R. Worsnop, and A. Virtanen

CONTRIBUTION OF GAS-PHASE ORGANIC ACIDS TO SECONDARY ORGANIC AEROSOL FORMATION IN THE PRESENCE OF AMMONIA

249

Ruiz-Jimenez, J., N. Zanca, S. Barua, G. Demaria, M. Salkinoja-Salonen, H. M. M. Siren, K. Hartonen and M.-L. Riekkola

SAMPLING AND ANALYSIS OF INDOOR AIR AND EMISSIONS FROM INSULATION MATERIALS

252

Havu, M., L. Kulmala, A. Riikonen, T. Viskari, and J. Järvi

SIMULATING URBAN SOIL CARBON DECOMPOSITION USING LOCAL WEATHER INPUT FROM A SURFACE MODEL

258

Heikkinen, L., K. Dällenbach, K. Luoma, J. Aalto, P. Rantala, D. R. Worsnop, M. Äijälä, and M. Ehn

SEASONAL VARIATION IN ORGANIC AEROSOL COMPOSITION IN THE FINNISH BOREAL FOREST

261

Heimsch, L., H. Vekuri, L. Kulmala, A. Lohila, M. Korhonen, O. Nevalainen, J. Rainne, T. Mäkel, J. Hatakka, J.-P. Tuovinen, T. Laurila, and J. Liski

CARBON BALANCE AT TWO FINNISH AGRICULTURAL GRASSLANDS WITH CONTRASTING SOIL TYPES

263

Heiskanen, L., M. Aurela, J.P. Tuovinen, T. Virtanen, S. Juutinen, A. Räsänen, T. Penttilä, and T. Laurila

GREENHOUSE GAS EXCHANGE OF A SUBARCTIC FEN: VARIATION OF FOUR PLANT COMMUNITY TYPES DURING TWO CONTRASTING GROWING SEASONS

266

Heitto A., C. Mohr, K. Lehtinen, and T. Yli-Juuti

A MODEL TO STUDY THE EFFECTS OF PARTICLE PHASE REACTIONS TO PARTICLES SIZE AND COMPOSITION EVOLUTION

270

Helin, A., H. Hakola, and H. Helln

ANALYSIS OF TERPENOIDS BY THERMAL DESORPTION-GAS CHROMATOGRAPHY-MASS SPECTROMETRY: A CASE STUDY OF DITERPENES

273

Helln, H., S. Schallhart, A. P. Praplan, T. Tykkä, M. Aurela, A. Lohila and H. Hakola

EMISSIONS AND AMBIENT CONCENTRATIONS OF ISOPRENE AND MONO- AND SESQUITERPENES AT A SUB-ARCTIC WETLAND

277

Hemmilä, M., U. Makkonen, G. Panagiotopoulou, H. Hakola, and H. Helln

AMINE AND GUANIDINE EMISSION MEASUREMENTS FROM BOREAL FOREST FLOOR

281

Holopainen, T. E., T. Kuhn, and H. Kokkola

IN-CLOUD SCAVENGING SCHEME FOR SECTIONAL AEROSOL MODULES

285

Hooda, R., K. Teinilä, H. Timonen, L. Salo, H. Kuuluvainen, T. Rönkkö, and A. Hyvärinen

ROADSIDE AIR QUALITY AT A SUB-URBAN SITE NEAR SOUTH DELHI

290

Hu, M., A. Lehtonen, F. Minunno, and A. Mäkel

ROADSIDE AIR QUALITY AT A SUB-URBAN SITE NEAR SOUTH DELHI

296

Hölttä, T. and A. Lintunen

MODEL OF HYDRAULIC FAILURE CAUSED BY WATER LOSS THROUGH BARK IN SCOTS PINE TREES

298

Isokääntä, S., B. Rosati, M. Bilde, and A. Virtanen
HYGROSCOPIC PROPERTIES OF DMS DERIVED AEROSOLS IN SMOG CHAM-
BER STUDY

301

Bian, J. P., Q. Zhang, H. Seppä, J. Raisanen, Z. Lu, P. Zhou, and R. Makkonen
DUST CONCENTRATIONS ROLE IN THE NORTHERN EXPANSION OF WES-
TERN AFRICAN MONSOON DURING THE MID-HOLOCENE PERIOD

304

Jokinen, T., K. Neitola, I. Ylivinkka, and M. Sipilä
CHEMICAL COMPOSITION OF AEROSOL PRECURSORS IN THE FINNISH SU-
BARCTIC

306

Joutsensaari, J., P. Yli-Pirilä, A. A. Waza, S. Bhutto, J. Kim, E. Kari, L. Hao, P.
Miettinen, and J. K. Holopainen
SECONDARY ORGANIC AEROSOL FORMATION VIA OZONOLYSIS OF GREEN
LEAF VOLATILES (GLV) AND TERPENES

308

Kangasluoma, J., R. Cai, J. Jiang, C. Deng, D. Stolzenburg, L. R. Ahonen, T. Chan,
Y. Fu, C. Kim, T. M. Laurila, Y. Zhou, L. Dada, J. Sulo, R. C. Flagan, M. Kulmala,
T. Petäjä, and K. Lehtipalo
OVERVIEW OF MEASUREMENTS AND CURRENT INSTRUMENTATION FOR
1-10 NM AEROSOL PARTICLE NUMBER SIZE DISTRIBUTIONS

312

Karttunen, S., M. Kurppa, and L. Järvi
ASSESSING THE EFFECT OF VEGETATION LAYOUT ON AEROSOL PAR-
TICLE CONCENTRATIONS WITHIN AN URBAN STREET CANYON USING
LARGE-EDDY SIMULATIONS

318

Keskinen, J.-P., R. Makkonen, and J. Lento
FCOE IN CMIP6

321

Keskinen, H., L. Heikkinen, I. Ylivinkka, P. A. Aalto, J. Aalto, E. Ezhova, K. Lehtipalo, M. Rätty, S. Santapukki, J. Kesti, J. Levula, M. Loponen, S. Rantanen, H. Laakso, R. Pilkottu, T. Matilainen, T. Salminen, M. Kulmala, T. Nieminen, and T. Petäjä
AUTUMNAL AEROSOL PM10 CONCENTRATION IN BOREAL FOREST AT
2005-2017

324

Kesti, J., E. Asmi, E.J. O'Connor, J. Backman, K. Budhavant, and . Gustafsson
PROCESSING OF AEROSOL SIZE DISTRIBUTIONS DURING THE TRANSPORT
OVER THE INDIAN OCEAN IN DIFFERENT SEASONS

328

Kohl, L., M. Koskinen, P. Mkiranta, T. Polvinen, M. Patama, S. Tenhoviirta, and M. Pihlatie
A CONTROLLED ENVIRONMENT CHAMBER SYSTEM FOR HIGH FREQUENCY
OF LEAF LEVEL CH₄ EXCHANGE MEASUREMENTS: SETUP, OPERATING
PRINCIPLES, AND INITIAL RESULTS

332

Kohonen, K-M., A. Vähä, M. Aurela, I. Mammarella, and T. Vesala
CARBONYL SULFIDE FLUX MEASUREMENTS OVER A RIVERS

334

Kokkonen, T. V., M. Kurppa, V.-M. Kerminen, Y. Wang, Z. Lin, Y. Chao, and M. Kulmala
SEASONAL VARIATION OF THE EFFECT OF HAZE ON THE URBAN BOUNDARY
LAYER HEIGHT IN BEIJING

337

Kontkanen, J., C. Yan, T. V. Kokkonen, L. Dada, C. Deng, Y. Fu, Y. Liu, J. Jiang, M. Kulmala, and P. Paasonen
ESTIMATING PARTICLE NUMBER EMISSIONS SIZE DISTRIBUTIONS IN BEIJING
BASED ON MEASURED PARTICLE SIZE DISTRIBUTIONS

339

Korhonen, J. F. J., N. Freistetter, J. Anttila, T. Vesala, and M. Pihlatie
INTEGRATING SOCIETY WITH SCIENCE

341

Korhonen, K. T. B. Kristensen, J. Falk, R. Lindgren, C. Andersen, R. L. Carvalho, V. Berg-Malmberg, A. Eriksson, C. Boman, J. Pagels, B. Svenningsson, M. Komppula, K. E. J. Lehtinen and A. Virtanen

SOLID BIOMASS COMBUSTION SOOT PROPERTIES RELATED TO THEIR ICE NUCLEATION ABILITY IN IMMERSION FREEZING

344

Korkiakoski, M., T. Penttil, T. Määttä, V. Hyöky, P. Pietikäinen, and A. Lohila
FIELD SCALE IRRIGATION EXPERIMENT TO INVESTIGATE METHANE EXCHANGE OF UPLAND FOREST SOIL IN NORTHERN FINLAND

349

Koskinen, M., A. Lohila, T. Laurila, P. Strakova, T. Penttilä, M. Pihlatie, and R. Laiho
REDOX IN IMPROVING ECOYSTEM MODELING UNDER ANOXIC CONDITIONS

353

Kubeka, J., V. Besel, T. Kurtn, and H. Vehkamäki
ATMOSPHERIC MOLECULAR CLUSTERS: PRESENCE OF WATER

356

Kudzotsa, I., H. Kokkola, J. Tonttila, and S. Romakkaniemi
RAPID REVERSAL OF GLOBAL WARMING THROUGH ARCTIC CLOUD SEEDING

358

Kurppa, M., M. Lange, H. Suominen, E. Oikarinen, R. Savvides, L. Järvi, and K. Puolamäki
APPLYING MACHINE LEARNING TO REPLICATE LARGE-EDDY SIMULATION RESULTS ON URBAN POLLUTANT DISPERSION

363

Kühn, T., K. Kupianen, T. Miinalainen, H. Kokkola, V.-V. Paunu, A. Laakso, J. Tonttila, R. Van Dingenen, K. Kulovesi, N. Karvosenoja, and K. E. J. Lehtinen
CLIMATIC IMPACTS OF BLACK CARBON MITIGATION IN THE ARCTIC

366

Köster, K., H. Aaltonen, E. Köster, C. Ribeiro-Kumara, X. Zhou, H. Zhang-Turpeinen, F. Berninger, and J. Pumpanen
SHORT AND LONG TERM EFFECTS OF FOREST FIRES ON THE STABILITY OF CARBON POOLS IN BOREAL FORESTS (BOREALFIRE)

370

Laitinen, T., E. Häkkinen, J. Chen, E. Siivola, M. Ehn, and M. Sipilä
FLOW TUBE EXPERIMENTS: SYSTEM VALIDATION AND MEASURING PARTICLE GROWTH AND UPTAKE OF DIFFERENT COMPOUNDS

373

Lampilahti, J., Z. Brasseur, M. Lampimäki, P. Poutanen, A. Manninen, A. Franck, M. Peltola, P. Hietala, Y. Wu, T. Petäjä, and M. Kulmala
AIRBORNE MEASUREMENTS OF AEROSOL PARTICLES DURING 2018 WINTER AND SPRING

377

Lampimäki, M., J. Ukkola, O. Laitinen, T. Vainio, L. Ahonen, J. Kangasluoma, E. Siivola, A. Samoylenko, G. Bart, S. Vainio, H. Liimatainen, and T. Petäjä
MEASUREMENTS OF NANOCELLULOSE AEROGEL FILTRATION PROPERTIES AND EXOSOMES SIZE-DISTRIBUTION

379

Lan, H., M. Jussila, K. Hartonen, and M.-L. Riekkola
DEVELOPMENT OF SELECTIVE MATERIALS FOR MINIATURIZED AIR SAMPLING TECHNIQUES

381

Leinonen, V., S. Heikkinen, T. Nieminen, T. Yli-Juuti, A. Virtanen, and S. Mikkonen
TRENDS OF PARTICLE NUMBER-SIZE DISTRIBUTION PARAMETERS IN MULTIPLE SITES

384

Leppänen, A., M. Raivonen, T. Markkanen, T. Aalto, T. Kleinen, X. Li, T. Vesala, A. Lohila, M. Nilsson, E. Humphreys
MODELING PEATLAND METHANE EMISSIONS ON FOUR SITES

387

Lheureux, V., L. Beck, H. Junninen, J. Brito, K. Sellegri, D. Worsnop, C. Flamant, M.A. Zaidan, J. Duplissy, T. Nieminen, and M. Kulmala
UNSUPERVISED MACHINE LEARNING APPLIED ON ATMOSPHERIC DATA FROM THE DACCIWA PROJECT

389

Li, H., M. Riva, P. Rantala, L. Heikkinen, K. Daellenbach, J. E. Krechmer, P.-M. Flaud, D. R. Worsnop, M. Kulmala, E. Villenave, E. Perraudin, M. Ehn, and F. Bianchi

CHEMICAL CHARACTERIZATION AND SOURCE APPORTIONMENT OF VOLATILE ORGANIC COMPOUNDS IN FOREST AREAS

393

Li, M., L. Wang, J. Liu, W. Gao, T. Song, Y. Sun, L. Li, X. Li, Y. Wang, L. Liu, K. R. Daellenbach, P. J. Paasonen, V.-M. Kerminen, M. Kulmala, and Y. Wang

EXPLORING THE REGIONAL POLLUTION CHARACTERISTICS AND METEOROLOGICAL FORMATION MECHANISM OF PM_{2.5} IN NORTH CHINA DURING 2013-2017

396

Li, X., O. Wahlroos, S. Haapanala, A. Ojala, J. Pumpanen, H. Vasander, T. Vesala, and I. Mammarella

CARBON DIOXIDE AND METHANE FLUXES FROM DIFFERENT SURFACE TYPES IN A CREATED URBAN WETLAND

398

Li, Z., A. Buchholz, A. Ylisirniö, L. Barreira, L. Hao, S. Schobesberger, T. Yli-Juuti, and A. Virtanen

IMPACT OF MOLECULAR-LEVEL VARIABILITY ON THE ISOTHERMAL EVAPORATION OF BIOGENIC SECONDARY ORGANIC AEROSOL PARTICLES

403

Liikanen, A. K., J. Hueber, D. Helmig, and A. P. Praplan

OZONE REACTIVITY MEASUREMENTS OF BIOGENIC VOLATILE ORGANIC COMPOUNDS

405

Lindfors, L., V. Hurry, and T. Hölttä

RELATIONSHIP BETWEEN EXTREME TEMPERATURE EVENTS IN THE WINTER, FREEZING INJURY AND FOLLOWING SUMMERS GROWTH ON PINE AND SPRUCE

408

Linkosalmi, M., M. Aurela, J.-P. Tuovinen, M. Peltoniemi, C. M. Tanis, A. N. Arslan, T. Markkanen, O. Nevalainen, J. Rainne, and T. Laurila

VEGETATION PHENOLOGY LINKED TO CO₂ FLUXES IN THREE NORTHERN PEATLANDS

410

Lintunen, A., Y. Preisler, I. Oz, X. Chen, D. Yakir, and T. Hölttä
BARK EVAPORATION AND CO₂ EXCHANGE IN A SEMI-ARID FOREST, IS-
RAEL

413

Liu, Ch., and A. Mäkelä
HYDRAULIC CAUSES OF THE PRODUCTION AND ABOVEGROUND GROWTH
DECLINES OF OLD SCOTS PINE

416

Luoma, K., J.V. Niemi, H. Timonen, M. Aurela, A. Helin, A. Kousa, T. Rönkkö, A.
Virkkula, and T. Petäjä
DECREASING TRENDS OF BLACK CARBON IN SOUTHERN FINLAND

420

Machacova, K., E. Vainio, O. Urban, and M. Pihlatie
SEASONAL DYNAMICS OF N₂O AND CH₄ FLUXES OF BOREAL TREE STEMS

423

Mahura, A., R. Nuterman, G. Nerobelov, M. Sedeeva, S. Smyshlayev, M. Savenets,
L. Pysarenko, S. Krakovska, S. Ivanov, S. Michaelides, I. Ruban, A.S. Sassi, R. Mak-
konen, A. Baklanov, T. Petäjä, S. Zilitinkevich, and M. Kulmala
INTEGRATED MULTI-SCALE MODELLING FOR METEOROLOGY-CHEMISTRY-
AEROSOLS INTERACTIONS

427

Mahura, A., T. Petäjä, H.K. Lappalainen, N. Altimir, I. Bashmakova, A. Borisova,
S.M. Noe, E-M. Duplissy, P. Haapanala, J. Bäck, L. Järvi, A. Ojala, J. Pumpanen, G.
Oblogov, A. Vasiliev, F. Pankratov, V. Shevchenko, P. Konstantinov, M. Varentsov,
S. Chalov, A. Baklanov, I. Ezau, S. Zilitinkevich, M. Kulmala
ARCTIC DATASETS IN THE INARS INTERNATIONAL COLLABORATION

432

Makkonen, R., and J. Liu
IDENTIFYING GLOBAL AEROSOL-CLIMATE INTERACTIONS THROUGH GEOS-
PATIAL NETWORKS

435

Mammarella, I., P. Alekseychik, D.V. Karpov, N.V. Filippova, T. Vesala, and E.D.
Lapshina
EDDY-COVARIANCE MEASUREMENTS OF CH₄ AND CO₂ FLUXES AT A BO-
REAL PEATLAND IN WEST SIBERIA

438

Marbouti, M., S. Jang, S. Becagli, T. Nieminen, G. Navarro, M. Sipilä, and M. Kulmala.

RELATIONSHIPS LINKING SATELLITE-RETRIEVED OCEAN COLOR DATA (CHLA-PP-PAR) WITH ATMOSPHERIC COMPONENTS (MSA, SA, HIO₃, HOM, AEROSOL CONCENTRATIONS IN 10, 50 AND 100 NM) IN ARCTIC SURROUNDING AREA

441

Martikainen I.N.J., A. Putkinen, J. Pumpanen, M. K. Pihlatie, and H. M. P. Siljanen
THE CONTRIBUTION OF PHYLLOSPHERIC MICROBES ON NITROUS OXIDE FLUXES OF NORWAY SPRUCE

445

Matkala L., P. Kolari, M. Aurela, J. Bäck, and L. Kulmala
EXTREME WEATHER EVENTS AND CARBON AND WATER FLUXES AT SUBARCTIC SCOTS PINE AND NORWAY SPRUCE SITES IN FINLAND

448

Mauranen, A., J. Mkel, T. Hölttä, Y. Salmon, and T. Vesala
COMPARISON OF STOMATAL CONDUCTANCE APPROACHES IN JSBACH

451

Meder, M., F. Graeffe, J. Shen, H. Virta, Y. Zhang, O. Garmash, O. Peräkyl, L. Qulver, and M. Ehn

CALIBRATING CHEMICAL IONIZATION MASS SPECTROMETERS WITH A DROPLET EVAPORATION BASED METHOD

454

Meinander, O., S. Chalov, H. Lappalainen, J. Ekman, K. Eleftheriadis, D. Frolov, A. Hyvärinen, V. Ivanov, N. Karvosenoja, K. Kupiainen, O. Popovicheva, I. Semenkov, L. Sogacheva, and The MSU Workshop Participants

ABOUT BLACK CARBON IN THE ARCTIC AND SIGNIFICANCE COMPARED TO HIGH-LATITUDE DUST SOURCES (FINNISH-RUSSIAN WORKSHOP AT THE LOMONOSOV MOSCOW STATE UNIVERSITY, 17-18 SEPTEMBER 2019, IN CO-OPERATION WITH MSU, INAR, PEEEX, MFA/IBA AND FMI)

457

Mielonen, T., T. Yli-Juuti, A. Virtanen, A. Hienola, T. Khn, J. Merikanto, A. Lipponen, A. Laakso, T. Bergman, H. Korhonen, P. Kolmonen, L. Sogacheva, M.R.A. Pitkänen, A. Arola, G.F.R de Leeuw, and H. Kokkola

CLIMATIC SIGNIFICANCE OF BIOGENIC AEROSOLS IN WARMING BOREAL FOREST: PART 2. SATELLITE OBSERVATIONS OF AEROSOLS AND CLOUDS

466

Miinalainen, T., H. Kokkola, K. E. J. Lehtinen, and T. Khn
CLIMATIC EFFECTS OF ANTHROPOGENIC AEROSOL EMISSIONS ORIGINATING FROM CHILE AND MEXICO

469

Mikkola J., V. Sinclair, and F. Bianchi
SLOPE AND VALLEY WINDS IN THE HIMALAYAS AS SIMULATED BY THE WEATHER RESEARCH AND FORECAST MODEL (WRF)

473

Mikkonen, S., Z. Nmeth, V. Varga, T. Weidinger, V. Leinonen, T. Yli-Juuti, and I. Salma
TIME TRENDS OF PARTICLE NUMBER CONCENTRATIONS IN BUDAPEST BETWEEN 2008 AND 2018

477

Mäki, M., P. Vestin, M. Roland, B. Tupek, K. Ryhti, J. Pumpanen, J. Heinonsalo, J. Bäck, and L. Kulmala
THE ACTIVITY OF ROOTS AND SOIL MICROBES ALONG A LATITUDINAL GRADIENT

480

Mäki, M., T. Mali, H. Helln, J. Heinonsalo, T. Lundell, and J. Bäck
COMPETITION PROMOTES RELEASE OF VOLATILE ORGANIC COMPOUNDS BY WOOD DECAYING FUNGI ON CONIFEROUS WOOD

483

Mänd, P., T. Hölttä, M. Mäki, P.Kupper, and J. Bäck
DO CLIMATE-DRIVEN CHANGES IN TREE HYDRAULICS AFFECT BVOC AND NOX EMISSIONS FROM SILVER BIRCHES?

486

Nevalainen, O., L. Kulmala, A. Lohila, L. Heimsch, H. Vekuri, T. Laurila, and J. Liski
CROP VEGETATION PARAMETERS FROM SENTINEL-2 FOR MONITORING CARBON UPTAKE BY AGRICULTURAL FIELDS

487

Nieminen, T., J. Heiskanen, V. Leinonen, O. Kurri, S. Mikkonen, T. Yli-Juuti, and M. Kulmala
CATEGORIZATION OF GROUND-BASED MEASUREMENT SITES BY AIR MASS SOURCE AREA, LAND-COVER TYPE AND POPULATION DENSITY

490

Nykänen, H., A. J. Rissanen, J. Turunen, T. Tahvanainen, and H. Simola
STABLE CARBON ISOTOPIC COMPOSITION TRANSITIONS OF PEAT CO-
LUMNS IN A PARTIALLY FORESTRY-DRAINED BOREAL BOG

492

Oivukkamäki, J., J. Atherton, S. Xu, A. Riikonen, and A. Porcar-Castell
DETECTING POTATO LEAF NUTRIENT CHANGES WITH LEAF LEVEL
FLUORESCENCE AND REFLECTANCE MEASUREMENTS

495

Ozon, M., A. Seppänen, J. Kaipio, and K. Lehtinen
PARAMETER ESTIMATION OF THE GENERAL DYNAMIC EQUATION FOR
AEROSOLS USING THE EXTENDED KALMAN SMOOTHER: APPROACH TO
STEADY STATE CASE

499

Pakarinen, O. H., G. Roudsari, B. Reischl, and H. Vehkamäki
EFFECT OF WATER CONFINEMENT ON ICE NUCLEATION

504

Paljakka T., S. Kovacs, K. Blumenstein, R. Kasanen, E. Terhonen, and T. Hölttä
THE DUTCH ELM DISEASE INFECTED FIELD ELMS IN DRY AND MOIST
CONDITIONS

507

Patama, M., L. Kohl, M. Koskinen, S. Tenhoviirta, and M. Pihlatie
AEROBIC METHANE EMISSIONS FROM BOREAL TREES: TEMPORAL VA-
RIATIONS AND THE EFFECTS OF STRESS

509

Peltola, O., P. Kolari, K. Lapo, I. Martinkauppi, C.K. Thomas, and T. Vesala
OBSERVING FINE-SCALE SPATIAL DETAILS OF ATMOSPHERIC MIXING
WITH DISTRIBUTED TEMPERATURE SENSING

512

Peräkylä, O., M. Riva, L. Heikkinen, L. Qulver, P. Roldin, and M. Ehn
VOLATILITY OF HIGHLY OXYGENATED MOLECULES (HOM) FROM ALPHA-
PINENE OXIDATION

516

Pichelstorfer, L., M. Rissanen, P. Roldin, T. Kurten, and M. Boy
FORMATION OF HOM FROM AVOCES AND ITS ATMOSPHERIC RELEVANCE

520

Praplan, A.P., S. Schallhart, T. Tykkä, A. Helin, and H. Helln
HYDROXYL RADICAL (OH) REACTIVITY OF BIRCH AND SPRUCE EMIS-
SIONS FOR IN SITU CONDITIONS

524

Pullinen, I., A. Ylisirniö, O. Visnen, L.Q. Hao, A. Buchholz, S. Schobesberger, Z. Li,
E. Kari, P. Miettinen, P. Yli-Pirilä, and A. Virtanen
SECONDARY ORGANIC AEROSOL FORMATION FROM α -PINENE VERSUS
REAL PLANT EMISSIONS

528

Kohl, L., M. Nurminen, J.J. Havisalmi, M. Koskinen, S. Gerin, V. Lindholm, K. Pel-
toniemi, A. Lohila, M. Pihlatie, and A. Putkinen
BIOTIC AND ABIOTIC DRIVERS OF SOIL CH₄ PRODUCTION AND OXIDA-
TION PROCESSES IN A NORTHERN BOREAL CATCHMENT

532

Raivonen, M., A. Leppänen, T. Markkanen, T. Aalto, T. Kleinen, X. Li, J. Mäkel, M.
Aurela, A. Lohila, K. Rautiainen, and T. Vesala
FROZEN SOIL IN A MODEL OF PEATLAND GAS TRANSPORT

535

Rajewicz, P.A., A. Riikonen, C. Zhang, J. Atherton, B. Fernandez-Marin, J. I. G.
Plazaola, and A. Porcar-Castell
CORRELATING LEAF-LEVEL SPECTRAL CHLOROPHYLL FLUORESCENCE
WITH PHOTOSYNTHESIS-CONTROLLING FACTORS DURING SPRING RECO-
VERY IN FINNISH BOREAL FOREST

538

Rantanen, M., J. Räisänen, V. A. Sinclair, J. Lento, and H. Järvinen
THE EXTRATROPICAL TRANSITION OF HURRICANE OPHELIA (2017) AS
DIAGNOSED WITH A GENERALIZED OMEGA EQUATION AND VORTICITY
EQUATION

542

Reischl, B., S. Turtola, G. Roudsari, O.H. Pakarinen, and H. Vehkamäki
TOWARDS UNDERSTANDING HETEROGENEOUS ICE NUCLEATION ON
REALISTIC SILVER IODIDE SURFACES FROM ATOMISTIC SIMULATION

545

Rissanen, K., A. Vanhatalo, Y. Salmon, J. Bäck, and T. Hölttä
TREE WATER RELATIONS AND CAMBIAL GROWTH AFFECT SCOTS PINE
(PINUS SYLVESTRIS) STEM VOC EMISSIONS

549

Roudsari, G., B. Reischl, O. H. Pakarinen, and H. Vehkamäki
ATOMISTIC SIMULATIONS OF ICE NUCLEATION ON SILVER IODIDE (0001)
SURFACES WITH DEFECTS

553

Lan, H., J. Ruiz-Jimenez, N. Zanca, G. Demaria, Y. Leleev, M. Jussila, K. Hartonen,
and M.-L. Riekkola
AERIAL DRONE, A USEFUL AND RELIABLE CARRIER FOR THE DETERMI-
NATION OF AIR GAS PHASE AND AEROSOL PARTICLE CHEMICAL COMPO-
SITIONS

558

Okuljar, M., J. Ruiz-Jimenez, O.-M. Sieti, G. Demaria, E. Zagatti, T. Liangsupree,
K. Hartonen, J. Heinonsalo, J. Bäck, T. Petäjä, and M.-L. Riekkola
CHARACTERIZATION OF PRIMARY BIOLOGICAL AEROSOL PARTICLES AT
THE BOREAL FOREST BY DIFFERENT METHODS

562

Ruuskanen, A., A. Leskinen, H. Kokkola, M. Komppula, and S. Romakkaniemi
THE EFFECT OF ATMOSPHERIC AEROSOL PARTICLES ON CLOUD ICING

566

Ryhti, K., S. Salko, J. Bäck, and L. Kulmala
SEASONAL DYNAMICS OF SCOTS PINE ROOT RESPIRATION IN FINLAND

569

Räisänen, J
EFFECT OF ATMOSPHERIC CIRCULATION ON RECENT TEMPERATURE
CHANGES IN FINLAND

573

Räty M., P. Aalto, K. Tabakova, H. Keskinen, M. Paramonov, L. Sogacheva, V.-M.
Kerminen, E. Ezhova, and M. Kulmala
THE EFFECT OF BOREAL FOREST ON CLOUDS AND PRECIPITATION BA-
SED ON LONG-TERM ATMOSPHERIC OBSERVATIONS

577

Rorup, B., L. Dada, R. Baalbaki, J. Kangasluoma, M. Kulmala, K. Lehtipalo and the CLOUD Collaboration

EFFECT OF PARTICLE COMPOSITION ON PSM CUT-OFFS DURING THE CLOUD EXPERIMENTS

580

Bhattacharjee, S., R. Pandit, T. Vesala, I. Mammarella, and G. Sahoo
MULTIFRACTAL ANALYSIS OF VELOCITY AND TEMPERATURE FLUCTUATIONS IN THE ATMOSPHERIC SURFACE LAYER OVER THE HYYTIL FOREST

583

Salmon, Y., A. Lintunen, M. Tian, H. Suhonen, T. Vesala, and T. Hölttä
THE ROLE OF LIVING BARK IN BETULA PENDULA ABILITY TO REFILL EMBOLISED XYLEM

588

Santala, M., and R. Makkonen
PARTICIPATORY CLIMATE COMMUNICATION PLATFORM: SERVICE FOR CITIZENS AND RESEARCHERS

591

Sarnela, N., J. Hakala, O. Kausiala, J. Mikkilä, T. Petäjä, M. Sipilä, and M. Kulmala
FIRST RESULTS OF MULTI-SCHEME CHEMICAL IONIZATION INLET MEASUREMENTS IN BOREAL FOREST

594

Schallhart, S., H. Li, P.A. Rantala, F. Bianchi, M. Ehn, and H. Helln
VOC FLUXES FROM A BOREAL FOREST MEASURED BY VOCUS PTR-TOF: A FIRST LOOK

598

Schiestl-Aalto P., Z.R. Stangl, L. Tarvainen, G. Wallin, J. Marshall, and A. Mäkel
USING A WHOLE TREE CARBON ISOTOPE MODEL TO EVALUATE MESOPHYLL CONDUCTANCE HYPOTHESES AND TO LINK WEATHER TO PHLOEM SUGAR ISOTOPIC COMPOSITION

601

Sami, S.
EFFECTS OF MARINE FUEL SULPHUR RESTRICTIONS ON PARTICLE PROPERTIES IN ATMOSPHERIC ENVIRONMENT

606

Shcherbacheva, A., T. Balehowsky, T. Helin, J. Kubecka, T. Olenius, M. Laine, H. Haario, T. Kurten, and H. Vehkamäki

Identification of molecular cluster evaporation rates, enthalpies and entropies by Monte Carlo method

611

Shen, ., X.He, W.Scholz, J.Them, G.Mario, M.Sipilä, K.Lehtipalo, and CLOUD collaboration

THE YIELD OF METHANESULFONIC ACID AND SULPHURIC ACID FROM THE OXIDATION OF DIMETHYL SULFIDE

632

Sillanpää, S., P. L. Fung, M. A. Zaidan AND T. Hussein

LONG-TERM ASSESSMENT OF AIR QUALITY IN HELSINKI, FINLAND

635

Sinclair, V. A., M. Rantanen, P. Haapanala, J. Räisänen, and H. Järvinen

THE STRUCTURE OF EXTRA-TROPICAL CYCLONES IN THE FUTURED

638

Skyttä, A., L. R. Ahonen, and J. Kangasluoma

DMA-MS ANALYSIS OF ALPHA-PINENE OXIDATION PRODUCTS

642

Stolzenburg, D., R. Cai, J. Kontkanen, and J.Kangasluoma

SUB-10 NM SIZE-DISTRIBUTION MEASUREMENTS IN HIGHLY CHALLENGING ENVIRONMENTS: AN OUTLOOK

647

Sulo, J., J. Kontkanen, P.Paasonen, J. Kangasluoma, N. Sarnela, L. Ahonen, T. Laurila, T. Jokinen, M. Kulmala, and K. Lehtipalo

TIME SERIES ANALYSIS OF LONG-TERM MEASUREMENTS OF 1-3 NM PARTICLE SIZE DISTRIBUTIONS AND AEROSOL PRECURSOR GASES FROM THE SMEAR II STATION

650

Svensson, J., J. Ström, and A. Virkkula

FILTER EXPERIMENTS WITH SOOT: INSIGHTS TO LIGHT-ABSORPTION MEASUREMENTS OF SNOW SAMPLES

654

Taipale, D., J. Aalto, P. Schiestl-Aalto, M. Kulmala, and J. Bäck
STAND AGE AND SEASON DEPENDENT IMPORTANCE OF INCLUDING THE
EMISSION OF MONOTERPENES FROM NEW SCOTS PINE FOLIAGE IN MO-
DELS

656

Taipale, U., T. S. Haapoja, A. Meyer-Brandis, V. Suonpää, and P. Söderlund
WHILE ART PERFORATES THE WALLS OF DATA SILOS: CLIMATE WHIRL
ARTS PROGRAM 2013-19 AND BEYOND

660

Tang, Y., P. Schiestl-Aalto, E. Sahlstedt, J. Bäck, and K. Rinne-Garmston
CLIMATE SIGNAL IN PINE NEEDLE SUGAR STABLE CARBON ISOTOPE RA-
TIOS FOR TWO SITES IN NORTHERN AND SOUTHERN FINLAND

666

Tenhovirta, S., L. Kohl, T. Polvinen., M. Koskinen, and M. Pihlatie
A PULSE LABELLING EXPERIMENT TO CONSTRAIN THE BIOCHEMICAL
PRECURSORS OF AEROBICALLY PRODUCED METHANE

668

Thakur, R. C., M. Mäki, H. Hellen, L. Beck, M. Sipilä, and J. Bäck
POTENTIAL SOURCES OF BIOGENIC VOLATILE ORGANIC COMPOUNDS IN
ARCTIC- FIRST RESULTS FROM NY-LESUND, SVALBARD

671

Tham, Y.J., N. Sarnela, I. Siddharth, L. Beck, A. Saiz-Lopez, and M. Sipilä
FIRST AMBIENT OBSERVATION OF HCLO₃ AND HCLO₄ IN THE ARCTIC EN-
VIRONMENTD

674

Tian, X., F. Minunno, T. Cao, M. Peltoniemi, T. Kalliokoski, and A. Mäkelä
EXTENDING THE RANGE OF APPLICABILITY OF THE SEMI-EMPIRICAL
ECOSYSTEM MODEL PRELES FOR VARYING FOREST TYPES AND CLIMATE

677

Tikkanen, V., R. Halonen, B. Reischl, and H. Vehkamäki
MOLECULAR DYNAMICS SIMULATIONS OF HOMOGENEOUS CO₂ NUCLEA-
TION

681

Tikkanen, O.-P., A. Buchholz, A. Ylisirniö, S. Schobesberger, A. Virtanen, and T. Yli-Juuti

ARE SOA VOLATILITY DISTRIBUTIONS ESTIMATED FROM ISOTHERMAL EVAPORATION AND FIGAERO-CIMS THERMOGRAM DATA SIMILAR?

684

Tonttila, J., H. Kokkola, A. Afzalifar, H. Korhonen, and S. Romakkaniemi
MODELLING PRECIPITATION ENHANCEMENT VIA HYGROSCOPIC SEEDING IN WARM AND MIXED-PHASE CLOUDS USING UCLALES-SALSA

688

Tsuruta, A., L. Backman, J. Hakkarainen, E. Kivimäki, H. Lindqvist, V. Kangasaho, M. Tenkanen, T. Markkanen, M. Raivonen, A. Reppänen, and T. Aalto

EUROPEAN METHANE BUDGETS ESTIMATED FROM CTE-CH₄ ATMOSPHERIC INVERSE MODEL

692

Tuovinen, S., J. Kontkanen, C. Yan, C. Deng, Y. Fu, K. R. Daellenbach, W. Du, Y. Liu, J. Jiang, and M. Kulmala

INVESTIGATING EFFECTIVE CONDENSATION SINK BASED ON HETEROGENEOUS NUCLEATION THEORY

695

Tuppi L., P. Ollinaho, M. Ekblom, V. Shemyakin, and H. Järvinen
ON EXTRACTING INFORMATION FROM CLOSURE PARAMETER CONVERGENCE TESTS USING OPENIFS

698

Uusitalo, H., J. Kontkanen, A. Demakova, M. Arshinov, T. Nieminen, and M. Kulmala

SIMULATIONS OF NEW PARTICLE FORMATION IN BOREAL FOREST USING CLUSTER DYNAMICS SIMULATION, PARAMETERIZATION AND MEASUREMENT RESULTS

704

Vakkari, V., E.J. O'Connor, and P.G. van Zyl
MEASUREMENTS OF AEROSOL PARTICLE DEPolarIZATION RATIO AT WELGEGUND, SOUTH AFRICA

708

Van Wittenberghe, S., N. Ignacio Garcia, B. Fernandez-Marn, A. Porcar-Castell, and J. Moreno

PHOTOSYNTHETIC ENERGY REGULATION UNDER EXCESSIVE LIGHT: THE QUICK IN VIVO ROLE OF XANTHOPHYLL POOL CONVERSIONS

710

Vekuri, H., A. Lohila, L. Kulmala, J-P. Tuovinen, J. Rainne, T. Mäkelä, J. Hatakka, E. Joki-Tokola, J. Liski, And T. Laurila

GREENHOUSE GAS FLUX MEASUREMENTS ON AN AGRICULTURAL GRASSLAND ON PEAT SOIL

713

Virkkula, A., J. Paatero, E. Asmi, H. Lihavainen, J. Svensson, M. Vestenius, P. Räisänen, A. Hienola, O. Meinander, H.-R. Hannula, S. Manninen, M. Ruppel, A. Korhola, J. Tissari, O. Sippula, P. Tiitta, M. Ihalainen, H. Lamberg, K. Kupiainen, M. Savolahti, V.-V. Paunu, and N. Karvosenoja

NOVEL ASSESSMENT OF BLACK CARBON IN THE EURASIAN ARCTIC (NABCEA): A SELECTION OF RESULTS AFTER THREE YEARS OF RESEARCH

716

Virman, M., M. Bister, V.A. Sinclair, J. Räisänen, and H. Järvinen

TEMPERATURE RESPONSE TO EVAPORATION OF STRATIFORM PRECIPITATION IN IDEALIZED WRF SIMULATIONS

722

Vähä, A., M. Aurela, S. Guseva, K.-M. Kohonen, A. Lindroth, A. Lorke, S. MacIntyre, J. Melack, A. Ojala, T. Vesala, M. Wallin, and I. Mammarella

CARBON DIOXIDE AND METHANE FLUXES OVER A BOREAL RIVER MEASURED WITH EDDY COVARIANCE

725

Wang, L., M. Li, J. Liu, J. Mao, W. Gao, T. Song, Y. Sun, L. Li, X. Li, Y. Wang, L. Liu, K. Daellenbach, P. Paasonen, V.-M. Kerminen, Y. Wang, and M. Kulmala

EXPLORING THE REGIONAL POLLUTION CHARACTERISTICS AND METEOROLOGICAL FORMATION MECHANISM OF PM_{2.5} AND O₃ IN NORTH CHINA DURING 2013-2017

728

Wang, Y., M. Riva, H. Xie, L. Heikkinen, and M. Ehn

FORMATION OF HIGHLY OXIDIZED MULTIFUNCTIONAL ORGANIC COMPOUNDS FROM CHLORINE ATOM INITIATED OXIDATION OF ALPHA-PINENE

731

Welti, A., A.A. Piedehierro, Y. Viisanen, A. Virtanen, K. Korhonen, and A. Laaksonen

DEPOSITION ICE NUCLEATION ON CLOUD SEEDING AGENTS

733

Wu, Y., Z. Brasseur, D. Castarde, P. Aalto, L. Hao, L. Heikkinen, N. Sarnela, P. Heikkilä, M. Kulmala, T. Petäjä, E. Thomson, and J. Duplissy

BIOGENIC AEROSOL AFFECT INP CONCENTRATION IN A BOREAL FOREST

736

Xavier. C, A. Rusanen, C. Dean, P. Zhou, L. Pichelstofer, P. Roldi, and M. Boy
AEROSOL MASS YIELDS OF SELECTED BIOGENIC VOLATILE ORGANIC COMPOUNDS - A THEORETICAL STUDY WITH NEAR EXPLICIT GAS-PHASE CHEMISTRY

737

Xu, S., J. Atherton, A. Riikonen, C. Zhan, J. Oivukkamäki, and A. Porcar-Castell
THE EFFECT OF CANOPY STRUCTURE AND PHYSIOLOGY ON CANOPY SOLAR-INDUCED CHLOROPHYLL FLUORESCENCE UNDER WATER STRESS IN POTATO

742

Yao, L., B.W. Chu, S.X. Wang, Y.H. Wang, X.L. Fan, Q.Z. Zha, J. Cai, W. Du, Y.C. Liu, H. Li, L. Wang, M. Ehn, T. Petäjä, Veli-Matti. Kerminen, D.R. Worsnop, M. Kulmala, and F. Bianchi.

GAS-PHASE CHEMISTRY OF HSO₅ AND SO₄ IN URBAN BEIJING, CHINA

745

Yli-Juuti, T., T. Mielonen, H. Kokkola, A. Arola, A. Lipponen, L. Heikkinen, T. Nieminen, M. Ehn, T. Petäjä, and A. Virtanen

CLIMATIC SIGNIFICANCE OF BIOGENIC AEROSOLS IN WARMING BOREAL FOREST: PART 1. IN SITU OBSERVATIONS ON ORGANIC AEROSOL

748

Ylisirniö A., L. Barreira, I. Pullinen, A. Buchholz, J. Jayne, J. Krechmer, D. Worsnop, A. Virtanen, and S. Scobesberger

SOLVING THE MYSTERY OF WILDLY DIFFERING RESULTS IN CALIBRATING FIGAERO TOF-CIMS DESORPTION TEMPERATURE WITH SATURATION VAPOUR PRESSURE

750

Ylivinkka, I., L. Dada, N. Sarnela, C. Yan, L. Yao, R. Baalbaki, T. Jokinen, T. Petäjä, V.-M. Kerminen, and M. Kulmala

SULFURIC ACID PROXY REVISED: THE EFFECT OF CRIEGEE INTERMEDIATES AND DIMERS

752

Zaidan, M.A., L. Dada, M.A. Alghamdi, H. Al-Jeelani, H. Lihavainen, A. Hyvärinen, and T. Hussein

MUTUAL INFORMATION INPUT SELECTOR AND PROBABILISTIC MACHINE LEARNING UTILISATION FOR AIR POLLUTION PROXIES

756

Zanca, T., J. Kubeka, E. Zapadinsky, M. Passananti, T. Kurtzn, and H. Vehkamäki

HOM CLUSTER FRAGMENTATION IN API-TOF MASS SPECTROMETERS

760

Zha, Q., D. Aliaga, O. Peräkylä, X. Chen, J. Enroth, L. Heikkinen, M. Sipilä, T. Petäjä, M. Kulmala, C. Mohr, and F. Bianchi

OBSERVATION OF HIGHLY OXYGENATED ORGANIC MOLECULES (HOM) ON TOP THE BOLIVIAN ANDES AT 5240M A.S.L.

765

Zhang, C., J. Atherton, and A. Porcar-Castell

A PROTOCOL FOR PROCESSING LONG-TERM FLUORESCENCE DATA OBTAINED FROM MONITORING PAM SYSTEM

768

Zhang, H., A. Korrensalo, N. Welti, A. M. Laine, E.-S. Tuittila, M. Maljanen, D. Elliott, T. Vesala, and A. Lohila

THE RESPONSE OF PEATLAND METHANE EMISSIONS TO WARMING

771

Zhang, Y., O. Peräkylä, C. Yan, L. Heikkinen, M. Äijälä, K. Daellenbach, Q. Zha, M. Riva, O. Garmash, H. Junninen, P. Paatero, D. R. Worsnop, and M. Ehn

BENEFITS OF FACTOR ANALYSIS ON SUB-RANGES OF MASS SPECTRA

773

Zhang-Turpeinen, H., M. Kivimäenpää, H. Aaltonen, F. Berninger, E. Köster, K. Köster, O. Menyailo, A. Prokushkin, and J. Pumpanen

WILDFIRE EFFECTS ON BVOC EMISSIONS FROM BOREAL FOREST FLOOR
ON PERMAFROST SOIL IN SIBERIA

776

Zhou P., J.-P. Keskinen, J. Bian, and R. Makkonen

A SIMULATION OF SOA OVER GREEN SAHARA IN MID-HOLOCENE PERIOD
WITH PRESCRIBED ISOPRENE AND MONOTERPENE EMISSIONS

781

Worsnop, D. R.

ATMOSPHERIC AEROSOL CHEMISTRY: CLIMATE AND AIR QUALITY

785

THE CENTER OF EXCELLENCE IN ATMOSPHERIC SCIENCE - FROM MOLECULAR AND BIOLOGICAL PROCESSES TO THE GLOBAL CLIMATE; OVERVIEW FOR YEAR 2019

M. KULMALA¹, A. LINTUNEN^{1,3}, Y. VIISANEN², J. BÄCK³, A. VIRTANEN⁴, M.-L. RIEKKOLA^{5,6}, T. VESALA¹, E. ASMI², A. ASMI², F. BIANCHI¹, M. BOY¹, M. DAL MASO^{1,7}, M. EHN¹, H. HAKOLA², J. HEINONSALO⁸, P. HARI³, K. HARTONEN⁵, A-P. HYVÄRINEN², K. HÄMERI¹, T. HÖLTTÄ³, L. JÄRVI¹, H. JÄRVINEN¹, J. KANGASLUOMA¹, H. KOKKOLA², J. KONTKANEN¹, J. KUJANSUU¹, A. LAAKSONEN², A. LAURI¹, T. LAURILA², K. LEHTIPALO¹, H. LIHAVAINEN², H.K. LAPPALAINEN¹, G. DE LEEUW^{1,2}, K. LEHTINEN⁴, A. LOHILA^{1,2}, R. MAKKONEN^{1,2}, I. MAMMARELLA¹, A. MÄKELÄ¹, D. MOISEEV¹, T. NIEMINEN^{1,3}, A. OJALA⁹, P. PAASONEN¹, T. PETÄJÄ¹, M. PIHLATIE¹, A. PORCAR-CASTELL³, J. PUMPANEN¹⁰, J. PULLIAINEN², A. PURSULA¹³, L. RIUTTANEN¹, S. ROMAkkANIEMI⁴, T. RUUSKANEN¹, S. SCHOBESBERGER⁴, V. SINGLAIR¹, M. SIPILÄ^{1,11}, H. VEHKAMÄKI¹, D.R. WORSNOP^{1,2,4,12}, T. YLI-JUUTI⁴, V.-M. KERMINEN¹ AND COE ATM TEAM

¹Institute for Atmosphere and Earth System Research / Physics, University of Helsinki, Finland

²Finnish Meteorological Institute, Helsinki, Finland

³Institute for Atmosphere and Earth System Research / Forest Sciences, University of Helsinki, Finland

⁴Department of Applied Physics, University of Eastern Finland, Kuopio, Finland

⁵Institute for Atmosphere and Earth System Research / Chemistry, University of Helsinki, Finland

⁶Department of Chemistry, University of Helsinki

⁷Department of Physics, Tampere University of Technology, Tampere, Finland

⁸Department of Environmental and Biological Sciences, University of Eastern Finland, Finland

⁹Department of Environmental Sciences, University of Helsinki, Finland

¹⁰Department of Environmental and Biological Sciences, University of Eastern Finland, Kuopio, Finland

¹¹Karsa Ltd, Helsinki, Finland

¹²Aerodyne Ltd, USA

¹³CSC-IT Centre for Science, Espoo, Finland

Keywords: ATMOSPHERIC PHYSICS, AEROSOLS, CLUSTERS, CLOUDS, ECOSYSTEM-ATMOSPHERE INTERACTIONS, BIOGEOCHEMICAL CYCLES, GLOBAL CLIMATE CHANGE, GHGS, VOCS, LONG-TERM MEASUREMENTS, SATELLITE DATA, SMEAR STATIONS, ICOS, MULTI-SCALE MODELS

INTRODUCTION

The Centre of Excellence in Atmospheric Science – from molecular and biological processes to the global climate (CoE ATM) has its last year ongoing. In this paper, we give an overview on the development of our research activities and summarize the main scientific achievements of year 2019.

The main scientific objective of the CoE ATM is to quantify the COBACC feedbacks in changing climate. In short, COBACC feedback loop offers system understanding of the interactions between the atmosphere and various ecosystems. Increasing CO₂ concentration in the atmosphere increases ecosystem production, but also air temperature via global warming. Healthy ecosystems remove CO₂ from the atmosphere in photosynthesis and store it in plant and soil biomass. The positive climate effect of ecosystems via carbon sink is supplemented by the release of volatile organic compounds capable of forming aerosols and subsequently clouds. Aerosols reflect solar radiation back to space thus cooling the globe, but they also scatter sun light, which increases photosynthesis and further ecosystem production. Our ultimate aim is to produce a quantitative estimate of the climate-biosphere feedback first for boreal and arctic climate regions and finally for the global climate.

More specifically, our aims during the ongoing CoE funding period 2017-2019 are:

1. To find out and quantify the main climatic feedbacks and forcing mechanisms related to aerosols, clouds, precipitation, air quality, biosphere-atmosphere and cryosphere-atmosphere interactions by:
 - Extension of the comprehensive, continuous and long-term observations of atmospheric composition (aerosols, ions, trace gases, clusters, greenhouse gases) to other arctic and boreal environments and to targeted field studies globally
 - Capacity building of atmospheric composition measurement and data interpretation in selected, currently underrepresented areas, such as Russia and China
 - Analyzing the potential impacts of climate change on ecosystem processes e.g. by experimenting in forested ecosystems using the highly instrumented world-class observatories
 - Unraveling the effects of disturbance mechanisms such as extreme weather events and wild fires on processes underlying GHG and BVOC fluxes between ecosystems and the atmosphere in boreal and arctic areas, including permafrost regions
2. To develop, refine and utilize the newest measurement techniques and modeling tools scaling from quantum chemistry to global Earth System Observations and Models by:
 - Chemical sensors further developed for monitoring of amines
 - Increased attention to primary biological aerosol particles from different ecosystems
 - Versatile and flexible solid phase microextraction based air sampling systems, further developed for in-situ analysis of different chemical compounds
 - Expansion of the ground-based observations to the atmospheric column with ground-based and satellite borne remote sensing and aircraft observations and integrating data analysis including new optical products such as SIF and PRI
 - Expansion and utilization of the unique time series on metabolic processes controlling the biogeochemical cycles in ecosystems
 - Improved observation capacity for OH reactivity, trace gases, atmospheric ions and clusters, radicals, atmospheric aerosols, and clouds
3. To create a deep and quantitative understanding on the role of atmospheric clusters and aerosol particles in local and global biogeochemical cycles of water, carbon, sulfur and nitrogen and their linkages to the atmospheric chemistry by:
 - Clarifying the amine reactions in the atmosphere and the effects on aerosol particle formation under atmospheric conditions by different chemical measurements
 - Clarifying and quantifying the contribution of ELVOCs to new particle formation and formation of secondary organic aerosols
 - Defining the most important physical and chemical factors controlling the cloud droplet activation of atmospheric aerosols and developing a simplified thermodynamic presentation to describe the activation
4. To integrate the results in the context of regional and global scale Earth system understanding by participating in international research initiatives:
 - CoE ATM has joined the European consortium of EC-Earth. The EC-Earth model is developed by over 20 institutes around Europe, and ATM CoE will pursue a significant role in the core development team. EC-Earth will provide a state-of-the-art global numerical laboratory for studying the main scientific questions of ATM CoE. ATM CoE will develop necessary processes in EC-Earth, including BVOC emissions, SOA formation and aerosol-cloud interactions. Furthermore, EC-Earth will be applied to quantify the COBACC feedback loops.
 - CoE ATM is participating Coupled Model Intercomparison Project phase 6 (CMIP6) with EC-Earth, both in terms of developing the CMIP6-version and providing CMIP6 simulations for the consortium. EC-Earth development at CoE ATM will ensure that the core processes and interactions of COBACC are adequately incorporated. The close integration to the CMIP6 process provides a link to following IPCC reports.

With these aims, CoE ATM addresses two of the most urgent global Grand Challenges: climate change and deteriorating air quality. As combustion inevitably emits both climate-warming greenhouse gases (GHG)

and mainly climate-cooling but health-deteriorating aerosols, these two Grand Challenges form an interlinked pair of wicked problems that must be solved in the coming decades. The remaining allowable net GHG emissions (i.e. “the carbon budget”) associated with the 1.5 °C and 2 °C temperature targets of the Paris Agreement are highly uncertain: estimates of the remaining carbon budget for the 1.5°C goal vary between -182 and 802 GtCO₂. Two major factors contributing to this uncertainty are the poorly constrained magnitudes of the cooling impact from anthropogenic aerosols partly counteracting the GHG warming, and the various feedbacks in the natural carbon cycle. A further uncertainty in allowable GHG emissions is associated with the possibility to partially counteract them with negative emissions, e.g. by managing carbon sequestration to terrestrial ecosystems. Air quality management falls largely outside international climate treaties, and may thus lead to unwanted climate impacts, as e.g. reductions in aerosol emissions cause additional warming. Our impact goal is to provide science-based facts to support policy and industrial design for clean and carbon-free green growth nationally, in Europe and overseas.

METHODS

The CoE ATM scientific approach is to combine i) continuous and comprehensive *in situ* observations in different types of environments or ecosystems and platforms, ii) ground- and satellite-based remote sensing, iii) targeted laboratory experiments and iv) multi-scale modeling efforts, in order to provide improved conceptual understanding over the relevant spatial and temporal scales. With this approach we are able to improve fundamental process understanding and to clarify the implications of the processes over the relevant spatial and temporal scales.

We have divided the work into four work packages that cover the relevant temporal and spatial scales. The work packages form a continuum from nano and micro scales to a regional scale, and further to a global scale. The comprehensive observations and hierarchical modeling tools, together with open data archives used in an integrative manner in combination with global GHG, aerosol and ecosystem networks, make it possible for us to study the different cycles and feedbacks.

INFRASTRUCTURE AND DATA MANAGEMENT

CoE ATM research infrastructure (INAR RI) belongs to the Finnish RI roadmap 2014–2020. With its research infrastructure and networks, CoE ATM acts as the backbone of the research in atmospheric sciences and atmosphere-biosphere interactions in Finland. CoE ATM is the national focal point of Finnish activities in three European research infrastructures: ICOS (Integrated Carbon Observation System), ACTRIS (Aerosols, Clouds, and Trace gases Research Infrastructure), and eLTER (European Long-term Ecosystem Research). At European level, ICOS head office and ACTRIS PPP office are run in Finland, the latter by the CoE ATM community, and the Advanced Community Project eLTER PLUS is also coordinated in Finland by the CoE ATM team in the University of Helsinki. Our national integration and co-location of environmental infrastructures also include AnaEE (ANALysis and Experimentation on Ecosystems).

CoE ATM operates five field stations in Finland: the four SMEAR (Station for Measuring Ecosystem-Atmosphere Relations) stations and GAW (Global Atmosphere Watch) station in Pallas-Sodankylä. The SMEAR II is the world leading station on ecosystem-atmosphere data due to its comprehensive research program and its unique time series of aerosol formation and biogeochemical fluxes. CoE ATM is also intensively involved in developing the GlobalSMEAR network. GlobalSMEAR serves as a facilitator for distributing and connecting the European Environmental research infrastructures (ICOS, ACTRIS, eLTER, AnaEE) as an integrated measurement concept beyond Europe. The aim of GlobalSMEAR is to establish a global in-situ station network based on the SMEAR concept. The global network would be based on a hierarchy of research stations, where the flagship stations would operate in a seamless collaboration with the flux stations and standard stations to achieve global and regional coverage. At the moment, there is five SMEAR stations (4 in Finland and 1 in Estonia), one SMEAR accredited station in Nanjing (China) called SORPES (Station for Observing Regional Process of Earth System), and one SMEAR concept station called

Beijing Haze -station. In addition, in the frame of the European EMME-CARE project we are in progress of setting up a new SMEAR concept station at Peya site in Cyprus. In 2019, we have received the first applications applying GlobalSMEAR membership that offers collaborative research that aims towards joint publications, annual data workshops and meetings, the development of services and exploring of the business opportunities based on the SMEAR data. In 2019, we have also introduced specific observation concept and roadmap (i.e. SMEAR concept) for marine environments.

Research laboratories include Aerosol Laboratories in the Universities of Helsinki and Eastern Finland and in Finnish Meteorological Institute, Ecophysiological laboratory and Laboratory for Analytical Chemistry in the University of Helsinki. Research is also done in the CERN Cloud Chamber, Leibniz-Institute for Tropospheric Research Laminar Flow Tube, Plant and reaction chamber facility at Forschungszentrum Jülich and European Synchrotron Radiation facility. In addition to ongoing field monitoring, field campaigns and laboratory data, we use large-scale remote sensing data of climate, and modelling at different spatial and temporal scales.

The climate modelling workflow is managed entirely under the CSC infrastructure. The climate modelling groups utilize the Sisu and Taito HPC infrastructure for model simulations, and CSC data infrastructure AVAA, IDA and Etsin. The international Earth System Grid Federation (ESGF) infrastructure is used to publish and acquire climate model simulation data (CMIP6) through national ESGF node at CSC implemented in Pouta virtual environment. The Earth System model data is centrally stored in dedicated CSC storage to ensure common access to all INAR groups.

CoE ATM's data policy follows the general guidelines of "Science Europe Principles on Open Access to Research Publications". The online-processed data from the SMEAR stations is inserted automatically into open SMEAR database (hosted by CSC). Manual processing and checking out of data are made by the responsible researchers. The final end-user data are periodically arranged into yearly datasets that are archived in long-term archive IDA and documented with persistent identifiers (URN) in metadata catalogue Etsin to improve the discoverability of the data. The primary data repository for end-users is SMEAR database, in which about 1800 environmental variables measured more or less continuously at the SMEAR stations are currently available. The data are accessible via the AVAA SmartSMEAR browser user interface (<https://avaa.tdata.fi/web/smart/smear>) and Application Programming Interface (API, documentation at <https://avaa.tdata.fi/web/smart/api>).

RESEARCH COLLABORATION AND STAKEHOLDERS BEYOND ACADEMIA

We have direct working connections with >2500 researchers (joint papers) in 800 universities and research institutes in more than 50 countries. We also have impact collaboration with 84 enterprises in terms of instrument, method and product testing and development (related to e.g. atmospheric aerosols, meteorology, air quality, emissions, Earth observation), expertise in environmental services and process understanding, emission measurements, and carbon accounting development. The CoE ATM predominantly acts as a coordinating body in the research activities taking the lead in directing the science, e.g. within European research infrastructures ICOS, ACTRIS, eLTER and AnaEE, and research initiatives like PEEEX (Pan-Eurasian EXperiment).

The PEEEX research network is currently covering ca 4000 researchers from Europe, Russia and China and over 30 official collaboration agreements with universities and research organizations located mostly in Russia and in China. The CoE ATM in the University of Helsinki has been active in China since 2012 with Nanjing University, Beijing University of Chemical Technology, Fudan University and Guangzhou Academy of Sciences. Also, collaboration with Government of Singapore, Nagoya University (Japan) and South-Korea's Capital city Seoul has started. To promote the PEEEX approach in China and in the frame Belt and Silk Road initiatives, PEEEX has published a separate PEEEX Belt and Silk Road agenda, which introduces the large research questions and research infrastructure relevant to Belt and Silk Road region.

CoE ATM is also a key partner in the CLOUD consortium at CERN. CoE ATM has participated to all the CLOUD campaigns, elucidating several new particle formation mechanisms. CoE ATM is also involved in the cloud and ice formation CLOUD experimental part. Also, our researchers from the Finnish Meteorological Institute and University of Helsinki have been collaborating in Antarctica research already for two decades. In addition to the Finnish owned Aboa, the groups are working in three other research stations: German station Neumayer, Argentine station Marambio, and Italian-French station Concordia. This year, we are also on board in a MOSAiC expedition on Polarstern ship. The ship is expected to freeze into the arctic sea ice and follow its drift while hundreds of scientists from 19 countries over 6 exchange phases will be performing measurements of Arctic environment: atmosphere, sea ice, ocean, biogeochemistry and ecosystem. The main aim of the MOSAiC is to significantly advance our understanding in Arctic climate system, comprehensively support climate models with observations and provide basis for policy making in climate change mitigation and adaptation.

The link from the ATM scientific breakthroughs towards innovations is established via a close co-operation with SMEs, especially with Airmodus Ltd., Karsa Ltd. and SMEAR Ltd. that are university spin off companies. Furthermore, Finnish Meteorological Institute and University of Helsinki have a strategic partnership with e.g. Vaisala Ltd. University of Helsinki and Finnish Meteorological Institute are partners in Cluster for Energy and Environment research consortium, CLEEN Ltd and contribute to the CLEEN research programs. We have several research projects in collaboration with enterprises and other communities. An example of these is a project boosting solutions for the agricultural sector in collaboration with the Baltic Sea Action Group (BSAG), Soilfood and Valio, in which we develop tools for expanding and monitoring carbon storage in arable soils. Another example is the MegaSense project that develops simple air quality sensors for citizens to be combined with the comprehensive SMEAR station network.

CoE ATM collaborates closely with CSC - IT Center for Sciences. This collaboration includes a computing platform, data infrastructure and data practises development: dedicated support persons located on-site in UH and FMI 2-3 days a week, support provided for software performance and installing, developing and running atmospheric science models and related post-processing of results, acquired hardware to Taito cluster and Pouta cloud platform to support atmospheric science, development and provision of Smart SMEAR web portal for easy and open data access, and planning and education on open data and data citation policies and practises.

The general public is reached through social media (Twitter accounts for INAR, PEEEX, GlobalSMEAR, ICOS, ACTRIS, study programs and individual researchers etc.), science-art collaboration, public events, open data tools targeted for the general public (Carbon Tree), open MOOC courses, teaching material available online, and through weather forecasts. Government agencies and decision makers include individual decision makers, government panels, Finnish parliament, and EU parliament. The most important NGOs are Baltic Sea Action Group, Compensate Foundation, Evangelical Lutheran Church of Finland, and cities and communities like Helsinki, Juupajoki, Salla, and Savukoski. Few concrete examples from this year are the start of Compensate that is a Finnish non-profit foundation that aims to reduce the amount of carbon dioxide in the atmosphere by collecting compensation payments for purchasing emissions reduction units. We collaborate with Compensate to find the most reliable and cost efficient ways to take in carbon from the atmosphere. Another example is the Energy and Climate Strategy Group of the Evangelical Lutheran Church of Finland that is chaired by Dr. Laura Riuttanen. The group prepared a programme for the Church in Finland to be carbon neutral in 2030.

RESEARCH HIGHLIGHTS

Ten of our researchers were selected as Thomson Reuters Highly Cited Researchers that are among the 1 % of the most cited researchers in their field in 2018: Markku Kulmala, Tuukka Petäjä, Veli-Matti Kerminen, Douglas Worsnop, Ari Laaksonen, Mikael Ehn, Mikko Sipilä, Heikki Junninen, Jonathan Duplissy, Mikael

Ehn and Siegfried Schobesberger. This is 25% of all the scientists (of any field) on that that list in Finland. In 2019, a new ERC starting grant was received in the CoE ATM by Federico Bianchi.

Research highlights of the CoE ATM for year 2019 covers various temporal and spatial scales. The highlights are divided into the aims of the funding period:

1. Climatic feedbacks and forcing mechanisms

- Our recent aerosol studies combining long term aerosol and satellite observations reveal a clear dependence on biogenic organic aerosol loadings with increasing temperature but the contribution of increased aerosol loadings to cloud properties is minor (Yli-Juuti et al., 2019, Mielonen et al., 2019)
- Panda (Polar and high altitude atmospheric research) group started long-term measurements at Ny-Ålesund, Svalbard, and at Värriö SMEAR I station in Finnish Lapland with mass spectrometers and cluster detectors. Panda performed a field campaign also at Neumayer III station, Antarctica, focusing on new particle formation from derivatives of marine phytoplankton emitted dimethyl sulphide, penguin colony emitted ammonia and galactic cosmic radiation. Results from 2019 work will be published in 2020-2021. In 2019, Panda coordinated and conducted altogether eight field campaigns around the world.
- In pristine environments, such as the Arctic, the amount of aerosol particles affects the cloud phase more than the aerosol type does (Filioglou et al., 2019)
- In the Arctic, the direct radiative forcing of black carbon (BC) emission reductions induces cooling and scales fairly well with the total global amount of BC emission strength reduction, but the aerosol indirect effects counter-act this cooling. Furthermore, natural variability in arctic cloud and snow cover introduce large uncertainties to these results (Kühn et al., in review)
- Sesquiterpene emissions from a northern boreal fen, Lompolojänkämä, in the Pallas-Yllästunturi National Park were very significant especially during the early growing season. They were exceeding monoterpene emissions during the whole summer.
- Alkylamines were measured from boreal forest floor from spring to fall in 2018. For most of the compounds maximum emissions were detected in July, for example DMA maximum emission rate in July were exceeding $1 \mu\text{g m}^{-2} \text{h}^{-1}$.
- Seasonal tree-stem N_2O flux measurements at SMEAR II station in Hyytiälä revealed that boreal spruce, birch and pine trees are sources of N_2O on an annual scale, and that the seasonality in tree-stem N_2O emissions are strongly connected to the physiological activity of the trees and the ecosystem as indicated in stem respiration and gross primary productivity (Machacova et al. 2019).
- We conducted the first long-term, ecosystem-level carbonyl sulphide (COS) flux measurements with eddy covariance technique in a boreal pine forest covering 32 months, over 5 years. We observed the annual (April-August) average net uptake of COS totaling 62.3 (gS/ha) with 48 % variability (submitted).
- We performed a chamber experiment using laboratory facilities provided by TOMCAT synchrotron beamline at Paul Scherrer Institute in Switzerland. Humid air (RH ~97 %) was led through the chamber including a needle with water stress. The preliminary results show that the water uptake of the needle was ~8 % (MS in preparation).
- Stomatal control can be understood by maximization of photosynthesis rate by balancing between stomatal and non-stomatal relations to photosynthesis (Salmon et al. in review, Lintunen et al. in review, Dewar et al. in preparation).
- According to the 2-year study following the clear-cut of a peatland forest, the CO_2 emissions from the clear-cut area are huge and overwhelm the N_2O emissions, which are also considerable if compared to the situation before the clear cut, in terms of global warming potential (Korkiakoski et al. 2019).
- Novel results of VOC and NO_x emissions from birch shoots at increased and ambient atmospheric humidity are shown. The effect of tree water status and osmotic potential on VOC emissions is discussed (see the abstract by Mänd et al. in this Proceedings).

- We characterized the factors that control the variation in leaf fluorescence spectra across time (Zhang et al. 2019) and species (Magney et al. 2019).
- The water use of pine tree in drained peatland is reduced at both high and low soil water table depths (Wang et al. in preparation).
- The local-scale CO₂ surface exchange in Helsinki was examined using urban land surface model SUEWS which for this purpose was developed to include the biogenic and anthropogenic CO₂ fluxes. In central Helsinki the most important sources are traffic but interestingly human respiration has also significant contribution and should be accounted for when modelling CO₂ emissions in cities and interpreting urban eddy covariance measurements (Järvi et al. 2019).
- The anthropogenic particle number emissions in Beijing are dictated by traffic emissions in nucleation mode size range, i.e. with diameters below 30 nm (Kontkanen et al., in preparation). The atmospheric growth of particles from nucleation mode traffic emissions and from atmospheric regional new particle formation events is the main source of accumulation mode particles (with diameters over 100 nm), which are largely responsible for the haze (Hakala et al., in preparation). During haze episodes in Beijing, a roughness sublayer can form below the turbulent mixing layer and remain isolated from the mixing layer for days, which suppresses the dilution and ventilation of air pollutants (Du et al., in preparation).

2. Development of new measurement techniques and modeling tools

- Miniaturized solid phase microextraction Arrow and in-tube extraction (ITEX) systems, including new selective and non-selective sorbent materials, were successfully applied for on-site sampling of outdoor and indoor air samples. These sampling tools enabled collection of air samples by exploiting also aerial drone as carrier, and ITEX, packed with polyacrylonitrile fibers, made fully automated continuous sampling with on-line quantitative gas chromatography – mass spectrometry analysis possible (Lan et al. 2019, Ruiz-Jimenez et al. 2019).
- Contributions to sub-10 nm particle size distribution measurements via characterization of the half-mini type mobility analyzer at reduced flow rates (Cai et al. 2018a), building of a optimized sub-10 nm differential mobility particle sizer (Kangasluoma et al. 2018) and related theoretical instrument analysis (Cai et al. 2019), introduction of new inversion methods for the particle size magnifier (Cai et al. 2018b), introduction of the methodology for determination of particle counter response times (Enroth et al. 2018), and review of the past developments in sub-3 nm particle counters and their calibrations (Kangasluoma and Attoui 2019).
- We have developed a statistical model for atmospheric cluster fragmentation in the mass spectrometric instrument that is able to reproduce experimental extent of fragmentation without any semi-empirical fitting parameters (Passananti, et al. 2019; Zapadinsky, et al. 2019).
- We have demonstrated that it is possible to tune spread-skill relationship of ensemble predictions systems using algorithmic approaches (Ekblom et al, in review).
- Contributing to vertical profiling studies of aerosols by developing post-processing algorithms for Halo Doppler lidars (Vakkari et al. 2019), and by testing the feasibility to use Unmanned Aerial Vehicles (UAV's) for atmospheric sciences (Barbieri et al., submitted)
- The newly developed sulphuric acid proxy, which takes into account the production by stabilized Criegee intermediates and losses due to dimer formation, follows well the diurnal cycle of measured sulphuric acid concentrations.
- Development of new (Riva et al., 2019a) and a first comparison of several existing (Riva et al., 2019b) instruments to measure VOC oxidation products were completed successfully.
- Precise measurements of plant-emitted methane (CH₄) require quantifying uncertainties and errors related to the gas analysis and measurement systems. We found that plant-emitted VOCs strongly interfere CH₄ concentration measurements by Fourier-transformed infrared spectroscopy (FTIR) but not the analysis by laser absorption spectroscopy (Kohl et al. 2019).
- We have developed greenhouse gas (GHG) measurement techniques, protocols and data harmonization within ICOS and other international projects, including advances in the eddy covariance (EC) method for methane and nitrous oxide (Nemitz et al., 2018), advances in EC data

processing (Sabbatini et al, 2018; Montagnani et al, 2018) and standardization of flux tower setup (Rebmann et al, 2018).

- To develop methodology to deliver new understanding for the interpretation of solar-induced chlorophyll fluorescence data, we presented innovative methodology to measure the fluorescence spectra of plant canopies (Atherton et al. 2019) and to quantify the physical and physiological factors that control it (Liu et al. 2019).
- Dendrometer measurements can be used to monitor tissue elasticity and permeability in winter conditions (Lindfors et al. 2019).

3. The role of atmospheric clusters and aerosol particles in local and global biogeochemical cycles of water, carbon, sulfur and nitrogen and their linkages to the atmospheric chemistry

- New aerosol formation mechanisms were found in the experiments performed in the CLOUD chamber (Lehtipalo et al., 2018) and in the field measurements in Antarctica (Jokinen et al., 2018). An increasing trend was found in the scattering efficiency of aerosol particles at SMEAR II during the last decade (Luoma et al., 2019). The concentrations of ice nucleating particles were measured at SMEAR II for the first time.
- In Tomsk, Siberia, the particle growth rates were smaller and the coagulation losses higher than in Hyytiälä, which causes lower survival probabilities for the newly formed particles and could partly explain the lower NPF frequencies observed in Siberia.
- The results from modelling monoterpene emissions from new Scots pine foliage suggest that the emission of monoterpenes from Finland is underestimated by ~20 Gg monoterpenes / year, and that the underestimation is especially severe during spring months when new particle formation is most frequent.
- Our laboratory studying realistic and complex VOC mixtures show that a) the complexity affects both the yields of single precursors and aerosol properties (Kari et al., 2019, Ylisirniö et al., submitted) and b) that the secondary organic aerosol evaporation is mainly limited by the vapor pressure of the compounds (Buchholz, et al. 2019, Buchholz et al., submitted Tikkanen et al., submitted), while particle-phase accretion chemistry may substantially lower that vapor pressure (D'Ambro et al., 2019), and the particle phase diffusion limitations can play a role in the partitioning of semivolatile vapors and at lowered temperatures (Li et al., submitted).
- The experimental and modelling investigations in a boreal forest environment show that the current mechanistic understanding of VOC oxidation and of the distribution of the oxidation products in the atmosphere can explain the observed nanoparticle growth (Mohr et al., 2019, Roldin et al., 2019)
- VOC emissions potentials from Scots pine depend on effects of soil moisture and cambial growth (Rissanen et al., in preparation). In addition to tree, forest floor has a substantial effect on stand-level VOC fluxes in spring and autumn, whereas in summer the effect is negligible (Mäki et al. 2019).
- Correlation was found between volatile organic compounds (VOCs) in gas phase and their presence in the primary biological aerosol particles by utilizing several statistical tools including machine learning (Okuljar et al., submitted).
- Investigating in South Asia, how brown carbon, a light absorbing aerosol, loses its light absorbing capacity by 84% due to photochemical oxidation during 6000 km transport from the Indo-Gangetic Plain to Indian Ocean (Dasari et al. 2019).

4. Earth system understanding

- Initial global quantification of COBACC feedback loop with the NorESM (Sporre et al., 2019)
- Assessment of mid-Holocene aerosol-chemistry using chemical transport model with focus on Green Sahara
- Participation in Coupled Model Intercomparison Project Phase 6 (CMIP6)
- The temperatures that are nowadays observed in Finland are systematically warmer than they would have been under similar atmospheric circulation four decades ago (Räsänen, 2019)
- Utilizing black carbon- and other aerosol measurements in Pallastunturi, Tiksi and Cape Baranova to validate global aerosol model outputs (Schacht et al. 2019).

- Related to weather system understanding, atmospheric observations and idealised simulations suggest that evaporation of stratiform precipitation and resulting subsidence may offer a new mechanism for deep convection's sensitivity to lower free-tropospheric moisture (Virman et al, 2018, Virman et al. in review)
- Precipitation associated with extra-tropical cyclones increases in a warmer climate and moves farther away from the cyclone centre indicating structural changes to mid-latitude weather systems (Sinclair et al, 2019).

EDUCATION, OTHER OUTCOMES AND SOCIETAL IMPACT

The special features of CoE ATM intensive courses include focus on real research questions, work in small groups with access to comprehensive long-term datasets, and use of the horizontal learning principle enabling everyone – students, supervisors, and lecturers – to adopt both the role of learner and teacher (Lauri et al., 2019). We found out that the motivation of both students and teachers increases upon use of real data and authentic scientific questions (Ruuskanen et al., 2018). Our education research and development team in the University of Helsinki does versatile and unique education development (see the CoE 2019 abstracts by Santala, Martikainen, Ruuskanen et al, Äijälä and Riuttanen) and new research projects are under planning.

In managing the revolutionary social systemic transitions necessary to answer the global climate change and unsustainability problems in the required brief timeframe, comprehensive education of citizens in climate and sustainability issues is of highly importance. The Climate University program, a collaboration of 11 Finnish universities, was recently established to re-imagine and reform Finnish climate education. Also few other new type of courses have been launched in year 2019. The CoE UH team was hosting the Climate Journey for the very first time. EIT Climate-KIC Journey summer school started its' Northern Path from Hyytiälä and explored the impact of climate change on various ecosystems and cities. Climates of Change course that focuses on gaining insight on art - atmospheric science collaboration was held in spring 2019.

Members of the CoE ATM received many awards during the past year: e.g. Academy of Finland award for the societal impact to associate prof. Mari Pihlatie, The Finnish Society of Forest Science Silver Cajander medal to prof. Timo Vesala, International Meteorological Organization prize to prof. Sergej Zilitinkevich.

Researchers from the Finnish Meteorological Institute and University of Helsinki are producing climate simulations for the world largest climate simulation programme for the first time. These climate simulations will be used in the 6th IPCC report that will be published in 2021-2022.

PEEX has participated the Arctic Circle initiated by the former President of Iceland, Ó.R. Grímsson, and International Arctic Forum hosted by Russian President V. Putin. The participation at these high level international dialogue forums provides important up-to-date information on the political discussions, especially on the Arctic and processes on environmental matters and concerns. Furthermore, PEEX has co-organized the Sofia Earth Forums (Helsinki, Finland), which are gathering experts of various disciplines and backgrounds to discuss practical solutions to Grand Challenges of the PEEX Science Plan. The forum organized in December 2019 is dedicated to the carbon neutrality, regulations and incentives, and is organized for the Finnish decision makers and experts. In September 2019, PEEX organized a special Finnish–Russian Workshop on Black Carbon and Arctic Dust in Moscow. In 2020, PEEX will organize an event called "Arena for the gap analysis of the existing Arctic Science Co-Operations" with the support from the Prince Albert Foundation in Monaco and a special session at EGU-2020 (European Geosciences Union) General Assembly.

To understand the processes behind the pollution phenomenon in megacities it is crucial to make long-term, continuous and comprehensive observations on aerosol particles, trace gases and atmospheric oxidants. By quantifying the processes, interactions and feedbacks within different air pollutants and ambient conditions, SMEAR concept can determine the most efficient steps towards reducing secondary air pollution, and thus clean the megacity air. INAR has been active in China since 2012 with Nanjing University, Beijing

University of Chemical Technology, Tsinghua University, Fudan University and Guangzhou Academy of Sciences. Also, collaboration with Government of Singapore, Nagoya University (Japan) and South-Korea's Capital city Seoul has started.

Our activities that aimed to popularize science and increase the knowledge of general public and decision makers on climate-related topic include: e.g. launching a new *kysyilmastosta.fi* ('ask about the climate') service, where anyone can ask anything about the climate and Finnish researchers representing various fields of science will provide answers in accessible language (project coordinator Risto Makkonen); participation in the Finnish delegation to finalize the report on climate change, desertification, land degradation, sustainable land management, food security, and greenhouse gas fluxes in terrestrial ecosystems by the Intergovernmental Panel on Climate Change (IPCC); organizing a policy discussion related to soil and sustainability as part of Science days; organizing a public event in Think corner on Carbon Sink and Carbon sink+.

Climate Whirl arts program was launched and art and science research and activities at the University of Helsinki, Hyytiälä Forestry Field Station began under its umbrella in 2013. The initiative was funded by Kone Foundation until the year 2018 and in 2019, Institute for Atmospheric and Earth System Research (the CoE team in UH) decided to continue and integrate the program to the activities of the research unit. Art-science activities in year 2019 include the artist residence of artist Josefina Nelimarkka in Hyytiälä, who is interested in Climate Change and aims to make the unseen visible at SMEAR II station; co-designing a mural on climate change together with urban artists to the streets of Helsinki (coordinator Stephany Mazon); as part of Climate Whirl arts program Finnish artist group IC-98 publishes a poetic counter-story called *IÄI* (located at an old forest at Hyytiälä and at Viikki Campus in Helsinki) in the end of 2019.

The further increase and develop our impact on society, the Faculty of Science invited Dr. Anneli Pauli to the position of Professor of Practice in Global Grand Challenges.

President of the republic of Finland Sauli Niinistö visited SMEAR II station in Hyytiälä this summer. He was interested to see our measurement station and hear about the ecosystem-atmosphere interaction research.

FUNDING

The Academy of Finland Centre of Excellence (grant no. 307331).

REFERENCES

- Atherton, J., Weiwei, L., Porcar-Castell, A. (2019). Nocturnal Light Emitting Diode Induced Fluorescence (LEDIF): A new technique to measure the chlorophyll a fluorescence emission spectral distribution of plant canopies in situ. *Remote Sensing of Environment* 231: 111137.
- Buchholz, A., Lambe, A., Ylisirniö, A., Li, Z., Tikkanen, O.-P., Faiola, C., Kari, E., Hao, L., Luoma, O., Huang, W., Mohr, C., Worsnop, D.R., Nizkorodov, S., Yli-Juuti, T., Schobesberger, S., Virtanen, A. (2019) Effect of RH and O:C ratio on α -pinene Secondary Organic Aerosol particle evaporation, *Atmos. Chem. Phys.*, 19, 4061-4073, doi.org/10.5194/acp-19-4061-2019.
- Cai, R., Attoui, M., Jiang, J., Korhonen, F., Hao, J., Petäjä, T., Kangasluoma, J. (2018a). Characterization of a high-resolution supercritical differential mobility analyzer at reduced flow rates. *Aerosol Sci Tech* 52:1332-1343.
- Cai, R., Mirme, S., Jiang, J., Kangasluoma, J. (2019). Parameters to determine the optimum performance of electrical mobility spectrometers for measurement of particle size distributions down to the cluster size. *J Aerosol Sci* 127:102-115.
- Cai, R., Yang, D., Ahonen, L. R., Shi, L., Korhonen, F., Petäjä, T., Zheng, J., Kangasluoma, J., Jiang, J. (2018b). Data inversion methods to determine sub-3 nm aerosol size distributions using the Particle Size Magnifier. *Atmos Meas Tech* 11:4477-4491.

- D'Ambro, E. L., Schobesberger, S., Gaston, C. J., Lopez-Hilfiker, F. D., Lee, B. H., Liu, J., Zelenyuk, A., Bell, D., Cappa, C. D., Helgestad, T., Li, Z., Guenther, A., Wang, J., Wise, M., Caylor, R., Surratt, J. D., Riedel, T., Hyttinen, N., Salo, V. T., Hasan, G., Kurtén, T., Shilling, J. E., Thornton, J. A. Chamber-based insights into the factors controlling epoxydiol (IEPOX) secondary organic aerosol (SOA) yield, composition, and volatility, *Atmos. Chem. Phys.*, 19, 11253-11265, doi.org/10.5194/acp-19-11253-2019, 2019.
- Dasari, S., Andersson A., Bikkina, S., Holmstrand, H., Budhavant, K., Satheesh, S., Asmi, E., Kesti, J., Backman, J., Salam, A., Singh Bisht, D., Tiwari, S., Hameed, Z., and Ö. Gustafsson (2019). Photochemical degradation affects the light absorption of water-soluble brown carbon in the SouthAsian outflow, *Science Advances* 5, 1, eaau8066, <https://doi.org/10.1126/sciadv.aau8066>.
- Enroth, J., Kangasluoma, J., Korhonen, F., Hering, S., Picard, D., Lewis, G., Attoui, M., Petaja, T. (2018). On the time response determination of condensation particle counters. *Aerosol Sci Tech* 52:778-787.
- Filioglou, M., Mielonen, T., Balis, D., Giannakaki, E., Arola, A., Kokkola, H., et al. (2019). Aerosol effect on the cloud phase of low-level clouds over the Arctic. *Journal of Geophysical Research: Atmospheres*, 124. <https://doi.org/10.1029/2018JD030088>
- Järvi, L., Havu, M., Ward, H.C., Bellucco, V., McFadden, J.P., Toivonen, T., Heikinheimo, V., Kolari, P., Riikonen, A., Grimmond, C.S.B., (2019). Spatial modelling of local-scale biogenic and anthropogenic carbon dioxide emissions in Helsinki. *J. Geophys. Res. – Atmospheres* 124, doi: 10.1029/2018JD029576.
- Jokinen, T., Sipilä, M., Kontkanen, J., Vakkari, V., Tisler, P., Duplissy, E. M., ... Kulmala, M. (2018). Ion-induced sulfuric acid–ammonia nucleation drives particle formation in coastal Antarctica, *Science advances*, 4, 11, eaat9744.
- Kangasluoma, J., Ahonen, L. R., Laurila, T., Cai, R., Enroth, J., Mazon, S., Korhonen, F., Aalto, P., Kulmala, M., Attoui, M., Petäjä, T. (2018). Laboratory verification of a new high flow differential mobility particle sizer, and field measurements in Hyytiälä. *J Aerosol Sci* 124:1-9.
- Kangasluoma, J. and Attoui, M. (2019). Review of sub-3 nm condensation particle counters, calibrations, and cluster generation methods. *Aerosol Sci Tech* 53:1277-1310.
- Kari, E., Hao, L., Ylisirniö, A., Buchholz, A., Leskinen, A., Yli-Pirilä, P., Nuutinen, I., Kuusalo, K., Jokiniemi, J., Faiola, C.L., Schobesberger, S., Virtanen, A. Potential dual effect of anthropogenic emissions on the formation of biogenic SOA, *Accepted to Atmos. Chem. Phys.*, October 2019.
- Kohl, L., Koskinen, M., Rissanen, K., Haikarainen, I., Polvinen, T., Hellén, H., Pihlatie, M. (2019). Technical note: Interferences of volatile organic compounds (VOCs) on methane concentration measurements. *Biogeosciences*, 16, 3319–3332.
- Korkiakoski M., Tuovinen J.-P., Penttilä T., Sarkkola S., Ojanen P., Minkinen K., Rainne J., Laurila T. and Lohila A. 2019. Greenhouse gas and energy fluxes in a boreal peatland forest after clearcutting. *Biogeosciences*, 16, 3703–3723, <https://doi.org/10.5194/bg-16-3703-2019>
- Lan, H., Holopainen, J., Hartonen, K., Jussila, M., Ritala, M., Riekkola, M.-L. (2019). Fully automated online dynamic in-tube extraction for continuous sampling of volatile organic compounds in air, *Anal. Chem.* 91, 8507.
- Lan, H., Zhang, W., Smått, J.-H., Koivula, R.T., Hartonen, K., Riekkola, M.-L. (2019). Selective extraction of aliphatic amines by functionalized mesoporous silica-coated solid phase microextraction Arrow, *Microchim. Acta* 186, 412.
- Lauri, A., T. Ruuskanen, L. Riuttanen, P. Hari and M. Kulmala (2019). Research-oriented intensive courses foster multidisciplinary atmospheric science. *WMO Global Campus Innovations: New Directions for Education and Training* (accepted for publication).
- Lehtipalo, K., Yan, C., Dada, L., Bianchi, F., Xiao, M., Wagner, R., ... Worsnop, D.R. (2018). Multicomponent new particle formation from sulfuric acid, ammonia, and biogenic vapors, *Science advances*, 4, 12.
- Lindfors, L., Atherton, J., Riikonen, A. and Hölttä, T., 2019. A mechanistic model of winter stem diameter dynamics reveals the time constant of diameter changes and the elastic modulus across tissues and species. *Agricultural and Forest Meteorology*, 272, pp.20-29.

- Liu W, Atherton J, Mottus M, Gastellu-Etchegorry J-P, Malenovský Z, Raunonen P, Åkerblom M, Mäkipää R, Porcar-Castell A (2019). Simulating solar-induced chlorophyll fluorescence in a boreal forest stand reconstructed from terrestrial laser scanning measurements. *Remote Sensing of Environment* 232:111274
- Luoma, K., Virkkula, A., Aalto, P., Petäjä, T., and Kulmala, M. (2019). Over a 10-year record of aerosol optical properties at SMEAR II, *Atmos. Chem. Phys.*, 19, 11363–11382.
- Machacova, K., Vainio E., Urban O., Pihlatie M. Seasonal dynamics of stem N₂O exchange follow the physiological activity of boreal trees. In press to *Nature Communications*.
- Magney TS, Frankenberg C, Köhler P, North GB, Davis T, Dold C, Dutta D, Fisher JB, Grossmann K, Harrington A, Hatfield J, Stutz J, Sun Y, Porcar-Castell A (2019) Disentangling changes in the spectral shape of chlorophyll fluorescence: implications for remote sensing of photosynthesis. *Journal of Geophysical research: Biogeosciences* DOI: 10.1029/2019JG005029
- Mäki, M., Aaltonen, H., Heinonsalo, J., Hellén, H., Pumpanen, J. and Bäck, J. (2019). Boreal forest soil is a significant and diverse source of volatile organic compounds. *Plant and Soil*, 441, 89-110.
- Mohr, C., Thornton, J. A., Heitto, A., Lopez-Hilfiker, F. D., Lutz, A., Riipinen, I., Hong, J., Donahue, N. M., Hallquist, M., Petäjä, T., Kulmala, M. and Yli-Juuti, T. Molecular identification of organic vapors driving atmospheric nanoparticle growth, *Nature Communications*, 10, 4442, 2019.
- Moisseev, D., Lautaportti, S., Alku, L., Tabakova, K., O'Connor, E.J., Leskinen, M., Kulmala, M. (2019). Inadvertent Localized Intensification of Precipitation by Aircraft, *JGR Atmospheres*, 124:4, 2094-2104.
- Montagnani, L., Grünwald, T., Kowalski, A., Mammarella, I., Merbold, L., Metzger, S., Sedlak, P. and Siebicke, L., 2018. Estimating the storage term in eddy covariance measurements: the ICOS methodology. *Int. Agrophys.*, 32, 551-567. doi: 10.1515/intag-2017-0037
- Nemitz, E., Mammarella, I., Ibrom, A., Aurela, M., Burba, G., Dengel, S., Gielen, B., Grelle, A., Heinesch, B., Herbst, M., Hörtnagl, L., Klemetsson, L., Lindroth, A., Lohila, A., McDermitt, D.K., Meier, P., Merbold, L., Nelson, D., Nicolini, G., Nilsson, M.P., Peltola, O., Rinne, J., and Zahniser, M., 2018. Standardization of eddy covariance flux measurements of methane and nitrous oxide. *Int. Agrophys.*, 32, 517-549. doi: 10.1515/intag-2017-0042
- Passananti, M., Zapadinsky, E., Zanca T., Kangasluoma, J., Myllys, N., Rissanen, M.P., Kurtén, T., Ehn, M., Attoui, M. and Vehkamäki, H. (2019) How Well Can We Predict Cluster Fragmentation Inside a Mass Spectrometer? *Chemical Communications*, Vol 5, pp. 5946-5949.
- Räisänen, J. (2019). Effect of atmospheric circulation on recent temperature changes in Finland. *Climate Dynamics*, 53(9), 5675-5687.
- Rebmann, C., Aubinet, M., Schmid H.P., Arriga, N., Aurela, M., Burba, G., Clement, R., De Ligne, A., Fratini, G., Gielen, B., Grace, J., Graf, A., Gross, P., Haapanala, S., Herbst, M., Hörtnagl, L., Ibrom, A., Joly, L., Kljun, N., Kolle, O., Kowalski, A., Lindroth, A., Loustau, D., Mammarella, I., Mauder, M., Merbold, L., Metzger, S., Mölder, M., Montagnani, L., Papale, D., Pavelka, M., Peichl, M., Roland, M., Serrano-Ortiz, P., Siebicke, L., Steinbrecher, R., Tuovinen, J.-P., Vesala, T., Wohlfahrt, G. and Franz, D., 2018. ICOS eddy covariance flux-station site setup: a review. *Int. Agrophys.*, 32, 439-455. doi: 10.1515/intag-2017-0044
- Riva, M., Ehn, M., Li, D., Tomaz, S., Bourgain, F., Perrier, S., & George, C. (2019a). CI-Orbitrap: An Analytical Instrument To Study Atmospheric Reactive Organic Species. *Analytical Chemistry*, 91(15), 9419-9423. doi:10.1021/acs.analchem.9b02093
- Riva, M., Rantala, P., Krechmer, J. E., Peräkylä, O., Zhang, Y. J., Heikkinen, L., Garmash, O., Yan, C., Kulmala, M., Worsnop, D., & Ehn, M. (2019b). Evaluating the performance of five different chemical ionization techniques for detecting gaseous oxygenated organic species. *Atmospheric Measurement Techniques*, 12(4), 2403-2421. doi:10.5194/amt-12-2403-2019
- Roldin, P., Ehn, M., Kurtén, T., Olenius, T., Rissanen, M. P., Sarnela, N., Elm, J., Rantala, P., Hao, L., Hyttinen, N., Heikkinen, L., Worsnop, D. R., Pichelstorfer, L., Xavier, C., Clusius, P., Öström, E., Petäjä, T., Kulmala, M., Vehkamäki, H., Virtanen, A., Riipinen, I., and Boy, M. (2019) The role of highly oxygenated organic molecules in the Boreal aerosol-cloud-climate system, *Nature Communication*, 10, 4370.

- Ruiz-Jimenez, J., Zanca, N., Lan, H., Jussila, M., Hartonen, K. and Riekkola, M.-L. (2019). Aerial drone as a carrier for new miniaturized air sampling systems. *Journal of Chromatography A* 1597, 202-208.
- Ruuskanen, T., H. Vehkamäki, L. Riuttanen and A. Lauri (2018). An Exploratory Study of the Learning of Transferable Skills in a Research-Oriented Intensive Course in Atmospheric Sciences. *Sustainability*, 10(5):1385. <https://doi.org/10.3390/su10051385>
- Sabbatini, S., Mammarella, I., Arriga, N., Fratini, G., Graf, A., Hörtnagl, L., Ibrom, A., Longdoz, B., Mauder, M., Merbold, L., Metzger, S., Montagnani, L., Pitacco, A., Rebmann, C., Sedlak, P., Sigut, L., Vitale, D. and Papale, D., 2018. Eddy covariance raw data processing for CO₂ and energy flux calculation at ICOS ecosystem stations. *Int. Agrophys.*, 32, 495-515. doi: 10.1515/intag-2017-0043
- Schacht, J., Heinold, B., Quaas, J., Backman, J., Cherian, R., Ehrlich, A., Herber, A., Huang, W. T. K., Kondo, Y., Massling, A., Sinha, P. R., Weinzierl, B., Zanatta, M., and I. Tegen (2019). The importance of the representation of air pollution emissions for the modeled distribution and radiative effects of black carbon in the Arctic, *Atmos. Chem. Phys.* 19, 11159–11183, <https://doi.org/10.5194/acp-19-11159-2019>.
- Sinclair, V. A., Rantanen, M., Haapanala, P., Räisänen, J. and Jarvinen, H. (2019) The characteristics and structure of extra-tropical cyclones in a warmer climate. *Weather Clim. Dynam. Discuss.* <https://doi.org/10.5194/wcd-2019-2>
- Vakkari, V., Manninen, A. J., O'Connor, E. J., Schween, J. H., van Zyl, P. G. and E. Marinou (2019). A novel post-processing algorithm for Halo Doppler lidars, *Atmos. Meas. Tech.* 12(2), 839–852, doi:10.5194/amt-12-839-2019.
- Virman, M., Bister, M., Sinclair, V. A., Räisänen, J. and Järvinen, H. (2018). A New Mechanism for the Dependence of Tropical Convection on Free-Tropospheric Humidity. *Geophysical Research Letters* 45(5), 2516-2523.
- Zapadinsky, E., Passananti, M., Myllys, N., Kurtén, T. and Vehkamäki, H. (2019) Modelling on Fragmentation of Clusters Inside a Mass Spectrometer. *Journal of Physical Chemistry A*, Vol 123 (2), pp.611–624.
- Zhang C, Atherton J, Peñuelas J, Filella I, Kolari P, Aalto J, Ruhanen H, Bäck J, Porcar-Castell A (2019) Do all chlorophyll fluorescence emission wavelengths capture the spring recovery of photosynthesis in boreal evergreen foliage? *Plant, Cell and Environment*, doi: 10.1111/pce.13620

ACTIVITIES OF THE ATMOSPHERE MODELLING GROUP IN 2019

M. BOY¹, P. ZHOU¹, M. BAYKARA¹, L. PICHELSTORFER¹, C. XAVIER¹, D. CHEN¹, P. CLUSIUS¹,
P. ROLDIN²

¹Institute for Atmospheric and Earth System Research (INAR) / Physics, P.O. Box 64, FI-00014 University of Helsinki, Finland

²Division of Nuclear Physics, Lund University, P.O. Box 118, 22100 Lund, Sweden

Keywords: ATMOSPHERE MODELLING, VOC, HOM, PRAM, AEROSOLS

INTRODUCTION AND OBJECTIVES

During the last year the main focus of the group was directed towards the formation and atmospheric impact of highly oxygenated organic molecules (HOM). In cooperation with Assist. Prof Pontus Roldin from Lund University we developed the novel near explicit chemical peroxy radical autoxidation mechanism PRAM, which enabled us to predict the HOM concentrations and their role in the formation of secondary organic aerosols (SOA) at the SMEAR II station in Hyytiälä, Finland. Further we applied PRAM together with the Master Chemical Mechanism (MCM) to predict the aerosol yields for various crucial biogenic volatile organic compounds (BVOC) and compared them, where available, with measured data from smog chamber and oxidative flow reactor experiments. Parallel we investigated the capability of our model system SOSAA to calculate the OH-reactivity and compared them with measurements.

METHODS

During the last year we applied different model systems (MALTE-BOX, SOSAA and ADCHEM) to tackle various scientific topics related to atmospheric chemistry and secondary organic aerosol formation. Detailed descriptions of these model systems including references and applications are available at the group website (<https://wiki.helsinki.fi/display/AMG/>) and only a very short introduction to the different models is provided next.

MALTE-BOX is the 0D version of the 1D model MALTE (Model to predict new Aerosol formation in Lower Troposphere - Boy et al., 2006). It consists of modules to calculate the gas-phase chemistry and aerosol dynamics. The peroxy radical autoxidation mechanism (Roldin et al., 2019) was incorporated alongside MCMv3.3.1. PRAM describes the evolution of peroxy radicals (RO₂) from the ozonolysis of monoterpenes driven by subsequent H-shifts and O₂ additions. The current version of PRAM considers HOM autoxidation for a fraction of the peroxy radicals formed during the ozonolysis of α -pinene and limonene and OH oxidation of α -pinene, β -pinene and limonene. The aerosol dynamics are simulated using the University of Helsinki Multicomponent Aerosol model (UHMA). The processes included in the model are nucleation, condensation, evaporation, coagulation and deposition. UHMA now supports an unlimited number of condensing vapours and the condensation algorithm considers both, the Kelvin effect and Raoult's law. New particle formation through neutral and ion-induced clustering of dimethyl amine / ammonia and H₂SO₄ molecules is simulated using the Atmospheric Cluster Dynamics Code (ACDC – Olenius et al, 2013), which is dynamically coupled to the aerosol dynamics model. A group contribution method based on Nannoolal et al. (2008) using the UManSysProp online system (Topping, 2016) is used to estimate the pure liquid saturation vapor pressures (p₀) of the organic compounds in MCMv3.3.1. For the PRAM species, p₀ is estimated using the functional group method SIMPOL (Pankow and Asher, 2008; Roldin et al., 2019).

SOSAA (model to Simulate the concentrations of Organic vapours, Sulphuric Acid and Aerosols) is a 1D chemical transport model comprised of boundary layer meteorology, biogenic emission of VOCs, gas-phase chemistry, aerosol dynamics and gas dry deposition (e.g. Boy et al., 2011; Zhou et al., 2014). The boundary layer meteorology is derived from SCAlar DIStribution (SCADIS; Sogachev et al., 2002), as described in Boy et al. (2011). The biogenic emission module is based on MEGAN (Model of Emissions of Gases and Aerosols from Nature, Guenther et al. 2012). A new module for dry deposition was recently implemented in SOSAA by Zhou et al. (2017a) and extended in Zhou et al. (2017b). The latter describe the explicit simulation of the loss of every compound in the model by dry deposition inside the canopy for all height levels. The gas-phase chemistry and aerosol dynamics are similar as in MALTE-BOX and also include PRAM and ACDC.

ADCHEM is a 2D-Lagrangian model for aerosol dynamics, gas phase chemistry and radiative transfer, which uses 1-order turbulence closure schemes to describe the air mass mixing in the vertical and horizontal direction perpendicular to the air mass trajectories (Roldin et al., 2011a). The model includes a novel aerosol dynamics and particle chemistry module that takes into account condensation and dissolution of over 1000 organic compounds. Further, ADCHEM provides a cloud microphysical module for aerosol-cloud droplet activation and dynamics; in-cloud aerosol processing and in- and below cloud scavenging of particles and gases; a 1D in-canopy model version of MEGAN and a detailed gas-phase chemistry scheme consisting of the Master Chemical Mechanism (MCMv3.3.1) and PRAM (Roldin et al., 2019).

RESULTS

In a study by Praplan et al. (2019) the total hydroxyl radical (OH) reactivity were measurement at the Station for Measuring Ecosystem-Atmosphere Relations (SMEAR II), a boreal forest site located in Hyytiälä, Finland, from April to July 2016. Total OH reactivity is not a simple function of a few variables but includes many complex processes involving sources and sinks that can change dramatically depending on the environmental conditions and the time of the year.

The averaged experimental total OH reactivity increased from April to June before decreasing in July because of more humid nights and lower radiation during the measurement period. The total OH reactivity diurnal pattern from May to July follows the one of biogenic compounds with high values during the night due to the low mixing height, even though emissions are lower at night. A suite of online and offline (O)VOCs measurements was used to calculate the known fraction of OH reactivity to compare it to the total OH reactivity measured. The missing fraction of the OH reactivity was also higher during the night, possibly due to a larger fraction of non-measured oxidation products, compared to day time, when the emissions are higher resulting in a larger fraction of known precursors. Oxidation products resulting from O₃ oxidation at night are not lost chemically (due to the very low levels of OH), which might explain the higher missing fraction of OH reactivity observed at night.

Nevertheless, as the data availability of (O)VOCs varies, the comparison between experimental and calculated OH reactivity is difficult but three different explanations can lead to high missing (unexplained) OH reactivity: 1) simply the lack of measurements, 2) not measuring oxidation products (only their precursors), and 3) not measuring the right class of compounds. Using the one-dimensional transport model SOSAA to estimate oxidation products concentrations from measured precursor concentrations for three periods of two to three days in various months (with most (O)VOC data availability) demonstrated that only a small fraction (up to ca. 9 %) of the missing reactivity can be explained by these oxidation products. On one hand, this is due to the absence in the model of degradation scheme for detected compounds in the ambient air (e.g. Δ^3 -carene, β -farnesene), but on the other hand it is also possible that

non-hydrocarbon compounds contribute to the OH reactivity as well. However, it might not be completely excluded that re-emissions of oxidation products of terpenes from surfaces are causing increases in OH reactivity. The model does not take into account this effect, as it only estimates concentrations of oxidation products based on the concentrations of their precursors.

More measurements of oxidised compounds and identification of non-terpene reactive compounds from emissions also from other sources than vegetation (e.g. soil) are required to better understand the reactivity and local atmospheric chemistry in the forest air in general, in particular during winter, spring, and autumn, when the forest air chemistry is not dominated by emissions from the vegetation.

In a study by Xavier and co-workers (2019) we modeled secondary organic aerosols (SOA) mass loadings from the oxidation (by O₃, OH and NO₃) of five representative biogenic volatile organic compounds: isoprene, α -pinene, limonene β -pinene and β -caryophyllene. The simulations were designed to replicate idealized smog chamber and oxidative flow reactors (OFR). The master chemical mechanism (MCM) together with PRAM, were used to simulate the gas-phase chemistry. The aim of this study was to compare the potency of MCM and MCM+PRAM in predicting secondary organic aerosol (SOA) formation. SOA yields were in good agreement with experimental values for chamber simulations when MCM+PRAM was applied, while a standalone MCM under-predicted the SOA yields. Compared to experimental yields, the OFR simulations using MCM+PRAM over-predicted SOA mass yields for BVOCs oxidized by O₃ and OH, probably owing to increased seed particle surface area used in the OFR simulations. Modelled SOA yields increased with decreasing temperatures and NO concentrations and vice-versa in agreement with the measurements.

The role of highly oxygenated organic molecules (HOM) in the Boreal aerosol-cloud-climate system was investigated by Roldin et al. (2019). Large amounts of volatile organic compounds (VOC) are transferred to the atmosphere from various natural (Guenther et al. 2012) and anthropogenic sources (Müller 1992), e.g.: trees and algae or vehicle emission, solvents and industrial sources. Peroxy radical autoxidation, involving intramolecular hydrogen shifts and oxygen molecule additions in several steps, can quickly (seconds to minutes) lead to the formation of highly oxygenated organic compounds after an initial reaction between a VOC and an oxidant (Ehn et al. 2014). Experiments showed that monoterpenes with endocyclic double bounds (e.g.: α -pinene or limonene) undergoing ozonolysis lead to high yields of HOM production. To a lower extent, monoterpenes oxidized by the hydroxyl radical (OH) form HOM too, while nitrogen monoxide (NO) may suppress the formation of HOM because it reacts with the peroxy radicals and terminate the autoxidation (Ehn et al. 2014; Jokinen et al. 2015; Berndt et al. 2016). The recently developed Peroxy Radical Autoxidation Mechanism PRAM describes the formation of HOM from the monoterpenes α -pinene, β -pinene, Δ^3 -carene and limonene. With PRAM and ACDC implemented in ADCHEM we could for the first time reproduce the HOM gas-phase composition (Fig. 1b) and measured and modelled median particle number size distributions at SMEAR II (Fig. 1a) (Roldin et al., 2019).

In this study we further showed that the combination of NPF and particle growth by biogenic HOM SOA has a profound but complex impact on the aerosol-cloud-climate system over the Boreal forest. In spring the HOM SOA increases the number of CCN with $\sim 10\%$ at cloud updraft velocities (w) in the range 0.3–5 m s⁻¹, which corresponds to water vapour supersaturations between $\sim 0.28\%$ and $\sim 0.84\%$. Furthermore, we estimated that the HOM SOA contributes to an average direct aerosol radiative forcing of -0.10 W m⁻². Thus, biogenic HOM SOA formation most likely contributes to climate cooling over the Boreal forest, both with and without the presence of clouds (Figure 1c and 1d). During typical spring-time conditions HOM SOA contributes to 18% of the modelled submicron particle mass at the SMEAR II station in Finland.

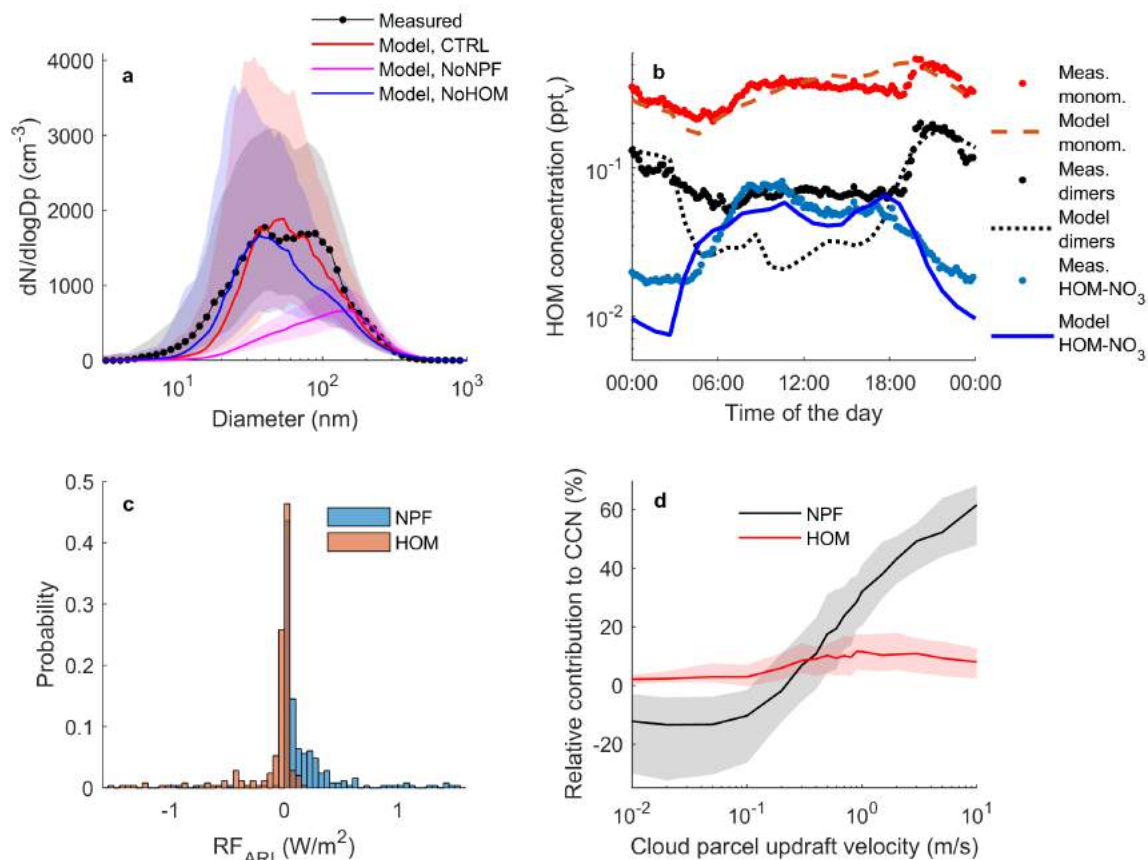


Figure 1: Model and measurement results for May 15-24, 2013 and April 15 to May 5, 2014 at SMEAR II (Roldin et al., 2019). a) median particle number size distributions, b) average diurnal trends of closed shell HOM monomers, HOM dimers and HOM-NO₃ concentrations, c) modelled top of the atmosphere direct aerosol radiative forcing probability distributions caused by NPF and HOM SOA formation, during clear sky conditions, d) relative fraction of the modelled CCN number concentrations caused by NPF and HOM SOA formation respectively. The model results were derived based on data from a control run (CTRL), a no NPF simulation (NoNPF) and a no HOM formation simulation (NoHOM). The shaded areas in a and d: 25th to 75th percentiles.

The net climate impact (i.e. cooling or warming) caused by NPF over the Boreal forest is more complex, and varies depending on the amount and type of clouds. Our model simulations revealed that the observed NPF can to a large extent, be explained by sulfuric acid clustering with ammonia. In spring the NPF upwind of SMEAR II contributes to $\geq 50\%$ of the number of CCN at cloud updraft velocities $\geq 3 \text{ m s}^{-1}$, but even reduces the number of CCN at updraft velocities $< 0.2 \text{ m s}^{-1}$. The NPF also causes a positive direct aerosol radiative forcing of on average $+0.15 \text{ W m}^{-2}$ at clear sky conditions. Thus, without clouds or during conditions with stratiform clouds with updraft velocities $< 0.2 \text{ m s}^{-1}$, NPF most likely results in climate warming, while in the presence of cumulus clouds (which typically have $w > 1 \text{ m s}^{-1}$) it will lead to optically thicker clouds and climate cooling. The combined effect of HOM formation and NPF over the Boreal forest is a substantial increase in the number concentration of CCN at cloud updraft velocities $> 0.2 \text{ m s}^{-1}$. However, at clear sky conditions the negative radiative forcing from HOM SOA formation is offset by the positive radiative forcing caused by the NPF.

We also demonstrated that the comprehensive PRAM mechanism may be substantially reduced. The reduced PRAM version can likely be used for realistic representations of HOM SOA formation in regional and global scale CTMs. However, before PRAM is used for large-scale CTM applications we recommend that the mechanism is evaluated also for other regions, e.g., over tropical forests and urban areas.

ACKNOWLEDGEMENTS

We acknowledge the support by the Academy of Finland (project no. 272041); the European Commission Horizon 2020 program (grant no. 654109); the European Research Council (638703-COALA, 227463-ATMNUCLE); the Swedish Research Council FORMAS (project no. 2014- 1445, 2015-749, 2018-01745); the Nordic Center of excellence eSTICC (eScience tools for investigating Climate Change in Northern High Latitudes); the CSC IT Center for Science in Espoo, Finland; the Centre for Scientific and Technical Computing at Lund University, LUNARC and the Swedish National Infrastructure for Computing, SNIC.

REFERENCES

- Berndt, T. et al.: Hydroxyl radical-induced formation of highly oxidized organic compounds, *Nat. Commun.* 7, 13677, 2016.
- Boy, M. et al.: MALTE - Model to predict new aerosol formation in the lower troposphere, *Atmos. Chem. Phys.*, 6(12), 4499–4517, 2006.
- Boy, M. et al.: SOSA — a new model to simulate the concentrations of organic vapours and sulphuric acid inside the ABL — Part 1: Model description and initial evaluation, *Atmos. Chem. Phys.*, 11, 43–51, 2011.
- Ehn, M. et al.: A large source of low-volatility secondary organic aerosol, *Nature*, 506(7489), 476–479, 2014.
- Guenther, A. et al.: The Model of Emissions of Gases and Aerosols from Nature version 2.1 (MEGAN2.1): an extended and updated framework for modelling biogenic emissions, *Geosci. Model Dev.*, 5, 1471–1492, 2012.
- Jokinen, T. et al.: Production of extremely low volatile organic compounds from biogenic emissions: measured yields and atmospheric implications, *Proc. Natl Acad. Sci. USA* 112, 7123–7128, 2015.
- Müller, J.-F., et al.: Geographical Distribution and Seasonal Variation of Surface Emissions and Deposition Velocities of Atmospheric Trace Gase, *J. of Geophysical Research: Atmospheres*, 97, (D4), 3787–3804, 1992.
- Nannoolal, Y. et al: Estimation of pure component properties part 3. Estimation of the vapor pressure of non-electrolyte organic compounds via group contribution and group interactions, *Fluid Phase Equilib.*, 269(1–2), 117–133, 2008.
- Olenius, T. et al.: Free energy barrier in the growth of sulfuric acid–ammonia and sulfuric acid–dimethylamine clusters, *J. Chem. Phys.* 139, 084312, 2013.
- Pankow, J. F. and Asher, W. E.: SIMPOL.1: a simple group contribution method for predicting vapor pressures and enthalpies of vaporization of multifunctional organic compounds, *Rev. Mex. Ciencias Farm.*, (8), 2773–2796, 2008.
- Praplan, A. P. et al.: Long-term total OH reactivity measurements in a boreal forest, *Atmos. Chem. Phys. Discuss.*, <https://doi.org/10.5194/acp-2019-122>, 2019.
- Roldin, P. et al.: Development and evaluation of the aerosol dynamics and gas phase chemistry model ADCHEM, *Atmos. Chem. Phys.*, 11, 5867–5896, 2011.
- Roldin, P., et al.: The role of highly oxygenated organic molecules in the Boreal aerosol-cloud-climate system, *Nature Commun.*, 10, 4370, <https://doi.org/10.1038/s41467-019-12338-8>, 2019.
- Sogachev, A. et al.: A simple three-dimensional canopy — planetary boundary layer simulation model for scalar concentrations and fluxes, *Tellus B: Chemical and Physical Meteorology*, 54, 784–819, 2002.
- Topping, D. et al.: UManSysProp v1.0: an online and open-source facility for molecular property prediction and atmospheric aerosol calculations, *Geosci. Model Dev.*, 9, 899–914, 2016.
- Xavier, C. et al.: Aerosol Mass yields of selected Biogenic Volatile Organic Compounds – a theoretical study with near explicit gas-phase chemistry, *Atmos. Chem. Phys. Discuss.*, doi.org/10.5194/acp-2019-424, 2019.
- Zhou, L. et al.: SOSAA—A new model to simulate the concentrations of organic vapours, sulphuric acid and aerosols inside the ABL—Part 2: Aerosol dynamics and one case study at a boreal forest site, *Boreal Env. Res.*, 19 (suppl. B), 237–256, 2014.
- Zhou, P. et al.: Simulating ozone dry deposition at a boreal forest with a multi-layer canopy deposition model, *Atmos. Chem. Phys.*, 17, 1361–1379, 2017a.
- Zhou, P. et al.: Boreal forest BVOC exchange: emissions versus in-canopy sinks, *Atmos. Chem. Phys.*, 17, 14 309–14 332, 2017b.

ECOSYSTEM PROCESSES – Activities in 2018-19

Bäck, J.^{1,4}, Hölltä, T.^{1,4}, Porcar-Castell, A.^{1,4}, Pihlatie, M.^{1,3,4}, Heinonsalo, J.^{1,4,7}, Mäkelä, A.¹, Vesala, T.^{2,4}, Aalto, J.², Adamczyk, B.⁶, Ahi, A.¹, Anttila, J.³, Atherton, J.¹, Berninger, F.¹, Chan, T.¹, Dominguez, M.¹, Kalliokoski, T.¹, Kohl, L.^{1,3}, Kolari, P.², Korhonen, J.F.J.^{1,3}, Koskinen, M.^{1,3}, Kulmala, L.^{1,7}, Kumpu, A.¹, Lintunen, A.¹, Lindfors, L.¹, Martikainen, I.^{3,5}, Matkala, L.¹, Mauranen, A.¹, Minunno, F.¹, Mäki, M.¹, Mänd, P.^{1,8}, Paljakka, T.¹, Patama, M.^{1,3}, Pumpanen, J.⁵, Putkinen, A.^{1,3}, Rajewicz, P.¹, Rissanen, K.¹, Salmon, Y.^{1,2}, Santalahti, M.⁴, Schiestl-Aalto, P.¹, Sietiö, O.-M.⁴, Taipale, D.^{1,2}, Tenhovirta, S.^{1,3}, Vainio, E.^{1,3}, Vanhatalo, A.¹ and Hari, P.¹ et al.

¹Institute of Atmospheric and Earth system Research/Forest Sciences, University of Helsinki, Finland

² Institute of Atmospheric and Earth system Research/ Physics, University of Helsinki, Finland

³Department of Agricultural Sciences, University of Helsinki, Finland

⁴Viikki Plant Science Centre (VIPS), University of Helsinki, Finland

⁵Dept. of Environmental and Biological Sciences, University of Eastern Finland, Kuopio, Finland

⁶Dept. of Food and Environmental Sciences, University of Helsinki, Finland

⁷Finnish Meteorological Institute, Helsinki, Finland

⁸Institute of Ecology and Earth Sciences, Department of Botany, University of Tartu, Estonia

The Ecosystem processes –team in the ATM Center of Excellence concentrates on the ecosystems' role in climate change. Our main results are highlighted in the FCoE Abstract Book. Most of the activities link to other themes as well, and only a brief summary is presented here.

The main aim has been to utilize the long-term measurements for building up a comprehensive understanding of the feedbacks and linkages between different compartments in the boreal ecosystems and the environment. In addition, short-term targeted campaigns, either in field or laboratory conditions, with variations of the driving forces, are used to pinpoint the key processes that need to be taken into account for model analysis and forecasting of the system changes.

Here some of the recent results are summarized under six sub-themes: Exchange of VOCs between ecosystems and atmosphere, Whole tree physiology, Methane and nitrous oxide exchange of forests, Optics of photosynthesis, Biogeochemical cycles, soil processes and element budgets, and Forest modeling.

1. EXCHANGE OF VOCs BETWEEN ECOSYSTEMS AND ATMOSPHERE (Bäck et al)

The PTR-MS is used to measure the emissions and concentrations of VOCs in forest stand both in small scale using enclosures, and in ecosystem scale with micrometeorological methods. Part of the work has been dealing with developing and optimizing the operations of field instrumentation, including various types of measurement chambers which enclose a confined part of ecosystem under observation, and enables the detailed analysis of dynamic features of gas exchange, including both inert GHGs and the reactive gases such as VOCs.

Transpiration regulates the emissions of water-soluble short-chained OVOCs in Scots pine (Rissanen et al)

In addition to the strong role of temperature in driving the VOC emissions from tree shoots and stem, tree water relations can be expected to influence the emissions from Scots pine. For example, on the one hand, Scots pine resin contains large amounts of monoterpenes, and the dynamics of resin storages depend at a long term on the tree water status (Rissanen et al. 2016, Rissanen et al. 2019). On the other hand, oxygenated VOCS methanol, acetaldehyde and acetone are water soluble, thus their transport within and release from the tree structures depend on the water-phase dynamics (Rissanen et al 2019).

Studying the interrelations between water availability, tree water relations and the VOC emissions from Scots pine shoots and stem has shown that even relatively small changes in soil moisture can change the stem emission potentials of monoterpenes, methanol and acetaldehyde. The soil moisture effect on monoterpenes is probably partly mediated through resin pressure that decreases with decreasing availability of water and can thus decrease the release of monoterpenes from the resin storage. The soil moisture effect on methanol and acetaldehyde is more likely a result of enhanced plant material degradation and anoxic conditions in soil that increase the production of acetaldehyde and methanol which can potentially be taken up in soil water. In addition, high water content in tree stem can decrease diffusion of oxygen, creating anoxic conditions and increasing acetaldehyde production locally. The emissions of methanol, acetaldehyde and acetone from the shoots also seem to be dependent on the water-phase dynamics, with strong correlations with transpiration. This suggests that the water-soluble compounds emitted from the shoots may be partly transported from branches, stem or all the way from soil, and released in transpiration (Rissanen et al 2019).

Seasonal and annual dynamics of VOC emissions from boreal forest soil (Mäki et al)

A number of studies have measured forest floor VOC fluxes using short measurement periods, while spatial and temporal variation of soil VOC exchange is unknown in various ecosystems (Mäki, 2019). In this thesis, we determined temporal variation and variability of VOC exchange between northern forest soils and the atmosphere using experimental set-ups and continuous measurements from eight years (Mäki, 2019). We found that forest floor VOC exchange was constant between years. The boreal forest floor was a substantial VOC source, as it accounted significantly to the total boreal forest monoterpene fluxes in spring and autumn and methanol fluxes in spring and early summer. Tree species influence forest floor VOC fluxes, as the *Pinus sylvestris* forest floor was a greater monoterpene source compared to the *Picea abies* forest floor, as decomposing *Pinus sylvestris* litter released large amount of monoterpenes from needle storage pools in boreal and hemiboreal climates. The boreal forest floor was also a substantial source of sesquiterpenes and this may influence atmospheric chemistry due to great formation potential of secondary organic aerosols. Finally, we show that VOC fluxes from the forest floor were mainly driven by temperature, soil moisture and relative humidity.

Long-term observations on pine forest VOC exchange (Ahi et al.)

The long-term observations using PTR-MS on stand level VOC exchange were analysed by Ahi et al (this issue, ms in preparation). The results clearly show a seasonal pattern in exchange, related to both environmental factors (temperature, light and moisture) and tree physiological features

(growth, onset of photosynthetic activity). The results will be used in detailed analysis on the temporary impacts of forest management activities that are executed at the SMEAR II stand in 2019-2020.

Stand, season and needle age as determinants for tree monoterpene emissions (Taipale et al)

Monoterpene emission models describe the variations in emission potentials only partially as a function of plant growth processes. We took the detailed measurements of monoterpene emissions from Scots pine during different seasons and covering several needle age classes, and set up to study how big contribution each of these would have on a larger scale (whole Finland). In addition, we evaluated how much these revised emission potentials could affect the new aerosol formation and growth. We utilised several years (2009-2011) of continuously measured emission rates of monoterpenes and chamber temperatures described and published in Aalto et al. (2014). We used two different Scots pine tree growth models to calculate the seasonal and yearly development of Scots pine needles, respectively. We conclude that if new Scots pine foliage is not considered in models, the whole growing season cumulative emissions of monoterpenes from southern Finland are underestimated by 57%, and in northern Finland by ~35%. For springtime the difference is even larger. The formation and growth rates of small particles would have the potential to increase by 98-258% and 60-255%, respectively, if the emissions from new Scots pine needles would be included into emission models.

Relationship between tree hydraulics, BVOC and NO_x emissions from silver birch (Mänd et al)

One of the open questions in climate research is the effect of increased humidity on the production of biogenic volatile signaling compounds (BVOCs) in northern forests, as future climate scenarios predict more humidity for northern latitudes. This is especially important since air humidity is one of the major factors determining nucleation events initiated by BVOCs, influencing cloud condensation and atmospheric haziness, while BVOCs also alter atmospheric reactivity. Preliminary experiments have shown that increased air humidity significantly reduces photosynthesis, total foliage area, foliage nutrient supply, tree height, stem volume, and transpiration, and humidified leaves are smaller respectively with lower mass per area, all affecting GPP. It is not known though, how this complex of changed factors affects the link between GPP and BVOCs.

We set up to measure the tree ecophysiology and emissions of BVOCs in a unique field experiment where air humidity is manipulated. Preliminary results suggest that tree hydraulic properties and environmental humidity do affect significantly leaf osmotic potential, which may lead also to changes in production of secondary carbon compounds, such as BVOCs. More NO_x emissions were detected during earlier phases of growing season.

2. WHOLE TREE PHYSIOLOGY (HÖLTTÄ ET AL.)

We have shown in both theoretical modelling studies as well as in field and laboratory studies that stomatal control can be understood by maximization of photosynthesis rate by balancing between stomatal and non-stomatal relations to photosynthesis. Increasing stomatal conductance increases

CO₂ concentration inside the leaf increasing the photosynthesis rate. However, at the same time increasing stomatal conductance decreases leaf water potential and leaf sugar content which decreases the photosynthesis rate for a given leaf internal CO₂ concentration (Salmon et al. in review, Lintunen et al. in review, Dewar et al. in preparation).

Stomatal control and photosynthesis, sink sugar usage as well as xylem and phloem transport have been incorporated into a realistic 3d structure of tree structure (Hölttä et al. in preparation)

We have modelled the water use of pine trees in drained peatland using the optimal stomatal control model. The cost of water in the optimal stomatal approach is seen to be the lowest at intermediate water table depths, and the water use of pine tree in drained peatland is reduced at both high (likely due to oxygen deficiency) and low soil water table depths (Wang et al. in preparation).

Dendrometer measurements have been interpreted in winter conditions when the stem is frozen. Diameter change of the stem has then been modelled to follow the temperature of ice with a time lag. The extent and time response due to temperature change of ice are interpreted to signify tissue elasticity and permeability, which are important parameters describing the state of winter acclimation (Lindfors et al. 2019).

3. METHANE AND NITROUS OXIDE EXCHANGE OF FORESTS (Pihlatie et al.)

Trees all around the world significantly contribute to the greenhouse gas methane (CH₄) and nitrous oxide (N₂O) emissions from forests (Barba et al., 2018; Machacova et al., 2016; Machacova et al., 2019). We showed that the tree stems of Scots pine, Norway spruce and Silver birch are net sources of N₂O on an annual scale and that the N₂O emissions strongly follow the physiological activity of the trees (Machacova et al., 2019). Our findings highlight that both CH₄ and N₂O exchange of trees should be accounted in the greenhouse gas budgets of forests. Most of research during the past decade has focused on quantifying the emissions of CH₄ and N₂O from tree stems, while the role of forest canopies remain unknown, mostly due to challenges accessing the canopies. Our earlier findings (Machacova et al., 2016) indicate that tree canopies may dominate the whole-tree emissions of both CH₄ and N₂O in a boreal forest, while at that time the processes remained unknown. To understand the canopy CH₄ and N₂O exchange processes, we constructed an automatized controlled climate chamber system for high frequency leaf-level CH₄ exchange measurements. The measurement system allows to assess plant gas exchange under controlled light, temperature, humidity and CO₂ environment with a minimal disturbance to the measured plant (Kohl et al., A). Based on our previous measurements we expect that the leaf-level CH₄ and N₂O emissions are small and requires high-precision gas analyzers. As part of the setup development, we found that plant-emitted volatile organic compounds (VOCs) interfere the gas analysis of CH₄ by FTIR analyzes, whereas no significant disturbances were found with laser spectrometers (Kohl et al., 2019). To finalize the setup, we are currently testing different materials (plastics, glues) used in constructing plant chambers in order to evaluate their possible emissions or uptake of CH₄ (Freistetter et al.).

Our initial experiments with tree saplings demonstrated that the shoots of different tree species emit CH₄ from distinct sources (N₂O not measured). Shoots of Scots pine and some birch species emitted

CH₄ that was mostly produced within the shoot, likely through aerobic CH₄ production. This leaf-level CH₄ emission showed a strong diurnal cycle that follows PAR irradiation and photosynthesis rate (Kohl et al., A). Shoot from *Betula nana* birch species, in contrast, showed emissions of soil-borne CH₄ that remained constant throughout day and night. The capacity of *Betula nana* saplings to transport CH₄ from the soil and X-ray imaging of the structure and volume of the conducting tree tissue are currently utilized in the development of gas transport model (Anttila et al.). We expect that future experiments utilizing different ¹³C-labelling experiments (Tenhovirta et al.) allows us to further disentangle shoot CH₄ emission processes, and to characterize their responses to environmental conditions (Patama et al.).

The core of the group is to understand the CH₄ and N₂O cycling dynamics in the whole soil-tree-atmosphere continuum and to upscale from single-tree processes to a catchment-scale. During 2019 extensive experiments were conducted in a gradient from a forest hilltop to a pristine peatland at Pallaslompola catchment, Finland, to understand the biotic and abiotic drivers of soil CH₄ production and oxidation processes and their seasonality, and to link the soil CH₄ dynamics to tree CH₄ exchange (Kohl et al., B). We also measure reductive-oxidative (redox) conditions in the soil profile in order to disentangle the changes in the CH₄ dynamics. We will use the soil redox status in soil process modelling, which will further feed to the soil-tree-atmosphere model development (Koskinen et al.). Additionally, we have pioneered with analyzing the role of phyllospheric microbes living on the leaves and needles of boreal trees and further quantified their role in N₂O fluxes. This new opening may reveal new aspects of the plant-microbe interactions, the role of trees in N₂O dynamics and nitrogen cycling in boreal forests (Martikainen et al.).

As a group we are constantly seeking ways to make our scientific results visible and understandable to the society and decision makers. Our mission is to bring the science to the society, and to make it accessible and understandable (Korhonen et al.).

4. OPTICS OF PHOTOSYNTHESIS (Porcar-Castell et al)

We seek to develop new methodologies and generate new understanding in views of establishing a quantitative connection between optical, biochemical, functional and structural traits of vegetation. We combine multiscale field experimentation with detailed laboratory experiments to elucidate the mechanistic connections both across space and time. Our most recent advances and ongoing work are summarized below.

a. Comparison of methods for estimation of leaf-level spectral fluorescence (Rajewicz et al.) The fluorescence spectra of leaves can be measured with the help of optical filters to excludes radiation above 650 nm so that the fluorescence spectra in the 650-800nm range can be measured. Importantly, factors like the geometry of the measurement or the morphology of the leaves can also interfere with the resulting spectra. In Rajewicz et al. (2019) we compared different methodologies to measure the fluorescence spectra of broadleaf and needle-like species. We found that the shape of the fluorescence spectra remains largely unaffected by the geometry of the measurement. In turn, the challenging morphology of the needles enhanced the reabsorption of red fluorescence.

b. R-Package for processing of long-term Monitoring PAM data (Zhang et al., this issue). Monitoring PAM fluorometers are ideal to follow diurnal and seasonal changes in photosynthetic

energy partitioning of leaves *in situ*. Although these measurements demand relatively low levels of supervision, the resulting data requires careful filtering to separate variations in fluorescence that are due to leaf-level physiological processes from those due to meteorological (dew, rain, snow), or physical factors (changes in sample area due to wind). In Zhang et al (**Abstract**) we present a processing flow for filtering the data as well as practical instructions for field implementation.

c. Nocturnal LED Induced fluorescence of whole plant canopies (Atherton et al.). In contrast to leaf-level measurements, the fluorescence emission of a plant canopy has been so far only measurable within narrow spectral windows (Solar Fraunhofer lines or telluric atmospheric absorption bands) where incoming solar irradiance is completely or strongly attenuated. Accordingly, the fluorescence spectra of whole plant canopies has remained elusive. We recently presented a ground breaking method (Atherton et al. 2019) to directly measure the fluorescence spectra of whole plant canopies. The novelty of the method lies in that measurements are conducted during nighttime using a commercial stage LED instead of the sun, allowing for retrieval of the whole fluorescence spectra. The method should find multiple applications for the interpretation of tower and satellite SIF data.

d. Canopy-level modelling and measurements of SIF with a low-weight dual field of view spectrometer (Atherton et al., Liu et al., Xu et al.)

Upscaling observations of solar-induced fluorescence (SIF) from the leaf to the canopy and beyond is not straightforward because new controls appear at each scale. In addition to leaf level physiology, factors like canopy structure, ground vegetation dynamics or atmospheric absorption processes can interfere with the signals recorded at the canopy level. However, lack of technology and quantitative methodologies have strongly limited the characterization of the potential impact of these factors. In this context, we have recently used a drone platform for multiscale measurements of SIF over various forests stands (Atherton et al. 2018) as well as in crops (Xu et al. this issue). This platform can be used to assess the impact of forest and crop structure on the top-of-canopy SIF signal, or to retrieve canopy parameters like the leaf angle distribution (Atherton et al. this issue). We also developed a quantitative framework for investigating the impact of forest structure on the SIF signal (Liu et al. 2019). Liu et al. used terrestrial laser scanner data to reconstruct a 3D model of a birch stand and coupled it to a canopy (DART) and leaf (Fluspect) radiative transfer models to conduct a sensitivity analysis of top-of-canopy SIF to physiological, biochemical and structural factors.

e. Spatiotemporal drivers of the leaf-level fluorescence signal

We characterize the processes that drive the intensity and spectral properties of the chlorophyll fluorescence signal at the leaf level. Temporally, we recently demonstrated that non-photochemical quenching controls the seasonal relationship between fluorescence and photosynthesis in top-canopy Scots pine needles (Zhang et al. 2019). Spatially, when considering leaves from different species, we found that both NPQ and foliar chlorophyll contents explain most of the variation in fluorescence properties (Magney et al. 2019). Spatiotemporally, Rajewicz et al. (this issue) investigates the factors that control the seasonal variation in fluorescence properties in a boreal ecosystem. In more detail, van Wittenberghe et al (this issue) reports on the mechanisms that drive the changes in fluorescence at time scales of seconds to minutes and their connection to changes in leaf reflectance.

We have also assessed the potential of SIF for precision agriculture using potato as a model species. We measured how diurnal variations in foliar physiology are coupled to canopy-level measurements of chlorophyll fluorescence in response to water stress (Xu et al. this issue). We found that diurnal changes in canopy structure (leaf angle distribution) were the main factor controlling the top-of-canopy SIF signal in response to water stress. Similarly, we investigated to what extent the effect of

foliar micro and macronutrients as well as heavy metals affect the leaf-level and top-of-canopy SIF (Oivukkamäki et al. this issue).

5. BIOGEOCHEMICAL CYCLES, SOIL PROCESSES AND ELEMENT BUDGETS

Biogeochemistry concerns cycling of elements in terrestrial as well as aquatic ecosystems by integrating physics, chemistry, geology and biology. Besides natural ecosystems, it also deals with systems altered by human activity such as forests under different management regimes, drained peatlands and lakes loaded by excess nutrients. The most important elements under study are carbon, nitrogen and phosphorus, which are vital for ecosystem functioning and processes such as photosynthesis, i.e. uptake of inorganic carbon by plants. Biogeochemistry focuses on interphases of scientific disciplines and by doing so, it also combines different research methods. We treat the ecosystems as open entities which are closely connected to atmosphere and where water is among the key transport mechanisms.

Disturbances and biogeochemistry (Köster, Pumpanen & Berninger et al)

The goal for Disturbances and Biogeochemistry team is to link the effects of different disturbances (fire, reindeer grazing) with the biogeochemical cycles in boreal and sub-arctic forests. We also work with effects of added charcoal (industrially produced biochar) on the C and N dynamics in boreal forests, and on growth of containerized planting stock.

Our study from northern boreal fire chronosequences (Yukon, Canada and Tura, Russia) showed that soils were warmer and drier, and soil C content was lower on recently burned areas. The depth of the active layer on top of permafrost was increasing rapidly after the fire. The thawing of near-surface permafrost directly affected the GHG fluxes (Köster et al., 2017a, Köster et al., 2018). We have also seen that forest fires may facilitate the decomposition of permafrost SOM by increasing the active layer depth, but on the same time increase the temperature sensitivity of decomposition - the SOM in the permafrost surface was less temperature sensitive than the SOM in the soil surface (Aaltonen et al., 2019a). We have also found that SOM in upland mineral soils at the permafrost surface could be mainly recalcitrant and its decomposition not particularly sensitive to changes resulting from fire (Aaltonen et al., 2019b).

Our study dealing with reindeer grazing in northern boreal forests (Värriö Strict Nature Reserve, Finnish Lapland) showed that grazing by reindeer significantly affected lichen and moss biomasses in these forests. Our results indicated that grazing by reindeer in the northern boreal forests affects the GHG emissions from the forest floor and these emissions largely depend on changes in vegetation composition (Köster et al., 2017b). Our study dealing with the addition of biochar to forest soil (Hyytiälä, Finland) showed that added biochar (with different treatments) had no significant effect on soil microbial biomass, the rates of N mineralization, nitrification and biological N fixation (Palviainen et al., 2018). The results suggest that wood biochar additions of 5–10 t ha⁻¹ to boreal forest soil does not cause strong effects and threat to the native soil C stocks because increase in soil CO₂ effluxes were rather small and vanished during the second year after biochar amendment (Palviainen et al., 2018). We have also found that biochar addition had no clear effect on soil total N, nor on the temperature sensitivity of soil respiration - the turnover time of soil C was unaffected by biochar addition (Zhao et al., 2019). These results indicate that from a C sequestration point of view,

biochar addition did not accelerate the mineralization of soil organic C, and could lead to higher stable C stocks in the surface soil layer.

Soil processes (Heinonsalo et al)

The research team of doc. Jussi Heinonsalo has the aim to investigate how soil C stocks are accumulated, affected by plant-microbial interactions and how stable soil organic matter (SOM) is formed. The research is intimately linked to investigation related to atmospheric feedbacks. Due to border-crossing approaches, the group works with close interaction with different departments at University of Helsinki as well as Finnish Meteorological Institute.

Earlier, the group has shown e.g. that plants cause drastic, direct changes in SOM decomposition (Kieloaho et al. 2016), understory dwarf shrubs species (*Calluna vulgaris*, *Vaccinium myrtillus* and *V.vitis-idaea*) alter SOM chemistry differently than Scots pine, mainly due to decrease in pH and increase in condensed tannin content in soil (Adamczyk et al. 2016) and from microbial perspective, soil fungal community structure at SMEARII station is species-rich and diverse also in deeper mineral soil horizons. Seasonally the community was shown to remain rather stable during growing season but drastic changes seem to occur between summer and winter seasons (Santalahti et al. 2016). The group also showed that fungal biomass is a large reservoir of amines, the community shift may cause release of fungal cell content (like amines) that are linked to atmospheric emissions (Kieloaho et al. 2016). The research combined microbiology and chemistry to be linked with atmospheric impacts of soil (e.g. GHG, amine, BVOC exchange).

During the last year, several important publications were published in e.g. New Phytologist and Nature Communications. In this research, fungal necromass, that is very abundant source of nitrogen (N)-rich organic matter in forest soils, was shown to form complexes with root-derived condensed tannins resulting in its decreased decomposability. This finding pinpoints a novel mechanism that would partly explain surprisingly slow decomposition rate of microbial litter (Adamczyk et al. 2019a). In a field experiment, using a three-year field experiment, the SOM decomposition and stabilization was compared in the presence of roots, with exclusion of roots but presence of fungal hyphae and with exclusion of both roots and fungal hyphae. Roots accelerate SOM decomposition compared to the root exclusion treatments, but also promote a different soil N economy with higher concentrations of organic soil N compared to inorganic soil N accompanied with the build-up of stable SOM-N. In contrast, root exclusion leads to an inorganic soil N economy (i.e., high level of inorganic N) with reduced stable SOM-N buildup. Based on these findings, a new framework was provided on how plant roots affect SOM decomposition and stabilization. (Adamczyk et al. 2019,b). Tree-root exclusion experiment also gave novel information on soil CO₂ sources and separation of autotrophic and heterotrophic soil respiration (Ryhti et al. manuscript under review). These result suggest that rather than a passive role as producer of litter, plants have a dynamic impact in SOM decomposition and formation, which is necessary to take into account in soil and ecosystem carbon modelling.

During the last year, Heinonsalo group has been active in establishing new experiments that focus on C sequestration in agricultural soils. The team continues with the same multidisciplinary way as described above and combine plant-microbial-soil interactions and soil C measurement with other

climatic feedbacks (mainly GHG gases) and modelling. Several new project are funded and new results are being produced to be presented later.

6. FOREST MODELLING (Mäkelä et al)

Methods for regional-scale monitoring and predicting forest carbon fluxes and stocks (Mäkelä et al)

The objective of this work is to develop methods that allow us to make large-scale predictions of the development of forest stocks and fluxes as influenced by climate and forest management. We have developed a model system, PREBAS, consisting of a climate-driven model (PRELES) of gross primary production (GPP) and linked this with a forest growth model (CROBAS) that can be run using either ground-based or satellite observations to initialise the model. The models are also being linked with the soil carbon model Yasso for the regional estimation of NEE. The model system has been linked to EO data provided by VTT, which includes novel EO data analysis results of forest variables needed for initialising the models (Mäkelä et al. *in prep*). Our estimates of the current growth of the growing stock in Finland are well in line with forest statistics (Holmberg et al. 2019), and our GPP and NEE results agree with flux tower measurements. The model system has also been linked to the multisource inventory data available with Luke (Härkönen et al. 2019, Mäkelä J. et al. 2019), and scenario results with climate scenarios have been input the Climate Guide web site maintained by FMI. The models are being applied in several projects, including the SRC project IBC-CARBON (Holmberg et al. 2019), Finnish Climate Panel (Kalliokoski et al. 2019b), forest management optimisation (Xue et al. 2019) and EU project Forest Flux.

Model development to incorporate old-growth and uneven-aged stands (Mäkelä et al)

This work aims at improving our growth models to be readily applicable to continuous cover management and old-growth stands which both have been suggested to contribute to climate change mitigation by means of increasing the total carbon sequestration of forests (Kalliokoski et al. 2016, Mäkelä et al. 2016). Empirical studies to support both objectives are have been completed (Kumpu et al. 2018, Kuusinen et al. 2019, Liu et al. *submitted*, Hu et al. *submitted*, Kumpu et al. *submitted*) or are underway (Liu et al. *in prep.*, Akujärvi et al. *in prep.*). A more detailed analysis of the interactions of crown structure and physiological processes could also help understand the decline of productivity with tree ageing (Mäkelä et al. *in press*).

Bayesian calibration of models (Minunno et al.)

A key part of the modelling work has been model calibration using inverse data-model fusion methods. We use Bayesian methods that allow us to combine both empirical and theoretical information in a flexible manner. We have calibrated PRELES for boreal sites (Minunno et al. 2016) and temperate and sub-tropical sites (Tian et al. *submitted*), and we have also used Bayesian model calibration of PRELES as a tool to analyse different ecosystem processes (Tian et al. *in prep*, Vernay et al. *submitted*). We have calibrated CROBAS for boreal sites (Minunno et al. 2019) and calibration to temperate forests is underway in EU project Forest Flux. We have analysed prediction uncertainties of the calibrated models in relation to climate model, climate scenarios, forest management scenarios,

uncertainty about impact processes and model parameter uncertainty (Kalliokoski et al. 2018, Mäkelä J. et al. 2019).

Climate change impacts and mitigation (Kalliokoski et al.)

Almost 70% of nations have indicated in their National Determined Contributions (NDCs) of Paris Agreement they will use the land based carbon dioxide removal (CDR) to reach their mitigation targets and overall of the 25% of the countries' current mitigation pledges as implied by NDCs are based on land use sector. Consistent land-use sector policy measures call for comprehensive accounting of uncertainties (Kalliokoski et al. 2019a) in the scenario projections and realization of improved forest management in specific region calls for reliable tools for projecting the impact of applied changes in forest management. Thus, the projections of forest development under different scenarios and with different modeling tools are important to evaluate (Kalliokoski et al. 2019b). In this study, we investigate the projections of six forest carbon models and compare the effect of their assumptions and parameterization e.g. on growth response after thinning, mortality, or accumulation of soil carbon (Kalliokoski et al. *in prep*). However, net climate impact of forest based mitigation includes also biophysical factors, e.g. albedo and secondary organic aerosols (SOA), and indirect carbon effects like avoided emissions through increased use of harvested wood products displacing fossil based energy and materials. In this work, we analyse the impact of different harvesting scenarios of Finnish forests on the radiative forcing (RF) accounting for all these different effects (Kalliokoski et al. *in prep*). This kind of comprehensive analysis is needed for generating understanding of the relative importance of different factors in the mitigation but also illuminating the key uncertainties of climate impacts of land use sector.

Within-season growth and phenology (Schiestl-Aalto et al.)

The objective of this work is to increase our understanding of the within-season timing of carbon acquisition and allocation to growth of the different plant components, in order to be able to analyse and predict the impacts of climate change on growth. A whole-tree model CASSIA has been developed earlier (Schiestl-Aalto et al. 2015) where temperature is the key environmental control (Schiestl-Aalto and Mäkelä 2017). Recently, information from within-season measurements of non-structural carbon compounds in different tree organs was incorporated in the model, which allowed us to make inferences about the annual carbon flux to root exudates (Schiestl-Aalto et al. 2019).

ACKNOWLEDGEMENTS

The Ecosystem processes team consists of >30 members, including ca. 20 graduate and post-graduate students, 10 post docs and 7 senior researchers. Funding was received from Academy of Finland (CoE grant, project grants and several fellowship grants), University of Helsinki, the EU-FP7 projects EXPEER, AnaEE, eLTER, ICOS; Marie Skłodowska-Curie Fellowship; the Doctoral Programmes in Atmospheric Sciences and in Sustainable use of renewable natural resources (ATM and AGFOREE, respectively); Nordforsk NCoEs CRAICC and DEFROST; Maj and Tor Nessling Foundation, Kone Foundation, The Finnish Foundation for Natural Resources, and Wihuri Foundation. An indication of our interdisciplinary approach is that most research themes overlap with themes studied by other teams in the FCoE. This has resulted e.g. in large numbers of joint publications and presentations, common field campaigns and joint doctoral training, and is highly acknowledged.

References

- Aaltonen, H., Köster, K., Köster, E., Berninger, F., Zhou, X., Karhu, K., Biasi, C., Bruckman, V., Palviainen, M., Pumpanen, J. (2019b). Forest fires in Canadian permafrost region: the combined effects of fire and permafrost dynamics on soil organic matter quality. *Biogeochemistry*, 143: 257-74.
- Aaltonen, H., Palviainen, M., Zhou, X., Köster, E., Berninger, F., Pumpanen, J., Köster, K. (2019). Temperature sensitivity of soil organic matter decomposition after forest fire in Canadian permafrost region. *Journal of Environmental Management*. 241: 637-644.
- Adamczyk, B., Sietiö, O.-M., Biasi, C. and Heinonsalo, J. (2019a) Interaction between tannins and fungal necromass stabilizes fungal residues in boreal forest soils. *New Phytologist* 223: 16–21, <https://doi.org/10.1111/nph.15729>
- Adamczyk, B., Sietiö, O.-M., Straková, P., Prommer, J., Wild, N., Hagner, M., Pihlatie, M., Fritze, H., Richter, A. and Heinonsalo, J. (2019b) Plant roots increase both decomposition and stable organic matter formation in boreal forest soil. *Nature Communications*, vol. 10: 3982, <https://doi.org/10.1038/s41467-019-11993-1>
- Adamczyk, B., Ahvenainen, A., Sietiö, O-M, Kanerva, S., Kieloaho, A.-J., Smolander, A., Kitunen, V., Saranpää, P., Laakso, T., Strakova, P. and Heinonsalo, J. (2016) The contribution of ericoid plants to soil nitrogen chemistry and organic matter decomposition in boreal forest soil. *Soil Biology & Biochemistry* 103, 394-404, <http://dx.doi.org/10.1016/j.soilbio.2016.09.016>.
- Akujärvi A., Minunno F., Peltoniemi M., Mäkelä A., Mäkipää R., Heikkinen R., Forsius M. 2019. The carbon sink capacity of boreal, old-growth Norway spruce stands. *In prep*.
- Atherton J, Liu E, Porcar-Castell A (2019) Nocturnal light emitting diode induced fluorescence (LEDIF): A new technique to measure the chlorophyll a fluorescence emission spectra distribution of plant canopies in situ. *Remote Sensing of Environment* 231:111137
- Atherton J, MacArthur A, Hakala T, Maseyk K, Robinson I, Liu W, Honkavaara E, Porcar-Castell A (2018) Drone measurements of solar-induced chlorophyll fluorescence acquired with a low-weight DFOV spectrometer system. *IGARSS IEEE, International Geoscience and Remote Sensing Symposium* 8834-8836
- Barba, J, Bradford, M., Brewer, P., Bruhn, D., Covey, K., van Haren, J., Megonigal, P., Mikkelsen, T., Pangala, S., Pihlatie, M., Poulter, B., Rivas-Ubach, A., Schadt, C., Terazawa, K., Warner, D., Zhang, Z., Vargas, R., Methane emissions from tree stems: a new frontier in the global carbon cycle. *New Phytologist* (2019) 222: 18–28.
- Holmberg, M., Aalto, T., Akujärvi, A., Arslan, A. N., Bergström, I., Böttcher, K., Lahtinen, I., Mäkelä, A., Markkanen, T., Minunno, F., Peltoniemi, M., Rankinen, K., Vihervaara, P. & Forsius, M. (2019) Ecosystem Services Related to Carbon Cycling - Modeling Present and Future Impacts in Boreal Forests. *Frontiers in plant science*. 10: 343-351.
- Hu M., Lehtonen A., Mäkelä A. 2019. Age effect on tree structure and carbon allocation in Scots pine and Norway spruce. *Submitted to Annals of Forest Science*.
- Härkönen, S., Neumann, M., Mues, V., Berninger, F., Bronisz, K., Cardellini, G., Chirici, G., Hasenauer, H., Koehl, M., Lang, M., Merganicova, K., Mohren, F., Moiseyev, A., Moreno, A., Mura, M., Muys, B., Olschofsky, K., Del Perugia, B., Rorstad, P. K., Solberg, B. , Thivolle-

- Cazat A, Trotsiuk V, Mäkelä, A. 2019. A climate-sensitive forest model for assessing impacts of forest management in Europe *Environmental Modelling & Software*. 115: 128-143
- Kalliokoski T., Mäkelä A., Fronzek T., Minunno F., Peltoniemi M. 2018. Decomposing sources of uncertainty in climate change projections of boreal forest primary production. *Agricultural and Forest Meteorology* 262: 192-205
- Kalliokoski T., Mäkinen H., Linkosalo T., Mäkelä A. 2016. Evaluation of stand-level hybrid PipeQual model with permanent sample plot data of Norway spruce. *Canadian Journal of Forest Research* 47:234-245.
- Kalliokoski, T., Aalto, T., Bäck, J., Ezhova, E., Franz, D., Haapanala, S., Juurola, E., Kerminen, V.-M., Kolari, P., Kulmala, L., Liski, J., Mammarella, I., Matkala, L., Petäjä, T., Rantala, P., Vesala, T., Kulmala M. 2019a. Carbon sink and CarbonSink+: from observations to global potential. 77 p. https://researchportal.helsinki.fi/files/125247979/Carbon_sink_and_CarbonSink_from_observations_to_global_potential_12062019.pdf
- Kalliokoski, T., Heinonen, T., Holder, J., Lehtonen, A., Mäkelä, A., Minunno, F., Ollikainen, M., Packalen, T., Peltoniemi, M., Pukkala, T., Salminen, O., Schelhaas, M.-J., Seppälä, J., Vauhkonen, J., Kanninen, M. 2019b. Skenaarioanalyysi metsien kehitystä kuvaavien mallien ennusteiden yhtäläisyyksistä ja eroista. *Suomen Ilmastopaneeli* 2/2019. 84 p.
- Kalliokoski, T., Heinonen, T., Holder, J., Lehtonen, A., Mäkelä, A., Minunno, F., Peltoniemi, M., Salminen, O., Schelhaas, M.-J., Seppälä, J., Kanninen, M. Ensemble of forest impact models for analysing the variability of carbon sink projections. In prep.
- Kalliokoski, T. Bäck, J., Kulmala, M., Mäkelä, A., Minkkinen, K., Paasonen, P., Berninger, F. et al. Mitigation impact of different harvesting scenarios of Finnish forests when albedo and aerosols are included together with trade-offs of carbon sequestration and avoided emissions. In prep
- Kieloaho, A.-J., Pihlatie, M., Dominguez Carrasco, M., Kanerva, S., Parshintsev, J., Riekkola, M.-L., Pumpanen, J. and Heinonsalo J. (2016) Stimulation of soil organic nitrogen pool: the effect of plant and soil organic matter degrading enzymes. *Soil Biology & Biochemistry* 96: 97-106.
- Kieloaho, A.-J., Pihlatie, M., Kulmala, M., Riekkola, M.-L., Parshintsev, J., Vesala, T. and Heinonsalo, J. (2017) Soil concentrations and soil-atmosphere exchange of alkylamines in a boreal Scots pine forest. *Biogeosciences*, 14, 1075–1091, 2017, doi:10.5194/bg-14-1075-2017.
- Kohl, L., Koskinen, M., Rissanen, K., Haikarainen, I., Polvinen, T., Pihlatie, M. (2019) Technical note: Interferences of volatile organic compounds (VOCs) on methane concentration measurements. *Biogeosciences*, 16, 3319–3332, 2019 doi.org/10.5194/bg-16-3319-2019
- Kumpu, A., Mäkelä, A., Pumpanen, J., Saarinen, J. & Berninger, F. 2018. Soil CO₂ efflux in uneven-aged and even-aged Norway spruce stands in southern Finland. *IForest*. 11: 705-712
- Kumpu A., Piispanen R., Berninger F., Saarinen J., Mäkelä A. 2019. Biomass and structure of uneven-aged Norway spruce stands in southern Finland. *Submitted to Forestry*.
- Kuusinen, N., Valkonen, S., Berninger, F. & Mäkelä, A. (2019) Seedling emergence in uneven-aged Norway spruce stands in Finland. *Scandinavian Journal of Forest Research*. 34: 200-207
- Köster, E., Köster, K., Berninger, F., Aaltonen, H., Zhou, X., Pumpanen, J. (2017a). Carbon dioxide, methane and nitrous oxide fluxes from a fire chronosequence in subarctic boreal forests of Canada. *Science of The Total Environment*, 601–602: 895-905.

- Köster, K., Köster E., Berninger F., Heinonsalo, J., Pumpanen J. (2017b). Contrasting effects of reindeer grazing on CO₂, CH₄ and N₂O fluxes in northern boreal forest floor. *Land Degradation and Development*, 29, 374-381.
- Köster, E., Köster, K., Berninger, F., Prokushkin, A., Aaltonen, H., Zhou, X., Pumpanen, J. (2018). Changes in fluxes of carbon dioxide and methane caused by fire in Siberian boreal forest with continuous permafrost. *Journal of Environmental Management*, 228: 405-415
- Lindfors, L., Atherton, J., Riikonen, A. and Hölttä, T., 2019. A mechanistic model of winter stem diameter dynamics reveals the time constant of diameter changes and the elastic modulus across tissues and species. *Agricultural and Forest Meteorology*, 272, pp.20-29.
- Liu C., Mäkelä A. 2019. Age-induced restraints to aboveground growth diverge amongst tree species in eastern Lapland. *Submitted to Tree Physiology*.
- Liu C., Berninger F., Hölttä T. Mäkelä A. 2019. Old Scots pine more susceptible to vapour deficit and less stimulated by irradiance in sap flow. *In prep*.
- Liu W, Atherton J, Mottus M, Gastellu-Etchegorry J-P, Malenovský Z, Raunonen P, Åkerblom M, Mäkipää R, Porcar-Castell A (2019). Simulating soilar-induced chlorophyll fluorescence in a boreal forest stand reconstructed from terrestrial laser scanning measurements. *Remote Sensing of Environment* 232:111274
- Machacova, K., Vainio, E., Urban, O., Pihlatie, M. 2019. Seasonal dynamics of stem N₂O exchange follow the physiological activity of boreal trees. *Nature Communications*, doi.org/10.1038/s41467-019-129
- Magney TS, Frankenberg C, Köhler P, North GB, Davis T, Dold C, Dutta D, Fisher JB, Grossmann K, Harrington A, Hatfield J, Stutz J, Sun Y, Porcar-Castell A (2019) Disentangling changes in the spectral shape of chlorophyll fluorescence: implications for remote sensing of photosynthesis. *Journal of Geophysical research: Biogeosciences* DOI: 10.1029/2019JG005029
- Minunno F, Peltoniemi M, Launiainen S, Aurela M, Mammarella I, Lindroth A, Lohela A, Minkkinen K, Mäkelä A 2016. Calibration and validation of a semi-empirical flux ecosystem model for coniferous forests in the Boreal region. *Ecological Modelling* 341:37-52.
- Minunno F., Peltoniemi M., Härkönen S., Kalliokoski T., Mäkinen H., Mäkelä A. 2019. Bayesian calibration of a carbon balance model PREBAS using data from permanent growth experiments and national forest inventory. *Forest Ecology and Management* 440: 208-257.
- Mäkelä A., Pulkkinen M., Mäkinen H. 2016. Bridging empirical and carbon-balance based forest site productivity - significance of below-ground allocation. *Forest Ecology and Management* 372:64-77.
- Mäkelä A., Grönlund L., Schiestl-Aalto P., Kalliokoski T., Hölttä T. 2019. Current-year shoot hydraulic structure in two boreal conifers – implications of growth habit on water potential. *Tree Physiology*. *In press*.
- Mäkelä A., Minunno F., Peltoniemi M., Sirro L., Häme T. 2019. Forest NPP and volume growth inferred from climate and satellite data at high spatial resolution. *In prep*.
- Mäkelä J., Minunno F., Aalto T., Mäkelä A., Markkanen T., Peltoniemi M. 2019. Uncertainty sources in simulated ecosystem indicators of the 21st century climate change. *Biogeosciences*. *Submitted*.
- Mäki, M. (2019). Volatile organic compound fluxes from northern forest soils. *Dissertationes Forestales*, 275, 1–52. <https://doi.org/10.14214/df.275>

- Palviainen, M., Berninger, F., Bruckman, V., Köster, K., Ribeiro Moreira de Assumpção, C., Aaltonen, H., Makita, N., Mishra, A., Kulmala, L., Adamczyk, B., Zhou, X., Heinonsalo, J., Köster, E., Pumpanen, J. (2018). Effects of biochar on carbon and nitrogen fluxes in boreal forest soil. *Plant and Soil*, 425: 71-85
- Rajewicz P, Atherton J, Alonso L, Porcar-Castell A (2019) Leaf-level spectral fluorescence measurements: comparing methodologies for broadleaves and needles. *Remote Sensing*, 11(5), 532
- Rissanen K., Hölttä T., Barreira L.F.M., Hyttinen N., Kurtén T., Bäck J. (2019). Temporal and Spatial Variation in Scots Pine Resin Pressure and Composition. *Frontiers in Forests and Global Change* 2:23.
- Rissanen K., Hölttä T., Vanhatalo A., Aalto J., Nikinmaa E., Rita H., Bäck J. (2016). Diurnal patterns in Scots pine stem oleoresin pressure in a boreal forest. *Plant Cell and Environment* 39: 527
- Ryhti, K., Kulmala, L., Pumpanen, J., Isotalo, J., Pihlatie, M., Helmisaari, H.-S., Leppälampi-Kujansuu, J., Kieloaho, A.-J., Bäck, J. and Heinonsalo, J. Partitioning of forest floor CO₂ emissions reveals the belowground interaction between different plant groups in a Scots pine (*Pinus sylvestris* L.) stand in southern Finland (under review in *Global Change Biology*)
- Santalahti, M., Sun, H., Jumpponen, A., Pennanen, T. and Heinonsalo, J. (2016) Seasonal and vertical dynamics of fungal communities in boreal Scots pine forest soil. *FEMS Microbiology Ecology*, Vol 92:11, DOI: <http://dx.doi.org/10.1093/femsec/fiw170>.
- Schiestl-Aalto, P., Kulmala, L., Mäkinen, H., Nikinmaa, E., Mäkelä, A. 2015. CASSIA – a dynamic model for predicting intra-annual sink demand and interannual growth variation in Scots pine. *New Phytologist* 206: 647–659 DOI: 10.1111/nph.13275
- Schiestl-Aalto P., Mäkelä A. 2017. Temperature dependence of needle and shoot elongation before bud break in Scots pine. *Tree Physiology* 37:316-325
- Schiestl-Aalto, P., Ryhti, K., Mäkelä, A., Peltoniemi, M., Bäck, J. & Kulmala, L. (2019) Analysis of the NSC Storage Dynamics in Tree Organs Reveals the Allocation to Belowground Symbionts in the Framework of Whole Tree Carbon Balance *Frontiers in forests and global change*. 2: p17
- Tian X., Minunno F., Schiestl-Aalto P., Chi J., Peichl M., Marshall J., Näsholm T., Peltoniemi M., Mäkelä A. 2019. Decomposing the impact of nitrogen-addition upon GPP in a boreal Scots pine forest. *In prep.*
- Tian X., Minunno F., Cao T., Peltoniemi M., Kalliokoski T., Mäkelä A. 2019. Extending the range of applicability of the semi-empirical ecosystem model PRELES for varying forest types and climate. *Submitted to Global Change Biology*.
- Vernay A., Tian X., Chi J., Linder S., Mäkelä A., Oren R., Peichl M., Stangl S.R., Tor-Ngern P., Marshall, J.D. 2019. Estimating canopy gross primary production from sapflux, phloem stable isotopes, and mesophyll conductance. *Submitted to New Phytologist*.
- Xue, H.L., Mäkelä, A., Valsta, L., Vanclay, J.K., Cao, T.J. 2019. Comparison of population-based algorithms for optimizing thinnings and rotation using a process-based growth model. *Scandinavian Journal of Forest Research* 34:458-468.
- Zhao, P., Palviainen, M., Köster, K., Berninger, F., Bruckman, V., Pumpanen, J. (2019). Effects of Biochar on Fluxes and Turnover of Carbon in Boreal Forest Soils. *Soil Science Society of America Journal*. 83: 126-136.

Zhang C, Atherton J, Peñuelas J, Filella I, Kolari P, Aalto J, Ruhanen H, Bäck J, Porcar-Castell A (2019) Do all chlorophyll fluorescence emission wavelengths capture the spring recovery of photosynthesis in boreal evergreen foliage? *Plant, Cell and Environment*, doi: 10.1111/pce.13620

ATMOSPHERIC PHYSICAL CHEMISTRY (COALA) GROUP HIGHLIGHTS

Mikael Ehn¹, Yanjun Zhang¹, Lauriane Quéléver¹, Otso Peräkylä¹, Liine Heikkinen¹, Mikko Äijälä¹, Olga Garmash¹, Mikko Äijälä¹, and Matthieu Riva^{1,2}

¹ Institute for Atmospheric and Earth System Research / Physics, Faculty of Science, University of Helsinki, Helsinki, 00140, Finland

² Univ Lyon, Université Claude Bernard Lyon 1, CNRS, IRCELYON, F-69626, Villeurbanne, France

Keywords. Mass spectrometry, SOA, HOM

INTRODUCTION

The “Atmospheric Physical Chemistry” group, also often called “COALA” group after the ERC grant with the same name, studies all aspects of the conversion of volatile organic compounds (VOC) into secondary organic aerosol (SOA). The oxidation of VOC form oxidation products (oxygenated VOC, OVOC) with various properties, e.g. volatility, depending on the VOC structure, the oxidant, and the atmospheric conditions. A particular focus in our group is the formation of low-volatile highly oxygenated organic molecules, HOM (Ehn et al., 2014). This abstract summarizes some of the main findings over the last year within our group.

RESULTS

On the topic of VOC oxidation, two major results were achieved concerning the formation of HOM under different conditions. Firstly, the autoxidation process (Crouse et al., 2013) was shown to be very sensitive to temperature in the case of alpha-pinene ozonolysis (Quéléver et al., 2019). Lowering temperature from 20 to 0 degrees Celsius caused a decrease in HOM yields of nearly two orders of magnitude under our experimental conditions. Secondly, HOM formation from aromatic compounds was shown to increase with higher exposure to hydroxyl radicals (OH) (Garmash et al., 2019, ACPD, in review). Earlier studies have only reported HOM yields from first generation oxidation products of VOC, and this study suggests that the potential of less oxygenated OVOC to form HOM can be significant. In addition to these, we also published a review in Chemical Reviews about HOM (Bianchi et al., 2019).

On the topic of instrument development and characterization, we performed the first parallel characterization of five different commonly used chemical ionization mass spectrometers (CIMS) for VOC and OVOC detection (Riva et al., 2019c). Our work was able to show that current instrumentation can map the majority of OVOC, but there are also certain ranges in the volatility distribution which are not properly covered. In addition, we developed a new type of CIMS by employing a chemical ionization inlet to an ultra high-resolution Orbitrap mass spectrometer (Riva et al., 2019a). This work will likely spur the community to consider shifting from the most commonly used time-of-flight mass spectrometers to Orbitraps, at least for certain applications.

On the topic of SOA formation and evolution, we have showed that the role of acidity in oligomer formation in organic aerosol is important also for monoterpene-derived aerosol (Riva et al., 2019b). The importance of acidity has earlier been mainly discussed in relation to isoprene. Monoterpene SOA formation can also be hampered by the presence of smaller molecules, such as isoprene (McFiggans et al., 2019). The effect arises both from the scavenging of OH by the smaller molecules as well as from the perturbation of gas-phase dimerization reactions. Finally, the aerosol at our Hyytiälä field station was characterized utilizing a combination of factorization and clustering algorithms applied to aerosol mass spectrometry data, yielding new insights into the sources of both organic and inorganic aerosol at the site (Äijälä et al., 2019).

ACKNOWLEDGEMENTS

This research was supported by the European Research Council (Grant 638703-COALA) and the Academy of Finland (grants 307331, 317380 and 320094).

REFERENCES

- Äijälä, M., Daellenbach, K. R., Canonaco, F., Heikkinen, L., Junninen, H., Petäjä, T., Kulmala, M., Prevot, A. S. H., & Ehn, M. (2019). Constructing a data-driven receptor model for organic and inorganic aerosol - a synthesis analysis of eight mass spectrometric data sets from a boreal forest site. *Atmospheric Chemistry and Physics*, *19*(6), 3645-3672. doi:10.5194/acp-19-3645-2019
- Bianchi, F., Kurtén, T., Riva, M., Mohr, C., Rissanen, M. P., Roldin, P., Berndt, T., Crouse, J. D., Wennberg, P. O., Mentel, T. F., Wildt, J., Junninen, H., Jokinen, T., Kulmala, M., Worsnop, D. R., Thornton, J. A., Donahue, N., Kjaergaard, H. G., & Ehn, M. (2019). Highly Oxygenated Organic Molecules (HOM) from Gas-Phase Autoxidation Involving Peroxy Radicals: A Key Contributor to Atmospheric Aerosol. *Chemical Reviews*, *119*(6), 3472-3509. doi:10.1021/acs.chemrev.8b00395
- Crouse, J. D., Nielsen, L. B., Jørgensen, S., Kjaergaard, H. G., & Wennberg, P. O. (2013). Autoxidation of Organic Compounds in the Atmosphere. *J. Phys. Chem. Lett.*, 3513-3520. doi:10.1021/jz4019207
- Ehn, M., Thornton, J. A., Kleist, E., Sipilä, M., Junninen, H., Pullinen, I., Springer, M., Rubach, F., Tillmann, R., Lee, B., Lopez-Hilfiker, F., Andres, S., Acir, I.-H., Rissanen, M., Jokinen, T., Schobesberger, S., Kangasluoma, J., Kontkanen, J., Nieminen, T., Kurten, T., Nielsen, L. B., Jørgensen, S., Kjaergaard, H. G., Canagaratna, M., Maso, M. D., Berndt, T., Petäjä, T., Wahner, A., Kerminen, V.-M., Kulmala, M., Worsnop, D. R., Wildt, J., & Mentel, T. F. (2014). A large source of low-volatility secondary organic aerosol. *Nature*, *506*(7489), 476-479. doi:10.1038/nature13032
- McFiggans, G., Mentel, T. F., Wildt, J., Pullinen, I., Kang, S., Kleist, E., Schmitt, S., Springer, M., Tillmann, R., Wu, C., Zhao, D. F., Hallquist, M., Faxon, C., Le Breton, M., Hallquist, A. M., Simpson, D., Bergström, R., Jenkin, M. E., Ehn, M., Thornton, J. A., Alfarra, M. R., Bannan, T. J., Percival, C. J., Priestley, M., Topping, D., & Kiendler-Scharr, A. (2019). Secondary organic aerosol reduced by mixture of atmospheric vapours. *Nature*, *565*(7741), 587-593. doi:10.1038/s41586-018-0871-y
- Quéléver, L. L. J., Kristensen, K., Jensen, L. N., Rosati, B., Teiwes, R., Daellenbach, K. R., Peräkylä, O., Roldin, P., Bossi, R., Pedersen, H. B., Glasius, M., Bilde, M., & Ehn, M. (2019). Effect of temperature on the formation of highly oxygenated organic molecules (HOMs) from alpha-pinene ozonolysis. *Atmospheric Chemistry and Physics*, *19*(11), 7609-7625. doi:10.5194/acp-19-7609-2019
- Riva, M., Ehn, M., Li, D., Tomaz, S., Bourgain, F., Perrier, S., & George, C. (2019a). CI-Orbitrap: An Analytical Instrument To Study Atmospheric Reactive Organic Species. *Analytical Chemistry*, *91*(15), 9419-9423. doi:10.1021/acs.analchem.9b02093
- Riva, M., Heikkinen, L., Bell, D. M., Peräkylä, O., Zha, Q., Schallhart, S., Rissanen, M. P., Imre, D., Petäjä, T., Thornton, J. A., Zelenyuk, A., & Ehn, M. (2019b). Chemical transformations in monoterpene-derived organic aerosol enhanced by inorganic composition. *npj Climate and Atmospheric Science*, *2*(1), 2. doi:10.1038/s41612-018-0058-0
- Riva, M., Rantala, P., Krechmer, J. E., Peräkylä, O., Zhang, Y. J., Heikkinen, L., Garmash, O., Yan, C., Kulmala, M., Worsnop, D., & Ehn, M. (2019c). Evaluating the performance of five different chemical ionization techniques for detecting gaseous oxygenated organic species. *Atmospheric Measurement Techniques*, *12*(4), 2403-2421. doi:10.5194/amt-12-2403-2019

ACTRIS – SHAPING THE FUTURE OF ATMOSPHERIC RESEARCH

P. HAAPANALA¹, M. PARAMONOV², E. JUUROLA¹, M. KULMALA¹, K. LEHTINEN³, H. KORHONEN², J. KESKINEN⁴, T. PETÄJÄ¹, H. HAKOLA², A. VIRTANEN³, M. DAL MASO⁴, and S. SORVARI SUNDET²

¹Institute for Atmospheric and Earth System Research, INAR, University of Helsinki

²Finnish Meteorological Institute

³University of Eastern Finland

⁴Tampere University

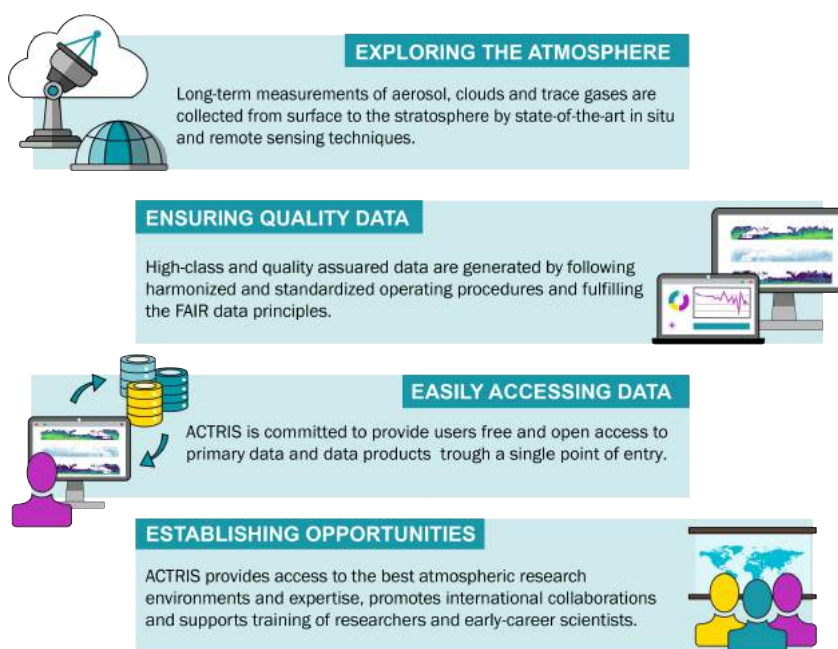
Keywords: RESEARCH INFRASTRUCTURE, AEROSOL, CLOUD MICROPHYSICS, TRACE GASES

INTRODUCTION

During the latest decades the improvements in means of analysing and sharing big data sets have made it possible to easily analyse complex data from across the globe. This requires inter-comparable data. The production of such data sets calls for wide networks producing harmonized data sets over large geographical area, and storing and delivering the data in a common way. This requires a lot of coordination.

International Research Infrastructures (RIs) are the European answer to these needs. They enable implementation of scientific instruments and networks that are too big for any nation to build alone. They also enable a more continuous funding scheme for large scale international operations.

AEROSOL, CLOUDS AND TRACE GASES RESEARCH INFRASTRUCTURE



The Aerosol, Clouds and Trace Gases Research Infrastructure (ACTRIS) is a pan-European research infrastructure producing high-quality data and information on short-lived atmospheric constituents and on the processes leading to the variability of these constituents in natural and controlled atmospheres. The general idea in ACTRIS is to pool together the efforts all around Europe in order to achieve better results than any nation alone could achieve. ACTRIS will not do research, but will provide data and other services that will enable researchers to produce better scientific results. The main objectives of ACTRIS are shown in the Figure 1.

Figure 1. Infographic on ACTRIS main objectives.

ACTRIS is planned to consist of National and Central Facilities. The National Facilities are the numerous existing and to-be-implemented measuring sites, mobile research platforms, simulation chambers and laboratories producing atmospheric data. The Central Facilities are Head Office, Data Centre and six Topical Centres for calibration of measurement instruments and operation support for different measurement instruments.

These six Topical Centres are:

- Centre for Aerosol In Situ Measurements
- Centre for Aerosol Remote Sensing
- Centre for Cloud In Situ Measurements
- Centre for Cloud Remote Sensing
- Centre for Reactive Trace Gases In Situ Measurements
- Centre for Reactive Trace Gases Remote Sensing

In the ACTRIS vision the nature of atmospheric research will be different than what it is today. The continuous atmospheric measurements will be performed and maintained by scientific engineers focusing on that task, and researchers around the world will use ACTRIS data for their research. This arrangement will free the researchers from operating and seeking funding for the long-term measurements, and grant them more time for utilising the data. Measurement campaigns and novel measurements will still be performed by the research scientists with the help of the station personnel at ACTRIS stations.

ACTRIS SERVICES

ACTRIS is currently in preparation and the plan is to set up ACTRIS by 2025. By that time ACTRIS will be fully established and providing its services in full capacity. During coming years, during the ACTRIS Implementation Phase, a comprehensive ACTRIS service catalogue will be developed. The services will be provided to all user communities, including both public and private sector.

The first and most obvious ACTRIS service is the data, which will be available for free via the ACTRIS Data Centre. The data will be inter-comparable due to common measurement and data processing protocols

and quality controlled via regular calibration of the instruments. Besides data delivery, the Data Centre provides virtual tools for processing the data online. The availability of the data will also allow new services to be built on the data. Another ACTRIS service is to provide supported access to the Topical Centres and to selected National Facilities via a competitive selection process. This way the most promising research projects will always have access to the best facilities and expertise available. Besides publicly funded research, access to ACTRIS facilities will also be available for commercial actors, which will enhance the public-private collaboration and lead to new science-based innovations. ACTRIS also provides training and education related to instruments and processing of atmospheric data. Furthermore, ACTRIS gives a stronger voice in the policy making for the related scientific communities.

HOW IS ACTRIS BEING IMPLEMENTED

The ACTRIS community has a long history of collaboration through various international projects, dating back to 1990's and early 2000's. From this background it is natural that ACTRIS is proceeding to become a more permanent and coordinated research infrastructure. ACTRIS was adopted on the European roadmap of new research infrastructures in 2016, with a deadline to start its operations within 10 years. The schedule of ACTRIS is, however, much faster, and aims at the establishment of ACTRIS as a legal entity and provision of first services in 2020-2021, and to ramp up the operations to full capacity by 2025. The schedule of ACTRIS is presented in figure 2.

ACTRIS lifecycle phases	Preparatory Phase			Implementation phase					Operational phase			
Framework	Project-based			transition	Legal entity - ACTRIS ERIC							
Support EC project	ACTRIS PPP			ACTRIS IMP					-			
Year	2017	2018	2019	2020	2021	2022	2023	2024	2025	2026	2027	2028

Figure 2. The schedule of ACTRIS and EC-projects supporting the implementation.

The legal model of ACTRIS is decided to be ERIC (European Research Infrastructure Consortium). This means that the members of ACTRIS will be the countries hosting ACTRIS facilities, not the research organizations. The countries will be represented through ACTRIS General Assembly and currently through its predecessor Interim ACTRIS Council, comprising of ministry and funding agency representatives from the participating countries, and being the highest decision making body in ACTRIS. Currently 17 countries are preparing ACTRIS at ministry level, and 5 more are involved in the process without ministry-level participation. The countries participating in ACTRIS are presented in Figure 3.

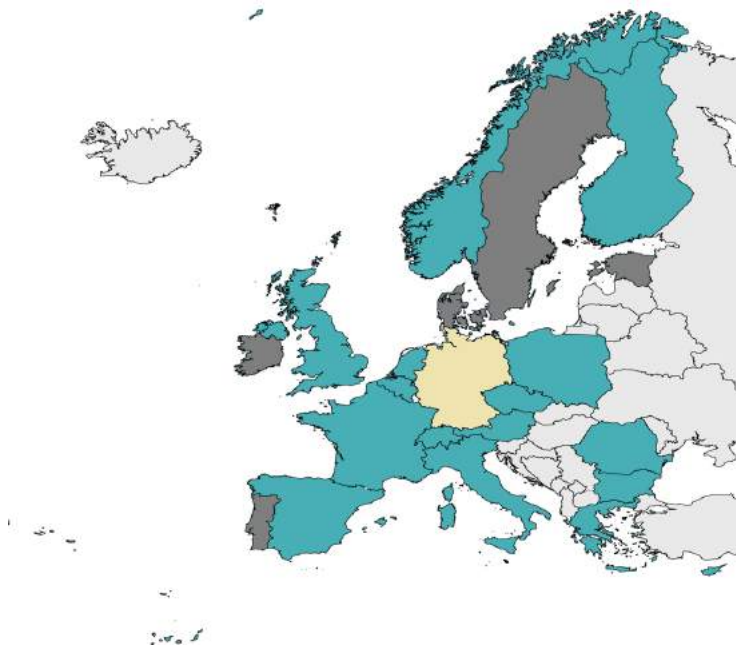


Figure 3. Countries involved in ACTRIS. Petrol blue: members of ACTRIS Interim Council; beige: observers, dark grey: countries have been committed to ACTRIS at the research organization-level or are in middle of negotiations.

Currently, the international coordination activities of ACTRIS are funded via three EC-funded projects: ACTRIS-2, EUROCHAMP 2020 and ACTRIS PPP (Figure 2). ACTRIS -2 and ACTRIS PPP project are ending this year and a new EC-funded project will start in the beginning of 2020: ACTRIS IMP. ACTRIS-2 has focused on scientific integration of the research communities around atmospheric aerosols, clouds and trace gases, and provides funding for trans-national access to 18 research facilities around Europe. EUROCHAMP 2020 does the same for research with atmospheric simulation chambers around Europe. ACTRIS PPP is a project to prepare the governance, legal, financial and operational frameworks needed for the fully fledged research infrastructure organisation. ACTRIS IMP will take ACTRIS into a new level of maturity and will set the needed structures for the implementation actions, both at the national and European level. The project builds on three main pillars: securing the long-term sustainability, implementing of ACTRIS functionalities, and positioning ACTRIS in the national, European and international science and innovation landscape. ACTRIS IMP will enable ACTRIS to respond to the users' needs and requirements.

Finnish partners are involved with a significant role in all these projects in the planned ACTRIS Central Facilities. The participating public research institutions are Finnish Meteorological Institute (FMI), University of Helsinki (UHEL), University of Eastern Finland (UEF) and Tampere University (TUNI). From private sector, instrument manufacturer Airmodus is involved.

- ACTRIS-2: FMI and UHEL partners, TUNI and Airmodus associated partners
- EUROCHAMP 2020: UEF and UHEL partners, Airmodus associated partner
- ACTRIS PPP: FMI coordinator, UHEL co-coordinator, UEF and TUNI associated partners
- ACTRIS IMP: FMI coordinator, UHEL co-coordinator, UEF and TUNI associated partners
- ACTRIS Head Office: Finland will lead ACTRIS
- ACTRIS Data Centre: FMI will participate with Cloudnet data unit
- Centre for Aerosol In Situ Measurements: UHEL will participate with sub-10nm particle measurements unit
- Centre for Cloud Remote Sensing: FMI will participate with a small Doppler Lidar data processing unit
- Centre for Reactive Trace Gases In Situ Measurements: UHEL will participate with instrument development and cluster measurements unit

Besides the participation in Central Facilities, Finland plans to include also a number of National Facilities in ACTRIS, including (but not limited to) all SMEAR stations, Pallas Atmosphere-Ecosystem Supersite, Utö Atmospheric and Marine Research Station, Mobile lidars and cloud radar, Kuopio Atmospheric Simulation Chambers, and TUNI Mobile Aerosol Laboratory.

ACKNOWLEDGEMENTS

ACTRIS has been / is currently supported by EC grants ACTRIS (2011-2015, #262254), ACTRIS-2, (2015-2019, #654109), EUROCHAMP 2020 (2017-2020, #730997) and ACTRIS PPP (2017-2019, #739530). The Finnish actions in ACTRIS are further supported by the Academy of Finland (2017-2019, #304013) and by the Ministry of Transport and Communication in Finland. We also thank the numerous past and ongoing national projects and programs for providing immense support for long-term atmospheric and aerosol research throughout Europe.

For more information about ACTRIS, please visit www.actris.eu.

MAIN RESEARCH TOPICS OF THE FMI AIR QUALITY GROUP IN 2019

HAKOLA H., HELIN A., HEMMILÄ M., KYLLÖNEN K., LIIKANEN A., MAKKONEN U.,
PRAPLAN A.P., SCHALLHART S., VIRKKULA A., HELLEN H.

Finnish Meteorological Institute, Air Quality, P.O. Box 503, FI-00101 Helsinki, Finland

Keywords: AIR QUALITY, ATMOSPHERIC CHEMISTRY, ALKYL AMINES, OH REACTIVITY,
OZONE REACTIVITY, VOCs, VOC EMISSIONS, WETLAND EMISSIONS, PAH

VOC, OH AND OZONE REACTIVITY MEASUREMENTS

In 2018 we measured volatile organic compounds (VOC) and OH reactivity at Pallas in Northern Finland on a sub-Arctic wetland. Seasonal changes and diurnal variations of total OH reactivity and mixing ratios of individual reactive compounds were studied as well as their emissions from the wetland. Data has been processed in 2019 and for the first time we found high sesquiterpene (SQT) emissions from wetland. Monoterpene (MT) emissions were generally less than 10% lower than isoprene emissions, but SQT emissions were surprisingly high exceeding MT emissions all the time (Fig.1). During early growing season SQT emission rates were about ten times higher than MT emission rates but this difference became smaller towards the end of a summer. However, also then SQT emission rates were still about twice as high as MT. Although the lifetimes of SQT is short, varying from minutes to hours, we could still detect them in ambient air also. The measured VOCs in the emission explained about half of the OH reactivity. The remaining reactivity is suspected to be caused by non-measured, direct emissions. Two manuscripts from fen VOC emissions and related OH reactivity measurements will be submitted by the end of 2019 (Schallhart et al. and Hellén et al.).

The OH reactivity was also measured from spruce and birch emissions for in situ conditions in Hyytiälä in summer 2019. The reactivity of the emissions was larger in June compared to July/August. The reactivity follows VOC and temperature diurnal pattern with a maximum during the day. The manuscript is under preparation by Praplan et al.

In order to get more information from the compounds we are missing, we also developed an O₃ reactivity instrument. It is now working with some limitations: high detection limits (ca. 19ppbv α -pinene equivalent) and challenges with mixtures of several compounds with different reactivity towards ozone (e.g. isoprene and sesquiterpenes) still need to be overcome. We continue to work with ozone reactivity instrument.

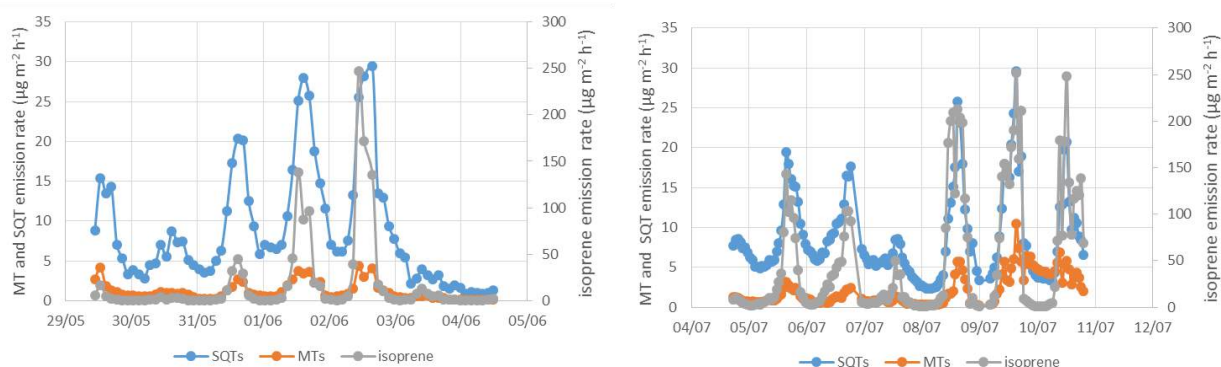


Figure 1: Measured emission rates of SQTs, MTs and isoprene from Lompolojänkää fen in Northern Finland in 2018 during early (left) and midsummer (right).

A METHOD TO MEASURE DITERPENES

Diterpenes are a class of chemical compounds composed of two monoterpene units with the molecular formula $C_{20}H_{32}$. Matsunaga et al. (2011) have measured the emissions of a diterpene, kaur-16-ene, from typical Japanese conifers, showing that these emissions are of the same magnitude as those of monoterpenes. Our measurement at Lompolojännkä fen and also many other studies show that we have not detected all the compounds causing OH reactivity. Diterpenes could be one group of compounds missing from reactivity calculations. Therefore we wanted to develop a method for diterpene analysis using a gas-chromatograph-mass-spectrometer. The method development and performance related experiments included, for example, desorption efficiency, sampling recovery and ozone reactivity tests. The method was also tested for real samples and multiple diterpenes could be detected in the emissions from pine needles and spruce twigs in laboratory conditions at 30 °C. The manuscript by Helin et al. will be submitted in 2019.

AMINE AND GUANIDINE SOIL EMISSION MEASUREMENTS

In our earlier study we measured amine concentrations in ambient air (Hemmilä et al. 2018). In that study we observed that different amines are likely to have different sources and that their seasonality is not the same for all the compounds. In order to get more information about amine sources, we conducted amine emission measurements from boreal forest floor in April, May, July and September in 2018. Monomethylamine (MMA), dimethylamine (DMA), trimethylamine (TMA), and diethylamine (DEA) had their maximum emissions in July, but guanidine had highest emissions already in the spring. In our earlier ambient air study (Hemmilä et al., 2018) we noticed that DMA and TMA had also their maximum ambient air concentrations in July. Diurnal variability of DMA emission rates are shown as an example in Fig. 2.

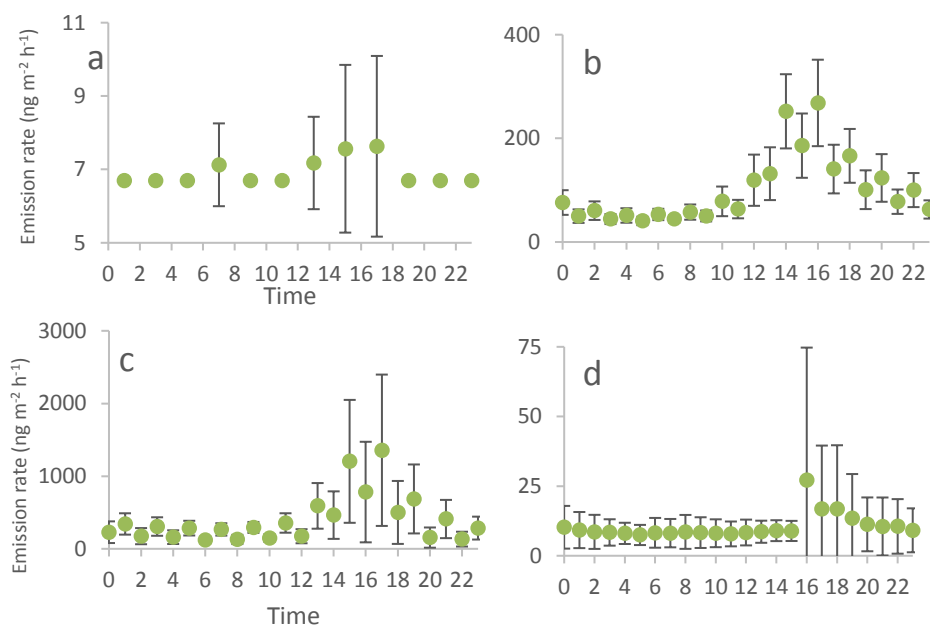


Figure 2. Diurnal variations of DMA emission rates from the boreal forest floor in April (a), May (b), July (c) and September (d).

NON-METHANE HYDROCARBON (NMHC) MEASUREMENTS ON UTÖ ISLAND

NMHCs were measured on Utö Island in Baltic Sea in Finland during 1994-2007 by collecting air samples in stainless steel canisters twice a week for further analysis in the laboratory. The results of these measurements are published in Laurila and Hakola, 1996 and Hakola et al., 2007. Later on from March 2018 to March 2019 VOCs were measured again, but this time using in situ gas-chromatograph with 2-hour time resolution.

Utö is an Atmospheric and Marine Research Station of Finnish Meteorological Institute (59° 46'50N, 21° 22'23E) at the outermost edge of the Archipelago Sea, facing the Baltic proper. The station is currently producing real-time, high-frequency measurements of the physical, chemical and biological features of the water column in the outermost archipelago and of atmospheric concentrations of trace gases and aerosols (<http://en-ilmatiiteenlaitos.fi/uto>). The description of the NMHC measurements conducted during 1994-2007 is in Hakola et al., 2007. During 2018-2019 an in-situ thermal desorption unit (Unity 2 + Air Server 2, Markes International ltd.) with a gas chromatograph (Agilent7890) and a mass spectrometer (Agilent 5975C) and a flame ionization detector was used.

The trend analysis conducted for the years 1994-2007 (Hakola et al., 2007) showed decreasing trends for the most reactive compounds, but no, or slightly increasing trends for ethane and propane. We now added the data from 2018 to this old dataset and the new trend analysis showed that decreasing trend for most of the compounds has strengthened, but there are few exceptions to this. The isoprene trend has increased during summer and i-butane and i-pentane concentrations have decreased less than n-isomers. These isomeric pairs have similar sources, they are all emitted as a result fuel evaporation and butanes also as a result of natural gas leakage. I-isomers react a bit slower with hydroxyl radicals in comparison with n-isomers and therefore the i/n-ratios are expected to be a little higher in remote areas. The increasing i/n-ratios have been observed also at Pallas in Northern Finland (Hellén et al., 2016) and one reason can be increased wood burning or natural gas usage, since these source categories have higher i/n ratios than traffic related emissions.

Ethane concentrations were higher at Pallas, Northern Finland, but all other NMHCs were most of the time higher on Utö.

TRENDS AND SOURCE APPORTIONMENT OF TRACE ELEMENTS IN PM AT PALLAS DURING THE LAST 22 YEARS

Atmospheric trace elements (Al, As, Cd, Co, Cr, Cu, Fe, Mn, Ni, Pb, V, Zn) in particulate matter have been measured at a sub-arctic site Pallas, Finland, since 1996. The results indicate a very low level of pollution as the measured concentrations are among the lowest measured in Europe. The annual average concentration during the whole time series 1996-2018 was from the lowest values to the highest Co<Cd<Cr<As<V<Ni<Cu<Mn<Pb<Zn<Al<Fe ranging from 0.02 to 20 ng m⁻³. For the priority pollutants As, Cd, Ni and Pb, the annual average concentration was 0.10, 0.02, 0.21 and 0.65 ng m⁻³, respectively, in 2018. The concentrations were compared with measurements at southern stations Hyytiälä, Virolahti and Ähtäri, and a clear south-to north decreasing gradient was clear for most elements; however the annual average concentration of Ni was in half of the studied years higher than concentrations measured in Hyytiälä and Ähtäri but lower than in Virolahti site. With source apportionment method, Ni as well as Cu, As and Co were found to be mostly associated to emissions from Kola Peninsula. Cd, Pb, V and Zn were attributed to long-range transported pollutants while Al, Fe and Mn were related to the soil origin. Gaseous Hg was included in the source analysis and was found almost purely in the background factor. Considering the full time series, trend analysis showed statistically significant decreasing trends for As, Cd, Co, Cu, Ni, Pb and V up to 64 % in the whole period. Since 2010, six elements (Cd, Co, Ni, Pb, V, Zn) continue the positive development of declining trends (P<0.05) with changes between 25 and 53 % in the period. No statistically significant increasing trends were observed. The manuscript by Kyllönen et al. will be submitted to Atmospheric Environment in December 2019.

TRENDS OF ATMOSPHERIC MERCURY

Atmospheric mercury measurements have now been conducted for over ten years at three background sites enabling for the first time to run a proper trend analysis of the time series. The results show that the concentrations are showing tendency for reduction, however, none of the trends are statistically significant. As mercury is a global pollutant with about 6 months lifetime in the atmosphere, the atmospheric concentrations are not only affected by the reduced emissions in Europe (and North America) but also the increased emissions in Asia. The trend analysis was calculated with the Generalized Least-Squares (GLS) regression with classical decomposition and AutoRegressive Moving Average (ARMA) errors applied for monthly mean values (Anttila and Tuovinen, 2010).

The atmospheric concentrations at the sub-arctic Pallas station are slightly higher than in the south, whereas the deposition of mercury follows the decreasing spatial trend from south to north, as typical for most pollutants (Fig. 3).

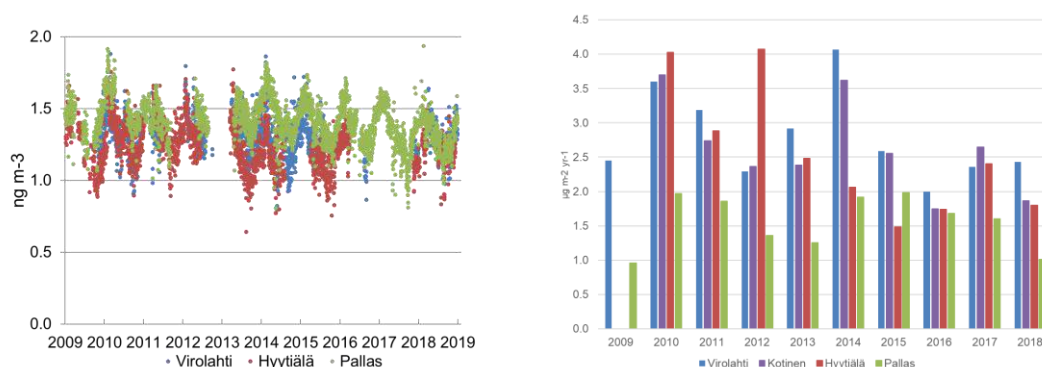


Figure 3: Daily total gaseous mercury (TGM) concentration (left) and annual Hg in deposition (right) in Finland during the last 10 years.

PAH MEASUREMENTS

Polycyclic aromatic hydrocarbons (PAHs) are particularly harmful compounds due to their carcinogenic effect on humans. PAHs are formed during the incomplete combustion of organic material, and are emitted into the atmosphere from several natural and anthropogenic emission sources. These compounds can exist in both gas and particulate phases in the atmosphere. Lighter, volatile PAHs consisting of two or three aromatic rings exist in the gas phase, whereas heavier compounds are incorporated into particles in the atmosphere. PAHs are usually collected on filters for 24 hours and therefore their atmospheric peak concentrations are not known. Therefore we developed a method to measure PAHs in the air using in situ TD-GC-MS with 1-hour time resolution. The developed method was found to be suitable for the volatile and semivolatile PAHs (Ryynälä J., 2019).

URBAN TERPENOID MEASUREMENTS

There are plenty of studies dealing with urban VOC concentrations, but not so many of the importance of biogenic VOCs in urban areas. We conducted a campaign at HSY street canyon station at Mäkelänkatu, Helsinki, measuring BVOCs and some newly identified aromatic hydrocarbons ($\text{C}_{10}\text{H}_{14}$, e.g. tetramethylbenzene) in addition to traditional anthropogenic hydrocarbons using an in situ thermodesorption gaschromatography- mass-spectrometry (TD-GC-MS). The data analysis is still ongoing, but we found relatively high concentrations of BVOCs.

MEASUREMENT CAMPAIGNS OUTSIDE FINLAND

While there is lots of data about BVOC concentrations from boreal areas, there is only very limited amount of data from the whole African continent. Together with the Department of Geosciences and Geography (UHEL) we conducted a measurement campaign to screen VOC concentrations from many different ecosystems in the area of the Taita station, Kenya. The major measured VOCs were isoprene, MBO and monoterpenoids, however the variability of the concentrations in the ecosystems was substantial and much more work is needed for getting a picture of the importance of BVOCs there.

We had also a campaign at Amazon together with the Max Planck Institute for Chemistry (Mainz, Germany) to measure ambient concentration of diterpenes during spring 2019. However, only monoterpenes, sesquiterpenes and some oxidation products were detected. The measurements at Amazon will continue in spring 2020.

AIR QUALITY MEASUREMENTS IN VIETNAM

A new air quality project has been started in Hanoi, Vietnam, in summer 2019. In the one-year project, daily filter samples are collected for the analysis of heavy metals, ions, EC/OC and levoglucosan in PM_{2.5} at two urban stations. Data will be used for source apportionment study to define the sources and their relative importance. So far, data on the chemical composition of PM is very scarce in Vietnam even though Hanoi and other cities in Vietnam are considered among the most polluted places in the world. The new project will give highly needed information to target air quality improvement policies for relevant sources.

REFERENCES

- Anttila P. & Tuovinen J.-P. 2010: Trends of primary and secondary pollutant concentrations in Finland in 1994–2007. *Atmos. Environ.* 44: 30–41.
- Hemmilä, M., Hellén, H., Virkkula, A., Makkonen, U., Praplan, A. P., Kontkanen J., Ahonen, L., Kulmala, M. and Hakola, H., *Atmospheric Chemistry and Physics*, 18 (2018) 6367–6380
- Laurila Tuomas and Hannele Hakola, 1996. Seasonal Cycle of C₂-C₅ hydrocarbons over the Baltic Sea and Northern Finland. *Atmospheric Environment*, 30, 1597-1607
- Hakola H., Hellén H. and Laurila T., 2006. Ten years of light hydrocarbon (C₂-C₆) concentration measurements in background air in Finland. *Atmospheric Environment* 40, 3621-3630
- Hellén H., Kouznetsov R., Anttila P., Hakola H., 2015. Increasing influence of easterly air masses on NMHC concentrations at the Pallas-Sodankylä GAW station. *Boreal Env. Res.* 20, 542-552.
- Matsunaga S., Chatani S., Nakatsuka S., Hiura T., 2011. Determination and potential importance of diterpene (kaur-16-ene) emitted from dominant coniferous trees in Japan. *Chemosphere* 87, 886-893.
- Ryynälä J., 2019: Measuring the Ambient Air Concentrations of Polycyclic Aromatic Hydrocarbons by Thermal Desorption-Gas Chromatography-Mass Spectrometry, Bachelor thesis, Metropolia University of Applied Science.

FUTURE EARTH FINLAND (FES)

M. HEMMILÄ, M. JUUSTILA, M. KULMALA

Institute for Atmospheric and Earth System Research / Physics, Faculty of Science, 00014 University of Helsinki, Finland

Keywords: NATIONAL COMMITTEE, CO-DESIGN, GLOBAL CHANGE, HEALTH

WHAT IS FUTURE EARTH FINLAND?

Future Earth Finland (FES) is the Finnish National Committee of Global Change Research. FES is representing Finland in international projects and organizations. The chair of the Committee is Markku Kulmala. The international Future Earth is a global network of scientists, researchers, and innovators collaborating for a more sustainable planet. The National Committee has been set by The Council of Finnish Academies

In Future Earth different sides of science are integrated to study global change in comprehensive perspectives. FES aims to enhance interdisciplinary global change research that will have an impact on society. The Committee co-designs its activities with end-users of research (f.ex. government, business, and civil society, Fig. 1).

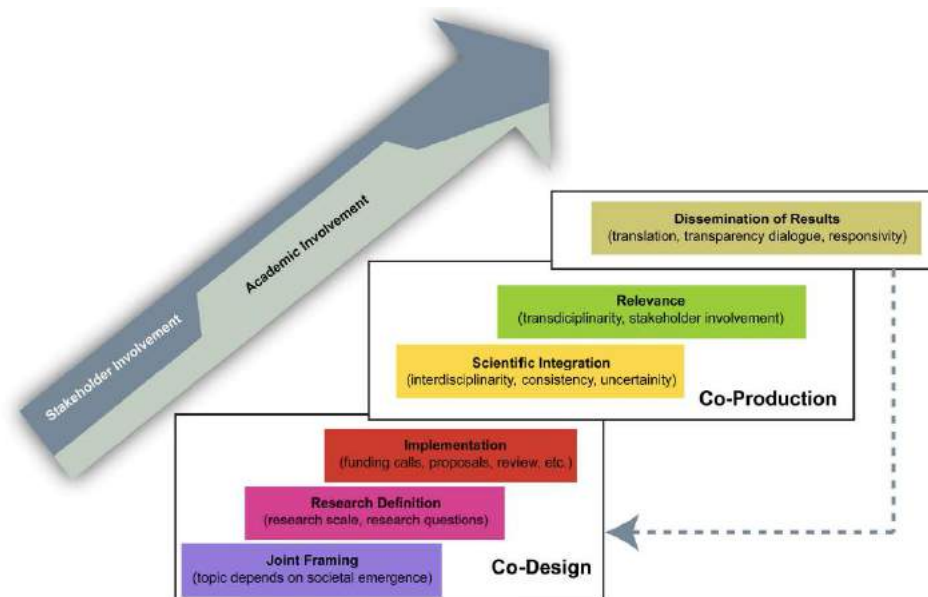


Figure 1. Co-design and co-production throughout the lifetime of a research project. Stakeholders here refer to people/organisations that influence or are influenced by the research. Adopted from Mauser et al., 2013.

FES 2019

The members of National Committee changed in June 2019. It has now members from Universities of Helsinki, Oulu and Turku, SYKE, HUS, Sitra, BSGA, Ministry of the Environment and LUT University.

Future Earth Finland has organized Global Change Symposium since 2015. The topics has been for example Renewable energy (2016) and Global Change and Food (2017). In year 2019, we have concentrated on climate change and health issues. FES will organize in 4th of November Global Change Symposium with One Health Finland (OHF) about Global Change and Health. It will be a panel seminar in Finnish to the public, and we are expecting ~100 participants. The panelists are experts in atmospheric sciences, biodiversity, virology and economy.

ACKNOWLEDGEMENTS

We thank The Council of Finnish Academies for the financial support.

REFERENCES

Mausser, W., Klepper, G., Rice, M., Schmalzbauer, B.S., Hackmann, H., Leemans, R., Moore, H. (2013) Transdisciplinary global change research: the co-creation of knowledge for sustainability, *Current Opinion in Environmental Sustainability*, 5 (3-4), 420-431

ACTIVITIES OF THE ATMOSPHERIC AEROSOLS GROUP OF THE FMI

A.-P. HYVÄRINEN¹, E. ASMI^{1,2}, M. AURELA¹, J. BACKMAN¹, D. BRUS¹, K. DOULGERIS¹, R.K. HOODA¹, J. KESTI¹, N. KIVEKÄS¹, A. KORPINEN¹, J. KUULA¹, O. MEINANDER¹, E. O'CONNOR¹, A. PIEDIHIERRO¹, S. SAARIKOSKI¹, H. SERVOMAA¹, J. SVENSSON^{1,3}, K. TEINILÄ¹, H. TIMONEN¹, S. TUKIAINEN¹, V. VAKKARI¹, A. WELTI¹

¹Atmospheric Composition Research, Finnish Meteorological Institute, Helsinki, P.O. Box 503, 00101 Finland.

²Servicio Meteorológico Nacional, Av. Dorrego 4019, Buenos Aires, Argentina.

³Grenoble

Keywords: Aerosol, Climate, Clouds, Measurements

INTRODUCTION

The Atmospheric Aerosols Research Group at the Finnish Meteorological Institute (FMI) studies the occurrence and properties of aerosols both in background- urban environments. Our objective is to enhance the understanding how aerosols affect climate, clouds and air quality. For this, the group utilizes state-of-the art instrumentation, and conducts measurements in the laboratory, in Finland, and in key locations around the globe. The group also contributes to the European Research Infrastructure for the observation of Aerosol, Clouds and Trace Gases, ACTRIS. For this, the group develops methods at its observing stations, exploratory platforms, and novel aerosol instrumentation.

METHODS

1. Primary and secondary emissions

In order to understand the chain from aerosol emissions to effects of aerosols on air quality and climate, the group has contributed to several studies on vehicle emissions from passenger cars (Pirjola et al. 2019, Simonen et al. 2019), busses (Järvinen et al. 2019), ships (Lehtoranta et al. 2019) and locomotive engines (Carbone et al. 2019). The results have highlighted the potential to mitigate both primary and secondary vehicle emissions with the use of cleaner fuels and after-treatment methods (Karjalainen et al. 2019). The group has also participated intercomparison studies between gravimetric impactors and electrical devices for emission studies (Salo et al. 2019).

A particular focus of the group's efforts have been understanding the role and linkages of black carbon in emissions, atmospheric composition, air quality and climate change. To this end, the group is developing metrics to illustrate a "Black Carbon Footprint", analogous to Carbon Footprint (Timonen et al. 2019).

2. Urban aerosols and air quality

One of the group's focus areas is urban air quality, and in particular the characterization of aerosol physical- and chemical composition. As major results, the group has characterized the variation of urban aerosol concentrations and chemical composition in Helsinki (Teinilä et al. 2019); and around the world (Saarikoski et al. 2019a, Pereira et al. 2019, de Jesus et al. 2019). Traffic- generated nanoparticles and their dispersion has also been studied, showing that traffic related nanoparticles can originate from combustion process formed by different pathways, but also from sources such as brake wear (Rönkkö et al. 2019). The concentrations of these nanoparticles decrease rapidly at road-side locations, mostly due to condensation and deposition processes (Kangasniemi et al. 2019).

3. Aerosols and climate

The group's continuous effort is to conduct long term observations of aerosols and clouds in key locations in Finland and internationally. In Finland, FMI's Pallastunturi Global Atmospheric Watch (GAW) station is under development to serve as a sub-Arctic supersite in ACTRIS. With an especial focus on black carbon (BC) measurements, the Pallastunturi station served as a platform for intercomparison measurements in the EMPIR Black Carbon project (<http://www.empirblackcarbon.com/>) at low BC concentrations. Pallastunturi site is also an integral part of the International Arctic Systems for Observing the Atmosphere (IASOA: www.iasoa.org, Uttal et al., 2015). For IASOA, the FMI is maintaining BC and other aerosol measurements also in Tiksi and Cape Baranova, in Arctic Russia. These data have recently been used to validate global aerosol model outputs (Schacht et al. 2019).

The group's other international activities are focused on key regions from the point of view of climate change or air quality, such as the Antarctic, southern Africa and South Asia. In a source-receptor site study in South Asia, it was found that brown carbon, a light absorbing aerosol, loses its light absorbing capacity by 84% due to photochemical oxidation during 6000 km transport from the Indo-Gangetic Plain to Indian Ocean (Dasari et al. 2019). Other key studies evidenced new particle formation followed by frequent apparent shrinking in Saudi Arabia (Hakala et al. 2019), and the first assessment of polar organic aerosols in southern Africa (Booyens et al. 2019).

The group continues to study also aerosol-cryosphere interactions, especially related to BC and high latitude dust. Currently measurements are being conducted in Sodankylä, and at two glaciers in Kyrgyzstan and Tajikistan. Importantly, we have developed a multiple scattering correction factor of quartz filters to improve the analyses of light-absorption in snow samples (Svensson et al. 2019). This will decrease the uncertainty of BC mass absorption coefficient (MAC) in snow.

To understand the fundamental aspects of aerosol formation, the group also studies ice nucleation and related parameters, such as amount of adsorbed water and contact angle in the laboratory. The mechanism how ice nucleates from surface adsorbed water is explored by correlating the amount of adsorbed water and the water-surface contact angle to the probability of ice nucleation.

4. Instrument- and method development

In order to keep abreast with state-of-the art science and methods, the group conducts both experimental and modeling development activities.

Vertical distribution of aerosol remains a major uncertainty in atmospheric sciences. The group has contributed to vertical profiling studies by developing post-processing algorithms for Halo Doppler lidars (Vakkari et al. 2019), and by developing of Unmanned Aerial Vehicles (UAV's) for atmospheric sciences (Barbieri et al. 2019).

Inexpensive miniature- and portable sized aerosol sensors have potential usage in aforementioned UAV's in addition to enabling measurement networks with a high spatial resolution. The group has studied the accuracy and applicability of these sensors. The results highlight that proper calibration and understanding individual sensor characteristics is required for reliable measurements (Kuula et al. 2019a, 2019b).

The utilization and application of Aerosol Chemical Speciation Monitors (ACSM's) is increasing in atmospheric sciences from being a campaign instrument to long term measurements. The group has contributed both to calibration studies of ACSM's (Freney et al. 2019), as well as testing a novel aerosol concentrator for detection of low concentration species using aerosol mass spectrometers (Saarikoski et al. 2019b).

CONCLUSIONS

The activities and results of the Atmospheric Aerosols Research Group at the Finnish Meteorological Institute (FMI), which are in line with the Finnish Center of Excellence in Atmospheric Science – From Molecular and Biological processes to The Global Climate –program, were presented.

ACKNOWLEDGEMENTS

Work was supported by the Academy of Finland Center of Excellence programme (grant no. 307331) and by Academy of Finland projects: C-MAIN, AAFIG, PARMAT, NABCEA,; by Ministry for Foreign Affairs: IBA-FIN-BCDUST, FINTAJ-2, FINKMET-2; by Business Finland projects: TAQIITA, BC-Footprint, CITYZER, by EU projects: ACTRIS-2, INTAROS, Euramet-Black Carbon, and by Maj and Tor Nessling foundation.

REFERENCES

- Alghamdi, M.A.; Al-Hunaiti, A.; Arar, S.; Khoder, M.; Abdelmaksoud, A.S.; Al-Jeelani, H.; Lihavainen, H.; Hyvärinen, A.; Shabbaj, I.I.; Almeahmadi, F.M.; Zaidan, M.A.; Hussein, T.; L.A. Dada (2019). A Predictive Model for Steady State Ozone Concentration at an Urban-Coastal Site, *Int. J. Environ. Res. Public Health* **16**, 258.
- Barbieri, L., Kral, S.T., Bailey, S.C.C., Frazier, A.E., Jacob, J.D., Reuder, J., Brus, D., Chilson, P.B., Crick, C., Detweiler, C., Doddi, A., Elston, J., Foroutan, H., González-Rocha, J., Greene, B.R., Guzman, M.I., Islam, A.L.H.A., Kemppinen, O., Lawrence, D., Pillar-Little, E.A., Ross, S.D., Sama, M., III, D.G.S., Schuyler, T.J., Shankar, A., Smith, S.W., Waugh, S., Dixon, C., Borenstein, S., and G.D. Boer (2019). Intercomparison of Small Unmanned Aircraft System (sUAS) Measurements for Atmospheric Science during the LAPSE-RATE Campaign, *Sensors* **19**, 2179.
- Booyens, W., Beukes, J. P., Van Zyl, P. G., Ruiz-Jimenez, J., Kopperi, M., Riekkola, M.-L., Jospovic, M., Vakkari, V. and L. Laakso (2019). Assessment of polar organic aerosols at a regional background site in southern Africa, *J. Atmos. Chem.*, doi:10.1007/s10874-019-09389-y.
- Carbone, S., Timonen, H., Rostedt, A., Happonen, M., Rönkkö, T., Keskinen, J., Ristimäki, J., Korpi, H., Artaxo, P., Canagaratna, M., Worsnop, D., Canonaco, F., S. H. Prévôt, A., Hillamo R., and S. Saarikoski (2019). Distinguishing fuel and lubricating oil combustion products in diesel engine exhaust particles, *Aerosol Science and Technology*, **53**:5, 594-607, DOI: 10.1080/02786826.2019.1584389.
- Dasari, S., Andersson A., Bikkina, S., Holmstrand, H., Budhavant, K., Satheesh, S., Asmi, E., Kesti, J., Backman, J., Salam, A., Singh Bisht, D., Tiwari, S., Hameed, Z., and Ö. Gustafsson (2019). Photochemical degradation affects the light absorption of water-soluble brown carbon in the SouthAsian outflow, *Science Advances* **5**, 1, eaau8066, <https://doi.org/10.1126/sciadv.aau8066>.
- Frenay, E., Zhang, Y., Croteau, P., et al. (2019). The second ACTRIS inter-comparison (2016) for Aerosol Chemical Speciation Monitors (ACSM): Calibration protocols and instrument performance evaluations, *Aerosol Science and Technology* **53**:7, 830-842, DOI: 10.1080/02786826.2019.1608901.
- Hakala, S., Alghamdi, M. A., Paasonen, P., Vakkari, V., Khoder, M. I., Neitola, K., Dada, L., Abdelmaksoud, A. S., Al-Jeelani, H., Shabbaj, I. I., Almeahmadi, F. M., Sundström, A.-M., Lihavainen, H., Kerminen, V.-M., Kontkanen, J., Kulmala, M., Hussein, T., and A.-P. Hyvärinen (2019). New particle formation, growth and apparent shrinkage at a rural background site in western Saudi Arabia, *Atmos. Chem. Phys.* **19**, 10537–10555, <https://doi.org/10.5194/acp-19-10537-2019>.
- de Jesus, A.L., M.M. Rahman, M. Mazaheri, H. Thompson, L.D. Knibbs, C. Jeong, et al. (2019). Ultrafine particles and PM_{2.5} in the air of cities around the world: are they representative of each other?, *Environ. Int.* **129**, pp. 118-135.
- Järvinen, A., Timonen, H., Karjalainen, P., Bloss, M., Simonen, P., Saarikoski, S., Kuuluvainen, H., Kalliokoski, J., Dal Maso, M., Niemi, J.V., Keskinen, J., and T. Rönkkö (2019). Particle emissions of Euro VI, EEV and retrofitted EEV city buses in real traffic, *Environmental Pollution* **250**, 708-716, doi.org/10.1016/j.envpol.2019.04.033.
- Kangasniemi, O., Kuuluvainen, H. Heikkilä, J. Pirjola, L., Niemi, J. V, Timonen, H., Saarikoski, S., Rönkkö, T. and M. Dal Maso (2019). Dispersion of a Traffic Related Nanocluster Aerosol Near a Major Road, *Atmosphere* **10**(6), 309, doi:10.3390/atmos10060309.

- Karjalainen, P., Rönkkö, T., Simonen, P., Ntziachristos, L., Juuti, P., Timonen, H., Teinilä, K., Saarikoski, S., Saveljeff, H., Lauren, M., Happonen, M., Matilainen, P., Maunula, T., Nuottimäki, J., and J. Keskinen (2019). Strategies To Diminish the Emissions of Particles and Secondary Aerosol Formation from Diesel Engines, *Environmental Science & Technology* **53** (17), 10408-10416, DOI: 10.1021/acs.est.9b04073.
- Kuula, J., Kuuluvainen, H., Niemi, J. V., Saukko, E., Portin, H., Kousa, A., Aurela, M., Rönkkö, T., and H. Timonen (2019a). Long-term sensor measurements of lung deposited surface area of particulate matter emitted from local vehicular and residential wood combustion sources, *Aerosol Science and Technology*, DOI: 10.1080/02786826.2019.1668909.
- Kuula, J., Kuuluvainen, H., Rönkkö, T., Niemi, J. V., Saukko, E., Portin, H., Aurela, M., Saarikoski, S., Rostedt, A., Hillamo, R., and H. Timonen (2019). Applicability of Optical and Diffusion Charging-Based Particulate Matter Sensors to Urban Air Quality Measurements, *Aerosol and Air Quality Research*, 10.4209/aaqr.2018.04.0143.
- Lehtoranta, K., Aakko-Saksa, P., Murtonen, T., Vesala, H., Ntziachristos, L., Rönkkö, T., Karjalainen, P., Kuittinen, N., and H. Timonen (2019). Particulate Mass and Nonvolatile Particle Number Emissions from Marine Engines Using Low-Sulfur Fuels, Natural Gas, or Scrubbers, *Environmental Science & Technology* **53**, 6, 3315-3322, DOI: 10.1021/acs.est.8b05555.
- Pereira G. M., Oraggio B., Teinilä K., Custódio D., Huang X., Hillamo R., Alves C. A., Balasubramanian R., Rojas N., Sanchez-Ccoyollo O., and P. Vasconcellos (2019). A comparative chemical study of PM10 in three Latin American cities: Lima, Medellín and São Paulo Air Quality, *Air Qual Atmos Health* **12**, 1141. <https://doi.org/10.1007/s11869-019-00735-3>.
- Pirjola, L., Kuuluvainen, H., Timonen, H., Saarikoski, S., Teinilä, K., Salo, L., Datta, A., Simonen, P., Karjalainen, P., Kulmala, K., and T. Rönkkö (2019). Potential of renewable fuel to reduce diesel exhaust particle emissions, *Applied Energy* **254**, 113636, 10.1016/j.apenergy.2019.113636.
- Rönkkö, T., and H. Timonen (2019). Overview of Sources and Characteristics of Nanoparticles in Urban Traffic-Influenced Areas, *Journal of Alzheimer's Disease* **72**, 1, 15-28.
- Saarikoski, S., Reyes, F., Vázquez, Y., Tagle, M., Timonen, H., Aurela, M., Carbone, S., Worsnop, D. R., Hillamo, R., and P. Oyola (2019a). Characterization of submicron aerosol chemical composition and sources in the coastal area of Central Chile, *Atmospheric Environment* **199**, 391-401, 10.1016/j.atmosenv.2018.11.040.
- Saarikoski, S., Williams, L. R., Spielman, S. R., Lewis, G. S., Eiguren-Fernandez, A., Aurela, M., Hering, S. V., Teinilä, K., Croteau, P., Jayne, J. T., Hohaus, T., Worsnop, D. R., and H. Timonen (2019b). Laboratory and field evaluation of the Aerosol Dynamics Inc. concentrator (ADIC) for aerosol mass spectrometry, *Atmos. Meas. Tech.* **12**, 3907–3920.
- Salo, L., Mylläri, F., Maasikmets, M., Niemelä, V., Konist, A., Vainumäe, K., Kupri, H.-L., Titova, R., Simonen, P., Aurela, M., Bloss, M., Keskinen, J., Timonen, H., and T. Rönkkö (2019). Emission measurements with gravimetric impactors and electrical devices: An aerosol instrument comparison, *Aerosol Science and Technology*, DOI: 10.1080/02786826.2019.1578858.
- Schacht, J., Heinold, B., Quaas, J., Backman, J., Cherian, R., Ehrlich, A., Herber, A., Huang, W. T. K., Kondo, Y., Massling, A., Sinha, P. R., Weinzierl, B., Zannata, M., and I. Tegen (2019). The importance of the representation of air pollution emissions for the modeled distribution and radiative effects of black carbon in the Arctic, *Atmos. Chem. Phys.* **19**, 11159–11183, <https://doi.org/10.5194/acp-19-11159-2019>.
- Simonen, P., Kalliokoski, J., Karjalainen, P., Rönkkö, T., Timonen, H., Saarikoski, S., Aurela, M., Bloss, M., Triantafyllopoulos, G., Kontses, A., Amanatidis, S., Dimaratos, A., Samaras, Z., Keskinen, J., Dal Maso, M., and L. Ntziachristos (2019). Characterization of laboratory and real driving emissions of individual Euro 6 light-duty vehicles – Fresh particles and secondary aerosol formation, *Environmental Pollution* **255**, 1, 113175, <https://doi.org/10.1016/j.envpol.2019.113175>.
- Svensson, J., Ström, J., and A. Virkkula (2019). Multiple scattering correction factor of quartz filters and the effect of filtering particles mixed in water: implications to analyses of light-absorption in snow samples, *Atmos. Meas. Tech. Discuss.*, <https://doi.org/10.5194/amt-2019-142>, accepted.
- Teinilä K., Aurela M., Niemi J., Kousa A., Petäjä T., Järvi L., Hillamo R., Kangas L., Saarikoski S., and H. Timonen (2019). Concentration variation of gaseous and particulate pollutants in the Helsinki

city centre — observations from a two-year campaign from 2013–2015, *Boreal Env. Res.* **24**: 115–136.

Timonen, H., Karjalainen, P., Aalto, P., et al. (2019). Adaptation of Black Carbon Footprint Concept Would Accelerate Mitigation of Global Warming, *Environmental Science & Technology Article*, DOI: 10.1021/acs.est.9b05586.

Vakkari, V., Manninen, A. J., O'Connor, E. J., Schween, J. H., van Zyl, P. G. and E. Marinou (2019). A novel post-processing algorithm for Halo Doppler lidars, *Atmos. Meas. Tech.* **12**(2), 839–852, doi:10.5194/amt-12-839-2019.

Zaidan, M.A.; Dada, L.; Alghamdi, M.A.; Al-Jeelani, H.; Lihavainen, H.; Hyvärinen, A., and T. Hussein (2019). Mutual Information Input Selector and Probabilistic Machine Learning Utilisation for Air Pollution Proxies. *Appl. Sci.* **9**, 4475.

AEROSOL SCIENCE AND TECHNOLOGY GROUP ABSTRACT

J. KANGASLUOMA, L. AHONEN, R. BAALBAKI, R. CAI, T. CHAN, L. DADA, J. ENROTH, J. HAATAJA, S. HOLM, E. HÄKKINEN, F. KESHAVARZ, M. LAMPIMÄKI, T. LAURILA, A. SKYTTÄ, D. STOLZENBURG, A. TOROPAINEN, Y. WU, P. AALTO, M. PASSANANTI, H. VEHKAMÄKI, T. PETÄJÄ

Institute for Atmospheric and Earth System Research / Physics, Faculty of Science, University of Helsinki, Finland

Keywords: heterogeneous nucleation, particle counter, differential mobility analyser, charging, particle size distribution

INTRODUCTION

Early 2019 a new group focusing on aerosol instrumentation and laboratory experimentation was established to INAR Helsinki lead by Juha Kangasluoma. The specific scientific topics of the group are currently aerosol charging, cluster mobility-mass measurements, heterogeneous nucleation, inversion procedures and general instrumental theory and measurement accuracy. This abstract collects the work by the group members from the past year.

PUBLISHED RESULTS ON 2018-2019 AND FUTURE WORK

Second half of the results from a prototype CPC workshop organized in Helsinki on 2017 were published by Enroth et al. (2018), who outlined the methods for comparable and reproducible CPC response time measurements and measured the response of the common commercial CPCs. Fast switching valve is the recommended method for the response time determination, and sheathed CPCs in general have the best response times. Another CPC workshop was organized in 2019 in Helsinki. The purpose of this workshop was focus on sub-10 nm particle size distribution measurements with several different techniques, e.g. PSM, sub-10 nm DMPS, CPC battery and temperature scanning water CPC. The workshop included laboratory measurements for one week, and another month of atmospheric measurements.

The PSM data inversion has been a challenge as long as the PSM has existed. Cai et al. (2018b) began tackling the problem with laboratory measurements and use of four different inversion methods. The size distributions inverted by the PSM were compared to a DMA-electrometer combination, and were in general in good agreement. Such laboratory data is missing the random noise and variation in the raw data, and this work is currently continued with analysis of atmospheric data using the four inversion methods.

Use of DMPS to the measurements of sub-10 nm particles has increased recently, and the accuracy of the measurements is still an open problem. Our group reports five advances in this front. Cai et al. (2018a) characterized the half-mini type DMA at low flow rates, i.e. in typical conditions at which it is operated as part of a DMPS system. Kangasluoma et al. (2018) constructed a DMPS optimized for sub-10 nm size distribution measurements, calibrated it and operated it in Hyytiälä. Cai et al. (2019) outlined the general parameters for characterizing and affecting any DMPS aimed at sub-10 nm size distribution measurements. Fu et al. (2019) outlined the general principles for designing a core sampling system that minimizes the sampling losses of the smallest particles. Last, Kangasluoma and Attoui (2019) reviewed the recent developments in sub-3 nm CPCs and their calibration methods. Future contributions from our group related to instrument development are building of a diluter that minimizes the particle losses during the dilution. With the current design, the losses are equivalent to a short capillary that can be theoretically predicted. We are characterizing a new high flow ultrafine CPC that increases the counting statistics in a DMPS system, and decreases counting uncertainties especially in the sub-10 nm size range. We are collecting a review type

paper for the sub-10 nm size distribution measurements that sets the stage for the future developments in this topic. Aerosol charging was identified as one of the major sources of uncertainty in the DMPS measurements, and our group has initiated experimental and theoretical efforts to understand and manipulate the particle charged fractions in aerosol chargers. Our group was involved in creating a standardized protocol for the measurement of particle formation and growth in chamber measurements. In addition, we are involved in a project aiming for creation of new type of particle filters from nanocellulose, which we demonstrated to be a suitable filtration material. Last, we are building a miniaturized CPC and its optics with the focus of extended unattended operation. Such CPC is aimed first at dense urban networks, and later on vertical atmospheric profiling with drones.

On heterogeneous nucleation research, we have three efforts ongoing. We are experimentally and theoretically examining what are the mechanisms affecting the observed preference to a certain charge state of the seed in a system of ionic liquids and diethylene glycol. This study also reveals if the PSM is suitable reactor for fundamental nucleation studies. Secondly, we are studying the applicability of the computational methods to reproduce experimental results from a nucleating NaCl-butanol-water system. Last, we are experimentally and theoretically quantifying binary water-diethylene nucleation inside the PSM.

To extend our capabilities in cluster characterizations, we are building and improving a DMA-MS system for the measurement of mass and mobility distributions. Earlier version of the current system was already utilized by Passananti et al. (2019), who demonstrated its suitability for cluster fragmentation analysis. Currently we study the suitability of the instrument for the analysis of oxidation products of VOCs and the potential of inferring structural information from them, and potential use for the characterization of nanoplastics. Our group also took the first steps in probing the potential particle phase reactions that the oxidized organics may undergo with the analysis of gas-phase products evaporated from particles made of oxidized organics.

Our group is heavily involved in the measurements established in BUCT in the beginning of 2018, contributing to the instrumentation and analysis of sub-10 nm particle dynamics (Zhou et al. 2019).

ACKNOWLEDGEMENTS

This work was supported by UHEL Faculty of Science support grant (75284140) and 3-year grant (75284132), and Finnish Academy of Science project (1325656)

REFERENCES

- Cai, R., Attoui, M., Jiang, J., Korhonen, F., Hao, J., Petäjä, T., Kangasluoma, J. (2018a). Characterization of a high-resolution supercritical differential mobility analyzer at reduced flow rates. *Aerosol Sci Tech* 52:1332-1343.
- Cai, R., Mirme, S., Jiang, J., Kangasluoma, J. (2019). Parameters to determine the optimum performance of electrical mobility spectrometers for measurement of particle size distributions down to the cluster size. *J Aerosol Sci* 127:102-115.
- Cai, R., Yang, D., Ahonen, L. R., Shi, L., Korhonen, F., Petäjä, T., Zheng, J., Kangasluoma, J., Jiang, J. (2018b). Data inversion methods to determine sub-3 nm aerosol size distributions using the Particle Size Magnifier. *Atmos Meas Tech* 11:4477-4491.
- Enroth, J., Kangasluoma, J., Korhonen, F., Hering, S., Picard, D., Lewis, G., Attoui, M., Petaja, T. (2018). On the time response determination of condensation particle counters. *Aerosol Sci Tech* 52:778-787.
- Fu, Y., Xue, M., Cai, R., Kangasluoma, J., Jiang, J. (2019). Theoretical and experimental analysis of the core sampling method: reducing diffusional losses in aerosol sampling line. *Aerosol Sci Tech* 53:793-801.

Kangasluoma, J., Ahonen, L. R., Laurila, T., Cai, R., Enroth, J., Mazon, S., Korhonen, F., Aalto, P., Kulmala, M., Attoui, M., Petäjä, T. (2018). Laboratory verification of a new high flow differential mobility particle sizer, and field measurements in Hyytiälä. *J Aerosol Sci* 124:1-9.

Kangasluoma, J. and Attoui, M. (2019). Review of sub-3 nm condensation particle counters, calibrations, and cluster generation methods. *Aerosol Sci Tech* 53:1277-1310.

Passananti, M., Zapadinsky, E., Zanca, T., Kangasluoma, J., Mylly, N., Rissanen, M. P., Kurten, T., Ehn, M., Attoui, M., Vehkamäki, H. (2019). How well can we predict cluster fragmentation inside a mass spectrometer? *Chem Commun* 55:5946-5949.

Zhou, Y., Dada, L., Liu, Y., Fu, Y., Kangasluoma, J., Chan, T., Yan, C., Chu, B., Daellenbach, K. R., Bianchi, F., Kokkonen, T., Liu, Y., Kujansuu, J., Kerminen, V. M., Petäjä, T., Wang, L., Jiang, J., Kulmala, M. (2019). Variation of size-segregated particle number concentrations in winter Beijing. *Atmospheric Chemistry and Physics Discussions*.

RESEARCH ACTIVITIES OF THE ATMOSPHERIC MODELING GROUP AT THE ATMOSPHERIC RESEARCH CENTRE OF EASTERN FINLAND

HARRI KOKKOLA¹, EEMELI HOLOPAINEN¹, INNOCENT KUDZOTSA¹, THOMAS KÜHN^{1,2},
ANTON LAAKSO¹, TERO MIELONEN¹, JUHA TONTTILA¹, ANTTI RUUSKANEN¹

¹Atmospheric Research Centre of Eastern Finland, Atmospheric Modelling Group,
P.O.Box 1627, Finnish Meteorological Institute, Kuopio, Finland.

²University of Eastern Finland, P.O.Box 1627, Finland

Keywords: AEROSOL, CLOUD, CLIMATE, MODELLING

INTRODUCTION

The Atmospheric Modelling group at the Atmospheric Research Centre of Eastern Finland does research on atmospheric composition, particularly atmospheric aerosol particles, and their effects on climate, health, and air quality. The main modelling tool in the group has been the sectional aerosol-cloud module SALSA which has been implemented in process scale (Pichelstorfer *et al.*, 2018), cloud scale (Ruuskanen *et al.*, 2019; Tonttila *et al.*, 2019) local/regional scale (Kurppa *et al.*, 2019), and global scale (Saponaro *et al.*, 2019).

METHODS

In cloud scale, we use the Large Eddy Simulations (LES) model UCLALES-SALSA which consists of the LES model UCLALES that simulates the dynamics of the boundary layer and the aerosol-cloud model SALSA which simulates the aerosol and cloud microphysics. In the UCLALES-SALSA model the aerosol properties are tracked through cloud processing from cloud droplet activation to precipitation formation and ice nucleation to melting and evaporation. It is a sectional model that includes separate size sections for interstitial aerosol, cloud droplets, precipitation droplets, and ice crystals. The model has been used to improve our understanding on aerosol-cloud interactions, especially aerosol effect on ice formation in clouds and the effect of aerosol on precipitation formation.

In global scale we have been using the ECHAM-HAMMOZ framework where SALSA has been implemented as an optional aerosol module (Kokkola *et al.*, 2018) alongside the modal scheme M7 (Tegen *et al.*, 2019). It solves the emissions, formation, transport, evolution, and removal of aerosol in the atmosphere and has been coupled to the radiation, and cloud formation in liquid, mixed, and ice phase clouds allowing for studying the aerosol direct and indirect effects. As our research within the Center of Excellence revolves around the effects of biogenic aerosol on climate, we have developed a detailed scheme for secondary organic aerosol formation, using the Volatility Basis Set scheme.

RESEARCH TOPICS

Icing is an atmospheric process where ice accumulates on surfaces. While several different icing processes exist, the most interesting related to atmospheric aerosol studies is in-cloud icing. This process can be caused either by liquid rain drops or cloud droplets freezing on impact with a surface.

Icing can cause damage to structures or financial losses. For example, wind energy power plants might have unplanned shutdown when large amounts of ice is accumulated on wind turbines. Flights might also get delayed/cancelled when weather conditions are such that favour icing on airplane surfaces. With well-structured forecasting models such unplanned events could be avoided.

The size distribution of the cloud and rain droplets have a significant effect on the icing efficiency of clouds. In addition, atmospheric aerosol have an influence on the size distribution of these hydrometeors as they influence the formation process of cloud droplets. We have investigated how much can aerosol concentrations affect the icing efficiency of clouds. Current forecasting models typically have simplified representation of droplets due to the lack of reliable measurement data for verifying the models. However, with the large eddy simulations model UCLALES-SALSA we can investigate in the aerosol effect on icing properties of clouds, in detail (Ruuskanen *et al.*, 2019).

Weather modification, particularly rain enhancement via cloud seeding by aerosol, is an increasingly active field of research due to the need to improve water security in many regions across the globe. Water shortage is a major challenge in arid regions and the problem in general is expected to get worse, given the present consumption rate and the effects of climate warming. UCLALES-SALSA is very well suited to study the effects of cloud seeding, because its design emphasizes the tracking of the features of the aerosol size distribution in both the activated and non-activated particle regimes. We have used our model to investigate the effects of hygroscopic seeding on warm marine stratocumulus clouds and convective mixed-phase clouds. Our model experiments suggest, that the effect of hygroscopic seeding via the warm precipitation process can be seen in our model experiments, but it is very weak. On the other hand, in suitable conditions, hygroscopic seeding above the melting layer may significantly increase the rime fraction of the total ice mass which in turn has the potential to produce at least an increase in the surface precipitation (Tonttila *et al.*, 2019).

In addition to weather modification by emitting aerosol to clouds, it has been suggested that aerosols can be used for counteracting climate warming by greenhouse gases. Such methods are, cirrus and low-level mixed-phase cloud seeding which focus especially over the Arctic region. These methods aim at altering the micro- and macro-physical properties of Arctic clouds so that they become more transparent to long-wave radiation emitted by the Earth's surface thus cooling the surface. Cooling over the Arctic would be beneficial as the rate of climate warming has been observed and forecasted to be fastest near the poles and hence immediate attention is warranted. In an ongoing project, we have used UCLALES-SALSA to investigate the efficacy of seeding both the cirrus and low-level mixed-phase clouds in the Arctic in an effort to reduce their lifetimes, spatial extent and optical thicknesses. We will make the first physically based estimates on the radiative forcing that can be achieved from seeding Arctic clouds (Kudzotsa *et al.*, 201).

Black Carbon (BC) affects the atmospheric radiation budget in several ways. While suspended in the air, BC absorbs incident solar radiation and thereby warms the surrounding air locally. The warming efficacy of BC is increased above strongly reflecting surfaces like snow and ice, while scattering aerosols are most effective above dark surfaces. After its deposition on ice or snow, BC continues to absorb radiation, thereby accelerating snowmelt. We have use the aerosol-climate model ECHAM-HAMMOZ (ECHAM6.3-HAM2.3-MOZ1.0) with the aerosol microphysics module SALSA to simulate the near-future impact of BC mitigation strategies on Arctic climate. Using specially generated aerosol emission scenarios, which are based on the ECLIPSE emission inventories. Our simulations indicate that the direct radiative forcing induces cooling and scales fairly well with the total global amount of BC emission strength reduction, but the aerosol indirect effects counter-act this cooling (Kühn *et al.*, 2019). One aspect affecting the transport of BC to the Arctic is the wet removal process which effectively affects the vertical profiles and the concentration of BC over the Arctic. To improve the estimates of BC climate forging, especially over the Arctic, we have developed a new wet deposition scheme for sectional aerosol models which was tested in the framework of ECHAM-HAMMOZ (Holopainen *et al.*, 2019)

In addition to anthropogenic aerosol, natural aerosol play a significant part in the global radiative balance and climate change as they set the base level of aerosol concentrations which can be perturbed by anthropogenic emissions. We have investigated the effect of increasing temperatures on the aerosol-cloud interaction, and estimated the significance of the plausible negative feedback in a warming climate. More specifically, we studied the causes of the positive correlation between aerosol properties, temperature and cloud properties over southern Finland where biogenic emissions are a significant source of atmospheric particles. This was achieved by comparing the temperature dependence of organic aerosol (OA) to satellite-

based observations to investigate the influence of changes in OA to cloud properties. Our results indicate that over southern Finland, biogenic emissions and the following biogenic aerosol optical depth increase as temperature increases. Over southern Finland, cloud effective radii decrease as temperature increases but the decrease is mainly caused by changes in synoptic meteorology and decrease in cloud top height.

ACKNOWLEDGEMENTS

Our work was funded by the ESA Living Planet Fellowship (ESA contract No. 4000112802/14/I-SBo), the Academy of Finland Centre of Excellence in Atmospheric Science (272041) and Academy Research Fellowship (250348, 256208) and Academy projects (287440, 308292, 283031, 309127, 285068), ERC Consolidator Grant ECLAIR (646857), the Nordic Center of Excellence eSTICC (sScience Tool for Investigating Climate Change in northern high latitudes) funded by Nordforsk (grant 57001), The Tiina and Antti Herlin (TAH) Foundation (project no. 20190133), Fortum Foundation (201800249), and the National Center of Meteorology, Abu Dhabi, UAE under the UAE Research Program for Rain Enhancement Science.

REFERENCES

- Holopainen E. (2019). On the effect of the wet deposition scheme on the simulated aerosol life-cycle in a global climate model, Master's Thesis, Aerosol physics research group, University of Eastern Finland, Department of Applied Physics, February 20, 2019
- Kokkola, H., Kühn, T., Laakso, A., Bergman, T., Lehtinen, K.E.J., Mielonen, T., Arola, A., Stadtler, S., Korhonen, H., Ferrachat, S., Lohmann, U., Neubauer, D., Tegen, I., Siegenthaler-Le Drian, C., Schultz, M.G., Bey, I., Stier, P., Daskalakis, N., Heald, C.L., and Romakkaniemi, S., SALSA2.0 (2019) The sectional aerosol module of the aerosol-chemistry-climate model ECHAM6.3.0-HAM2.3-MOZ1.0, *Geosci. Model Dev.*, 11, 3833-3863, <https://doi.org/10.5194/gmd-11-3833-2018>
- Kudzotsa, I., Kokkola, H., Tonttila, J., Romakkaniemi, S., Rapid reversal of global warming through Arctic cloud seeding, in Proceedings of 'the Center of Excellence in Atmospheric Sciences (CoE ATM) -From Molecular and Biological Processes to the Global Climate' Annual Meeting 2019.
- Kurppa, M., Hellsten, A., Roldin, P., Kokkola, H., Tonttila, J., Auvinen, M., Kent, C., Kumar, P., Maronga, B., and Järvi, L. (2019). Implementation of the sectional aerosol module SALSA2.0 into the PALM model system 6.0: model development and first evaluation, *Geosci. Model Dev.*, 12, 1403-1422, <https://doi.org/10.5194/gmd-12-1403-2019>
- Kühn, T., Kupiainen, K., Miinalainen, T., Kokkola, H., Paunu, V.-V., Laakso, A., Tonttila, J., van Dingenen, R., Kulovesi, K., Karvosenoja, N., and Lehtinen, K.E.J. (2019) Climatic impacts of black carbon mitigation in the Arctic, in Proceedings of 'the Center of Excellence in Atmospheric Sciences (CoE ATM) -From Molecular and Biological Processes to the Global Climate' Annual Meeting 2019.
- Mielonen, T., Yli-Juuti, T., Virtanen, A., Hienola, A., Kühn, T., Merikanto, J., Lipponen, A., Laakso, A., Bergman, T., Korhonen, H., Kolmonen, P., Sogacheva, L., Pitkänen, M.R.A., Arola, A., de Leeuw, F.R., Kokkola, H., Climatic significance of biogenic aerosols in warming boreal forests, in Proceedings of 'the Center of Excellence in Atmospheric Sciences (CoE ATM) -From Molecular and Biological Processes to the Global Climate' Annual Meeting 2019.
- Pichelstorfer, L., Stolzenburg, D., Ortega, J., Karl, T., Kokkola, H., Laakso, A., Lehtinen, K. E. J., Smith, J. N., McMurry, P. H., and Winkler, P. M. (2018). Resolving nanoparticle growth mechanisms from size- and time-dependent growth rate analysis, *Atmos. Chem. Phys.*, 18, 1307-1323, <https://doi.org/10.5194/acp-18-1307-2018>
- Ruuskanen, A., Leskinen, A., Kokkola, H., Komppula, M., and Romakkaniemi, S. (2019). The effect of atmospheric aerosol particles on cloud icing rate, in Proceedings of 'the Center of Excellence in Atmospheric Sciences (CoE ATM) -From Molecular and Biological Processes to the Global Climate' Annual Meeting 2019.
- Tegen, I., Neubauer, D., Ferrachat, S., Siegenthaler-Le Drian, C., Bey, I., Schutgens, N., Stier, P., Watson-Parris, D., Stanelle, T., Schmidt, H., Rast, S., Kokkola, H., Schultz, M., Schroeder, S., Daskalakis, N., Barthel, S., Heinold, B., and Lohmann, U. (2019) The global aerosol-climate model

ECHAM6.3–HAM2.3 – Part 1: Aerosol evaluation, *Geosci. Model Dev.*, 12, 1643-1677, <https://doi.org/10.5194/gmd-12-1643-2019>, 2019.

- Tonttila, J., Kokkola, H., Afzalifar, A., Korhonen H., Romakkaniemi, S. (2019) Modelling precipitation enhancement via hygroscopic seeding in warm and mixed-phase clouds using UCLALES-SALSA, in Proceedings of 'the Center of Excellence in Atmospheric Sciences (CoE ATM) -From Molecular and Biological Processes to the Global Climate' Annual Meeting 2019.
- Saponaro, G., Sporre, M. K., Neubauer, D., Kokkola, H., Kolmonen, P., Sogacheva, L., Arola, A., de Leeuw, G., Karset, I. H. H., Laaksonen, A., and Lohmann, U. (2019). Evaluation of aerosol and cloud properties in three climate models using MODIS observations and its corresponding COSP simulator, and their application in aerosol-cloud interaction, *Atmos. Chem. Phys. Discuss.*, <https://doi.org/10.5194/acp-2019-631>, in review.

SUMMARY ON THE ACTIVITIES OF THE ATMOSPHERIC AEROSOLS AND IONS GROUP DURING YEAR 2018-2019

J. KONTKANEN, P. AALTO, R. BAALBAKI, Z. BRASSEUR, J. DUPLISSY, T. JOKINEN, J. LAMPILAHTI, M. LAMPIMÄKI, K. LEINO, K. LUOMA, M. OKULJAR, B. RÖRUP, J. SULO, D. WIMMER, Y. WU and K. LEHTIPALO

Institute for Atmospheric and Earth System Research / Physics, Faculty of Science, University of Helsinki, Helsinki, Finland

Keywords: AEROSOL PARTICLES, NEW PARTICLE FORMATION, ICE NUCLEATION

INTRODUCTION

Atmospheric aerosols and ions group (AIGG) is a research group at the Institute for Atmospheric and Earth System Research (INAR) of the University of Helsinki focusing on measurements of atmospheric aerosol particles. AIGG performs measurements of physical properties of aerosol particles in different environments, including both long-term monitoring and shorter-term intensive campaigns. In addition, AIGG performs laboratory experiments to investigate different aerosol processes in a well-controlled environment and to perform instrumental development. The main aim of the group is to improve our understanding of atmospheric aerosol processes, including new particle formation (NPF), cloud droplet formation, ice nucleation and aerosol-radiation interactions. This knowledge can help to reduce the uncertainties related to the climate effects of atmospheric aerosol particles. The following abstract introduces the latest progress of AIGG in atmospheric and laboratory experiments.

ATMOSPHERIC MEASUREMENTS

During 2018-2019 AIGG contributed to long-term field measurements at stations belonging to SMEAR (Station for Measuring Ecosystem-Atmosphere Relations) network and participated in intensive campaigns in several locations around the world.

One of the main focuses of AIGG was studying the first steps of atmospheric NPF in different environments. Sulo et al. (abstract in the collection) analyzed almost 4 years of data on size distribution of sub-3 nm nanoparticles measured with a Particle Size Magnifier (PSM) at the SMEAR II station in Hyytiälä, continuing the earlier work of Kontkanen et al. (2017). They compared nanoparticle concentrations to measurements of precursor gas concentrations with a Chemical Ionization Atmospheric Pressure interface Time of Flight Mass Spectrometer (CI-APi-TOF) and found that the concentration highly oxidized organic molecule (HOM) dimers correlated strongest with the nanoparticle concentrations. Furthermore, Jokinen et al. (abstract in the collection) deployed for the first time a PSM, a CI-APi-TOF, and a Neutral cluster and Air Ion Spectrometer (NAIS) at the SMEAR I station in Värriö, Eastern Lapland for studying the concentrations of nanoparticles and precursor gases in clean Arctic air masses. On the other hand, Okuljar et al. (abstract in the collection) analyzed PSM, NAIS and CI-APi-TOF measurements from an urban environment at the SMEAR III station in Helsinki. They compared the long-term measurements at SMEAR III to measurements performed at a nearby street canyon during an intensive campaign in spring 2018, and found that traffic produces a significant number of sub-3 nm particles at the both sites. Long-term measurements of aerosols and trace gases were also started at Qvidja farm in southwestern Finland and Tomsk in Siberia.

In addition to long-term measurements, NPF was studied during intensive measurements campaigns in different environments around the world. Jokinen et al. (2018) performed measurements with a PSM, a NAIS, and a CI-APi-TOF in Aboa, Antarctica, and found that nucleation is explained by ion-induced nucleation of sulfuric acid and ammonia. Baalbaki et al. (abstract in the collection) studied NPF using the

same instruments in a very different environment, at Cyprus. They found that NPF is frequent at the site (~60% of the days) but further data analysis is still needed to resolve the NPF mechanism. Wimmer et al. (2018) published the first observations of NPF at the Amazon region: they observed eight NPF events at the pasture site during the wet season. Furthermore, to get more insights into vertical and horizontal extent of NPF, Lampilahti et al. (abstract in the collection) and Leino et al. (2019) performed particle size distribution measurements at different altitudes in the vicinity of the SMEAR II station using a Cessna aircraft. They presented the first vertical profile of sub-3nm particles. They observed NPF occurring inside the boundary layer, but they also found freshly formed particles in a layer between the residual layer and the free troposphere. Further aircraft measurements were performed in Lapland in summer 2019.

Other main research focuses of AIGG were aerosol-radiation interactions and ice nucleation. Luoma et al. (2019) analyzed 10-years of data on aerosol optical properties at SMEAR II and found statistically significant trends for the PM₁₀ scattering and absorption coefficients, single-scattering albedo, and backscatter fraction. The trends indicate that the scattering efficiency of aerosol particles has increased during the last decade at SMEAR II. Brasseur et al. (abstract in the collection) studied ice nucleation at SMEAR II by collecting filter samples at different heights (at the ground level, at 35 m high tower and in the free troposphere using flight measurements) during spring 2018 and analyzed them with an INSEKT (Ice Nucleation Spectrometer of the Karlsruhe Institute of Technology). They did not observe a difference between ice nucleating particle (INP) concentrations measured at the ground level and at 35 m. However, in the free troposphere, INP concentrations were clearly lower than in the boundary layer. Wu et al (abstract in the collection) also investigated the concentration of INP at SMEAR II during spring 2018 but they used a second-generation Portable Ice Nucleation Chamber (PINCii) to count INPs. They found that INP concentration correlates with aerosol particle surface area concentration and that high INP concentrations are connected with regional-scale transport.

LABORATORY EXPERIMENTS

The laboratory work of AIGG included instrumental development and testing as well as participating in measurements performed at the CLOUD (Cosmics Leaving OUtdoor Droplets) facility at CERN. Measurements in the CLOUD chamber allow for studying NPF mechanisms in highly-controlled conditions. Lehtipalo et al. (2019) studied multicomponent nucleation involving HOMs, sulfuric acid and ammonia and were able to reproduce particle formation observed in daytime in boreal forests from the combination of these vapors. Stolzenburg et al. (2018) on the other hand studied particle growth in the CLOUD chamber in the presence of organic compounds. They found that that slower autoxidation rate of organic compounds at lower temperature is compensated by their reduced volatility. In addition to studying NPF mechanisms, measurements in the CLOUD chamber can also be used for instrumental verification purposes. Rörup et al. (abstract in the collection) studied the composition dependency of the cut-off size of the PSM in the CLOUD chamber, continuing the previous work by Kangasluoma et al. (2016). They found that while the cut-off size of the PSM agrees well with the NAIS in pure inorganic systems, in organic systems the cut-off size of the PSM is shifted to larger sizes. Lampimäki et al. (abstract in the collection) studied the filtration efficiency of cellulose based nanofibers (CNF) using Condensation Particle Counters (CPCs). They observed that CNF filters perform well for particles between 10 and 500 nm.

CONCLUSIONS

During the last year AIGG has participated in laboratory experiments and long- and short-term field measurements in different environments. The main focus of the research has been studying atmospheric NPF using instruments capable of measuring freshly-formed nanoparticles and their precursor gases. In addition, AIGG has investigated aerosol-cloud-radiation interactions using field measurements at SMEAR II. During 2018-2019 our group was very active also in ice nucleation studies, which is a totally new research area for the group. AIGG has also contributed to instrumental development and testing. Current and future efforts of AIGG include participating in large measurement campaigns, such as MOSAiC expedition and

CLOUD14 campaign, while at the same time continuing to take care of and improve our long-term field measurements.

ACKNOWLEDGEMENTS

The work is supported by Academy of Finland Centre of Excellence project (grant no. 307331).

REFERENCES

- Jokinen, T., Sipilä, M., Kontkanen, J., Vakkari, V., Tisler, P., Duplissy, E. M., ... Kulmala, M. (2018). Ion-induced sulfuric acid–ammonia nucleation drives particle formation in coastal Antarctica, *Science advances*, **4**, 11, eaat9744.
- Kangasluoma, J., Samodurov, A., Attoui, M., Franchin, A., Junninen, H., Korhonen, F., Kurtén, T., Vehkamäki, H., Sipilä, M., Lehtipalo, K., Worsnop, D. R., Petäjä, T., and Kulmala, M. (2016). Heterogeneous nucleation onto ions and neutralized ions: insights into sign-preference, *J. Phys. Chem. C*, **120**, 13, 7444–7450.
- Kontkanen, J., Lehtipalo, K., Ahonen, L., Kangasluoma, J., Manninen, H. E., Hakala, J., Rose, C., Sellegri, K., Xiao, S., Wang, L., Qi, X. M., Nie, W., Ding, A. J., Yu, H., Lee, S., Kerminen, V. M., Petäjä, T., Kulmala, M. (2017). Measurements of sub-3nm particles using a particle size magnifier in different environments: from clean mountain top to polluted megacities, *Atmos. Chem. Phys.* **17**, 2163 – 2187.
- Lehtipalo, K., Yan, C., Dada, L., Bianchi, F., Xiao, M., Wagner, R., ... Worsnop, D.R. (2018). Multicomponent new particle formation from sulfuric acid, ammonia, and biogenic vapors, *Science advances*, **4**, 12.
- Leino, K., Lampilahti, J., Poutanen, P., Väänänen, R., Manninen, A., ... Kulmala, M. (2019). Vertical profiles of sub-3 nm particles over the boreal forest, *Atmos. Chem. Phys.*, **19**, 4127–4138.
- Luoma, K., Virkkula, A., Aalto, P., Petäjä, T., and Kulmala, M. (2019). Over a 10-year record of aerosol optical properties at SMEAR II, *Atmos. Chem. Phys.*, **19**, 11363–11382.
- Stolzenburg, D., Fischer, L., Vogel, A. L., Heinritzi, M., Schervish, M., Simon, M., ... Winkler, P (2018). Rapid growth of organic aerosol nanoparticles over a wide tropospheric temperature range, *Proceedings of the National Academy of Sciences*, **115**, 37, 9122-9127.
- Wimmer, D., Buenrostro Mazon, S., Manninen, H. E., Kangasluoma, J., Franchin, A., ... Petäjä, T. (2018). Ground-based observation of clusters and nucleation-mode particles in the Amazon, *Atmos. Chem. Phys.*, **18**, 13245–13264.

PRESENT ACTIVITIES OF INAR IN ASIA

J. KUJANSUU¹, T. PETÄJÄ¹, H.K. LAPPALAINEN¹, F. BIANCHI¹, J. KANGASLUOMA¹, C. YAO¹, and M. KULMALA¹

¹INAR, University of Helsinki, Finland.

Keywords: HAZE Beijing, Nanjing, JirLATEST, Guangzhou, Singapore, Japan, South Korea

INTRODUCTION

The rapid, large-scale urbanization and industrialization of Asia, and especially China, are unique in history. For example, China's air pollution situation has worsened dramatically during the last 2–3 decades as emissions from industry, energy production and traffic have increased. Highly non-linear processes, such as atmospheric chemistry and aerosol dynamics, can transform the urban pollution cocktail, Chemical Cocktail (Kulmala 2015), and generate secondary pollution, such as ultrafine particles and ozone. The fact that new particle formation can occur in polluted megacities, such as Beijing, suggests that there are several major physical and chemical mechanisms in a megacity atmosphere that have not been recognized before.

To understand the processes behind the pollution phenomenon in megacities it is crucial to make long-term, continuous and comprehensive observations on aerosol particles, trace gases and atmospheric oxidants (Kulmala *et al.*, 2015). Recent advances in theoretical understanding has made it possible to explain how enhanced pollution decreases atmospheric turbulence and mixing, reducing the boundary layer height and causing further enhancement of pollution levels (Petäjä *et al.*, 2016). These recent advancements, together with local government support, provide platform to clarify the Chemical Cocktail of Asian megacities.

AIMS

By quantifying the processes, interactions and feedbacks within different air pollutants and ambient conditions, SMEAR concept can determine the most efficient steps towards reducing secondary air pollution, and thus clean the megacity air. The main focus should be on secondary pollution like new particle formation (NPF) and gas-to-particle conversion, since NPF can produce 60-80% of aerosol number load in very polluted megacities (see Kulmala *et al.*, 2016b).

Main scientific question that SMEAR concept can answer is:

- **What are the key processes related to gas-to-particle conversion and atmospheric boundary layer (BL) dynamics in megacity environments?**

Answers will provide crucial knowledge to:

- a) why atmospheric new particle formation (NPF) occur in polluted conditions where the ratio between the condensation sink and particle growth rate is approximately 10 times too high in order to be explained with present knowledge.

- b) how are Boundary Layer (BL) dynamics and formation of the chemical cocktail in the BL interacting with each other?
- c) are there new and effective oxidation pathways?
- d) what are the relative role of different compounds, such as inorganics, organosulphates, organonitrates and other organic compounds, in participating atmospheric gas-to-particle conversion (GTP) and NPF?
- e) how is black carbon and other particulate matter affecting the stability of BL?

FUTURE PROSPECTS

SMEAR concept relies on continuous, comprehensive observations of atmospheric composition and fluxes combined with detailed description of meteorology. This research ideology has been proven in SMEAR II (*Station for Measuring Earth system-Atmosphere Relations*, Hyytiälä, Finland). The SMEAR network was extended to the city of Helsinki, Finland, in 2005, when SMEAR III (Järvi et al. 2009) was established to examine the urban environment. Knowledge from both SMEAR II and III are the backbone in SMEAR concept projects in Asia.

INAR has been active in China since 2012 when Nanjing University collaboration started with JirLATEST project station. After successful research activities in Nanjing, Beijing University of Chemical Technology (BUCT) requested our help to understand haze phenomenon in Beijing. BUCT project HAZE Beijing started at 2017 and station was ready at January 2018. First report to Mayor of Beijing has been submitted and the Mayor Chen Jining also visited INAR in Helsinki at early October 2019. INAR has also been active in Shanghai since 2015 with Fudan University, and late 2018 Guangzhou Academy of Sciences contacted INAR to upgrade their existing measurement station network up-to SMEAR concept level. During the summer of 2019 INAR trained first patch of scientist from Guangzhou in SMEAR II station in Hyytiälä. Upgrading of the stations will start at early 2020 from Guangzhou-city and then continue to Nanling forest station, Shenzhen-city, Macao-city and Hong Kong-city stations. Also, Government of Singapore has been interested to understand new second generation air pollutants, caused by VOCs, in visibly clean urban environment. Many new chemical compounds in air are invisible, but do have human health effects. Negotiations are in final stage and project will start at early 2020 together with National University of Singapore. In Japan, Nagoya University contacted INAR at early 2019 and requested help to upgrade their existing Hokkaido-station to SMAR status. First visits have been done and project will start at 2020. Also, INAR has been in contact with newly appointed Environmental Minister of Japan for deeper collaboration that the Government of Finland is supporting. As a final note, Ambassador of South-Korea in Finland have visited INAR at early 2019 and requested INAR's help to understand environmental conditions of Capital city Seoul. This possibility is still in its early stages and nothing concrete has not been decided yet.

The measurements in Asia and in Finland provide a unique basis to diversify the existing aerosol, trace-gas and GHG measurements into different environments which, besides enhancing our scientific understanding, will provide crucial information for regional air quality models, basis for education activities and decision making process in national and local levels. SMEAR concept can also find out long-term changes and trends in Asia. With combined efforts, SMEAR concept is able to connect atmospheric data with surface data and to find out combinations and trends that have not been discovered during earlier research campaigns in Asia.

ACKNOWLEDGEMENTS

Financial support of the BUCT project come from Beijing Municipality Government Fund. Financial support for the JirLATEST comes from Jiangsu Province Government Fund. Financial support of the Guangzhou project comes from the Guangdong Province Government Fund. Financial support for the Nagoya University project comes from the Government of Japan International Collaboration Fund.

REFERENCES

- Hari P. et al. (2016) Conceptual design of a measurement network of the global change. *Atmos. Chem. Phys.*, **16**, 1017–1028.
- Huang R.-J. et al. (2014) High secondary aerosol contribution to particulate pollution during haze events in China. *Nature*, **514**, 218–221.
- Järvi L. et al. (2009). The urban measurement station SMEAR III: Continuous monitoring of air pollution and surface-atmosphere interactions in Helsinki, Finland. *Boreal Environmental Research* 14 (Suppl. A), 86-109
- Kulmala M. (2015) China's choking cocktail. *Nature*, **526**, 497–499.
- Kulmala M. et al. (2016a) On secondary new particle formation in China. *Front. Environ. Sci. Eng.*, **10**, doi:10.1007/s11783-016-0850-1.
- Kulmala M. et al. (2016b) On the mode-segregated aerosol particle number concentration load: contributions of primary and secondary particles in Hyytiälä and Nanjing. *Boreal Env. Res.*, **21**, 319–331.
- Petäjä T. et al. (2016b) Enhanced air pollution via aerosol boundary layer feedback in China. *Sci. Rep.*, **6**, 18998.

VERIFYING THE POTENTIAL OF CLIMATIC-FRIENDLY AGRICULTURE IN FINLAND

L. KULMALA^{1,2}, A. LOHILA^{1,3}, T. AALTO¹, T. LAURILA¹, J. HEINONSALO^{1,2}, T. VISKARI¹, I. FER¹, O. NEVALAINEN¹, L. HEIMSCH¹, H. VEKURI¹, J. MÄKELÄ¹, M. AURELA¹, J. LISKI¹

¹ Finnish Meteorological Institute, Helsinki, Finland.

² Institute for Atmospheric and Earth System Research / Forest Sciences, Faculty of Agriculture and Forestry, University of Helsinki, Finland.

³ Institute for Atmospheric and Earth System Research / Physics, Faculty of Science, University of Helsinki, Finland.

Keywords: CARBON CYCLE, EDDY COVARIANCE, REMOTE SENSING, YASSO, PECAN

INTRODUCTION

The targets of the Paris climate agreement cannot be reached by cutting greenhouse gas emission (GHG) alone but also effective ways to remove carbon dioxide (CO₂) from the atmosphere are critically needed (Millar et al. 2017, Minasny et al. 2017). Today, agricultural soils are in general sources of carbon, intensively managed and cover notable areas. Nevertheless, changes in management practices can turn these soils into sinks of atmospheric CO₂ (Paustian et al. 2016). These so-called climate-smart or climate-friendly agricultural practices have high potential for storing the carbon into soil (Paustian et al. 2016). This potential has also been widely recognized among decision makers.

The most important methods to increase soil carbon sequestration in agricultural lands include 1) soil amendments (such as manure, biochar and compost), 2) careful selection of crops (such as deep rooted plants, perennial species, cover crops), 3) high biodiversity of flora, fauna and other forms of life, 4) nutrient management and liming in unproductive agricultural lands, 5) rotational and no-tilling farming, 6) agroforestry, and 7) improved grazing. Even if the benefits of these practices are widely known, they are not commonly applied yet in Nordic countries due to lack of incentives and research in local climate.

In addition to climate change mitigation, a growing soil carbon content provides other benefits: It improves soil resilience, yield and other ecosystem services since it enhances the soil structure (Bronick and Lal 2004), increases the water retention (Rawls et al. 2003), and decreases the need for fertilization (Pan et al. 2009). Nevertheless, the agricultural practices sequestering carbon into soil may have also other climatic impacts. They change soil moisture, temperature and the quality and quantity of organic matter, which affect microbial activity possibly enhancing the production of nitrous oxide (N₂O) and methane (CH₄). To ensure that the overall effect is still favourable, it is important to estimate the net climatic effect.

The effects of different practices are varying because agricultural lands are dissimilar in terms of age, cultivation history, soil properties and climate. While it is not possible to use the laborious and instrument-intensive GHG exchange and soil measurements on all fields, it is necessary to develop a general and inexpensive yet reliable method to estimate the climatic impacts of the practices for policies, carbon markets and product footprints. Insufficient verification methodologies are currently a major barrier to investing in climate-smart farming practices (Vermeulen et al. 2019). Thus, our aim is to develop a verification methodology of cultivation taking into account the specific features of the Nordic agriculture.

METHODS

FMI currently measures the greenhouse gas fluxes at four agricultural sites in Finland (Fig 1). Eddy covariance measures net ecosystem CO₂ exchange at Qvidja farm in Parainen, Southern Finland, and at Ruukki in Siikajoki, Central Finland. In addition, manual chamber measurements are carried out at all

sites. Varying climate-friendly management practices are tested at the sites including increased biodiversity, agroforestry, soil amendments, fertilization type and intensity, and in the case of grasslands, also increased cutting height.

The core of the verifying methodology will be a calculator that describes the stocks (vegetation, soil) and fluxes (photosynthesis, plant and microbial respiration, plant growth, litter production, harvest, leaching) of carbon in agricultural fields according to the Guidelines and Good Practice Guidance of the Intergovernmental Panel on Climate Change (IPCC). Other relevant climate impacts resulting from methane, nitrous oxide and albedo are also accounted for. We build the calculator by combining suitable models for vegetation and the decomposition of soil organic matter, such as Yasso (Tuomi et al. 2011).

The calculator will estimate sequestered carbon units, their longevity and the other climate impacts using input data from ordinary farms (soil and vegetation characteristics, farming practices) as well as weather and remote sensing data. To ensure the reliability of these estimates, we develop a data assimilation method to adjust the calculator to various available soil, vegetation and greenhouse gas flux data from study sites and databases. As a platform for the calculator, we will utilize the Predictive Ecosystem Analyzer (PEcAn) running several ecosystem models.

The methodology will be calibrated using available data from FMI, co-operators and advanced Carbon Action farms (n=40) with varying farming practises including a tailored carbon farming experiment. The calculator is further verified at Carbon Action farms (n=108) spread across Finland.



Figure 1: Agricultural sites accompanied with flux measurements by FMI

EXPECTED RESULTS

The calculator will be used for scientific purposes such as earth system models but the calculated units of sequestered carbon will be also needed in policies, carbon markets and product footprints.

ACKNOWLEDGEMENTS

SITRA, Business Finland, Maj and Tor Nessling foundation, Tiina and Antti Herlin Foundation and Strategic Research Council (SRC) at the Academy of Finland are acknowledged for financial support. We thank the owners of Qvidja farm and Kilpiä farm, staff at FMI and Ruukki research station (Luke) for practical help and Baltic Sea Action Group for the active co-operation with different stakeholders such as farmers.

REFERENCES

- Dietze, M. C. (2017), Prediction in ecology: a first-principles framework. *Ecol Appl*, 27: 2048-2060. doi:10.1002/eap.1589
- Millar RJ et al. (2017) *Nature Geoscience* 10: 741–747. <https://doi.org/10.1038/NGEO3031>
- Minasny B et al (2017) *Geoderma* 292: 59–86. <https://doi.org/10.1016/j.geoderma.2017.01.002>
- Pan G et al. (2009) *Agriculture, Ecosystems & Environment* 129: 344-348 <https://doi.org/10.1016/j.agee.2008.10.008>
- Paustian K et al. (2016) *Nature* 532(7597): 49–57. <https://doi.org/10.1038/nature17174>
- Pihlatie, M et al. (2013). *Agricultural and Forest Meteorology* 171/172: 124–136. <https://doi.org/10.1016/j.agrformet.2012.11.008>
- Rawls WJ et al. (2003) *Geoderma* 116: 61-76. [https://doi.org/10.1016/S0016-7061\(03\)00094-6](https://doi.org/10.1016/S0016-7061(03)00094-6)
- Tuomi M et al. 2011 *Ecological Modelling* 222: 709–718 <https://doi.org/10.1016/j.ecolmodel.2010.10.025>
- Vermeulen et al. (2019) *Nature Sustainability* <https://doi.org/10.1038/s41893-018-0212-z>

“STATION FOR MEASURING EARTH SURFACE – ATMOSPHERE RELATIONS” CONCEPT GlobalSMEAR INITIATIVE

HANNA K. LAPPALAINEN¹, JONI KUJANSUU¹, HEIKKI JUNNINEN², ANTON RUSANEN¹,
NURIA ALTIMIR¹, ALEXANDER MAHURA¹, LEENA JÄRVI¹, FEDERICO BIANCHI¹, JUHA
KANGASLUOMA¹, STEFFEN NOE³, TIMO VIHMA⁴, PTTERI UOTILA¹, JAANA BÄCK¹, TIMO
VESALA¹, TUUKKA PETÄJÄ¹ AND MARKKU KULMALA¹

- 1) Institute for Atmospheric and Earth System Research (INAR)/ Physics, Faculty of Science,
University of Helsinki, 00014 Helsinki, Finland
- 2) University of Tartu, Estonia
- 3) Estonian University of Life Sciences (EULS), Estonia
- 4) Finnish Meteorological Institute, Finland

Key words: climate change, air quality, atmospheric – ecosystem in-situ observations, atmosphere – Earth surface interaction and feedbacks, megacities, the Arctic marine environments

1. INTRODUCTION

The Grand Challenges (GC), like climate change, urban air pollution, clean water and food security, are interlinked, but current observations are fragmented (Kulmala 2015, Kulmala et al. 2015, Kulmala 2018). For the future aspiration we need an integrated approach together with the comprehensive, continuous and coordinated observation system “a Global Earth Observatory to better understand the land - atmosphere interaction and feedbacks lined to GC, to reduce uncertainties, to improve urban air quality and to mitigate and adapt effectively (Kulmala 2018). The “Station for Measuring Earth Surface – Atmosphere Relations”, the GlobalSMEAR, is a bottom-up initiative by the Institute for Atmospheric and Earth System Research (INAR), University of Helsinki (Hari and Kulmala 2005, Hari et al. 2017, Kulmala 2018, www.atm.helsinki.fi/globalsmear). The aim of the GlobalSMEAR is to establish a global in-situ station network based on the SMEAR concept. The global network would consist of the SMEAR flagship stations together the different standard, flux and advanced stations (Hari et al. 2017, Kulmala 2018). The GlobalSMEAR technical model is built on a state-of-the-art in-situ observation methods, instrument technology, data system, comprehensive data analysis methods, a development and design carried out at the Stations Measuring Ecosystem Atmospheric relations (SMEAR II) station in Hyytiälä, Finland starting from 1995. The SMEAR II serves as a prototype for the GlobalSMEAR flagship station and represents the most advanced and comprehensive in-situ station worldwide. Currently the SMEAR II is carrying out standardized observations over 1200 parameters (including concentrations and fluxes) 24/7 on different ecosystems: boreal forest, wetland and lakes and is contributing to several European ESFRIs (ICOS, ACTRIS, AnaEE, eLTER) and Earth Observation systems and networks such as WMO GAW and GEO-GEOSS. Recently we have been focused on the further development of different elements (station network concept, customer journey line, building up new stations, networking and identification of new services and end users) needed for the GlobalSMEAR implementation (Kulmala 2018).

2. CURRENT APPROACH

Architecture of the hierarchic station network and data systems structure

We have formulated an architecture for the hierarchic, integrated in situ station network. As a whole, the global observation network would be based on a hierarchy of research stations, where the flagship stations would operate in a seamless collaboration with the flux stations and standard stations to achieve global and regional coverage (Hari et al. 2017). A station network of 1000 or more well-equipped ground-based stations around the world would be able to track the changes in the environmental conditions in various ecosystems and to continuously provide observational evidence to understand the factors affecting the grand challenges. The proposed approach would complete coverage from ground stations to observations of Earth’s conditions and complete the satellite based information by resolving processes or fluxes, or trace the hundreds more

compounds of interest (Kulmala 2018). In addition, we have just introduced specific observation concept and roadmap, how to improve the marine atmospheric in situ data availability to better understand the most important atm. processes, how to improve the in situ station network to better understand the linkages between the marine Arctic and Eurasian continent and how to improve the observational coverage needed for improved atmospheric and ocean re-analyses (Vihma et al. 2019).

In an operational phase the GlobalSMEAR station network would deliver big data. At the moment the data coming from the University of Helsinki hosted SMEAR stations is collected and filed at the CSC – IT Center For Science Ltd. systems (www.csc.fi/csc) and the open data access is provided by a web interface (avaa.tdata.fi/web/smart). The components contributing to European research infrastructures and to WMO GAW rely on their respective data services. In the future we need to find technical and juridical (IPR, data ownership) solutions on the data collection, filing and on the open data access for the new GlobalSMEAR data. This is work in progress and is part of the ongoing INAR Beijing Haze project.

Service Concept for upgrading of an existing in situ stations and establishing a new station

In 2018 we carried out a Climate-KIC “GlobalSMEAR” project aimed at the GlobalSMEAR upscaling and for the service concept design. In this project we discussed the GlobalSMEAR service concept, markets and marketing, competition advantages and barriers in the international RI landscape and how the well-structured processes would enable us to give a support to the customer / end-user during the process starting from planning and construction until the operation phases of a new station. We introduced a modular service concept for the upgrading of instruments and measurements of an existing station or building a new station. The modules and services are flexible and can be tailored for local requirements, environments (forest, peatland, lake, agriculture land, tundra, maritime coastal line, urban) and for different purposes (climate change monitoring, air quality monitoring, different early warning systems such as fence-line observations for of hazardous volatile pollutants or dispersion of epidemic compounds). The training of the technical experts and education on the data analysis methods were included as fundamental part of the SMEAR service concept.

As a continuation of the Climate-KIC - GlobalSMEAR upscaling project, INAR has submitted a proposal called “Detailed Monitoring to Verify the Future Healthy - Clean Cities and Carbon Neutrality in Urban Environment” with University of Tartu, Estonian University of Life Sciences and Cyprus Institute to ClimateKIC Call on the innovation and demonstration projects focused on healthy, clean cities in Europe. The aim of our proposal is to co-design a SMEAR-European model (C40 cities, carbon neutrality frameworks) and to improve the customer process towards a new operational SMEAR station by using lessons-learned from the current operational SMEAR (benchmarked) stations in Finland, Estonia, Cyprus and in China.

New SMEAR stations and the GlobalSMEAR member network

At the moment we have five SMEAR stations out of which SMEAR I-IV stations operate in Finland and SMEAR-Estonia in Järvelja, Estonia. We also have a SMEAR accredited SORPES (Station for Observing Regional Process of Earth System) station in Nanjing, China. It has been operational since 2010. However, the number of the new and accredited SMEAR stations is increasing. In May 2017 an investment of a value of 10 MEUR was granted to INAR to establish a new station at the Beijing University of Chemical Technology (BUCT; Beijing, China). In collaboration with BUCT we constructed the SMEAR concept station instrumentation and a data system in Beijing. This new “Beijing Haze” station has been operational since January 2018. In Europe, INAR is a partner in an EU Horizon2020 EMME-CARE Teaming project together with the Cyprus Institute (CyI), Max Planck Institute for Chemistry (MPIC) and Commissariat à l’Energie Atomique (CEA). In the frame of the EMME-CARE project we are in progress setting up a new observation site at Peysa site in Cyprus following the SMEAR concept. These new and other SMEAR accredited stations are addressing a need for a coordinated GlobalSMEAR member network. In 2019 we have received the first applications applying the GlobalSMEAR membership. The membership offers collaborative research that aims towards joint publications, annual data workshops and meetings, the development of services and exploring of the business opportunities based on the SMEAR data.

Promoting the SMEAR concept and further networking

Starting from 2012, we have promoted GlobalSMEAR in different international conferences (EGU, ISAR, IASC etc.) and forums (Arctic Circle) and established an extensive contact network, especially, in China and Russia (see also Kujansuu et al. of this proceedings). Our current China contact network covers ca 30 universities and city administrations. The main interest in China market is on urban air quality monitoring including indoor air quality. The Chinese Ecosystem Research Network (CERN) station network for the ecosystem monitoring is part of global eLTER network. CERN / eLTER provides a standardized station network that could be upgraded to the towards SMEAR network by including an atmospheric component to the measurement setups. Our contacts and network in China are also actively involved with the Silk Road Economic Belt Initiative. Silk Road Economic Belt has interest for establishing new environmental observation systems along the Silk Road transport corridors and cities and opens opportunities for the new GlobalSMEAR stations (Lappalainen et al. 2018). The Russia contact network, covering over 30 universities and research organizations, is being built upon the Pan-Eurasian Experiment (PEEX) Programme coordinated by INAR (see also Lappalainen et al. of this proceedings). For example, recently established collaboration with Roshydromet provides potential for upgrading their meteorological station network.

3. FUTURE PROSPECTS

The GlobalSMEAR is mainly based on academic franchising and have different upscaling plans, end-users and end-user interests in Europe, in Eurasia, in Asia, in the Eastern Mediterranean and the Middle East (EMME) region, in Africa and in the Arctic regions. In Europe the main interest is to use advanced monitoring systems and RI on verifying the carbon neutrality and urban air quality, in Asia on the urban air and environmental pollution and in the Arctic context on climate change and teleconnections. In addition the upscaling the GlobalSMEAR in these frameworks, the new openings for the SMEAR station concept are foreseen on mobile phone apps and the use of machine learning techniques. The MegaSense programme by the Univ.Helsinki, started in 2017, is aimed at these directions and gathers and fuses spatially variable gas and particulate measurements from the atmospheric instruments, commercial air quality transmitters, dense low-cost sensor arrays, and consumer wearables utilizing 4G and 5G technologies. The machine learning techniques are used for the calibration of a high number of low-quality and low-cost sensors with a small number of highly accurate SMEAR stations. The credibility of MegaSense concept and potential is huge and is currently emerged through City of Helsinki Air Quality projects Urban Sense, and EU Healthy Outdoor Premises for Everyone UIA HOPE, and through International pilots. The European potential and end users and EU-wide clean and smart cities strategies, are at the moment, indicated by the SMart URban Solutions for air quality, disasters and city growth (SMURBS, 2018-2021, UHEL as a partner).

REFERENCES

- Hari, P. & Kulmala, M. 2005: Station for Measuring Ecosystem–Atmosphere Relations (SMEAR II). *Boreal Env. Res.* 10: 315–322.
- Hari, P., Petäjä, T., Bäck, J., Kerminen, V.-M., Lappalainen, H.K. Vihma, T., Laurila, T., Viisanen, Y., Vesala, T., and Kulmala M., 2016. Conceptual design of a measurement network of the global change, *Atmos. Chem. Phys.*, 16, 1017-1028, doi:10.5194/acp-16-1017-2016.
- Kulmala, M., Lappalainen, H.K., Petäjä, T., Kurten, T., Kerminen, V.-M., Viisanen, Y., Hari, P., Bondur, V., Kasimov, N., Kotlyakov, V., Matvienko, G., Baklanov, A., Guo, H., Ding, A., Hansson, H.-C., and Zilitinkevich, S., 2015. Introduction: The Pan-Eurasian Experiment (PEEX) – multi-disciplinary, multi-scale and multi-component research and capacity building initiative, *Atmos. Chem. Phys.*, 15, 13085-13096, doi:10.5194/acp-15-13085-2015
- Kulmala Markku China’s Chocking Air Coctail, *Nature Comment*, *Nature* 526, 497–499, 2015, doi:10.1038/526497a
- Kulmala, M., Lappalainen, H. K., Petäjä, T., Kurten, T., Kerminen, V.-M., Viisanen, Y., Hari, P., Sorvari, S., Bäck, J., Bondur, V., Kasimov, N., Kotlyakov, V., Matvienko, G., Baklanov, A., Guo, H. D., Ding, A., Hansson, H.-C., and Zilitinkevich, S.: Introduction: The Pan-Eurasian Experiment (PEEX) – multidisciplinary, multiscale and multicomponent research and capacity-building initiative, *Atmos. Chem. Phys.*, 15, 13085–13096, <https://doi.org/10.5194/acp-15-13085-2015>, 2015.

Kulmala Markku Build a global Earth observatory, Nature Comment, Nature 553, 21-23, 2018, doi: 10.1038/d41586-017-08967-y

Lappalainen, H.K., Kulmala, M., Kujansuu, J., Petäjä, T., Mahura, A., de Leeuw, G., Zilitinkevich, S., Juustila, M., Kerminen, V-M., Bornstein, B., Zhang Jiahua, Xue Yong, Qiu Yubao, Liang Dong, Liu Jie & Guo Huadong (2018) The Silk Road agenda of the Pan-Eurasian Experiment (PEEX) program, Big Earth Data, 2:1, 8-35, doi: 10.1080/20964471.2018.1437704.

Pan Eurasian Experiment (PEEX) Science Plan (2016). Editors Lappalainen H.K., Kulmala M. & Zilitinkevich S. http://www.atm.helsinki.fi/peex/images/PEEX_SP_27052015.pdf

Vihma, T., Uotila, P., Sandven, S., Pozdnyakov, D., Makshtas, A., Pelyasov, A., Pirazzini, R., Danielsen, F., Chalov, S., Lappalainen, H. K., Ivanov, V., Frolov, I., Albin, A., Cheng, B., Dobrolyubov, S., Arkhipkin, V., Myslenkov, S., Petäjä, T., and Kulmala, M.: Towards an advanced observation system for the marine Arctic in the framework of the Pan-Eurasian Experiment (PEEX), Atmos. Chem. Phys., 19, 1941–1970, <https://doi.org/10.5194/acp-19-1941-2019>, 2019.

PAN-EURASIAN EXPERIMENT (PEEX) PROGRAMME – ACTIVITIES IN 2019 AND FUTURE PROSPECTS

H.K. LAPPALAINEN^{1,2,5}, T.PETÄJÄ^{1,13}, V-M. KERMINEN¹, A. MAHURA¹, N. ALTIMIR¹, E. EZHOVA¹, R. MAKKONEN^{1,2}, I. BASHMAKOVA¹, J. KUJANSUU¹, A. LAURI¹, S. MAZON¹, A. BORISOVA¹, F. BIANCHI¹, T. LAURILA², J. BÄCK¹, T. VIHMA², P. UOTILA¹, L. SOGACHEVA², G. DE LEEUW², L. HEININEN¹, S. CHALOV³, P. KONSTANTINOV³, N.CHUBAROVA³, O. POPOCHOVA³, M. ARSHINOV⁴, B. BELAN⁴, V. GENNADINIK⁵, Y. QIU⁶, I. EZAU⁷, V. MELNIKOV⁵, G. MATVIENKO⁴, A. DING⁸, A. BAKLANOV⁹, Y.VIISANEN², N. KASIMOV⁵, H. GUO⁶, V. BONDUR¹⁰, S. ZILITINKEVICH^{1,2,5,11}, M. KULMALA^{1,5}

¹⁾ Institute for Atmospheric and Earth System Research (INAR)/ Faculty of Science, Physics, University of Helsinki (UHEL), Helsinki, Finland.

²⁾ Finnish Meteorological Institute (FMI), Helsinki, Finland

³⁾ Moscow State University (MSU), Moscow, Russia

⁴⁾ Institute of Atmospheric Optics, Tomsk 634055, Russia

⁵⁾ University of Tyumen, Russia

⁶⁾ Institute of Remote Sensing and Digital Earth, Chinese Academy of Sciences, Beijing 100101, China

⁷⁾ Nansen Environmental and Remote Sensing Center, NERSC, Norway

⁸⁾ Institute for Climate and Global Change, Research & School of Atmospheric Sciences, Nanjing University, 210023 Nanjing, China

⁹⁾ World Meteorological Organization, 1211 Genève, Switzerland

¹⁰⁾ AEROCOSMOS Research Institute for Aerospace Monitoring, Moscow, Russia

¹¹⁾ Dept. of Radiophysics, Nizhny Novgorod State University, Russia

Keywords climate change, air quality, multidisciplinary approach, multiscale research, grand challenges, arctic-boreal, land-atmosphere interactions, Arctic Ocean, observation networks

1. INTRODUCTION

Pan-Eurasian Experiment (PEEX) Programme (www.atm.helsinki.fi/peex), initiated by the University of Helsinki INAR together with five main partners from Russia and China, is an international, multidisciplinary, multiscale bottom up initiative, established in autumn 2012. PEEX is an asset for INAR and its co-partners to have high international visibility, to attract further research collaboration and to upscale the scientific impact in various arenas. PEEX is built on four main pillars: Research Agenda (RA), Research Infrastructure (RI) development, capacity building activities and societal impact making. The PEEX geographical focus is on the northern high latitudes (Arctic, boreal) and on China and the new Silk Road Economic Belt regions. The PEEX research network is currently covering ca 4000 researchers coming from Europe, Russia and China and over 30 official collaboration agreements with universities and research organizations located mostly in Russia and in China (www.atm.helsinki.fi/peex/index.php/mou). PEEX framework is motivated by the all scales research approach, high quality RI and big data, education and training of the next generation of scientists and experts, participating processes aimed at the fast tract policy making and increasing awareness of the highly connected environmental challenges. All these aspects are needed for solving grand challenges, like climate change and air quality, and ensuring the ecosystem services now and for the future (Kulmala et al. 2015, Kulmala 2015).

2. ACTIVITIES AND RESULTS IN 2019

2.1 Research Agenda

The PEEX scientific focus is on understanding of large-scale feedbacks and interactions between the land - atmosphere - ocean continuum under the changing climate of the Northern high latitudes (Kulmala et al. 2015, Lappalainen et al. 2014; 2015; 2016; 2018) and on the transport and transformation of air pollution in China. The backbone of the research work has been the Finnish Center of Excellence in “Atmospheric Science - From Molecular and Biological processes to the Global Climate”. In addition, PEEX research results have been published the PEEX Special Issue in J. Atmospheric Chemistry and Physics (www.atmos-chem-phys.net/special_issue395.html), in the Journal “Geography, Environment, Sustainability”

(ges.rgo.ru/jour) and in the J. Big Data (journalofbigdata.springeropen.com). In order to coordinate and facilitate the research approach, PEEEX has organized science conferences in Helsinki, St. Petersburg, Moscow and Beijing in years 2012-2018 (for conference proceedings see the Finnish Aerosol Research Report Series www.atm.helsinki.fi/FAAR/index.php?page=series).

In 2019 PEEEX started comprehensive analysis on the first results over last five years based on the published peer review papers and results attained from the PEEEX geographical domain. The aim of the analysis is to study the state-of-the-art research outcome versus the PEEEX large-scale research questions addressed by the Science Plan (Lappalainen et al. 2015). To facilitate the direct input from the research community, we have asked researchers to answer to a form where they could list their main scientific results and activities considered relevant to PEEEX region and also include ancillary information such as type of activity or geographical extend. The preliminary metadata database covers information from over 400 scientific papers and the analysis is in progress. The key gaps of current understanding and future research needs will be discussed from the system point of view, from the land ecosystems, atmosphere, ocean & river systems and society perspectives.

In addition PEEEX coordinates research activities such as bi lateral research collaboration, subprograms and projects together with the partners from Russia and China and from the Europe and Nordic countries.

In Russia, the most important research activities are the Baikal Selenga Network (BaSeNet) (www.atm.helsinki.fi/peex/index.php/baikal-selenga-network-basenet) - PEEEX subprogram and several bi-lateral research projects (www.atm.helsinki.fi/peex/index.php/projects). New openings, having high regional and global relevance, are related to permafrost dynamics in Siberia and the environmental health issues in the Russian Arctic under changing climate (Melnikov et al. 2018, Kasimov et al. 2018). The analysis of the borehole temperature datasets in Nadym and modelling of the permafrost evolution has been carried out in collaboration with the University of Tyumen. Observations confirm high sensitivity of permafrost dynamics in the discontinuous permafrost area near Nadym to snow thickness and warming, resulting in accelerated thaw during recent years with extreme summer temperatures and winter precipitation (Kukkonen et al. submitted). Dynamics of permafrost in Russia are also analyzed in the frame of the “Permafrost dynamics & Mechanisms, pathways and patchiness of the Arctic ecosystem responses and adaptation to changing climate” (CLIMECO) project funded by the Academy of Finland. The medical-geographical analysis of spatio-temporal distribution and changes in pattern of naturally-dependent and socially important diseases under the changing climate and economic development of the Russian Arctic with focus on Yamalo-Nenets Autonomous Okrug is performed in collaboration with Moscow State University. The studies of climatic factors leading to the recent anthrax outbreak emphasize the importance of precipitation dynamics in the region (Ezhova et al. paper in preparation). There are also ongoing joint research in hydrological observations (Vihma et al, 2019) and modelling of the water ecosystems of the Fennoscandia and NW Russia, Baltic and White Seas (collaboration with Northern Water Problems Institute, Karelia); on diagnosis and numerical simulation of the atmospheric boundary layer dynamics and the Arctic terrestrial ecosystems state under anthropogenic stress; physical models of extreme marine weather events caused by climate change in the Arctic zone in the first half of the 21st century (with Institute of Numerical Mathematics, Moscow); evaluation of accumulated ecological damage for forest ecosystems in Russia and Finland based on forest inventories, SMEAR stations fluxes, remote sensing data processing, monetary evaluation (with Scientific Research Center for Ecological Safety, St.Petersburg); measurements and modelling of spatio-temporal variability of atmospheric mercury in the Russian Arctic (with Kola Science Centre, Apatity); online integrated multi-scale modelling (for NW Russia, Kola, Scandinavia, and Arctic) of direct, indirect, combined effects of aerosols on meteorology and atmospheric composition (with Russian State Hydrometeorological University/ St.Petersburg State University, St. Petersburg).

In China, the joint PEEEX research is coordinated as an integral part of the GlobalSMEAR approach (see the Lappalainen et al. GlobalSMEAR abstract of this proceedings) and is connected to the analysis of the new SMEAR standardized measurements done in China. The most active partners are the Nanjing University (NJU), the Beijing University of Chemical Technology (BUCT,) and the Institute of Remote

Sensing and Digital Earth, Chinese Academy of Sciences (RADI-CAS). The research together with NJU is carried under the “Joint international research laboratory of Atmospheric and Earth System Sciences” JirLATEST (jirlatest.nju.edu.cn/main.htm). JirLATEST also includes organization of joint workshops and student training. In addition, INAR has also published several papers together with Nanjing University based on the data from the SMEAR benchmarked station called “Station for Observing Regional Processes of the Earth System” (SORPES-NJU). The new Beijing Haze station hosted by BUCT is the first urban mega city station based on the SMEAR concept and has been constructed in 2018-2019. The first datasets are currently analyzed and first report for Mayor of Beijing has been submitted. The RADI-INAR / PEEEX collaboration is implemented in a frame of the Digital Belt and Road Program (DBAR), INAR named as International Center of Excellence (ICoE) in Helsinki of DBAR, abbreviate the “DBAR-ICoE- Helsinki”. To promote the PEEEX approach in China and in the frame Belt and Silk Road initiatives, PEEEX has published a separate PEEEX Belt and Silk Road agenda, which introduces the large research questions and research infrastructure relevant to Belt and Silk Road region (Lappalainen et al. 2018).

In the European and Nordic scale the most recent PEEEX activity coordinated by INAR has been FutArcSoc (*Future Arctic: Feedbacks and System Understanding of, Scenarios and Innovation Insights for, Development of Arctic Societies*) proposal and a new cross disciplinary research concept outlined for the EU Horizon 2020 Cryospheric Call in 2018 and, a modified version, for the NordForsk “*Multidisciplinary Research Projects Call*”(submitted in Nov 2019). The FutArcSoc introduces a research concept for analyzing the feedbacks & system understanding of Arctic environment, scenarios & innovation insights for the future development of Arctic societies. The concept takes into account growing pressure and gaps in knowledge of local and global communities due to rapidly changing Arctic environment and the international geopolitical and geo-economic landscapes. FutArcSoc concept is addressing on the most relevant topical issues and the main opportunities for development, as well as how research infrastructure could be used more effectively across national borders and programs. The added value of the concept is the inter- and transdisciplinary research approach combined with the holistic system analysis and with the currently missing aspects such as societal security to the analysis (Heininen et al. in preparation).

2.2 Research Infrastructure development in the PEEEX region

2.2.1 In situ observations

The basic principles of the PEEEX *in situ* observation network based on the SMEAR (Stations Measuring the Earth Surface – Atmosphere Relations) concept has been introduced by Hari et al. (2016), Kulmala et al. (2016) and, for the marine environments by Vihma et al. (2019). The PEEEX RI mission is to fill in the observational gap especially in the Northern Eurasian region, to expand the PEEEX / GlobalSMEAR observation networks in Russia and China, and to promote the Arctic Ocean *in situ* observation concept in the Arctic RI forums such as Arctic Council SAON WG and Group on Earth Observations (GEO) Cold Regions Initiative (GEO CRI) framework, and PEEEX was already involved in the co-lead board for this global effort for the new implementation for the next three years from 2020 to 2022. The PEEEX RI mission finds synergy with and is contributing the international Arctic RI projects like EU Horizon-2020 iCUPE (*Integrative and Comprehensive Understanding on Polar Environments*; www.atm.helsinki.fi/icupe) coordinated by INAR (Petäjä et al., 2019 paper in preparation) and INTAROS (*Integrated Arctic Observation System*; www.nersc.no/project/intaros) coordinated by the Nansen Environmental and Remote Sensing Center (Norway).

In Russia, the PEEEX RI collaboration is currently built on the existing *in situ* stations networks. PEEEX has introduced, in collaboration with INTAROS, the Russian *in situ* station e-Catalogue (www.atm.helsinki.fi/peex/index.php/peex-russia-in-situ-stations-e-catalogue, a living document). The catalogue is aimed at enhancing the research collaboration and data exchange between researchers. It also provides guidelines (co-locations etc. aspects) when stations selected for a station upgrading or new stations are initiated. PEEEX continues expanding the contact network and new stations are invited to join the station network. At the moment, new data from Russia is mostly attained from the bi-lateral field campaigns, the most recent ones being “*Land – atmosphere feedback loops over Northern Eurasia /New Particle Formation*

in Siberia “ (in collaboration with V.E. Zuev Institute of Atmospheric Optics) and the long-term measurements on the green-house gases fluxes at the Mukhrino Field Station West Siberia (in collaboration with the Yugra State University). Since 2019 the novel multicomponent study of air and water pollution in Moscow metropolis is implemented under PEEEX umbrella. PEEEX also provides topical framework for environmental, climate and meteorological education activities between the Moscow State University (MSU) PEEEX Office and RosHydroMet. The example of such approach is Baikal Selenga Network (BaSeNet) which is a separate subprogram in PEEEX aiming at investigating and quantifying the waterborne transport of matter under changing hydro-climatic conditions on large drainage basin scales (Karthe et al., 2019).

In China, the PEEEX RI is an integral part of the GlobalSMEAR / Global Observatory approach (Kulmala 2015, 2018) and has the primary focus on the air quality in Chinese megacities and large metropolitan areas. Starting in 2012, we have made preliminary market analysis and established an extensive contact network in China. Our current China contact network covers ca. 30 universities and city administrations. The main interest in Chinese market is on urban air quality monitoring including indoor air quality. However, the Chinese Ecosystem Research Network (CERN) for ecosystem monitoring, as a part of global eLTER network, provides a standardized station network that could be upgraded to the SMEAR network. In case of CERN the ecosystem measurement could be complemented by the SMEAR atmospheric component. Our contacts in China are also actively involved with the Belt and Road Initiative, which has potential for establishing new SMEAR flagship stations along the Silk Road transport corridors and cities (SMEAR Upscaling Plan – ClimateKIC internal strategy document).

2.2.2 PEEEX Modelling Platform

PEEX-MP (www.atm.helsinki.fi/peex/index.php/modelling-platform) introduces an ensemble of the models from micro- to global scales. The future aim is to establish a seamless modelling framework from nano-scale modelling to Earth system models and to introduce community-based services for data mining and for demonstrating air pollution events at multi-scales in selected regions of Arctic-boreal-domain. Currently, PEEEX-MP includes more than 30 different models with more than 100 members of the network. The models have varied coverage of different Earth system components, such as atmosphere-hydrosphere-pedosphere-biosphere and processes such as physical-chemical-biological. The models used for realization of the PEEEX research agenda include: Earth System Models (EC-Earth, MPI-ESM, CESM, HadGEM2-ES); online integrated meteorology and atmospheric composition models (Enviro-HIRLAM, WRF-Chem); multi-scale atmospheric chemical transport models (SILAM, CAM-Chem, TOMCAT-GLOMAP, GEOS-Chem, EurCTM, ATMES, MMAD&IT, FLEXPART); ocean-sea-ice models (HYCOM-CICE, HBM, SWAN); models for atmosphere-vegetation-ecosystems processes and interactions (AVIM2, SOSAA, Agro-C, CH4MOD, CNMM-DNDC, SIM-BIM, EmpBVOC), large eddy simulation models (PALM, LESNIC, UCLALES-SALSA); inverse modelling tools (FLEXPART, CTDAS, IMDAF) and others. At INAR, in particular, the multi-scale and -processes modelling approach is realized through demonstration and application of the EC-Earth, Enviro-HIRLAM and MALTE-Box models, which are actively used in research tasks and science education (courses, trainings, schools) considering PEEEX research agenda and knowledge transfer.

2.2.3 Satellite observations

Satellites provide information complementary to in situ observation and modelling. Where in situ observation can provide much detail from continuous observation representative for a specific location, satellites provide less detail but with large spatial coverage with up to daily repeat cycle, and several observations each day. In general, the satellite data are column-integrated quantities and sometimes this can be obtained also for several individual layers, whereas detail on the vertical structure is available from satellite-based lidars. Satellite data are often used to constrain models, to test models or, vice versa, models are used for better understanding of satellite observations or improve the retrieval results by providing a priori information. It is noted that satellite-based instrument provides limited information and the retrieval is under-constrained and often assumptions are needed to find a solution. The retrieval results are validated with reference data from ground-based instruments and observation networks are established for this purpose, such as the global sunphotometer network AERONET established by NASA (Holben et al., 1998),

with sites all over the PEEEX study area, complemented with networks in China such as CARSNET, CARE-China and SONET. Satellites are used in China with RADII as primary partner and in Russia with (AEROCOSMOS) as primary partner. Strong cooperations on the use of satellite data and ground-based reference data exist in particular between Finnish Meteorological Institute (FMI) and several research institutes and universities in China, The current activities in Europe are a cooperation between FMI and the Royal Netherlands Meteorological Institute (KNMI) with a focus on atmospheric observations. Different types of satellites are used, providing information on aerosols, clouds, surface properties, trace gases and greenhouse gases. Such data has recently been used to study the spatial and temporal distribution of aerosols in China (de Leeuw et al., 2018), spanning a period of two decades showing the effect of national programs to reduce air pollution with a clear decrease since 2011 (Sogacheva et al., 2018a; 2018b). A satellite-based model has been developed to monitor PM_{2.5} concentrations (Zhang et al., 2019) and several studies are made together with Chinese colleagues on the occurrence of haze, contributions of natural and anthropogenic contributions to air pollution in China, chemical transformation of aerosols, aerosol-cloud interaction, etc. Furthermore satellites are used to study aerosols, trace gases and greenhouse gases over Eurasia, their relation to the occurrence of forest fires and transport of absorbing aerosol to the Arctic where they affect snow and ice properties, and vegetation/atmosphere interaction (de Leeuw et al, in preparation).

2.3 Capacity Building Activities, Outreach and Knowledge Transfer

The PEEEX education is a cross-section activity, which covers the training of young scientists, organization of specific winter and summer schools, and the expert training targeted towards more technical aspects of measurement, modelling, and assessment techniques and running operations including data management aspects of field stations, running models, performing assessments. Most of these activities have been implemented as an integral part of UHEL-INAR's Masters and Doctoral programs. In addition, we have several short- and long-term visiting scientists, including young researchers, at INAR from the PEEEX collaborating institutes, from Belarus, Russia, Ukraine, etc. The MODEST (*Doctoral Program Modernization of Doctoral Education in Science and Improvement Teaching Methodologies*; www.atm.helsinki.fi/peex/index.php/projects/174-modest-project) project for the 2018-2021 (Erasmus+ Capacity Building in the Field of Higher Education Program) is aimed at modernization of doctoral education in Science in European countries and Armenia, Belarus, and Russia and provides new contact network of students from Eastern Europe interested in atmospheric sciences for INAR and PEEEX. The Finnish-Russian FIRST+ PEEEX-AC (*Pan-Eurasian EXperiment – Academic Challenge*; www.atm.helsinki.fi/peex/index.php/projects/183-pan-eurasian-experiment-academic-challenge-peex-ac-network) networking project is aimed at strengthen international added value and prestige of the Finnish Universities educational system, to share knowledge, experience and promote state-of-the-art research and educational tools; and boost the PEEEX international collaboration. Under the PEEEX, annually the spring and autumn schools are organized at the Hyttiälä forestry station (www.atm.helsinki.fi/peex/index.php/education). In June 2019, the research training course (www.atm.helsinki.fi/peex/images/Summary_ClimEco-ResTraining_Jun2019_vfinal.pdf) on seamless integrated modelling took place in Tyumen (Russia) and workshop on the PhD programmes and University education in Helsinki (Finland) as part of ClimEco and MODEST projects, respectively. In addition, the research training intensive course (www.rshu.ru/3170) and young scientist summer school (worldslargerivers.boku.ac.at/wlr/index.php/ysss.html) on multi-scales and –processes modelling, observations, and assessments are planned in Russia for April and August 2020 in St.Petersburg and Moscow, respectively (as part of AoF ClimEco and FIRST+ PEEEX-AC projects). Mini-crash-courses on aspects of the PhD education/programmes and building Nordic/Finnish Centers of Excellences and their linkage to PEEEX will be organized in March 2020 (Moscow, Russia) and training educational workshop in May 2020 (Hyttiälä, Finland).

Starting 2016 PEEEX has been active member of the Universities of Arctic (U-Arctic) community. PEEEX has been named as one of the U-Arctic thematic networks called as “Arctic-Boreal Hub” (www.uarctic.org/organization/thematic-networks/arctic-boreal-hub). U-Arctic facilitates active Arctic network of researchers and students. A new education and outreach project “Climate change Effects on Nature and Society in the Arctic (CENSArctic) started under the thematic network in 2019. The goals of the

project are to provide unique educational opportunities for students at the circumpolar North, to enhance human capacity, and to expand a crucial interdisciplinary knowledge in the North by providing new e-learning tools and by running a summer school on climate change effects on nature and society in the Arctic. U-Arctic collaboration has also motivated PEEEX to provide good information flows between communities. PEEEX is currently releasing (3-4 times per year) the PEEEX-Arctic-Boreal-e-Newsletter (www.atm.helsinki.fi/peex/index.php/newsletters), PEEEX Blog (peexhq.home.blog), PEEEX Twitter (twitter.com/PEEX_News) and continuous news line “News & Events” (www.atm.helsinki.fi/peex). These tools serve as a multi-functional platform for everyone to share their news on their latest research results, upcoming events, reports of the site visits etc. in the community.

2.4 Societal Impact Making

PEEX has been participated the Arctic Circle initiated by the former President of Iceland, Ó.R. Grímsson, and International Arctic Forum hosted by Russian President V. Putin. The participation at these high level international dialogue forums provides important up-to-date information on the political discussions, especially on the Arctic and processes on environmental matters and concerns. Participation to these forums supports PEEEX keep up the momentum in the societal impact making. Furthermore, PEEEX has co-organized the Sofia Earth Forums (Helsinki, Finland), which are gathering experts of various disciplines and backgrounds to discuss practical solutions to Grand Challenges of the PEEEX Science Plan. The December 2019 forum is dedicated to the carbon neutrality, regulations and incentives and is organized for the Finnish decision makers and experts at a high level.

The black carbon has been the topic of high relevance and impact and has been addressed several times by the Finnish President S. Niinistö in the Arctic collaboration discussion. In September 2019 PEEEX organized a special Finnish–Russian Workshop on “*Back Carbon and Arctic Dust*” (Moscow, RU) part of the “*Black carbon in the Arctic and significance compared to dust sources*” (IBA-FIN-BCDUST) project coordinated by the Finnish Meteorological Institute (FMI). In 2020, as a continuation of the impact processes INAR / PEEEX will organize an event called “*Arena for the gap analysis of the existing Arctic Science Co-Operations (AASCO)*” with the support from the Prince Albert Foundation in Monaco. Moreover, the PEEEX special session “*Pan-Eurasian EXperiment (PEEX) – Observation, Modelling and Assessment in the Arctic-Boreal Domain*” (meetingorganizer.copernicus.org/EGU2020/session/35931) is scheduled at the EGU-2020 (European Geosciences Union; www.egu2020.eu; 3-8 May 2020) General Assembly with a series of splinter meetings on the PEEEX - Observations, Modelling, Impact on Society, Education/Knowledge Transfer - Platforms.

FUTURE PROSPECTS

Climate change together with the growing economic activities and traffic connected to the China Belt and Road Initiative are increasing pressures on the Arctic, Northern Eurasian environments and the Silk Road Economic Belt and Road region. There is an urgent need to improve the analysis of the atmospheric and environmental pollution in these regions, their sources and to quantify the role of local and transported pollution emissions at the region (Lappalainen et al. 2018, Petäjä et al. 2019 submitted). PEEEX, together with GlobalSMEAR, provide all-round tools and research framework to find solutions the environmental problems at the regional and global scales.

ACKNOWLEDGEMENTS

A major part of the PEEEX work in years 2010–2019 has been based on the in-kind contribution and continuous collaboration of several European, Russian and Chinese research universities/institutes via supporting active participation to the PEEEX meetings, conferences organized in Helsinki and Hyytiälä (Finland), Moscow and St.Petersburg (Russia) and Beijing (China). In addition, we would like to acknowledge the support or funding from the following bodies: Finnish Cultural Foundation, Grant: Prof.

Markku Kulmala “International Working Groups”; Russian Mega-Grant No. 11.G34.31.0048 (University of Nizhny Novgorod), Academy of Finland contract 259537, Beautiful Beijing (Finland-China collaboration project) funded by TEKES, EU project InGOS, NordForsk Nordic Centre of Excellence of CRAICC (no 26060), NordForsk CRAICC-PEEX (amendment to contact 26060) and NordForsk PEEX-CRUCIAL (2016-2017) projects. 7), Russian Fund for Basic Research project 18-05-60219 and Russian Scientific foundation project 19-77-30004 (research activities in Moscow).

REFERENCES TO-BE-CHECKED – REFENCES TO BE ADDED

Alekseychik, P., Lappalainen, H. K., Petäjä, T., Zaitseva, N., Heimann, M., Laurila, T., ... Kulmala, M. (2016). Ground-based station network in Arctic and Subarctic Eurasia: an overview. *Geography, Environment and Sustainability*, 9(2). https://doi.org/10.15356/2071-9388_02v09_2016_06

Boy, M., Thomson, E. S., Acosta Navarro, J.-C., Arnalds, O., Batchvarova, E., Bäck, J., Berninger, F., Bilde, M., Dagsson-Waldhauserova, P., Castarède, D., Dalirian, M., de Leeuw, G., Dragosics, M., Duplissy, E.-M., Duplissy, J., Ekman, A. M. L., Fang, K., Gallet, J.-C., Glasius, M., Gryning, S.-E., Grythe, H., Hansson, H.-C., Hansson, M., Isaksson, E., Iversen, T., Jonsdottir, I., Kasurinen, V., Kirkevåg, A., Korhola, A., Krejci, R., Kristjansson, J. E., Lappalainen, H. K., Lauri, A., Leppäranta, M., Lihavainen, H., Makkonen, R., Massling, A., Meinander, O., Nilsson, E. D., Olafsson, H., Pettersson, J. B. C., Prisle, N. L., Riipinen, I., Roldin, P., Ruppel, M., Salter, M., Sand, M., Seland, Ø., Seppä, H., Skov, H., Soares, J., Stohl, A., Ström, J., Svensson, J., Swietlicki, E., Tabakova, K., Thorsteinsson, T., Virkkula, A., Weyhenmeyer, G. A., Wu, Y., Zieger, P., and Kulmala, M.: Interactions between the atmosphere, cryosphere and ecosystems at northern high latitudes, *Atmos. Chem. Phys.*, 2018, doi.org/10.5194/acp-2018-733.

Che, H., Zhang, X.-Y., Xia, X., Goloub, P., Holben, B., Zhao, H., Wang, Y., Zhang, X.-C., Wang, H., Blarel, L., Damiri, B., Zhang, R., Deng, X., Ma, Y., Wang, T., Geng, F., Qi, B., Zhu, J., Yu, J., Chen, Q., and Shi, G.: Ground-based aerosol climatology of China: aerosol optical depths from the China Aerosol Remote Sensing Network (CARSNET) 2002–2013, *Atmos. Chem. Phys.*, 15, 7619-7652, [doi:10.5194/acp-15-7619-2015](https://doi.org/10.5194/acp-15-7619-2015), 2015.

de Leeuw, G., Sogacheva, L., Rodriguez, E., Kourtidis, K., Georgoulias, A. K., Alexandri, G., Amiridis, V., Proestakis, E., Marinou, E., Xue, Y., and van der A, R.: Two decades of satellite observations of AOD over mainland China using ATSR-2, AATSR and MODIS/Terra: data set evaluation and large-scale patterns, *Atmos. Chem. Phys.*, 18, 1573-1592, doi.org/10.5194/acp-18-1573-2018, 2018.

Hari, P., Petäjä, T., Bäck, J., Kerminen, V.-M., Lappalainen, H.K., Vihma, T., Laurila, T., Viisanen, Y., Vesala, T., and Kulmala M., 2016. Conceptual design of a measurement network of the global change, *Atmos. Chem. Phys.*, 16, 1017-1028, [doi:10.5194/acp-16-1017-2016](https://doi.org/10.5194/acp-16-1017-2016).

Karthe D., Chalov S., Gradel A., Kusbach A. Special issue «Environment change on the Mongolian plateau: atmosphere, forests, soils and water». *GEOGRAPHY, ENVIRONMENT, SUSTAINABILITY*. 2019;12(3):60-65, doi.org/10.24057/2071-9388-2019-1411.

Kasimov N.S., Kotlyakov V.M., Krasnikov D.N., Krayukhin A.N., Tikunov V.S. NATIONAL ATLAS OF THE ARCTIC. *GEOGRAPHY, ENVIRONMENT, SUSTAINABILITY*. 2018;11(1):51-57, doi.org/10.24057/2071-9388-2018-11-1-51-57.

Kulmala, M., Lappalainen, H.K., Petäjä, T., Kurten, T., Kerminen, V.-M., Viisanen, Y., Hari, P., Bondur, V., Kasimov, N., Kotlyakov, V., Matvienko, G., Baklanov, A., Guo, H., Ding, A., Hansson, H.-C., and Zilitinkevich, S., 2015. Introduction: The Pan-Eurasian Experiment (PEEX) – multi-disciplinary, multi-scale and multi-component research and capacity building initiative, *Atmos. Chem. Phys.*, 15, 13085-13096, [doi:10.5194/acp-15-13085-2015](https://doi.org/10.5194/acp-15-13085-2015)

Kulmala M., 2015: China’s choking cocktail, *Nature*, 526, 497–499.

Kulmala, M., Lappalainen, H. K., Petäjä, T., Kurten, T., Kerminen, V.-M., Viisanen, Y., Hari, P., Sorvari, S., Bäck, J., Bondur, V., Kasimov, N., Kotlyakov, V., Matvienko, G., Baklanov, A., Guo, H. D., Ding, A., Hansson, H.-C., and Zilitinkevich, S.: Introduction: The Pan-Eurasian Experiment (PEEX) – multidisciplinary, multiscale and multicomponent research and capacity-building initiative, *Atmos. Chem. Phys.*, 15, 13085–13096, <https://doi.org/10.5194/acp-15-13085-2015>, 2015.

Kulmala M., 2018: Build a global Earth observatory, *Nature*, 553, 21-22

Lappalainen, H.K., Kulmala, M., Kujansuu, J., Petäjä, T., Mahura, A., de Leeuw, G., Zilitinkevich, S., Juustila, M., Kerminen, V.-M., Bornstein, B., Zhang Jiahua, Xue Yong, Qiu Yubao, Liang Dong, Liu Jie & Guo Huadong (2018) The Silk Road agenda of the Pan-Eurasian Experiment (PEEX) program, *Big Earth Data*, 2:1, 8-35, doi: 10.1080/20964471.2018.1437704.

Lappalainen, H.K., Petäjä, T., Kujansuu, J., and Kerminen, V.-M. et al. 2014 : Pan-Eurasian Experiment (PEEX) – a research initiative meeting the grand challenges of the changing environment of the northern Pan-Eurasian arctic-boreal areas, *J. Geography Environment Sustainability*, 2(7), 13-48, doi.org/10.24057/2071-9388-2014-7-2-13-48.

Lappalainen, H. K., Kerminen, V.-M., Petäjä, T., Kurten, T., Baklanov, A., Shvidenko, A., Bäck, J., Vihma, T., Alekseychik, P., Andreae, M. O., Arnold, S. R., Arshinov, M., Asmi, E., Belan, B., Bobylev, L., Chalov, S., Cheng, Y., Chubarova, N., de Leeuw, G., Ding, A., Dobrolyubov, S., Dubtsov, S., Dyukarev, E., Elansky, N., Eleftheriadis, K., Esau, I., Filatov, N., Flint, M., Fu, C., Glezer, O., Gliko, A., Heimann, M., Holtslag, A. A. M., Hörrak, U., Janhunen, J., Juhola, S., Järvi, L., Järvinen, H., Kanukhina, A., Konstantinov, P., Kotlyakov, V., Kieloaho, A.-J., Komarov, A. S., Kujansuu, J., Kukkonen, I., Duplissy, E.-M., Laaksonen, A., Laurila, T., Lihavainen, H., Lisitzin, A., Mahura, A., Makshtas, A., Mareev, E., Mazon, S., Matishov, D., Melnikov, V., Mikhailov, E., Moiseev, D., Nigmatulin, R., Noe, S. M., Ojala, A., Pihlatie, M., Popovicheva, O., Pumpanen, J., Regerand, T., Repina, I., Shcherbinin, A., Shevchenko, V., Sipilä, M., Skorokhod, A., Spracklen, D. V., Su, H., Subetto, D. A., Sun, J., Terzhevik, A. Y., Timofeyev, Y., Troitskaya, Y., Tynkkynen, V.-P., Kharuk, V. I., Zaytseva, N., Zhang, J., Viisanen, Y., Vesala, T., Hari, P., Hansson, H. C., Matvienko, G. G., Kasimov, N. S., Guo, H., Bondur, V., Zilitinkevich, S., and Kulmala, M.: Pan-Eurasian Experiment (PEEX): towards a holistic understanding of the feedbacks and interactions in the land–atmosphere–ocean–society continuum in the northern Eurasian region, *Atmos. Chem. Phys.*, 16, 14421–14461, <https://doi.org/10.5194/acp-16-14421-2016>, 2016.

Lappalainen H.K., Altimir N., Kerminen V., Petäjä T., Makkonen R., Alekseychik P., Zaitseva N., Bashmakova I., Kujansuu J., Lauri A., Haapanala P., Mazon S.B., Borisova A., Konstantinov P., Chalov S., Laurila T., Asmi E., Lihavainen H., Bäck J., Arshinov M., Mahura A., Arnold S., Vihma T., Uotila P., de Leeuw G., Kukkonen I., Malkhazova S., Tynkkynen V., Fedorova I., Hansson H.C., Dobrolyubov S., Melnikov V., Matvienko G., Baklanov A., Viisanen Y., Kasimov N., Guo H., Bondur V., Zilitinkevich S., Kulmala M. Pan-Eurasian Experiment (PEEX) program: An overview of the first 5 years in operation and future prospects. *GEOGRAPHY, ENVIRONMENT, SUSTAINABILITY*, 11(1):6–19, 2019, doi.org/10.24057/2071-9388-2018-11-1-6-19.

Melnikov, V., Gennadinik, V., Kulmala, M., Lappalainen, H. K., Petäjä, T., and Zilitinkevich, S.: Cryosphere: a kingdom of anomalies and diversity, *Atmos. Chem. Phys.*, 18, 6535–6542, doi.org/10.5194/acp-18-6535-2018, 2018.

Sogacheva, L., de Leeuw, G., Rodriguez, E., Kolmonen, P., Georgoulias, A. K., Alexandri, G., Kourtidis, K., Proestakis, E., Marinou, E., Amiridis, V., Xue, Y., and van der A, R. J.: Spatial and seasonal variations of aerosols over China from two decades of multi-satellite observations – Part 1: ATSR (1995–2011) and MODIS C6.1 (2000–2017), *Atmos. Chem. Phys.*, 18, 11389–11407, doi.org/10.5194/acp-18-11389-2018, 2018.

Sogacheva, L., Rodriguez, E., Kolmonen, P., Virtanen, T. H., Saponaro, G., de Leeuw, G., Georgoulias, A. K., Alexandri, G., Kourtidis, K., and van der A, R. J.: Spatial and seasonal variations of aerosols over China from two decades of multi-satellite observations – Part 2: AOD time series for 1995–2017 combined from ATSR ADV and MODIS C6.1 and AOD tendency estimations, *Atmos. Chem. Phys.*, 18, 16631–16652, doi.org/10.5194/acp-18-16631-2018, 2018.

Pan Eurasian Experiment (PEEX) Science Plan (2016). Editors Lappalainen H.K., Kulmala M. & Zilitinkevich S. http://www.atm.helsinki.fi/peex/images/PEEX_SP__27052015.pdf

Vihma, T., Uotila, P., Sandven, S., Pozdnyakov, D., Makshtas, A., Pelyasov, A., Pirazzini, R., Danielsen, F., Chalov, S., Lappalainen, H. K., Ivanov, V., Frolov, I., Albin, A., Cheng, B., Dobrolyubov, S., Arkhipkin, V., Myslenkov, S., Petäjä, T., and Kulmala, M.: Towards an advanced observation system for the marine Arctic in the framework of the Pan-Eurasian Experiment (PEEX), *Atmos. Chem. Phys.*, 19, 1941–1970, <https://doi.org/10.5194/acp-19-1941-2019>, 2019.

Xin, J., Wang, Y., Pan, Y., Ji, D., Liu, Z., Wen, T., Wang, Y., Li, X., Sun, Y., Sun J., Wang P., Wang G., Wang X., Cong Z., Song T., Hu B., Wang L., Tang G., Gao W., Guo Y., Miao H., Tian S., Wang L.; The Campaign on Atmospheric Aerosol Research Network of China: CARE-China; *Bull. Amer. Meteor. Soc.*, 96(7), 1137–1155, 2015.

INAR EDUCATION RESEARCH AND DEVELOPMENT

A. LAURI¹, T. M. RUUSKANEN¹, L. RIUTTANEN¹, M. ÄIJÄLÄ¹ and M. SANTALA¹

¹Institute for Atmospheric and Earth System Research INAR, University of Helsinki,
P.O. Box 64, FI-00014 Helsinki, Finland.

Keywords: climate education, pedagogy, education development, interdisciplinarity.

INTRODUCTION

INAR education research and development team was formally established in October 2019. The team is developing the multi- and interdisciplinary education in atmospheric sciences based on pedagogical approaches and theories created and/or adopted in INAR.

LEARNING ON RESEARCH-ORIENTED INTENSIVE COURSES

INAR has a 20-year old tradition in organizing research-oriented intensive courses. Recently we have reported both the pedagogical concept and learning outcomes of such courses (Lauri et al., 2019; Ruuskanen et al., 2018). The courses are usually 10-12 days long and often held on research stations such as SMEAR II (Kulmala and Hari, 2005). The special features of these courses include focus on real research questions, work in small groups with access to comprehensive long-term datasets, and use of the horizontal learning principle enabling everyone – students, supervisors, and lecturers – to adopt both the role of learner and teacher (Lauri et al., 2019). We found out that the motivation of both students and teachers increases upon use of real data and authentic scientific questions (Ruuskanen et al., 2018).

CLIMATE UNIVERSITY AND ONLINE EDUCATION

Climate change is an example of a wicked problem where education collaboration across borders is needed (Lehtonen et al, 2018). We at INAR also recognise that the fundamental societal, technical and economic transformations needed to answer the challenges surrounding climate change requires not only educating atmospheric researchers at INAR, but also educating the society at large. To broaden the teaching of climate topics to the entire Finnish higher education field, a new collaborative, national program, Climate University (blogs.helsinki.fi/climateuniversity) was established in 2018. The nationwide program is coordinated by INAR and includes in total 11 Finnish universities. Based on a needs assessment survey, Climate University will focus on the themes of *multidisciplinarity*, *holistic thinking*, *data and statistics based decision-making*, *science communication*, *private sector collaboration* and *consumer perspective*, as well as the viewpoint of *ethics and values* driving human behaviour and choices (Äijälä and Riuttanen, 2019).

The new Climate University open online courses will follow the same principles as the 2016 produced Climate.now (www.climatenow.fi), an online climate course currently running in seven universities in Finland (Martikainen, 2019). The six new Climate University courses of 2020 are: (1) Systems thinking, “Systemschange.now”; (2) Basics of sustainability, “Sustainable.now”; (3) Industry collaboration projects “Solutions.now”; (4) Climate education for high schools “Climate.now for schools”; (5) Climate data and statistics, and (6) Science communication. The new courses will be offered at several Finnish universities already on the fall semester of 2020.

Besides Climate University, INAR has been active in development of new online learning modules both locally and internationally. Together with partners in eight Nordic and Baltic countries we are creating new online courses and modules in topics related to interdisciplinary Arctic studies, air quality, and statistical tools for climate and atmospheric sciences. With local University of Helsinki digital leap funding we are building five online courses covering the topics in basic studies in meteorology and hydrospheric geophysics.

In the newly founded master's programme EnCHiL (Nordic Master in Environmental Changes at Higher Latitudes), INAR together with Swedish and Icelandic partners is combining online education with classroom and field studies in a joint-degree programme level (EnCHiL, 2019).

KYSYILMASTOSTA.FI

INAR Edu-Team together with INAR ESM group have developed and implemented a new social media based approach for science outreach. Public web service Kysyilmastosta.fi was launched in January 2019, and it enables direct communication between citizens and researchers on climate related questions (Santala, 2019). Citizens can ask question, and researcher answer to them. The questions will be used for future research purposes: they will be analyzed for the development of climate education (Santala and Makkonen, 2019), and new research projects will be made based on them.

TEACHERS' CLIMATE CHANGE FORUM

Teachers' Climate Change Forum was held in Hyytiälä in August 2019 (<https://www.helsinki.fi/en/science-education/teachers-climate-change-forum-2019>). The forum was organized in collaboration with INAR and University of Helsinki Science Education Centre. 31 international teachers arrived from all around the world to study and discuss climate change teaching in schools.

CLIMATE-KIC JOURNEY

University of Helsinki INAR was hosting EIT Climate-KIC Journey for the first time in August 2019. Climate Journey is the world's largest climate summer school (<https://journey.climate-kic.org/>). In August 2019, 40 students from all around Europe gathered to Hyytiälä for one week to study the basics of climate change and climate science. We shared the host position together with Aalto University, and from Hyytiälä the students continued to Aalto Otaniemi campus.

ART-SCIENCE COLLABORATION

Atmospheric sciences have a long history of art-science collaboration, Climate Whirl concept (Juurola et al., 2014) is based on www.carbotree.fi -portal that was launched ten years ago in 2009. Recent new openings are on the frontier of education (Ruuskanen et al., 2019). INAR has started organizing joint course with the University of the Arts Theater Academy where students with different backgrounds from meteorology, aerosol physics, environmental ecology, geophysics to dance, sound design, dance pedagogy etc study climate change from different perspectives. This mutually fruitful collaboration has been motivating for both science and art participants, climate change is an example of when a set of answers that are focused on principles and physical processes behind the problem is not enough for the information to be received by non-scientists.

CONCLUSIONS

INAR education research and development team does versatile and unique education development and new research projects are under planning.

ACKNOWLEDGEMENTS

Academy of Finland is acknowledged for centre of excellence funding and national doctoral programme funding, which have been used to arrange and develop research-intensive courses. Nordic council of ministers, especially its Nordic Master and Nordplus programmes are acknowledged for funding various educational, pedagogical, and online learning projects. NordForsk is acknowledged for funding Nordic intensive courses and a Nordic graduate school CBACCI. Tiina and Antti Herlin foundation is acknowledged for funding Kysyilmastosta.fi and Magnus Ehnrooth Foundation for the Teachers Climate Change Forum. Climate University is funded by the Ministry of Education and Culture Finland, Finnish Innovation Fund Sitra and participating universities.

REFERENCES

- EnCHiL (2019). Nordic Master in Environmental Changes at Higher Latitudes. <http://enchil.net/>
- Hari, P. and M. Kulmala (2005). Stations for Measuring Ecosystem-Atmosphere Relations (SMEAR II). *Boreal Environ. Res.*, 10:315–322.
- Juurola, E., J. F. J. Korhonen, L. Kulmala, P. Kolari, U. Taipale, J. Rasinmäki, T. Ruuskanen, T. Haapoja, J. Bäck, J. Levula, L. Riuttanen, E.-M. Kyrö, I. Dzhedzhev, E. Nikinmaa, T. Vesala and M. Kulmala (2014). Knowledge transfer of climate-ecosystem-interactions between science and society — Introducing the Climate Whirl concept. *Boreal Environ. Res.* 19 (suppl. B):406-411.
- Lauri, A., T. Ruuskanen, L. Riuttanen, P. Hari and M. Kulmala (2019). Research-oriented intensive courses foster multidisciplinary atmospheric science. *WMO Global Campus Innovations: New Directions for Education and Training* (accepted for publication).
- Lehtonen, A., A. Salonen, H. Cantell and L. Riuttanen (2018). A pedagogy of interconnectedness for encountering climate change as a wicked sustainability problem. *Journal of cleaner production*, 199:860-867.
- Martikainen, J. (2019). *Säteilypakote-käsitteen oppiminen Ilmasto.nyt-kurssilla*. Pro gradu –tutkielma. Helsingin yliopisto. <https://helda.helsinki.fi/handle/10138/305177>
- Ruuskanen, T., H. Vehkamäki, L. Riuttanen and A. Lauri (2018). An Exploratory Study of the Learning of Transferable Skills in a Research-Oriented Intensive Course in Atmospheric Sciences. *Sustainability*, 10(5):1385. <https://doi.org/10.3390/su10051385>
- Santala, M. (2019). *Osallistava toimintamalli ilmastoviestintään: verkkopalvelu kansalaisille ja tutkijoille*. Pro gradu –tutkielma. Helsingin yliopisto. <https://helda.helsinki.fi/handle/10138/303433>
- Santala, M. and R. Makkonen (2019): *Participatory climate communication platform: service for citizens and researchers*, ATM FCoE abstracts, 2019.
- Äijälä, M. and L. Riuttanen (2019): *Co-creating new climate education in Finnish universities*, ATM FCoE abstracts, 2019.
- Ruuskanen, T., Kallinen, A., Lauri, A., Riuttanen, L. and Vehkamäki, H., (2019): *Integration of art and science, facing climate change together*, ATM FCoE abstracts, 2019.

EARTH SYSTEM MODELING: OVERVIEW OF ACTIVITIES

R. MAKKONEN^{1,2}, A. MAHURA¹, J.-P. KESKINEN¹, P. ZHOU¹, J. BIAN¹, M. SANTALA¹, J. LENTO³,
A. RUSANEN¹, C. XAVIER¹, J. HAUTALA¹

¹Institute for Atmospheric and Earth System Research / Physics, Faculty of Science,
University of Helsinki, Helsinki, Finland

²Climate System Research unit, Finnish Meteorological Institute, Helsinki, Finland

³ IT Center for Science Computing (CSC), Espoo, Finland

Keywords: Earth System Modelling, Global- Climate- Regional- Scales and Processes Modelling,
Outreach and Knowledge Transfer, HPC Migration

INTRODUCTION

The Earth System modeling groups focuses on development and application of Earth System and climate models as well as tools around model workflows. The main tools of the group are EC-Earth, MPI-ESM, NorESM, Enviro-HIRLAM and their submodels. Model applications range from paleoclimate experiments to future climate assessments. The group has strong co-operation with Dynamic Meteorology and Atmospheric Modeling groups of ATM FcoE.

RECENT RESEARCH ACTIVITIES

The Earth System Modelling (ESM) group is participating in the Coupled Model Intercomparison Project Phase 6 (CMIP6). The group focuses on experiments with interactive aerosols and chemistry (Keskinen et al., FCOE2019), but also provides simulations for AMIP-style experiments (prescribed aerosols, fixed sea surface temperatures). The results from CMIP6 simulations will be published in Finnish Earth System Grid Federation node, which is built on the Center for Science Computing (CSC) infrastructure. The CMIP6 is expected to support the sixth assessment report of IPCC (AR6).

The group is also focusing on mid-Holocene aerosols and aerosol-climate interactions, in particular, the “Green Sahara” regime. Putian et al. (FCOE2019) simulated mid-Holocene aerosols and chemistry with offline chemical transport model TM5. The simulations focus is on significant changes in dust-vegetation-domain during Green Sahara. During Green Sahara scenario, dust emissions from Sahara were reduced even by 50-80% due to increased vegetation in Northern Africa. At the same time, vegetation itself emitted aerosols and precursors, which partly counteracted the dust-decrease. While dust reduction has been suggested as one of the drivers of Green Sahara, the vegetation emissions have so far been omitted in scientific literature.

Following the aerosol-climate studies in mid-Holocene, Bian et al. (FCOE2019) apply the coupled climate model EC-Earth to investigate role of aerosols on West-African Monsoon (WAM). The aerosol-fields simulated in Putian et al. (FCOE2019) have been incorporated into EC-Earth, and several coupled simulations have been performed to isolate the effects of aerosols and vegetation on Green Sahara and related feedbacks. Preliminary analysis shows that aerosols do play a major role in WAM extent and intensity during mid-Holocene. While the studies focus on mid-Holocene, several key features could play a role in future development of Sahel/Sahara region.

Global aerosol-climate model ECHAM-HAM has been used to quantify the short-term (weeks to months) effects of supervolcanic eruptions on tropical superstorms. Preliminary results show that there is

intensification of such storms at higher latitudes and weakening at lower latitudes. Some higher latitude coastal regions may experience particularly strong storms. In the future, the impact of eruption location (low- vs. mid-latitudes, Northern vs. Southern hemispheres) and timing (season) will be assessed.

To efficiently handle, reduce and analyse extensive amounts of ESM generated data (even in the order of terabytes during a relatively short simulation) a research tool was elaborated (Makkonen et al., FCOE2019). Whilst typical postprocessing includes monthly averaging and selected time-series at observation sites, a significant amount of valuable information is lost in the process. We have generated a Python-based clustering software, which provides data reduction methods as well as analysis for geospatial networks and interactions. The algorithms identify spatially homogeneous clusters in geospatial gridded datasets, e.g. climate model output. In addition to clustering, the software can detect mutual information between any clusters in two distinct datasets, allowing e.g. network identification and interactions. The algorithms can be applied to identify aerosol-cloud-climate interactions in climate model data as well as satellite products.

In collaboration with Nordic TRAKT-project (TRAKT, 2019), ESM group has provided analysis of IPCC AR5 future climate scenarios in Kola Peninsula and surrounding domain, as well as applied Earth System model EC-Earth results in assessing meteorological conditions relevant for air pollution episodes. The analysis focused on identifying meteorological conditions (wind, daily precipitation) which enable poor local/regional air quality conditions. For winter pollution episode, the Enviro-HIRLAM model was run in a downscaling chain from regional-subregional- to urban scales at resolutions of 15-5-2.5 km to simulate meteorology and atmospheric composition for the Northern Fennoscandia and Kola Peninsula domains. The analysis focused on identifying small-scale features characteristic for meteorology and pollution in selected regions at dominating low winds conditions, when direct and indirect aerosols are also activated in model simulations.

The group participated in the EU FP7 BACCHUS project on extensive multi-model global Cloud Condensation Nuclei (CCN) simulation experiment (Fanourgakis et al., 2019). The combined analysis of 16 global models indicated that models typically underestimate aerosol and CCN concentrations. The model diversity was high especially for total particle concentration, but also CCN concentrations were highly diverse over tropics, polar regions and oceans.

In collaboration with Norwegian teams, ESM group participated in quantifying BVOC-aerosol-climate feedbacks in an ESM framework (Sporre et al., 2019). Quantifying the COBACC feedback loop revealed that, at least in NorESM, the climate impacts can be significant. In the model experiments, global annual BVOC emissions increased over 60%, when considering doubling of CO₂ and corresponding climate change. This led to stronger cloud forcing (-0.43 W m⁻²) and more negative aerosol direct forcing (-0.06 W m⁻²). While the BVOC-SOA-CCN pathway seems important in NorESM, the model showed only minor feedback via the SOA-GPP loop. Results can be highly model specific, and e.g. Rap et al. (2018) reported strong feedbacks via the SOA-GPP components. The ESM group provided further quantification of global Earth System feedback loops in Boy et al. (2019).

ESM group has also participated in quantifying air pollution and related mortality impacts of Nordic emissions (Im et al., 2019), as well as global anthropogenic aerosol forcing via multi-model experiments with simplified aerosols (Fiedler et al., 2019).

A series of studies on multi-scale modelling and analysis of aerosols feedbacks and interactions in Arctic-boreal domain, aerosols influence on regional scale with zooming to selected metropolitan areas, cases of transboundary pollution from continuous sources of emissions over Kola vs. Fennoscandia, occurrence of elevated black carbon episodes vs. forest fires, and mesoscale resolution radar data assimilation were realised and ongoing (see more Mahura et al., FCOE2019). In these the Enviro-HIRLAM (Environment – High Resolution Limited Area Model) and HARMONIE (HIRLAM-ALADIN Research for Meso-scale Operational NWP In Europe) modelling system are employed. These studies are done in close collaboration with partners involved into Enviro-PEEX on ECMWF project.

OUTREACH AND KNOWLEDGE TRANSFER

The ESM group has initialised new mechanisms for climate research communication. Kysyilmastosta.fi, coordinated at ESM group, provides a public service for climate related questions. The online platform provides a direct communication channel between climate scientists and society. Visitors can post questions about climate, asking for example more details on recent climate news, climate research, or misconceptions about climate change. The questions in the service will be thoroughly analyzed in the future (Santala et al., FCOE2019) and there will be new research made based on selected questions. The platform was launched in January 2019, and there are already more than 100 questions asked.

The models (including MALTE-Box, Boy et al., FCOE2019) are also demonstrated and promoted to the Universities/Institutions science education, and especially to younger generation of researchers, through organization of research training intensive courses and young scientist schools. In particular, the research training weeks for students on multi-scale and -processes integrated modelling took place at the UHEL-INAR (Apr 2019; peexhq.home.blog/2019/06/19/student-training-visit-at-inar) and the University of Tyumen (UTMN, Tyumen, Russia, Jun 2019; www.atm.helsinki.fi/peex/images/Summary_ClimEco-ResTraining_Jun2019_vfinal.pdf). Next trainings are scheduled for Apr and Aug 2020 at the Russian State Hydrometeorological University (RSHU, St.Petersburg; ums.rshu.ru) and Moscow State University (MSC, Moscow; worldslargerivers.boku.ac.at/wlr/index.php/ysss.html), respectively. During these events, the models will be employed for small-scale research projects to be realised by groups of students.

MIGRATION MODELS TO NEW HPC PLATFORM

The ESM group, as a very active user/customer of the CSC computing facilities and resources, in summer 2019 started preparations for migration of their models and corresponding input data and simulation results into new computing and data management environment. Instead of Sisu & Taito High Performance Computing (HPC) systems based on CRAY-XC40, new ones to be in use. In particular, since Sep 2019 Puhti HPC (Atos BullSequana X400) became available (note, Mahti with Atos BullSequana XH2000 is planned for beginning 2020). Since Oct 2019, CSC central data repository called Allas became accessible as well. It has 12 PB of storage capacity, and it can be used to transfer, store, share, and analyse data. In addition to trainings on new systems organized by CSC (and provided useful basic information, guides and materials; docs.csc.fi), the ESM group is also arranging internal practical workshops (“mini-crash-courses”) to learn and practice on how more effectively to work and use new environment.

ACKNOWLEDGEMENTS

This work was supported by the Academy of Finland Centre of Excellence (grant no. 272041), for other funding sources, see individual ATM FCoE abstracts.

REFERENCES

- Bian et al.: Dust concentrations' role in the northern expansion of Western African monsoon during the Mid-Holocene period, ATM FCoE abstracts, 2019.
- Boy, M., Thomson, E. S., Acosta Navarro, J.-C., Arnalds, O., Batchvarova, E., Bäck, J., Berninger, F., Bilde, M., Brasseur, Z., Dagsson-Waldhauserova, P., Castarède, D., Dalirian, M., de Leeuw, G., Dragosics, M., Duplissy, E.-M., Duplissy, J., Ekman, A. M. L., Fang, K., Gallet, J.-C., Glasius, M., Gryning, S.-E., Grythe, H., Hansson, H.-C., Hansson, M., Isaksson, E., Iversen, T., Jonsdottir, I., Kasurinen, V., Kirkevåg, A., Korhola, A., Krejci, R., Kristjansson, J. E., Lappalainen, H. K., Lauri, A., Leppäranta, M., Lihavainen, H., Makkonen, R., Massling, A., Meinander, O., Nilsson, E. D., Olafsson, H., Pettersson, J. B. C., Prisle, N. L., Riipinen, I., Roldin, P., Ruppel, M., Salter, M., Sand, M., Seland, Ø., Seppä, H., Skov, H., Soares, J., Stohl, A., Ström, J., Svensson, J., Swietlicki, E., Tabakova, K., Thorsteinsson, T., Virkkula, A., Weyhenmeyer, G. A., Wu, Y., Zieger, P., and Kulmala, M.: Interactions between the atmosphere, cryosphere, and ecosystems at northern

- high latitudes, *Atmos. Chem. Phys.*, 19, 2015-2061, <https://doi.org/10.5194/acp-19-2015-2019>, 2019.
- Fanourgakis, G. S., Kanakidou, M., Nenes, A., Bauer, S. E., Bergman, T., Carslaw, K. S., Grini, A., Hamilton, D. S., Johnson, J. S., Karydis, V. A., Kirkevåg, A., Kodros, J. K., Lohmann, U., Luo, G., Makkonen, R., Matsui, H., Neubauer, D., Pierce, J. R., Schmale, J., Stier, P., Tsigaridis, K., van Noije, T., Wang, H., Watson-Parris, D., Westervelt, D. M., Yang, Y., Yoshioka, M., Daskalakis, N., Decesari, S., Gysel-Beer, M., Kalivitis, N., Liu, X., Mahowald, N. M., Myriokefalitakis, S., Schrödner, R., Sfakianaki, M., Tsimpidi, A. P., Wu, M., and Yu, F.: Evaluation of global simulations of aerosol particle and cloud condensation nuclei number, with implications for cloud droplet formation, *Atmos. Chem. Phys.*, 19, 8591-8617, <https://doi.org/10.5194/acp-19-8591-2019>, 2019.
- Fiedler, S., Kinne, S., Huang, W. T. K., Räisänen, P., O'Donnell, D., Bellouin, N., Stier, P., Merikanto, J., van Noije, T., Makkonen, R., and Lohmann, U.: Anthropogenic aerosol forcing – insights from multiple estimates from aerosol-climate models with reduced complexity, *Atmos. Chem. Phys.*, 19, 6821-6841, <https://doi.org/10.5194/acp-19-6821-2019>, 2019.
- Im, U., Christensen, J. H., Nielsen, O.-K., Sand, M., Makkonen, R., Geels, C., Anderson, C., Kukkonen, J., Lopez-Aparicio, S., and Brandt, J.: Contributions of Nordic anthropogenic emissions on air pollution and premature mortality over the Nordic region and the Arctic, *Atmos. Chem. Phys.*, 19, 12975–12992, <https://doi.org/10.5194/acp-19-12975-2019>, 2019.
- Keskinen et al.: FCoE in CMIP6, ATM FCoE abstracts, 2019.
- Makkonen et al.: Identifying global aerosol-climate interactions through geospatial networks, ATM FCoE abstracts, 2019.
- Putian et al.: A simulation of SOA over Green Sahara in Mid-Holocene period with prescribed isoprene and monoterpene emission, ATM FCoE abstracts, 2019.
- Santala et al.: Participatory climate communication platform: service for citizens and researchers, ATM FCoE abstracts, 2019.
- Sporre, M. K., Blichner, S. M., Karset, I. H. H., Makkonen, R., and Berntsen, T. K.: BVOC–aerosol–climate feedbacks investigated using NorESM, *Atmos. Chem. Phys.*, 19, 4763-4782, <https://doi.org/10.5194/acp-19-4763-2019>, 2019.
- TRAKT, 2019: Esau I., L. Bobylev, V. Donchenko, V. Gorny, N. Gnatiuk, A. Kiselev, S. Kritsuk, H.K. Lappalainen, P. Konstantinov, A. Mahura, R. Makkonen, A. Manvelova, V. Masloboev, V. Miles, T. Petäjä, P. Poutanen, M. Varentsov, T. Wolf, S. Zilitinkevich, M. Kulmala (2019): An Integrated Approach To Produce Transferable Knowledge For High-Resolution Environmental Impact Assessment. *To be submitted to Geography, Environment, Sustainability (GES) journal*.
- Mahura A., Nuterman R., Nerobelov G., Sedeeva M., Smyshlyaev S., Savenets M., Pysarenko L., Ivanov S., Michaelides S., Ruban I., Sassi A.S., Makkonen R., Baklanov A., Petäjä T., Zilitinkevich S., Kulmala M. (FCOE2019): Integrated multi-scale modelling for meteorology-chemistry-aerosols interactions.

VÄRI-PROJECT AND DEVELOPMENT OF VÄRRIÖ STATION

K. NEITOLA¹, J. MUKKALA², A.-P. HYVÄRINEN³, J. BÄCK⁴ and T. PETÄJÄ¹

¹Institute for atmospheric and earth system research / Physics, Faculty of Science, University of Helsinki, Finland.

²Itä-Lapin kuntayhtymä, Kuumaniemenkatu 2 A, Kemijärvi, Finland.

³Finnish Meteorological Institute, Erik Palmenin aukio 1, P.O. box 503, Helsinki, Finland.

⁴¹Institute for atmospheric and earth system research /Forest Sciences, Faculty of Agriculture and Forestry, University of Helsinki, Finland.

Keywords: VÄRRIÖ STATION, SMEAR I, OUTREACH.

INTRODUCTION

Värriö research station (67.7383°, 29.6109°, 370 m a.s.l.) is located in eastern Lapland, 6 km from the Russian border in the Värriö strict nature reserve. The station was founded in 1967 as a biological station and SMEAR I station was founded there on 1992 to investigate pollution originating in the Kola Peninsula smelteries (Kyrö *et al.*, 2014). Due to the original purpose of large predator research done at the biological station, information about the station was very limited to the local population, where one of the main livelihoods was reindeer herding. Local technicians have managed the station over the years, without any scientists working at the site, except for short visits. This has limited the overall scientific development of the instrumentation, co-operation with foreign research groups and overall number of publications originating from the station. To increase the general knowledge of the research done at the station and make use of the high-level data for the local communities and livelihood, a VÄRI-project started in autumn 2018, in collaboration with INAR and the union of municipalities of Eastern Lapland (Itä-Lapin kuntayhtymä). EU funds the project in collaboration with the Coalition of Lapland (Lapin Liitto). The main aim of the 2-year project is to increase general knowledge of the research done at the station for the local population, as well as equip some of the results for the local companies to use. The funding has enabled hiring a scientist working at the station to further develop the measurements, co-operation and publications, as well as provide scientific products for the local businesses.

METHODS

The VÄRI-project aims to improve the general knowledge of the station and the research by participating in local events with own booth and presentations, as well as presenting obtained data on screens in, for example municipality buildings and other local hot spots. The data includes various historical weather data (max. and min. temperatures and snow depths, etc.) and climate change data (CO₂ conc., mean temperature increase, decrease of snow cover-days), as well as near-real-time data (meteorological parameters, aerosol particle characteristics, etc.).

The project includes workshops for the local businesses to brainstorm how to apply some of the results from the research to the use of the businesses. One of easiest solutions is to promote the ultra-clean atmosphere for the tourism businesses in a marketing form: Figure 1 shows an increase in life expectancy for tourists arriving from various places in Europe, for spending one week in the clean atmosphere of the Eastern Lapland. The data is calculated using University of Chicago's Energy Policy Institute's Air Quality Life Index (AQLI) data for life expectancy and decrease of it, due to atmospheric aerosols. A carbon-footprint-

compensation program is being developed for the Eastern Lapland, where the arriving tourists can compensate their traveling footprint. The idea is to plant the forests in the opening in Eastern Lapland, left by old fields and other openings without plans to be forested. Recommendations to grow trees and forests that can be used, for example, in construction or furniture material will be given in the compensation program, to increase the duration of the carbon cycle.

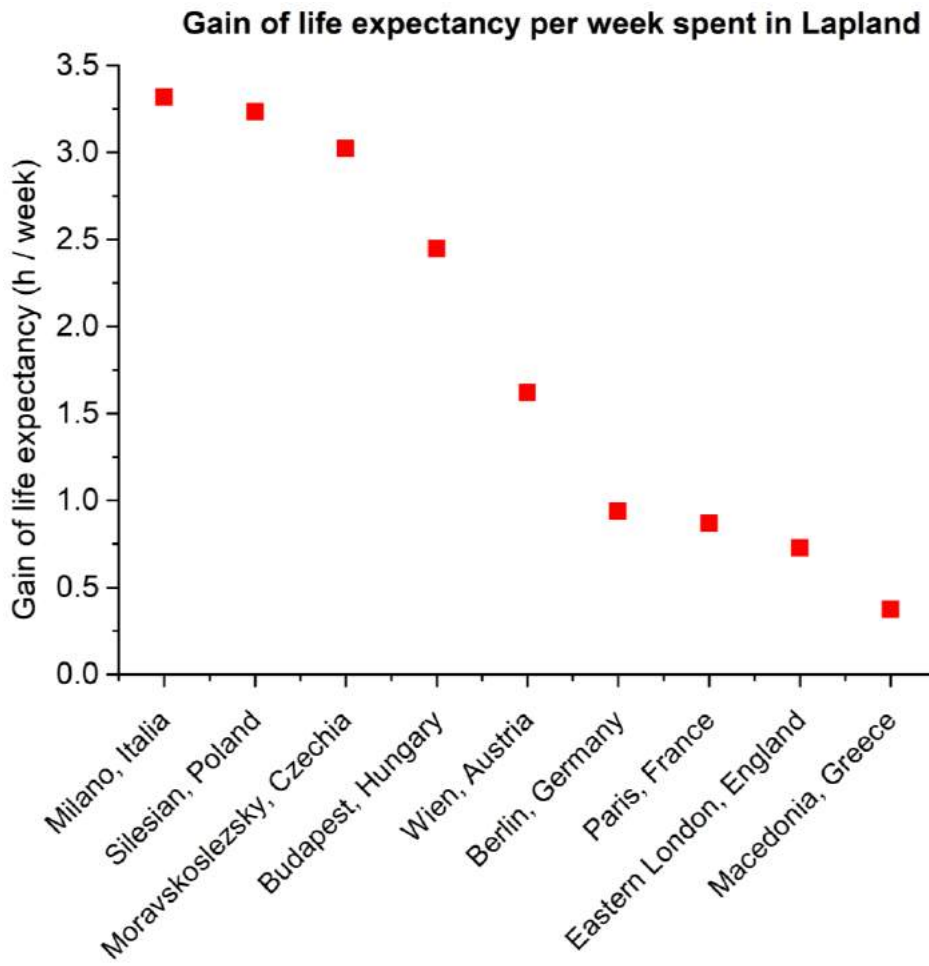


Figure 1. Gain in life expectancy per week spent in Eastern Lapland due to the cleaner atmosphere for tourists arriving from various places in Europe.

Other methods of increasing the knowledge is to invite groups and people related to the projects to the station during a visiting day on spring 2020. Co-operation with other research station in Lapland will be done to learn from their outreach experiences.

Co-operation with a local high school has already started, with a visit to the station by the students and teacher. The co-operation will continue further with a planned climate change-course, organized by the high school and Värriö research station staff.

Hiring a scientist to the station has already increased the ability to have instruments at the station, that demand more educated manpower. CI-Api-ToF (Jokinen *et al.*, 2012) was placed at the station in autumn 2018 and it has been measuring since. A Single Particle Soot Photometer (SP2) was measuring at the station throughout the summer season. The instrument was placed at the station by the Finnish Meteorological Institute (FMI) to investigate effect of aging of soot particles between Värriö station and FMI Pallas station in western Lapland originating from the forest fires in Russia. Plans have been made to increase the instrumentation towards cloud properties and place those on top of the Värriö fell, to increase understanding

of aerosol-cloud activation processes. The station will be advertised in the scientific community to cooperate with foreign researcher and research groups to further increase the scientific results and publication numbers.

CONCLUSIONS

The VÄRI-project has potential to increase the general knowledge of local communities of the research conducted at the Värriö research station and create scientific products for the use of local livelihood and businesses. The funding also enables further development of the research conducted at the station and increase it's visibility in the scientific community. We will make Värriö great again!

ACKNOWLEDGEMENTS

This work was funded by the Lapin Liitto – EAKR (European Regional Development Fund) with several comembers, grant number A74910.

REFERENCES

- AQLI: <https://aqli.epic.uchicago.edu/the-index/>
- Jokinen, T., Sipilä, M., Junninen, H., Ehn, M., Lönn, G., Hakala, J., Petäjä, T., Mauldin III, R.L., Kulmala, M. and Worsnop, D.R. (2012) Atmospheric sulfuric acid and neutral cluster measurements using CI-API-TOF, *Atmos. Chem. Phys.* 12, 4117-4125.
- Kyrö, E.-M., Väänänen, R., Kerminen, V.-M., Virkkula, A., Petäjä, T., Asmi, A., Dal Maso, M., Nieminen, T., Juhola, S., Shcherbinin, A., Riipinen, I., Lehtipalo, K., Keronen, P., Aalto, P.P., Hari, P. and Kulmala, M. (2014) Trends in new particle formation in Eastern Lapland, Finland: effect of decreasing sulfur emissions from Kola Peninsula, *Atmos. Chem. Phys.* 14, 4383-4396.

OVERVIEW OF THE ACTIVITIES WITHIN GLOBAL ATMOSPHERE–EARTH SURFACE FEEDBACKS GROUP

T. NIEMINEN, E. EZHOVA, A. DEMAKOVA, E.-M. DUPLISSY, J. HEISKANEN,
V. LHEUREUX, S. B. MAZON, M. RÄTY, K. TABAKOVA, D. TAIPALE, H. UUSITALO,
I. YLIVINKKA, M. ZAIDAN, V.-M. KERMINEN, and M. KULMALA

Institute for Atmospheric and Earth System Research (INAR), University of Helsinki, Helsinki, Finland

INTRODUCTION

The research done in the Global atmosphere–Earth surface feedbacks (GAEA) group is aiming to identify and analyse the regionally and globally important interactions and feedback mechanisms in the atmosphere – Earth surface continuum. Kulmala et al. (2014) have previously investigated the COBACC (Continental Biosphere-Aerosol-Cloud-Climate) feedback loop, in which the biosphere carbon sink and aerosol source are linked with each other via photosynthesis, primary productivity, production of volatile organic compounds (VOC) and the subsequent formation of secondary organic aerosols (SOA). The recent work done within GAEA group is involved with the emissions of precursor vapours and the initial steps of SOA formation, characterizing the atmospheric composition over West Africa based on airborne observations of trace gas and particle concentrations and composition, quantifying the airmass source areas and spatial representativeness of ground-based measurement sites, as well as analyzing the impact of environmental change on disease outbreaks observed in Siberia.

CURRENT RESEARCH ACTIVITIES

Trees emit a variety of VOCs, but the emission strengths and the chemical composition of the emitted VOCs depend on physical, environmental and biological conditions. Taipale et al. (abstract in these proceedings) have investigated the importance of taking into account the monoterpene emissions from new Scots pine foliage as a function of the season, stand age and tree provenance. They found that the emission of monoterpenes from Finland is underestimated by circa 20 Gg of monoterpenes per year, and that the underestimation is largest during spring months when also atmospheric new particle formation (NPF) occurs most frequently. Taking into account in models the monoterpene emissions from the expanding conifers foliage can lead to increases in the formation and growth rates of small particles by 98-258% and 60-255%, respectively.

Besides organic vapours, sulphuric acid has been identified as an important species for atmospheric NPF (Kulmala et al., 2013). Proxy variables for estimating sulphuric acid concentrations have been developed (Petäjä et al., 2009; Mikkonen et al., 2011). Ylivinkka et al. (abstract in these proceedings) have developed a revised sulphuric acid proxy which takes into account production of sulphuric acid from SO₂ oxidation by stabilized Criegee intermediates (Mauldin et al., 2012) as well as the formation of sulphuric acid dimer molecules. Based on comparison to long-term measurements of sulphuric acid during 2016–2019 at the SMEAR II station, the newly developed proxy agrees with measured concentrations better especially during nighttime.

Two recent reviews (Kerminen et al., 2018; Nieminen et al., 2018) of the current knowledge on atmospheric new particle formation (NPF) show that NPF occurs on regional scales across all continental environments in the lower troposphere, even though with a highly varying frequency. One area where NPF has been observed, but detailed long-term studies are lacking, is the boreal forest in Siberia. Demakova et al. (abstract in these proceedings) analyzed the particle number-size distribution measurement data during 2015–2018 from Fonovaya station near Tomsk. They observed the number of NPF events to be highest in March, especially in clear sky conditions, but the total number of events to be lower than at another boreal forest site in Hyytiälä SMEAR II in Finland. Uusitalo et al. (abstract in these proceedings) analyzed and compared NPF observations in Tomsk and Hyytiälä using cluster dynamics simulations with ACDC (McGrath et al., 2012). They found high summertime temperatures typical for Siberia could be one reason for the infrequent NPF in this area. Also, the ratio of the particle growth rates to their coagulation losses is lower in Tomsk compared to Hyytiälä. This lowers the survival probability of particles growing to larger sizes.

Assessing the spatial representativeness of atmospheric measurements performed on a fixed-location site is important for interpreting the measurement data. Nieminen et al. (abstract in these proceedings) have devised a framework for describing the variability and representativeness of a given measurement location in terms of land-cover type and level of anthropogenic influence.

Lheureux et al. (abstract in these proceedings) have applied machine learning methods to analyze the large measurement datasets obtained within the DACCWA project (Knippertz et al., 2015). The data includes observations of basic meteorology, trace gas and particle concentrations, particle chemical composition, as well as mass spectra of sub-2 nm clusters. Several clusters with distinct characteristics of aerosol and trace gas properties have been identified during individual flight tracks by utilizing the k-means algorithm. Comparing the geographical locations and altitudes where these clusters were observed provides information on the local emission sources and the effect of long-range transport of air pollutants.

The Arctic is currently one of the most rapidly changing environments due to global climate change. Ezhova et al. (abstract in these proceedings) analyzed the connections between permafrost thawing and observations of anthrax outbreaks in North Western Siberia. These disease outbreak events were connected both with the conditions (temperature and precipitation amount) during the winter preceding the outbreak as well as the lack of precipitation in the summer when the outbreaks occurred.

ACKNOWLEDGEMENTS

This work was supported by the Academy of Finland Centre of Excellence (project number 307331).

REFERENCES

- Kerminen, V.-M., Chen, X., Vakkari, V., Petäjä, T., Kulmala, M., Bianchi, F. (2018). Atmospheric new particle formation and growth: review of field observations. *Environ. Res. Lett.* 13, 103003.
- Knippertz, P., Coe, H., Chiu, J.C., Evans, M.J., Fink, A. H., Kalthoff, N., Liousse, C., Mari, C., Allan, R.P., Brooks, B., Danour, S., Flamant, C., Jegede, O.O., Lohou, F., Marsham, J.H. (2015). The DACCWA Project: Dynamics–Aerosol–Chemistry–Cloud Interactions in West Africa. *Bull. Amer. Meteor. Soc.* 96, 1451–1460.
- Kulmala, M., Kontkanen, J., Junninen, H., Lehtipalo, K., Manninen, H. E., Nieminen, T., Petäjä, T., Sipilä, M., Schobesberger, S., Rantala, P., Franchin, A., Jokinen, T., Järvinen, E., Äijälä, M., Kangasluoma, J., Hakala, J., Aalto, P. P., Paasonen, P., Mikkilä, J., Vanhanen, J., Aalto, J., Hakola, H., Makkonen, U., Ruuskanen, T., Mauldin, R. L., Duplissy, J., Vehkamäki, H., Bäck, J., Kortelainen, A., Riipinen, I., Kurtén, T., Johnston, M. V., Smith, J. N., Ehn, M., Mentel, T. F.,

- Lehtinen, K. E. J., Laaksonen, A., Kerminen, V.-M., and Worsnop, D. R. (2013). Direct Observations of Atmospheric Aerosol Nucleation. *Science* 339, 943–946.
- Kulmala, M., Nieminen, T., Nikandrova, A., Lehtipalo, K., Manninen, H. E., Kajos, M. K., Kolari, P., Lauri, A., Petäjä, T., Krejci, R., Hansson, H.-C., Swietlicki, E., Lindroth, A., Christensen, T. R., Arneth, A., Hari, P., Bäck, J., Vesala, T., Kerminen, V.-M. (2014). CO₂-induced terrestrial climate feedback mechanism: From carbon sink to aerosol source and back. *Boreal Environ. Res.* 19 (suppl. B), 122–131.
- Mauldin, R. L., Berndt, T., Sipilä, M., Paasonen, P., Petäjä, T., Kim, S., Kurtén, T., Stratmann, F., Kerminen, V.-M., and Kulmala, M. (2012). A new atmospherically relevant oxidant of sulphur dioxide. *Nature* 488, 193–196.
- McGrath, M. J., Olenius, T., Ortega, I. K., Loukonen, V., Paasonen, P., Kurtén, T., Kulmala, M., and Vehkamäki, H. (2012). Atmospheric Cluster Dynamics Code: a flexible method for solution of the birth-death equations. *Atmos. Chem. Phys.* 12, 2345–2355.
- Mikkonen, S., Romakkaniemi, S., Smith, J. N., Korhonen, H., Petäjä, T., Plass-Duelmer, C., Boy, M., McMurry, P.H., Lehtinen, K. E. J., Joutsensaari, J., Hamed, A., Mauldin III, R. L., Birmili, W., Spindler, G., Arnold, F., Kulmala, M., and Laaksonen, A. (2011). A statistical proxy for sulphuric acid concentration. *Atmos. Chem. Phys.* 11, 11319–11334.
- Nieminen, T., Kerminen, V.-M., Petäjä, T., Aalto, P. P., Arshinov, M., Asmi, E., Baltensperger, U., Beddows, D. C. S., Beukes, J. P., Collins, D., Ding, A., Harrison, R. M., Henzing, B., Hooda, R., Hu, M., Hörrak, U., Kivekäs, N., Komsaare, K., Krejci, R., Kristensson, A., Laakso, L., Laaksonen, A., Leitch, W. R., Lihavainen, H., Mihalopoulos, N., Németh, Z., Nie, W., O’Dowd, C., Salma, I., Sellegri, K., Svenningsson, B., Swietlicki, E., Tunved, P., Ulevicius, V., Vakkari, V., Vana, M., Wiedensohler, A., Wu, Z., Virtanen, A., Kulmala, M. (2018). Global analysis of continental boundary layer new particle formation based on long-term measurements, *Atmos. Chem. Phys.* 18, 14737–14756.
- Petäjä, T., Mauldin, I., R. L., Kosciuch, E., McGrath, J., Nieminen, T., Paasonen, P., Boy, M., Adamov, A., Kotiaho, T., and Kulmala, M. (2009). Sulfuric acid and OH concentrations in a boreal forest site. *Atmos. Chem. Phys.* 9, 7435–7448.

AIR QUALITY RESEARCH GROUP AT INAR/PHYSICS

P. PAASONEN¹, T. HUSSEIN^{1,2}, J. CAI^{1,3}, L. DADA¹, W. DU^{1,3}, K. DÄLLENBACH¹, B. FOREBACK¹,
P.-L. FUNG¹, S. HAKALA¹, J. KONTKANEN¹, M. LI^{1,4,5}, A. SHAHIRYER¹, S. TUOVINEN¹,
L. WANG^{1,4} and L. XINYANG¹

¹Institute for Atmospheric and Earth System Research / Physics, Faculty of Science, University of Helsinki, Finland.

²Department of Physics, The University of Jordan, Amman 11942, Jordan.

³Aerosol and Haze Laboratory, Beijing Advanced Innovation Center for Soft Matter Science and Engineering, Beijing University of Chemical Technology, Beijing 100029, China

⁴State Key Laboratory of Atmospheric Boundary Layer Physics and Atmospheric Chemistry (LAPC), Institute of Atmospheric Physics, Chinese Academy of Sciences, Beijing, 100029, China

⁵University of the Chinese Academy of Sciences, Beijing, 100049, China

Keywords: AIR QUALITY, AEROSOL, CLIMATE, EXPOSURE.

INTRODUCTION

Air quality research group at INAR/Physics started in the beginning of 2019. Most of the group members belonged earlier to the Aerosol-Cloud-Climate-Interactions (ACCI) group. The group has two main research themes: Air quality – weather – climate interactions, and Air quality and exposure. The former investigates air quality in terms of its drivers, impacts and interactions from local/regional scale to regional/global scale, whereas the latter investigates the exposure and impacts of local scale air quality and focuses the air quality to a citizen scale.

AIR QUALITY – WEATHER – CLIMATE INTERACTIONS

Our research on air quality interactions has concentrated on the air quality situation in and around Beijing, China. In regional scale, Wang et al. (*abstract in this collection*) investigated the ozone (Liu et al., 2019) and PM_{2.5} (Wang et al., 2019) concentrations and their connections to synoptic and local meteorological factors at 58 North-Chinese cities, based on the data collected by the Ministry of Environmental Protection (MEP) of China during years 2013-2017. Liu et al. (2019) showed that the summer time (April-October) ozone concentrations in North Chinese cities increased from 2013 to 2017, and that the variation in synoptic circulation patterns could explain only 40 % of the observed increase. Local meteorological conditions, such as temperature, RH and wind direction, was defined to cause 40-60 % of the day-to-day variation in ozone concentrations in almost all studied cities. On the contrary, the PM_{2.5} concentrations and the duration of severe PM_{2.5} pollution episodes were observed to decrease considerably from 2013 to 2017 (Wang et al., 2019). Especially, the annual number of large scale pollution days covering most of the studied North-China area decreased notably. The contribution of synoptic circulation to the reduced PM_{2.5} concentrations was estimated to be 64 % in summer and 45 % in winter.

Hakala et al. (*abstract in this collection*) studied the aerosol particle number size distributions as a function of time the air mass has spent over the densely populated areas in North-China. The analysis showed that in clean air masses particles in nucleation mode (diameters < 30 nm) dominate the size distributions and the diameter of the particles observed at the measurement station at the Beijing University of Chemical Technology (BUCT) increases with increasing time the air mass has spent over densely populated area. The results showed clear analogy with the evolution of particle size distributions in rural Boreal environment depicted as a function of time spent over forested areas (Tunved et al., 2006). The evolution of particle populations affected by new particle formation (NPF) within air masses circulating to and over high

emission areas is analysed further with the methodology applied by Hakala et al. (2019, and *manuscript in preparation*) for observations in Hada Al Sham, Saudi-Arabia. In Saudi-Arabia, the detailed analysis of air mass trajectories showed that the observed decrease in mode mean diameter after NPF and initial growth, previously suggested to result from shrinkage of the particles, is likely caused by variations of the particle growth rates due to air masses travelling over areas with different levels of aerosol precursor emissions.

We studied anthropogenic aerosol emissions from data recorded at BUCT with two separate approaches. Cai et al. (*abstract in this collection*) studied the contributions of different anthropogenic aerosol sources with positive matrix factorisation method (PMF) applied for organic aerosol mass and particle number size distributions. The analysis segregated the traffic emissions from light and heavy duty vehicles, cooking emissions and regional and secondary aerosols. The method can be applied to quantify the contributions of these sources on aerosol pollution. With another method, developed by Kontkanen et al. (*abstract in this collection*), we resolved the locally representative number size distribution of the emitted aerosol particles. This analysis clearly demonstrated the dominance of nucleation mode particles from traffic emissions on anthropogenic primary sources. This method makes it possible to distinguish the traffic emissions from particles formed in regional NPF events and quantify their significance for aerosol production. Du et al. (*manuscript in preparation*) investigated the composition and concentrations of aerosols at the ground level and in mast at 260 m of altitude. They showed that, during haze episodes, a roughness sublayer with height below 300 m can remain unmixed with the turbulent mixing layer for several days, weakening the dilution of the ground level pollution.

NPF events are observed frequently in conditions with high condensation/coagulation sink for aerosol precursor vapours and freshly formed clusters, which should in theory prevent the occurrence of NPF events (Kulmala et al., 2017). We conducted both experimental and theoretical analyses to find out the reasons for the observed NPF. Du et al. (*abstract in this collection*) investigated the chemical composition of particles acting as the condensation sink (CS) at the BUCT site. They reported that the mass fraction of organic compounds is higher on NPF days than on other days. Tuovinen et al. (*abstract in this collection*) studied how the contact angle in heterogenous nucleation can impact the uptake of vapours by pre-existing particles. They showed that certain types of chemical properties of the seed particle and the vapour can lead to relatively high contact angles, which can, in theory, significantly reduce the effectiveness of the CS.

Foreback et al. (*abstract in this collection*) analysed the atmospheric composition and meteorological conditions at BUCT site during the Chinese New Year festivities in 2018 and 2019. They showed that in 2018 the peak in concentrations of several pollutants (e.g. PM, BC, SO₂, CO) was much more pronounced than in 2019, but the explanation for the difference is under investigation. By comparing the BUCT data with the MEP data from other Beijing sites during the previous years, they analysed the typical patterns of air quality conditions during the festival seasons.

AIR QUALITY AND EXPOSURE

Our urban air quality research was conducted in co-operation with Finnish Meteorological Institute (FMI), Helsinki Region Environmental Authority (HSY), city of Helsinki and instrument manufacturers (Vaisala, Pegasor), as well as the Computer Science department of the University of Helsinki and the Nanjing University in China. In Helsinki Air Quality Testbed project (HAQT) we developed a hierarchical observation system for air pollutants, containing of SMEAR-type research stations, authority network and complementary sensor network, all integrated with fusion model FMI-ENFUSER to present and predict the air quality conditions with 12 m spatial and 1 h temporal resolution (Johansson 2019; Paasonen et al., 2019; Petäjä et al., 2019). Similar approach was applied in Nanjing mega-city in China, within a Vaisala-lead project Nanjing Air Quality Testbed (NAQT) with FMI, Nanjing University and other Chinese partners. This work is expanded further with a dense network of portable and stationary low-cost sensors within the Healthy Outdoor Premises for Everybody project (HOPE). In these projects, we derived proxies for new air quality parameters, such as black carbon (BC), particle number concentration (N), lung deposited surface area (LDSA) and atmospheric oxidative capacity in terms of sulphuric and nitric acid concentrations. These parameters were measured at the research station and/or authority network stations, and the proxies were

derived with parameters that are detected with complementary and/or low-cost sensor network. This makes it possible to estimate the new air quality parameters also with the high resolution data from FMI-ENFUSER. The derivation of the proxies during the HAQT project was described by Paasonen et al. (2019) and proxy derivation within the HOPE project by Fung et al. (*abstract in this collection*), who also used multiple conditional mean imputation with simple BC proxy to fill in the missing air quality data.

The urban air quality work described above is conceptualized and presented to different stakeholders in projects like MegaSense (<https://www.helsinki.fi/en/researchgroups/sensing-and-analytics-of-air-quality>) and SMURBS (Smart Urban Solutions for air quality, disasters and city growth; smurbs.eu).

ACKNOWLEDGEMENTS

Our work is supported by Academy of Finland (grant numbers 307331 and 316114) and European Research Council (ATM-GTP; grant number 742206), EU Urban Innovative Actions via HOPE project (grant number UIA03-240), EC project SMURBS (grant number 689443) under ERA-PLANET H2020SC5-15-2015, Doctoral Programme in Atmospheric Sciences (ATM-DP) at the University of Helsinki, Swiss National Science postdoc mobility grant (P2EZP2_181599), the National Key R&D Program of China (2017YFC0209503, 2017YFC0209505 & 2017YFC0210003), the National Science Foundation of China (21876094) and the National Natural Science Foundation of China (91644213, 41730106, 41505133 & 41775162), National research program for key issues in air pollution control (DQGG0101), the program of China Scholarships Council, the Regional innovations and experimentations funds AIKO, governed by the Helsinki-Uusimaa Regional Council (project HAQT, AIKO014) and Business Finland – Vaisala project NAQT (Business Finland diary number 4109/31/2017).

REFERENCES

- Hakala, S., Alghamdi, M. A., Paasonen, P., Vakkari, V., Khoder, M. I., Neitola, K., Dada, L., Abdelmaksoud, A. S., Al-Jeelani, H., Shabbaj, I. I., Almeahmadi, F. M., Sundström, A.-M., Lihavainen, H., Kerminen, V.-M., Kontkanen, J., Kulmala, M., Hussein, T. and Hyvärinen, A.-P. (2019). New particle formation, growth and apparent shrinkage at a rural background site in western Saudi Arabia, *Atmos. Chem. Phys.*, **19**, 10537–10555.
- Johansson, L. (2019). Impact and benefit of HAQT network on ENFUSER AQ modelling system, **Deliverable 3-2** for HAQT – Helsinki metropolitan Air Quality Testbed -project.
- Kulmala, M., Kerminen, V. M., Petäjä, T., Ding, A. J. and Wang, L. (2017). Atmospheric Gas-to-Particle Conversion: why NPF events are observed in megacities, *Faraday Discuss.*, **200**, 271-288.
- Liu, J., Wang, L., Li, M., Liao, Z., Sun, Y., Song, T., Gao, W., Wang, Y., Li, Y., Ji, D., Hu, B., Kerminen, V.-M., Wang, Y., and Kulmala, M. (2019). Quantifying the impact of synoptic circulations on ozone variations in North China from April–October 2013–2017, *Atmos. Chem. Phys. Discuss.*, in review.
- Paasonen, P., Timonen, H., Saukko, E., Laakso, M., Shahriyer, A., Kangasluoma, J., Luoma, K., Kuula, J., Niemi, J.V. and Petäjä, T. (2019). Recommendations for new AQ observations to improve AQ situational awareness, **Deliverable 4-2** for HAQT – Helsinki metropolitan Air Quality Testbed -project.
- Petäjä, T., Paasonen, P., Timonen, H., Laakso, M., Saukko, E., Niemi, J.V. (2019). AQ network utilization roadmap based on HAQT results, **Deliverable 6-1** for HAQT – Helsinki metropolitan Air Quality Testbed -project.
- Tunved, P., H.-C. Hansson, V.-M. Kerminen, J. Ström, M. Dal Maso, H. Lihavainen, Y. Viisanen, P. P. Aalto, M. Komppula and M. Kulmala (2006). High Natural Aerosol Loading over Boreal Forests, *Science*, **312**, 261-263.
- Wang, L., M. Li, J. Liu, W. Gao, T. Song, Y. Sun, L. Li, X. Li, Y. Wang, L. Liu, K. Dällenbach, P. Paasonen, V.-M. Kerminen, M. Kulmala and Y. Wang (2019). Exploring the regional pollution characteristics and meteorological formation mechanism of PM_{2.5} in North China during 2013-2017, *Env. Int.*, **2382**.

BIOGEOCHEMISTRY RESEARCH GROUP / FC₀E TEAM ABSTRACT

JUKKA PUMPANEN¹, HEIDI AALTONEN², FRANK BERNINGER¹, HEM RAJ BHATTARAJ¹, CHRISTINA BIASI¹, KAJAR KÖSTER², EGLE KÖSTER², MAIJA MARUSHCHAK³, MARJA MALJANEN¹, MARJO PALVIAINEN², HANNU NYKÄNEN¹, HENRI SILJANEN¹, NARASINHA SHURPALI¹, CAROLINA VOIGT⁴, HUIZHONG ZHANG-TURPEINEN¹ AND XUAN ZHOU²,

¹Department of Environmental and Biological Sciences, University of Eastern Finland, P.O. Box 1627, FI-70211 Kuopio, Finland

²Department of Forest Sciences, P.O. Box 27, FI-00014 University of Helsinki, FINLAND

³Department of Biological and Environmental Science, University of Jyväskylä, Jyväskylä, Finland

⁴Department of Geography, University of Montréal, Montréal, Québec, Canada

Keywords: GREENHOUSE GASES, NITROUS ACID, PERMAFROST, PEATLANDS

INTRODUCTION

The research activities of the biogeochemistry (BGC) group of the University of Eastern Finland have focused in 2019 on the processes underlying carbon dioxide (CO₂), nitrous oxide (N₂O), nitric acid (HONO), biogenic volatile organic compounds (BVOCs) as well as methane (CH₄) fluxes between the soil and the atmosphere. All of these gases are closely associated with the atmospheric chemistry. CO₂, N₂O and CH₄ affect climate by directly contributing to the radiation balance of the atmosphere while the reactive gases contribute to the formation of secondary organic aerosols (SOA), which act as cloud condensation nuclei (CCN) thus increasing the formation of clouds.

The formation and consumption of these gases are related to changes in vegetation and soil which the BGC group is investigating in several ongoing projects funded by the Academy of Finland including for example; “Ammonia oxidizing microbes and factors regulating their occurrence and activity in acidic boreal and Arctic peat soils (AMOBORA), PI Henri Siljanen”, “The origin of nitrous acid (HONO) emissions from northern soils and linkages to nitrogen cycle processes, PI Marja Maljanen”, and “Methane and algae trough zooplankton to valuable food, PI Hannu Nykänen” and “Long term effects of fire on carbon and nitrogen pools and fluxes in the arctic permafrost and subarctic forests (ARCTICFIRE), PI Jukka Pumpanen and “Constraining uncertainties in the permafrost-climate feedback / Consortium: COUP, PI Christina Biasi”. Here, we present the most important findings of the projects carried out in the BGC group from the last year 2018-2019.

HONO-project

Tropospheric removal of pollutants initiated by the hydroxyl radical (OH) is a key process in atmospheric chemistry. In the lower atmosphere, OH production is linked to photolysis of nitrous acid (HONO), and it has been suggested that soil contributes strongly to the production of atmospheric HONO. However, factors controlling HONO production in soils are poorly known. Bhattaraj et al. (2019) reported for the first time that HONO production in agricultural soil could be related to the germination and early development of wheat, one of the most important agricultural crops in the world. They observed that the release of Nitrite (NO₂⁻) released from the germinating seeds increased the HONO production. Given the significant area of agricultural lands globally, the emission of HONO from initial growth phase of wheat should be considered as a mechanism contributing to the OH production in the atmosphere.

Source: Bhattaraj H.R. et al. 2019. Germinating wheat promotes the emission of atmospherically significant nitrous acid (HONO) gas from soils. *Soil Biology and Biochemistry* 136: 107518

AMOBORA-project

Bare peat surfaces created by frost action and wind erosion in permafrost peatlands have been shown to emit high amounts of nitrous oxide (N₂O), the third most significant greenhouse gas (GHG) warming the atmosphere. With global warming, emissions of N₂O are expected to increase in Arctic permafrost peatlands. Siljanen et al. (2019) investigated nitrification, ammonia (NH₄) oxidizer populations and N₂O production in vegetated and bare peat soils from four distant Arctic geographic locations. They showed through a combination of molecular analyses and group-specific inhibitor assays that NH₄ oxidation, the first step in nitrification, is mainly performed by ammonia-oxidizing archaea (AOA). The results indicated that high N₂O emissions from these ecosystems are mostly resulting from nitrification mediated by very few archaeal species. The arctic peat soils in this study were the first natural environments where high N₂O emissions have been linked to AOA. Any changes in archaeal nitrification induced by global warming will therefore impact on N₂O emissions from the permafrost peatlands.

Source: Siljanen H. et al. 2019. Archaeal nitrification is a key driver of high nitrous oxide emissions from arctic peatlands. *Soil Biology and Biogeochemistry*. 137:107539

METHANE-project

The sediments of small boreal humic lakes are important carbon stores and GHG sources. However, the composition and structuring mechanisms of their microbial communities are not well known. Rissanen et al. 2019 analyzed the vertical profiles of microbial biomass and the bacterial and archaeal community composition in sediments of a small boreal lake. The results showed that even though microbial biomass decreased with sediment depth, viable microbes were present throughout the sediment profiles. The vertical stratification patterns of the bacterial and archaeal communities resembled those in marine sediments with well-characterized groups (e.g. *Methanomicrobia*, *Proteobacteria*, *Cyanobacteria*, *Bacteroidetes*) dominating in the surface sediment and being replaced by poorly-known groups (e.g. *Bathyarchaeota*, *Aminicenantes* and *Caldiserica*) in the deeper layers. The results also suggested that, similar to marine systems, the deep bacterial and archaeal communities were consisting of species that are able to tolerate low energy conditions. Methanotrophs were rare indicating that these sediments rich in methane are important methane emitters.

Source: Rissanen et al. 2019. Vertical stratification of bacteria and archaea in sediments of a small boreal humic lake. *FEMS Microbiology Letters* 366(5): 1-11.

ARCTICFIRE-project

About 24%, 23 million km², of the land area in the Northern Hemisphere, including most of the boreal forests, is underlain by permafrost. About 1% of boreal forests are exposed to fire annually, which affects the soil and permafrost under them. Thawing of permafrost increases the depth of the active layer containing large amounts of organic matter which decomposition could release GHGs and other atmospherically important gases including Biogenic Volatile Organic Compounds (BVOCs). Zhang-Turpeinen et al. 2019, studied in the recent paper long-term effects of wildfire on forest floor BVOC emission rates along a wildfire chronosequence in a *Larix gmelinii* forest in central Siberia. The forest floor was a source of BVOCs in all forest age classes but the BVOC emissions were lower in the recently burnt forests and the emissions increased along with forest succession. Fire-induced permafrost thawing and subsequent increase in soil organic matter exposed to decomposition did not increase BVOC emissions. The results indicated that the potential increase in the frequency of forest fires as a result of climate warming may affect the BVOC emissions from boreal forest floor.

In the same project, the effect of forest fires on permafrost soils were characterized using soil organic matter (SOM) chemical fractionation and incubation experiments to reveal the effects on SOM quality and decomposition (Aaltonen et al. 2019a,b). The chemical fractionation showed that the effect of fire on SOM

quality in upland forest soils with underlying permafrost was restricted to the first 5-10 cm of the soil surface while no changes in SOM quality were observed in deeper soil. However, fire decreased the SOM quality and increased the temperature sensitivity of decomposition. Further, when the effects of fire on microbial community were studied from the same soils (Zhou et al. 2019), we observed that fires changed the microbial population structure and increased the relative abundances of genes associated C degradation and anammox metabolic processes, resulting in those fire-affected bacteria acted as C and N decomposers. Overall, wildfires affected the GHG and BVOC fluxes between the forest floor and the atmosphere, and the changes in GHG fluxes and soil were transient and recovered to the pre-fire levels during the time >100 years time frame of our study.

Sources: Aaltonen H. et al. 2019. Forest fires in Canadian permafrost region: the combined effects of fire and permafrost dynamics on soil organic matter quality. *Biogeochemistry*. <https://doi.org/10.1007/s10533-019-00560-x>.

Aaltonen H. et al. 2019. Temperature sensitivity of soil organic matter decomposition after forest fire in Canadian permafrost region. *Journal of Environmental Management*. <https://doi.org/10.1016/j.jenvman.2019.02.130>.

Zhang-Turpeinen H., et al. 2019 Wildfire effects on BVOC emissions from boreal forest floor on permafrost soil in Siberia. *Science of the Total Environment*. Accepted.

Zhou X. et al. 2019. The impact of wildfire on microbial C:N:P stoichiometry and the fungal-to-bacterial ratio in permafrost soil. *Biogeochemistry*. <https://doi.org/10.1007/s10533-018-0510-6>.

COUP and DEFROST-project

Permafrost peatlands are biogeochemical hot spots in the Arctic due to their large carbon stocks. The thawing of permafrost could expose part of these old carbon stocks to decomposition releasing GHGs but it is highly uncertain how much and at which time span GHGs will be released. Voigt et al. 2019 used a novel experimental approach using intact mesocosms to simulate permafrost thaw and measured the GHG production and consumption in the peat columns with chamber measurements and soil GHG concentration profile measurements as well as radiocarbon (¹⁴C) dating. The measurements showed sustained decomposition and GHG production from permafrost but the oxidation of CH₄ in the peat column prevented the CH₄ release to the atmosphere. Under dry conditions, peatlands strengthen the permafrost-carbon feedback by adding CO₂ fluxes but at the same time they showed a strong CH₄ sink capacity which potentially compensates part of the permafrost CO₂ losses over long time scales.

Source: Voigt et al. 2019. Ecosystem carbon response of an Arctic peatland to simulated permafrost thaw. *Global Change Biology* 25: 1746-1764.

INDO-NORDEN Project

As a part of this project, two review papers on biofuel production from biomass and agricultural residues are published in high impact journals. Brief conclusions from one of these review are given below.

The bioethanol production technologies are close to full maturity for the thermochemical biofuels and in early commercial prototype phase for bioethanol production. Nevertheless, further research and development is needed for the thermochemical biofuels on the material selection for different parts in production and instrumentation to make them more resistant to harsh process conditions. Also, extensive research has been carried out to make different bioethanol process steps more efficient – development of various pre-treatment methods, enzyme development for enhanced hydrolysis, re-research for more tolerant yeasts capable of fermenting different sugars. Value addition and perspective, cost saving measures can be achieved with the application of different combined processing technologies such as SSF, SSCF and CBP

and by using residues from bioethanol process to produce additional products like bio-chemicals, fertilizer, heat and energy by applying integrated biorefinery approach.

Source: M.Raud, T.Kikas, O.Sippula, and N.J.Shurpali. Potentials and challenges in lignocellulosic biofuel production technology. *Renewable and Sustainable Energy Reviews* Volume 111, September 2019, Pages 44-56

CAPTURE Project

As a part of this project, Narasinha Shurpali was invited to be a part of the FLUXNET CH₄ synthesis activity. The coordination activity and some basic synthesis results were published in a paper. Here is a brief overview of the synthesis activity.

This paper describes the formation of, and initial results for, a new FLUXNET coordination network for ecosystem-scale methane (CH₄) measurements at 60 sites globally, organized by the Global Carbon Project in partnership with other initiatives and regional flux tower networks. The objectives of the effort are presented along with an overview of the coverage of eddy covariance (EC) CH₄ flux measurements globally, initial results comparing CH₄ fluxes across the sites, and future research directions and needs. Annual estimates of net CH₄ fluxes across sites ranged from $-0.2 \pm 0.02 \text{ g C m}^{-2} \text{ y}^{-1}$ for an upland forest site to $114.9 \pm 13.4 \text{ g C m}^{-2} \text{ y}^{-1}$ for an estuarine freshwater marsh, with fluxes exceeding $40 \text{ g C m}^{-2} \text{ y}^{-1}$ at multiple sites. Average annual soil and air temperatures were found to be the strongest predictor of annual CH₄ flux across wetland sites globally. Water table position was positively correlated with annual CH₄ emissions, although only for wetland sites that were not consistently inundated throughout the year. The ratio of annual CH₄ fluxes to ecosystem respiration increased significantly with mean site temperature. Uncertainties in annual CH₄ estimates due to gap filling and random errors were on average $\pm 1.6 \text{ g C m}^{-2} \text{ y}^{-1}$ at 95% confidence, with the relative error decreasing exponentially with increasing flux magnitude across sites. Through the analysis and synthesis of a growing EC CH₄ flux database, the controls on ecosystem CH₄ fluxes can be better understood, used to inform and validate Earth system models, and reconcile differences between land-surface model- and atmospheric-based estimates of CH₄ emissions.

Source: Knox et al., FLUXNET-CH₄ Synthesis Activity: Objectives, Observations, and Future Directions. 2019. *Bulletin of the American Meteorological Society*. Online journal. <https://doi.org/10.1175/BAMS-D-18-0268.1>

REFERENCES:

Aaltonen H., Köster K., Köster E., Berninger F., Zhou X., Karhu K., Biasi C., Bruckman V., Palviainen M. and Pumpanen J. 2019. Forest fires in Canadian permafrost region: the combined effects of fire and permafrost dynamics on soil organic matter quality. *Biogeochemistry*. <https://doi.org/10.1007/s10533-019-00560-x>.

Aaltonen H., Zhou X., Köster E., Berninger F., Pumpanen J. and Köster K. 2019. Temperature sensitivity of soil organic matter decomposition after forest fire in Canadian permafrost region. *Journal of Environmental Management*. <https://doi.org/10.1016/j.jenvman.2019.02.130>.

Bhattarai H.R., Liimatainen M., Nykänen H., Kivimäenpää M., Martikainen P.J. and Maljanen M. 2019. Germinating wheat promotes the emission of atmospherically significant nitrous acid (HONO) gas from soils. *Soil Biology and Biochemistry* 136: 107518

Knox et al., FLUXNET-CH₄ Synthesis Activity: Objectives, Observations, and Future Directions. 2019. *Bulletin of the American Meteorological Society*. Online journal. <https://doi.org/10.1175/BAMS-D-18-0268.1>

Raud M., Kikas T., Sippula O., and Shurpali. N.J. 2019. Potentials and challenges in lignocellulosic biofuel production technology. *Renewable and Sustainable Energy Reviews* Volume 111: 44-56

Rissanen A.J., Peura S., Mpamah P.A., Taipale S., Tirola M., Biasi C., Mäki A., Nykänen H. et al. 2019. Vertical stratification of bacteria and archaea in sediments of a small boreal humic lake. *FEMS Microbiology Letters* 366(5): 1-11

Siljanen H.M.P., Alves R.J.E., Ronkainen J.G., Lamprecht R.E., Bhattarai H.M., Bagnound A., Marushchak M.E., Martikainen P.J., Schleper C. and Biasi C. 2019. Archaeal nitrification is a key driver of high nitrous oxide emissions from arctic peatlands. *Soil Biology and Biogeochemistry* 137:107539

Zhang-Turpeinen H., Kivimäenpää M., Aaltonen H., Berninger F., Köster E., Köster K., Menyailo O., Prokushkin A., and Pumpanen J. 2019. Wildfire effects on BVOC emissions from boreal forest floor on permafrost soil in Siberia. *Science of the Total Environment*. Accepted.

Zhou X., Sun H., Pumpanen J., Sietiö O.-M., Heinonsalo J., Köster K. and Berninger F. 2019. The impact of wildfire on microbial C:N:P stoichiometry and the fungal-to-bacterial ratio in permafrost soil. *Biogeochemistry*. <https://doi.org/10.1007/s10533-018-0510-6>.

Voigt C., Marushchak M.E., Mastepanov M., Lamprecht R.E., Christensen T.R., Dorodnikov M., Jackowicz-Korczynski, Lindgren A., Lohila A., Nykänen H., Oinonen M., Oksanen T., Palonen V., Treat C.C., Martikainen P.J. and Biasi C. 2019. Ecosystem carbon response of an Arctic peatland to simulated permafrost thaw. *Global Change Biology* 25: 1746-1764.

ACKNOWLEDGEMENTS

We acknowledge the funding support from The Centre of Excellence in Atmospheric Science - From Molecular and Biological processes to The Global Climate. We also acknowledge the Academy of Finland projects no. 286685, 290315, 297735, 140964, 291691.

ELTER RI DRIVES ECOSYSTEM RESEARCH FORWARD IN EUROPE

T. RASILO¹, M. KAUKOLEHTO², M. MIRTL² and J. BÄCK¹

¹INAR/Forest sciences, University of Helsinki,
P.O. Box 27, 00014 University of Helsinki, Finland.

²Helmholtz Centre for environmental Research GmbH – UFZ,
Permoserstraße 15, 04318 Leipzig, Germany.

Keywords: Ecosystem research, Research Infrastructures, eLTER.

INTRODUCTION

Research infrastructures (RIs) are supported in European Union under the ESFRI (European Strategy Forum for Research Infrastructures) concept. The ESFRI produces a RI roadmap which has been updated last time in 2018. In the 2018 update, one of the new Roadmap infrastructures was eLTER (European Long-Term Ecosystem, Critical Zone and Socio-ecological Research Infrastructure), which was supported by 18 (CHECK) ministries (Expression of Support) and 162 research institutions (Memorandum of Understanding). The pan-European eLTER RI will this enter a new phase where its future services and structure will be defined over the next 10 years.

As a next step, the EU Commission approved significant funding for the eLTER for the period of 2020-2024. The two projects, eLTER PPP and eLTER PLUS, got altogether 14 million euros from the EU for developing and building eLTER RI. The overall purpose of the eLTER RI is to provide a pan-European integrated research infrastructure of long-term research sites for use in the fields of ecosystem, critical zone and socio-ecological research. With this, eLTER aims to secure and strengthen scientific excellence through the highest quality interoperable services in close interaction with related European and global research infrastructures.

SCIENTIFIC BACKGROUND

The world faces many Grand Challenges, identified in the EU's 7th Environment Action Programme (e.g., Steffen *et al.*, 2015), including those posed by climate change, biodiversity loss, and water and soil pollution. These multiple stressors act simultaneously over a range of temporal and spatial scales, resulting in significant loss of ecosystem services that eventually affect societal well-being and humanity. While immediate impacts sometimes receive considerable attention, little is known about their long-term and systemic effects and cross-scale interactions. Closing these knowledge gaps requires an improved, transdisciplinary understanding of the multifaceted environmental system, in order to develop appropriate mitigation measures. This is the fundamental justification for the eLTER RI.

The design of eLTER RI addresses the scientific challenges with a unique Whole System Approach, which combines two conceptual frameworks, applicable from plot to landscape scale (Figure 1). These frameworks are the Press Pulse Dynamic Model as horizontal component (Collins *et al.*, 2011) and the spatially-nested hierarchical feedback paradigm of Macrosystems Ecology as a vertical component (Heffernan *et al.*, 2014).

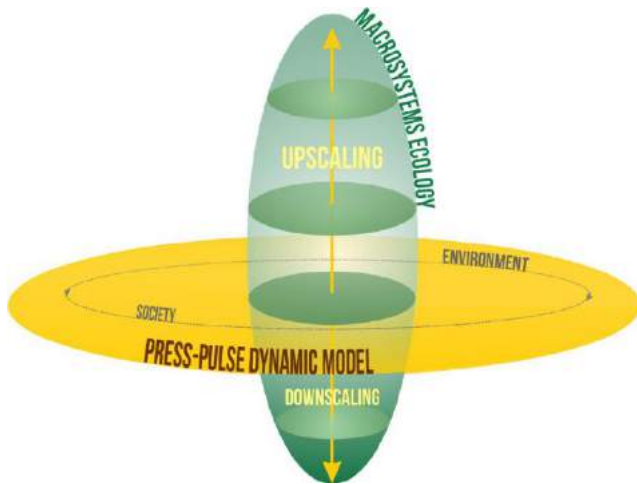


Figure 1. The conceptual framework of eLTER's Whole System Approach combining Macrosystems Ecology and the Press-Pulse Dynamic model (PPD) to facilitate a holistic approach to ecosystems and socio-ecological research. The macrosystems ecology frame emphasises the importance of nested hierarchical research and dependence of ecological phenomenon at a given scale on dynamics occurring at larger or smaller spatial scales (Pulliam and Johnson, 2002). The PPD model provides a framework for understanding interactions and feedbacks between socio-economic systems and biophysical systems over time.

The eLTER Whole System Approach encompasses the Earth system and related disciplines from geosphere to the hydrosphere, and from biosphere and socio-econosphere to atmosphere. This will allow strong links to other European environmental RIs.

DESIGN OF eLTER RI

eLTER RI will be a distributed infrastructure and comprise of National Research Infrastructures, i.e., sites of different categories, and European level Central Services. The sites and eLTSER Platforms form the *in situ* backbone of eLTER RI through which eLTER will implement the Whole System research. At each eLTER *in-situ* facility, all major system components are covered by eLTER Standard Observations. The planned categories range from fully instrumented eLTER Master Sites to Regular Sites covering major ecosystem processes and finally to Satellite Sites for specific purposes (these might be less equipped or extensive, but serve special purposes such as increasing coverage, enabling upscaling or monitoring larger scale processes). In addition, eLTSER Platforms have largest spatial extend and focus on investigating human society - environment interactions in the long term. Thus, they act as regional anchoring points for integrated, policy-relevant natural scientific and socio-ecological system research. eLTER Sites and eLTSER Platforms are built on existing LTER Europe network of over 400 sites. The aim is gradually increase the number of sites and platforms up to 250 sites.

Central Services of eLTER RI are expected be Head Office, Service Portal and thematic Topic Centres. They will providing coordination, strategic development and outreach of the whole RI (Head Office) as well as access to sites and data (Service Portal). The Topic Centres are designed to ensure the support of the science case, integrate the different elements and function of the RI and provide focus for the outreach and interoperability with related RIs and research communities. According the current plan, they will focus on technological development, capacity building and data processing.

THE NEW eLTER PROJECTS

The design will be complemented and implementation started with the two new projects, eLTER PPP and eLTER PLUS, funded by European Commission. Both projects will start in February 2020 and last for five years.

The main aim of the Preparatory Phase project, eLTER PPP, is to prepare for implementation and operation of eLTER RI. Thus, the project will further the operational, technical and strategic development at the existing sites in Europe to meet the current challenges of global change with holistic, systemic observations and analysis of environmental trends. Harmonized methods and research approaches will be designed, access to data will be facilitated and a wide range of user groups, from research to policy, will receive comprehensive support. eLTER PPP is coordinated by the Helmholtz-Centre for Environmental Research (UFZ) in Germany. There is 27 institutions from 24 countries participating eLTER PPP (Table 1).

The University of Helsinki in Finland will coordinate the Advanced Community project, eLTER PLUS. The main aim of eLTER PLUS is to further open and expand the network, engage current and new users from both academia and industry, offer an excellent training site for students to enhance their international contacts, and further integrate the operations of advanced cross-disciplinary and transdisciplinary research as reflected by the eLTER Sites and eLTER Platforms experimental design and Standard Observation framework. This Advanced Community Project will conduct a performance test of the emerging eLTER RI, challenging, assessing and strengthening its operations. Selected sites and platforms in terrestrial, freshwater and coastal ecosystems will be used to study ecosystem integrity, impacts of climate change, and endangered ecosystem services at a pan-European scale. In eLTER PLUS, there are 32 participants from 23 countries (Table 1).

Country	Participant	eLTER PPP	eLTER PLUS
FI	University of Helsinki	x	x
FI	Finnish Environmental Institute	-	x
FI	CSC IT Center for Science Ltd.	-	x
AU	Environmental Agency Austria	x	x
AU	University of Natural Resources and life sciences	-	x
BE	Research Institute Nature and Forest	x	x
BG	Pensoft Publishers	x	x
BG	The Institute of Biodiversity and Ecosystem Research	x	x
CH	Swiss Federal Research Institute WSL	x	x
CZ	Global Change Research Institute	x	x
DK	University of Copenhagen	x	x
ES	Spanish National Research Council	x	x
FR	National Centre for Scientific Research	x	x
GE	Helmholtz Centre for Environmental Research GmbH – UFZ	x	x
GE	Forschungszentrum Jülich GmbH	-	x
GE	Senckenberg Gesellschaft für Naturforschung	x	x
GR	Technical University of Crete	x	x
HU	Centre for Ecological Research of the Hungarian Academy of Sciences	x	x
IL	Ben-Gurion University of Negev	x	x
IL	Israel Institute of Technology	x	x
IT	National Research Council of Italy	x	x
IT	University of Milan	-	x
LV	University of Latvia	x	x
NL	Sovon Dutch Centre for Field Ornithology	x	-
PO	European Regional Centre for Ecohydrology of the Polish Academy of Sciences	x	x
PT	Research Centre in Biodiversity and Genetic Resources	-	x
PT	FCiências.ID – Associação para a Investigação e Desenvolvimento de Ciências	x	x
RO	University of Bukarest	x	x
RS	BioSense Institute	x	x
SE	Swedish University of Agricultural Sciences	x	x
SI	Research Centre of the Slovenian Academy of Sciences and Arts	x	x

SK	Institute of Landscape Ecology of the Slovak Academy of Sciences	x	x
UK	UK Centre for Ecology and Hydrology	x	x

Table 1. Partners participating eLTER PPP and eLTER PLUS.

MISSION OF eLTER

eLTER RI will fill the critical gap for top-class in answering grand challenges related to biodiversity loss and land use change, climate change and greenhouse gases and to eutrophication and pollution, especially reactive nitrogen in the environment at continental scale. It will offer access to integrated research sites and their local expert teams. Easy access to long-term data as well as data products, models and analysis tools are also important outcomes of eLTER RI. In addition it can provide support for ground-truthing and remote sensing service development and for development of new observation technologies and approaches. eLTER RI will also contribute to the scientific community through education and training programs and by supporting research project design. Overall, eLTER RI will provide information on the state of European ecosystems and impacts of pressures to support policy makers at continental and local level.

ACKNOWLEDGEMENTS

eLTER PPP and eLTER PLUS projects will be supported by European commission. The work so far has been supported by European Commission (projects eLTER H2020, Advance_eLTER), by Academy of Finland (Centre of Excellence in Atmospheric Sciences) and by Faculty of Agriculture and Forestry of University of Helsinki.

REFERENCES

- Collins, S., et al (2011). An Integrated Conceptual Framework for Social Ecological Research. *Frontiers in Ecology and the Environment* 9, 351–357.
- Heffernan J.B., et al (2014). Macrosystems ecology: understanding ecological patterns and processes at continental scales. *Frontiers in Ecology and the Environment* 12, 5–14.
- Pulliam, H. R. and Johnson, B. R., (2002). Ecology's New Paradigm: What Does It Offer Designers and Planners?, in: Johnson, B. R. & Hill, K. (eds.) *Ecology and Design: Frameworks for Learning*. (Island Press, Washington) pp. 51-84.
- Steffen, W., et al. (2015). Planetary boundaries: Guiding human development on a changing planet. *Science* 347, 1259855.

RECENT DEVELOPMENTS IN THE ANALYSIS OF OUTDOOR AND INDOOR AIR

M.-L. RIEKKOLA^{1,2}, K. HARTONEN^{1,2}, J. RUIZ-JIMENEZ^{1,2}, H. LAN^{1,2}, M. JUSSILA¹, N. ZANCA^{1,2}, S. BARUA¹, G. DEMARIA¹, E. ZAGATTI¹, T. LIANGSUPREE¹, Y. LELEEV¹, M. SALKINOJA-SALONEN¹, AND H. M. M. SIREN¹

¹ University of Helsinki, Department of Chemistry, P.O. Box 55, 00014 University of Helsinki, Finland.

² Institute for Atmospheric and Earth System Research, P.O. Box 55, 00014 University of Helsinki, Finland.

Keywords: MINIATURIZED AIR SAMPLING, MATERIALS, AERIAL DRONE, BIOAEROSOLS.

INTRODUCTION

Microextraction techniques, solid phase microextraction (SPME) Arrow and in-tube extraction (ITEX), have been utilized for outdoor and indoor air sampling. They are very suitable for on-site sampling of air samples (for example as sampling tools of aerial drone) due to their small size, simplicity and compatibility with the chromatographic analysis techniques [Ruiz-Jimenez et al. 2019, Lan, Zhang et al. 2019]. An appropriate material used as sorbents in sampling devices can ensure favorable interactions between the material and analytes resulting in the highest possible sensitivity. However, depending on the application purposes, from selective extraction of target compounds from a complex matrix to universal screening of organic compounds in atmospheric air, specific or non-specific materials can be employed. Due to the limited number of commercial sorbent material options, new selective and non-selective materials are needed to ensure e.g. the best sorption capacity, physical and chemical stability [Lan et al. 2019]. Passive sampling of gaseous air can be done with SPME Arrow and active (dynamic) sampling with exhaustive ITEX technique, from which the latter is more suitable for quantitative work [Lan, Holopainen et al. 2019]. Different small accessories can be attached to the sampling system before ITEX to remove unwanted components (water, ozone, particles, etc.). These miniaturized sampling tools are also applicable for indoor air quality studies to reveal, for example, chemistry behind the health problems faced in 'sick' houses. For very low volatile and polar compounds, a cryogenic sampling is then preferred.

Primary biological aerosol particles (PBAPs), defined as solid particles derived from biological organisms, have most probably an important impact on aerosol-climate interactions, but their role in the earth system includes still high uncertainties. The chemical composition of PBAPs in aerosol particles can be studied by collecting them onto filters followed by liquid chromatography – mass spectrometry (HPLC-MS). Together with their DNA concentration and microorganism-DNA data, further information can be obtained about their abundances in different particle size fractions at the boreal forest region, helping to understand better their biosphere-atmosphere interactions [Okuljar et al. 2019].

METHODS

SPME Arrow and ITEX were used and developed for miniaturized air sampling. Ordered mesoporous silica (OMS) materials with various pore sizes and pore-channel structures were prepared via hydrolytic sol-gel process and surface grafting approach. SPME Arrows were coated with these materials by dipping method. For ITEX, organic and inorganic nanofibers, prepared by electrospinning and electroblowing, were applied as the packing materials.

A remote controlled drone (Geodrone X4L, Videodrone, Finland) was equipped with a sampling box, which allowed simultaneous sampling of outdoor air with multiple ITEX and SPME Arrow systems that could be remotely operated. The weight of sampling box with the pump was about 1.4 kg, which allowed a total flight time of 35 min. The applicability of aerial drone as platform for miniaturized air sampling systems was evaluated in three different campaigns. The first two campaigns took place at the SMEAR II station in

Hyytiälä, the first from the 22nd to 26th of October 2018, and the second from the 1st to 12th of July 2019. The third measurements were carried out at Qvidja site (60°17'42.6"N 22°23'32.3"E) at Parainen from the 24th of July 2019 to the 10th of September 2019.

Indoor air of 'sick' houses from Nummela and Vantaa were studied together with the insulation materials used in these buildings. Samples of condensed/frost water of the air were collected with e-collector (cryogenic sampler). SPME Arrow and ITEX were also applied to collect gas phase compounds in indoor air and from insulation materials. Commercial PDMS-DVB and Carbon WR were used here as sorbents for the SPME Arrow. ITEX was packed with laboratory-made polyacrylonitrile (PAN) fibers.

For bioaerosol study, samples were collected at SMEAR II station in autumn 2017 using a Dekati PM10 impactor for the sampling of four particle size fractions (< 1.0, 1–2.5 μm , 2.5–10 μm and > 10 μm). After ultrasound-assisted extraction, HPLC - electrospray ionization (ESI) - triple quadrupole mass spectrometer (QQ-MS) was employed for the determination of free saccharides and amino acids. Total nucleic acids were extracted from the filters with a commercial DNA extraction kit. The bacterial and fungal DNA amounts in the filter samples were quantified with qPCR.

CONCLUSIONS

Outdoor air samples: For SPME Arrow, acid treated OMS materials decreased the pore size and reduced the sample capacity, while the selectivity was increased. OMS with small pore size and 2D channels restricted the water molecules more effectively. [Lan, Zhang et al., 2019] Polyacrylonitrile (PAN)-ITEX exhibited the highest extraction affinity to alcohols, aldehydes, and ketones because of rich amine and imide groups on the surface of the PAN nanofibers. ITEXs packed with inorganic nanofibers were selective with small sample capacity due to their physical and chemical surface structures, e.g. inaccessible pore size and weak functional groups. [Lan, Holopainen et al., 2019]

By using ITEX packed with PAN fibers, fully automated continuous sampling was established and the system was on-line connected to gas chromatography – mass spectrometry (GC/MS) for automated desorption and quantitative analysis [Lan, Holopainen et al. 2019]. Packed ITEX was durable and could withstand over 1500 sampling and desorption cycles. The performance of the automated dynamic ITEX-GC/MS system was proved by two successful long time campaign for unattended outdoor air analysis in Kumpula Campus, Helsinki. Typical air sample chromatogram obtained with this system is shown in Figure 1.

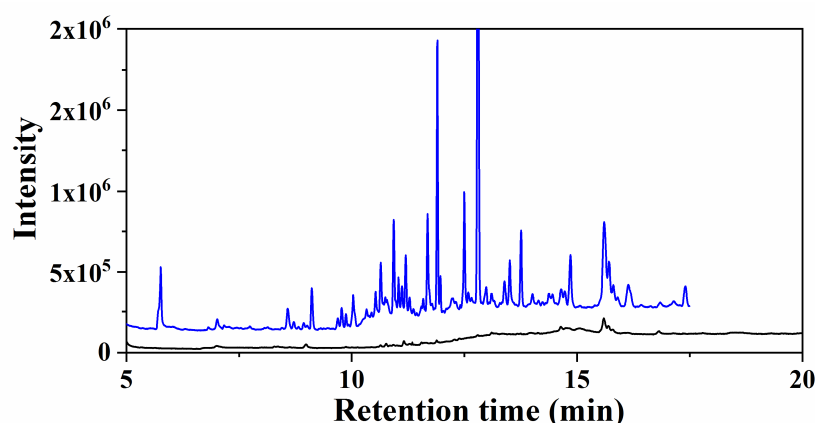


Figure 1. GC-MS chromatograms with the automated dynamic PAN-ITEX-GC/MS system. Blue line means the chromatogram of 2 hours air sampling (200 mL min⁻¹ flow rate, sampling volume 24 L) and the black line is the background chromatogram of ITEX system.

The microextraction sampling tools (SPME Arrow and ITEX) proved to be excellent for aerial drone. [Ruiz-Jimenez, Zanca, Lan et al., 2019] Their remote operation was smooth and reliable. Different accessories to remove particles, water and ozone before ITEX were functioning well. Drone sampling could easily be made in places with difficult access and at different altitudes to get vertical concentration profiles in addition to horizontal ones. A proper quality assurance/quality control (QA/QC), was developed to ensure reliable and quantitative results. By using the internal standard addition, the reproducibility of Arrow-to-Arrow and ITEX-to-ITEX was clearly improved.

Indoor air samples: Many more chemical compounds were found from indoor air of ‘sick’ houses in Nummela and in Vantaa compared to healthy reference house in Tampere. Amounts were highest in Vantaa house. Highly polar (not much retention in reversed phase column) and high molecular mass compounds were found to be present in Vantaa house when samples were analyzed with HPLC-QqQ-MS. Samples collected from Vantaa house included also more compounds with molecular mass higher than 800. [Ruiz-Jimenez, Zanca, Barua et al., 2019]

Water (moisture) had a great effect on the number of compounds and on their amounts emitted from the insulation materials. Higher number of compounds were emitted from the cellulose wool compared to glass wool. These compounds were mostly of low volatility (most likely more polar and more water soluble). Increase of the amount of water further enhanced this effect. Many of the compounds increased their intensity with water amount and a few compounds behaved completely in an opposite way. This proved that at the high moisture conditions, insulation materials produce more chemicals to indoor air, and/or compounds are more easily mobilized/transported in air. [Ruiz-Jimenez, Zanca, Barua et al., 2019]

Primary biological aerosol particles: Correlation was found between the VOCs in gas phase and their presence in the PBAPs. Individual multiple linear regression models were established for the different particle sizes based on variations in the microorganism species in the samples. In all cases, explained variance of the models was over 92.0%. It was, however, impossible to find a single correlation between microbiological composition and the aerosol particle size. Up to three different trends were obtained for pseudomonas, fungi–bacteria and total amount of DNA in the samples. Discriminant analysis provided correct classification of 85.0 % of the samples. The use of neural network for the classification of the samples allowed the correct classification of 78.5 % of the samples. Finally, a clear relationship was seen between the environmental and meteorological variables and the microbiological and chemical composition of the aerosols. [Okuljar et al. 2019]

ACKNOWLEDGEMENTS

This work was supported by the Academy of Finland Centre of Excellence program (project no. 307331).

REFERENCES

- Lan, H., Zhang, W., Smått, J.-H., Koivula, R.T., Hartonen, K., Riekkola, M.-L. (2019). Selective extraction of aliphatic amines by functionalized mesoporous silica-coated solid phase microextraction Arrow, *Microchim. Acta* **186**, 412.
- Lan, H., Holopainen, J., Hartonen, K., Jussila, M., Ritala, M., Riekkola, M.-L. (2019). Fully automated online dynamic in-tube extraction for continuous sampling of volatile organic compounds in air, *Anal. Chem.* **91**, 8507.
- Okuljar, M., Ruiz-Jimenez, J., Sietiö, O.-M., Demaria, G., Zagatti, E., Liangsupree, T., Hartonen, K., Heinonsalo, J., Bäck, J., Petäjä, T. and Riekkola, M.-L. (2019). Chemical and microbiological characterization of primary biological aerosol particles at the boreal forest. Manuscript will be submitted to *Atmos. Chem. Phys.*

Ruiz-Jimenez, J., Zanca, N., Lan, H., Jussila, M., Hartonen, K. and Riekkola, M.-L. (2019). Aerial drone as a carrier for new miniaturized air sampling systems. *Journal of Chromatography A* **1597**, 202-208.

Ruiz-Jimenez, J., Zanca, N., Barua, S., Demaria, G., Salkinoja-Salonen, M., Siren, H.M.M., Hartonen, K. and Riekkola, M.-L. (2019). Sampling and analysis of indoor air and emissions from insulation materials. Presentation at FCoE seminar in Helsinki, 25.-26.11. 2019.

INTEGRATION OF ART AND SCIENCE, FACING CLIMATE CHANGE TOGETHER

T. RUUSKANEN¹, A. KALLINEN², A. LAURI¹, L. RIUTTANEN¹, H VEHKAMÄKI¹

¹Institute of Atmospheric Sciences and Earth System Research – Physics, University of Helsinki, Finland

²Theatre Academy, University of the Arts Helsinki, Finland

Keywords: education, collaboration,

INTRODUCTION

Physical sciences are working towards solutions on questions that require collaboration over field of science as well as other boarders. Communication on climate change is an example of when a set of answers that are focused on principles and physical processes behind the problem is not enough for the information to be received by non-scientists. Facing climate change causes can cause defense mechanisms such as denialism and shutting down, and Hulme (2015) concludes that we cannot find solutions only based on fact but it is also crucial to cultivate adequate spaces of public encounter and listening. Head and Harada (2017) found out that climate change scientists often emphasize dispassion, suppress painful emotions, use humour and switch off from work to protect themselves. Davenport (2017) recommend facing feelings such as worry, anger and regret and fostering and practicing resilience e.g. in the form of transformational leadership that supports hope and action. Art can provide an alternative path for climate change, it activates viewers more than engagement or participatory activities (Sommer et al., 2019).



Figure 1. Climate of Change –course students built a ‘Maja’ in the Hyytiälä old dining hall (in middle of picture above) where they could together safely face climate change storms. Artistic illustration by Timo Tikka.

EDUCATION ACTIONS

University of Helsinki and Arts University organize joint intensive courses emphasizing dialogue, communication and language. How is information about climate change and its impacts communicated and understood? How can this be utilized in society to promote solutions? What kind of feelings do we experience when facing climate change and can we turn them into an asset? Joint transdisciplinary courses enable master and doctoral students to explore and share methods from art and science in order to identify and work with synergies, and support transdisciplinary communication as well as enable adopting new ways of working from other communities that have different traditions and practices. The collaboration was piloted in spring 2018 with Think Like a Forest residential course in Vallisaari (<https://blogs.helsinki.fi/vallisaari/>). Climates of Change course in spring 2019 continued the collaboration and focuses on gaining insight on art - atmospheric science collaboration.

AIMS OF COLLABORATION

The courses aim at: 1) Exchange of skills and knowledge; Participation, discussions and group work reveal practical means to address climate change and foster ideas of how artistic and scientific work contribute to working towards solutions of climate change. 2) Creation of new practices: Emphasizing integration, this transdisciplinary workshop will support emerging new practices in short and long term. 3) Empowering; Students rightly view climate change as a phenomenon of complex factors. They express anxiety and powerlessness in relation to it. We support students in becoming the agents of change. Students gain skills, information and experiences for different forms of working cultures.

CONCLUSIONS

In our experiences bringing students from different backgrounds together, building an atmosphere of trust and collaboration among the diverse group the students has been very productive. The course participants faced climate changes eco-anxiety and –hope on personal as well as societal level. Working together has been inspiring and activating as the teachers and students have shared different approaches and gained new insights from one another.

ACKNOWLEDGEMENTS

The Atmospheric master and Atmospheric doctoral programs have supported this work.

REFERENCES

- Head and Harada (2017) Keeping the heart a long way from the brain: The emotional labour of climate scientists, *Emotion, Space and Society*, 24. 34-41. <https://doi.org/10.1016/j.emospa.2017.07.005>.
- Hulme (2015). (Still) disagreeing about climate change: Which way forward?. *Zygon*. 50. 893-905. 10.1111/zygo.12212.
- Sommer, Klöckner, Andreas (2019) Does activist art have the capacity to raise awareness in audiences?— A study on climate change art at the ArtCOP21 event in Paris. *Psychology of Aesthetics, Creativity, and the Arts*.

DYNAMIC METEOROLOGY: AN OVERVIEW

V.A. SINCLAIR¹, M. BISTER¹, M. EKBLÖM¹, J. HAUTALA, H. JÄRVINEN¹, J. LENTO², J. MIKKOLA, M. RANTANEN¹, J. RÄISÄNEN¹, I. STATNAIA¹, L. TUPPI¹ and M. VIRMAN¹

¹ Institute for Atmospheric and Earth System Research / Physics, Department of Physics, University of Helsinki, Helsinki, Finland.

² CSC – IT Center for Science, Espoo, Finland.

Keywords: ATMOSPHERIC CIRCULATION, CONVECTION, ENSEMBLE PREDICTION, EXTRA-TROPICAL CYCLONES, MICROPHYSICS, OPEN-IFS.

INTRODUCTION

Dynamic meteorology is the branch of fluid dynamics concerned with the meteorologically significant motions of the atmosphere. It forms the primary scientific basis for weather and climate prediction, and thus plays a primary role in atmospheric sciences. The research performed by the dynamic meteorology group covers a range of topics and current key aims are:

1. Develop in-depth physical understanding of meteorological phenomena, such as deep convection and high impact extra-tropical storms, and apply this knowledge to improve numerical weather prediction models and hence weather forecasts.
2. Develop ensemble prediction and algorithmic parameter estimation techniques together with open source software packages to permit further improvement of numerical weather forecast models.
3. Quantify how weather events such as extra-tropical cyclones and heat waves will change as the climate warms.
4. Assess the accuracy of the current generation of coupled climate models, understand inter-model variations and factors that affect regional temperature changes.

Our research is performed in collaboration with multiple national and international groups. We have active collaborations with the Finnish Meteorological Institute (FMI), the University of Lappeenranta, the European Centre for Medium Range Weather Forecasting (ECMWF), the University of Reading (UK) and the University of Bergen. We collaborate with other FCoE research teams, for example the Multiscale Modeling - from processes to the Earth System group as well as different aerosol measurement groups to whom we bring meteorological expertise. Members of the dynamic meteorology research group have recently contributed to a highly successful education export project, co-arranged with FMI and funded by the World Bank. Below we provide summaries of recent research studies and activities performed within the group. We start by giving a general overview to the main tools used in our group.

RESEARCH TOOLS

OpenIFS is a global model and is a portable version of the world leading Integrated Forecast System (IFS) developed and used for operational forecasting at ECMWF. OpenIFS has the same

dynamical core, physical parameterizations, land-surface scheme and wave model as the full IFS. OpenIFS can be used as a standard weather forecast model, in climate mode, and in idealised configurations such as a single column model or as an aqua-planet. OpenIFS was launched in 2013 and our group was one of the first worldwide to implement OpenIFS into our research and teaching. We are very active in the OpenIFS user community and OpenIFS is one of our most important tools.

The Weather Research and Forecasting (WRF) model is a complementary tool to OpenIFS. WRF is a non-hydrostatic, fully open access, mesoscale model developed by NCAR's Mesoscale and Microscale Meteorology Laboratory, USA. WRF has a range of physical parameterizations schemes implemented for different processes, has the option for nested domains and idealised situations can be set up in Cartesian geometry. We use WRF for idealised simulation and for high resolution simulations (e.g. 1 km grid spacing) over complex terrain.

Coupled Model Intercomparison Project is an internationally agreed standard experimental framework for studying the output of coupled atmosphere-ocean general circulation models. CMIP5 (phase 5) is the most current and extensive of the CMIPs, the data from which is openly available and includes output from over 40 different climate models. This data has been used in our group to assess how realistic the models are in simulating the recent past, particularly in Finland, and to investigate future projections.

Reanalysis are a blend of observations and model state and as such give a gridded, long-term global data set which can be considered our best estimate of the atmospheric state at any given time. We have previously used ERA-Interim in many studies. In summer 2019, our group downloaded over 20 Tbytes of ECMWF's newest reanalysis, ERA5, which is now available for all researchers in INAR to access and use.

Observations, for example, SYNOP station data, radiosonde soundings and satellite based estimated of precipitation are also used.

Infrastructure: Many of our activities are reliant on large data sets, powerful computing resources and thus the support of CSC – IT Center for Science. Our group has developed an excellent and highly beneficial working relationship with the division's application specialist from CSC - Juha Lento.

PHYSICS OF DEEP CONVECTION

Atmospheric deep convection is the mechanism behind showers of rain and many severe weather phenomena, such as thunderstorms, hurricanes, tornadoes and flash floods. It is also the main source of water vapour in the free-troposphere. The processes controlling the physics of deep convection need to be understood and parameterized in order to produce accurate weather forecasts and climate predictions. In our group, we study the fundamental, yet not properly understood, relationship between deep convection and lower tropospheric humidity. The mechanism behind this relationship has been studied extensively, yet models still struggle to represent it accurately.

In the first part of this project, an analysis of sounding and precipitation data was conducted (Virman et al., 2018). Results from the analysis suggest a new mechanism to explain the relationship between deep convection and lower tropospheric humidity was found. More specifically, after precipitation in dry areas robust lower tropospheric warm anomalies were observed, whereas in moist areas these warm anomalies were absent. Our results suggest that the warm anomalies may be the result of subsidence below a layer of strong evaporation of precipitation. In the second part (Virman et al., 2019), idealised WRF simulations were conducted to study the temperature structures associated with evaporation of stratiform precipitation, which often occurs associated with deep convection. The simulations showed that evaporation of stratiform precipitation and

resulting subsidence warming causes lower tropospheric warm anomalies, which are qualitatively similar to the observed ones in the first part of this project.

As lower tropospheric warm anomalies are known to inhibit deep convection, we believe that evaporation of precipitation is a key mechanism in controlling the formation of future deep convection and should be accounted for in both models and theories of convective phenomena (see Virman *et al.* in this issue for more information).

DYNAMICS OF MID-LATITUDE WEATHER SYSTEMS

OpenIFS has been used to investigate (1) the dynamics of Hurricane Ophelia which underwent extra-tropical transition, (2) the synoptic-dynamic evolution of windstorm Mauri which caused 2 deaths in northern Finland in 1982 and (3) how the structure, vertical motion and precipitation associated with extra-tropical cyclones in the future will change as the climate warms. As well as cyclonic, low pressure systems we have also analysed the heatwave of 2018 in Finland using reanalysis and observations.

Hurricane Ophelia: Tropical cyclones are generally driven by the latent heat release in the deep, moist convection, while extratropical cyclones, in turn, develop primarily from the meridional temperature and moisture gradients at mid-latitudes (i.e. baroclinic instability). For this reason, understanding the relative importance of different forcing mechanisms on tropical cyclones which transform into extratropical storms is of great importance. In this study, the contributions of different forcing terms affecting Hurricane Ophelia's (2017) extratropical transition are analysed, with the focus primarily on the transition and extratropical phases of the storm. The main result was that diabatic heating, dominated by the latent heat release in the frontal clouds, was the leading forcing for the intensification of Ophelia as a post-tropical cyclone. More details are available in (Rantanen *et al.*, 2019).

Windstorm Mauri: Reanalysis data and OpenIFS simulations were used to study windstorm Mauri which caused considerable damage in northern Finland on 22 September 1982. Forecasters speculated that this windstorm was related to Hurricane Debby, a category four hurricane. Hurricane Debby underwent extra-tropical transition which resulted in ridge building and an acceleration of the jet stream but ex-Debby did not re-intensify immediately. Instead ex-Debby travelled rapidly across the Atlantic as a diabatic Rossby wave. When ex-Debby approached the UK, it moved ahead of an upper-level trough and rapid re-intensification began. Ex-Debby then underwent 24 hours of rapid deepening before affecting northern Finland as storm Mauri. Turbulent mixing behind the cold front and convectively driven downdrafts in the warm sector were found to enhance the wind gusts over Northern Finland. We conclude that Hurricane Debby likely contributed to some extent to the development of storm Mauri but many other factors, such as the interaction with the upper level trough near the UK, were of equal importance. All of the OpenIFS forecasts diverged from reanalysis after only two days indicating that the event was characterised by intrinsic low predictability and strong sensitivities. More details are available in (Laurila *et al.*(2019)).

Extra-tropical cyclone structure in the future: Two idealised experiments are performed with OpenIFS configured as an aqua-planet: a control simulation and one in which sea surface temperatures are uniformly warmed by 4 K. All extra-tropical cyclones are tracked and cyclone centred composites are created. The results show that warming does not increase the median intensity of extra-tropical cyclones but that the strongest cyclones intensify. The amount of precipitation associated with the cyclones increases by almost 50% and the location of the precipitation moves further downstream away from the cyclone centre. These results indicate that the spatial structure of extra-tropical cyclones may change in the future as the climate. More details are available in (Sinclair *et al.*(2019a)).

The 2018 heat wave in Finland: We used surface SYNOP observations, radio soundings and ERA-Interim reanalysis data to quantify the heat wave of summer 2018, identify the synoptic-scale weather patterns associated with it, and determine how high in the atmosphere the anomalous warmth extended. May and July 2018 were exceptionally warm whereas June was not abnormally warm. The 2-m temperature anomalies in May at all considered stations exceeded 4.3°C. In July, the temperature anomalies were most extreme in northern Finland with Sodankylä having a 5.5°C positive anomaly. In both May and July, the anomalous warmth was associated with high pressure and extended throughout the depth of the troposphere - up to 10 km. The surface sensible and latent heat fluxes were above the climatological average, but the Bowen ratio did not differ notably from the climatological mean suggesting that surface processes such as soil moisture did not play a decisive role in the anomalous warmth. More details are available in (Sinclair *et al.* (2019b)).

ENSEMBLE PREDICTION AND PARAMETER ESTIMATION

Ensemble predictions (ENS) in meteorology are operationally applied to assess the day-to-day uncertainties of weather predictions, or "predict the predictability". These uncertainties are due to unavoidable small errors in the initial state and the model formulation. Over the past five or so years, our group has pioneered the use of ENS to assess uncertainties in model closure parameters. All geophysical prediction models contain such parameters and a handful of them are critically important for the forecast quality (Berner *et al.*, 2017). To this end, we have developed algorithmic parameter estimation techniques, foremost the ensemble prediction and parameter estimation system (EPPES), which has proven to shift the effort of model tuning from the domain of human learning to the domain of expert assisted machine learning. In academia, running ensemble predictions is tedious due to the huge number of simulations needed to gauge the small but highly non-linear model parameter space. A recent innovation from our group is a software package called OpenEPS, which facilitates administration of the model runs, output file post-processing, and parameter estimation, and opens new opportunities to apply ENS outside operational centres.

OpenEPS has been applied to study the convergence of closure parameters in OpenIFS. To investigate convergence of closure parameters requires a large number of optimization experiments to be run, each with a slightly different set-up. Here OpenEPS shows its value: a large number of slightly different ensemble prediction experiments can be run with a minimal amount of manual work. From the wealth of convergence tests we have performed, we can draw conclusions on what would be the most efficient way to tune the chosen closure parameters, which in our recent work have been parameters related to convection. A medium-sized ensemble of ~ 20 members lead to computationally cheap but stable enough convergence, and short forecasts of 24 hours seem to maximize the resolution of the cost function. (Tuppi *et al.*, 2019)

Building on the previous work of estimating closure parameters, we have developed an algorithmic method for optimizing stochastic parameters in an ensemble forecasting system. An ensemble forecasting system is optimal when the relationship between the spread of the ensemble members and the skill of the ensemble mean are on average equal. Here, the target is to optimize parameters regulating the amplitude of stochastic physics parameters and uncertainties of initial values such that the spread-skill relationship of the ensemble system is optimal. We use a cost function based on filter likelihood and an optimizer based on differential evolution. We have demonstrated our method with the idealized model Lorenz'95. (Ekblom *et al.*, 2019)

UNDERSTANDING SOURCES OF PREDICTABILITY AT THE SUB-SEASONAL TIMESCALE

Sudden stratospheric warmings (SSWs) are the most prominent phenomena taking place in the wintertime polar stratosphere. During a major SSW event the zonal mean zonal winds at 10 hPa and 60°N reverse from westerlies to easterlies (i.e. negative) and the stratospheric temperature rises by several tens of Kelvins over the course of a few days. SSWs have been shown to be related to an enhancement of tropospheric forced planetary wave packets that propagate upward into the stratosphere and interact with the mean flow. They deposit westward angular momentum (Eliassen-Palm convergence) which leads to the deceleration and breaking down of the polar night jet. This in turn has the possibility of influencing global modes. In particular, it leads to the development of the negative phase of the Northern Annular Mode (NAM), shifting tropospheric storm tracks southward and making northern and central Europe affected by cold Arctic air masses. This is why SSWs are considered a potential source of predictability at the extended-range timescale since the stratosphere tends to be more predictable than the troposphere. It is therefore important to understand the factors that control variability of the polar vortex.

In this study we investigate the role of the tropospheric forcing in the occurrence of the SSW that took place in February 2018, its predictability and teleconnection with the Madden-Julian Oscillation (MJO) by analysing the ECMWF ensemble forecast initialised on 1 February. The purpose of the study is to analyse the atmospheric circulation in stratosphere and troposphere before and during the SSW of 2018 and clarify the driving mechanisms focusing on the amplification of upward wave activity injection into the stratosphere before the SSW onset.

EFFECT OF ATMOSPHERIC CIRCULATION ON RECENTLY OBSERVED TEMPERATURE CHANGES

The climate changes that we observe in the real world result from a combination of two factors. On one hand, climate is affected by changes in external forcing such as the atmospheric composition. On the other hand, the non-linear dynamics of the climate system generate substantial internal variability. A separation between forced change and internal variability would be valuable, for example, when testing climate models for their ability to simulate climate response to increasing greenhouse gas concentrations.

In extratropical latitudes, most of the internal climate variability results from variations in the atmospheric circulation. On the other hand, global climate models suggest that forced changes in atmospheric circulation should be relatively small. If this also holds for the real world, most of the apparent circulation changes that have been observed during the last few decades have probably resulted from internal variability. Thus, we probably get a better idea of the underlying forced climate change by subtracting the effect of the circulation changes from the observed climate changes.

We have tested this idea for monthly mean temperature trends in Finland in the years 1979-2018, using a trajectory-based approach to quantify the effect of atmospheric circulation on the observed temperatures (Räsänen, 2019). The results indicate that atmospheric circulation has only had a very modest effect on annual mean warming in Finland, but it has substantially modified the changes in some individual months. In particular, changes in circulation explain the lack of observed warming in June and about a half of the very large warming in December. The residual trends obtained by subtracting the circulation-related change from observations are robustly positive in all months of the year. Thus, the temperatures that are nowadays observed in Finland are systematically warmer than they would have been under similar atmospheric circulation four decades ago, with an annual mean difference of about 2°C.

SUPERVOLCANOES AND STORMS

The global aerosol-climate model ECHAM-HAM has been used to quantify the short-term (weeks to months) effects of supervolcanic eruptions on tropical superstorms. Preliminary results show that there is an intensification of such storms at higher latitudes and weakening at lower latitudes. Some higher latitude coastal regions may experience particularly strong storms. In the future, the impact of the eruption location (low- vs. mid-latitudes, Northern vs. Southern hemisphere) and timing (season) will be assessed.

REFERENCES

- Berner, J. et al. (2017) Stochastic Parameterization: Toward a New View of Weather and Climate Models. *Bull. Amer. Meteorol. Soc.*, **98**, 565-587.
- Ekblom, M., Tuppi, L., Shemyakin, V., Laine, M., Ollinaho, P., Haario, H., and Järvinen, H. (2019). Algorithmic tuning of spread-skill relationship in ensemble forecasting systems. *Q. J. R. Meteorol. Soc.*, in review.
- Laurila, T., Sinclair, V. A., and Gregow, H. (2019). Transition of Hurricane Debby (1982) and the subsequent development of an Intense Windstorm over Finland. *Mon. Wea. Rev.* Accepted October 2019. doi: 10.1175/MWR-D-19-0035.1
- Sinclair, V. A., Mikkola, J., Rantanen, M. and Räisänen, J. (2019) The summer 2018 heatwave in Finland. *Weather* doi: 10.1002/wea.3525
- Sinclair, V. A., Rantanen, M., Haapanala, P., Räisänen, J. and Jarvinen, H. (2019) The characteristics and structure of extra-tropical cyclones in a warmer climate. *Weather Clim. Dynam. Discuss.* <https://doi.org/10.5194/wcd-2019-2>, in review, 2019.
- Rantanen, M., Räisänen, J., Sinclair, V. A., Lento, J. and Järvinen, H. (2019). The extratropical transition of Hurricane Ophelia (2017) as diagnosed with a generalised omega equation and vorticity equation *Tellus A*, in review.
- Räisänen, J. (2019). Effect of atmospheric circulation on recent temperature changes in Finland. *Climate Dynamics*, **53(9)**, 5675-5687.
- Tuppi, L., Ollinaho, P., Ekblom, M., Shemyakin, V. and Järvinen, H. (2019). On extracting information from closure parameter convergence tests using OpenIFS *Manuscript, to be submitted*.
- Virman, M., Bister, M., Sinclair, V. A., Räisänen, J. and Järvinen, H. (2018). A New Mechanism for the Dependence of Tropical Convection on Free-Tropospheric Humidity *Geophysical Research Letters* **45(5)**, 2516-2523.
- Virman, M., Bister, M., Sinclair, V. A., Räisänen, J. and Järvinen, H. (2019). Vertical temperature structure associated with evaporation of stratiform precipitation in idealized WRF simulations *J. Atmos. Sci.* in review

ARCTIC, POLAR AND HIGH ALTITUDE ATMOSPHERIC RESEARCH AT INAR IN 2019

M. SIIPIÄ¹ and F. BIANCHI¹

¹Institute for Atmospheric and Earth System Research, University of Helsinki

Keywords: Nucleation, Free Troposphere, Polar atmosphere, Arctic, Antarctic, Mass spectrometry, Ions, Pre-industrial

INTRODUCTION

A significant fraction (>50%) of cloud condensation nuclei (CCN) in the atmosphere arises from new-particle formation (Dunne *et al.*, 2016) where 35% are directly formed in the free troposphere (Merikanto *et al.*, 2009). While particle nucleation has been observed almost everywhere in the atmosphere, the mechanisms governing this process are still poorly understood, especially at high altitude in the free troposphere and during the pre-industrial time.

Laboratory experiments and quantum chemical calculations have identified potential candidates that may play this role, including ions (Kirkby *et al.*, 2011), sulfuric acid (H₂SO₄) and ammonia (NH₃) (Kirkby *et al.*, 2011; Jokinen *et al.*, 2018), amines (Almeida *et al.*, 2013; Bianchi *et al.*, 2014), and a possibly wide range of oxygenated organic molecules (Bianchi *et al.*, 2019; Ehn *et al.*, 2014; Riccobono *et al.*, 2014). In addition to that, recent studies have shown that nucleation of pure highly oxygenated organic molecules (HOM) without sulphuric acid is possible (Bianchi *et al.*, 2016; Kirkby *et al.*, 2016; Tröstl *et al.*, 2016).

Despite the recent instrument developments, only a few studies have observed new-particle formation in remote locations and even fewer have managed to measure down to 1 nm in size using instruments such as the Neutral cluster Air Ion Spectrometer (NAIS). Still more limited number of previous studies have measured the chemical composition of the growing clusters (Sipilä *et al.*, 2016; Jokinen *et al.*, 2018). Therefore, while multi-decadal research has confirmed that new-particle formation is important, results are yet insufficient to allow for a reasonable evaluation of the mechanisms in order to improve the accuracy of new-particle formation representation in models. A detailed framework that unifies the particles' physical properties and the chemical composition of key vapours is required to understand from first principles the fundamental pathways by which new-particle formation occurs in the atmosphere. The new instrumental advances present a unique opportunity to determine the chemical ingredients responsible for nucleation and cluster growth in the atmosphere and PANDA utilizes this opportunity by carrying out short-term (few months) campaigns and long-term permanent measurements with mass spectrometers and cluster and particle detection instrumentation.

WORK PERFORMED

In the year 2019 several intensive campaigns have been carried out in the Arctic and polar regions. Sites include Ny-Ålesund, Svalbard; Neumayer III, Queen Maud Land, Antarctica; Marambio Base, Antarctic Peninsula and recently started MOSAIC expedition on board Polarstern research vessel. Furthermore, SMEAR I and II stations were upgraded and a field campaign was carried out in Qvidja agricultural site. Also laboratory experiments in CERN CLOUD chamber have been performed. Below a short summary of each campaign.

Ny-Ålesund

In Ny-Ålesund, Svalbard “Polar and High altitude atmospheric research group” (PANDA) performed first comprehensive field campaign between February – August 2017. The key research question was to understand the role of phytoplankton dimethyl sulphide (DMS) emissions, ammonia as well as the possible

role of organic vapours and iodine species in new particle formation and growth in the polar Arctic atmosphere.

In that campaign, we utilized a suite of instrumentation for detection of particle precursor vapours – such as sulfuric acid and methane sulphonic acid (oxidation products of DMS), iodic acid and highly oxidized organic molecules (HOM) – chemical composition of cluster ions, and concentrations and size distributions of neutral and charged small clusters. Panda works closely with CNR – Italy, Alfred Wegener Institute (AWI) Germany and Stockholm University, who provide supporting data on aerosol size distributions, cloud activation, meteorology and marine phytoplankton productivity.

Since 2017 campaign we started continuous long-term monitoring of ion cluster and neutral particle size distribution with NAIS in April 2018 and long term monitoring of particle precursor vapour concentrations and ion cluster composition with a switching ion/NO₃⁻CI-API-TOF in April 2019. Measurements provide information on mechanisms and intensity of secondary cluster and particle formation. They serve also as a valuable comparison to data collected on board Polarstern during MOSAIC expedition (See later).

First results on details of secondary aerosol formation around Svalbard Archipelago will be published early 2020. Further information can be found from 2018 proceedings (Beck et al., 2018).

Neumayer III

An intensive 3 month campaign in German Antarctic research station Neumayer III was conducted between mid November 2018 and end of February 2019. To prepare for the campaign we shipped a measurement container for our equipment in preceding season (2017-2018). Two members of Panda group (M. Sipilä, L. Beck) participated to the campaign. Setup was almost identical to one deployed in Ny-Ålesund during 2017 campaign. Research aimed in deeper understanding of relevance of ion-induced sulfuric acid – ammonia nucleation we observed earlier (2014-2015) in Finnish Aboa research station (Jokinen et al., 2018). Since Neumayer, unlike Aboa, is located on the coast with nearby sea ice and a large emperor penguin colony, we hoped to see effects of enhanced iodine emissions from sea ice and ammonia emissions from penguin colony. Besides new particle formation from DMS and iodine derivatives as well as ammonia, we investigated formation of small particles and clusters together with their chemical composition during snowstorms. Results from the Neumayer expedition will be reported during 2020. Further information can be found from Beck et al. (these proceedings, 2019).

Marambio

Argentinian base Marambio, located in Antarctic peninsula is an ideal place for aerosol formation studies since it receives airmasses both from permanently ice-covered Weddell sea and from permanently open ice-free Southern Ocean. After the first intensive campaign in early 2018 we have continued with long-term ion and neutral cluster / particle measurements with NAIS. Work is carried out in collaboration with Finnish Meteorological Institute and Servicio Meteorológico Nacional Argentina. First reports from the work performed are foreseen in late 2020.

MOSAIC

Mosaic is a multinational and multidisciplinary experiment where the German research icebreaker Polarstern drifts with the Arctic sea ice over a full year. Polarstern sailed in September 2019 and connected to sea ice in early October 2019. Campaign runs until September/October 2020. INAR/PANDA contributes to expedition by providing manpower and equipment, including CI-API-TOF, NAIS, PSM etc. First results are expected late 2020 and publications 2021.

Värriö – SMEAR I

During 2019, SMEAR I station at Värriö strict nature reserve in Finnish Lapland was upgraded by a CI-API-TOF. Analysis of the data from the first summer season is ongoing and results will be reported early 2020. Further information can be found from Jokinen et al. (these proceedings, 2019)

Hyytiälä - SMEAR II

Hyytiälä SMEAR II station was upgraded by a Karsa MION-API-TOF mass spectrometer. MION is a multiple ionization system that allows the use of several reagent ions with the one single instrument. We operate the system with nitrate (NO₃⁻) and bromide (Br⁻) ionization as well as without ionization (natural ion clusters). Preliminary results can be found from Sarnela et al. (these proceedings, 2019).

Qvidja

Intensive measurement campaign was performed at Qvidja agricultural site in Parainen, southern Finland, utilizing ion/CI-API-TOF, PSM, NAIS etc. Aim was to focus on impacts of agriculture on new particle formation. Measurements started in March 2019 and are still ongoing. The campaign has been performed in collaboration with Tampere University of Applied Sciences.

CLOUD – CERN

As in every fall, PANDA contributes to CLOUD experiment in CERN. This year the focus is in ice nucleation rather than in new particle formation. CLOUD-14 experiments started in late September 2019. Analysis of results from CLOUD-12 and CLOUD-13 has been finalized and publications regarding details of e.g. iodic acid nucleation are expected by the end of the year.

ACKNOWLEDGEMENTS

This work was supported by the Academy of Finland (306853, 296628, 310627, 272041) and European Research Council (ERC-StG GASPARCON 714621).

REFERENCES

- Almeida, J., *et al.*, (2013) *Nature* 502, 359-363.
Bianchi, F., *et al.*, (2014) *Environ. Sci. Technol.* 48, 13675-13684.
Bianchi, F., *et al.*, (2016) *Science* 6289, 1109-1112.
Dunne *et al.*, (2016) *Science* 354, 1119-1124.
Ehn, M., *et al.*, (2014) *Nature* 506, 476-479.
Jokinen T., *et al.* (2018) *Science Advances* vol. 4 , no. 11 , 9744.
Kirkby, J., *et al.*, (2011) *Nature* 476, (7361), 429-433.
Kirkby, J., *et al.*, (2016) *Nature* 10.1038/nature17953.
Merikanto, J., *et al.* (2009) *Atmos. Chem. Phys.* 9 (21), 8601–8616.
Riccobono, F., *et al.* (2014) *Science* 344, 717-721.
Sipilä, M., *et al.* (2016) *Nature* 537(7621), 532-534.
Tröstl, J., *et al.*, (2016) *Nature* 10.1038/nature18271

AN OVERVIEW OF UNIVERSITY OF HELSINKI COMPUTATIONAL AEROSOL PHYSICS GROUP ACTIVITIES IN 2019

HANNA VEHKAMÄKI, DINA ALFAOURI VITUS BESEL, ROOPE HALONEN, FATEMEH KESHAVARZ, JAKUB KUBECKA, THEO KURTÉN, OLLI PAKARINEN, MONICA PASSANANTI, BERNHARD REISCHL, GOLNAZ ROUDSARI, ANNA SHCHERBACHEVA, VALTTERI TIKKANEN, TOMMASO ZANCA AND EVGENI ZAPADINSKY

Institute for Atmospheric and Earth System Research, Faculty of Science, FI-00014 University of Helsinki, Finland

Keywords: PARTICLE FORMATION, MOLECULAR CLUSTERS, SULPHURIC ACID, AMINES, AMMONIA, ORGANIC ACIDS, MASS SPECTROMETRY, ICE NUCLEATION

FRAGMENTATION OF ATMOSPHERIC CLUSTERS IN MASS SPECTROMETERS

Mass spectrometers such as Atmospheric Pressure interface Time of Flight (APi-ToF) and the Chemical Ionization APi-ToF (CI-APi-ToF) are currently the only tools that can be used to detect molecules and small clusters involved in the first stages of new particle formation at the low concentration they are present in the atmosphere. Understanding cluster fragmentation in these instruments is necessary for retrieving the actual ambient cluster distributions from measurements. We have developed a statistical model for the cluster fragmentation inside mass spectrometric instruments. In this model, the charged clusters move through the Atmospheric Pressure interface (APi) under applied constant and uniform electrical field (defined by the settings of the instrument). The fate of cluster is simulated as a random process involving collisions with carrier gas, energy transfer and fragmentation. To validate the model, we conducted experiments by producing negatively charged sulphuric acid clusters using electrospray Ionization and selected negatively charged three acid clusters using a Differential Mobility Analyser to inject into the APi-ToF. We studied fragmentation in the three vacuum chambers of the APi where an electric field is applied to guide the ions through the interface. We evaluated the effects of the voltages applied to the electrodes to the fragmentation rate. Both experiments and simulations indicate clusters are mainly fragmented at the interface between the first and second chamber, and the model captures the observed extent of fragmentation well (Zapadinsky *et al.* 2019, Passananti *et al.* 2019). We have also contributed to a ion mobility-mass spectrometry study of iodine pentoxide–iodic acid hybrid cluster anions observed during nucleation events in coastal regions. These clusters were shown to be relatively stable against dissociation inside mass spectrometers, and they can become sufficiently hydrated for iodine pentoxide to convert to iodic acid. Water sorption beyond this level is not significant, indicating that the clusters do not form nanometer-scale droplets in the atmosphere (Ahonen *et al.* 2019).

CONFIGURATIONAL SAMPLING FOR MOLEUCLAR CLUSTERS

Configurational sampling has been a main bottleneck in quantum chemical studies of noncovalently bonded molecular clusters relevant to the atmosphere, restricting the size and chemical variety of clusters studied. We have developed a systematic sequence of preoptimizations, re-optimizations, filtering, sampling/selection processes to search for minimum energy configurations using as an example clusters containing guanidine and sulfuric acid, which have a large number of different bonding patterns. We present a cost-effective strategy for representing hydrogen bonding and proton transfer, that play a key role in atmospheric clustering, using rigid molecules and ions in different protonation states (Kubečka *et al.* 2019)

REALISTIC COLLISION KINETICS

Collisions of molecules and clusters drive atmospheric new particle formation and growth. The collisions have usually been described using kinetic gas theory which assumes spherical non-interacting particles, and may significantly underestimate the collision rate for most atmospherically relevant molecules due to neglect of attractive long-range dipole-dipole interactions which enhance collision probability. We studied the statistics of collisions of sulfuric acid molecules in a vacuum using atomistic molecular dynamics (MD) simulations. We found that the effective collision cross section of the H₂SO₄ molecule, as described by an optimised potentials for liquid simulation (OPLS) is enhanced by a factor of 2.2 at 300 K compared with kinetic gas theory. This value is very close to the enhancement factor deduced from comparison between experimental formation rates of clusters containing sulfuric acid and calculated formation rates using hard-sphere kinetics. We also find that the Langevin model of capture, based on the attractive part of the atomistic intermolecular potential of mean force, yields reasonable approximations for the enhancement factor (Halonen *et al.* 2019).

ATMOSPHERIC PARTICLE FORMATION STUDIES INVOLVING ORGANIC COMPOUNDS

We have revealed that at ppt level piperazine, an alternative to the widely used monoethanolamine in post-combustion CO₂ capture, can significantly enhance sulphuric acid -based particle formation in the atmosphere. The enhancing potential of piperazine is higher than that of dimethylamine and monoethanolamine, and but lower than that of putrescine. Participation in the particle formation pathway can significantly alter the environmental impact of piperazine compared to only considering oxidation pathways, which yield carcinogenic nitrosamines (Ma *et al.* 2019). We have also contributed to a detailed chemistry and aerosol modelling study to investigate the impact of newly formed particles on the aerosol-cloud-climate system over the Boreal forest in Finland. This study shows for the first time that particle formation over the Boreal forest, a phenomenon observed and intensively studied for more than two decades, results in a climate warming in case of low to moderated updraft velocities. Until now it has been widely assumed that particle formation will cool the planet and thus counteract the effect of greenhouse gases (Roldin *et al.* 2019).

ACKNOWLEDGEMENTS

This work was supported by the Academy of Finland (Center of Excellence program project no. 307331, ARKTIKO project 285067 ICINA), European Research Council (Grant 692891-DAMOCLES) and University of Helsinki, Faculty of Science (ATMATH project). We thank CSC – IT Center for Science in Espoo, Finland, for computing time.

REFERENCES

- Ahonen, L., Li, C., Kubečka, J., Iyer, S., Vehkamäki, H., Petäjä, T., Kulmala, M. and Hogan, C. Jr. (2019) Ion Mobility-Mass Spectrometry of Iodine Pentoxide-Iodic Acid Hybrid Cluster Anions in Dry and Humidified Atmosphere. *Journal of Physical Chemistry Letters*, Vol 10, pp. 1935-1941.
- Halonen, R., Zapadinsky, E., Kurtén, T., Vehkamäki, H. and Reischl, B. (2019) Rate enhancement in collisions of sulfuric acid molecules due to long-range intermolecular forces *Atmospheric Chemistry and Physics*, Vol.19, 13355–13366.
- Kubečka, J., Besel, V., Kurtén, T., Myllys, N., Vehkamäki, H. (2019) Configurational Sampling of Non-Covalent (Atmospheric) Molecular Clusters: Sulfuric Acid and Guanidine. *Journal of Physical Chemistry A*, Vol 123, pp. 6022–6033
- Ma, F., Xie, H-B., Elm, J., Shen, J., Chen, J. and Vehkamäki, H (2019).: Piperazine Enhancing Sulfuric Acid Based New Particle Formation: Implications for the Atmospheric Fate of Piperazine. *Environmental Science & Technology*, Vol 53, pp. 8785-8795.

- Passananti, M., Zapadinsky, E., Zanca T., Kangasluoma, J., Myllys, N., Rissanen, M.P., Kurtén, T., Ehn, M., Attoui, M. and Vehkamäki, H. (2019) How Well Can We Predict Cluster Fragmentation Inside a Mass Spectrometer? *Chemical Communications*, Vol 5, pp. 5946-5949.
- Roldin, P., Ehn, M., Kurtén, T., Olenius, T., Rissanen, M.P., Sarnela, N., Elm, J., Rantala, P., Hao, L., Hyttinen, N., Heikkinen, L., Worsnop, D., Pichelstorfer, L., Xavier, C., Clusius, P., Öström, E., Petäjä, T., Kulmala, M., Vehkamäki, H., Virtanen, A., Riipinen, I. and Boy, M. (2019) The role of highly oxygenated organic molecules in the Boreal aerosol-cloud-climate system. *Nature Communications*, Vol 10, 4370.
- Zapadinsky, E., Passananti, M., Myllys, N., Kurtén, T. and Vehkamäki, H. (2019) Modelling on Fragmentation of Clusters Inside a Mass Spectrometer. *Journal of Physical Chemistry A*, Vol 123 (2), pp. 611–624.

INTEGRATED CARBON OBSERVATION SYSTEM (ICOS) FINLAND

T. VESALA¹, E. VAINIO², H. AALTONEN³, M. AURELA³, J. HATAKKA³, L. JÄRVI¹, P. KERONEN¹, P. KOLARI¹, H. KORHONEN³, M. KORKIAKOSKI³, L. LAAKSO³, T. LAURILA³, K. LEHTINEN^{3,4}, A. LESKINEN³, A. LOHILA^{1,3}, I. MAMMARELLA¹, A. OJALA^{2,5}, E.-S. TUITTILA⁶

¹ INAR Institute for Atmospheric and Earth System Research / Physics, Faculty of Science, University of Helsinki, Finland

² INAR Institute for Atmospheric and Earth System Research / Forest Sciences, Faculty of Agriculture and Forestry, University of Helsinki, Finland

³ Finnish Meteorological Institute, Helsinki, Finland

⁴ Department of Applied Physics, Faculty of Science and Forestry, University of Eastern Finland, Kuopio, Finland

⁵ Ecosystems and Environment Research Programme, Faculty of Biological and Environmental Sciences, University of Helsinki, Finland

⁶ School of Forest Sciences, Faculty of Science and Forestry, University of Eastern Finland, Joensuu, Finland

Keywords: GREENHOUSE GASES, LONG TERM OBSERVATIONS, CLIMATE CHANGE, DISTRIBUTED RESEARCH INFRASTRUCTURE

INTRODUCTION

Climate change is one of the most challenging global problems, and deeper understanding of its driving forces requires full quantification of the greenhouse gas (GHG) emissions and sinks, and the controlling mechanisms. This yields for high-precision long-term observations of GHGs. ICOS (Integrated Carbon Observation System) is a European scale distributed infrastructure for on-line, *in-situ* monitoring of GHGs. The mission of ICOS is to enable research to understand the GHG perturbations. Through ICOS, we can detect changes in regional GHG fluxes, early warning of negative developments and the response of natural fluxes to extreme climate events, and reduce uncertainties in Earth System models. ICOS aims to establish a template for the future development of similar integrated and operative GHG observation networks beyond Europe.

The ICOS network uses established routines and protocols for observations, and produces long-term, continuous and high-quality data for needs of research on climate change and biogeochemical cycles. All data produced within ICOS is quality controlled and will be freely, openly and easily available.

ICOS will reach its full operationality by 2020, when all the current more than 130 stations are labelled, i.e. obtaining ICOS certificate, according to commonly agreed standards. ICOS Research Infrastructure (RI) consists presently of national networks in 12 countries, including ICOS-Finland.

ICOS-FINLAND NATIONAL NETWORK

ICOS-Finland studies the sinks and sources of GHGs in typical boreal ecosystems focusing on coniferous forests and peatlands, but including also unique sites of a lake and an urban environment. ICOS-Finland has in total 13 measurement sites presently in operation, of which four are Atmospheric stations (ATM), four Ecosystem stations (ECO), and five Associated ECO stations (Fig. 1). So far seven stations have received

the ICOS label for standardised measurements: Pallas-Sammaltunturi (ATM), Utö (ATM), Hyytiälä SMEAR II (ATM), Hyytiälä SMEAR II (ECO), Siikaneva (ECO), Värriö (Associated ECO), Lettosuo (Associated ECO). The ECO stations measure turbulent GHG and latent (evapotranspiration) and sensible heat fluxes by flux towers, by eddy covariance method (EC) (Aubinet et al., 2012), together with auxiliary meteorological, ecophysiological and soil parameters (Franz et al., 2018). The ATM stations measure precise concentrations of GHGs above the atmospheric surface layer by tall towers or on the sea shore (Rödenbeck et al., 2009).

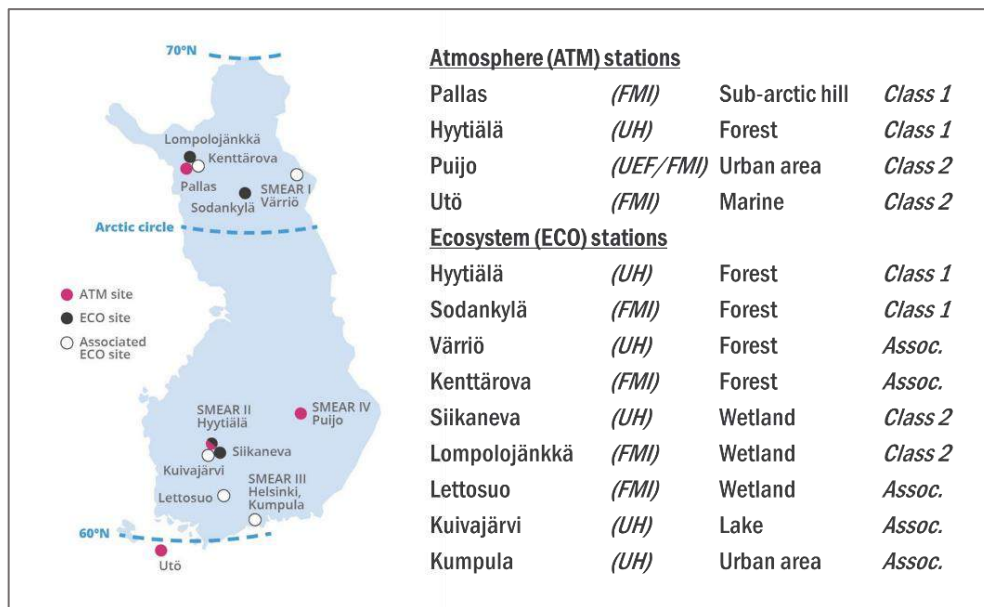


Fig. 1. ICOS-Finland station network in 2019.

ICOS-Finland has been established by three national partners – University of Helsinki (UH), Finnish Meteorological Institute (FMI), and University of Eastern Finland (UEF). ICOS-Finland has obtained funding from the Academy of Finland since 2010.

ICOS-Finland is part of INAR RI. INAR RI acts as an umbrella RI, taking care of the implementation and national coordination of the following ESFRIs (the European Strategy Forum on Research Infrastructures): ICOS (Integrated Carbon Observation System), ACTRIS (Aerosol, Clouds, and Trace Gases Research Infrastructure), eLTER (European Long-term Ecosystem Research) and AnaEE (Infrastructure for Analysis and Experimentation on Ecosystems). INAR RI is on the national roadmap.

ICOS- Finland within INAR RI brings together top-level scientists studying GHGs and biogeochemical cycles, and also provides a platform for facilitating education and training. ICOS- Finland (and the whole INAR RI) stresses the importance of the close collaboration between atmospheric physicists and forest and environmental scientists, involved in the joint Centre of Excellence and numerous research projects, joint teaching and education, and the joint use of RI. ICOS-Finland has connections to major companies in the field, e.g. Aerodyne (carbonyl sulphide measurements, USA), NEON Inc. (measurement strategies, USA) and LI-COR (GHG measurements; USA). In Finland, several prototypes of gas analyzers have been tested under demanding northern field conditions and ICOS expertise has been utilized by St1 energy company in its plans to verify afforestation impacts on net carbon uptake.

RECENT RESULTS

The success of Finnish atmospheric and ecosystem research is largely based on the long-term, comprehensive and continuous data. The longest methane (CH_4) EC flux record of 13 years is measured at Siikaneva (ECO), and the longest carbon dioxide (CO_2) EC flux record on a lake is 7 years data from Lake Kuivajärvi (Associated ECO). ICOS Finland is a pioneer in Finland in harmonisation and standardisation of GHG flux and concentration measurements, and in combining measurements of greenhouse gas concentrations and surface fluxes. The expertise of ICOS-Finland (UH and FMI) has been utilized in establishing two flux towers in Siberia: one on a West-Siberian peatland site being the only flux tower in the core of the West-Siberian plateau (Alekseychik et al. 2017), and the other one on coastal tundra zone in north-eastern Siberia, at the seashore of Laptev Sea (Tuovinen et al. 2019).

Researchers and technicians of ICOS-Finland have played a significant role in standardization of *in-situ* observations. A standard for EC measurements has been submitted to the World Meteorological Organisation (WMO), and ECO station protocols were published in the format of scientific articles in the open-access journal International Agrophysics (<http://www.international-agrophysics.org/Issue-4-2018,7048>) in 2018.

New research publication within ICOS-Finland concluded that clear-cutting at Lettosuo (Associated ECO site) drained peatland forest results in large CO_2 emissions (Fig 2.; Korkiakoski et al. 2019). Before the harvest, the annual NEE at the site was close to zero. The soil turned into a small source of CH_4 and a substantial source of N_2O – this change produced a 100-year GWP of about 10% of that due to the increased NEE at the site.

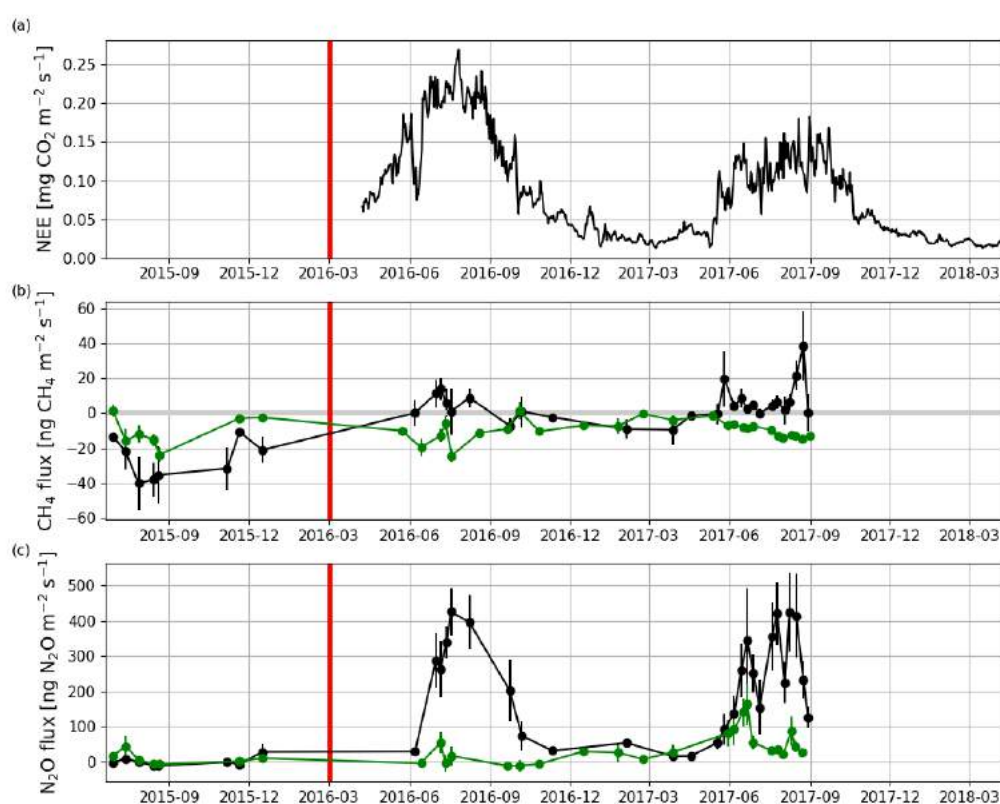


Fig. 2. a) Net ecosystem exchange (NEE; daily means from eddy covariance) at the clear-cut area, and forest floor fluxes of (b) CH_4 and (c) N_2O (hourly means from soil chambers) at the clear-cut (black) and control (green) areas at Lettosuo (Associated ECO) drained peatland forest. The time of the clear-cutting is shown by the red vertical line.

At ICOS-Finland urban site Kumpula (Associated ECO site), together with planned new ICOS-Finland site in the Helsinki city centre, biogenic and anthropogenic CO₂ emissions in Helsinki were studied by a surface-flux model (Surface Urban Energy and Water Balance Scheme) and EC (Järvi et al. 2019). Distinct spatial variation in the CO₂ was demonstrated (Fig. 3). In Kumpula, traffic is the dominant CO₂ source but summertime vegetation partly offsets traffic-related emissions. In the city centre, emissions from traffic and human metabolism dominate and the vegetation effect is minor due to the low proportion of vegetation surface cover (22%).

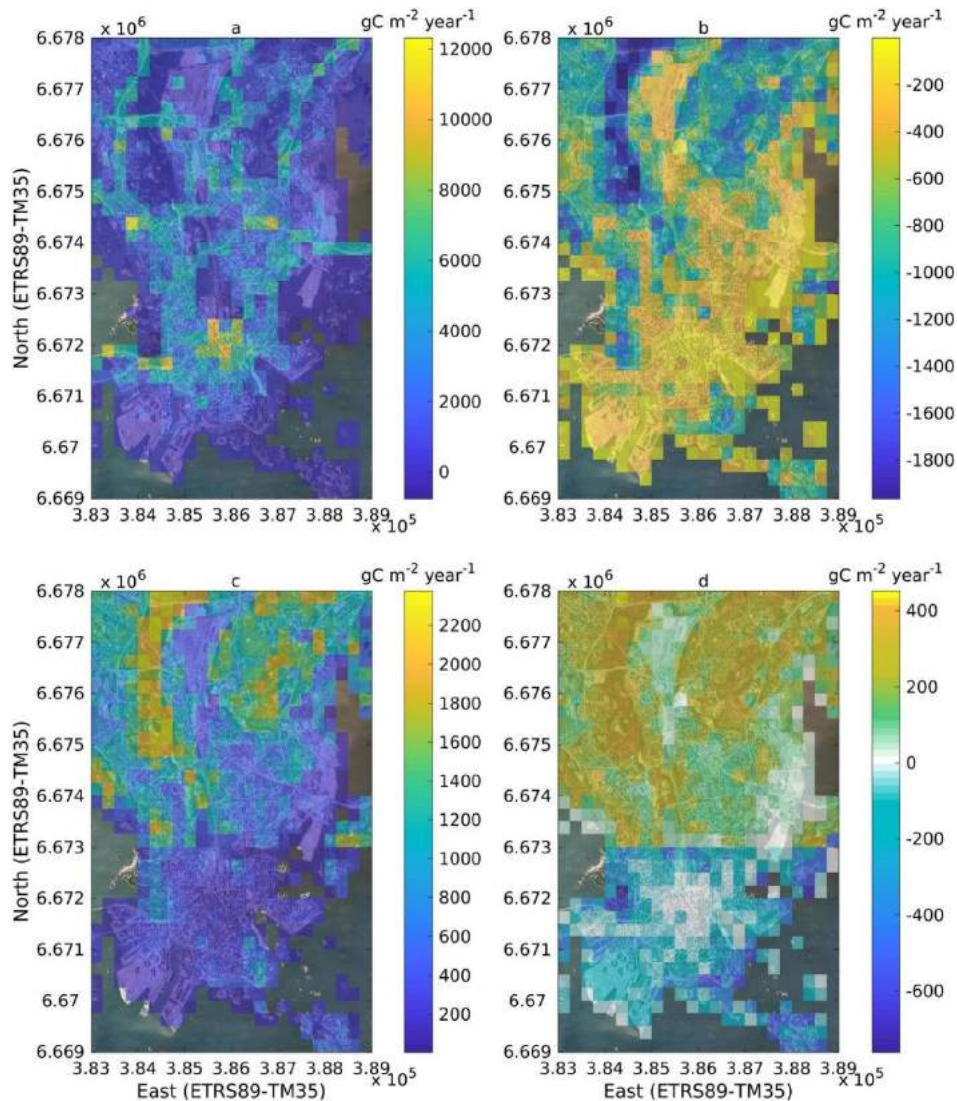


Fig. 3. Annual cumulative (a) net CO₂ flux (F_c), (b) photosynthesis (F_{pho}), (c) respiration (F_{res}), and (d) biogenic net CO₂ ($F_{c,bio}$) flux for 2012. All have units g C m⁻² year⁻¹, but scale differs between maps. (Järvi et al. 2019)

FUTURE PERSPECTIVES

The rest of the measurement stations of ICOS-Finland are estimated to obtain the official ICOS label by spring 2020. New possible sites planned for the next 5-years (2020–2024) are: agricultural site SMEAR-Agri (ECO Class 2), Helsinki city centre Torni (urban), Tvärminne sea shore, Siikaneva 2 (bog), Hyytiälä forest clear-cut site, restored peatland site (these 5 would be Associated ECO sites), as well as M/S Silja Serenade (ocean). Also there is a tentative plan to upgrade Siikaneva (fen) from Class 2 to 1.

ACKNOWLEDGEMENTS

The ICOS-Finland research network is financially supported by the Academy of Finland (281255, 319871), the Ministry of Transport and Communications, the Ministry of Education and Culture.

REFERENCES

- Alekseychik, P. et al. (2017). Net ecosystem exchange and energy fluxes measured with the eddy covariance technique in a western Siberian bog, *Atmos. Chem. Phys.*, 17, 9333–9345.
- Aubinet, M., Vesala, T. & Papale, D. (Eds.) (2012) *Eddy covariance: a practical guide to measurement and data analysis*. Springer Science & Business Media, 438 p.
- Erkkilä K.-M., Ojala A., Bastviken D., Biermann T., Heiskanen J.J., Lindroth A., Peltola O., Rantakari M., Vesala T., and Mammarella I. (2018). Methane and carbon dioxide fluxes over a lake: comparison between eddy covariance, floating chambers and boundary layer method, *Biogeosciences*, 15, 429–445.
- Franz, D. et al. (2018). Towards long-term standardised carbon and greenhouse gas observations for monitoring Europe's terrestrial ecosystems: a review, *International Agrophysics*, 32(4), 439–455.
- Järvi L., Havu M., Ward H.C., Bellucco V., McFadden J.P., Toivonen T., Heikinheimo V., Kolari P., Riikonen A., and Grimmond C.S.B. (2019). Spatial modeling of local-scale biogenic and anthropogenic carbon dioxide emissions in Helsinki. *Journal of Geophysical Research: Atmospheres*, 124(15), 8363–8384.
- Korkiakoski, M. et al. (2019). Greenhouse gas and energy fluxes in a boreal peatland forest after clear-cutting, *Biogeosciences*, 16, 3703–3723.
- Rödenbeck, C. et al. (2009). A two-step scheme for high-resolution regional atmospheric trace gas inversions based on independent models. *Atmos. Chem. Phys.*, 9, 5331–5342.
- Tuovinen, J.-P., Aurela, M., Hatakka, J., Räsänen, A., Virtanen, T., Mikola, J., Ivakhov, V., Kondratyev, V., and Laurila, T. (2019). Interpreting eddy covariance data from heterogeneous Siberian tundra: land-cover-specific methane fluxes and spatial representativeness, *Biogeosciences*, 16, 255–274.

MICROMETEOROLOGY, GREENHOUSE GASES, BIOGEOCHEMICAL CYCLES AND URBAN METEOROLOGY RESEARCH TEAM: OVERVIEW OF SCIENTIFIC ACTIVITIES

T. VESALA^{1,2}, L. JÄRVI^{1,3}, A. LOHILA^{1,4}, I. MAMMARELLA¹, T. ASLAN¹, R. DEWAR¹, T. GRÖNHOLM¹, M. HAVU¹, P. HIETALA¹, P. KERONEN¹, K.-M. KOHONEN¹, T.V. KOKKONEN¹, P. KOLARI¹, M. KURPPA¹, S. KARTTUNEN¹, A. LEPPÄNEN¹, X. LI¹, A. MARCHIONNE¹, O. PELTOLA^{1,4}, M. RAIVONEN¹, Ü. RANNIK¹, P. RANTALA¹, G. SAHOO¹, Y. SALMON¹, J. STRÖMBERG¹, R. TAIPALE¹, H. ZHANG¹, A. VÄHÄ¹, T. LAURILA⁴, J. PULLIAINEN⁴, A. OJALA⁵, E.-S. TUUTTILA⁶, T. HÖLTTÄ², M. PIHLATIE⁷ and J. BÄCK²

¹INAR/Physics, University of Helsinki

²INAR/Forest Sciences, University of Helsinki

³Helsinki Institute of Sustainability Science, University of Helsinki

⁴Finnish Meteorological Institute

⁵Department of Environmental Sciences, University of Helsinki

⁶University of Eastern Finland

⁷Department of Agricultural Sciences, University of Helsinki

Keywords: Turbulent fluxes, greenhouse gases, carbon cycle, water cycle, carbonyl sulphide, boreal forest, lake, peatland, eddy covariance, lake model, urban, LES

INTRODUCTION

The coupling of the Earth's surface and the overlying atmosphere through mass and energy fluxes has an important role in atmospheric chemistry and physics in addition to boundary layer meteorology and ecosystem research. Micrometeorology, Greenhouse gases and Biogeochemical cycles group of University of Helsinki aims at increasing the fundamental understanding of biosphere-atmosphere interactions in different ecosystems and to apply the gained information for practical applications and purposes. The group has a comprehensive experience on ecosystem scale flux measurements carried out by means of micrometeorological techniques. Long term and continuous measurements are performed over forest, peatland and freshwater ecosystems and in urban environment. The work is done in close co-operation with other FCoE research teams from University of Helsinki (Ecosystem processes, Soil Dynamics), from Finnish Meteorological Institute (Greenhouse gases), as well as with other national and international collaborators. In 2017 a new University of Helsinki project ATMATH started, which is strengthening collaboration between profs. Antti Kupiainen and Matti Lassas (both in Department of Mathematics and Statistics) and prof. Hanna Vehkamäki. We report below summaries of recent research studies and activities performed within the group.

METHODOLOGICAL ASPECTS AND DEVELOPMENTS

Advances in Eddy Covariance method

During last year the research group has been actively involved in several activities related to greenhouse gas (GHG) measurement techniques, protocols and data harmonization within ICOS and other international projects. The work includes advances in the eddy covariance (EC) method for methane and nitrous oxide (Nemitz et al., 2018), advances in eddy covariance (EC) data processing (Sabbatini et al, 2018; Montagnani et al, 2018) and standardization of flux tower setup (Rebmann et al, 2018).

The EddyUH software, developed in our group, is the state of art tool for EC flux data processing, and at moment counts more than 400 external users. In a recent study (Mammarella et al., 2016), we have carried out an inter-comparison between EddyUH and EddyPro (the software developed by *LI-COR* Biosciences), aiming to estimate the flux uncertainty due to the use of different software packages and to evaluate the

most critical processing steps, determining the largest deviations in the calculated fluxes. In recent study (Rannik et al., 2016), we have reviewed different methods used to estimate random uncertainties of flux measurements by the eddy covariance technique using measured turbulent and simulated artificial records.

Finally, an international field instrument intercomparison was implemented at Lake Vanajavesi (Finland) in January-May 2016 (Potes et al., 2017) and at Alqueva Reservoir (Portugal) in June-September 2017. The aim is to evaluate the performance of a new eddy covariance (EC) instrument called IRGASON (Campbell Scientific), with a separated and standard EC system for reference (Metek + LI-7200). The IRGASON integrates an open-path gas analyzer and a sonic anemometer into the same sensing volume, thus eliminating sensor separation in comparison to the traditional open-path EC setup. However, the first studies made using the IRGASON yielded some unrealistic results (e.g. night-time CO₂ uptake over lakes and vegetation), which seems to be related to a “missing” gas analyser spectroscopic correction (Bogoev et al., 2014).

ECOSYSTEM PROCESSES AND FLUX STUDIES

Boreal forest and carbonyl sulphide flux

The long-term dynamics of the biospheric exchange of (carbonyl sulphide) COS is partly unknown. We conducted the first long-term, ecosystem-level COS flux measurements with eddy covariance technique in a boreal pine forest covering 32 months, over 5 years. Fluxes from hourly to yearly scales are reported and the aim is to reveal controlling factors and the level of inter-annual variability. The spring recovery of the flux is mostly governed by the air temperature and the onset of the uptake varied 2 weeks. The significant reduction of the summer COS flux under large water vapour pressure deficit occurred, which is reported here the first time at the ecosystem scale. The maximum COS uptake varied 13 % and its timing varied by 7 weeks. The fraction of the nocturnal uptake remained 21% at maximum. We observed the annual (April-August) average net uptake of COS totaling 62.3 (gS/ha) with 48 % variability.

Greenhouse gas exchange over lake

Freshwaters bring a notable contribution to the global carbon budget by emitting both carbon dioxide (CO₂) and methane (CH₄) to the atmosphere. Since 2010 our research activities is carried out at the comprehensive and unique measurement platform Lake-SMEAR, located in the small boreal Lake Kuivajärvi, close to Hyytiälä Forestry Field Station in Southern Finland. Lake-SMEAR includes direct and indirect flux measurements of CO₂ and CH₄ and other auxiliary measurements over the lake and in the water (Mammarella et al., 2015). We aim to assess the current global CO₂ evasion estimates from lakes to the atmosphere by comparing parameterizations for gas transfer velocity k and the significance of wind and heat flux to the gas transfer especially in small lakes (Heiskanen et al, 2014). Global estimates of freshwater emissions traditionally use a wind speed based gas transfer velocity k (e.g. Cole and Caraco, 1998), for calculating diffusive flux with the boundary layer method (BLM). Such simple parameterizations are also often used in lake models including carbon cycle related processes (e.g. Stepanenko et al., 2016). For slightly soluble gases, like CO₂ and CH₄, k is mainly controlled by water-side turbulence. We investigate the relationship between water-side turbulence and the air-water gas transfer velocity k using in-situ measurements performed at Lake Kuivajärvi in Southern Finland. Direct measurements of water-side turbulent velocity fluctuations were obtained with an Acoustic Doppler Velocimeter (ADV), from which water surface dissipation of turbulent kinetic energy (ε) was calculated. Simultaneous observations of k were obtained using measurements of CO₂ and CH₄ fluxes performed with eddy covariance and floating chamber methods, together with dissolved gas concentrations (pCO₂ and pCH₄) measured at the water surface. Field measurements of k are compared to the small-eddy model and other theoretical approaches, which relate the efficiency of a gas to escape from the water-air interface (e.g. the gas transfer velocity) to near-surface water turbulence expressed, for an homogenous surface layer, by ε (Mammarella et al., 2019). Other recent studies include two important aspects: 1) the effect of water clarity on thermal stratification of a lake, which in turn affects lake-atmosphere heat exchange and further gas transfer (Heiskanen et al., 2015); 2) comparison of fluxes of CH₄ and CO₂ measured during a

two week campaign at Lake-SMEAR using different techniques, including eddy covariance, floating chambers, and direct measurements of water turbulence and k (Erkkilä et al., 2018). The agreement between different methods were fairly good, and recent parameterizations for k , including both wind and heat fluxes (Heiskanen et al., 2014; Tedford et al., 2014), were superior in comparison with more simple ones (e.g. Cole and Caraco, 1998).

Campaign at River Kitinen

Whereas the database of (long-term) direct greenhouse gas (GHG) flux measured by the eddy-covariance technique is consistently growing for lakes, the list of published datasets for rivers is limited to 30 days on a boreal river. However, direct measurements and accompanying process studies are inevitable to fill the gaps in knowledge. We conducted a river case study based on a joint measurement campaign (KITEX) in June-September 2018 at River Kitinen, Sodankylä, Finland, aiming to improve our understanding of river-atmosphere GHG exchange. The campaign followed a multi-method approach addressing turbulent GHG fluxes, water turbulence and chemistry, gas concentrations in the water, limnological parameters and catchment sampling. The campaign formed also a proof of concept for the respective methodology. We also evaluated the bulk transfer approaches for H and LE fluxes using EC flux measurements. The aim is to contribute to the understanding of the driving processes and magnitudes of H and LE exchange over rivers and to further constrain how different heat flux components contribute to the energy balance of a river. Results shall contribute to a better representation of the physical processes and dynamics of river turbulent heat fluxes within regional and global modelling.

West Siberia peatland flux measurements

In order to fill one of the major observational gaps, we have established recently a new eddy covariance flux tower at the raised bog wetland site at the Mukhrino field station in Khanty–Mansi Autonomous Okrug (Russia). The flux tower for energy, carbon dioxide fluxes is the first one in West Siberian peatlands (with the nearest one being ZOTTO 1000 km to the east). The fluxes obtained in summer-2015, combined with the available meteorological, soil and vegetation data are used to study the diurnal and seasonal variations of fluxes, as well as to determine ecosystem annual budgets of energy and carbon at this typical Siberian middle taiga bog site (Alekseychik et al., 2017). The measurements continued in 2016. In 2018, a CH₄ open-path analyser was added to the EC system, and currently flux measurements until 2019 are analysed (Mammarella et al, this issue).

Greenhouse gas fluxes from peatland forestry

In Finland, drained peatlands are an important part of the operational forestry with their areal share of total forestry land of 25%. We have studied the impacts of traditional forestry regeneration, i.e. clear-cutting, on the GHG and energy fluxes in Lettosuo site in Tammela, southern Finland, using the eddy covariance and chamber methods (Korkiakoski et al., 2019). According to the 2-year study following the clear-cut, the CO₂ emissions from the clear-cut area are huge and overwhelm the N₂O emissions, which are also considerable if compared to the situation before the clear cut, in terms of global warming potential.

We have also established a new measurement site on a nutrient rich peatland forest, Ränskälänkorpi in Asikkala in cooperation with the Natural Resource Institute Finland. The eddy covariance fluxes of CO₂ are measured on top of a 29 m telescopic mast. In addition, six automatic chambers are monitoring the fluxes of CO₂, CH₄ and N₂O from the soil. Both Lettosuo and Tammela sites will be, together with Hyytiälä site, part of the new Academy of Finland project BiBiFe, lead by prof. Jaana Bäck, which will study the biophysical and biogeochemical impacts of forest harvesting or thinning.

LABORATORY STUDIES

Modelling of water vapour exchange by plants

Vesala et al. (2017) theoretically showed that high water tension inside trees can cause transpiration to turn into the condensation of the water vapour from atmosphere inside to the stomata even below 100 %

relative humidity. To confirm the hypothesis, we performed a chamber experiment using laboratory facilities provided by TOMCAT synchrotron beamline at Paul Scherrer Institute (PSI) in Switzerland. This beamline is developed for a micro-structural imaging of biological matters and reconstructed CT scans provide a detailed information of the internal structure of the sample. A pine needle was placed inside a small flow-through chamber (volume ~0.5 dl). The CT scan was first performed at room humidity (~40 %). Then, the humid air (RH ~97 %) was led through the chamber for one hour and scanning was repeated. By comparing the results, we were able to calculate the increase of water volume inside the puffed needle. The preliminary results show that the water uptake of the needle was ~8 %. The value is surprisingly similar to the results of Limm et al. (2009) who reported that submerging a leaf in water for 180 minutes can increase the leaf water content by 2-11 % depending on the species.

MODELLING STUDIES

Modelling of the urban atmosphere

Urban areas cause a challenge for atmospheric modelling due to the highly variable surface form and function. These include the 3-dimensional roughness elements, such as buildings and trees, and anthropogenic activities creating highly spatially variable emission sources. In recent study we examined the spatial and temporal variations of local-scale CO₂ emissions in central Helsinki (Järvi et al. 2019) using land surface model SUEWS (*Surface Urban Energy and Water balance*, Järvi et al. 2011). The results show traffic being the largest CO₂ source with highly spatially variable emission pattern. The second largest contributor to CO₂ emissions is human metabolism because of the large amount of commuters in central Helsinki on workdays. The same model was also used to examine long term changes in urban water balance in Vancouver, Canada (Kokkonen et al. 2018), and the effect of haze on urban hydrological cycle in Beijing (Kokkonen et al. 2019). The latter study found an increase in low precipitation events but not on appearance of flash floods.

The most promising tool to model urban atmosphere is large eddy simulation (LES) which can account for the complex structure of urban surfaces. We use and participate to the development of LES model PALM (Maronga et al. 2015) with the focus particularly on the high spatial and temporal variability of air quality within urban landscapes (Kurppa et al. 2018). We have added sectional aerosol module to PALM and good correspondence is found with size distribution observations in Cambridge, UK (Kurppa et al. 2019).

Wetland methane model

We developed a model of peatland methane emissions, HIMMELI (Helsinki Model of Methane build-up and emission) that simulates fluxes of CH₄, CO₂ and O₂ between peatland and the atmosphere (Raivonen et al. 2017, Peltola et al. 2018, Susiluoto et al. 2018). It is not a full model of peatland carbon cycling but can be used as the CH₄ emission module of e.g. a biosphere model. Currently, we are using combination of HIMMELI and JSBACH, the land surface model of MPI-ESM (Kleinen et al. 2019), for several studies done in collaboration with the Carbon Cycle group of FMI.

In order to validate the CH₄ and CO₂ fluxes simulated by the JSBACH+HIMMELI combination on pristine peatlands, we are running site-level simulations on a set of temperate and boreal peatland sites. Preliminary results show reasonable agreement between the modelled and observed fluxes. JSBACH+HIMMELI is used in larger scale as well, for simulating CH₄ emissions of European pristine peatlands in project VERIFY that aims to develop a system to estimate GHG emissions to support countries' emission reporting. As drained, managed peatlands are a major source of GHG emissions, we are also developing the model combination to be able to reliably simulate GHG fluxes of forested and agricultural peatlands and the effects of different management practices on the emissions.

As part of the global fluxnet CH₄ synthesis work, facilitated by the U.S. Powell center, we have recently started elaborating the HIMMELI model to make it applicable for partitioning a given flux of methane into oxidation and production. Such partitioning would be highly helpful to better understand the dynamics of

net CH₄ emission, and the environmental variables controlling it and explaining the site-to-site differences.

ACKNOWLEDGEMENTS

The financial supports by the Academy of Finland Centre of Excellence program (project no 272041), Academy of Finland projects ICOS-FINLAND, Academy Professor projects (1284701 and 1282842) and EU projects RINGO and VERIFY are gratefully acknowledged.

REFERENCES

- Alekseychik, P., Mammarella, I., Karpov, D., Dengel, S., Terentieva, I., Sabrekov, A., Glagolev, M., and Lapshina, E.: Net ecosystem exchange and energy fluxes measured with eddy covariance technique in a West Siberian bog. *Atmos. Chem. Phys.*, 17, 9333-9345, doi:10.5194/acp-2017-43, 2017.
- Erkkilä, K.-M., Ojala, A., Bastviken, D., Biermann, T., Heiskanen, J. J., Lindroth, A., Peltola, O., Rantakari, M., Vesala, T., and Mammarella, I.: Methane and carbon dioxide fluxes over a lake: comparison between eddy covariance, floating chambers and boundary layer method, *Biogeosciences*, <https://doi.org/10.5194/bg-15-429-2018>, 2018.
- Järvi, L., Rannik, Ü., Kokkonen, T.V., Kurppa, M., Karppinen, A., Kouznetsov, R.D., Rantala, P., Vesala T., Wood, C.R. (2018). Uncertainty of eddy covariance flux measurements over an urban area based on two towers. *Atmos. Meas. Tech.* 11, 5421-5438, doi: 10.5194/amt-11-5421-2018.
- Järvi, L., Havu, M., Ward, H.C., Bellucco, V., McFadden, J.P., Toivonen, T., Heikinheimo, V., Kolari, P., Riikonen, A., Grimmond, C.S.B., (2019). Spatial modelling of local-scale biogenic and anthropogenic carbon dioxide emissions in Helsinki. *J. Geophys. Res. – Atmospheres* 124, doi: 10.1029/2018JD029576.
- Kleinen, T., Mikolajewicz, U. and Brovkin, V. (2019). Terrestrial methane emissions from Last Glacial Maximum to preindustrial. *Climate of the Past Discussions*, doi: 10.5194/cp-2019-109.
- Kokkonen, T.V., Grimmond, C.S.B., Oke, T., Christen, A., Järvi, L. (2018). The effect of urbanization and densification on long-term water balance in Vancouver. *Water Resour. Res.* 54 (9), 6625-6642, doi: 10.1029/2017WR022445.
- Kokkonen, T.V., Grimmond, C.S.B., Murto, S., Liu, H., Sundström, A.-M., Järvi, L. (2019). Simulation of effect of the radiative effect of haze on the urban hydrological cycle using reanalysis data in Beijing. *Atmos. Chem. Phys.* 19, 7001-7017, doi: 10-5194/acp-19-7001-2019.
- Korkiakoski M., Tuovinen J.-P., Penttilä T., Sarkkola S., Ojanen P., Minkkinen K., Rainne J., Laurila T. and Lohila A. (2019). Greenhouse gas and energy fluxes in a boreal peatland forest after clearcutting. *Biogeosciences*, 16, 3703–3723, <https://doi.org/10.5194/bg-16-3703-2019>.
- Kurppa, M., Hellsten, A., Roldin, P., Kokkola, H., Tonttila, J., Auvinen, M., Kent, C., Kumar, P., Maronga, B., Järvi L. (2019). Implementation of the sectional aerosol module SALSA2.0 into the PALM model system 6.0: Model development and first evaluation. *Geosci. Mod. Dev.* 12, 1403-1422, doi: 10.5194/gmd-12-1403-2019.
- Kurppa, M., Hellsten, A., Auvinen, M., Vesala, T., Raasch, S., Järvi, L. (2017). Ventilation and Air Quality in City Blocks Using Large Eddy Simulation - Urban Planning Perspective. *Atmosphere* 9 (2), 65, doi: 10.3390/atmos9020065.
- Limm, E. B., Simonin, K. A., Bothman, A. G., and Dawson, T. E. (2009). Foliar water uptake: a common water acquisition strategy for plants of the redwood forest. *Oecologia*, 161(3), 449–459. doi:10.1007/s00442-009-1400-3.
- Mammarella, I., A. Vähä, K.-M. Erkkilä, J. Heiskanen, A. Ojala, M. Rantakari, T. Vesala and G. Katul, (2019). In-situ evaluation of the relationship between lake surface turbulence and air-water gas transfer velocity at a small lake in Finland. *Manuscript*
- Montagnani, L., Grünwald, T., Kowalski, A., Mammarella, I., Merbold, L., Metzger, S., Sedlak, P. and Siebicke, L., 2018. Estimating the storage term in eddy covariance measurements: the ICOS methodology. *Int. Agrophys.*, 32, 551-567. doi: 10.1515/intag-2017-0037.

- Nemitz, E., Mammarella, I., Ibrom, A., Aurela, M., Burba, G., Dengel, S., Gielen, B., Grelle, A., Heinesch, B., Herbst, M., Hörtnagl, L., Klemedtsson, L., Lindroth, A., Lohila, A., McDermitt, D.K., Meier, P., Merbold, L., Nelson, D., Nicolini, G., Nilsson, M.P., Peltola, O., Rinne, J., and Zahniser, M., 2018. Standardization of eddy covariance flux measurements of methane and nitrous oxide. *Int. Agrophys.*, 32, 517-549. doi: 10.1515/intag-2017-0042.
- Peltola, O., Raivonen, M., Li, X., and Vesala, T (2018). Technical note: Comparison of methane ebullition modelling approaches used in terrestrial wetland models. *Biogeosciences*, 15, 937-951, doi: 10.5194/bg-15-937-2018.
- Raivonen, M., Smolander, S., Backman, L., Susiluoto, J., Aalto, T., Markkanen, T., Mäkelä, J., Rinne, J., Peltola, O., Aurela, M., Lohila, A., Tomasic, M., Li, X., Larmola, T., Juutinen, S., Tuittila, E.-S., Heimann, M., Sevanto, S., Kleinen, T., Brovkin, V., and Vesala, T. (2017). HIMMELI v.1.0: Helsinki Model of MEthane buiLd-up and emISSION for peatlands. *Geoscientific Model Development*, 10, 4665-4691, doi: 10.5194/gmd-10-4665-2017.
- Rebmann, C., Aubinet, M., Schmid H.P., Arriga, N., Aurela, M., Burba, G., Clement, R., De Ligne, A., Fratini, G., Gielen, B., Grace, J., Graf, A., Gross, P., Haapanala, S., Herbst, M., Hörtnagl, L., Ibrom, A., Joly, L., Kljun, N., Kolle, O., Kowalski, A., Lindroth, A., Loustau, D., Mammarella, I., Mauder, M., Merbold, L., Metzger, S., Mölder, M., Montagnani, L., Papale, D., Pavelka, M., Peichl, M., Roland, M., Serrano-Ortiz, P., Siebicke, L., Steinbrecher, R., Tuovinen, J.-P., Vesala, T., Wohlfahrt, G. and Franz, D., 2018. ICOS eddy covariance flux-station site setup: a review. *Int. Agrophys.*, 32, 439-455. doi: 10.1515/intag-2017-0044.
- Sabbatini, S., Mammarella, I., Arriga, N., Fratini, G., Graf, A., Hörtnagl, L., Ibrom, A., Longdoz, B., Mauder, M., Merbold, L., Metzger, S., Montagnani, L., Pitacco, A., Rebmann, C., Sedlak, P., Sigut, L., Vitale, D. and Papale, D., 2018. Eddy covariance raw data processing for CO₂ and energy flux calculation at ICOS ecosystem stations. *Int. Agrophys.*, 32, 495-515. doi: 10.1515/intag-2017-0043.
- Susiluoto, J., Raivonen, M., Backman, L., Laine, M., Mäkelä, J., Peltola, O., Vesala, T., and Aalto, T. (2018). Calibrating a wetland methane emission model with hierarchical modeling and adaptive MCMC. *Geoscientific Model Development*, 11, 1199-1228, doi:10.5194/gmd-11-1199-2018.
- Vesala, T., Sevanto, S., Grönholm, T., Salmon, Y., Nikinmaa, E., Hari, P. and Hölttä, T. (2017) Effect of leaf water potential on internal humidity and CO₂ dissolution: Reverse transpiration and improved water use efficiency under negative pressure. *Front. Plant. Sci.* 8:54, doi: 10.3389/fpls.2017.00054.

FOCUS OF THE RESEARCH OF UEF TEAM, YEAR 2019

A. Virtanen¹, T. Yli-Juuti¹, S. Schobesberger¹, K. Lehtinen¹, S. Mikkonen¹

¹Department of Applied Physics, University of Eastern Finland, Yliopistoranta 1, 70210 Kuopio, Finland

Keywords: SOA, AEROSOL-CLOUD INTERACTION, VOC OXIDATION

INTRODUCTION

The persistent uncertainties related to aerosol radiative forcing in the changing climate can be related both to unknowns in process level details, and to the gap between the detailed understanding of processes, and their representation in large scale models. Hence, systematic work connecting process level information and large scale models is needed to take the step from understanding atmospheric aerosol properties and loadings to quantifying their true impact on climate forcing. Recently, the aim of our activities at UEF have been directed to bridge this gap especially for aerosol-cloud interaction, and our methodological starting point of the process-level experimental investigations have been strongly guided by and conducted with the ultimate aim of improving climate models and reducing uncertainty.

METHODS

Our methodological tool pack is spanning from carefully planned laboratory scale measurements and process modelling targeted to investigate the central aerosol properties (e.g. Buchholz et al., 2019, Li et al., 2019, Tikkanen et al., 2019, Schobesberger et al., 2018, Mohr et al., 2019, D'Ambro et al., 2019) to aerosol-climate modelling (Kuhn et al., 2019), intensive field campaigns, and long term atmospheric observations combining the remote sensing and in-situ measurements (e.g. Yli-Juuti et al., 2019, Leinonen et al., 2019). Our main research topics are related to atmospheric organic aerosols, from precursor vapour emissions to aerosol-cloud interaction. In our laboratory studies we are focusing for example on the investigations of the effect of complexity of precursor gases (e.g. real plant emissions, or combustion emissions) on the properties of formed aerosol or on the yields of specific precursors (Kari et al., 2019, Ylisirniö et al., 2019). We are currently improving our capabilities to use novel statistical analysis methods both in laboratory and atmospheric data analysis (Joutsensaari et al., 2018, Mikkonen et al., 2019, Isokääntä et al., 2019). A good example of our "bridging the scales" approaches is our development of new methods to quantify the vapour pressures of organic oxidation products by combining laboratory measurements and process modelling. The process level information is then implemented both to the process models to investigate the effects of uncertainties in volatility on the number of CCN formed in the atmosphere, and to large scale climate models (ECHAM) to investigate the effect of volatility description on aerosol forcing. One of our special focus areas is to combine the mitigation policies and climate models to increase the societal relevance of our research (Kühn et al., 2019).

COLLABORATION

The group's excellent research facilities and wide collaborative network allow us to integrate the laboratory and outdoor measurements with theories and models in order to understand and predict the impacts of human-caused and natural changes on climate. Our main collaborators related to the current and near future activities are listed below:

- FCoE teams
- Prof. Ilona Riipinen, Stockholm University, Sweden
- Prof. Douglas Worsnop, Aerodyne Research, USA
- Prof. Joel Thornton, University of Washington, USA

- Prof. Sergey Nizkorodov, University of California, Irvine, USA
- Assist. Prof. Claudia Mohr, Stockholm University, Sweden
- Prof. Heikki Junninen, University of Tartu, Estonia
- Prof. Gordon McFiggans, University of Manchester; Great Britain
- Prof. Frank Stratmann, Leibniz Institute for Tropospheric Research, Germany
- Prof. Imre Salma, Eötvös Loránd University, Hungary
- Assoc. Prof. James Blande, UEF, Finland
- Prof. Kati Kulovesi, UEF, Finland
- Assoc Prof. Aku Seppänen, UEF, Finland
- H2020 project FORCeS Team
- CLOUD collaboration

ACKNOWLEDGEMENTS

This work was supported by the Academy of Finland Centre of Excellence (grant no 307331) and Academy of Finland project nos. 299544 and, 309142, 310682, 317373, 325647.

REFERENCES

- Buchholz, A., Lambe, A., Ylisirniö, A., Li, Z., Tikkanen, O.-P., Faiola, C., Kari, E., Hao, L., Luoma, O., Huang, W., Mohr, C., Worsnop, D.R., Nizkorodov, S., Yli-Juuti, T., Schobesberger, S., Virtanen, A. Effect of RH and O:C ratio on a-pinene Secondary Organic Aerosol particle evaporation, *Atmos. Chem. Phys.*, 19, 4061-4073, doi.org/10.5194/acp-19-4061-2019, 2019a.
- Buchholz, A., Ylisirniö, A., Huang, W., Mohr, C., Canagaratna, M., Schobesberger, S., Virtanen, A. Deconvoluting FIGAERO-CIMS thermal desorption profiles using Positive Matrix Factorisation to identify chemical and physical processes during particle evaporation, submitted to *Atmos. Chem. Phys.*, October 2019b.
- D'Ambro, E. L., Schobesberger, S., Gaston, C. J., Lopez-Hilfiker, F. D., Lee, B. H., Liu, J., Zelenyuk, A., Bell, D., Cappa, C. D., Helgestad, T., Li, Z., Guenther, A., Wang, J., Wise, M., Caylor, R., Surratt, J. D., Riedel, T., Hyttinen, N., Salo, V. T., Hasan, G., Kurtén, T., Shilling, J. E., Thornton, J. A. Chamber-based insights into the factors controlling epoxydiol (IEPOX) secondary organic aerosol (SOA) yield, composition, and volatility, *Atmos. Chem. Phys.*, 19, 11253-11265, 2019.
- Isokääntä I., Kari E., Buchholz A., Hao L., Schobesberger S., Virtanen A., and Mikkonen S.: Comparison of dimension reduction techniques in the analysis of mass spectrometry data. Submitted to *Atmos. Meas. Tech.* 2019.
- Kari, E., Hao, L., Ylisirniö, A., Buchholz, A., Leskinen, A., Yli-Pirilä, P., Nuutinen, I., Kuuspalo, K., Jokiniemi, J., Faiola, C.L., Schobesberger, S., Virtanen, A. Potential dual effect of anthropogenic emissions on the formation of biogenic SOA, Accepted to *Atmos. Chem. Phys.*, October 2019.
- Kühn, T., Kupiainen, K., Miinalainen, T., Kokkola, H., Paunu, V.-V., Laakso, A., Tonttila, J., Van Dingenen, R., Kulovesi, K., Karvosenoja, N., and Lehtinen, K. E. J. (2019) Effects of Black Carbon Mitigation on Arctic Climate. *Atmos. Chem. Phys. Discuss.*, in review, doi:10.5194/acp-2019-864.
- Leinonen, V., Heikkinen, S., Nieminen, T., Yli-Juuti, T., Virtanen, A., and Mikkonen, S. Trends of particle number-size distribution parameters, in Proceedings of 'the Center of Excellence in

Atmospheric Sciences (CoE ATM) -From Molecular and Biological Processes to the Global Climate' Annual Meeting 2019, 2019.

- Li, Z, Tikkanen, O.-P., Buchholz, A., Hao, L., Kari, E., Yli-Juuti T., and Virtanen, A. Effect of decreased temperature on the evaporation of α -pinene secondary organic aerosol particles, Submitted to Earth and Space Chem., September 2019.
- Mikkonen, S., Pitkänen, M. R. A., Nieminen, T., Lipponen, A., Isokääntä, S., Arola, A., and Lehtinen, K. E. J. Technical note: Effects of uncertainties and number of data points on line fitting – a case study on new particle formation, Atmos. Chem. Phys., 19, 12531–12543, [doi:10.5194/acp-19-12531-2019](https://doi.org/10.5194/acp-19-12531-2019), 2019.
- Mohr, C., Thornton, J. A., Heitto, A., Lopez-Hilfiker, F. D., Lutz, A., Riipinen, I., Hong, J., Donahue, N. M., Hallquist, M., Petäjä, T., Kulmala, M. and Yli-Juuti, T. Molecular identification of organic vapors driving atmospheric nanoparticle growth, Nature Communications, 10, 4442, 2019.
- Roldin, P., Ehn, M., Kurten, T., Olenius, T., Rissanen, M.P., Östrom, E., Sarnela, N., Rantala, P., Hao, L., Hyttinen, N., Heikkinen, L., Worsnop, D., Pichelstorfer, L., Petäjä, T., Kulmala, M., Virtanen, A., Riipinen, I., Boy, M. Constraining the sources, sinks and contribution of highly oxygenated molecules to the growth of new particles over the Boreal forest region, Nature Communications, 10, 4370, 2019.
- Tikkanen, O.-P., Buchholz, A., Ylisirniö, A., Schobesberger, S., Virtanen, A., and Yli-Juuti, T. Comparing SOA volatility distributions derived from isothermal SOA particle evaporation data and FIGAERO-CIMS measurements, Submitted to Atmos. Chem. Phys., October 2019.
- Ylisirniö, A., Buchholz, A., Mohr, C., Li, Z., Barreira, L., Lambe, A., Faiola, C., Kari, E., Yli-Juuti, T., Nizkorodov, S., Worsnop, D., Virtanen, A., and Schobesberger S. Composition and volatility of SOA formed from oxidation of real tree emissions compared to single VOC-systems., Submitted to Atmos. Chem. Phys., October 2019.
- Yli-Juuti, T., Mielonen, T., Kokkola, H., Arola, A., Lipponen, A., Heikkinen, L., Nieminen, T., Ehn, M., Petäjä, T. and Virtanen, A., Climatic significance of biogenic aerosols in warming boreal forest: part 1. In situ observations on organic aerosol, in Proceedings of 'the Center of Excellence in Atmospheric Sciences (CoE ATM) -From Molecular and Biological Processes to the Global Climate' Annual Meeting 2019, 2019.

CO-CREATING NEW CLIMATE EDUCATION IN THE FINNISH UNIVERSITIES

M. ÄIJÄLÄ, L. RIUTTANEN

Institute for Atmospheric and Earth System Research, University of Helsinki, Helsinki, 00560, Finland

Keywords: climate change education, education development

INTRODUCTION

In our ever faster changing world, in addition to population and economic growth also the environmental crises are accelerated. Solving the climate and sustainability emergencies demands a rapid response from human societies (IPCC, 2018). Not only do we need to urgently rebuild our fossil-based energy production, industry, transportation and agriculture, but a critical examination of many prevailing societal and economic paradigms seems unavoidable. In managing such revolutionary social systemic transition in the required brief timeframe, comprehensive education of citizens in climate and sustainability issues is a key to change, specifically in democratic states and societies.

Although a traditional forerunner in the field of education, also Finland needs to create a solid program for climate change and sustainability education of its citizens. To date, a multitude of inspiring individual projects and programs have sprung up in the recent few years, and individual higher education courses exist in the Finnish universities (Liljeström and Monni, 2015), but their scale and reachability remains on average limited and is often constrained in funding and/or expertise. Specifically in higher education, silo mentality and lack of multidisciplinary remains a challenge in climate education (Lehtonen and Cantell, 2015). Thus, wider and more comprehensive programs on climate change and sustainability education are needed to bring together the best practices, ideas and experts and to pool contributions of individual actors for improved resource efficiency and maximal societal impact.

Recently, the nationwide Climate University project (blogs.helsinki.fi/climateuniversity) was established to advance climate and sustainability in Finnish higher education, in collaboration with schools and the working life. To accommodate the wide variety of needs of universities, students and teachers from all parts of Finland, online learning and digital materials were chosen as the basis for the new climate education. All learning materials would also be open access to maximise their outreach and availability. These principles were already piloted in the Climate.now project in 2016 (www.climatenow.fi) and the Climate.now courses are currently run in seven universities in Finland (Martikainen, 2019). Considering the high-level expertise and resources available from all the major participating universities, we foresee Climate University has the potential to thoroughly reshape and re-create the Finnish climate education field.

METHODS

To incorporate the finest ideas both from inside and outside of the academic community, collaborative re-imagining was selected as the working method for creating the new climate and sustainability education schemes. To accomplish gathering the experts' ideas, a workshop was held where major themes of climate education were discussed, starting from the question of "what kind of expertise (education) is needed in the near future, in order to answer the challenges of climate change and sustainability?" From the talks, a preliminary list of important topics (see the Results section) was compiled.

This preliminary agenda was then expanded and elaborated on, in the form of 'needs assessment' survey for the Climate University community. This comprehensive survey, conducted in January to March 2019, received 49 responses and yielded useful quantitative data and comments for planning of the activities and materials of the Climate University program. The survey and its results, summarised in Results, are available

in more detail in the needs assessment report (Äijälä, 2019), available online. Based on the results of the survey, plans for activities and materials of the Climate University were then drafted.

The core of the Climate University program consists of 9 workshops for further educating teachers and staff in higher education and in collaborating schools, NGO's and private sector. Overall, two large massive open online courses (MOOCs) would be produced along with smaller courses and additions to existing climate education online materials. Within these frames, the Climate University community was given rather free hand to decide how to best advance climate education.

RESULTS & DISCUSSION

From the preliminary talks in the opening workshop of Climate University, the following important themes emerged:

Multidisciplinarity – crossing the traditional borders of natural (or technical, engineering) vs human (sociological) sciences is necessary.

Holistic understanding of the grand challenges is required, and specifically, systems thinking is important. It is important to try to see the bigger picture and not look at the challenges from a single, narrow angle.

Impactful decisions are based on *data and statistics*, to but it is equally important to keep in mind the personal, *human perspective (choices, values, ethics, and principles)* and create an emotional connection to the challenges, to bring about change in the society.

Science communication is key. Academic knowledge needs to be communicated to the decision makers, but academics equally *need to understand political decision-making.*

Including the private sector and markets in answering the challenges and considering finances and the economics is needed, and (green technology) business opportunities and innovations need to be recognized. However, focusing too much on innovations and technical solutions may hinder grasping the bigger picture of the challenges.

Consumer perspective is important to consider – green choices need to be made easy. *Sustainability education* (in e.g. circular economy) in schools is necessary, to *educate responsible citizens and customers* of the future.

These were then further charted in the needs assessment survey, which surveyed the estimated education material needs and expertise of the participants' organisations. Additionally, open format text answers were allowed for commenting the themes and planned activities of Climate University and for proposing new ideas and themes additional to those mentioned above. Based on the analysis of the survey answers, the following themes and suggestions stood out (Äijälä, 2019): (1) *inter-disciplinarity* and *holistic understanding* were considered the ones with most pressing need for education material. In connection to these, *systemic thinking* was often specifically mentioned. (2) An "introduction to sustainability" type of course was proposed in multiple open answers, as it seems this type of a basic course is missing from many university level curricula. (3) A project course for collaboration between universities and the private sector, as well as (4) an online course on the basics of climate change for high schools were both considered necessary from the perspective of encouraging interactions between the academia and other equally important sectors of the society. Finally, there were several suggestions for smaller, additional material packages (5) on topics such as: science communication, Arctic or Nordic perspectives, scientific basis of climate change, values and ethics modules, statistical tools and data course, climate anxiety and philosophy, nexus of sustainable development goals.

To accommodate the list of topics highlighted by the survey participants, plans for the following new Climate University courses were drafted (Table 1).

Course name	Topic	Size	Level	Themes
Systemchange.now	Systems thinking in global challenges.	5 cr	Master	Systemic change, multidisciplinary, holism, impactful decisions
Sustainable.now	Introduction to sustainability in climate change	5 cr	Bachelor	Multidisciplinary, values and ethics, consumer perspective, citizen responsibility
Solutions.now	Project course in private sector collaboration	5 cr	Master	Private sector and markets, Consumer perspective
Climate.now for schools	High school level course on basics of climate change	2 cr	High school	Multidisciplinary, values and ethics, sustainability education, science communication
Climate data and statistics	Statistical tools for analysing climate data	5 cr	Master	Data and statistics
Science communication	Science communication in climate topics	1 cr	Bachelor	Science communication, values and ethics

Table 1. Climate University program new courses and their basic information.

The proposed courses thus cover the topics highlighted in the needs assessment and offer a solid foundation for climate education in Finnish higher education, while also contribution to climate and sustainability education in schools and the private sector. Additionally to the new courses and education materials, Climate University also provides additional, continuous education, and has helped educate hundreds of teachers, experts, workers and students in workshops organised across Finland. The Climate University community has already formed an active network of Finnish higher education organisations and active collaborators from high schools, NGOs and private companies.

While the work for renewal of climate education is still ongoing, the Climate University program is off to a promising start. The agenda to design future climate education in an open, transparent and inclusive way has certainly encouraged openness, new thinking and genuine collaboration across the traditional academic silos – something that is not be taken for granted.

ACKNOWLEDGEMENTS

The Climate University is funded for years 2019-2020 by the Ministry of Education, The Finnish Innovation Fund Sitra, The universities of Helsinki, Jyväskylä, Oulu, Tampere and Turku, the Aalto University, the LUT-University, University of Eastern Finland and the Lahti, Metropolia and Turku Universities of Applied Sciences.

REFERENCES

Climate University blog. blogs.helsinki.fi/climateuniversity (last accessed 18.Oct.2019)

IPCC (editors: Hoegh-Guldberg, O., Jacob, D., Taylor, M., Bindi, M., Brown, S., Camilloni, I., Diedhiou, A., Djalante, R., Ebi, K., and Engelbrecht, F) (2018). Impacts of 1.5 °C global warming on natural and human systems.

Lehtonen A. and Cantell H. (2015). Suomen ilmastopaneeli, raportti 1/2015: Ilmastokasvatus osaamisen ja vastuullisen kansalaisuuden perustana. Available online at <https://www.ilmastopaneeli.fi/wp-content/uploads/2018/10/Ilmastokasvatuksen-raportti-9.6.2015.pdf> (last accessed 18.Oct.2019)

Liljeström E. and Monni S. Ilmastoalan yliopisto-opetuksen nykytila Suomessa. Sitra-commissioned report by Benviroc Oy. (2015). Available online at https://media.sitra.fi/2017/02/27175124/Ilmastoalan_yliopisto_opetuksen_nykytila_suomessa-2.pdf (last accessed 18.Oct.2019)

Martikainen J. (2019) Säteilypakote-käsitteen oppiminen Ilmasto.nyt-kurssilla. Pro Gradu Thesis, University of Helsinki. Available online at <http://hdl.handle.net/10138/305177> (last accessed 25.Oct. 2019).

Äijälä M. (2019). Climate University: Assessment of needs report, available online at https://blogs.helsinki.fi/climateuniversity/files/2019/06/CU_needs_assessment.pdf (last accessed 17.Oct. 2019).

WITHIN-CANOPY VARIATION OF VOC EMISSIONS FROM SCOTS PINE CANOPY

J. AALTO^{1,2}, E. SIIVOLA², P. KOLARI² and J. BÄCK³

¹SMEAR II, Hyytiälä Forestry Field Station, Juupajoki, University of Helsinki

²Institute for Atmospheric and Earth System Research / Physics

Faculty of Science, University of Helsinki, Finland

³Institute for Atmospheric and Earth System Research / Forest Sciences, Faculty of Agriculture and Forestry, University of Helsinki, Finland

Keywords: HYDROCARBONS, PLANT-ATMOSPHERE EXCHANGE, PLANT EMISSIONS

INTRODUCTION

Boreal forests are the most significant source of volatile organic compounds (VOCs) in Northern Europe, emissions originating both from trees and forest floor. The VOCs are reactive trace gases that participate in chemical reactions in the atmosphere, thus affecting aerosol formation and climate.

In field conditions, VOC emissions are typically measured on top of the tree canopies, under unshaded conditions (for example Aalto et al. 2014; 2015). However, the responses of VOC synthesis and emissions on environmental factors lower in the canopy may differ from those detected under unshaded conditions, mainly because the needles lower in the canopy have physically and physiologically acclimated to different conditions than those located upper in the canopy.

The overall aim of this study was to characterize the spatial variability of VOC emissions from different parts of Scots pine canopy and explain the processes and phenomena affecting those.

METHODS

Measurements were conducted at SMEAR II measurement station, in Southern Finland. A dynamic shoot enclosure equipped with eight light sensors and temperature sensor was installed to lower part of the canopy, and the detected VOC emission rates were compared to those measured on top of the canopy. Proton transfer reaction – quadrupole mass spectrometer was used as VOC detector. The measurements were continued over several days, after which the enclosure located lower in the canopy was moved to another location to the canopy. In total, five data sets were measured during two summers, in 2011 and 2013.

RESULTS

Acetaldehyde and acetone emission rates were comparable between the lower parts of canopy and top of the canopy (fig. 1). Methanol emission rates were comparable in 2013, but in 2011 the pine shoot located in top of the canopy emitted clearly higher amounts of methanol than those located lower in the canopy (fig. 1). Monoterpene emission rates were comparable in 2011, but in 2013 the pine shoots located in lower parts of the canopy emitted clearly higher amounts of monoterpenes than those located lower in the canopy (fig. 1). Temperature responses (β parameters) for all studied compounds were equal between the shoots located lower and upper in the canopy.

In 2011 the monoterpene emission capacities under standardized conditions (hybrid algorithm, $T=30\text{ }^{\circ}\text{C}$ and $\text{PPFD}=1000\text{ }\mu\text{mol m}^{-2}\text{ s}^{-1}$) were roughly comparable between the top and the lower parts of the canopy, although lower parts of the canopy exhibited somewhat higher pool emission potential than the top parts of the canopy (fig. 2). However, in 2013 data the monoterpene emission capacity lower in the canopy was more than double compared to that of the top part of the canopy (fig. 2). Again, pool emission potential

comprised about half of the total monoterpene emission potential in the lower parts of the canopy, while in the top parts of the canopy the pool emission potential is only about one third of the total monoterpene emission potential.

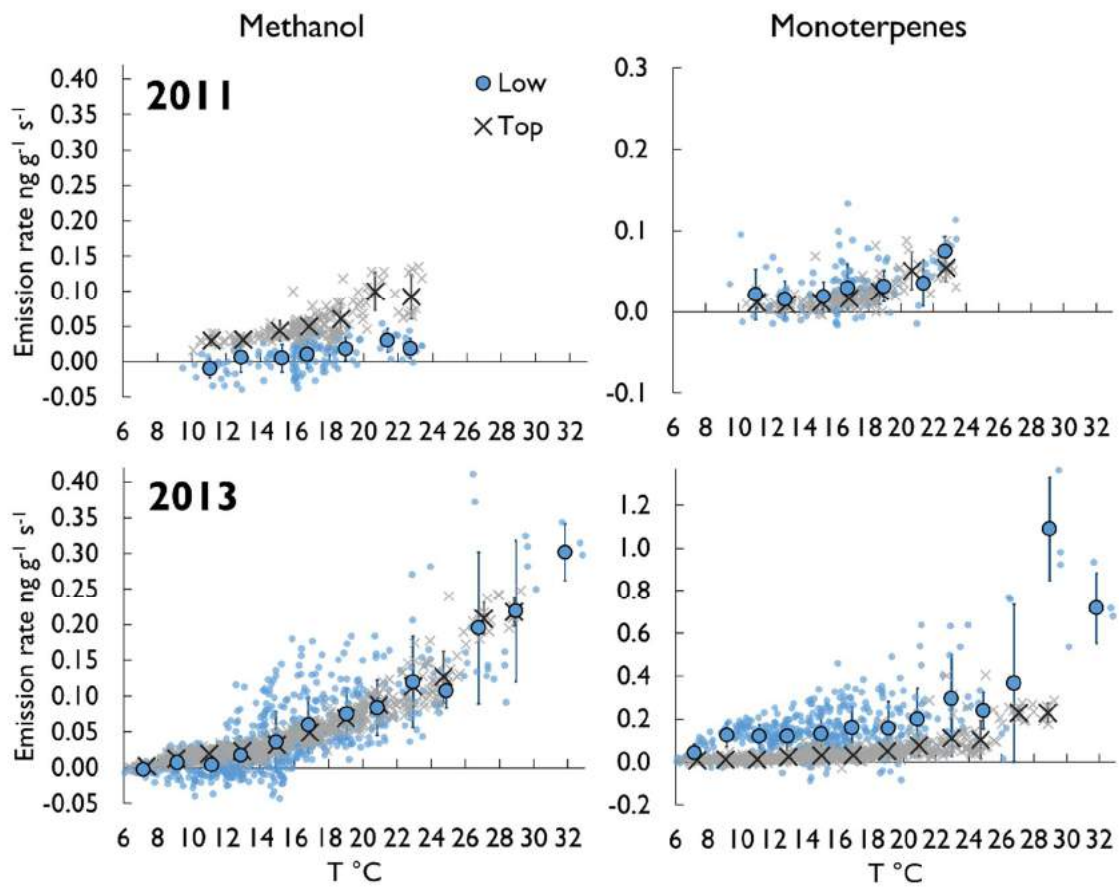


Figure 1. Relation between temperature and VOC emission rates (methanol and monoterpenes) in different parts of canopy. The upper panel is for 2011 data and the lower panel is for 2013 data. Large circles and crosses represent the mean emission rates within 2 degree bins. The error bars represent standard deviation within the temperature bins. The light grey and blue marks represent individual closures.

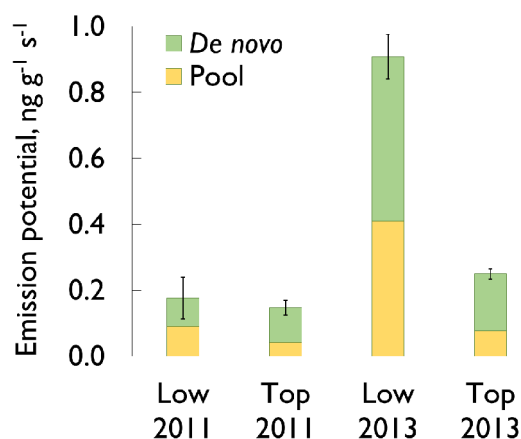


Figure 2. *De novo* and pool monoterpene emission potentials obtained using hybrid model for both study years and parts of the canopy. The error bars represent the 95 % confidence intervals around the total emission potential.

CONCLUSIONS

To our knowledge, these data are the most extensive set of results explaining the within-canopy VOC emission variability to date. The overall conclusion is that the lower parts of canopy release about the same amount of VOCs to atmosphere when compared to the top parts of the canopy. On the other hand, because the lower parts of canopy receive less radiation than the top parts of canopy, it's obvious that the lower parts of canopy have higher capacity per needle mass or area unit to produce and release VOCs than the top parts of canopy. There is no specific need for taking into account the canopy light environment and the effect of needle location on emission capacity in modelling efforts, if we can assume that higher emission capacity of lower parts of the canopy in general compensates the lower radiation availability. However, because that assumption is extremely strong and contains high risk of failure, we recommend that in modeling applications one should carefully consider the role of VOCs emitted by lower parts of the canopy.

ACKNOWLEDGEMENTS

The work was supported by the Academy of Finland Center of Excellence programme (grant no. 307331).

REFERENCES

- Aalto, J., P. Kolari, P. Hari, V.-M. Kerminen, P. Schiestl-Aalto, H. Aaltonen, J. Levula, E. Siivola, M. Kulmala and J. Bäck (2014). New foliage growth is a significant, unaccounted source for volatiles in boreal evergreen forests. *Biogeosciences* **11**, 1331-1344.
- Aalto, J., A. Porcar-Castell, J. Atherton, P. Kolari, T. Pohja, P. Hari, E. Nikinmaa, T. Petäjä and J. Bäck (2015). Onset of photosynthesis in spring speed up monoterpene synthesis and leads to emission bursts. *Plant, Cell & Environment* **38**.

FIRE-INDUCED CHANGES IN QUALITY OF SOIL ORGANIC MATTER IN BOREAL PERMAFROST REGION OF CANADA

H. AALTONEN¹, M. PALVIAINEN¹, X. ZHOU¹, E. KÖSTER¹, F. BERNINGER², J. PUMPANEN³, K. KÖSTER¹

¹Department of Forest Sciences, University of Helsinki, PO Box 27 (Latokartanonkaari 7), Fi-00014, Finland

²Department of Environmental and Biological Sciences, University of Eastern Finland, PL 111, FI- 80101 Joensuu, Finland

³Department of Environmental and Biological Sciences, University of Eastern Finland, PL 1627, FI-70211, Kuopio, Finland

Keywords:

INTRODUCTION

The soils in the Northern Hemisphere permafrost area contain around 50% of the global soil carbon (C) (Davidson and Janssens, 2006). Due to warming climate this significant frozen C pool is becoming vulnerable: one fourth of this storage could thaw by the end of the century, exposing previously frozen soil organic matter (SOM) to decomposition. (Davidson and Janssens, 2006). The degradation of frozen SOM would lead to additional release of greenhouse gases; a positive feedback to global warming. Currently permafrost soils are vastly covered by boreal forests acting as C sinks. However, the frequency of boreal forest fires has been on the rise in the last decades and fires further advance the permafrost thaw. The possible greenhouse gas emissions from these soils are, among other factors, dependent on the effects of fire on soil properties and the quality of permafrost SOM itself.

METHODS

Four differently aged fire chronosequences were established in the Canadian boreal forest permafrost region. The study areas were located along the Dempster Highway in Yukon and Northwest territories. Soil samples were collected from soil pits from the depths of 5, 10, 30 and 50 cm. We also measured the soil organic layer depth, active layer depth, ground- and tree biomass, species composition and species coverage.

We conducted chemical fractionation of SOM with water, ethanol and sulphuric acid extractions to determine the different SOM pools (such as sugars, waxes and fats and lignin) and compare the proportional size of the fractions between time since last fire occurrence. We also analyzed ¹⁵N and ¹³C isotopic of soil samples with an elemental analyser (FlashEA 1112 Series, Thermo Fischer Scientific, Waltham, MA) coupled to an isotope ratio mass spectrometer (IRMS, DELTA plusXP[®], Thermo Electron Fischer Scientific, Waltham, MA). In addition we performed an incubation experiment in a climatic chamber (24 h in 1, 7, 13 and 19 °C) to determine the soil temperature sensitivity (Q_{10}) and the soil heterotrophic respiration rates and microbial metabolic quotient qCO_2 , the respiration rate per microbial biomass C.

CONCLUSIONS

Our results showed that fire increased the active layer depth (seasonally freezing and thawing layer) on top of permafrost, indicating permafrost thaw. Fires also decreased the soil organic layer depth, thus affecting the SOM quality and quantity. The proportional size of the most labile SOM fractions (water- and ethanol soluble) were decreased in the 5 cm depth after the latest fire compared to older fire areas. This was also observed as increased temperature sensitivity Q_{10} as more recalcitrant matter may be assumed to have higher Q_{10} values due to kinetic theory. In addition soils were enriched with heavier isotopes post-fire. We found no significant changes in the heterotrophic soil respiration rates, but fire appeared to increase the microbial

metabolic quotient, meaning that the microbial efficiency was decreased: more accumulated C was used for respiration than microbial growth. Forest fire may advance greenhouse gas emissions from permafrost soils due to enhanced permafrost thaw. However, fires also increase the proportional amount of recalcitrant SOM, which could reside in the soil for long periods. According to this chronosequence, the effects of fire on SOM and permafrost depth are temporary and reach the original status with forest succession. If the fire frequency increases, the forest rotation time becomes shorter and less C will be stored in the soil (Kaipainen et al. 2004; Hoy et al. 2016). At the same time labile C may be lost in fire, while simultaneously recalcitrant C is formed. This could decrease the CO₂ emissions from post-fire soils. In these upland mineral soils, the SOM quality at permafrost surface appeared reasonably low.

ACKNOWLEDGEMENTS

This study was supported by the Academy of Finland (Projects No. 286685, 294600, 307222).

REFERENCES

- Davidson EA, Janssens IA (2006) Temperature sensitivity of soil carbon decomposition and feedbacks to climate change. *Nature* 440:165–173.
- Kaipainen T, Liski J, Pussinen A, Karjalainen T (2004) Managing carbon sinks by changing rotation length in European forests. *Environ Sci Policy* 7:205–219.
- Hoy EE, Turetsky MR, Kasischke ES (2016) More frequent burning increases vulnerability of Alaskan boreal black spruce forests. *Environ Res Lett* 11:095001.

IMPACTS OF SUB-CANOPY REMOVAL ON STAND LEVEL VOLATILE ORGANIC COMPOUNDS (VOC) EXCHANGE

A. AHI¹, J. BÄCK¹, J. AALTO²,

¹Institute of Atmosphere and Earth system Research/Forest Sciences, University of Helsinki, Finland

² Institute of Atmosphere and Earth system Research/Dept. of Physics, University of Helsinki, Finland

Keywords: Volatile Organic Compounds (VOCs), Sub-canopy thinning, Monoterpene, Methanol.

INTRODUCTION

Removal of sub-canopy trees is a common type of forest management practiced in Finland (Vesala *et al.*, 2005), also referred to as undergrowth thinning. It is employed to meet various objectives such as improving yields of residual overstory trees, increasing resilience to drought, enhancing ecosystem processes, and promoting forest gross primary productivity (D'Amato *et al.*, 2013; Shen *et al.*, 2019; Zeide, 2004). After thinning, remaining trees have access to higher resources, therefore their growth rate increases (Vesala *et al.*, 2005). Thinning, however, can also be a source of disturbance to the forest ecosystem, as it, for example, modifies understory vegetation and creates establishment sites for colonizing species (Dodson *et al.*, 2008). Due to such contradictory implications, it is important to examine the consequences of thinning on the forest ecosystem and microclimate.

A significant consequence of sub-canopy removal is its effect on the forest stand level emission of volatile organic compounds (VOCs) to the atmosphere (Räisänen *et al.* 2008). VOCs are involved in plant growth, development, reproduction, defence, and function as communication media within and between plants (Laothawornkitkul *et al.*, 2009). These plant-released VOCs have high chemical reactivity with large mass emission rate from vegetation into the atmosphere (Laothawornkitkul *et al.*, 2009); therefore, they are major determinants of atmospheric gas composition that have important implications for the Earth's climate (Koppmann, 2007). Volatile isoprenoids such as monoterpenes and isoprene are particularly important among VOCs because of their high reactivity in the atmosphere and their contribution to the total plant emission (Niinemets *et al.*, 2009).

Recently, studies have begun to measure VOCs fluxes using mainly proton transfer reaction mass spectrometry, quantifying VOCs emissions, and describing how they affect microclimate (e.g., Rantala *et al.*, 2015; Schallhart *et al.*, 2018). Yet the long-term concentrations of VOCs in the air above the canopy is still rare. Those few studies that focus on VOCs concentrations look into the concentration on a short-term perspective. For example, Lappalainen *et al.* (2009) study seasonal changes of VOC concentration in the upper canopy of a boreal forest for merely two consecutive years. Similarly, Rinne *et al.* (2005) study VOC concentration analyzing daily and diurnal changes only during one summer month. Others have looked at the VOC emission from soil (see Peñuelas *et al.*, 2014), not from the forest stand. Motivated by this gap in the literature, we set out to study the long-term concentrations of VOCs above a boreal forest from May 2010 to August 2019. In addition, we investigate the possible effect of a sub-canopy thinning, which was performed in spring 2019 in the site where our measurements have been conducted, on VOC concentration.

METHODS

VOC measurements have long been conducted at SMEAR II in Hyytiälä, southern Finland. Hyytiälä is located in the boreal region, with the dominant tree species as Scots pine (*Pinus sylvestris*), with some

Norway spruce (*Picea abies*) and some broadleaved trees such as European aspen (*Populus tremula*), birch (*Betula* sp.), and rowan (*Sorbus aucuparia*; see Hari and Kulmala (2005) for a detailed description of the station and the surrounding nature). The canopy height is 18m and the stand density is approximately 1300ha^{-1} (Schallhart et al., 2018). To do the measurement, the proton transfer reaction quadrupole mass spectrometer (PTR-MS, manufactured by Ionicon Analytik GmbH, Innsbruck, Austria) has been used, which measures different masses from a measurement level at a tower standing at 33.6 meter height. Out of 27 masses measured by PTR-MS, we analysed six masses: methanol, acetaldehyde, acetone, isoprene, toluene, and monoterpenes.

CONCLUSIONS

In SMEAR II station, VOCs have been measured for more than a decade. In this research, we study measurements from May 2010 to August 2019. To the best of the authors' knowledge, these measurements are the longest, relatively continuous VOCs measurement from a forest stand. As an example, we present monoterpene concentrations in Figure 1a. Since in spring 2019 the stand underwent a sub-canopy thinning, to understand whether the thinning had any effects on monoterpene concentrations, we compare the concentrations in June 2018 with those in June 2019 (see Figure 1b). As can be seen, concentrations during June 2019 are noticeably higher than those in June 2018. However, other environmental variables such as temperature, soil water content and moisture, and light play a role in VOC emissions from trees. Therefore, whether this is due to sub-canopy thinning or other factors need to be scrutinized further.

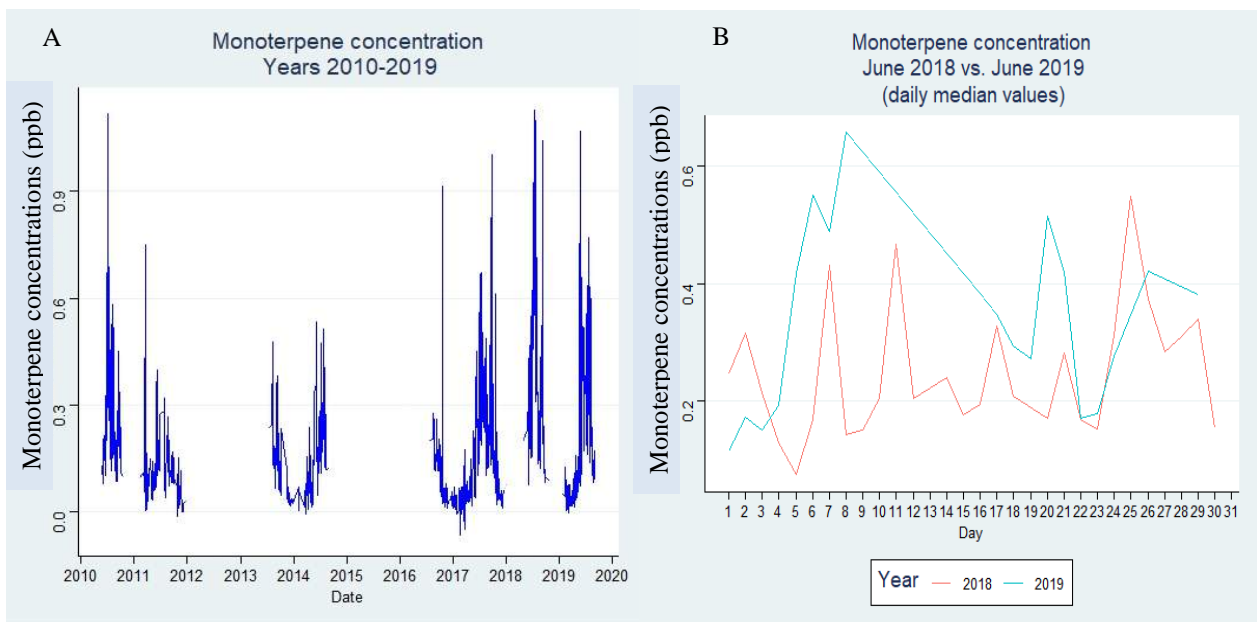


Figure 1. Concentration of monoterpene a) Daily median values of monoterpene concentration from May 2010 to August 2019, b) Comparison of median values of monoterpene concentration in June 2018 with those in June 2019.

ACKNOWLEDGEMENTS

This work was financed by the Academy of Finland (CoE grant, project grant no 324259).

REFERENCES

D'amato, A.W., J.B. Bradford, S. Fraver, and B.J. Palik. (2013). Effects of thinning on drought vulnerability and climate response in north temperate forest ecosystems. *Ecological Application*, 23, 1735–1742.

- Hari, P. and Kulmala, M.: Station for Measuring Ecosystem–Atmosphere Relations (SMEAR II), *Boreal Environmental Research*, 10, 315–322, 2005.
- Koppmann, R. (2007). *Volatile Organic Compounds in the Atmosphere*, Oxford, Blackwell Publishing.
- Laothawornkitkul, J., Taylor, J. E., Paul, N. D., & Hewitt, C. N. (2009). Biogenic volatile organic compounds in the Earth system. *New Phytologist*, 183(1), 27-51.
- Lappalainen, H. K., Sevanto, S., Bäck, J., Ruuskanen, T. M., Kolari, P., Taipale, R., ... & Hari, P. (2009). Day-time concentrations of biogenic volatile organic compounds in a boreal forest canopy and their relation to environmental and biological factors. *Atmospheric Chemistry and Physics*, 9(15), 5447-5459.
- Niinemets, Ü., Monson, R. K., Arneth, A., Ciccioli, P., Kesselmeier, J., Kuhn, U., ... & Staudt, M. (2010). The leaf-level emission factor of volatile isoprenoids: caveats, model algorithms, response shapes and scaling. *Biogeosciences*, 7(6), 1809-1832.
- Peñuelas, J., Asensio, D., Tholl, D., Wenke, K., Rosenkranz, M., Piechulla, B., & Schnitzler, J. P. (2014). Biogenic volatile emissions from the soil. *Plant, cell & environment*, 37(8), 1866-1891.
- Räisänen, T., Ryyppö, A., and Kellomäki, S. (2008). Impact of timber felling on the ambient monoterpene concentration of a Scots pine (*Pinus sylvestris* L.) forest. *Atmospheric Environment*, 42(28), 6759-6766.
- Rantala, P., Aalto, J., Taipale, R., Ruuskanen, T. M., & Rinne, J. (2015). Annual cycle of volatile organic compound exchange between a boreal pine forest and the atmosphere. *Biogeosciences*. 12, 5753-5770.
- Rinne, J., Ruuskanen, T. M., Reissell, A., Taipale, R., Hakola, H., & Kulmala, M. (2005). On-line PTR-MS measurements of atmospheric concentrations of volatile organic compounds in a European boreal forest ecosystem. *Boreal environment research*, 10(5), 425-436.
- Schallhart, S., Rantala, P., Kajos, M. K., Aalto, J., Mammarella, I., Ruuskanen, T. M., & Kulmala, M. (2018). Temporal variation of VOC fluxes measured with PTR-TOF above a boreal forest. *Atmospheric Chemistry and Physics*, 18(2), 815-832.
- Shen, C., Nelson, A. S., Jain, T. B., Foard, M. B., & Graham, R. T. (2019). Structural and Compositional Responses to Thinning over 50 Years in Moist Forest of the Northern Rocky Mountains. *Forest Science*, 1-11.
- Vesala, T., Suni, T., Rannik, Ü., Keronen, P., Markkanen, T., Sevanto, S., ... & Ojansuu, R. (2005). Effect of thinning on surface fluxes in a boreal forest. *Global Biogeochemical Cycles*, 19(2).
- Zeide, B. (2004). Optimal stand density: a solution. *Canadian Journal of Forest Research*, 34(4), 846-854.

NOVEL AEROSOL DILUTER MINIMIZING SIZE DEPENDENT LOSSES DOWN TO 1 NM PARTICLE SIZE

L. R. AHONEN¹, R. BAALBAKI¹, F. KORHONEN, J. VANHANEN, J. KANGASLUOMA^{1,2} and T. PETÄJÄ¹

¹Institute for Atmospheric and Earth System Research / Physics, Faculty of Science, University of Helsinki, Finland

²Aerosol and Haze Laboratory, Beijing Advanced Innovation Center for Soft Matter Science and Engineering, Beijing University of Chemical Technology, Beijing, China

Keywords: SUB 10 NM SAMPLING, DILUTION, CPC.

INTRODUCTION

In any experiment aiming to characterize properties of aerosol particles, the sampling line and its characterization plays an important role in getting reliable data. The sampling line should be designed according to the properties of particles of interest. The size of these particles governs effective diffusional, inertial and gravitational losses and the specifics of optimal sampling line. Therefore 1 nm and 10 μm particles should not share the same sampling line. The smallest aerosol particles diffuse most rapidly and thereby lost to the surfaces of the sampling lines. Larger particles on the other hand are more sensitive to bends and horizontal sections in the sampling line due to their increased inertia and mass making them unable to follow fluid flow and causing them to settle or deposit in the line.

Measurement of the nanoparticle concentrations is often conducted with the condensation particle counting (CPC) technique. CPCs are single particle counting instruments with upper limit of accurate concentration measurement in the range of 10^4 - 10^5 cm^{-3} . In many different measurements, such as car emission or some industrial applications, the particle concentration can easily exceed 10^5 cm^{-3} , which makes the concentration measurement without some kind pre-treatment inaccurate. Further, often most of these particles are smaller than 10 nm in size. Thus, accurate measurements in such systems require particle transport lines, which are characterized for particle losses, and particle concentration dilution upstream of the CPC. Most aerosol diluters are based on mixing particle-free air with the sample.

We have been developing a new nanoparticle sampling system optimized for sub 10 nm particles, which is equipped with a core sampling system and adjustable dilution. The dilution is conducted in very short space with minimized section of reduced flowrate making any size dependent losses in the size range of interest minimal. We characterize the sampling system in the laboratory, and perform computational fluid dynamic CFD model to further verify the design

DESIGN AND APPROACH

The main goal for the design was to get order of ten-to-one dilution without distorting the initial particle population of the sample. This meant minimalizing the diffusional losses still achieving the expected dilution fraction. Secondary goal was to keep design compact taking as little space as possible in front of the instrument it is coupled with. This enables us to easily implement diluter to existing measurement locations.

Starting point of the design was self-contained sampling box that was described in Kangasluoma et al. (2016). Sampling system consisted core sampling to maximize penetration efficiency of small aerosol particles, Zero-measurement as diagnostic test for the used instrument and switchable ion filter with cut-off size of 4.5 nm. We wanted to keep these functionalities while incorporation dilution to the system. We also

wanted to go from self-contained unit to a separate control box which allows more flexibility with installations.

When sampling nanoparticles that are smaller than 10 nm, careful design of the sampling line becomes crucial in order to minimize the diffusional losses. In a tubular and laminar flow, the particle concentration profile becomes parabolic with time. The diffusional losses in laminar pipe flow depends on flow rate length of the particle if fluid properties are kept constant. A common way of estimating the diffusion losses in the sampling lines is by using the Gormley and Kennedy equation (Gormley and Kennedy, 1949).

Result was a cylindrical dilution/sampling piece that attaches between the instrument and its sampling line with standard sized pipe fittings. Design is modular allowing it to be used either with or without dilution. Sample is taken from the middle of the stream and excess flow collected radially around the concave cone shaped probe. This shortens the space required to make sampling without disturbing the flow upstream of the tip of the probe. To extend usable size range towards micrometer sized particle sampling is kept close to isokinetic in order to mitigate over- or under sampling.

Making enough dilution means that flowrate of the sample, which is taken from the core sampling, needs to be pretty small. In order to keep losses acceptable, the distance between core sampling and the region where particle free air is introduced to the flow is kept extremely small. Particle free air is introduced radially into the flow. Because the entire mixed flow is passed through the diluter, uniform mixing of the particle concentration in the flow is not essential. In this type of use this is an advantage, since particles are initially travelling in the middle of the tubular flow after dilution, surrounded by particle free flow. The total flow rate exiting the diluter $Q_{total} = Q_{sample} + Q_{dilution}$ is fixed and determined by the instrument that diluter is coupled with. This limits the maximum to dilution ratio to be around order of magnitude. Dilution systems where sample is mixed with particle free air and then small sample is taken from the mixed flow don't have this limitation. We decided to compromise the maximum dilution ratio in order to optimize penetration efficiency for small aerosol particles which is the key feature.

MODELLING

Preliminary model has been already run with robust and computationally light turbulent model. Fluid flow in the diluter was simulated with Finite Element Method (FEM) using COMSOL 5.3 software. We used Turbulent Flow interface from the CFD module to solve velocity and pressure fields for incompressible flow. The Reynolds number is well within laminar region in the main channel, which particle's encounter while passing through the diluter. Outside these areas, there is, most likely, regions where turbulence occur. Reynolds-Averaged Navier–Stokes (RANS) turbulence model type with $\kappa - \epsilon$ turbulence model was used to take this into account. For the walls, no slip condition is used as a boundary condition in the main channel. In turn, slip condition is used downstream of the radial core sampling in the outflow and before the radial dilution in a clean air inflow. In addition, transport of diluted species package was used to visualize the actual dilution. Our system consists of channels with great differences in dimensions which forced us to use pronouncedly fine mesh. The same CAD drawings were used to create flow domains in the simulation as was used to machine the physical parts. Geometry was slightly modified for the simulation to allow efficient meshing by forming composite faces where continuous surface was defined in unnecessary many pieces. The final model needs to be run with turbulent model that is better suited for solving flow in proximity of walls. In addition, a particle tracing model will be added to model penetration efficiency for a wide particle size range

INITIAL RESULTS

Based on the preliminary results magnitude of the dilution ratio is measured to be close to a ten-to-one dilution which have been the target value. Additionally, there is only moderate additional losses introduced by the diluter unit (Figure 1). This is measured with NiCr – oxide particles that are size selected with HalfMini DMA (Fernández de la Mora and Kozłowski, 2013). Based on the initial model the flow profile

seems to be well-centered in the tube channel and the sample taken prior to the dilution is sampled in middle of the stream. The sample is initially in middle the flow after is mixed with the dilution air (Figure 2).

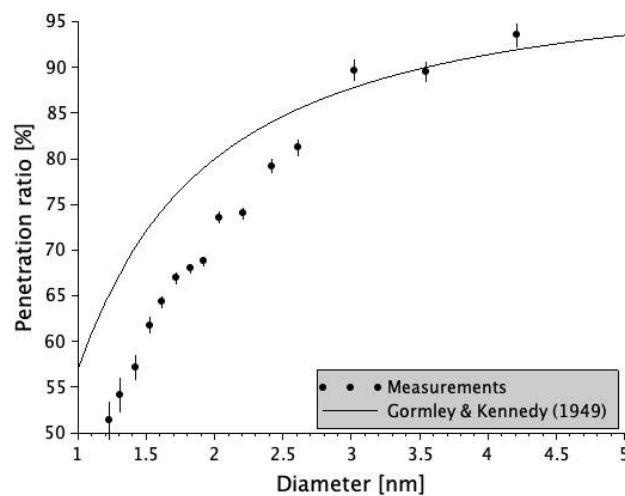


Figure 1 Measured penetration efficiency of as function of particles size and rough estimate based on Gormley-Kennedy equation.

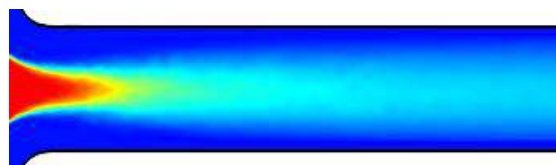


Figure 2 Simulated concentration of a tracer species in arbitrary units just after sample is mixed with dilution air.

ACKNOWLEDGEMENTS

This work was supported by the Academy of Finland (grants 307331 and 316114).

REFERENCES

- Fernández de la Mora, J., and Kozlowski, J.: Hand-held differential mobility analyzers of high resolution for 1–30nm particles: Design and fabrication considerations, *J Aerosol Sci*, 57, 45-53, 10.1016/j.jaerosci.2012.10.009, 2013.
- Gormley, P. G., and Kennedy, M.: Diffusion from a Stream Flowing through a Cylindrical Tube, *Proceedings of the Royal Irish Academy. Section A: Mathematical and Physical Sciences*, 52, 163-169, 1949.
- Kangasluoma, J., Franchin, A., Duplissy, J., Ahonen, L., Korhonen, F., Attoui, M., Mikkilä, J., Lehtipalo, K., Vanhanen, J., Kulmala, M., and Petäjä, T.: Operation of the Airmodus A11 nano Condensation Nucleus Counter at various inlet pressures and various operation temperatures, and design of a new inlet system, *Atmos. Meas. Tech.*, 9, 2977-2988, 10.5194/amt-9-2977-2016, 2016.

SULFURIC ACID - DIMETHYLAMINE CLUSTERS FRAGMENTATION INSIDE AN ATMOSPHERIC PRESSURE INTERFACE TIME OF FLIGHT MASS SPECTROMETER

D. ALFAOURI¹, N. MYLLYS², J. KUBEČKA¹, T. ZANCA¹, E. ZAPADINSKY¹, L. AHONEN¹, J. KANGASLUOMA¹, M. PASSANANTI^{1,3}, and H. VEHKAMÄKI¹

¹Institute for Atmospheric and Earth System Research / Physics, Faculty of Science, University of Helsinki, Finland

²Department of Chemistry, University of California, Irvine, USA

³Dipartimento di Chimica, Università di Torino, Italy

Keywords: ATMOSPHERIC CLUSTERS, CLUSTER FRAGMENTATION, SULFURIC ACID, DIMETHYLAMINE, PLANAR-DIFFERENTIAL MOBILITY ANALYSER, API-TOF MS

INTRODUCTION

Mass spectrometry has been used to study the chemical composition of the species involved in new particle formation (NPF). Detection of the elemental composition of several atmospheric clusters at ambient low concentrations was done using the Chemical Ionization Atmospheric Pressure interface Time Of Flight mass spectrometer (CI-API-TOF) (Jokinen *et al.*, 2012). Although this instrument can provide important information on atmospheric clusters, careful consideration of data interpretation and analysis should take place. Due to the reduced stability of clusters in comparison to molecules, clusters can undergo transformations inside the instrumentation more easily. Some of the factors causing fragmentation and/or evaporation of molecules from clusters include; chemical ionization process, energetic collisions and low pressure inside the instrument. Previous studies have shown that theoretical models predict higher cluster concentration in comparison to concentrations that were measured by API-TOF mass spectrometer. Reasons for such deviations could be due to the cluster fragmentation processes inside the instrument (Olenius *et al.*, 2013).

In many cases, acid-base nucleation mechanism involves sulfuric acid and amines clusters (Jokinen *et al.*, 2012). In this study, we investigated clusters of dimethylamine and sulfuric acid using an instrumental set-up consisting of planar-Differential Mobility Analyser (planar-DMA) and ElectroSpray Ionizer (ESI) coupled with the Atmospheric Pressure interface Time-Of-Flight Mass Spectrometry (APi-TOF MS). Our main interest was to identify the clusters that fragment inside the APi-TOF, quantify the amount of fragmented clusters and compare our findings to theoretical fragmentation data obtained with a statistical model (Zapadinsky *et al.*, 2019). Combining these data, we could be able to reconstruct a mass spectrum of the cluster ions detected, removing the artefacts due to the fragmentation.

METHODS

Molecular ions were generated using the ESI operating in negative mode, then injected into the planar-DMA and finally detected by the APi-TOF mass spectrometer. Three different solution concentrations were tested with three different ratios of sulfuric acid to dimethylamine; 100mM/50mM, 50mM/25mM, and 10mM/5mM respectively, all solutions were prepared in methanol and water with a ratio of 4:1 (v:v, CH₃OH:H₂O).

We simulated the fragmentation of sulfuric acid and dimethylamine clusters using our statistical model which describes the cluster ions trajectory through the APi-TOF and their collisions with carrier gas

molecules. Those collisions may cause the fragmentation of the cluster ions inside the instrument if they convey sufficient energy (Zapadinsky et al., 2019).

CONCLUSION

We identified the cluster ions formed with the ESI and the ones that underwent fragmentation inside the APi-TOF MS in both the experiments and using the model. In negative mode, the solution that produced a larger number of clusters was the one with concentration of 50mM/100mM dimethylamine/sulfuric acid concentration, the results of which are shown below. Figure 1 shows a mass defect plot of the 13 cluster ions detected by the APi-TOF MS.

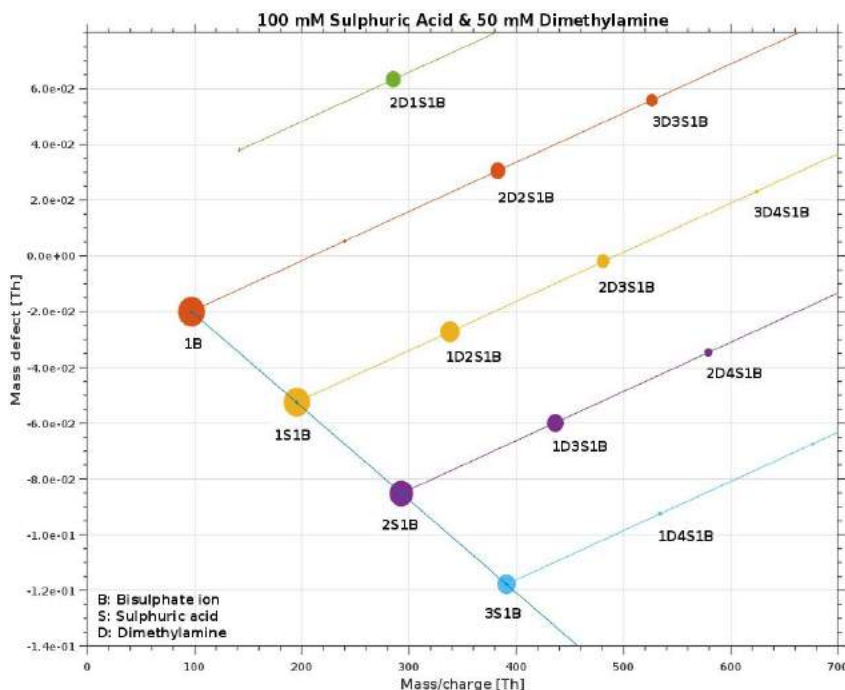


Figure 1: Mass defect (Th) versus mass/charge (Th) for a sample of 50mM/100mM dimethylamine/sulfuric acid in methanol to water ratio of 4:1 v:v.

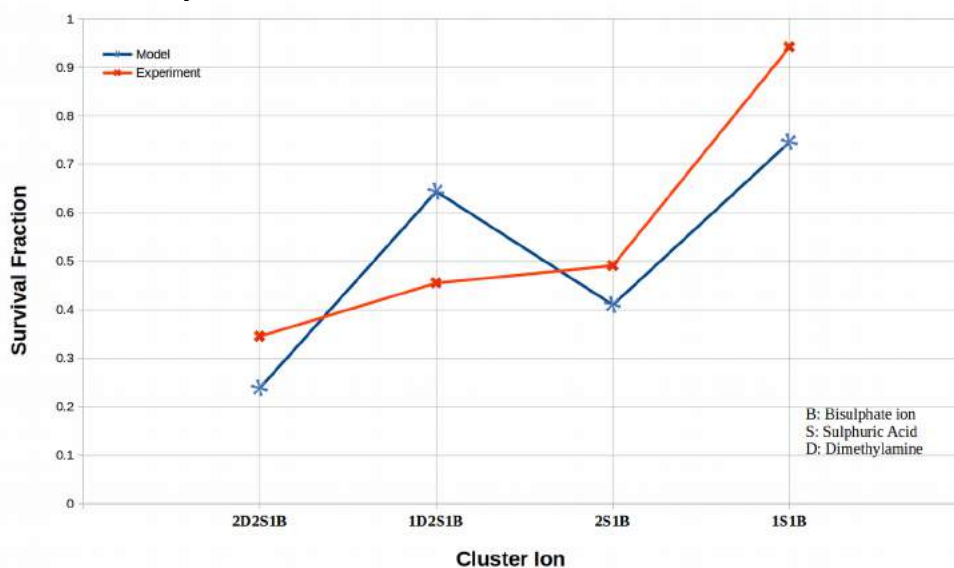


Figure 2: Survival fraction calculated from model and experiments of four selected cluster ions of sulfuric acid and dimethylamine.

The combination of the DMA and the APi-TOF MS data allow us to distinguish between original cluster ions and fragments. From our experiments we observed that all cluster ions from our sample, that went into the APi-TOF MS underwent fragmentation to some extent. We quantified experimentally the fragmentation of four selected sulfuric acid-dimethylamine clusters and simulated their fragmentation using our statistical model. As Figure 2 shows, the survival fraction of the selected clusters calculated from the experiments are in good agreement with the values calculated from our model. The results of the model gave us an important insight into the fragmentation of the charged clusters, which is of great importance for the reconstruction of the mass spectrum that does not contain artefacts due to the fragmentation.

ACKNOWLEDGEMENTS

This work is being funded by the ERC Project 692891-DAMOCLES, Academy of Finland, ATMATH Project. We thank the CSC-IT Center for Science in Espoo, Finland, for computational resources.

REFERENCES

- Jokinen, T., *et al.* (2012). Atmospheric sulphuric acid and neutral cluster measurements using CI-APi-TOF. *Atmos. Chem. Phys.* **12**, 4117-4125.
- Zapadinsky, E., *et al.* (2019). Modeling on Fragmentation of Clusters inside a Mass Spectrometer. *J. Phys. Chem. A*, **123**, 611-624.
- Olenius, T., Schobesberger, S., Kupiainen-Määttä, O., Franchin, A., Junninen, H., Ortega, I. K., Kurtén, T., Loukonen, V., Worsnop, D.R., Kulmala, M. and Vehkamäki, H. (2013). Comparing simulated and experimental molecular cluster distributions. *Faraday Discuss.* **165**, 75-89.

The Southern hemisphere high ALTitude Experiment on particle Nucleation And growth (SALTENA) campaign at Mount Chacaltaya: Transport simulations and footprint clustering

D. ALIAGA¹, V. SINCLAIR¹ Z. QIAOZHI¹, M. ANDRADE¹, C. MOHR³, F. BIANCHI¹,

¹ Institute for Atmospheric and Earth System Research/Physics, Faculty of Science, University of Helsinki, 00014 Helsinki, Finland.

² Universidad Mayor de San Andres, LFA-IIF-UMSA, Laboratory for Atmospheric Physics, Campus Universitario Cota Cota calle 27, Edificio FCPN piso 3, Casilla 4680, La Paz, Bolivia

³ Department of Environmental Science and Analytical Chemistry (ACES), Stockholm University, 10691 Stockholm, Sweden

Keywords: trajectory analysis, new particle formation, free-tropospheric aerosols, particle source clustering analysis

INTRODUCTION

Atmospheric aerosols affect climate directly by interacting with the incoming solar radiation, and indirectly via acting as cloud condensation nuclei (CCN), thus impacting the cloud albedo and lifetime. A significant fraction of atmospheric CCN arises from new particle formation (NPF), with 35 % of the CCN being directly formed in the free troposphere (Merikanto et al., 2009).

Motivated by the results from Rose et al. (2015) showing frequent NPF events at the Chacaltaya station (CHC, 5240 m a.s.l) located in Bolivia, we conducted The Southern hemisphere high ALTitude Experiment on particle Nucleation And growth (SALTENA) (December 2017 – June 2018). The goal is to complement the findings of Rose et al. (2015) by constraining the driving factors of NPF events in terms of chemistry, source regions and meteorological conditions. The focus is on (1) understanding the influence of the nearby city of El Alto – La Paz on NPF events at the station, and (2) comparing NPF events with different air mass sources. In order to provide the proper framework for understanding the different chemical signatures and aerosol properties measured at the site during the campaign, we use the Weather Research and Forecasting Model (WRF) simulations, the Lagrangian particle dispersion model (FLEXPART) and clustering analysis to classify the air mass sources and meteorological conditions.

METHODS

Given the complex topography of the site and the proximity of the nearly-two-million-inhabitant city of La Paz, the accuracy of the simulation is seminal to isolate the influence of the city and to identify other source regions. We therefore run high resolution four-domain telescoping-nest simulations with the WRF model with initial and boundary conditions from CFSv2.

On the WRF output, we use the Lagrangian particle dispersion model (LPDM) FLEXPART-WRF (v3.3.2) Brioude et al. (2013) in backward mode, modelling the release of 20 thousand particles each hour at the CHC station back in time 4 days (see e.g. Sturm et al. (2013)). This is done for the entire measurement period. The simulations with FLEXPART take into account particle

advection both horizontally and vertically by mean wind and parameterizes turbulent mixing and deep convection.

Furthermore, we regrid the FLEXPART output to a log polar grid and cluster the the footprints using the k-means clustering algorithm. The clustering was performed on the time series of residence times on the log polar regridded domain, maintaining the vertical levels so that the altitude is also resolved.

CONCLUSIONS

We have successfully clustered the air mass influences at the Chacaltaya measuring cite during the SALTENA campaign. These results will inform further analysis of the campaign measurements. The results are an enhancement on analysis previously done with HYSPLIT, because FLEXPART enables us to capture the complicated mountain meteorology.

Our methodology has successfully identified both transport patterns that are dominated by large scale circulation and stochastic processes occurring on a shorter scale. Moreover, we can resolve the relative contribution of air masses influenced by e.g. cities (La Paz), boundary layer, shallow convection and free troposphere.

References

- Brioude, J., Arnold, D., Stohl, A., Cassiani, M., Morton, D., Seibert, P., Angevine, W., Evan, S., Dingwell, A., Fast, J. D., Easter, R. C., Pisso, I., Burkhardt, J., and Wotawa, G. (2013). The Lagrangian particle dispersion model FLEXPART-WRF version 3.1. *Geoscientific Model Development*, 6(6):1889–1904.
- Merikanto, J., Spracklen, D. V., Mann, G. W., Pickering, S. J., and Carslaw, K. S. (2009). Impact of nucleation on global CCN. *Atmospheric Chemistry and Physics*, 9(21):8601–8616.
- Rose, C., Sellegri, K., Velarde, F., Moreno, I., Ramonet, M., Weinhold, K., Krejci, R., Ginot, P., Andrade, M., Wiedensohler, A., and Laj, P. (2015). Frequent nucleation events at the high altitude station of Chacaltaya (5240 m a.s.l.), Bolivia. *Atmospheric Environment*, 102:18–29.
- Sturm, P., Tuzson, B., Henne, S., and Emmenegger, L. (2013). Tracking isotopic signatures of CO₂ at the high altitude site Jungfraujoch with laser spectroscopy: Analytical improvements and representative results. *Atmos. Meas. Tech.*, 6(7):1659–1671.

ICE NUCLEATION ACTIVITY OF SOA PARTICLES FROM BOREAL FOREST

A. A. PIEDEHIERRO¹, A. WELTI¹, A. VIRTANEN², A. BUCHHOLZ², K. KORHONEN², I. PULLINEN², I. SUMMANEN² and A. LAAKSONEN^{1,2}

¹ Finnish Meteorological Institute, Helsinki, Finland

² Department of Applied Physics, University of Eastern Finland, Kuopio, Finland

Keywords: SOA particles, ice nucleation, α -pinene, boreal forest, aerosol-cloud interaction.

INTRODUCTION

Secondary organic aerosol (SOA) particles are produced in the atmosphere from oxidation of volatile compounds (VOCs) and subsequent condensation of the reaction products (Hallquist *et al.*, 2009). SOA constitutes a large portion of the submicron particulate mass in the lower troposphere with most of the VOC precursors emitted from biogenic sources (Kanakidou *et al.*, 2005; Jimenez *et al.*, 2009). There is evidence about ice nucleation (IN) activity of SOA: oxidized organic matter has been found in ice particle residuals from cirrus clouds (Cziczo *et al.*, 2004), and modelling studies suggest that viscous SOA could be an important ice nucleating particle (Murray *et al.*, 2010). The phase state of SOA, which depends on temperature and relative humidity (Zobrist *et al.*, 2008), seems to be a key factor responsible for their IN properties. However, the role of SOA particles in cloud activation and especially their importance in ice cloud formation remains poorly understood.

METHODS

We report preliminary results from the SINE campaign (SOA Ice Nucleation Experiment) carried out at the University of Eastern Finland Aerosol Physics Laboratory. The SINE campaign was focused on studying the IN properties of SOA formed from boreal forest emissions. SOA was produced from α -pinene (one of the most common VOCs found in boreal forests) with different oxygen-to-carbon (O:C) ratios (0.5, 0.8, 1.0) in an oxidation flow reactor by ozonolysis or photo oxidation. The size distribution and composition of the generated particle population was monitored by a scanning mobility particle sizer and an aerosol mass spectrometer. As a proxy for real trees emissions, SOA particles were also generated from pine-needle oil. The ice nucleation efficiency of the produced SOA particles was explored between 210 and 240K and from ice to water saturation using the Spectrometer for Ice Nuclei (SPIN). SOA particles were size selected with a differential mobility analyzer at 100nm and the relative humidity of the sample entering the SPIN was set to 40%, 10%, or <1% RH.

To investigate the effect of SOA formation conditions on IN activity, we also performed IN experiments using an atmospheric simulation chamber to ensure more atmospheric relevant conditions. In these experiments real plant emitted VOCs were used in addition to the α -pinene and pine-needle oil experiments.

RESULTS

The ice nucleation efficiency is reported as activated fraction (AF): ratio of number of particles counted as ice crystals respect to total number of particles. Results from α -pinene SOA particles produced in an oxidation flow reactor are shown in Figure 1.

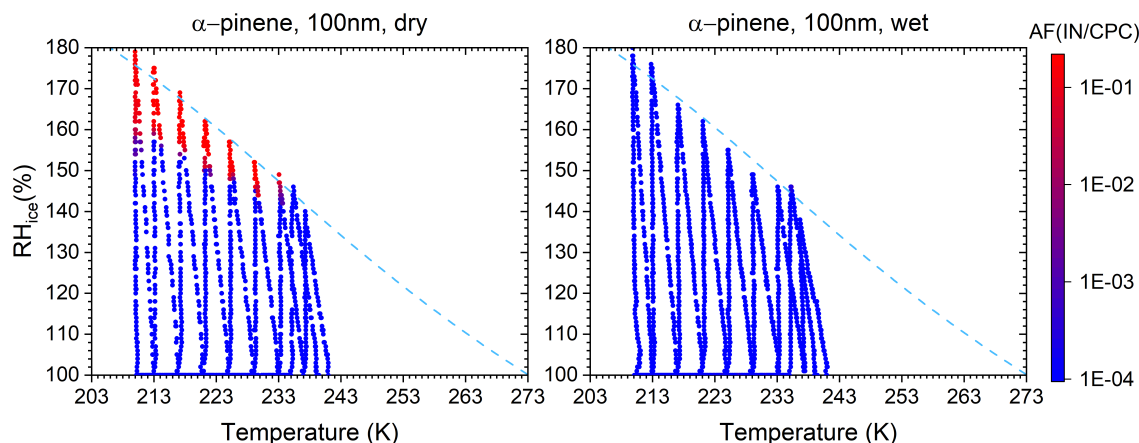


Figure 1: Ice active fraction as function of T and RH_i of 100 nm α -pinene SOA particles measured with the sample dried to 10% RH (left) or without drying (40% RH, right). High activity is indicated in red colors and low or no activity in blue.

SOA particles produced from α -pinene showed a clear activation for high RH_i and temperatures below 233K when they were dried before measurements in SPIN (Fig. 1, left). The transition from non active to active ice nuclei appears at RH_i values that approximate a constant relative humidity value respect to water. However, their IN activity disappears when the relative humidity of the SOA particle sample remains high before measuring (Fig. 1, right). The same behavior was detected for the different O:C ratios of α -pinene SOA particles.

CONCLUSIONS

Preliminary results show that the relative humidity of the SOA sample is the major factor controlling the phase state and therefore enabling ice activation. Regarding the O:C ratio, studied precursor VOCs, and SOA formation conditions (flow tube vs atmospheric simulation chamber) results indicate that they had a negligible effect on ice formation from α -pinene SOA.

ACKNOWLEDGEMENTS

This work was supported by the Academy of Finland, C-Main project (grant no. 309141), and the Center of Excellence programme (grant no. 307331).

REFERENCES

- Cziczo, D., P. DeMott, S. Brooks, A. Prenni, D. Thomson, D. Baumgardner, J. Wilson, S. Kreidenweis, and D. Murphy, (2004). Observations of organic species and atmospheric ice formation. *Geophys. Res. Lett.*, **31**, L12116.
- Hallquist, M., J. C. Wenger, U. Baltensperger, Y. Rudich, D. Simpson, *et al.*, (2009). The formation, properties and impact of secondary organic aerosol: current and emerging issues. *Atmos. Chem. Phys.*, **9**, 5155-5236.
- Jimenez, J. L., M. R. Canagaratna, N. M. Donahue, *et al.*, (2009). Evolution of organic aerosols in the atmosphere. *Science*, **365**, 1525-1529.
- Kanakidou, M., J. H. Seinfeld, S. N. Pandis, I. Barnes, F. J. Dentener, M. C. Facchini, R. Van Dingenen, B. Ervens, A. Nenes, C. J. Nielsen, E. Swietlicki, J. P. Putaud, Y. Balkanski, S.

- Fuzzi, J. Horth, G. K. Moortgat, R. Winterhalter, C. E. L. Myhre, K. Tsigaridis, E. Vignati, E. G. Stephanou, and J. Wilson, (2005). Organic aerosol and global climate modelling: a review. *Atmos. Chem. Phys.*, **5**, 1053-1123.
- Koop, T., J. Bookhold, M. Shiraiwa, and U. Poschl, (2011). Glass transition and phase state of organic compounds: Dependency on molecular properties and implications for secondary organic aerosols in the atmosphere. *Phys. Chem. Chem. Phys.*, **13(43)**, 19238-19255.
- Murray, B. J., T. W. Wilson, S. Dobbie, Z. Cui, S. M. Al-Jumur, O. Mohler, M. Schnaiter, R. Wagner, S. Benz, M. Niemand, H. Saathoff, V. Ebert, S. Wagner, and B. Karcher, (2010). Heterogeneous nucleation of ice particles on glassy aerosols under cirrus conditions. *Phys. Chem. Chem. Phys.*, **8**, 5221-52
- Zobrist, B., C. Marcolli, D. A. Pedernera, and T. Koop, (2008). Do atmospheric aerosols form glasses? *Nat. Geosci.*, **3**, 233-237.

MODELLING METHANE FLOWS BETWEEN SOIL, TREES, AND ATMOSPHERE

J.V. ANTTILA^{1,3}, T. HÖLTTÄ², M. KOSKINEN^{1,2,4}, A. LEPPÄNEN³, M. RAIVONEN³, A. LOHILA^{3,4}, T. VESALA³, M. PIHLATIE^{1,2,5}

¹ Department of Agricultural Sciences, Faculty of Agriculture and Forestry, University of Helsinki, Finland.

² Institute for Atmospheric and Earth System Research / Forest Sciences, Faculty of Agriculture and Forestry, University of Helsinki, Finland.

³ Institute for Atmospheric and Earth System Research / Physics, Faculty of Science, University of Helsinki, Finland.

⁴ Finnish Meteorological Institute, Helsinki, Finland.

⁵ Viikki Plant Science Centre (ViPS), University of Helsinki, Finland.

Keywords: modelling, methane, transport processes

INTRODUCTION

Currently, the process-based understanding of methane flows to the atmosphere from natural soil is lacking. Vegetation forms a large poorly characterised component in the global biogeochemical methane budget. We aim to study the methane transport in the soil, and between the soil, trees and the atmosphere, by utilising process-based mathematical modelling.

In particular, we aim to answer two questions: a) how is methane transported within a plant from the root compartment to the stem and canopy compartments, and b) to which degree are differences in methane fluxes between similar sites explained by differences in underlying methane production, oxidation, and transport processes. Both research questions are approached by modifying existing mathematical models, and parameterising the models based on recent field and laboratory measurements.

METHODS

The methodology of this project consists of dynamical modelling of production, consumption, and transport processes in soil and inside vegetation. The models used here are reaction–diffusion–advection -type, which are, for the most part, treated numerically by finite-difference methods. The starting points to our work are two published models: a) a carbon dioxide stem transport and efflux model (Hölttä and Kolari, 2009), and b) the Helsinki Model of METHANE buiLd-up and emIssion from peatlands model (HIMMELI) (Raivonen *et al.*, 2017), which are used here to study a) the within-plant transport of methane and efflux from different tree parts, and b) the variability of methane flux with respect to variability in methane production and oxidation components, respectively.

The within-stem transport model, developed by Hölttä and Kolari (2009), was originally used for studying CO₂ transport, production, and efflux from pine stem. Initially, we aim to make the necessary modifications to use the model to study methane flow in *Betula nana*. Most importantly, we need to include the root compartment, originally not considered in the model, since we believe

roots are of specific importance in aerenchymatous plants (*e.g. B. nana, B. pubescens*), in which the methane mostly occupies the aerated space because of its low solubility. The model flux output, with appropriate parameterisation, will be compared to measured fluxes from an experimental laboratory setting. The main aim in the long-term is to generalise the model for use in quantifying methane fluxes in various future projects.

The HIMMELI model describes methane flow from anaerobic layers of peatland soil to the atmosphere through vegetation, and aerated and oxidising soil layers. Methane production and maximum oxidation capacity are required as inputs to the model, but these are rarely measured at any field site. The question addressed here is, can we infer these two from measured flux profiles, based on a model. Oxidation potential is described by a simple maximum value parameter V_{\max} in a two-substrate Michaelis-Menten function. Methane production is more complicated, since the model input is given as daily values. However, based on the few existing measurements, methane production is readily approximated by the positive part of a sinusoidal curve. Thus, a parameterised function $f(t) = \max[\beta, \alpha \cdot \sin(2\pi t/\phi)]$ can be used to generate methane production curves such that the parameter α defines the maximum production level. With this simplification, the problem is reduced to simple two-parameter inference, amenable to optimisation through forward simulations of the model. This approach still remains to be tested in practice, but may shed light on differences in methane fluxes between seemingly similar field sites.

FUTURE PROSPECTS

This project started very recently, on *2019-09-01*, and thus no conclusions are available at this point. Results are expected within one year. Extensions and modifications to the models and their computer implementations will be useful concerning future modelling objectives in the associated research groups.

ACKNOWLEDGEMENTS

This work is supported by the Centre of Excellence in Atmospheric Science and the European Research Council.

REFERENCES

- Hölttä, T., Kolari, P. (2009). Interpretation of stem CO₂ efflux measurements *Tree Physiology*, **29**, 1447-1456.
- Raivonen, M., Smolander, S., Backman, L., Susiluoto, J., Aalto, T., Markkanen, T., Mäkelä, J., Rinne, J., Peltola, O., Aurela, M., Lohila, A., Tomasic, M., Li, X., Larmola, T., Juutinen, S., Tuittila, E.-S., Heimann, M., Sevanto, S., Kleinen, T., Brovkin, V., Vesala, T. (2017). HIMMELI v1.0: Helsinki Model of Methane build-up and emission from peatlands *Geosci. Model Dev.*, **10**, 4665-4691.

BIOPHYSICAL AND BIOGEOCHEMICAL RESPONSES OF BOREAL FOREST TO THINNING: A MODEL-ASSISTED REVIEW

T. ASLAN¹, K. HAAHTI², A.J. KIELOAHO², A. LEHTONEN², T. GRÖNHOLM¹, O. PELTOLA³, I. MAMMARELLA¹ and S. LAUNIAINEN²

¹Institute for Atmospheric and Earth System Research, Department of Physics, University of Helsinki, Finland.

²Natural Resources Institute Finland, Helsinki, Finland.

²Finnish Meteorological Institute, Helsinki, Finland.

Keywords: carbon balance, energy balance, forest management.

INTRODUCTION

Thinning is a standard practice in boreal forestry. In even-age management, it is commonly done 2-3 times during the rotation period of 60-120 years with the aim to manage between-tree competition and allocate resources to value growth of the remaining trees.

Thinning reduces stand basal area and canopy leaf-area index, and changes the vertical foliage distribution and species composition. Opening of the canopy leads to immediate changes in micro-climatic conditions that consequently triggers various changes in physical and biological processes (Banerjee and Linn, 2018; Launiainen et al. 2016). Our knowledge on the biophysical and biogeochemical responses to thinning, at ecosystem scale, still rely on separate field experiments (Vesala et al. 2005; Lagergen et al. 2008; Lindroth et al. 2018) and modeling (Gonzalo et al. 2007; Collalti et al. 2018). What is urgently lacking is more holistic understanding of climate-relevant thinning impacts, in which the consolidated effects of management on radiation balance and albedo, water and energy cycles, primary productivity and carbon balance are comprehensively described. It is of great importance for designing and implementing better forestry practices for climate change mitigation.

To develop a better understanding of biophysical and biogeochemical impacts of thinning we, (1) broadly review existing literature on short-term (0 - 3 years post-harvest) thinning responses of surface-atmosphere exchange, (2) complement the literature review by predictions of a vertically-resolved soil-vegetation-atmosphere transfer model (Launiainen et al. 2015), and use the model results to discuss the mechanisms underlying commonly observed thinning responses, and address potential differences among the empirical studies.

METHODS

We use a 1-dimensional multi-layer, multi-species soil-vegetation-atmosphere transfer model APES (Atmosphere-Plant Exchange Simulator), which describes forest ecosystem components (e.g. plant species, bottom layer vegetation and soil) as independent objects that contain the conservation equations of mass and energy, and structural and functional properties of the respective part of the ecosystem (Launiainen et al. 2015).

RESULTS

Analyses and results of this study are still under progress.

REFERENCES

- Banerjee, T., & Linn, R. (2018). Effect of vertical canopy architecture on transpiration, thermoregulation and carbon assimilation. *Forests*, 9(4), 198.
- Collalti, A., Trotta, C., Keenan, T. F., Ibrom, A., Bond-Lamberty, B., Grote, R., ... & Anav, A. (2018). Thinning can reduce losses in carbon use efficiency and carbon stocks in managed forests under warmer climate. *Journal of advances in modeling earth systems*, 10(10), 2427-2452.
- Garcia-Gonzalo, J., Peltola, H., Briceno-Elizondo, E., & Kellomäki, S. (2007). Changed Thinning Regimes May Increase Carbon Stock Under Climate Change: A Case Study from a Finnish Boreal Forest. *Climatic Change* , 81 (3-4), 431-454.
- Lagergren, F., Lankreijer, H., Kuchera, J., Cienciala, E., Mölder, M., & Lindroth, A. (2008). Thinning effects on pine-spruce forest transpiration in central Sweden. *Forest Ecology and Management* , 255 (7), 2312-2323.
- Launiainen, S., Katul, G. G., Lauren, A., & Kolari, P. (2015). Coupling boreal forest CO₂, H₂O and energy flows by a vertically structured forest canopy–Soil model with separate bryophyte layer. *Ecological modelling*, 312, 385-405.
- Launiainen, S., Katul, G. G., Kolari, P., Lindroth, A., Lohila, A., Aurela, M., ... & Vesala, T. (2016). Do energy fluxes and surface conductance of Boreal coniferous forests in Europe scale with leaf area ?. *Global Change Biology* , 22 (12), 4096-4113.
- Lindroth, A., Holst, J., Heliasz, M., Vestin, P., Lagergren, F., Biermann, T., ... & Mölder, M. (2018). Effects of low thinning on carbon dioxide fluxes in a mixed hemiboreal forest. *Agricultural and Forest Meteorology* , 262 , 59-70.
- Vesala, T., Suni, T., Rannik, Ü., Keronen, P., Markkanen, T., Sevanto, S., ... & Ojansuu, R. (2005). Effect of thinning on surface fluxes in a boreal forest. *Global Biogeochemical Cycles*, 19(2).

THE PALLAS SUMMER 2019 AEROSOL BLACK CARBON CAMPAIGN

E. ASMI¹, J. BACKMAN¹, H. SERVOMAA¹, A.-P. HYVÄRINEN¹, M. GINI¹, K. ELEFTHERIADIS²,
T. MÜLLER³, Y. KONDO⁴ and P. QUINCEY⁵

¹Finnish Meteorological Institute, Helsinki, Finland

²National Center for Scientific Research “Demokritos”, Athens, Greece

³Leibniz Institute for Tropospheric Research, Leipzig, Germany

⁴National Institute of Polar Research, Tokyo, Japan

⁵National Physical Laboratory, Teddington, United Kingdom

Keywords: AEROSOL ABSORPTION, MEASUREMENT STANDARD, PALLAS STATION, BC.

INTRODUCTION

Globally, aerosol particles cool the climate by directly scattering the solar radiation and via their impacts on cloud radiative properties. A fraction of these particles, commonly referred to as “the Black Carbon (BC) aerosol”, however instead absorbs the solar radiation and consequently causes atmospheric heating. In Polar Regions of particular importance is also the BC cryospheric effect via the snow and ice albedo reduction which further accelerates the heating effect (AMAP, 2011). The BC aerosol is also a major threat to human health and has shown better correlation with negative health impacts than the Particulate Mass (PM), which is the currently regulated aerosol component of the Air Quality (AQ).

A plausible explanation to why the AQ-regulation is currently not applied to the BC is the lack of standardization of the common BC measurement techniques. The existing direct techniques to measure aerosol absorption include: filter-based absorption photometers, photoacoustic and photothermal interferometry. In addition, the aerosol absorption can be calculated from simultaneous extinction and scattering measurements. Filter-based photometers are globally the most commonly utilized technique to determine the aerosol absorption and further the equivalent aerosol black carbon (eBC) mass concentration. For the latter one, an instrument and wavelength specific Mass Absorption Cross-section (MAC) needs to be applied.

The BC concentrations are subject to large measurement uncertainties, both due to the instruments internal inaccuracies but also due to their sensitivity to various aerosol properties, such as the particle size (e.g. Nakayama et al., 2010; Müller et al., 2011). The challenging aim of the 16ENV02 Black Carbon project on metrology for light absorption by atmospheric aerosols is to bring the standardisation in the field of BC measurements. The project team develops and characterizes filter-free absorption measurement methods and black carbon standard reference materials (SRMs), representative of the atmospheric aerosols, aiming at developing a traceable, primary method for determining the aerosol absorption coefficients at specific wavelengths along with a validated transfer standard for the field use.

The summer 2019 Pallas field campaign was the first attempt to apply the new knowledge and methodologies and test them in the field conditions. The specific aim of the campaign was to elucidate the methodological differences and challenges that could be encountered in an extremely clean environment, such as the Arctic.

METHODS

The Pallas aerosol absorption measurement campaign was run during one month: 19.6 – 17.7.2019. During this time period, the aerosol absorption and scattering coefficients were measured using various

instruments. The majority of them were filter-based absorption photometers but in addition the aerosol absorption was measured using the extinction minus scattering technique and the refractory black carbon mass concentration and size distribution determined using the SP2 high-intensity laser technique (Table 1). The instruments were calibrated and intercompared in the beginning, middle and end of the campaign using atomizing solutions of ammonium sulphate (purely scattering) and Aquadag® (Aqueous Deflocculated Acheson Graphite) that is mainly consisting of highly absorbing elemental carbon.

The core instruments are summarized in Table 1. In addition to these aerosol optical measurements, the continuous air quality (part of the EU EMEP programme), aerosol particle (part of the EU ACTRIS) and greenhouse gas (part of EU ICOS) measurements are run at the Pallas site. More information on site, measurements and previous publications can be found at: <https://en.ilmatieteenlaitos.fi/pallas-atmosphere-ecosystem-supersite>.

Instrument	Manufacturer	Time resolution applied [s]
Multi-angle absorption photometer (MAAP)	Thermo	60
Aethalometer AE33	Magee Sci.	60
Aethalometer AE31	Magee Sci.	60
Microaethalometer MA200	Magee Sci.	60
COSMOS	NIPR	60
PSAP	Radiance Res.	1
Aurora 4000	Ecotech	10
Nephelometer TSI	TSI	300
CAPS ex	DMT	5
CAPS ssa	DMT	1
Soot Particle Absorption Photometer (SP2)	DMT	1

Table 1. Instrumentation used in Pallas campaign to measure the absorbing and BC aerosol.

The meteorology at the site is monitored with a Vaisala weather station. Air mass back trajectories at the arrival level of 500 m a.s.l. for the campaign period were calculated using a HYSPLIT 4 model (Draxler and Hess, 1997). CDC1 were used as a meteorological data input for the model runs and a new trajectory was started every 6 h calculating 72 h backwards.

Data from each instrument were corrected for the artefacts based on the latest literature recommendations. These included truncation corrections for nephelometers, filter spot size and scattering corrections for PSAP and AE31, wavelength discrepancies corrections for PSAP and MAAP, flow corrections, and finally a conversion to STP (0°C; 101325 Pa) conditions when needed.

CONCLUSIONS

The campaign could be roughly divided into two parts: Before July 8 the air masses were mainly clean Arctic with persistent low pressure passes and several days of precipitation. Concentrations were low and wet scavenging removed efficiently the aerosols leading to a scattering coefficient in the range 0 to 5 Mm⁻¹. After July 8 weather became dry while the air masses turned to north-east with the origin in the northern Russian coastal and Arctic regions. The aerosol scattering coefficient increased to >5 Mm⁻¹, reaching the maximum values of around 20 Mm⁻¹ (Figure 1).

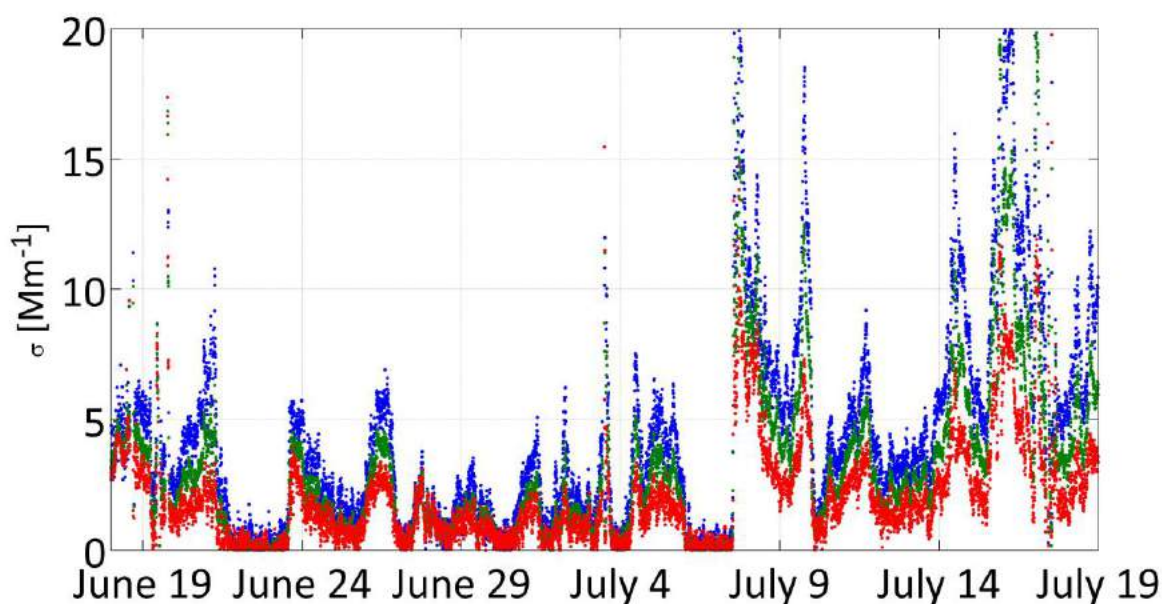


Figure 1. Aerosol scattering coefficient at blue, green and red (450 nm, 550 nm and 700 nm) wavelength during the campaign.

The fraction of aerosol absorption remained low during the whole campaign. The average single scattering albedo at the wavelength of 637 nm was 0.93 being indicative of a highly scattering aerosol type. This was calculated based on the TSI nephelometer and MAAP data.

There were clear differences between the instruments corresponding to changes in aerosol size, type and concentrations. This is to some extent in line with previous findings (e.g. Nakayama et al., 2010; Müller et al., 2011). For example, the change of the air mass type on July 8 affected the ratio of the AE33 and the MAAP (Figure 2).

In summary, all methods for measuring the particle absorption suffered from sensitivity issues at such low concentrations. The lowest eBC concentrations were measured with COSMOS and MAAP and the highest with the aethalometers and PSAP. The residual BC (from SP2) was 20-50% of the eBC that was measured by the different filter based methods.

Data analysis is still on-going and the presented results are preliminary. Our analysis aims at understanding the observed differences between the instruments in challenging field conditions which are subject to multiple changes. The final goal is to present the benefits and the challenges of different measurement techniques along with the associated uncertainties in field operating conditions in the Arctic.

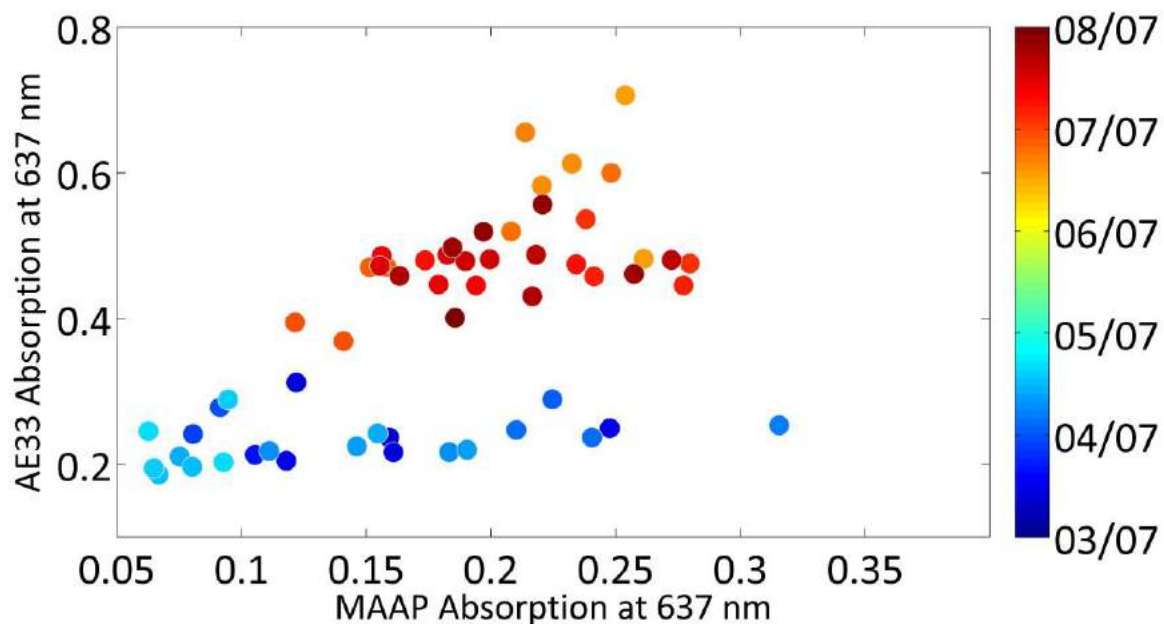


Figure 2. Hourly averaged aerosol absorption coefficient at 637 nm wavelength measured with AE33 and MAAP during five consecutive days between July 4 and July 8.

ACKNOWLEDGEMENTS

The EMPIR initiative is co-funded by the European Union’s Horizon 2020 research and innovation programme and the EMPIR Participating States. The research presented here was funded by the 16ENV02 Black Carbon project. Research also received funding from the European Union’s Horizon 2020 research and innovation program under grant agreement no. 654109 (ACTRIS) and the Academy of Finland Centre of Excellence program (project number 307331).

REFERENCES

- AMAP (2011) The Impact of Black Carbon on Arctic Climate. By: Quinn, P.K. et al., Arctic Monitoring and Assessment Programme (AMAP), Oslo, 72 pp.
- Draxler, R. R. and Hess, G. D.: Description of the HYSPLIT_4 modeling system. NOAA Tech. Memo. ERL ARL-224, NOAA Air Resources Laboratory, Silver Spring, MD, USA, 24 pp., 1997.
- Nakayama, T., et al.: Size-dependent correction factors for absorption measurements using filter-based photometers: PSAP and COSMOS, *Journal of Aerosol Science* 41(4): 333-343, 2010.
- Müller, T., et al.: Characterization and intercomparison of aerosol absorption photometers: result of two intercomparison workshops, *Atmos. Meas. Tech.*, 4, 245–268, 2011.

HEURISTIC METHODS TO CORRECT FOR WAVELENGTH OFFSET EFFECTS IN DUAL FIELD OF VIEW SPECTROMETER SYSTEMS

J. ATHERTON¹, S. XU^{1,2} and A. PORCAR-CASTELL¹

¹ Optics of Photosynthesis Laboratory, Institute for Atmospheric and Earth System Research (INAR)/ Forest Sciences, Faculty of Agriculture and Forestry, University of Helsinki, PO Box 27, 00014 FINLAND.

² State Key Laboratory of Remote Sensing Science, Jointly Sponsored by Beijing Normal University and Institute of Remote Sensing and Digital Earth of Chinese Academy of Sciences, Beijing 100875, China.

Keywords: SIF, remote sensing.

INTRODUCTION

Dual field of view (DFOV) spectrometer systems are used to measure sun-induced fluorescence (SIF) and reflectance in the field from proximal and remote platforms. At their core, these systems consist of two separate fiber optic assemblies connected to a spectrometer. The downwelling (DW) light flux, quantified as irradiance, is collected with a skyward pointing fiber optic cable assembly topped with an optical diffuser. The upwelling flux (UW), which is the scattered (reflected) and fluoresced light from the forest canopy, is quantified as radiance with a separate fiber optic cable assembly, usually in bare fiber mode.

In the ideal system the spectral calibration, and resulting wavelength scales, for upwelling and downwelling assemblies are identical. In reality, variation in tolerances of optical components can cause a difference in the spectral response of UW and DW assemblies. The result of this effect is that UW and DW spectra are measured on slightly different wavelength scales. Although this difference is typically small (e.g. of similar magnitude to the spectral sampling interval of the sensor), it causes an issue for Fluorescence Line Depth (FLD) based retrievals of SIF which require high resolution measurements of irradiance and radiance at precisely the same wavelengths. Therefore in systems with a difference in spectral calibration between UW and DW measurements, a correction is required to remove this difference for reasonable estimates of SIF. (From here, we refer to this problem as the offset correction). Unfortunately offset correction is not trivial, as to spectrally shift one of the measurements relative to the other so as to place them on the same wavelength scale requires an upsampling of the offset signal to higher spectral resolution.

Deconvolution can potentially be used to reconstruct a higher resolution spectrum given knowledge of the spectral response function (S) however the problem is ill-posed, even when S is known. The problem is further complicated for hyperspectral instruments, such as DFOV SIF systems, as S typically changes shape across the measurement space. Such issues motivated the development of the super-resolution approach which uses iterative spline-based interpolation to reconstruct higher resolution satellite spectra from lower resolution data (Zhao, 2010).

We tested a simple single step interpolation and a 2 step method inspired by Zhao (2010) for offset correction in DFOV data. We used simulated data with known error statistics to assess the techniques.

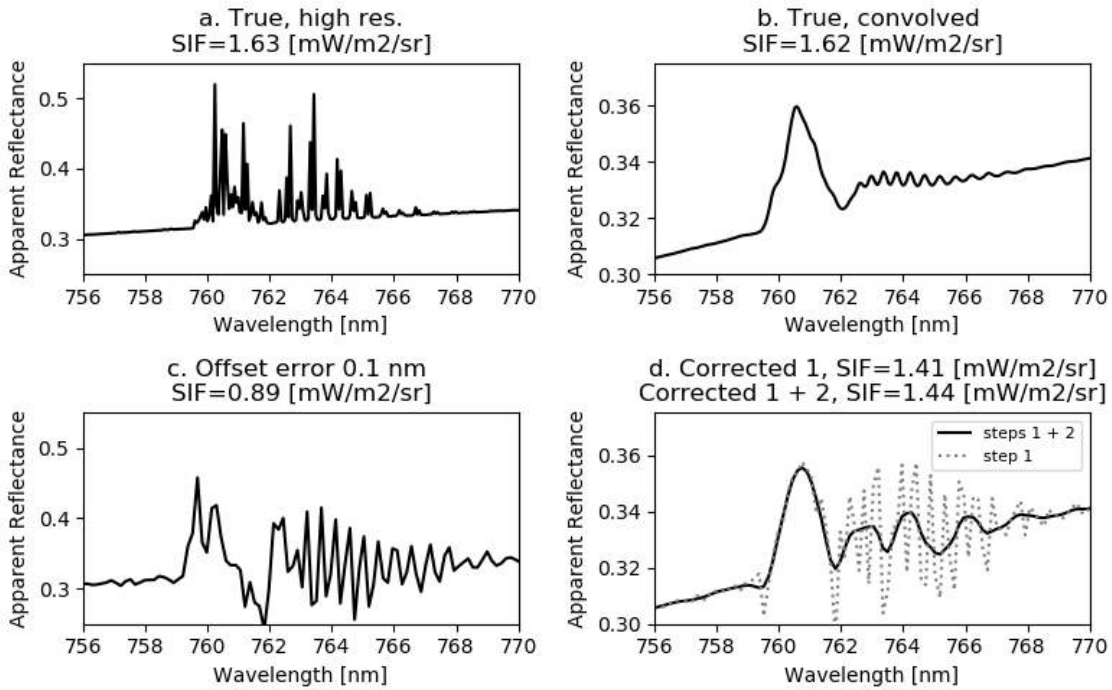


Figure 1: Apparent reflectance spectra for simulated data in the O_2A feature.

METHODS AND ALGORITHM

The offset issue is visible in the ratio of UW to DW measurements, known as the apparent reflectance spectrum, which appears *rough* when calculated with offset data (fig. 1c) in the O_2A region of the spectrum. However if our data were uncorrupted at moderate spectral resolutions of approximately 0.5 nm typical of DFOV SIF systems, the apparent reflectance spectrum is smooth (fig. 1b). Hence the 2 step method works by forcing this smoothness in the apparent reflectance spectrum using spline interpolation. The smoothness occurs due to two reasons, firstly the inherent reflectance of forest canopies is smooth. Secondly, in the infilled oxygen absorption regions which are potentially non-smooth (fig. 1a), smoothness is apparent in downsampled observations (fig. 1b) due to the filtering effect of convolution with S . For this second reason, this method should be applied with caution to higher resolution ($\text{FWHM} \lesssim 0.1$ nm) data.

The algorithm starts by assuming the spectral sampling of measurements E and L are offset by a small known amount ϵ , these offset data are E^1 and L^1 . E^1 and L^1 each have their own wavelength scale (λ) where $\lambda_E + \epsilon = \lambda_L$. The objective of the algorithm is to estimate E at λ_L . In the first step, E^1 is interpolated and evaluated at the radiance wavelengths, λ_L resulting in the initial correction, E^2 . Next, an additional second smoothing step using splines is then applied to apparent reflectance calculated with this first guess. Finally corrected irradiance (E^3) is estimated by back calculating from the smooth reflectance and measured radiance (L). The method was implemented in MATLAB, the initial step used the PCHIP algorithm and the second step used *fit* function with the *smoothingSpline* option for the added control of smoothing parameter, p .

We used simulated data to test the *offsetCorrection* method. We modelled true radiance using a high resolution irradiance spectrum from MODTRAN and reflectance and fluorescence simulations from the SCOPE model (Van der Tol, 2009) as:

$$L = \rho \frac{E}{\pi} + SIF. \quad (1)$$

Algorithm 1 Two step interpolation algorithm for offset correction. Python method calls are on right hand side of algorithm.

```
1: procedure OFFSETCORRECTION( $\lambda_E, E^1, L^1, \epsilon, p$ )
2:    $\lambda_L \leftarrow \lambda_E + \epsilon$ 
3:    $E^2(\lambda_L) \leftarrow \text{INTERPOLATE}(\lambda_L, \lambda_E, E)$ 
4:    $\rho_a^2 \leftarrow \frac{\pi L}{E^2}$ 
5:    $\rho_a^3 \leftarrow \text{SPLINESMOOTH}(\lambda_L, p, \rho_a^2)$ 
6:    $E^3 \leftarrow \frac{\pi L}{\rho_a^3}$ 
7:   return  $E^2, E^3$ 
```

Next we shifted the wavelength scale of E by 0.1 nm relative to L , added normally distributed noise and convolved spectra with a gaussian kernel of FWHM = 0.31 nm to simulate measured data at a lower resolution. We retrieved fluorescence using the 3FLD method at the O_2A feature. p was set to the default value, 0.99.

RESULTS AND CONCLUSIONS

Results of the offset correction are shown in fig 1d. The method reproduces the lower resolution apparent reflectance spectrum with only a small error, likewise for SIF. The simulations suggest that the first step interpolation does an adequate job in reconstructing the apparent reflectance spectrum. The second step then acts as refinement to this initial estimate and improves the result further. Also of note, although not shown here, as the noise increases the added value of the second step likely decreases as the spline begins to suffer from overfitting. Therefore we suggest that unless the noise characteristics are well known, as in the simulated case here, then a simple 1 step interpolation is likely preferable.

ACKNOWLEDGEMENTS AND CONTRIBUTIONS

This work was supported by the Academy of Finland (grant numbers 319211, 304097).

REFERENCES

- C. Van der Tol, W. Verhoef, J Timmermans, A Verhoef, and Z Su (2009). An integrated model of soil-canopy spectral radiances, photosynthesis, fluorescence, temperature and energy balance. *Biogeosciences*, **6:12**, 3109-3129.
- Huijie Zhao, Guorui Jia, and Na Li (2010). Transformation From Hyperspectral Radiance Data to Data of Other Sensors Based on Spectral Superresolution *IEEE TRANSACTIONS ON GEOSCIENCE AND REMOTE SENSING*, **48:11**, 3903-3912.

TOWARDS UNDERSTANDING THE MECHANISMS OF NEW PARTICLE FORMATION IN THE EASTERN MEDITERRANEAN

R. BAALBAKI¹, M. PIKRIDAS², T. JOKINEN¹, T. LAURILA¹, L. DADA¹, A. MAISSER², K. NEITOLA², A. CHRISTODOULOU², F. UNGA², K. LEHTIPALO¹, J. KANGASLUOMA¹, G. BISKOS², T. PETÄJÄ¹, JEAN SCIARE² and M. KULMALA¹

¹ Institute for Atmospheric and Earth System Research/Physics, Faculty of Science, University of Helsinki, P.O. Box 64, 00014 Helsinki, Finland

² The Energy, Environment and Water Research Center (EEWRC), The Cyprus Institute, P.O. Box 27456, CY-1645 Nicosia, Cyprus

Keywords: New particle formation, Eastern Mediterranean

Email: rima.baalbaki@helsinki.fi

INTRODUCTION

Atmospheric new particle formation (NPF) is a large source of global aerosol particle number load and cloud condensation nuclei (CCN) (Merikanto et al., 2009). Therefore, it has been the focus of a multitude of research studies in the past 20 years ranging from atmospheric observations to chamber experiments and conceptual and modelling studies. These studies aim to understand the NPF mechanism, its characteristics, how and when NPF takes place and eventually how it affects global climate.

The conditions governing NPF have been shown to vary in different environments. These conditions are unique in the Eastern Mediterranean and Middle East (EMME) region. This region lies at the crossroads of three continents receiving precursor gases and aerosols from continental, maritime and desert-dust pollution sources. The surrounding complex orography affects atmospheric dynamics and boundary layer processes on different scales. Further, the dry and hot weather throughout most of the year with strongly increasing heat extremes sets off intense photochemistry (Lelieveld et al., 2002; Lelieveld et al., 2016). All these factors nominate the Mediterranean area as a hotspot for atmospheric and climate change research in general and atmospheric nucleation in specific. In this context and within the framework of the Eastern Mediterranean and Middle East – Climate and Atmosphere Research Centre (EMME-CARE) project, we performed a one-year-long campaign to study atmospheric NPF at a background site in Cyprus. Here we present a brief overview of the results measured during this campaign.

METHODS

The measurement site is located at the Cyprus Atmospheric Observatory (CAO), a rural background station, close to the villages of Agia Marina and Xyliatos (33.05° E–35.03° N; 532m above sea level). The site is far away from any major local pollution sources except for some traffic from the nearby department of forests fire brigade.

In this campaign, we used four instruments to study NPF: an Airmodus A11 Nano Condensation Nucleus Counter (nCNC) system, a Neutral cluster and Air Ion Spectrometer (NAIS), a scanning mobility particle sizer (SMPS; Grimm, model 5400) and a Chemical Ionization Atmospheric-Pressure-interface – Time-Of-Flight (CI-APi-TOF) mass spectrometer. The first three instruments measure particle size distribution and were deployed at the site for a period of one year. The nCNC is composed of a Particle Size Magnifier (PSM) and a Condensation Particle Counter (CPC) and is capable of measuring particle size distribution of sub 3nm particles (Vanhanen et al., 2011). The NAIS measures the size distribution of aerosol particles between 2 and 42 nm and the mobility distributions of air ions between 0.8 nm and 42nm (Hanna E

Manninen et al., 2016; Mirme & Mirme, 2013). The SMPS is composed of a differential mobility analyzer (DMA) and a CPC. It was used to obtain the size distribution of aerosol particles from 10 nm to 700 nm. The CI-API-TOF measures the chemical composition of precursor molecules and clusters (Jokinen et al., 2012) and was operated for 10 days during this campaign. Complementary meteorological data and criteria gas pollutants data were available from the CAO nearby measurements container.

The data from the three particle sizing instruments was used to reconstruct the full particle size distribution plots between 1 and 700 nm (Figure 1). These plots were used to categorize measurement days into NPF event days, non-event days and undefined days following based on previously reported classification schemes (Buenrostro Mazon et al., 2009; Dal Maso et al., 2005; Hirsikko et al., 2007; H. E. Manninen et al., 2010). Further, calculations of particle formation rates (J), growth rates (GRs) in various size ranges, condensation sink (CS) and coagulation sink (coagS) were calculated following the protocol presented by Kulmala et al. (2012).

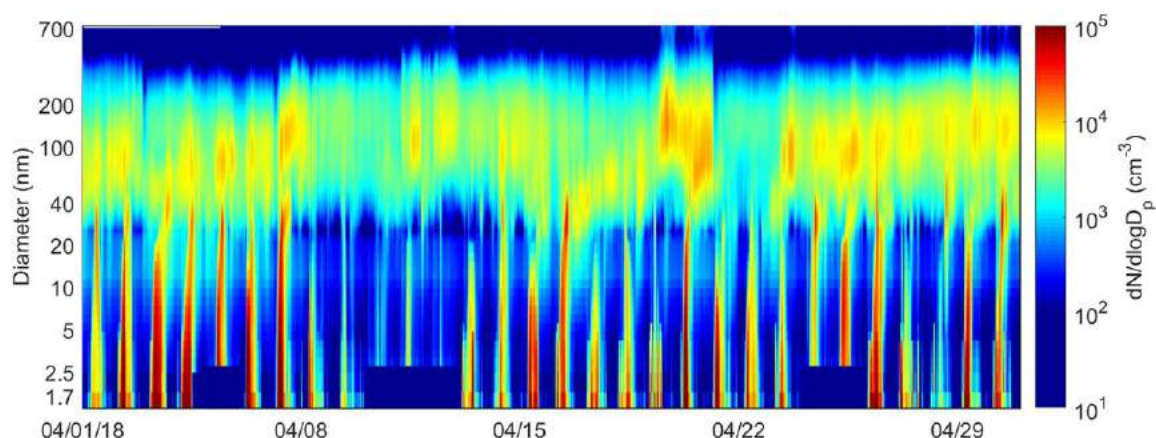


Figure 1. Example of the constructed particle number size distribution from three instruments as recorded for the month of April.

RESULTS

We investigated the particle size distributions looking for NPF events from Jan 27, 2018 to Jan 26, 2019. The total number of classified days was equal to 251 with 14 days excluded from the classification because of missing or invalid/bad. During the whole measurement period, 58% of the days were event days and 36% were clear non-event days (Figure 2).

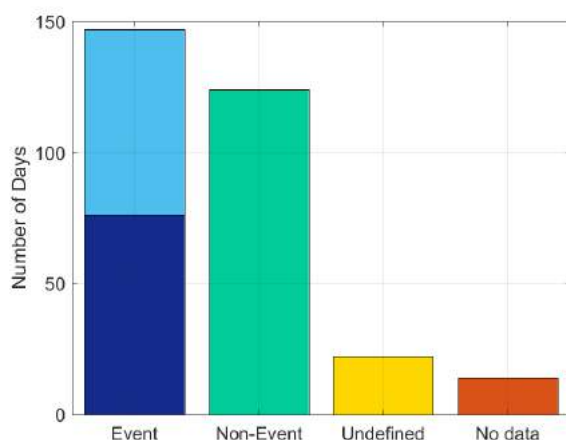


Figure 2. A one year classification of new particle formation events at AgiaMarina-Xyliatos.

We found that NPF is most frequent during the spring season mainly during the month of March and April (Figure 3). This could probably be linked to the increased biogenic activity during spring and the onset of intense photochemistry. We did not find a clear minima in NPF frequency in summer similar to data reported in other sites but the month with the least NPF frequency were August and September (Figure 3).

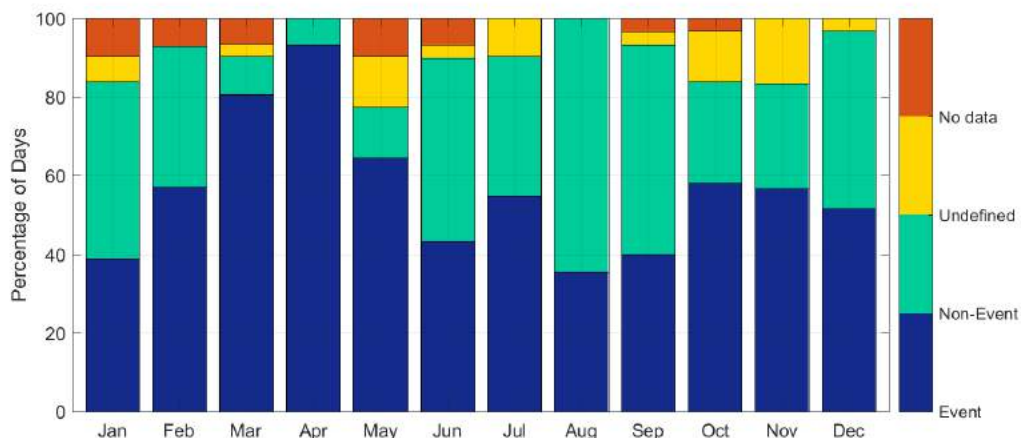


Figure 3. Monthly variation in the percentage of NPF occurrence at AgiaMarina-Xyliatos.

Multiple factors are well known to influence NPF occurrence. Those factors are solar radiation, temperature, pre-existing aerosol loading (represented by condensation sink), relative humidity, gas-phase sulfuric acid concentration (calculated using a proxy), and wind direction (Kerminen et al., 2018). Additionally other factors like wind speed, clearness index, O₃ concentrations, NO_x concentrations can play a role in explaining NPF occurrence. In an attempt to explain the observed seasonal variability in NPF occurrence, we investigated the aforementioned factors during different seasons, mainly focusing on the two month with the highest and lowest NPF occurrence. We found out that relative humidity was the only factor that had a clear relationship with NPF occurrence where it is higher during the month with the lowest occurrence except during August. None of the other factors could explain why we have a minimum in NPF during August and September. This minima could be explained by a lack of ammonia which is needed to stabilize the initial clusters as explained by Pikridas et al. (2012). Otherwise it could be linked to less biogenic volatile organic compounds (VOCs) released during these month when the plants are under stress from dry conditions.

Taking each month apart, NPF seemed to generally occur at higher temperature, higher pressure, higher SO₂, lower RH and lower wind speed while NO_x, O₃, CO, condensation sink, radiation, and wind direction did not seem to have a clear effect on NPF occurrence.

Further comprehensive data analysis of aerosol formation rates, growth rates, precursor gases will be shown to understand the mechanisms that favors or disfavors particle nucleation in the EMME region. This knowledge will help unfold the characteristics of aerosol nucleation in yet another environment leading to a better understanding of aerosol dynamics and their effect on the climate.

ACKNOWLEDGEMENTS

This work was supported by European Commission through EMME-CARE (Project ID: 763699), European Research council through ATM-GTP (Project ID: 742206) and Academy of Finland through CoE-ATM (Project ID: 307331).

REFERENCES

- Buenrostro Mazon, S., Riipinen, I., Schultz, D. M., Valtanen, M., Dal Maso, M., Sogacheva, L., et al. (2009). Classifying previously undefined days from eleven years of aerosol-particle-size distribution data from the SMEAR II station, Hyytiälä, Finland. *Atmos. Chem. Phys.*, 9(2), 667-676. <https://www.atmos-chem-phys.net/9/667/2009/>
- Dal Maso, M., Kulmala, M., Riipinen, I., Wagner, R., Hussein, T., Aalto, P. P., & Lehtinen, K. E. J. B. E. R. (2005). Formation and growth of fresh atmospheric aerosols: eight years of aerosol size distribution data from SMEAR II, Hyytiälä, Finland. *10*(5), 323.
- Hirsikko, A., Bergman, T., Laakso, L., Dal Maso, M., Riipinen, I., Hörrak, U., & Kulmala, M. (2007). Identification and classification of the formation of intermediate ions measured in boreal forest. *Atmos. Chem. Phys.*, 7(1), 201-210. <https://www.atmos-chem-phys.net/7/201/2007/>
- Jokinen, T., Sipilä, M., Junninen, H., Ehn, M., Lönn, G., Hakala, J., et al. (2012). Atmospheric sulphuric acid and neutral cluster measurements using CI-API-TOF. *Atmos. Chem. Phys.*, 12(9), 4117-4125. <https://www.atmos-chem-phys.net/12/4117/2012/>
- Kerminen, V.-M., Chen, X., Vakkari, V., Petäjä, T., Kulmala, M., & Bianchi, F. (2018). Atmospheric new particle formation and growth: review of field observations. *Environmental Research Letters*, 13(10), 103003. <http://dx.doi.org/10.1088/1748-9326/aadf3c>
- Kulmala, M., Petäjä, T., Nieminen, T., Sipilä, M., Manninen, H. E., Lehtipalo, K., et al. (2012). Measurement of the nucleation of atmospheric aerosol particles. *Nature Protocols*, 7(9), 1651-1667. <https://doi.org/10.1038/nprot.2012.091>
- Lelieveld, J., Berresheim, H., Borrmann, S., Crutzen, P. J., Dentener, F. J., Fischer, H., et al. (2002). Global Air Pollution Crossroads over the Mediterranean. *Science*, 298(5594), 794-799. <http://science.sciencemag.org/content/sci/298/5594/794.full.pdf>
- Lelieveld, J., Proestos, Y., Hadjinicolaou, P., Tanarhte, M., Tyrllis, E., & Zittis, G. (2016). Strongly increasing heat extremes in the Middle East and North Africa (MENA) in the 21st century. *Climatic Change*, 137(1), 245-260. journal article. <https://doi.org/10.1007/s10584-016-1665-6>
- Manninen, H. E., Mirme, S., Mirme, A., Petäjä, T., & Kulmala, M. (2016). How to reliably detect molecular clusters and nucleation mode particles with Neutral cluster and Air Ion Spectrometer (NAIS). *Journal of Atmospheric Measurement Techniques*, 9(8), 3577-3605.
- Manninen, H. E., Nieminen, T., Asmi, E., Gagné, S., Häkkinen, S., Lehtipalo, K., et al. (2010). EUCAARI ion spectrometer measurements at 12 European sites – analysis of new particle formation events. *Atmos. Chem. Phys.*, 10(16), 7907-7927. <https://www.atmos-chem-phys.net/10/7907/2010/>
- Merikanto, J., Spracklen, D. V., Mann, G. W., Pickering, S. J., & Carslaw, K. S. (2009). Impact of nucleation on global CCN. *Atmos. Chem. Phys.*, 9(21), 8601-8616. <https://www.atmos-chem-phys.net/9/8601/2009/>
- Mirme, S., & Mirme, A. (2013). The mathematical principles and design of the NAIS—a spectrometer for the measurement of cluster ion and nanometer aerosol size distributions. *Journal of Atmospheric Measurement Techniques*, 6(4), 1061-1071.
- Pikridas, M., Riipinen, I., Hildebrandt, L., Kostenidou, E., Manninen, H., Mihalopoulos, N., et al. (2012). New particle formation at a remote site in the eastern Mediterranean. *Journal of Geophysical Research: Atmospheres*, 117(D12). <https://agupubs.onlinelibrary.wiley.com/doi/abs/10.1029/2012JD017570>
- Vanhanen, J., Mikkilä, J., Lehtipalo, K., Sipilä, M., Manninen, H. E., Siivola, E., et al. (2011). Particle Size Magnifier for Nano-CN Detection. *Aerosol Science and Technology*, 45(4), 533-542. <https://www.tandfonline.com/doi/abs/10.1080/02786826.2010.547889>

FIRST REFRACTORY BLACK CARBON MEASUREMENTS ON THE EAST ANTARCTIC PLATEAU

J. BACKMAN¹, A. VIRKKULA¹, T. RAATIKAINEN¹, P.P. AALTO², A. LUPI³, P. CRISTOFANELLI⁴
L. CAIAZZO^{5,6} and R. TRAVERSI⁶

¹Atmospheric composition research, Finnish Meteorological Institute,
Helsinki, Finland.

²Institute for Atmospheric and Earth System Research (INAR), University of Helsinki, Helsinki, Finland

³CNR-ISP, Bologna, Italy

⁴CNR-ISAC, Bologna, Italy

⁵INFN and Physics Dept., University of Florence, Italy

⁶Dept. of Chemistry "Ugo Schiff", University of Florence, Italy

Keywords: BLACK CARBON, ANTARCTICA, POLLUTION, AEROSOLS.

INTRODUCTION

Antarctica is the continent with the least anthropogenic influence in the world. Just X % of the world's population live in the southern hemisphere where 80 % of the Earth's ocean surface-area is and is surrounded by the notoriously stormy southern ocean where virtually no commercial shipping lanes are to be found. Under the Antarctic treaty, Antarctica has no permanent settlements and is generally restricted to research visits only.

The atmospheric lifetime of aerosol particles is in the order of a few days to a couple of weeks depending on the setting (Raes et al., 2000). Compared to the timescales of interhemispheric mixing, the aerosols lifetime in the atmosphere is short (Verma, 2000). Typically pollutants mix within the hemisphere in a few weeks to a few months. Interhemispheric mixing typically takes much longer, a year or two, and is well studied using measurements of long lived trace gases such as CO₂ (Jacob, 1999). This means that aerosols over Antarctica should primarily originate from the southern hemisphere.

Black carbon aerosols originate from incomplete combustion of carbonaceous matter such as various fossil fuels and biomass burning. Much of the black carbon found in the atmosphere is of anthropogenic origin with the only major source of natural origin being naturally occurring wildfires (REF). Another unique feature of atmospheric black carbon is that it is chemically inert in the atmosphere and doesn't change its ability to absorb light during atmospheric transport. This makes black carbon a very good tracer for air-masses arriving from over land. Given the remote location of Antarctica and the atmospheric lifetime of aerosols the concentrations of black carbon are expected to be very low. The concentration of BC in polar areas important as BC is detrimental to the snow and ice sheets ability to reflect solar radiation and keep surface temperatures cool (Wiscombe & Warren, 1980).

The station is ideal for studying very clean air as the air masses that arrive at the station are one of the cleanest on Earth. This is mainly due to two facts. First, due to the high elevation and close proximity to the pole, air masses that arrive at the station subside from higher up in the atmosphere and are not advected along the surface where most of the air pollution originates. Secondly, most of the man-made air pollution is emitted in the northern hemisphere where the majority of the Earth's population live.

During the summer campaign 2018-2019 of the Austral summer a Single Particle Soot Photometer (SP2) was deployed at the Italian and French Antarctic research station Concordia. The station is located on the east Antarctic inland plateau 3233 m above mean sea level and some 1000 km from the coast and is one of only three all year around stations on inland plateau; see Figure 1.

METHODS

The SP2 is a highly sensitive instrument which is able to detect the occurrence of soot (black carbon) in a single aerosol particle down to a size of around 70 nm in size. This is equivalent to about 0.2 fg of black carbon. The SP2 operating principal is based on a high power intra-cavity infrared laser beam through which the sample aerosol is directed. The infrared laser beam, 1064 nm, causes the light absorbing black carbon aerosol particles to heat up by absorption of infrared light to the point of incandescence. The incandescing particles are then detected by photodetectors; one by one, by saving the traces of the particles in the detectors sampled by a digital oscilloscope. The amplitude of the incandescence signal is proportional to the BC mass and sensing this BC in this way is referred to as refractory BC (rBC, Petzold et al., 2013)

The instrument is not limited to detecting only light absorbing particles because non-absorbing particles scatter the IR laser's light. This allows for the detection and distinction of particles that absorb light, scatter light, or both. A later improvement of the SP2 included a position sensitive detector which allows for the estimation of optical size of the shell surrounding black carbon containing aerosol particles before the coating evaporates (Gao et al., 2007).

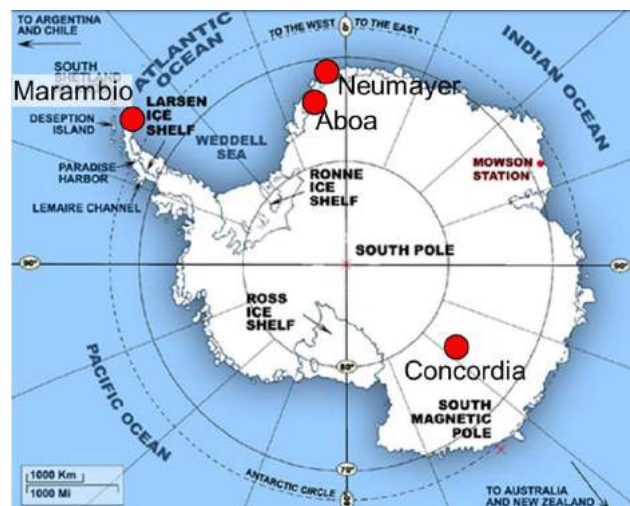


Figure 1. The location of the French Italian research station Concordia located on the East-Antarctic inland plateau. Also shown in the figure are stations where the Finnish Meteorological Institute and Institute for Atmospheric and Earth System Research (INAR) of University of Helsinki are conducting research.

The instrument is calibrated using particles of known size and density. The detectors sensitive to incandescing particles were calibrated using a Differential Mobility Analyser (DMA) and the reference material Aquadag which has a known density in the size range that the SP2 is sensitive to. Aquadag is a highly absorbing reference material which behaves very much like ambient soot although the density differs and the instrument response can be non-linear at large particles masses. Ammonium sulphate was used to calibrate the detector that is sensitive to elastically scattered light from the IR laser.

RESULTS

The instrument was deployed at Concordia (Figure 1) from 30 of November 2018 to 3 of January 2019. The sample flow was drawn through the common inlet used for the differential mobility particle sizer

(DMPS) which operates at the site. The SP2 was connected to the same line to have a high enough sample flow in the line do avoid unnecessarily high diffusional losses as the flow rate of the SP2 was only 0.12 volumetric litres per minute (vlpn). An extra flow of 0.5 vlpn was drawn to a T-piece just before the instrument to keep diffusional losses at a minimum. The particle losses in the sampling line before the SP2 instrument was estimated to be insignificant for the size range of the instrument.

A summary of the measured particle number concentrations and rBC mass concentrations during the duration of the measurements is given in Table 1. The mass concentration of light absorbing particles are very low, as expected. However, they vary from day to day and there are clear events with clean and very clean air when the mass concentrations can decrease by an order of magnitude for a couple of days. Figure 2 depicts the variation in the rBC mass concentration differentiated into different types of aerosol particles based on their optical properties during the measurement period.

Particle type	Particle number concentration (1/cm ³)	rBC mass concentration (ng/cm ³)
Scattering	5.01	-
Absorbing	0.11	0.12
Mixed	0.23	0.90

Table 1. Particle concentrations according to optical classification by the SP2. Scattering comprise only particles that only scatter light; no incandescence signal. Absorbing comprise particles that only register in the incandescence channels. Mixed particles both scatter and absorb the IR laser's light.

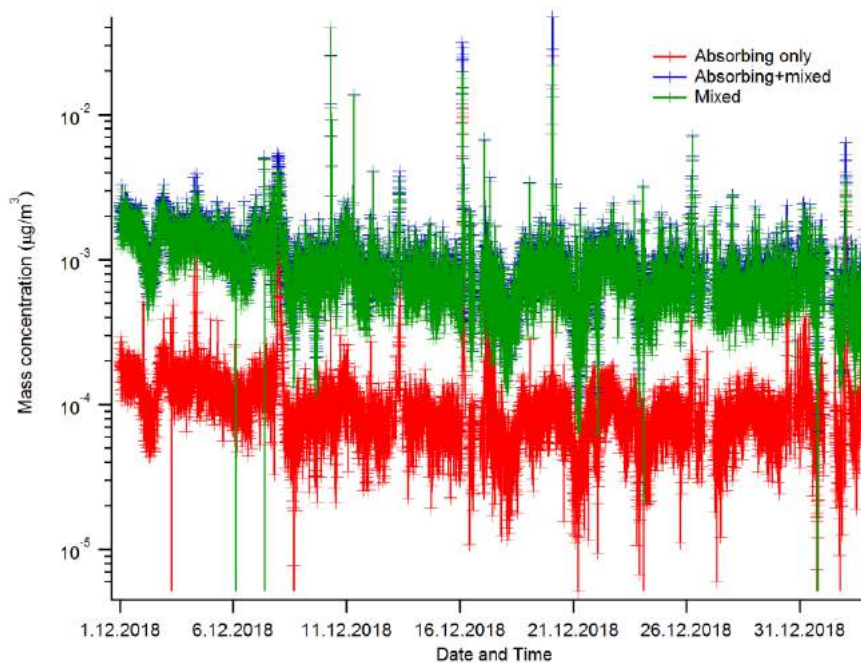


Figure 2. Mass concentration of rBC aerosol during the campaign assuming a density of 1.8 g/cm³ for rBC. The red markers show the mass concentration of only absorbing rBC aerosol particles. The green markers show the rBC mass concentration of particles that also scatter light. The blue markers show the total rBC mass concentration.

As can be seen from the figure, there are events when the total mass concentration of rBC drop for an extended period of time. Several such events occurred from the beginning of the campaign until it ended on in the beginning of January. Further meteorological analyses, as well as ozone data, will be needed to uncover if these events occur due to transport along the surface from the coast or large scale circulation involving subsidence of air-masses from higher up in the atmosphere.

CONCLUSIONS

The SP2 instrument was successfully deployed for just over one month at the Concordia station in Antarctica. As expected, the concentrations were very low and, on average, the rBC mass concentrations were 1.02 ng/cm^3 . Although the concentrations were low, they were by no means steady. Several episodes with cleaner air occurred during the campaign lasting up to a day. The origin of these clean episodes remains to be investigated.

ACKNOWLEDGEMENTS

Field measurements at Concordia Station were made possible by the joint French–Italian Concordia Program, which established and currently runs the permanent Concordia station at Dome C. We thank the Italian polar programme PNRA (Programma Nazionale di Ricerca in Antartide) and the French polar Institute (Institut Paul Emile Victor, IPEV). In particular, this work was supported by the PNRA project LTCPAA (Long-Term Measurements of Chemical and Physical Properties of Atmospheric Aerosol at Dome C, PNRA 2015/AC3). The Academy of Finland Center of Excellence program (project number 272041) is also acknowledged.

REFERENCES

- Daniel J. Jacob (1999). *Introduction to Atmospheric Chemistry*, (Princeton University Press).
- Gao, R. S., Schwarz, J. P., Kelly, K. K., Fahey, D. W., Watts, L. A., Thompson, T. L., and Worsnop, D. R. (2007). A Novel Method for Estimating Light-Scattering Properties of Soot Aerosols Using a Modified Single-Particle Soot Photometer. *Aerosol Science and Technology*, **41**(2), 125–135. <https://doi.org/10.1080/02786820601118398>
- Petzold, a., Ogren, J. a., Fiebig, M., Laj, P., Li, S. M., Baltensperger, U., and Zhang, X. Y. (2013). Recommendations for reporting black carbon measurements. *Atmospheric Chemistry and Physics*, **13**, 8365–8379. <https://doi.org/10.5194/acp-13-8365-2013>
- Raes, F., Dingenen, R. Van, Elisabetta, V., Wilson, J., Putaud, J. P., Seinfeld, J. H., & Adams, P. (2000). Formation and cycling of aerosols in the global troposphere. *Developments in Environmental Science*, **34**, 4215–4240. [https://doi.org/10.1016/S1474-8177\(02\)80021-3](https://doi.org/10.1016/S1474-8177(02)80021-3)
- Verma, A. (2000). An introduction to automatic differentiation. *Current Science*, **78**(7), 804–807. <https://doi.org/10.1002/pamm.200310012>
- Wiscombe, W. J., & Warren, S. G. (1980). A model for the spectral albedo of snow. II: Snow Containing Atmospheric Aerosols. *Journal of Atmospheric Sciences*. [https://doi.org/10.1175/1520-0469\(1980\)037<2734:AMFTSA>2.0.CO;2](https://doi.org/10.1175/1520-0469(1980)037<2734:AMFTSA>2.0.CO;2)

BLOWING SNOW PRODUCING HALOGEN ION CLUSTERS IN ANTARCTICA

L. BECK¹ and M. SIPILÄ¹

¹Institute for Atmosphere and Earth System Research, Department of Physics, University of Helsinki, Finland

Keywords: HALOGENS, IONS, ANTARCTICA, BLOWING SNOW.

INTRODUCTION

Previous studies have demonstrated that blowing snow in polar environments is a significant source of sea salt aerosol as well as halogens (Yang et al., 2008, Giordano et al., 2018). Within the Antarctic boundary layer, the aerosol composition is containing a high fraction of chlorine and sodium, which is clearly linked to high wind speeds due to local meteorological conditions (Giordano et al., 2018). During our campaign in Antarctica at Neumayer Station III, we observed a high amount of particles and ions during blowing snow events and were able to detect the chemical composition of those ions.

METHODS

In order to measure the particle concentration as well as particle size distribution, we used a setup of instruments including the Neutral cluster and Air Ion Spectrometer (NAIS, Manninen et al., 2009) as well as a Particle Size Magnifier (PSM, Vanhanen et al. 2011) and an Atmospheric Pressure interface - Time-of-Flight (APi-TOF, Tofwerk A.G., Junninen et al, 2010). The measurements were carried out at Neumayer Station III in Antarctica (70°40' S, 008°16' W) next to Atka Bay at the Weddell Sea between November 2018 and February 2019.

CONCLUSIONS

When the wind speed was reaching a certain threshold and the snow on the surface had the right density to be transported by the wind, we observed a rapid increase in ion- and particle concentration from a couple of hundreds up to several thousand per cm³. Additionally we measured a variety of ions and ion clusters containing halogens. Those phenomena have also been observed at other polar environments, though the circumstances such as the critical wind speed, leading to the increasing amount of ions, is highly dependent on the location itself. Further details will be presented in near future.

ACKNOWLEDGEMENTS

This work was supported by European Research Council (GASPARCON, grant No. 714621).

REFERENCES

- Junninen, H. et al. (2010) A high-resolution mass spectrometer to measure atmospheric ion composition. *Atmos. Meas. Tech.* **3**, 1039–1053.
- Giordano, M. R. et al. (2018) The importance of blowing snow to halogen-containing aerosol in coastal Antarctica: influence of source region versus wind speed, *Atmos. Chem. Phys.*, **18**, 16689-16711.
- Manninen, H. et al. (2009) Long-term field measurements of charged and neutral clusters using Neutral cluster and Air Ion Spectrometer (NAIS). *Bor. Env. Res.* **14**, 591-605.
- Vanhanen, J. et al. (2011) Particle Size Magnifier for Nano-CN Detection. *Aerosol Sci. Technol.* **45**, 533-542.
- Yang, X. et al. (2008). Sea salt aerosol production and bromine release: Role of snow on sea ice, *Geoph. Res. Let.* **35**, L16815.

COMPUTATIONAL STUDIES ON NEW PARTICLE FORMATION INVOLVING CHARGED SULFURIC ACID - AMMONIA CLUSTERS

V.BESEL¹, J. KUBEČKA¹, T. KURTÉN² AND H. VEHKAMÄKI CHAPMAN¹

¹Institute for Atmospheric and Earth System Research, University of Helsinki, Gustav Hällströmin katu 2, 00560 Helsinki, Finland.

²Institute for Atmospheric and Earth System Research, University of Helsinki, A.I. Virtasen aukio 1, 00560 Helsinki, Finland.

Keywords: configurational sampling, molecular clusters, atmospheric chemistry.

INTRODUCTION

Atmospheric aerosol particles have impact onto the global climate in various ways. They scatter and absorb radiation or can act as cloud condensation nuclei. A bulk of the aerosol particles in the atmosphere are formed by gas-to-particle nucleation (Merikanto, 2009). However, the exact process of single molecules forming cluster, which subsequently can grow into particles, remains largely unknown. Recently, sulfuric acid has been identified to play a key role in this new particle formation enhanced by other compounds such as organic acids (Zhang, 2010) or ammonia (Anttila, 2005). We conducted a computational study for identifying characteristics of cluster formation and nucleation involving sulfuric acid and ammonia in neutral, positive and negative mode.

METHODS

We use a layered approach for the configurational sampling of molecular cluster starting from utilizing a genetic algorithm in order to explore the whole potential energy surface (PES) of the cluster for all geometrical minima, however, with very unreliable energies. The structures are further optimized with a semi-empirical method, DFT on the ω B97X-D level of theory, with filtering after each step, to obtain the global minimum configuration.

Further, high level of theory (DLPNO-CCSD(T)) is used for obtaining electronic energies and together with DFT frequency analysis the Gibbs free energies of formation are calculated. These are passed to the Atmospheric Cluster Dynamics Code (ACDC) (McGrath, 2012) which calculates the fluxes of molecular clusters and a nucleation rate.

CONCLUSIONS

We determined global minima for sulfuric acid - ammonia clusters with $(H_2SO_4)_m(NH_3)_m$ for neutral clusters (*c.f.* fig. 1), with $(H_2SO_4)_m(HSO_4)^-(NH_3)_n$ for positively charged clusters and with $(H_2SO_4)_m(NH_4)^+(NH_3)_n$ for negatively charged clusters, where $m < 7$. We omitted structures which have been shown to be unstable or from minor role in previous studies. (Olenius, 2013)

Further, we present formation rates, steady state concentrations and fluxes (Cf. fig. 1) of these clusters calculated with ACDC and discuss how a new configurational sampling procedure and more precise quantum chemistry methods have changed these ACDC results in comparison to previous studies and how these results fare in comparison to experimental results.

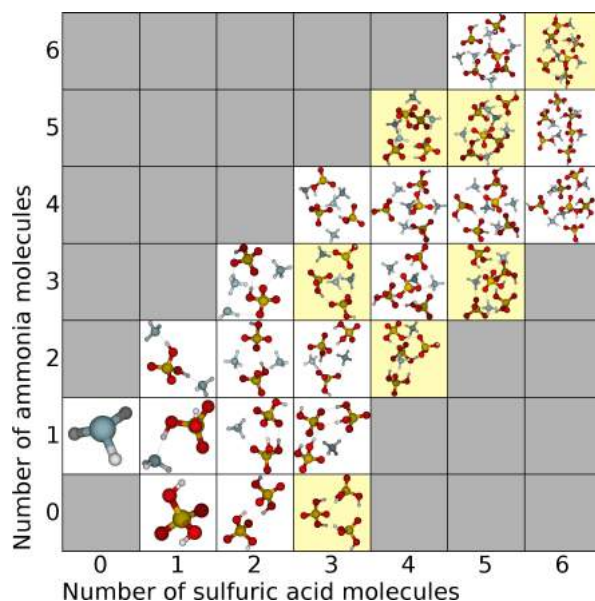


Figure 1: The global minima for neutral sulfuric acid-ammonia cluster found

ACKNOWLEDGEMENTS

This work is supported by the European Research Council project 692891-DAMOCLES, Academy of Finland, ATMATH project. We would like to thank also CSC–Finnish IT Centre for access to computer cluster and computational resources.

REFERENCES

- J. Merikanto, D. V. Spracklen, G. W. Mann, S. J. Pickering, and K. S. Carslaw (2009). Impact of nucleation on global CCN. *Atmos. Chem. Phys.*, **9**, 8601-8616.
- R. Zhang (2010) Getting to the Critical Nucleus of Aerosol Formation. *Science*, **328**, 1366-1367.
- T. Anttila, H. Vehkamäki, I. Napari, M. Kulmala (2005). Effect of ammonium bisulphate formation on atmospheric water-sulphuric acid-ammonia nucleation. *Boreal Env. Res.*, **10**, 523.
- M.J. McGrath, T. Olenius, I.K. Ortega, V. Loukonen, P. Paasonen, T. Kurten, M. Kulmala (2012). Atmospheric Cluster Dynamics Code: a flexible method for solution of the birth-death equations. *Atmos. Chem. Phys.*, **12**, 2355.
- T. Olenius, O. Kupiainen-Määttä, I.K. Ortega, T. Kurten, H. Vehkamäki (2013). Free energy barrier in the growth of sulfuric acid-ammonia and sulfuric acid-dimethylamine clusters. *J. Chem. Phys.*, **139**, 084312.

DEGRADATION OF NANOPLASTICS IN WATER: IMPACT ON GASEOUS AND AQUEOUS PHASE ORGANIC CARBON.

A. BIANCO¹, P. A. ALPERT², P. CORRAL ARROYO², J. DOU³, F. SORDELLO⁴, K. WITTE², B. WATTS², U. K. KRIEGER³, M. AMMANN², D.V. VIONE⁴ and M. PASSANANTI^{1,4}

¹ Institute for Atmospheric and Earth System Research/Physics, Faculty of Science, University of Helsinki, FI-00014, Finland.

² Paul Scherrer Institute, Laboratory of Environmental Chemistry, 5232 Villigen PSI, Switzerland.

³ Institute for Atmospheric and Climate Science, ETH Zürich, 8092 Zürich, Switzerland

⁴ Dipartimento di Chimica, Università di Torino, Via Pietro Giuria 5, 10125, Torino, Italy

Keywords: plastic pollution, nanoplastics, environmental chemistry, photodegradation

INTRODUCTION

Previous studies have shown the ubiquitous presence in the biosphere of microplastics (MPs), plastic fragments with size lower than 5 mm, due to years of improper disposal of plastic materials, mismanagement and negligent littering. Only recently, the presence of nanoplastics (NPs) in oceans and in atmospheric particulate matter has been demonstrated (Ter Halle et al., 2017, Allen et al., 2019) and it is still unclear what it could be their environmental impact. NPs have size lower than 1 μm and, due to their density, they are expected to float at the surface of the oceans and interact with both atmosphere and bulk water. Therefore, NPs can absorb sunlight and react with oxidants in the gas and in the liquid phase. Most of the studies focus on surface modification using different approaches, mainly based on infrared spectroscopy or microscopy. However, as far as we know, little information is reported concerning degradation and photodegradation products released in both aqueous and gaseous phase. In this study, we evaluated the reactivity of NPs dispersed in water towards gas-phase and liquid-phase oxidants. In particular, we investigated the reaction between ozone and NPs dispersed in waters; this system can be representative of both NPs in aerosols and at the surface of oceans. Moreover, we studied the oxidation of NPs induced by light and/or hydroxyl radical, one of the stronger oxidants in the environment.

METHODS

At first, interaction between PS-NPs (polystyrene nanoparticles) and light or ozone was investigated, using commercially available NPs. PS-NPs suspended in MilliQ water were a) irradiated with UVC lamps or b) exposed to air flow containing 400 ppb of ozone. A significant uptake of ozone into the PS-NPs was observed, also for short-term exposure (19h). This result highlights that NPs at the surface of water can interact with oxidants in the gas phase, such as ozone. PS-NPs were also analyzed by STXM/NEXAFS (scanning transmission X-ray microscopy coupled to near-edge X-ray absorption fine structure spectroscopy) in order to investigate surface and bulk modifications. Experiments a) and b) show a general increase of oxygenated function, confirming that PS-NPs dispersed in water react with both light and ozone, leading to a chemical change of NPs. Analysis of the gas phase evidence the formation of benzaldehyde and butanal.

Since polystyrene represents less than 10% of the world plastic demand (Plastics- the Facts, 2018), the degradation of different NPs particles was investigated in aquatic environment. Commercially available NPs and MPs were dispersed in Milli-Q water and were exposed to UVA light (355 nm) in the presence and in the absence of hydrogen peroxide 1mM. The formation of degradation products induced by direct light absorption, reaction with photogenerated hydroxyl radicals or hydrogen peroxide, was studied by ESI-DMA-APiTOF MS (electrospray ionization – differential mobility analyser – atmospheric pressure interface time of flight mass spectrometry). NPs degradation leads to the formation of small carboxylic acids; in particular, formate and acetate were observed for all the investigated polymers. Other compounds, with mass

weight up to 200 Da, were observed. Figure 1 reports the formation kinetics of degradation products for the UVA irradiation of PS-NPs in water in the presence of hydrogen peroxide as source of hydroxyl radicals. However, any degradation products was observed at high mass, excluding the breakup of large segment of the polymer chain. Preliminary results suggest that polymer oxidation takes place little by little at chain extremities but further investigations are needed to confirm this hypothesis.

CONCLUSIONS

NPs and MPs are not inert and they can react with both compounds in the gas and liquid phase. Their degradation in aquatic environment, representative of atmospheric and surface water, is triggered by the reaction with oxidants (ozone, hydroxyl radical) and sunlight. These degradation processes are still poorly understood, however we demonstrated that they can release soluble compounds that could have an impact on DOM (dissolved organic matter), with a potential and completely unexplored effect of carbon cycle.

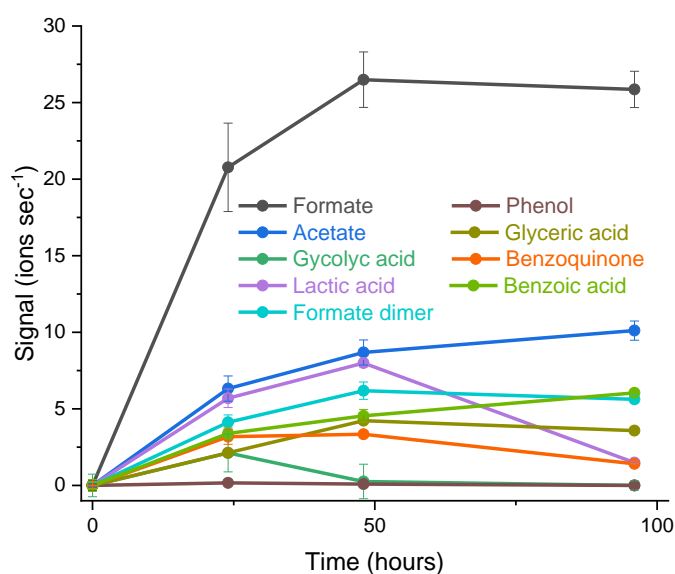


Figure 1. Release of degradation products in water by UVA irradiation of polystyrene nanoparticles in the presence of hydrogen peroxide as source of hydroxyl radicals.

ACKNOWLEDGEMENTS

This study was supported by the University of Helsinki (3 year research grants, n.75284135). The STXM/NEXAFS experiments were carried out at PoLux under the proposal n.20180904.

REFERENCES

- [1] Ter Halle, A., Jeanneau, L., Martignac, M., Jardé, E., Pedrono, B., Brach, L., Gigault, J., 2017. Nanoplastic in the North Atlantic subtropical gyre. *Environmental science & technology* 51, 13689–13697.
- [2] Allen, S., Allen, D., Phoenix, V.R., Le Roux, G., Durántez Jiménez, P., Simonneau, A., Binet, S., Galop, D., 2019. Atmospheric transport and deposition of microplastics in a remote mountain catchment. *Nature Geoscience* 12, 339–344.
- [3] Plastics - the Facts 2018. <https://www.plasticseurope.org>

VERTICAL PROFILE OF ICE NUCLEATING PARTICLE CONCENTRATIONS IN A BOREAL ENVIRONMENT

Z. BRASSEUR¹, J. SCHNEIDER², J. LAMPILAHTI¹, P. POUTANEN¹, M. PELTOLA¹, A. FRANCK¹, M. LAMPIMÄKI¹, A. MANNINEN¹, P. HIETALA¹, F. KORHONEN¹, K. HÖHLER², O. MÖHLER², B. BERTOZZI², T. SCHORR², N. UMO², F. VOGEL², M. KULMALA¹, T. PETÄJÄ¹ AND J. DUPLISSY¹

¹Institute for Atmospheric and Earth System Research, University of Helsinki, 00014 Helsinki, Finland

²Institute of Meteorology and Climate Research, Karlsruhe Institute of Technology, 76021 Karlsruhe, Germany

Keywords: ice nucleating particles, boreal environment, vertical profile.

INTRODUCTION

The impact of aerosol particles on the formation and properties of clouds is one of the largest remaining sources of uncertainty in climate change projection. Some aerosol particles can act as ice nucleating particles (INPs) by initiating the formation of ice crystals in clouds through heterogeneous ice nucleation. Although aerosol particle properties have been studied for decades, their ability to act as INP remains poorly understood (IPCC, 2013).

A measurement campaign (HyICE2018) was organized in southern Finland from mid-February to mid-June 2018. The main objectives of this campaign were to characterize the INP properties in a boreal environment. The campaign took place in the forest area of Hyytiälä at the University of Helsinki research station SMEARII.

During the HyICE2018 campaign, the Institute for Atmospheric and Earth System Research (INAR) and the Karlsruhe Institute of Technology (KIT) deployed a significant instrumentation in order to study the vertical profile of INP concentrations.

METHODS

Airborne measurements were performed to quantify INP concentrations in the boundary layer and in the free troposphere. A typical measurement flight lasted 3 hours during which the plane flew above SMEARII station from altitudes of 300 m up to 3000 m. The INP concentrations were measured using aerosol filter samples collection and different filter were used for each atmospheric layer. In addition, two sampling sites were installed at SMEARII: one at ground level and another in the 35 m tower. The plane was also equipped for aerosol physical properties investigation.

The INP content of aerosol filter samples was analyzed with the INSEKT (Ice Nucleation Spectrometer of the Karlsruhe Institute of Technology), a device developed to study the immersion freezing mode of ice nucleation (Schiebel, 2017). The aerosol samples collected on filters were suspended in clean water and pipetted in small volumes into a freezing array. The samples were cooled with a constant cooling rate while a camera detected brightness changes of the volumes related to their freezing. INSEKT is able to measure INP concentrations in a temperature range from 273 K to 248 K, which is relevant to study drop freezing conditions within supercooled mixed-phase clouds. The results obtained are in the form of temperature spectra of INP concentrations.

RESULTS AND CONCLUSIONS

During the campaign, 38 flights were realized between the 7th of March to the 19th of May 2018. Preliminary results show no substantial difference between INP concentrations measured at ground level, in the tower and in the boundary layer. On the other hand, INP concentrations measured in the free troposphere were always lower than the three latter mentioned. An example of typical result is shown in Figure 1.

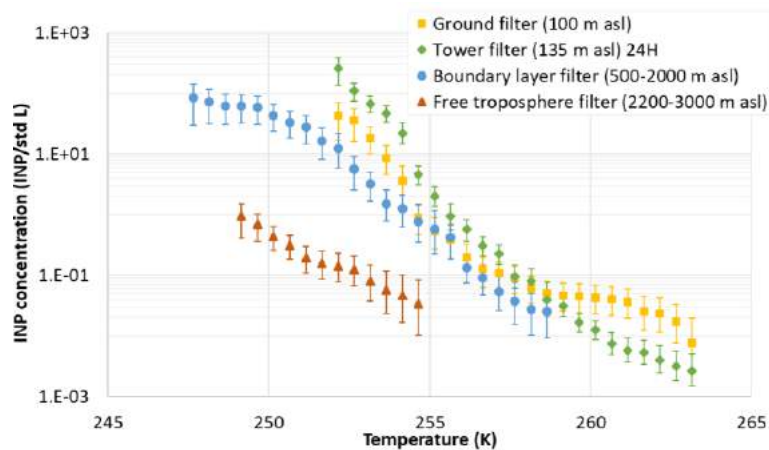


Figure 1. Temperature spectra of INP concentrations measured on the 14th of May 2018

ACKNOWLEDGEMENTS

This work was supported by the Academy of Finland Center of Excellence and the BIOFUTURE2025 project; it also received funding from the EU's 2020 programme via ACTRIS-2 Integrating Activities and iCUPE projects. Many thanks to the whole HyICE team and the facility staff at the Hyytiälä forestry research station.

REFERENCES

- IPCC, *Climate Change 2013: The Physical Science Basis. Contribution of Working Group I to the Fifth Assessment Report of the Intergovernmental Panel on Climate Change*. Cambridge University Press, Cambridge, United Kingdom and New York, NY, USA, 1535 pp, 2013
- Schiebel, T., 2017: *Ice nucleation activity of soil dust aerosols*. Ph.D. thesis, Karlsruhe Institute of Technology

DECONVOLUTING FIGAERO-CIMS THERMAL DESORPTION PROFILES WITH POSITIVE MATRIX FACTORISATION (PMF)

A. BUCHHOLZ¹, A. YLISIRNIÖ¹, W. HUANG², C. MOHR³, M. CANAGARATNA⁴,
D. R. WORSNOP⁴, S. SCHOBESBERGER¹, and A. VIRTANEN¹

¹Department of Applied Physics, University of Eastern Finland, Kuopio, Finland.

²Institute of Meteorology and Climate Research, Karlsruhe Institute of Technology, Karlsruhe, Germany

³Department of Environmental Science and Analytical Chemistry, Stockholm University, Stockholm, Sweden.

⁴Center for Aerosol and Cloud Chemistry, Aerodyne Research, Inc., Billerica, MA, USA.

Keywords: FIGAERO, PMF, VOLATILITY, SECONDARY ORGANIC AEROSOL.

INTRODUCTION

To understand the impact of secondary organic aerosol (SOA) on the earth's climate and human health, we need to know more about the chemical and physical properties of these particles and how they evolve with time in the atmosphere. The filter inlet for gases and aerosols (FIGAERO) together with a chemical ionisation mass spectrometer (CIMS) is a very useful tool for this endeavour. It has been applied around the world for ambient measurements and laboratory studies giving new insights into the overall chemical composition of aerosol particles and the processes involved in their formation and aging (e.g. Le Breton et al., 2018; Lee et al., 2018; Mohr et al., 2017). But in addition, the thermal desorption behaviour of each detected ion is recorded by this instrument. These ion thermograms can be related to the volatility of the detected compounds. So far, mostly the peak desorption temperature (T_{\max}) has been used for that purpose (e.g. Wang and Hildebrandt Ruiz, 2018). But a single T_{\max} value does not take the presence of isomers with different volatility or thermal decomposition processes into account which will cause multi-modal features or a general broadening of the ion thermograms (D'Ambro et al., 2017; Lopez-Hilfiker et al., 2015).

These difficulties in the analysis may be one reason why mostly bulk chemical composition and volatility have been discussed for FIGAERO-CIMS measurements and detailed thermal desorption profile data has been widely ignored. Another reason may be the complexity of the datasets. For each desorption cycle, hundreds of mass spectra are recorded and need to be compared. In previous studies, a few marker compounds/ions were selected and analysed in more detail (e.g. "pinic acid" in Lopez-Hilfiker et al. (2015) or C₈H₁₂O₅ in Schobesberger et al. (2018)).

We are the first to utilise Positive Matrix Factorisation (PMF) to perform a full and detailed analysis of the characteristics of all ion thermograms in a FIGAERO-CIMS dataset. PMF is a mathematical model which represents a complex dataset (here multiple ion thermograms/mass spectra) by a small number of factors (factor mass spectra) with varying contributions (factor thermograms).

METHODS

The investigated dataset consists of FIGAERO-CIMS samples of aerosol particle of different starting compositions (aerosol types) representing atmospheric conditions. These were then exposed to different length (0.25 h or 4 h) of isothermal evaporation under dry or wet conditions (relative humidity of < 2% or 80%, respectively) prior to the measurements with a FIGAERO-CIMS system using iodide-adduct ionisation (Aerodyne Research Inc., Lopez-Hilfiker et al., 2014, Lee et. al., 2014). The change in particle size during isothermal evaporation was measured as another independent measure of particle volatility. More details about this dataset can be found in Buchholz et al. (2019).

Note that the FIGAERO-system always sampled the residual particles after different lengths of prior isothermal evaporation. If the dominant process is indeed isothermal evaporation, the change in a single ion

thermogram towards higher desorption temperatures is then caused by isomers of higher volatility being removed before the sample is collected. Lower volatility compounds stay behind and will be detected.

RESULTS AND DISCUSSION

The isothermal evaporation measurements yield a direct measure of the volatility of the investigated SOA types and are discussed in detail in Buchholz et al. (2019). One important finding in this study was that wet conditions always enhanced the observed isothermal evaporation. Low-OC SOA particles exhibit roughly the same amount of isothermal evaporation after 4 h under dry as after 0.25 h under wet conditions. This information can be used to help with the interpretation and validation of the PMF results in general and specifically with understanding the effect of particulate water.

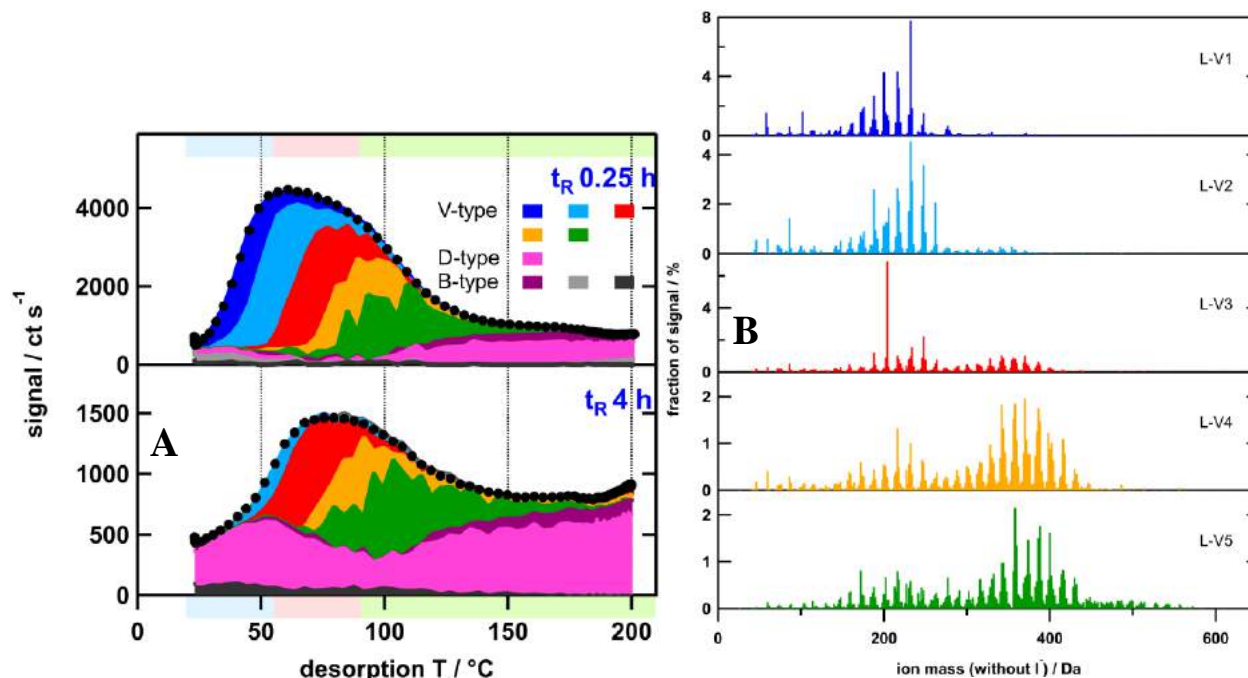


Figure 1: Left (A): Contribution of PMF factors to the total thermogram of low-OC SOA particles after 0.25 and 4 h of isothermal evaporation under wet conditions ($RH = 80\%$). Right (B): Corresponding factor mass spectra of the V-type factors (D- and B-type factors are omitted). The colour code is the same in both panels.

With PMF we identified three types of factors with distinct peak shape and behaviour in all datasets: volatility classes (V-type factors) were separated from background (B-type factors) and decomposition dominated parts of the signal (D-type factors). The V-type factors were characterised by their T_{max} values which did not change between samples if isothermal evaporation was the dominant process in the particles. Instead, the changes in particle composition with increasing prior isothermal evaporation were explained by decreasing the contribution of the V-type factors with the lowest T_{max} values (i.e., the most volatile ones, dark and light blue factors in Figure 2 A). Thus, we can indeed interpret the V-type factors as volatility classes, i.e., compounds with a similar volatility (desorption behaviour) are grouped into one factor. If the chemical composition of the particles had changed by another process than isothermal evaporation (here aqueous phase chemistry), PMF identified a new unique factor directly showing which ions/compounds were affected by the observed process.

The factor mass spectra give insights into the changes in particle composition which are not visible in the overall OC ratios for the particles. With decreasing volatility (increasing T_{max} values), the factor mass spectra show a stronger contribution of signals at molecular weights of >300 Da and more than 10 C atoms (Figure 2 B). Many of the lower M_w ions show contributions to multiple factors indicating that they most likely stem from direct desorption at low and from thermal decomposition of low volatility compounds at high desorption temperature.

This new approach to analyse FIGAERO-CIMS thermal desorption profile data can be applied to all kinds of FIGAERO-CIMS datasets and is not limited to laboratory studies. For ambient data, it enables a deeper analysis of the composition beyond source apportionment. The additional information on volatility changes has important implications for the further fate of aerosol particles in the atmosphere (i.e., will they persist or quickly evaporate). Also, the volatility class information derived from PMF V-type factors can be used for a straight-forward integration of results based on FIGAERO observations into (process) models.

ACKNOWLEDGEMENTS

We thank the European Research Council (ERC StG QAPPA 335478), the Academy of Finland Centre of Excellence program (decision 307331) and the Academy of Finland (grants 299544, 317373, and 310682) for financial support.

REFERENCES

- Buchholz, A., Lambe, A.T., Ylisirniö, A., Li, Z., Tikkanen, O.P., Faiola, C., Kari, E., Hao, L., Luoma, O., Huang, W., Mohr, C., Worsnop, D.R., Nizkorodov, S.A., Yli-Juuti, T., Schobesberger, S., Virtanen, A., 2019. Insights into the O: C-dependent mechanisms controlling the evaporation of α -pinene secondary organic aerosol particles. *Atmos. Chem. Phys.* 19, 4061–4073. <https://doi.org/10.5194/acp-19-4061-2019>
- D'Ambro, E.L., Lee, B.H., Liu, J., Shilling, J.E., Gaston, C.J., Lopez-Hilfiker, F.D., Schobesberger, S., Zaveri, R.A., Mohr, C., Lutz, A., Zhang, Z., Gold, A., Surratt, J.D., Rivera-Rios, J.C., Keutsch, F.N., Thornton, J.A., 2017. Molecular composition and volatility of isoprene photochemical oxidation secondary organic aerosol under low- and high-NO_x conditions. *Atmos. Chem. Phys.* 17, 159–174. <https://doi.org/10.5194/acp-17-159-2017>
- Le Breton, M., Wang, Yujue, Hallquist, Å.M., Pathak, R.K., Zheng, J., Yang, Y., Shang, D., Glasius, M., Bannan, T.J., Liu, Q., Chan, C.K., Percival, C.J., Zhu, W., Lou, S., Topping, D., Wang, Yuchen, Yu, J., Lu, K., Guo, S., Hu, M., Hallquist, M., 2018. Online gas- and particle-phase measurements of organosulfates, organosulfonates and nitrooxy organosulfates in Beijing utilizing a FIGAERO ToF-CIMS. *Atmos. Chem. Phys.* 18, 10355–10371. <https://doi.org/10.5194/acp-18-10355-2018>
- Lee, B.H., Lopez-Hilfiker, F.D., D'Ambro, E.L., Zhou, P., Boy, M., Petäjä, T., Hao, L., Virtanen, A., Thornton, J.A., 2018. Semi-volatile and highly oxygenated gaseous and particulate organic compounds observed above a boreal forest canopy. *Atmos. Chem. Phys.* 18, 11547–11562. <https://doi.org/10.5194/acp-18-11547-2018>
- Lopez-Hilfiker, F.D., Mohr, C., Ehn, M., Rubach, F., Kleist, E., Wildt, J., Mentel, T.F., Carrasquillo, A.J., Daumit, K.E., Hunter, J.F., Kroll, J.H., Worsnop, D.R., Thornton, J.A., 2015. Phase partitioning and volatility of secondary organic aerosol components formed from α -pinene ozonolysis and OH oxidation: The importance of accretion products and other low volatility compounds. *Atmos. Chem. Phys.* 15, 7765–7776. <https://doi.org/10.5194/acp-15-7765-2015>
- Mohr, C., Lopez-Hilfiker, F.D., Yli-Juuti, T., Heitto, A., Lutz, A., Hallquist, M., D'Ambro, E.L., Rissanen, M.P., Hao, L., Schobesberger, S., Kulmala, M., Mauldin, R.L., Makkonen, U., Sipilä, M., Petäjä, T., Thornton, J.A., 2017. Ambient observations of dimers from terpene oxidation in the gas phase: Implications for new particle formation and growth. *Geophys. Res. Lett.* 44, 2958–2966. <https://doi.org/10.1002/2017GL072718>
- Schobesberger, S., D'Ambro, E.L., Lopez-Hilfiker, F.D., Mohr, C., Thornton, J.A., 2018. A model framework to retrieve thermodynamic and kinetic properties of organic aerosol from composition-resolved thermal desorption measurements. *Atmos. Chem. Phys.* 18, 14757–14785. <https://doi.org/10.5194/acp-18-14757-2018>
- Wang, D.S., Hildebrandt Ruiz, L., 2018. Chlorine-initiated oxidation of alkanes under high-NO conditions: Insights into secondary organic aerosol composition and volatility using a FIGAERO-CIMS. *Atmos. Chem. Phys.* 18, 15535–15553. <https://doi.org/10.5194/acp-18-15535-2018>

Source apportionment of fine particulate matters by physical and chemical markers during the non-heating season in Beijing, China

Jing Cai^{1,2}, Biwu Chu^{1,2,3,4}, Lei Yao^{1,2}, Chao Yan^{1,2}, Liine M. Heikkinen^{1,2}, Feixue Zheng¹, Chang Li¹, Xiaolong Fan¹, Yonghong Wang^{1,2}, Tom V. Kokkonen^{1,2}, Tommy Chan^{1,2}, Ying Zhou¹, Lubna Dada^{1,2}, Yongchun Liu¹, Hong He^{3,4}, Shaojun Zhang⁵, Pauli Paasonen^{1,2}, Joni T Kujansuu^{1,2}, Tuukka Petäjä^{1,2}, Juha Kangasluoma^{1,2}, Federico Bianchi^{1,2}, Yele Sun⁶, Philip. L. Croteau⁷, Douglas R. Worsnop⁷, Veli-Matti Kerminen^{1,2}, Wei Du^{1,2*}, Markku Kulmala^{1,2*}, Kaspar R. Daellenbach^{1,2*}

1 Aerosol and Haze Laboratory, Beijing Advanced Innovation Center for Soft Matter Science and Engineering, Beijing University of Chemical Technology, Beijing 100029, China

2 Institute for Atmospheric and Earth System Research, Faculty of Science, University of Helsinki, Helsinki 00014, Finland

3 Center for Excellence in Regional Atmospheric Environment, Institute of Urban Environment, Chinese Academy of Sciences, Xiamen 361021, China

4 State Key Joint Laboratory of Environment Simulation and Pollution Control, Research Center for Eco-Environmental Sciences, Chinese Academy of Sciences, Beijing 100085, China

5 School of Environment, Tsinghua University, Beijing 100084, China

6 State Key Laboratory of Atmospheric Boundary Layer Physics and Atmospheric Chemistry, Institute of Atmospheric Physics, Chinese Academy of Sciences, Beijing 100029, China

7 Aerodyne Research, Inc., Billerica, MA 01821, USA

Key words: Source apportionment, Beijing, ACSM, SMPS

Introduction

Sources of fine particulate matters are of importance to control air pollution and haze in China. Though source apportionment studies has been conducted by numerous studies in China¹⁻³, there are not too many researches applying both chemical and physical properties to identify sources in particle mass and number concentrations, which resulting in much less information of primary sources are provided. In this study, both particle chemical and physical markers were applied in the same site during non-heating season. By positive matrix factorization (PMF) analysis with organic markers (OA-PMF) as well as size distributions (Size-PMF), similar source types and contributions from size and mass contribution were resolved, including light duty vehicle emissions (LDV-related), heavy duty vehicle emissions (HDV-related), cooking emissions (cooking-related) as well as regional sources.

Methods

For this study, data were collected in Beijing University of Chemical and Technology (BUCT), Beijing, China from April 6 to Jul 2, 2018. A Time-of-Flight Aerosol Chemical Species Monitor (ACSM) equipped with a PM_{2.5} aerodynamic lens and standard vaporizer as well as a Scanning Mobility Particle Sizer (SMPS) were performed in a rooftop of a 5-floor teaching building. Non-refractory species (including sulfate, nitrate, ammonium, chloride and organics) in PM_{2.5} and particle size from 20 to 680 nm were measured by those two instruments, respectively. PM_{2.5} concentration, boundary layer height as well as the traffic flow data near the sampling site were also measured. PMF as well as multilinear engine 2 (ME-2) methods were performed to solve the number and mass contributions of fine particulate matters and organic aerosols (OA) during the sampling period.

Results

By PMF methods, LDV-related particles were found to exhibit the dominating size of 20 nm and average concentration of $2.4 \times 10^3 \text{ cm}^{-3}$. After converting to mass concentration with the density of 1.5 g/cm^3 , LDV-related could contribute $0.79 \text{ } \mu\text{g/m}^3$ on average. It also exhibited similar diurnal pattern of the LDV vehicle flow at nearest intersections. However, HDV-related particles showed a dominating size peak of 100 nm and $5.5 \times 10^3 \text{ cm}^{-3}$, exhibiting similar diurnal HDV patterns, which concentrated to travel during nighttime due to the daytime restrictions⁴. HDV-related particles also had a good correlation with BC plus HOA from OA-PMF from ACSM ($r = 0.65$).

The peak of cooking-related particle sizes were around 40 nm with the number concentration of $5.5 \times 10^3 \text{ particles/cm}^3$. The cooking-related particles of Size-PMF showed very similar diurnal patterns with OA-PMF analysis with one peak during the lunchtime the other during the dinner time. Discrepancies from the converted mass from Size-PMF and OA-PMF can be explained by the high relative ionization efficiencies (RIEs) for cooking particles.

Regional sources from Size-PMF and secondary particles (sulfate, nitrate, ammonium plus secondary organic aerosols) in OA-PMF exhibited strong correlation ($r = 0.93$) with a slope of 1.1, suggesting that those particles with larger size can come from regional and secondary processes.

Overall, this studies applied both chemical and physical fingerprints to identify and quantify the sources in both mass and number levels of fine particulate matters in Beijing, China during the non-heating season. It can provide detailed information for the primary sources of particles for further researches.

References

1. Sun, Y.; Du, W.; Fu, P.; Wang, Q.; Li, J.; Ge, X.; Zhang, Q.; Zhu, C.; Ren, L.; Xu, W.; Zhao, J.; Han, T.; Worsnop, D. R.; Wang, Z., Primary and secondary aerosols in Beijing in winter: sources, variations and processes. *Atmospheric Chemistry and Physics* **2016**, *16*, (13), 8309-8329.
2. Sun, Y.; Du, W.; Wang, Q.; Zhang, Q.; Chen, C.; Chen, Y.; Chen, Z.; Fu, P.; Wang, Z.; Gao, Z.; Worsnop, D. R., Real-Time Characterization of Aerosol Particle Composition above the Urban Canopy in Beijing: Insights into the Interactions between the Atmospheric Boundary Layer and Aerosol Chemistry. *Environ Sci Technol* **2015**, *49*, (19), 11340-7.
3. Sun, Y.; Xu, W.; Zhang, Q.; Jiang, Q.; Canonaco, F.; Prévôt, A. S. H.; Fu, P.; Li, J.; Jayne, J.; Worsnop, D. R.; Wang, Z., Source apportionment of organic aerosol from 2-year highly time-resolved measurements by an aerosol chemical speciation monitor in Beijing, China. *Atmospheric Chemistry and Physics* **2018**, *18*, (12), 8469-8489.
4. Yang, D.; Zhang, S.; Niu, T.; Wang, Y.; Xu, H.; Zhang, K. M.; Wu, Y., High-resolution mapping of vehicle emissions of atmospheric pollutants based on large-scale, real-world traffic datasets. *Atmospheric Chemistry and Physics* **2019**, *19*, (13), 8831-8843.

TRANSMISSION OF CHARGED NANOPARTICLES THROUGH AN ADVERSE AXIAL ELECTRIC FIELD AND ITS IMPROVEMENT

R. CAI^{1,2}, J. KANGASLUOMA¹, and J. JIANG²

¹ Institute for Atmospheric and Earth System Research, Faculty of Science, University of Helsinki, Helsinki, Finland.

²School of Environment, Tsinghua University, Beijing, China.

Keywords: NANOPARTICLE, ELECTRICAL LOSS, DIFFUSIONAL LOSS, DMA.

INTRODUCTION

In aerosol studies, it is often encountered that charged nanoparticles or ions are transported against an adverse electric field. For instance, when classifying them according to their electrical mobility using a differential mobility analyzer, charged particles and ions migrate along with the electric field in the classification region and then against the adverse electric field in the sample outlet (or inlet in some cases). Their electrostatic losses can be reduced using a specially designed sample outlet or inlet inside which the adverse electric field is axially parallel. Based on the same principle, the electrical mobility filter (EMF) that can segregate charged particles using an adjustable adverse axial electric field.

Theoretical analysis of nanoparticle penetration through the adverse axial electric field considering both particle diffusion and electrostatic migration is needed, especially for sub 10 nm particles. Previously, several models were used for characterizing the transmission efficiency of charged particles through an axial electric field. Bezantakos et al. (2015) used a semi-empirical formula considering both electrostatic and diffusional losses. In this formula, four parameters were used to fit experimentally measured transmission efficiency. Different values were obtained for these parameters when instrumental working conditions are different, which limits the application of this semi-empirical formula.

Based on sound theoretical derivation, Tammet (2015) proposed an analytical solution for the transmission efficiency of non-diffusive particles which is a function of one dimensionless parameter. A conceptual model based on single particle tracking is proposed by Tammet (2015) as an example to illustrate how to simulate particle diffusion in an electric field; however, examination on the feasibility of the model was not reported, and there was no further discussion on the transmission efficiency evaluated using the model. Following Tammet (2015), we study the transmission of charged particles and ions through an adverse axial electric field inside an ESD tube when considering both particle diffusion and electrostatic migration.

METHODS

Electric field

The adverse electric field is axially uniform due to the linearly changing electric potential on the surface of the tube, which is achieved using electrostatic dissipative (ESD) materials. The electric field inside the ESD tube is solved analytically.

Numerical model

A numerical model is proposed to estimate particle transmission efficiency through the adverse electric field. This model is derived based on the two assumptions/approximations as follows:

- 1) The air flow profile remains the same along the axial direction of the cylindrical tube.

- 2) The axial length where particles move as a result of the radial electric field is negligible compared to the total length of the tube.

In the numerical model, particle diffusion and electrostatic losses are simulated step by step. For the DMA sample outlet, the transmission efficiency is simulated in 5 steps. Diffusion losses are simulated before, within, and after the adverse electric field; and electrostatic migration of particles are simulated at the entrance and exit of the electric field. Particle cross-sectional concentration profiles are numerically solved after each step of diffusion or electrical migration. After that, particle transmission efficiency through the tube is obtained by calculating integral of concentration flux at the exit of the tube and divide it by that at the entrance of the tube. For the EMF, the transmission efficiency is simulated by 9 steps because the electric field is more complicated than that of the DMA sample outlet.

Simplified analytical model

To save the computational expense, an additional assumption is added when the electric field is short compared to the total tube length:

- 3) The electric field does not affect the diffusive loss rate.

Based on assumptions 1) – 3), a simplified analytical model is proposed. In this simplified analytical model, the electrostatic loss and diffusion of particles are considered in two separate steps: the first step considering only particle diffusion and the second step considering only the electrostatic loss. In the first step, the particle concentration profile as a result of diffusion is calculated at the exit of the entire tube (Gormley and Kennedy 1949). In the second step, the effect of the electric field is simplified as only removing particles outside the threshold radius for electrical loss without changing the trajectories of particles inside it.

Monte Carlo method

The Monte Carlo method is based on tracking the trajectories of individual particles. The flow field is either estimated using an approximate model for the entrance flow (Targ 1951) or simply assumed to be the Hagen-Poiseuille or plug flow. Since this Monte Carlo method is based on single particle tracking within the flow and electric fields, it does not rely on assumptions 2) and 3). Thus, this Monte Carlo method is considered to be more accurate than the numerical model and the simplified analytical model.

Experiments

The transmission efficiencies of ions through the ESD tube with different adverse field lengths were experimentally studied. Monodisperse tetra-heptyl ammonium ions (THA⁺) with an electrical mobility diameter of ~1.48 nm were generated using electrospray and subsequently classified using a half-mini DMA. The voltage on the DMA inner electrode was -300 V, and the external electrode was grounded. The sample outlet of the half-mini DMA was modified such that the voltages of the outlet tube was also -300 V. The classified ions were measured by two aerosol electrometers upstream and downstream of the ESD tube.

Application example

Based on the above models and experiments, the ESD tube (POM-C, Ensinger Inc.) was used to increase the transmission efficiency through the sample outlet of a mini-cy DMA. The insulation Delrin used between the central electrode and the original metal outlet tube was replaced with a rigid ESD tube. Ions with an electrical mobility diameter of 1.48 nm were used to characterize the penetration efficiencies of the DMA.

CONCLUSIONS

The numerical model agrees with the Monte Carlo method unless the electric field is too short to be axially uniform (length/radius < 4) or the tube length before the electric field is much shorter than the entrance length of the air flow. The simplified analytical model is valid when the adverse electric field is relatively short compared to the total tube length. If the assumptions in developing the proposed model are significantly violated, the Monte Carlo method which requires higher computational expenses can be used instead to estimate the transmission efficiency. Both the proposed models and the Monte Carlo method were applied for an electrical mobility filter and the sample outlet of a differential mobility analyzer. Under the typical conditions for these devices, the transmission efficiency estimated using the proposed models agrees well not only with the Monte Carlo method (a mean absolute difference smaller than 1%) and but also with the measured transmission efficiencies for sub-6 nm particles. By replacing the commonly used Delrin insulator at the sample outlet of a mini-cy DMA with an ESD tube to reduce electrostatic loss, the penetration efficiency of 1.48-nm ions under typical operating conditions (a sheath flow rate of 25 L·min⁻¹ and an aerosol flow rate of 1.5 L·min⁻¹) was increased by 50%, because using the ESD tube decreased the adverse electrostatic field.

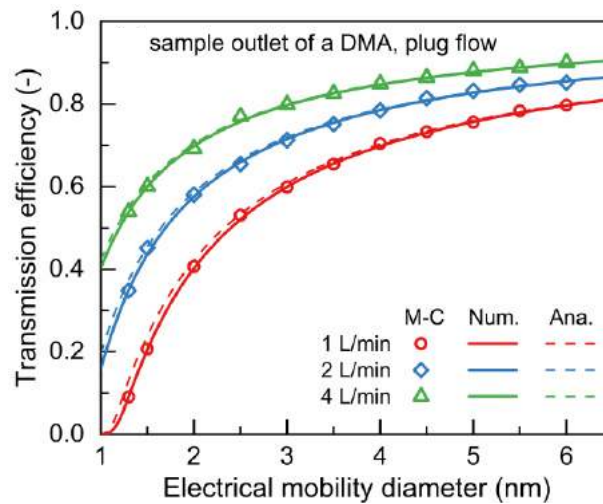


Figure 1. Comparison of the Monte Carlo method (M-C), numerical model (Num.) and the simplified analytical model (Ana.).

ACKNOWLEDGEMENTS

This work was supported by the National Key R&D Program of China (2017YFC0209503) and the National Natural Science Foundation of China (21876094).

REFERENCES

Tammet, H. (2015). The Aspiration Method for the Determination of Atmospheric-Ion Spectra. *Aerosol Sci Technol*, **49**, 220-228.

UNDERSTANDING THE INVERSION METHODS FROM SUB-3 NM PARTICLE NUMBER CONCENTRATION DATA IN BEIJING, CHINA

T. CHAN^{1,2}, J. KANGASLUOMA^{1,2}, R. CAI³, L. YILIANG⁴, Y. ZHOU², L. AHONEN¹, J. SULO¹, L. WANG⁴ and M. KULMALA^{1,2}

¹Institute for Atmospheric and Earth System Research/Physics Faculty of Science, University of Helsinki, P.O. Box 64, 00014 Helsinki, Finland

²Aerosol and Haze Laboratory, Beijing University of Chemical Technology, Beijing 100029, China

³State Key Joint Laboratory of Environment Simulation and Pollution Control, School of Environment, Tsinghua University, 100084 Beijing, China

⁴Shanghai Key Laboratory of Atmospheric Particle Pollution and Prevention (LAP3), Department of Environmental Science and Engineering, Fudan University, Shanghai 200433, China.

Keywords: aerosol particles, particle size magnifier, inversion methods, sub-3nm

INTRODUCTION

Knowledge of the particle number size distribution (PNSD) of atmospheric aerosol particles is an important component to understand cloud formation, nucleation, formation and growth rates. This is especially important in the sub-3 nm range because of the growth of particles directly coming from the gas phase. A common problem of any PNSD studies, the inversion of the measured data to a proper size distribution from particle number concentration, is challenging. This is even more so of the measurements at sub-3 nm range due to its complexity and due to the simple fact that not many measurements at this range has been properly measured in the environment. This study examines various PNSD inversion methods using the Particle Size Magnifier (PSM, Airmodus Oy, Finland), which determines the PNSD based on the relationship between the particle number concentration and a varying saturator flow rate. Although the uncertainties of the size distribution prior to data inversion and after inversion has been addressed (Kangasluoma & Kontkanen, 2017; Cai *et al.*, 2018), understanding both the measured data prior to inversion and the uncertainties faced when measuring in the environment are not well understood.

METHODS

We looked at data prior to inversion, during inversion and after inversion. More specifically, prior to inversion, we saw how each individual scan looks like data (i.e. a scan, ranging from 0.1 litres per minute to 1.3 litres per minute) and applied a discard method to remove scans which are deemed bad, based on a statistical hypothesis test (p value). During inversion, we introduced four methods to invert measured data: step-wise and kernel methods, introduced by Lehtipalo *et al.* (2014); the Hagen and Alofs linear inversion method (Hagen & Alofs, 1983); and the expectation–maximization algorithm, the latter two introduced by Cai *et al.* (2018). In this study, we used data measured from the Beijing University of Chemical Technology, in Beijing, China. This site is situated in an urban environment of central Beijing. This site allows for useful understanding of how each inversion method allocates the measured particle number concentration into their respective size bin. Particularly, we separated the event-types into three categories: new particle formation, non-new particle formation and haze. The measurement period used in this study was from 15 Jan. to 15 Mar., which was during the winter heating period.

REFERENCES

- Cai R, Yang D, Ahonen LR, Shi L, Korhonen F, Ma Y, Hao J, Petäjä T, Zheng J, Kangasluoma J. 2018.** Data inversion methods to determine sub-3 nm aerosol size distributions using the particle size magnifier. *Atmospheric Measurement Techniques* **11**(7): 4477-4491.
- Hagen DE, Alofs DJ. 1983.** Linear inversion method to obtain aerosol size distributions from measurements with a differential mobility analyzer. *Aerosol Science and Technology* **2**(4): 465-475.
- Kangasluoma J, Kontkanen J. 2017.** On the sources of uncertainty in the sub-3 nm particle concentration measurement. *Journal of Aerosol Science* **112**: 34-51.
- Lehtipalo K, Leppä J, Kontkanen J, Kangasluoma J, Franchin A, Wimmer D, Schobesberger S, Junninen H, Petaja T, Sipila M. 2014.** Methods for determining particle size distribution and growth rates between 1 and 3 nm using the Particle Size Magnifier. *Boreal Environment Research*.

DECADAL TRENDS OF ATMOSPHERIC OXIDANTS AT THE BOREAL FOREST IN FINLAND

D. CHEN¹, P. ZHOU¹, P. ROLDIN², T. NIEMINEN¹, M. BAYKARA AND M. BOY¹

¹Institute for Atmospheric and Earth System Research / Physics, Faculty of Science, University of Helsinki, Finland

²Division of Nuclear Physics, Lund University, P.O. Box 118, 22100 Lund, Sweden

Keywords: chemistry transport model, decadal trend, atmospheric oxidants

INTRODUCTION

The atmospheric oxidation capacity is strongly influenced by the hydroxyl radical (OH), ozone (O₃) and the nitrate radical (NO₃) concentrations, however, real-time measurement data of OH and NO₃ are only available at few sites during certain campaigns. The sulfuric acid (H₂SO₄) concentration is an important indicator for the new particle formation event frequency over the long term. The 1-dimensional chemical-transport model SOSAA (Boy et al., 2011) was validated to simulate OH concentration with reasonable results in earlier publications (Boy et al., 2011, Petäjä et al., 2013). In this study, 12-years simulation with the SOSAA model were performed for the years 2007-2018 to investigate the atmospheric oxidants trends at SMEAR II, Hyytiälä, Finland.

METHODS

The SOSAA version applied in this study is based on the version applied in the study by Zhou et al. (2017), which includes a new module to simulate the dry deposition of gases, besides the existing modules for meteorology, BVOCs emission, chemistry and aerosol. However, here we turned the aerosol module off to save computational time. For our simulations, we used SOSAA with 51 logarithmic scaled layers from 0-3000 m. Meteorological data and trace gases including CO, NO, NO₂, SO₂ and ozone are provided as input from the SMEAR II station. These gases come mainly from anthropogenic sources and by constraining them by measurements we aim to consider the most important anthropogenic impact, thus no emission inventory is required. For biogenic emission, our BVOCs module is retrieved from the MEGAN model. Inorganic gas emission from biogenic sources are not considered but are proved to be minor from prior studies (Kesik et al., 2005). Methane concentration is assumed to have a fixed increasing trend. We used the MCM mechanism to calculate the gas-phase chemistry, considering all species which react with O₃, OH or NO₃ in Hyytiälä and are known to have a significant concentration. With this model, we are able to simulate the vertical profile and flux of atmospheric compositions.

CONCLUSIONS

Although ozone is also one of the main oxidants, it is read in from measurement, thus we only focus on the OH and NO₃ radical. From the input data, we see a strong declining trend for SO₂ and NO₂, and we did set a fixed increase of 6 ppt per year for CH₄. Monoterpenes, which are major contributor for OH sink, are modelled with the BVOCs emission module based on MEGAN. For the 12 years period, OH concentration shows a weak increase, but it has strong fluctuations through the years. Figure 1 shows the time series from year 2007 to 2018 for OH. Therefore it's still difficult to provide a guess for OH future change under current climate changing trends. We also modelled NO₃, which showed an obvious decrease, which is probably connected with the reduce of NO₂ emissions in Europe.

With the model simulations for more than one decade, we aim to understand how the atmospheric oxidants change through climatic patterns in northern European boreal forest. The oxidants in boreal forest have a strong impact on H₂SO₄ concentration, which is crucial to understand decadal trends of new particle formation at a single site, and further on a global scale. Previous studies did use proxies for OH based on UVB and other parameters. By considering the gas-phase chemistry by MCM, we aim to provide another

measure for OH concentration in the long term. Based on this, we can provide a long term trend of H₂SO₄. Existing measurement of NO₃ concentration are quite rare, there are also methods to approximate, and with this study we could provide an estimate on the NO₃ trend over the long term.

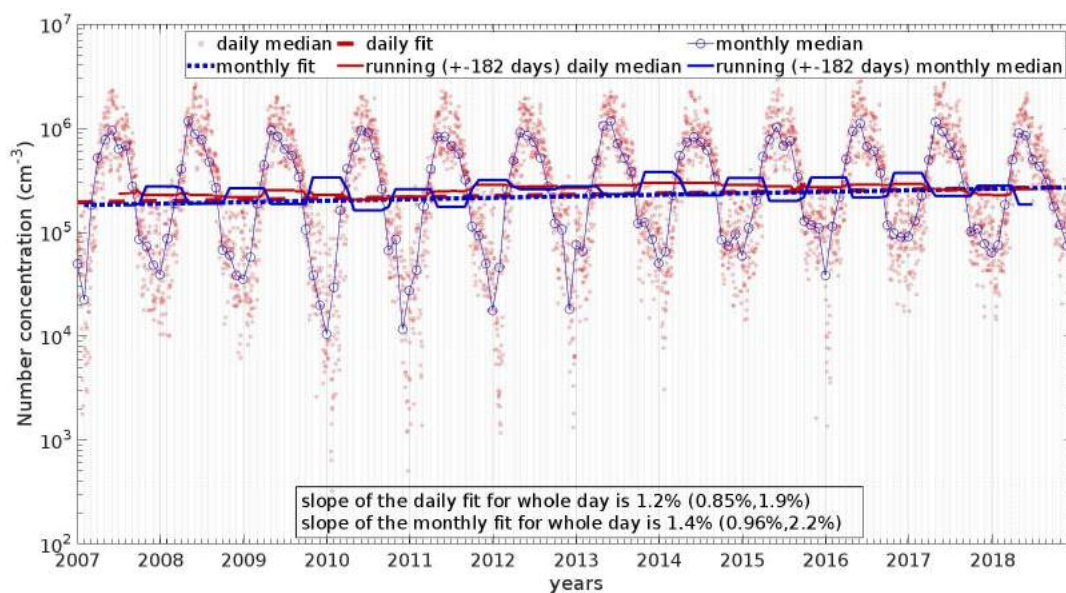


Fig. 1 Time series of OH concentration for the years 2007 – 2018. Dots represent model data, solid lines represent running mean over 365 days, and dashed lines represent linear regression for data in the log-scale. Plots in red represent daily median data, while data in blue represent monthly median data.

ACKNOWLEDGEMENTS

We acknowledge the support of the Academy of Finland Center of Excellence program (272041), the China Scholarship Council (CSC), and we want to thank the CSC – IT Center for Science Ltd for computational resources.

REFERENCES

- Boy, M., Sogachev, A., Lauros J. et al.: SOSA – a new model to simulate the concentrations of organic vapours and sulphuric acid inside the ABL – Part 1: Model description and initial evaluation, *Atmos. Chem. Phys.*, 11, 43-51, 2011.
- Kesik, M., Ambus, P., Baritz, R. Et al.: Inventories of N₂O and NO emissions from European forest soils, *Biogeosciences*, 2, 353-375, 2005.
- Mogensen, D., Smolander, S., Sogachev, et al.: Modelling atmospheric OH-reactivity in a boreal forest ecosystem, *Atmos. Chem. Phys.*, 11, 9709-9719, 2011.
- Boy, M., Mogensen, D., Smolander, S., Zhou, L., Nieminen, T., Paasonen, P., Plass-Dülmer, C., Sipilä, M., Petäjä, T., Mauldin, L., Berresheim, H. and Kulmala, M.: Oxidation of SO₂ by stabilized Criegee intermediate (sCI) radicals as a crucial source for atmospheric sulfuric acid concentrations, *Atmospheric Chemistry and Physics*, doi:10.5194/acp-13-3865-2013, 2013.a
- Zhou, P., Ganzeveld, L., Taipale, D. et al.: Boreal forest BVOC exchange: emissions versus in-canopy sinks, *Atmos. Chem. Phys.*, 17, 14309-14332, 2017.

A PROPOSED AEROSOL INDEX (AI) BASED ON 1-YEAR OBSERVATION OF AEROSOL SIZE DISTRIBUTION IN BEIJING

Biwu Chu^{1,2,3}, Lubna Dada^{1,2}, Juha Kangasluoma^{1,2}, Tuukka Petäjä^{1,2,4}, Veli-Matti Kerminen¹, Markku Kulmala^{1,2,4}

¹Institute for Atmospheric and Earth System Research / Physics, Faculty of Science, University of Helsinki, Finland

²Aerosol and Haze Laboratory, Beijing Advanced Innovation Center for Soft Matter Science and Engineering, Beijing University of Chemical Technology, Beijing, China

³State Key Joint Laboratory of Environment Simulation and Pollution Control, Research Center for Eco-Environmental Sciences, Chinese Academy of Sciences, Beijing 100085, China

⁴Joint International Research Laboratory of Atmospheric and Earth System Sciences, School of Atmospheric Sciences, Nanjing University, Nanjing 210023, China

Keywords: AIR QUALITY, AEROSOL NUMBER CONCENTRATION, CONDENSATION SINK, NEW PARTICLE FORMATION, HAZE.

INTRODUCTION

In China, the high concentrations of various gas precursors, i.e. SO₂, NO_x, NH₃, and Volatile organic compounds (VOCs) (X. G. Liu et al., 2013; L. Wang et al., 2015; Ye et al., 2011; Zou et al., 2015) have resulted in high concentrations of secondary inorganic and organic species in fine particles (PM_{2.5}) during haze formation (Z. Wang et al., 2012; Yang et al., 2011; Zhao et al., 2013). However, the occurrence frequencies of NPF events in high condensation sink (CS) environments of China were higher than those in low aerosol-loading environments (Peng et al., 2014). Meanwhile, the observed formation rate (FR) of new particles was one to two orders of magnitude higher for NPF in China than that at rural/urban sites in western countries, resulting in high number concentration of nano-particles (Chu et al., 2019; Yao et al., 2018). At present, air quality index (AQI) was used to represent the air quality for the cocktail of gas pollutants and particulate matter (or highly complex air pollution). In AQI, only mass concentration of fine particles (PM_{2.5}) was include for characterize aerosol. And at a large fraction of time, especially when the pollution happened, the primary pollutant was usually PM_{2.5}. In the past decades, more and more comprehensive measurement of aerosols were carried out in China, and therefore, we may deserve a more comprehensive aerosol index (AI). In this study, an AI was proposed based on 1-year observation of aerosol size distribution in Beijing, in which particle number concentration, condensation sink, and PM_{2.5} mass concentrations are considered.

METHODS

The results presented in this study are collected at a comprehensive measurement station in urban Beijing (N 33.94°, E 116.30°) between 23rd of January and 31st December 2018. The observation station is located on the western campus of Beijing University of Chemical Technology (BUCT), which is 400 m to the west of the West Third Ring Road and surrounded by residential and commercial areas (Lu et al., 2019; Zhou et al., 2019). Particle number concentration and size distribution were monitored with a suite of instruments, including a Particle Size Magnifier (PSM) to measure small particles in the range of 1.5 – 2.5 nm (Vanhanen et al., 2011), a diethylene glycol (DEG) SMPS to measure 1.5 – 6 nm particles (Cai, Chen, Hao, & Jiang, 2017; Jiang, Chen, Kuang, Attoui, & McMurry, 2011), a Particle Size Distribution (PSD) to detect particles from 3 nm to 10 μm (J. Q. Liu, Jiang, Zhang, Deng, & Hao, 2016), and a neutral cluster and air ion spectrometer (NAIS) to monitor the 0.8 – 20 nm ions and 2 – 20 nm particles (Mirme & Mirme, 2013).

These data were mainly used to calculate the concentration sink (CS), particle formation and growth rates (Kulmala et al., 2012), and to identify NPF events with the method introduced by Dal Maso et al. (2005).

The AI was calculated similarly as AQI, while the detail method of AQI calculation can be found in the Chinese national air quality standard GB3095-2012, and HJ 633-2012. Three parameters determinate AI in this study, i.e. particle number concentration, condensation sink, and PM_{2.5} mass concentration. To calculate the AI, we first need to set levels for each parameter, which might be quite subjective. The levels were set mainly according to the statistical distributions of each parameter at different type of days, i.e. NPF days, haze days and the other days in this study. The levels of PM_{2.5} are kept the same as the Chinese national air quality standard GB3095-2012. The optimized level standards are listed in Table 1.

Table 1. Aerosol Index Standard

Level	Aerosol index grade (AIG)	Particle number concentration (particles/cm ³)	Condensation sink (s ⁻¹)	PM _{2.5} mass concentration (μg/m ³)
1	0	0	0	0
2	50	1e4	0.01	35
3	150	7e4	0.06	115
4	300	2e5	0.16	250
5	500	3e5	0.26	500

Then, AI could be calculated following the four steps listed below:

1. Collect and calculated the three parameters in Table 1.
2. Compare each parameter with the standard in Table 1, and find the lowest level that higher than or equal with the concentration (H) and the highest level that lower than the concentration (L). For example, if PM_{2.5} mass concentration is 20μg/m³, then the H level is 2 and the L level is 1.
3. Calculate the individual aerosol index (IAI) for each parameter i:

$$IAI_i = AIG_L + \frac{C_i - S_{L,i}}{S_{H,i} - S_{L,i}} (AIG_H - AIG_L)$$

where AIG_L and AIG_H are the aerosol index grade for level L and level H in Table 1, respectively; $S_{H,i}$ and $S_{L,i}$ are the standard values of parameter i for level H and level L in Table 1, respectively; C_i is the measured or calculated value of parameter i.

4. Calculate the AI from IAI of the three parameters:

$$AI = \max(AI_i)$$

Similar as the definition of primary pollutant, the parameter which has the highest IAI is called the primary factor.

CONCLUSIONS

According to whether NPF and haze events happened or not, the days were classified into three groups, i.e. NPF days, haze days, and the other days without NPF and haze during the observation period. AI and primary parameters in these three groups, as well as AQI during a 5-month period are shown in Figure 1 as an example. Generally, AI followed the trend of AQI well. Since PM_{2.5} is usually the pollutant than determinates the AQI and more parameters of aerosol are included in AI than AQI, the AI was always higher than AQI. The small peaks of AI above AQI indicate periods with high particle number concentration or high particle surface area concentration. During the observation period, NPF mainly happened when the primary factor was the particle number concentration, while there was still a small fraction of NPF happened when the primary factor was CS. Haze mainly happened when AQI showed a high peak and the primary factor was the PM_{2.5} mass concentration, while there was also a small fraction of haze happened when the primary factor is CS. On average, about 70% of the NPF, haze and other days happened with primary factor to be particle number concentration, PM_{2.5} mass concentration, and CS, respectively. So the application of AI in this study maybe also used to classify the types of pollution. Besides the urban environment, we also

applied the AI calculation to the observation at a forest station in Hyytiala, where long period of observation of particle size distribution and NPF classification is available (Dada et al., 2017; Mäkelä et al., 1997). The AI seemed also separate the events (i.e. NPF) well, although the AI calculation methods was developed based on the observation of aerosol size distribution in Urban Beijing.

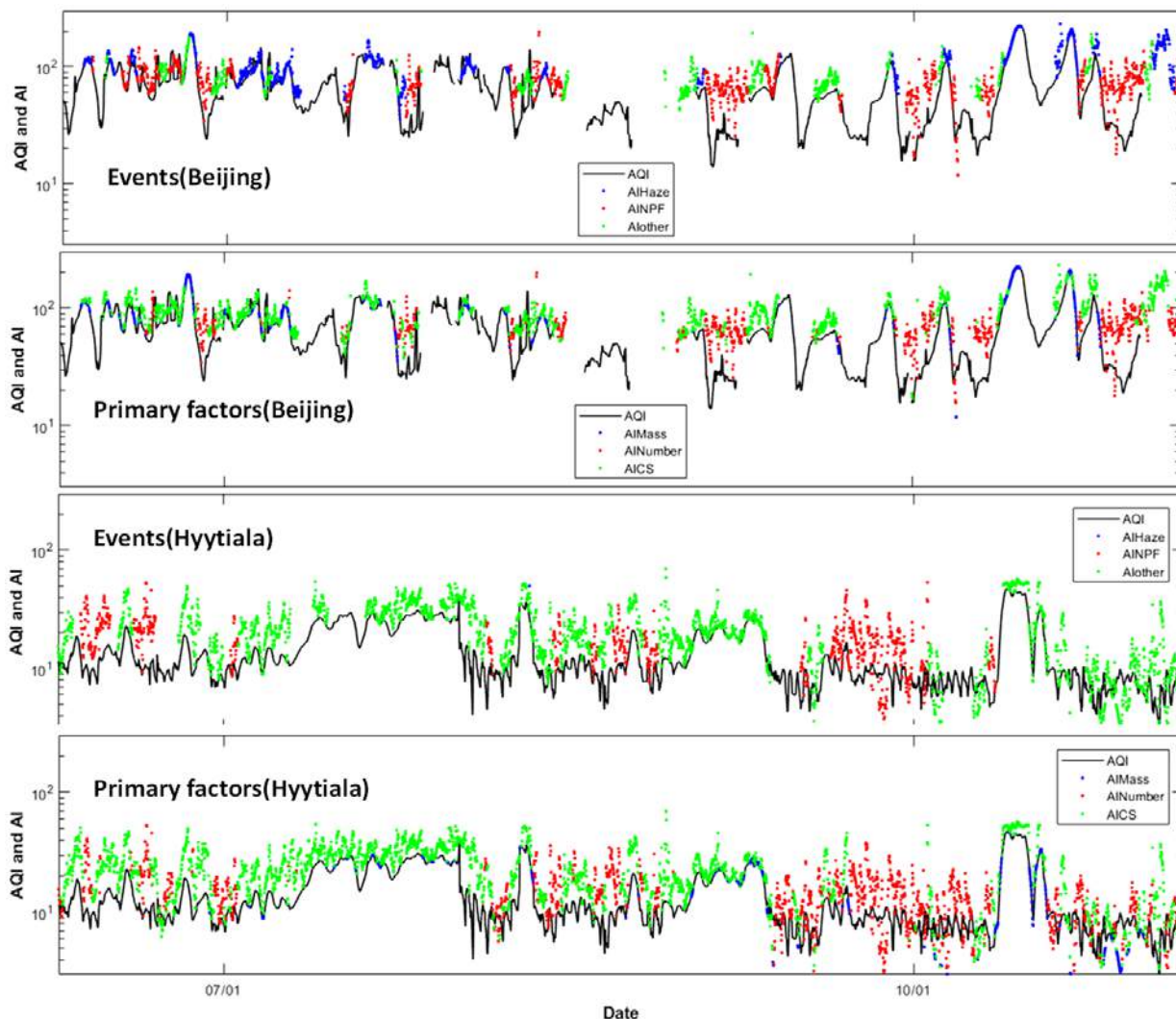


Figure 1. AQI (black line), AI (points) in the urban station of Beijing, China and forest station of Hyytiala, Finland. The AI points are classified by different types of days, i.e. NPF, haze and the other days, in ‘Events’ picture, while classified by the primary factors, i.e. particle number concentrations, CS, and $PM_{2.5}$ mass concentrations, in ‘Primary factors’ picture.

ACKNOWLEDGMENTS

This work was supported by Beijing Advanced Innovation Center for Soft Matter Science and Engineering, Beijing University of Chemical Technology, Academy of Finland (1251427, 1139656, 296628, 306853, Finnish centre of excellence 1141135), and the EC Seventh Framework Program and European Union’s Horizon 2020 program (ERC, project no.742206 “ATM-GTP”).

REFERENCES

Cai, R. L., Chen, D. R., Hao, J. M., & Jiang, J. K. (2017). A miniature cylindrical differential mobility analyzer for sub-3 nm particle sizing. *Journal of Aerosol Science*, *106*, 111-119. doi: 10.1016/j.jaerosci.2017.01.004

- Chu, B. W., Kerminen, V. M., Bianchi, F., Yan, C., Petaja, T., & Kulmala, M. (2019). Atmospheric new particle formation in China. *Atmospheric Chemistry and Physics*, *19*(1), 115-138. doi: 10.5194/acp-19-115-2019
- Dada, L., Paasonen, P., Nieminen, T., Mazon, S. B., Kontkanen, J., Perakyla, O., . . . Kulmala, M. (2017). Long-term analysis of clear-sky new particle formation events and nonevents in Hyytiala. *Atmospheric Chemistry and Physics*, *17*(10), 6227-6241. doi: 10.5194/acp-17-6227-2017
- Dal Maso, M., Kulmala, M., Riipinen, I., Wagner, R., Hussein, T., Aalto, P. P., & Lehtinen, K. E. J. (2005). Formation and growth of fresh atmospheric aerosols: eight years of aerosol size distribution data from SMEAR II, Hyytiala, Finland. *Boreal Environment Research*, *10*(5), 323-336.
- Jiang, J., Chen, M., Kuang, C., Attoui, M., & McMurry, P. H. (2011). Electrical Mobility Spectrometer Using a Diethylene Glycol Condensation Particle Counter for Measurement of Aerosol Size Distributions Down to 1 nm. *Aerosol Science and Technology*, *45*(4), 510-521. doi: 10.1080/02786826.2010.547538
- Kulmala, M., Petaja, T., Nieminen, T., Sipila, M., Manninen, H. E., Lehtipalo, K., . . . Kerminen, V. M. (2012). Measurement of the nucleation of atmospheric aerosol particles. *Nature Protocols*, *7*(9), 1651-1667. doi: 10.1038/nprot.2012.091
- Liu, J. Q., Jiang, J. K., Zhang, Q., Deng, J. G., & Hao, J. M. (2016). A spectrometer for measuring particle size distributions in the range of 3 nm to 10 μ m. *Frontiers of Environmental Science & Engineering*, *10*(1), 63-72. doi: 10.1007/s11783-014-0754-x
- Liu, X. G., Li, J., Qu, Y., Han, T., Hou, L., Gu, J., . . . Hu, M. (2013). Formation and evolution mechanism of regional haze: a case study in the megacity Beijing, China. [Article]. *Atmospheric Chemistry and Physics*, *13*(9), 4501-4514. doi: 10.5194/acp-13-4501-2013
- Lu, Y., Yan, C., Fu, Y., Chen, Y., Liu, Y., Yang, G., . . . Wang, L. (2019). A proxy for atmospheric daytime gaseous sulfuric acid concentration in urban Beijing. *Atmos. Chem. Phys.*, *19*(3), 1971-1983. doi: 10.5194/acp-19-1971-2019
- Mäkelä, J. M., Aalto, P., Jokinen, V., Pohja, T., Nissinen, A., Palmroth, S., . . . Kulmala, M. (1997). Observations of ultrafine aerosol particle formation and growth in boreal forest. *Geophysical Research Letters*, *24*(10), 1219-1222.
- Mirme, S., & Mirme, A. (2013). The mathematical principles and design of the NAIS - a spectrometer for the measurement of cluster ion and nanometer aerosol size distributions. *Atmospheric Measurement Techniques*, *6*(4), 1061-1071. doi: 10.5194/amt-6-1061-2013
- Peng, J. F., Hu, M., Wang, Z. B., Huang, X. F., Kumar, P., Wu, Z. J., . . . He, L. Y. (2014). Submicron aerosols at thirteen diversified sites in China: size distribution, new particle formation and corresponding contribution to cloud condensation nuclei production. *Atmospheric Chemistry and Physics*, *14*(18), 10249-10265. doi: 10.5194/acp-14-10249-2014
- Vanhänen, J., Mikkilä, J., Lehtipalo, K., Sipila, M., Manninen, H. E., Siivola, E., . . . Kulmala, M. (2011). Particle Size Magnifier for Nano-CN Detection. *Aerosol Science and Technology*, *45*(4), 533-542. doi: 10.1080/02786826.2010.547889
- Wang, L., Wen, L., Xu, C., Chen, J., Wang, X., Yang, L., . . . Zhang, Q. (2015). HONO and its potential source particulate nitrite at an urban site in North China during the cold season. *Science of The Total Environment*, *538*, 93-101. doi: 10.1016/j.scitotenv.2015.08.032
- Wang, Z., Wang, T., Guo, J., Gao, R., Xue, L. K., Zhang, J. M., . . . Wang, W. X. (2012). Formation of secondary organic carbon and cloud impact on carbonaceous aerosols at Mount Tai, North China. *Atmospheric Environment*, *46*, 516-527. doi: 10.1016/j.atmosenv.2011.08.019
- Yang, F., Tan, J., Zhao, Q., Du, Z., He, K., Ma, Y., . . . Zhao, Q. (2011). Characteristics of PM_{2.5} speciation in representative megacities and across China. *Atmospheric Chemistry and Physics*, *11*(11), 5207-5219. doi: 10.5194/acp-11-5207-2011
- Yao, L., Garmash, O., Bianchi, F., Zheng, J., Yan, C., Kontkanen, J., . . . Wang, L. (2018). Atmospheric new particle formation from sulfuric acid and amines in a Chinese megacity. *Science*, *361*(6399), 278-281. doi: 10.1126/science.aao4839

- Ye, X. N., Ma, Z., Zhang, J. C., Du, H. H., Chen, J. M., Chen, H., . . . Geng, F. H. (2011). Important role of ammonia on haze formation in Shanghai. *Environmental Research Letters*, 6(2), 024019. doi: 10.1088/1748-9326/6/2/024019
- Zhao, P. S., Dong, F., He, D., Zhao, X. J., Zhang, X. L., Zhang, W. Z., . . . Liu, H. Y. (2013). Characteristics of concentrations and chemical compositions for PM_{2.5} in the region of Beijing, Tianjin, and Hebei, China. [Article]. *Atmospheric Chemistry and Physics*, 13(9), 4631-4644. doi: 10.5194/acp-13-4631-2013
- Zhou, Y., Dada, L., Liu, Y., Fu, Y., Kangasluoma, J., Chan, T., . . . Kulmala, M. (2019). Variation of size-segregated particle number concentrations in winter Beijing. *Atmos. Chem. Phys. Discuss.*, 2019, 1-31. doi: 10.5194/acp-2019-60
- Zou, Y., Deng, X. J., Zhu, D., Gong, D. C., Wang, H., Li, F., . . . Wang, B. G. (2015). Characteristics of 1 year of observational data of VOCs, NO_x and O₃ at a suburban site in Guangzhou, China. *Atmospheric Chemistry and Physics*, 15(12), 6625-6636. doi: 10.5194/acp-15-6625-2015

THE ROLE OF NH₃ AND DMA IN NEW PARTICLE FORMATION IN A BOREAL FOREST ENVIRONMENT

Petri Clusius¹, Tinja Olenius², Jonas Elm³, Pontus Roldin⁴, Hanna Vehkamäki¹ and Michael Boy¹

¹Institute for Atmospheric and Earth System Research (physics) / University of Helsinki

²Department of Environmental Science and Analytical Chemistry (ACES), Stockholm University

³Department of Chemistry and iClimate, Aarhus University

⁴Division of Nuclear Physics, Department of Physics, Lund University

Contact: petri.clusius@helsinki.fi.

Keywords: ATMOSPHERIC MODELLING, NEW PARTICLE FORMATION, MALTE-BOX, ACDC.

INTRODUCTION

In boreal forest new particle formation (NPF) has been observed to be dependent on sulfuric acid (Kerminen et al., 2018). Under usual lower boundary layer conditions, sulfuric acid alone is too unstable to produce the formation rates observed. The role of ammonia and amines as a stabilizer for initial molecular clusters has been studied extensively throughout this millennium. From chamber experiments and theory we know that together with sulfuric acid they are able to produce stable clusters of at least 1 nm (Almeida et al., 2013; Olenius et al., 2013). We have used the model ACDC (Atmospheric Cluster Dynamics Code) (McGrath et al., 2012) and quantum chemical data (see Methods) to quantitatively estimate the formation rates at measured ambient conditions in Hyytiälä, Finland, and further simulated the particle growth due to other condensable vapours.

METHODS

ACDC calculates molecular cluster formation by simulating monomer and cluster collisions and evaporation. The evaporation rates are derived from quantum chemical calculations (DLPNO-CCSD(T)/avtz// ω B97X-D/6-31++G(d,p) for dimethylamine (DMA) and RICC2/aug-cc-pV(T+d)Z //B3LYP/CBSB7 for NH₃) of Gibbs free energies of each cluster composition. ACDC is incorporated in MALTE-box (Boy et al., 2006), a zero-dimensional model that uses meteorological, chemical and particle measurement data and simulates the chemistry, most notably reactions that involve radicals and Volatile Organic Compounds (VOCs), and aerosol dynamics. The model also includes the newly developed Peroxy Radical Autoxidation Mechanism PRAM (Roldin et al., 2019) to estimate the concentration of Highly Oxygenated Organic molecules (HOM).

We have used measurements from Hyytiälä, Finland from April 2018 as input for the model. Individual days were simulated by applying respective measurements as input, and additional 24-hour simulations were made where 10-day hourly mean levels were used as the input. We also studied how much additional DMA would be needed to bring the modelled formation rates and particle numbers in agreement with the observations. Since no measurement data of DMA was available, ammonia levels multiplied by a factor was used as time series.

CONCLUSIONS

We have found that the observed ammonia and sulfuric acid levels in Hyytiälä strongly affect the NPF rate in the model. Typically the measured levels of ammonia do not produce strong enough formation of new particles in the model to reproduce the observed particle concentrations. However, the events are captured by the model, even if the formation is considerably lower, and by applying 10-day mean values of meas-

ured quantities, a typical event day size distribution can be simulated by increasing the concentration of ammonia within 1–2 standard deviations of the 10 day mean or sulfuric acid by one standard deviation (figure 1).

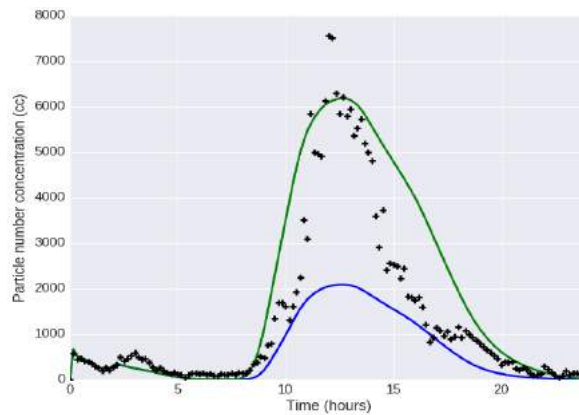


Figure 1: Comparing modelled and measured number concentrations of 3–15 nm size range in Hyytiälä, April 3–13, 2018. The first model run (blue) uses 10 day hourly mean values for input data; in the second run (green) sulfuric acid concentration was one standard deviation above mean. Typical event day particle number concentration from the same 10 day period is shown with black markers.

Also, additional DMA in trace quantities was able to bring the modelled formation rates in agreement with observations. The fraction of DMA to NH_3 was in the order of 0.01–0.1, depending on the ammonia levels (Figure 2). This corresponds to DMA levels of 1–10 ppt, which is in agreement with earlier measurements from Hyytiälä (Hemmilä et al., 2018).

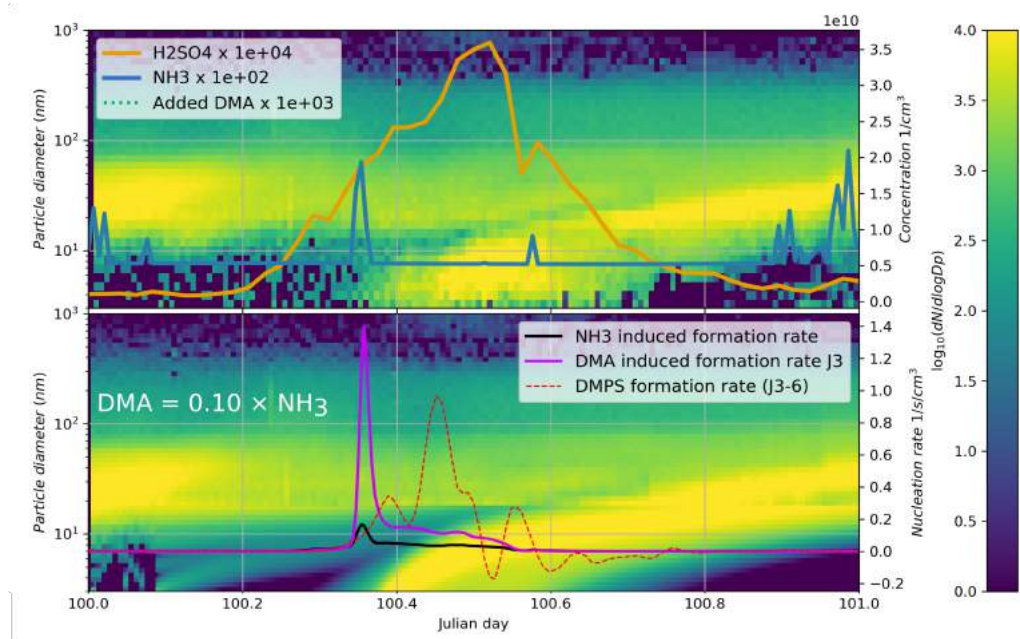


Figure 2: Additional DMA in small quantities is able to get the modelled 1–15 nm particles and formation rates in agreement with the observations. Here 0.2–0.8 ppt of DMA was used in the model, following ammonia trend, on April 10th, 2018. The modelled formation time series depends on the peak in DMA and therefore does not coincide temporally with measured J_3 , but the magnitude is similar.

OUTLOOK

New quantum chemical data for H₂SO₄-NH₃ cluster free energies, obtained with more advanced methods (DLPNO-CCSD(T)/aug-cc-pVTZ/ωB97X-D/6-31++G**) (Myllys et al., 2019) suggests that pure two-component clusters are even less-favourable than what the previous data showed. This means that we should look into the effects of amines and other strong bases in stabilization of sulfuric acid clusters. Also three-component reactions H₂SO₄-NH₃-X could well be plausible mechanism for new particle formation.

REFERENCES

- Almeida, J., Schobesberger, S., Kürten, A., Ortega, I.K., Kupiainen-Määttä, O., Praplan, A.P. et al. Molecular understanding of sulphuric acid-amine particle nucleation in the atmosphere *Nature*. 2013;502(7471):359-363.
- Boy, M., Hellmuth, O., Korhonen, H., Nilsson, E.D., ReVelle, D., Turnipseed, A. et al. MALTE -- model to predict new aerosol formation in the lower troposphere *Atmos. Chem. Phys.*. 2006;6(12):4499-4517.
- Hemmilä, M., Hellén, H., Virkkula, A., Makkonen, U., Praplan, A.P., Kontkanen, J. et al. Amines in boreal forest air at SMEAR II station in Finland *Atmos. Chem. Phys.*. 2018;18(9):6367-6380.
- Kerminen, V.-M., Chen, X., Vakkari, V., Petäjä, T., Kulmala, M., Bianchi, F. Atmospheric new particle formation and growth: review of field observations *Environ. Res. Lett.*. 2018;13(10):103003.
- McGrath, M.J., Olenius, T., Ortega, I.K., Loukonen, V., Paasonen, P., Kurtén, T. et al. Atmospheric Cluster Dynamics Code: a flexible method for solution of the birth-death equations *Atmos. Chem. Phys.*. 2012;12(5):2345-2355.
- Myllys, N., Kubečka, J., Besel, V., Alfaouri, D., Olenius, T., Smith, J.N. et al. Role of base strength, cluster structure and charge in sulfuric-acid-driven particle formation *Atmos. Chem. Phys.*. 2019;19(15):9753-9768.
- Olenius, T., Kupiainen-Määttä, O., Ortega, I.K., Kurtén, T., Vehkamäki, H. Free energy barrier in the growth of sulfuric acid-ammonia and sulfuric acid-dimethylamine clusters *The Journal of Chemical Physics*. 2013;139(8):084312.
- Roldin, P., Ehn, M., Kurtén, T., Olenius, T., Rissanen, M.P., Sarnela, N. et al. The role of highly oxygenated organic molecules in the Boreal aerosol-cloud-climate system *Nat. Commun.*. 2019;10(1):

EXPERIMENTAL RESEARCH AND ANALYSIS OF ATMOSPHERIC AEROSOL AND ITS PRECURSORS IN SIBERIAN BOREAL FOREST

A.DEMAKOVA¹, E.EZHOVA¹, O.GARMASH¹, M. ARSHINOV², B.BELAN², T.PETAJA¹ and M.KULMALA¹

¹Institute for Atmospheric and Earth System Research/Physics (INAR), Helsinki, Finland.

²V.E. Zuev Institute of Atmospheric Optics of Siberian Branch of the Russian Academy of Science (IAO SB RAS), Tomsk, Russia

Keywords: NEW PARTICLE FORMATION, BOREAL FOREST, AEROSOL.

INTRODUCTION

New Particle Formation (NPF) is a process in which a large number of particles is formed in the atmosphere with the help of gas-to-particle conversion of low-volatile vapours and also by clustering. There is a lot of research done on NPF in different environments (Kerminen *et al.*, 2018), including experimental and theoretical aspects. Many studies were focused, for example, on the observed character of NPF in different atmospheric environments, including particle formation rates (FRs) and growth rates (GRs), the chemistry of atmospheric NPF, the thermodynamics and kinetics of NPF. Experiments related to NPF observations were done earlier on Fonovaya station near Tomsk, Russia, but the number of experiments is not enough. We are in process of establishing new observations in Siberia. According to the experimental data from SMEAR II station in Finland (Dada *et al.*, 2017), circumstances for NPF in Siberia should be practically ideal. However, limited amount of experiments show that this statement is not true and NPF are less frequent in Siberia than SMEAR II station (Wiedensohler *et al.*, 2018). The aim of the research is to understand why NPF are rare in Siberia.

METHODS

The site of research is Fonovaya station in Siberia, Tomsk region, Russia. The Diffusion battery Particle Sizer system (DPS) and gas analyzers were measuring aerosols and trace gases since 2015 year, but data from those instruments were not enough for understanding the nature of NPF events in Siberia. That is why the instruments Neutral cluster Air Ion Spectrometer (NAIS) (Manninen H. *et al.*, 2016) and Particle Size Magnifier (PSM) (Vanhanen J. *et al.*, 2011) were shipped and installed on Fonovaya station. The measurements with those instruments started from July 2019, but it takes more time to get enough data for the research. For data processing programming languages such as Matlab and Python are used.

RESULTS

The data since 2015 to June 2018 from DPS and gas analysers was processed. Several things were identified during this processing. First, the number of NPF events has the highest value in March. Second, the concentrations of trace gases, such as sulfur dioxide, nitrogen dioxide and nitrogen oxide have higher values during NPF events. Third, the concentrations of those gases in general are much higher in Siberia than in SMEAR II station in Finland. Next, the NPF events are more frequent when the sky is clear.

CONCLUSIONS

Now the data processing is continuing. The next step is to explore the air mass trajectories and to understand from where the air mass comes to the station, is it from an urban or boreal area. Also, comparison with data from SMEAR Estonia is planned.

For future research, such instruments as Chemical Ionisation Atmospheric Pressure interface Time-Of-Flight (CI-API-TOF) and Differential Mobility Particle Sizer (DMPS) will be shipped to Fonovaya station for measuring the chemical composition of the atmosphere at Fonovaya station.

The big experimental research on Fonovaya station in Siberian boreal forest is taking place. The experiment is currently underway, and getting more data is necessary for understanding why NPF is rare in Siberia.

ACKNOWLEDGEMENTS

This work was supported by ERC ATM-GTP grant, project (ATM-GTP/ERC) that has received funding from the European Research Council (ERC) under the European Union's Horizon 2020 research and innovation programme (grant agreement no. 742206)

REFERENCES

1. Kulmala M. *et al.*, (2013). Direct Observations of Atmospheric Aerosol Nucleation. *Science*, 339(6122), 943-946. <https://doi.org/10.1126/science.1227385>
2. Kerminen V.-M. *et al.*, (2018). Atmospheric new particle formation and growth: Review of field observations. *Environmental Research Letters*. 13. 10.1088/1748-9326/aadf3c.
3. Vanhanen J. *et al.*, (2011) Particle Size Magnifier for Nano-CN Detection, *Aerosol Science and Technology*, 45:4, 533-542, DOI: 10.1080/02786826.2010.547889
4. Junninen H. *et al.*, (2010) A high-resolution mass spectrometer to measure atmospheric ion composition, *Atmos. Meas. Tech.*, 3, 1039-1053, <https://doi.org/10.5194/amt-3-1039-2010>.
5. Manninen H. *et al.*, (2016) How to reliably detect molecular clusters and nucleation mode particles with Neutral cluster and Air Ion Spectrometer (NAIS), *Atmos. Meas. Tech.*, 9, 3577-3605, <https://doi.org/10.5194/amt-9-3577-2016>, 2016.
6. Wiedensohler A. *et al.* (2018). Infrequent New Particle Formation over the Remote Boreal Forest of Siberia. *Atmospheric Environment*. 200. 10.1016/j.atmosenv.2018.12.013.
7. Dada, L. *et al.* (2017), Long-term analysis of clear-sky new particle formation events and nonevents in Hyytiälä, *Atmospheric Chemistry and Physics*, vol. 17, no. 10, pp. 6227-6241. <https://doi.org/10.5194/acp-17-6227-2017>

CONNECTIONS OF NON-STRUCTURAL CARBON COMPOUNDS AND PHOTOSYNTHESIS IN BOREAL WOODY PLANTS

M.R. DOMÍNGUEZ-CARRASCO¹, L. KULMALA^{1,2}, P. SCHIESLT-AALTO¹, P. KOLARI²,
E. JUUORLA², T. HÖLTTÄ¹, J. HEINONSALO^{1,2}, J. BÄCK¹

¹Institute for Atmospheric and Earth System Research / Forest Sciences

Faculty of Agriculture and Forestry, P.O. Box 27, FIN-00014, University of Helsinki, Finland.

²Finnish Meteorological Institute, Helsinki, Finland.

Keywords: carbohydrates, modelling, annual cycle, photosynthetic acclimation

INTRODUCTION

Finnish forest is a boreal forest that mainly tree species of *Pinus sylvestris*, *Picea abies*, *Betula pendula* and *Betula pubescens* and a sub-canopy of dwarf shrubs, mosses and lichens species (Goulden, M. L. et al., 1997) (Moren, A. S. et al., 2000); (Kulmala, L. et al., 2009). Seasonality of temperature and solar radiation are large in boreal zone, with winters characterized to be cold, dry and fairly dark periods while in the contrast, growing seasons are short, rather warm and with long daily light hours. It has been shown that temperature and light are the main external drivers of patterns of photosynthesis (Kolari, P. et al., 2014). Although, Mäkelä et al. (2004) showed that photosynthetic capacity is strongly connected with a delay temperature effect, called by Mäkelä as the state photosynthetic acclimation (S) (Makela, A. et al., 2004). This effect occur under conditions of strong seasonality of temperature, as it is the case of Finnish forests. Changes in the state of photosynthetic acclimation suggest that internal mechanisms influencing photosynthesis, though, these internal mechanisms are poorly understood, overall under natural conditions. In photosynthesis, plants synthesize from atmospheric CO₂ molecules of sugars. Part of these sugars not fixed in the biomass, are called non-structural-carbon (NSC) compounds, playing different roles in plants. (metabolic, osmotic reactions, transport, energy storage, etc. NSC molecules can be transformed from one to another depending on physiological necessities, in a, so called, sugar-starch turnover, that regulates for instance, trees water-uptake, of water loss, or recovering from embolism (Holttä, T. et al., 2018). It has also shown that NSC concentration play a role in inhibiting photosynthesis (Mcdowell, N. G., 2011; Nakano, H. et al., 2000; Franck, N. et al. 2006; Lemoine, R. et al., 2013; Schaberg, P. G., 2000), nevertheless, the mechanism remains rather well known. There is a lack of experimental studies boarding the yearly relationship NSC and photosynthesis under natural conditions without stress in boreal forest ecosystem.

In this project, we aim to investigate the relationship between the concentrations of non-structural carbohydrate and photosynthesis. We hypothesize that the NSC concentration is connected to the rate of photosynthesis in an intra- and inter-specific manner and that NSC content and the rate of photosynthesis are connected also in normal field conditions over a seasonal cycle with natural variation in temperature, soil moisture, radiation, and CO₂ atmosphere concentration.

For the purpose, we 1) measured photosynthesis and NSC concentrations of Scots pine (*Pinus sylvestris*) seedlings and dwarf shrubs bilberry (*Vaccinium myrtillus*), lingonberry (*Vaccinium vitis-idaea*), and heather (*Calluna vulgaris*) in a controlled microcosms laboratory experiment, and 2) derived the annual pattern of photosynthetic potential of Scots pine from continuous field measurements and connected it to NSC concentrations in leaves over three full growing season in southern Finland.

METHODS

Our experimental procedure was divided in two measurement groups, one carried out under laboratory conditions, made on 9 months old plant shoots that we called i) Microcosm experiment; and the other one was done on adult Scots pine trees at Smear II station (Southern Finland), that we called ii) Field experiment.

In Microcosm experiment, we used four replicates of 9 months old plant species: a) *Vaccinium vitis-idaea* L. (Lingonberry), b) *Vaccinium myrtillus* L. (Bilberry), c) *Calluna vulgaris* (L.) Hull (Heather), and d) *Pinus sylvestris* L. (Pine). Seeds grew up in app. 178 cm³ cuvettes with isolated sub-chambers for roots and the aerial part of the plant. They were under laboratory conditions for 9 months, at stable temperature (18-4°C/ for day to night), stable PAR intensity of 170 $\mu\text{mol m}^{-2} \text{s}^{-1}$, and a day length of 18 hours. We carried out measurements of CO₂ exchange in microcosm cuvettes following a method developed by Pumpanen, (Pumpanen, J. S. et al., 2009} } }). A synthetic air gas circulated for 30 min. inside the sub-chambers of the cuvettes, after which it was collected and analyzed the content of CO₂ mass. We calculated the difference between the CO₂ mass in the inlet and outlet gas flow. The rate of photosynthesis (*P*) was calculated as the difference between the rate of respiration of shoot in dark conditions and the total net exchange of CO₂ concentration during light conditions, assuming that respiration was the same during dark and light conditions. See more details of the CO₂ and exchange measurements and calculations (Pumpanen, 2009, 2018). For more details in the experimental method, see (Adamczyk, J. et al., 2016) (Pumpanen, J. S. et al., 2009) and (Kulmala, L. et al., 2018) (Kulmala, L. et al., 2018)

In Field experiment, we took samples of 3 to 4 mature Scots pine at Smear II station in southern Finland every 3-4 weeks in the growing seasons 2008, and 2015; and during the whole year in 2009. For the three studied years, we also used continuous chamber measurements of CO₂ exchange in Scots pine branches (see details of chamber measurements modifications)(Kolari, P. et al., 2014). We fitted optimal stomatal control model and Farquhar model to the measurements and used the gained parameters in further analysis.

Needles and leaves samples was collected from both experiment groups. We lyophilized the samples in a Christ Gamma 2-16 LSC Freeze dryer (Christ Gamma 2-16 LSC; SciQuip Ltd, Merrington, UK), and grinded them (2000-230 Geno/Grinder; Spex SamplePred, USA). We extracted the content of soluble sugars and starch with different methods. The concentration of soluble sugars was done in a chromatograph-mass spectrometer (Agilent 7890B GC/5977A MSD) with a method developed in the Natural Resources Institute Finland, (LUKE). The concentration of starch was analysed in the University of Helsinki, with a spectrophotometer (UV-1650 PC, Shimadzu) at 510 nm of wave length, using K-TSTA Total Starch Assay Kit (Megazyme Internation Ireland, Wicklow, Ireland).

PRELIMINARY RESULTS

In the microcosms experiment, there was a negative and intraspecific relationship between glucose and fructose with the rate of photosynthesis especially with the dwarf shrubs. Nevertheless, the low number of samples per species statistical significance was rarely found. Starch was the only carbohydrate with which the rate of photosynthesis showed a interspecific relationship indicating that the higher was the starch concentration, the lower was photosynthesis. It was seen similarities in the relation between NSC and photosynthesis, differing between evergreen species and deciduous species. But to give general conclusions are needed further analysis.

In the field experiment, it was seen clear and negative connections between the sum of soluble sugars (overall the sum of glucose, fructose and sucrose) and photosynthesis rate of mature pine trees. It was also seen a relation between the rate soluble sugar/starch and photosynthesis rate, in autumn and winter the rate increase while the photosynthesis activity decrease, while in spring the rate soluble sugar/starch decrease when photosynthesis increased.

Finally, we did a linear mix model to compare the effect on photosynthesis capacity of variables as temperature, the state of photosynthetic acclimation and the concentration of soluble sugars. Our results

showed that the main driver is the effect of the state of photosynthetic acclimation, and also soluble sugar content improve the model, suggesting that internal process are involve in the photosynthesis capacity.

ACKNOWLEDGEMENTS

Work was supported by the Helsinki University Funds, and the Academy of Finland (grant no. 277623) and Academy of Finland Center of Excellence programme (grant no. 307331).

REFERENCES

- Adamczyk, J., Deregowska, A., Skoneczny, M., Skoneczna, A., Kwiatkowska, A., Potocki, L., . . . Wnuk, M. (2016). Adaptive response to chronic mild ethanol stress involves ROS, sirtuins and changes in chromosome dosage in wine yeasts. *Oncotarget*, *7*(21), 29958-29976.
- Franck, N., Vaast, P., Genard, M., & Dauzat, J. (2006). Soluble sugars mediate sink feedback down-regulation of leaf photosynthesis in field-grown *Coffea arabica*. *Tree Physiology*, *26*(4), 517-525. doi:DOI 10.1093/treephys/26.4.517
- Goulden, M. L., & Crill, P. M. (1997). Automated measurements of CO₂ exchange at the moss surface of a black spruce forest. *Tree Physiology*, *17*(8-9), 537-542.
- Holtta, T., Dominguez Carrasco, M. D. R., Salmon, Y., Aalto, J., Vanhatalo, A., Back, J., & Lintunen, A. (2018). Water relations in silver birch during springtime: How is sap pressurised? *Plant Biol (Stuttg)*, *20*(5), 834-847. doi:10.1111/plb.12838
- Kolari, P., Chan, T., Porcar-Castell, A., Back, J., Nikinmaa, E., & Juurola, E. (2014). Field and controlled environment measurements show strong seasonal acclimation in photosynthesis and respiration potential in boreal Scots pine. *Front Plant Sci*, *5*, 717. doi:10.3389/fpls.2014.00717
- Kulmala, L., Carrasco, M. D. D., & Heinonsalo, J. (2018). The differences in carbon dynamics between boreal dwarf shrubs and Scots pine seedlings in a microcosm study. *Journal of Plant Ecology*, *11*(5), 709-716. doi:10.1093/jpe/rtx051
- Kulmala, L., Pumpanen, J., Vesala, T., & Hari, P. (2009). Photosynthesis of boreal ground vegetation after a forest clear-cut. *Biogeosciences*, *6*(11), 2495-2507.
- Lemoine, R., La Camera, S., Atanassova, R., Dedaldechamp, F., Allario, T., Pourtau, N., . . . Durand, M. (2013). Source-to-sink transport of sugar and regulation by environmental factors. *Front Plant Sci*, *4*, 272. doi:10.3389/fpls.2013.00272
- Makela, A., Hari, P., Berninger, F., Hanninen, H., & Nikinmaa, E. (2004). Acclimation of photosynthetic capacity in Scots pine to the annual cycle of temperature. *Tree Physiology*, *24*(4), 369-376.
- McDowell, N. G. (2011). Mechanisms Linking Drought, Hydraulics, Carbon Metabolism, and Vegetation Mortality. *Plant Physiology*, *155*(3), 1051-1059. doi:10.1104/pp.110.170704
- Moren, A. S., & Lindroth, A. (2000). CO₂ exchange at the floor of a boreal forest. *Agricultural and Forest Meteorology*, *101*(1), 1-14.
- Nakano, H., Muramatsu, S., Makino, A., & Mae, T. (2000). Relationship between the suppression of photosynthesis and starch accumulation in the pod-removed bean. *Australian Journal of Plant Physiology*, *27*(2), 167-173.
- Pumpanen, J. S., Heinonsalo, J., Rasilo, T., Hurme, K. R., & Ilvesniemi, H. (2009). Carbon balance and allocation of assimilated CO₂ in Scots pine, Norway spruce, and Silver birch seedlings determined with gas exchange measurements and C-14 pulse labelling. *Trees-Structure and Function*, *23*(3), 611-621.
- Schaberg, P. G. (2000). Winter photosynthesis in red spruce (*Picea rubens* Sarg.): Limitations, potential benefits, and risks. *Arctic Antarctic and Alpine Research*, *32*(4), 375-380. doi:Doi 10.2307/1552385

**GROUND BASED AND AIRBORNE
MEASUREMENTS OF AEROSOL AND CLOUD PROPERTIES DURING
PALLAS CLOUD EXPERIMENT 2017**

K.M. DOULGERIS¹, K. NEITOLA¹, A.HIRSIKKO¹, C. KELESHIS², P. VOUTERAKOS², G.
SCHAUFELBERGER³, M.WEISS⁴, J. SCIARE² and D.BRUS¹

¹Finnish Meteorological Institute, Erik Palménin aukio 1, FI-00101, Helsinki, Finland

²The Cyprus Institute, Konstantinou Kavafi Street 20, 2121 Aglantzia, Nicosia, Cyprus

³Airclip Service GmbH & Co KG, Am Eiswurlager 24, DE-01189, Dresden, Germany

⁴Palas GmbH Greschbachstraße 3b, DE-76229, Karlsruhe, Germany

Keywords: aerosol, cloud, UAV, Pallas

INTRODUCTION

Aerosol particles and their interaction with the properties of atmospheric clouds still remains one of the most persistent sources of uncertainty in the estimates of anthropogenic climate forcing. The understanding of the impact of aerosol-cloud-precipitation interactions has been proven very difficult. Cloud properties (e.g. albedo, precipitation rate and lifetime) depend, amongst other factors, on the number concentration of aerosol particles and on their chemical composition (Komppula, 2005; Lihavainen, 2008).

Continuous, semi-long term, ground based, in-situ measurements of low level clouds were conducted during the Pallas Cloud Experiments (PaCE) in autumn of 2017 at Pallas Atmosphere - Ecosystem Supersite in northern Finland. Our main motivation during the campaign was to investigate aerosol-cloud interactions using in-situ measurements techniques (Doulgeris *et al.*, 2018). In addition, from September 18th until 30th the intensive Unmanned Aerial Vehicles (UAV) part of the campaign took place. During this period clouds were still warm and it was safe to fly through them.



Fig.1 Pallas Atmosphere-Ecosystem Supersite located in Finnish sub-Arctic region (67°58' N, 24°07' E)

METHODS

The 7th Pallas Cloud Experiment took place at the Pallas Atmosphere-Ecosystem Supersite – Sammallunturi Global Atmospheric Watch (GAW) station (67°58' N, 24°07' E) in Finnish sub-Arctic region during fall and winter 2017 (Fig. 1). Sammallunturi station is located on a top of an arctic fjell (560 m a.s.l.) and it is during the fall about 50 % of time inside low level clouds which allow us direct measurements of aerosol-cloud interaction.

All meteorological data at the station were measured by Vaisala FD12P weather sensor (Hataka *et al.*, 2003). The Cloud, Aerosol and Precipitation Spectrometer probe (CAPS, DMT, CO, USA) was installed on the roof top of Sammallunturi station to measure the cloud droplets. CAPS, includes three instruments: the Cloud Imaging Probe (CIP, 12.5 μm -1.55 mm), the Cloud and Aerosol Spectrometer (CAS-DPOL, 0.51-50 μm) with depolarization feature, and the Hotwire Liquid Water Content Sensor (Hotwire LWC, 0 - 3 g/m^3). In this abstract, due to similar size range with UAV instruments we used only CAS probe, see Fig. 2.

The airborne measurements took place within the FMI's reserved TEMPO D airspace PALLAS that is centered around the Sammallunturi station with boundaries of 7 km and ceiling limit FL80 (1994 m MSL). Three teams deployed UAVs - the Finnish Meteorological Institute (FMI), the Cyprus Institute (CYI) and Airclip Service GmbH & Palas GmbH - to measure airborne in-situ aerosol and cloud physical properties together with meteorological parameters (table 1).

team	Type of UAV	Aerosol/cloud instruments	Meteorological parameters sensors
FMI	Multicopter hexacopter	2 x TSI CPC 3007 (cut off $D_{50} = 7$ and 14 nm)	RH, T, P
CYI	Fixed wing	OPS (0.5-17 μm , 16 channels)	RH, T, P
AirClip & Palas	Multicopter X-octacopter	Palas Fidas Fly200 (0.17 – 18 μm , 255 channels)	

Table 1. General information regarding the UAV teams that participated in the PaCE campaign.

Obtained aerosol, cloud and meteorological datasets were compared to ground based measurements on top-hill Sammallunturi station, balloon soundings, and concurrent continuous remote-sensing instrumentation.



Figure 2. The CAPS probe as it was installed on the roof of Sammallunturi measurement site during PaCE2017.



Figure 3. From left to right, the CYI team with the fixed wing plane, the Airclip Service GmbH Multirotor X-octocopter and the FMI Multirotor hexacopter.

RESULTS

Several successful flights were performed during the campaign. In this work, we will present an example case when UAVs were measuring below, through and above a low level homogeneous cloud. The same cloud was sampled also at Sammaltunturi station during the day.

Figure 4a presents vertical profiles of the total aerosol counts as they were measured during September 25th by UAVs. Also the total aerosol counts are shown as references as they were measured from the total and the gas inlet at the station. In Figure 4b, the size distribution of the homogeneous cloud as it was measured during the UAVs flights along with the size distribution of the cloud as it was measured at the station. Agreement in both cases was considered good.

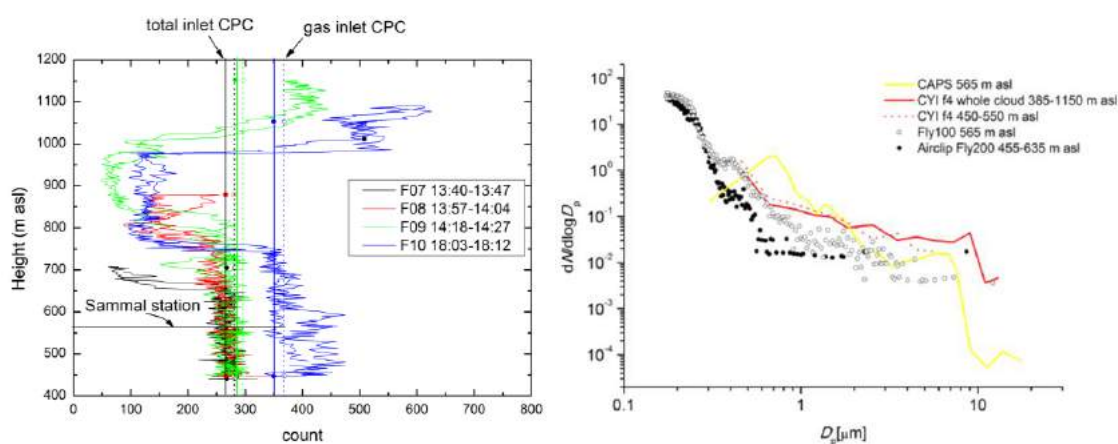


Figure 4. The total aerosol count as it was measured by the UAV along with the total aerosol counts as they were measured at the Sammaltunturi station (gas and total inlet). Also, the size distribution of the in cloud particles as they were measured from UAVs and the in-situ cloud probe (CAPS, Palas Fly100) at the Sammaltunturi station are shown.

Figure 5 presents the meteorological profiles of RH and temperature as they were measured from airborne measurements (UAVs and balloon sounding). The temperature decreases until the UAV came out of the cloud and entered to sunny conditions according to both sensors from FMI and CYI UAVs. Balloon sounding demonstrates similar behaviour, however there was noticed a difference around 5 °C above the cloud between UAVs sensors and sounding. Relative humidity was around 100% when the UAV and the balloon were flying through the cloud and it suddenly drops to RH below 10% above the cloud. All sensors agreed, however we should take into respect the different response time of each sensor and the drift of balloon position by wind.

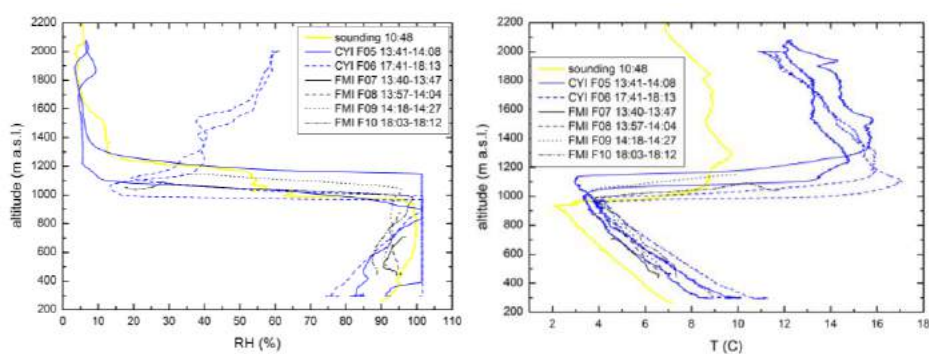


Figure 5. Relative humidity and temperature vertical profile as they were measured by UAV sensors and balloon sounding

ACKNOWLEDGEMENTS

This work was supported by KONE foundation, Nordforsk Contract number 26060, CRAICC Amendment on CRAICC-PEEX Collaboration, Academy of Finland project: Greenhouse gas, aerosol and albedo variations in the changing Arctic (project number 269095), Academy of Finland Center of Excellence program (project number 272041), BACCHUS (EU 7th Framework program), Natural Environment Research Council (NERC), grant number NE-L011514-1 and ACTRIS-2, the European Research Infrastructure for the observation of Aerosol, Clouds, and Trace gases. This project has received funding from the European Union's Horizon 2020 research and innovation programme under grant agreement No 654109.

REFERENCES

- Doulgeris, K.M. and D. Brus (2018). In-situ measurements of low level clouds during Pallas cloud experiments, in Proc. of FCOE 2018, Kuopio, Finland.
- Hatakka, J., T. Aalto, V. Aaltonen, M. Aurela, H. Hakola, M. Komppula, T. Laurila, H. Lihavainen, J. Paatero, K. Salminen and Y. Viisanen (2003). Overview of the atmospheric research activities and results at Pallas GAW station, *Boreal Environ. Res.*, **8**, 365–384
- Komppula, M., Lihavainen, H. and Kerminen, V.-M. (2005). Measurements of cloud droplet activation of aerosol particles at a clean subarctic background site, *J. Geophys. Res.*, **110**, D06204.
- Lihavainen, H., Kerminen, V.-M., Komppula, M., Hyvarinen A.-P., Laakia J., Saarikoski S., Makkonen, U. Kivekas, N., Hillamo, R., Kulmala, M. and Viisanen, Y. (2008). Measurements of the relation between aerosol properties and microphysics and chemistry of low level liquid water clouds in Northern Finland *Atmos. Chem. Phys.*, **8**, 6925-6938, <https://doi.org/10.5194/acp-8-6925-2008>

UNDERSTANDING NEW PARTICLE FORMATION EVENTS UNDER HIGH CONDENSATION SINK CONDITIONS

WEI DU^{1,2}, LUBNA DADA², KASPAR DÄLLENBACH², JING CAI², MARKKU KULMALA² et al.

¹ Aerosol and Haze Laboratory, Beijing Advanced Innovation Center for Soft Matter Science and Engineering, Beijing University of Chemical Technology, Beijing, China

² Institute for Atmospheric and Earth System Research / Physics, Faculty of Science, University of Helsinki, Finland

Keywords: NEW PARTICLE FORMATION, EFFECTIVE CONDENSATION SINK, SURVIVAL PROBABILITY, CHEMICAL COMPOSITION.

INTRODUCTION

Atmospheric aerosols play an important role in affecting global radiation balance, climate and human health. As the critical source of particles on a global scale, New particle formation (NPF) attract a wide range of attention (Chu et al., 2019; Zhang et al., 2012; Kulmala et al., 2004). In the traditional view, high particle concentration inhibited the formation and growth of nucleation particles because of the high condensation sink (CS). However, the observation of NPF events in the highly polluted areas bring challenges to traditional theory. A possible way to explain this is that the scavenging of molecules by pre-existing particles is less effective than it is in theory, which means that the calculated CS could be overestimated. For a known vapor, CS is calculated based on the size and concentration of pre-existing particles. The particle shape, phase and chemical composition were assumed to be constant. However, large amounts of studies have shown that the chemical composition of atmospheric aerosols varied with particle size and PM concentration levels. The hygroscopicity, mixing state, and even the shape of particles is strongly depended on chemical composition. Thus, particle chemical composition might have influence on CS. In this study, the measurements of particle number size distribution and chemical composition were conducted in urban Beijing from March 1st, 2018 to March 1st, 2019. We investigated the variation of chemical composition with calculated CS, then discussed the differences of particle chemical composition between NPF days and non-NPF days, and further gave possible explanations that CS is less effective than predicted.

METHODS

The sampling site is located in the west campus of Beijing University of Chemical and Technology (BUCT, 39° 56'31" N, 116°17'50" E), near the West Third Ring Road of Beijing. A Scanning Mobility Particle Sizer (SMPS, TSI) and a Differential Mobility Particle Spectrometer (DMPS, TSI) were conducted to measure the particle number size distribution in the size range from 14 to 737 nm and 6 to 840 nm, respectively. Non-refractory chemical compositions of fine particles, including organic, sulfate, nitrate, ammonium, and chloride, were measured by an online Aerosol Chemical Speciation Monitor (ACSM, Aerodyne Research Inc.) equipped with PM_{2.5} leas. Two different diameters were used in parallel throughout this study including mobility diameter (D_m) for SMPS and DMPS measurements and vacuum aerodynamic diameter (D_{va}) for ACSM measurements. Assuming spherical particles, D_{va} approximately equals particle density (ρ_{comp}) times D_m (DeCarlo et al., 2004). We classified NPF events following the method introduced by Dal Maso, et al. (2005). The detailed information of calculating formation rates (J), growth rates (GR) were reported in Yan et al. (2019, in preparation).

CONCLUSIONS

With slopes higher than 0.9, the calculated mass concentration based on SMPS and DMPS correlated well with the mass measured by ACSM. Although the size range of SMPS is slightly different with that of DMPS, the calculated CS based on these two instruments were almost the same during the comparison period from May 30th to July 1st, 2018. During our observation periods, non-refractory fine particles (NR-PM_{2.5}) varied dramatically from 1.0 to 364.4 $\mu\text{g m}^{-3}$ with the average concentration of 42.4 $\mu\text{g m}^{-3}$. CS correlated well with NR-PM_{2.5}, varying from 1.1×10^{-3} to 1.4×10^{-1} s⁻¹ with average value of 2.9×10^{-2} s⁻¹. Almost

concentration of all chemical species increased significantly with the increasing of CS. When the CS was lower than $1.0 \times 10^{-2} \text{ s}^{-1}$, chemical composition kept relatively stable, dominated by Org (~50%). When the CS was higher than $1.0 \times 10^{-2} \text{ s}^{-1}$, the fraction of secondary inorganic aerosols (SIA) increased obviously from 45% to 68%. Accounting for 33% of total mass, NO₃ was the most important species driven the increasing of SIA.

When the CS is lower than $8.0 \times 10^{-3} \text{ s}^{-1}$, NPF was observed almost every day. As the increasing of the CS, NPF frequency decreased obviously. Thus, half of the NPF events were observed when the CS is lower than $1.0 \times 10^{-2} \text{ s}^{-1}$. According to theoretical predictions, NPF was not detectable under high CS conditions. However, there were 30% of NPF events were detected when the CS is higher than $2.0 \times 10^{-2} \text{ s}^{-1}$ although the frequency was lower than 40%. We then investigated the chemical composition of the pre-existing particles between 10:00 to 14:00. In general, higher mass fraction of Org were obtained during NPF days.

ACKNOWLEDGEMENTS

The work is supported by Academy of Finland via Center of Excellence in Atmospheric Sciences (project no. 272041) and European Research Council via ATM-GTP 266 (742206). This research has also received funding from Academy of Finland (project no. 316114 & 315203) as well as the Doctoral Programme in Atmospheric Sciences at the University of Helsinki. Partial support from the National Key R&D Program of China (2017YFC0209503 & 2017YFC0209505), the National Science Foundation of China (21876094) and the National Natural Science Foundation of China (91644213 & 41730106) is acknowledged. Moreover, this research received support from the Swiss National Science postdoc mobility grant (P2EZP2_181599).

REFERENCES

- Chu, B., Kerminen, V.-M., Bianchi, F., Yan, C., Petäjä, T., and Kulmala, M.: Atmospheric new particle formation in China, *Atmos. Chem. Phys.*, 19, 115-138, 10.5194/acp-19-115-2019, 2019.
- Dal Maso, M., Kulmala, M., Riipinen, I., Wagner, R., Hussein, T., Aalto, P. P., and Lehtinen, K. E. J.: Formation and growth of fresh atmospheric aerosols: eight years of aerosol size distribution data from SMEAR II, Hyytiälä, Finland, *Boreal Environ. Res.*, 10, 323-336, 2005.
- DeCarlo, P. F., Slowik, J. G., Worsnop, D. R., Davidovits, P., and Jimenez, J. L.: Particle Morphology and Density Characterization by Combined Mobility and Aerodynamic Diameter Measurements. Part 1: Theory, *Aerosol Sci. Tech.*, 38, 1185-1205, 10.1080/027868290903907, 2004.
- Kulmala, M., Vehkamäki, H., Petäjä, T., Dal Maso, M., Lauri, A., Kerminen, V. M., Birmili, W., and McMurry, P. H.: Formation and growth rates of ultrafine atmospheric particles: a review of observations, *J. Aerosol Sci.*, 35, 143-176, 10.1016/j.jaerosci.2003.10.003, 2004.
- Zhang, R., Khalizov, A., Wang, L., Hu, M., and Xu, W.: Nucleation and growth of nanoparticles in the atmosphere, *Chemical reviews*, 112, 1957-2011, 10.1021/cr2001756, 2012.

CHANGES IN AEROSOL LOADING RELATED TO AIRMASSES PASSING OVER DECREASING SEA ICE ARE EVIDENT IN NORTHERN SCANDINAVIA

E.-M. DUPLISSY¹, T. NYGÅRD², S. HAKALA¹, R. VÄÄNÄNEN¹, V. SINCLAIR¹, V.-M. KERMINEN¹, T. PETÄJÄ¹ and M. KULMALA¹

¹Institute for Atmospheric and Earth System Research (INAR), University of Helsinki, Helsinki, Finland

²Finnish Meteorological Institute, Helsinki, Finland

Keywords: AEROSOL LOADING, ARCTIC SEA ICE, ATMOSPHERIC CIRCULATION, ACCUMULATION MODE.

INTRODUCTION

Decreasing sea ice will change the sources and sinks of aerosols in the Arctic when more open sea surface is exposed. At the same time, the changes in sea ice can have an effect on large-scale atmospheric circulation and vice versa. Here we show, i) how the aerosol concentrations and size distributions change in the continental Arctic with respect to the time that air masses spend over sea ice or open ocean before entering our site in Eastern Lapland, Finland, and ii) how the atmospheric large-scale circulation and variability changes the situation. We also speculate about the changes in aerosol-cloud interactions in the future based on the results.

METHODS

We calculated linear regressions to median aerosol concentrations and mode peak diameters at SMEAR I station in Värriö, Eastern Lapland, as a function of time over sea ice (TOSI), time over open sea (TOOS) and time over land (TOL). The data was divided into summer (Jun-Sep) and winter (Oct-May). The choice of these months is justified by two facts: October-May is approximately the period when Värriö has snow cover and the sea ice has minimum area in September. In the analysis we used aerosol size distribution data from DMPS (Differential Mobility Particle Sizer), SO₂ concentration data, HYSPLIT 96 hour back-trajectories, sea ice concentration data from NSIDC (National Snow and Ice Data Center) and daily AO indices. TOL and SO₂ were used in order to reduce the effect of land and sulphur emissions from Kola (Kyrö, 2014). In our trajectory calculations, we took into account only those trajectories that had spent >90% of their travel time North of Värriö. We also used Self Organizing Map (SOM) method to create 12 representing mean sea level pressure (MSLP) and total cloud water maps (nodes 1-16) over the Scandinavia and sea areas north of it. We used this method to differentiate the effect of atmospheric dynamics on the aerosol loading in northerly air masses.

CONCLUSIONS

During summer, the total aerosol number, Aitken mode and accumulation mode concentrations were decreasing with increasing time the air mass spent over the sea ice by -8.9, -5.3 and -1.6 cm⁻³h⁻¹, respectively. The Aitken mode diameter was decreasing -0.3 nm/h and the accumulation mode diameter -0.5 nm/h. Accumulation mode concentration and diameter increased by +0.8 cm⁻³h⁻¹ and +0.3 nm/h, respectively, as a function of TOOS. During winter there was a decrease in total, nucleation mode and Aitken mode concentrations (-1.3, -0.3, -0.6 cm³/h, respectively) as a function of TOSI. Accumulation mode concentration and diameter were decreasing by -0.4 cm⁻³h⁻¹ and -0.2 nm/h as a function of TOOS. In winter, the accumulation mode was increasing with increasing sea ice area by 1.2⁻⁴ cm⁻³km⁻² in the Kara and Barent's Seas. In summertime, the accumulation mode concentration did not have as clear dependency with the sea ice area as during winter.

From the above values one can see, that the accumulation mode decreased with increasing TOSI in summer and decreased with increasing TOOS in winter, *i.e.* the decrease of Arctic sea ice had an opposite effect to the concentrations of potential CCN (=accumulation mode) during summer and winter. The increased amount of potential CCN due to less sea ice will probably pose a cooling effect on climate through aerosol-cloud interactions in summer. In winter, however, the clouds have much more complex effects on the radiative balance in the Arctic due to surface snow cover, polar night and longwave radiative cooling (Quinn, 2008). Thus, the increase in potential CCN might still lead to cooling effect on climate through aerosol-cloud interactions. However, the SOM maps show that under certain atmospheric conditions the concentrations of potential CCN can be different from this main observation.

More detailed comparison of SOM nodes and aerosol concentrations revealed interesting features. In winter, those nodes which had more negative AO values compared to other nodes with similar atmospheric circulation pattern, had accumulation modes dominating over other modes and generally higher aerosol concentrations compared with nodes with more positive AO index. Aitken mode dependency on TOOS in winter varied from node to node but was generally negative in those nodes where accumulation mode dominated and positive where Aitken mode dominated or both accumulation and Aitken mode had similar concentrations. While in most nodes the accumulation mode was decreasing with increasing TOOS similarly as for the entire winter data, there was especially one node (8) which stood up with opposite trend. In this node, the MSLP over entire region was very homogenous, cloud water anomaly was slightly negative (air mass drier than average), and lower than average wind speeds. This was also the only node with positive temperature dependency in accumulation mode during winter, which probably also partly explains the increase in accumulation mode with increasing TOOS.

Clearly, Arctic sea ice has a strong impact on aerosol concentrations in Eastern Lapland and the decreasing sea ice most likely will change the aerosol population in the continental Arctic. Thus, the changes in the sea ice extent and the time that the air parcel spends over sea ice can have an influence on the aerosol-cloud interactions in the continental Arctic. The overall strength and sign of the radiative forcing cannot be assessed based on our results, but our data suggests that decreasing sea ice seems to have a cooling effect through the changes in the aerosol-cloud interactions.

REFERENCES

- Kyrö, E.-M. et al. (2014). Trends in new particle formation in eastern Lapland, Finland: effect of decreasing sulfur emissions from Kola Peninsula. *Atmos. Chem. Phys.*, **14**, 4383-4396.
- Quinn, P.K. et al. (2008). Short-lived pollutants in the Arctic: their climate impact and possible mitigation strategies. *Atmos. Chem. Phys.*, **8**, 1723-1735.

Sources and processes contributing to PM_{2.5} in Beijing

Kaspar R. Daellenbach^{1,2}, Jing Cai^{1,2}, Feixue Zheng¹, Chao Yan^{1,2}, Yonghong Wang^{1,2}, Biwu Chu^{1,2,3}, Liine Heikkinen², Tommy Chan^{1,2}, Simo Hakala², Juha Kangasluoma^{1,2}, Haiyan Li², Ying Zhou¹, Joni Kujansuu^{1,2}, Tuukka Petäjä^{1,2,4}, Veli-Matti Kerminen², Federico Bianchi^{1,2}, Douglas R. Worsnop⁵, Yongchun Liu¹, Markku Kulmala^{1,2}

¹ Aerosol and Haze Laboratory, Beijing Advanced Innovation Center for Soft Matter Science and Engineering, Beijing University of Chemical Technology, Beijing, China

² Institute for Atmospheric and Earth System Research / Physics, Faculty of Science, University of Helsinki, Finland

³ Research Center for Eco-Environmental Sciences, Chinese Academy of Science, Beijing, China

⁴ Joint International Research Laboratory of Atmospheric and Earth System Sciences, Nanjing University, Nanjing, China

⁵ Aerodyne Research Inc., Billerica, Massachusetts 01821, USA.

Keywords: Aerosol Mass Spectrometry, Source apportionment, Secondary Organic Aerosol, Haze.

INTRODUCTION

Particulate matter (with a diameter smaller than 2.5 μm , PM_{2.5}) is a major risk factor to human health and causes globally nearly 8% of all deaths (Lelieveld et al., 2015; 2017, Burnett et al., 2018). It has been established that secondary aerosol, formed from gas phase precursors through oxidation in the atmosphere, contribute a large fraction to PM in many environments (Zhang et al., 2011). Recent publications revealed that secondary inorganic (SIA) and organic aerosol (SOA) are a major contributor during haze episodes in heavily polluted environments in China (Huang et al., 2014; Elser et al., 2016; Sun et al., 2018). However, knowledge on SOA, such as its sources and formation, in polluted environments is limited. For deepening our understanding of SOA's role in forming haze, we started studying the chemical composition of PM_{2.5} at a newly established observational site in Beijing.

METHODS

For this study, data was collected at the newly established measurement site at Beijing University of Chemical Technology (BUCT), Beijing, China. Since February 2018 a Time-of-Flight Aerosol Chemical Speciation monitor (ToF-ACSM, Fröhlich et al., 2013) is monitoring the non-refractory PM_{2.5} (NR-PM_{2.5}) concentration and its composition (organic aerosol: OA, nitrate: NO₃, ammonium: NH₄, sulphate: SO₄, chloride: Cl). The chemical analyses of PM_{2.5} are complemented by an Aethalometer measuring black carbon concentrations (BC, AE33, Drinovec et al., 2015) and an online x-ray fluorescent instrument (Skyray) measuring trace element concentrations. Additionally, trace gases and meteorological parameters complete the atmospheric observations. The mass spectral information of OA is used for source apportionment using a statistical unmixing model, termed positive matrix factorization (PMF, Paatero and Tapper, 1994, solved by multilinear engine 2, Paatero, 1999).

RESULTS AND CONCLUSIONS

While we observe highest daily average concentrations of NR-PM_{2.5} reaching more than 250 $\mu\text{g}/\text{m}^3$, also rather clean days occur (Fig. 1, 2). Our measurements show that OA contributes most to NR-PM_{2.5} at rather low PM_{2.5} concentrations, while secondary inorganic aerosol (SIA) constituents such as ammonium (NH₄, nitrate (NO₃), and sulphate (SO₄) dominate at high NR-PM_{2.5} concentrations (Fig. 1). Chloride (Cl) contributes only a small fraction to NR-PM_{2.5}, yet its concentration shows the strongest seasonality with elevated concentrations during winter. This behavior is consistent with its interpretation as a marker for coal combustion, commonly used for residential heating (Elser et al., 2014).

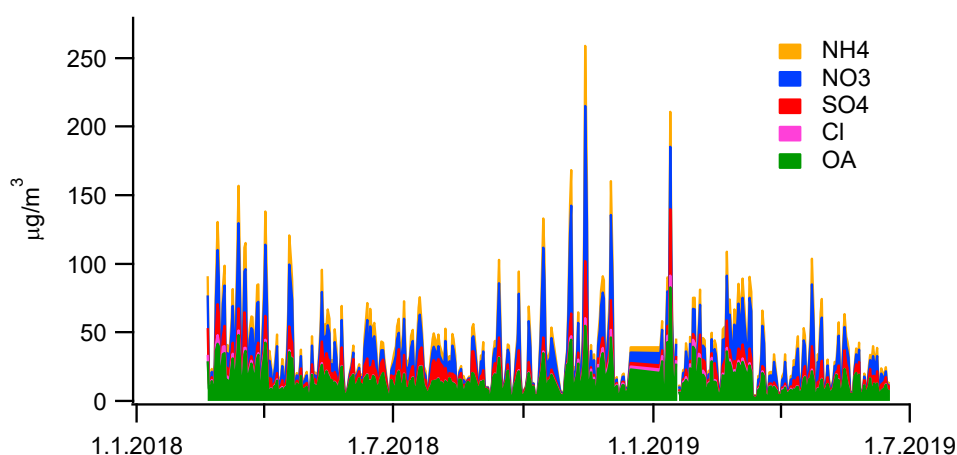


Figure 1: Chemical composition of NR-PM_{2.5} (daily average, NH₄, NO₃, SO₄, OA, and Cl).

We quantify the contribution of several sources to primary OA (POA, traffic, cooking, and residential heating represented by coal combustion, biomass burning, Fig. 2) by performing PMF using a priori information on their chemical composition (from Elser et al., 2014). As opposed to traffic and residential heating POA, cooking POA correlates neither with gas-phase combustion markers (NO_x or CO) nor with black carbon (BC) (Fig. 3). CCOA correlates well with both chloride as well as a component retrieved from trace element PMF analysis, which is related to solid fuel combustion. Additionally, we separate and quantify the contribution of SOA (Fig. 2). In agreement with previous research (Huang et al., 2014; Elser et al., 2014; Sun et al., 2018), we find that SOA is a main contributor to OA in Beijing, especially during haze.

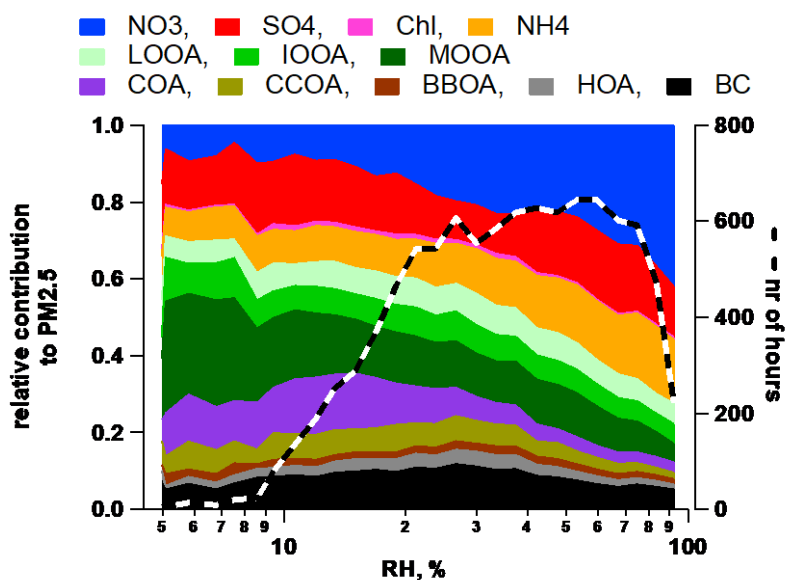


Figure 2: Relative contribution of aerosol sources/components to NR-PM_{2.5}+BC.

We further examine the nature of SOA by further separating it into tentatively three groups of yet unknown origin (less oxygenated OOA, LOOA, intermediate oxygenated OOA, IOOA, and more oxygenated OOA, MOOA). IOOA and LOOA correlate with residential heating emissions, while MOOA correlates well with sulphate. This indicates that different sources as well as processes are the determining drivers of these SOA components. We observe that at increasing relative humidity (RH) the SOA/POA ratio increases. Additionally, the sulfur oxidation ratio is enhanced at increasing RH. Overall, this is in agreement with a prominent role of heterogeneous formation pathways contributing to secondary organic

and inorganic aerosol. Increasing NR-PM_{2.5} concentrations coincide with increasing relative contributions of SOA and SIA (NH₄, NO₃, SO₄) corroborating the important role of secondary aerosol for haze.

This study overall, shows the important role of secondary PM, including SOA. Furthermore, several SOA components with distinct temporal behavior could be identified which indicates the importance of various SOA sources and formation processes throughout the year. Further research should focus on identifying the main SOA sources and quantifying their contribution to SOA.

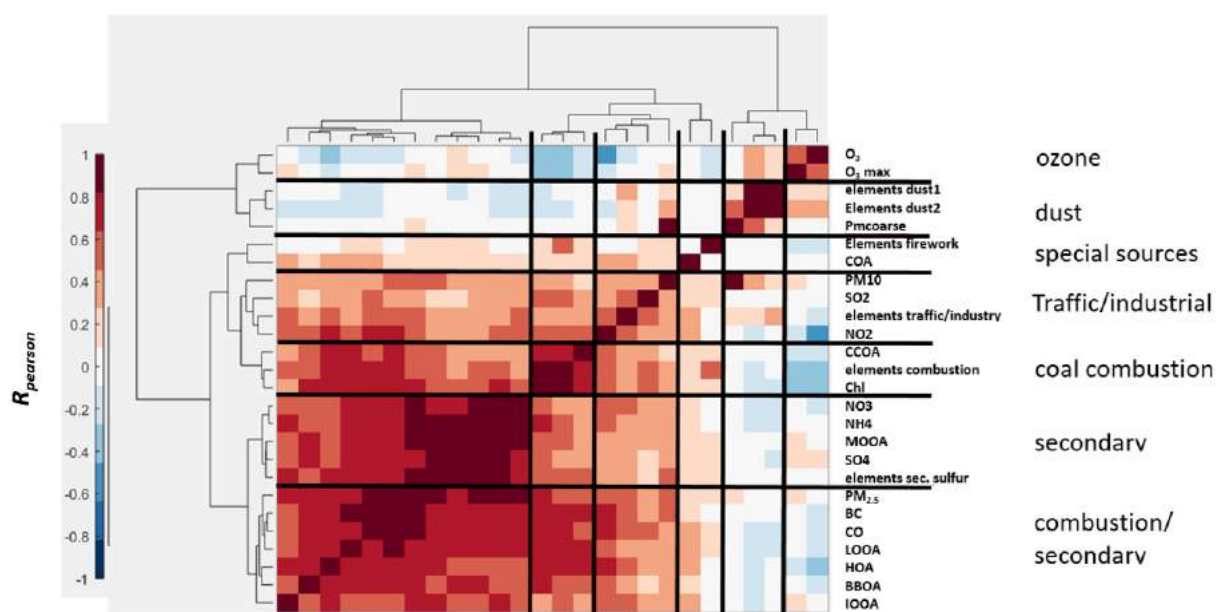


Figure 3: Clustegramm of the time series of resolved OA and trace element sources as well as other aerosol constituents (NH₄, NO₃, SO₄, Cl, OA, BC) and gas-phase air pollutants (CO, NO_x, O₃, SO₂).

ACKNOWLEDGEMENTS

This work is supported by the Swiss National Science Foundation grant P2EZP2_181599, Academy of Finland via Center of Excellence in Atmospheric Sciences (project no. 272041) and the European Research Council via ATM-GTP 266 (742206).

REFERENCES

- Burnet et al. (2018). Global estimates of mortality associated with longterm exposure to outdoor fine particulate matter, *Proc. Nat. Acad. Sci.*, 115, 9592-9597.
- Elser, M., et al. (2016). New insights into PM_{2.5} chemical composition and sources in two major cities in China during extreme haze events using aerosol mass spectrometry, *Atmos. Chem. Phys.*, 16, 3207-3225.
- Fröhlich et al. (2013). The ToF-ACSM: a portable aerosol chemical speciation monitor with TOFMS detection, *Atmos. Meas. Tech.*, 6, 3225-3241.
- Huang, R.-J., et al. (2014). High secondary aerosol contribution to particulate air pollution during haze events in China, *Nature*, 514, 218-222.

- Sun et al., (2018). Source apportionment of organic aerosol from 2-year highly time-resolved measurements by an aerosol chemical speciation monitor in Beijing, China, *Atmos. Chem. Phys.*, 18, 8469-8489.
- Drinovec et al. (2015). The “dual-spot” Aethalometer: an improved measurement of aerosol black carbon with real-time loading compensation, *Atmos Meas. Tech.*, 8, 1965-1979.
- Lelieveld et al. (2015). The contribution of outdoor air pollution sources to premature mortality on a global scale, *Nature*, 525.
- Lelieveld et al. (2017). Chemists can help to solve the air-pollution health crisis, *Nature*, 551.
- Zhang et al. (2011) Ubiquity and dominance of oxygenated species in organic aerosols in anthropogenically-influenced Northern Hemisphere midlatitudes, *Geophys. Res. Lett.*, 34, L13801.

ALGORITHMIC TUNING OF SPREAD-SKILL RELATIONSHIPS IN ENSEMBLE FORECASTING SYSTEMS

M. EKBLÖM¹, L. TUPPI¹, V. SHEMYAKIN², M. LAINE³, P. OLLINAHO³, H. HAARIO², H. JÄRVINEN¹

¹ Institute for Atmospheric and Earth System Research/Physics, University of Helsinki, Helsinki, Finland.

² School of Engineering Science, Lappeenranta University of Technology, Lappeenranta, Finland

³ Finnish Meteorological Institute, Helsinki, Finland

Keywords: ensemble forecasting, stochastic optimization, Lorenz'95.

INTRODUCTION

In weather forecasting ensemble weather prediction systems are used to approximate uncertainties of the forecasts. These uncertainties arise from incomplete knowledge in model formulation, initial conditions, and in boundary conditions, which all lead to forecast errors accumulating over forecast lead time (Leutbecher and Palmer, 2008).

Numerical weather prediction models contain parametrization schemes (and corresponding model parameters) of sub-grid scale processes. Ensemble prediction systems also contain stochastic physics parameters, which account for uncertainties in the model formulation. Both model physics parameters and stochastic physics parameters are important. Here, the focus will be on the uncertainties related to stochastic physics parameters and the initial conditions. We will denote the parameters regulating the amplitude of stochastic physics and the uncertainties of the initial conditions as 'spread parameters'.

In this study, we will study the problem of optimizing these spread parameters in an ensemble prediction system with an idealized model. We will use an algorithmic approach with filter likelihood as a cost function and differential evolution as an optimizer.

METHODS

The target is to optimize the spread parameters of an ensemble forecasting system such that the spread-skill relationship of the ensemble prediction is optimal. We use filter likelihood as a cost function for optimizing the spread parameters. Filter likelihood, see e.g. (Hakkarainen *et al.*, 2013), compares the ensemble forecasts against the observations taking into account any errors of the observations. Solonen and Järvinen (2013) studied the connection between the filter likelihood and how it balances the skill and the spread of the ensemble. This means that good filter likelihood values correspond to good verification metrics, such as continuous ranked probability score, rank histogram, and relationship between spread and skill.

We use an algorithmic approach based on differential evolution algorithm (Shemyakin and Haario, 2018) to optimize the spread parameters with the filter likelihood as a target function.

The approach is demonstrated using an implementation with an idealized model, Lorenz 95 (Lorenz, 1996; Wilks, 2005). We use two versions of the model: a full version of the model used for generation of synthetic observations and a parametrized model with stochastic physics used as the forecast

model. The aim is to optimize two stochastic physics parameters and a third parameter controlling the amplitude of the initial uncertainties using the algorithmic approach such that the ensemble prediction system is optimal.

We will look at how different aspects, such as ensemble size and DE population size, affect the convergence of the algorithmic method.

CONCLUSIONS

We have presented an algorithmic approach for optimizing spread parameters in an ensemble prediction system. The implementations using the model Lorenz'95 suggest that an algorithmic approach for tuning spread parameters in an ensemble prediction system is possible in an idealized case.

ACKNOWLEDGEMENTS

This work was supported by Academy of Finland (project n:o 313828), the Vilho, Yrjö and Kalle Väisälä Foundation, the Academy of Finland Center of Excellence programme (grant no. 307331), Doctoral Programme in Atmospheric Sciences of University of Helsinki, and the Academy of Finland Centre of Excellence of Inverse Modelling and Imaging (decision number 312122).

REFERENCES

- Hakkarainen J., Solonen A., Ilin A., Susiluoto J., Laine M., Haario H., Järvinen H., (2013). A dilemma of the uniqueness of weather and climate model closure parameters. *Tellus A: Dynamic Meteorology and Oceanography*, **65(1)**, 20147, doi:10.3402/tellusa.v65i0.20147.
- Leutbecher M. and Palmer T. N., (2008). Ensemble forecasting. *Journal of Computational Physics*, **227 (7)**, 3515-3539, doi:10.1016/j.jcp.2007.02.014..
- Lorenz E. N. (1996). Predictability: A problem partly solved. In Proc. Seminar on predictability, volume 1.
- Shemyakin V. and Haario H., (2018). Online identification of large-scale chaotic systems. *Nonlinear Dynamics*, 1-15, doi:10.1007/s11071-018-4239-5.
- Solonen A. and Järvinen H., (2013). An approach for tuning ensemble prediction systems. *Tellus A. Dynamic Meteorology and Oceanography*, **65(1)**,20594, doi:10.3402/tellusa.v65i0.20594.
- Wilks D. S., (2005). Effects of stochastic parametrizations in the Lorenz'96 system. *Quarterly Journal of the Royal Meteorological Society*, **131(606)**,389-407, doi:10.1256/qj.04.03.

FAAR abstract instructions and template

Please read carefully - the text contains instructions for abstract preparation

THE ROLE OF PRECIPITATION FOR THE RECENT OUTBREAK OF ANTHRAX IN SIBERIA

E. EZHOVA¹, D. ORLOV², E. SUHONEN¹, S. MALKHAZOVA², V. GENNADINIK³, D. DROZDOV⁴,
D. KAVERIN⁵, I. KUKKONEN⁶, H. LAPPALAINEN¹, V. MELNIKOV⁴, T. PETÄJÄ¹,
V.-M. KERMINEN¹, S. ZILITINKEVICH⁷, T. CHRISTENSEN⁸, and M. KULMALA¹

¹Institute for Atmospheric and Earth System Research, University of Helsinki, Helsinki, PO Box 64
00014, Finland.

²Department of Medical Geography, Lomonosov Moscow State University, Moscow, Russia.

³Cryology and cryosophy center, University of Tyumen', Tyumen', Russia.

⁴Department of monitoring and information-geosystem modeling of cryolithozone, Earth Cryosphere
Institute, Siberian Branch, Russian Academy of Sciences, Moscow, Russia.

⁵Institute of Biology of Komi Science Center of Russian Academy of Science, Syktyvkar, Russia.

⁶Department of Geoscience and Geography, University of Helsinki, Helsinki, PO Box 64 00014, Finland.

⁷Finnish Meteorological Institute, Helsinki, Finland.

⁸Department of Bioscience, Aarhus University, Denmark.

Keywords: PERMAFROST, ANTHRAX, PRECIPITATION, SIBERIA.

INTRODUCTION

North-Western Siberia is one of the most rapidly warming sites in the Northern Hemisphere (Serreze *et al.*, 2000). In 2016, a severe anthrax outbreak happened at the Yamal Peninsula, Russia (Popova *et al.*, 2016). Anthrax is a bacterial disease caused by *B. Antracis*. In vegetative form, the bacteria are vulnerable to the environmental conditions, such as heating and freezing. At the same time, spores are highly resistant and can survive unfavourable conditions over dozens of years (Malkhazova *et al.*, 2018). The spores of *B. Antracis* can be found in soil. Climatic factors are known to play an important role triggering and influencing spread of anthrax. In this study, we perform analysis of these factors and their effect on the recent outbreak in Siberia.

In this study, we focus on several factors: active layer thickness and precipitation. Numerous probes of soil taken prior to the outbreak were free of bacteria, therefore, the main hypothesis is that anthrax outbreak was caused by permafrost thawing and revival of old spores. We study the rates of thaw and potential factors influencing thaw, such as air temperature and snow thickness. In addition, we consider summer precipitation, as dry weather is a well-known factor favouring spread of disease.

METHODS

The analysis is based on the observational data sets from 2005-2018. Medical data on the localization and intensity of outbreak are available from the Department of Medical Geography, Moscow State University. The data on active layer thickness is available from the Continuous Active Layer Monitoring program site (CALM). Meteorological data archive from nine official WMO stations was downloaded from the weather forecast site (www.rp5.ru).

We investigated temporal dynamics of active layer thickness from several CALM sites within 200 km from the outbreak location to assess the process of permafrost thaw in the region. We further performed analysis

FAAR abstract instructions and template

Please read carefully - the text contains instructions for abstract preparation

of the related meteorological data in order to explain the observed dynamics. We calculated freezing and thawing degree-days from air temperature and estimated corresponding indices for soil, taking into account the effect of snow thickness. In addition, we analysed dynamics of summer precipitation in the region.

RESULTS

Our study shows that the active layer thickness in the region was continuously increasing starting from 2010. The thaw rate was especially high in the discontinuous permafrost area near Nadym. Dynamics of active layer can be mainly explained by the temperature factor in the area underlain by continuous permafrost, while snow thickness appeared to be an additional factor significantly affecting active layer thickness in the region of discontinuous permafrost.

Summer precipitation displays a strong decreasing trend in the area of outbreak localization, while nearby areas were less affected and some of them even show an opposite trend. This drought is likely an important factor contributing to the spread of disease, which was completely overlooked before the present study.

CONCLUSIONS

We have investigated climatic factors contributing to outbreak of anthrax in Siberia. We found that a rapid permafrost thaw in the region was a consequence of the temperature and winter precipitation dynamics, when soil surface was effectively insulated by the thick snow cover during cold years. Therefore, opposite to the hypothesis suggested in mass media, this outbreak was not the result of one hot summer. In addition, we revealed a drastic drop in summer precipitation during the year of outbreak, which likely contributed to the fast spread of the disease.

ACKNOWLEDGEMENTS

This study is part of the Pan-Eurasian Experiment program. This work was supported by the Academy of Finland Centre of Excellence under grant 307331.

REFERENCES

- Malkhazova S., Mironova V., Shartova N., Orlov D. (2019) *Mapping Russia's Natural Focal Diseases: History and Contemporary Approaches*. Springer Series: Global Perspectives on Health Geography, (Springer International Publishing AG).
- Popova A.Yu., Demina Yu.V., Ezhlova E.B., Kulichenko A.N., Ryazanova A.G., Maleev V.V., Ploskireva A.A., Dyatlov I.A., Timofeev V.S., Nechepurenko L.A. and Khar'kov V.V. (2016) Outbreak of Anthrax in the Yamalo-Nenets Autonomous District in 2016, Epidemiological Peculiarities, *Problemy Osobo Opasnykh Infektsii [Problems of Particularly Dangerous Infections]* **4**, 42. (In Russ.).
- Serreze, M. C., Walsh, J. E., Chapin III, F. S., Osterkamp, T., Dyrgerov, M., Romanovsky, V., Oechel, W. C., Morison, J., Zhang, T. and Barry, R. G. (2000) Observational evidence of recent change in the northern high-latitude environment, *Clim. Change* **46**, 159.

COMPARISON OF MODEL PREDICTIVE PERFORMANCES FOR NORDIC GRASSLANDS

I. FER¹, M.C. DIETZE², TONI VISKARI¹, JARMO MÄKELÄ¹, LIISA KULMALA¹, JARI LISKI¹,
MATTI VIKINKOSKI³, MIKKO KAASALAINEN³, TUULA AALTO¹

¹Climate System Research, Finnish Meteorological Institute, Erik Palménin aukio 1 FI-00560 Helsinki, Finland

²Department of Earth and Environment, Boston University, 685 Commonwealth Ave, Boston MA 02215, United States of America

³Department of Mathematics, Tampere University, PO Box 553, 33101 Tampere, Finland

Keywords: Bayesian model selection, posterior predictive loss, uncertainty, grasslands

INTRODUCTION

Process-based simulation models are important tools for predicting the future state and functioning of grassland ecosystems under the changing climate. There are many models, each formulating different hypotheses about how these ecosystems work. Past studies have found large variability in outputs from different models. In such cases, it is a typical approach to compare model performances against some test data and select or rank the models according to metrics that minimize model error while accounting for model complexity. Such selection procedures usually consider only errors that arise from model parameters (i.e. they try to find an optimum in penalizing models for larger number of parameters while favouring for smaller validation errors). However, while making future predictions other errors come into play such as errors in the model drivers. For selecting models that have better predictive performance rather than fitting the existing data, different skill metrics should be used (Vehtari and Ojanen, 2012; Hooten and Hobbs, 2015).

METHODS

In this study, we will use a suite of process-based simulation models that span a wide spectrum of complexity (Table 1): random walk (null model, embodies no process understanding), BASGRA (least complex), BASGRA_N, BASGRA_N-YASSO, BASGRA_N-CoSMo, BASGRA_N-CoSMo-YASSO, STICS, LPJml, LPJ-GUESS (most complex). We will couple these models to an ecological bioinformatics-toolbox, called Predictive Ecosystem Analyzer in order to enable a reproducible multi-model comparison exercise.

Model	# of parameters	# of drivers	IC/SU	Reference
BASGRA	79	5	IC	van Oijen et al., 2005 Höglind et al., 2016
BASGRA_N	112	5	IC	Persson et al., 2019 Höglind et al., in press
STICS	48	6	IC	Brisson et al., 2008 Jégo et al., 2013
LPJml	62	11	SU	Schaphoff et al. 2018a,b von Bloh et al., 2018
LPJ-GUESS	98	9	SU	Lindeskog et al., 2013 Olin et al., 2015

Table 1. Models used in this study. IC/SU: Whether model uses initial conditions (IC) or spin up (SU). BASGRA_N-YASSO, BASGRA_N-CoSMo, BASGRA_N-CoSMo-YASSO are under development. Note that number of parameters and drivers can change between different modeling protocols.

Next, we will generate synthetic data sets from each model with different length, frequency, and errors. We will perform goodness-of-fit (accounting for parameter errors) and goodness-of-prediction model selection (accounting for initial condition, driver and process errors in addition) at Nordic grassland sites for yield simulations under different scenarios. We hypothesize that common goodness-of-fit metrics (e.g. RMSE, DIC) are biased toward too complex models as they ignore other sources of errors in model comparison, whereas goodness-of-prediction metrics (e.g. posterior predictive loss) are not as they balance validation error and total predictive uncertainty.

ACKNOWLEDGEMENTS

This work was supported by CARBO-CREDIT (49402-201039) and MULTA projects.

REFERENCES

- Brisson, N., Launay, M., Mary, B., Beaudoin, N. (2008) Conceptual Basis, Formalisations and Parameterization of the STICS Crop Model Éditions QUAE. Versailles, France.
- Hooten, M. B. and Hobbs, N. T. (2015), A guide to Bayesian model selection for ecologists. *Ecological Monographs*, 85: 3-28. doi:10.1890/14-0661.1
- Höglind, M., Van Oijen, M., Cameron, D., Persson, T., 2016. Process-based simulation of growth and overwintering of grassland using the BASGRA model. *Ecol. Model.* 335, 1–15.
- Jégo, G., Bélanger, G., Tremblay, G.F., Jing, Q., Baron, V.S. (2013) Calibration and performance evaluation of the STICS crop model for simulating timothy growth and nutritive value. *Field Crops Res.* 151, 65–77.
- Lindeskog, M., Arneth, A., Bondeau, A., Waha, K., Seaquist, J., Olin, S., and Smith, B. (2013) Implications of accounting for land use in simulations of ecosystem carbon cycling in Africa, *Earth Syst. Dynam.*, 4, 385–407, doi:10.5194/esd-4-385-2013
- Olin, S., Lindeskog, M., Pugh, T. A. M., Schurgers, G., Wårlind, D., Mishurov, M., et al. (2015). Soil carbon management in large-scale Earth system modelling: implications for crop yields and nitrogen leaching. *Earth System Dynamics*, 6(2), 745-768. doi:10.5194/esd-6-745-2015.
- Persson, T., Höglind, M., Van Oijen, M., Korhonen, P., Palosuo, T., Jégo, G., Virkajärvi, P., Bélanger, G., Gustavsson, A.-M. (2019) Simulation of timothy nutritive value: A comparison of three process-based models. *Field Crops Research* 231, 81–92. <https://doi.org/10.1016/j.fcr.2018.11.008>
- Schaphoff, S., von Bloh, W., Rammig, A., Thonicke, K., Biemans, H., Forkel, M., Gerten, D., Heinke, J., Jägermeyr, J., Knauer, J., Langerwisch, F., Lucht, W., Müller, C., Rolinski, S., and Waha, K. (2018a) LPJmL4 – a dynamic global vegetation model with managed land – Part 1: Model description, *Geosci. Model Dev.*, 11, 1343–1375, <https://doi.org/10.5194/gmd-11-1343-2018>
- Schaphoff, S., Forkel, M., Müller, C., Knauer, J., von Bloh, W., Gerten, D., Jägermeyr, J., Lucht, W., Rammig, A., Thonicke, K., and Waha, K. (2018b) LPJmL4 – a dynamic global vegetation model with managed land – Part 2: Model evaluation, *Geosci. Model Dev.*, 11, 1377–1403, <https://doi.org/10.5194/gmd-11-1377-2018>
- van Oijen, M., Höglind, M., Hanslin, H.M., Caldwell, N. (2005) Process-based modeling of timothy regrowth. *Agron. J.* 97 (5), 1295–1303.
- Vehtari, A. and Ojanen J. (2012), A Survey of Bayesian predictive methods for model assessment, selection and comparison. *Statistics Surveys*, 6: 142-228. doi: 10.1214/12-SS102
- von Bloh, W., Schaphoff, S., Müller, C., Rolinski, S., Waha, K., and Zaehle, S.: Implementing the nitrogen cycle into the dynamic global vegetation, hydrology, and crop growth model LPJmL (version 5.0) (2018) *Geosci. Model Dev.*, 11, 2789–2812, <https://doi.org/10.5194/gmd-11-2789-2018>.

IDENTIFICATION OF INTERFERING CH₄ AND VOCS EMISSIONS FROM CH₄ FLUX MEASUREMENT SET-UP MATERIALS

N.C. FREISTETTER^{1,2}, L. KOHL^{1,2}, T. POLVINEN^{1,2}, M. KOSKINEN^{1,2,4} and M. PIHLATIE^{1,2,3}

¹Institute for Atmospheric and Earth System Research / Forest Sciences, Helsinki, Finland

²Department of Agricultural Sciences, Faculty of Agriculture and Forestry, University of Helsinki, Helsinki, Finland

³Viikki Plant Science Centre, University of Helsinki, Helsinki, Finland⁵Department of Agricultural Sciences, Faculty of Agriculture and Forestry, University of Helsinki, Helsinki, Finland

⁴Finnish Meteorological Institute, Helsinki, Finland

Keywords: methane, VOC, flux, material testing.

INTRODUCTION

Research groups studying methane (CH₄) fluxes from biological systems use a variety of analysers and materials to construct flux chambers and setups that measure CH₄ concentrations. The fluxes and the concentration changes measured are often small over the short period of one closure, which can be as short as a few minutes. Thus, an error-free measurement is crucial to a meaningful interpretation of the data. In addition to the interference of volatile organic compounds (VOCs) emitted from plant materials to the spectroscopic analysis of CH₄ (Kohl et al., 2019), we observed a strong distortion of measurements by what we assume to be emissions from materials of the set-up. Herein, we aim to conduct systematic tests to compare the non-biological CH₄ sources and interfering VOC emissions of various materials used in flux chamber systems. The primary goal is to identify direct CH₄ emission rates of the setup materials, to track the change of those emission rates over time from ‘fresh out of the box’ to drying out of the materials, and to follow the effect of storage conditions (e.g. temperature) on the emissions. We also aim to identify which non-CH₄ VOCs are erroneously interpreted as CH₄ by the analysers, and to compare the results from different analysers. Eventually we aim at providing emission rates per dry mass of the tested material and recommendations of safe materials for flux chambers or the measurement setups.

METHODS

We will measure the potentially CH₄ and VOC emitting materials (Table 1) in a closed loop system connected to multiple CH₄ analysers (Picarro G2301 and depending on availability G2201i, LGR UGGA, LiCor Li-8710). The materials will be weighted into plastic polypropylene storage boxes (0.8L), from now on called chambers, and the sample surface area will be estimated. The chambers are connected to a 16-position flowpath selector valve (VICI Valco Instruments Co. Inc., Houston) that connects one chamber at a time to the gas loop. A Controllino Maxi programmable controller is driving the Valco flowpath selector upon an automated sequence, and actuates the valves that switch between closure and flushing mode of the

set-up (Figure 1). Emission rates of CH₄ will be measured at room temperature during 15 minutes closures. Before each closure, the chambers will be flushed for 10 minutes with ambient air. After the initial fresh-out-of-the-box measurement on day 1, samples will be re-analysed after one and three weeks after storage (a) in the lab at room temperature and at low humidity, and (b) in the cold room at +4°C and high humidity.

Material	Manufacturer
Vacuum grease	Sigma-Aldrich vacuum grease 18405-250G
Empty chambers	Hobby Life Demirel Plastik airtight storage boxes 0.8L
Polymer sealant	Soudal Fix-All Turbo SMX Hybrid Polymer
Epoxy glue	Henkel Adhesives LOCTITE Power Epoxy Universal
Adhesive deformable pads	Bostik Blu-Tack
Instance glue	Henkel Adhesives LOCTITE Super Glue Control
Tubing	SMC polyurethane tubes TU0604 aquamarin blue, 6x4
Shoot chamber cover foil	PTFE foil

Table 1. Uncompleted list of materials that will be tested for CH₄ and VOC emission rates.

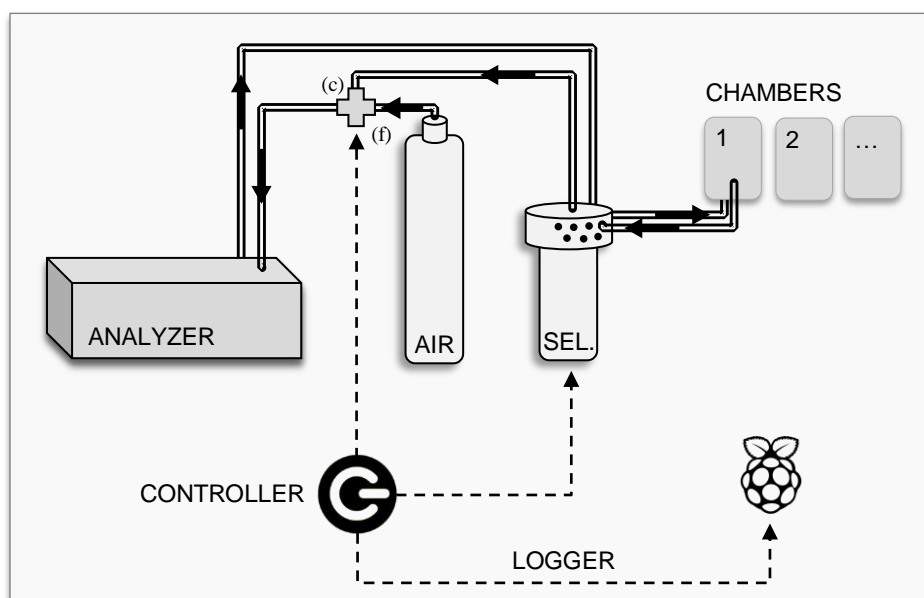


Figure 1. Schematic of experimental set-up for testing methane (CH₄) and volatile organic compound (VOC) emission rates from different materials. Up to 16 chambers can be connected to the VICI flowpath selector (SEL.) to be measured by the Picarro G2301 (ANALYZER) or other analysers. The Controllino programmable controller (CONTROLLER) actuates the selector and the three-way valve to switch between flush (f) with air (AIR) or closure (c). At the same time, the controller holds serial communication with a Raspberry Pi (LOGGER), which saves the logs to a file.

EXPECTED RESULTS

We expect to obtain a complete emission rate estimate from all tested materials and the effects of drying and temperature to the emissions of these materials. We also expect that the experiment will be helpful for the research community and will aid scientists in their decision making when constructing measurement systems. The results will complete our analysis of the interference of different VOCs on the spectroscopic analysis of CH₄.

ACKNOWLEDGEMENTS

This project has received funding from the European Research Council (ERC) under the European Union's Horizon 2020 research and innovation program (grant agreement number 757695) and the Academy of Finland (grant numbers 319329 and 2884941). Markku Koskinen received a fellowship from the Maj and Tor Nessling foundation.

REFERENCES

Kohl, L., M. Koskinen, K. Rissanen, I. Haikarainen, T. Polvinen, H. Hellén and M. Pihlatie (2019). Technical note: Interferences of volatile organic compounds (VOCs) on methane concentration measurements, *Biogeosciences*, **16**, 3319–3332.

MISSING DATA IMPUTATION AS SIMPLE PROXY OF URBAN BLACK CARBON IN HELSINKI, FINLAND

P.L. FUNG¹, M.A. ZAIDAN¹, S. SILLANPÄÄ¹ and T. HUSSEIN^{1,2}

¹Institute for Atmospheric and Earth System Research/Physics, University of Helsinki, 00560 Helsinki, Finland.

²Department of Physics, The University of Jordan, Amman 11942, Jordan.

Keywords: simple proxy, missing data, black carbon.

INTRODUCTION

Missing data has been one of the major challenges in understanding the nature of air pollution. The common reasons for incomplete datasets are instrument failure, data corruption or human error in data acquisition. Rubin (1976) classified incomplete data according to their generating mechanisms. The missing data mechanism of air quality data sets is generally random (MAR), in the sense that the probability that a value is missing does not depend on the missing value (Junninen *et al.*, 2004). Under MAR, the complete case analysis no longer relies on a random sample of the source population and selection bias is likely to occur (Donders *et al.*, 2006). In time series analysis, this problem can be huge because excluding incomplete observations may corrupt temporal structures such as autocorrelation, trends, and seasonality. Here we fill up the air quality missing data with multiple conditional mean imputation by a proxy of other air pollutant variables.

METHODS

In this study, we developed a simple black carbon ($\mu\text{g}/\text{m}^3$, BC) proxy model with maximum three predictor variables. We included lung deposited surface area ($\mu\text{m}^2/\text{m}^3$, LDSA) in all the models. We added one of the nitrogen oxide type variables (NO, NO₂, NO_x) as an optional variable. The above two aerosol and gas variables are highly correlated with BC. Meteorological variables (temperature, relative humidity and wind speed). We performed ordinary least-squared (OLS) linear regression. In case of a model with p predictor variables, the generalized OLS regression model writes:

$$Y = \beta_0 + \sum_{i=1}^p \beta_i X_i + \varepsilon \quad (1),$$

where Y is the response variable, β_0 is the intercept of the model, β_i and X_i correspond to the i^{th} regression coefficient and i^{th} predictor variable of the model, and ε is the random error with expectation 0 and variance σ^2 .

We applied an extra regularization by using ‘bisquare’ weight function, which is also known as robust fitting. This is an alternative to the traditional OLS regression when data are contaminated with outliers. We ran the regression for each of the model and obtain its evaluation attributes, which includes the adjusted coefficient of determination ($\text{adj}R^2$), mean absolute error (MAE) and root mean square error (RMSE). Multiple imputation were completed by bootstrapping method. Original data set is divided into 50 subsets each including 80% of the data set. Separate models are developed to each subset and the regression coefficients and evaluation attributions are calculated as arithmetic means from these model parameters. We ranked the models by $\text{adj}R^2$, followed by MAE and RMSE.

We classified A definition of thermal seasons was used. Spring and autumn are the periods when daily average temperatures are between 0°C and 10°C, and winter and summer are when the temperatures are below 0°C and above 10°C, respectively. According to the definition, 171, 102, 274 and 183 days were defined as winter, spring, summer and autumn, respectively, in year 2017 and 2018 in total. Workdays and

holidays (weekends and public holidays) were classified for each of the four seasons since they perform differently in terms of traffic rates and corresponding air pollutants concentration (Järvi *et al.*, 2008). 502 workdays and 228 holidays were identified. Altogether, the classification generates eight cases and proxies were developed separately.

SITE DESCRIPTION AND DATA TREATMENT

We used data of year 2017 and 2018 in SMEAR III station. This SMEAR III urban background station is situated in Kumpula about 4 km northeast of the Helsinki centre. Air quality data are measured on the 31-m-high, triangular lattice tower located on a rocky hill at 26 m above sea level) next to the University of Helsinki buildings and the Finnish Meteorological Institute. Next to the tower stands an air-conditioned measurement container, where the aerosol particle and the trace gas measurement instrumentation is located. In addition, basic meteorological measurements are made from the rooftop of Physicum building in the University of Helsinki (Järvi *et al.*, 2009).

BC mass concentrations were measured by a multi-angle absorption photometer (MAAP) Thermo Scientific 5012 with a PM₁₀ inlet. The MAAP determines absorbance from particles deposited on the filter, which was then converted to BC mass concentration by using a fixed 6.6 m²/g mass absorption coefficient at 637 nm. LDSA concentration were calculated from Differential Mobility Particle Sizer (DMPS) with deposition efficiency and summing up the total LDSA concentration of the aerosol. The conversion equation was first introduced in the human respiratory tract model on the ICRP report by Bair in 1994. NO_x, NO and NO₂ in Kumpula were measured with Themo TEI42S.

As for meteorological data, air temperature was measured with a platinum resistant thermometer Pt-100 and air humidity with a Platimun resistance thermometer and thin film polymer sensor Vaisala DPA500 from the roof of the University of Helsinki Building. On the same roof, horizontal wind speed was measured by a Vaisala cup anemometer.

PRELIMINARY RESULTS

Table 1. Best performing OLS regression simple proxy results for the eight classifications in Kumpula, where X are the predictor variables in the models, β are the regression coefficients and SE are the standard errors of the regression coefficients. WD stands for workdays and H represents holidays.

	Winter			Spring			Summer			Autumn		
	X	β	SE	X	β	SE	X	β	SE	X	β	SE
WD	LDSA	0.98	0.08	LDSA	0.95	0.011	LDSA	0.96	0.011	LDSA	0.94	0.010
	NO	0.04	0.003	NO _x	0.11	0.006	NO _x	0.10	0.006	NO _x	0.11	0.006
				RH	-0.00	0.000	RH	-0.00	0.000	Temp	-0.00	0.000
	adjR ²	0.88				0.88			0.88			0.88
	MAE	0.006				0.022			0.022			0.020
	RMSE	0.25				0.27			0.27			0.27
H	LDSA	0.93	0.010	LDSA	0.98	0.008	LDSA	0.90	0.010	LDSA	0.96	0.009
	NO _x	0.11	0.006	NO	0.04	0.003	NO	0.03	0.004	NO	0.04	0.002
	Temp	-0.00	0.000	Temp	-0.00	0.000				WS	-0.01	0.002
	adjR ²	0.88				0.88			0.77			0.88
	MAE	0.020				0.006			0.006			0.007
	RMSE	0.27				0.26			0.34			0.25

All models except holidays in summer attained a good correlation (adjR² over 85%). RMSEs generate a similar result as in adjR². MAEs are generally higher in workdays (over 0.02) than in holidays. It appears that when NO_x was used in the model, MAE is higher. In some classifications (workdays in winter and holidays in summer), meteorological variables do not help improve the accuracy of the models. For weekdays in autumn, holidays in winter and holidays in spring, temperature contributed in the model

accuracy. Relative humidity was used in weekdays in spring and summer while wind speed (Table. 1). Figure 1 shows the overall correlation of proxy BC and measured BC in all cases. The overall adjR² is over 80%.

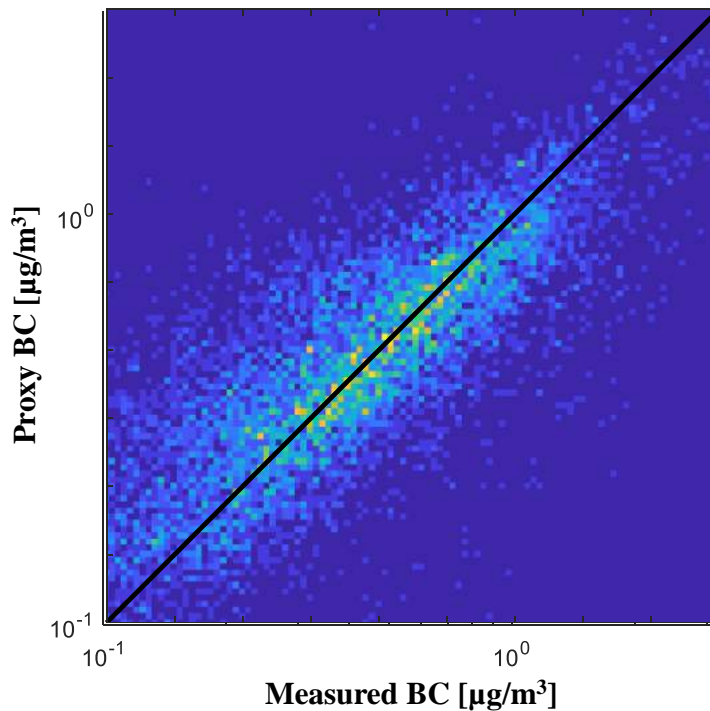


Figure 1. Scatter plot of proxy BC and measured BC in $\mu\text{g}/\text{m}^3$, colored by the density of the data points. The black bold line represents 1:1 gradient. The two axes are in logarithm scale.

ACKNOWLEDGEMENTS

This work was supported by the EU Urban Innovative Actions via HOPE project (grant number UIA03-240).

REFERENCES

- Bair, W. J. (1994). The Revised International Commission on Radiological Protection (ICRP) Dosimetric Model for the Human Respiratory Tract—An Overview. *The Annals of Occupational Hygiene*, 38(inhaled_particles_VII), 251–256.
- Donders, A. R. T., van der Heijden, G. J. M. G., Stijnen, T., & Moons, K. G. M. (2006). Review: A gentle introduction to imputation of missing values. *Journal of Clinical Epidemiology*, 59(10), 1087–1091. <https://doi.org/10.1016/j.jclinepi.2006.01.014>
- Järvi, L., Junninen, H., Karppinen, A., Hillamo, R., Virkkula, A., Mäkelä, T., ... Kulmala, M. (2008). Temporal variations in black carbon concentrations with different time scales in Helsinki during 1996-2005. *Atmospheric Chemistry and Physics*, 8(4), 1017–1027. <https://doi.org/10.5194/acp-8-1017-2008>
- Järvi, Leena, Hannuniemi, H., Hussein, T., Junninen, H., Aalto, P. P., Hillamo, R., ... Kulmala, M. (2009). The urban measurement station SMEAR II: Continuous monitoring of air pollution and surface-atmosphere interactions in Helsinki, Finland. *Boreal Environment Research*, 14(SUPPL. A), 86–109.
- Junninen, H., Niska, H., Tuppurainen, K., Ruuskanen, J., & Kolehmainen, M. (2004). Methods for imputation of missing values in air quality data sets. *Atmospheric Environment*, 38(18), 2895–2907. <https://doi.org/10.1016/j.atmosenv.2004.02.026>
- Rubin, D. B. (1976). Inference and Missing Data. *Biometrika Trust*, 63(3), 581–592. <https://doi.org/10.1186/1471-2105-12-432>

EFFECT OF OZONE ON HOM FORMATION IN OXIDATION OF TOLUENE

O. GARMASH¹, M.P. RISSANEN², M. RIVA³, O. PERÄKYLÄ¹, P. RANTALA¹ and M. EHN¹

¹Institute for Atmospheric and Earth System Research/Physics, University of Helsinki, Finland

²Aerosol Physics Laboratory, Physics Unit, Faculty of Engineering and Natural Sciences, University of Tampere, Tampere, Finland

³Univ Lyon, Université Claude Bernard Lyon 1, CNRS, IRCELYON, 69626, Villeurbanne, France

Keywords: HOM, TOLUENE, SECONDARY ORGANIC AEROSOL, MASS SPECTROMETRY

INTRODUCTION

Secondary aerosol formation is an important source of particulate matter in the atmosphere. Secondary processes include new particle formation and particle growth through condensation. Many recent studies have shown that oxidation products of organic compounds known as highly oxygenated organic molecules (HOM) play an important role in both of these processes (Bianchi *et al.*, 2019, Ehn *et al.*, 2014).

HOM form in a rapid autoxidation process through peroxy radical isomerisation and subsequent O₂ addition following the first oxidation step. This pathway is known to occur in hydroxyl radical (OH) and ozone (O₃) - initiated oxidation of biogenically-emitted volatile organic compounds (VOC), such as isoprene, monoterpenes and sesquiterpenes (Jokinen *et al.*, 2015, Jokinen *et al.*, 2016). Recently, this oxidation pathway was also observed in OH oxidation of aromatic VOC, which primarily originate from anthropogenic sources (Garmash *et al.*, 2019, Molteni *et al.*, 2018, Wang *et al.*, 2017).

Laboratory simulations of atmospheric oxidation can help us to evaluate the role of a specific VOC in the atmosphere. A lot of experimental work on secondary organic aerosol (SOA) formation in oxidation of aromatic VOC have been conducted; however, the results varied significantly between the experiments (Hildebrandt *et al.*, 2009, Ng *et al.*, 2007). One possible explanation are the different experimental conditions that affect the formation rate and composition of HOM and other oxidation products. We tested this hypothesis and shown that the HOM formation in oxidation of benzene, the simplest aromatic VOC, is dependent on OH concentration (Garmash *et al.*, 2019). At high OH concentration, multiple OH oxidation steps occur which leads to an increase in total HOM molar yield as well as to change in HOM chemical composition.

In this study, we continue to explore how different experimental conditions affect HOM formation and test the effect of ozone in oxidation of toluene. Most of the methods of OH radical generation either require the presence of O₃ or produce it as a by-product. In oxidation of any aromatic VOC, after the initial OH attack, some of the oxidation products lose aromaticity and retain some double bonds. Double bonds make a compound reactive towards O₃. As the reaction with ozone progresses few orders of magnitude slower than with OH, high concentration of O₃ and longer residence times may make ozonolysis a competitive reaction. By varying the concentration of ozone, while maintaining the OH concentration constant, we attempt to test if any of the HOM are produced via secondary ozonolysis reaction. The results from this work will be useful to advance our understanding on HOM formation in atmospheric simulation chambers and extend this knowledge to the ambient atmosphere.

METHODS

The oxidation experiments were conducted in 2 m³ PTFE COALA chamber at the University of Helsinki. The chamber was operated in continuous flow regime with the residence time of approximately 40 min. The measurement set-up schematic is shown in Figure 1.

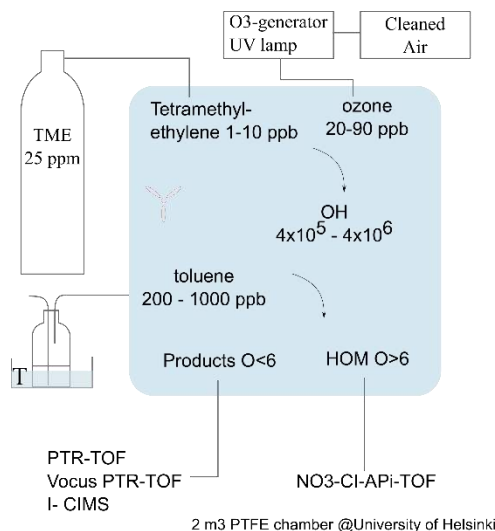


Figure 1. Schematic of the experimental set-up in COALA chamber.

The toluene was fed by flowing 1 mlpm of N₂ through a temperature-controlled glass vial, after which it was mixed into the clean air going to the chamber. To initiate the oxidation of toluene, OH radicals were produced from reaction of tetramethylethylene (TME) with ozone. TME and ozone were fed from separate lines to the chamber. In order to ensure a single OH attack to toluene, we operated at high toluene concentrations, 200-1000 ppb. The TME concentration was kept at 1-10 ppb, while ozone at 20-90 ppb, resulting in OH concentrations 4×10⁵ - 4×10⁶ cm⁻³. To test the effect of ozone on the formation of HOM, we varied the ratio between TME and ozone in order to maintain a constant OH concentration.

To measure HOM, we used nitrate-based chemical ionization atmospheric pressure interface time-of-flight mass spectrometer, CI-API-TOF (Jokinen *et al.*, 2012). Toluene and TME concentrations were measured using proton transfer time-of-flight mass spectrometer (PTR-TOF) that uses H₃O⁺ ionization scheme. We also monitored the lower oxygenated oxidation products using Vocus PTR-TOF and low-pressure iodide chemical ionization mass spectrometer.

RESULTS AND CONCLUSION

In order to determine the role of ozone in our experiments, we first had to eliminate the effect of OH on the HOM yield. In HOM yield calculations, we considered the most abundant HOM: C₇ monomers and C₁₄ dimers. The results showed a constant HOM yield at OH concentrations of 4×10⁵ - 4×10⁶ cm⁻³ and nearly-constant ozone concentration of 40-50 ppb. Preliminary analysis revealed that HOM molar yield increased with increasing ozone concentration from 20 ppb to 90 ppb while OH was kept below 10⁶ cm⁻³. Future work will focus on exploring if secondary reactions with ozone are responsible for this increase and if a change in chemical composition of HOM can be seen as a response. The results of this work will be helpful in advancing our understanding of HOM formation in urban areas and in interpreting results from atmospheric simulation chambers.

ACKNOWLEDGEMENTS

This work was supported by Academy of Finland Centre of Excellence program (project no 272041, 307331), European Research Council (COALA grant 638703), and the Doctoral Programme in Atmospheric Sciences (ATM-DP) at the University of Helsinki. We also thank the tofTools team for providing tools for mass spectrometry data analysis.

REFERENCES

- Bianchi, F., *et al.* (2019). *Chemical Reviews*, 119, 3472-3509.
- Ehn, M., *et al.* (2014). *Nature*, 506, 476-9.
- Garmash, O., *et al.* (2019). *Atmos. Chem. Phys. Discuss.*, 2019, 1-33.
- Hildebrandt, L., *et al.* (2009). *Atmos. Chem. Phys.*, 9, 2973-2986.
- Jokinen, T., *et al.* (2015). *Proc Natl Acad Sci U S A*, 112, 7123-8.
- Jokinen, T., *et al.* (2016). *Boreal Environment Research*, 21, 262-273.
- Jokinen, T., *et al.* (2012). *Atmos. Chem. Phys.*, 12, 4117-4125.
- Molteni, U., *et al.* (2018). *Atmos. Chem. Phys.*, 18, 1909-1921.
- Ng, N. L., *et al.* (2007). *Atmos. Chem. Phys.*, 7, 3909-3922.
- Wang, S., *et al.* (2017). *Environmental Science & Technology*, 51, 8442-8449.

EFFECT OF AIR MASS HISTORY ON THE OBSERVED PARTICLE NUMBER SIZE DISTRIBUTION IN BEIJING

S. HAKALA^{1,2}, P. PAASONEN², V. VAKKARI³, C. DENG², Y. FU², J. JIANG², J. KANGASLUOMA^{1,2}, T. PETÄJÄ^{1,2,4}, J. KUJANSUU^{1,2}, C. YAN^{1,2}, F. BIANCHI^{1,2}, K. DÄLLENBACH^{1,2}, Y LIU¹, L. DADA^{1,2}, M. KULMALA^{1,2}

¹Aerosol and Haze Laboratory, Beijing Advanced Innovation Center for Soft Matter Science and Engineering, Beijing University of Chemical Technology, Beijing, China

²University of Helsinki, Department of Physics, Finland

³Finnish Meteorological Institute, Finland

⁴Joint International Research Laboratory of Atmospheric and Earth System Sciences, Nanjing University, Nanjing, China

Keywords: aerosol particles, new particle formation, size distribution, haze

INTRODUCTION

Despite ongoing pollution control measures, serious haze episodes remain a problem in Beijing, China. It is well established that the majority of particle mass during haze originates from secondary production rather than direct particle emissions. However, it remains largely unclear whether the eventually haze-forming particles were initially produced in new particle formation (NPF) events or emitted directly from primary sources. Some studies suggest that NPF is the main driver of haze formation as haze episodes are consistently preceded by NPF events in Beijing (Guo et al., 2014). While this connection clearly exists, it does not prove a causality between the two events: In Beijing NPF events are found to occur in clean northerly air masses which lowers the condensation sink, and since haze events are, by definition, preceded by clean periods they also become preceded by NPF events. One of the things obscuring the interpretation of the connection between NPF and haze is the highly varying appearance of the produced particle number size distributions by NPF events in Beijing. In some occasions, the newly formed particles clearly grow towards large sizes, where they start significantly contributing to the submicron particle mass, while in other cases the particles do not seem to grow past some modest size at all. Additionally, sometimes a sudden jump towards larger sizes is seen in the number size distribution, which makes the origin of these larger particles disputable. Such jumps can be related to sudden changes of air mass at the measurement site. In this study, we analyze particle number size distributions observed in Beijing as a function of different metrics describing the history of the arriving air masses. Our analysis shows that a simple metric describing the exposure of an air mass to anthropogenic emissions can be a powerful tool in explaining the observed size distributions. In addition, our results give further confirmation towards the contribution of NPF in the formation of haze.

METHODS

The particle number size distribution measurements were conducted at the Beijing University of Chemical Technology, Beijing, China during 16 Jan 2018 – 28 Mar 2019. The particle number size distribution of 1 nm–10 µm particles was measured with a homemade diethylene glycol scanning mobility particle sizer (DEG-SMPS) and a homemade particle size distribution (PSD) system. The DEG-SMPS measured particles between 1–6.5 nm (electric mobility diameter), while the PSD system, consisting of two scanning mobility particle sizers and an aerodynamic particle sizer, covered the rest of the range. 72-hour air mass back trajectories and potential emission sensitivities were calculated hourly for the whole measurement

period using a Lagrangian particle dispersion model FLEXPART version 9.02 (Stohl et al., 2005). European Centre for Medium-Range Weather Forecasts (ECMWF) operational forecast with 0.15 degree horizontal resolution, 137 vertical levels and 1 h temporal resolution was used as input data to FLEXPART. In order to estimate the anthropogenic influence on the air masses, we calculated cumulative population density values for the hourly trajectories by integrating population density data (Gridded Population of the World, Version 4, Revision 10, Year 2015) along the trajectory paths (see Fig. 1). The integration only included points where the trajectory height was less than 2 km above ground level. This threshold was used to approximate the height where the air mass is significantly affected by surface activities.

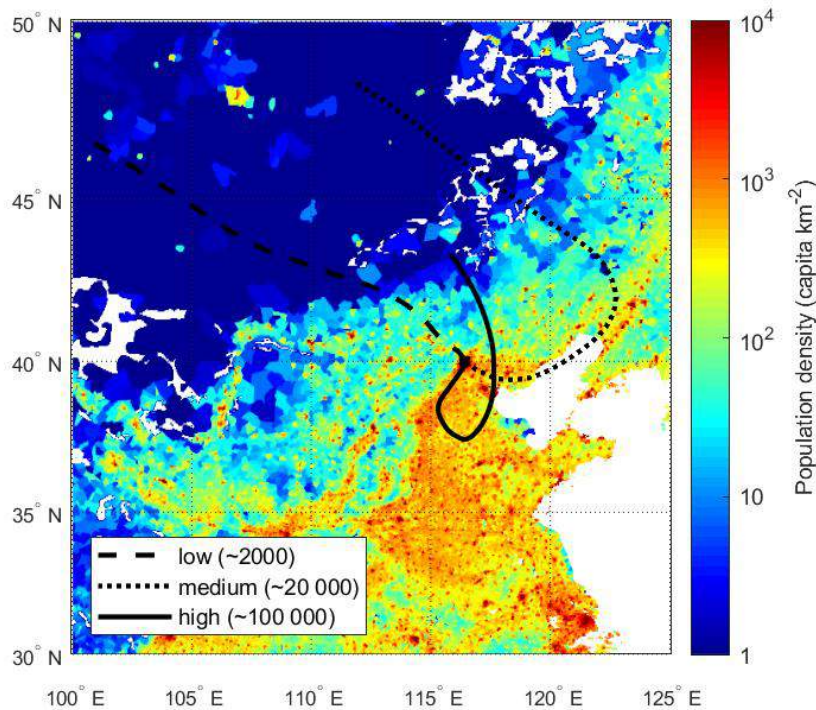


Figure 1. A population density map of north-eastern China displaying example trajectories with different cumulative population density values.

RESULTS

In Figure 2 we show examples of air mass trajectories at the onset of selected NPF events (NPF + 0 h) that eventually lead (or are followed by) haze formation. From this figure, we can see that NPF events typically take place in clean air masses that arrive from the sparsely populated areas located north of Beijing. During these periods the condensation sink is low, which is beneficial for the formation of new particles. As the development towards haze begins, we start to see a southern loop in the trajectories, meaning that circulation over more populated and polluted regions in the south has occurred. This increased exposure to anthropogenic emissions likely allows for more rapid and longer-lasting particle growth, which will contribute towards the formation of haze.

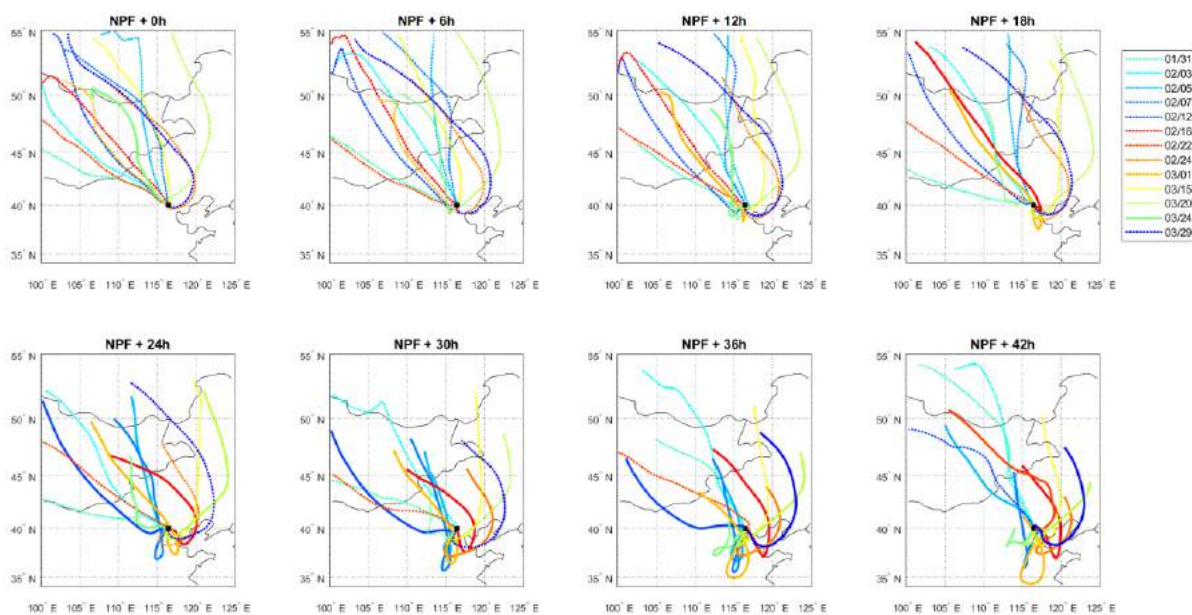


Figure 2. 60-h Back trajectories for 13 selected cases where an NPF event is followed by haze. The text above the panels indicates the trajectory release time in time after NPF on the days shown in the legend (mm/dd 2018). The trajectory lines turn from dotted to solid if the trajectory release occurs during haze (i.e. hourly median visibility has been ≤ 10 km.) In most of the cases, the haze development seems to be related to a southern loop over more polluted areas. However, even in the last panel (NPF+42 h), the air mass source regions (trajectory end points) at NPF - 18 h clearly reside within the clean regions in the north. Therefore, it is likely that NPF has also occurred in these air masses.

In figure 3 we compare the median particle number size distributions and the cumulative population density values of two different types of NPF events: those which show continuous growth (left panel) and those where the growth appears to seize in Beijing (right panel). In both cases the initial NPF takes place in clean air masses where the cumulative population density value is relatively low, but the later development is seen to differ significantly. In the case of continuous growth, the cumulative population density value is seen to increase simultaneously with increasing particle size, indicating the growth-favoring development of a southern loop, as seen in figure 2. Consistently, in the cases where the growth is disrupted also the cumulative population density values stays low. During these days, the source region of the arriving air masses stays in the northerly region where both the concentrations of condensable vapors and the spatial extent of the NPF area is likely to be limited. It is, however, important to note that while the particle growth is limited in Beijing, the particles are most likely to continue growing as they are transported further south within the polluted urban region. This is to say that although these particular NPF events do not produce haze-forming particles in Beijing, they might still contribute to haze formation somewhere else.

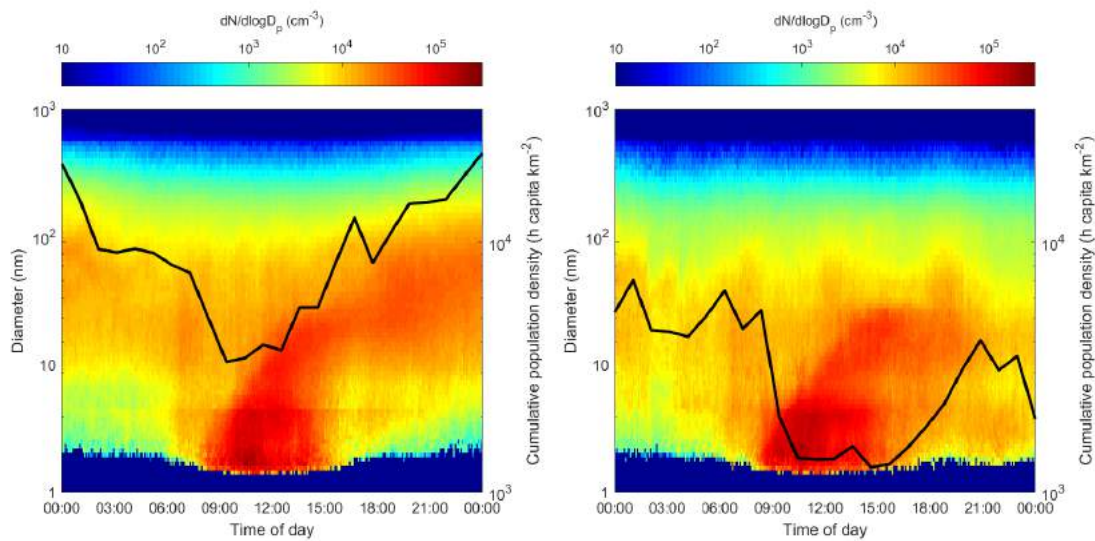


Figure 3. Comparison of the median particle number size distributions and the cumulative population density values (black line; right y-axis) of two different types of NPF events.

In figure 4, we present the observed particle size distribution as a function of the cumulative population density for the whole measurement period. Despite the varying appearance of particle growth events as a function of time, the particle size distribution can be seen to represent continuous and steady growth when sorted based on the air mass history. Essentially, this figure gives a simple estimation of the size distribution development as observed along an air mass travelling over the highly populated region. The fact that the number of larger particles (diameter > 50 nm) is low with low cumulative population density values suggests that these larger particles are neither formed in cleaner air masses nor emitted directly from local primary sources in significant amounts. Instead, the larger haze-forming particles seem to result from the growth of the smaller ones. The fact that the obtained particle number size distribution closely resembles that of an NPF event points towards an important role of the growth of nucleation mode (diameter < 30 nm) particles in haze formation.

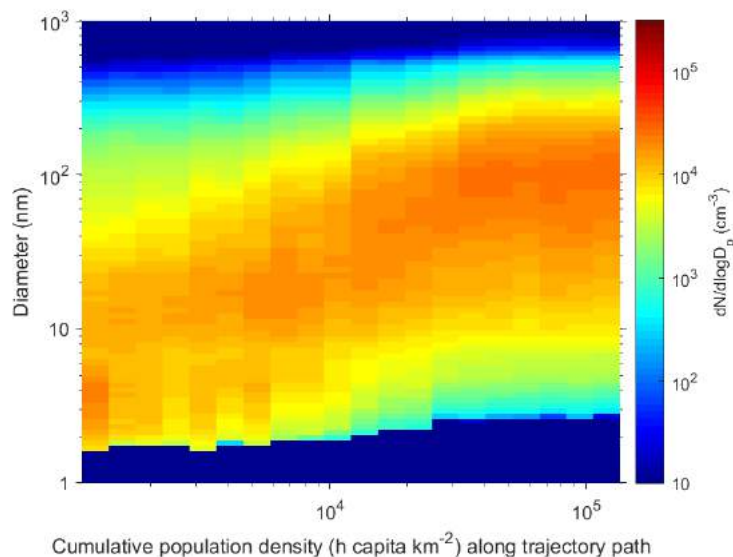


Figure 4. Median particle number concentrations as a function of cumulative population density along trajectory path.

A similar approach, as in Figure 4, was used by Tunved et al. (2006) to study the evolution of aerosol properties in Finland as a function of the time the arriving trajectories had spent over land. In that study, the observed particle mass and size was found to increase as a function of trajectory time over land, which was considered to represent the importance of biogenic emissions from boreal areas for particle growth. The cumulative population density, used in this study, can be considered as a proxy for the cumulative influence from anthropogenic emissions, since the population density and the intensity of such emissions are closely related. This suggest that anthropogenic emissions provide fuel for the growth of pre-existing nucleation mode particles, and that this growth, rather than direct particle emissions, is the principal source of larger (> 100 nm) particles which typically start to contribute significantly to particulate mass.

ACKNOWLEDGEMENTS

This study was funded the Academy of Finland Centre of Excellence program (projects 272041 and 307331), the European Research Council (ERC) under the European Union's Horizon 2020 research and innovation program (ATM-GTP, grant agreement 742206) and the Doctoral Programme in Atmospheric Sciences (ATM-DP, University of Helsinki).

REFERENCES

- Guo, S., Hu, M., Zamora, M. L., Peng, J. F., Shang, D. J., Zheng, J., Du, Z. F., Wu, Z., Shao, M., Zeng, L. M., Molina, M. J., and Zhang, R. Y.: Elucidating severe urban haze formation in China, *P Natl Acad Sci USA*, 111, 17373-17378, 10.1073/pnas.1419604111, 2014.
- Stohl, A., Forster, C., Frank, A., Seibert, P., and Wotawa, G.: Technical note: The Lagrangian particle dispersion model FLEXPART version 6.2, *Atmos. Chem. Phys.*, 5, 2461-2474, 2005.
- Tunved, P., Hansson, H. C., Kerminen, V. M., Strom, J., Dal Maso, M., Lihavainen, H., Viisanen, Y., Aalto, P. P., Komppula, M., and Kulmala, M.: High natural aerosol loading over boreal forests, *Science*, 312, 261-263, 10.1126/science.1123052, 2006.

RATE ENHANCEMENT IN COLLISIONS OF SULFURIC ACID MOLECULES DUE TO LONG-RANGE INTERMOLECULAR FORCES

R. HALONEN¹, E. ZAPADINSKY¹, T. KURTÉN², H. VEHKAMÄKI¹ AND B. REISCHL¹

¹ Institute for Atmospheric and Earth System Research / Physics, Faculty of Science, University of Helsinki, P.O. Box 64, FI-00014, Finland.

²Institute for Atmospheric and Earth System Research / Chemistry, Faculty of Science, University of Helsinki, P.O. Box 55, FI-00014, Finland.

Keywords: Rate coefficients, molecular dynamics, chemical reaction dynamics, new particle formation.

INTRODUCTION

Collisions of molecules and clusters play a key role in determining the rate of atmospheric new particle formation and growth. Traditionally the statistics of these collisions are taken from kinetic gas theory assuming spherical non-interacting particles (with hard-sphere radius R calculated using the bulk liquid density), which may significantly underestimate the collision coefficients for most atmospherically relevant molecules. Such systematic errors in predicted new particle formation rates will also affect large-scale climate models.

METHODS

We have studied the statistics of collisions of sulfuric acid molecules in vacuum by atomistic molecular dynamics simulations. We have benchmarked two classical force fields (by Ding *et al.* (2003) and Loukonen *et al.* (2010)) against experimental and ab initio data and determined that the OPLS force field by Loukonen *et al.* (2010) was able to describe the geometry and vibrational spectra of the isolated sulfuric acid molecule, as well as the geometry and binding free energy of the sulfuric acid dimer.

The simulations were carried out in the NVE ensemble, as the colliding molecules constitute a closed system (in atmospheric conditions collisions with the carrier gas are rare on the time scale of collisions between sulfuric acid molecules). In order to determine the molecules' collision probability P as a function of impact parameter and relative velocity, the following setup was used: first, two sulfuric acid molecules were placed in the simulation box, separated by 100 Å along x and the impact parameter b was set along the z direction, ranging from 0 to 17.5 Å in steps of 0.5 Å. For a collision of two identical molecules with molecular mass m , the relative velocities v follow the Maxwell-Boltzmann distribution with reduced mass $\mu = m/2$. For each value of the impact parameter and the relative velocity, 1000 simulations were carried out starting with different initial atomistic velocities, to ensure good sampling. A successful collision event is determined by formation of one or more hydrogen bonds between the sulfuric acid molecules. The statistics of the collision probabilities obtained from the atomistic simulations are shown in Fig. 1.

Additionally, we have used the classical Langevin model of capture to analytically calculate the critical impact parameter b_c (above which the reaction is inaccessible i.e. $P = 0$, otherwise $P = 1$) for a collision complex with a spherically symmetric long-ranged attractive interaction decaying with r^{-6} . The magnitude of the attractive interaction between two H₂SO₄ molecules is determined

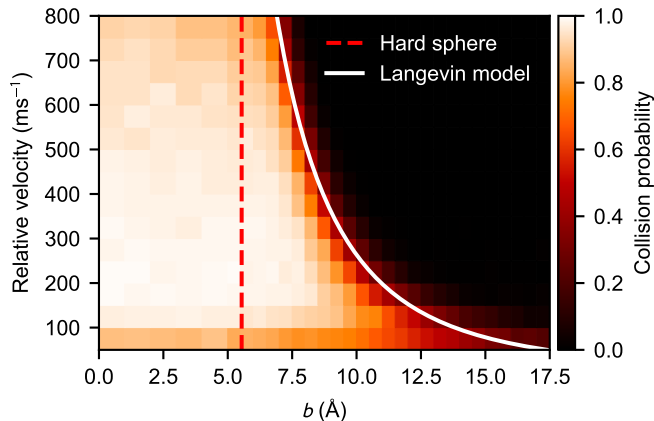


Figure 1: Heat map of the collision probability of sulfuric acid molecules plotted as a function of impact parameter b and relative velocity v obtained from molecular dynamics simulation. The impact parameter equivalent to the hard-sphere collision area ($b = 2R$) and the critical impact parameter obtained from the Langevin capture model are indicated by the dashed red and the solid white lines, respectively.

by calculating the potential of mean force from a well-tempered metadynamics simulation (Tribello, 2014).

The canonical collision rate coefficient is calculated by integrating over both the relative velocity distribution $f(v)$ and b^2 as

$$\beta = \pi \int_0^\infty dv \int_0^\infty db^2 v f(v) P(b, v). \quad (1)$$

To examine the difference between the rate coefficients obtained with atomistic simulations and Langevin modelling, we have calculated the enhancement factor over the kinetic gas theory of hard spheres as

$$W = \frac{\beta}{\beta_{\text{HS}}}, \quad (2)$$

where β_{HS} is the hard sphere collision rate for which $b_c = 2R$.

CONCLUSIONS

We have found that the effective collision cross section of the H_2SO_4 molecule, as described by an OPLS-All Atom force field, is significantly larger than the hard-sphere diameter assigned to the molecule based on the liquid density of sulfuric acid. As a consequence, the actual collision coefficient is enhanced by a factor 2.2 at 300 K, compared to kinetic gas theory. This enhancement factor obtained from atomistic simulation is consistent with the discrepancy observed between experimental formation rates of clusters containing sulfuric acid and calculated formation rates using hard sphere kinetics (Kürten, 2014; Lehtipalo, 2016; Kürten, 2018).

At a temperature range from 250 to 400 K (see Fig.2), the rate enhancement factor is monotonously decreasing with increasing temperature, however the drop is less than 20 %. We also note that the enhancement factor obtained from the Langevin model using the attractive part of the intermolecular potential is a bit overestimated due to the imperfect treatment of the anisotropic dipole-dipole interaction, yet in the atmospherically relevant temperature range the factor is within 30 % of the result from the atomistic simulation, at a fraction of the computational cost.

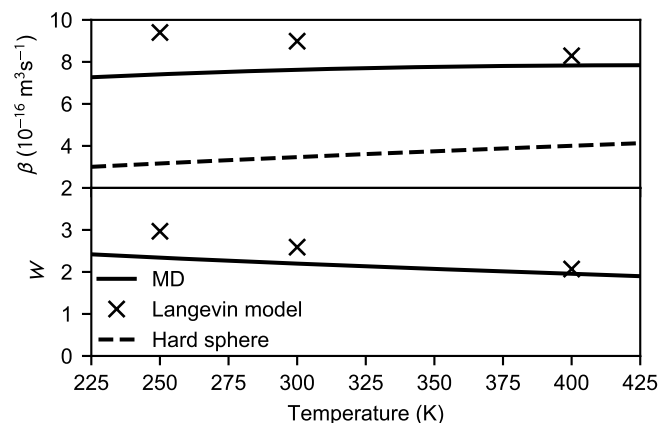


Figure 2: Collision rate coefficient β (upper panel) and the enhancement factor W (lower panel) as a function of temperature calculated for the hard-sphere, MD, and Langevin approaches.

In the future, the atomistic collision modelling approach presented in this work can be applied to other atmospherically relevant molecules, clusters, or ions, exhibiting dipoles of varying magnitude – and in some cases several times larger than the one of the sulfuric acid molecule – to help understand the effect of long-range interactions in cluster formation rates. However, before we can quantitatively assess the influence of collision rate enhancement on atmospheric new particle formation rates obtained from cluster dynamics models, it is necessary to obtain the enhancement factors for all the relevant collisions between clusters of different sizes and composition, as the pathway for growth may change – a formidable task, even if only the simplest acid-base clusters were considered.

ACKNOWLEDGEMENTS

This work was supported by the European Research Council (project 692891 DAMOCLES), Academy of Finland (Academy Research Fellow project 1266388 and ARKTIKO project 285067 ICINA), and University of Helsinki, Faculty of Science ATMATH project. Computational resources were provided by CSC–IT Center for Science, Ltd., Finland.

REFERENCES

- Ding, C.G., Taskila, T., Laasonen, K., and Laaksonen, A., (2003). Reliable potential for small sulfuric acid-water clusters. *Chem. Phys.*, **287**, 7–19.
- Kürten, A., Jokinen, T., Simon, M., Sipilä, M., Sarnela, N., Junninen, H., Adamov, A., Almeida, J., Amorim, A., Bianchi, F., *et al.*, (2014). Neutral molecular cluster formation of sulfuric acid–dimethylamine observed in real time under atmospheric conditions. *Proc. Natl. Acad. Sci. USA.*, **111**, 15019–15024.
- Kürten, A., Li, C., Bianchi, F., Curtius, J., Dias, A., Donahue, N.M., Duplissy, J., Flagan, R.C., Hakala, J., Jokinen, T., Kirkby, J., Kulmala, M., Laaksonen, A., Lehtipalo, K., Makhmutov, V., Onnela, A., Rissanen, M.P., Simon, M., Sipilä, M., Stozhkov, Y., Tröstl, J., Ye, P., and McMurry, P.H., (2018). New particle formation in the sulfuric acid–dimethylamine–water system: reevaluation of CLOUD chamber measurements and comparison to an aerosol nucleation and growth model. *Atmos. Chem. Phys.*, **18**, 845–863.
- Lehtipalo, K., Rondo, L., Kontkanen, J., Schobesberger, S., Jokinen, T., Sarnela, N., Kürten, A.,

- Ehrhart, S., Franchin, A., Nieminen, T. *et al.*, (2016). The effect of acid–base clustering and ions on the growth of atmospheric nano-particles. *Nat. Commun.*, **7**, 11594.
- Loukonen, V., Kurtén, T., Ortega, I.K., Vehkamäki, H., Pádua, A.A.H., Sellegri, K. and Kulmala, M., (2010). Enhancing effect of dimethylamine in sulfuric acid nucleation in the presence of water – a computational study. *Atmos. Chem. Phys.*, **10**, 4961–4974.
- Tribello, G.A. and Bonomi, M. and Branduardi, D. and Camilloni, C. and Bussi, G., (2014). Plumed 2: New feathers for an old bird. *Comput. Phys. Commun.*, **185**, 604–613.

CONTRIBUTION OF GAS-PHASE ORGANIC ACIDS TO SECONDARY ORGANIC AEROSOL FORMATION IN THE PRESENCE OF AMMONIA

L.Q. HAO¹, E. KARI¹, J. JOKINIEMI², D. R. WORSNOP^{1,3} and A. VIRTANEN¹

¹Department of Applied Physics, University of Eastern Finland, Kuopio, Finland

²Department of Environmental and Biological Sciences, University of Eastern Finland, Kuopio FI-70211, Finland

³Department of Physics, University of Helsinki, P.O. 64, Finland

Keywords: AMMONIA, SECONDARY ORGANIC AEROSOL, AEROSOL MASS SPECTROMETER

INTRODUCTION

The largest uncertainty in prediction of global warming is related to negative solar radiative forcing associated with aerosols (IPCC, 2013). Secondary organic aerosols (SOA) is one of the dominant component of atmospheric organic aerosol. Ammonia (NH₃) is ubiquitous in the atmosphere as a base compound. It has been come to be realized that NH₃ is involved in SOA formation (Na et al., 2007, Babar et al., 2017). This work presents the results of SOA formation from photooxidation of α -pinene in the presence of ammonia in the nucleation and seeded experiments. The results will have potential applications in studying SOA formation mechanism and the impact of SOA on climate forcing.

METHODS

The SOA formation experiments were carried out in a 29 m³ iLmari environmental chamber in 2018 (Leskinen et al., 2015). Experimental procedure has been presented in Kari et al. (2017; 2019). Two sets of experiments were designed (Table 1). In experimental group 1, SOA were formed from photooxidation reaction of α -pinene at low concentration in the presence of ammonium sulfate seeds. In experimental group 2, SOA was produced in the chamber from photooxidation of high-concentration α -pinene without adding seeds. Hydrogen peroxide (H₂O₂) was evaporated and flowed into chamber to act as an OH source. UV-lamps (340nm) were applied to irradiate H₂O₂ to generate OH radicals. The time evolution of α -pinene and other gas compounds was monitored by an on-line high-resolution proton transfer reaction mass spectrometer (HR-PTR-MS, Ionicon Analytik). The size-resolved chemical composition of aerosol particles were measured directly with an on-line high-resolution time-of-flight aerosol mass spectrometer (HR-Tof-AMS, DeCarlo et al., 2006). Particle size distributions were measured using a scanning mobility particle sizer (SMPS; TSI 3081 DMA + 3775 CPC).

	Experiment	a-Pinene(ppb)	AS seed surface ($\mu\text{m}^2/\text{cm}^3$)	OH exposure ($\#/\text{cm}^3 \text{ s}$)
Seeded SOA Exp.	E0314	4.13	2.96E7	1.21E+11
	E0315	4.15	4.30E7	1.23E+11
	E0316	4.84	2.16E7	1.26E+11
Nucleated SOA Exp.	E0322	100	0	-
	E0326	100.94	0	1.30E+11
	E0327	107.26	0	1.34E+11

Table 1 Summary of conductions in two sets of experiments

RESULTS AND DISCUSSION

In the nucleation experiments (left panels, Fig. 1), we have observed rapid increase of SOA formation in mass concentrations after the photooxidation reaction was enabled. After the SOA concentrations

reached the maximum, its concentration started to decline because of particle deposition on the chamber wall and possible aerosol evaporation. In contrast, the mass concentrations of ammonium component were still increasing when SOA masses decreased. Together taking into account the fact that aerosol wall deposition loss was present, our results suggest new production of ammonium salts.

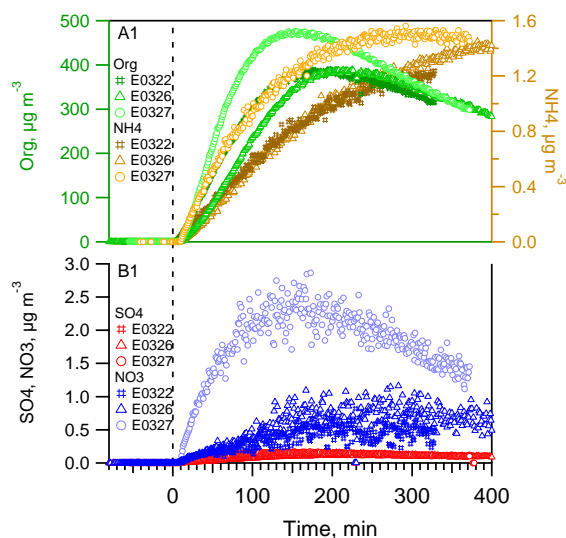


Figure 1. The time series of organic (left axis), ammonium (top panels, right axis), sulfate and nitrate (bottom panels) in nucleation experiments. The time zero marks the start of photooxidation reactions after UV lights were switched on.

To explore the mechanism of ammonium formation, we examined the organic acids in the gas phase. Figure 2 shows the correlation between the concentration of organic mono- and di-carboxylic acids in the gas phase and the ammonium mass concentration in the particle phase. Except for pinonic acid, we have observed the excellent correlation of the two components with correlation coefficients being $r^2 > 0.9$. The good correlation of the organic acids with ammonium salt suggests that they played a role in the formation of ammonium. For pinonic acid, its vapor pressure is about 4 to 5 order of magnitude lower than those of C1-C5 monoacids, which explains its different behavior from other organic acids.

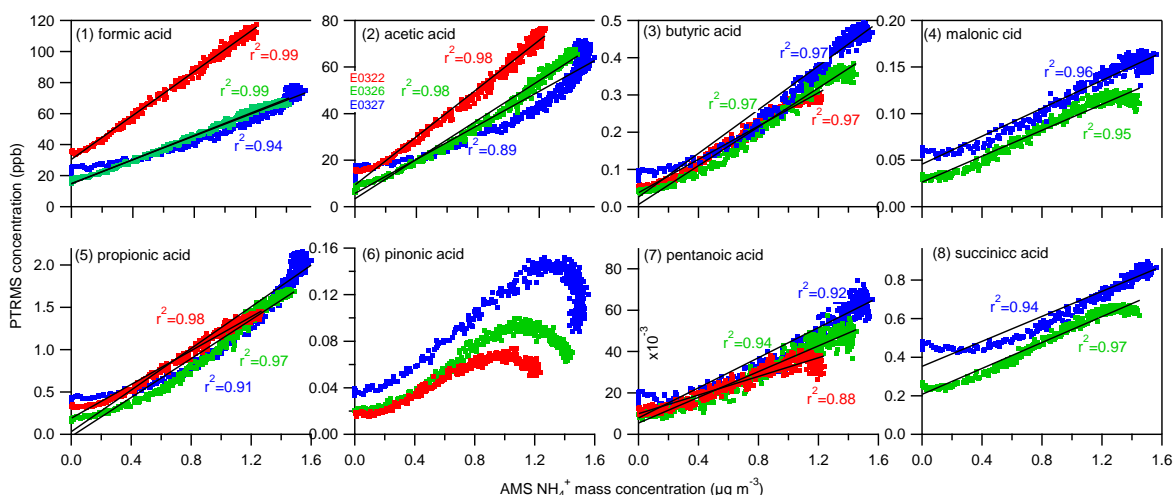


Figure 1. The correlation between gas-phase organic mono- and di-carboxylic acids measured by PTRMS and particle phase ammonium salt measured by AMS in the nucleated SOA.

CONCLUSIONS

The SOA experiments was conducted from photooxidation reaction of α -pinene in the presence of ammonia in a chamber. The organic mono- and di-carboxylic acids formed in the photooxidation of α -pinene in the gas phase played a role in the ammonium formation in the SOA particles through acid-base reaction, and thus contributed to SOA formation. The changes in aerosol mass, size and chemical composition due to the ammonia-SOA interaction can potentially lead to aerosol direct and indirect impacts on climate change.

ACKNOWLEDGEMENTS

This work was supported by The Academy of Finland Center of Excellence programme (grant no 307331), the European Research Council (ERC Starting Grant 335478) and EUROCHAMP2020 project (grant no 730997).

REFERENCES

- Babar, Z.B., Park, J., Lim H. (2017). Influence of NH₃ on secondary organic aerosols from the ozonolysis and photooxidation of α -pinene in a flow reactor, *Atmos. Environ.*, **164**, 71.
- DeCarlo, P. F., Kimmel, J. R., Trimborn, A., Northway, M. J., Jayne, J. T., Aiken, A. C., Gonin, M., Fuhrer, K., Horvath, T., Docherty, K., Worsnop, D. R. and Jimenez, J. L.(2006). Field-Deployable, High-Resolution, Time-of-Flight Aerosol Mass Spectrometer, *Anal. Chem.*, **78**, 8281.
- IPCC 2013. Climate change 2013: The physical science basis. Intergovernmental panel on Climate Change, Cambridge University Press, New York.
- Kari, E., Hao, L.Q., Yli-Pirilä, P., Leskinen, A., Kortelainen, M., Grigonyte, J., Worsnop, D.R., Jokiniemi, J., Sippula, O., Faiola, C.L., and Virtanen, A. (2017). The effect of pellet boiler exhaust on secondary organic aerosol formation from α -pinene, *Environ. Sci. Technol.* **51**, 1423.
- Kari, E., Hao, L., Ylisirniö, A., Buchholz, A., Leskinen, A., Yli-Pirilä, P., Nuutinen, I., Kuuspalo, K., Jokiniemi, J., Faiola, C., Schobesberger, S., and Virtanen, A. (2019). Dual effect of anthropogenic emissions on the formation of biogenic SOA, *Atmos. Chem. Phys. in print*.
- Leskinen, A., Yli-Pirilä, P., Kuuspalo, K., Sippula, O., Jalava, P., Hirvonen, M.-R., Jokiniemi, J., Virtanen, A., Komppula, M., and Lehtinen, K. E. J. (2015). Characterization and testing of a new environmental chamber, *Atmos. Meas. Tech.*, **8**, 2267.
- Na K., Song C., Switzer C., Cocker D.R. (2007). Effect of ammonia on secondary organic aerosol formation from α -pinene ozonolysis in dry and humid conditions, *Environ Sci Technol*, **41**, 6096.

SAMPLING AND ANALYSIS OF INDOOR AIR AND EMISSIONS FROM INSULATION MATERIALS

J. RUIZ-JIMENEZ^{1,2}, N. ZANCA^{1,2}, S. BARUA¹, G. DEMARIA¹, M. SALKINOJA-SALONEN¹,
H. M. M. SIREN¹, K. HARTONEN^{1,2} AND M.-L. RIEKKOLA^{1,2}

¹University of Helsinki, Department of Chemistry, P.O.Box 55, 00014 University of Helsinki, Finland.

² Institute for Atmospheric and Earth System Research, P.O.Box 55, 00014 University of Helsinki, Finland.

Keywords: INDOOR AIR, MATERIAL EMISSIONS, SAMPLING, ANALYSIS.

INTRODUCTION

Outdoor air quality in Finland is among the best ones in the world. However, we are suffering of low indoor air quality with the most striking health problems related to the dampness of the house caused by mold and mildew (sick building syndrome, SBS) (Spengler et al., 2001). This can be due to the too well isolated energy efficient buildings, possible water damages, water damaged materials and other physical and chemical parameters related for example to ventilation. Other chemical and microbiological emissions can result from the incompatible constructing materials especially if they are at high humidity, and from chemicals used for maintenance of the building (e.g. chemicals used for cleaning) (Rao et al., 2012). In worst cases, the ‘sick’ house can damage the health of the whole family (especially children), create huge economical problems and make the life unbearable (The Human Microbiome Project Consortium, 2012). As the outdoor air temperature and humidity (also the amount of rains, storms and floods) in Finland will be increased in the future due to the climate change, these indoor air problems will most likely come more serious.

METHODS

Indoor air of ‘sick’ houses from Nummela (not inhabited) and Vantaa (still inhabited) were studied together with the insulation materials used in these two buildings. Outdoor air samples were also collected for comparison as well as reference samples from the ‘healthy’ buildings.

Samples were collected using cryogenic sampler (e-collector) to trap compounds with condensed/frost water of the air obtained onto the surface of the sampler metal box that was cooled with dry ice. After the sampling when the sampler warmed up, the collected water was rinsed into the glass vial for further treatment and analysis. Solid phase microextraction Arrow (SPME Arrow) and in-tube extraction (ITEX) were utilized for the collection of gas phase compounds in indoor air and insulation material emissions. Commercial PDMS-DVB and Carbon WR were used as sorbents for the SPME Arrow, and ITEX was packed with laboratory-made polyacrylonitrile (PAN) fibers. Insulation materials were placed into the headspace vials for analysis.

Analyses for the gas phase and insulation materials were done with gas chromatography – mass spectrometry (GC-Q-MS; m/z 30-300 and GC-Q-TOFMS; m/z 50-600) and for condensate/frost water samples with liquid chromatography – mass spectrometry (HPLC-QQQ-MS; m/z 50-1500). Columns used in the GC were InertCap for Amines (30 m x 0.25 mm i.d.) from GL Sciences and HP-5MS (30 m x 0.25 mm i.d.) from Agilent Technologies. Reversed phase separation with Poroshell C-18 column (3.0 x 50 mm, 2.7 µm) was used in HPLC. Electron impact (EI) and chemical ionization (CI) with methane were used with the GC-MS and positive and negative electrospray (ESI) with the HPLC-MS. Spectral processing for qualitative analysis included NIST MS library search, retention index (RI) comparison, fungal metabolite

screening using database of 474 mycotoxins and fungal metabolites (Nielsen et al., 2003), accurate mass information, MS-MS database (Metlin) and characteristic fragments.

CONCLUSIONS

Indoor air

Gas phase analysis of indoor air in Vantaa and Nummela houses revealed that only a small number of compounds were collected by SPME Arrow and analyzed with GC-MS (Figure 1). Totally 33 compounds could be identified from Vantaa house and 42 from Nummela (16 of those were found from both).

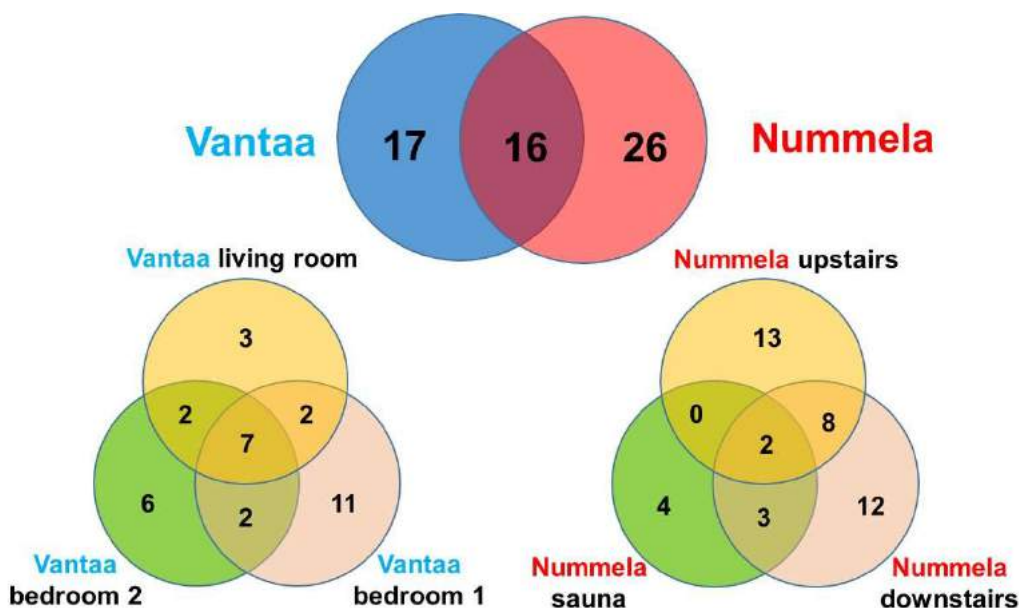


Figure 1. Number of identified compounds found in the gas phase samples of the ‘sick’ houses in Vantaa and Nummela. SPME Arrow sampling and analysis with GC-Q-TOFMS. About 35% of all detected compounds remained unidentified.

In-tube extraction (ITEX) has a great potential for active indoor air sampling due to its relatively large sorbent amount (enables high air flow-rates) and exhaustive nature (easy quantification). As an example, GC-MS chromatogram is shown in Figure 2 for the indoor air sample obtained with ITEX.

Using cryogenic collection (condensed/frost indoor air water), much higher number of compounds were detected than with sorbent collection of gas phase (see Figure 3). Totally, 546 compounds were found from Vantaa house and 254 from Nummela house. The same 194 compounds were found in both houses. More compounds were detected from living room compared to the other rooms. In addition, clearly higher number of compounds was present in Vantaa (inhabited) than in Nummela (not inhabited) due to human activities inside house.

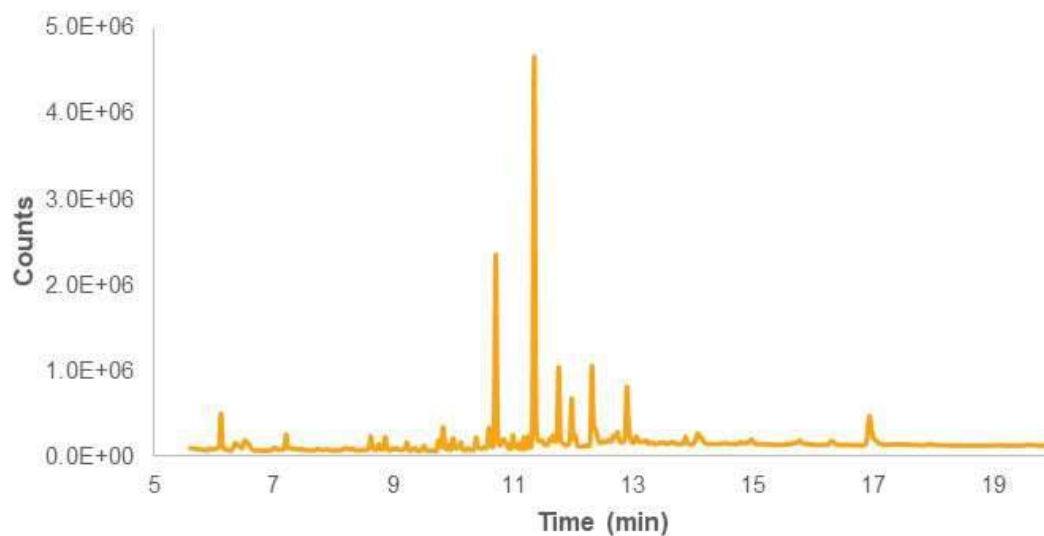


Figure 2. GC-Q-MS chromatogram of indoor air sample collected with ITEX using laboratory-made PAN fibers as adsorbent. 48 VOCs were identified using standards and 29% of those were hydrocarbons, 25% alcohols, 20% acids and derivatives, 13% aldehydes, 11% ketones and 2% halogenated compounds.

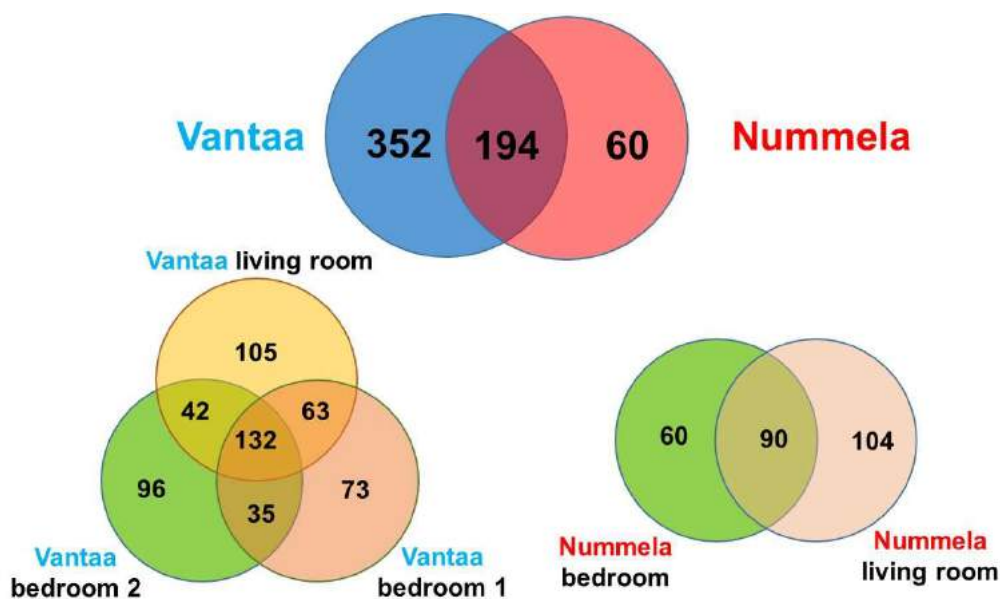


Figure 3. Number of different compounds found in the condensed/frost water samples of the indoor air from 'sick' houses in Vantaa and Nummela. Samples analysed by HPLC-QQQ-MS using ESI+.

Chemical load was much higher in Nummela and Vantaa houses compared to healthy reference Tampere house, being highest in Vantaa house (Figure 4). Lower graphs in Figure 4 (red circles) demonstrate that highly polar (not much retention in reversed phase column) and high molecular mass compounds were present in Vantaa house. Similar type of compounds were present in Vantaa bedroom 2 but not in bedroom

1 when samples were analyzed with HPLC-QQQ-MS using negative ESI (data not shown). In addition, samples collected from Vantaa house included also more compounds with molecular mass higher than 800.

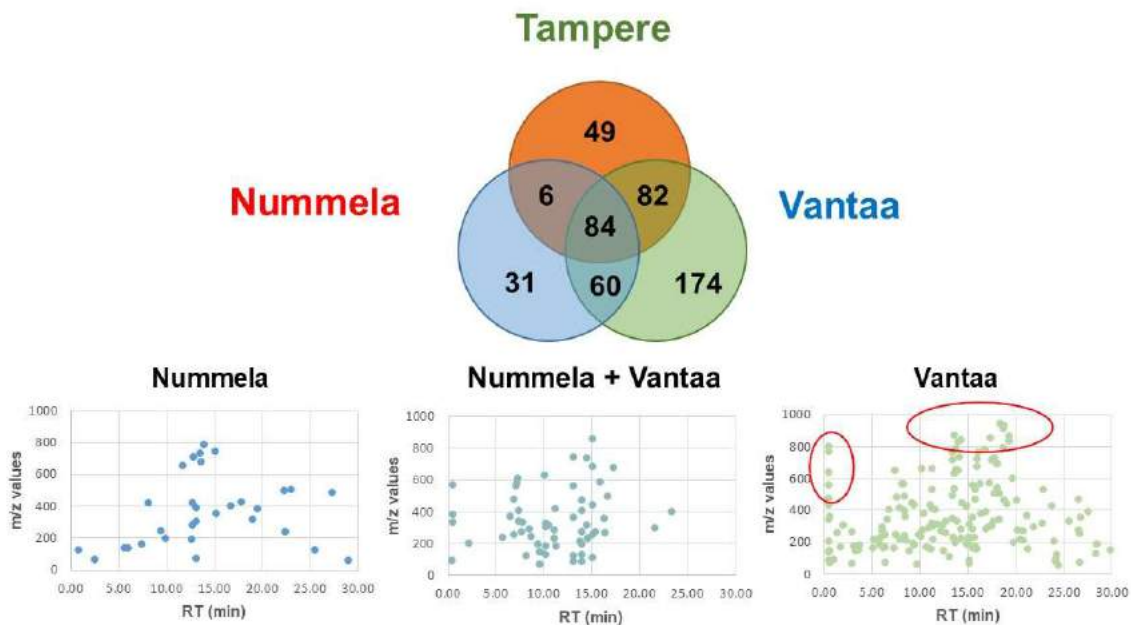


Figure 4. Number of compounds found in indoor air samples of Nummela, Vantaa and Tampere (healthy reference) houses and distribution of these compounds according to their retention times and m/z values. Condensed/frost water from indoor air analysed by HPLC-QQQ-MS using ESI+.

Material emissions

Water (moisture) affected greatly the number of compounds and their amounts emitted by the insulation materials (Figure 5). Higher number of compounds were emitted from the cellulose wool compared to glass wool. Also these compounds were mainly of higher volatility (most likely more polar and more water soluble). Increase of the amount of water added further enhanced this effect. Most of the compounds increased their intensity with water amount and some compounds behaved completely in an opposite way. This shows that at the moist conditions, insulation materials produced more chemicals to indoor air, and/or compounds are more easily mobilized/transported in gas phase. Especially the cellulose wool is more prone to microbial attack, and a high amount of flame retardants need to be added to it. Humidity has earlier been found to affect the chemical emissions from the waterborne materials like floor varnish and wall paint (Fang et al., 1999). Increase of the humidity from 0% to 50% has resulted in elevated emissions of VOCs from the carpet, sealant and wall paint in the studies of Wolkoff (1998). More recently, Markowicz and Larsson (2015) obtained an increase in VOC concentrations due to a high humidity. In addition, in this study temperature had a stronger effect on the cellulose wool. Increase of temperature from 22°C to 80°C raised the number of detected compounds from 30 to 161 with cellulose wool and from 22 to only 39 with glass wool.

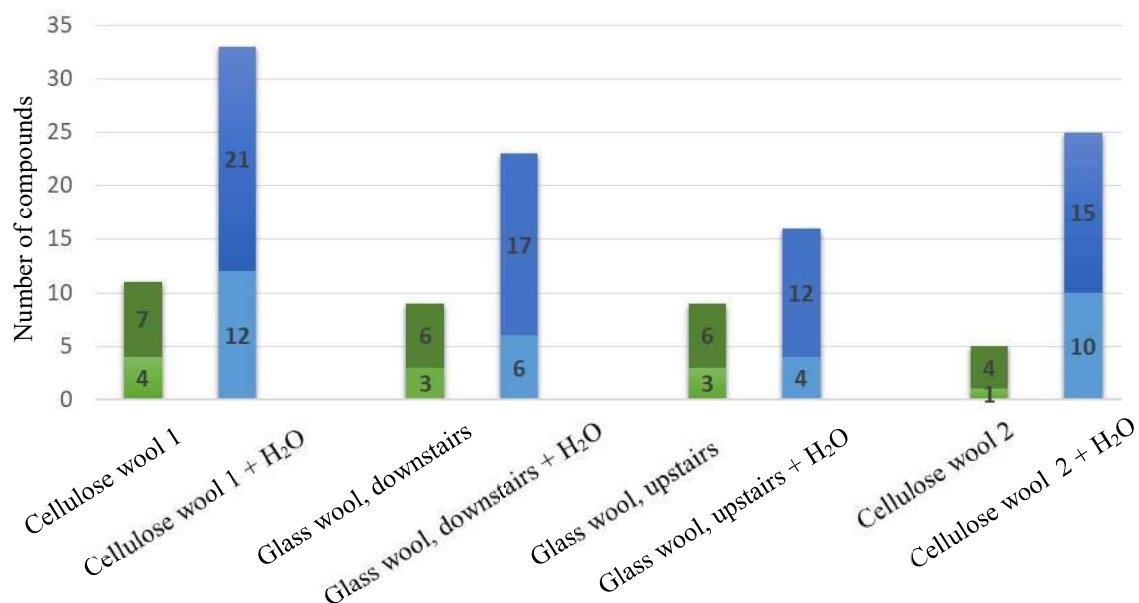


Figure 5. Number of compounds found in the emissions from the insulation materials (500 mg of glass wool or cellulose wool) with and without addition of 200 μ L of water. Samples were pre-heated at 40 C (5 min) followed by 5 min SPME Arrow extraction and GC/MS analysis. Lighter color means higher volatility (RI<1000) and darker color means lower volatility (RI>1000).

Compounds emitted from the insulation materials of Vantaa and Nummela houses were collected with commercial SPME Arrow (DVB-PDMS) at room temperature for 5 min. Totally 187 compounds were identified with GC-Q-TOFMS using chemical ionization. These compounds included, for example, N'-Nitrosonornicotine, 4-Hydroxystyrene, Pyrazinamide, Diethylcarbamazine, 2-Phenylbutyric acid, Benzaldehyde, 2,5-Dimethyl-3-mercaptotetrahydrofuran, Procainamide, 2,6-nonadienal, Pelargonaldehyde, Perillyl alcohol, Acetophenone, Hexanamide, 2-Propenyl propyl disulfide, 6-Chloroindole, 4-Heptyloxyphenol and 2-Mercaptobenzothiazole. Several mycotoxins, detected at low concentrations (Table 1), indicates that low volatile and nonvolatile compounds could be transported (be mobile) in the air via air moisture or as aqueous aerosols (Salo et al., 2019).

Table 1. Hazardous compounds (at low concentrations) found from the gas phase of the insulation materials at different temperatures. Sample 0.25 g. Amount of water added 0.5 mL.

Name	GHS Hazard	80°C	40°C	20°C
Aflatoxicol I	330,350,360	X		
Aflatoxin B1	330,340,350	X	X	X
Aflatoxin B2 a	330,350	X		
Aflatoxin G2 a	330,351	X		
Ochratoxin B	335	X	X	X
Fumonisin B2	330,335,351	X		
Fumonisin B1	351	X		
Cytochalasin A	330,361	X	X	
Cytochalasin H	330,361	X		
Cytochalasin D	361	X	X	X
Paxillin	331,335	X	X	
Antimycin A2	331	X		
Antimycin A1	331	X	X	
Apicidin	330	X		
1,3-Benzendiol	341,351	X		
Benzoic acid	372	X	X	X
Pyrogallol	341	X	X	X
Tyramine	335	X	X	
Kojic acid	351	X		
Baccatin III	335,350	X		

ACKNOWLEDGEMENTS

This work was supported by the Academy of Finland Centre of Excellence program (project no. 307331).

REFERENCES

- Fang L., Clausen G. and Fanger P.O. (1999). Impact of temperature and humidity on chemical and sensory emissions from building materials. *Indoor Air* **9**, 193-201.
- Markowicz P. and Larsson L. (2015). Influence of relative humidity on VOC concentrations in indoor air. *Environ. Sci. Pollut. Res.* **22**, 5772–5779.
- Nielsen K.F. and Smedsgaard J. (2003). Fungal metabolite screening: database of 474 mycotoxins and fungal metabolites for dereplication by standardised liquid chromatography–UV–mass spectrometry methodology. *Journal of Chromatography A* **1002**, 111–136.
- Rao, C. Y., Burge, H. A. and Chang, J. C. (1996) Review of quantitative standards and guidelines for fungi in indoor air. *Journal of the Air & Waste Management Association* **46**, 899-908.
- Salo M.J., Marik T., Mikkola R., Andersson M.A., Kredics L., Salonen H. and Kurnitski J. (2019). *Penicillium expansum* strain isolated from indoor building material was able to grow on gypsum board and emitted guttation droplets containing chaetoglobosins and communesins A, B and D. *Journal of Applied Microbiology* **127**, 1135-1147.
- Spengler, J. D., Samet, J. M. and McCarthy, J. F. (2001). *Indoor air quality handbook*, (McGraw-Hill Professional).
- The Human Microbiome Project Consortium, (2012). Structure, function and diversity of the healthy human microbiome. *Nature* **486**, 207-214.
- Wolkoff, P. (1998). Impact of air velocity, temperature, humidity, and air on long-term VOC emissions from building products. *Atmospheric Environment* **32**, 2659-2668.

SIMULATING URBAN SOIL CARBON DECOMPOSITION USING LOCAL WEATHER INPUT FROM A SURFACE MODEL

M. HAVU¹, L. KULMALA^{2,3}, A. RIIKONEN^{1,3}, T. VISKARI², and J. JÄRVI^{1,4}

¹Institute for Atmospheric and Earth System Research /Physics, University of Helsinki, Finland.

²Finnish Meteorological Institute, Helsinki, Finland.

³Institute for Atmospheric and Earth System Research /Forest, University of Helsinki, Finland.

⁴Helsinki Institute of Sustainability Science, University of Helsinki, Finland.

Keywords: SUEWS, URBAN, YASSO, SOIL

INTRODUCTION

There is a need to reduce carbon from the atmosphere due to climate warming. Cities in particular are interested to know ways to reduce their emissions and how much carbon could be sequestered by their own vegetation and soil. However, vegetation and soil in urban ecosystems can act very differently than in natural ecosystems and therefore, studies are needed to understand the biogenic carbon cycle in urban areas. In this study, the urban microclimate and biogenic carbon cycle through urban vegetation and soil is modelled using an urban land surface model SUEWS (Järvi et al., 2019) and the carbon storage in soil with carbon soil model Yasso (Liski et al., 2005). SUEWS is specially created to work in urban areas, whereas Yasso has been created for natural ecosystem and used also in agriculture (Karhu et al., 2012). Yasso has also been used before in urban areas in a general way (Rasinmäki et al., 2014) but in this study the purpose is to fine tune the model for urban areas. The first step is to evaluate both models in Viikki, Helsinki. Measurements of carbon dioxide and sap flow flux are going to be used to evaluate the carbon dioxide and evaporation components in the model SUEWS. Yasso is evaluated against soil carbon measurements.

METHODS

The surface Urban Energy and Water Balance Scheme (SUEWS, Järvi et al., 2011) is traditionally used to model energy and water balances in cities but now it includes also biogenic and anthropogenic carbon dioxide surface exchange. SUEWS has seven surface types: paved, buildings, evergreen trees/shrubs, deciduous trees/shrubs, grass, bare soil and water, that need to provide for the model as an input. It also needs other site specific characteristics such as building and tree heights. Common meteorological variables are used to force the model, such as, wind speed, wind direction, air temperature, pressure, precipitation and shortwave radiation. In this study, SUEWS is used to simulate biogenic carbon dioxide fluxes. Photosynthesis is estimated with empirical canopy-level model, which depends upon maximum photosynthesis, leaf area index, air temperature, specific humidity, soil moisture deficit and shortwave radiation (Järvi et al., 2019). Soil and vegetation respiration is simply estimated with its exponential relation to air temperature (Järvi et al., 2012).

The soil carbon model Yasso15 version (Järvenpää et al., 2019, In preparation) is used to simulate the stock of soil carbon and the changes in the amount of soil carbon in urban areas. Yasso has four groups that decompose at different rates: compounds soluble in ethanol (E), or in water (W), and compounds hydrolysable in acid (A) and neither soluble nor hydrolysable at all (N). The mass loss of these compounds depend on climate conditions, mainly temperature and precipitation. There is also a mass flow towards recalcitrant humus (H). Litter decomposition is based on a large litter bag dataset that has been gathered around the globe and it will not be altered in this study. The initial amount of carbon can be calculated from loss-on-ignition (LOI) that has been measured in the beginning of the study period. If the soil types are known, then the A, W, E, N and H classes can be further specified. Yasso is forced with local meteorology, but only with annual precipitation, annual temperature and its amplitude.

SUEWS is run over a 200x200 m² size area in two locations in Viikki, Helsinki (Riikonen et al., 2011) for years 2003-2016. The first year is a spin-up period and the others will be used for the model evaluation. The model is forced with meteorology primarily from Kumpula and secondarily from Helsinki-Vantaa Airport. Viikki has two test streets where they have studied intensely carbon and water fluxes (Riikonen et al., 2016, 2017) for 2002-2014. The parameters used in SUEWS photosynthesis model are based on leaf-level photosynthetic response measurements from street trees in Viikki in 2007-2009. The same parameters control also evaporation via stomatal conductance (Järvi et al., 2019). The modelled evaporation will be evaluated against sap flow measurements and modelled soil moisture against soil moisture observations.

Yasso model is evaluated against soil carbon (based on LOI) measurements. Soil carbon was measured at the beginning of the study period and later every few years (Riikonen et al., 2017) by taking soil samples. The model initialisation is possible because the soil type and structure are known when the trees were planted in 2002. Yasso requires air temperature data and this will be obtained from SUEWS which will provide the local 2 meter air temperature.

RESULTS

Using air temperature measured at Helsinki-Vantaa airport Yasso model compares well with the loss-on-ignition (LOI) measurements (Figure 1). The street was built in 2002, when the new soil contained a lot of carbon. Yasso is able to model the initial carbon loss and its subsequent stabilization well, with about a third of initial carbon remaining after 2005. The next step is to run SUEWS and evaluate it by comparing it against measurements. Finally, SUEWS will provide the local air temperature, which will be used to force Yasso.

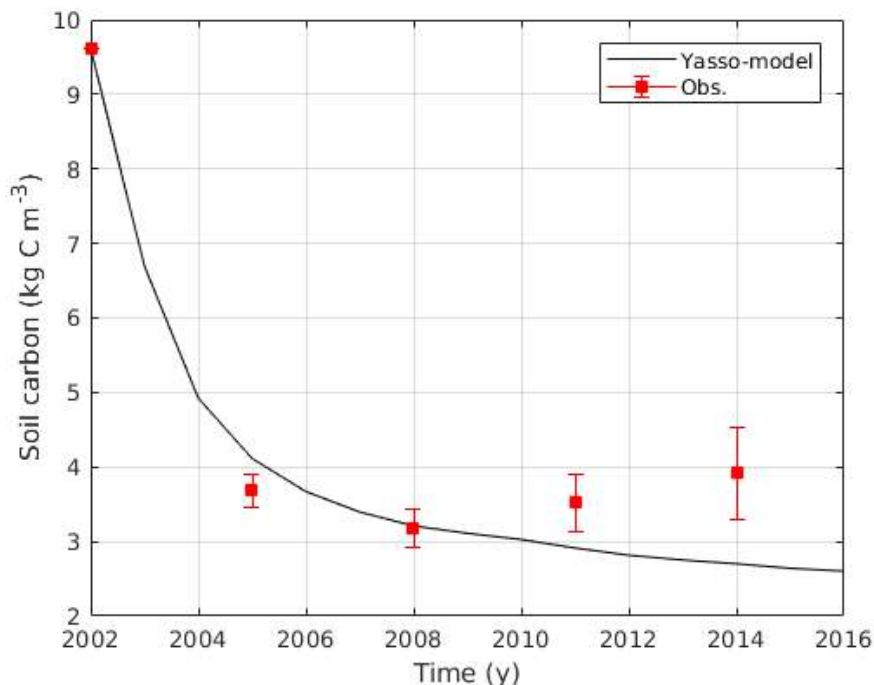


Figure 1. Modelled and measured average carbon stock in soil (\pm SD).

ACKNOWLEDGEMENTS

This work is supported by Tiina and Antti Herlin Foundation grant, the Academy of Finland the Center of Excellence programme (no. 307331), the Academy of Finland projects ICOS-Finland (no. 319871) and CarboCity (no. 321527).

REFERENCES

- Järvenpää, M., A. Repo, A. Akujärvi, M. Kaasalainen, and J. Liski. Soil carbon model Yasso15 - Bayesian calibration using worldwide litter decomposition and carbon stock data. Manuscript in preparation
- Järvi, L., C. Grimmond, and A. Christen (2011). The surface urban energy and water balance scheme (SUEWS): Evaluation in Los Angeles and Vancouver, *J. Hydrol.*, **411** (3-4), 219–237.
- Järvi, L., A. Nordbo, H. Junninen, A. Riikonen, J. Moilanen, E. Nikinmaa, and T. Vesala (2012). Seasonal and annual variation of carbon dioxide surface fluxes in Helsinki, Finland, in 2006–2010, *Atmos. Chem. Phys.*, **12**, 8475–8489.
- Karhu, K., A. I. Gärdenäs, J. Heikkinen, P. Vanhala, M. Tuomi, and J. Liski (2012). Impacts of organic amendments on carbon stocks of an agricultural soil—comparison of model-simulations to measurements. *Geoderma*, **189**, 606-616.
- Liski, J., T. Palosuo, M. Peltoniemi, and R. Sievänen (2005). Carbon and decomposition model Yasso for forest soils. *Ecological Modelling*, **189**(1-2), 168-182.
- Riikonen, A., L. Lindén, M. Pulkkinen, and E. Nikinmaa (2011). Post-transplant crown allometry and shoot growth of two species of street trees. *Urban forestry & urban greening*, **10**(2), 87-94.
- Riikonen, A., L. Järvi, and E. Nikinmaa (2016). Environmental and crown related factors affecting street tree transpiration in Helsinki, Finland. *Urban ecosystems*, **19**(4), 1693-1715.
- Riikonen, A., J. Pumpanen, M. Mäki, and E. Nikinmaa (2017). High carbon losses from established growing sites delay the carbon sequestration benefits of street tree plantings—A case study in Helsinki, Finland. *Urban forestry & urban greening*, **26**, 85-94.
- Rasinmäki, J and R. Känkänen (2014). Kuntien hiilitasekartoitus osa 1: Helsingin, Lahden, Turun, Vantaan ja Espoon maankäyttösektorin kasvihuonekaasupäästöt, hiilinielut ja hiilivarastot. *Helsingin kaupungin ympäristökeskus* **9**.

SEASONAL VARIATION IN ORGANIC AEROSOL COMPOSITION IN THE FINNISH BOREAL FOREST

L. HEIKKINEN¹, K. DÄLLENBACH¹, K. LUOMA¹, J. AALTO², P. RANTALA¹, D. WORSNOP^{1,3},
M. ÄIJÄLÄ¹, and M. EHN¹

¹Institute for Atmospheric and Earth System Research / Physics, University of Helsinki, Helsinki, Finland.

²Institute for Atmospheric and Earth System Research / Forest Sciences, University of Helsinki, Helsinki, Finland.

³Aerodyne Research Inc., Billerica, MA, USA.

Keywords: ORGANIC AEROSOL, AEROSOL CHEMICAL SPECIATION MONITOR (ACSM), POSITIVE MATRIX FACTORIZATION (PMF).

INTRODUCTION

During the last decades, a vast scientific effort has been targeted in organic aerosol (OA) research due to the large contribution of OA to the tropospheric particulate matter, worldwide (Jimenez et al., 2009). Due to the complexity of OA formation pathways and chemistry, many scientific questions have remained open especially regarding the role of OA in the Earth's climate system (Kanakidou et al., 2005; Shrivastava et al., 2017). Organic aerosol can be emitted directly in particulate form (primary organic aerosol, POA) from various sources such as fossil fuel combustion or biomass burning. Alternatively, it can form secondarily (secondary organic aerosol, SOA) in the atmosphere from condensable vapours. These condensable vapours are in turn yielded from atmospheric oxidation processes involving volatile organic compounds (VOCs) and atmospheric oxidants, such as ozone, hydroxyl and nitrate radicals. Biogenic VOCs are major SOA precursors. Monoterpenes represent a group of them that are of high importance in global biogenic SOA production. To help improve and constrain climate modelling efforts and understanding the aerosol sensitivity of our climate, comprehensive long-term high-quality observational data are of utmost importance. Furthermore, measurements in climate sensitive environments, such as the boreal forest, are critical (Kulmala, 2018). Detailed measurements regarding atmospheric composition are conducted at the Station Measuring Atmosphere – Ecosystem Relations (SMEAR II) that is located within the Finnish boreal forest (Hari and Kulmala, 2005). It serves as the measurement site for the current study from where we analysed eight years of on-line recorded OA mass spectra to gain better understanding of the seasonal trends in OA sources and composition aiming to narrow down the biogenic contribution of forest emissions to the OA loading. To our understanding, the data presented in this study represents the longest time series of OA composition ever recorded online in the boreal environment.

METHODS

The measurements were conducted utilizing on-line mass spectrometry with an Aerosol Chemical Speciation Monitor (ACSM, Aerodyne Research Inc., USA; Ng et al., 2011). The instrumentation provides a mass spectrum of non-refractory sub-micron aerosol chemical components every half an hour with a unit mass resolution. The measurements took place between March 2012 and September 2019. The mass spectra acquired represents the bulk mass spectra comprising of ion fragments produced in the instrument via aerosol flash vaporization (600 °C) and electron impact ionization (70 eV). Generally, the largest peaks obtained in ambient measurements are CO_2^+ (m/Q 44 Th) and $\text{C}_2\text{H}_3\text{O}^+$ (m/Q 43 Th). Their abundances in the mass spectrum can be used as a proxy of the degree of aerosol oxygenation (Aiken et al., 2006). Few ions recorded in the mass spectrum can be attributed with specific emissions. For example, relatively high C_4H_9^+ (m/Q 57 Th) signals have been generally detected in urban areas and can be associated with traffic emissions (Zhang et al., 2005). $\text{C}_2\text{H}_4\text{O}_2^+$ (m/Q 60 Th) on the other hand is a known ion resulting from levoglucosan fragmentation. It can be traced to biomass burning emissions (Alfarra et al., 2007).

We started the analysis by investigating the seasonal behaviour of known marker ions of m/Q 57 Th and m/Q 60 Th as well as the relationship between m/Q 44 Th and m/Q 43 Th. When an understanding of the general OA mass spectral seasonal variation was gained, we targeted for quantifying the contributions of different OA types to the total OA mass concentration. For this purpose, we utilized positive matrix factorization (PMF) with a multilinear engine (ME-2; Paatero, 1999). This sort of analysis enables extraction of a number of factors comprising of temporally correlating species. These factors contain information regarding their sources, chemical properties and atmospheric ageing. The PMF analysis was conducted with Source Finder (SoFi Pro, Datalystica, Switzerland; Canonaco et al., 2013) code package deployed in the Wavemetrics Igor Pro software.

CONCLUSIONS

The mass fraction of organic aerosol (OA) in the sub-micron particulate matter measured below the Finnish boreal forest canopy often exceeded 80% during summers and even during cold seasons, when the inorganic aerosol concentration was at highest, organics still made up nearly half of the aerosol mass. The sum of (anthropogenic) POA factors remained low throughout the year (mass fraction below 25%). The POA maximum was generally recorded in February. The main source of OA at SMEAR II could be attributed to the forest emissions. This fresh SOA mass concentration was highest at summer. More work is needed to connect the biogenic SOA to different formation pathways.

ACKNOWLEDGEMENTS

We acknowledge the Academy of Finland via Center of Excellence in Atmospheric Sciences (project no. 272041) and ERC-Stg COALA.

REFERENCES

- Jimenez, Jose L., et al. "Evolution of organic aerosols in the atmosphere." *Science* 326.5959 (2009): 1525-1529.
- Kanakidou, M., et al. "Organic aerosol and global climate modelling: a review." *Atmospheric Chemistry and Physics* 5.4 (2005): 1053-1123.
- Shrivastava, Manish, et al. "Recent advances in understanding secondary organic aerosol: Implications for global climate forcing." *Reviews of Geophysics* 55.2 (2017): 509-559.
- Kulmala, Markku. "Build a global Earth observatory." (2018): 21.
- Hari, P., and Kulmala, M. "Station for measuring ecosystem-atmosphere relations (SMEAR II)." *Boreal Environment Research* 10 (2005), 315-322.
- Ng, Nga L., et al. "An Aerosol Chemical Speciation Monitor (ACSM) for routine monitoring of the composition and mass concentrations of ambient aerosol." *Aerosol Science and Technology* 45.7 (2011): 780-794.
- Aiken, Allison C., et al. "O/C and OM/OC ratios of primary, secondary, and ambient organic aerosols with high-resolution time-of-flight aerosol mass spectrometry." *Environmental Science & Technology* 42.12 (2008): 4478-4485.
- Zhang, Qi, et al. "Hydrocarbon-like and oxygenated organic aerosols in Pittsburgh: insights into sources and processes of organic aerosols." *Atmospheric Chemistry and Physics* 5.12 (2005): 3289-3311.
- Alfarra, M. Rami, et al. "Identification of the mass spectral signature of organic aerosols from wood burning emissions." *Environmental science & technology* 41.16 (2007): 5770-5777.
- Paatero, Pentti. "The multilinear engine—a table-driven, least squares program for solving multilinear problems, including the n-way parallel factor analysis model." *Journal of Computational and Graphical Statistics* 8.4 (1999): 854-888.
- Canonaco, F., et al. "SoFi, an IGOR-based interface for the efficient use of the generalized multilinear engine (ME-2) for the source apportionment: ME-2 application to aerosol mass spectrometer data." *Atmospheric Measurement Techniques* 6.12 (2013): 3649-3661.

CARBON BALANCE AT TWO FINNISH AGRICULTURAL GRASSLANDS WITH CONSTRASTING SOIL TYPES

L. HEIMSCH¹, H. VEKURI¹, L. KULMALA^{1,2}, A. LOHILA^{1,2}, M. KORAKOSKI¹, O.
NEVALAINEN¹, J. RAINNE¹, T. MÄKELÄ¹, J. HATAKKA¹, J.-P. TUOVINEN¹, T. LAURILA¹ and J.
LISKI¹

¹ Finnish Meteorological Institute, Climate System Research, P.O. Box 503, FI-00101, Helsinki, Finland.

² Institute for Atmospheric and Earth System Research / Forest Sciences, Faculty of Agriculture and Forestry, University of Helsinki, Finland.

³ Institute for Atmospheric and Earth System Research / Physics, Faculty of Science, University of Helsinki, Finland.

Keywords: AGRICULTURE, CO₂ FLUXES, CLIMATE.

INTRODUCTION

Modern intensive agriculture is globally the second largest anthropogenic source of carbon emissions to the atmosphere, after industry and fossil fuel combustion, contributing more than 10% to the GHG emissions (Houghton & Nassikas 2017, Le Quéré et al. 2017, Lal 2016). Conventional intensive management practices are the main cause of high emissions in agriculture. Frequent ploughing, monocropping, intensive use of agrochemicals, and deforestation are the main contributors to the loss of soil organic matter and CO₂ emissions from land use. At the same time as modern agriculture is being a significant emission source, one of the most potential tools to mitigate climate change is the sequestration of carbon from the atmosphere into the agricultural soils (Minasny et al. 2017).

It is well known that topsoil layer and especially humus-rich mineral soils can store more carbon than atmosphere and vegetation together. Therefore, increasing the amount of SOM in the agroecosystems, by applying enhanced management practices such as no-tillage, high biodiversity and cover cropping, agricultural soils would not only help to mitigate climate change but also to restore soil quality and fertility (Jastrow et al. 2007, Yang et al. 2019). On the other hand, cultivation of peat soils is well known for causing net CO₂ emissions into the atmosphere. Methods to reduce these emissions are currently sought. To understand the carbon dynamics on different agricultural sites and to verify soil carbon and ecosystem models, continuous long-term monitoring of GHG fluxes is essential at such managed ecosystems.

METHODS

Continuous CO₂ flux measurements using Eddy covariance method have been conducted at Qvidja farm on mineral (clay) soil forage grassland in Parainen, southern Finland (60.29550°N, 22°39281°E) since the spring 2018. Another agricultural flux measurement site was established at peat soil grassland, in Ruukki, located in Siikajoki, western Finland (64.68399°N, 25.10632°E) in the summer 2019.

The size of the experimental field in Qvidja is about 16 ha, and it has been in agricultural use for decades. Past years, it has been cultivated under conventional management practices. However, since the beginning of the flux measurements, some of the carbon farming practices are applied more on the field. The field is mainly surrounded by forests in the northern, as well as eastern and western sides. In the south of the field, there is a wetland area covering about 15 ha. The field in Ruukki has also been in conventional agricultural

use, and forage grass is cultivated approximately on half of the experimental field which is about 25 ha. The whole field is peat soil with the depth varying from 0.4 to 0.7 m.

Eddy covariance (EC) measurements are conducted on both experimental sites with Li-7200 CO₂/H₂O analyser by LI-COR Inc. (Nebraska, US), which observes the CO₂ and H₂O mixing ratios, and an uSonic-3 Scientific anemometer by METEK GmbH (Bristol, UK), which measures the wind components and air temperature at the height of 2.30 m at both sites.

EC measurements are supported by meteorological observations right next to the flux towers. These include soil moisture measurements, and soil temperature at the depths of 0.05 m, 0.1 m and 0.3 m. Furthermore, global and reflected solar radiation and net radiation, as well as photosynthetically active radiation (PAR) are measured at both experimental sites. Also, precipitation, air temperature and humidity are continuously recorded. Further measurements in both locations include chamber measurements, leaf area index and other vegetation measurements, as well as biomass and soil sampling. Satellite data is also utilised in data analysis.

CONCLUSIONS

The annual carbon balance was estimated to be negative at the southern site i.e. the site acted as an overall sink of carbon even in the dry and hot year 2018. Calculations were based on the flux (Fig. 1) and biomass data. However, the seasonal CO₂ fluxes were greatly dependent on weather conditions and management options. Results from 2019 are still collected and analysed but it seems that the latter growing season accompanied with a bit higher precipitation and lower temperatures, as well as higher cutting height was more favorable for carbon uptake in Qvidja than 2018. Even though the nighttime CO₂ emissions were higher at the peat site compared to the mineral site, the carbon balance during the growing season 2019 seemed to be negative also there, i.e. the peat site acted also as a carbon sink especially during the warm season. After data analysis, the national potential to reduce the annual GHG emissions by enhancing carbon sequestration of grasslands will be further concerned based on these results.

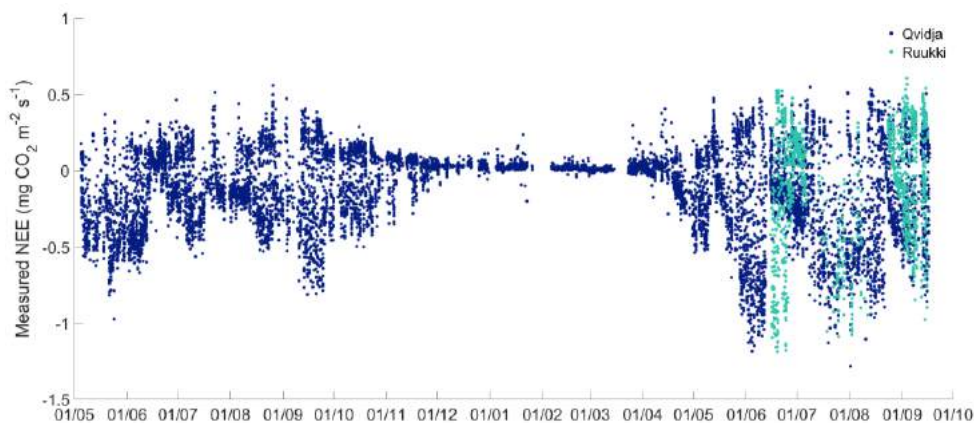


Figure 1. Measured NEE in Qvidja from the 3rd of May 2018 to the 15th of September 2019 and in Ruukki from the 13th of June 2019 to the 15th of September 2019. Negative values indicate net CO₂ uptake and positive values net CO₂ release.

ACKNOWLEDGEMENTS

SITRA, Business Finland, Strategic Research Council (SRC) at the Academy of Finland and the Finnish Centre of Excellence Programme by Academy of Finland are acknowledged for financial support.

REFERENCES

- Jastrow, J.D., Amonette, J.E., Bailey, V.L. (2007). Mechanisms controlling soil carbon turn-over and their potential application for enhancing carbon sequestration. *Climatic Change* 80, 5–23.
- Houghton, R.A., Nassikas, A.A. (2017). Global and regional fluxes of carbon from land use and land cover change 1850–2015. *Global Biochemical Cycles* 31, 456–472.
- Lal, R. (2016). Beyond COP21: Potential and challenges of the “4 per Thousand” initiative. *Journal of Soil and Water Conservation* 71, 20A–25A.
- Le Quéré, C. et al. (2017). Global Carbon Budget 2017. *Earth System Science Data Discussions*, 1–79.
- Yang, Y., Tilman, D., Furey, G., Lehman, C. (2019). Soil carbon sequestration accelerated by restoration of grassland biodiversity. *Nature Communications* 10, 718.

GREENHOUSE GAS EXCHANGE OF A SUBARCTIC FEN: VARIATION OF FOUR PLANT COMMUNITY TYPES DURING TWO CONTRASTING GROWING SEASONS

L. HEISKANEN¹, M. AURELA¹, J.-P. TUOVINEN¹, T. VIRTANEN², S. JUUTINEN², A. RÄSÄNEN², T. PENTTILÄ³, T. LAURILA¹

¹Finnish Meteorological Institute, Helsinki, Finland

²Department of Environmental Sciences, University of Helsinki, Finland

³Natural Resources Institute Finland (LUKE), Helsinki, Finland

Keywords: GREENHOUSE GAS, FLUX, FEN, MICROTOPOGRAPHY

INTRODUCTION

Current global warming is causing arctic regions to warm two to three times faster than the rest of the world (IPCC 1.5°C Special report, 2018). The northern peatlands form one of the largest carbon pools in the biosphere and the release of the stored carbon stays low because of the cold and wet climatic conditions, but as the climate warms these conditions could change (Tarnocai et al. 2009). If this happens, more of the stored organic carbon can be released into the atmosphere, which in turn would enhance the warming, thus creating a positive feedback loop. Therefore, understanding the carbon cycle processes of the northern peatlands is crucial for estimating the future climate scenarios.

The ecosystem-atmosphere exchange of CO₂ and CH₄ were measured using both eddy covariance (EC) and chamber methods on a subarctic fen in Kaamanen, northern Finland, during 2017 and 2018. During 2018 a drought period affected the fen ecosystem in July-August, which introduced an opportunity to compare normal 2017 growing season to more extreme climate conditions.

The measurements were conducted as part of CAPTURE-project (Carbon dynamics across Arctic landscape gradients: past, present and future). The objective of the continuous eddy covariance flux measurements was to assess the mean greenhouse gas (GHG) balances of the fen in an ecosystem scale, while the manual chamber measurements were used for estimating the growing season GHG exchange separately for the ecosystem's four main plant community types (PCTs).

METHODS

The Kaamanen mesotrophic flark fen (N69°8.435', E27°16.189', 155 m a.s.l.) has varying hummock and hollow microtopography that comprises of four main plant communities (Maanavilja et al., 2011): 1) Ericales-Pleurozium community grows on top of the dry hummocks and 2) *Betula nana*-Sphagnum grows on the hummock margins. The wet hollows are dominated by 3) *Trichophorum tussocks* and 4) *Carex-Scorpidium* communities. These four plant communities vary in their appearance due to the differences in moisture conditions, water table level (WTL) and nutrient availability, and they also vary notably in their GHG exchange.

The EC method provides continuous data from the entire fen ecosystem, while the flux chamber measurements add more detailed information about the plant community carbon dynamics. The EC measurement system at 5 m measurement height consisted of a sonic anemometer (METEK USA-1), a CO₂ analyzer (LI-COR LI-7000) and a CH₄ analyzer (LGR RMT-200), while the manual chamber flux measurements were conducted with Picarro G2401 gas analyzer.

Vegetation types were mapped in detail around the fen EC tower fetch area during both growing seasons. The mapping consisted of plant species coverage observations, soil sample collection and pH measurements along transects. Drone imaging of the plant communities and land cover types were also conducted during the growing seasons.

RESULTS AND CONCLUSIONS

The growing season at the Kaamanen fen started in the end of May 2018 which was a few weeks earlier than in 2017. The growing season 2018, especially July, was warmer and drier than in 2017. The water table level measured at the fen dropped 10 to 15 cm in all plant communities during the 2018 drought period compared to the previous year.

The differences in carbon dynamics between the PCTs of the fen were quite evident, which can be seen from the chamber measurements (Figure 1). The water table level gradient from the wet flarks (average WTL: +2 cm) to dry string tops (average WTL: -50 cm) largely controls the vegetation composition and consequent carbon fluxes.

The CO₂ respiration (R) and gross primary productivity (GPP) were smallest in the wet plant communities and largest in the dry ones (Figure 1). However, the net ecosystem exchange (NEE) was much smaller in magnitude than R and GPP in all PCTs. In 2018 R and GPP were larger in all plant communities. The NEE of the drier communities shifted to a sink or a smaller source in 2018, and vice versa for the wet communities, however the uncertainties were noticeable. The CH₄ emissions were smallest on top of the dry strings, while the other three plant communities had quite similar fluxes, but the emissions decreased slightly from 2017 to 2018.

The annual cumulative carbon balance, inferred from the fluxes measured by the EC method, of the Kaamanen fen was $-0.1 \pm 3.8 \text{ g C m}^{-2} \text{ yr}^{-1}$ in 2017 and $1.3 \pm 2.7 \text{ g C m}^{-2} \text{ yr}^{-1}$, when both CO₂ and CH₄ fluxes were taken into account (Figure 2). In 2017 the annual cumulative CO₂ flux added up to $-8.5 \pm 1.9 \text{ g C m}^{-2} \text{ yr}^{-1}$, while the annual cumulative CH₄ flux was $8.4 \pm 1.9 \text{ g C m}^{-2} \text{ yr}^{-1}$. In 2018 the annual cumulative CO₂ flux was slightly smaller $-5.6 \pm 1.2 \text{ g C m}^{-2} \text{ yr}^{-1}$, and likewise the annual cumulative CH₄ flux was smaller $6.9 \pm 1.5 \text{ g C m}^{-2} \text{ yr}^{-1}$. On average Kaamanen fen has been a CO₂ sink of $-21.5 \text{ g C m}^{-2} \text{ yr}^{-1}$, during 1997-2002 (Aurela et al., 2004), and a CH₄ source of $6.0 \text{ g C m}^{-2} \text{ yr}^{-1}$ during 2010-2017 (data not published).

The annual carbon balance of the fen in 2018 was affected by the earlier onset of photosynthesis in spring, which increased the annual sink, and the drought event that in turn decreased the carbon sink.

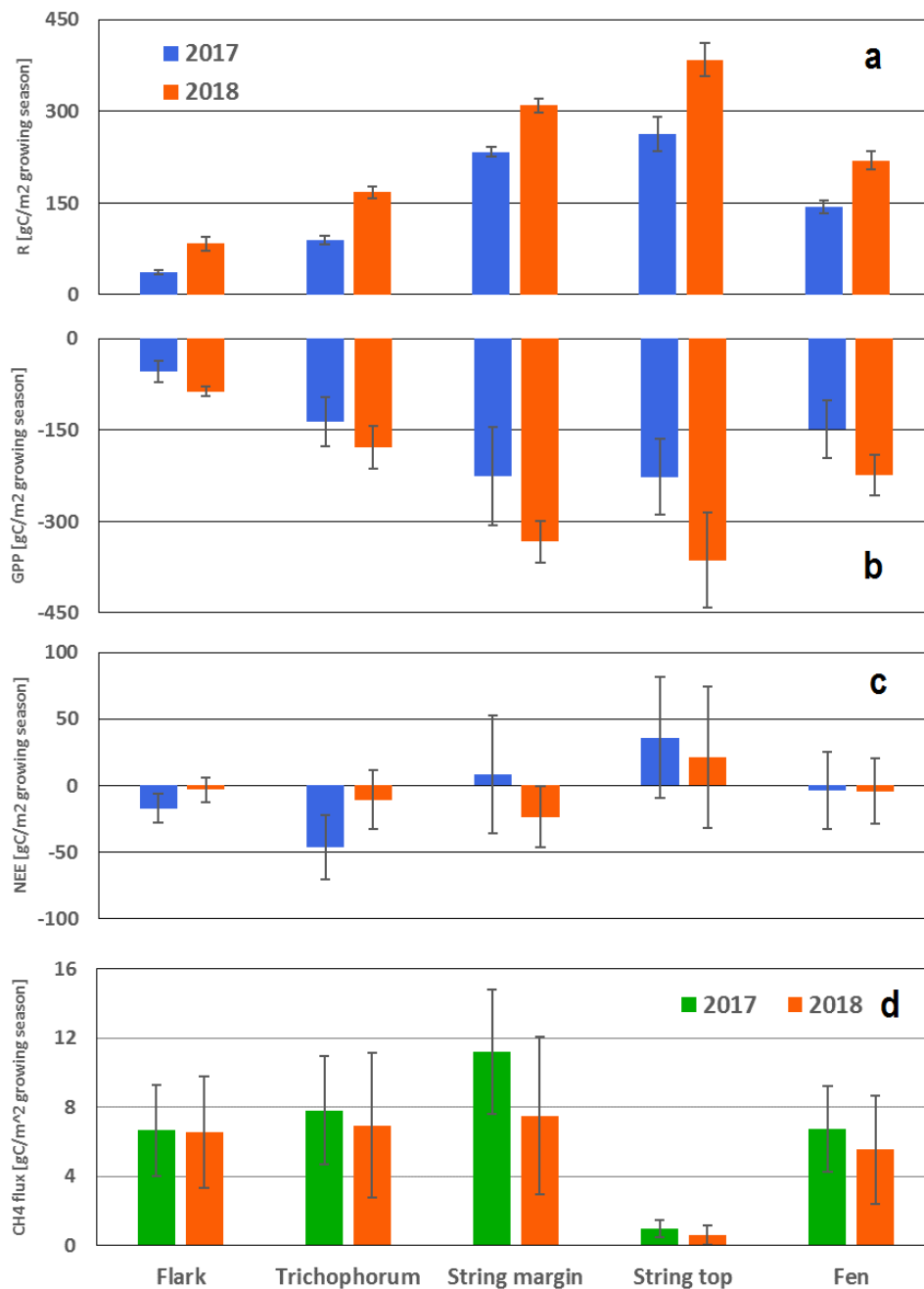


Figure 1: Growing season carbon fluxes of the plant communities and fen from chamber measurements: respiration (a), gross primary productivity (b), net ecosystem exchange (c) and methane flux (d). Negative values indicate carbon sink from the atmosphere to the ecosystem. The whiskers represent the standard deviation among the four replicates of each plant community type.

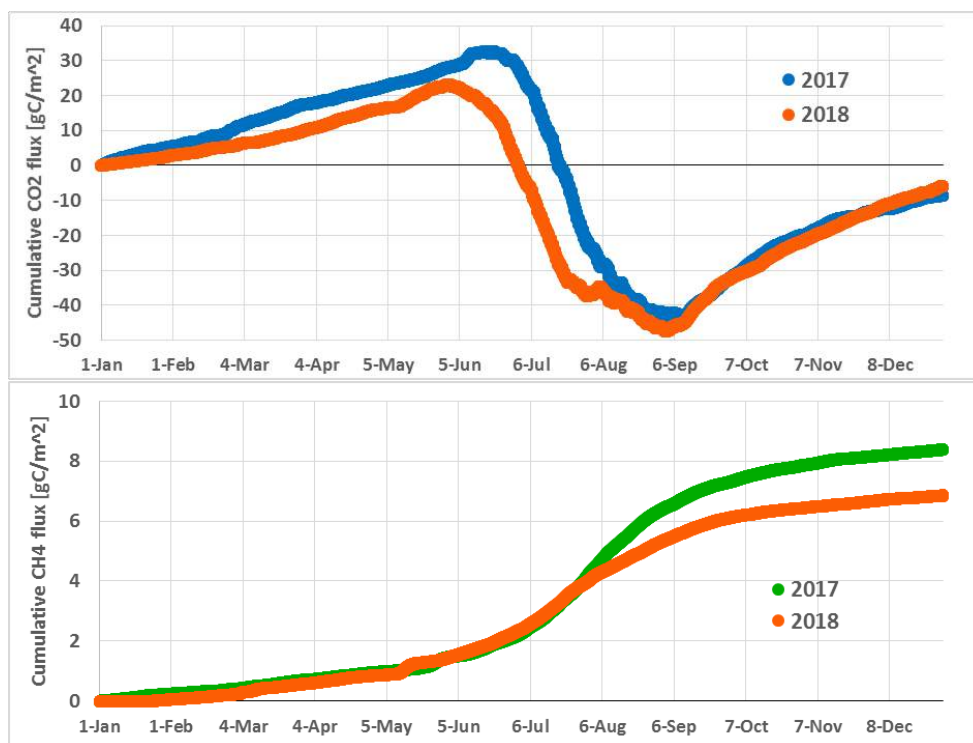


Figure 2: Cumulative CO₂ (top) and CH₄ (bottom) fluxes measured at the fen with EC method.

ACKNOWLEDGEMENTS

This work was supported by the Finnish Academy *CAPTURE-project (Carbon dynamics across Arctic landscape gradients: past, present and future)* Grant no. 296423 and Academy of Finland Centre of Excellence program (project number 307331).

REFERENCES

- Aurela, M., Laurila, T. and Tuovinen, J.-P. 2004. The timing of snow melt controls the annual CO₂ balance in a subarctic fen. *Geophys. Res. Lett.* 31, L16119, doi:10.1029/2004GL020315.
- IPCC, 2018: Global Warming of 1.5°C. An IPCC Special Report on the impacts of global warming of 1.5°C above pre-industrial levels and related global greenhouse gas emission pathways, in the context of strengthening the global response to the threat of climate change, sustainable development, and efforts to eradicate poverty [Masson-Delmotte, V., P. Zhai, H.-O. Pörtner, D. Roberts, J. Skea, P.R. Shukla, A. Pirani, W. Moufouma-Okia, C. Péan, R. Pidcock, S. Connors, J.B.R. Matthews, Y. Chen, X. Zhou, M.I. Gomis, E. Lonnoy, T. Maycock, M. Tignor, and T. Waterfield (eds.)]. In Press.
- Maanavilja, L., Riutta, T., Aurela, M., Pulkkinen, M., Laurila, T., Tuittila, E-T. 2011. Spatial variation in CO₂ exchange at a northern aapa mire. *Biogeochemistry* 104:325–345.
- Tarnocai C et al. 2009. Soil organic carbon pools in the northern circumpolar permafrost region. *Glob Biogeochem Cycl* 23.

A MODEL TO STUDY THE EFFECTS OF PARTICLE PHASE REACTIONS TO PARTICLE'S SIZE AND COMPOSITION EVOLUTION

A. HEITTO¹, C. MOHR², K. LEHTINEN^{1,3} and T. YLI-JUUTI¹

¹Department of Applied Physics, University of Eastern Finland, Finland

²Department of Environmental Science and Analytical Chemistry, Stockholm University, Sweden.

³Finnish Meteorological Institute, Kuopio, Finland

Keywords: MABNAGO, OLIGOMERIZATION, DECOMPOSITION

INTRODUCTION

Many physical and chemical reactions take place in secondary organic aerosol particles (SOA) in the atmosphere, changing the properties, composition and potentially reflecting to changes in particle size. Among these reactions is oligomerization, where monomers combine forming bigger oligomer molecules. Studies have shown, that oligomers can cover a notable fraction of SOA particle's mass (Denkenberger et al., 2007; Dommen et al., 2006). The formed oligomers tend to be less volatile than the monomers they are formed from and thus through oligomerization also the volatile monomer compounds, that would usually mostly stay in the gas phase, can contribute to the growth of SOA particles. Also, the reverse process where larger molecules decompose to smaller ones can happen and the resulting molecules may evaporate from the particle due to their higher volatility. To study how these two processes, oligomerization and decomposition, affect particle size evolution in the atmosphere, we are developing models that describe these processes in addition to particle phase acid-base chemistry.

METHODS

We are simultaneously developing two different models. MABNAGO (Model for Acid-Base chemistry in Nanoparticle Growth with Oligomerization) which is developed further from MABNAG (Model for acid-base chemistry in nanoparticle growth, Yli-Juuti et al. 2013), is a monodisperse particle population growth model that uses concentrations of condensing gases, RH, ambient temperature and preset oligomerization and decomposition rates to calculate the time evolution of particle's composition and size. The model also considers the dissociation and protonation between acids and bases in the particle phase using Extended Aerosol Inorganics Model (E-AIM; Clegg and Seinfeld, 2006a, b) In the model water and bases are assumed always to be in equilibrium state between gas and particle phase. Mass fluxes of other compounds to and from the particles are determined based on their gas phase concentrations and their dissociation and composition dependent equilibrium vapor concentrations, solved with E-AIM.

The other model is mostly similar to MABNAGO, with the exception of not using E-AIM to calculate acid-base chemistry. Instead no organic acids or bases are included and the amount of inorganic bases is assumed to be equal to the amount of inorganic acids in the particle. As E-AIM is not included in this second model, we assume an ideal mixture when calculating equilibrium vapor pressures of the organic vapors.

At the moment the model system can consist of water, ammonia, sulfuric acid, nitric acid and multiple organic compounds, their number varying between simulations. The condensing organic compounds can include amines as well as organic compounds that can be assigned as acids, oligomer forming monomers, decomposing compounds or non-reactive compounds. The initial composition of the particles in simulations is 40 sulfuric acid molecules and corresponding amount of water and ammonia. With this setting the initial diameter is approximately 2 nanometers. The properties of the organic model

compounds are specified based on Chemical Ionization Mass Spectrometry (CIMS) measurements from the Hyytiälä measurement station (Mohr et al., 2019) presented with volatility basis set (VBS). The number of model compounds that are affected by oligomerization and/or decomposition is varied between simulations. With these simulations we aim to investigate how much particle growth could be affected by particle phase reactions and how the extent of such possible effects compares to the uncertainties in measured gas phase concentrations and estimated saturation vapor concentrations of condensing organic compounds.

RESULTS

In Figure 1 we present an example from our particle growth simulations. In these simulations, the condensing compounds included four non-reactive compounds and two semi-volatile compounds that could form a low-volatile compound through oligomerization and the bulk phase oligomerization. The oligomerization rates were varied between the simulations. These results suggest that oligomerization can affect particle growth significantly.

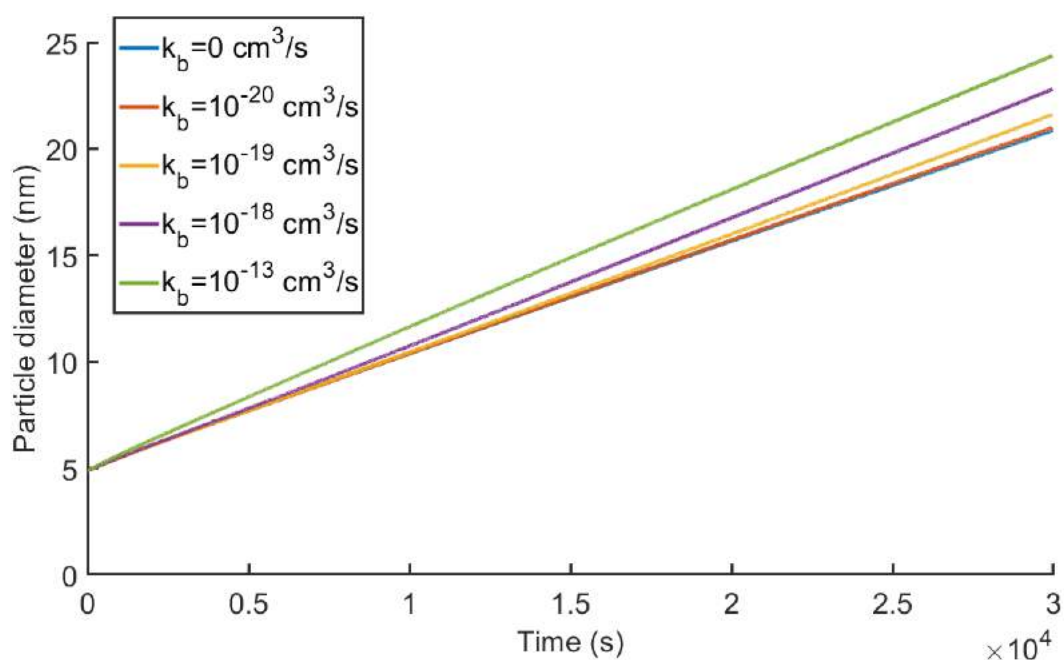


Figure 1. Diameter of a particle as a function of time in simulations where the condensing compounds included two semi-volatile compounds that could form a low-volatile compound in the particle phase through oligomerization. Five simulations with different bulk phase oligomerization rates (k_b) are shown.

ACKNOWLEDGEMENTS

This work was supported by the Academy of Finland Center of Excellence programme (grant no. 307331) and the Academy of Finland (project no. 299544).

REFERENCES

- Denkenberger K., Moffet R., Holecek J., Rebotier T., and Prather K. (2007), Real-Time, Single-Particle Measurements of Oligomers in Aged Ambient Aerosol Particles, *Environ. Sci. Technol.*, **41**, 5439-5446.

- Dommen J., Metzger A., Duplissy J., Kalberer M., Alfarra M. R., Gascho A., Weingartner E., Prevot A. S. H., Verheggen, B., and Baltensperger U. (2006). Laboratory observation of oligomers in the aerosol from isoprene/NO_x photooxidation, *Geo. Phys. Res. Lett.*, **33**, L13805.
- Yli-Juuti T., K. Barsanti, L. Hildebrandt Ruiz, A.-J. Kieloaho, U. Makkonen, T. Petäjä, T. Ruuskanen, M. Kulmala, and I. Riipinen (2013). Model for acid-base chemistry in nanoparticle growth (MABNAG), *Atmos. Chem. Phys.*, **13**, 12507–12524.
- Clegg, S. L. and J. H. Seinfeld (2006a). Thermodynamic models of aqueous solutions containing inorganic electrolytes and dicarboxylic acids at 298.15 K. 1. The acids as non-dissociating components, *J. Phys. Chem. A*, **110**, 5692–5717.
- Clegg, S. L. and J. H. Seinfeld (2006b). Thermodynamic models of aqueous solutions containing inorganic electrolytes and dicarboxylic acids at 298.15 K. 2. Systems including dissociation equilibria, *J. Phys. Chem. A*, **110**, 5718–5734.
- Mohr C., Thornton J. A., Heitto A., Lopez-Hilfiker F. D., Lutz A., Riipinen I., Hong J., Donahue N. M., Hallquist M., Petäjä T., Kulmala M. and Yli-Juuti T. (2019). Molecular identification of organic vapors driving atmospheric nanoparticle growth, *Nature Communications*, **10**, 4442.

ANALYSIS OF TERPENOIDS BY THERMAL DESORPTION-GAS CHROMATOGRAPHY-MASS SPECTROMETRY: A CASE STUDY OF DITERPENES

A. HELIN¹, H. HAKOLA¹ and H. HELLÉN¹

¹Atmospheric Composition Research, Finnish Meteorological Institute, Helsinki, FI-00101, Finland

Keywords: DITERPENES, TERPENOIDS, EMISSIONS.

INTRODUCTION

During the past decades, terpenoids have been studied quite intensively in boreal forest areas. Most previous studies have focused on isoprene (C₅), monoterpenoids (C₁₀, MTs) and sesquiterpenoids (C₁₅, SQTs), however, there are no studies on diterpenoids (C₂₀, DTs) in ambient air or in enclosure emissions in boreal areas. In recent years, DTs have been observed e.g. in ambient air in Amazon and in Japan (Matsunaga et al., 2012; Yee et al., 2018), and in branch enclosure emissions in the Mediterranean (Haberstroh et al., 2018; Yáñez-Serrano et al., 2018).

Diterpenes have been observed in essential oil samples of typical boreal forest trees, such as Norway spruce and Scots pine (Kanerva et al., 2008), thus it could be speculated that these compounds might be present also in the gas phase. However, DTs are very low volatile and very reactive compounds, which might make their analysis challenging. Few studies that have detected DTs in gaseous samples have used e.g. sorbent tubes for sampling prior to thermal desorption (or solvent desorption) - gas chromatography mass - spectrometry (TD-GC-MS) (Haberstroh et al., 2018; Matsunaga et al., 2012; Yáñez-Serrano et al., 2018). However, those studies did not present any detailed information about method validation or performance parameters, making it difficult to evaluate the suitability of the methods for the analysis of DTs.

In this study, a thermal desorption-gas chromatography-mass spectrometry (TD-GC-MS) method following sorbent tube sampling was developed for the determination of monoterpenoids (MTs), sesquiterpenoids (SQTs) and diterpenoids (DTs) in branch enclosure emissions. The method development and performance related experiments included, for example, desorption efficiency, sampling recovery and ozone reactivity tests. In addition, dynamic headspace sampling of terpenoids emitted from spruce twigs and pine needles was studied under laboratory conditions.

METHODS

The analytes included in the standards consisted of nine MTs, six SQTs, three DTs and three other VOCs. Only three commercially available DTs (ent-kaurene, cembrene and 3-methylene-5- α -androstane (MA)) could be obtained for this study.

The stainless-steel multiphase adsorbent (Tenax TA/Carbopack B) tubes used in this study were either purchased directly from PerkinElmer Inc. (Waltham, MA, USA) or prepared manually in the laboratory. With these sorbent tubes, the sampling flow rate used throughout this study was typically 80-100 mL/min.

The analyses were performed by using TD-GC-MS. The TD-GC-MS consisted of an automatic TD unit (TurboMatrix 350) connected to a GC (Clarus 680) coupled to a quadrupole MS (Clarus SQ 8 T), all units purchased from PerkinElmer Inc. (Waltham, MA, USA). The cold trap in TD and column in GC were Tenax TA/Carbopack B and Elite-5MS (60 m x 0.25 mm, film thickness 0.25 μ m), respectively (both from PerkinElmer Inc., Waltham, MA, USA). In the primary desorption, the sorbent tube was desorbed for 5 min at 300 °C at a flow rate of 50 mL/min of helium. The desorbed compounds were trapped into a cold trap held at 20 °C during the primary desorption. In the secondary desorption, the cold trap was rapidly heated to 300 °C and held for 1 min. The GC oven temperature program was as follows: 60 °C (held for 2 min),

then to 300 °C at 8 °C/min and 300 °C (held for 15 min). In MS, electron ionization at 70 eV was used. Total ion chromatogram (TIC) was scanned in *m/z* range 50-350 and selected ion recording (SIR) time windows with quantifier and qualifier ions were applied for the target analytes.

The method development and validation tests included e.g. desorption efficiency, sampling recovery and ozone reactivity tests. Desorption efficiency was tested by performing two consecutive desorptions from the same analyte loaded (*c*=40-200 ng) sorbent tube. The sampling recovery was tested with two different inlet lines (a 15 m long Teflon tubing (i.d. 1/8 in.) and a 1 m long heated stainless steel tube (i.d. 1/16 in., heated to ca. 150 °C)) and with a branch enclosure cuvette (a ca. 6.2 L Teflon bag). The experimental setup used in sampling recovery tests was similar as in Hellén et al. (2012). The main flow rate in inlet sampling line recovery tests was 1.0 L/min. In the cuvette recovery tests, three different flow rates were tested (1.0, 2.0 and 6.7 L/min). The ozone reactivity tests were done by loading sorbent tube with analytes (*c*=40-200 ng) and by purging the tube with 0-24 L of either 0 ppb or 40 ppb of ozone.

The real sample application test was a dynamic headspace sampling of compounds emitted by Scots pine needles or Norway spruce twigs in a closed flow-through chamber upon heating. The plant material samples were heated in 5-10 °C step from 30 to 70 °C. The results were handled with focus on DTs. The unknown compounds in samples were identified based on both retention index (RI) values and mass spectra comparison to NIST mass spectra database and/or Adams (2007) library. The non-target compounds were quantified in relation to standard analytes.

CONCLUSIONS

The first steps in the TD-GC-MS method development were to verify the desorption efficiency and the chromatographic separation of the terpenoids. The desorption efficiency was $\geq 99.8\%$ for all compounds at 300 °C for 5 min. The chromatographic separation of all analytes was considered to be adequate since the peaks were baseline separated.

The analytical method validation results were considered to be adequate. The intermediate precision (*n*=22 during 4.5 months period) was acceptable for all compounds (*RSD*<10%). The expanded measurement uncertainty with 95% confidence level varied between 17-40%, which was considered to be fit-for-purpose. The limit-of-quantification (LOQ) values (expressed as absolute amount in sorbent tube) were the lowest for monoterpenoids (13-88 pg) and for sesquiterpenes (33-198 pg), and the highest for caryophyllene oxide (340 pg) and diterpenes (287-518 pg). If assuming a sample volume of 5 L in offline sampling, the LOQ values were approximately 0.5-2.8 pptv for MTs, 0.8-7.5 pptv for SQTs and 5.1-9.3 pptv for DTs.

The sampling recovery results are shown in Fig. 1. The recoveries were acceptable (within 100±20%) for all compounds and with both inlet lines tested (Fig. 1a). For example, with the 1 m long heated stainless steel (SS) line, the recoveries of MTs, SQTs and DTs were on average 89±1%, 88±2%, 86±1%, respectively. Also, the cuvette recoveries were acceptable for MTs and SQTs with all flow rates tested (Fig. 1b). The recoveries of DTs were acceptable in the flow rate range of 2.0-6.7 L/min, but with the lowest flow rate tested the residence time inside the cuvette was too long for these compounds (Fig. 1b). Collectively, the sampling recovery results were promising as they indicated that typical inlet line and cuvette materials can be used also with DTs.

Since some terpenoids are highly reactive towards ozone and the ozone reaction rate coefficients (*k*_{O₃}) of DTs are highly uncertain, experiments focusing on analyte stability upon ozone exposure were conducted. The O₃=0 ppb tests were done for obtaining a reference level and the O₃=40 ppb tests in order to estimate the possible losses caused by ozone. Overall, the results were reasonable in the sense that the compounds that had the greatest reported *k*_{O₃} values were subsequently lost the fastest. However, the results also indicated that the literature *k*_{O₃} values of some DTs might be underestimated. For example, as can be seen in Fig. 2, the decline in slope was more rapid as the *k*_{O₃} increased in the order of camphene, limonene and caryophyllene, however, ent-kaurene *k*_{O₃} value is somewhat lower than would be expected based on the slope decline. Based on results obtained from literature retrieved ln(*k*_{O₃}) values plotted as a function of the

slopes obtained from the ozone purging experiments, the estimated experimental k_{O_3} value for ent-kaurene was $(1.4 \pm 8.2) \times 10^{-15}$. This was roughly two orders of magnitude higher than the literature k_{O_3} value (see Fig. 2), which demonstrates that the ozone reactivity contribution of DTs might be underestimated.

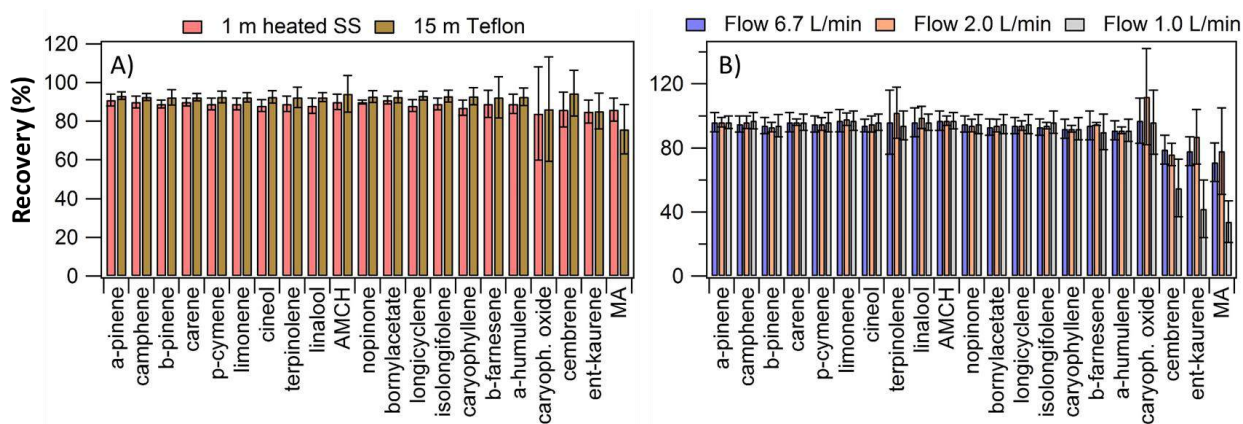


Figure 1. The sampling recovery experiment results from a) the inlet lines and b) the cuvette bag. The error bars represent reproducibility ($n=3-9$).

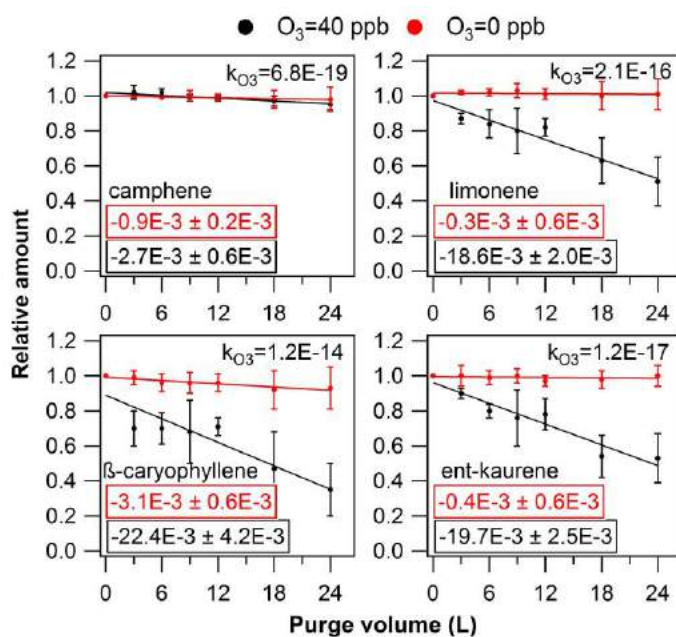


Figure 2. Selected examples from the ozone exposure experiments presented as relative amount of compound in sorbent tube as a function of purge volume. The values in boxes are the linear regression fit slopes (\pm uncertainty) of corresponding conditions (either $O_3=0$ or $O_3=40$ ppb). The compound specific literature k_{O_3} values are presented in the plots as well. The error bars represent reproducibility ($n=3$).

Multiple diterpenes could be detected in the emissions from pine needles and spruce twigs. However, these were detected mainly at the highest temperatures tested and eventually in quite low concentrations. In emissions from spruce twigs, 13 DTs and one unidentified compound ($C_{19-20}H_{28-30}$) were detected. In emissions from pine needles, five DTs and eight other similar high molecular weight compounds ($C_{18-20}H_{26-32}O_{0-2}$) were detected. Collectively, the identified compounds in these samples included e.g. rimuene, cembrene, sandaracopimaradiene, 13-epi-manool oxide and abietadiene.

Emission rate coefficients were calculated in order to evaluate the relative amount of DTs emitted in comparison to MTs and SQTs (Fig. 3). These results are semi-quantitative and the uncertainties are high.

At 30 °C, the emission rates of DTs were approximately one-to-three orders of magnitude lower than those of MTs and SQTs. The emission rates increased as the temperature was increased and at 60 °C, the emission rates of DTs were only 5-to 42-fold lower than those of MTs and SQTs. In relative terms, the increase in DTs emissions was more drastic than the increase in MTs and SQTs emissions as the temperature increased.

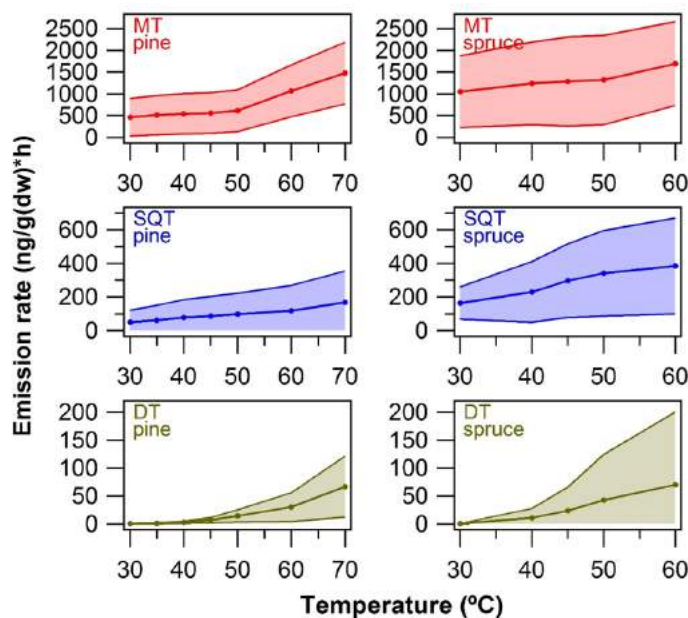


Figure 3. Terpenoid semi-quantitative emission rates (average \pm standard deviation) from pine needles and spruce twigs as a function of oven temperature in the dynamic headspace extraction experiments.

ACKNOWLEDGEMENTS

This work was supported by the Academy of Finland project (no. 316151) and Academy of Finland via the Center of Excellence in Atmospheric Sciences (grant no. 307331).

REFERENCES

- Adams, R.P. (2007). *Identification of essential oil components by gas chromatography/mass spectrometry*, (Allured Publishing Corporation Carol Stream, IL).
- Haberstroh, S., Kreuzwieser, J., Lobo-do-Vale, R., Caldeira, M.C., Dubbert, M. and Werner, C. (2018). Terpenoid emissions of two Mediterranean woody species in response to drought stress. *Front. Plant Sci.* **9**, 1071.
- Hellén, H., Kuronen, P. and Hakola, H. (2012). Heated stainless steel tube for ozone removal in the ambient air measurements of mono- and sesquiterpenes. *Atmos. Environ.* **57**, 35.
- Kanerva, S., Kitunen, V., Loponen, J. and Smolander, A. (2008). Phenolic compounds and terpenes in soil organic horizon layers under silver birch, Norway spruce and Scots pine. *Biology and Fertility of Soils* **44**, 547.
- Matsunaga, S.N., Chatani, S., Nakatsuka, S., Kusumoto, D., Kubota, K., Utsumi, Y., Enoki, T., Tani, A., and Hiura, T. (2012). Determination and potential importance of diterpene (kaur-16-ene) emitted from dominant coniferous trees in Japan. *Chemosphere* **87**, 886.
- Yáñez-Serrano, A., Fasbender, L., Kreuzwieser, J., Dubbert, D., Haberstroh, S., Lobo-do-Vale, R., Caldeira, M. and Werner, C. (2018). Volatile diterpene emission by two Mediterranean Cistaceae shrubs. *Scientific Reports* **8**, 6855.
- Yee, L.D., Isaacman-VanWertz, G., Wernis, R.A., Meng, M., Rivera, V., Kreisberg, N.M., Hering, S.V., Bering, M.S., Glasius, M., Upshur, M.A., Gray Bé, A., Thomson, R.J., Geiger, F.M., Offenberger, J.H., Lewandowski, M., Kourtchev, I., Kalberer, M., de Sá, S., Martin, S.T., Alexander, M.L., Palm, B.B., Hu, W., Campuzano-Jost, P., Day, D.A., Jimenez, J.L., Liu, Y., McKinney, K.A., Artaxo, P., Viegas, J., Manzi, A., Oliveira, M.B., de Souza, R., Machado, L.A.T., Longo, K. and Goldstein, A.H. (2018). Observations of sesquiterpenes and their oxidation products in central Amazonia during the wet and dry seasons. *Atmos. Chem. Phys.* **18**, 10433.

EMISSIONS AND AMBIENT CONCENTRATIONS OF ISOPRENE AND MONO- AND SESQUITERPENES AT A SUB-ARCTIC WETLAND

H. HELLÉN¹, S. SCHALLHART¹, A.P. PRAPLAN¹, T. TYKKÄ¹, M. AURELA¹, A. LOHILA^{1,2} and H. HAKOLA¹

¹Finnish Meteorological Institute, P.O. Box 503, 00101 Helsinki, Finland

²Institute for Atmospheric and Earth System Research

INTRODUCTION

Wetlands cover an area of about 2% of the total land surface area of the world and are most common in the boreal and tundra zones. More than half of the global wetlands are in the Far North. Northern wetlands are important sinks for carbon dioxide and sources of methane, but knowledge on their volatile organic compound (VOC) emissions is very limited. Currently we know that northern wetlands are high isoprene emitters (Janson and Serves, 1998; Haapanala *et al.*, 2006; Hellén *et al.*, 2006; Holst *et al.*, 2010), but very little is known about the physiological and environmental regulations of isoprene fluxes especially in colder subarctic environments and even less is known on the emissions of other VOCs. We have studied VOC emissions and their ambient concentrations at a sub-Arctic wetland (Lompolojänkämä), which is an open, nutrient-rich sedge fen (Lohila *et al.*, 2015), and a part of the Pallas-Sodankylä Global Atmosphere Watch (GAW) station.

METHODS

The emission measurement setup consisted a 60 x 60 x 25 cm FEP chamber, which was flushed with 4 L min⁻¹ of VOC-free air. For in situ analysis, the VOC samples were collected directly into a cold trap of the thermal desorptor - gas chromatograph - mass spectrometer (TD-GC-MS) via a 21 m heated fluorinated ethylene propylene (FEP) tubing for 30 min every two hour in May-June and every hour in July. Offline samples were taken in the end of July using Tenax TA/Carbopack B adsorbent tubes and samples were analysed later in the laboratory of the Finnish Meteorological Institute. Three different stainless steel frames located close to the measurement cabin in the middle of the fen were used for the emission measurements.

Ambient air samples were collected through a 21 m long heated FEP tubing (od. ¼ inch, id. 1/8 inch). VOCs in a 40 mL min⁻¹ subsample were collected from the main inlet flow for 30 minutes every hour or every other hour directly in the cold trap of the thermal-desorption unit. Samples were taken at the height of 1.5 m in the middle of the fen.

RESULTS

Earlier studies have shown that isoprene is emitted from wetlands (Jansson and de Serves, 2009; Haapanala *et al.*, 2006; Hellén *et al.*, 2006) and it turned out to be the most abundant compound in the current study also (Table 1). Monoterpene (MT) emissions were generally less than 10 % of the isoprene emissions, but sesquiterpenes (SQT) emissions were surprisingly high exceeding MT emissions all the time.

MT and isoprene emissions were higher in July than early summer concomitant with temperature, but this was not the case with SQTs (Table 1). High early summer emissions of SQTs could be due to compounds produced in soil and trapped in frozen soil and snow cover during winter. Aaltonen *et al.* (2012) measured VOCs in the snow cover in a boreal forest in southern Finland and found both MTs and SQTs in snow with decreasing trend from soil surface to top layer of snow indicating soil as a source for terpenoids. These

compounds can then be released to the air when snow melts and ground thaws. Additional proof for trapped SQTs is that the emissions are well correlated (exponential, $R^2=0.78$) with soil temperature in early summer, when soil temperature was below 15°C and vegetation was sparse. Exponential correlation with air temperature inside the chamber at the same time was clearly lower ($R^2=0.56$). Later, new growth affected the emissions, correlation with soil temperature weakened and correlation with chamber temperature increased. For MTs and especially for isoprene chamber temperature had better correlation also in early summer indicating stronger effect of new growth also then.

	F1 (29.5.-4.6.)	F2 (6.-7.6.)	F1 (4.-10.7.)	F3 (12.-13.7.)	F1(T) (30.7.-2.8.)
T [°C]	14	7	20	26	29
PAR [$\mu\text{mol m}^{-2} \text{s}^{-1}$]	540	290	560	720	530
CT*CL	0.25	0.04	0.27	0.89	0.86
SQTs [$\mu\text{g m}^{-2} \text{h}^{-1}$]	8.8	2.1	8.7	7.3	2.5
MTs [$\mu\text{g m}^{-2} \text{h}^{-1}$]	1.1	0.2	2.1	3.0	0.9
Isoprene [$\mu\text{g m}^{-2} \text{h}^{-1}$]	18	0.2	49	82	90

Table 1. Mean temperature (T), photosynthetic active radiation (PAR), temperature and light activity coefficient (CT*CL, Guenther *et al.*, 1993) and emission rates of monoterpenes (MTs), sesquiterpenes (SQTs) and isoprene during the various sampling periods. N=number of samples. F1=frame 1, F2=frame 2, F3=frame 3 and F1(T)=tube samples from frame 1.

The emission pattern of both MTs and SQTs varied during the measurements. The most abundant SQT was cadinene until β -cadinene exceeded it in August (cadinenes are tentative identifications). We identified altogether 19 SQTs, but we had standards for only 8 of them. The rest were tentatively identified and quantified based on their mass spectra and retention indexes.

Both MT and SQT emissions were dependent on temperature as shown in Fig. 1. The β -coefficient (as described by Guenther *et al.*, 1993) for MTs was $0.08 \text{ }^\circ\text{C}^{-1}$ which is close to $0.09 \text{ }^\circ\text{C}^{-1}$ often observed for terrestrial plants. The coefficient for SQTs was lower ($0.05 \text{ }^\circ\text{C}^{-1}$). Lower values ($0.02\text{-}0.06 \text{ }^\circ\text{C}^{-1}$) of SQTs were also found for Norway spruce emissions (Hakola *et al.*, 2017).

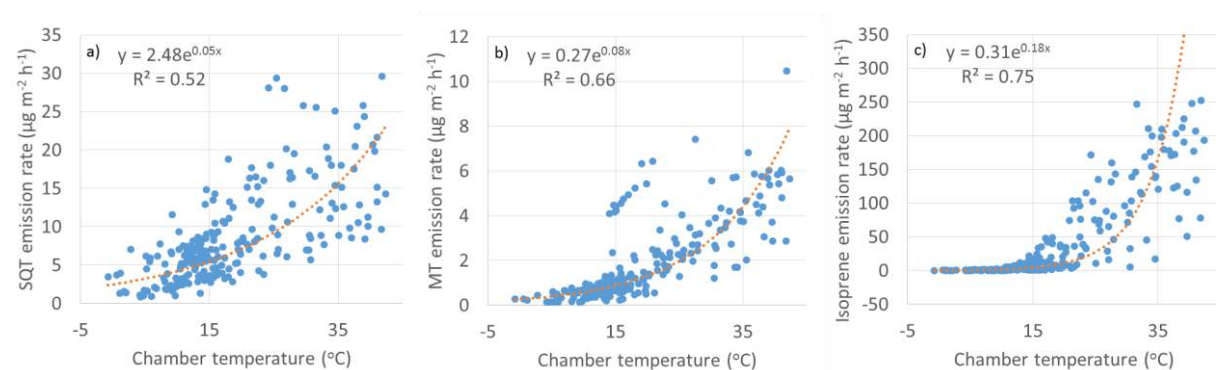


Figure 1. Exponential correlation of temperature with emission rates of a) SQTs, b) MTs and c) isoprene.

Ambient air concentrations were measured in three periods over the growing season as shown in Table 2. Isoprene concentrations increased from May to July similar to their emission rates, but MT concentrations

were high also in the beginning of the growing season. In 8th of May there were still 40 cm of snow and in 21st of May no snow was detected anymore. Highest daily means in May for both MTs and SQTs were measured during this snow melting period. Aaltonen *et al.* (2012) have shown that VOCs produced under the snow cover by for example microbes and decaying litter remain in the snow cover with quite high concentrations and are released to the air when snow is melting and ground thaws. Melting influences also the surrounding forest and may cause higher emissions also there.

	May (8.-27.5.) N=142	June (12.-30.6.) N=103	July (1.-3.7.) N=28
T [°C]	10	11	16
O ₃ (ppb)	39	31	27
SQTs [pptv]	7	3	21
MTs [pptv]	350	58	560
Isoprene [pptv]	3	5	87

Table 2. Ambient air concentrations of sesquiterpenes (SQTs), monoterpenes (MTs) and isoprene. N=number of samples

The SQTs measured in ambient air were not the same as measured in the emissions of the fen, but the most abundant compounds in air were α -copaene and β -caryophyllene. β -Caryophyllene is a very fast reacting compound, its lifetime is only of a few minutes, and it was only minor fraction (<2%) of fen emissions. It is the main SQT in Norway spruce emissions (Hakola *et al.*, 2017). Therefore it is likely that nearby spruce forest can also be a SQT source. Other possible close by sources are mountain birches (Haapanala *et al.* 2009) and Scots pines (Tarvainen *et al.* 2005). Cadinene was the main SQT in the emissions and it was detected in ambient air too. Although MT and SQT emissions from the fen were quite considerable, they were not the only emissions affecting atmospheric concentrations, but surrounding forests contribute as well.

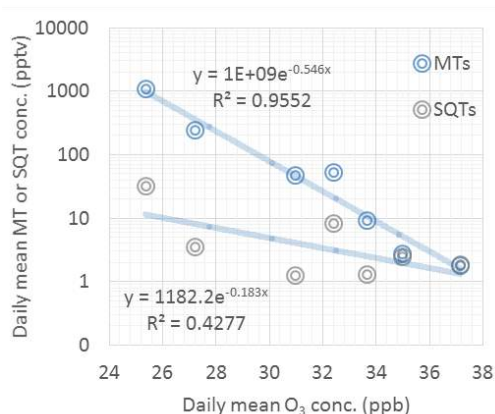


Figure 2. Exponential correlation of daily mean ozone concentrations with daily mean MT and SQT concentrations during the ambient air measurements in June and July in 2018.

Vertical ozone fluxes measured above forests are explained at least partly by stomatal uptake and non-stomatal sinks including chemical reactions with the BVOCs (Wolfe *et al.* 2011). We found that daily mean MT and SQT concentrations had negative exponential correlation with ozone concentrations as shown in Fig. 2. This indicates that BVOC emissions have strong impact on ozone concentrations at this remote sub-Arctic site. However, the dependence was detected only in June and July. In May MT concentrations were

high, but no correlation was observed. The reason could be that during that time the main MT source impacting our measurements was very close by, perhaps in the snow cover on the fen as discussed earlier, while impact of VOCs on ozone concentrations is a more regional phenomenon. In June and July, due to low emissions at the fen, the main source of MTs was expected to be more regional (e.g. surrounding coniferous forests). Lifetimes of MTs in relation to ozone reaction are of a few hours for most of the MTs.

CONCLUSIONS

Even though isoprene was the main terpenoid emitted from the fen, sesquiterpene emissions were significant as well especially during the early growing season. Changes in light and temperature were explaining most of the seasonal changes of isoprene, but for sesquiterpenes emissions were controlled by other factors as well, which was shown for example by decreasing emission potentials over the growing season. High early summer emissions of SQTs indicated that the compounds trapped in frozen soil and snow cover during winter could be a strong source of these compounds when the soil thaws.

Although isoprene, MT and SQT emissions from the fen were quite considerable, they were not the only emissions affecting their atmospheric concentrations at the Lompolojänkkä fen, but surrounding forest contributed as well. Strong correlation of daily mean ambient air concentrations of MTs and SQTs with ozone concentrations indicated that BVOC emissions from the wetlands and surrounding forests also have strong impacts on ozone levels at this site.

ACKNOWLEDGEMENTS

The research was supported by the Academy research fellow project (Academy of Finland, project 275608) and Academy of Finland via the Center of Excellence in Atmospheric Sciences (grant no. 307331).

REFERENCES

- Aaltonen, H., Pumpanen, J., Hakola, H., Vesala, T., Rasmus, S., and Bäck, J.: Snowpack concentrations and estimated fluxes of volatile organic compounds in a boreal forest, *Biogeosciences*, 9, 2033–2044, <https://doi.org/10.5194/bg-9-2033-2012>, 2012.
- Guenther, A. B., Zimmerman, P. R., Harley, P. C., Monson, R. K., and Fall, R.: Isoprene and monoterpene emission rate variability: Model evaluation and sensitivity analyses, *J. Geophys. Res.*, 98(D7), 12,609, 1993.
- Haapanala, S., Rinne, J., Pystynen, K.-H., Hellén, H., Hakola, H., and Riutta, T.: Measurements of hydrocarbon emissions from a boreal fen using the REA technique, *Biogeosciences*, 3, 103–112, 2006.
- Haapanala, S., Ekberg, A., Hakola, H., Tarvainen, V., Rinne, J., Hellén, H., and Arneth, A.: Mountain birch – potentially large source of sesquiterpenes into high latitude atmosphere, *Biogeosciences*, 6, 2709–2718, <https://doi.org/10.5194/bg-6-2709-2009>, 2009.
- Hakola, H., Tarvainen, V., Praplan, A. P., Jaars, K., Hemmilä, M., Kulmala, M., Bäck, J., and Hellén, H.: Terpenoid and carbonyl emissions from Norway spruce in Finland during the growing season, *Atmos. Chem. Phys.*, 17, 3357–3370, [doi:10.5194/acp-17-3357-2017](https://doi.org/10.5194/acp-17-3357-2017), 2017.
- Hellén, H., Hakola, H., Pystynen, K.-H., Rinne, J., and Haapanala, S.: C₂-C₁₀ hydrocarbon emissions from a boreal wetland and forest floor, *Biogeosciences*, 3, 167–174, <https://doi.org/10.5194/bg-3-167-2006>, 2006.
- Holst, T., Arneth, A., Hayward, S., Ekberg, A., Mastepanov, M., Jackowicz-Korczynski, M., Friborg, T., Crill, P. M., and Bäckstrand, K.: BVOC ecosystem flux measurements at a high latitude wetland site, *Atmos. Chem. Phys.*, 10, 1617–1634, <https://doi.org/10.5194/acp-10-1617-2010>, 2010.
- Janson, R. and De Serve, C.: Isoprene emissions from boreal wetlands in Scandinavia, *J. Geophys. Res.*, 103, 25 513–25 517, 1998.
- Lohila A, Penttilä T, Jortikka S, Aalto T, Anttila P, Asmi E, Aurela M, Hatakka J, Hellen H, Henttonen H, Hänninen P, Kilkki J, Kyllönen K, Laurila T, Lepistö A, Lihavainen H, Makkonen U, Paatero J, Rask M, Sutinen R, Tuovinen J, Vuorenmaa J. and Viisanen Y.: Preface to the special issue on integrated research of atmosphere, ecosystems and environment at Pallas. *Boreal Env. Res.* 20: 431–454, 2015.
- Tarvainen V., Hakola H., Hellén H., Bäck J., Hari P. and Kulmala M.: Temperature and light dependence of the VOC emissions of Scots pine. *Atmospheric Chemistry and Physics*, 5, 1–10, 2005.
- Wolfe G. M., Thornton J. A., McKay M., Goldstein, A. H.: Forest-atmosphere exchange of ozone: sensitivity to very reactive biogenic VOC emissions and implications for in-canopy photochemistry, *Atmos. Chem. Phys.* 11, 7875–7891, [DOI: 10.5194/acp-11-7875-2011](https://doi.org/10.5194/acp-11-7875-2011), 2011.

AMINE AND GUANIDINE EMISSION MEASUREMENTS FROM BOREAL FOREST FLOOR

M. HEMMILÄ, U. MAKKONEN, G. PANAGIOTOPOULOU, H. HAKOLA, H. HELLÉN

Finnish Meteorological Institute, PL 503, 00101 Helsinki, Finland

Keywords: AMINES, FOREST FLOOR EMISSIONS, GUANIDINE, MARGA-MS

INTRODUCTION

Amines are gaseous bases, whose general formula is RNH_2 , R_2NH or R_3N . Models have shown that they could affect aerosol particle formation with sulfuric acid (Kurtén et al. 2008, Paasonen et al. 2012). Atmospheric aerosol particles affect the climate, because they can act as cloud condensation nuclei (CCN) (IPCC 2014). They also scatter and absorb sun radiation. Amines also affect hydroxyl radical (OH) reactivity and via that to the atmospheric chemistry (Hellén et al. 2014, Kieloaho et al. 2013). In a recent study, organobase, guanidine, has shown even more efficient aerosol particle formation with sulfuric acid than amines (Myllys et al. 2018). Guanidine is a catabolite of arginine, and it has been found for example in urine (Marascau et al. 1992, Van Pilsum et al., 1956). Arginine concentrations have been detected in boreal forest in Alaska, USA (Werdin-Pfisterer et al., 2009).

In our earlier study we measured amine concentrations in ambient air (Hemmilä et al. 2018). In that study we observed that different amines are likely to have different sources and that their seasonality is not the same for all the compounds. In this abstract we present preliminary results of forest floor amine and guanidine emissions.

METHODS

Forest floor emission measurements were performed at SMEAR II station in Hyytiälä, Southern Finland (61°51'N, 24°17'E, 180 m a.s.l., Hari and Kulmala, 2005) since March 2018 about one week per month. Emissions were measured using static flow through technique with a polymethylmethacrylate chamber (60 cm * 60 cm * 80 cm). Chamber was flushed with amine free air at the flow of 25 L min⁻¹. We used an oxalic acid filter to remove bases from the air that went to the chamber. Samples from the chamber air were taken using MARGA (Monitor for AeRosols and Gases in Ambient air, Metrohm-Applikon, Schiedam, Netherlands) (ten Brink et al. 2007), which is an on-line ion chromatograph (IC) connected to sampling system. In addition of this the MARGA system was connected to an electrospray ionization quadrupole mass spectrometer (MS, Shimadzu LCMS-2020, Shimadzu Corporation, Kyoto, Japan) to improve sensitivity of amine measurements. For more detailed description, see Hemmilä et al. (2018). We have added to the measurement method also guanidine. Sampling air flow was 16.7l/min and sampling time was 1 hour.

RESULTS AND DISCUSSION

We measured amine and guanidine emissions from the boreal forest floor in April, May, July and September in 2018. In Fig. 1 the average emission rates are shown for every month. MMA, DMA, TMA, and DEA had their maximum emissions in July, but guanidine had highest emissions already in the spring. In our earlier ambient air study (Hemmilä et al., 2018) we noticed that DMA and TMA had also their maximum ambient air concentrations in July. In that study MMA had its maximum ambient air concentrations in the spring, but here the highest emission rates from the forest floor were measured in the summer.

We compared measured emission rates to aerosol concentrations of different size distributions and also new particle formation event days, but we could not find correlation with them.

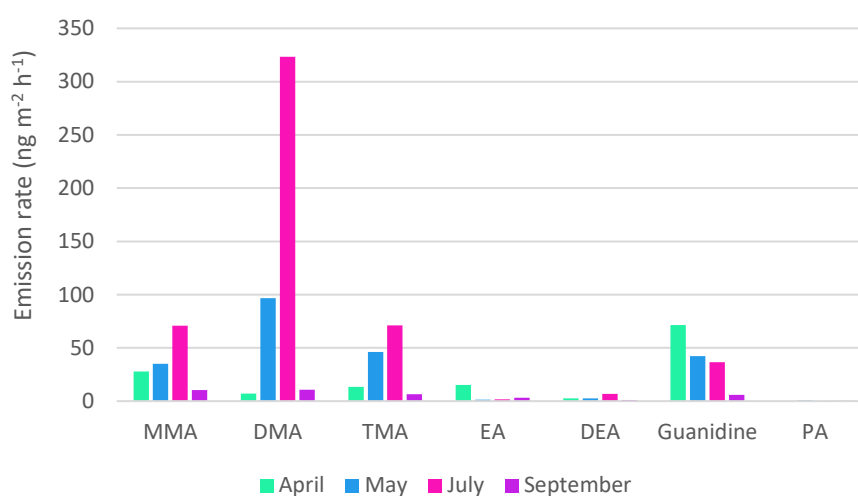


Figure 1. Average amine and guanidine emission rates ($\text{ng m}^{-2} \text{h}^{-1}$) in different months.

In May and July, the diurnal variation of amine emission rates, especially for DMA, followed temperature (Fig. 2a and b). The temperature dependence was best, when DMA and guanidine emissions were plotted against temperature measured two hours earlier (Fig. 3, Table 1), for TMA we did not detect as clear difference. Reason for this could be that TMA evaporates easier than DMA. It is also possible that it takes some time for DMA emissions to react to the temperature changes of the chamber air. For example, temperature of soil surface layer, which could be a source of these compounds, is expected to follow ambient air temperature changes slowly behind. This also indicates, that soil could be the main source of DMA and guanidine, but for TMA source could be for example surface vegetation, which responds faster to the changes of the air temperature.

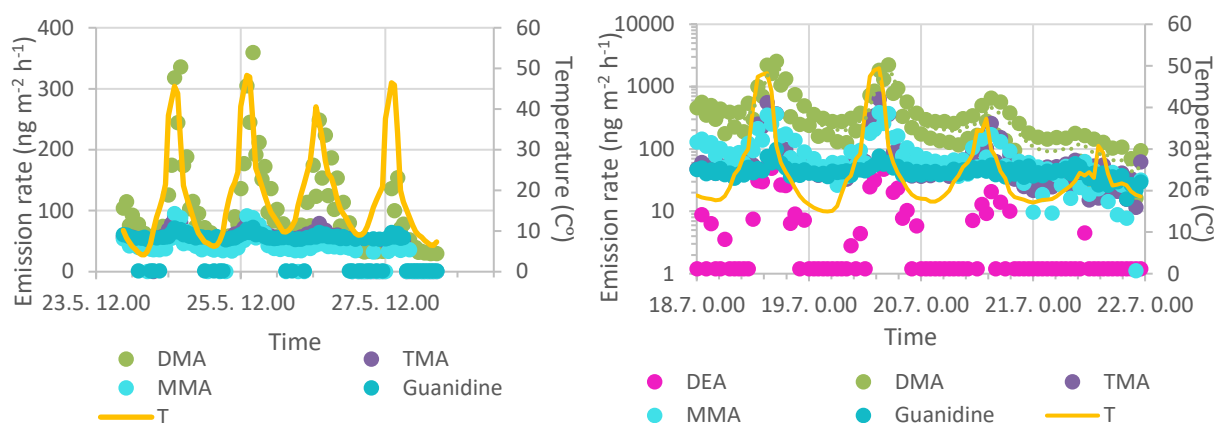


Figure 2. Time series of amine and guanidine emissions and temperature of the chamber in May and July 2018.

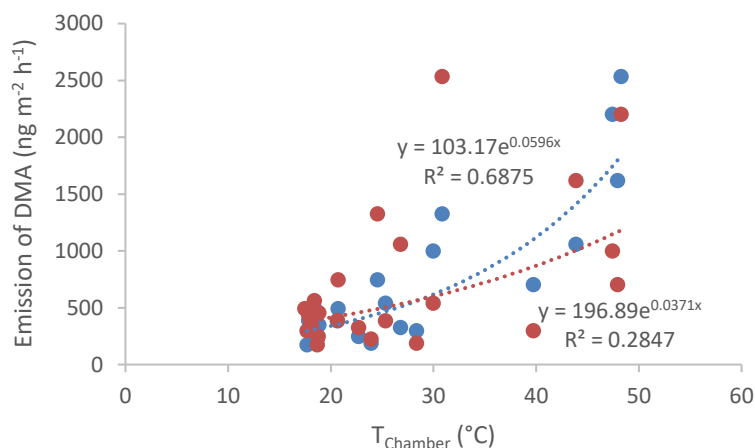


Figure 3. Exponential correlation of DMA emission rates with temperature measured at the same time (red) and two hours earlier (blue) on 18th of July.

Table 1. Calculated daily emission potentials of DMA (exponential function), TMA and guanidine (linear function) at temperature 20 °C Emission potentials with R²-value <0.4 has been marked as red.

Date	DMA			TMA		Guanidine		
	Emission potential (ng m ⁻² h ⁻¹)	R ²	R ² without temperature move	Emission potential (ng m ⁻² h ⁻¹)	R ²	Emission potential (ng m ⁻² h ⁻¹)	R ²	R ² without temperature move
24.5.	107	0.86	0.64	60	0.48	52	0.28	0.18
25.5.	98	0.86	0.64	59	0.72	49	0.35	0.35
26.5.	96	0.70	0.50	57	0.58	50	0.19	0.11
27.5.	50	0.73	0.38	22	0.47	28	0.37	0.41
18.7.	340	0.69	0.28	51	0.58	40	0.61	0.15
19.7.	271	0.78	0.41	61	0.66	43	0.68	0.56
20.7.	187	0.16	0.15	55	0.31	43	0.057	0.097
21.7.	69	0.05	0.0055	37	0.0047	39	0.17	0.0068

CONCLUSIONS

Amine emission measurements were performed from boreal forest floor. In July 2018 several amines were emitted with higher emission rates than in spring. In May and July diurnal variation of the emissions followed the variation of the temperature. Especially DMA emissions were high, which is in line with our earlier ambient air amine measurements at the site (Hemmilä et al., 2018). Also guanidine emissions were detected both in spring and summer. To our best knowledge, this is the first time amine and guanidine emissions has been quantified from the forest floor.

ACKNOWLEDGEMENTS

The financial support of the Academy of Finland Centre of Excellence program (project no. 272041) and the Academy research fellow project by H. Hellén (275608) are gratefully acknowledged.

REFERENCES

- Hari, P. and Kulmala, M., *Boreal Environment Research*, 10 (2005) 315-322
- Hellén, H., Kieloaho, A.-J. and Hakola, H., *Atmospheric Environment*, 94 (2014) 192-197
- Hemmilä, M., Hellén, H., Virkkula, A., Makkonen, U., Praplan, A. P., Kontkanen J., Ahonen, L., Kulmala, M. and Hakola, H., *Atmospheric Chemistry and Physics*, 18 (2018) 6367-6380
- IPCC, *The Intergovernmental Panel on Climate Change: Climate Change 2013: The Physical Science Basis*. Cambridge University Press, New York, 2013
- Kieloaho, A.-J., Hellén, H., Hakola, H., Manninen, H.E., Nieminen, T., Kulmala, M. and Pihlatie, M., *Atmospheric Environment*, 80 (2013) 369-377
- Kurtén, T., Loukonen, V., Vehkamäki, H. and Kulmala, M., *Atmospheric Chemistry and Physics*, 8 (2008) 4095-4103
- Marescau, B., Deshmukh, D. R., Kockx, M., Possemiers, I., Qureshi, I. A., Wiechert, P., De Deyn, P. P., *Metabolism: Clinical and Experimental*, 41 (1992) 526-532
- Myllys, N., Ponkkonen, T., Passananti, M., Elm, J., Vehkamäki, H. and Olenius, T., *The Journal of Physical Chemistry A*, 122 (2018) 4717-4729
- Paasonen, P., Olenius, T., Kupiainen, O., Kurtén, T., Petäjä, T., Birmili, W., Hamed, A., Hu, M., Huey, L. G., Plass-Duelmer, C., Smith, J. N., Wiedensohler, A., Loukonen, V., McGrath, M. J., Ortega, I. K., Laaksonen, A., Vehkamäki, H., Kerminen, V.-M., and Kulmala, M., *Atmospheric Chemistry and Physics*, 12 (2012) 9113-9133
- ten Brink, H. M., Otjes, R., Jongejan, P., and Slanina, J., *Atmospheric Environment* 41 (2007) 2768-2779
- Van Pilsum, J. F., Martin, R. P., Kito, E., Hess, J., *The Journal of Biological Chemistry*, 222 (1956) 225-236
- Werdin-Pfisterer, N.R., Kielland, K., and Boone, R.D., *Soil Biology and Biochemistry*, 41 (2009) 1210-1220.

IN-CLOUD SCAVENGING SCHEME FOR SECTIONAL AEROSOL MODULES

T.E. HOLOPAINEN¹, T. KÜHN^{1,2} and H. KOKKOLA¹

¹ Atmospheric Modelling Group, Finnish Meteorological Institute, Atmospheric Research Centre of Eastern Finland, P.O.Box 1627, Finland.

² Aerosol Research group, Department of Applied Physics, University of Eastern Finland, Kuopio, P.O. Box 1627, Finland.

Keywords: climate modelling, wet deposition, in-cloud scavenging.

INTRODUCTION

Atmospheric aerosols affect the climate directly by reflecting and absorbing radiation and indirectly through aerosol-cloud interactions. Thus, in order to estimate the radiation budget of the Earth correctly, the aerosol concentrations have to be modelled correctly, which is, among others, affected by aerosol transport. Especially with respect to the Arctic, the simulated black carbon (BC) concentrations show large intermodel variability (Kipling *et al.*, 2016). One of the possible sources of this problem is wet deposition (Liu *et al.*, 2011; Bourgeois *et al.*, 2011). At high latitudes, BC in particular, has been shown to be a major warming agent and its mitigation has been proposed as a possible means to slow Arctic warming (Stone *et al.*, 2014). Here we developed a wet deposition scheme for sectional aerosol models, which calculate the in-cloud scavenging rates from the simulated number of activated cloud droplets. For the ice clouds the same thing was done according to Tabazadeh *et al.* (2002) where the in-cloud scavenging rates are calculated based on the number of nucleated ice particles which in turn is calculated from the surface area of each size class. The sensitivity of the new in-cloud scavenging scheme was then tested using ECHAM-HAM-SALSA simulations with varying the BC emission size distribution and hygroscopicity.

METHODS

This study uses the newest version of ECHAM-HAMMOZ (ECHAM6.3-HAM2.3- MOZ1.0) (Stier *et al.*, 2005). ECHAM-HAMMOZ uses different microphysics packages to characterize aerosol populations. To test our new wet deposition scheme and the sensitivity of the model we used the Sectional Aerosol module for Large Scale Applications (SALSA) in our model simulations. The detailed description of the newest SALSA version, SALSA2.0, is done by Kokkola *et al.* (2018).

The old wet deposition scheme for SALSA includes in-cloud and below cloud scavenging and, if the precipitation evaporates below the cloud, the subsequent release of aerosols back into the atmosphere (Bergman *et al.*, 2012). The in-cloud scavenging parameters are a function of aerosol size and they are presented in detail by Bergman *et al.* (2012). Below-cloud scavenging is a function of aerosol concentration, collection efficiency and area of precipitation. The below cloud parametrization is presented in detail by Croft *et al.* (2009).

The new in-cloud nucleation scavenging for sectional aerosol modules for liquid clouds was implemented following the modal method by Croft *et al.* (2010). However, instead of computing the amount of scavenged aerosols from the total amount of formed CDNC, the fractions of activated particles for each size bin were directly obtained from the cloud activation scheme by Abdul-Razzak and Ghan (2002). This method was then enhanced to take into account the insoluble core in the

particles. For ice clouds the in-cloud nucleation scavenging coefficients were calculated according to Tabazadeh et al. (2002). The fractions were then calculated from the surface area of the wet particles in each monodisperse size bins. The old and new wet deposition simulations are denoted in the comparisons as "baserun_wd1" and "baserun_wd3" respectively. In these studies we use the BC emission distribution prescribed in the ECHAM-HAMMOZ model.

The sensitivity for the new sectional scavenging was then tested using different sensitivity studies. In our model the BC is emitted to insoluble population so first we investigated how sensitive our new wet scavenging scheme is to the emission size distribution of BC in this population. These studies were done so that first all of the BC emissions were directed to size range 0.7-1.7 μm in the insoluble population. This study is referred to as "BC_0.7-1.7 μm ". Secondly the emissions were directed to insoluble size range of 50-96.7 nm. This study is referred to as "BC_50-100nm". The hygroscopicity studies included a simulation where all of the BC was directed to soluble size bins which is referred to as "BC_emi_to_sol". This massively increases the hygroscopicity of BC thus increasing the activation and deposition of these particles.

The simulations were done with ECHAM-HAMMOZ for the year 2010 using 3-hourly data output, after a 6 month spin-up. The emissions were obtained from the ACCMIP (Emissions for Atmospheric Chemistry and Climate Model Intercomparison Project) emission inventories. In particular, RCP4.5 (Representative Concentration Pathways) was selected. The model meteorology was nudged towards meteorological observations of ECMWF (European Centre for Medium-Range Weather Forecasts), and the sea surface temperature (SST) and sea ice cover (SIC) were also prescribed. SST and SIC were obtained from monthly mean climatologies from AMIP (Atmospheric Model Intercomparison Project).

RESULTS

We compare the modelled vertical profiles with the measurements done in two different aircraft campaigns: TC4 (Toon *et al.*, 2010), which is near the primary sources and Spring ARCTAS NASA DC-8 (Jacob *et al.*, 2010), which is near the Arctic. Figure 1 shows the vertical profile of BC simulated with the old and new wet deposition scheme and the vertical profile measured in the aircraft campaigns TC4 and Spring ARCTAS NASA DC-8.

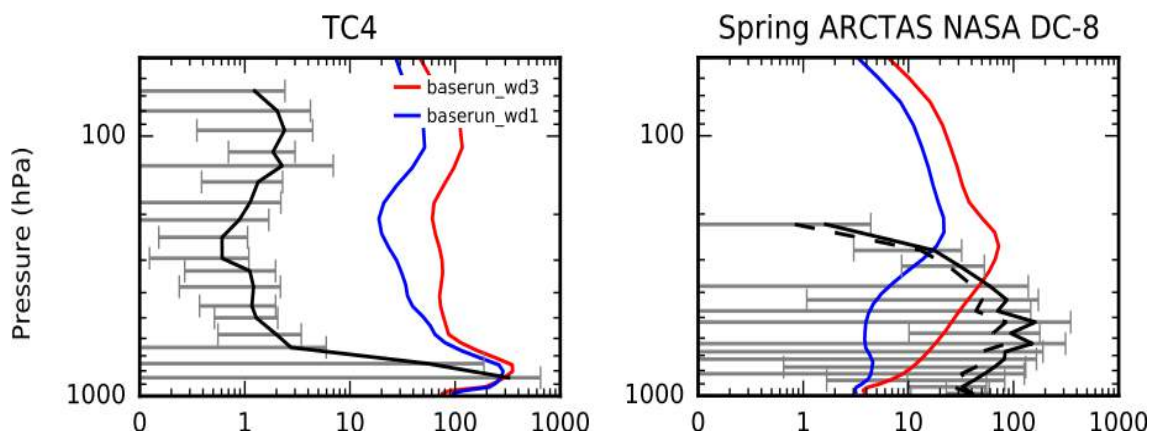


Figure 1: The vertical profile of BC simulated with the old and new wet deposition scheme and the vertical profile measured in the aircraft campaigns TC4 and Spring ARCTAS NASA DC-8.

From the Figure 1 we can see that the new wet deposition scheme overestimates the BC concentration near the source areas and performs more better in the Arctic. To increase the efficiency of the new method near the source regions we wanted to test what affects the vertical profiles by

using sensitivity simulations. Figure 2 shows the vertical profile of BC simulated with the different sensitivity studies and the vertical profile measured in the aircraft campaigns TC4 and Spring ARCTAS NASA DC-8.

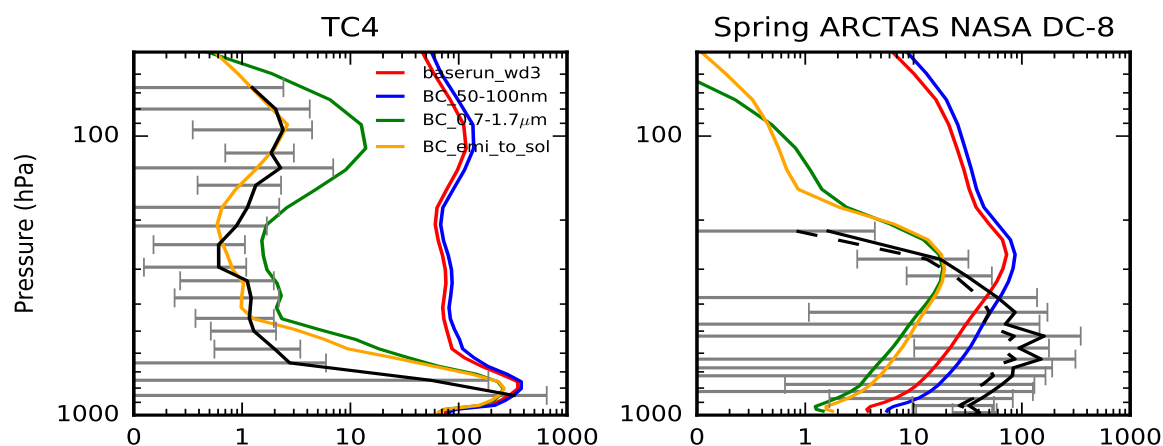


Figure 2: The vertical profile of BC simulated with the different sensitivity studies and the vertical profile measured in the aircraft campaigns TC4 and Spring ARCTAS NASA DC-8.

One notable difference between the baserun and the sensitivity studies can be seen in the size distribution study where the BC emissions are directed to the insoluble size range of 0.7-1.7 μm . This is due to the fact that when the BC is in larger size bins the deposition of these particles is faster. Second notable difference can be seen in the sensitivity testing where the BC is directed straight to the soluble size bins. This increases the hygroscopicity of these particles and they can activate more efficiently. The BC particles are insoluble but after aging with sulphate or OC they become soluble and can activate. Thus it might be reasonable to assume that the BC can in fact be emitted to soluble population.

ACKNOWLEDGEMENTS

The financial support from the Academy of Finland Center of Excellence (grant no. 307331), Academy of Finland research projects no. 317390 and 285389, and the strategic funding from University of Eastern Finland are gratefully acknowledged.

The ECHAM-HAMMOZ model is developed by a consortium composed of ETH Zurich, Max Planck Institut für Meteorologie, Forschungszentrum Jülich, University of Oxford, the Finnish Meteorological Institute and the Leibniz Institute for Tropospheric Research, and managed by the Center for Climate Systems Modeling (C2SM) at ETH Zurich.

REFERENCES

- Stier, P., J. Feichter, S. Kinne, E. Vignati, J. Wilson, L. Ganzeveld, I. Tegen, M. Werner, Y. Balkanski, M. Schulz, O. Boucher, A. Minikin and A. Petzold (2005). The aerosol-climate model ECHAM5-HAM. *Atmospheric Chemistry and Physics*, **5**, 1125–1156.
- Bergman, T., V.-M. Kerminen, H. Korhonen, K. J. Lehtinen, R. Makkonen, A. Arola, T. Mielonen, S. Romakkaniemi, M. Kulmala and H. Kokkola (2012). Evaluation of the sectional aerosol microphysics module SALSA implementation in ECHAM5-HAM aerosol-climate model. *Geoscientific model development*, **5**, 845–868.
- Kokkola, H., T. Kuhn, A. Laakso, T. Bergman, K. E. J. Lehtinen, T. Mielonen, A. Arola, S. Stadtler, H. Korhonen, S. Ferrachat, U. Lohmann, D. Neubauer, I. Tegen, C. Siegenthaler-Le Drian, M. G. Schultz, I. Bey, P. Stier, N. Daskalakis, C. L. Heald and S. Romakkaniemi (2018). SALSA2.0: The sectional aerosol module of the aerosol-chemistry-climate model ECHAM6.3.0-HAM2.3-MOZ1.0. *Geoscientific Model Development*, **11**, 3833–3863.
- Abdul-Razzak, H. and Ghan, S. (2002). A parameterization of aerosol activation 3. Sectional representation. *Journal of Geophysical Research*, **107**, 1–6.
- Kokkola, H., M. Vesterinen, T. Anttila, A. Laaksonen and K. E. J. Lehtinen (2008). Technical note: Analytical formulae for the critical supersaturations and droplet diameters of CCN containing insoluble material. *Atmospheric Chemistry and Physics*, **8**, 1985–1988.
- Tabazadeh, A., Y. S. Djikaev and H. Reiss (2008). Surface crystallization of supercooled water in clouds. *National Academy of Sciences*, **99**, 15 873–15 878.
- Croft, B., U. Lohmann, R. V. Martin, P. Stier, S. Wurzler, J. Feichter, R. Posselt, C. Hoose, U. Heikkilä, A. van Donkelaar and S. Ferrachat. (2010). Influences of in-cloud aerosol scavenging parameterizations on aerosol concentrations and wet deposition in ECHAM5-HAM. *Atmospheric Chemistry and Physics*, **10**, 1511–1543.
- Toon, O. B., Starr, D. O., Jensen, E. J., Newman, P. A., Platnick, S., Schoeberl, M. R., Wennberg, P. O., Wofsy, S. C., Kurylo, M. J., Maring, H., Jucks, K. W., Craig, M. S., Vasques, M. F., Pfister, L., Rosenlof, K. H., Selkirk, H. B., Colarco, P. R., Kawa, S. R., Mace, G. G., Minnis, P., and Pickering, K. E. (2010). Planning, implementation, and first results of the Tropical Composition, Cloud and Climate Coupling Experiment (TC4). *Journal of Geophysical Research: Atmospheres*, **115**
- Jacob, D. J., Crawford, J. H., Maring, H., Clarke, A. D., Dibb, J. E., Emmons, L. K., Ferrare, R. A., Hostetler, C. A., Russell, P. B., Singh, H. B., Thompson, A. M., Shaw, G. E., McCauley, E., Pederson, J. R., and Fisher, J. A. (2010). The Arctic Research of the Composition of the

Troposphere from Aircraft and Satellites (ARCTAS) mission: design, execution, and first results. *Atmospheric Chemistry and Physics*, **10**, 5191–5212.

Kipling, Z. and Stier, P. and Johnson, C. E. and Mann, G. W. and Bellouin, N. and Bauer, S. E. and Bergman, T. and Chin, M. and Diehl, T. and Ghan, S. J. and Iversen, T. and Kirkevåg, A. and Kokkola, H. and Liu, X. and Luo, G. and van Noije, T. and Pringle, K. J. and von Salzen, K. and Schulz, M. and Seland, Ø. and Skeie, R. B. and Takemura, T. and Tsigaridis, K. and Zhang, K. (2016). What controls the vertical distribution of aerosol? Relationships between process sensitivity in HadGEM3–UKCA and inter-model variation from AeroCom Phase II *Atmospheric Chemistry and Physics*, **16**, 2221–2241.

Liu, Junfeng and Fan, Songmiao and Horowitz, Larry W. and Levy II, Hiram (2011). Evaluation of factors controlling long-range transport of black carbon to the Arctic. *Journal of Geophysical Research: Atmospheres*, **116**.

Bourgeois, Q. and Bey, I. (2011). Pollution transport efficiency toward the Arctic: Sensitivity to aerosol scavenging and source regions. *Journal of Geophysical Research*, **116**, D08213.

Stone, R., Sharma, S., Herber, A., Eleftheriadis, K., and Nelson, D. (2014) A characterization of Arctic aerosols on the basis of aerosol optical depth and black carbon measurements. *Elem Sci Anth*, **2**, p.000 027.

ROADSIDE AIR QUALITY AT A SUB-URBAN SITE NEAR SOUTH DELHI

R. HOODA¹, K. TEINILÄ¹, H. TIMONEN¹, L. SALO², H. KUULUVAINEN², T. RÖNKKÖ² and A. HYVÄRINEN¹

¹Finnish Meteorological Institute, Atmospheric Composition Research, FI-00560, Helsinki, Finland.

²Tampere University, Physics Unit, Aerosol Physics Laboratory, P.O. Box 692, FI-33101 Tampere, Finland.

Keywords: EMISSIONS, COMPOSITION, SIZE-DISTRIBUTION, BOUNDARY LAYER.

INTRODUCTION

Air pollutants impact on both local and regional scale, causing adverse health effects (Pope and Dockery, 2006), decreasing visibility (Watson, 2002), and influencing the climate (IPCC, 2013). Rapid industrialization and economic growth coupled with a high population density have made south Asia (especially the Indian sub-continent) a region of increasing vulnerability to these adverse impacts. While, urban air quality has shown deterioration due to the presence of very high concentrations of local emissions, the regional scale air quality is impacted by primary emissions from a range of sources (Hooda et al., 2018) and due to formation of secondary aerosols by the pre-cursor species (Aggarwal et al., 2013). Since the last two decades air quality has been a major concern in India (Balakrishnan et al., 2019). The densely populated Indo-Gangetic Plain (IGP) is a particularly high emission region in India. Traffic emissions are an important contributor to these emissions, causing severe air pollution especially during the winter seasons when the atmospheric boundary layer is low (Hooda et al., 2016), and are associated strongly with adverse health effects. The diesel particulate and gaseous emissions are recently shown to be specifically harmful and the diesel engine exhaust are classified as carcinogenic to humans (IARC 2012). In addition to reduction of lung function, increase in blood pressure and enhancement of cancer risk in the lung, Siddique et al. (2011) have studied in eastern India that chronic exposure to vehicular pollution even tend to prevail attention-deficit hyperactivity disorder (ADHD) in childhood populations. A study in Delhi attributed all-natural cause mortality and morbidity to increase in the vehicular population (Rizwan et al., 2013). Thus, characterization of typical primary and secondary traffic -generated aerosols in the region could be an important attempt to fingerprint vehicular emissions. In the present work, we have studied high-resolution diurnal variability of chemical, physical and optical aerosol properties by deploying state-of-the-art instruments at a roadside.

METHODS

The measurements were conducted at Gual Pahari (28°25'N, 77°08'E, 254 m asl) about 25 km south of Delhi (Hyvärinen et al., 2010; Kulmala et al., 2011). The surroundings of Gual Pahari represent a semi-urban environment (Hooda et al., 2016). The site is in the IGP (Indo-Gangetic Plain) which is one of the most populated area with over 900 million inhabitants. The IGP is a highly fertile agricultural area but also rapidly developing region of the Indian sub-continent and is recognized to be among the global pollution hotspots of aerosols and trace gases (Moorthy et al., 2016).

During the campaign of two months in winter season of year 2018–2019, the measurement instruments were installed in a mobile laboratory that was stationed near high traffic roadside. A PM_{2.5} inlet (Digitel) system was mounted 1.5–2 meter above the mobile van roof and it was 4–5 meter above ground level for air sampling to the instruments.

The Time-of-Flight Aerosol Chemical Speciation Monitor (ToF-ACSM; Aerodyne Research Inc.) is designed for long-term monitoring of submicron aerosol composition with high temporal resolution. The concentrations of organics, nitrate, sulphate, ammonium and chloride were measured with ToF-ACSM. Particle size-distributions were measured with Scanning Mobility Particle Sizers (SMPS; TSI Inc.) and

FAAR abstract

Electrical Low-Pressure Impactor, ELPI+ (Dekati Ltd.). The SMPS has a Differential Mobility Analyzer (DMA, TSI 3071) for particle size selection and a Condensation Particle Counter (CPC, TSI 3775) to measure the particle number concentration. The scanned size range in this study was from 7 to 250 nm (mobility diameter). Total concentration of Lung deposited surface area (LDSA) was measured with Pegasor AQ™ urban sensor. Changes in PM concentration were measured with Dekati® eFilter™ as well as with a low-cost sensor (indigenously assembled in Finnish Meteorological Institute), and a novel sensor for measuring particulate matter from traffic (Tampere University) was also used. A seven-wavelength (370 nm to 950 nm) Aethalometer (Magee Scientific AE-31) was used for measuring absorption coefficient (σ_{ap}) and equivalent black carbon (eBC) at $\lambda=880$ nm. Corrections of the multiple scattering of the light within the filter fibers and the “shadowing” effect of the aerosol particles that occurs as the filter gets more highly loaded were performed using the procedure described by Weingartner et al. (2003). The measurements of gaseous pollutants (e.g., NO₂, NO, NO_x, O₃, CO, SO₂) and particulate matter (PM_{2.5} and PM₁₀) were conducted using Horiba real-time analysers. The primary meteorological parameters were observed using WXT (Vaisala). The traffic volumes for cars, trucks and buses were manually calculated for three days between 07:00 hrs and 23:00 hrs in February. The traffic volume calculations were done shortly after the campaign and are represent the typical traffic pattern at the road.

CONCLUSIONS

The meteorological conditions during the measurements period were typical of winter season in a tropical region with day temperature less than 15°C and night temperature between 4 and 10°C, and wind speed was very low with below 2 ms⁻¹. The measurement site was influenced by anthropogenic emission sources i.e. biomass and fossil fuel combustion, traffic, industrial activities and secondary aerosol formation as also concurred from the previous findings of the area (Hyvärinen et al., 2010; Hooda et al., 2016).

The particulate matter (PM_{2.5} and PM₁₀) at the monitored site was ranged between 150 to 475 $\mu\text{g m}^{-3}$ and 250 to 700 $\mu\text{g m}^{-3}$, respectively. Both these parameters have concentrations that exceed the 24-hour levels of National Ambient Air Quality standard in India which are 60 $\mu\text{g m}^{-3}$ and 100 $\mu\text{g m}^{-3}$, respectively (CPCB, 2009). The high resolution (2 minutes) diurnal variability is presented as an example for ToF-ACSM (Fig. 1). The measured particle chemical composition showed that organics with typical concentrations ranging from 50 to 100 $\mu\text{g m}^{-3}$ are the major chemical component in PM_{2.5} (Fig. 1).

The main components of submicron particles were organic matter (52% of PM₁) and BC (14% of PM₁). The contribution of inorganic ions was higher (34%) than typically observed in clean environments. The main inorganic ions were nitrate (13%) and ammonium (10%). The contribution of chloride was 6% and sulphate 5%. The relative fraction corroborates well with earlier findings (Hooda et al., 2016) in the same region. The organics show a typical cycle of apparent peaks in the morning and evening hours, but consistent high levels throughout the day, except in the afternoon. This indicates that biomass burning activities might be a prevailing factor.

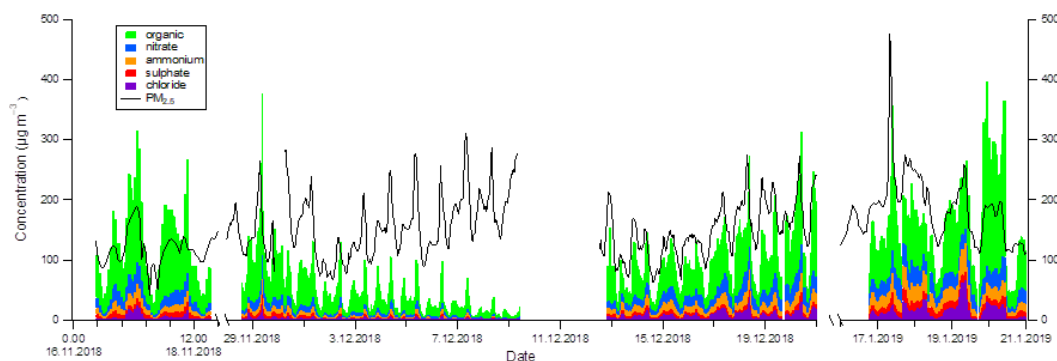


Figure 1. High resolution diurnal variability with ToF-ACSM at Gual Pahari road-side location.

FAAR abstract

Figure 2a shows stable black carbon levels, although high, imply no change in traffic emissions over the course of the day, except in the afternoon time. Black carbon peaks during night time are concurrent with high concentrations of organics, this could be due to heavy-duty diesel vehicles emissions (Zheng et al., 2015). The levels of AAE elevated in the morning and evening times might imply emissions from both the biomass activities and traffic while during noon time the low levels ranged between 1.0 and 1.2 might suggest traffic emissions (Fig. 2b).

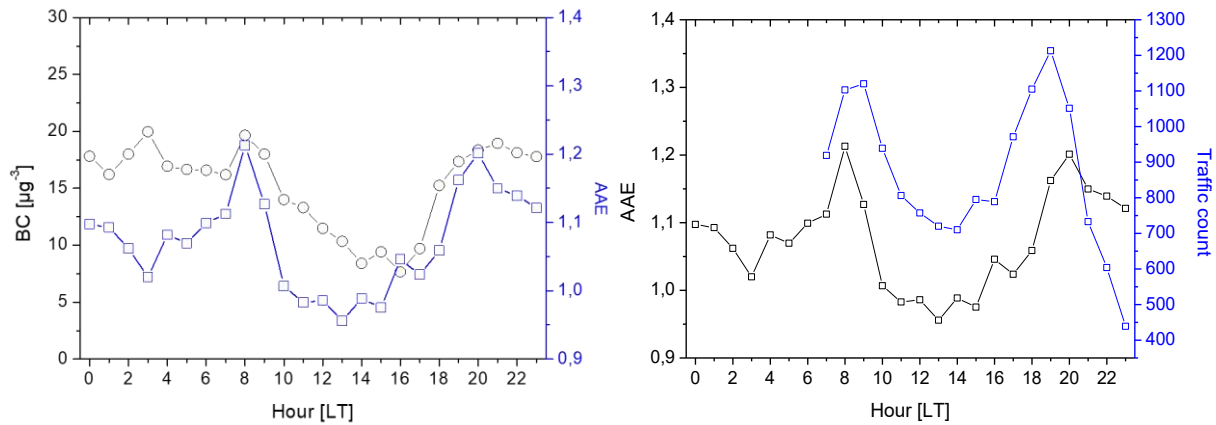


Figure 2. a) Diurnal variability of black carbon concentration and Absorption Ångström exponent; b) AAE and traffic volume

But interestingly it is noted that the concentrations of all the measured species are typically lower during afternoon and that can also be attributed to a deep mixing layer depth and dilution of local pollutants (Fig. 3).

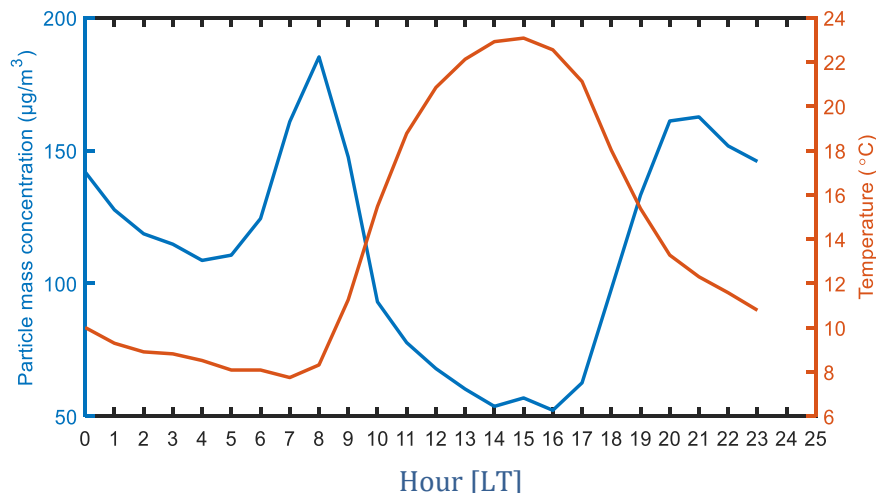


Figure 3. Diurnal variability of mass concentration with temperature.

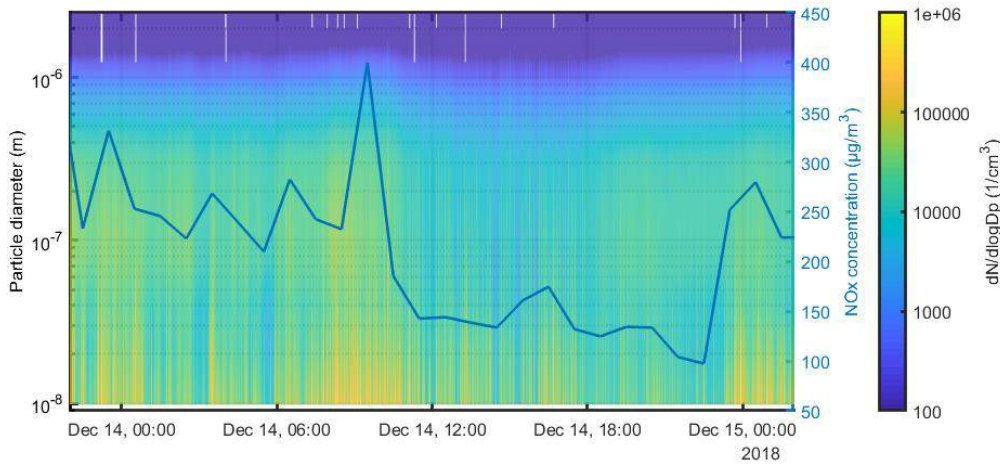


Figure 4. Particle number concentration and NO_x concentration.

Figure 4 shows that particle number concentration depends on the abundance of local sources (traffic) when presented simultaneously with NO_x levels, while particle mass concentration depends more on the boundary layer dynamics. Time series of particle number and mass concentrations illustrates that most of the variables measured at the site have seen with a distinct diurnal variation. Particle mass concentration was minimum during the day between 13:00 hrs and 16:00 hrs while number concentration was minimum during the day between 13:00 hrs and 16:00 hrs, and after midnight between 01:00 hrs and 04:00 hrs. These results indicate that the levels of aerosols at this roadside are influenced by dilution due to dynamics of the boundary layer and variability in emissions from the traffic (Fig. 3 & 4).

The findings can be highlighted with the following points:

1. The present study gave, new information on Indian roadside ambient particles;
2. High resolution-time aerosol chemistry in conjunction with physical properties, however, primary (fossil fuel vs biomass burning) and secondary emission distinction yet to be examined;
3. Significantly high levels of Cl⁻ and NH₄⁺ at a sub-urban site and elevated SO₂ at noon time;
4. Particle number significantly affected by small sized particles (<30 nm) but soot (70-100 nm) and accumulation (~200 nm) modes can also be important;
5. Fresh aerosol more during day whilst aged during the night;
6. Consistently high BC levels and AAE variability.

The future task, given the fact that IGP is having a complex geography, heterogeneity in sources and varying atmospheric dynamics, will be enriched in terms of fingerprint primary and secondary emissions using entire data set and modelling tools.

ACKNOWLEDGEMENTS

This work 'TAQIITA' was supported by the Business Finland and Department of Biotechnology, Govt. of India. The partial funding support of Dekati Oy, Pegasor Oy, Neste and HSY, and technical support of TERI and IOCL is also acknowledged.

REFERENCES

- Aggarwal, S.G., Kawamura, K., Umarji, G.S., Tachibana, E., Patil, R.S., Gupta, P.K. (2013). Organic and inorganic markers and stable C-, N-isotopic compositions of tropical coastal aerosols from megacity Mumbai: sources of organic aerosols and atmospheric processing. *Atmos. Chem. Phys.* 13, 4667–4680
- Balakrishnan, K. et al. (2019). The impact of air pollution on deaths, disease burden, and life expectancy across the states of India: the Global Burden of Disease Study 2017, *Lancet Planet Health* 2019; 3: e26–39, [http://dx.doi.org/10.1016/S2542-5196\(18\)30261-4](http://dx.doi.org/10.1016/S2542-5196(18)30261-4).
- CPCB, 2009. National Ambient Air Quality Standards, Notification, Central Pollution Control Board, Government of India, New Delhi, India.
- Hooda, R. K., A.-P. Hyvärinen, M. Vestenius, S. Gilardoni, V. P. Sharma, E. Vignati, M. Kulmala, and H. Lihavainen (2016). Atmospheric aerosols local-regional discrimination for a semi-urban area in India, *Atmos. Res.*, 168, 13–23, doi:10.1016/j.atmosres.2015.08.014.
- Hooda, R. K., Kivekäs, N., O'Connor, E. J., Collaud Coen, M., Pietikäinen, J.-P., Vakkari, V., et al. (2018). Driving factors of aerosol properties over the foothills of central Himalayas based on 8.5 years continuous measurements. *J Geophysical Research: Atmospheres*, 123, 13,421–13,442. <https://doi.org/10.1029/2018JD029744>.
- Hyvärinen, A.-P., Lihavainen, H., Komppula, M., Panwar, T.S., Sharma, V.P., Hooda, R.K., Viisanen, Y., (2010). Aerosol measurements at the Gual Pahari EUCAARI station: preliminary results from in-situ measurements, *Atmos. Chem. Phys.*, 10,7241–7252.
- IARC. Press release 213. Diesel Engine Exhaust Carcinogenic,12/6/2012.
- IPCC, 2013, Climate Change 2013: *The Physical Science Basis. Contribution of Working Group I to the Fifth Assessment Report of the IPCC*, (eds Stocker, T.F.et al.), Cambridge University Press, Cambridge, United Kingdom.
- Kulmala, M., Asmi, A., Lappalainen, H.K., Baltensperger, U., Brenguier, J.-L. et al. (2011). General overview: European Integrated project on Aerosol Cloud Climate and Air Quality interactions (EUCAARI)—integrating aerosol research from nano to global scales. *Atmos. Chem. Phys.* 11, 13061–13143.<http://dx.doi.org/10.5194/acp-11-13061-2011>.
- Moorthy, K. K., Satheesh, S. K., Sarin, M. M., and Panday, A. K. (2016). South Asian aerosols in perspective: Preface to the special issue. *Atmospheric Environment*, 125, 307–311, doi:10.1016/j.atmosenv.2015.10.073.
- Pope III, C. A. and Dockery, D. W. (2006). Health effects of fine particulate air pollution: lines that connect, *J. Air Waste Manage.*, 56, 709– 742, <https://doi.org/10.1080/10473289.2006.10464485>.
- Rizwan, S.A., Nongkynrih, B., Gupta, S.V. (2013). Air pollution in Delhi: Its Magnitude and Effects on Health, *Ind. J. Comm. Med.* 38: 4–8.
- Siddique, S., Banerjee, M., Ray, M.R. et al. (2011). Attention-deficit hyperactivity disorder in children chronically exposed to high level of vehicular pollution, *Eur J Pediatr*, 170: 923. <https://doi.org/10.1007/s00431-010-1379-0>.
- Watson, J. G. (2002). Visibility: Science and Regulation, *J. Air Waste Manage.*, 52, 628–713, <https://doi.org/10.1080/10473289.2002.10470813>.

FAAR abstract

Weingartner, E., H. Saathoff, M. Schnaiter, N. Streit, B. Bitnar, and U. Baltensperger (2003). Absorption of light by soot particles: Determination of the absorption coefficient by means of aethalometers, *J. Aerosol Sci.*, 34, 1445– 1463.

Zheng, X. et al. (2015). Characteristics of On-road Diesel Vehicles: Black Carbon Emissions in Chinese Cities Based on Portable Emissions Measurement, *Environ. Sci. Technol.*, 49, 13492–13500.

AGE EFFECT ON TREE STRUCTURE AND CARBON ALLOCATION IN SCOTS PINE AND NORWAY SPRUCE

M. HU^{1,2}, A. LEHTONEN³, F. MINUNNO¹ and A. MÄKELÄ^{1,2}

¹Department of Forest Sciences, University of Helsinki, P.O. Box 27, Helsinki FI-00014, Finland.

²Institute for Atmospheric and Earth System Research / Forest Sciences, Faculty of Agriculture and Forestry, University of Helsinki, Finland.

³Natural Resources Institute Finland (Luke), Latokartanonkaari 9, FI-00790 Helsinki Finland.

Keywords: age group, pipe model, biomass proportion, empirical coefficients.

INTRODUCTION

Carbon allocation patterns are considered to be an important factor for forest growth prediction when using process-based models. Structure equations derived by pipe model theory have been incorporated in many process-based models. However, more data concerning old-growth trees would be needed to test the reliability and generality of the structure equations. We hypothesized that the parameters used in the PMT-based structure equations are species specific and independent of tree age. The objectives of this study were (1) to provide information for further developing the models of biomass allocation in aboveground components; (2) to test the age-independence of the regularities of tree structure used in process-based models. We tested the hypothesis in 122 Scots pine and 142 Norway spruce individual trees from 4 age groups. If an age-dependence is detected, we will modify the parameters of the equations regarding to our hypothesis. This will allow us to further develop carbon allocation models of old trees (Mäkelä 1997, Minunno et al. 2019).

MATERIALS AND METHODS

The material used in this study was collected from southern Finland in 1988-1990 by the Finnish Forest Research Institute (Metla, now Natural Resources Institute Finland, Luke) (VAPU data set). It consists of 122 Scots pine (including 25 young, 41 middle-aged, 34 mature and 22 old trees) and 146 Norway spruce (including 9 young, 79 middle-aged, 34 mature and 20 old trees) sample trees. VAPU data set consists of field measurements of branch, foliage and stem biomass and height information along the stem among other measurements. The proportions of aboveground tree biomass were studied on 122 Scots pine and 142 Norway spruce sample trees. Biomass was measured for samples and then up-scaled for individual trees by empirical models. Linear mixed models were used to test the age effect on the structure equations where age was considered as a fixed factor and plot number as random effect.

RESULTS

For both species, the biomass proportions changed throughout the age-sequence while the regularities of the structure were rather stable in the whole data set. Stem mass was the main aboveground carbon pool in each stand and the proportion increased with increasing age, while proportions of both branch and foliage decreased. For the biomass within the crown, for both species, the proportion of foliage and branch biomass from the total aboveground biomass decreased with growing crown length while that of stem biomass increased. However, in the whole tree level the pattern was the opposite, the proportion of stem biomass decreased with increasing crown ratio, while the proportion of branch and foliage increased.

Age-dependence of biomass proportions in old trees was detected for Scots pine in the hypothesized equations while no age-dependence was found for Norway spruce. Moreover, for both species stem form below the crown followed a prescribed dependence on crown ratio rather than tree age.

CONCLUSIONS

The regularities of tree structure suggested by pipe model theory are rather stable over their development, and hence, the biomass proportions are predictable in Scots pine and Norway spruce. Furthermore, with either the stable coefficients in Norway spruce or the more age-independent coefficients in Scots pine, we can estimate the forest growth variables by simple measurements. This could save the fieldwork that is essential in practice.

ACKNOWLEDGEMENTS

This study was supported by Academy of Finland, Strategic Research Council (research project: Integrated Biodiversity Conservation and Carbon Sequestration in the Changing Environment [IBC-CARBON]).

REFERENCES

- Mäkelä A. (1997). A carbon balance model of growth and self-pruning in trees based on structural relationships. *Forest Science*, 43(1), 7-24.
- Chapman, D.H. (1975). Optical scattering from combustion aerosols, *J. Aerosol Science* **36**, 3456.
- Minunno F., Peltoniemi M., Härkönen et al. (2019) Bayesian calibration of a carbon balance model PREBAS using data from permanent growth experiments and national forest inventory. *Forest Ecology and Management*, 440(15), 208-257.

MODEL OF HYDRAULIC FAILURE CAUSED BY WATER LOSS THROUGH BARK IN SCOTS PINE TREES

T. HÖLTTÄ¹ and A. LINTUNEN^{1,2}

¹Institute for Atmospheric and Earth System Sciences INAR/Forest Sciences, P.O. Box 27, FIN-00014, University of Helsinki, Finland

² Institute for Atmospheric and Earth System Sciences INAR/Physics, P.O. Box 27, FIN-00014, University of Helsinki, Finland

Keywords: bark evaporation, hydraulic failure, tree mortality, xylem

INTRODUCTION

Large scale tree mortality during extensive drought periods has become (and are predicted to become) more common in our changing climate, but exact mechanism(s) leading to tree death during drought are not well understood. Two main candidates for tree mortality have been carbon starvation and hydraulic failure (McDowell et al. 2008). In carbon starvation, the tree's carbon balance is negative for a prolonged period due to extensive stomatal closure and the subsequent decrease in photosynthetic production. In hydraulic failure, extensive embolism formation occurs, i.e. the conduits transporting water from soil to leaves become air-filled (Tyree and Sperry 1989). If embolism formation exceeds a critical threshold, the tree is unable to recover after the drought.

Typically the role of bark evaporation is not considered when the water balance of trees is calculated. Neglecting water loss through the bark is a reasonable assumption because the majority of tree water loss is occurring through the stomata in the leaves. However, during severe drought, the stomata close, and water loss from the leaves is restricted to water loss through the cuticles (Cochard 2019). Water loss through the bark is also important in deciduous trees when leaves are shed, and can account to even 5 % of total annual water loss (Oren and Pataki 2001).

In this study, the water loss rate through the bark in different sized branches of Scots pine and silver birch were measured in controlled laboratory conditions where air temperature and relative humidity could be controlled. Measurements were conducted on 12 branches of Scots pine ranging in diameter between 3 mm and 40 mm. Based on these measurements, results and allometric equations predicting the relations between tree height, total bark area, and total volume of a tree taken from Hölttä et al. (2013), the time required for hydraulic failure caused by water loss through the bark was calculated when it was assumed that the tree would not be able to obtain any water from the soil.

METHODS

The differential equation for the rate of change in amount of water in tree (dm_{water}/dt) due to evaporation through the bark is

$$\frac{dm_{water}}{dt} = - \frac{C m_{water} A_{bark} D}{m_{dry}} \quad (\text{Eq 1})$$

I.e. water loss rate per bark surface area (A_{bark}) and VPD (D) is assumed to be linearly proportional water content, m_{dry} is the dry mass, where C is a the constant of proportionality ($C = \text{water loss rate per unit bark surface area per VPD (g m}^{-2} / (\text{g m}^{-3}))$). Setting water content to saturation at time $t=0$ to a value of two times dry mass (i.e. $m_{water,sat} = 2 * m_{dry}$), and integrating yields

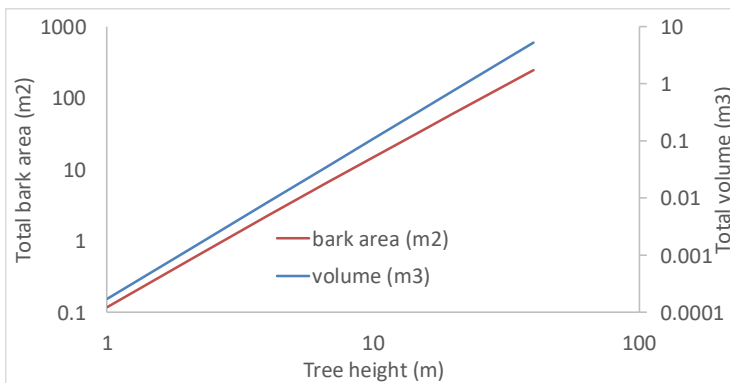
$$m_{water} = m_{water,sat} \exp\left(- \frac{C A_{bark} D}{m_{dry}} t\right) \quad (\text{Eq 2})$$

The time taken for hydraulic failure can be calculated from Eq. 2 by solving the time t ($=t_{hydr_fail}$), when $m_{water} = m_{water,RWC=50\%}$. i.e. hydraulic failure is assumed to be reached when the RWC (=relative water content) = 50 % (Rosner et al. 2018).

$$t_{hydr_fail} = -\frac{m_{dry}}{CA_{bark}D} \ln(m_{water,sat}/m_{water,RWC} \%) \quad (\text{Eq. 3})$$

The allometric equations in Hölttä et al. (2013) lead to predictions on total volume and bark surface area for a Scots pine tree as a function of tree height (Fig. 1). The dry mass per unit volume of wood is assumed to be 60% times the density of water. The amount of water at saturation is assumed to be equal to the dry mass.

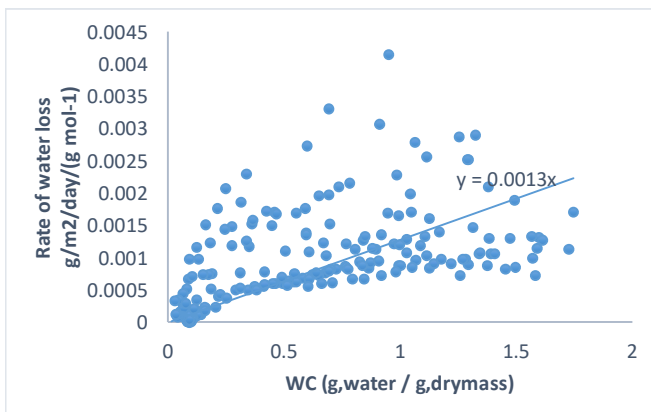
Fig 1. Predictions of total tree bark area, and total tree volume as a function of tree height from Hölttä et al. (2013).



RESULTS AND DISCUSSION

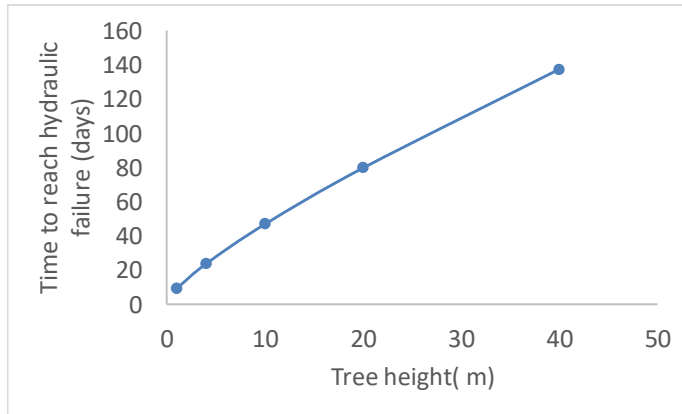
Figure 2 shows the water loss rate through the bark as a function of relative water content.

Fig. 2. water loss rate through the bark as a function of relative water content



The constant C is thus $0.0013 \text{ g m}^{-2} \text{ day}^{-1}(\text{g m}^{-3})^{-1}$. Assuming a VPD of 5 g m^{-3} and that the evaporation rate through the bark is not dependent on branch/stem size, the time taken for hydraulic failure for trees of different sized is shown in Fig. 3.

Fig.3. The time taken for hydraulic failure assuming water loss occurs only through the bark and no water is available from the soil.



Smaller trees reach hydraulic failure much earlier than large trees. Given our simple parameterization, i.e. that evaporation rate per surface area is not dependent on branch/stem size, the differences in time taken to reach hydraulic failure are due to differences in the ratio of the water amount in the tree (proportional to tree volume) divided by the bark surface area.

ACKNOWLEDGEMENTS

This work is supported by the Academy of Finland post-doctoral grant 310375 and Centre of Excellence grant 307331.

REFERENCES

- Cochard, H. (2019). A new mechanism for tree mortality due to drought and heatwaves. *bioRxiv*, 531632.
- Hölttä, T., Kurppa, M., & Nikinmaa, E. (2013). Scaling of xylem and phloem transport capacity and resource usage with tree size. *Frontiers in plant science* 4, 496.
- McDowell, N., Pockman, W. T., Allen, C. D., Breshears, D. D., Cobb, N., Kolb, T., ... & Yezzer, E. A. (2008). Mechanisms of plant survival and mortality during drought: why do some plants survive while others succumb to drought?. *New phytologist*, 178(4), 719-739.
- Oren, R., & Pataki, D. E. (2001). Transpiration in response to variation in microclimate and soil moisture in southeastern deciduous forests. *Oecologia*, 127(4), 549-559.
- Rosner, S., Johnson, D.M., Voggeneder, K. and Domec, J.C., (2019). The conifer-curve: fast prediction of hydraulic conductivity loss and vulnerability to cavitation. *Annals of Forest Science*, 76(3), p.82.
- Tyree, M. T., & Sperry, J. S. (1989). Vulnerability of xylem to cavitation and embolism. *Annual review of plant biology*, 40(1), 19-36.

HYGROSCOPIC PROPERTIES OF DMS DERIVED AEROSOLS IN SMOG CHAMBER STUDY

S. ISOKÄÄNTÄ¹, B. ROSATI², M. BILDE², and A. VIRTANEN¹

¹Department of Applied Physics, University of Eastern Finland, FI-70210, Kuopio, Finland.

²Department of Chemistry, University of Aarhus, DK-8000, Aarhus C, Denmark.

Keywords: DMS, HTDMA, SMOG CHAMBER, HYGROSCOPICITY

INTRODUCTION

Dimethyl sulfide (DMS) has been suggested to be a major contributor to produce aerosol particles in marine environments (Andreae & Raemdonck, 1983; Charlson et al., 1987). In marine environments, DMS is produced as a breakdown product of dimethylsulfoniopropionate (DMSP), which is produced not only by the metabolism of phytoplankton, but also by the air exposure of corals. When released to the atmosphere, DMS is then further oxidised to form sulphate aerosols. Sulphate aerosols formed through the oxidation of DMS can further act as cloud condensation nuclei, which influence to cloud albedo and radiative forcing. Indeed, modelling studies have shown that the DMS emissions affect the cloud microphysical properties and that the changes coincide with the times when phytoplankton blooms occur (Thomas et al., 2010).

On the other hand, both corals and the occurrence of phytoplankton blooms are highly dependent on the current climatic conditions, and therefore affected by climate change. It is, hence, important to study new particle formation from oxidation products of DMS and investigate the properties of these secondary particles. The oceans cover more than 70% of the surface of the Earth and thus the impact of DMS derived particles may be critical albeit until now completely unknown. In addition, different meteorological parameters, like temperature and humidity, might have major effects on the nucleation potential and volatility of the DMS derived particles. In this study, the properties of DMS derived aerosols were investigated in a smog chamber where different atmospheric conditions (e.g. different seasons) can be simulated.

METHODS

The physical and chemical properties of the nucleated DMS aerosols are investigated at Aarhus university during an intensive campaign (11.2-11.3.2019). The experiments took place in the AURA-chamber (see detailed description e.g. in Kristensen et al., (2017)), which allows to investigate how different temperatures (-15°C/0°C/20°C) and relative humidities (RH = 0% and 70%) affect the properties of aerosol particles formed from the DMS precursor. We investigated different aerosol properties, including e.g. chemical composition, size distributions, hygroscopicity and CCN activity. This abstract presents the preliminary results of the hygroscopic properties of small aerosol particles in the size range from 10 nm to 50 nm produced at different temperatures, when the smog chamber humidity was held approximately constant (~70%). In the chamber, H₂O₂ was photolyzed to produce OH radicals, and 200 ppb of DMS were injected to the chamber prior to the addition of the oxidant in each experiment. The hygroscopicity of the smallest sizes ($d_{dry} = 10-20$ nm) was investigated with a nano-HTDMA, and short description of the instrument is available in Tikkanen et al. (2018). Larger sizes were measured with a commercially available long-HTDMA (Brechtel).

RESULTS

Figure 1 shows the hygroscopic growth factors (GF) at RH=80% for the different sizes and chamber temperatures. The different sizes were not measured simultaneously, as the freshly nucleated particles are

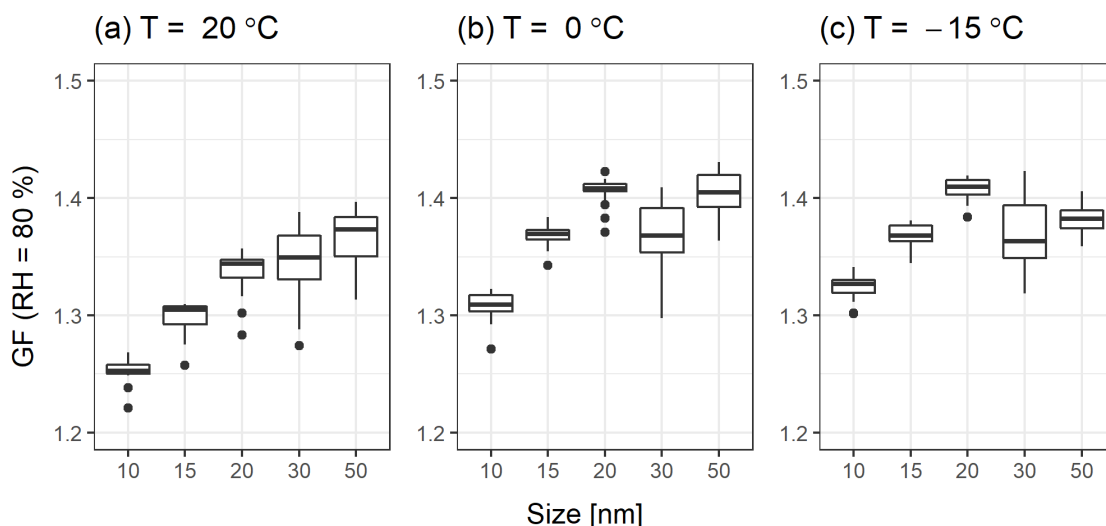


Figure 1. Growth factors (GF) for the particles at chamber temperatures of (a) 20°C, (b) 0°C and (c) -15°C. Sizes up to 20 nm were measured with the nano-HTDMA while 30 nm and 50 nm were measured with the long-HTDMA. The relative humidity in the chamber was 70% and the relative humidity inside the HTDMAs was held at 80%.

small and grow gradually. At 20°C, for example, the delay between the first measurement of 10 and 50 nm sizes was approximately 100 minutes. Solid horizontal lines for each size show the median, and the box shows the limits between the first (Q1) and third quartile (Q3). Black dots outside the boxes are values larger or smaller than $3 \times \text{IQR}$ ($\text{IQR} = \text{Q3} - \text{Q1}$). At 20°C (Fig. 1a), we see that GFs are larger for the larger sizes, being around 1.25 for 10 nm and 1.37 for the 50 nm particles. When inspecting the GFs at colder temperatures (Fig. 1b and 1c) we note that the GFs are increased. To untangle the Kelvin effect that significantly affects particles in this size range, we additionally calculated the hygroscopicity parameter, κ , to be able to compare the different sizes (Petters and Kreidenweis, 2007). The κ values are illustrated in Fig. 2. Contrarily to the GF results, the hygroscopicity parameter at $T = 20^\circ\text{C}$ is comparable throughout the measured size range and lies approximately between 0.45-0.50 for all dry sizes. However, for the colder temperatures the hygroscopicity of the particles in the nano-HTDMA range is significantly increased,

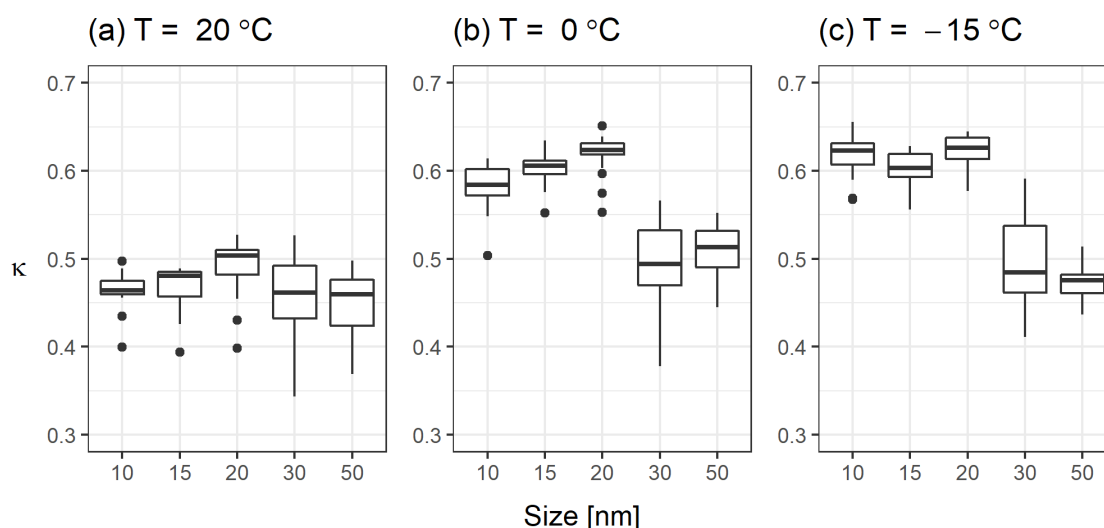


Figure 2. Hygroscopicity parameter κ for the particles at chamber temperatures of (a) 20°C, (b) 0°C and (c) -15°C. Sizes up to 20 nm were measured with the nano-HTDMA while 30 nm and 50 nm were measured with the long-HTDMA. The relative humidity in the chamber was 70% and the relative humidity inside the HTDMAs was held at 80%.

indicating that the chemical composition of the particles might be different at colder temperatures. Besides, the hygroscopicity of the larger sizes (30 and 50 nm) also shows a concurrent increase in κ with decreasing temperatures, but the differences are not as pronounced as for the smaller sizes. Increasing hygroscopicity in the small size range could indicate that e.g. fewer organic compounds with lower hygroscopicity such as MSA (methanesulfonic acid), having $\kappa = 0.36$ at 90% RH at room temperature (Johnson et al., 2004), are condensing onto the particles. Additionally, another cause for higher κ -values at the colder temperatures may be a change in the DMS oxidation pathway, thus resulting into a completely different aerosol particle with different chemical composition (see, e.g., Fig. 3 in Barnes et al., 2006). Further analysis is currently ongoing to investigate the chemical properties of these particles.

ACKNOWLEDGEMENTS

This work was supported by the Academy of Finland (Finnish Center of Excellence, grant no 307331; AquBor, grant no 317373).

REFERENCES

- Andrea, M. O., and H. Raemdonck, H. (1983). Dimethyl sulfide in the surface ocean and the marine atmosphere: a global view. *Science*, 221, 4621, 744-747.
- Barnes, I., Hjort, J., and N. Mihalopoulos (2006). Dimethyl sulfide and dimethyl sulfoxide and their oxidation in the atmosphere. *Chem. Rev.*, 106, 940-975.
- Charlson, R. J., Lovelock, J. E., Andreae, M.O and S. G. Warren (1987). Oceanic phytoplankton, atmospheric Sulphur, cloud albedo and climate. *Nature*, 326, 655-661.
- Johnson, G. R., Ristovski, Z. and L. Morawska (2004). Method for measuring the hygroscopic behavior of lower volatility fractions in an internally mixed aerosol. *Aerosol Science*, 35, 443-455.
- Kristensen, K., Jensen, L., N. Glasius, M., and M. Bilde (2017). The effect of sub-zero temperature on the formation and composition of secondary organic aerosol from ozonolysis of alpha-pinene. *Environ. Sci.: Processes Impacts*, 19, 1220-1234.
- Petters, M. D. and S. M. Kreidenweis (2007). A single parameters representation of hygroscopic growth and cloud condensation nucleus activity. *Atmos. Chem. Phys*, 7, 1961-1971.
- Thomas, M., A., Suntharalingam, P., Pozzoli, L., Rast, S., Devasthale, A., Kloster, S., Feichter, J., and T. M. Lenton, (2010). Quantification of DMS aerosol-cloud-climate interactions using the ECHAM5-HAMMOZ model in a current climate scenario. *Atmos. Chem. Phys*, 10, 7425-7438.
- Tikkanen, O-P., Väisänen, O, Hao., L., Holopainen, E., Wang., H., Lehtinen., K. E. J. and T. Yli-Juuti (2018), *Aerosol. Sci. Technol.*, 52, 9, 971-983.

DUST CONCENTRATIONS' ROLE IN THE NORTHERN EXPANSION OF WESTERN AFRICAN MONSOON DURING THE MID-HOLOCENE PERIOD

J.P. BIAN^{1*}, Q. ZHANG², H. SEPPÄ³, J. RAISANEN¹, Z. LU⁴, P. ZHOU¹, and R. MAKKONEN^{1,5}

¹Institute for Atmospheric and Earth System Research /Physics, University of Helsinki, Finland

²Department of Physical Geography, Stockholm University, Sweden

³Department of Geophysics and Geography, University of Helsinki, Finland

⁴Department of Physical Geography and Ecosystem Science, Lund University, Sweden

⁵Finnish Meteorological Institute, Helsinki, Finland

Keywords: MID-HOLOCENE, WESTERN AFRICAN MONSOON, DUST CONCENTRATIONS

INTRODUCTION

The Sahara desert was covered with vegetation during the “Green Sahara” period (11,000 to 4,000 years before the present). The “Green Sahara” was caused by the stronger Western African Monsoon (WAM) circulation, which was ultimately driven by orbital factors and further enhanced by regional factors like aerosols and vegetation cover. In this research, we focus on the mid-Holocene epoch (6,000 years before the present) and conduct related general circulation modelling (GCM) via the EC-Earth platform (IFS+NEMO). For most of the previous efforts of the mid-Holocene researches, the difficulties were caused by unrealistic incorporation of dust concentrations and multi aerosols resources in the simulations. So providing more realistic distributions of aerosols during the Mid-Holocene period could improve their feedback in the large-scale atmosphere-ocean circulations.

METHODS

Our researches set up methodological framework of EC-Earth platform, and simulate the mid-Holocene and pre-industrial dust concentrations without the prescribed vegetation background. Then we conduct the analysis of dust concentrations-climate interactions and feedback during mid-Holocene period, and quantify the synergistic effect of aerosols on northern expansion of WAM circulation and enhancement of precipitation in the Sahara region.

CONCLUSIONS

Previous researches gave the conclusion that dust concentrations played no difference in WAM circulation and precipitation during the Mid-Holocene period when there was no Sahara vegetation background existed (Pausata et al. 2016; Tierney et al. 2017; Hopcroft et al. 2019). By providing more realistic distributions of dust concentrations during the mid-Holocene period, we find that from the comparison between the control (MH_CNTRL) and dust concentrations (MH_AEROSOL) simulations (Fig. 1a), there is a five degrees' northern shift of WAM circulation and increased precipitation in the Sahara under the new aerosol background (Fig. 1b). Forced by new dust concentrations distribution patterns during the mid-Holocene period, the Northern Atlantic (NA)'s warming and enhancement of African Easterly Jet (AEJ) promote strengthened WAM circulation and mid-to-low moist convection, which forces the northern expansion of monsoon and increases rainfall in the Sahara. Moreover, we work further explores the indirect role of dust concentrations and multi

aerosols resources through unveiling surface properties that are important for vegetation-albedo-climate feedback and WAM circulation.

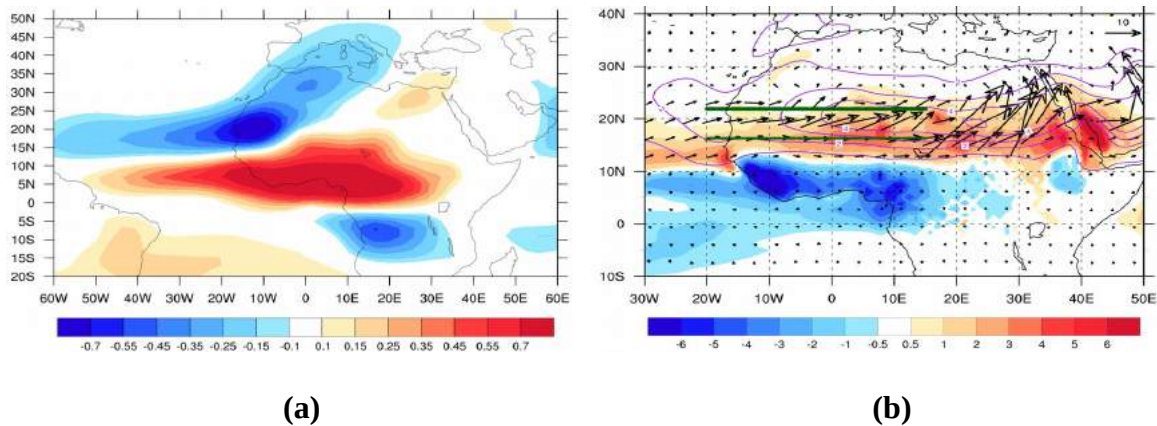


Figure 1. Difference between MH_CNTRL and MH_AEROSOL during the summer season (Jun-Sep). (a) Averaged aerosol optical depth (AOD) at 550 nm; (b) Precipitation (color, units: mm/day), moisture fluxes at 925 hPa (vector, units: (10m/s). (g/kg)), and relative humidity at 925 hPa (contour, units: %). The horizontal green lines represent the maximum northward extent of the WAM in the MH_CNTRL (thin) and MH_Aerosol (thick) simulations.

REFERENCES

- Pausata, Francesco SR, Gabriele Messori, and Qiong Zhang. "Impacts of dust reduction on the northward expansion of the African monsoon during the Green Sahara period." *Earth and Planetary Science Letters* 434 (2016): 298-307.
- Tierney, Jessica E., Francesco SR Pausata, and Peter B. deMenocal. "Rainfall regimes of the Green Sahara." *Science advances* 3.1 (2017): e1601503.
- Hopcroft, Peter O., and Paul J. Valdes. "On the Role of Dust-Climate Feedbacks During the Mid-Holocene." *Geophysical Research Letters* 46.3 (2019): 1612-1621.

CHEMICAL COMPOSITION OF AEROSOL PRECURSORS IN THE FINNISH SUBARCTIC

T. JOKINEN^{1*}, K. NEITOLA¹, I. YLIVINKKA¹ AND M. SIPILÄ¹

¹Institute for Atmospheric and Earth System Research / Physics, Faculty of Science, P.O. Box 64
00014 University of Helsinki, Finland.

Keywords: Subarctic, Measurements, Precursors, New Particle Formation, Mass Spectrometry

INTRODUCTION

The subarctic region offers climate with some of the most extreme temperature variations on the planet and is warming twice as fast compared to the global average. The boreal forest (taiga) covers most of the subarctic, being the largest land biome in the world. The forest-atmosphere ecosystems link closely to one another. We started measurements at the SMEAR I station located in Värriö (67°46'N, 29°36'E) in eastern Lapland, Finland (e.g. Kyrö et al., 2014), in order to start permanent deployment of aerosol precursor measurements in the Finnish subarctic. The data analysed for this abstract comes from the spring and summer of 2019. The measurements concentrate in the measurements of aerosol precursor vapours using mass spectrometer using nitrate ions for chemical ionization.

A high-resolution mass spectrometer, CI-APi-TOF for neutral molecules, is analysing the precursor vapour concentration including sulphuric acid (H₂SO₄), methane sulfonic acid (MSA) and iodic acid (HIO₃). Jokinen et al., 2012, describes the instrumentation in details. We aim first to identify days when new particles form and then analyse what compounds dominate the mass spectra during these days. We are also interested in what happens in the gas phase if very clean days with very few particles present are compared to the high pollution airmasses from the Kola Peninsula. The results are the first longer period ambient measurement of aerosol precursor gases from the Finnish subarctic covering the period of midnight sun in midsummer.

RESULTS AND DISCUSSION:

New particle formation (NPF) days are detected few times a month at SMEAR I. One example of a NPF days I give in Fig. 1 when new particles were observed to form on a day in June. We studies the chemical composition of NPF participating compounds during this day using the nitrate CI-APi-ToF. With this instrument, we measured elevated concentrations of several condensing vapours during the event (Fig 2 A and B). In the neutral compound analysis, sulphuric acid (SA), malonic acid (MA), methane sulfonic acid (MSA) and iodic acid (HIO₃) were detected during this event. Abundant quantities of highly oxygenated molecules or other oxidized organic compounds were recorded also. During this one day, not a single compound dominated the spectrum and much deeper analysis will be conducted in the future in order to find out the exact chemical composition of molecular clusters at this site.

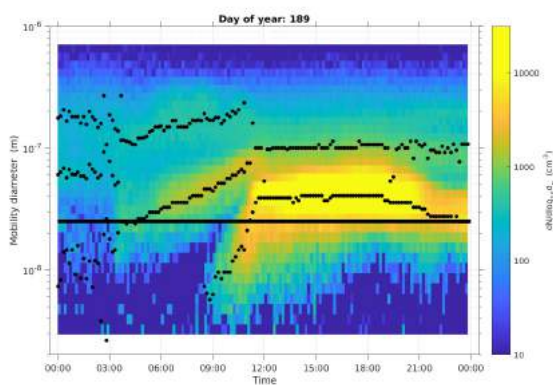


Figure 1. New particle formation event observed in Värriö, SMEAR I station in June 2019. The observation is collected from an DMPS system and it represents the mobility size distribution of small particles.

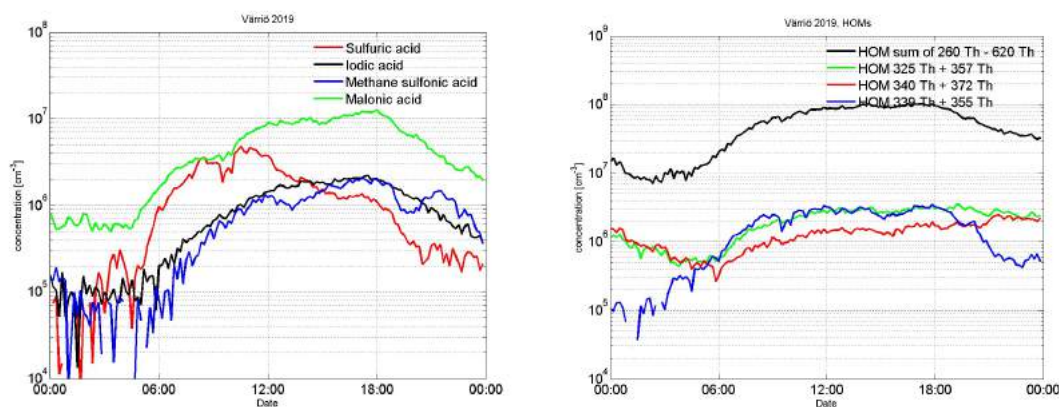


Figure 2. A) panel on the left represents the measured concentrations of sulfuric acid (red), iodic acid (black), methane sulfonic acid (blue) and malonic acid (green). B) the panel on the right represents the estimated concentrations of selected highly oxygenated compounds (HOM) and their sum (black). Green HOMs are RO₂-radical signals, red HOMs are closed shell monomer (C₁₀) products and the blue ones are organic nitrates. All concentrations are calculated using a preliminary calibration factor from sulfuric acid calibration.

ACKNOWLEDGEMENTS:

We are grateful to the European Research Council (ERC) that funds the research program GASPARCON, grant agreement ID: 714621 and we thank the personnel of SMEAR I station for technical help during the measurements.

REFERENCES:

- Kyrö E.M., Väänänen R., Kerminen V.-M., Virkkula A., Petäjä T., Asmi A., Dal Maso M., Nieminen T., Juhola S., Shcherbinin A., Riipinen I., Lehtipalo K., Keronen P., Aalto P.P., Hari P. & Kulmala M. Trends in new particle formation in eastern Lapland, Finland: effect of decreasing sulfur emissions from Kola Peninsula. *Atmos. Chem. Phys.* 14: 4383–4396, 2014.
- Jokinen, T., Sipilä, M., Junninen, H., Ehn, M., Lönn, G., Hakala, J., Petäjä, T., Mauldin III, R. L., Kulmala, M., and Worsnop, D. R.: Atmospheric sulphuric acid and neutral cluster measurements using CI-APi-TOF, *Atmos. Chem. Phys.*, 12, 4117-4125, <https://doi.org/10.5194/acp-12-4117-2012>, 2012.

SECONDARY ORGANIC AEROSOL FORMATION VIA OZONOLYSIS OF GREEN LEAF VOLATILES (GLV) AND TERPENES

J. JOUTSENSAARI¹, P. YLI-PIRILÄ², A.A. WAZA¹, S. BHUTTO¹, J. KIM¹, E. KARI¹, L. HAO¹, P. MIETTINEN¹ and J.K. HOLOPAINEN²

¹Department of Applied Physics, University of Eastern Finland, P.O. Box 1627, FI-70211 Kuopio, Finland

²Department of Environmental and Biological Sciences, University of Eastern Finland, P.O. Box 1627, FI-70211 Kuopio, Finland

Keywords: Secondary organic aerosol, green leaf volatiles, terpenes.

INTRODUCTION

Atmospheric aerosols have a strong but highly uncertain influence on the Earth's radiation balance and climate (IPCC, 2013). Formation of secondary organic aerosols (SOA) by oxidation of volatile organic compounds (VOC) in the troposphere is one of the main sources of atmospheric aerosols, contributing ca. 60 % of total organic aerosol mass. On the global scale, VOC emissions from vegetation (i.e., biogenic VOC) to the atmosphere constitute about 90% of all global VOC emissions (Guenther et al., 1995) and thus they are important precursors for SOA. The main biogenic VOCs contributing tropospheric SOA formation are isoprene and monoterpenes such as α -pinene, β -pinene, and limonene.

Green leaf volatiles (GLVs) are an important group of oxygenated biogenic VOCs, which are mainly emitted from leaves of plants, e.g., wheat, oilseed rape, grape and birch trees (Scala et al., 2013; Ameye et al., 2018). GLVs are especially released after wounding and other damage of leaves and the odor of cut grass and damaged green leaves is mainly from GLV compounds. Typical GLV compounds detected in atmosphere are *cis*-3-hexenyl acetate, *cis*-3-hexenol and *cis*-3-hexenal. In an ecosystem level, GLVs are active in plant-plant and plant-insect communications and interactions, e.g., they repel herbivores and attract their natural enemies. In general, a burst of GLVs is immediately (0-5 min) released from plants after the damage whereas terpenes are typically released with a delay (hours). GLVs are typically highly reactive with atmospheric oxidants (typical lifetimes in minutes or hours) and thus they readily form both SOA and ozone when realized to troposphere.

To understand better effects of GLVs on SOA formation in the atmosphere, there is a need for controlled chamber experiments using multicomponent VOC mixtures. In this study, we have investigated SOA formation from oxidation of three individual GLV compounds (*trans*-2-hexenal, *cis*-3-hexenol and *cis*-3-hexenyl acetate), their mixtures, and mixtures of GLVs and monoterpenes (MT) (α -pinene and mixture of monoterpenes) via ozonolysis at humid conditions (RH ~50 %).

METHODS

We have conducted several ozonolysis experiments using GLVs and terpenes as precursors for SOA formation. The experimental system used in this study consists of a Teflon reaction chamber (volume 9.8 m³), VOC and ozone injection systems and gas and particle analyzers. At the beginning the experiments, the ozone-enriched air was introduced into the chamber to achieve target ozone concentration (ca. 200 ppb). Then, GLV and monoterpene compounds were injected into the chamber by a cleaned and dried carrier gas. VOC solutions were injected two times into the chamber during one experiments: the 1st injection at the start time of the experiment and the 2nd injection 1-1.5 hour later. The target concentration of each VOC injection was 40 ppb for the 1st injection and 40-80 ppb for the 2nd injection. The GLVs used in this study were *trans*-2-hexenal (HAL), *cis*-3-hexanol (HOL), *cis*-3-hexenyl acetate (CHA) and a mixture of them.

Furthermore, α -pinene and a terpene mixture (MT-mixture) consisted of α -pinene, sabinene, limonene, β -myrcene, ocimene, linalool and β -caryophyllene were used in some experiments. Summary of the experiments, used precursors and their concentrations are shown in Table 1.

Concentrations of injected VOC and various gas-phase intermediates and products formed during experiments were determined continuously with a proton transfer reaction - mass spectrometer (PTR-MS) and off-line with a gas chromatography mass spectrometer (GC-MS). Furthermore, O_3 , SO_2 , NO_x concentrations in the chamber was continuously measured with gas monitors. The formation and growth of SOA particles were investigated by measuring number size distributions and total concentrations with a scanning mobility particle sizer (SMPS).

Table 1. Summary of the chamber experiments: number of the experiment (Exp. no.), injected VOCs, their volumes and concentrations, and ozone (O_3) peak concentrations for the 1st and 2nd VOC injections.

Exp. no.	Terpene	GLV	1 st VOC injection		2 nd VOC injection	
			VOC volume / concentration	Peak O_3 (ppb)	VOC volume / concentration	Peak O_3 (ppb)
1	-	HAL	2.0 μ L / 43 ppb	44	2.0 μ L / 43 ppb	42
2	-	HOL	2.0 μ L / 42 ppb	220	4.0 μ L / 84 ppb	193
3	-	CHA	2.6 μ L / 41 ppb	203	5.2 μ L / 82 ppb	178
4	α -pinene	-	2.6 μ L / 41 ppb	212	2.6 μ L / 41 ppb	186
5	α -pinene	HAL	MT: 2.6 μ L / 41 ppb GLV: 2.0 μ L / 43 ppb	204	GLV: 4.0 μ L / 86 ppb	176
6	α -pinene	HOL	MT: 2.6 μ L / 41 ppb GLV: 2.0 μ L / 42 ppb	200	GLV: 4.0 μ L / 84 ppb	153
7	α -pinene	CHA	MT: 2.6 μ L / 41 ppb GLV: 2.6 μ L / 41 ppb	211	GLV: 5.2 μ L / 82 ppb	172
8	α -pinene	GLV-mix	MT: 2.6 μ L / 41 ppb GLV: 2.0 μ L / 39 ppb	235	GLV: 4.0 μ L / 78 ppb	190
9	MT-mix	-	2.8 μ L / 41 ppb	208	2.8 μ L / 41 ppb	183
10	MT-mix	HAL	MT: 2.8 μ L / 41 ppb GLV: 2.0 μ L / 43 ppb	205	GLV: 4.0 μ L / 86 ppb	194
11	MT-mix	HOL	MT: 2.8 μ L / 41 ppb GLV: 2.0 μ L / 42 ppb	215	GLV: 4.0 μ L / 84 ppb	180
12	MT-mix	CHA	MT: 2.8 μ L / 41 ppb GLV: 2.6 μ L / 41 ppb	230	GLV: 5.2 μ L / 82 ppb	180
13	MT-mix	GLV-mix	MT: 2.8 μ L / 41 ppb GLV: 2.0 μ L / 39 ppb	220	GLV: 4.0 μ L / 78 ppb	189

RESULTS AND DISCUSSION

Figure 1 shows results of SOA formation from a typical GLV experiment (HOL) and a α -pinene experiment. In the HOL experiment, only a minor particle formation (ca. 300 cm^{-3}) was observed after the 1st VOC injection (42 ppb) although VOC concentration was decreased substantially due to ozonolysis reactions. After the 2nd injection of HOL (84 ppb), slightly stronger SOA formation occurred. The total particle number concentration (Ntot) increased to ca. 4000 cm^{-3} , however total particle mass concentration (Mtot) was still very low (below $1 \mu\text{g m}^{-3}$). Minor SOA formation (ca. 1400 cm^{-3} , $0.3 \mu\text{g m}^{-3}$) was also for CHA whereas practically no particle formation was observed for HAL. The reaction rate constant of HAL with ozone is about 1/40 that of HOL (Mellouki et al., 2015) and, thus, SOA formation from HAL is very low.

In contrast, a very intensive new particles formation (NPF) occurred during the ozonolysis of α -pinene. After the 1st injection of α -pinene (41 ppb), Ntot increased very rapidly to ca. $9 \times 10^4 \text{ cm}^{-3}$ and Mtot to ca. $45 \mu\text{g m}^{-3}$. The 2nd injection (41 ppb) did not produce clear NPF anymore but increased Mtot to ca. $130 \mu\text{g m}^{-3}$ because formed organic mass mainly condensed onto existing particles.

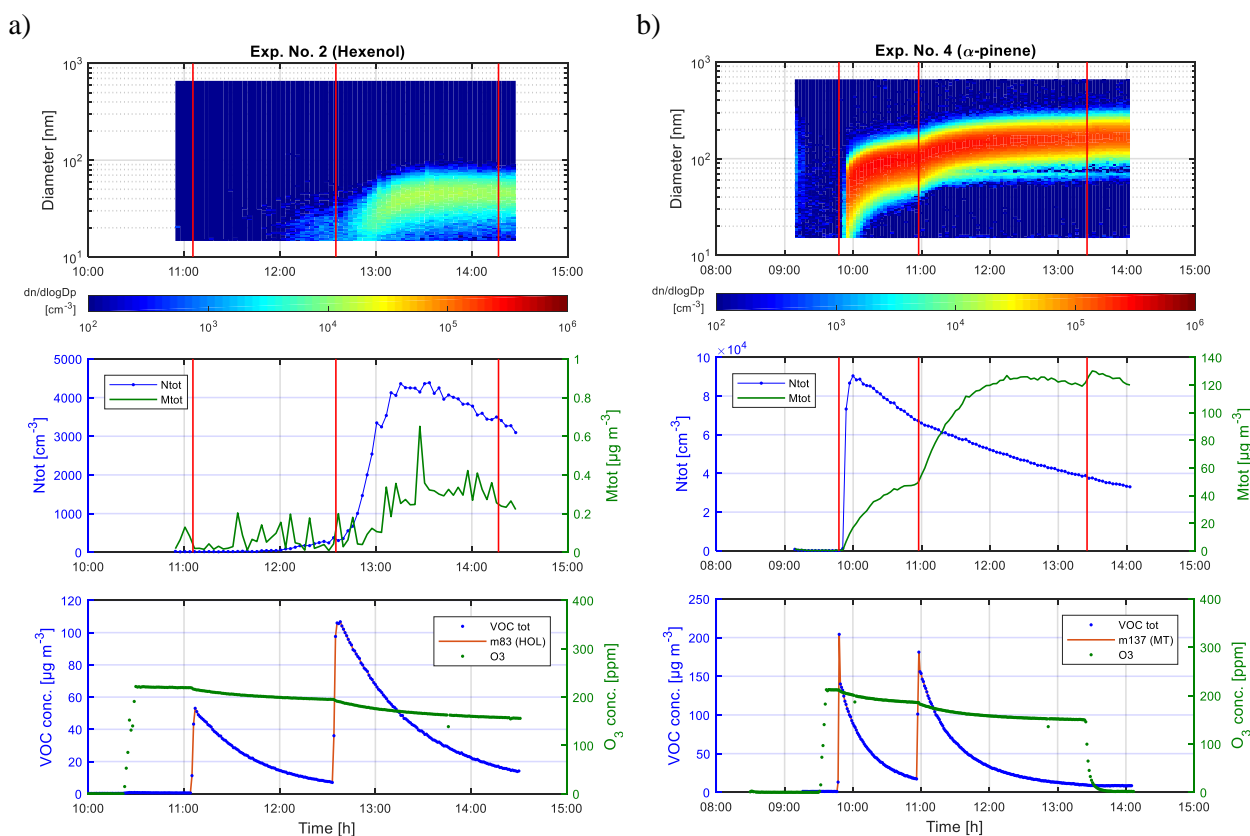


Figure 1. SOA formation from a) hexenol (HOL) and b) α -pinene experiments. The 1st panel shows particle number size distribution, the 2nd panel total particle number (Ntot) and mass (Mtot) concentrations, and the 3rd panel total VOC concentration (VOC tot), concentrations of certain PTR-MS mass peaks (m83, m137, etc.) and ozone concentration (O_3) during the experiment. Red vertical lines indicate times of the first VOC, the second VOC and TME injections into the chamber.

In the next set of the experiments, we studied the effect of a mixture of α -pinene and GLV on SOA formation. In the α -pinene/GLV experiments, a clear NPF was observed after the 1st VOC injection when both MT and GLV were injected together. The N_{tot} and M_{tot} values were very similar to those measured in the pure α -pinene experiment. During the 2nd injection of HOL and CHA, a clear increase in organic mass together a decrease in O₃ concentration was observed. In contrast, no clear change in N_{tot}, M_{tot} and O₃ concentrations can be seen after the 2nd injection of HAL due to its very low reaction rate with ozone. Very similar results were also observed in MT-mixture/GLV than α -pinene/GLV experiments. However, more particles in counts but less in mass has formed in the MT-mixture experiments than α -pinene experiments.

CONCLUSIONS

The results shows that MTs produce SOA more efficiently than GLVs due to higher reactivity with ozone. However, studied GLVs have also a substantial effect on SOA formation except HAL, which has very low reactivity with ozone. GLVs can also reduce NPF by acting as scavengers for oxidant without forming substantial amount of condensable species needed in NPF.

ACKNOWLEDGEMENTS

The study was financially supported by the strategic funding of the University of Eastern Finland and the Academy of Finland (decisions no. 307331 and no. 250215).

REFERENCES

- Ameye, M., Allmann, S., Verwaeren, J., Smagghe, G., Haesaert, G., Schuurink, R. C., and Audenaert, K.: Green leaf volatile production by plants: a meta-analysis, *New Phytologist*, 220, 666-683, doi:10.1111/nph.14671, 2018.
- Guenther, A., Hewitt, C. N., Erickson, D., Fall, R., Geron, C., Graedel, T., Harley, P., Klinger, L., Lerdau, M., McKay, W. A., Pierce, T., Scholes, B., Steinbrecher, R., Tallamraju, R., Taylor, J., and Zimmerman, P.: A global model of natural volatile organic compound emissions, *J. Geophys. Res. Atmos.*, 100, 8873-8892, 1995.
- IPCC: Climate Change 2013: The Physical Science Basis. Contribution of Working Group I to the Fifth Assessment Report of the Intergovernmental Panel on Climate Change, Cambridge University Press, Cambridge, United Kingdom and New York, NY, USA, 1535 pp., 2013.
- Mellouki, A., Wallington, T. J., and Chen, J.: Atmospheric Chemistry of Oxygenated Volatile Organic Compounds: Impacts on Air Quality and Climate, *Chemical Reviews*, 115, 3984-4014, 10.1021/cr500549n, 2015.
- Scala, A., Allmann, S., Mirabella, R., Haring, M. A., and Schuurink, R. C.: Green leaf volatiles: a plant's multifunctional weapon against herbivores and pathogens, *International journal of molecular sciences*, 14, 17781-17811, 10.3390/ijms140917781, 2013.

OVERVIEW OF MEASUREMENTS AND CURRENT INSTRUMENTATION FOR 1-10 NM AEROSOL PARTICLE NUMBER SIZE DISTRIBUTIONS

J. Kangasluoma^{1,2}, R. Cai^{2,3}, J. Jiang³, C. Deng³, D. Stolzenburg^{2,4}, L. R. Ahonen², T. Chan², Y. Fu³, C. Kim^{5,6}, T. M. Laurila², Y. Zhou¹, L. Dada², J. Sulo², R. C. Flagan⁵, M. Kulmala^{1,2}, T. Petäjä², K. Lehtipalo^{2,7}

¹Aerosol and Haze Laboratory, Beijing Advanced Innovation Center for Soft Matter Science and Engineering, Beijing University of Chemical Technology, Beijing, China

²Institute for Atmospheric and Earth System Research / Physics, Faculty of Science, University of Helsinki, Finland

³State Key Joint Laboratory of Environment Simulation and Pollution Control, School of Environment, Tsinghua University, Beijing, China

⁴Faculty of Physics, University of Vienna, 1090 Vienna, Austria

⁵Division of Chemistry and Chemical Engineering, California Institute of Technology, 1200 East California Boulevard, Pasadena, California 91125, USA

⁶School of Civil and Environmental Engineering, Pusan National University, Busan 46241, Republic of Korea

⁷Finnish Meteorological Institute, Erik Palménin aukio 1, 00560 Helsinki, Finland

Keywords: particle number size distribution, instrumentation, uncertainty

INTRODUCTION

Sub-10 nm particles exist in various environments, often in systems in which vapors transform into particles. This process begins with the formation of molecular clusters and continues with the subsequent condensation of vapors and particle growth. Such processes are observed for example in the atmosphere, industrial applications, combustion, and is the basis of several nanomaterial synthesis methods (e.g. Alanen et al. 2015; Kulmala et al. 2004; Nosko et al. 2017; Wang et al. 2017). The process of particle formation and growth can take place in systems with wide range of dynamics, creating a need for instrument optimization for specific systems. For instance, measurement of particle formation in the Arctic environment requires very low particle concentration detection limits and good sensitivity, while the process can be relatively slow due to very low precursor concentrations (Wiedensohler et al. 1994). Measurements on board aircraft or cars call for optimized instrument response time (Rönkkö et al. 2017; Wehner et al. 2015). In industrial and combustion processes, and even in some heavily polluted environments, the particle concentrations can be too high for some of the current instrument capable for sub-10 nm particle measurements (Tang et al. 2017). In some laboratory experiments, the only required instrumental characteristics is high size resolving power (Fernandez de la Mora and Barrios-Collado 2017). It is therefore obvious that careful selection of the available instrumentation is crucial for a successful measurement. Furthermore, all measurements include random and systematic uncertainties, which depend on the measurement method and particle number size distribution (PNSD) to be characterized. This manuscript aims to assess various aspects of sub-10 nm PNSD measurements, and provide suggestions for instrument selection based on quantitative analysis. We focus only on the instrumental aspects of sub-10 nm PNSD measurements, i.e. ion mobility distributions, total particle number concentrations, or any subsequent parameter calculated based on the sub-10 nm size distribution data, such as particle formation and growth rates are not discussed.

In the forthcoming manuscript, our goal is to provide overall view on the status of the 1-10 nm PNSD measurements. We first describe briefly the general operation principles of the current instruments used for sub-10 nm PNSD measurements. Then we present PNSDs measured from three different sites, which represent the current state-of-the-art sub-10 nm PNSD measurements. This is followed by a literature review on publications that report measurements of sub-10 nm PNSDs using at least two concurrent

instruments. After the PNSD measurement overview, we discuss the measurement uncertainties. Our aim is to assess thoroughly the relevant parameters affecting the measurement accuracy. At the end, with the description of the concentration and sizing uncertainties, we make recommendations on selecting sets of instruments for various applications.

METHODS

Our analysis is structured as follows:

- review of current instrumentation with focus on electrical mobility spectrometers and condensation particle counting methods,
- review of previous literature on sub-10 nm PNSD measurements in which at least two instruments have been used concurrently to obtain comparison of the measured distributions,
- analysis of three state-of-the-art sub-10 nm PNSD measurements from Hyytiälä, Beijing and CLOUD chamber
- analysis of measurement uncertainties focus on electrical mobility spectrometers and condensation particle counting methods
- overview of the future challenges for the community to improve the measurement capabilities and accuracy

RESULTS

Two types of results are presented: measurements from Beijing and a table compiling the uncertainties.

Beijing

Continuous measurements were established at the Beijing University of Chemical Technology west campus inside urban Beijing in the beginning of 2018 (Zhou et al. 2019). For the long-term sub-10 nm PNSD measurements, the station includes the PSM, NAIS and DMPS, and also for our selected measurement period an SMPS, which is a combination of DEG SMPS, another twin SMPS and APS, covering the whole size range from 1 nm to 1 μm from Tsinghua University (Liu et al. 2016). The instruments are located on 5th floor of the building, sampling either through a window (PSM, NAIS, 1 – 6 nm part of the Tsinghua SMPS) or from the roof (DMPS and 6 nm – 1 μm part of the Tsinghua SMPS). The PSM is sampling with a core sampling system with a 1.3 m line. The NAIS sampling line is about 1 m long, and is located next to the PSM. The DMPS samples with a 2.5 μm preimpactor and drier in the sampling line, and covers the size range of 6 – 840 nm with a single DMA by measuring in two flow modes with a TSI 3772 as the detector. Thus, the DMPS is not fully optimized for the sub-10 nm size range. The DEG SMPS is around 5 m away from the PSM and NAIS, also utilizing core sampling, while the Tsinghua SMPS is a twin SMPS with the ultrafine part utilizing the TSI nanoDMA and TSI 3776 as the detector.

Based on the data we identified two characteristic types of days regarding their typical conditions, namely those affected by haze (high contribution of super-micron particles) and new particle formation event days (high concentration of ultrafine particles followed by their growth towards larger sizes). Therefore, as the corresponding PNSDs were very different, we separated the data accordingly. We selected 14 NPF event days and 31 haze days in 2018 for the comparison. Similarly, as for Hyytiälä, median PNSD and hourly PNSDs for one days are presented. In Beijing, we expect that the particle composition is mostly sulfuric acid-dimethyl amine in around 1-2 nm (Yao et al. 2018), while at some larger size it is expected that also oxygenated organics participate to particle formation but the exact size ranges and contributions are unknown. We can make the following observations from Figure 3: during NPF, in the size range from 3 nm to 8 nm the NAIS detects larger size distribution function than the DEG SMPS. The DEG SMPS and the PSM exhibit an agreement within a factor of 3, and the trends of the measured PNSDs agree

quite well. Based on the discussion on the sources of uncertainties in these measurements, this agreement between the PSM and DEG SMPS can be considered fairly good. During haze time, the detection limit of the DEG SMPS is too high to detect particles below 3 nm, while the PSM still reports elevated sub-3 nm particle concentrations. The observation of persistent existence of sub-3 nm particles even during times of high condensation sink is an interesting observation that will be examined further in the future.

Figure 4 presents three PNSD comparisons on 25.12.2018 at 8, 12 and 14 which was an NPF event day. As in Fig.3, the NAIS detects in all cases larger size distribution function of about a factor of 1-5 than the DEG SMPS. Especially in the morning but also throughout the day, the PSM detects clearly larger size distribution function than the DEG SMPS, depending on the size the PSM exceeding the DEG SMPS with a factor of more than 10. Possible reasons for this observation include for example particle composition that is not easily detected with DEG, which would increase the cut-off of the DEG SMPS, while the distribution measured by the PSM would be only shifted along the diameter axis. Another possibility is strongly decreased charging efficiency because of the particle composition, which, however, we cannot speculate further due to lack of suitable data.

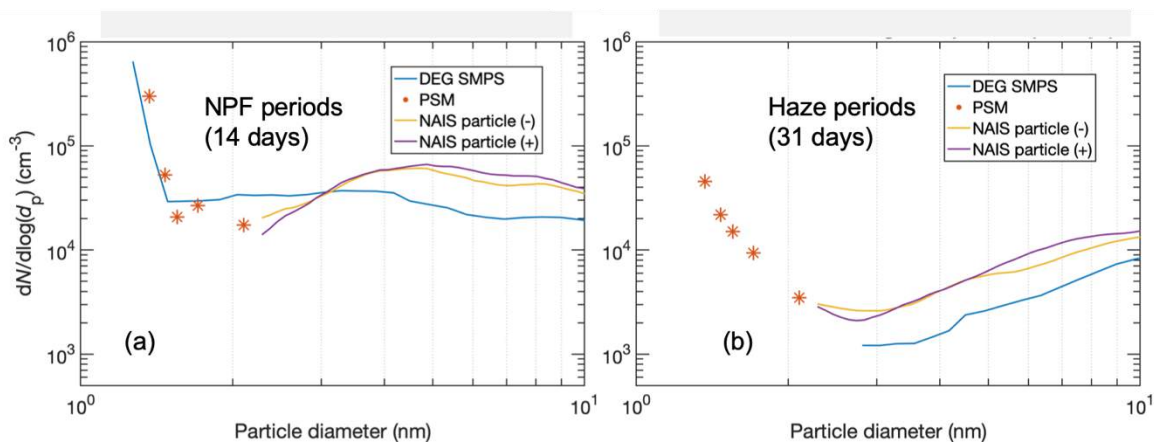


Figure 3. Median size distributions over selected (a) NPF periods and (b) haze periods during 2018 measured in urban Beijing.

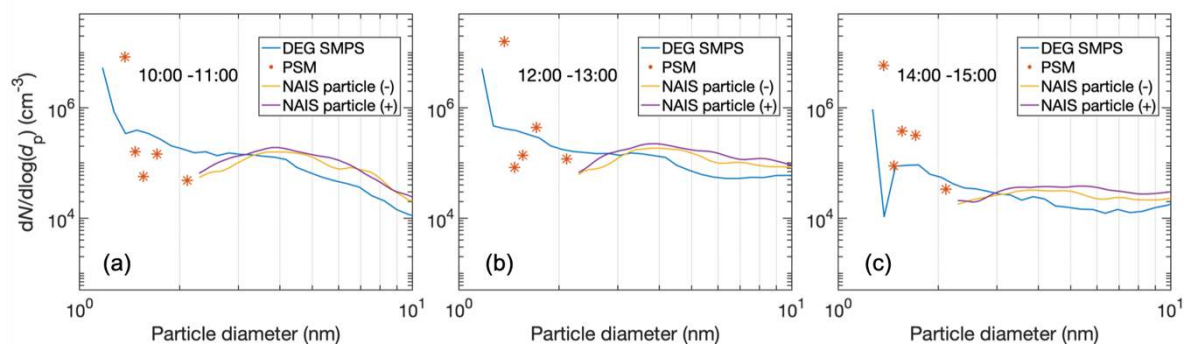


Figure 4. Median size distributions over one hour during (a) 10:00 – 11:00, (b) 12:00 – 13:00 and (c) 14:00 – 15:00 on 24-Feb-2018 in urban Beijing. The event started around 7:30 and ended approximately 15:00 on 24-Feb-2018

Table 1. Summary of the concentration and sizing inaccuracy sources

Source	Physical/chemical source	Affects	Instrument	Magnitude	Comment
Unknown line penetration	Diffusion	Concentration	All instruments	Depends on sampling design, negligible if well-designed or characterized, significant for sub-3 nm without characterization	For a size classified particle linear effect to inverted concentration. Impossible to correct for total concentration measurement
Unknown charging efficiency	Charger ion-particle interactions	Concentration	EMS	Highly uncertain, possibly at least up to $\pm 50\%$	Linear effect to inverted concentration, can vary in different environments
Instrument size resolution	Diffusion for DMA, vapor-particle interactions for CPC, size distribution change over the transfer function or cut-off width	Concentration, size	All instruments	Concentration $\pm 0-20\%$. Size: $\pm 0.5/R\%$ (FWHM of transfer function).	Sizing uncertainty related to transfer function and cut-off, concentration uncertainty to systematic sizing error
CPC cut-off	Vapor-particle interactions	Concentration, size	CPCs, SMPS	Concentration: Highly system dependent. Size: from ± 0.1 nm to ± 1 nm.	For A11 and CPCb, sizing based on cut-off curve accuracy. For EMS, lowest detectable particle size depends on cut-off
Counting statistics	Random spatial distribution of particles in air	Concentration	EMS	Scales with \sqrt{N} , up to $\pm 100\%$ at low concentration	Random (not systematic) effect to inverted concentration
Inversion	Assumption of infinite resolution, low counting statistics	Concentration, size	All instruments	Up to $\pm 30\%$	Depends strongly on PNSD

CONCLUSIONS

In this overview, we studied the previous literature in which sub-10 nm PNSDs are measured at least with two independent instruments, presented new PNSD data from three sites, and showed that the current PNSD measurements contain some sources of uncertainties that are larger than expected, or unknown sources we cannot account for currently. Due to these uncertainties, significant discrepancies exist in the observed PNSDs between the instruments, especially during times of relatively low concentrations. Depending on the measurement, a multiplier factor between lowest and highest size distribution function can vary from 1 up to 10 and more, typically being the highest if one of the instruments detects low concentrations, or is at its detection limit. According to the presented uncertainty assessment, we estimated this factor to be about maximum of 2-4, suggesting our analysis quite well captures the observed deviations between the size distribution functions reported in the literature. Generally, in size range between 3-10 nm, the NAIS seems to always detect the largest size distribution function, while SMPS systems the lowest. In the sub-3 nm size

range, the PSM generally observes larger size distribution function than the EMS. Overall, we can state that the general trends observed in the PNSDs usually agree quite well, while some systematic discrepancies are included in the obtained PNSDs, of which sources remain ambiguous.

We discussed six separate sources for uncertainty for the measurements of sub-10 nm PNSDs that are: particle transport losses, charging efficiency, DMA sizing, CPC cut-off, statistical counting and inversion uncertainty. Of these, the total uncertainties are likely dominated by the charging and in the sub-3 nm size, contributed also by the CPC cut-off and statistical counting uncertainty. Particle transport losses can be efficiently minimized by using the core sampling system, while uncharacterized and/or poorly designed sampling lines can lead to losses of even 95% and more. Uncertainties due to the assumption of zero width for the instrument transfer function or detection efficiency curves are limited to maximum of around 5-20%.

Based on the general characteristics of the instruments and typical systems in which sub-10 nm particles are observed, we outline general suggestions for selecting. The selection of instruments should be based on selecting a suitable combination of instruments by optimizing the response time, detection limit and size range. Individual instruments can/should be optimized for given applications for optimum performance. Generally, above size distribution function values of 10^4 $dN/d\log D_p$ at 2 nm the uncertainties would be reduced by reduced charging and sizing uncertainties, and below that by also increased counting statistics.

REFERENCES

Alanen, J., Saukko, E., Lehtoranta, K., Murtonen, T., Timonen, H., Hillamo, R., Karjalainen, P., Kuuluvainen, H., Harra, J., Keskinen, J., Ronkko, T. (2015). The formation and physical properties of the particle emissions from a natural gas engine. *Fuel* 162:155-161.

Fernandez de la Mora, J. and Barrios-Collado, C. (2017). A bipolar electrospray source of singly charged salt clusters of precisely controlled composition. *Aerosol Sci Tech* 51:778-786.

Kulmala, M., Vehkamäki, H., Petaja, T., Dal Maso, M., Lauri, A., Kerminen, V. M., Birmili, W., McMurry, P. H. (2004). Formation and growth rates of ultrafine atmospheric particles: a review of observations. *J Aerosol Sci* 35:143-176.

Liu, J., Jiang, J., Zhang, Q., Deng, J., Hao, J. (2016). A spectrometer for measuring particle size distributions in the range of 3 nm to 10 μ m. *Front Env Sci Eng* 10:63-72.

Nosko, O., Vanhanen, J., Olofsson, U. (2017). Emission of 1.3-10 nm airborne particles from brake materials. *Aerosol Sci Tech* 51:91-96.

Rönkkö, T., Kuuluvainen, H., Karjalainen, P., Keskinen, J., Hillamo, R., Niemi, J. V., Pirjola, L., Timonen, H. J., Saarikoski, S., Saukko, E., Jarvinen, A., Silvennoinen, H., Rostedt, A., Olin, M., Yli-Ojanpera, J., Nousiainen, P., Kousa, A., Dal Maso, M. (2017). Traffic is a major source of atmospheric nanocluster aerosol. *P Natl Acad Sci USA* 114:7549-7554.

Tang, Q., Cai, R., You, X., Jiang, J. (2017). Nascent soot particle size distributions down to 1 nm from a laminar premixed burner-stabilized stagnation ethylene flame. *P Combust Inst* 36:993-1000.

Wang, Y., Kangasluoma, J., Attoui, M., Fang, J. X., Junninen, H., Kulmala, M., Petaja, T., Biswas, P. (2017). Observation of incipient particle formation during flame synthesis by tandem differential mobility analysis-mass spectrometry (DMA-MS). *P Combust Inst* 36:745-752.

Wehner, B., Werner, F., Ditas, F., Shaw, R. A., Kulmala, M., Siebert, H. (2015). Observations of new particle formation in enhanced UV irradiance zones near cumulus clouds. *Atmos Chem Phys* 15:11701-11711.

Wiedensohler, A., Aalto, P., Covert, D., Heintzenberg, J., McMurry, P. (1994). Intercomparison of Four Methods to Determine Size Distributions of Low-Concentration ($\sim 100 \text{ cm}^{-3}$), Ultrafine Aerosols ($3 < D_p < 10 \text{ nm}$) with Illustrative Data from the Arctic. *Aerosol Sci Tech* 21:95-109.

Yao, L., Garmash, O., Bianchi, F., Zheng, J., Yan, C., Kontkanen, J., Junninen, H., Mazon, S. B., Ehn, M., Paasonen, P., Sipila, M., Wang, M. Y., Wang, X. K., Xiao, S., Chen, H. F., Lu, Y. Q., Zhang, B. W., Wang, D. F., Fu, Q. Y., Geng, F. H., Li, L., Wang, H. L., Qiao, L. P., Yang, X., Chen, J. M., Kerminen, V. M., Petaja, T., Worsnop, D. R., Kulmala, M., Wang, L. (2018). Atmospheric new particle formation from sulfuric acid and amines in a Chinese megacity. *Science* 361:278-281.

Zhou, Y., Dada, L., Liu, Y., Fu, Y., Kangasluoma, J., Chan, T., Yan, C., Chu, B., Daellenbach, K. R., Bianchi, F., Kokkonen, T., Liu, Y., Kujansuu, J., Kerminen, V. M., Petäjä, T., Wang, L., Jiang, J., Kulmala, M. (2019). Variation of size-segregated particle number concentrations in winter Beijing. *Atmospheric Chemistry and Physics Discussions*.

ASSESSING THE EFFECT OF VEGETATION LAYOUT ON AEROSOL PARTICLE CONCENTRATIONS WITHIN AN URBAN STREET CANYON USING LARGE-EDDY SIMULATIONS

S. KARTTUNEN¹, M. KURPPA¹ and L. JÄRVI^{1,2}

¹ Institute for Atmospheric and Earth System Research / Physics, Faculty of Science, University of Helsinki, P.O. Box 68, 00014 Helsinki, Finland

²Helsinki Institute of Sustainability Science, University of Helsinki, 00014 Helsinki, Finland

Keywords: air quality, vegetation, street trees, hedges, street canyon, urban planning, ventilation, particulate matter

INTRODUCTION

The increase in computational resources creates a potential in utilizing high resolution air quality modelling to support urban planning. The possibility to solve the flow field and air quality related processes down to a one-meter scale and beyond allows the city planners and researchers to test the effects of different city planning scenarios on the very local air quality as well as wind and thermal comfort.

The large-eddy simulation (LES) is currently the most promising tool to study the local effects of different city planning scenarios on various environmental issues, such as air quality, wind and thermal comfort. Development of LES models has been active in recent years. One example is the PALM model system (Maronga et al., 2019), which incorporates various model components designed specifically for urban applications. These include, for example, a plant canopy model and a sectional aerosol model SALSA (Maronga et al., 2019; Kurppa et al., 2019).

The effect of urban vegetation on air quality has been found to be a two-fold question. Whilst in parks and open road configurations trees are effective in reducing pollutant concentrations by dry deposition to tree leaves, previous studies have shown that the decreased ventilation due to the aerodynamic effects of vegetation canopy seems to play a bigger role than the dry deposition in street canyons. An extensive review of the previous studies is available in Abhijith et al. (2017).

The study aims to combine high resolution flow modelling together with a sectional aerosol model SALSA to assess effects of different street vegetation configurations on local scale air quality. Simulations are conducted on a wide street canyon with high traffic rates for which six different street and vegetation configurations are considered. The analysis focuses on the pedestrian level number and mass concentrations, the differences in the particle size distributions and ventilation performance.

METHODS

The study area is described by a 50 to 58 meter wide and approximately 800 meter long street canyon surrounded by three to seven story buildings.

The simulations are conducted for six different street configurations, each with different vegetation layouts. Scenarios S0, S2A, S2B and S2C incorporated a 54-meter wide street canyon while scenario S1 used 58-meter wide and scenario S3 used a 50-meter wide street canyon. The vegetation configurations applied in each scenario are listed in Table 1. The simulations are performed for

Scenario	Tree rows	Tree species	Hedges
S0	0	-	-
S1	4	<i>Tilia × vulgaris</i>	-
S2A	3	<i>Tilia × vulgaris</i>	-
S2B	3	<i>Tilia × vulgaris</i>	Below outermost trees
S2C	3	<i>Tilia × vulgaris</i> (middle), <i>Sorbus intermedia</i> (outermost)	-
S3	2	<i>Tilia × vulgaris</i>	-

Table 1: The vegetation configurations used in the study. *Tilia × vulgaris* had a height of 15 meters, *Sorbus intermedia* 9 meters and hedges 0.75 meters.

two wind directions, 8° and 82° with respect to the street canyon. Moderate wind conditions and a neutral stratification are applied.

Traffic lanes are defined as pollutant source areas, covering 41-48% of the street canyon surface area. The emission factors used represented a high traffic rate (3660 vehicles per hour) with a vehicle fleet and technologies projected for year 2030. Moderate background concentration estimates are used as boundary conditions for the aerosol model.

The numerical approach used the PALM model system with a LES-LES self nesting approach. The simulations were initialized with a precursor run. A finer grid resolution (1 m horizontally and 0.75 m vertically) child domain of size $768 \times 384 \times 72$ grid points is embedded in a coarser resolution (3 m in each direction) parent domain of size $384 \times 192 \times 64$ grid points. The aerosol model is solved only for the child domain in order to reduce computational costs. Each simulation are run for 1 hr 10 mins and data only from the last 60 mins is used.

KEY FINDINGS

The key finding is that the vegetation increases pedestrian level PM10 mass concentrations within the street canyon compared to the vegetation-free case by 52% to 74%, depending on the scenario. The decrease in the street canyon ventilation is found to play more important role than the dry deposition of pollutants into vegetation. This is consistent with the majority of the previous studies (Abhijith et al., 2017).

For particle number concentrations this increase is significantly lower, from 7% to 18%. The dry deposition is more effective for smaller particles which dominate the particle number concentration. A decrease in particle number concentrations was observed for approximately sub-50 nm particles.

The best scenario and vegetation configuration in terms of air quality seems to depend on which measure is given the most weight. In terms of PM2.5 and PM10 concentrations, scenario S2C which incorporates a variable-height tree canopy disturbs the ventilation performance of the pollutants the least whilst in terms of smaller particles the scenarios with more vegetation content such as S1 and S2B show better performance.

ACKNOWLEDGEMENTS

This work was done in collaboration with the City of Helsinki. Work was supported by the Academy of Finland Centre of Excellence (project no. 307331) and Helsinki Metropolitan Region Urban Research Program.

REFERENCES

- Abhijith K.V., Kumar P., Gallagher J., McNabola A., Baldauf R., Pilla F., Broderick B, Di Sabatino S., Pulvirenti B. (2017) Air pollution abatement performances of green infrastructure in open road and built-up street canyon environments – A review *Atmospheric Environment*, **162**, 71-86, doi:10.1016/j.atmosenv.2017.05.014
- Kurppa M., Hellsten A., Roldin P., Kokkola H., Tonttila J., Auvinen M., Kent C., Kumar P., Maronga B., Järvi L. (2019) Implementation of the sectional aerosol module SALSA2.0 into the PALM model system 6.0: Model development and first evaluation *Geosci. Mod. Dev.*, **12**, 1403-1422, doi:10.5194/gmd-12-1403-2019
- Maronga B., Banzhaf S., Burmeister C., et al. (2019) Overview of the PALM model system 6.0 *Geosci. Mod. Dev.*, doi:10.5194/gmd-2019-103

STATUS OF FCOE PARTICIPATION IN CMIP6 USING EC-EARTH

J.-P. Keskinen¹, R. Makkonen¹, and J. Lento²

¹Institute for Atmospheric and Earth System Research (INAR) / Physics, University of Helsinki, Finland.

²CSC – IT Center for Science Ltd.

Keywords: CMIP6, AerChemMIP, EC-Earth, earth system modelling

INTRODUCTION

The Coupled Model Intercomparison Project (CMIP) is considered an integral part of climate science. It is organised under the World Climate Research Programme’s Working Group on Coupled Modelling. Started more than 20 years ago, CMIP has now entered its sixth phase (CMIP6) (Eyring et al., 2016). The Finnish Centre of Excellence in Atmospheric Science (FCoE) takes part in CMIP6 through the contribution from the Institute for Atmospheric and Earth System Research (INAR) at the University of Helsinki. The participation in CMIP6 simulations is done using the EC-Earth earth system model as a part of the EC-Earth consortium and in a very close coordination with the Finnish Meteorological Institute (FMI), the Royal Netherlands Meteorological Institute (KNMI), and the Barcelona Supercomputing Centre (BSC).

CMIP6

In order to participate in CMIP6, all models are required to complete a small set of common experiments called Diagnostic, Evaluation, and Characterisation of Klima (DECK) and a historical simulation spanning the years between 1850 and 2014. The DECK simulation consist of an atmosphere only simulation (amip), a pre-industrial control simulation (piControl), an abrupt quadrupling of CO₂ concentration simulation (abrupt-4xCO₂), and a 1 % per year CO₂ concentration increase simulation (1pctCO₂). The DECK experiments provide continuity between past and future phases of CMIP and allow the evaluation of model characteristics. Performing the historical simulation allows to assesses the ability of the model to simulate climate and its variability.

The more specific scientific questions will be addressed through several topical model intercomparison projects (MIPs). CMIP6 includes a wide variety of MIPs with topics ranging from land use to geoengineering and from clouds to paleoclimate. The FCoE will participate only in the Aerosols and Chemistry MIP (AerChemMIP) (Collins et al., 2017), a MIP focusing on the quantifying the climate and air quality impacts of aerols and chemically reactive gases. Figure 1 illustrates both the structure of CMIP6. FCoE’s AerChemMIP participation will be done in as a part of the EC-Earth consortium and in a very close cooperation with FMI, KNMI, and BSC.

EC-EARTH

In order to participate in CMIP6, the climate model EC-Earth (Hazeleger et al., 2012) will be used to perform the simulations in FCoE’s contribution. The model has been developed within a consortium consisting of 27 research institutions in 10 different European countries. EC-Earth is based on and uses as its atmospheric component the Integrated Forecasting System (IFS), developed

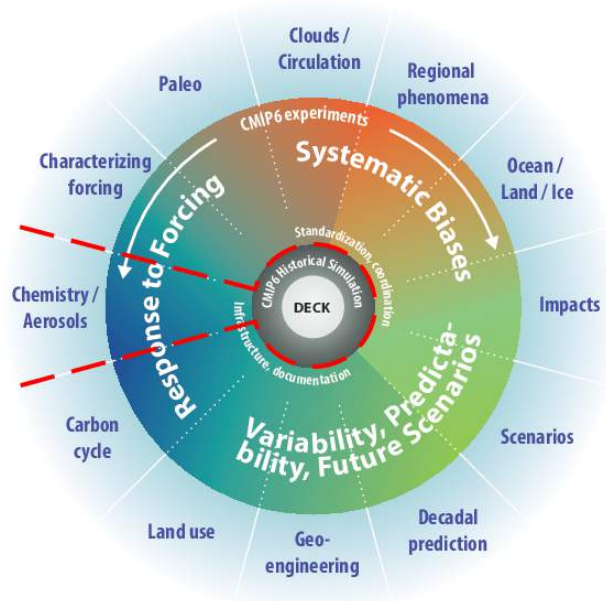


Figure 1: Structure of CMIP6. The participation of FCoE is highlighted with red colour.

by the European Centre for Medium-Range Weather Forecasts (ECMFW). In the AerChemMIP version of EC-Earth, the other model components are the Ocean model NEMO and the aerosol-chemistry transport model TM5. The composite models are coupled together using the OASIS coupler.

Since the participation in CMIP5, the previous phase of CMIP, EC-Earth has been through substantial development. At the moment of the writing of this abstract, the implementation of new features has been completed and the development concentrates on tuning of the model. The final CMIP6 version of EC-Earth is scheduled for November 2018 and a model description paper is expected during the year 2019.

TIMELINE FOR CMIP6 EXPERIMENTS

The first simulations for CMIP6 using EC-Earth are expected to start soon after the tuning of the model has been finished in the end of 2018. Due to the structure of CMIP6, the first simulation will be piControl from the DECK. The historical simulation will be started as soon as suitable initial conditions are available from piControl. In similar manner, the scenario simulations can be started as soon as the initial conditions from the historical simulation are available. The simulation results will be distributed through the Earth System Grid Federation (ESGF) (Cinquini et al., 2014).

Depending on the model configuration and the computational platform, EC-Earth is able to produce up to 2-20 simulated years per day. This means that model configurations with higher performance might be able to finish their first simulations during 2018. The model configuration used at the University of Helsinki for AerChemMIP involves a larger number of coupled fields between the atmospheric and the aerosol-chemistry component and for this reason approximately two simulated years per day are expected. The first CMIP6 simulations carried out by the University of Helsinki are hence expected to start at the beginning of 2019 and the first results are expected in mid-2019. The simulations will be carried out using the CSC - IT Center for Science Ltd's Sisu supercomputer (Cray XC40). The created data will be distributed using an ESGF data node set up in collaboration with FMI and CSC.

ACKNOWLEDGEMENTS

This study was supported by Academy of Finland Centre of Excellence program (project no. 272041). CSC – IT Center for Science is acknowledged for providing HPC infrastructure for CMIP6.

REFERENCES

- Cinquini, L., Crichton, D., Mattmann, C., Harney, J., Shipman, G., Wang, F., Ananthakrishnan, R., Miller, N., Denvil, S., Morgan, M., Pobre, Z., Bell, G. M., Doutriaux, C., Drach, R., Williams, D., Kershaw, P., Pascoe, S., Gonzalez, E., Fiore, S., and Schweitzer, R. (2014). The Earth System Grid Federation: An open infrastructure for access to distributed geospatial data. *Future Generation Computer Systems*, 36:400–417.
- Collins, W. J., Lamarque, J.-F., Schulz, M., Boucher, O., Eyring, V., Hegglin, M. I., Maycock, A., Myhre, G., Prather, M., Shindell, D., and Smith, S. J. (2017). AerChemMIP: quantifying the effects of chemistry and aerosols in CMIP6. *Geoscientific Model Development*, 10(2):585–607.
- Eyring, V., Bony, S., Meehl, G. A., Senior, C., Stevens, B., Stouffer, R. J., and Taylor, K. E. (2016). Overview of the Coupled Model Intercomparison Project Phase 6 (CMIP6) experimental design and organisation. *Geoscientific Model Development*, 9:1937–1958.
- Hazeleger, W., Wang, X., Severijns, C., Ștefănescu, S., Bintanja, R., Sterl, A., Wyser, K., Semmler, T., Yang, S., van den Hurk, B., van Noije, T., van der Linden, E., van der Wiel, K., Ștefănescu, S., Bintanja, R., Sterl, A., Wyser, K., Semmler, T., Yang, S., van den Hurk, B., van Noije, T., van der Linden, E., and van der Wiel, K. (2012). EC-Earth V2.2: Description and validation of a new seamless earth system prediction model. *Climate Dynamics*, 39(11):2611–2629.

AUTUMNAL AEROSOL PM10 CONCENTRATION IN BOREAL FOREST AT 2005-2017

H. KESKINEN^{1,2}, L. HEIKKINEN¹, I. YLIVINKKA^{1,2}, P. A. AALTO¹, J. AALTO^{1,2}, E. EZHOVA¹, K. LEHTIPALO¹, M. RÄTY¹, S. SANTAPUKKI¹, J. KESTI³, J. LEVULA^{1,2}, M. LOPONEN^{1,2}, S. RANTANEN^{1,2}, H. LAAKSO^{1,2}, R. PILKOTTU^{1,2}, T. SALMINEN^{1,2}, T. MATILAINEN^{1,2}, M. KULMALA¹, T. NIEMINEN¹ AND T. PETÄJÄ¹

¹Institute for Atmospheric and Earth System Research / Physics, Research/Forest
Faculty of Science, University of Helsinki, Finland

²Hyytiälä Forestry Field Station, Korkeakoski, Finland

³Finnish Meteorological Institute (FMI), Helsinki, Finland

Keywords: LONG-TERM MEASUREMENTS, AEROSOL MASS CONCENTRATION

INTRODUCTION

The air that we breathe consists of, among gases, particulate matter (PM). The mixture of gases and particles is called aerosol. When the inhaled particles end up in our respiratory system, they may cause serious health hazards such as asthma or cardiovascular diseases (Pope et al., 2002). Tragic events, such as the Great Smog of London in December 1952 that led to the death of approximately 12,000 people, has evoked a need to monitor and regulate PM concentrations (Bell and Davis, 2001). Nowadays, they are reported on-line worldwide. The mass concentration of particles with (aerodynamic) diameter less than 10 μm is called ‘coarse mode particles’ PM10. Here, we report for the first time long-term (2005-2017) autumnal (September, October and November (SON)) variations of PM10 measured with the gravimetric impactor, on-line mass analyzer SHARP and aerosol mass concentration derived from number size distribution measurements in Hyytiälä, SMEARII, Finland (Hari and Kulmala, 2005).

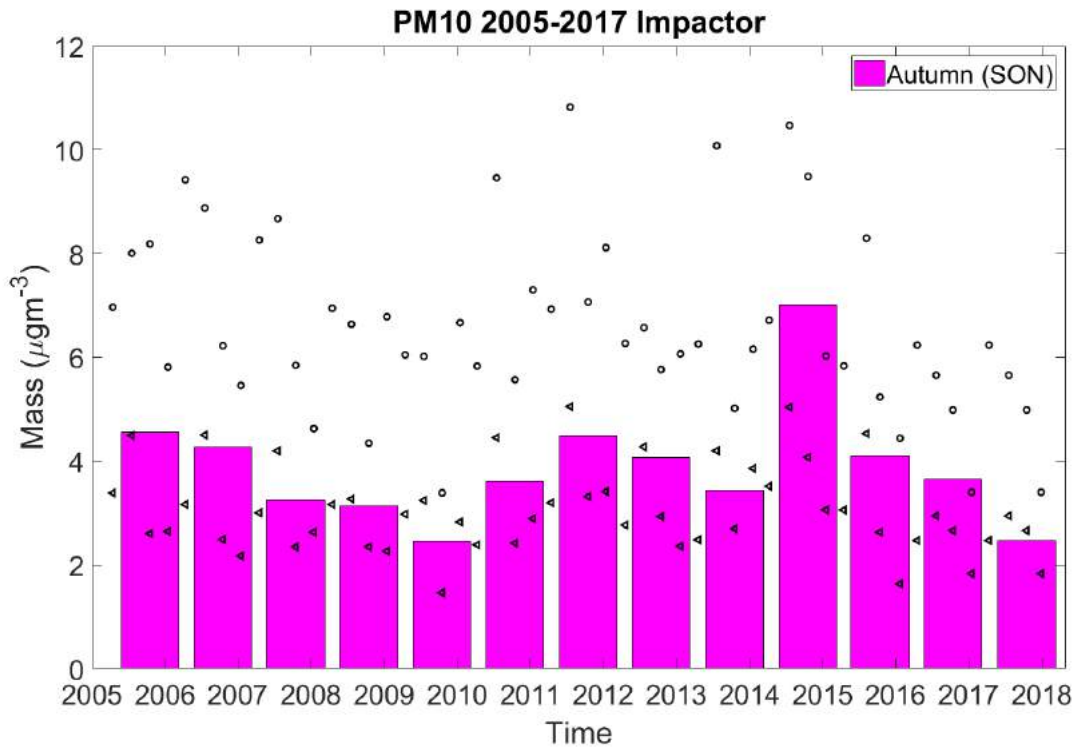
METHODS

Measurements are performed at SMEAR II (Station for Measuring Ecosystem-Atmosphere Relations) located in Hyytiälä in southern Finland (61°51'N, 24°17'E; 181 m a.s.l.; Hari and Kulmala 2005). Particulate samples were started to collect with gravimetric impactor (Berner and Lurzer, 1980) in late 1990's. The impactor has unheated TSP inlet with a stainless-steel tube. The aerosol mass concentration for PM10, PM2.5 and PM1 can also be estimated by using the number size distributions measured with Differential Scanning Mobility Sizer (DMPS) and Aerosol Particle Sizer (APS). This instrument set-up used at SMEARII is described in detail by Aalto et al. (2001). Third method Synchronized Hybrid Ambient Real-time Particulate Monitor SHARP (Thermo Scientific, Model 5030) is, a real-time particulate monitor and the measurements started at 2012. SHARP combines light scattering photometry and β -ray attenuation for continuous PM10 measurement. SHARP utilizes proprietary digital filtering for continuous mass calibration of the nephelometric measurement of PM10. However, the mass concentration is relatively low in Hyytiälä, which may be problematic for high-resolution online measurements.

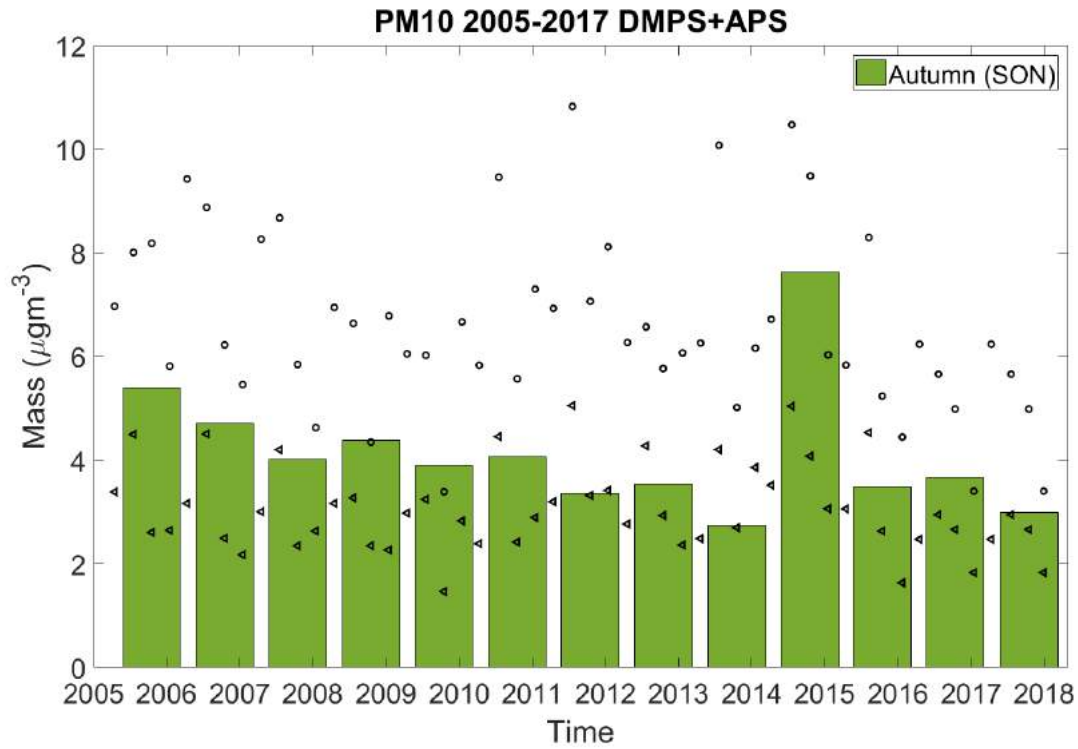
CONCLUSIONS

Autumnal mean PM10 concentration was 4.5-5.1 $\mu\text{g m}^{-3}$ in 2005-2017. In comparison, Laakso et al. (2003) observed the PM10 concentration of 6.9 $\mu\text{g m}^{-3}$ for the years 1999-2002. Thus, the PM10 concentration decreased from the value in 1999-2002. In autumn, the boreal forest starts to be less active, and the effects of the new EU-regulation on ambient air quality might affect on the concentrations. In figure 1 we see the

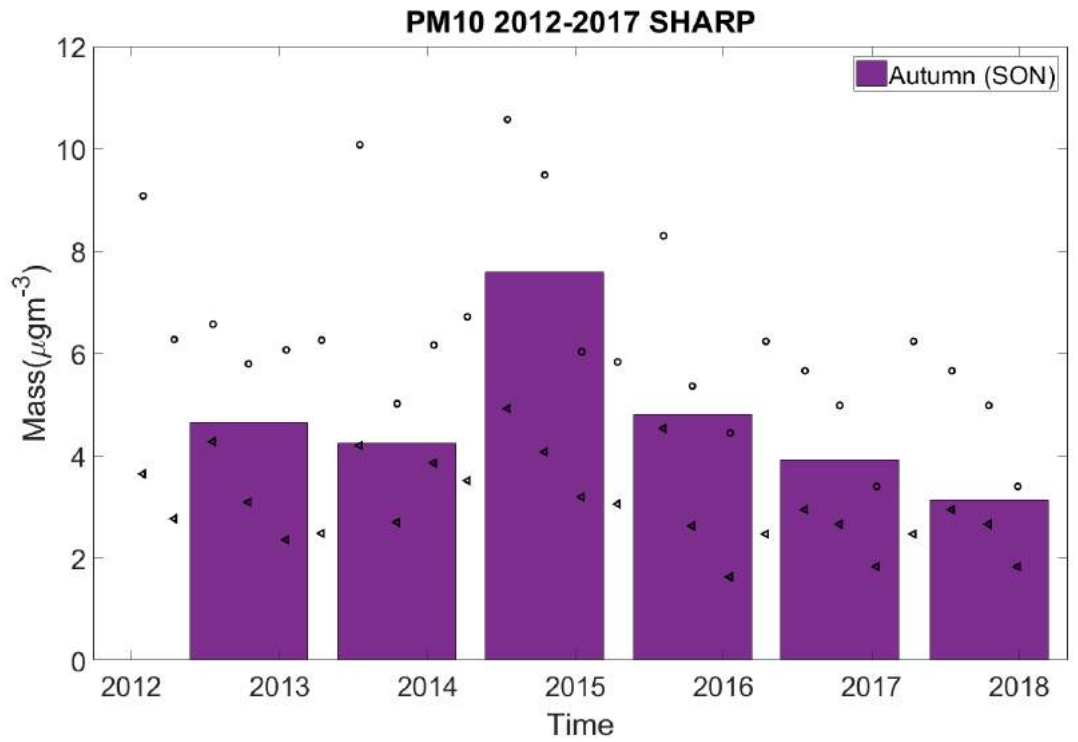
median PM10 concentrations measured by impactor (a), DMPS+APS(b) and SHARP(c). One can see that there is a certain maximum in autumn 2014. The reason for the high PM concentrations in 2014 was a six-month-long (from 31st of August 2014 until 27th of February 2015) eruption of the Bardarbunga volcano. It was the largest eruption in Iceland since the devastating Laki eruption in 1783-84. Very recently, the same eruption in Autumn 2014 was observed also by an Aerosol Chemical Speciation Monitor (ACSM) at SMEARII (Heikkinen et al., 2019).



a)



b)



c)

Figure 1. Autumnal median PM10 concentrations and their 25 and 75 quartile ranges measured with the impactor (a), DMPS+APS (b) and SHARP (c).

ACKNOWLEDGEMENTS

Thanks for the money: ACTRIS, ECAC, Academy of Finland (307331, 272041)

REFERENCES

Aalto, P., Hämeri, K., Becker, E., Weber, R., Salm, J., Mäkelä, J. M., Hoell, C., O'Dowd, C. D., Karlsson, H., Hansson, H., Väkevä, M., Koponen, I. K., Buzorius, G., Kulmala, M., 2001: Physical characterization of aerosol particles during nucleation events. *Tellus*, 53B, 344–358.

Bell M.L. and Devra Lee Davis, Reassessment of the Lethal London Fog of 1952: Novel Indicators of Acute and Chronic Consequences of Acute Exposure to Air Pollution, *Environmental Health Perspectives* • VOLUME 109 | SUPPLEMENT 3 | June 2001

Berner, Axel & Luerzer, Christian. (1980). Mass size distributions of traffic aerosols at Vienna. *The Journal of Physical Chemistry*. 84. 10.1021/j100453a016.

Hari, P. and Kulmala, M.: Stations for Measuring Ecosystem – Atmosphere Relations (SMEAR II). Boreal Environ. Res., 10, 315–322, 2005.

Heikkinen et al., 2019, submitted.

Laakso, L., Hussein, T., Aarnio, P., Komppula, M., Hiltunen, V., Viisanen, Y., Kulmala, M., 2003: Diurnal and annual characteristics of particle mass and number concentrations in urban, rural and Arctic environments in Finland. *Atmos. Environ.*, 37, 2629–2641.

Pope, C.R., Burnett, R., M.J., T., Calle, E., Krewski, D., Ito, K., Thurston, G., 2002. Lung cancer, cardiopulmonary mortality, and long-term exposure to fine particulate air pollution. *Journal of the American Medical Association* 287, 1132–1141.

PROCESSING OF AEROSOL SIZE DISTRIBUTIONS DURING THE TRANSPORT OVER THE INDIAN OCEAN IN DIFFERENT SEASONS

J. KESTI¹, E. ASMI¹, E.J. O'CONNOR¹, J. BACKMAN¹, K. BUDHAVANT² and Ö. GUSTAFSSON³

¹ Finnish Meteorological Institute, Helsinki, Finland.

²Maldives Climate Observatory-Hanimaadhoo, Maldives Meteorological Services, Maldives.

³Department of Environmental Science and Analytical Chemistry, The Bolin Centre for Climate Research, Stockholm University, Stockholm, Sweden.

Keywords: AEROSOL NUMBER SIZE DISTRIBUTION, WET SCAVENGING, ASIAN AEROSOL, LONG-RANGE TRANSPORT.

INTRODUCTION

The aerosol emissions are highest in Asia (Lelieveld *et al.*, 2001; Zhang and Reid, 2010; Van Donkelaar *et al.*, 2010). Aerosol particles from the emissions can be transported long distances to remote locations such as the Maldives. Aerosol particle processes during the long-range transport, such as growth, aging and the removal processes, need accurate modeling to predict future climate reliably.

Wet scavenging is a significant removal process of aerosol particles from the atmosphere. In the process raindrops and snow flakes transport particles to the ground. The efficiency of the process depends inter alia on the precipitation intensity and aerosol particle size. The wet scavenging processes have still huge uncertainties in atmospheric models (Liu *et al.*, 2012). To increase knowledge about wet scavenging, we need to investigate how efficiently precipitation removes aerosol particles from the atmosphere and in which size ranges the removal is most efficient.

The climate in the Maldives presents two distinct seasons: northeast (NE) and southwest (SW) monsoon. During the NE monsoon, the air masses arriving to the Maldives are mainly transported from the Indian subcontinent and thus bringing polluted air. During the SW monsoon, the air masses are transported over the Indian Ocean bringing moist marine air consisting mostly of natural aerosols. Local aerosol sources are minor at the Maldives, so it is an ideal site for studying the impact of precipitation on long-range aerosol transport. In this study, the interaction between meteorological phenomena and aerosol long-range transport are investigated by analysing the seasonal and long-term behaviour of aerosol properties. The study also provides knowledge about longer-term aerosol particle properties in the area, where there are no published multi year aerosol particle studies.

METHODS

The measurements were conducted at the Maldives Climate Observatory of Hanimaadhoo (MCOH, 6°78 N, 73°18 E). The observatory is located in the northern part of the Maldives. The terrain is very flat, and the observatory is surrounded by forest, which mostly consists of palm trees.

We used two different data sets. The first measurement period was during 2004–2008 (Period 1). Fine aerosol particles in a size range of 10–500 nm were measured with a Scanning Mobility Particle Sizer (SMPS) with time resolution of 5 minutes. The second measurements were conducted during

Season	Mean total number concentration ($1/\text{cm}^3$)	Median total number concentration ($1/\text{cm}^3$)
NE monsoon, east Period 1	1666 ± 819	1745
NE monsoon, east Period 2	1915 ± 470	1849
NE monsoon, west Period 1	879 ± 422	772
NE monsoon, west Period 2	1615 ± 527	1562
SW monsoon, marine Period 1	268 ± 114	250
SW monsoon, marine Period 2	379 ± 256	332

Table 1: Particle total number concentrations measured in Period 1 and 2. Air masses are divided to easterly and westerly based on their route to the Maldives during NE monsoon. In the marine air masses during SW monsoon we discriminated the trajectories which have sidetracked over land.

2014–2017 (Period 2) using a Differential Mobility Particle Sizer (DMPS), which measured particles in a size range of 7–800 nm with a time resolution of 10 minutes.

We calculated 14-day air mass back trajectories with the NOAA HYSPLIT (Hybrid Single-Particle Lagrangian Integrated Trajectory) (Draxler and Hess, 1998) model 4.9 to estimate the air mass origin. The meteorological fields for the model runs were taken from the global GDAS 1° (Global Data Assimilation System) dataset from the National Center for Atmospheric Research as (Kanamitsu, 1989). We calculated hourly trajectories and cumulative rainfall along the trajectory for the both measurement periods.

CONCLUSIONS

We observed the highest aerosol particle total number concentrations during the NE monsoon, when the source of particles is India and the Indo-Gangetic plain (Table 1). We further divided the air masses to western and eastern based on whether they have travelled from the western or eastern side of the Indian subcontinent to the Maldives. We observed a major difference in particle total number concentrations in western air masses between Period 1 and 2 (Table 1). One explanation for the difference could be the more frequent intensive rainfall events in Period 1. The measured aerosol size distributions did not show a significant difference between the two origins and transport routes.

During the SW monsoon, the aerosol total number concentrations were only about a quarter of the values measured during the NE monsoon (Table 1). The accumulation mode particles were removed efficiently by precipitation, while the nucleation mode concentration remained similar or slightly increased (in Period 2), with more rainfall (Figure 1).

The results showed an increase in particle total number concentration between the two measurement periods, both in NE and SW monsoon seasons. This increase was partly explained by the environmental factors, such as the differences in air mass routes and in the amount of rainfall, but a remaining fraction suggested a possible increase in aerosol number in the source. This could be due to increasing emissions in Asia.

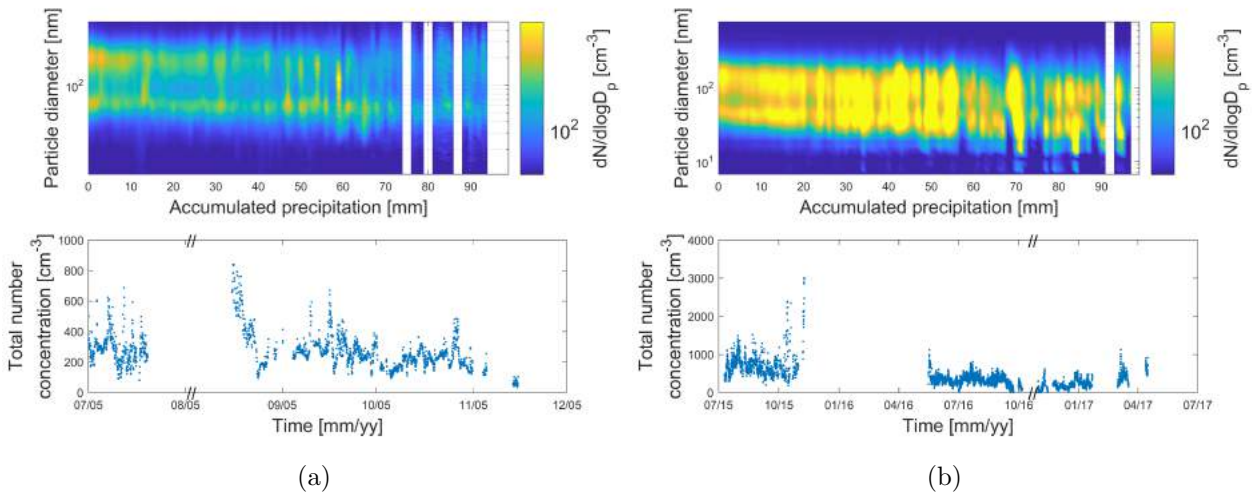


Figure 1: Effect of accumulated rainfall on measured particle size distribution and total number concentration time series during SW monsoon season in (a) Period 1, and (b) Period 2. In the upper figure on the x-axis is the accumulated rainfall (mm) during four days before the air mass arrived to the measurement site, on the y-axis is the particle diameter (nm) and the concentration $dN/d\log(d_p)$ (cm^{-3}) is in colour. In the lower figure on the x-axis is time $mm\,yy^{-1}$ and on the y-axis is the total number concentration (cm^{-3}). All data are in hourly resolution, and the particle size distribution data are averaged to 1 mm rain bins.

ACKNOWLEDGEMENTS

The staff working at the Climate Observatory of Hanimaadhoo is acknowledged for maintenance of the measurements.

REFERENCES

- Draxler, R.R. and Hess, G.D. (1998). An overview of the HYSPLIT_4 modelling system for trajectories. *Aust. Meteorol. Mag.*, **47**, 4.
- Kanamitsu, M. (1989). Description of the NMC global data assimilation and forecast system. *Weather Forecasting*, **4**, 3.
- Lelieveld, J., Crutzen, P.J., Ramanathan, V., Andreae, M.O., Brenninkmeijer, C.A.M., Campos, T., Cass, G.R., Dickerson, R.R., Fischer, H., De Gouw, J.A., and others (2001). The Indian Ocean experiment: widespread air pollution from South and Southeast Asia. *Science*, **291**, 5506.
- Liu, X., Easter, R.C., Ghan, S.J., Zaveri, R., Rasch, P., Shi, X., Lamarque, J.-F., Gettelman, A., Morrison, H., Vitt, F., and others (2012). Toward a minimal representation of aerosols in climate models: Description and evaluation in the Community Atmosphere Model CAM5. *Geosci. Model Dev.*, **5**, 3.
- Van Donkelaar, A., Martin, R.V., Brauer, M., Kahn, R., Levy, R., Verduzco, C. and Villeneuve, P.J. (2010). Global estimates of ambient fine particulate matter concentrations from satellite-based aerosol optical depth: development and application. *Environ. Health Perspect.*, **118**, 6.
- Zhang, J. and Reid, J.S. (2010). A decadal regional and global trend analysis of the aerosol optical

depth using a data-assimilation grade over-water MODIS and Level 2 MISR aerosol products.
Atmos. Chem. Phys., **10**, 22.

A CONTROLLED ENVIRONMENT CHAMBER SYSTEM FOR HIGH FREQUENCY OF LEAF LEVEL CH₄ EXCHANGE MEASUREMENTS: SETUP, OPERATING PRINCIPLES, AND INITIAL RESULTS

LUKAS KOHL^{1,2}, MARKKU KOSKINEN^{1,2,3}, PAIVI MÄKIRANTA⁴, TATU POLVINEN^{1,2}, MARJO PATAMA^{1,2,5}, SALLA TENHOVIRTA^{1,2,5}, and MARI PIHLATIE^{1,2,5}

¹Department of Agricultural Sciences, University of Helsinki, Finland

²Institute for Atmospheric and Earth System Research / Forest Sciences, Finland

³Finnish Meteorological Institute, Helsinki, Finland

⁴Finnish Institute of Natural Resources (Luke), Helsinki, Finland

⁵Viikki Plant Science Centre, University of Helsinki, Finland

Keywords: Methane, Plant, controlled environment.

INTRODUCTION

Plant shoots can emit small amounts of methane (CH₄), which, on a global scale, may constitute a major yet so far unaccounted CH₄ source (Carmichael et al., 2014; Kepler et al., 2006). Shoot CH₄ emission can originate from multiple source processes, including transported CH₄ produced by microorganisms in soils and core wood, and aerobic CH₄ production in foliage (Carmichael et al., 2014). So far, few measurements of shoot CH₄ emissions have been conducted in mature forest trees (Machacova et al., 2016), and it remains unclear whether shoot CH₄ emission from distinct source processes vary with environmental parameters.

This lack of data is likely due to the technical difficulty of measuring shoot trace gas fluxes. CH₄ flux measurements require static enclosure that recirculate air between the enclosed volume and a CH₄ analyser. The enclosed plant shoots, however, rapidly fixate all available CO₂ and transpired water increases the humidity of the enclosed air to the point where condensation on the chamber walls occurs. In addition, chambers exposed to sunlight heat up rapidly. These three factors (CO₂, humidity, temperature) thus can significantly change the conditions in the chamber and the observed flux rates.

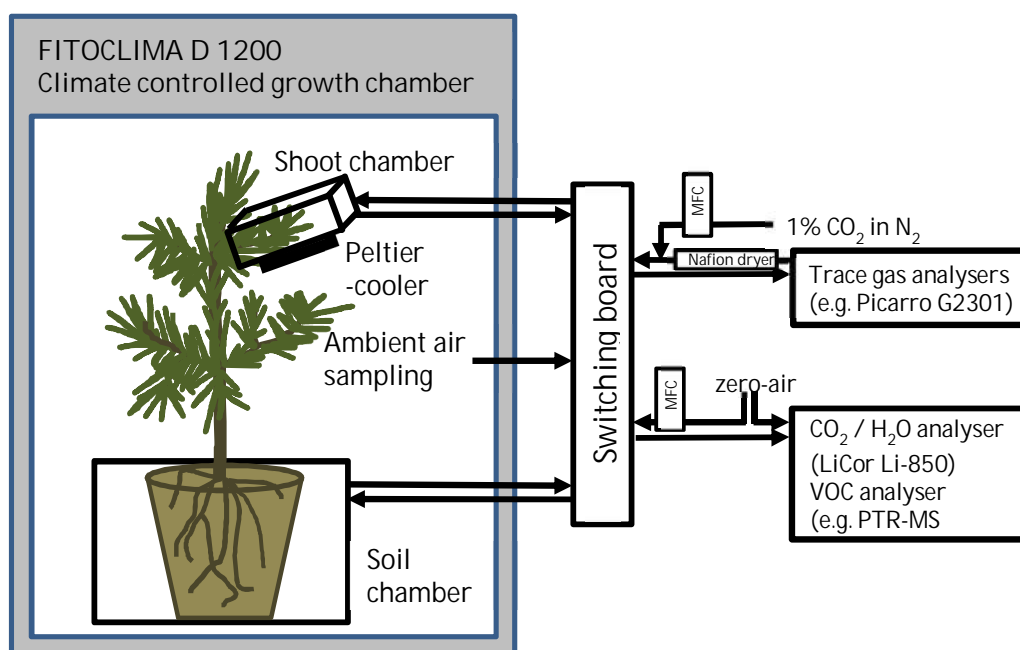


Figure 1. Overview of the climate chamber system used for trace gas flux measurements.

METHODS

We constructed a chamber system to study how leaf level fluxes of CH₄ and other trace gases respond to environmental factors like dark-light-cycles, temperature, drought, or CO₂ concentrations (Figure 1). Tree saplings are located in a FITOCLIMA D 1200 plant growth chamber to for PAR, temperature and humidity control and equipped with a measurement chamber to quantify CH₄ exchange in a closed loop setup with a Picarro G2301 CH₄ analyser. The system was further customized to control temperature, CO₂, and humidity control in the measurement chamber. The system allows the detection of CH₄ flux rates of on the order of 1 nmol CH₄ h⁻¹ and can conduct high frequency (< 15 min) measurements of CH₄ emissions rates from small shoots (<5g foliage biomass).

Initial measurements were conducted with Scots pine, downy birch, and silver birch saplings. Trees were placed inside the chamber and exposed to natural diurnal light patterns (maximum PAR ~1000 μmol m⁻² sec⁻¹), moderate relative humidity (40-70% relative humidity) and constant temperature (10 or 15 C).

RESULTS AND DISCUSSION

Our initial experiments demonstrated that the shoots of different tree species emit CH₄ from distinct sources. Shoots of Scots pine and some birch species emitted CH₄ produced within the shoot, likely through aerobic CH₄ production, which showed a strong diurnal cycle that follows irradiation and photosynthesis rates. Shoot from some birch species, in contrast, showed emissions of soil-borne CH₄ that remained constant throughout day and nighttime. We expect that future experiment with this unique setup will allow to further disentangle shoot CH₄ emissions and to characterize their response to environmental conditions including light, temperature, and relative humidity.

ACKNOWLEDGEMENTS

This project has received funding from the European Research Council (ERC) under the European Union's Horizon 2020 research and innovation program (grant agreement number 757695) and the Academy of Finland (grant numbers 319329 and 2884941). Markku Koskinen received a fellowship from the Maj and Tor Nessling foundation.

REFERENCES

- Carmichael, M. J., Bernhardt, E. S., Bräuer, S. L., & Smith, W. K. (2014). The role of vegetation in methane flux to the atmosphere: Should vegetation be included as a distinct category in the global methane budget? *Biogeochemistry*, *119*(1–3), 1–24. <https://doi.org/10.1007/s10533-014-9974-1>
- Keppeler, F., Hamilton, J. T. G., Braß, M., & Röckmann, T. (2006). Methane emissions from terrestrial plants under aerobic conditions. *Nature*, *439*(7073), 187–191. <https://doi.org/10.1038/nature04420>
- Machacova, K., Bäck, J., Vanhatalo, A., Halmeenmäki, E., Kolari, P., Mammarella, I., et al. (2016). Pinus sylvestris as a missing source of nitrous oxide and methane in boreal forest. *Scientific Reports*, *6*(September 2015), 1–8. <https://doi.org/10.1038/srep23410>

CARBONYL SULFIDE FLUX MEASUREMENTS OVER A RIVER

K-M. KOHONEN¹, A. VÄHÄ¹, M. AURELA², I. MAMMARELLA¹ and T. VESALA^{1,3}

¹ Institute for Atmospheric and Earth System Research/ Physics, University of Helsinki, Helsinki, Finland.

² Finnish Meteorological Institute, Helsinki, Finland.

³ Institute for Atmospheric and Earth System Research/ Forest Sciences, University of Helsinki, Helsinki, Finland.

Keywords: CARBONYL SULFIDE, FLUX, EDDY COVARIANCE, RIVER.

INTRODUCTION

Carbonyl sulfide (COS) flux measurements are growing in popularity as they are tested as a way to measure photosynthesis. However, the global COS budget is not closed and there is either a too large sink or a too small source in the global budget models (Whelan *et al.*, 2018). At global scale, the main source of COS are the oceans where it is produced photochemically from chromophoric dissolved organic matter (CDOM) and by a light-independent production that has been linked to sulfur radical formation (Lennartz *et al.*, 2017). There is also an indirect source through dimethylsulfide (DMS) and carbon disulfide (CS₂), that are partially oxidized to COS in the atmosphere. Earlier studies suggest that these processes most likely also occur in freshwater ecosystems (Richards *et al.*, 1991; Richards *et al.*, 1994). Dissolved COS is also destroyed in water by abiotic hydrolysis at a rate determined by pH, salinity and temperature, and to a small extent by photosynthesis of algae.

In this study, we measured COS exchange over River Kitinen in Sodankylä. Our direct COS eddy covariance (EC) flux measurements over a river are the first of its kind. EC measurements over a river are unique in general, as yet only one study on carbon dioxide (CO₂) fluxes over a river with EC technique has been published (Huotari *et al.*, 2013). For the global COS budget to be more accurate, an estimate of the freshwater emissions is urgently needed (Whelan *et al.*, 2018).

METHODS

Measurements were done at River Kitinen, close to Finnish Meteorological Institute Sodankylä observatory (67° 22' N, 26° 37' E) from beginning of June until end of September in 2018. Flux measurements were done over the river from a 2.0 m tall tower, approximately 10 m away from the shoreline, using the EC technique. Wind speed in three dimensions was measured with METEK USA-1 ultrasonic anemometer and mixing ratios of COS, CO₂, carbon monoxide (CO) and water vapor (H₂O) were measured with Aerodyne mini-QCLS. All measurements were done at 10 Hz frequency. Fluxes were processed using EddyUH software (Mammarella *et al.*, 2016) using the suggested data processing steps presented in Kohonen *et al.*, (2019).

RESULTS

We observed a distinguishable diurnal cycle in COS exchange during the whole measurement period, with negative fluxes observed during the night and positive during the day. During nighttime

hydrolysis is destroying COS in the water and thus there is a downward flux observed. In daytime, COS is produced by photochemical reactions from CDOM and this reaction surpasses the sink due to hydrolysis. Overall, the median COS flux over the whole period was slightly positive, 0.45 pmol m⁻²s⁻¹. This is quite close to the observed ocean fluxes, that vary between -0.09 and 0.54 pmol m⁻²s⁻¹ (Lennartz *et al.*, 2017).

CONCLUSIONS

River Kitinen acted as a small source of COS during the measurement campaign in summer 2018. However, there was a distinguishable diurnal pattern observed with positive fluxes during the day due to photochemical production and negative fluxes during nighttime due to hydrolysis. Further analysis is needed to find out the most important environmental factors driving the COS exchange between freshwater and atmosphere.

ACKNOWLEDGEMENTS

Special thanks to Rigel Kivi, Sami Haapanala and Risto Taipale for all their technical support and help during the campaign. This study was supported by the Academy of Finland Center of Excellence (307331) and Academy Professor projects 284701 and 282842, ICOS-Finland (281255) and the Vilho, Yrjö and Kalle Väisälä foundation.

REFERENCES

- Huotari, J., Haapanala, S., Pumpanen, J., Vesala, T. and Ojala, A. (2013). Efficient gas exchange between a boreal river and the atmosphere. *Geophysical Research Letters*, **40(21)**, 5683-5686.
- Kohonen, K.-M., Kolari, P., Kooijmans, L. M. J., Chen, H., Seibt, U., Sun, W. and Mammarella, I. (2019). Towards standardized processing of eddy covariance flux measurements of carbonyl sulfide. *Atmospheric Measurement Techniques Discussions*
- Lennartz, S. T., Marandino, C. A., von Hobe, M., Cortes, P., Quack, B., Simo, R., Booge, D., Pozzer, A., Steinhoff, T., Arevalo-Martinez, D. L., Kloss, C., Bracher, A., Röttgers, R., Atlas, E. and Krüger, K. (2017). Oceanic emissions unlikely to account for the missing source of atmospheric carbonyl sulfide. *Atmospheric Chemistry and Physics*, **17(1)**, 385–402.
- Mammarella, I., Peltola, O., Nordbo, A., Järvi, L. and Rannik, Ü. (2016). Quantifying the uncertainty of eddy covariance fluxes due to the use of different software packages and combinations of processing steps in two contrasting ecosystems. *Atmospheric Measurement Techniques*, **9(10)**, 4915–4933.
- Richards, S. R., Kelly, C. a. and Rudd, John W. M. (1991). Organic volatile sulfur in lakes of the Canadian Shield and its loss to the atmosphere. *Limnology and Oceanography*, **36(3)**, 468–482.
- Richards, A. S. R., Rudd, J. W. M. and Kelly, C. A. (1994). Organic volatile sulfur in lakes ranging in sulfate and dissolved salt concentration over five orders of magnitude. *Limnol. Oceanogr.*, **39(3)**, 562–572.
- Whelan, M. E., Lennartz, S., Gimeno, T. E., Wehr, R., Wohlfahrt, G., Wang, Y., Kooijmans, L.M.J, Hilton, T. W., Belviso, S., Peylin, P., Commane, R., Sun, W., Chen, H., Kuai, L., Mammarella, I., Maseyk, K., Berkelhammer, M., Li, K-F., Yakir, D., Zumkehr, A., Katayama, Y., Ogée, J., Spielmann, F.M., Kitz, F., Rastogi, B., Kesselmeier, J., Marshall,

J. , Erkkilä, K-M. , Wingate, L. , Meredith, L.K. , He, W. , Bunk, R. , Launois, T. , Vesala, T. , Schmidt, J.A. , Fichot, C. G. , Seibt, U. , Saleska, S. , Saltzman, E.S. , Montzka, S.A. , Berry, J. A. and Campbell, J.E. (2018). Reviews and syntheses: Carbonyl sulfide as a multi-scale tracer for carbon and water cycles. *Biogeosciences*, **15**(12), 3625–2657.

SEASONAL VARIATION OF THE EFFECT OF HAZE ON THE URBAN BOUNDARY LAYER HEIGHT IN BEIJING

T. V. KOKKONEN^{1,2}, M. KURPPA¹, V.-M. KERMINEN¹, Y. WANG¹, Z. LIN², Y. CHAO^{1,2} and M. KULMALA^{1,2}

¹Institute for Atmospheric and Earth System Research / Physics, University of Helsinki, Finland.

²Aerosol and Haze Laboratory, Beijing Advanced Innovation Center for Soft Matter Science and Engineering, Beijing University of Chemical Technology, China.

Keywords: BOUNDARY LAYER HEIGHT, HAZE, AIR POLLUTION.

INTRODUCTION

The air pollution is attenuating incoming solar radiation leading to a decreased surface energy availability. This leads to lower boundary layer height (BLH) which forces the pollution emission to a smaller volume further increasing the pollutant concentrations. This forms a vicious feedback cycle between the particulate pollution and boundary layer height. Even though the effect of haze on the reduction of urban boundary layer height in Beijing is rather well-known phenomena, most of the previous research has focused on the winter (Ding *et al.*, 2016; Gao *et al.*, 2015; Liu *et al.*, 2018), since this season is often also the most polluted time of the year. Therefore, there are still significant knowledge gaps in the seasonal variation of the effect of haze on the urban boundary layer height.

METHODS

The analyses of the BLH in this study focused on the meteorological variables measured at the rooftop of a campus building at the west campus of the Beijing University of Chemical Technology (BUCT) for the year 2018, supplemented with the surface energy balance modelling conducted with Surface Urban Energy and Water Balance Scheme (SUEWS; Järvi *et al.*, 2011). All of the meteorological variables were hourly averaged prior usage.

SUEWS has seven surface types (paved, buildings, evergreen and deciduous trees/shrubs, grass, bare soil and water), which are separately simulated but dynamic interaction between the surfaces is allowed. The latent heat flux is calculated from the Penman–Monteith equation (Penman, 1948; Monteith, 1948) and the sensible heat flux is calculated as a residual from other energy balance components (Järvi *et al.*, 2011).

CONCLUSIONS

The average daytime boundary layer height during clean conditions was the highest in spring (2000 m) autumn (1700 m), while the lowest in winter (1550 m). Also, the effect of haze on the BLH was the highest in spring (48 %) and autumn (56 %), while having substantially smaller effect in summer (18 %). This is presumably related to the seasonal variation of the magnitude of the surface heat fluxes. The SUEWS modelling showed that the effect of haze is the greatest when the surface heat flux was rather small, but there was enough incoming solar radiation to enable vertical mixing, which is lifting the boundary layer height. In summer time there were high surface heat fluxes indicating that there is enough surface energy available to enable the BLH diurnal profile even when the haze is attenuating the incoming solar radiation. This is partly explaining why the late autumn, winter and early spring time is also the most polluted time of the year. Even if the pollutant emission would be constant throughout the year, this season would be the most polluted due to the substantial effect of the radiative effect of haze on the urban boundary layer height through the modification of the surface energy availability.

ACKNOWLEDGEMENTS

This research was supported by Academy of Finland via Center of Excellence in Atmospheric Sciences (project no. 272041) and European Research Council via ATM-GTP 266 (742206). This research has also received funding from Doctoral Program of Atmospheric Sciences (ATM-DP) at the University of Helsinki.

REFERENCES

- Ding, A. J., Huang, X., Nie, W., Sun, J. N., Kerminen, V. M., Petäjä, T., Su, H., Cheng, Y. F., Yang, X. Q., Wang, M. H., Chi, X. G., Wang, J. P., Virkkula, A., Guo, W. D., Yuan, J., Wang, S. Y., Zhang, R. J., Wu, Y. F., Song, Y., Zhu, T., Zilitinkevich, S., Kulmala, M., and Fu, C. B. (2016). Enhanced haze pollution by black carbon in megacities in China, *Geophys Res Lett*, 43, 2873-2879, 10.1002/2016gl067745.
- Gao, Y., Zhang, M., Liu, Z., Wang, L., Wang, P., Xia, X., Tao, M., and Zhu, L. (2015). Modeling the feedback between aerosol and meteorological variables in the atmospheric boundary layer during a severe fog-haze event over the North China Plain, *Atmos. Chem. Phys.*, 15, 4279-4295, 10.5194/acp-15-4279-2015.
- Järvi, L., S. Grimmond, and A. Christen (2011). The Surface Urban Energy and Water Balance Scheme (SUEWS): Evaluation in Los Angeles and Vancouver, *J. Hydrol.*, **411**, 219–237.
- Liu, Q., Jia, X., Quan, J., Li, J., Li, X., Wu, Y., Chen, D., Wang, Z., and Liu, Y. (2018). New positive feedback mechanism between boundary layer meteorology and secondary aerosol formation during severe haze events, *Sci Rep-Uk*, 8, 6095, 10.1038/s41598-018-24366-3.
- Monteith, J. L. (1965). Evaporation and the environment, *Symp. Soc. Exp. Biol.*, 19, 205–234.
- Penman, H. L. (1948). Natural evaporation from open water, bare soil and grass, *P. Roy. Soc. Lond. A Mat.*, 193, 120–145, 10.1098/rspa.1948.0037.

ESTIMATING PARTICLE NUMBER EMISSIONS SIZE DISTRIBUTIONS IN BEIJING BASED ON MEASURED PARTICLE SIZE DISTRIBUTIONS

J. KONTKANEN¹, C. YAN^{1,2}, T. V. KOKKONEN¹, L. DADA¹, C. DENG³, Y. FU³, Y. LIU², J. JIANG³, M. KULMALA^{1,2}, P. PAASONEN¹

¹Institute for Atmospheric and Earth System Research / Physics, Faculty of Science, University of Helsinki, Helsinki, Finland

²Aerosol and Haze Laboratory, Beijing Advanced Innovation Center for Soft Matter Science and Engineering, Beijing University of Chemical Technology, Beijing, China

³State Key Joint Laboratory of Environment Simulation and Pollution Control, School of Environment, Tsinghua University, Beijing, China

Keywords: PARTICLE NUMBER EMISSIONS, NEW PARTICLE FORMATION, AIR QUALITY

INTRODUCTION

Currently, many urban regions suffer from high levels of particulate matter. This is due to the large emissions of particles from different sources, including the emissions of primary particles from traffic and other pollution sources (Brines *et al.*, 2015), and the production of secondary particles by new particle formation (NPF) (Guo *et al.*, 2014). The knowledge of the number size distribution of particles originating from different sources is needed to estimate their impacts on human health and climate (WHO, 2013; Stocker *et al.*, 2013). In this study, we introduce a new method to determine the size distribution of particle number emissions, including both primary emissions and the production of particles by NPF, by using the measured particle size distributions. We apply this method to particle size distribution data measured in Beijing, China, to estimate the average particle number emissions in a Chinese megacity.

METHODS

Our method is based on determining emissions E ($\text{m}^{-2} \text{s}^{-1}$) to a column extending from the ground to the top of the boundary layer by solving the following balance equation for each size bin i :

$$\frac{d(N_i \times BLH)}{dt} = E_i + BLH \times GR \times N_{i-1} / \Delta d_{p,i-1} - BLH \times GR \times N_i / \Delta d_{p,i} - BLH \times \text{Coag}S_i \times N_i \quad (1)$$

Here N_i is the number concentration of particles in the size bin i , BLH is the boundary layer height, GR is the particle growth rate, $\Delta d_{p,i}$ is the width of the size bin i , and $\text{Coag}S_i$ is the coagulation sink for particles in this bin. Thus, the term on the left-hand side of Eq. (1) describes the observed change in the column particle number concentration, the second and the third terms on the right hand-side describe the growth into and out of the size bin i , and the last term describes the losses due to coagulation. For the smallest size bin ($i = 1$), the term describing the growth into the size bin is omitted, and thus the emissions to the first size bin also include the production of particles by NPF.

We applied this method to particle size distribution data measured with a Diethylene Glycol Scanning Mobility Particle Sizer (DEG-SMPS; Jiang *et al.*, 2011; Cai *et al.*, 2017) and a custom-made Particle Size Distribution (PSD; Liu *et al.*, 2016) system at the measurement station of Beijing University of Chemical Technology during January 2018 – March 2019. The station is located in the western part of Beijing ($39^\circ 56' 31'' \text{N}$, $116^\circ 17' 50'' \text{E}$), close to the 3rd Ring Road of Beijing. We calculated particle number emissions to 17 particle size bins with the lower limit d_p and the upper limit $d_p \times 4/3$, between 5 and 706 nm. For GR we used a constant value of 3 nm/h for all the size bins, which corresponds to typical GR observed at the station. We determined the average diurnal cycle of particle number emission size distributions on NPF event and non-event days. Our assumption is that by averaging long enough data set, we can avoid the effect of transport on the estimated particle number emissions.

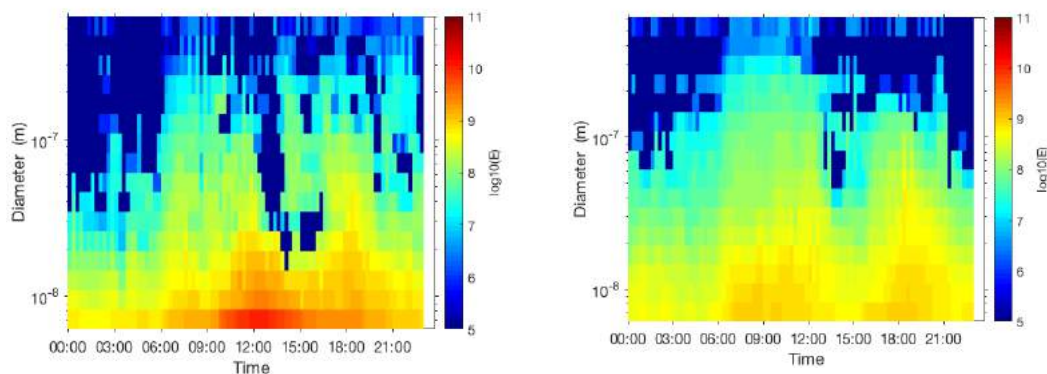


Figure 1. Average diurnal variation of particle number emission size distributions on NPF event days (left) and non-event days (right).

RESULTS

The average diurnal variations of particle number emission size distributions on NPF event days and non-event days are presented in Fig. 1. On both event and non-event days, emissions from traffic are clearly observed during morning and evening rush hours (06:00–13:00 and 16:00–22:00). These emissions are highest at sizes between 5 and 30 nm, demonstrating that traffic is an important source of nucleation mode particles in Chinese megacities. In addition, on NPF event days, a high number of nucleation mode particles is produced by atmospheric clustering during daytime (09:00–18:00). However, a more detailed analysis is still needed to quantitatively separate the effects of NPF and primary emissions on particle production in Beijing.

CONCLUSIONS

We introduce a new method to estimate the size distribution of particle number emissions, including both primary emissions and production of particles by atmospheric NPF, by using measured particle size distribution data. We apply this method to measurements performed in Beijing, China, during January 2018 – March 2019, and determine the average particle number emission size distribution between 5 and 706 nm. Our results show that particle number emissions in Beijing are dominated by direct emissions of sub-30 nm particles from traffic and the production of nucleation mode particles by atmospheric NPF.

ACKNOWLEDGEMENTS

The work is supported by Academy of Finland (grant nos. 307331 and 316114) and European Research Council (ATM-GTP; grant no. 742206).

REFERENCES

- Brines, M. *et al.* (2015). Traffic and nucleation events as main sources of ultrafine particles in high-insolation developed world cities, *Atmos. Chem. Phys.* **15**, 5929–5945.
- Cai, R. *et al.* (2017). A miniature cylindrical differential mobility analyzer for sub-3 nm particle sizing, *Journal of Aerosol Science*, **106**, 111–119.
- Guo, S. *et al.* (2014). Elucidating severe urban haze formation in China, *PNAS* **111**, 49, 17373–17378.
- Jiang, J. *et al.* (2011). Electrical Mobility Spectrometer Using a Diethylene Glycol Condensation Particle Counter for Measurement of Aerosol Size Distributions Down to 1 nm, *Aerosol Science and Technology* **45**, 510-521.
- Liu, J. *et al.* (2016). A spectrometer for measuring particle size distributions in the range of 3 nm to 10 μ m, *Frontiers of Environmental Science & Engineering* **10**, 63-72.
- Stocker, T. *et al.* (2013). IPCC, 2013: climate change 2013: the physical science basis. Cambridge University Press, 1535 pp.
- WHO (World Health Organization) (2013). Review of Evidence on Health Aspects of Air Pollution – REVIHAAP project, Technical Report, World Health Organization.

INTEGRATING SOCIETY WITH SCIENCE

J.F.J. KORHONEN^{1,2}, N. FREISTETTER^{1,2}, J. ANTTILA^{1,3}, T. VESALA³ AND M. PIHLATIE^{1,2,4}

¹Environmental Soil Science, Department of Agricultural Sciences, Faculty of Agriculture and Forestry, University of Helsinki, Finland

²Institute for Atmospheric and Earth System Research / Forest Sciences, Faculty of Agriculture and Forestry, University of Helsinki, Finland

³Institute for Atmospheric and Earth System Research / Physics, Faculty of Science, University of Helsinki, Finland

⁴Viikki Plant Science Centre (ViPS), University of Helsinki, Finland

Keywords: scientific communication, decision making, public outreach, societal change.

MOTIVATION

In an ideal society, decision making is based on scientific knowledge. However, as the amount of knowledge increases, producing new significant knowledge becomes more and more difficult and the results are less and less generalizable. Complexity of the research also means that for common people who are not specialized in the field, it can be difficult to understand the scientific research and to trust the scientific results. This means that the bottleneck of making scientifically informed decisions is shifting from producing new scientific knowledge to strengthening the interaction between the scientific community and the society.

VISION

In order to be used in the society, scientific knowledge must exist, it must be accessible, it must be understandable and it must be received with either understanding, or in good faith in science. Making good science and making science (data and publications) accessible are basic requirements for scientific research today. Making science understandable and delivering the message is typically carried out by a field of its own, science communications. Being interesting or entertaining is also a priority for science communications. Science communication is often carried out in collaboration with media experts. Understanding science means both understanding scientific principles and procedures, as well as understanding scientific knowledge and results. Complete understanding of results is not necessary, as long as scientific process is transparent, and the main principles behind the results are understood. This requires trust in that researchers do not have hidden agendas, and while accepting that errors happen in science, the scientific method in general is a sound foundation for knowledge.

We postulate four stages of interaction between the scientific community and the society:

0. Current situation in so-called developed countries: Unidirectional science communications done by media experts in collaboration with scientists.
1. Integrating science with society. Direct unidirectional science communications done by the scientific community, in collaboration with media experts.
2. Communalization of science. Communication is bidirectional, and there is genuine interaction between the society and scientists.
3. Society is integrated with science. Scientific results must be taken into account in all decision making, whenever possible.

There may be stages before stage 0, but they are not considered here. For example developing countries may be in these stages, and while it is recognized that lack of integration of science to society is probably one of their largest problems when it comes to societal progress, these stages cannot be addressed here.

At stage 0, Scientists typically have difficulties in explaining things in a way, a non-scientist can comprehend. Science communications therefore is mainly carried by media experts. i.e. journalists, who interview scientists, interpret their results and communicate the understood to the public in the shortest and most comprehensible way. This saves researchers valuable time, but messages are being interpreted twice, first by the journalist, then by the public. This can also have great advantages, as often the details interesting to a scientist are not very interesting to the general public. On the other hand, this way of communication can cause misinterpretation, blurring of important messages or the complete loss of the essential implication.

At stage 1, the scientific community communicates directly with the general public. Here, the scientist becomes the media expert. Or rather said, the journalist is a person with scientific background that is directly working in the field he is reporting about. Developing both, the mindset of a scientist and one of a science communicator is a challenge that requires a lot of time and practice. As the educational standard level rises in developed countries, more and more people graduate at Master's or PhD level and thus, not only understand scientific messages better. The abundance of academics could lead to an abundance of scientific journalists or science communicators.

At stage 2, bidirectional interaction between the scientific community and general public will be a significant part of science communications. This goal requires bringing science to where people are, and make people comfortable to visit research institutions. Digital networks are a good tool for communication to start with, but hands-on experience on science would have an even stronger impact.

Artists potentially play an important role at achieving this stage 2, as art is the common language between people at an emotional level, no matter the level of scientific background. Artistic research typically concerns the same basic questions as scientific research, but instead of trying to give definite answers, artistic research tries to raise questions and awareness through emotions. As with science, the independent nature of arts must be respected, and financial resources should be allocated so that artists are able to do their work.

At stage 3, the interaction between the science and society is so deep, that it is not anymore clear what is being integrated into which: science with society, or society with science. The best knowledge is taken into account in the society at private and public decision making. While a major part of decision making is value-based, scientific knowledge still helps to achieve the values.

ACTION

Stage 0. The current activities should be continued, as different kind of science communication is not exclusive, but supportive.

Stage 1. A YouTube channel will be established by a person with research background, for doing a well-prepared talk-show-type science program that tries to be entertaining, while keeping the focus on substance. While the research done within the CoE research community is largely related to climate change, and climate change is a grand challenge, the idea of the channel is not concentrate on that subject. Neither is the idea of the channel is not to advertise our research community, or to sell anything, or try to convince anybody about anything. The main idea is to get people familiar and closer to science, and provide foundation for bi-directional communication between the scientific community and the general public.

Stage 2. This stage requires a lot of work and resources. The continuation of the Climate whirl (www.climatewhirl.fi; Juurola et al., 2014) umbrella is essential part of our activities. Preferably more

workshops can be organized, as well as do-it-yourself courses. Courses for building your own soil CO₂ emission and tree stem water flow (sapflow) measurement systems, including some ecology are under consideration.

Stage 3. Hopefully this will happen during the lifetime of the authors.

REFERENCES

Juurola, E., Korhonen, J. F. J., Kulmala, L., Kolari, P., Taipale, U., Rasinmaki, J., Ruuskanen, T., Haapoja, T., Back, J., Levula, J., Riuttanen, L., Kyro, E. M., Dzhedzhev, I., Nikinmaa, E., Vesala, T., and Kulmala, M. (2014): Knowledge transfer of climate-ecosystem-interactions between science and society - Introducing the Climate Whirl concept, *Boreal Environment Research*, **19**, 406-411.

SOLID BIOMASS COMBUSTION SOOT PROPERTIES RELATED TO THEIR ICE NUCLEATION ABILITY IN IMMERSION FREEZING

K. KORHONEN¹, T.B. KRISTENSEN², J. FALK², R. LINDGREN³, C. ANDERSEN⁴, R.L. CARVALHO^{3, a}, V. BERG-MALMBORG⁴, A. ERIKSSON⁴, C. BOMAN³, J. PAGELS⁴, B. SVENNINGSSON², M. KOMPPULA⁵, K.E.J. LEHTINEN¹ AND A. VIRTANEN¹

¹University of Eastern Finland, Department of Applied Physics, P.O. box 1627, FI-70211 Kuopio, Finland

²Lund University, Department of Physics, SE-22100, Lund, Sweden

³Umeå University, Thermochemical Energy Conversion Laboratory, SE-90187, Umeå, Sweden

⁴Lund University, Ergonomics and Aerosol Technology, Box 118, Lund SE-22100, Sweden

⁵Finnish Meteorological Institute, Atmospheric Research Centre of Eastern Finland, P.O. box 1627, FI-70211 Kuopio, Finland

^a Now at: Centre for Environmental and Marine Studies, University of Aveiro, Department of Environment and Planning, PT-3810-193, Aveiro, Portugal

Keywords: Immersion freezing, SPIN, Combustion emissions, Cookstoves.

INTRODUCTION

The particulate matter (PM) emissions from various combustion processes have a well-known direct effect on air quality and routinely observed effect on radiative forcing, yet their indirect contribution to the latter remains less understood. The ice nucleating (IN) ability is an important property of particulate matter, because it contributes to formation of cirrus clouds in the upper troposphere and stratosphere, which further affects the atmospheric reflectivity. The IN abilities of many natural and anthropogenic PM emissions have not yet been extensively studied and reported.

The IN efficiencies of biomass-fired cookstove emissions were studied using a portable ice nuclei counter SPIN (**SP**ectrometer for **I**ce **N**uclei) as a part of the SUSTAINED (**S**alutary **U**meå **S**tudy of **A**erosols **I**n **B**iomass **C**ook **S**tove **E**missions) experiment campaign. A few selected experiments included intentional modification of combustion conditions. This abstract focuses on five special cases where the combustion efficiency of one cookstove was modified, and it resulted in elevated soot production and significant increase in ice nucleation ability in two cases. Possible links between physical and chemical properties of the emission particles and their ice nucleating ability were investigated via extensive online characterization of the sample aerosol that supported the observations from the SPIN.

EXPERIMENT METHODOLOGY

Sample emissions were generated using a modified version of water boiling test (WBT, version 4.2.4), where 5 litres of water were first heated to boiling point (cold start phase) and then kept boiling for 45 minutes (simmering phase). The emissions were injected to a 15 m³ aerosol storage chamber after preliminary dilution and desiccation to <5% relative humidity. Prior to starting the experiment sequences on the SPIN, the chamber was filled to 10-100 µg m⁻³ mass concentration over a time that roughly represented one full combustion cycle on a pellet stove that was used in experiments with modified combustion conditions.

The setup for ice nucleation experiments in this study is presented in detail by Korhonen et al. (2019). The size-selected accumulation mode (250-500 nm) soot particles were sampled from the aerosol storage chamber and introduced to the SPIN at constant $RH_w = 115\%$, for immersion/condensation freezing (Vali et al, 2015). The sampling temperature was scanned over a range from -32 °C down to -41 °C and the T-scans were repeated 2-4 times for each experiment, before aerosol processes inside the storage chamber reduced the number concentration too low, below 30 cc⁻¹, for sampling on the SPIN. A condensation particle counter (CPC, Airmodus A20) was run parallel to the SPIN for calculation of the ice-activated fraction:

$$\alpha = \frac{N_{ice}}{N_{CPC}}$$

where N_{ice} is the background-corrected (i.e. background signal subtracted from the total signal) concentration of ice crystals detected by the SPIN and N_{CPC} is the concentration of sample particles detected by the CPC.

Particle number size distributions were measured directly from the sample line using a fast particle analyser (FPA, Cambustion DMS 500) during the WBTs, and then from the chamber using an SMPS system (classifier TSI 3082 + condensation particle counter TSI 3775) during the ice nucleation experiments. The presented six physical and chemical properties of biomass combustion emissions were measured using versatile instrumentation that produced supportive data to the ice nucleation experiments. The ability of particles as cloud condensation nuclei (CCN), κ_a , was measured using a CCN counter (CCNC, Droplet Measurement Technologies) and effective density with an aerosol particle mass analyzer (APM, Kanomax). A seven-wavelength aethalometer (Magee Scientific AE33) was used in parallel with a high-resolution time-of flight soot particle aerosol mass spectrometer (SP-AMS, Aerodyne Inc.), for measuring black carbon (BC) concentrations and chemical composition of the particles, respectively.

The five special experiments were carried out with a forced-draft gasifier stove (FDGS) and Swedish softwood pellets that were used as a reference fuel in the experiment campaign. The secondary air supply of the cookstove was intentionally blocked in two experiments, which impaired combustion efficiency and increased soot production. Three experiments were carried out using modified combustion conditions with alternative cooking pot height. In other words, the cooking pot was set above its designated height during operation, which led to elevated soot production during combustion.

RESULTS AND DISCUSSION

Modification of combustion conditions increased the ice nucleating ability of the emission particles significantly in two out of five experiments. Figure 1 shows results from all five cases and comparison to homogeneous freezing test on highly diluted ammonium sulphate droplets. The highest ice activity was observed in an experiment where cooking pot height was modified (green dots in Fig. 1), when 10^{-3} ice-activated fraction occurred at 5.9 °C higher temperature than what was required for homogeneous freezing. Another experiment with blocked secondary air supply of the FDGS (red dots in Fig.1) produced corresponding activated fraction at approximately 4 °C higher than homogeneous freezing. When these experiments were repeated without intentionally changing anything, the ice nucleation activity decreased with blocked secondary air (blue dots in Fig.1) and particles from two cooking pot height experiments (yellow and magenta dots in Fig.1) did not produce 10^{-3} activated fraction that was distinguishable from homogeneous freezing. This indicates that very minor changes in combustion conditions can have a dramatic effect on ice nucleating activity of the emission particles.

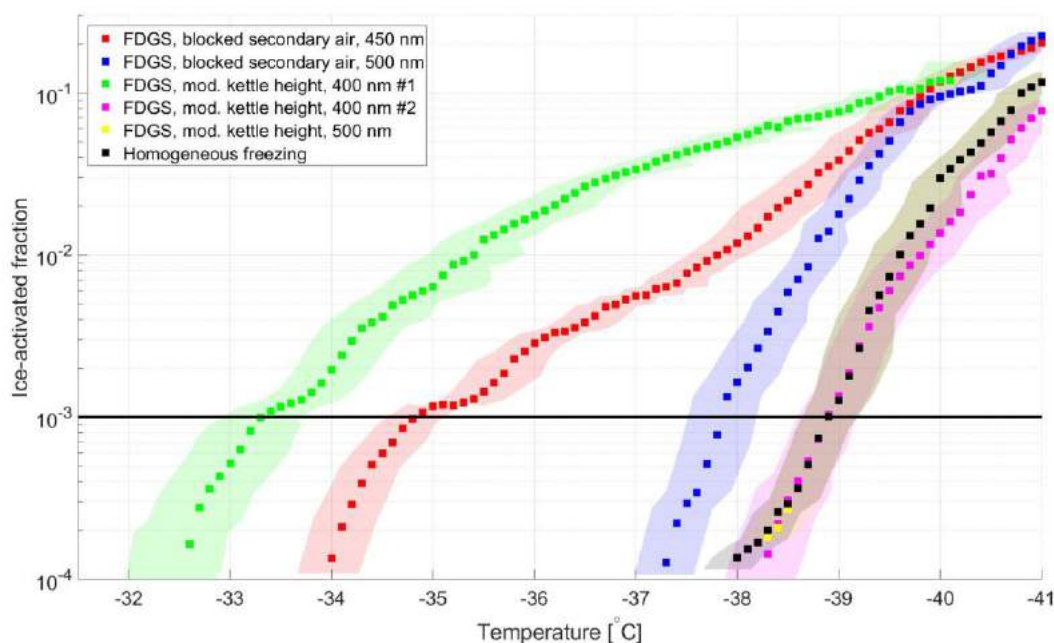


Figure 1: Ice-activation spectra of emissions from combustion of Swedish softwood pellets in a forced-draft gasifier stove, with modified combustion conditions at $RH_w = 115\%$. Each shaded area of respectful colour represents \pm one standard deviation on sample temperature during each observation. The solid black line presents the 10^{-3} activation. The ice-activation spectrum for homogeneous freezing test is included for comparison.

The connection between ice nucleating ability and certain physical and chemical properties was investigated using the extensive online measurement to support the ice nucleation experiments. The CCNC and the APM measured the CCN activity (κ_a) and effective density (ρ_e) values, respectively, for quasi-disperse 350 nm particles. The particles showed very low κ_a values, and effective density typical for refractory black carbon particles (Rissler et al., 2013). An elevated absorption of ultraviolet light was observed in two cases, the B450 and the B500, associated with increased fraction of mid-carbon range species that were also observed with the SP-AMS. Further analysis on chemical properties revealed that the fraction of refractory oxygen, such as surface oxides, varied only little between the experiments (see bottom panel of Fig.2).

The detailed analysis of above-mentioned physical and chemical properties of studied emission particles does not reveal any clear correlation to their ice nucleating abilities. Only a weak trend was observed in the fraction of refractory oxygen species (bottom panel of Fig.2), but it is questionable whether it is significant or not. Our investigation shows that either the studied aerosol properties do not determine the ice nucleating ability, or the ability is due to a complex combination of multiple particle properties. Further studies are needed before a firm conclusion can be drawn.

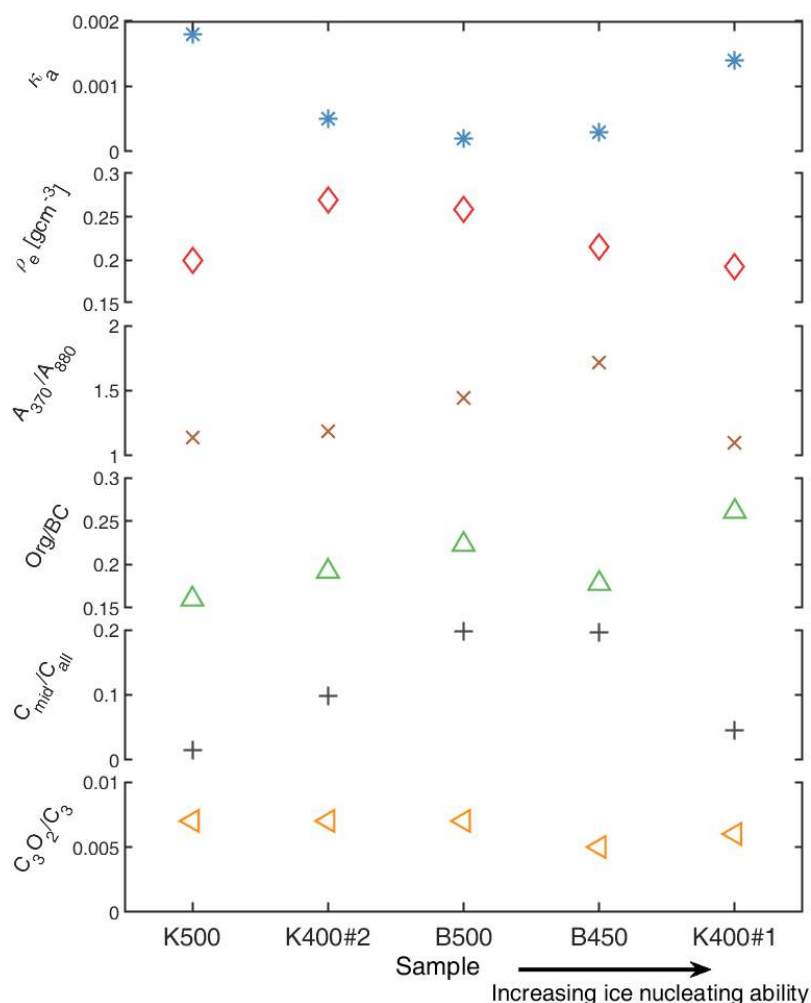


Figure 2: Physical and chemical properties of soot particles in five cases presented in Figure 1. The five cases presented have been re-ordered in a way so that the samples with higher ice nucleating ability are located further to the right. The properties from the top to the bottom represent the hygroscopicity (κ_a), effective density (ρ_e), ratio between the absorption at a wavelength of 370 nm versus 880 nm (A_{370}/A_{880}), ratio of organic aerosol mass to refractive BC mass (Org/BC), indirect qualitative information about the nanostructure (C_{mid}/C_{all}) and relative abundance of refractory oxygen species ($C_{3O_2^+}/C_{3^+}$). The two uppermost panels are for quasi-monodisperse soot particles with a mobility diameter of 350 nm, while the other properties are inferred for polydisperse aerosol. Letters K and B refer to modified cooking pot height and blocked secondary air experiments, respectively, in labels of the x-axis.

SUMMARY AND CONCLUSIONS

The SUSTAINED experiment campaign provided an excellent framework for studying IN abilities of cookstove emissions and possible relations between the IN ability and physico-chemical properties of the studied emission particles. One of our main findings was that even a modest variability in combustion conditions, even when performed under well-controlled laboratory conditions without making any intentional changes between repeated experiments, may affect the IN potential of particulate emissions significantly.

This study shows that biomass-fired cookstove emissions may have a potential as an atmospherically relevant source of IN particles. Particles that have a high IN potential were produced in cooking simulations which may well represent daily real-life usage by at least 500 million people in sub-Saharan Africa alone. It is worth noting that the studied emissions were relatively fresh, and atmospheric aging processes can further increase the IN potential.

The relation between the IN abilities of biomass-fired cookstove emissions and their physico-chemical properties, however, remains an open question because no clear correlation was found in our study. Therefore, the conclusion of this analysis is that the studied particle properties cannot define their IN ability alone, and the IN ability may be due to complex combinations of multiple properties of soot particles. We recommend further studies to explore the link between properties of combustion soot particles and their ice nucleation activity.

ACKNOWLEDGEMENTS

This work has been supported by Academy of Finland, Centre of Excellence (grant no. 272041), North-Savo Council - European Regional Development Fund's (project no. A32350), Swedish Research Council FORMAS (Dnr. 942-2015-1385, 2015-992 and 2013-01023) and Swedish Research Council VR (projects 2018-04200 and 2013-05021). T.B. Kristensen acknowledges grant no. 2017-05016 from VR and R. Carvalho the Postdoctoral grant JCK-1516 funded by the Kempe Foundation.

REFERENCES

Korhonen, K., Kristensen, T.B., Falk, J., Lindgren, R., Andersen, C., Carvalho, R. L., Berg-Malmborg, V., Eriksson, A., Boman, C., Pagels, J., Svenningsson, B., Komppula, M., Lehtinen, K. E. J., and Virtanen, A.: Ice nucleating ability of particulate emissions from solid biomass-fired cookstoves: an experimental study, *Atmos. Chem. Phys. Discuss.*, <https://doi.org/10.5194/acp-2019-890>, in review, 2019.

Rissler, J., Messing, M. E., Malik, A. I., Nilsson, P. T., Nordin, E. Z., Bohgard, M., Sanati, M and Pagels, J.: Effective density characterization of soot agglomerates from various sources and comparison to aggregation theory. *Aer. Sci. Tech.*, 47(7), 792-805, doi: 10.1080/02786826.2013.791381, 2013.

Vali, G., DeMott, P.J., Möhler, O. and Whale, T.F., Technical Note: A proposal for ice nucleation terminology, *Atmos. Chem. Phys.*, 15, 10263–10270, doi:10.5194/acp-15-10263-2015, 2015.

FIELD SCALE IRRIGATION EXPERIMENT TO INVESTIGATE METHANE EXCHANGE OF UPLAND FOREST SOIL IN NORTHERN FINLAND

M. KORCIAKOSKI¹, T. PENTTILÄ², T. MÄÄTTÄ¹, V. HYÖKY³, P. PIETIKÄINEN³ and A. LOHILA^{1,4}

¹Finnish Meteorological Institute, Atmospheric Composition Research, P.O. Box 503, FI-00101, Helsinki, Finland

²Natural Resources Institute Finland, Viikinkaari 4, FI-00790, Helsinki, Finland

³Metsähallitus Luontopalvelut, Pallasjärven toimipiste, Pallaksentie, Muonio, Finland

⁴Institute for Atmospheric and Earth System Research/Physics, Faculty of Science, University of Helsinki, P.O. Box 68, FI-00014 Helsinki, Finland

Keywords: ch₄ oxidation, ch₄ production, flux, chamber technique.

INTRODUCTION

Boreal forests and peatlands store a large amount of carbon (C) and interact with the atmosphere by exchanging greenhouse gases (GHGs) which are the main drivers of climate warming. Both forests and wetlands fix atmospheric carbon dioxide (CO₂) in photosynthesis and release it in the decomposition of dead organic matter. On the other hand, pristine wetlands are net emitters of methane (CH₄) due to the anoxic conditions favouring the methane-producing bacteria, while upland forest soils consume atmospheric methane due to predominance of methane-oxidising bacteria.

In addition to wet peatlands, mineral upland forest soils can occasionally be flooded and temporarily act as a source of methane (Savage *et al.*, 1997; Christianssen *et al.*, 2012; Lohila *et al.*, 2016). In annual terms, this source can be significant as weather conditions may cause the flooding to last a considerable proportion of the active season and because often the forest coverage within a typical boreal catchment is much higher than that of wetlands. After upscaling to a regional scale, even a small CH₄ emission in upland forest soil becomes significant. Furthermore, as precipitation may increase during summer and autumn in northern latitudes (Jylhä *et al.*, 2009), this flooding-induced source of methane may be activated more frequently in the future. This source is accounted for in the models of global methane emissions, but there are recent observation-based indications that its magnitude may be severely underestimated, suggesting that the total annual emissions from upland forest soils in wet years may be nearly as large as those from northern peatlands (Lohila *et al.* 2016).

The aim of this experiment was to irrigate forest soil in northern Finland to see the impact of excess soil moisture on CH₄ exchange. We also aimed at reaching moisture levels in which the soil would turn to CH₄ source, as was observed at the site during a very wet summer of 2011.

METHODS

The experiment was set up in the Kenttäröva forest in Kittilä, within the Pallas-Yllästunturi National Park in northern Finland, located on a hill-top plateau, ca. 60 m above the surrounding plains. The site is a spruce forest (*Hylocomium-Myrtillus* type) with some *Betula pubescens*, *Populus tremula* and *Salix caprea*. The main species of the ground floor are *Vaccinium myrtillus*, *Empetrum nigrum*, *Vaccinium vitis-idaea* and the

forest mosses *Pleurozium schreberi*, *Hylocomium splendens*, and *Dicranum polysetum*. The soil type at the site is podzolic till. The snow cover maximum in Finland has often been observed at the Kenttäröva forest site, with an average annual maximum value of 104 cm (81–125 cm) in 2008–2014.

The wetting experiment consisted of control and irrigation areas, which both had four different types of chamber plots. Both areas included four old chamber plots where CH₄ fluxes have been measured since 2016. Next three chamber plots were surrounded by open-top chambers (OTC) to slightly increase the temperature in the plot. The last six plots were divided into litter exclusion and litter addition plots. In litter exclusion plots, a litter collector was installed on top of the plots. The litter was collected and weighted bi-weekly, and distributed evenly on the litter addition plots. Also, the litter exclusion plots were measured with and without the vegetation layer. Root exclusion fabric was installed in the 40 cm deep soil pits dug around the litter exclusion plots. This was done to prevent the below-ground litter input into the plot.

The irrigation was performed with two sprinklers and one irrigation caused on average 9 mm of rain. Forest floor was irrigated every weekday in summer 2018 and three times a week in summer 2019. However, due to the drought in 2018, the site was irrigated twice every day corresponding to 18 mm of rain.

The CH₄ flux measurements were made with the closed-chamber technique by using opaque rectangular chamber (50 x 50 x 37 cm, length x width x height) with a permanently installed steel collar in the soil. The chamber was closed for 5 minutes and a 50 m long tubing was used to transfer the sample air into a cavity ring-down spectroscopy gas analyser (Picarro G1300, Picarro Inc., USA) to acquire CH₄ mixing ratios with 5 second time resolution.

RESULTS

In summer (JJA) 2018, 5 cm soil temperatures at the irrigation area were on average 1 °C higher than at the control area (Fig. 1), but the temperatures were variable at both areas. Also, in 2019 the mean temperatures were similar in both areas. There were no significant differences in soil temperatures between the heated and non-heated plots.

Soil moisture was on average 6.5% and 3.7% higher on the irrigated area in summers 2018 and 2019 (Fig. 1), respectively. Outside irrigation and rainfall events the soil moistures (volumetric water content, %) varied mostly between 15–25% in the irrigation area and 8–15% in the control area. Irrigation typically raised soil moisture immediately by 4–20% (Fig. 2), but usually it returned to the pre-irrigation range within a day.

The initial analysis showed only one CH₄ emission case measured at end of June 2019. However, the mean CH₄ sink in Jun-Jul period was smaller at the irrigated area (2018: $-169 \mu\text{g CH}_4 \text{ m}^{-2} \text{ h}^{-1}$, 2019: $-198 \mu\text{g CH}_4 \text{ m}^{-2} \text{ h}^{-1}$) than at the control area (2018: $-300 \mu\text{g CH}_4 \text{ m}^{-2} \text{ h}^{-1}$, 2019: $-259 \mu\text{g CH}_4 \text{ m}^{-2} \text{ h}^{-1}$) during both years (Fig. 3).

The mean cumulative summertime CH₄ sinks between different plot types varied somewhat. The litter addition and heated plots in the irrigation area had on average 237 and 134 mg CH₄ m⁻² smaller sink than the area mean in 2018. However, in 2019, only the litter addition plots had noticeably smaller CH₄ sink while the other plot types had rather similar CH₄ sinks. In the control area, in 2018, only the long term plots had noticeably larger sink ($-554 \text{ mg CH}_4 \text{ m}^{-2}$, area mean: $-384 \text{ mg CH}_4 \text{ m}^{-2}$) than the other plots. On the other hand, the CH₄ uptake rate was on average smaller in litter exclusion plots ($-240 \text{ mg CH}_4 \text{ m}^{-2}$) than the rest of the plot types, which were close to the area mean ($-384 \text{ mg CH}_4 \text{ m}^{-2}$). In 2019, all the plot types at the control area had similar CH₄ uptake rates.

CONCLUSIONS

Dry summers made the conditions for the wetting experiment difficult. Irrigating the forest floor with an amount that corresponded to 18 mm was not enough to increase the soil moisture more than 25% at best for

a short time as the dry and warm conditions caused the water to evaporate quickly. However, the irrigated area never dried up completely before the next irrigation; therefore, the soil moisture stayed higher than at the control area. Also, this higher soil moisture decreased CH₄ oxidation and, as a result, CH₄ sink was smaller at the irrigated area than at the control area. Even though the amount of irrigation was decreased in 2019, the CH₄ sink stayed around the same at the irrigated area but decreased at the control area. This can be explained by higher precipitation sum over summer 2019 compared to 2018.

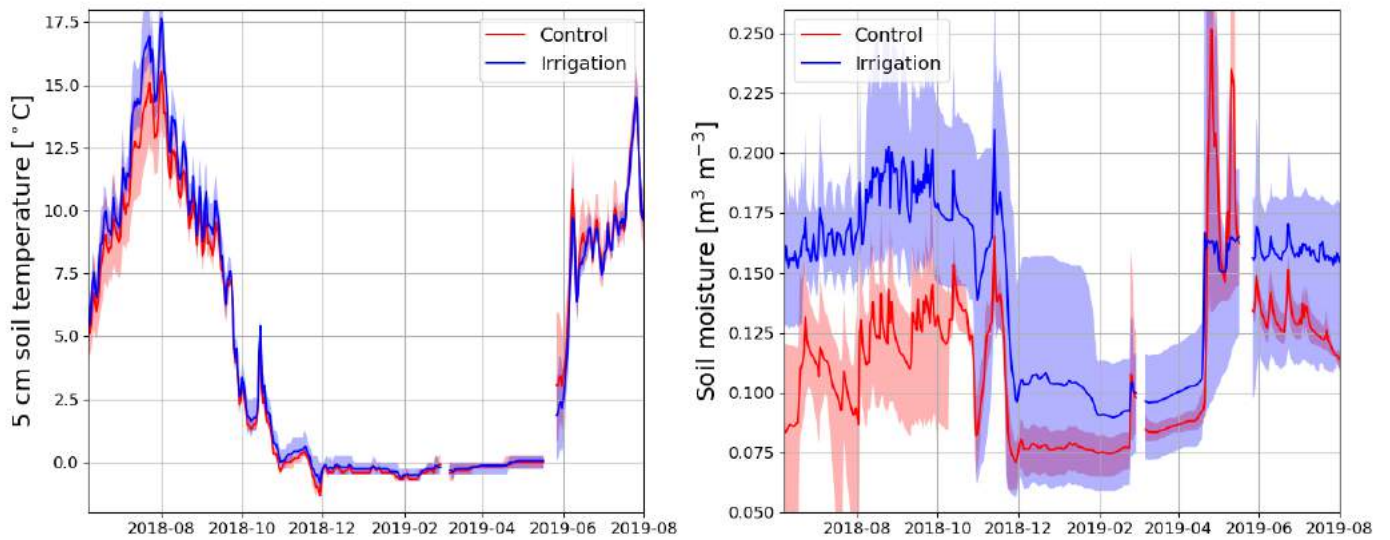


Figure 1. Daily mean 5 cm soil temperature (left) and 5 cm soil moisture (right) and their minimum and maximum values at the irrigated (blue) and control (red) area (n = 3–12).

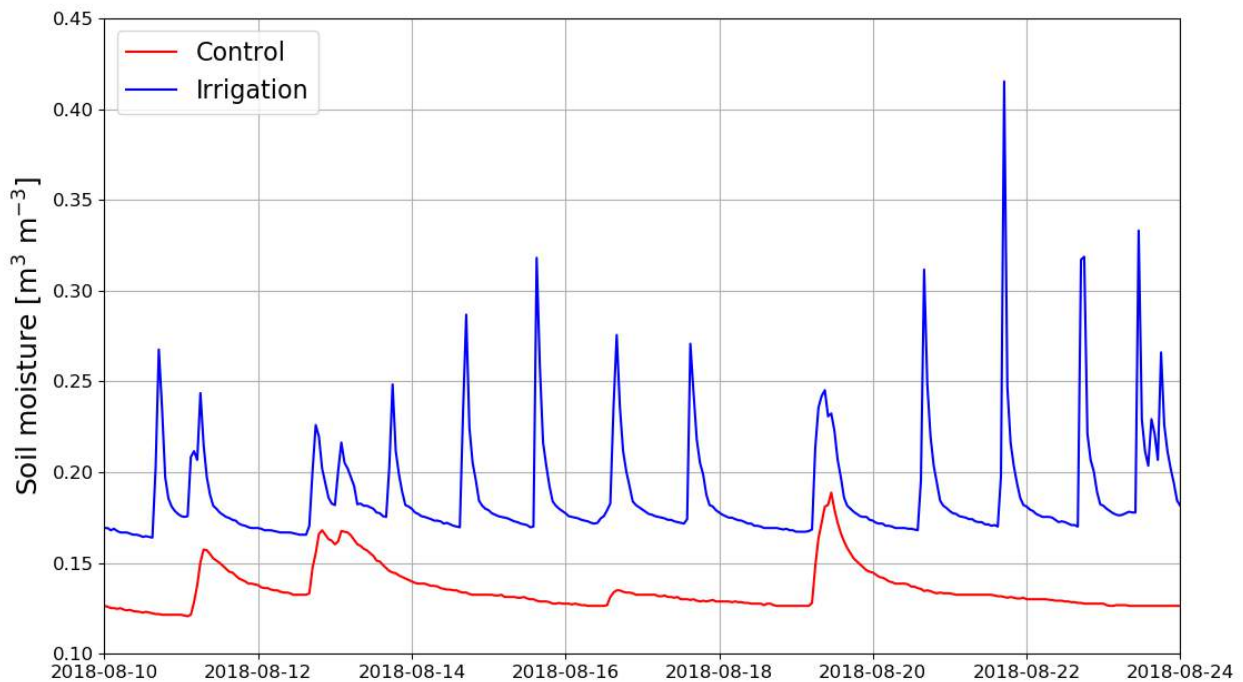


Figure 2. Daily mean 5 cm soil moisture measured at one of the chamber plots at the irrigated (blue) and control (red) area in 10-24 August 2018.

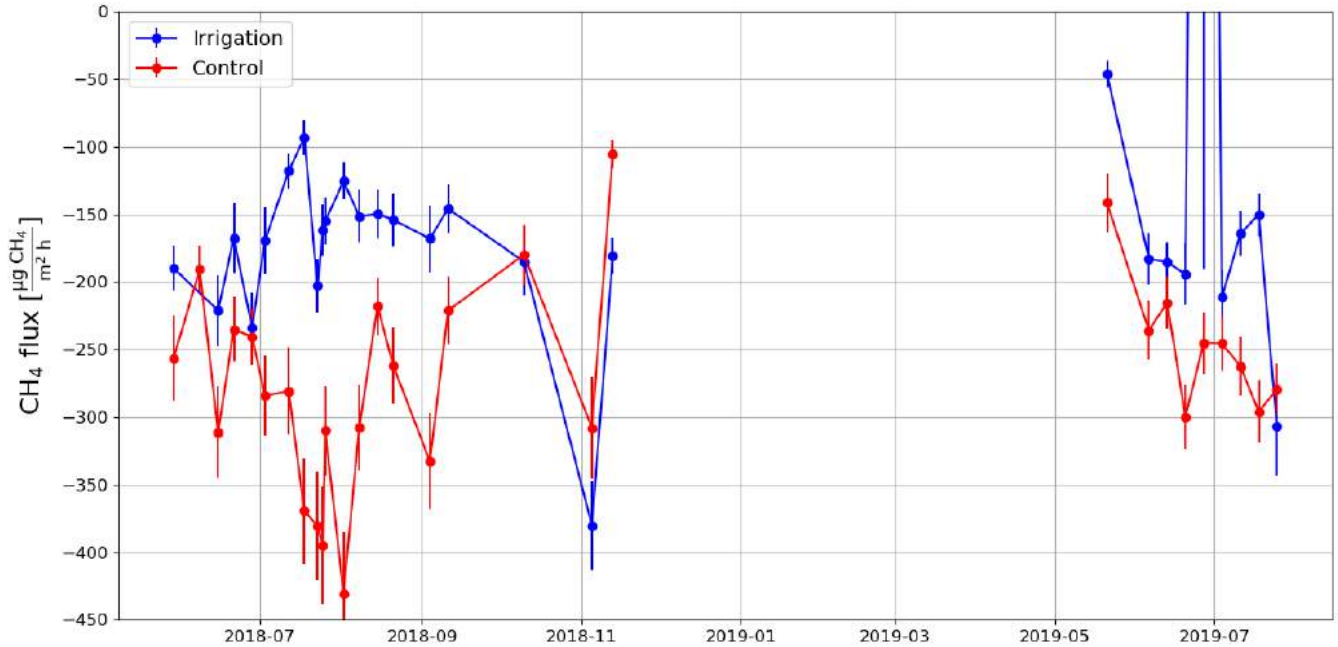


Figure 3. Daily mean (n = 13) CH₄ fluxes and their standard error of the means measured at the irrigated (blue) and control (red) area during summers 2018 and 2019.

ACKNOWLEDGEMENTS

This work was supported by the Academy of Finland (grant no. 308511).

REFERENCES

- Savage, K., Moore, T.R. and P. M. Crill (1997). *Methane and carbon dioxide exchanges between the atmosphere and northern boreal forest soils*. J. Geophys. Res. 102, D24, 29279–29288.
- Lohila, A., Aalto, T., Aurela, M., Hatakka, J., Tuovinen, J.-P., Kilkki, J., Penttilä, T., Vuorenmaa, J., Hänninen, P., Sutinen, R., Viisanen, Y. and T. Laurila (2016). *Large contribution of boreal upland forest soils to a catchment-scale CH₄ balance in a wet year*, Geophys. Res. Lett., 43(6), 2946–2953.
- Christiansen, J. R., Vesterdal, L. and P. Gundersen (2012). *Nitrous oxide and methane exchange in two small temperate forest catchments—Effects of hydrological gradients and implications for global warming potentials of forest soils*. Biogeochemistry, 107, 437–454.
- Jylhä, K., Ruosteenoja, K., Räisänen, J., Venäläinen, A., Tuomenvirta, H., Ruokolainen, L., Saku, S. and S. Seitola (2009). *Changing climate in Finland: estimates for adaptation studies*. ACCLIM project report 2009. Finnish Meteorological Institute, Reports.

REDOX IN IMPROVING ECOSYSTEM MODELING UNDER ANOXIC CONDITIONS

M. KOSKINEN^{1,2,3}, A. LOHILA^{1,3}, T. LAURILA³, P. STRAKOVA⁴, T. PENTTILÄ⁴, M. PIHLATIE^{2,3}, R. LAIHO⁴

¹ Finnish Meteorological Institute, Greenhouse Gases Research Group, Helsinki, Finland

²Institute for Atmospheric and Earth System Research, University of Helsinki, Finland

³Environmental Soil Science, Department of Agricultural Sciences University of Helsinki, Finland

⁴Natural Resources Institute Finland, Helsinki, Finland

Keywords: REDOX, PEATLANDS, GREENHOUSE GASES, WATER QUALITY.

INTRODUCTION

Globally, peatlands cover 4,500,000 km² of the Earth (Yu et al., 2010). Pristine peatlands are a major source of methane (CH₄) (Huttunen et al., 2003b). At the same time, they are one of the largest terrestrial stores for carbon and a net sink for carbon dioxide (CO₂). Drainage of peatlands has been done on an estimated area of 500,000 km² worldwide (Joosten, 2009). The reasons for draining peatlands have varied in different parts of the world. In the boreal region, the most common cause for drainage has been forestry. In the temperate and tropical regions, agriculture and peat excavation have been the most common goals. Drainage has been connected to harmful environmental effects world wide including eutrophication and turbidisation of water courses, massive carbon loss from the soil and loss of biodiversity. On the other hand, efforts to mitigate these negative effects, eg. ecological restoration by means of rewetting, have caused their own problems, such as leaching of nutrients and organic carbon and increased CH₄ emissions (eg. Koskinen et al., 2016; Koskinen et al., 2017).

Under current peatland forestry practices, the most usual chain of operations for forest renewal is clear-cutting followed by ditch maintenance, possibly additional drainage and then planting of seedlings. This causes drastic changes in soil conditions as first the water level (WTL) rises when the transpiring vegetation is removed and then WTL goes deeper again as the effects of ditch maintenance and transpiration by the renewed vegetation start to take hold. This causes first release of soluble phosphorus (P), dissolved organic carbon (DOC) and nitrogen (N) (Nieminen et al., 2017) and possibly CH₄ (Huttunen et al., 2003a) from the soil as reducing conditions reach the top peat layers. After the renewal of vegetation as oxidising conditions again prevail, leading to CO₂ release from the soil. Recent research indicates that forestry-drained peatlands cause water-course loading of nitrogen even without further forestry operations such as logging, fertilisation and ditch maintenance (Nieminen et al., 2018b). Recently, research efforts have been directed to so-called continuous cover forestry on drained peatlands as an alternative to the conventional force-based renewal chain (Nieminen et al., 2018a). In this model, only a portion of the stand volume is removed at a time and ditch maintenance is not necessary. At the same time, the aim is to keep WTL high enough to limit peat decomposition and thus reduce the CO₂ emissions and C losses from the soil. In the global scale, there is growing interest in so-called paludiculture, where crops are grown on peatlands that have a high WTL. This is done to minimise the loss of soil carbon and to mitigate nitrous oxide (N₂O) emissions connected to a deep WTL and intensive agricultural use. The key question in paludiculture is how to minimise both the N₂O and CO₂ emissions and simultaneously CH₄ emissions and aqueous carbon and nutrient losses connected to

a high WTL. All of these processes are dependent on the reductive-oxidative (redox) conditions of the soil and thus assessing the multiple, simultaneous reactions requires understanding of redox processes. Decision-making on the use of peatlands need to be evidence-based and optimised for protection of biodiversity, climate, water quality, and livelihoods. Current ecological models fail to represent the complexities of chemical reactions that lie behind the effects of both drying and rewetting of peatlands and thus cannot reliably predict the outcomes of operations.

Reduction-oxidation (redox) reactions are central to the adsorption and release of carbon and nutrients in all soils. Different electron acceptors are used by microbes to gain energy according to their availability and ease of use. The presence and status of different electron acceptors and donors affects the availability of electrons in the soil. The redox conditions in soils can be described by the electric potential compared to a standard hydrogen electrode. Recent developments in measurement methods have enabled continuous field measurements of redox potential. As redox reactions are key to carbon dioxide (CO₂) and methane (CH₄) emissions and the release of phosphorus (P), ammonia (NH₄-N) and dissolved organic carbon (DOC) from peat soils, the redox state of peatlands could be used to improve models that predict the functioning of these ecosystems under different water table regimes.

In this project and its proposed extension, we aim to improve existing ecosystem models in their capacity to predict outcomes of operations on peat soils, such as clear cut, partial harvest, restoration and gradual increase in WTL by ditches filling in by themselves. This will be attained by creating a module to predict which anoxic redox reactions are taking place in the soil at a given time based on the composition of the peat and the hydrological regime. Initial data is available from a two-year measurement campaign on drained and undrained mesotrophic peatlands.

METHODS

Redox probes with sensors at five depths (5, 15, 25, 35, 45cm) were deployed at the Lakkasuo mire (61°47,7' N, 24°18,5' E) in three different drainage regimes (undrained (UD), short-term drainage (STD), long-term drainage (LTD)) on a mesotrophic part of the mire complex. Three probes per treatment were used. Water-table level (WTL) and soil temperature (ST) were also recorded at the same spots. The measurement campaign started in August 2014 and continued until fall 2016.

For the modeling, wider field measurements on several drained and undrained peatlands in Southern and Northern Finland are being conducted; laboratory experiments in micro- and mesocosm scale to study the effects of peat properties on redox conditions and redox conditions on element release and carbon cycling are being planned. The capability of the PHREEQC model (Parkhurst and Appelo, 2013) to predict the release of elements in the experiments will be tested and the model will be used to provide ecosystem-scale models with redox species and reactions.

CONCLUSIONS

The initial results from Lakkasuo reveal that the connection between WTL and redox potential is complex. On the STD and LTD plots, rising WTL leads to falling redox potential, whereas on the UD plot, rising WTL often causes rising redox potential in permanently inundated peat layers. These differences probably reflect the different hydrological status of the plots: on the drained plots (STD, LTD), the source of water is mainly precipitation, as the plot is cut off from its surrounding watershed; whereas on the undrained plot, a significant portion of the water comes from the surrounding mineral soil, possibly bringing with it reducible compounds the rainwater does not have.

ACKNOWLEDGEMENTS

This work is supported by the Maj and Tor Nessling Foundation, and by the Academy of Finland (grant 289116).

REFERENCES

- Huttunen, Jari T., Hannu Nykänen, Pertti J. Martikainen, and Mika Nieminen (2003a). “Fluxes of nitrous oxide and methane from drained peatlands following forest clear-felling in southern Finland”. In: *Plant and Soil*, pp. 457–462. DOI: <https://doi.org/10.1023/A:1026035427891>.
- Huttunen, Jari T., Hannu Nykänen, Jukka Turunen, and Pertti J. Martikainen (2003b). “Methane emissions from natural peatlands in the northern boreal zone in Finland, Fennoscandia”. In: *Atmospheric Environment* 37.1, pp. 147–151. ISSN: 13522310. DOI: 10.1016/S1352-2310(02)00771-9.
- Joosten, H. (2009). *The Global Peatland CO₂ Picture: peatland status and drainage related emissions in all countries of the world*. English. URL: <https://www.cabdirect.org/cabdirect/abstract/20093336601> (visited on 09/17/2019).
- Koskinen, Markku, Liisa Maanavilja, Mika Nieminen, Kari Minkkinen, and Eeva-Stiina Tuittila (2016). “High methane emissions from restored Norway spruce swamps in southern Finland over one growing season”. In: *Mires and Peat* 17.2, pp. 1–13.
- Koskinen, Markku, Teemu Tahvanainen, Sakari Sarkkola, Meseret Walle Menberu, Ari Laurén, Tapani Sallantausta, Hannu Marttila, Anna-Kaisa Ronkanen, Miia Parviainen, Anne Tolvanen, Harri Koivusalo, and Mika Nieminen (2017). “Restoration of nutrient-rich forestry-drained peatlands poses a risk for high exports of dissolved organic carbon, nitrogen, and phosphorus”. In: *Science of the Total Environment* 586, pp. 858–869. DOI: 10.1016/j.scitotenv.2017.02.065.
- Nieminen, M., H. Hökkä, R. Laiho, A. Juutinen, A. Ahtikoski, M. Pearson, S. Kojola, S. Sarkkola, S. Launiainen, S. Valkonen, T. Penttilä, A. Lohila, M. Saarinen, K. Haahti, R. Mäkipää, J. Miettinen, and M. Ollikainen (Sept. 2018a). “Could continuous cover forestry be an economically and environmentally feasible management option on drained boreal peatlands?” In: *Forest Ecology and Management* 424, pp. 78–84. ISSN: 0378-1127. DOI: 10.1016/j.foreco.2018.04.046.
- Nieminen, M., S. Sarkkola, S. Hellsten, H. Marttila, S. Piirainen, T. Sallantausta, and A. Lepistö (2018b). “Increasing and Decreasing Nitrogen and Phosphorus Trends in Runoff from Drained Peatland Forests—Is There a Legacy Effect of Drainage or Not?” In: *Water, Air, and Soil Pollution* 229.8. ISSN: 15732932. DOI: 10.1007/s11270-018-3945-4.
- Nieminen, M., S. Sarkkola, and A. Laurén (May 2017). “Impacts of forest harvesting on nutrient, sediment and dissolved organic carbon exports from drained peatlands: A literature review, synthesis and suggestions for the future”. In: *Forest Ecology and Management* 392, pp. 13–20. ISSN: 0378-1127. DOI: 10.1016/j.foreco.2017.02.046.
- Parkhurst, David L. and C.A.J. Appelo (2013). *Description of input and examples for PHREEQC version 3: a computer program for speciation, batch-reaction, one-dimensional transport, and inverse geochemical calculations*. Tech. rep. Reston, VA, p. 519. URL: <http://pubs.er.usgs.gov/publication/tm6A43>.
- Yu, Zicheng, Julie Loisel, Daniel P. Brosseau, David W. Beilman, and Stephanie J. Hunt (2010). “Global peatland dynamics since the Last Glacial Maximum: GLOBAL PEATLANDS SINCE THE LGM”. In: *Geophysical Research Letters* 37.13. ISSN: 00948276. DOI: 10.1029/2010GL043584.

ATMOSPHERIC MOLECULAR CLUSTERS: PRESENCE OF WATER

J. KUBEČKA¹, V. BESEL¹, T. KURTÉN¹ and H. VEHKAMÄKI¹

¹Institute for Atmospheric and Earth System Research (INAR),
University of Helsinki, Helsinki, Finland.

Keywords: molecular clusters, quantum chemistry, configurational sampling, new-particle formation.

INTRODUCTION

Atmospheric aerosol studies are about understanding atmospheric molecular chemistry, aerosol physics, but also about aerosol formation. Single atmospheric molecules collide with each other forming molecular clusters which might then grow into aerosols by condensation of other molecules. In order to study new-particle formation (NPF) by theoretical methods, the structural properties of molecular cluster have to be known. Therefore, configurational sampling method is required. We present our configurational sampling approach. Moreover, since we have systematic approach for studying molecular clusters, we focus on larger systems or try to include water (*i.e.*, humidity) into our calculations.

METHODS

We have developed the Jammy Key for Configurational Sampling program (JKCS) which is a program that operates with all files (structures, outputs etc.) and 3rd-party computational programs needed to search for a global minimum (and also low-lying local minima) structure(s).

The process is based on the so called ‘building up’ approach. The whole Potential Energy Surface (PES) is explored on Molecular Mechanics (MM) level by methods utilizing neural networks, genetic algorithm, machine learning *etc.* In this work, we selected the Artificial Bee Colony (ABC) genetic algorithm (Karaboga and Basturk, 2012) implemented in the program ABCcluster (Zhang and Dolg, 2015; Zhang and Dolg, 2016). Further, several re-optimization, filtering or sampling/selection steps are used to obtain just a few molecular structures which are the energetically lowest lying local minima on the desired level of theory.

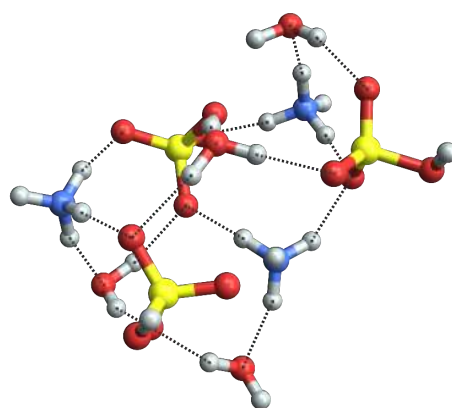


Figure 1. Molecular structure of sulfuric acid-ammonia-water cluster. Spot the bridging of hydrogen bonds via water molecules. Color coding: sulfur = yellow, nitrogen = blue, oxygen = red, hydrogen = white.

We have already utilized the program for configurational sampling of several types of clusters. However, now, we focus on understanding the presence of water in molecular clusters. In the atmosphere, water has

orders of magnitude higher concentration than other studied molecules. And, water molecule might work as a bridge for hydrogen bond interaction between two distant molecules (see example in Figure 1). Thus, does water play an important role in stabilization of molecular clusters? Or, has water presence just minor effect in the beginning of new-particle formation?

CONCLUSIONS

We have found a way for systematic configurational sampling of atmospheric molecular clusters. The configurational sampling approach has been recently published by Kubečka *et al.* (Kubečka *et al.*, 2019). We discuss the main obstacles of configurational sampling or global minima search, how to treat those obstacles and why the high level of theory evaluation of molecular clusters is required. Moreover, we present an application of our universal protocol for configurational sampling on several systems containing molecules such as sulfuric acid, ammonia, guanidine, highly oxygenated molecules, water etc. The Jammy Key for Configurational Sampling (JKCS) program has been released for public usage.

Finally, using Atmospheric Cluster Dynamics Code (ACDC) (McGrath *et al.*, 2012), we also briefly discuss population dynamics of several cluster systems involved in new-particle formation. Now, our main focus are molecular cluster structures containing also water, and thus, we can understand overall effect of humidity on new-particle formation.

ACKNOWLEDGEMENTS

This research is supported by the European Research Council project 692891-DAMOCLES, Academy of Finland and ATMATH project. We would like to thank also CSC – Finnish IT Centre for access to computer clusters.

REFERENCES

- Karaboga, D., and B. Basturk (2008). *App. Soft Matter*, **8**, 687-697.
- McGrath, M. J., T. Olenius, I. K. Ortega, V. Loukonen, P. Paasonen, T. Kurtén, M. Kulmala, and H. Vehkamäki (2012). *Atmos. Chem. Phys.*, **12**, 2345.
- Zhang, J., and M. Dolg (2015). *Phys. Chem. Chem. Phys.*, **17**, 24173-24181.
- Zhang, J., and M. Dolg (2016). *Phys. Chem. Chem. Phys.*, **18**, 3003-3010.
- Kubečka, J., V. Besel, T. Kurtén, N. Mylly, and H. Vehkamäki (2019). *J. Phys. Chem. A*, **28**, 6022-6033.

Rapid Reversal of Global Warming Through Arctic Cloud Seeding.

I. KUDZOTSA^a, H. KOKKOLA^a, J. TONTTILA^a, S. ROMAkkANIEMI^a

^a*Finnish Meteorological Institute, Atmospheric Research Centre of Eastern Finland, Kuopio, Finland.*

Key Words: Arctic clouds, Cirrus seeding, Aerosol-cloud interactions, Ice melting.

INTRODUCTION

Climate change continues to be the greatest challenge threatening our future and our planet Earth. It is mainly attributed to anthropogenic emissions of carbon dioxide into the atmosphere, which then causes global warming (Boucher and Randall, 2013). There are two main categories of mechanisms that have been proposed, which can potentially counteract the CO₂ induced warming. The first category aims at sequestering carbon dioxide either from the emission sources (Carbon Capture and Storage, CCS) or from the atmosphere (Carbon Dioxide Removal, CDR). The second category, the solar radiation management (SRM) aims at altering the radiation balance of the Earth. One SRM method which has received much attention is the artificial injection of aerosol particles or their precursor gases into the stratosphere, where they can reflect solar radiation back to space and hence cooling the Earth (Laakso et al., 2017). However; since these SRM methods reduce shortwave radiation reaching the earth, this has a side effect of reducing the global radiation and precipitation budgets (Ferraro et al., 2014). Another widely proposed SRM method is the whitening of low-level stratocumulus clouds over oceans, which targets shortwave radiation with very strong local effect (Maalick et al., 2014). These have also been shown to be less effective in cooling the climate than initially anticipated (Partanen et al., 2012). Therefore, other techniques of directly counteracting global warming, which have smaller impact on global solar radiation and precipitation budget have been mooted (Muri et al., 2014). Such methods are, cirrus and low-level mixed-phase cloud seeding which focus especially over the Arctic region (Storelvmo et al., 2013; Lohmann and Gasparini, 2017). These methods aim at altering the micro- and macro-physical properties of these clouds so that they become more transparent to long-wave radiation emitted by the Earth's surface thus cooling the surface. Cooling over the Arctic would be beneficial as the rate of climate warming has been observed and forecasted to be fastest near the poles (Boucher and Randall, 2013) and hence immediate attention is warranted.

If the theoretical hypotheses and implications of this mechanism are successfully materialized, then this mechanism is preferable over the above mentioned geoengineering techniques because it proffers minimum side effects on our climate system and speeds up the reversal of global warming. However, only few a studies have examined the effectiveness of this methods and those have been performed using global-scale climate models, which are not well suited for simulating cloud-scale processes that occur very much within the sub-grid scales of global models. Consequently, some questions pertaining to these

mechanisms still remain unanswered, both on the global and the cloud-resolving scales. These include: how tropical convection and circulation would be affected; which geographical regions are ideal targets for seeding; what is the optimal seeding frequency and what are the transport mechanisms of the seeded ice nucleating particles (INP) (Lohmann and Gasparini, 2017)?

The main goal of this work is to investigate: the microphysical and dynamical effects of cirrus and low-level cloud seeding in the Arctic region and to establish its implication on the radiative balance of the Earth and to develop parameterizations for GCMs. The specific objectives that will be addressed in this work are as follows.

- **O1:** To identify suitable INPs and altitudes for optimal cirrus seeding.
- **O2:** To establish the effective microphysical and dynamical mechanisms of heterogeneous ice nucleation in Arctic clouds.
- **O3:** To establish whether, with the typical humidity amounts or conditions in the Arctic middle to upper troposphere, heterogeneously nucleated ice crystals can indeed grow large enough to precipitate or sediment leading to significant dissipation of cirrus Arctic clouds.
- **O4:** To investigate the efficacy of a combination of cirrus and low-level mixed-phase cloud seeding on cooling the Arctic region and to establish the most efficient technique between the two.

The ultimate objective of this study will be to provide an estimate for the maximum potential of Arctic cirrus and low-level cloud seeding to reduce climate warming over the Arctic areas.

METHODS

The tasks in this work focus on different aspects of the formation and evolution of heterogeneously nucleated cirrus clouds and INP seeded low-level clouds over the Arctic region and aim at answering to research questions set out by the objectives stated above. The research will be achieved by using our state-of-the-art Large Eddy Simulator called UCLALES-SALSA (Tonttila et al., 2017). The first task will be aimed at addressing the first objective. Here, the implementation of the ice-phase microphysics in SALSA will be validated against observational data available from relevant campaigns conducted in the Arctic region, such as the Indirect and Semi-Direct Aerosol Campaign (ISDAC) (Ghan et al., 2007) and the Mixed Phase Arctic Clouds Experiment (M-PACE) (Verlinde et al., 2007) campaigns. It is appreciated that very few reliable observations are available for the Arctic region mainly due to its limiting weather conditions. Different ice nucleation techniques will be explored or developed to identify the most relevant ones for the Arctic scenarios. During this task, different INPs will be tested to identify the IN species and median sizes most suitable for an effective seeding process. Bismuth triiodite, Silveriodite, metallic dust and soot have been suggested as effective ice-nucleating agents.

The other main hypothesis in this work is that effective Arctic cloud seeding would promote the glaciation of both cirrus and low-level mixed-phase clouds particularly due to the Bergeron-Findeisen process (which is a process whereby ice crystals in mixed-phase

clouds grow rapidly at the expense of cloud droplets) and subsequently lead to increased sedimentation and precipitation and resulting in thinning and depletion of the cloud lifetime, coverage and optical thicknesses. However, it is not well understood whether the typical relative humidities and water contents that characterize the usually dry Arctic atmosphere would be adequate and conducive enough to facilitate this postulation and if so, the main microphysical and dynamical mechanisms through which this proposed crystal growth would take place will be explored. This will be done by conducting sensitivity tests that can isolate the importance of different microphysical process involved in the nucleation, growth, precipitation and dissipation of such clouds. Furthermore, the amount of needed seeding material will be optimized and estimates will be given on how much effort would be needed to expand seeding over the whole Arctic.

The ultimate goal of this work is to be able to quantify or estimate the maximum radiative forcing achievable through Arctic cirrus and low-level mixed-phase cloud seeding. Different idealized scenarios will be simulated under different conditions for the amount of radiation, moisture and temperature profiles and initial particulate aerosol loading in order to resolve the most important parameters and processes which affect cloud's radiative properties and evolution. Here, special attention shall be given to how liquid water is partitioned between liquid cloud droplets and ice crystals. In general, ice crystals are expected to grow readily at the expense of the liquid droplets leading to more solid precipitation and hence depletion of cloud's spatial extent, lifetime and optical thickness. The radiative forcing caused by these changes will be assessed by conducting sensitivity tests in which radiation is either partially or completely switched off from the simulation. Switching off or artificially controlling/prescribing the crystal/droplet number concentration in the simulations helps understanding how different changes in cloud properties affect the radiation balance of the domain. As a result, the radiative forcing, if any, caused by the seeding process will be quantified and the main mechanisms and pathways responsible will be understood.

CONCLUSIONS

It is well known that the representation of clouds in general still needs improvement in climate models and ice-phase clouds are the most poorly represented. This has remained the largest contribution to the uncertainties associated with the simulation of the current and future climate and the Arctic or Polar regions are the most poorly represented. In this work, some parameterizations for ice nucleation and ice-phase cloud seeding shall be developed and recommended for global climate modeling.

ACKNOWLEDGEMENTS

This work is supported by The Tiina and Antti Herlin (TAH) Foundation (project no. 20190133).

References

- Boucher, O. and D. Randall, 2013: Climate change 2013: The physical science basis. contribution of working group i to the fifth assessment report of the intergovernmental panel on climate change, (ipcc). *Cambridge University Press, Cambridge, United Kingdom and New York, NY, USA.*, **5th**.
- Ferraro, A. J., E. J. Highwood, and A. J. Charlton-Perez, 2014: Weakened tropical circulation and reduced precipitation in response to geoengineering. *Environmental Research Letters*, **9** (1), 014 001.
- Ghan, S., et al., 2007: Indirect and semi-direct aerosol campaign (isdac).
- Laakso, A., H. Korhonen, S. Romakkaniemi, and H. Kokkola, 2017: Radiative and climate effects of stratospheric sulfur geoengineering using seasonally varying injection areas. *Atmospheric Chemistry and Physics*, **17** (11), 6957.
- Lohmann, U. and B. Gasparini, 2017: A cirrus cloud climate dial? *Science*, **357** (6348), 248–249.
- Maalick, Z., H. Korhonen, H. Kokkola, T. Kühn, and S. Romakkaniemi, 2014: Modelling artificial sea salt emission in large eddy simulations. *Phil. Trans. R. Soc. A*, **372** (2031), 20140 051.
- Muri, H., J. E. Kristjánsson, T. Storelvmo, and M. A. Pfeffer, 2014: The climatic effects of modifying cirrus clouds in a climate engineering framework. *Journal of Geophysical Research: Atmospheres*, **119** (7), 4174–4191.
- Partanen, A.-I., H. Kokkola, S. Romakkaniemi, V.-M. Kerminen, K. E. Lehtinen, T. Bergman, A. Arola, and H. Korhonen, 2012: Direct and indirect effects of sea spray geoengineering and the role of injected particle size. *Journal of Geophysical Research: Atmospheres*, **117** (D2).
- Storelvmo, T., J. E. Kristjánsson, H. Muri, M. Pfeffer, D. Barahona, and A. Nenes, 2013: Cirrus cloud seeding has potential to cool climate. *Geophysical Research Letters*, **40** (1), 178–182.
- Tonttila, J., Z. Maalick, T. Raatikainen, H. Kokkola, T. Kühn, and S. Romakkaniemi, 2017: Uclales-salsa v1. 0: a large-eddy model with interactive sectional microphysics for aerosol, clouds and precipitation. *Geoscientific Model Development*, **10** (1), 169.
- Verlinde, J., et al., 2007: The mixed-phase arctic cloud experiment. *Bulletin of the American Meteorological Society*, **88** (2), 205–222.

APPLYING MACHINE LEARNING TO REPLICATE LARGE-EDDY SIMULATION RESULTS ON URBAN POLLUTANT DISPERSION

M. KURPPA¹, M. LANGE², H. SUOMINEN², E. OIKARINEN², R. SAVVIDES², L. JÄRVI^{1,3}
and K. PUOLAMÄKI^{1,2}

¹Institute of Atmospheric and Earth System Research/Physics, Faculty of Science, University of Helsinki, Finland.

²Department of Computer Science, University of Helsinki, Finland.

³Helsinki Institute of Sustainability Science, University of Helsinki, Finland.

Keywords: LES, machine learning, air quality, urban

INTRODUCTION

Urban pedestrian-level air quality is characterised as highly variable. This stems especially from temporally and spatially variable pollutant sources, such as cars and chimneys, and the turbulent nature of flow that transports air pollutants. Urban structures, i.e., buildings and vegetation, effectively modify the flow and generate turbulence.

In order to resolve the complex pollutant concentration fields, high-resolution modelling is needed, for which the large-eddy simulation (LES) is the most promising method. However, to apply LES for example for urban planning purposes, both high computational resources and expertise are needed.

To develop faster and computationally cheaper predictive models, application of machine learning techniques in air quality studies has increased rapidly in the past few years. Several studies have used multiple linear regression (MLR, see Krecl et al. (2019) for a review) or more advanced methods such as Random Forest (e.g., Krecl et al. (2019)) or deep neural networks (Kim et al., 2019) to predict air pollutant concentrations based on observed values. Still, high-resolution LES that implicitly resolves the impact of urban structures on pollutant dispersion has not yet been employed in predictive model development.

This study utilises LES data output from Kurppa et al. (2018) with the aim to develop a predictive statistical model for hourly averaged street level pollutant concentrations in a complex urban environment. Furthermore, the importance of different predictor variables is assessed.

METHODS

Kurppa et al. (2018) investigated the impact of city-block orientation and variation in the building height and shape on the dispersion of traffic-related pollutants using the LES model PALM (Maronga et al., 2015). Specifically, LES simulations were conducted applying four alternative city-planning solutions and under two different meteorological conditions. Air pollutant dispersion was studied by applying a Lagrangian particle model and representing air pollutants as inert air parcels that follow the air flow and do not interact with any surface.

As a first step, different type of features or predictor variables of the simulation environment were defined for each (x, y) -point in the simulation domain, such as street width, height of the nearest building and particle emission strength. Then, different predictive models, including linear models, regression tree, and Random Forest, were trained and tested with different data combinations.

CONCLUSIONS

Fig. 1 display an example on the hourly-averaged particle density in one urban planning scenario at $z = 4$ m from LES and the corresponding prediction using regression tree algorithm, respectively. The wind is from south-west.

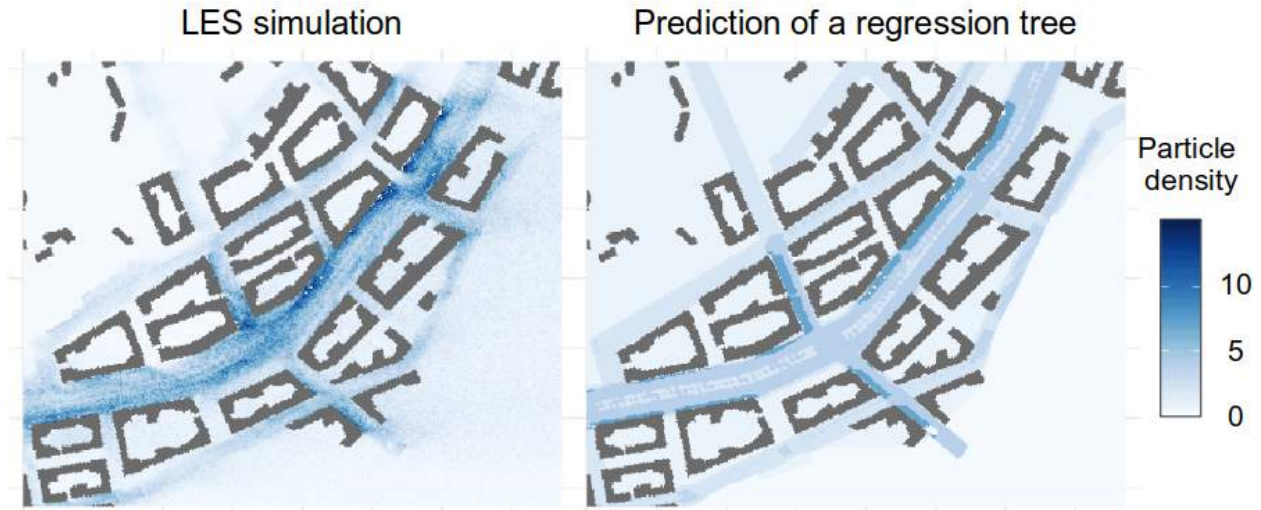


Figure 1: Hourly averaged particle densities in the city planning solutions V_{J-J} in Kurppa et al. (2018) at 4 m above ground. Left: LES simulation output. Right: prediction using a regression tree algorithm. Wind is from south-west.

In this example, the prediction captured successfully the accumulation of particles on the western side and northern part of the boulevard as well lower concentrations below street trees in the middle of the boulevard. However, other details were not predicted. The most important predictor is the particle emission, which was generally observed with all models. Nevertheless, features such as whether a point (x, y) is within a courtyard or not, or tree height were shown important.

The study is on-going and further investigations are needed to find the most accurate model and most important features, as well as to reliably estimate the accuracy of the estimates in new environments. The learned models may offer a way to replace computationally costly LES simulations in some applications. The models could be also be used to help to understand the relevant emergent interactions relevant to the spread of pollutants in urban environment.

ACKNOWLEDGEMENTS

This work was supported by the Doctoral Programme in Atmospheric Sciences (ATM-DP, University of Helsinki), the Academy of Finland (decisions 326280 and 326339) and Centre of Excellence (project no. 307331), and Helsinki Metropolitan Region Research Program.

REFERENCES

- Kim et al. (2019). Development of a daily PM_{10} and $PM_{2.5}$ prediction system using a deep long short-term memory neural network model. *Atmospheric Chemistry and Physics*, **19**, 12935-12951.
- Kurppa et al. (2018). Ventilation and Air Quality in City Blocks Using Large-Eddy Simulation—Urban Planning Perspective. *Atmosphere*, **9**(2), 65.

- Krecl et al. (2019). Modelling urban cyclists' exposure to black carbon particles using high spatiotemporal data: A statistical approach. *Science of the Total Environment*, **679**, 115-125.
- Maronga et al. (2015). The Parallelized Large-Eddy Simulation Model (PALM) version 4.0 for atmospheric and oceanic flows: model formulation, recent developments, and future perspectives. *Geosci. Model Dev.*, **8**, 2515–2551.

CLIMATIC IMPACTS OF BLACK CARBON MITIGATION IN THE ARCTIC

T. KÜHN^{1,2}, K. KUPIANEN³, T. MIINALAINEN¹, H. KOKKOLA², V.-V. PAUNU³, A. LAAKSO², J. TONTTILA², R. VAN DINGENEN⁴, K. KULOVESI⁵, N. KARVOSENOJA³, and K.E.J. LEHTINEN^{1,2}

¹Department of Applied Physics, University of Eastern Finland (UEF), Kuopio, Finland.

²Finnish Meteorological Institute (FMI), Kuopio, Finland.

³Finnish Environment Institute (SYKE), Helsinki, Finland.

⁴European Commission, Joint Research Centre (JRC), Ispra (VA), Italy

⁵Department of Law, University of Eastern Finland (UEF), Joensuu, Finland.

Keywords: Arctic, black carbon, climate modelling, aerosol.

INTRODUCTION

Global warming is one of the main concerns of the 21st century. Mitigation measures, however, are only slowly being implemented and greenhouse gas emissions continue to increase on a global scale. According to the fifth assessment report of the IPCC, the global mean surface temperature is likely to increase by 1.5°C or more until the end of the century compared to pre-industrial times. Arctic surface temperatures are increasing much faster and the effects of this increase, like e.g. retreat of arctic sea ice and extended permafrost thawing, affect the Arctic already now [Kirtman et al., 2013]. In order to slow Arctic warming on a short to medium time scale, the mitigation of short-lived climate pollutants (SLCP) has been widely considered. The projected 2°C increase until 2050 may be decreased by up to 0.5° if maximum SLCP mitigation was implemented globally [AMAP 2015, Stohl et al., 2015], half of which are attributed to reductions in black carbon (BC). At the same time, SLCP mitigation has many positive co-benefits, like e.g. increased human health and crop yields, also in source regions that are not directly affected by the changing arctic climate. However, there are still many sources of uncertainty. For instance, the relative amount of substance reaching the Arctic is usually greater if the source is close by, but on the other hand the emission strengths in regions close to the Arctic are already small to begin with, so it is unclear which mitigation measures are most effective and if these should be the same everywhere. Additionally many pollutants are usually co-emitted by one source, so even if only one substance is targeted by a mitigation measure, other emissions will be reduced as well (not all of which may lead to cooling). This makes the overall effect of a mitigation measure hard to assess. Here we investigate how maximum BC mitigation in different regions of the globe affects BC concentrations and radiative forcings in the Arctic.

METHODS

We use the aerosol-climate model ECHAM-HAMMOZ (ECHAM6.3-HAM2.3-MOZ1.0) with the aerosol microphysics module SALSA [Kokkola et al., 2018] to simulate the near-future impact of BC mitigation strategies on Arctic climate. We use specially generated aerosol emission scenarios, which are based on the ECLIPSEv5a emission inventories. In our study, we compare 5 emission scenarios for the year 2030: (1) the emissions following the current legislation (CLE), (2) CLE + BC mitigation in the Arctic council (AC8) member states, (3) CLE + BC mitigation in AC8 and active observers, (4) CLE + BC mitigation in AC8 and all observers, and (5) CLE + global BC mitigation. The simulation results are compared to a reference simulation for the year 2010. All simulations are run over 30 model years, plus half a year of spin-up. Here we are only interested in aerosol effects, all other parameters, in particular greenhouse gas concentrations, sea surface temperature, and sea ice extent, are held fixed at 2010 values.

Figure 1 shows the reduction in BC emissions for the different scenarios. Compared to the current legislation, mitigation of BC in the Arctic Council member states has only a fairly small impact on total global anthropogenic BC emissions, while a global implementation can reduce the anthropogenic BC emissions by 81%. However, as the atmospheric lifetime of aerosol particles is of the order of one to two

weeks, BC mitigation in regions within or close to the Arctic affect BC column burdens in the Arctic much more directly than source regions far away. This is clearly visible in Fig. 2: BC emission reductions in the Arctic Council member and observer states, most of which are very close to the Arctic, contribute almost 50% of the globally possible reduction in Arctic BC column burden. Furthermore, source regions close to the Arctic have a stronger effect on BC concentrations close to the surface, while source regions further away rather affect BC concentrations aloft. As BC deposition strongly depends on the concentrations close to the surface, the reduction in BC deposition on Arctic snow and ice due to mitigation in the Arctic Council member and observer states is even more pronounced (not shown).

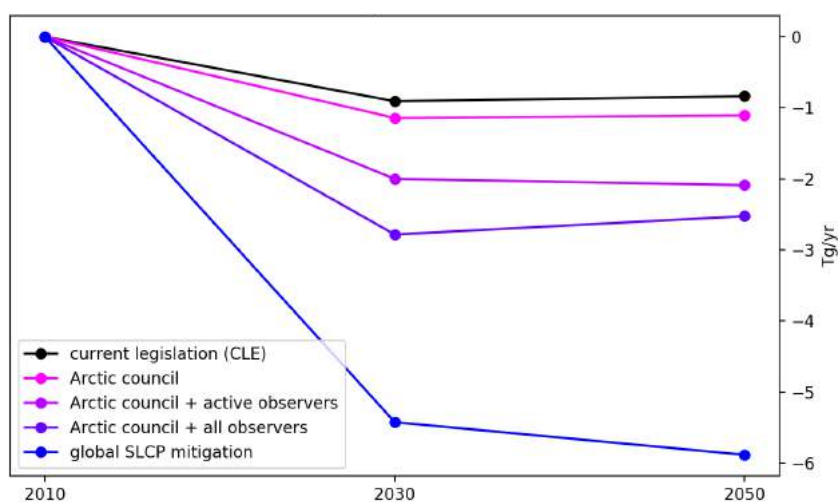


Figure 1: Reduction in the total global amount of yearly emitted BC for the different scenarios.

Figure 3 shows the aerosol direct radiative forcing (RF) in the Arctic due to BC mitigation in the different scenarios. BC mitigation shows a general cooling effect which scales pretty well with the total global amount in BC emission reduction. The relative contribution of the Arctic Council member and observer states to the RF is comparably small, because BC concentrations above cloud contribute to the RF more strongly, which means that remote sources, which contribute more to BC concentrations in the upper atmosphere affect the RF more.

If aerosol-cloud interactions are taken into account in the radiative forcing calculations (effective radiative forcing; ERF), the picture changes quite drastically. Figure 4 shows the ERF over the Arctic for the different scenarios. All scenarios show a warming compared to 2010, with no apparent ordering of the scenarios in with respect to the strength of BC emission reduction. In addition, the ERF values are accompanied by uncertainties of the order of ± 2 W/m², which are even larger than the ERF values themselves. This happens because the reduction in Arctic BC and organic carbon (OC) concentrations reduces the amount of cloud condensation nuclei, which induces a warming effect and hence counter-acts the cooling effect of the direct aerosol effect. The uncertainties in the ERF are caused by natural variability in cloud and snow cover.

This work has recently been submitted to Atmospheric Chemistry and Physics and is currently under review [Kühn et al., *under review*, 2019].

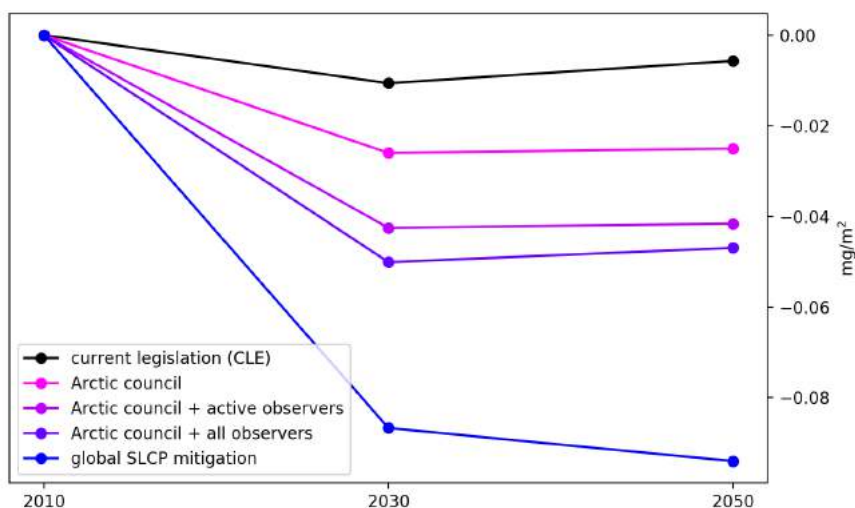


Figure 2: Average BC column burden over the Arctic (60-90°N) for the different scenarios.

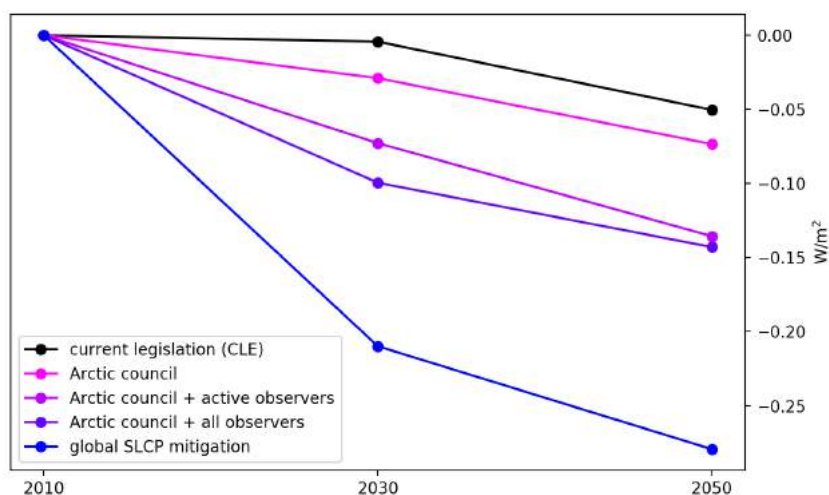


Figure 3: Arctic (60-90°N) aerosol direct radiative forcing due to reduction of BC and co-emitted species for the different scenarios.

CONCLUSIONS

In order to assess the efficacy of black carbon (BC) mitigation in slowing Arctic warming, we performed a set of simulations with different emission scenarios, which implemented BC mitigation measures in a successively larger region of the globe. We find that the relative contribution of source regions close to the Arctic to Arctic BC burdens and deposition is stronger than that of remote source regions. Direct radiative forcings, however scale fairly well with the global total reduction in BC emission strength. The effective radiative forcing, which takes aerosol-cloud interactions into account, shows no clear signal with respect to the BC emission reduction strength and is accompanied by very large uncertainties.

ACKNOWLEDGEMENTS

This work was supported by the Academy of Finland, grant no. 286613 and the Centre of Excellence (grant no. 272041). The authors wish to acknowledge CSC – IT Center for Science, Finland, for computational resources.

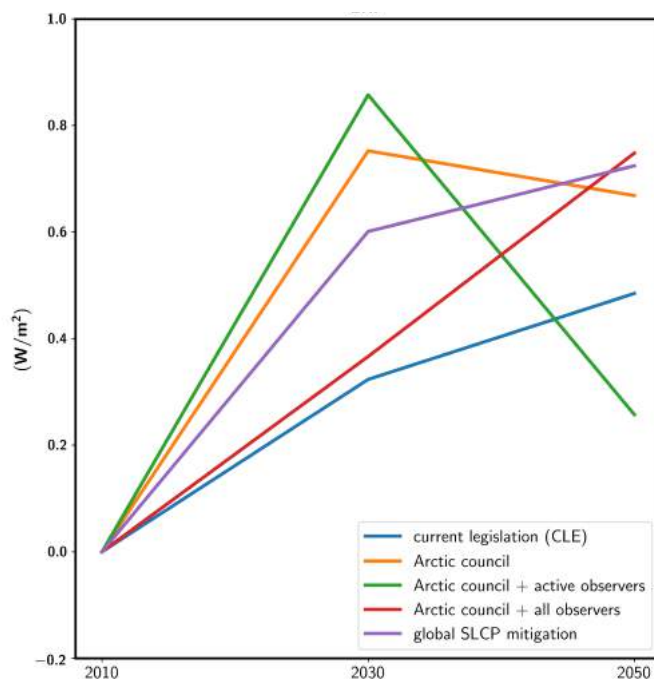


Figure 4: Arctic effective radiative forcing (ERF) due to reduction of BC and co-emitted species for the different scenarios.

REFERENCES

AMAP, 2015. *AMAP Assessment 2015: Black carbon and ozone as Arctic climate forcers*. Arctic Monitoring and Assessment Programme (AMAP), Oslo, Norway.

Kirtman, B., S.B. Power, J.A. Adedoyin, G.J. Boer, R. Bojariu, I. Camilloni, F.J. Doblas-Reyes, A.M. Fiore, M. Kimoto, G.A. Meehl, M. Prather, A. Sarr, C. Schär, R. Sutton, G.J. van Oldenborgh, G. Vecchi and H.J. Wang (2013). *Near-term Climate Change: Projections and Predictability*. In: *Climate Change 2013: The Physical Science Basis. Contribution of Working Group I to the Fifth Assessment Report of the Intergovernmental Panel on Climate Change*. Cambridge University Press, Cambridge, United Kingdom and New York, NY, USA.

Kokkola, H., Kühn, T., Laakso, A., Bergman, T., Lehtinen, K. E. J., Mielonen, T., Arola, A., Stadtler, S., Korhonen, H., Ferrachat, S., Lohmann, U., Neubauer, D., Tegen, I., Siegenthaler-Le Drian, C., Schultz, M. G., Bey, I., Stier, P., Daskalakis, N., Heald, C. L., and Romakkaniemi, S.: SALS2.0: *The sectional aerosol module of the aerosol–chemistry–climate model ECHAM6.3.0-HAM2.3-MOZ1.0*, Geoscientific Model Development, 11, 3833–3863, <https://doi.org/10.5194/gmd-11-3833-2018>, <https://www.geosci-model-dev.net/11/3833/2018/>, 2018.

Kühn, T., Kupiainen, K., Miinalainen, T., Kokkola, H., Paunu, V.-V., Laakso, A., Tonttila, J., Van Dingenen, R., Kulovesi, K., Karvosenoja, N., and Lehtinen, K. E. J.: *Effects of Black Carbon Mitigation on Arctic Climate*, Atmos. Chem. Phys. Discuss., <https://doi.org/10.5194/acp-2019-864>, in review, 2019.

Stohl, A., Aamaas, B., Amann, M., Baker, L. H., Bellouin, N., Berntsen, T. K., Boucher, O., Cherian, R., Collins, W., Daskalakis, N., Dusinska, M., Eckhardt, S., Fuglestvedt, J. S., Harju, M., Heyes, C., Hodnebrog, Ø., Hao, J., Im, U., Kanakidou, M., Klimont, Z., Kupiainen, K., Law, K. S., Lund, M. T., Maas, R., MacIntosh, C. R., Myhre, G., Myriokefalitakis, S., Olivie, D., Quaas, J., Quennehen, B., Raut, J.-C., Rumbold, S. T., Samset, B. H., Schulz, M., Seland, Ø., Shine, K. P., Skeie, R. B., Wang, S., Yttri, K. E., and Zhu, T. (2015). *Evaluating the climate and air quality impacts of short-lived pollutants*. Atmos. Chem. Phys., 15, 10529-10566, doi:10.5194/acp-15-10529-2015.

SHORT AND LONG TERM EFFECTS OF FOREST FIRES ON THE STABILITY OF CARBON POOLS IN BOREAL FORESTS (BOREALFIRE)

KAJAR KÖSTER¹, HEIDI AALTONEN¹, EGLE KÖSTER¹, CHRIS RIBEIRO-KUMARA¹, XUAN ZHOU¹, HUIZHONG ZHANG-TURPEINEN², FRANK BERNINGER³, JUKKA PUMPANEN²

¹Department of Forest Sciences, P.O. Box 27, FI-00014 University of Helsinki, FINLAND, email: kajar.koster@helsinki.fi, heidi.m.aaltonen@helsinki.fi, egle.koster@helsinki.fi, christine.ribeiro@helsinki.fi, xuan.zhou@helsinki.fi,

²Department of Environmental and Biological Sciences, University of Eastern Finland, P.O. Box 1627, FI-70211 Kuopio, Finland, email: jukka.pumpanen@uef.fi, huizhong.zhang@uef.fi

³Department of Environmental and Biological Sciences, University of Eastern Finland, PL 111, FI-80101 Joensuu, Finland, email: frank.berninger@uef.fi

Keywords: FOREST FIRE, GHG EXCHANGE, PERMAFROST, DISTURBANCES

INTRODUCTION

Boreal forests, which are to a large extent located on permafrost soils, are a crucial part of the climate system because of their large soil carbon (C) pool. Even small change in this pool may change the terrestrial C sink in the arctic into a source with consequent increase in CO₂ concentrations. About 1% of boreal forests are exposed to fire annually, which affects the soil and permafrost under them. Thawing of permafrost increases the depth of the active layer containing large C and N stocks. In addition to temperature, the decomposition of soil organic matter depends on its chemical composition which may also be affected by fires.

AIMS

The aim of this project is to study the short and long term effects of fire on the stability of C pools in boreal forests - how boreal forests soils respond to rising temperature and increasing fire frequency. These responses largely determine the present and future role of boreal forests on global C cycle. Climate will change the fire regimes, which will deeply affect the C turnover of boreal forests.

METHODS

The long term effects of fire will be studied based on chronosequences, where forest stands with similar soil type but different fire history will be compared to study biogeochemical changes following the fire.

The short term effects of fires and the effect of different fire severity on SOM turnover will be studied on experimental burning areas.

The study will be based on three different main datasets: 1) chronosequence at different fire sites (explore time since fire + climate), 2) experimental burning site, 3) lab experiments.

The study areas (fire chronosequences) are located: 1) Canada – permafrost and non-permafrost soils in Yukon and Northwest Territories (Inuvik, Eagle Plains, Dawson, Carmacs, Whitehorse); 2) Russia – permafrost and non-permafrost soils in Tura and Zotino); 3) Finland – non permafrost areas in the surrounding of Värriö subarctic research station (SMEAR I station); 4) Estonia – non-permafrost areas in the surrounding of Vihterpalu (North-West Estonia).

Experimental burnings (short term effects of fire) are performed in Canada, on the Canadian Boreal Community FireSmart Project sites and the old International Crown Fire Modelling Experiment (ICFME) sites, close to Fort Providence, NWT. Experimental burnings have been conducted there since 1997.

We have studied the effect of forest fires on soil greenhouse gas fluxes (CO₂, CH₄ and N₂O) using portable chambers. The amount of easily decomposable and recalcitrant fractions in soil organic matter were determined with water, ethanol and acid extraction. Also, changes in microbial community structure and composition have been analyzed with next generation pyrosequencing. We have also studied the effects of wildfires on Biogenic Volatile Organic Compound (BVOC) and nitric acid (HONO) emissions from soils in Värriö and in Centra Siberia using portable chambers, Tenax tubes, GC-MS and LOPAP®-03 (Long Path Absorption Photo Meter).

OUR RECENT RESEARCH HIGHLIGHTS ARE AS FOLLOWS:

- In our recent study by Aaltonen et al. (2019a) we determined how heterotrophic soil respiration (Rh), originating from the decomposition of SOM, and the Q₁₀ of this process vary between different depths over the years following a forest fire in permafrost-affected soils. How the microbial biomass and qCO₂ are affected by the fire, and what are the most important factors affecting the Q₁₀ of SOM decomposition. The results indicate that forest fires may facilitate the decomposition of permafrost SOM by increasing the active layer depth, but on the same time fire increased the temperature sensitivity of decomposition. The SOM in the permafrost surface was less temperature sensitive than the SOM in the soil surface. The post-fire decreases in ground vegetation were reflected in the SOM temperature sensitivity shortly after fire but seemed to return to original levels with forest succession. The fire also increased the microbial qCO₂, and these changes partly explain the lack of significant decrease in heterotrophic soil respiration after fire, as the microbes may use more C for respiration in the recently burned areas compared with the older areas. Even though fires increased the active layer depth, the decrease in SOM quality caused by fire may limit the decomposition rate to some degree.

- In our recent paper by Aaltonen et al. (2019b) we studied how the proportions of insoluble (recalcitrant) and soluble (labile) fractions in soil organic matter (SOM) change as a result of forest fire in the active layer on permafrost, and what are the most important factors (active layer depth, soil temperature, biomass, C/N ratio) explaining the size of insoluble (recalcitrant) fractions of SOM post-fire. The SOM fraction ratios reverted towards pre-fire status with succession. Changes in SOM were less apparent deeper in the soil. Best predictors for the size of recalcitrant SOM fraction were active layer depth, vegetation biomass and soil C/N ratio, whereas microbial biomass was best predicted by the size of the recalcitrant SOM fraction. Results indicated that SOM in upland mineral soils at the permafrost surface could be mainly recalcitrant and its decomposition not particularly sensitive to changes resulting from fire.

- In our recent paper by Zhou et al. (2019), we studied the impact of wildfire on microbial C:N:P stoichiometry and the fungal-to-bacterial ratio in permafrost soils. The results of the study indicate that forest wildfire increased the active layer depth and subsequently decreased soil moisture and vegetation coverage. This consequently led to a decrease in the microbial C and N contents as well as the F:B ratios. However, the C:N:P ratios in the microbial biomass remained relatively constant over time following a wildfire, indicating homeostatic regulation. Wildfire also failed to affect the microbial communities in the deep soil layers. These results indicate a complex interaction between the decomposer community, resource availability, and successional stage. Forest wildfire either shifted the microbial diversity or suppressed the microbial growth rate for several decades.

Recent publications of the group on the fire effects on forest carbon and nitrogen cycles:

1. Aaltonen, H., Palviainen, M., Zhou, X., Köster, E., Berninger, F., Pumpanen, J., Köster, K. (2019a). Temperature sensitivity of soil organic matter decomposition after forest fire in Canadian permafrost region. *Journal of Environmental Management*. 241: 637-644.
2. Aaltonen, H., Köster, K., Köster, E., Berninger, F., Zhou, X., Karhu, K., Biasi, C., Bruckman, V., Palviainen, M., Pumpanen, J. (2019b). Forest fires in Canadian permafrost region: the combined effects of fire and permafrost dynamics on soil organic matter quality. *Biogeochemistry*, 143: 257-74.
3. Zhou, X., Sun, H., Pumpanen, J., Sietiö, O.-M., Heinonsalo, J., Köster, K., Berninger, F. 2019. The impact of wildfire on microbial C:N:P stoichiometry and the fungal-to-bacterial ratio in permafrost soil. *Biogeochemistry*, 142: 1-17.
4. Parro, K., Köster, K., Jögiste, K., Seglinš, K., Sims, A., Stanturf, J.A., Metslaid, M., 2019. Impact of post-fire management on soil respiration, carbon and nitrogen content in a managed hemiboreal forest. *Journal of Environmental Management* 233, 371-377.
5. Köster, E., Köster, K., Berninger, F., Prokushkin, A., Aaltonen, H., Zhou, X., Pumpanen, J., 2018. Changes in fluxes of carbon dioxide and methane caused by fire in Siberian boreal forest with continuous permafrost. *Journal of Environmental Management* 228, 405-415.

ACKNOWLEDGEMENTS

We acknowledge the Academy of Finland projects: no. 286685 “Long term effects of fire on carbon and nitrogen pools and fluxes in the arctic permafrost and subarctic forests” and no. 294600 “Short and long term effects of forest fires on the stability of carbon pools in boreal forests”.

FLOW TUBE EXPERIMENTS: SYSTEM VALIDATION AND MEASURING PARTICLE GROWTH AND UPTAKE OF DIFFERENT COMPOUNDS

LAITINEN, T., HÄKKINEN, E., CHEN, J., SIIVOLA, E., EHN, M. and SIPILÄ, M.

Institute for Atmospheric and Earth System Research (INAR), University of Helsinki, Finland.

Keywords: Aerosols, particle growth, flow tube, mass spectrometry

INTRODUCTION

New particle formation at the nature has been observed world wide (Kulmala 2004). Measurements can be made directly from the atmosphere with different instruments (i.e. mass spectrometry), but laboratory measurements are needed to study the happenings in more depth. A flow tube or flow chambers are found to be useful reactors for studying the properties of nucleating particles (Sipilä 2010). Generally in the flow chambers the chamber is filled with different gases and then they are let to react within each other at the expose of UV-light. Meanwhile the changes are monitored with i.e. mass spectrometric means and particle size distribution measurements. The flow tubes have constant flow of gases through them while the tube is also exposed to UV-lights so that photolysis of different compounds can be performed. Generally, one problem with the current instrumentation is that the residence time of the flow tube is often too small to make atmospheric relevant measurements in some cases, i.e. measuring sulphuric acid nucleation (Nieminen 2010). Our aim was to design, construct and put in action a flow tube that has transfer time through it closer to a tens of seconds than a second, has cooling and temperature controlling capabilities, suitable radiation everywhere in the tube and contamination free measurements. These corner stones of flow tube design will make possible i.e. studying of sulphuric acid-ammonia-amine pathways in more depth.

METHODS AND DISCUSSION

Experiments were carried out in INAR physics laboratory at University of Helsinki, Finland with the recently build-up flow tube. The schematic of the tube can be seen in Figure 1.

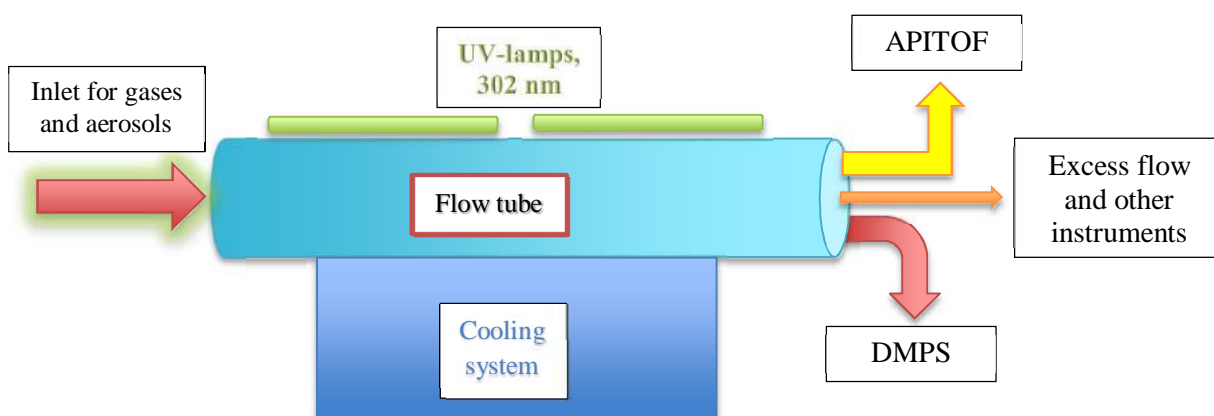


Figure 1. Schematic of the flow tube.

The tube is “lightened” with 12 UV-lamps, which cover nearly whole length of the tube. The lamps emit peak radiation at around 302 nm UV-B wavelength (see Figure 2. for lamp spectra), which is suitable to produce many different atmospherically relevant photochemical reactions in the tube i.e.:

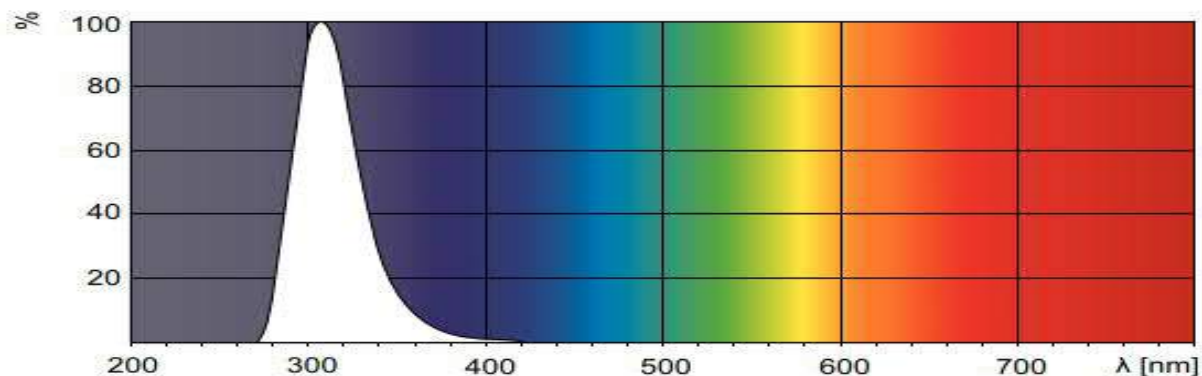
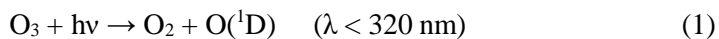


Figure 2. Flow tube UV-lamps emission range from 290-320 nm. Peak at 302 nm. Notice that there are no emission in 254 nm as in regular Hg-lamps. This particular lamp was also chosen since it has very high quantum yield for reaction 1.

The formed hydroxyl radical can initiate the oxidation process of the hydrocarbons in the atmosphere. An example of this is demonstrated in the Figure 3. In Fig. 3 can be seen that around 40 nm particles are formed in the flow tube by introducing gases of 15 lpm synthetic air, 33 mlpm, of alpha-pinene and 100 mlpm of O₃ (equals average of 40 ppb of O₃ in the flow tube) to it. In this experiment the particles coming out the flow tube were introduced to heating oven of up to 200 °C. The heating effect can be seen in Figure 4. After the oven, the particles were introduced to the ApiTOF (Atmospheric pressure interface time-of-flight mass spectrometer) to measure the oxidation products of alpha-pinene (Figure 5). ApiTOF used negative chemical ionization as an ionization method.

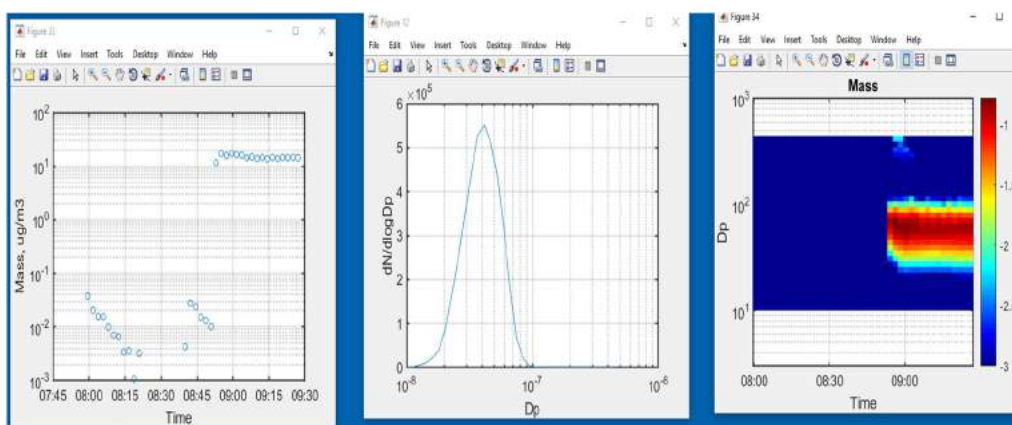


Figure 3. About 40 nm particles formed in the flow tube through oxidation of alpha-pinene.

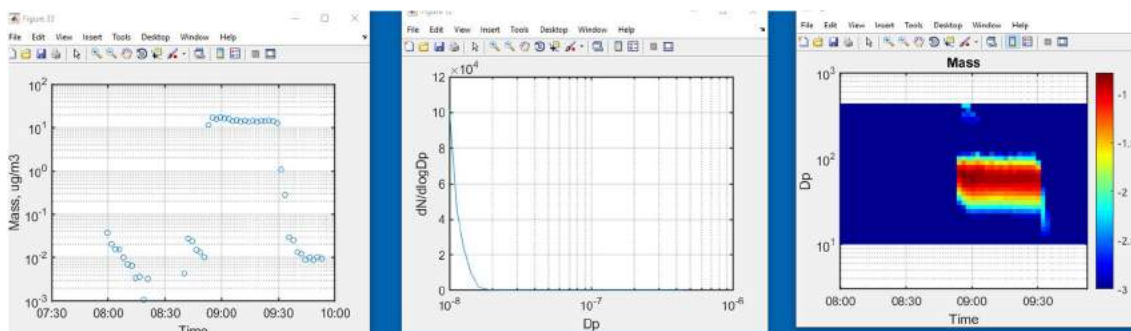


Figure 4. 40 nm particles formed in the flow tube and introduced to 200 °C oven directly from flow tube. Particle size and mass dropped dramatically after the oven.

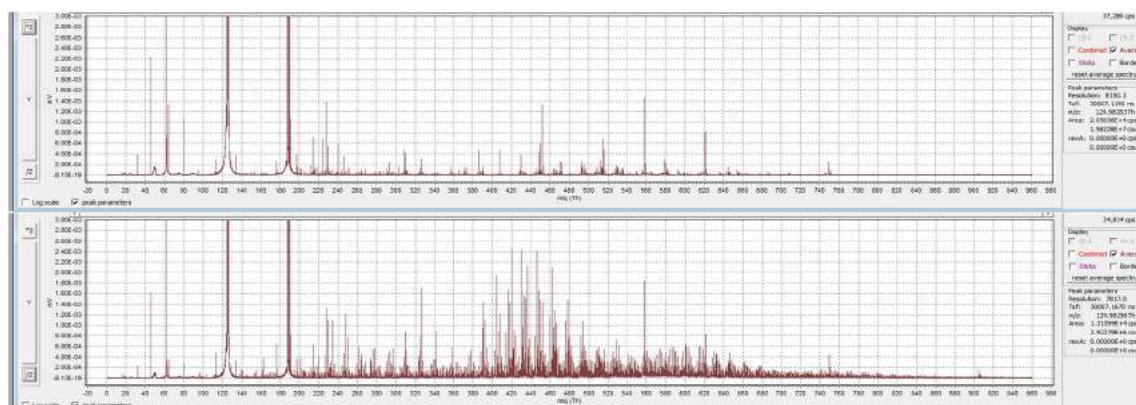


Figure 5. Mass spectra of alpha-pinene oxidation of 40 nm particles before and after vaporization of 200 °C oven.

During these above experiments the flow tube temperature was kept at room temperature (around 23 °C). The temperature and RH can have a huge effect for reactions that take place in the system. Figure 6 is presenting of RH relation to amine reaction at different reaction times. The flow tube is build inside of a frame, which is insulated so that the temperature can be kept constant, independent of heat burden that the UV-lamps will provide to the system. The system has a build-up cooling system, which can go down to -10 °C itself, and can reach about 0 °C inside of the flow tube while all the UV-lamps are on. Also, all the used gas or aerosol flows are cooled at the same temperature before entering the tube. The inner surfaces of the insulated flow tube chamber were covered with mirror-polished stainless steel to maximize the evenly distributed UV-radiation all over the tube.

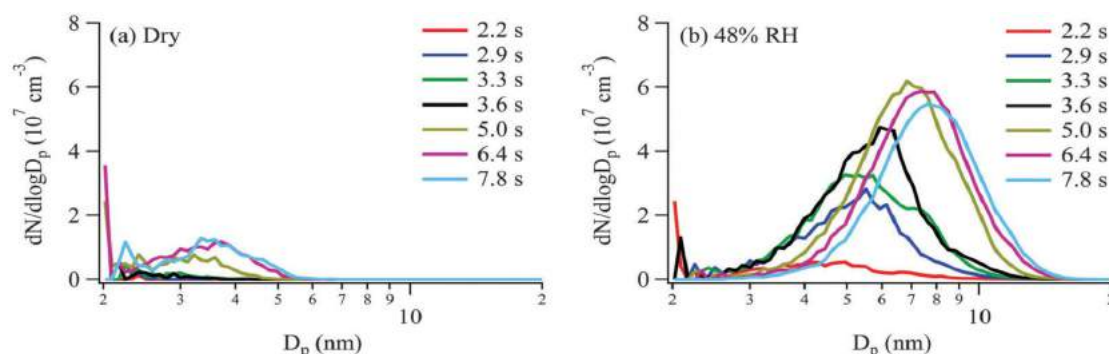


Figure 6. The effect of RH in particle size in the flow tube at different reaction times of amines.

CONCLUSIONS

The constructed flow tube is tested to be a suitable tool for studying the varying conditions of clusters and growing particles. The flow tube is constructed so that all possible contamination sources are minimized/terminated. Flow tube itself is quartz, inlet and outlet flanges stainless steel and all sealants for the sensors or connections either are enamel or Viton (which is also avoided until the very end). The idea was to make a Cadillac quality flow tube, and based on our results we succeed. The measurements will go further on with flow tube in the future for example by trying to solve the particle uptake of low volatile explosives and sulphuric acid and dimethylamine oxidation reactions and other particle formation studies. Idea is also to monitor the reactions taking place at different lengths and spots inside of the flow tube.

ACKNOWLEDGEMENTS

This work was supported by the Academy of Finland grant.

REFERENCES

- Kulmala M., Vehkamäki H., Petäjä T., Dal Maso M., Boy M., Lauri A., Kerminen V.-M., Birmili, W., McMurry P.H. (2004). Formation and growth rates of ultrafine atmospheric particles: a review of observations. *J. Aerosol. Sci.* 35, 143.
- Nieminen, T., Lehtinen, K. E. J., and Kulmala, M. (2010). On condensational growth of clusters and nanoparticles in sub-10 nm size range, *Atmos. Chem. Phys. Discuss.*, 10, 1693.
- Sipilä, M., Berndt, T., Petäjä, T., Brus, D., Vanhanen, J., Stratmann, F., Patokoski, J., Mauldin III, R.L., Hyvärinen, A.-P., Lihavainen, H. and Kulmala, M. (2010). The role of sulfuric acid in atmospheric nucleation, *Science*, 327, 1243.

AIRBORNE MEASUREMENTS OF AEROSOL PARTICLES DURING 2018 WINTER AND SPRING

Janne Lampilahti¹, Zoé Brasseur¹, Markus Lampimäki¹, Pyy Poutanen¹, Antti Manninen², Anna Franck¹, Maija Peltola³, Paula Hietala¹, Yusheng Wu¹, Tuukka Petäjä^{1,4} and Markku Kulmala^{1,4,5}

¹Institute for Atmospheric and Earth System Research / Physics, Faculty of Science, University of Helsinki, Finland.

²Finnish Meteorological Institute, Helsinki, Finland.

³Laboratoire de Météorologie Physique (LaMP), Université Clermont Auvergne, France.

⁴Joint International Research Laboratory of Atmospheric and Earth System Sciences, Nanjing University, Nanjing, China.

⁵Aerosol and Haze Laboratory, Beijing Advanced Innovation Center for Soft Matter Science and Engineering, Beijing University of Chemical Technology, Beijing, China.

Keywords: airborne measurements, new particle formation, boundary layer
Contact: janne.lampilahti@helsinki.fi

Introduction

Atmospheric aerosols affect health and climate. The properties of atmospheric aerosols are governed by complex processes that are not well understood.

We measured the particle number-size distribution down to 1.5 nm, collected filter samples and measured meteorological parameters onboard a Cessna 172 aircraft during the 2018 winter and spring in Hyytiälä, Finland.

Methods

The airborne measurement campaign was between March-May 2018 in Hyytiälä, Finland. Table 1 summarizes the instrumentation used. A forward facing inlet sampled the air into the main sampling line, while the airspeed was kept at 130 km/h. An onboard scientific operator manually maintained the flow rate at 50 L/min in the main sampling line.

Table 1. Instrumentation onboard the Cessna 172. PNC = particle number concentration, PNSD = particle number size distribution.

Instrument	Measured variable
PSM	>1.5 nm PNC
TSI 3776 CPC	>3 nm PNC
SMPS	10-400 nm PNSD
TSI 3330 OPS	0.3-10 µm PNSD
Rotronic HygroClip-S	Relative humidity
PT100	Temperature
Vaisala PTB100B	Pressure
Li-Cor Li-840	CO ₂ and H ₂ O concentration
GPS receiver	Latitude, longitude and altitude
Filter collection	Ice nucleating particle concentrations

The instruments were mounted on a rack inside the airplane cabin and they sampled the air from the main sampling line through core inlets. The filters collecting ice nucleating particles were in series with the main sampling line. Measurement flights were flown in the morning and in the afternoon. Each flight lasted roughly 2.5 h and consisted of 20-40 km long segments over Hyytiälä at different altitudes between 100-3000 m above ground.

Conclusions

The total particle number concentration was roughly an order of magnitude higher inside the boundary layer compared to above. During new particle formation events the particle number concentration showed significant variability horizontally. However, separate particle layers were observed above the BL.

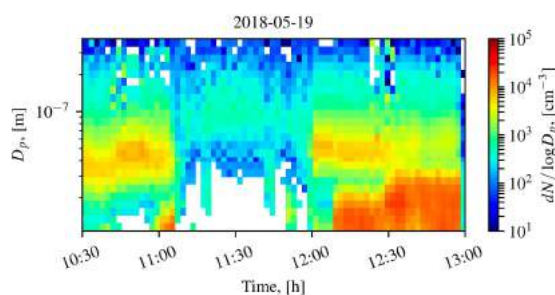


Figure 1. SMPS measurements from the morning flight on May 19, 2018 showing a NPF event.

Acknowledgements: This work was supported by the European Research Council via ERC-Advanced Grant ATM-GTP (742206), the European Commission via projects H2020-INFRAIA-2014-2015 project ACTRIS-2 (Aerosols, Clouds, and Trace gases Research InfraStructure), H2020 research and innovation 345 programme under grant agreement No 689443 (ERAPLANET) via project iCUPE (Integrative and Comprehensive Understanding on Polar Environments), FP7 project BACCHUS (Impact of Biogenic versus Anthropogenic emissions on Clouds and Climate: towards a Holistic UnderStanding, FP7-603445), Academy of Finland via Centre of Excellence in Atmospheric Sciences (272041) and NanoBiomass (307537).

MEASUREMENTS OF NANOCELLULOSE AEROGEL FILTRATION PROPERTIES AND EXOSOMES SIZE-DISTRIBUTION

M. LAMPIMÄKI¹, J. UKKOLA², O. LAITINEN², T. VAINIO¹, L. AHONEN¹, J. KANGASLUOMA¹, E. SIIVOLA¹, A. SAMOYLENKO³, G. BART³, S. VAINIO³, H. LIIMATAINEN², and T. PETÄJÄ¹

¹ Institute for Atmospheric and Earth System Research (INAR)
University of Helsinki, 00014 Helsinki, Finland

² Faculty of Technology, University of Oulu
90220 Oulu, Finland

³ Faculty of Biochemistry and Molecular Medicine, Biocenter Oulu, InfoTech Oulu, University of Oulu, Borealis Biobank, Oulu University Hospital, 90220 Oulu, Finland

Keywords: CELLULOSE, AEROGEL, FILTER, EXOSOME, DMPS

INTRODUCTION

Cellulose based nanofibers (Sirviö *et al.* 2015) can be shaped in porous filter structures (i.e. aerogels and membranes) for enrichment and classification of nanoscale biomass material, such as exosomes that are 30-100 nm in size. Exosomes are nature present nano- and micrometer size vesicles, which provide promising new biomaterial source for different research areas, including medicine (Jella *et al.* 2014; Krause *et al.* 2015; Krause *et al.* 2018). Exosomes present also potential for interactions with biological aerosol particles found in the atmosphere (Pratt *et al.* 2017). Here we have studied filtration efficiencies of nanocellulose aerogels as well as the size distribution of milk, renal cell and sweat based exosomes using Differential Mobility Particle Sizer (DMPS) setups.

METHODS

The nanocellulose nanofiber (CNF) aerogels were produced from the aqueous dispersions having variable solid contents (0.2 - 1.0 %-w/w). The CNF was fabricated from a milk container board (MCB) using deep eutectic solvent system. The material was flash-frozen with liquid nitrogen and dried, resulting in an aerogel. Each filter type was categorized by the mass-% of the nanocellulose in comparison to the deionized water. The use of nanocellulose as air filters was studied with NaCl particles within the 10 nm - 500 nm size range. Samples were mounted to copper bushings for the filtration efficiency studies. Two Condensation Particle Counters (CPC's) for the filtered and reference flows were employed in the setup. Milk-, renal cell carcinoma- (RCC, Renca) and sweat derived exosomes were studied up to 300 nm size range by nebulizing diluted solutions into aerosol phase.

CONCLUSIONS

The experiments demonstrate that the increase in solid content mass-% in CNF aerogels yields better filtration efficiencies. In general, CNF filters performed well within the 10-500 nm size range and very high filtration efficiency was achieved already for the 0.5 m% MCB sample (Figure 1).

The results also suggest that DMPS can be used to access exosomes size distribution and concentration in aerosol phase. Concentration profiles for diluted sweat exosomes and renca exosomes are shown in Fig. 2. Concentration maxima were observed below 100 nm in all samples. The results will be compared with the other nanoparticle size-distribution and concentration characterization methods.

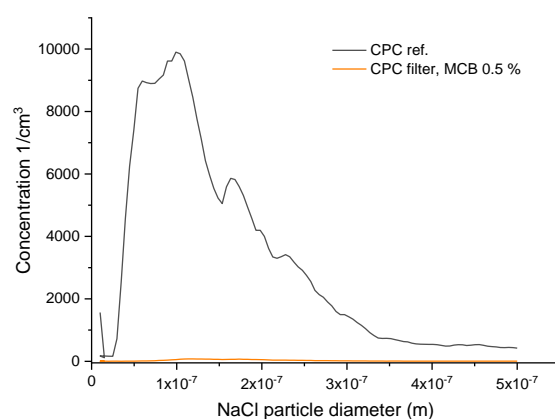


Figure 1. NaCl particle filtration experiment of nanocellulose aerogel sample with 0.5 m-% solid MCB content.

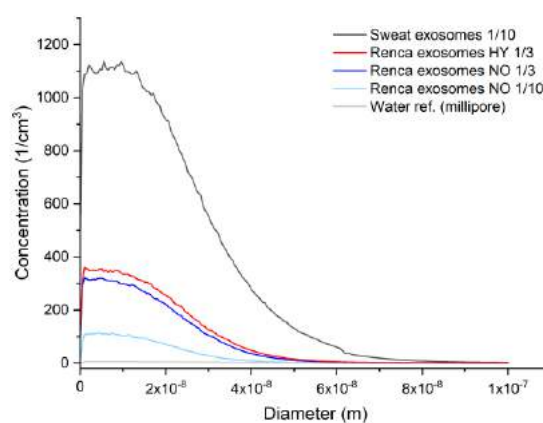


Figure 2. Concentration profiles for diluted sweat exosomes, renca exosomes and water reference (Millipore).

ACKNOWLEDGEMENTS

This research is supported by the Academy of Finland BioFuture2025 project NanoBiomass (307537).

REFERENCES

- J. Sirviö, M. Visanko and H. Liimatainen (2015). Deep eutectic solvent system based on choline chloride-urea as a pre-treatment for nanofibrillation of wood cellulose. *Green Chemistry*, **17** (2015) 3401.
- K. Jella, S. Rani, L. O'Driscoll, B. McClean, J. Byrne, F. Lyng. (2014). Exosomes are involved in mediating radiation-induced bystander signaling in human keratinocyte cells. *Radiat. Res.* **181**, 138.
- M. Krause, Rak-Raszewska, A. Naillat, F. Saarela, U. Schmidt, C. Ronkainen, VP. Bart. G. Ylä-Herttuala, S. Vainio SJ. (2018). Exosomes as secondary inductive signals involve in kidney organogenesis. *J Extracell Vesicles.* **7**,1422675.
- M. Krause, Samoylenko, A. Vainio, SJ. (2015). Exosomes as renal inductive signals in health and disease, and their application as diagnostic markers and therapeutic agents. *Front Cell Dev Biol.* **20**;3:65.
- K. Pratt, P. DeMott, J. French, Z. Wang, D. Westphal, A. Heymsfield, C. Twohy, A. Prenni and K Prather. (2009). In situ detection of biological particles in cloud ice-crystals, *Nat. Geosci.* **2**, 398–401.

Development of selective materials for miniaturized air sampling techniques

Hangzhen Lan, Matti Jussila, Kari Hartonen, Marja-Liisa Riekkola

Department of Chemistry and Institute for Atmospheric and Earth System Research, P.O. Box 55, FI-00014, University of Helsinki, Finland

Keywords: Miniaturized air sampling; Microextraction technique; Selective material; Mesoporous silica; Polymeric nanofibers; Volatile organic compounds

Introduction

Employment of new sorbent materials to immobilize miniaturized air samplers (MAS) and extend their applicability have become a trend in analytical chemistry. Nanomaterials with porous structures, diverse surface chemistries, and specific physical and chemical properties allow them to capture a certain compound or a group of compounds based on size exclusion and chemical selectivity. MAS, that enables air sampling with minimized operation steps and analytical errors, have been widely used. Furthermore, small devices are particularly suitable for automation. New approaches, combining selective materials, microextraction devices, advanced controlling systems, and platforms, have the potential to provide comprehensive and time-dependent information of analytes of interests and contribute to other sciences. This work was focused on the development and application of selective materials as coating and/or packing materials in the miniaturized devices that can be exploited for quantitative analysis of volatile organic compounds (VOCs) in air.

Methods

Solid phase microextraction (SPME) Arrow and in-tube extraction (ITEX) were selected as miniaturized air sampler. Ordered mesoporous silica (OMS) materials are good alternatives to classical sorbents due to their well-defined pore-size distribution, pore structure, and modifiable surface characteristics. OMSs and functionalized OMSs with different mesopore sizes and multidimensional pore-channel structures were synthesized via hydrolytic sol-gel process and surface grafting approach. They were coated on bare SPME Arrows by dipping method. Nanofibers featured excellent permeability, uniform diameter, rich surface functional groups, and good thermal stability that predicted their applicability as the packing material of ITEX. Organic and inorganic nanofibers were

prepared via electrospinning and electroblowing techniques. The nanofibers packed ITEXs were fabricated by sequentially packing deactivated silicon wool, nanofibers, deactivated silicon wool, and spring into an empty ITEX tube.

Conclusions

Pore size of OMS is the decisive parameter for efficient sampling of small amines from air. Under the ideal and dry (<1% humidity) conditions, competing compounds did not interfere with the interaction between amines and OMS. Pore size and surface acidity of the OMS materials determined the sampling efficiency for amines when the sampling time (10 min) was far from equilibrium. Acidity enhanced OMSs decreased the pore size and consequently reduced the loading capacity, but increased selectivity. On the other hand, the hydrophilic nature of OMSs predicted that the sampling performance of OMS coatings would drop dramatically when working in a high humidity atmosphere due to the occupation of extraction sites by water molecules. Interestingly, OMS with smaller pore size and 2D channels can restrict the water molecules more effectively when compared to other materials.

The nanofibers packed ITEXs were tested with a wide range of VOCs, which are with different polarity, volatility, and molecular mass, and are widely distributed in the atmosphere and present at trace level concentrations. Polyacrylonitrile (PAN)-ITEX exhibited the highest extraction affinity to alcohols, aldehydes, and ketones due to the rich amine and imide group on the surface of PAN nanofibers. Inorganic nanofibers packed ITEXs were only selective to few compounds with small extraction capacity which can be interpreted by their physical and chemical structures, e.g. inaccessible pore size and weak surface functional groups.

Acknowledgements

Financial support was provided by China Scholarship Council (H.L., Grant No. 201508330310) and the Academy of Finland Centre of Excellence program (Grant No. 307331).

References

H. Lan, W. Zhang, J.-H. Smått, R.T. Koivula, K. Hartonen, M.-L. Riekkola, Selective extraction of aliphatic amines by functionalized mesoporous silica-coated solid phase microextraction Arrow, *Microchimica Acta*, 186 (2019) 412.

H. Lan, J. Holopainen, K.M. Hartonen, M. Jussila, M. Ritala, M.-L. Riekkola, Fully automated online dynamic in-tube extraction for continuous sampling of volatile organic compounds in air, *Analytical Chemistry*, 91 (2019) 8507-8515.

J. Ruiz-Jimenez, N. Zanca, H. Lan, M. Jussila, K. Hartonen, M.-L. Riekkola, Aerial drone as a carrier for miniaturized air sampling systems, *Journal of Chromatography A*, 1597 (2019) 202-208.

TRENDS OF PARTICLE NUMBER-SIZE DISTRIBUTION PARAMETERS IN MULTIPLE SITES

V. LEINONEN¹, S. HEIKKINEN¹, T. NIEMINEN², T. YLI-JUUTI¹, A. VIRTANEN¹, and S. MIKKONEN^{1,3}

¹Department of Applied Physics, University of Eastern Finland, Kuopio, Finland.

²Institute for Atmospheric and Earth System Research, University of Helsinki, Helsinki, Finland

³Department of Environmental and Biological Sciences, University of Eastern Finland, Kuopio, Finland

Keywords: Dynamic linear modelling, trend analysis, aerosol size distribution

INTRODUCTION

The measurement network of atmospheric aerosols provides knowledge on the processes behind aerosol formation and atmospheric aging of aerosols. Current collaboration networks, such as the European Research Infrastructure for the observation of Aerosol, Clouds and Trace Gases (ACTRIS) and the Atmospheric Radiation Measurement (ARM), provide data from a large number of atmospheric variables and their evolution in time. Comparison studies, where measurements conducted all over the world are combined, give a comprehensive illustration of the long-term trend and seasonality of parameters describing aerosol size distribution. These studies are needed for evaluating the effects of both anthropogenic emission reductions and natural changes in aerosol formation caused by the changing climate.

In this study, we use the particle number-size-distribution data from Nieminen et al. (2018) and extended with open data that can be downloaded from the ACTRIS database (actris.nilu.no). The aim of the study was to investigate the evolution of particle mode (nucleation, Aitken, and accumulation) parameters: geometric mean diameter, geometric standard deviation, and number concentration of the mode during the measured time series.

METHODS

The same particle size distribution data from several atmospheric measurement sites introduced in Nieminen et al. (2018) was used. In addition to these datasets, we downloaded data from the ACTRIS database to complement the data from the same sites with measurements made after analysis of Nieminen et al. (2018) and also data from sites that were not available for their study. We have included sites that contain more than four years of size distribution measurements to enable seasonality to be estimated from time series. The whole dataset consists of measurements from 22 different sites between the years 1996 and 2018, most datasets starting after 2005. Visual inspection of the data has been performed to remove incorrect parts of the data before further data analysis.

Particle number-size distribution parameters have been estimated from the size distribution data for each time point separately by applying a mode fitting algorithm (Hussein et al., 2005). Briefly, the algorithm fits one to three log-normal modes for the number size distribution by minimizing the squared distance between measured distribution and fit. Resulting mode parameters (geometric mean diameter, geometric standard deviation, and number concentration of particles) were averaged over a day to create daily time series for each representative mode (nucleation mode, Aitken mode, and accumulation mode).

Trends for each mode parameter for each mode have been estimated using Dynamic Linear Modeling (Petris, Petrone, & Campagnoli, 2009) using existing Matlab-toolbox (Laine, Latva-Pukkila, & Kyrölä, 2014). In addition to the trend estimation, the model estimates also the seasonality in time series.

RESULTS

We analysed the trend for 22 sites, which are mostly located in Europe. Trend and seasonality have been analysed and compared between sites. Figure 1 shows the trend for particle number concentrations in three modes in Hyytiälä between 1996 and 2018. A decrease in number concentrations was observed in all three modes. The largest decrease was seen in nucleation mode, where the decrease was on average 18%/10 years. In Aitken mode, the decrease was 14%/10 years and in accumulation mode, 13%/10 years on average.

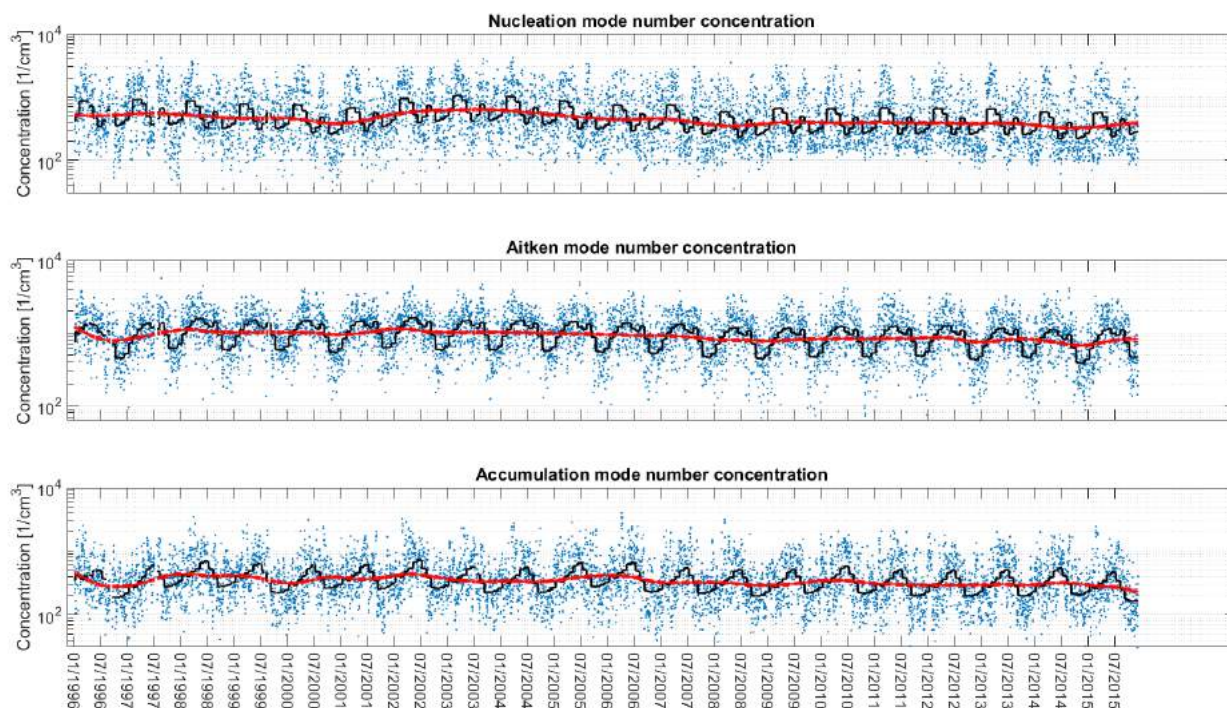


Figure 1 Number concentrations in nucleation, Aitken, and accumulation mode in Hyytiälä between 1998-2015. Blue points show the fitted daily values of the number of particles in three modes. Red line shows the Dynamic Linear Model trend estimate for the number concentration. Black line represents the trend estimate + seasonal estimate.

Similar decreasing trends in the number concentrations were also observed in most (18/22) measurement sites in Europe. Four sites (Hohenpeissenberg, Mukteshwar, Pallas, and Zeppelin), which have low number concentrations, showed some increase in number concentrations during the observed time.

Further analysis of the data will concentrate on analysing the differences in observed trends between sites. What can explain the difference in magnitude of decrease and how the location of the site will affect the decrease observed?

ACKNOWLEDGEMENTS

This work was supported by The Nessling foundation and The Academy of Finland Centre of Excellence (grant no 307331).

We acknowledge the data providers and data from ACTRIS database. ACTRIS project has received funding from the European Union's Horizon 2020 research and innovation programme under grant agreement No 654109.

REFERENCES

- Hussein, T., Dal Maso, M., Petäjä, T., Koponen, I. K., Paatero, P., Aalto, P. P., ... Kulmala, M. (2005). Evaluation of an automatic algorithm for fitting the particle number size distributions. *Boreal Environment Research*, *10*(5), 337–355.
- Laine, M., Latva-Pukkila, N., & Kyrölä, E. (2014). Analysing time-varying trends in stratospheric ozone time series using the state space approach. *Atmospheric Chemistry and Physics*, *14*(18), 9707–9725. <https://doi.org/10.5194/acp-14-9707-2014>
- Nieminen, T., Kerminen, V.-M., Petäjä, T., Aalto, P. P., Arshinov, M., Asmi, E., ... Kulmala, M. (2018). Global analysis of continental boundary layer new particle formation based on long-term measurements. *Atmospheric Chemistry and Physics*, *18*(19), 14737–14756. <https://doi.org/10.5194/acp-18-14737-2018>
- Petris, G., Petrone, S., & Campagnoli, P. (2009). *Dynamic linear models with R*. Springer-Verlag.

Modeling peatland methane emissions on four sites

A. LEPPÄNEN¹, M. RAIIVONEN¹, T. MARKKANEN², T. AALTO², T. KLEINEN³, X. LI¹, T. VESALA¹, A. LOHILA^{1,2}, M. NILSSON⁴, E. HUMPHREYS⁵

¹INAR/Physics, University of Helsinki, Finland.

²Finnish Meteorological Institute, Helsinki, Finland.

³MPI for Meteorology, Hamburg, Germany.

⁴Swedish University of Agricultural Sciences, Sweden.

⁵Carleton University, Canada.

Keywords: peatland, methane, JSBACH, modeling

INTRODUCTION

Wetlands account for roughly one third of total methane emissions. Methane is produced in anoxic conditions below the water table. The production rate depends on temperature and therefore may be affected by climate change. After production methane is transported to the atmosphere by either diffusion, plant transport or by ebullition. Also, methane may be oxidized to carbon dioxide.

HIMMELI (Helsinki Model of METHane buiLd-up and emIssion for peatlands) is a model simulating production, oxidation and transport of methane using a layered peat column (Raivonen *et al.*, 2017; Susiluoto *et al.*, 2018). Oxygen and carbon dioxide processes and fluxes are also included in the model. HIMMELI takes anoxic respiration rate, leaf area index, soil temperature profile and water table depth as an input.

HIMMELI is used with JSBACH, the land surface component of the MPI Earth System Model, which provides the inputs (Kleinen *et al.*, 2019). JSBACH is forced by meteorological data. The anoxic respiration rate is calculated by YASSO soil carbon model.

The aim of the study is to test and validate HIMMELI/JSBACH combination with measurements from different sites and to find out the areas that need and can be developed further.

METHODS

So far four sites have been studied.

Site	Location	Type
Siikaneva	61°49' N, 24°11' E	oligothropic fen
Degerö	64°11' N, 19°33' E	nutrient-poor minerogenic mire (fen)
Mer Bleue	45°18' N, 75°45' W	ombrotrophic bog
Lompolojännkä	68°0' N, 24°13' E	open, nutrient-rich sedge fen

Table 1: Study sites

The fraction of anoxic respiration that produces methane in HIMMELI has been changed from original 0.5 to 0.17 based on comparisons with measurements.

The model was run in two configurations for each site: oxic soil respiration was either calculated by HIMMELI or JSBACH. In the latter case actually the minimum of the two respirations was taken

to prevent e.g. negative concentrations in HIMMELI. Also, because JSBACH does not calculate respiration by layer the respiration was given the same distribution as calculated by HIMMELI.

First we ran JSBACH for years 1956-2015. Then the standalone soil-carbon model Cbalone was run for 3500 years with forcing from the last 30 years of the first JSBACH run cycled. Finally, JSBACH was run for years 1986-2015 starting from the carbon pools from the Cbalone run. Although the observations were newer than 2005 the run was started in 1986 to give the methane concentrations and possibly other variables time to stabilize.

PRELIMINARY RESULTS

For Siikaneva the model is able to reproduce the yearly cycle of methane emission well except for large overestimation during spring. Also, for Degerö the yearly cycles appear similar except for overestimation outside winter. The model overestimates the emission for Mer Bleue during late summer and early autumn. Lompolojännkä is similar to Siikaneva with overestimation during spring and underestimation during summer.

There is much less difference between the sites in the modeled emissions than in the measurements especially during summer and autumn. Also, the model is not currently able to predict the correct order of the magnitude of the mean emission for different sites.

For every site, emissions are higher with oxic respiration calculated by HIMMELI. This is likely because HIMMELI respiration is larger and larger oxic respiration results in less oxygen available for methane oxidation. The difference in emissions is largest for Mer Bleue.

Next steps are to run more sites and study also the CO₂ flux.

ACKNOWLEDGEMENTS

This work was supported the SRC of Academy of Finland project SOMPA (312932), and EU-H2020 project VERIFY (776810) and University of Helsinki, Faculty of Science ATMATH project.

REFERENCES

- Kleinen, T., Mikolajewicz, U. and Brovkin, V. Terrestrial methane emissions from Last Glacial Maximum to preindustrial *Climate of the Past Discussions*, doi: 10.5194/cp-2019-109.
- Raivonen, M., Smolander, S., Backman, L., Susiluoto, J., Aalto, T., Markkanen, T., Mäkelä, J., Rinne, J., Peltola, O., Aurela, M., Lohila, A., Tomasic, M., Li, X., Larmola, T., Juutinen, S., Tuittila, E.-S., Heimann, M., Sevanto, S., Kleinen, T., Brovkin, V., and Vesala, T. (2017). HIMMELI v1.0: Helsinki Model of Methane build-up and emission for peatlands *Geosci. Model Dev.*, **10**, 4665-4691.
- Susiluoto, J., M. Raivonen, L. Backman, M. Laine, J. Mäkelä, O. Peltola, T. Vesala and T. Aalto Calibrating a wetland methane emission model with hierarchical modeling and adaptive MCMC *Geosci. Model Dev.*, **11**, 1199-1228.

UNSUPERVISED MACHINE LEARNING APPLIED ON ATMOSPHERIC DATA FROM THE DACCIWA PROJECT

V. LHEUREUX¹, L. BECK¹, H. JUNNINEN^{1,2}, J. BRITO³, K. SELLEGRI⁴, D. WORSNOP^{1,5}, C. FLAMANT⁶, M.A. ZAIDAN¹, J. DUPLISSY^{1,7}, T. NIEMINEN¹ and M. KULMALA¹

¹Institute for Atmospheric and Earth System Research, University of Helsinki, Helsinki, Finland

²Institute of Physics, University of Tartu, Tartu, Estonia

³Ecole des Mines de Douai, Douai, France

⁴Observatoire de Physique du Globe de Clermont-Ferrand, Clermont-Ferrand, France

⁵Aerodyne Research, Inc, Billerica, MA, United States

⁶LATMOS - Laboratoire Atmosphères, Milieux, Observations Spatiales

⁷Helsinki Institute of Physics, Helsinki, Finland

Keywords: Atmospheric particulates, Atmospheric Chemistry, Statistical Methods, Clustering, DACCIWA

INTRODUCTION

In this study we applied unsupervised machine learning algorithms and statistical methods for analyzing data measured during a 20 days flight-campaign in Africa (Togo, Ghana and Benin) as part of the DACCIWA (Dynamics-Aerosol-Chemistry-Cloud Interactions in West Africa) project. DACCIWA aimed to investigate the influence of anthropogenic and natural emissions on the atmospheric composition over South West Africa and to assess their impact on human and ecosystem health and agricultural productivity (Deroubaix et al, 2019). Multiple measurement devices were used on board of three aircrafts as well as on ground-base site (Ivory Coast, Togo) to provide spatial information. The objective of this work was to analyse the characteristics of each clustered data obtained from unsupervised machine learning.

DATA AND METHODS



Illustration 1: Harbour view from ATR-42 during the flight campaign

In this project we used data from the ATR-42 from Meteo-France (Brito et al, 2018). During this campaign realised from 29.06.16 to 16.07.2016, 20 flights were done at different times in the day (in the morning or in the afternoon). The typical flight duration was close to 2h30 and the ranging altitude was from 200 meters to more than 6000 meters. These collected data include trace gas concentrations from standard gas monitor (Ozone, NO₂, NO, NO_x, SO₂) and from a new CI-Xray APiTOF (Sulfuric acid), particle composition (AMS data organics, NO₃, SO₄, NH₄, Chl) and particle number concentration and number-size distribution (CPC and SMPS). Initial data processing was done in order to prepare suitable datasets for inputs to the machine learning algorithms: we performed data quality checking to remove erroneous measurement data, and time averaging of all the datasets to common time resolution (all the devices don't have the same measurement frequency). Data averaging time was decided taking into account the high flight speed of the aircraft (suggesting short data averaging time) and the need to have high enough signal-to-noise ratio of the averaged data (suggesting longer averaging time). AMS and gas phase species data were averaged in 40 s time resolution. APiTOF data were mass calibrated and extracted. We use TofTools (Junninen et al, 2012) to analyze the APiTOF mass spectra : mass calibration to efficiently relate time of flight to ion mass, peak identification and unit-mass-resolution extraction.

An unsupervised machine learning approach aims to understand the atmospheric composition in different locations and at different altitudes. For example to observe the impact from anthropogenic urban pollution on remote areas. For this, K-means algorithm is applied to the data both from individual flights and on the whole combined dataset from all the flights. K-means clustering aims to partition the dataset into K clusters: K refers to the number of centroids, representing the center of the clusters. Every data point is allocated to the nearest cluster, minimising the distances between datapoints within the cluster and at the same time maximising the distance between different clusters.

K-means algorithm was applied on the the measured trace gases data om flight 24. The ideal number of clusters was determined for each flight based on the evaluation on several indexes, that are elbow, DBI, silhouette, describing the intra- and inter-cluster distances between datapoints for different number of clusters. In order to understand the contributions of different clusters, we compared the distribution of each measured variable between the clusters. For example, a cluster with high concentrations of NO_x may be associated to emissions from anthropogenic pollution sources. An example of the location of the clusters along the track of one flight is shown in Figure 2.

RESULTS

K-means algorithm is functional and looks coherent. However, the less variables are in inputs, the more meaning has the notion of distance between points for clustering.

K-means clustering typically works effectively on lower dimensional space. Since there are many measurement data involved (e.g. gas phases concentration, AMS concentrations and number-size distribution – 11 variables in total), a dimensionality reduction method is required for effective analysis. First, the correlation between measured variables are searched. For example, we found that the correlations between NO_x, NO₂ and NO concentrations are very similar. It means that we can remove some of similar variables since they may have similar contribution. After that, the second approach is to apply Principal Component Analysis (PCA). PCA is a technique for feature extraction with the aim to identify and remove the least important variables, in order to keep only the most informational ones. PCA permits to considerably reduce the dimensionality of the dataset while keeping the majority of the information. In the example of flight number 24, we kept the first three of new principal components, corresponding in 80% of the original dataset. In this case, it allows us to visualize the dispersion of these points in 3-dimension grid as shown in Figure 1. In the principal component space, we can then perform effectively K-means clustering. Different colours in Figure 1 represent different clusters. For each cluster, the data index is tracked, and we can correlate these clusters to the original data sets.

Observation of the dataset in 3D after PCA algorithm

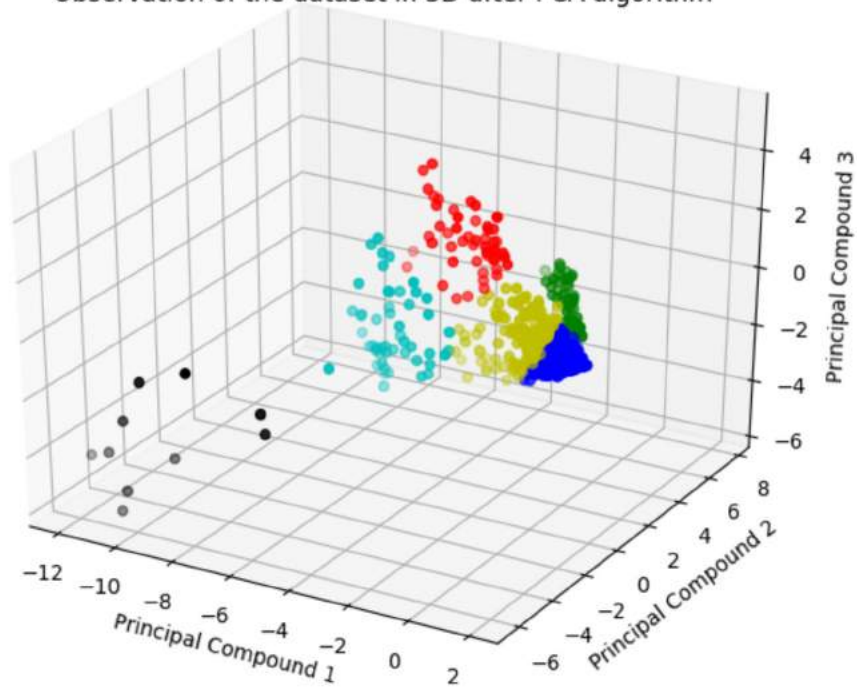


Figure 1: Observation of the cluster in 3D after PCA and K-means. Each colored cluster has different properties. The dimension are the 3 Principal Compounds returned by PCA algorithm

Figure 2 shows the result of the clustering with 6 clusters (the optimal number of clusters found for this flight). Each data point is associated with a coloured label, which may be unique in its atmospheric characteristic. The next step is to produce statistical analysis to understand each cluster atmospheric characteristic.

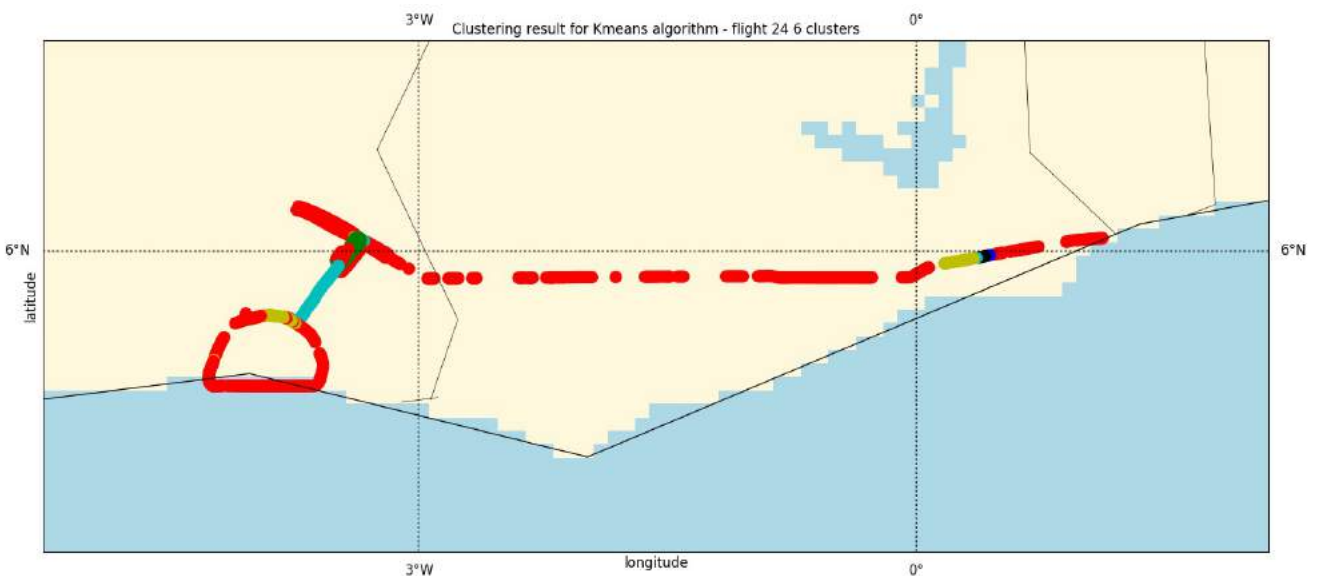


Figure 2: The track of flight number 24 on 06.07.2016. The colors indicate the clustering of datapoints using k-means algorithm with six clusters.

REFERENCES

Brito, J., Freney, E., Dominutti, P., Borbon, A., Haslett, S.L, Batenburg, A.M, Colomb, A., Dupuy, R., Denjean, C., Burnet, F., Bourriane, T., Deroubaix, A., Sellegri, K., Borrmann, S., Coe, H., Flamant, C., Knippertz, P., and Schwarzenboeck, A. (2018). Assessing the role of anthropogenic and biogenic sources on PM1 over southern West Africa using aircraft measurements. *Atmos. Chem. Phys.*, 18, 757–772.

Deroubaix, A., Menut, L., Flamant, C., Brito, J., Denjean, C., Dreiling, V., Fink, A., Jambert, C., Kalthoff, N., Knippertz, P., Ladkin, R., Mailler, S., Maranan, M., Pacifico, F., Pigué, B., Siour, G., and Turquety, S. (2019). Diurnal cycle of coastal anthropogenic pollutant transport over southern West Africa during the DACCIWA campaign. *Atmos. Chem. Phys.*, 19, 473–497.

Junninen, H. (2013). Data cycle in Atmospheric Physics : From detected millivolts to understanding the atmosphere. Report Series in Aerosol Science, 145.

CHEMICAL CHARACTERIZATION AND SOURCE APPORTIONMENT OF VOLATILE ORGANIC COMPOUNDS IN FOREST AREAS

HAIYAN LI¹, MATTHIEU RIVA², PEKKA RANTALA¹, LIINE HEIKKINEN¹, KASPAR DAELLENBACH¹, JORDAN E. KRECHMER³, PIERRE-MARIE FLAUD^{4,5}, DOUGLAS WORSNOP³, MARKKU KULMALA¹, ERIC VILLENAVE^{4,5}, EMILIE PERRAUDIN^{4,5}, MIKAEL EHN¹ and FEDERICO BIANCHI¹

¹Institute for Atmospheric and Earth System Research / Physics, Faculty of Science, University of Helsinki, Finland

²Department of Geophysics, University of Munster, Killarney, Kerry, Republic of Ireland.

²Univ. Lyon, Université Claude Bernard Lyon 1, CNRS, IRCELYON, F-69626, Villeurbanne, France.

³Aerodyne Research Inc., Billerica, Massachusetts 01821, USA.

⁴Univ. Bordeaux, EPOC, UMR 5805, F-33405 Talence Cedex, France.

⁵CNRS, EPOC, UMR 5805, F-33405 Talence Cedex, France.

Keywords: Volatile organic compounds, atmospheric oxidation, PMF, Vocus PTR-TOF.

INTRODUCTION

Organic aerosol (OA) constitutes a large fraction of atmospheric particles, having significant impacts on climate change, air quality, and human health. On the global scale, secondary OA (SOA) is the largest source of OA, significantly contributed by atmospheric oxidation of biogenic volatile organic compounds (BVOCs). While considerable studies have been conducted to investigate atmospheric chemistry of BVOCs over the past few years (Atkinson and Arey, 2003; Baltensperger et al., 2005), an incomplete understanding of BVOCs oxidation still exists and leads to large uncertainties in quantitative estimates of air quality and climate effects of atmospheric aerosols.

Atmospheric oxidation of BVOCs produces a large variety of organic species, with the volatility ranging from gas-phase volatile species, to semi-volatile and low volatility organic compounds (SVOC and LVOC), to extremely low volatility organic compounds (ELVOC) largely present in the particle phase (Donahue et al., 2012). Due to the complex physical-chemical properties of these species, it is challenging to provide a comprehensive characterization of the complex organic mixtures, especially at molecular-formula level. Recently, Vocus PTR-TOF (proton transfer reaction time-of-flight mass spectrometry) was developed with a new chemical ionization source and focusing ion-molecule reactor (Krechmer et al., 2018). With the improved measurement precision and detection limits, Vocus PTR-TOF allows measurements of VOC reaction products and intermediates in addition to many volatile precursors.

METHODS

To gain a better understanding of VOC variations and their oxidation processes, ambient measurements using Vocus PTR-TOF were performed at two forest sites, SMEAR II station and the French Landes forest. Both stations are known with high emissions of terpenes which are highly reactive in the atmosphere, thus providing a good opportunity to investigate biogenic oxidation processes. The SMEAR II station is located in a boreal forest in southern Finland. The vegetation nearest to the measurement site was a homogeneous Scots pine forest where some birch, poplar, and Norway spruce grow below the canopy. Anthropogenic influence at the site is low. The largest nearby city is Tampere, located 60 km to the site. The campaign at

SMEAR II station lasted from early April to late August, 2019. The Landes forest is situated at the European Integrated Carbon Observation System (ICOS) station at Bilos in southwestern France along the Atlantic coast, ~40 km southwest from the nearest urban area of the Bordeaux metropole. The forest is largely composed of maritime pines. The measurements in Landes forest took place from 8 to 20 July, 2018.

CONCLUSIONS

Due to the greatly improved detection efficiency compared to traditional PTR instruments, the Vocus PTR-TOF identifies a large amount of gas-phase signals with elemental composition categories including CH, CHO, CHN, CHS, CHON, CHOS, and others. Multiple hydrocarbons are detected, with carbon numbers up to 20. Particularly, we report the first direct observations of low-volatility diterpenes in the ambient air. Various types of terpene reaction products and intermediates are also characterized. Generally, the more oxidized products from terpene oxidations show a broad peak in the day due to the strong photochemical effects, while the less oxygenated products peak in the early morning and/or in the evening.

With the novel approach of mass spectral binning combined with positive matrix factorization (binPMF), source characterization of VOCs were conducted to identify different sources or processes. Factors related to isoprene, monoterpenes, sesquiterpenes, and the less oxidized or more oxidized processes are resolved.

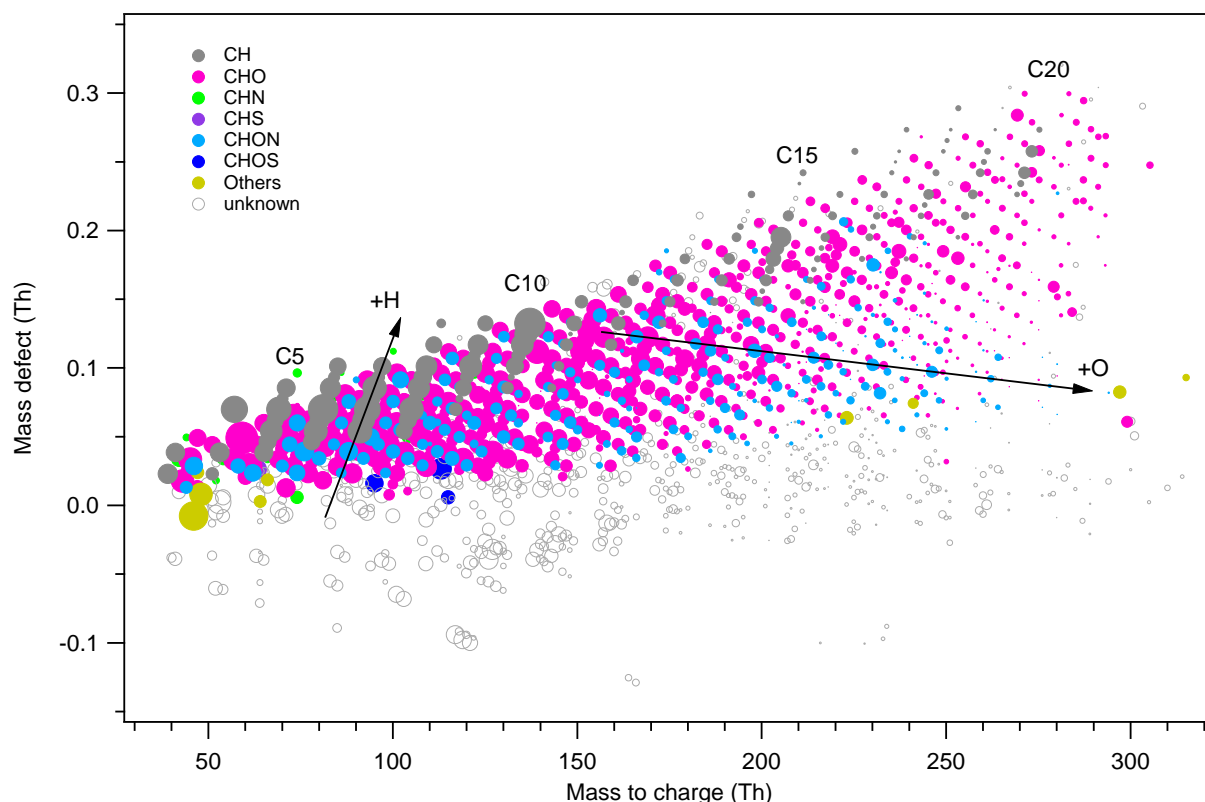


Figure 1. Mass defect plot of the ions identified by high-resolution analysis of Vocus PTR-TOF data set. The x-axis shows the mass to charge ratio and the y-axis shows the mass defect, which is the deviation of the accurate mass from the nominal mass. Data points in (a) are color-coded by ion family (CH, CHO, CHN, CHS, CHON, CHOS) and sized by the logarithm of peak area.

ACKNOWLEDGEMENTS

This work was supported by the European Research Council under grants 742206 ATM-GP and 638703 COALA, and the Academy of Finland (project numbers 317380 and 320094). The authors would like to thank the PRIMEQUAL programme for financial support (ADEME, convention #1662C0024). This study has also been carried out with financial support from the French National Research Agency (ANR) in the frame of the Investments for the future Programme, within the Cluster of Excellence COTE (ANR-10-LABX-45) of the University of Bordeaux. Special thanks to Dr Elena Ormeño-Lafuente (IMBE) for the loan of the BVOC calibration gas cylinders and Dr Christophe Chipeaux and Dr Denis Loustau (ISPA-INRA) for their precious help in providing meteorological data and access to ICOS station facility.

REFERENCES

- Atkinson, R., & Arey, J. (2003). *Atmos Environ*, 37, 197-219.
Baltensperger et al. (2005). *Faraday Discussions*, 130, 265-278.
Donahue et al. (2012). *Atmos. Chem. Phys.*, 12, 615-634.
Krechmer et al. (2018). *Analytical Chemistry*, 90, 12011-12018.

**EXPLORING THE REGIONAL POLLUTION CHARACTERISTICS AND
METEOROLOGICAL FORMATION MECHANISM OF PM_{2.5} IN NORTH CHINA DURING
2013-2017**

MINGGE LI^{1,7}, LILI WANG^{1,3}, JINGDA LIU^{1,8}, WENKANG GAO¹, TAO SONG¹, YANG SUN¹,
LIANG LI⁴, XINGRU LI⁶, YONGHONG WANG³, LILI LIU⁵, KASPAR R. DAELLENBACH³, PAULI J
PAASONEN³, VELI-MATTI KERMINEN³, MARKKU KULMALA³, YUESI WANG^{1,2,7,8}

¹State Key Laboratory of Atmospheric Boundary Layer Physics and Atmospheric Chemistry (LAPC),
Institute of Atmospheric Physics, Chinese Academy of Sciences, Beijing, 100029, China

²Centre for Excellence in Atmospheric Urban Environment, Institute of Urban Environment, Chinese
Academy of Science, Xiamen, Fujian 361021, China

³Institute for Atmospheric and Earth System Research / Physics, Faculty of Science, University of
Helsinki, Finland

⁴China National Environmental Monitoring Center, Beijing, 100012

⁵Tianjin Institute of Meteorological Science, Tianjin 300074, China

⁶Department of Chemistry, Analytical and Testing Center, Capital Normal University, Beijing 100048,
China

⁷University of the Chinese Academy of Sciences, Beijing, 100049, China

⁸Department of Atmospheric Physics, Nanjing University of Information Science & Technology, Nanjing,
210044, China

ABSTRACT

In the last decade, North China (NC) has been one of the most populated and polluted regions in the world. The regional air pollution has had a serious impact on people's health; thus, all levels of government have implemented various pollution prevention measures since 2013. Based on multi-city in situ environmental and meteorological data, as well as the meteorological reanalysis dataset from 2013 to 2017, regional pollution characteristics and meteorological formation mechanisms were analyzed to provide a more comprehensive understanding of the evolution of PM_{2.5} in NC. The domain-averaged PM_{2.5} was 79±17 µg m⁻³ from 2013 to 2017, with a decreasing rate of 10 µg m⁻³ yr⁻¹. Two automatic computer algorithms were established to identify 6 daily regional pollution types (DRPTs) and 48 persistent regional pollution events (PRPEs) over NC during 2014-2017. The average PM_{2.5} concentration for the Large-Region-Pollution type (including the Large-Moderate-Region-Pollution and Large-Severe-Region-Pollution types) was 113±40 µg m⁻³, and more than half of Large-Region-Pollution days and PRPEs occurred in winter. The PRPEs in NC mainly developed from the area south of Hebei. The number of Large-Region-Pollution days decreased notably from 2014 to 2017, the annual number of days varying between 194 and 97 days, whereas a slight decline was observed in winter. In addition, the averaged PM_{2.5} concentrations and the numbers and durations of the PRPEs decreased. Lamb-Jenkinson weather typing was used to reveal the impact of synoptic circulations on PM_{2.5} across NC. Generally, the contributions of the variations in circulation to the reduction in PM_{2.5} levels over NC between 2013 and 2017 were 64% and 45% in summer and winter, respectively. The three most highly polluted weather types were types C, S and E, with an average PM_{2.5} concentration of 137±40 µg m⁻³ in winter. Furthermore, three typical circulation dynamics were categorized in the peak stage of the PRPEs, namely, the southerly airflow pattern, the northerly airflow pattern and anticyclone pattern; the averaged relative humidity, recirculation index, wind speed and boundary layer height were 63%, 0.33, 2.0 m s⁻¹ and 493 m, respectively. Our results imply that additional emission reduction measures should be implemented under unfavorable meteorological situations to attain ambient air quality standards in the future.

Keywords: North China, PM_{2.5}, Regional pollution events, Identification of regional pollution type, Meteorological formation mechanism

ACKNOWLEDGEMENTS

This work was partially supported by the grant of National Key R&D Plan (Quantitative Relationship and Regulation Principle between Regional Oxidation Capacity of Atmospheric and Air Quality 2017YFC0210003), the National Natural Science Foundation of China (No. 41505133&41775162), National research program for key issues in air pollution control (DQGG0101) and the program of China Scholarships Council. Special thanks to the National Earth System Science, Data Sharing Infrastructure, and National Science & Technology Infrastructure of China. We thank European Research Council via ATM-GTP 266 (742206), and Academy of Finland Centre of Excellence in Atmospheric Sciences (grant number: 272041).

CARBON DIOXIDE AND METHANE FLUXES FROM DIFFERENT SURFACE TYPES IN A CREATED URBAN WETLAND

Xuefei Li¹, Outi Wahlroos², Sami Haapanala³, Jukka Pumpanen⁴, Harri Vasander⁵,
Anne Ojala^{1,5,6}, Timo Vesala^{1,5} and Ivan Mammarella¹

¹Institute for Atmospheric and Earth System Research (INAR)/Physics, University of Helsinki, Finland

²University of Turku, Turku, Finland

³Suvilumi, Orahuhdantie 2 B, 00680 Helsinki, Finland

⁴Department of Environmental and Biological Sciences, University of Eastern Finland, Finland

⁵INAR/Forest Sciences, Faculty of Agriculture and Forestry, University of Helsinki, Finland

⁶Ecosystems and Environment Research Programme, Faculty of Biological and Environmental Sciences, University of Helsinki, Finland

Keywords: greenhouse gas, surface type, urban wetland, annual balance, artificial neural network

INTRODUCTION

Wetlands can take up carbon dioxide (CO₂) through emergent and submerged vegetation but they are also important sources of methane (CH₄), a greenhouse gas more potent than CO₂ when considered over a 100-year horizon (Stocker et al., 2014). The exchange of greenhouse gases (GHG) such as CO₂ and CH₄ between atmosphere and ecosystem have direct influence on the atmospheric concentration of these gases, thus besides the ecosystem services that wetland provide, the GHG budget of constructed wetlands should be accounted for according to international agreements such as the Kyoto protocol. Urban wetlands have received extensive attention globally and their societal and economical importance have been evaluated whereas their climate impact is still largely overlooked except for only a few studies (e.g. Morin et al., 2014).

The objective of this study is to investigate how CO₂ and CH₄ surface-atmosphere exchange vary with seasonality and spatial heterogeneity and what the annual radiative forcing of these gases are in a constructed urban wetland near town Nummela, Municipality of Vihti, Southern Finland. The studied Gateway wetland was designed and implemented to serve the purposes of stormwater quality treatment, creating an urban park, as well as supporting biodiversity. Besides taking advantage of ecosystem-scale EC measurements, we also parse the variability of gas exchange induced by surface heterogeneity (open water and vegetated area) using diffusional flux modeling and footprint modelling overlapped on a high-resolution surface map. To illustrate how the urban wetland functions as a source or a sink of GHG equivalents, we calculate separately the sustained global warming potential (SGWP) of CO₂ and CH₄ over a hundred-year horizon in each surface type.

METHODS

Study site

Our study site is a created stormwater wetland Gateway, located by an eutrophicated Lake Enäjärvi in the District of Nummela, Municipality of Vihti, Southern Finland (60.3272°N, 24.3369°E). The wetland has a total area of 7 hectares. The wetland was constructed in 2010 at the mouth of a 550 hectare largely urbanized (35 % impervious) watershed of Stream Kilsoi. It consists of an inlet stilling pond, a meandering shallow water area with three habitat islands, and an outlet pond.

Measurements and data analysis

A 2.9 m eddy covariance tower was established in the autumn of 2012 on the southern side of the wetland. The EC set-up included a 3D-sonic anemometer (uSonic-3, Metek, Elmshorn, Germany) to measure the three wind speed components and sonic temperature, a gas analyser (LI-7200, Li-Cor Inc., Lincoln, Nebraska, USA) which measures CO₂ and H₂O mixing ratio and a TDL gas analyser (TGA100A, Campbell Scientific Inc., USA) to measure CH₄ mixing ratio at the frequency of 10 Hz. The post-processing of the EC flux data has been done with EddyUH post-processing software (Mammarella et al., 2016).

We used an artificial neural network (ANN) technique to gap-fill half-hourly flux data using meteorological variables (Moffat et al., 2007).

Local weather conditions were recorded with a Vaisala WXT weather transmitter (WXT520, Vaisala Oyj, Finland) at the inlet monitoring station. Water monitoring stations were set up at the inlet (60.3283° N, 24.3356° E) and at the outlet (60.3281° N, 24.3377° E) of the wetland. Water temperature as well as Water level, water turbidity, oxygen concentration, conductivity and pH were measured continuously with 10-minute interval. The concentration of dissolved carbon dioxide ([CO₂]) and dissolved methane ([CH₄]) were measured.

Diffusive gas exchange from the open water was calculated using boundary layer model and gas transfer velocity was estimated using exiting method (Cole and Caraco, 1998).

Estimating zone fluxes and radiative forcing

By combining EC tower and diffusive flux from the open-water, the following model can be derived

$$F_{EC} = F_{water} \times f_{water} + F_{veg} \times f_{veg} \quad (1)$$

where F_{EC} is the flux measured by EC tower, F_{water} and F_{veg} stands for the flux from open-water and vegetated area, respectively, f_{water} and f_{veg} are the footprint-weighted spatial fraction of open-water and vegetated area. In this study, ebullition was neither measured nor calculated, so the flux from water was only represented by the diffusive flux. We calculated the sustained global warming potential (SGWP) for CO₂ and CH₄ over a hundred-year horizon in each surface type. Since CH₄ is a more potent greenhouse gas, we multiply the emission of CH₄ by a factor of 45 to convert it to kg CO₂-eq m² yr⁻¹ (Neubauer and Megonigal, 2015).

RESULTS

		Ecosystem	Water	Vegetation
Flux (g C m ⁻²)	CO ₂	8 [-18.9, 34.9]	297.5	-39.5 [-70.8, -8.1]
	CH ₄	3.9 [3.8, 4.1]	1.7	4.3 [4.1, 4.5]
SGWP (kg CO ₂ -eq m ⁻²)	CO ₂	0.03 [-0.07, 0.13]	1.09	-0.14 [-0.26, -0.03]
	CH ₄	0.23 [0.22, 0.24]	0.10	0.26 [0.25, 0.27]

Table 1: Annual CO₂ and CH₄ exchange from different surface zones and their sustained global warming potential (SGWP). Ecosystem, water and vegetation represent flux and SGWP measured or calculated from the ecosystem by EC tower, from open water and from vegetated area. The numbers in the square bracket represent the 95% confidence interval of the average. No error bounds are reported for flux and SGWP from water as they are modelled using gas concentration in the water and meteorological measurements.

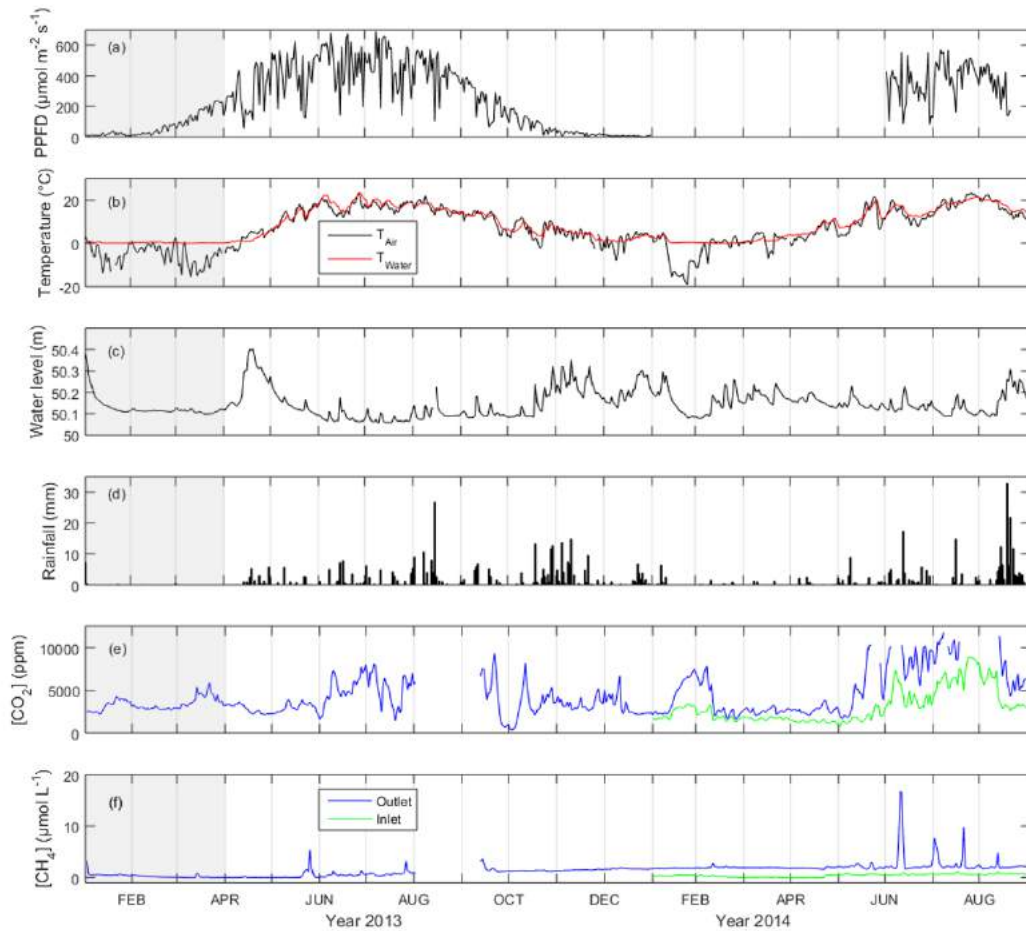


Figure 1: The daily-average of (a) photosynthetic photon flux density (PPFD), (b) air and water temperature, (c) water level, (d) rainfall, (e) CO₂ concentration and (f) CH₄ concentration from inlet and outlet of Nummela wetland from January 2013 to August 2014. The grey zone indicates the ice-covered period.

The seasonal variation of environmental variables are shown in Fig. 1.

A footprint distribution was modeled for each half hour when an eddy flux measurement was collected at the EC tower. The open-water area accounted for 10 % to 16 % of the total wetland area within the footprint while the rest was comprised of wetland vegetation. When weighted with footprint distribution, f_{water} ranged from 0 to 25.5 % and f_{veg} from 74.5 % to 100 %.

CO₂ flux showed strong diel pattern in summer with CO₂ uptake during daytime and release in the night, which was controlled by photosynthetic activity. The CO₂ flux from the vegetated area had higher maximum uptake than the EC measurements carried out over the whole constructed wetland. In the winter, the CO₂ fluxes from both tower and vegetation were similar. CH₄ flux also showed diel patterns in the summer with much larger variability than those from CO₂ flux. CH₄ emission in general was higher in daytime than in nighttime. In the daytime in summer, CH₄ flux from the vegetated area was higher than the flux measured from the tower while there was no difference during the nighttime. The summer peak daytime flux from tower ($18.9 \text{ nmol m}^{-2} \text{ s}^{-1}$) and vegetated area ($24.7 \text{ nmol m}^{-2} \text{ s}^{-1}$) was 2.4 times and 3.3 times higher than the nighttime flux ($7.5 \text{ nmol m}^{-2} \text{ s}^{-1}$), respectively. This can be understood as daytime CH₄ flux is linked with

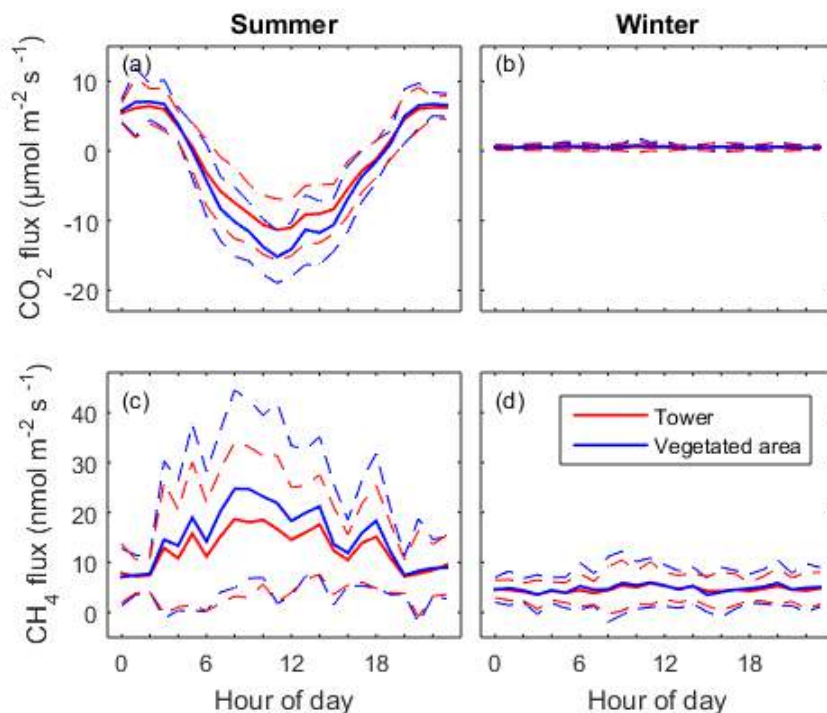


Figure 2: Mean diel pattern of the half-hourly net CO₂ and CH₄ fluxes in summer ((a) and (c)) and in winter ((b) and (d)). The dashed lines represent the standard deviation. Red lines indicate measurement from EC tower and the blue lines show the fluxes modelled for vegetated area.

photosynthesis while nighttime CH₄ flux is controlled by other processes like diffusion, ebullition and convection between the soil, water and atmosphere. In winter there was small (on average 4.6 nmol m⁻² s⁻¹) but constantly positive CH₄ flux without obvious diel pattern (Fig. 2).

To obtain the climate forcings from each land surface type, we calculated the half-hourly and annual gas fluxes from the vegetated area using footprint-weighted spatial fraction, ecosystem fluxes and diffusive fluxes from the open water. The annual median value of footprint-weighted spatial extent was used to calculate the annual fluxes, which showed open-water area was a CO₂ source (297.5 g C-CO₂ m⁻² yr⁻¹) and vegetated area was a CO₂ sink (-39.5 C-CO₂ m⁻² yr⁻¹). Both open-water and vegetated area were CH₄ sources but the CH₄ emission from vegetated area was higher than open-water area, being 4.26 and 1.73 g C-CO₂ m⁻² yr⁻¹, respectively. Open water has contributed large amount of CO₂ emission into the atmosphere through diffusion (1.09 kg CO₂-eq m⁻² yr⁻¹) whereas the CH₄ emission was relatively small (0.104 kg CO₂-eq m⁻² yr⁻¹). Vegetated area was a small sink of CO₂ but the cooling effect of vegetation by CO₂ uptake was relatively small (-0.145 kg CO₂-eq m⁻² yr⁻¹) compared to its CH₄ emission (0.256 kg CO₂-eq m⁻² yr⁻¹). Overall, the ecosystem had a small warming effect with 0.263 kg CO₂-eq m⁻² yr⁻¹ of which 89 % was contributed by CH₄ (Table 1).

CONCLUSIONS

Urban wetlands have received global attention as a nature-based urban runoff management solution for sustainable cities, as they provide cost efficient flood control and water quality mitigation as well as many ecological and cultural services. In the meantime, the climate impact of urban wetlands should also be considered. Wetting a landscape may enhance the CO₂ sequestration in the

ecosystem, whereas CH₄ can be emitted due to the anaerobic conditions in the soil after wetting. Furthermore, heterogeneity induced in newly created urban wetland may contribute differently to the overall climate impact. In the present study, for the first time a full annual carbon balance of an urban stormwater wetland in the boreal region was evaluated and the radiative forcing from heterogeneous landscapes were presented. We found that, during the monitored period at the study wetland, both the open water area and the vegetated area within the created wetland were carbon sources, and thus the urban wetland had a net climate warming effect, the monitored fourth year after the wetland establishment. The radiative forcing effect of the open-water area exceeded the vegetated area, which indicated that limiting open-water surfaces and setting a design preference for areas of emergent vegetation in the establishment of urban wetlands can be a beneficial practice when considering only the climate impact of a created urban wetland. In the meanwhile, we also emphasize that the value of urban wetlands should not be determined solely by GHG radiative forcing. The values of urban wetlands in other areas e.g. flood control, pollutant removal, biodiversity, recreation and education are as well of paramount importance to human society.

ACKNOWLEDGEMENTS

This research was supported by the EU Life+11 ENV/FI/911 Urban Oases project grant, Academy of Finland, Academy Professor projects (312571 and 282842), ICOS-Finland (281255), the Maa- ja vesiteknikan tuki ry, the Ministry of the Environment of Finland and the Municipality of Vihti.

REFERENCES

- Anderson, F. E., Bergamaschi, B., Sturtevant, C. et. al: Variation of energy and carbon fluxes from a restored temperate freshwater wetland and implications for carbon market verification protocols, *Journal of Geophysical Research-Biogeosciences*, 121, 777-795, 2016.
- Stocker, T. F., Qin, D., Plattner, G. K. et. al: *Climate Change 2013: The Physical Science Basis*, 1-1535 pp., 2014.
- Morin, T. H., Bohrer, G., Frasson, R. et. al: Environmental drivers of methane fluxes from an urban temperate wetland park, *Journal of Geophysical Research-Biogeosciences*, 119, 2188-2208, 10.1002/2014jg002750, 2014.
- Mammarella, I., Peltola, O., Nordbo, A. et. al: Quantifying the uncertainty of eddy covariance fluxes due to the use of different software packages and combinations of processing steps in two contrasting ecosystems, *Atmospheric Measurement Techniques*, 9, 4915-4933, 2016.
- Moffat, A. M., Papale, D., Reichstein, M. et. al: Comprehensive comparison of gap-filling techniques for eddy covariance net carbon fluxes, *Agricultural and Forest Meteorology*, 147, 209-232, 2007.
- Cole, J. J., and Caraco, N. F.: Atmospheric exchange of carbon dioxide in a low-wind oligotrophic lake measured by the addition of SF₆, *Limnology and Oceanography*, 43, 647-656, 1998.
- Neubauer, S. C., and Megonigal, J. P.: Moving Beyond Global Warming Potentials to Quantify the Climatic Role of Ecosystems, *Ecosystems*, 18, 1000-1013, 2015.

IMPACT OF MOLECULAR-LEVEL VARIABILITY ON THE ISOTHERMAL EVAPORATION OF BIOGENIC SECONDARY ORGANIC AEROSOL PARTICLES

Z. LI¹, A. BUCHHOLZ¹, A. YLISIRNIÖ¹, L. BARREIRA¹, L. HAO¹,
S. SCHOBESBERGER¹, T. YLI-JUUTI¹, A. VIRTANEN¹

¹ Department of Applied Physics, University of Eastern Finland, Kuopio, Finland.

Keywords: secondary organic aerosol, molecular composition, isothermal evaporation

INTRODUCTION

Atmospheric oxidation of biogenic volatile organic compounds (BVOCs) can lead to a complex mixture of condensable organic vapours spanning a wide range of functionalities and structures, and hence volatilities. Volatility is one key aspect, which governs the partitioning of organic constituents between gas and particulate phase. Some of these organics can therefore contribute to the mass concentration of secondary organic aerosol (SOA).

Intensive studies have been conducted to understand the evaporation behaviour of α -pinene SOA under various humidity conditions (Vaden *et al.* 2011, Yli-Juuti *et al.* 2017, Buchholz *et al.* 2019). All of these measurements have consistently reported slower SOA evaporation compared to that derived from yield-based Volatility Basis Set (VBS) parametrizations, suggesting a significant impact of viscous phase state and unexpectedly low-volatility organics on particle evaporation. However, little is known about the evaporation of SOA from BVOC precursors other than α -pinene. To better understand the volatility of SOA, especially when resulting from forest emissions, it is important to carry out isothermal evaporation measurements with a wide range of monoterpenes and sesquiterpenes characteristic for those environments.

METHODS

Here, α -pinene and a mixture of farnesenes and bisabolenes (SQTmix) were chosen to generate two types of SOA for isothermal evaporation measurements. Farnesenes and bisabolenes are major sesquiterpenes emitted from boreal trees (Hakola *et al.* 2017). SOA with similar O:C ratios was generated by photooxidation in a Potential Aerosol Mass (PAM) flow reactor. Monodisperse SOA particles with 80 nm selected by Nano-DMA were supplied into a 100-L Residence Time Chamber (RTC) for isothermal evaporation under different RH conditions (dry, 40% and 80%) at room temperature (293 K). The size-selection also lead to a dilution of gas phase compounds, initiating particle evaporation. After filling, the RTC was closed off to allow undisturbed particle evaporation and periodically opened for particle characterisation (Fig. 1).

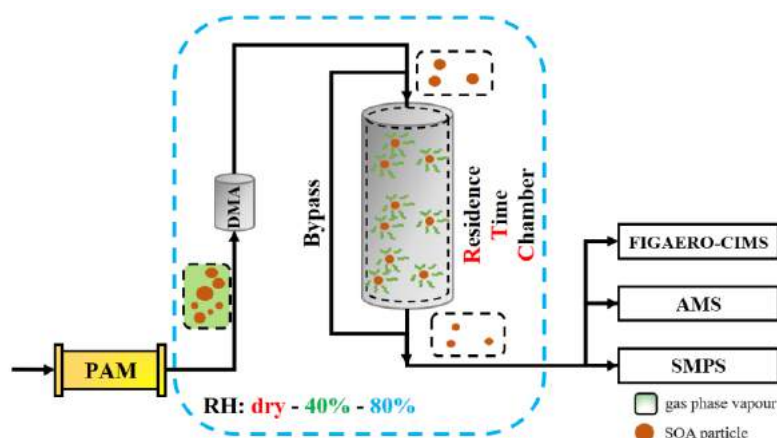


Figure 1. Schematic diagram of the set-up for evaporation experiments of SOA particles.

During sampling, the particle size was monitored with a Scanning Mobility Particle Sizer (SMPS). Additionally, the particle composition was characterised with a High-Resolution Time-of-Flight Aerosol Mass Spectrometer (HR-ToF-AMS) and a Chemical Ionization Mass Spectrometer coupled with a Filter Inlet for Gases and Aerosols (FIGAERO-CIMS) using iodide-adduct ionisation. This system also reveals

the particles thermal desorption behaviour characterised by the median desorption temperature T_{median} of the particulate mass from the FIGAERO filter.

RESULTS AND CONCLUSIONS

Evaporation of particles was faster at higher RH for both SOA systems, due to the plasticization effect of water and the enhanced bulk diffusivity. Although the bulk elemental compositions of particles (derived from AMS data) were comparable between α -pinene and SQTmix SOA, the particle evaporation rates were different at a set RH (Fig. 2). The implied differences in the volatility distributions most likely stem from the variability of detailed molecular composition, which is not represented by the particle bulk O:C ratios.

Samples collected with the FIGAERO-CIMS represent the chemical composition at the beginning (20 min, 'fresh') and later phases (3 to 4 hours) of the particle evaporation, respectively. Inconsistent with the observed differences in the isothermal evaporation, similar values of T_{median} are observed for both types of 'fresh' SOA particles, i.e. irrespective of precursor identity. However, larger fractions of high molecular weight compounds ($MW_{[M+I]} > 300$ Da) were observed in the 'fresh' α -pinene case, whereas compounds with higher oxidation state were found in the 'fresh' SQTmix case. Inconsistencies between particle volatility inferred by mass spectrometry measurements and the particle volatility evident by observations of decreasing particle size (Fig. 2) will be further explored.

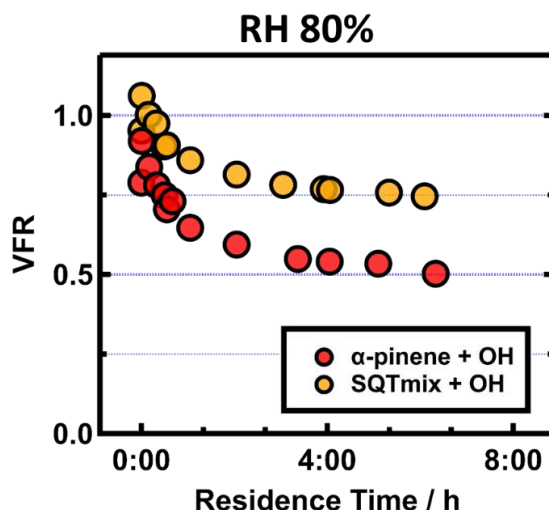


Figure 2. Volume fraction remaining (VFR) of α -pinene (yellow) and SQTmix SOA (red) particles at 80% RH.

ACKNOWLEDGMENTS

This work was supported by the European Research Council (ERC starting grant 335478) and Academy of Finland (grant no. 259005, 299544, 307331, 310682).

REFERENCES

- Buchholz A., Lambe A.T., Ylisirniö A., Li Z., Tikkanen O.-P., Faiola C., Kari E., Hao L., Luoma O. & Huang W. 2019. Insights into the O: C-dependent mechanisms controlling the evaporation of α -pinene secondary organic aerosol particles. *Atmospheric Chemistry and Physics* 19: 4061-4073.
- Hakola H., Tarvainen V., Praplan A.P., Jaars K., Hemmilä M., Kulmala M., Bäck J. & Hellén H. 2017. Terpenoid and carbonyl emissions from Norway spruce in Finland during the growing season. *Atmospheric Chemistry and Physics* 17: 3357-3370.
- Vaden T.D., Imre D., Beranek J., Shrivastava M. & Zelenyuk A. 2011. Evaporation kinetics and phase of laboratory and ambient secondary organic aerosol. *Proc Natl Acad Sci U S A* 108: 2190-2195.
- Yli-Juuti T., Pajunoja A., Tikkanen O.P., Buchholz A., Faiola C., Vaisanen O., Hao L., Kari E., Perakyla O., Garmash O., Shiraiwa M., Ehn M., Lehtinen K. & Virtanen A. 2017. Factors controlling the evaporation of secondary organic aerosol from alpha-pinene ozonolysis. *Geophysical Research Letters* 44: 2562-2570.

OZONE REACTIVITY MEASUREMENTS OF BIOGENIC VOLATILE ORGANIC COMPOUNDS

A. K. LIIKANEN¹, J.HUEBER², D.HELMIG², A. P. PRAPLAN¹

¹Finnish Meteorological Institute, P.O. Box 503, 00101 Helsinki, Finland

²Institute of Arctic and Alpine Research, University of Colorado, Campus Box 450
Boulder, CO 80309-0450 USA

Keywords: Biogenic Volatile Organic Compounds (BVOC), ozone reactivity.

INTRODUCTION

Volatile organic compounds (VOC) play important role in atmospheric chemistry as precursors of ozone and secondary organic aerosols (SOA) (Atkinson, 2000). VOCs originate from biogenic sources such as trees and other vegetation, and from anthropogenic sources. The annual VOC flux is estimated to be 1150 TgC, consisting of 44% isoprene and 11% monoterpenes which are biogenic VOC (BVOC) (Guenther et al., 1995). Once released in air, VOCs react with ozone (O₃) and atmospheric radicals, like hydroxyl radical (OH) and the nitrate radical (NO₃) forming SOA among other reactions (Kulmala et al., 2013). VOCs have a significant impact also on air quality and human health and better understanding of their reactions with atmospheric oxidants is needed on predicting future atmospheric condition and related climate phenomena (Lelieveld et al., 2008).

In terms of reactivity, OH radical is important during daytime, NO₃ during night but O₃ concentrations can be abundant during the whole day (Atkinson and Arey, 2003). Quantifying total OH reactivity has developed in past years but comparison between individually detected OH sinks unveils a considerable missing reactivity (Yang et al., 2016), particularly in forested areas missing OH reactivity can be as high as 58-89% (Nölscher et al., 2012). Investigation of detailed emission characteristics of BVOCs is important as all regions are subjected to increasing temperature, which further affects plant emissions (Kulmala 2013). Even though OH is the most important oxidant in the atmosphere, O₃ and NO₃ contribute to atmospheric VOC chemistry, especially at night. Reactivities for O₃ and NO₃ have been investigated by modelling studies but emission measurements are rare. Matsumoto (2014) has developed a system to measure total O₃ reactivity and published results of O₃ measurements from vegetation. Also Prof Helmig (University of Colorado) has been developing such system and conducted O₃ reactivity measurements from tree emissions and ambient air (to be published). Simultaneous measurements of O₃ and OH reactivities with new instruments can bring additional information to the atmospheric VOC chemistry.

METHODS

The system is based on the work of Matsumoto (2014) and Prof. Detlev Helmig. A schematic of the setup is presented in Fig. 1. The total ozone reactivity (R_{O_3}) is obtained from the comparison of O₃ levels in the sampled air before and after the reactor, which consists of 2 to 4 glass bottles (2.5 l each). In fig. 2. is presented formula to calculate R_{O_3} from the measurements.

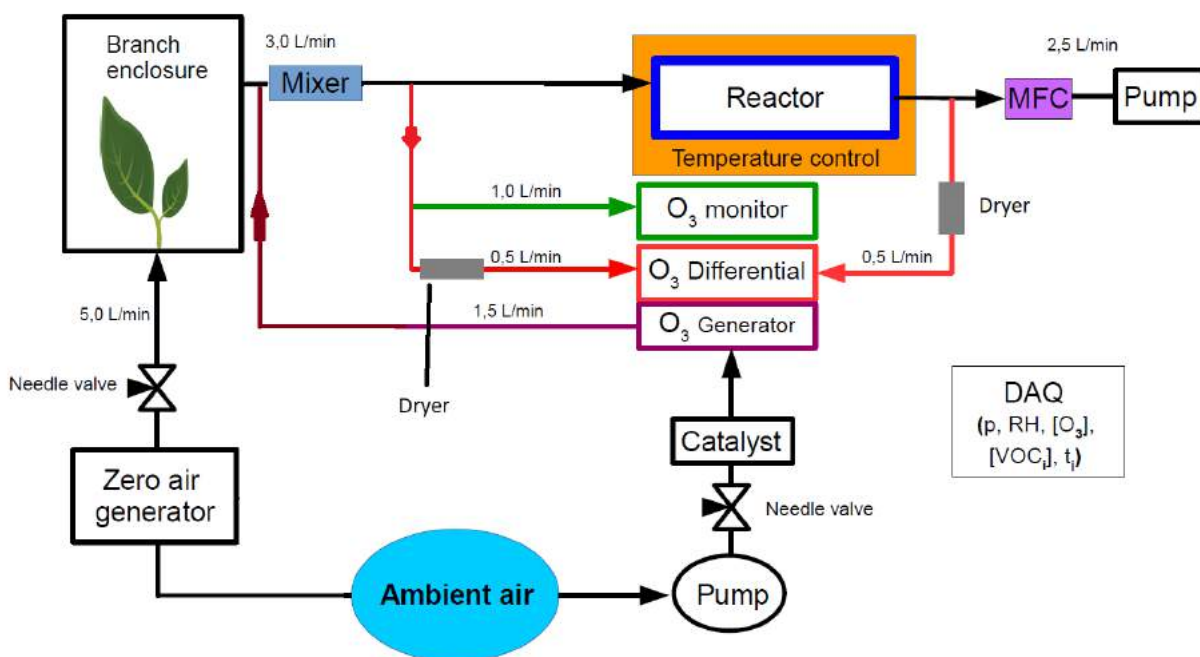


Figure 1: Schematic of the ozone reactivity measurement setup. Values of flows can be altered depending on desired conditions.

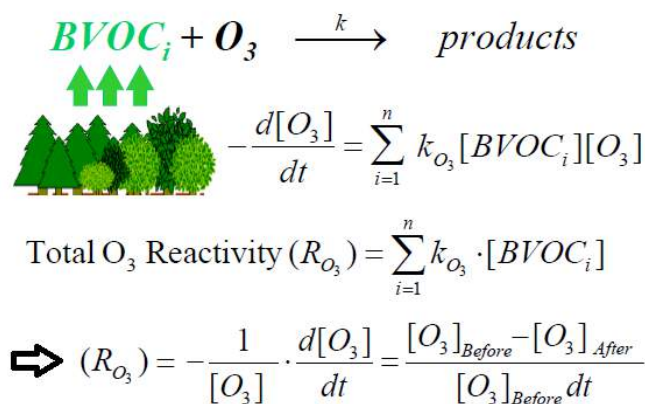


Figure 2: Derivation of the formula to calculate total ozone reactivity from the measurements (Poster presentation of P. Jeong-Hoo, 2013).

Typical flow values are indicated in Fig. 1, but these need to be modified depending on the type of sample measured. Due to the different reaction rate of various compounds with ozone, the residence time in the reactor needs to be adjusted (e.g. short residence time for reactive compounds), which can be difficult to achieve for mixtures of compounds with very different reaction rate values. The system needs also to be characterized to correct R_{O_3} from errors caused by O_3 wall losses. In addition, water vapour can cause artefacts in ozone analyzer, especially rapid changes in relative humidity, thus additional dryers before inlets of ozone analyzer are used.

With the setup depicted in Fig. 1, the system's detection limit for emission measurements with stable conditions is $4.4 \cdot 10^{-5} \text{ s}^{-1}$ (which corresponds to roughly 0.15 ppb, 19 ppb and 125 ppb of β -caryophyllene, α -pinene and isoprene respectively). This is why ambient air measurements are difficult due to generally

lower concentrations and more challenging conditions. Nevertheless, direct emission measurements are conducted with enclosure systems. Branches from a tree are enclosed in Teflon film enclosures and the reactivity of the emissions is measured using a dynamic flow through technique (Hakola et al., 2006). A zero air generator is used for producing VOC- and oxidant-free incoming air for the enclosure. VOCs and O₃ reactivity are measured from the outgoing air.

CONCLUSIONS

Preliminary results show that this method can be used to measure ozone reactivity for relatively high concentrations or BVOCs. This is suitable for reactivity measurements from emissions but makes measurement in ambient conditions challenging. Furthermore the instrument needs to be carefully characterized (e.g. wall losses, water interference) in order to avoid any bias in the results. Emission measurements in the boreal forest and Arctic tundra will be performed in the future to verify that the chemical characterization from these emissions are consistent with the observed reactivity.

ACKNOWLEDGEMENTS

This work is supported by Academy of Finland (decision 307797).

REFERENCES

- Atkinson, R., (2000). Atmospheric chemistry of VOCs and NO_x. *Atmos. Environ.* 34 (39), 2063-2101.
- Atkinson, R., Arey, J., (2003). Atmospheric degradation of volatile organic compounds. *Chem. Rev.* 103 (34), 4605-4638.
- Guenther, A., C. N. Hewitt, D. Erickson, R. Fall, C. Geron, T. Graedel, P. Harley, L. Klinger, M. Lerdau, W. A. McKay, T. Pierce, B. Scholes, R. Steinbrecher, R. Tallamraju, J. Taylor, and P. Zimmerman (1995). A global model of natural volatile organic compound emissions. *J. Geophys. Res.*, 100, 8873-8892.
- Hakola, H., V. Tarvainen, J. Bäck, H. Ranta, B. Bonn, J. Rinne, and M. Kulmala (2006). Seasonal variation of mono- and sesquiterpene emission rates of Scots pine. *Biogeosciences*, 3, 93-101.
- Kulmala, M., T. Nieminen, R. Chellapermal, R. Makkonen, J. Bäck, and V.-M. Kerminen (2013). Climate Feedbacks Linking the Increasing Atmospheric CO₂ Concentration, BVOC Emissions, Aerosols and Clouds in Forest Ecosystems, pp. 489-508. *Springer Netherlands, Dordrecht*.
- Lelieveld, J., T. M. Butler, J. N. Crowley, T. J. Dillon, H. Fischer, L. Ganzeveld, H. Harder, M. G. Lawrence, M. Martinez, D. Taraborrelli, and J. Williams (2008). Atmospheric oxidation capacity sustained by a tropical forest, *Nature*, 452, 737-740.
- Matsumoto, J. (2014). Measuring Biogenic Volatile Organic Compounds (BVOCs) from Vegetation in Terms of Ozone Reactivity. *Aerosol Air Qual. Res.*, 14, 197-206.
- Nölscher, A. C., J. Williams, V. Sinha, T. Custer, W. Song, A. M. Johnson, R. Axinte, H. Bozem, H. Fischer, N. Pouvesle, G. Phillips, J. N. Crowley, P. Rantala, J. Rinne, M. Kulmala, D. Gonzales, J. Valverde-Canossa, A. Vogel, T. Hoffmann, H. G. Ouwersloot, J. Vila-Guerau de Arellano, and J. Lelieveld (2012). Summertime total OH reactivity measurements from boreal forest during HUMPPA-COPEC 2010. *Atmos. Chem. Phys.*, 12, 8257-8270.
- Yang, Y., M. Shao, X. Wang, A. C. Nölscher, S. Kessel, A. Guenther, and J. Williams (2016). Towards a quantitative understanding of total OH reactivity: A review. *Atmos. Environ.*, 134, 147-161.

RELATIONSHIP BETWEEN EXTREME TEMPERATURE EVENTS IN THE WINTER, FREEZING INJURY AND FOLLOWING SUMMERS GROWTH ON PINE AND SPRUCE

L. LINDFORS^{1,2}, V. HURRY² and T. HÖLTTÄ¹

¹Institute for Atmospheric and Earth System Research / Forest Sciences
Faculty of Agriculture and Forestry, University of Helsinki, Finland

²Department of Forest Genetics and Plant Physiology at Swedish University of Agricultural Sciences (SLU) / Umeå Plant Science Centre.

Keywords: Climate change, freezing injury, elastic modulus, dynamic modelling.

INTRODUCTION

Conifers are the most abundant plants in the northern hemisphere where very low temperatures occur frequently. Knowledge of the impact of winter on boreal ecosystem is limited, even though it constitutes a significant part of the year. Many studies have recently highlighted the important role of various biological and ecological processes that take place in the winter (Brooks et al. 2011). For instance, winter can play a significant role in the net carbon exchange between forest ecosystems and the atmosphere (Monson et al 2006) despite frozen soil and low air temperatures. Conifers and other perennial plants in the boreal region undergo metabolic process of cold acclimation in advance of sub-zero temperatures to achieve cold hardiness. Cold hardened living cells in plants are able to avoid freezing, partly due to the chemical properties of the ice, that occupies intercellular spaces in trees in the winter. Ice has a desiccative effect on the cells which causes them to shrink as their water content decreases. Decrease in the water content also decreases the equilibrium freezing temperature of the cell sap. As the chemical potential of ice is temperature dependent (Rajashekar and Burke, 1982), lower temperatures cause the living cells to shrink to ever smaller diameters. This mechanism is also known to cause small but measurable shrinking of tree stem diameter and it has been used to study tree physiology in the winter (Zweifel and Häsler, 2000). Cold hardening also protects the photosynthetic apparatus from the sub-freezing temperatures, which is particularly harmful when combined with high light. In the spring rapid de-hardening must occur in order for the trees to be able to maximize carbon uptake during the short growing period. Winter survival requires a well-timed adaptation that is driven by temperature and phenology. Budburst, which is a critical for this adaptation, has been predicted to take place approximately 10 days earlier in 2051–2080 than in 1971–2000 in northern Europe (Olsson 2017). Frequency of early freezing injury in the spring for spruce has been predicted to increase, that is caused by the earlier de-hardening and late freezing temperatures (Schlyter et al. 2006).

The aim of this project is to study extreme temperature events in the winter and to identify events of freezing injury in pine and spruce trees by monitoring the elastic modulus of the tree. Freezing injuries will be compared to how the trees grew on the following summer. This will help us understand how pine and spruce may have different sensitivity on climate change.

METHODS

The relationship between extreme temperature events, freezing injury and following summer's growth rates will be studied at three experimental forests. For pine the relationship will be studied at Hyytiälä and Värriö stations in Finland and for spruce at Svartberget station in Sweden. On each station several trees are measured with dendrometers to monitor how stem of the trees changes during the winter. New dendrometer system was recently (10/2019) purposely-build to serve this project (see picture 1) at the Svartberget station, which belongs to ICOS infrastructure and to the Swedish University of Agricultural Sciences. Diameter change measurements as well as tree temperature data will be used to estimate the elastic modulus of the

stem with 1-3 day temporal interval, for each tree separately. The estimation will be done using a recently published mechanistic dynamic model (Lindfors et al. 2019), in combination with machine learning algorithm. The model simulates the water exchange between living cells and ice through a semi-permeable membrane, which is driven by changes in ice temperature and chemical potential of ice.



Picture 1. An illustration of how the new dendrometer measurement system was set-up on four spruce stems at the Svartberget experimental forest in north Sweden. The white shelters around the trees protect sensors and sensor-holding-frames from sunlight, rain, snow and falling ice. The same trees also include sap flow measurements, which are installed under the metallic wrap around the trees, found under the white shelters. The white box on top of a pole holds a data logger that collects data from the sensors.

ACKNOWLEDGEMENTS

This work was supported by the Finnish Cultural Foundation and the Kalle and Dagmar Vålímáa fund.

REFERENCES

- Brooks, P. D., P. Grogan, P. H. Templer, P. Groffman, M.G. Öquist and J. Schimel (2011). Carbon and nitrogen cycling in snow-covered environments. *Geography Compass*, 5(9), 682-699.
- Monson, R. et al. (2006). *Nature* 439, 711-714.
- Monson, R. K., D. L. Lipson, S. P. Burns, A.A. Turnipseed, A.C. Delany, M.W. Williams and S.K. Schmidt (2006). Winter forest soil respiration controlled by climate and microbial community composition. *Nature*, 439(7077), 711.
- Rajashekar, C.B. and M.J. Burke (1982). Liquid water during slow freezing based on cell water relation and limited experimental testing. In: Li, P.H., Sakai, A. (Eds.), *Plant Cold Hardiness and Freezing Stress—Mechanisms and Crop Implications*. Academic Press, New York, pp. 211–221.
- Schlyter, P., I. Stjernquist, L. Barring, A.M. Jönsson and C. Nilsson (2006). Assessment of the impacts of climate change and weather extremes on boreal forests in northern Europe, focusing on Norway spruce. *Climate Research*, 31(1), 75-84.
- Olsson, C., S. Olin, J. Lindström and A.M. Jönsson (2017). Trends and uncertainties in budburst projections of Norway spruce in Northern Europe. *Ecology and evolution*, 7(23), 9954-9969.
- Zweifel, R. and R. Häsler (2000). Frost-induced reversible shrinkage of bark of mature subalpine conifers. *Agric. For. Meteorol.* 102, 213–222.

VEGETATION PHENOLOGY LINKED TO CO₂ FLUXES IN THREE NORTHERN PEATLANDS

M. LINKOSALMI¹, M. AURELA¹, J.-P. TUOVINEN¹, M. PELTONIEMI², C. M. TANIS¹, A. N. ARSLAN¹, T. MARKKANEN¹, O. NEVALAINEN¹, J. RAINNE¹ and T. LAURILA¹

¹Finnish Meteorological Institute (FMI), 00101 Helsinki, Finland.

²Natural Resources Institute Finland (LUKE), Helsinki, Finland.

Keywords: Vegetation phenology, CO₂ fluxes, peatlands.

INTRODUCTION

Boreal peatlands store high amounts of terrestrial carbon (C) accumulated due to limited decomposition rates in anaerobic conditions (Gorham, 1991). The worldwide coverage of boreal peatlands is about 3% of the total land area, but as a C storage, their portion is as much as 30% of the global C pool (Gorham, 1991; Turunen et al., 2002). The changing climate and land use changes can, however, affect the greenhouse gas exchange of the peatland ecosystems. To better understand these phenomena and the factors affecting them, we studied the vegetation phenology and the related carbon dioxide (CO₂) fluxes in three northern natural peatlands. Vegetation phenology refers to the seasonal changes in plant physiology, biomass and leaf area (Migliavacca et al., 2011; Sonnentag et al., 2011 & 2012; Bauerle et al., 2012). Bud burst, development of the leaves, flowering and senescence are examples of the phenological events that can be easily detected visually. The phenology is affected by many abiotic factors, such as precipitation, temperature, radiation and water availability (Bryant and Baird, 2003; Körner and Basler, 2010). The seasonal variations in leaf area, stomatal conductance, photosynthesis and respiration further affect the gas exchange between the plant and atmosphere (Richardson et al., 2013). The climate change may affect the abiotic factors and thus change the soil and vegetation features (Richardson et al., 2013; Migliavacca et al., 2012), and further the gas exchange between the plant and atmosphere. Greenness indices derived from digital camera images have been associated with vegetation activity and C uptake in forests and peatlands (e.g. Sonnentag et al., 2012; Peichl et al., 2015; Linkosalmi et al., 2016; Peltoniemi et al., 2017). Digital camera observation is an inexpensive, continuous and effective tool for monitoring vegetation phenology, it provides vegetation community or even species level information on the changes in the vegetation. Further, these near-surface measurements can be used as verification of remote sensing products or ecosystem models.

METHODS

We monitored the vegetation phenology with digital cameras (StarDot Netcam SC 5) in three northern peatlands: Halssiaapa in Sodankylä (N67°22.117', E26°39.244', 180m a.s.l.), Lompolojänkkä in Pallas area (N67°59.842', E24°12.569', 269m a.s.l.) and Kaamanen (N69°08.435', E27°16.189', 155m a.s.l.). Images were taken every 30 minutes and transferred automatically to a remote server. The cameras were adjusted in an angle of 45° and facing north. The cameras were shooting mostly the ground vegetation, but also the sky was visible in the images. The images from year 2015 to 2019 were then analyzed with the FMIPROT, a toolbox for image processing for phenological and meteorological purposes (see description in Tanis et al., 2018). Colour fraction indices were derived from the images with the program. Here, we mainly used the Green Chromatic Coordinate (GCC):

$$GCC = \frac{\Sigma G}{\Sigma R + \Sigma G + \Sigma B}$$

where ΣG , ΣR , ΣB are the sums of green, red and blue channel indices of all pixels comprising an image. In addition to a more general picture of the vegetation (including many vegetation types), also more specific Regions of Interest (ROIs) were chosen based on different vegetation groups. We only analysed the images during the growing season and daytime. The GCC was then combined with meteorological measurements and CO₂ flux data. The ecosystem–atmosphere CO₂ exchange was measured by the micrometeorological eddy covariance (EC) method, which provides continuous CO₂ data averaged on an ecosystem scale. Also, supporting meteorological variables, such as air and soil temperature, air and soil humidity, water table level and different radiation components, were measured at all sites.

CONCLUSIONS

The start and the end of the growing season are clearly visible in the development of greenness: the GCC starts to increase when the vegetation begins to grow in the spring and it declines when the autumn senescence appears. When the vegetation evolves, also the photosynthesis starts. Thus, the development of GCC and GPP go well in line in springtime and during the growing season. Also, incidents in abiotic factors affect the GCC development. For example, cold spring delays the development of GCC or cold periods during the growing season affects the GCC. The effect of the composition of the vegetation is visible, when the GCC of different sites are compared: The Lompolojännkä is the richest in nutrients and this reflects the vegetation and thus, the site produces highest GCC values.

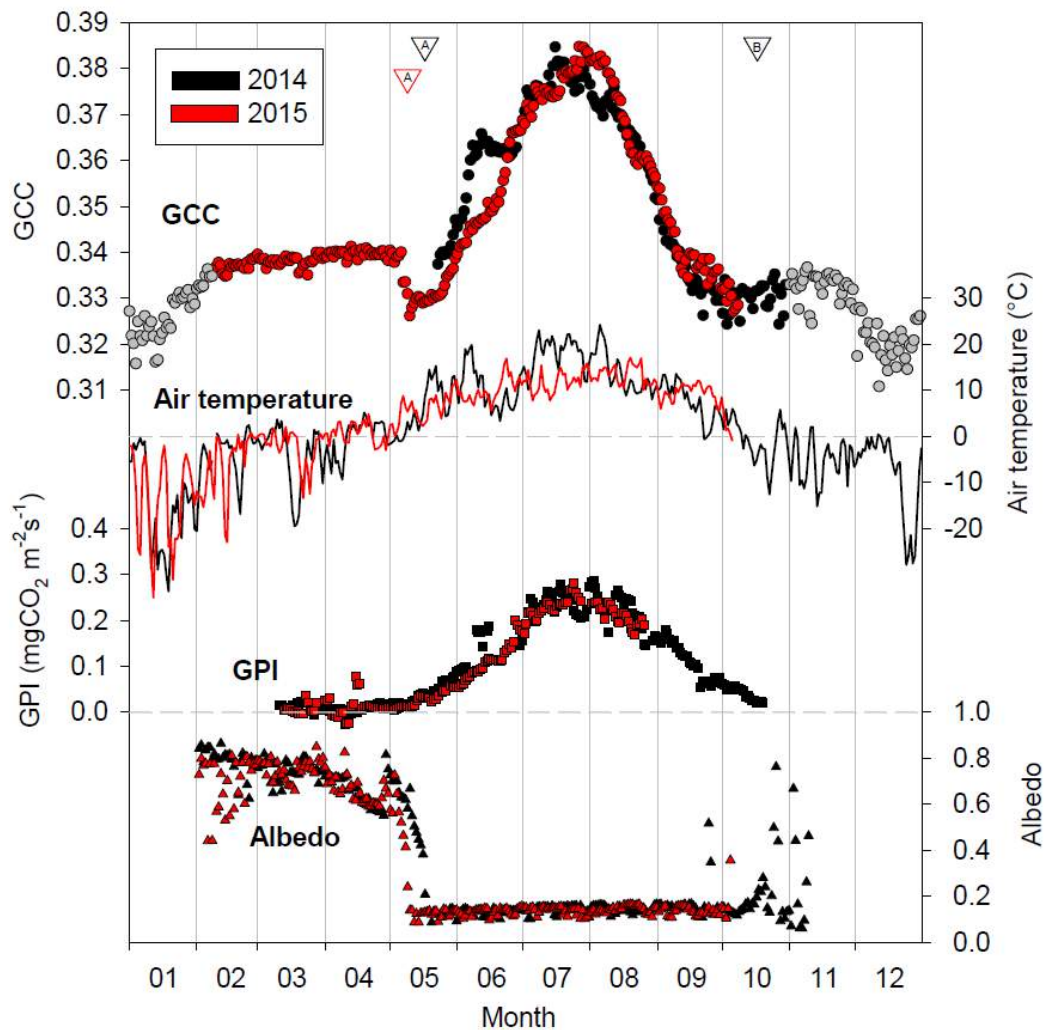


Figure 1. Example of the mean daytime GCC, daily mean air temperature, gross photosynthesis index (GPI) and albedo in 2014–2015 in Halssiaapa, previously presented in Linkosalmi et al., 2016. GPI indicates the maximal photosynthetic activity in optimal radiation conditions (see Aurela et al., 2001). The (A) indicates the dates of snow melt and (B) snow appearance. The grey circles indicate the wintertime data in an insufficient light level.

ACKNOWLEDGEMENTS

This work was supported by the European Commission through EU Life+ project MONIMET Project (LIFE12ENV/FI/000409) during 2013–2017.

REFERENCES

- Aurela, M., J.-P. Tuovinen and T. Laurila (2001). Net CO₂ exchange of a subarctic mountain birch ecosystem, *Theor. Appl. Climatol.* **70**, 135–148.
- Bauerle, W.L., R. Oren, D.A. Way, S.S. Qian, P.C. Stoy, P.E. Thornton, J.D. Bowden, F.M. Hoffman and R.F. Reynolds (2012). Photoperiodic regulation of the seasonal pattern of photosynthetic capacity and the implications for carbon cycling, *P. Natl. Acad. Sci. USA* **109**(22), 8612–8617.
- Bryant, R. G. and A.J. Baird (2003). The spectral behaviour of Sphagnum canopies under varying hydrological conditions, *Geophys. Res. Lett.* **30**(3), 1134–1138.
- Gorham, E. (1991). Northern peatlands: Role in the carbon cycle and probable responses to climatic warming, *Ecological Applications* **1**(2), 182–195.
- Körner, C. and D. Basler (2010). Warming, photoperiods, and tree phenology response, *Science* **329**, 278.
- Linkosalmi, M., M. Aurela, J.-P. Tuovinen, M. Peltoniemi, C.M. Tanis, A.N. Arslan, P. Kolari, K. Böttcher, T. Aalto, J. Rainne, J. Hatakka and Laurila, T. (2016). Digital photography for assessing the link between vegetation phenology and CO₂ exchange in two contrasting northern ecosystems, *Geosci. Instrum. Meth.* **5**, 417–426.
- Migliavacca, M., M. Galvagno, E. Cremonese, M. Rossini, M. Meroni, O. Sonnentag, G. Manca, F. Diotri, L. Busetto, A. Cescatti, R. Colombo, F. Fava, U. Morra di Cella, E. Pari, C. Siniscalco, C., and A. Richardson (2011). Using digital repeat photography and eddy covariance data to model grassland phenology and photosynthetic CO₂ uptake, *Agr. Forest Meteorol.* **151**, 1325–1337.
- Migliavacca, M., O. Sonnentag, T.F. Keenan, A. Cescatti, J. O’Keefe, and A.D. Richardson (2012). On the uncertainty of phenological responses to climate change, and implications for a terrestrial biosphere model, *Biogeosciences* **9**, 2063–2083.
- Peichl, M., O. Sonnentag and M.B. Nilsson (2015). Bringing color into the picture: Using digital repeat photography to investigate phenology controls of the carbon dioxide exchange in a boreal mire, *Ecosystems* **18**, 115–131.
- Peltoniemi, M., M. Aurela, K. Böttcher, P. Kolari, J. Loehr, J. Karhu, M. Linkosalmi, C.M. Tanis, J.-P. Tuovinen and A.N. Arslan (2018). Webcam network and image database for studies of Phenological changes of vegetation and snow cover in Finland, image time series from 2014 to 2016, *Earth Syst. Sci. Data* **10**, 173–184.
- Richardson, A. D., T.F. Keenan, M. Migliavacca, Y. Ryua, O. Sonnentag, and M. Toomey (2013). Climate change, phenology, and phenological control of vegetation feedbacks to the climate system, *Agr. Forest Meteorol.* **169**, 156–173.
- Sonnentag, O., M. Detto, R. Vargas, Y. Ryu, B.R.K. Runkle, M. Kelly, and D.D. Baldocchi (2011). Tracking the structural and functional development of a perennial pepperweed (*Lepidium latifolium* L.) infestation using a multi-year archive of webcam imagery and eddy covariance measurements, *Agr. Forest Meteorol.* **151**, 916–926.
- Sonnentag, O., K. Hufkens, C. Teshera-Sterne, A.M. Young, M. Friedl, B.H. Braswell, T. Milliman, J. O’Keefe and A.D. Richardson (2012). Digital repeat photography for phenological research in forest ecosystems, *Agr. Forest Meteorol.* **152**, 159–177.
- Tanis, C.M., M. Peltoniemi, M. Linkosalmi, M. Aurela, K. Böttcher, T. Manninen and A.N. Arslan (2018). A system for acquisition, processing and visualization of image time series from multiple camera networks, *Data*, **3**.
- Turunen, J., E. Tomppo, K. Tolonen and A. Reinikainen (2002). Estimating carbon accumulation rates of undrained mires in Finland – application to boreal and subarctic regions, *The Holocene* **12**, 69–80

BARK EVAPORATION AND CO₂ EXCHANGE IN A SEMI-ARID FOREST, ISRAEL

A. LINTUNEN^{1,2}, Y. PREISLER³, I. OZ³, X. CHEN⁴, D. YAKIR³, and T. HÖLTTÄ²

¹Institute for Atmospheric and Earth System Research / Physics, University of Helsinki

²Institute for Atmospheric and Earth System Research / Forest Sciences, University of Helsinki

³Weizmann Institute of Science, Israel

⁴Key Laboratory of Vegetation Restoration and Management of Degraded Ecosystems, South China Botanical Garden, Chinese Academy of Sciences

Keywords: DROUGHT, BARK EVAPORATION, LENTICELL, STEM PHOTOSYNTHESIS.

INTRODUCTION

Plants need a protective barrier to avoid water loss due to the water potential gradient between the inner plant parts and the surrounding environment. Plant parts that have secondary growth, such as tree stems, are isolated with outer bark. However, the bark cannot totally isolate the plant from the surrounding environment, as oxygen diffusion through the lenticels in the bark is required for respiration to take place and CO₂ to diffuse out. Lenticels are static pores that act as air channels that intersperse the outer bark (Groh *et al.*, 2002; Geigenberger, 2003; Rosner and Kartusch, 2003; Lenzian, 2006; Wittmann and Pfanz, 2008). In contrast to stomatal control, gas exchange through the bark is only regulated by long-term structural changes. Thus, we hypothesize that the ratio of gas exchange through bark to the whole tree gas exchange is proportionally large and physiologically important during periods of drought when gas exchange in leaves is minimized with closed stomata, but lenticels remain open.

METHODS

The research site is located in a semi-arid forest in Israel, next to a desert. Five pairs of *Pinus halepensis* trees were measured (one branch per tree, see Fig. 1) for 3 to 120 days at a control and irrigated site right next to each other in summer 2019. The irrigation started in May 2017. Pre-dawn water potential is 2 MPa lower in control trees compared to irrigated trees during the summer months. Stomata are (nearly) closed in trees of the control site during the dry summer months, whereas they are open in the trees of the irrigated site.

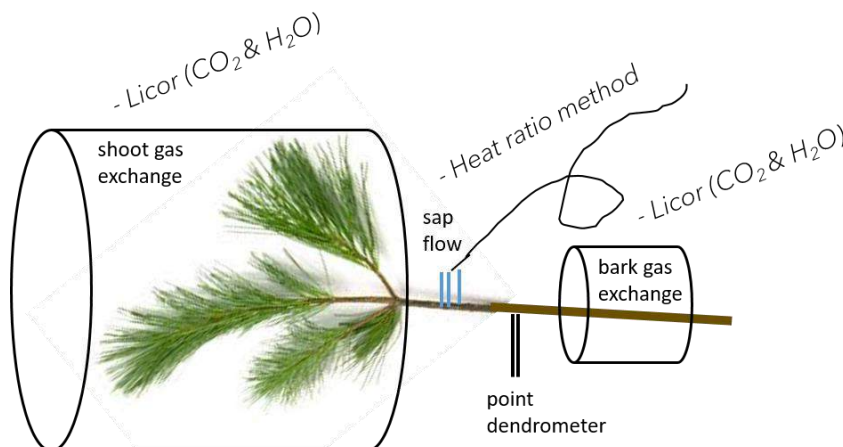


Figure 1. The measurement setup in a branch. From each intact sample branch, we measured exchange of CO₂ and water vapour from a needle-bearing shoot and from a branch segment without any needles. From the same branch, also sap flow (heat ratio method) and branch diameter changes (point dendrometers) were measured.

PRELIMINARY RESULTS

Evaporation and CO₂ emission were observed from all measured branches (Fig. 2). CO₂ emission was always higher in the irrigated trees. Also evaporation through bark was in most cases (but not always) higher in irrigated than in control trees.

Evaporation through bark and transpiration from shoots per surface area were of similar size in the control trees, because the stomata in the shoots were closed. In the irrigated trees, transpiration per needle area was 20-fold compared to control trees or compared to evaporation through bark. Photosynthesis per needle area was 13-fold compared to bark photosynthesis in irrigated trees, whereas the difference was typically small in control trees.

Evaporation through bark was dependent on vapour pressure deficit (VPD) similarly in control and irrigated trees, and from June to September. There was water uptake by branches during some nights when VPD was low. Bark CO₂ emission was dependent on temperature. Control trees had always low CO₂ emission through the bark, whereas the emission from the irrigated trees decreased clearly from June to September, probably due to decreasing growth respiration.

The aim is to compare these measurements to measurements from Hyytiälä, and to scale both bark evaporation and photosynthesis to whole tree level to have an idea of their physiological importance for trees in dry conditions.

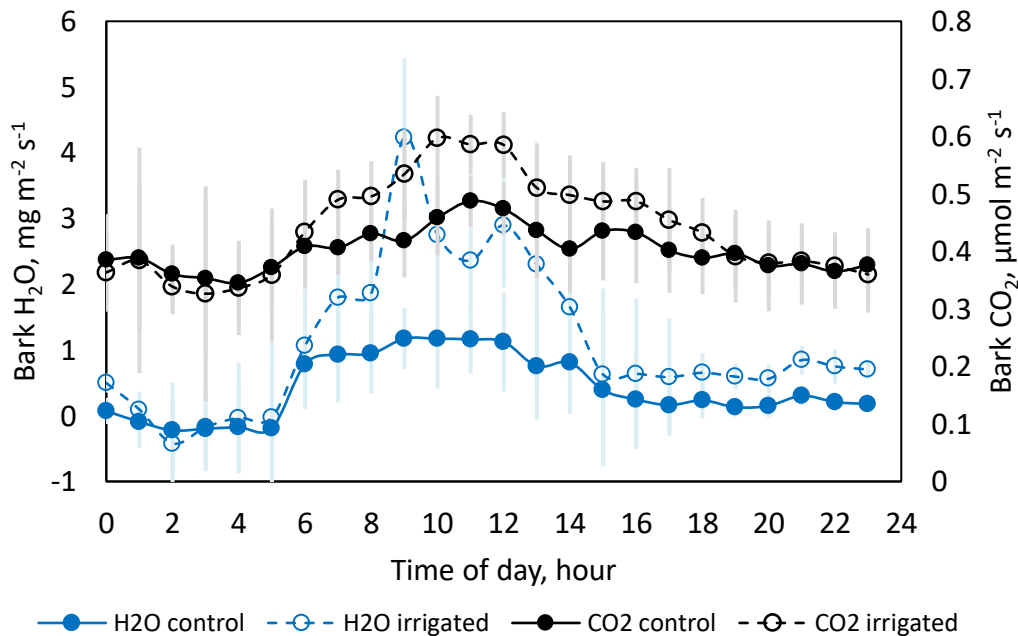


Figure 2. Evaporation and CO₂ emission through bark in a branch of a control tree and in a branch of an irrigated tree between 10th and 12th of June in 2019. Hourly averages of three days measurements are shown together with standard deviation.

ACKNOWLEDGEMENTS

Heikki Laakso, Juho Aalto and Tommy Chan are acknowledged for building the mobile gas exchange measurement system used in this study. This work is supported by the Academy of Finland post-doctoral grant 310375 and Centre of Excellence grant 307331.

REFERENCES

- Geigenberger, P. (2003). Response of plant metabolism to too little oxygen. *Curr. Opin. Plant Biol.* **6**, 247-256.
- Groh, B., Hubner, C. and K.J. Lenzian (2002). Water and oxygen permeance of phellems isolated from trees: the role of waxes and lenticels. *Planta* **215**, 794-801.
- Lenzian, K.J. (2006). Survival strategies of plants during secondary growth: barrier properties of phellems and lenticels towards water, oxygen, and carbon dioxide. *J. Exp. Bot.* **57**, 2535-2546.
- Rosner, S. and B. Kartusch (2003). Structural changes in primary lenticels of Norway spruce over the seasons. *IWA Journal* **24**, 105-116.
- Wittmann, C. and H. Pfanz (2008). Antitranspirant functions of stem periderms and their influence on cortical photosynthesis under drought stress. *Trees* **22**, 187-196.

HYDRAULIC CAUSES OF THE PRODUCTION AND ABOVEGROUND GROWTH DECLINES OF OLD SCOTS PINE

Ch. LIU^{1,2} and A. MÄKELÄ^{1,2}

¹Department of Forest Sciences, University of Helsinki, Helsinki, Finland

²Institute for Atmospheric and Earth System Research (INAR), University of Helsinki, Helsinki, Finland

Keywords: hydraulic resistance hypothesis; sapwood-specific conductivity; sap flow density.

INTRODUCTION

In order to test one of the most supported hypotheses on production and aboveground growth declines, namely the hydraulic resistance hypotheses (HRH) (Ryan & Yoder 1997; Koch *et al.*, 2004; Ryan *et al.*, 2006), we hypothesized and investigated the correlations 1) between height and sapwood-specific conductivity in branches and 2) among sap flow density, vapour deficit and irradiance in young/short and old/tall Scots pine (*Pinus sylvestris*, L.), a dominant species of boreal forest, in northern and southern Finland. Precedent works have inspired on the first correlation (e.g. West *et al.*, 1999; Tyree & Zimmermann, 2002; Olson *et al.*, 2014), but controversies still exist HRH alone or combined with nutrition (e.g. Wright *et al.*, 2004; Merilo *et al.*, 2009; Rämö *et al.*, 2012; Osnas *et al.*, 2013). Meanwhile, despite the optimization models of stomatal control have provided prototypic insights (e.g. Cowan & Farquhar, 1977; Hari *et al.*, 1986; Hari & Mäkelä, 2003; Dewar *et al.*, 2018), modelling the dynamics of sap flow responding to environmental factors on fine temporal scales is much less abundant. Thus, a quantitative study to describe the whole-tree hydraulic dynamics regarding ageing effects is of necessity. Such necessity is ampler in boreal forest, where significant changes in temperature and precipitation are likely to occur through this century by whichever Representative Concentration Pathway (RCP; IPCC, 2014). Our hypotheses are

1. The sapwood-specific conductivity of the branches atop the crowns is negatively correlated with height;
2. The young Scots pine has more effective stomatal control against vapour deficit than does the old; and
3. The water transport of the young Scots pine reacts to irradiance by a higher magnitude than that of the old.

METHODS

There were two study sites, the northern (N) one for testing Hypothesis 1 and the southern (S) one for Hypotheses 2 and 3. The N site was located near the Värriö Research Station (VRS), University of Helsinki (UH) and Station I for Measuring Forest Ecosystem-Atmosphere Relations (SMEAR I; 67.7°N, 29.6°E), and the S site near the Hyytiälä Forest Station (HFS), UH and SMEAR II (61.8°N, 24.3°E). Five or six sample trees for each of the age groups, young or old, were selected in each site. The young trees were typically no older than 70 and the old no younger than 140. Fieldwork was conducted during July and August 2017 and June and July 2018 in the N and S sites, respectively.

For Hypothesis 1, the two-year-old segments of the topmost branches were used in measurement. There were three replicates at each height. The configuration and computation followed Grönlund *et al.* (2016) (see Table 1 for all the algebraic notation):

$$K_S = \frac{Ql}{\rho gha}$$

Tree-average K_S over the three replicates was used in the subsequent analyses.

Table 1. Algebraic notation in this work. In Status, C = constant, P = parameter, V = variable.

Name	Status	Meaning	Typical unit
K_S	V	Sapwood-specific conductivity	$\text{m}^3 \text{m}^{-1} \text{Pa}^{-1} \text{s}^{-1}$
Q	V	Flow rate, averaged every 15 min over 2 h	g s^{-1}
d	V	Branch sample under-bark diameter	cm
l	V	Branch sample length	cm
a	V	Branch sample cross-section area	cm^2
ρ	C	KCl solution density	kg m^{-3}
g	C	Gravitational acceleration	m s^{-2}
h	V	Water head height	m
E	V	Transpiration rate	$\text{mol m}^{-2} \text{s}^{-1}$
A	V	Photosynthetic rate	$\text{mol m}^{-2} \text{s}^{-1}$
t	V	Time	s or 10-min
g_s	V	Stomatal control	m s^{-1}
λ	P	Marginal water cost of carbon gain	mol mol^{-1}
ζ	P	Reflecting λ and atmospheric $[\text{CO}_2]$	--
D	V	Vapour deficit	mol m^{-3}
I	V	Photosynthetic photon flux rate (PPFD)	$\text{mmol m}^{-2} \text{s}^{-1}$
J	V	Whole-tree average sap flow density	m s^{-1}
τ	P	Elapsed time between E and J	10-min
β	P	Fitted coefficients; subscripts follow the notation above	(varying)

For Hypotheses 2 and 3, the optimization models of stomatal control were simplified to enable empirical testing, where the time point of optimized stomatal status was defined as (Cowan and Farquhar, 1977; Hari *et al.*, 1986)

$$\arg \min_t \int_{t_1}^{t_2} (E(t) - \lambda A(t)) dt$$

and the optimal stomatal conductance at that time can be written as

$$g_s = (\sqrt{\zeta/D} - 1) f_I(I)$$

and thus

$$E = 1.6 g_s D = 1.6 D (\sqrt{\zeta/D} - 1) f(I) \equiv f_D(D) f_I(I)$$

Considering light response $f(I)$ is usually expressed in a function with decreasing slope towards an asymptote (saturation) (e.g. Hari & Mäkelä, 2003), both $f_D(D)$ and $f_I(I)$ can be approximated empirically by power function provided D is large enough to have (-1) omitted and I not extremely high to saturate the light-response curve. Therefore, there is

$$E = \beta_0 D^{\beta_D} I^{\beta_I}$$

To substitute E by J , τ (typically < 120 min) was accounted in the following autoregressive log-log model applied to each sample tree

$$\ln J_t = \beta'_0 + \beta_D \ln D_{t-\tau} + \beta_I \ln I_{t-\tau}$$

Having removed the best explanatory lag that allowed the highest adjusted R^2 among all the tested τ values, we fitted it again on the age-group level by introducing a categorical factor (B , $B = 0$ for young and $B = 1$ for old trees). In this analysis of covariance (ANCOVA), all the seven possibilities of B affecting single or multiple coefficients were tested along with a general model without B .

The measurement of J basically followed Granier (1987) and Lu *et al.*, (2004), and the definition of baseline voltage followed Oishi *et al.*, (2008). Four pairs of probes at NW, SW, SE and NE were installed into each sample tree. For each sector, the correction by Clearwater *et al.*, (1999) was applied when the sapwood depth was thinner than probe length, and the scaling by the gamma distribution was conducted when the sapwood was thicker than probe length (Berdanier *et al.*, 2016). The whole-tree sapwood density was the mean of that of each direction weighted by the central angles. The data were averaged every ten minutes.

D was calculated from the air temperature, relative humidity and I directly available as PPFD measured at SMEAR II at heights of 16.8 m and 33.6 m (for the young and the old sample trees, respectively).

CONCLUSIONS

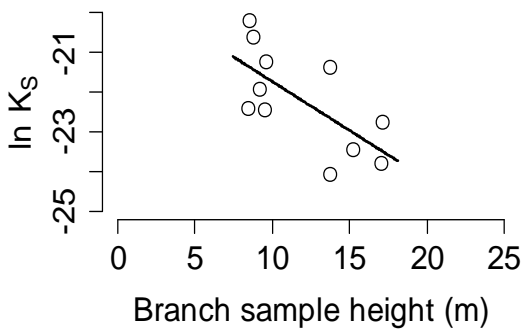


Figure 1. Correlation between $\ln K_s$ of topmost branches of Scots pine and their height. Of the fitted line, Slope = -0.246 , adjusted $R^2 = 0.404$, $P = 0.02$.

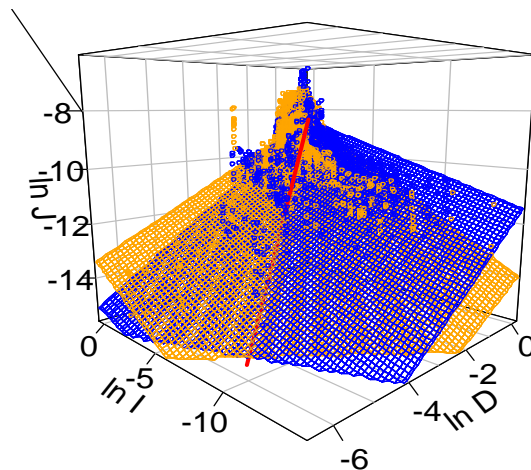


Figure 2. Correlation among $\ln J$, $\ln D$ and $\ln I$ of young (blue) and old (orange) Scots pine. The fitted planes intersect at the red line. Of all coefficients $P < 0.001$.

The sapwood-specific conductivity of topmost branches was found significantly decreasing with height (Figure 1), supporting Hypothesis 1. In the ANCOVA, the best-performing model was with B affecting the coefficients of D and I but not the intercept. Hence, the sap flow density of old Scots pine was more driven by D while that of young more by I (Figure 2). These results support Hypotheses 2 and 3 within, however, particular ranges related to the partial derivatives of J to D or I . These results provide insights into 1) the impacts of mechanical tissues' growth and local xeric conditions on fine branch conductivity, 2) the decline of whole-tree leaf- to sapwood-area ratio with tree height as a compensation for higher evaporative demand and 3) a faster decline of the slope of light response of old Scots pine after the initial value.

ACKNOWLEDGEMENTS

This work was technically supported by all staff of VRS and HFS, UH, and financially by the Finnish Society of Forest Sciences (SMS) Expenditure Grant 201810042 to Ch. L. and by the Academy of Finland 312635 to A. M.

REFERENCES

- Berdanier, A.B., C.F. Miniati and J.S. Clark (2016). Predictive models for radial sap flux variation in coniferous, diffuse-porous and ring-porous temperate trees, *Tree Physiology* **36**(8), 932-941.
- Clearwater, M.J., F.C. Meinzer, J.L. Andrade, G. Goldstein and N.M. Holbrook (1999). Potential errors in measurement of nonuniform sap flow using heat dissipation probes, *Tree Physiology* **19**(10), 681-687.
- Cowan, I.R. and G.D. Farquhar (1977). Stomatal function in relation to leaf metabolism and environment. In: *Integration of Activity in the Higher Plant* (ed. D.H. Jennings), (Cambridge University Press, Cambridge, U.K.).
- Dewar, R., A. Mäkelä, T. Hölttä, B. Medlyn and T. Vesala (2018). New insights into the covariation of stomatal, mesophyll and hydraulic conductances from optimization models incorporating nonstomatal limitations to photosynthesis, *New Phytologist* **217**(2), 571-585.
- Granier, A. (1987). Evaluation of transpiration in a Douglas-fir stand by means of sap flow measurements, *Tree Physiology* **3**(4), 309-320.
- Grönlund, L., T. Hölttä and A. Mäkelä (2016). Branch age and light conditions determine leaf-area-specific conductivity in current shoots of Scots pine, *Tree Physiology* **36**(8), 994-1006.
- Hari, P. and A. Mäkelä (2003). Annual pattern of photosynthesis in Scots pine in the boreal zone, *Tree Physiology* **23**(3), 145-155.
- Hari, P., A. Mäkelä, E. Korpilahti and M. Holmberg (1986). Optimal control of gas exchange, *Tree Physiology* **2**(1-3), 169-175.
- IPCC (2014). *Climate Change 2014: Synthesis Report, Contribution of Working Groups I, II and III to the Fifth Assessment Report of the Intergovernmental Panel on Climate Change*, (IPCC, Geneva, Switzerland).
- Koch, G.W., S.C. Sillett, G.M. Jennings and S.D. Davis (2004). The limits to tree height, *Nature* **428**(6985), 851.
- Lu, P., L. Urban and P. Zhao (2004). Granier's thermal dissipation probe (TDP) method for measuring sap flow in trees: theory and practice, *Acta Botanica Sinica (English Edition)* **46**(6), 631-646.
- Merilo, E, I. Tulva, O. Räm, A. Kükit, A. Sellin and O. Kull (2009). Changes in needle nitrogen partitioning and photosynthesis during 80 years of tree ontogeny in *Picea abies*, *Tree* **23**(5), 951-958.
- Oishi, A.Ch., R. Oren and P.C. Stoy (2008). Estimating components of forest evapotranspiration: a footprint approach for scaling sap flux measurements, *Agricultural and Forest Meteorology* **148**(11), 1719-1732.
- Olson, M.E., T. Anfodillo, J.A. Rosell, G. Petit, A. Crivellaro, S. Isnard, C. León-Gómez, O. Alvarado-Cárdenas and M. Castorena (2014). Universal hydraulics of the flowering plants: vessel diameter scales with stem length across angiosperm lineages, habits and climates, *Ecology Letters* **17**(8), 988-997.
- Osnas, J.L., J.W. Lichstein, P.B. Reich and S.W. Pacala (2013). Global leaf trait relationships: mass, area, and the leaf economics spectrum, *Science* **340**(6133), 741-744.
- Räm, O., E. Kaurilind, L. Hallik and E. Merilo E (2012). Why does needle photosynthesis decline with tree height in Norway spruce? *Plant Biology* **14**(2), 306-314.
- Ryan, M.G., N. Phillips, B.J. Bond (2006). The hydraulic limitation hypothesis revisited, *Plant, Cell & Environment* **29**(3), 367-381.
- Ryan, M.G. and B.J. Yoder (1997). Hydraulic limits to tree height and tree growth, *Bioscience* **47**(4), 235-242.
- Tyree, M.T. and M.H. Zimmermann (2002). *Xylem Structure and the Ascent of Sap* (2nd Ed.), (Springer-Verlag Berlin Heidelberg, New York, U.S.A.).
- West, G.B., J.H. Brown and B.J. Enquist (1999). A general model for the structure and allometry of plant vascular systems, *Nature* **400**(6745), 664.

DECREASING TRENDS OF BLACK CARBON IN SOUTHERN FINLAND

K. LUOMA¹, J.V. NIEMI², H. TIMONEN³, M. AURELA³, A. HELIN³, A. KOUSA², T. RÖNKKÖ⁴, A. VIRKKULA^{1,3}, T. PETÄJÄ¹

¹Institute for atmospheric and Earth system research / Physics, Faculty of Science, University of Helsinki, P.O. Box 68, 00014 Helsinki, Finland.

²Helsinki region environmental services authority, P.O. Box 100, 00066 Helsinki, Finland.

³Atmospheric Composition Research, Finnish Meteorological Institute, P.O. Box 503, 00101, Helsinki, Finland.

⁴ Aerosol Physics, Faculty of Natural Sciences, Tampere University of Technology, P.O. Box 692, 33101 Tampere, Finland

Keywords: BLACK CARBON, LONG-TERM TREND, AIR QUALITY

INTRODUCTION

Black carbon (BC) is highly absorbing carbonaceous material emitted in combustion processes. BC is one of the most notable warming agents in global warming (Bond et al., 2013). However, compared to greenhouse gases, the lifetime of BC in the atmosphere is short and therefore decreasing BC emissions would have a rather fast effect on the radiative forcing. BC can also be used as an indicator about air quality. World Health Organization (WHO) reported that combustion related particulate matter (PM) has more adverse health effects than PM from other sources (Krzyżanowski et al., 2005). Since BC is a by-product of combustion, observing BC in addition to PM gives additional information about the health effects of PM (Janssen et al., 2012).

In the Helsinki metropolitan area in southern Finland, the main sources of BC are traffic and wood burning (Helin et al., 2018). Also, part of the observed BC in southern Finland is long-range transport originating from Europe (Hienola et al., 2013). Due to the new emission standards, the emissions from traffic have decreased and we expect to see this in the BC data. Here, we show how the long-term trends of BC relate to the trends of other monitored air pollutants.

METHODS

The Helsinki region environmental services authority (HSY) has measured the BC concentration at various sites in the Helsinki metropolitan area (60° 10' N, 24° 56' E). The longest BC time series in Helsinki have been observed at a city centre site since 2011 and at an urban background site since 2012. The site in the city centre is located next to a busy street close to a busy intersection so the site is highly influenced by traffic. The urban background site is located in the downtown area, but further away from busy streets.

BC measurements conducted at the SMEAR II station since 2006 by the University of Helsinki were also included in this study. SMEAR II is located in Hyttiälä (61° 50' N, 24° 17' E) in southern Finland about 200 km north from Helsinki. Here the SMEAR II station represents a regional background site. There are no significant local sources around the station and the closest bigger cities Tampere and Jyväskylä are located about 60 and 100 km away from the station.

At the sites that were located in the Helsinki metropolitan area, the BC concentration was measured with a Multi-Angle Absorption Photometer (MAAP, Thermo model 5012). At SMEAR II the BC concentration

was measured with a MAAP since 2013 and before that with an Aethalometer (Magee Scientific model AE-31). Here, the term BC refers to the so-called equivalent black carbon (eBC), which indicates that the BC concentration was measured by optical means.

Also, measurements of NO_x and total mass of particulate matter smaller than 2.5 µm (PM_{2.5}) were used in this study. At the sites that are located in Helsinki, PM_{2.5} concentrations were measured with continuous PM monitors and at SMEAR II the PM_{2.5} was measured offline by collecting particles in a cascade impactor. The NO_x measurements were conducted with chemiluminescence analyzers.

The trends were analysed by using a seasonal Kendall test described by Gilbert (1987). The seasonal Kendall test determines the trend from monthly median values. The test estimates the slope of the trend and tests if the trend is statistically significant.

CONCLUSIONS

The concentration of BC had a statistically significant decreasing trend at all of the sites and the trends are presented in Table 1. The absolute decrease was most notable at the city centre, where the trend was -0.04 µg m⁻³ yr⁻¹. The decrease is probably due to reducing emissions from traffic. At the background sites, which do not have local sources in vicinity, the trends were smaller; -0.02 and -0.01 µg m⁻³ yr⁻¹ at the urban and regional background sites, respectively.

To compare how the trend of BC relates to the trends of other air pollutants, the trend analysis was also conducted for NO_x and PM_{2.5}, and the results are also presented in Table 1. The BC concentration decreased relatively about 6 % yr⁻¹ at all the sites that is quite similar to the trend of the NO_x, decreased from 7 to 4 % yr⁻¹. The trend of PM_{2.5} concentration decreased relatively about 3 % yr⁻¹, which is less than the relative decrease for BC and NO_x. Therefore, we can conclude that especially the amount of combustion related particles, which especially are hazardous for health, have decreased in southern part of Finland.

Table 1. The trends for BC, NO_x and PM_{2.5}, measured at the city centre, the urban background and the regional background sites. The trends were statistically significant (p-value < 0.5) for all the variables at all the sites. Table presents the absolute trends (in units of µg m⁻³ yr⁻¹) and the relative trends (in units of % yr⁻¹). The relative trends were determined by dividing the absolute trend by the overall median of the variable.

	City centre (trend/year)	Urban background (trend/year)	Regional background (trend/year)
BC	-0.04 µg m ⁻³ -6 %	-0.02 µg m ⁻³ -6 %	-0.01 µg m ⁻³ -6 %
NO _x	-3.11 µg m ⁻³ -7 %	-0.80 µg m ⁻³ -5 %	-0.04 µg m ⁻³ -4 %
PM _{2.5}	-0.24 µg m ⁻³ -3 %	-0.20 µg m ⁻³ -4 %	-0.09 µg m ⁻³ -3 %
Years included	2011, 2013 - 2018	2012 - 2018	2006 - 2018

ACKNOWLEDGEMENTS

This work was supported by the Academy of Finland Centre of Excellence in Atmospheric Science (grant no. 307331) and the Regional innovations and experimentations funds AIKO governed by the Helsinki Regional Council (project HAQT, AIKO014).

REFERENCES

- Bond, T. C., Doherty, S. J., Fahey, D. W., Forster, P. M., Berntsen, T., DeAngelo, B. J., Flanner, M.G., Ghan, S., Kärcher, B., Koch, D. & Kinne, S. (2013). Bounding the role of black carbon in the climate system: A scientific assessment. *Journal of Geophysical Research: Atmospheres*, 118(11), 5380-5552.
- Gilbert, R. O. (1987). *Statistical methods for environmental pollution monitoring*. John Wiley & Sons.
- Helin, A., Niemi, J. V., Virkkula, A., Pirjola, L., Teinilä, K., Backman, J., Aurela, M., Saarikoski, S., Rönkkö, T., Asmi, E., & Timonen, H. (2018). Characteristics and source apportionment of black carbon in the Helsinki metropolitan area, Finland. *Atmospheric environment*, 190, 87-98.
- Hienola, A. I., Pietikäinen, J.-P., Jacob, D., Pozdun, R., Petäjä, T., Hyvärinen, A.-P., Sogacheva, L., Kerminen, V.-M., Kulmala, M., and Laaksonen, A. (2013). Black carbon concentration and deposition estimations in Finland by the regional aerosol–climate model REMO-HAM, *Atmospheric Chemistry and Physics*, 13, 4033-4055.
- Janssen, N. A., Hoek, G., Simic-Lawson, M., Fischer, P., Keuken, M., Atkinson, R. W., Anderson, H.R., Brunekreef, B. & Cassee, F. R. (2011). Black carbon as an additional indicator of the adverse health effects of airborne particles compared with PM10 and PM2.5. *Environmental Health Perspectives*, 119, 1691-1699.
- Krzyżanowski, M., Kuna-Dibbert, B., & Schneider, J. (Eds.). (2005). *Health effects of transport-related air pollution*. WHO Regional Office Europe.

SEASONAL DYNAMICS OF N₂O AND CH₄ FLUXES OF BOREAL TREE STEMS

K. MACHACOVA¹, E. VAINIO^{2,3}, O. URBAN¹, and M. PIHLATIE^{2,3,4}

¹ Global Change Research Institute of the Czech Academy of Sciences, Belidla 4a, CZ-60300 Brno, Czech Republic

² Environmental Soil Science, Department of Agricultural Sciences, University of Helsinki, PO Box 56, FI-00014 Helsinki, Finland.

³ Institute for Atmospheric and Earth System Research/Forest Sciences, University of Helsinki, PO Box 27, FI-00014 Helsinki, Finland.

⁴ Viikki Plant Science Centre (ViPS), University of Helsinki, PO Box 56, FI-00014 Helsinki, Finland

Keywords: METHANE, NITROUS OXIDE, FOREST, GHG EXCHANGE

INTRODUCTION

Boreal forest soils are a natural source of nitrous oxide (N₂O) and a sink of methane (CH₄). N₂O is naturally produced within soils in a wide range of nitrogen (N) turnover processes, including mainly nitrification and denitrification processes. While N₂O production is predominant, N₂O can also be reduced to N₂ in the denitrification processes (Wrage et al. 2001; Smith et al. 2003; Rütting et al. 2011). According to the traditional paradigm CH₄-oxidizing bacteria (methanotrophs) function in aerobic soil layers, while CH₄-producing archaea (methanogens) require anaerobic conditions. Thus, methanotrophy is a prevailing process in dry soils, while methanogenesis predominates in wet soils.

In general, trees can contribute to ecosystem N₂O and CH₄ exchange (1) by transporting the gases from soil to the atmosphere (Pihlatie et al. 2005; Machacova et al. 2013; Pangala et al. 2015), (2) by producing these gases in situ in the plant tissues (Smart & Bloom 2001; Keppler et al. 2006), (3) by consuming these gases from the atmosphere (Machacova et al. 2017; Haikarainen et al. 2019), or (4) indirectly by altering the soil biochemical or physical conditions, and thus the CH₄ production and consumption, as well as N turnover processes (Yu & Chen 2009; Praeg et al. 2017). Regarding the transportation processes, both N₂O and CH₄ are suggested to be transported in the transpiration stream (Pihlatie et al. 2005; Machacova et al. 2013; Barba et al. 2019). However, while N₂O is well water-soluble (Yu et al. 1997), CH₄ is not and thus it can also be transported in air-filled pore-space (Armstrong 1980), such as aerenchymatic tissues common in wetland plants (Armstrong et al. 1994).

Recent research has revealed that not only herbaceous plants but also trees can be significant sources of both N₂O and CH₄ (Machacova et al. 2016; Wen et al. 2017; Barba et al. 2019). Ecologically relevant studies on the N₂O exchange of mature trees growing in natural field conditions are rare. Tree CH₄ exchange is mainly studied at the temperate zone, while the trees at the boreal zone has not gained much attention. Furthermore, studies on the seasonality of the tree CH₄ and N₂O fluxes have been lacking. Here, we quantified the stem N₂O and CH₄ fluxes year-round from the dominant boreal trees: Scots pine (*Pinus sylvestris*), Norway spruce (*Picea abies*), as well as downy and silver birch (*Betula pubescens* and *B. pendula*).

METHODS

We measured the stem fluxes of N₂O and CH₄ from mature pine, spruce and birch trees from June 2014 to May 2015 at the SMEAR II (*Station for Measuring Ecosystem-Atmosphere Relations*) Hyytiälä ICOS (*Integrated Carbon Observation System*) site. We selected three plots with naturally different soil moisture

(*volumetric water content*, VWC). At the wet (mean annual VWC $0.81 \text{ m}^3 \text{ m}^{-3}$) and moderately wet (VWC $0.40 \text{ m}^3 \text{ m}^{-3}$) plots we measured fluxes from three trees per each species, and at the dry plot (VWC $0.21 \text{ m}^3 \text{ m}^{-3}$) from three pines (no other tree species were present). Together with the tree stems, we measured the forest floor N_2O and CH_4 fluxes at the study plots. There were three forest-floor-flux points both at the wet and moderately wet plot, and six points at the dry plot. The forest floor fluxes were measured always at the same time with the tree flux measurements at each plot.

The fluxes of both the stems and the forest floor were measured with closed chamber technique. The stem chambers were attached ca. 0.2 m above the soil. We used two types of stem chambers: cylindrical, covering a stem surface area of $0.083\text{--}0.258 \text{ m}^2$, and box-chambers consisting of two boxes, covering a total area of 0.0176 m^2 . The soil chambers were covering a forest floor area of 0.298 m^2 (wet and moderately wet plots) or 0.116 m^2 (dry plot). During the chamber closure, manual head-space-air samples were taken with syringes, stored in glass vials, and analysed with gas chromatograph. The fluxes were calculated from the sample N_2O and CH_4 mixing ratios by using linear fit (for details of the chamber measurements, sample analyses and flux calculation, see Machacova et al. 2019).

One round of measurements from all the three plots were performed in 1–2 weeks, and all the plots were measured at least once a month – except for November and January when the conditions did not allow measurements. The fluxes of the missing months were estimated with linear interpolation using the adjacent months. The most intensive measurement period was from June to August.

In addition to the flux measurements, several environmental parameters were monitored at the site, such as soil VWC, soil and air temperature, GPP, and PAR. Soil temperature and stem CO_2 effluxes as well as ecosystem gross primary productivity (GPP) and evapotranspiration were considered as indicators of physiological activity of the trees. There was a continuous snow cover at the site from mid-December to early April.

CONCLUSIONS

All the studied tree species were on average net sources of N_2O and CH_4 at the annual scale. There was significant seasonal dynamics in the stem N_2O exchange connected to the tree physiological activity. All the studied species emitted N_2O during spring and summer (April–September), and the fluxes decreased in October (Fig. 1). Trees were exchanging small amounts of N_2O even during the dormant season, showing both small emissions and uptake, and started to emit N_2O again in March (Fig. 1).

The CH_4 exchange was more variable between the species, but the fluxes were mostly low (small emission/uptake) during the winter season. However, the birches at the wet plot started emitting again large amounts of CH_4 already in January. The CH_4 fluxes of birch and pine trees were clearly connected to the soil moisture, while the spruce fluxes not so visibly. The forest floor was mainly a sink of CH_4 , except for the wet plot which was a significant source of CH_4 in June–July, and a small source for the rest of the year. For N_2O , the forest floor was a source independently of soil moisture.

We found a strong positive correlation with evapotranspiration, which supports our hypothesis that N_2O is taken up from the soil by roots, then transported into the above-ground tree tissues in xylem via the transpiration stream. Based on the results, we suggest that there are different mechanisms driving the N_2O than CH_4 exchange of the stems.

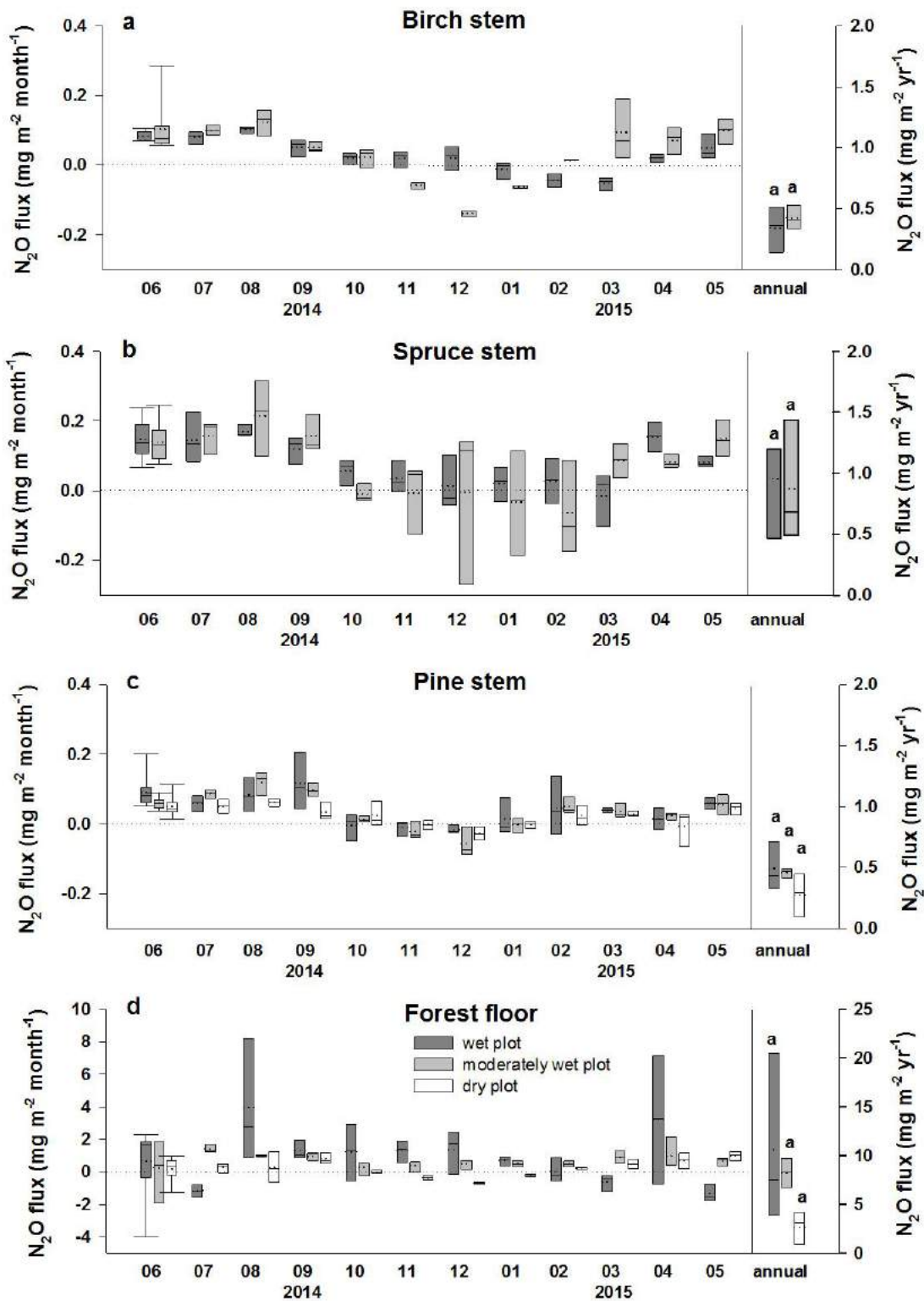


Fig. 1. Monthly and annual N_2O fluxes ($\text{mg m}^{-2} \text{ month}^{-1}$, $\text{mg m}^{-2} \text{ yr}^{-1}$, respectively) from stems of (a) birch, (b) spruce, (c) pine, and (d) forest floor between June 2014 and May 2015. Positive fluxes indicate emission, negative fluxes uptake. The solid line marks the median value, broken line the mean, box boundaries the 25th and 75th percentiles, and whiskers the 10th and 90th percentiles. Statistically significant differences among annual fluxes at $p < 0.05$ are indicated by different letters.

ACKNOWLEDGEMENTS

This research was supported by the Czech Science Foundation (17-18112Y), the Ministry of Education, Youth and Sports of the Czech Republic within the National Programme for Sustainability (LO1415), EU FP7 project ExpeER (Grant Agreement 262060), Emil Aaltonen Foundation, Academy of Finland Research Fellow projects (292699, 263858, 288494), The Academy of Finland Centre of Excellence (projects 1118615, 272041), ICOS-Finland (281255), and the European Research Council (ERC) under the European Union's Horizon 2020 research and innovation programme (Grant Agreement 757695). We thank Marian Pavelka, Jiří Dušek, Stanislav Stellner, Jiří Mikula, Marek Jakubík, Janne Levula and Matti Loponen for technical support and Uwe Großmann for IT support in data processing.

REFERENCES

- Armstrong W. (1980). Aeration in higher plants, *Advances in Botanical Research* 7, 225–332.
- Armstrong et al. (1994). Mechanisms of flood tolerance in plants, *Acta Botanica Neerlandica* 43, 307–358.
- Keppler F, Hamilton JTG, Brass M, Rockmann T. (2006). Methane emissions from terrestrial plants under aerobic conditions, *Nature* 439, 187–191.
- Machacova, K., Papen, H., Kreuzwieser, J. & Rennenberg, H. (2013). Inundation strongly stimulates nitrous oxide emissions from stems of the upland tree *Fagus sylvatica* and the riparian tree *Alnus glutinosa*. *Plant Soil* 364, 287–301.
- Machacova, K. et al. (2016). *Pinus sylvestris* as a missing source of nitrous oxide and methane in boreal forest. *Sci. Rep.* 6, 23410.
- Machacova, K., Maier, M., Svobodova, K., Lang, F. & Urban, O. (2017). Cryptogamic stem covers may contribute to nitrous oxide consumption by mature beech trees. *Sci. Rep.* 7, 13243.
- Machacova K., Vainio E., Urban O., and Pihlatie M. (2019). Seasonal dynamics of stem N₂O exchange follow the physiological activity of boreal trees, *Nature Communications*, in press.
- Pangala SR, Hornibrook ERC, Gowing DJ, Gauci V (2015). The contribution of trees to ecosystem methane emissions in a temperate forested wetland. *Global Change Biology* 21, 2642–2654.
- Pihlatie, M., Ambus, P., Rinne, J., Pilegaard, K. & Vesala, T. (2005). Plant-mediated nitrous oxide emissions from beech (*Fagus sylvatica*) leaves. *New Phytologist* 168, 93–98.
- Rütting, T., Boeckx, P., Müller, C. & Klemmedtsson, L. (2011). Assessment of the importance of dissimilatory nitrate reduction to ammonium for the terrestrial nitrogen cycle. *Biogeosciences* 8, 1779–1791.
- Smart, D. R. & Bloom, A. J. (2001). Wheat leaves emit nitrous oxide during nitrate assimilation. *Proc. Natl Acad. Sci. USA* 98, 7875–7878.
- Smith, K. A. et al. (2003) Exchange of greenhouse gases between soil and atmosphere: interactions of soil physical factors and biological processes. *Eur. J. Soil. Sci.* 54, 779–791.
- Wen, Y., Corre, M. D., Rachow, C., Chen, L. & Veldkamp, E. (2017). Nitrous oxide emissions from stems of alder, beech and spruce in a temperate forest. *Plant Soil* 420, 423–434.
- Wrage, N., Velthof, G. L., van Beusichem, M. L. & Oenema, O. (2001). Role of nitrifier denitrification in the production of nitrous oxide. *Soil Biol. Biochem.* 33, 1723–1732.
- Yu, K. W., Wang, Z. P. & Chen, G. X. (1997). Nitrous oxide and methane transport through rice plants. *Biol. Fert. Soils* 24, 341–343.
- Yu, K. & Chen, G. (2009) in *Nitrous Oxide Emissions Research Progress* (eds Sheldon, A. I. & Barnhart, E. P.) 85–104 (Nova Science Publishers, Hauppauge, NY, USA, 2009).

INTEGRATED MULTI-SCALE MODELLING FOR METEOROLOGY-CHEMISTRY-AEROSOLS INTERACTIONS

A. MAHURA¹, R. NUTERMAN², G. NEROBELOV^{3,4}, M. SEDEEVA^{3,4}, S. SMYSHLYAEV³,
M. SAVENETS⁵, L. PYSARENKO⁵, S. KRAKOVSKA⁵, S. IVANOV⁶, S. MICHAELIDES⁷,
I. RUBAN⁶, A.S. SASSI⁶, R. MAKKONEN^{8,1}, A. BAKLANOV^{9,2}, T. PETÄJÄ¹, S. ZILITINKEVICH¹,
and M. KULMALA¹

¹Institute for Atmospheric and Earth System Research (INAR), Faculty of Science, Physics / University of Helsinki (UH), P.O.Box 64, Helsinki, FI-00014, Finland.

²University of Copenhagen (UCPH), Niels Bohr Institute (NBI), Juliane Maries Vej 30, Copenhagen, DK-2100, Denmark.

³Russian State Hydrometeorological University (RSHU), Malookhtinskiy Prospekt, 98, St. Petersburg, 175176, Russia.

⁴Saint-Petersburg State University (SPBU), Universitetskaya Naberegnaya 7-9, St. Petersburg, 199034, Russia.

⁵Ukrainian Hydrometeorological Institute (UHMI), Prospekt Nauki 37, Kyiv, 03028, Ukraine.

⁶Odessa State National Environmental University (OSNEU), Lvivska Street 15, Odessa, 65016, Ukraine.

⁷The Cyprus Institute (CyI), 20 Konstantinou Kavafi Street 20, Nicosia, 2121, Cyprus.

⁸Climate System Research unit, Finnish Meteorological Institute (FMI), Helsinki, Finland.

⁹World Meteorological Organization (WMO), 7 bis, Avenue de la Paix, 1211 Geneva 2, Switzerland.

Keywords: Online Integrated Modelling, Meteorology – Chemistry – Aerosols, Direct/ Indirect/ Aerosol Effects, Pollution, PEEEX, Enviro-HIRLAM, HARMONIE

INTRODUCTION

The development and application of on-line integrated meteorology-chemistry-aerosols modelling systems is expected to be able to handle and study many existing processes and interactions, which is difficult to investigate using the off-line modelling approach. In particular, aerosols can cause various complex effects in the atmosphere at different temporal and spatial scales. This depends on origin, chemical composition, lifetime, size, shape, optical properties, etc. The modelling platform is important component of the PEEEX (Pan-Eurasian EXperiment programme; www.atm.helsinki.fi/peex) research infrastructure. In particular, the Enviro-HIRLAM/ HARMONIE models can be applied for multi-scale and –processes studies on interactions and feedbacks of meteorology vs aerosols/chemistry; aerosols vs. cloud formation and radiative forcing; boundary layer parameterizations; urbanization processes impact on changes in urban weather and climate; assessments for human and environment; improving prediction of extreme weather/ pollution events; etc. All these can be studied at different spatial (urban-subregional-regional) and temporal scales. In addition, added value to analysis is obtained through integration of modelling results into GIS environment for further risk/vulnerability/consequences/etc. studies.

METHODS AND RESULTS

The Environment – High Resolution Limited Area Model (Enviro-HIRLAM; Baklanov et al., 2017) is continued to be developed as a fully online integrated numerical weather prediction (NWP) and atmospheric chemical transport (ACT) modelling system. In our studies, it is used in the research mode. Note, that the NWP part developed by HIRLAM consortium (Undén et al., 2002) and the Enviro-components/modules were developed in collaboration with the Universities from different countries (see all references in Baklanov et al., 2017). The HIRLAM-ALADIN Research for Meso-scale Operational NWP In Europe (HARMONIE) combines elements from the global IFS/Arpege model (Déqué et al., 1994) with the ALADIN non-hydrostatic dynamics (Bénard et al., 2010). At high horizontal resolutions (<2.5 km), the forecast model and analysis system are basically linked with AROME model from Météo-France (Seity et al., 2011; Brousseau et al., 2011). Physical parametrizations from ALARO, HIRLAM (Undén et al., 2002) and ECMWF are applicable in this framework.

Aerosols Feedbacks and Interactions in Arctic-Boreal Domain

To study aerosol feedbacks and interactions at regional scale in the Arctic-boreal domain, the Enviro-HIRLAM model was employed (Mahura et al., 2019a, 2019b). It is run in a long-term mode for reference and aerosols effects (direct, indirect, combined included) and at resolution of 15-5 km. Meteorology and atmospheric composition output (at 40 model levels) are simulated simultaneously. The initial and boundary conditions are taken from ECMWF; and anthropogenic, biogenic, and natural emissions are pre-

processed. Analysis of variability for basic statistics (average, median, max, min, standard deviation) was performed for all model runs and differences between the model runs (Fig. 1). In winter, the differences between runs are less pronounced for average concentration in the Arctic regions compared with other regions (Fig1-a1,a2); but these differences are observed for max concentration, and especially for the Siberia and Ural regions of Russia (Fig. 1-a4). The average sulphur dioxide monthly concentration is larger over mid-latitudes (presence of anthropogenic sources), but maximum is also observed due to long-range atmospheric transport (Fig. 1-b1,b2). The average particular matter concentration is lower in the Arctic compared with mid-latitudes, but their composition is dominated by sea salt aerosols (Fig 1-b3,b4).

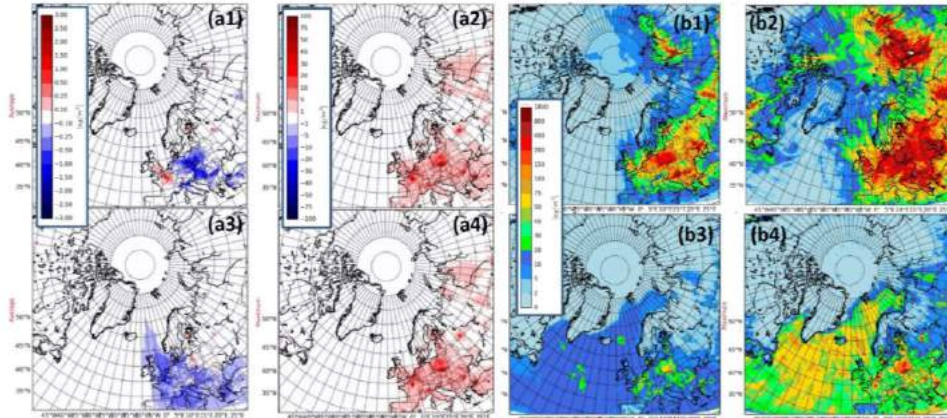


Figure 1: Enviro-HIRLAM: (a) Difference fields between CTRL&DAE (a1,a2) and CTRL&IDAE (a3,a4) model runs for monthly (January) averaged (a1,a3) and maximum (a2,a4) concentration of black carbon, BC (in $\mu\text{g}/\text{m}^3$); (b) January (12 UTC) monthly averaged (b1,b3) and maximum (b2,b4) simulated concentration (in $\mu\text{g}/\text{m}^3$) of SO_2 (b1,b2) and $\text{PM}_{2.5}$ (b3,b4) for control run.

Aerosols on Regional Scale and Zooming to Urban Areas

To study influence of aerosols on meteorological parameters for winter and summer months (January and August 2010), the Enviro-HIRLAM model was run in several modes: reference/control, CTRL (without any aerosols effects included), DAE (Direct Aerosols Effects), IDAE (InDirect Aerosols Effects), and DAE+IDAE (combined both direct and indirect effects included) (Nerobelov et al., 2019a, 2019b). The geographical area in focus is Scandinavia and North-West Russia (including zooming for metropolitan areas of St. Petersburg, Moscow and Helsinki) (Fig. 2). It was found that aerosol influence was stronger during August 2010. On regional scale, DAE decreased air temperature and total cloud cover during both months. IDEA and DAE+IDAE increased these parameters during the same period. DAE decreased specific humidity in January and increased in August, when IDEA and DAE+IDAE increased in January and decreased in August. All 3 aerosol effects decreased precipitation in both months.

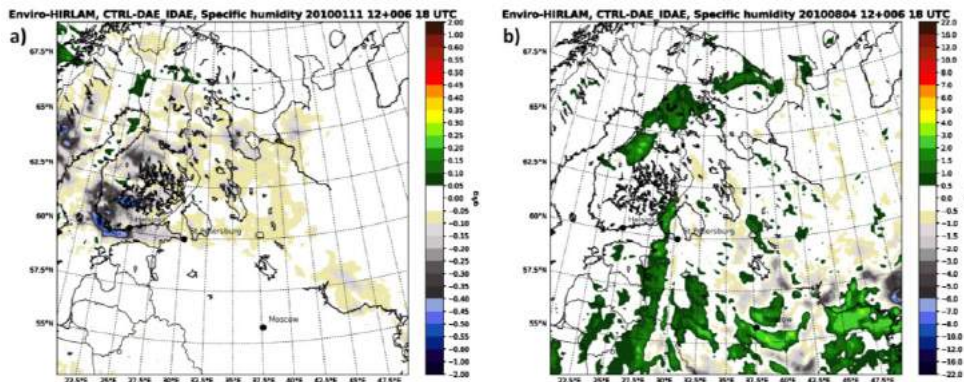


Figure 2: Enviro-HIRLAM: Difference fields between CTRL&DAE+IDAE model runs for specific humidity (in g/kg) for (a) 11 Jan 2010, 18 UTC and (b) 4 Aug 2020, 18 UTC.

At zooming on urban areas, for August, DAE decreased air temperature in St. Petersburg and Helsinki, but increased in Moscow. IDAE decreased it in St. Petersburg and increased (max 2-4°C) in other cities. Combined effect decreased air temperature in cities, but highest was in St.Petersburg. At the same time, DAE decreased total cloud cover in these cities, but IDAE and combined effects - increased. Moreover, 3

effects decreased specific humidity and precipitation (max 6 g/kg & 10 mm, respectively). In January, DAE decreased all parameters in 3 cities, except for precipitation in St. Petersburg. IDAE and combined effects increased all parameters, except for precipitation in Helsinki and for air temperature in Moscow.

Transboundary Pollution over Kola vs. Fennoscandia

To evaluate atmospheric pollution via continuous emissions of the sulphur dioxide (SO₂) from the sources of the Kola Peninsula (Russia) and deposition of sulphates on surfaces of water bodies of the Kola and Fennoscandia, the Enviro-HIRLAM and GIS (QuantumGIS - QGIS) research tools were employed (Sedeeva et al., 2019a; 2019b). Spatial-temporal changes of pollutants via variations in different meteorology-pollution fields (air temperature, wind speed and direction, precipitation, concentration, deposition) were analysed for January and August 2010. The modelled fields of SO₂ concentration and SO₄ dry deposition were integrated into GIS environment (Fig. 3a). Here, it became possible to estimate cases: when Ambient Air Standard (AAS for SO₂) was exceeded, and when the transboundary pollution took place. The max amounts of deposited sulphates on surfaces of several water bodies/reservoirs were calculated in GIS environment (Fig. 3b). Analysis showed that transboundary pollution was observed more frequently in August compared to January. Specific meteorological conditions in August such as anticyclonic circulation led to accumulation of SO₂ over Kola's territories than Fennoscandia. Often, when the SO₂ concentration had its maximum, it coincided with time of higher air temperatures. During period studied, AAS for SO₂ was exceeded 13 times: only one case over territory of Norway (Kirkenes), the rest – over different cities of the Kola Peninsula. The max value identified is more than 300 ppb. The number of cases as well as values of the sulphates' wet deposition were higher in Aug 2010. For Fennoscandia, the max value of deposited sulphates over surfaces of water reservoirs was observed on territory of Finland (47 and 2.4 kg/km² during Aug and Jan 2010, respectively). The min deposition was observed over Swedish water reservoirs (5.6 and 0.6 kg/km² during Aug and Jan 2010, respectively).

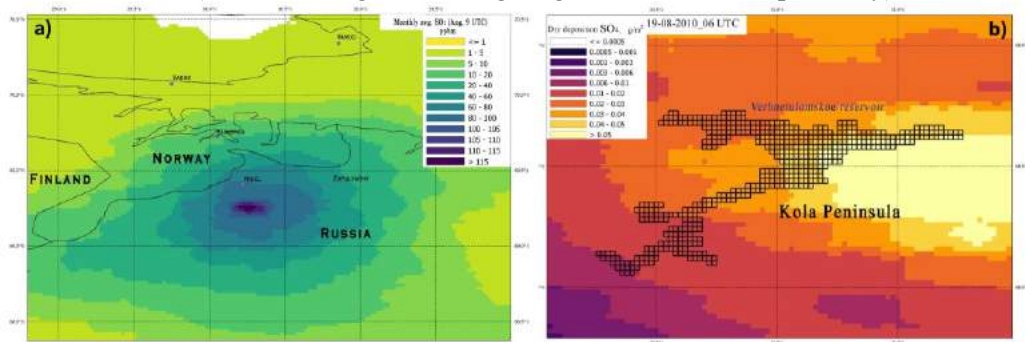


Figure 3: Enviro-HIRLAM: Modelled patterns of spatial distribution of (a) monthly averaged SO₂ concentration (in ppb) for August 2010 at 09 UTC /with focus on the Northern Fennoscandia and Kola Peninsula/, and (b) SO₄ dry deposition (in g/m²) on 19 Aug 2010 at 06 UTC /with focus on the Verkhnetulomskoe reservoir of the Kola Peninsula, Russia/.

Elevated Black Carbon Episodes vs. Forest Fires

To identify potential sources of black carbon (BC) emissions associated with forest fires and to link these to a series of elevated pollution episodes, the Enviro-HIRLAM model was used (Savenets et al., 2019). The elevated pollution levels were observed over several regions of Ukraine during 7-17 Aug 2010 (Fig. 4). These were a result of remote atmospheric transport of pollution from the north-east sector towards Ukraine. Intense fires observed during July-August on territory of Russia. However, stationary anticyclonic conditions with high air temperatures, low moisture content, frequent absence of clouds and continuous droughts facilitated severe forest fires occurred during 2-18 Aug. In overall, BC concentrations near burning areas exceeded 700 ppb (400 ppb for accumulation mode and 300 ppb for coarse mode). During initial period (2–6 Aug) the dominated circulation patterns caused atmospheric transport from burning areas towards north, east and south, and therefore, Ukraine was minimally affected by these emissions and elevated pollution levels. The first polluted air masses with high BC content appeared on 7 Aug and concentrations reached 150 ppb (for accumulation mode) and 80 ppb (for coarse mode). Because of typical for anticyclone clockwise air movement, it caused additional pollution transport towards Ukraine during 13-16 Aug. A clear fingerprint of BC atmospheric transport from forest fires was observed up to 2000 km away from the sources. Moreover, analysis of vertical profiles for BC content

showed the prevailing transport within the lowest 3-km layer (up to 700 hPa). Rarely, but BC was also observed up to 550 hPa level. Because of regular temperature inversions, these prevented pollution from faster dispersion and elevated concentrations were more frequently observed at the near-ground levels.

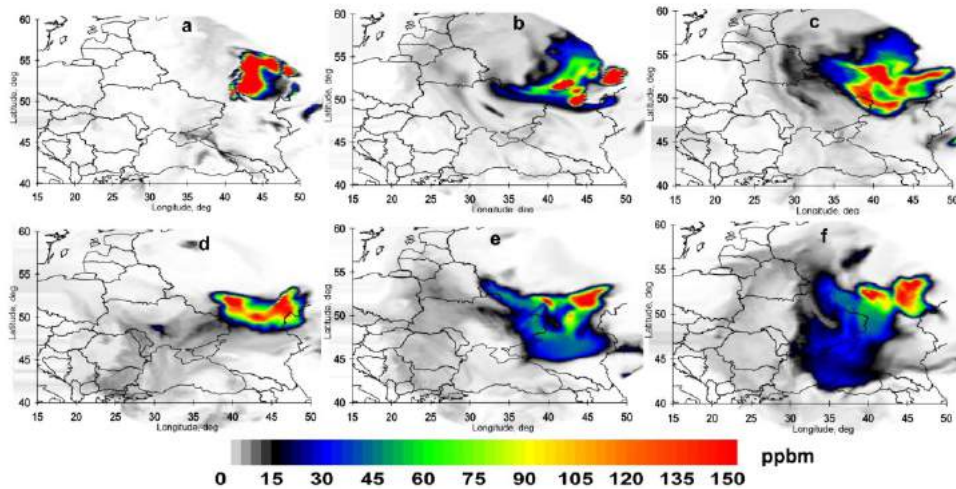


Figure 4: Enviro-HIRLAM: Spatial distribution of the black carbon (for the accumulation mode) during selected episodes of elevated concentrations at the near-surface level and dominated atmospheric transport from the north-east sectors at (a) 00 UTC on 3 Aug, (b) 18 UTC on 7 Aug, and at 06 UTCs on (c) 8 Aug, (d-e-f) 13-14-15 Aug 2010.

Mesoscale Resolution Radar Data Assimilation

The pre-processing approach was adopted for the radar reflectivity data assimilation (DA) in the HARMONIE NWP model (Ivanov et al., 2019). It creates a 3D regular grid where horizontal size of meshes coincides with horizontal resolution of the model. It minimizes a representative error associated with the discrepancy between resolutions in informational sources. After such pre-processing, the horizontal structure functions and their gradients for radar reflectivity maintain sizes and shapes of precipitation patterns similar to those of original data. The method showed improvement of precipitation prediction within radars' location areas in both the rain rates and spatial pattern. It redistributes precipitable water with smoother values over common domain since the control runs show, among several sub-domains with increased and decreased values, correspondingly; and it also reproduces the mesoscale belts and cell patterns of sizes from a few to ten km in precipitation fields (Fig. 5).

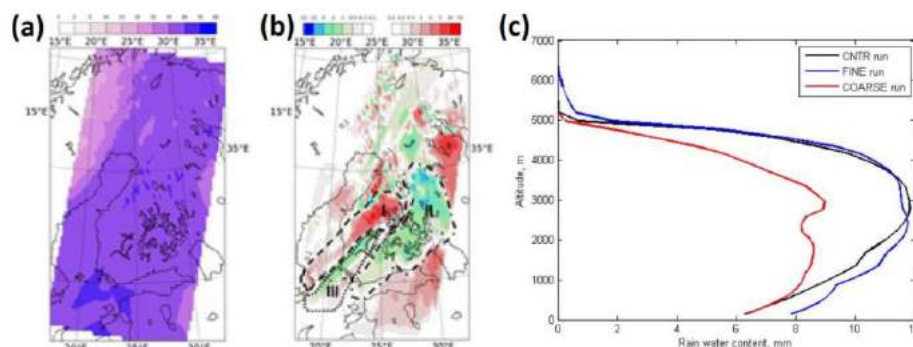


Figure 5: HARMONIE: (a) Modelled spatial distribution of precipitable water over territory of Finland in focus; (b) Impact of mesoscale radar data assimilation /areas I, II, and III outline specific regions in redistributing of precipitable water/; (c) Vertical profiles of rain water in the atmosphere for different model runs.

Due to such DA, the model simulated larger water content in mid-troposphere (within 1-6 km depth layer & major variations at 2.5-3 km). Thus, the DA system in the convection-permitting HARMONIE model has been developed by involving radar reflectivity measurements. The focus was on optimizing inner parameters used in pre-processing. To pursue a compatibility between the model resolution and smoothed radar observation density, the “cube-smoothing” approach was used. It produces presentation of radar measurements on a regular grid at a resolution equal to that of the model’s grid. This ensures equivalent presentation of precipitation (reflectivity) structures in both model and observation in a sense of equally preserving the scales of precipitation patterns. From a spectral point of view for spatial frequencies (wave

numbers), this implies an equal cut-off of a high-frequency band in model-observation fields. It leads to minimization of, at least, one component of the forecast error associated with the representativeness error.

CONCLUDING REMARKS

The models are planned to be further continued developed and applied as part of the Enviro-PEEX on ECMWF HPC (*“Pan-Eurasian EXperiment (PEEX) Modelling Platform research and development for online coupled integrated meteorology-chemistry-aerosols feedbacks and interactions in weather, climate and atmospheric composition multi-scale modelling”*) & CSC (*“Enviro-HIRLAM seamless modelling of meteorology-chemistry-aerosols interactions and feedbacks on multi-scales”*) projects as well as other ongoing/planned Horizon-2020, FP9, Nordic, AoF, etc. research projects and applied for different research tasks according to the PEEX Science Plan (PEEX, 2015). The emphasis continued to be on evaluation and testing of the online integrated approach for in-depth sensitivity analyses of mechanisms, relationships, feedbacks, interactions, etc. between chemistry-aerosols and meteorology and assessment studies in a changing climate. Moreover (see Makkonen et al., FCOE2019), science education component (as part of the PEEX Educational Platform) for the Enviro-HIRLAM model is also realised, and in particular, through organization and carrying out of the research training weeks. The latest trainings took place in April 2019 (Helsinki; Enviro-PEEX project) and June (Tyumen, Russia; AoF ClimEco project), and next ones to be carried out in April (St.Petersburg, FIRST+ PEEX-AC project) and August 2020 (Moscow, ClimEco & MegaCity projects) in Russia. Due to recent CSC’s upgrade to new HPC system, the Enviro-HIRLAM model is also migrating to new platform and computing environment (i.e. instead of using Sisu’s CRAY XC based, the Puhti/Mahti’s Atos BullSequana will be used) as well as new data storage (Allas).

ACKNOWLEDGEMENTS

Thanks to the Centre for Scientific Computing (CSC; www.csc.fi/csc) for technical support and advice. The CSC and ECMWF supercomputing facilities (CRAY-XC40) were used as part of the CSC and Enviro-PEEX projects. The ECMWF boundary conditions, meteorological and air quality observations/datasets were used for application, validation and verification of the models. The work was supported by Enviro-PEEX on ECMWF; AoF ClimEco; AoF Center of Excellence programme, CoE-ATM (grant no. 307331); and others projects.

REFERENCES

- Baklanov, A., Smith Korsholm, U., Nuterman, R., Mahura, A., Nielsen, K. P., Sass, B. H., Rasmussen, A., Zakey, A., Kaas, E., Kurganskiy, A., Sørensen, B., and González-Aparicio, I. (2017): Enviro-HIRLAM online integrated meteorology-chemistry modelling system: strategy, methodology, developments and applications (v7.2), *Geosci. Model Dev.*, 10, 2971-2999
- Bénard, P., Vivoda, J., Mašek, J., Smolíková, P., Yessad, K., Smith, Ch., Brožková, R., Geleyn, J.-F. (2010), Dynamical kernel of the Aladin-NH spectral limited-area model: Revised formulation and sensitivity experiments. *Q.J.R. Met. Soc.*, 136: 155-169
- Brousseau, P., Berre, L., Bouttier, F. and Desroziers, G. (2011), Background-error covariances for a convective-scale data-assimilation system: AROME-France 3D-Var. *Q.J.R. Meteorol. Soc.*, 137: 409-422
- Déqué M., Dreveton C., Braun A., Cariolle D. (1994): The ARPEGE-IFS atmosphere model: a contribution to the French community climate modelling. *Climate Dynamics* 10: 249-266
- Ivanov S. et al. (2019): Mesoscale resolution radar data assimilation in the Harmonie model. *Manuscript in preparation.*
- Mahura et al. (2019a): Aerosol feedbacks and interactions at regional scale in Arctic-boreal domain. *Manuscript in preparation.*
- Mahura A. et al. (2019b): Enviro-PEEX: integrated multi-scale and multi-processes modelling of meteorology-chemistry-aerosols feedbacks and interactions in weather, climate and atmospheric composition. *Manuscript in preparation.*
- Makkonen R., A. Mahura, J.-P. Keskinen, P. Zhou, J. Bian, M. Santala, J. Lento, A. Rusanen, X. Carlton, J. Hautala (FCOE2019): Earth System Modeling: Overview Of Activities.
- Nerobelov G., A. Mahura, R. Nuterman, S. Mostamandy, S. Smyshlyaev (2019a): Online integrated modeling on regional scale in North-West Russia: estimating of aerosols impact on meteorological parameters. *Submitted to the RSHU Sci.Reports journal.*
- Nerobelov G., A. Mahura, R. Nuterman, S. Smyshlyaev (2019b): Online-integrated modeling of aerosols feedbacks for the St. Petersburg, Moscow and Helsinki metropolitan areas. *Manuscript in preparation.*
- PEEX (2015): Pan-Eurasian Experiment, PEEX Science Plan. Eds. H.K. Lappalainen, M. Kulmala, S. Zilitinkevich. ISBN 978-951-51-0587-5, ISBN 978-951-51-0588-2 (on-line), 307p, www.atm.helsinki.fi/peex/images/PEEX_SP_27052015.pdf
- Savenets M. et al. (2019): Estimation of elevated black carbon periods/ episodes using Enviro-HIRLAM. *In preparation.*
- Sedeeva M., Mahura A., Nuterman R., Mostamandi S., Smyshlyaev S. (2019a): Modelling and GIS evaluation of regional pollution from Kola peninsula?. *Submitted to the RSHU Scientific Reports journal.*
- Sedeeva M., Mahura A., Nuterman R., Smyshlyaev S. (2019b): Enviro-HIRLAM modeling and GIS evaluation of pollution in Northern Fennoscandia and North-West Russia. *Manuscript in preparation.*
- Seity Y., P. Brousseau, S.Malardel, G. Hello, P. Benard, F. Bouttier, C. Lac, V. Masson (2011): The AROME-France Convective-Scale Operational Model, *MWR*, 139, 976-991
- Uden, P., L. Rontu, H. Järvinen, P. Lynch, J. Calvo, G. Cats, J. Cuhart, K. Eerola, etc. (2002): HIRLAM-5 Scientific Documentation. Dec 2002, HIRLAM-5 Project Report, SMHI.

ARCTIC DATASETS IN THE INAR'S INTERNATIONAL COLLABORATION

A. MAHURA¹, T. PETÄJÄ¹, H.K. LAPPALAINEN¹, N. ALTIMIR¹, I. BASHMAKOVA¹,
A. BORISOVA¹, S.M. NOE², E-M. DUPLISSY¹, P. HAAPANALA¹, J. BÄCK¹, L. JÄRVI¹, A. OJALA¹,
J. PUMPANEN¹, G. OBLOGOV³, A. VASILIEV³, F. PANKRATOV⁴, V. SHEVCHENKO⁵,
P. KONSTANTINOV⁶, M. VARENTSOV⁶, S. CHALOV⁶, A. BAKLANOV^{7,8}, I. EZAU⁹,
S. ZILITINKEVICH^{1,11}, and M. KULMALA¹

¹ Institute for Atmospheric and Earth System Research (INAR), Faculty of Science, Physics / University of Helsinki (UH),
P.O.Box 64, Helsinki, FI-00014, Finland.

² Estonian University of Life Sciences (EULS), Tartu, Estonia.

³ Institute of Earth Cryosphere, Tyumen Scientific Center, Siberian Branch RAS (IEC TSC SB RAS), Tyumen, Russia.

⁴ Kola Science Centre, Russian Academy of Sciences (KSC RAS), Apatity, Russia.

⁵ P.P. Shirshov Institute of Oceanology, Russian Academy of Sciences (SIO RAS), Moscow, Russia.

⁶ Moscow State University (MSU), Moscow, Russia.

⁷ World Meteorological Organization (WMO), Geneva, Switzerland.

⁸ University of Copenhagen (UCPH), Niels Bohr Institute (NBI), Copenhagen, Denmark.

⁹ Nansen Environmental & Remote Sensing Centre (NERSC), Bergen, Norway.

¹⁰ Finnish Meteorological Institute (FMI), Helsinki, Finland.

Keywords: Arctic datasets, research infrastructures, in-situ observations, PEEEX e-Catalogue, INTAROS, iCUPE, Data and Information Access Services

INTRODUCTION

The INAR is leading the Pan-Eurasian EXperiment (PEEX; www.atm.helsinki.fi/peex) initiative as an international, multi-disciplinary, multi-scale programme focused on solving interlinked global challenges influencing societies in the regions of the Northern Eurasia, including selected Arctic regions. The PEEEX Research Infrastructure's (RI) building blocks are linked to in-situ observations, remote sensing/ satellite monitoring, data systems and modelling activities. The RI has 3 components: observation component, data component and modelling component. According to the PEEEX Science Plan (PEEX, 2015) the RI main aims are: (i) to establish and sustain long-term, continuous and comprehensive ground-based, air/seaborne research infrastructures linked with remote-sensing data; (ii) to develop new datasets with continuous, comprehensive data flows; and (iii) to implement validated and harmonized data products for models of different spatio-temporal scales and –processes in focus. Observations networks will produce large volume of raw data to be pre/processed and analysed as well as delivered in a form of datasets (or products) to the research and stakeholders/end-users communities. Several steps taken are discussed here, and include an overview (as PEEEX-e-Catalogue) of measurement capacity of existing stations, linkages to Integrated Arctic Observation System (INTAROS) and Integrative and Comprehensive Understanding on Polar Environments (iCUPE).

METHODS AND RESULTS

In-Situ Atmospheric-Ecosystem Collaborating Stations

Although more than 200 stations are presented in the PEEEX regions of interest, but so far only about 60+ Russian stations have metadata information available (peexdata.atm.helsinki.fi - under request). The station metadata enables to categorize stations in a systematic manner and to connect them to international observation networks, such as the World Meteorological Organization - Global Atmosphere Watch Programme (WMO-GAWP), China Ecosystem Research Network (CERN), and perform standardization of data formats. As part of the INAR activities with Russian partners, an electronic catalogue was published (PEEX, 2019; as a living document; last updated in June 2019) to be updated with new information on stations and new stations joining the PEEEX network). The e-catalogue (www.atm.helsinki.fi/peex/index.php/peex-russia-in-situ-stations-e-catalogue) introduces information on measurements and contacts of the Russian stations in the collaboration network. The catalogue aim is to

promote research collaboration and stations as partners of the collaboration network and to give wider visibility to the stations activities.

Integrated Arctic Observation System

From 200+ stations (in total) 11 Russian stations in the Arctic region were selected for the Integrated Arctic Observation System (INTAROS; intaros.nersc.no) Atmospheric, Terrestrial and Cryospheric parts/themes. The updated metadata were obtained for these measurement stations located within the Russian Arctic territories. Metadata include basic information, physico-geographical and infrastructure description of the sites and details on atmosphere and ecosystem (soils–forest–lakes–urban–peatland–tundra) measurements. For the atmospheric part, the measurements for meteorological parameters such the air temperature, relative humidity, wind speed and direction, precipitation; and for the terrestrial and cryospheric parts, the measurements for temperature profiles of the soil/ peat layers, and soil/ peat temperature profile down to the bed rock (bore hole) can be provided. Measurements at these sites represent more local conditions of immediate surrounding environment and datasets (as time-series) are available under request.

To demonstrate ("show case") capabilities of observational s capabilities, the detailed analysis results for selected Russian station (Marre-Sale) was performed. These include inter-annual, month-to-month and diurnal cycle variabilities of meteorological and ecosystem parameters, which are underlying climatic and environmental changes observed in the Arctic regions of Russia. Moreover, trends of selected meteorological parameters were also analysed for about 100 meteorological stations located in the northern and Arctic latitudes.

In total, about 50 datasets (including those from UHEL/INAR: links to SMEAR-I station meteorology-pollution-ecosystem data and PEEEX-e-catalogue metadata for in-situ atmospheric-ecosystem collaborating stations of Russia) are presented now in the INTAROS web-based catalogue (catalogue-intaros.nersc.no/dataset) by organizations contributed, related research themes/ topics, data formats, and types of licenses (majority under the Creative Common Attribution). Themes includes atmosphere, ocean, sea ice, marine ecosystem, terrestrial, glaciology, natural hazards, and community-based monitoring. As for SMEAR-I (Station for Measuring Atmosphere-Ecosystem Relations) station, being a part of the INAR activities, it was set up in 1991. Programme includes meteorological (wind speed and direction, air temperature and relative humidity), radiation (global, reflected, net), chemistry/aerosols (CO₂, SO₂, O₃, NO_x, etc.); ecosystem, photosynthesis, irradiance related measurements (detailed information on measured parameters including instruments - www.atm.helsinki.fi/SMEAR/index.php/smear-1/measurements).

Integrative and Comprehensive Understanding on Polar Environments

The datasets (in total about 20) as products for researchers, decision- and policy makers, stakeholders and end-users communities will be produced as part of the Integrative and Comprehensive Understanding on Polar Environments (iCUPE; www.atm.helsinki.fi/icupe/index.php) activities. All these datasets are expected to be publicly available for different applications. Focusing on the Arctic region territories, the planned datasets will include novel data on anthropogenic contaminants in snow and ice cores and organic contaminants in the air-snow-water; concentrations of different chemical species and aerosols as well as their characteristics including vertical profiles; various atmosphere-hydrosphere-cryosphere-etc. related parameters in the Arctic based on ground-airborne-satellite-etc. platforms; near-real time parameters of the Arctic Research Infrastructures; others. Some datasets will focus on selected areas in northern latitudes, others - on geographical locations (measurement sites). A list of expected datasets is presented at <https://www.atm.helsinki.fi/icupe/index.php/datasets/list-of-datasets-as-deliverables>.

These planned datasets are promoted to larger science and public communities through so-called dataset "teasers" (www.atm.helsinki.fi/icupe/index.php/submitted-datasets). For Arctic regions, these include "promotional" materials on fractional snow cover area in selected sites of Svalbard islands; proxies for mixing layer height, condensation sink and gross primary production; dataset for ground-validation of precipitation measurements in high-latitudes; atmospheric mercury speciation and isotope observations; time series of lake size changes; concentration of organic contaminants, mercury and other heavy metals in annual snow and shallow core records; source apportionment of organic aerosols including source regions; occurrence, transport and exchange fluxes of emerging organic contaminants; small-scale vertical

and horizontal variability of the atmospheric boundary layer aerosol using unmanned aerial systems; absorption coefficient/ equivalent black carbon standardized dataset for long term impacts; continuous vertical observation of aerosol and cloud properties; and others. These also include those from the iCUPE Russian collaborators for the Russian Arctic: atmospheric mercury measurements at Amderma station; elemental and organic carbon over the north-western coast of the Kandalaksha Bay of the White Sea; micro-climatic features and Urban Heat Island intensity in cities of Arctic region; and others.

Since Dec 2018, so far, datasets on emerging organic contaminants in air/snow/water, anthropogenic contaminants in snow/ice cores, near-real time aerosol absorption measurements from selected regions/ locations of the Arctic were delivered (www.atm.helsinki.fi/icupe/index.php/datasets/delivered-datasets), and more are expected during 2019-2020. Majority of archived datasets (as products) are directly linked (and downloadable) at website, and corresponding Read-Me files are available with detailed description and metadata information included. Following data management plan, UHEL will maintain these datasets accessibility, and the raw data to be hosted and maintained by the datasets providers.

Selected datasets are also to be tested and integrated into several platforms. One of these is linked to COPERNICUS services. COPERNICUS is the largest data provider. To facilitate and standardize access to Copernicus data, there are 5 cloud-based online platforms known as the Data and Information Access Services (DIAS). These will provide mass storage and handling of data as well as centralized access to data, processing tools, and relevant information. The DIAS platforms (CREODIAS - creodias.eu; SOBLOO - sobloo.eu; MundiWebServices - mundiwebservices.com; ONDA - www.onda-dias.eu/cms; and WEKEO - www.wekeo.eu) allow users to explore, process, and download Copernicus data and information as well as have ability to process and combine with data from other sources. It is also possible to develop and host new applications in the cloud. Other tested platforms for pre/post-processing/analysis data include the Virtual Laboratory, VLab (vlab.geodab.org) Google Earth Engine (earthengine.google.com), Polar Thematic Exploitation Platform, Polar-TEP (portal.polartep.io), EUROGEOSS Geo Discovery and Access Broker (www.eurogeoss-broker.eu). Moreover, datasets can be also interlinked with the INTAROS web-catalogue (catalog-intaros.nersc.no/dataset).

CONCLUDING REMARKS

All types of observations (in-situ, satellite, etc.) are of critical importance for understanding processes and changes occurred in different environments including atmosphere, hydrosphere, biosphere, etc. All produced datasets are of practical importance and applicability for various models verification, and in particular those of the PEEEX-Modelling-Platform (www.atm.helsinki.fi/peex/index.php/modelling-tools-demonstration). Moreover, the PEEEX, INTAROS and iCUPE datasets and catalogues will be demonstrated and promoted during upcoming research training events such as intensive courses and young scientist summer schools (Apr and Aug 2020, in St.Petersburg and Moscow, Russia) on multi-scale processes modelling, observations and assessments for environmental applications.

ACKNOWLEDGEMENTS

The work was supported through the PEEEX programme activities, Horizon-2020 INTAROS and iCUPE and AoF ClimEco projects; AoF Center of Excellence programme (CoE-ATM; grant no. 307331); and others projects.

REFERENCES

- PEEX (2015): Pan-Eurasian Experiment, PEEEX Science Plan. Eds. H.K. Lappalainen, M. Kulmala, S. Zilitinkevich. ISBN 978-951-51-0587-5, ISBN 978-951-51-0588-2 (on-line), 307p, www.atm.helsinki.fi/peex/images/PEEX_SP_27052015.pdf
- PEEX (2019): PEEEX In-Situ Atmospheric-Ecosystem Collaborating Stations – Russian Federation ; e-Catalogue, version of June 2019; https://www.atm.helsinki.fi/peex/images/PEEX_catalogue_June_2019_Optimized_Locked.pdf
- Mahura A., T. Petäjä, H.K. Lappalainen, G. Oblogov, A. Vasiliev, A. Borisova, I. Bashmakova, N. Altimir, S. Chalov, P. Konstantinov, J. Bäck, L. Järvi, A. Ojala, J. Pumpanen, S.M. Noe, E-M. Duplissy, F. Pankratov, V. Shevchenko, M. Varentsov, A. Baklanov, I. Ezau, S. Zilitinkevich, and M. Kulmala (2019): Linking PEEEX with Russian Arctic observations and datasets. Abstracts Book of the Arctic Year of the Polar Prediction (YOPP) Science Workshop (14-16 Jan 2019, Helsinki, Finland), pp. 50-51
- Mahura A., H.K. Lappalainen, G. Oblogov, A. Vasiliev, A. Borisova, I. Bashmakova, N. Altimir, S. Chalov, P. Konstantinov, J. Bäck, T. Petäjä, S. Zilitinkevich, and M. Kulmala (2019): Russian Arctic in the PEEEX Observational System. Geophysical Research Abstracts, Vol. 21, EGU2019-10987
- Mahura A., R. Makkonen, P. Poutanen, H.K. Lappalainen, T. Petäjä, M. Boy, M. Kulmala, S. Zilitinkevich (2019): TRANSferable Knowledge and Technologies: Measuring Ecosystem-Atmosphere Relations and Multi-Scale Modelling for Assessment and Management of Environmental Impact. Geophysical Research Abstracts, Vol. 21, EGU2019-12584

IDENTIFYING GLOBAL AEROSOL-CLIMATE INTERACTIONS THROUGH GEOSPATIAL NETWORKS

R. MAKKONEN^{1,2}, J. LIU¹

¹Climate System Research unit, Finnish Meteorological Institute, Helsinki, Finland

²Institute for Atmospheric and Earth System Research / Physics, Faculty of Science, University of Helsinki, Finland

Keywords: Global aerosol, aerosol-climate interactions, network analysis

INTRODUCTION

Climate models provide an fruitful platform for generating Big Data: Coupled Model Intercomparison Project Phase 5 (CMIP5) produced already several petabytes of data, while ongoing CMIP6 is expected to surpass with potentially tens of petabytes. Large climate datasets allow application of novel data science methods, and increasing model complexity and interactivity allows exploration of undisclosed patterns, interactions and feedback mechanisms. Fountalis et al. (2014) proposed a network-analysis framework for studying climate variable patterns. The process involves identification of geographical regions based on e.g. homogeneity of a certain variable. The established regions can be further considered as nodes, and network analysis can be used to find the interconnections in the coupled system.

Global aerosol-climate models are able to produce several terabytes of data even during one-year simulation. During subsequent post-processing, there is an urgent need for reducing the amount of data, usually by reduction of temporal resolution. However, temporal averaging distorts the data, hindering the analysis of e.g. aerosol–cloud–climate interactions. Constructing spatial nodes based on variable homogeneity is one mechanism for spatial dimension reduction, while it also allows for analyzing the interactions among aerosol and precursor sources, aerosol formation, and clouds. Furthermore, cluster detection helps to assess model performance against observations, identifying e.g. spatial shifts in simulated responses to a perturbation.

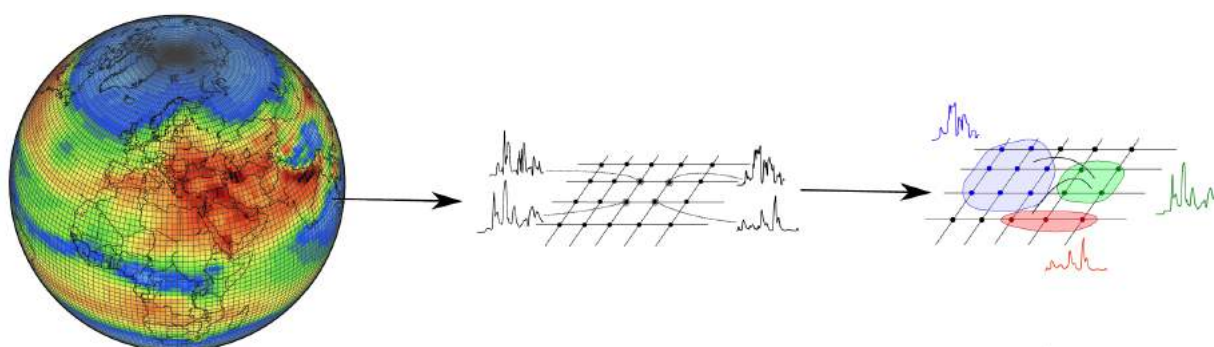


Figure 1. Initial 2D/3D regional/global geospatial datasets are produced by Earth System Models (atmosphere, land, ocean, biosphere, ...) or observations (satellite datasets). Second, the temporal behaviour can be further processed (averaging, removal of trends or seasonal cycle), or the time series can be combined with other variables. The goal of geospatial clustering is to identify continuous regions that share common factors, e.g. similar response to perturbations. Homogeneity of a region can be assessed via e.g. covariance or mutual information metrics.

METHODS

We have developed a Python-based software package which contains modules for 1) automatic cluster (node) detection from geospatial datasets and 2) network generation using correlations of the corresponding (lagged) time series. The software package reads in NetCDF-files as inputs, and provides data and figures (including maps) of detected clusters as output. The software can then detect networks between established nodes or analyze node correlation to separately given time series.

Here we present selected results of potential applications of network analysis of aerosol-climate connection. For example model input, we use ECHAM-HAM aerosol-climate model (Zhang et al., 2012).

RESULTS

In our example, we have chosen to cluster single vertical level (atmospheric column integral) data acquired from models and observations during the period 2001-2010. We deseasonalize the data throughout the period and consider only monthly anomalies. Figure 1 shows an example of clustering based on simulated cloud condensation nuclei (CCN) data (0.2% supersaturation) over oceans. In this case, the algorithm requires a minimum correlation between any two gridcell timeseries. The size of the domains is a direct consequence of selected parameter values for required homogeneity (minimum correlation).

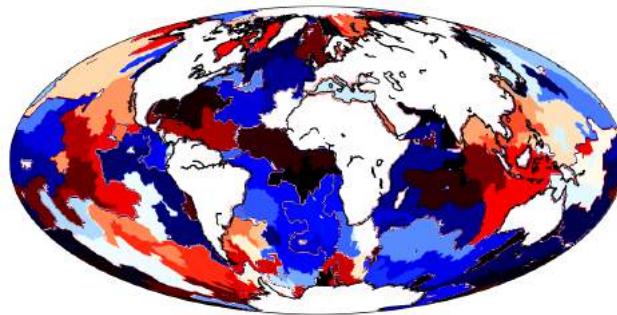


Figure 2. An example of detected clusters of monthly CCN concentration anomalies simulated by ECHAM-HAM during 2001-2010. An individual cluster would show similar response to e.g. emission or climate changes in that region. The colors only guide to distinguish different clusters.

We have applied the algorithm to anomalies in climate (temperature, precipitation) aerosol sources (anthropogenic and biogenic emissions, sea spray, dust), aerosol concentrations, and cloud properties. This allows us to detect spatial responses to perturbations and later, given a set of sensitivity simulations, attributing the aerosol-climate responses to e.g. emission sectors. Further, we have used the methodology to pinpoint certain issues in the model not being able to capture the observed anomalies.

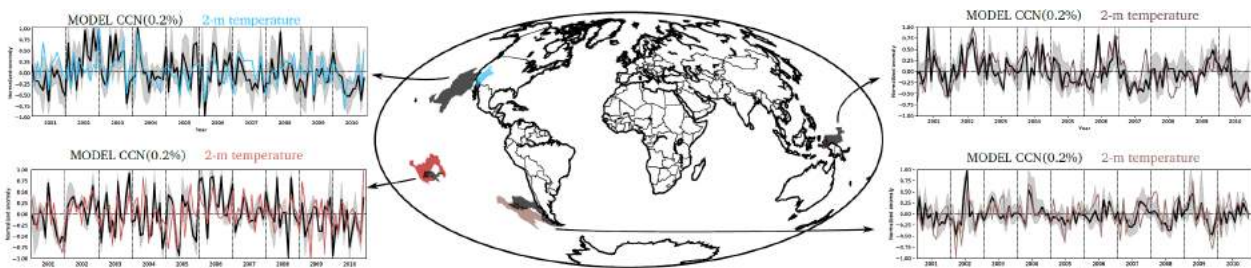


Figure 3. Examples of connecting clusters identified in two datasets, simulated CCN (black/grey) and 2-meter temperatures (coloured).

After clustering of two datasets, the tool can identify connections between clusters (Figure 3). This can be thought as a network with individual clusters as nodes, and connections in networks can be identified from cluster properties (correlation, mutual information etc.). The simulated CCN seems to be closely connected (positive correlation) to temperature in several areas, specifically close to outflow regions of continents (note that the analysis is only done for above-ocean-CCN). The strong connection could be linked to e.g. increased biogenic or wildfire emissions.

ACKNOWLEDGEMENTS

This work was supported by the Nordic Centre of Excellence eSTICC and Academy of Finland Centre of Excellence (grant no. 272041). R.M. would like to thank Athanasios Nenes for fruitful discussions.

REFERENCES

- Fountalis, I., Bracco, A. & Dovrolis, C (2014). *Clim. Dyn.*, 42: 879.
- Zhang, K. et al. (2012). The global aerosol-climate model ECHAM-HAM, version 2: sensitivity to improvements in process representations, *Atmos. Chem. Phys.* **12**, 8911–8949.

EDDY-COVARIANCE MEASUREMENTS OF CH₄ AND CO₂ FLUXES AT A BOREAL PEATLAND IN WEST SIBERIA

MAMMARELLA I.¹, ALEKSEYCHIK P.^{1,2}, KARPOV D.V.³, FILIPPOVA N.V.³, VESALA T.¹ and LAPSHINA E.D.³

¹ Institute for Atmospheric and Earth System Research INAR / Physics, Faculty of Science, University of Helsinki, Finland

² Natural Resources Institute Finland (LUKE), Helsinki, Finland

³Yugra State University, Russian Federation

Keywords: West Siberia, middle taiga, peatland ecology, carbon dioxide flux, methane flux, eddy-covariance

INTRODUCTION

Boreal peatlands, covering a large fraction of the northern hemisphere, are an important terrestrial carbon pool, whose size is estimated to be around 500 ± 100 Pg of organic carbon integrated over the entire peat depth (Yu, 2012). Photosynthesis and respiration of plant and microbial communities regulate the size of this pool. However, peatlands are also prone to rapid ecological changes related to climate, which modify the interaction between hydrology, carbon cycle, vegetation cover and micro-topography. Detailed knowledge of the processes governing the carbon exchange in northern peatlands over the course of a growing season is limited, especially with respect to the impact of relevant environmental variables.

While continuous and long-term time series of methane (CH₄) and carbon dioxide (CO₂) fluxes are already available from several boreal peatland sites in Europe, measurements of this kind are rare in Siberia (Peltola et al, 2019). This is mainly due to the lack of developed measurement sites with the infrastructure suitable for continuous monitoring of the ecosystem-atmosphere exchange processes, and frequent inaccessibility of key ecological zones and biomes. In Western Siberia, the range of CH₄ emission rates are largely uncertain, because discontinuous and short-term observations (static chamber technique) have been often used to derive regional and long-term methane emission rates (e.g. Glagolev et al., 2011; Sabrekov et al., 2011).

This study was motivated by the need and interest to fill the Siberian observational gap by establishing the eddy-covariance (EC) measurement setup in a typical West Siberian peatland. In April 2018 we have started EC measurements of methane fluxes at the Mukhrino raised bog in addition to the energy and CO₂ fluxes which were established already in 2015 (Aleksyechik et al, 2017). The objective of the project is to provide more insights into carbon cycle and greenhouse gas exchange dynamics at the wetland bog site close the Mukhrino station and to construct a long-term dataset of fluxes measured according to standardized protocols.

METHODS

Mukhrino Field Station (MFS) in the center of Western Siberia (Khanty-Mansiysk Autonomous District, Russia, <http://mukhrinostation.wordpress.com>) was established as a part of the UNESCO chair “Environmental Dynamics and Global Climate Change” of Yugra State University in 2009. MFS is located in a mixed forest/floodplain/peatland landscape 30 km South-west from the city of Khanty-Mansiysk (60°53' N; 68°42' E) on the left terrace of the Irtysh river (Figure 1).

The research activities at MFS are conducted, firstly, in peatland, and, secondly, in Irtysh floodplain. The peatland site is representative of the pristine carbon-accumulating mire ecosystems of the West Siberian Middle taiga zone. These mires cover about 60 % of the land surface of this zone, and are mainly represented by the oligotrophic rain-fed variety, bogs. Also, native old dark coniferous and mixed forests, as well as wetland and meadow graminoid vegetation in vast flood plains of Irtysh and Ob rivers are represented. The immediate vicinity of the measurement setup (the eddy-covariance footprint area) presents a complex mosaic of typical raised bog surfaces covers (hollow-hummock complexes, flarks and ponds). The hummocks are sparsely populated by pine trees ranging between 1-4 m in height. These features are found in a large proportion of the regional mires.

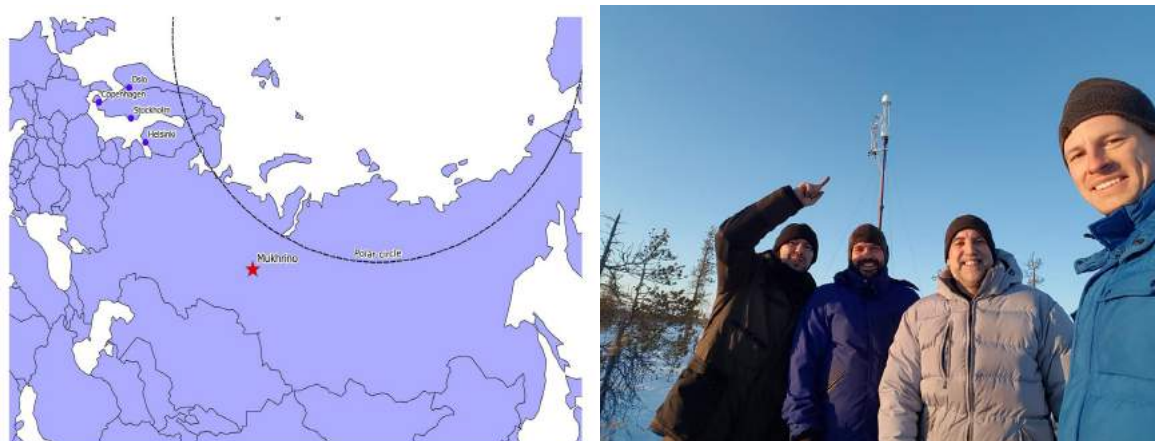


Figure 1. A map showing the Mukhrino station location (on the left) and a photo of the EC tower with us (Pavel Alekseychik and Ivan Mammarella) and our Russian collaborators (on the right).

Automatic weather station provides many parameters both in a wet hollow and in a pine-dwarf shrub-sphagnum ecosystem of oligotrophic mire, including air and soil temperature profiles, air and soil moisture, solar radiation (direct and reflected), wind speed and direction, precipitation, atmospheric pressure. Eddy-covariance (EC) measurements were launched in 2015. Currently, the EC system consists of a LI-7500 gas analyzer and a Gill R3 anemometer, providing the estimates of CO₂ and energy fluxes. The system was expanded in 2018 with the LI-7700 methane analyzer. Data processing and quality control are done in full compliance with the accepted routines; eddy-covariance data is analyzed with the EddyUH software (Mammarella et al. 2016). No similar measurements have been brought out anywhere else in the West-Siberian region; the nearest stations with equivalent setup are located approx. 1000 km to the East and South-East.

CONCLUSIONS

On average, the bog acted as net CO₂ sink and CH₄ source during the analyzed period (Fig. 2). Fluxes of CH₄ have similar magnitude as measured in Finnish peatlands (e.g. Rinne et al, 2018), having an emission peak up to 0.1 $\mu\text{mol m}^{-2} \text{s}^{-1}$ during the thawing period in May, and ranging between 0.05 and 0.1 $\mu\text{mol m}^{-2} \text{s}^{-1}$ during the summer. Largest daytime CO₂ uptake happened during July and August. The flux magnitude was somehow lower than what was measured in the more wet summer 2015 (Alekseychik et al, 2017), but larger than the dry year of 2016 (data not shown), pointing at the importance of the water availability control for the ecosystem.

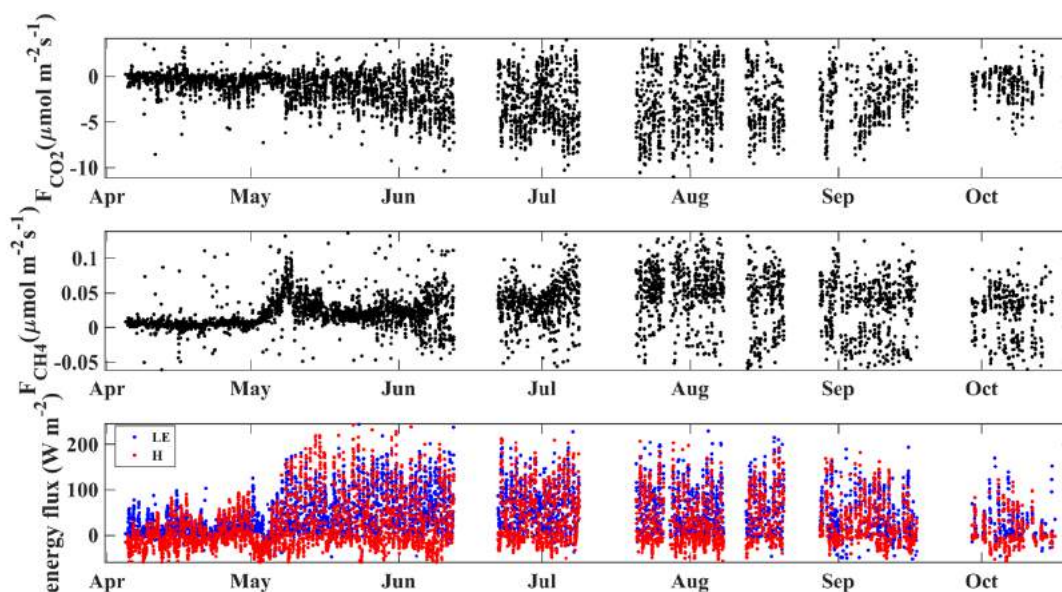


Figure 2. Time series of EC turbulent fluxes of CO₂, CH₄, sensible (H) and latent heat (LE) measured in 2019.

ACKNOWLEDGEMENTS

This work was supported by the INTERACT project GHG-FLUX+ and by the Academy of Finland Centre of Excellence program (grant 307331).

REFERENCES

- Alekseychik, P., Mammarella, I., Karpov, D., Dengel, S., Terentieva, I., Sabrekov, A., Glagolev, M., and Lapshina, E., 2017. Net ecosystem exchange and energy fluxes measured with the eddy covariance technique in a western Siberian bog, *Atmos. Chem. Phys.*, 17, 9333-9345, <https://doi.org/10.5194/acp-17-9333-2017>.
- Glagolev, M., Kleptsova, I., Filippov, I., Maksyutov, S., and Machida, T., 2011. Regional methane emission from West Siberia mire landscapes, *Environ. Res. Lett.*, 6, 045214
- Mammarella, I., Peltola, O., Nordbo, A., Järvi, L., and Rannik, Ü., 2016. Quantifying the uncertainty of eddy covariance fluxes due to the use of different software packages and combinations of processing steps in two contrasting ecosystems, *Atmos. Meas. Tech.*, 9, 4915-4933, [doi:10.5194/amt-9-4915-2016](https://doi.org/10.5194/amt-9-4915-2016)
- Peltola, O., and co-authors, 2019. Monthly gridded data product of northern wetland methane emissions based on upscaling eddy covariance observations, *Earth Syst. Sci. Data*, 11, 1263–1289, <https://doi.org/10.5194/essd-11-1263-2019>
- Rinne, J., Tuittila, E.-S., Peltola, O., Li, X., Raivonen, M., Alekseychik, P., Haapanala, S., Pihlatie, M., Aurela, M., Mammarella, I., and Vesala, T., 2018. Temporal variation of ecosystem scale methane emission from a boreal fen in relation to temperature, water table position, and carbon dioxide fluxes. *Global Biogeochemical Cycles*, 32, 1087–1106. <https://doi.org/10.1029/2017GB005747>
- Sabrekov, A. F., Glagolev, M. V., Kleptsova, I. E., Machida, T., and Maksyutov, S. S., 2013. Methane emission from mires of the West Siberian taiga, *Eurasian Soil Sci.*, 46, 1182–1193, <https://doi.org/10.1134/s1064229314010098>
- Yu, Z. C.: Northern peatland carbon stocks and dynamics: a review, *Biogeosciences*, 9, 4071–4085, <https://doi.org/10.5194/bg-9-4071-2012>, 2012.

RELATIONSHIPS LINKING SATELLITE-RETRIEVED OCEAN COLOR DATA (CHLA-PP-PAR) WITH ATMOSPHERIC COMPONENTS (MSA, SA, HIO₃, HOM, AEROSOL CONCENTRATIONS IN 10, 50 AND 100 NM) IN ARCTIC SURROUNDING AREA

M. MARBOUTI¹, S. JANG², S. BECAGLI³, T. NIEMINEN¹, G. NAVARRO⁴, M. SIPILÄ¹, M. KULMALA¹

¹Institute for Atmospheric and Earth System Research / Physics, Faculty of Science, University of Helsinki, Finland.

²Division of Environmental Science and Engineering, Pohang University of Science and Technology, Pohang, South Korea.

³Department of Chemistry, University of Florence, Sesto Fiorentino, 50019 Florence, Italy.

⁴Departamento de Ecología y Gestión Costera, Instituto de Ciencias Marinas de Andalucía (ICMAN-CSIC), Puerto Real, 11510 Cádiz, Spain.

Keywords: New particle formation, Chlorophyll a, oceanic primary production, photosynthetically active radiation, methanesulfonic acid, Sulfuric acid, highly oxidized molecules, aerosol concentrations.

INTRODUCTION

New particle formation (NPF) and the growth of particles in the atmosphere are crucial processes which have great impact on climate by contributing to the concentration of cloud condensation nuclei (CCN). Because marine aerosols and clouds can have direct and indirect impact on the Earth's radiation budget, it is known that particle formation process is important in climate regulation. The total particle number concentration in regional background conditions is very likely to be dominated by NPF especially in pristine regions such as Arctic atmosphere. Still some parts of new particle formation and growth are remained elusive. There are many ongoing laboratory experiments and field measurements concerning this topic. However, still there is a lack of data and evidence on detailed particle formation processes under natural atmospheric conditions. There are many source compounds for new particle formation and growth in the atmosphere in remote ocean such as sulfuric acid (SA), methane sulfonic acid (MSA), highly oxidized molecules (HOMs), and HIO₃. Dimethyl sulfide (DMS) produced by marine phytoplankton is the most abundant form of sulfur released into the atmosphere from the ocean (Stefels et al., 2007). DMS may have an impact on the radiative balance of the earth (Bates et al., 1987; Simo, 2001). The potential role of marine DMS in adjusting climate was introduced by Quinn et al. (2011). They highlighted that atmospheric DMS is rapidly oxidized by hydroxyl radicals and is then transformed into SA and MSA, both of which may contribute to the formation of new particles and CCN (Jang, 2016). HOMs exist in the atmosphere as forms of ion or neutral species in the gas phase (Ehn et al., 2012; Bianchi et al., 2016) and main source of HOMs is the oxidation of terpenes, which are biogenically emitted volatile organic compounds. In recent years, the importance of HOM in the atmosphere have received much interest, with studies finding that they can have significant impacts on both aerosol particle number and mass. Some previous studies revealed that HOMs can play a critical role in new particle formation process due to their low vapor pressures (Tröstl et al., 2016, Kirkby 2016) even though there is no SA in the atmosphere. It is known that oxidized iodine species can also play a role in the new particle formation, but their sources in the Arctic remain unclear (Mahajan et al., 2010; Allan et al., 2015). Coastal areas are known as the most productive area for iodine species where most of iodine production dominated by seaweeds, but also open ocean environment can produce iodine-containing compounds from as well as Arctic and Antarctic sea ice (Atkinson et al., 2012). In the sea-ice region, marine phytoplankton and sea-ice algae, especially diatoms, are responsible for the iodine production (Saiz-Lopez et al., 2015). Some of iodine oxides are formed following photolysis of reactive iodine precursors and atmospheric ozone, but most of iodine in sea-ice areas is produced by diatoms trapped within brine channels of sea ice and released to the atmosphere owing to porous property of sea ice (Saiz-

Lopez et al., 2015). It remains uncertain whether the particle formation by iodine oxide is important in remote ocean area and has relevant contribution to the atmospheric conditions.

In this study, we examined the relationships linking atmospheric in-situ data of MSA, SA, HIO₃, HOM and aerosol concentrations (with sizes of 10nm, 50nm and 100nm) with satellite-derived chlorophyll a (Chl-a), oceanic primary production (PP), and Photosynthetically Active Radiation (PAR) also as a function of sea ice concentration and extent during two time spans – the phytoplankton bloom period, April-May 2017 (30th March-1st June) and post-phytoplankton bloom; June – July 2017 (2nd June- 4th August) – in two ocean domains; Greenland and Barents sea.

METHODS

Sampling site

Field measurements were performed at Gruvebadet laboratory in Ny Ålesund (78.9° N, 11.9° E), ca. 1.5 km south from the main village (Figure 1a). A trajectory analysis was performed to identify primary source areas of atmospheric vapours and aerosols sampled at Ny Ålesund (Figure 1b). Based on trajectory analysis we divided source areas to three sectors (Figure 1a). Barents Sea with 25%, Greenland Sea with 28% and sea ice area with 44% contribution to air mass origin. The sea ice is largely dominant (about 44%) but as it is not possible to measure beneath of sea ice, so our approach cannot be used to study this area (sea ice algae). Therefore, we focus on Barents and Greenland seas.

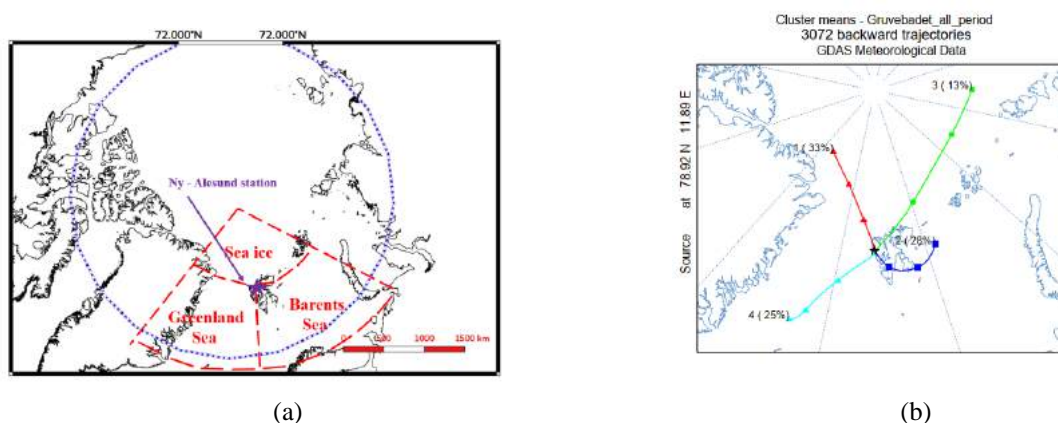


Figure 1. (a) A map of the Arctic region with the sampling site. The three main source regions for airmasses reaching Ny Ålesund are defined with red dash lines. (b) Air masses origin as indicated by a cluster analysis of the 3-day backtrajectories at 50 m starting at Ny Ålesund for 30th March to 4th August 2017.

Sampling methods

The MSA, SA, HIO₃ and HOMs were measured by a nitrate ion Chemical Ionization – Atmospheric Pressure interface - Time-of-Flight - mass spectrometer (CI-APi-ToF) described in Jokinen et al. (2012) and used in numerous previous field and laboratory studies (e.g Kirkby et al., 2016).

Satellite data and calculation of primary production

Eight-day (8D) average of PAR from the Level-3 MODIS-Aqua data sets are calculated from the NASA's Ocean Color website (<http://oceancolor.gsfc.nasa.gov/>) with a spatial resolution of 4 km. Chl-a (8D) were downloaded from OC-CCI website (<http://www.esa-oceancolour-cci.org>). The OC-CCI is a long-term, consistent and error-characterized dataset generated from merged normalized remote-sensing reflectance derived from four satellite sensors: SeaWiFS, MODIS, MERIS, and VIIRS. In this work, we have used OC-CCI v3.0, where more data have been included (VIIRS and SeaWiFS LAC). Primary Production data (8D)

were downloaded from <http://www.science.oregonstate.edu/ocean.productivity/index.php>. We used the Eppley-VGPM algorithm. The time series were computed in the two selected domains by spatially averaging the 4 km 8-day datasets. Missing values in Arctic regions are mainly due to either cloudiness or algorithm failure. However, overall there are enough cloud-free data to describe the evolution of Chl-a and PAR for our sampling site. Also monthly average of sea ice concentration anomalies and sea ice extent (SIE) were added to this study.

Ocean color time series affected by Barents and Greenland Seas and sea ice properties

The evolution of the 8-day average ocean color parameters (PP, PAR, Chl-a) for Barents and Greenland seas around of Ny Ålesund are calculated. Also monthly average of sea ice concentration anomalies and sea ice extent (SIE) were calculated and shown for April-May period and June-July period in Figure 2 and 3 to add more knowledge about sea ice melting time for year 2017 in two dominant seas. Pattern of ocean color parameters in two ocean domains in two periods was changed and connections between sea ice situation and the early phytoplankton bloom in Greenland and Barents Seas was found.

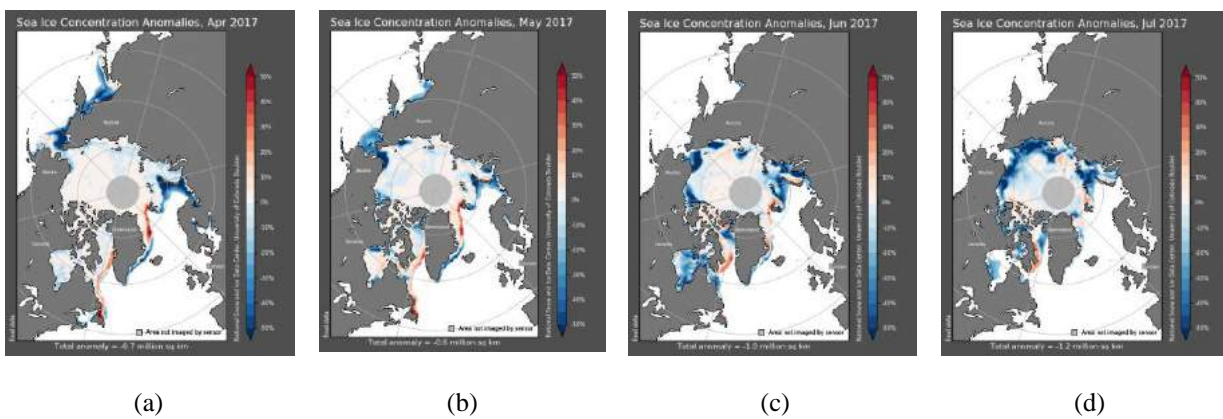


Figure 2. Monthly sea ice concentration anomalies in (a) April (b) May (c) June; (d) July in 2017.

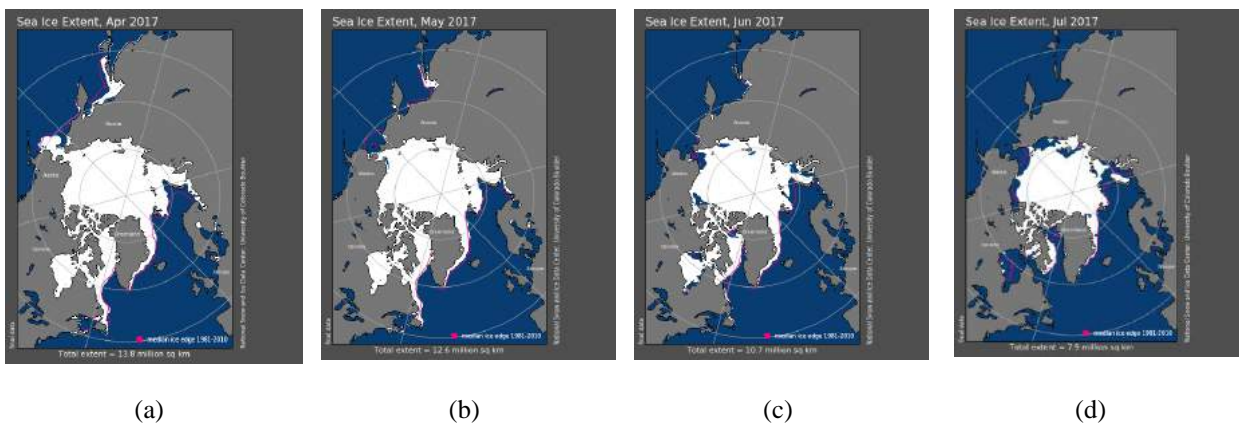


Figure 3. Monthly sea ice extents in (a) April (b) May (c) June; (d) July in 2017.

Correlation between biologic parameters and atmospheric components in April-May (phytoplankton bloom time) and June-July 2017 (post - phytoplankton bloom time).

Atmospheric measurements (MSA, SA, HIO₃, HOM, aerosol concentrations (10nm, 50nm, 100nm)) were from end of March until first of August. The period was divided to two period of bloom time (April-May) and post-bloom time (June-July) in Arctic. Correlation plots between atmospheric components and biogenic parameters were calculated in two time periods and in two ocean domains. 21 correlation plots were analysed that high correlations were found in our result that emphasis role of ocean color parameters in atmospheric components. We call R square as significant, if $P < 0.05$.

CONCLUSIONS

We investigated the relationships among Chl-a concentration, PP, PAR and atmospheric variables (MSA, SA, HIO₃, HOM, aerosol concentrations (10nm, 50nm, 100nm)) at Ny Ålesund, Svalbard islands. Atmospheric measurements at Ny Ålesund station and satellite-based measurements of Chl-a, PAR and calculations of primary production at the potential source area located in two ocean domains (Barents and Greenland Seas) based on air mass back-trajectories were used in the analysis. Monthly sea ice anomalies and sea ice extent during April–July were added to this study. The results showed that there are different relationships for different ocean domains (Greenland and Barents seas) and different seasons. Ocean color controlling factors for atmospheric components in both seas were calculated and new findings between sea ice properties, early phytoplankton bloom and ocean domains were presented

ACKNOWLEDGEMENTS

This work was supported by Institute for Atmospheric and Earth System Research (INAR), Helsinki university.

REFERENCES

- Allan, J. D. et al (2015). Iodine observed in new particle formation events in the Arctic atmosphere during ACCACIA. *Atmospheric Chemistry and Physics* **15**. Pages 5599–5609.
- Bates, T.S., Charlson, R.J., Gammon, R.H. (1987). Evidence for the climatic role of marine biogenic sulphur. *Nature* **329**, 319e321.
- Bianchi, F., Garmash, O., He, X., Yan, Ch., Iyer, S., Rosendahl, I., Xu, Zh., Rissanen, M. P., Riva, M., Taipale, R., Sarnela, N., Petäjä, T., Worsnop, D.R., Kulmala, M., Ehn, M., Junninen, H (2016). The role of highly oxygenated molecules (HOMs) in determining the composition of ambient ions in the boreal forest. *Atmospheric Chemistry and Physics* **17**. 13819–13831.
- Ehn, M., Kleist, E., Junninen, H., Petäjä, T., Lönn, G., Schobesberger, S., Dal Maso, M., Trimborn, A., Kulmala, M., Worsnop, D. R., Wahner, A., Wildt, J., Mentel, Th. F. (2012). Gas phase formation of extremely oxidized pinene reaction products in chamber and ambient air. *Atmos. Chem. Phys* **12**, 5113–5127.
- Jokinen, T., Sipilä, M., Junninen, H., Ehn, M., Lönn, G., Hakala, J., Petäjä, T., Mauldin III, R. L., Kulmala, M., and Worsnop, D. R., (2012). Atmospheric sulphuric acid and neutral cluster measurements using CI-API-TOF, *Atmospheric Chemistry & Physics* **12**, 4117–4125.
- Kirkby, J. et al (2016). Ion-induced nucleation of pure biogenic particles. *Nature* **533**, pages 521–526.
- Mahajan, A.S., Shaw, M., Oetjen, H., Hornsby, K. E., Carpenter, L. J., Kaleschke, L., Tian, X., Lee, J. D., Moller, S. J., Edwards, P., Commane, R., Ingham, T., Heard, D. E., Plane, M.C. (2010). Evidence of reactive iodine chemistry in the Arctic boundary layer. *Journal of geophysical research atmospheres* **115**.
- Quinn, P. K. et al (2016). The case against climate regulation via oceanic phytoplankton sulphur emissions. *Nature* **480**, pages 51–56.
- Saiz-Lopez, A., Blaszcak-Boxe, C. S. and Carpenter, L. J. (2015). A mechanism for biologically induced iodine emissions from sea ice. *Atmospheric Chemistry and Physics* **15**, 9731–9746.
- Simo, R., 2001. Production of atmospheric sulfur by oceanic plankton: biogeo-chemical, ecological and evolutionary links. *Trends Ecol. Evol.* **16**, 287–294.
- Stefels, J., Steinke, M., Turner, S., Malin, G., Belviso, S., (2007). Environmental constraints on the production and removal of the climatically active gas dimethylsulphide (DMS) and implications for ecosystem modeling. *Biogeochem* **83**, 245–275.
- Tröstl, J. et al (2016). The role of low-volatility organic compounds in initial particle growth in the atmosphere. *Nature* **533**, pages 527–531.
-

THE CONTRIBUTION OF PHYLLOSPHERIC MICROBES ON NITROUS OXIDE FLUXES OF NORWAY SPRUCE

I.N.J. MARTIKAINEN^{1,2}, A. PUTKINEN^{2,3}, J. PUMPANEN¹, M.K. PIHLATIE^{2,3}, and H.M.P. SILJANEN¹,

¹Biogeochemistry Research Group, Department of Environmental and Biological Sciences
University of Eastern Finland
Kuopio, P.O. Box 1627, Finland.

²Environmental Soil Science, Department of Agricultural Sciences, University of Helsinki
P.O. Box 56, Finland.

³Institute for Atmospheric and Earth System Research / Forest Sciences
University of Helsinki, P.O. Box 27, Finland.

Keywords: NITROUS OXIDE, PHYLLOSPHERE, NOSZ,

INTRODUCTION

Nitrous oxide (N₂O) is the third most significant greenhouse gas with stratospheric ozone depleting ability (Myhre 2013). N₂O is produced mostly as a byproduct of microbial metabolism, but it is also released from anthropogenic sources, like biomass and fossil fuel combustion, which have increased its atmospheric concentration from preindustrial time. In the biosphere N₂O is consumed only by microbial process, where it is reduced to dinitrogen gas with nitrous oxide reductase (nos) enzyme. N₂O reduction happens mostly in anoxic, but potentially also in microaerophilic conditions (Deesloover 2014).

Current climate models show that we still lack the knowledge of all possible sinks of N₂O. One potential, yet not studied sink could be the phyllospheric microbiota of trees. This hypothesis is supported by the evidence that birch stems and cryptogamic stem covers are able to consume N₂O (Machakova 2017) and *nosZ*-gene coding nitrous oxide reductase has been extracted from spruce (Siljanen, unpublished data). In addition, phyllospheric microbes are known to be able to form aggregates and biofilms on leaf surfaces, the inner parts of which provide anoxic environment suitable for N₂O reduction (Monier & Lindow 2003, Wessel 2014).

Aim of this study was to quantify N₂O consumption potential of Norway spruce branches from different parts of Finland and to isolate and identify N₂O consuming microbe species from branches. In our study we wanted to differentiate the functioning and diversity of microbes living on the plant surfaces (epiphytic) and inside the plant (endophytic).

METHODS

Phyllospheric samples were collected in the beginning of June 2019 from three locations; from Viikki, Helsinki; Puijo, Kuopio and from Kenttäröva, Kittilä. In each location, a top part of a branch was taken from nine spruce trees, branches from three trees forming one sample. All the trees were growing on mineral soil and branches were collected from approximately 1.5 meters above ground. Branches were placed into incubation bottles containing fresh water media (FWM), in which they were thoroughly shaken to release epiphytic microbes to the media. In a laboratory the branches and needles were taken out from the bottles and relocated into new incubation bottles containing FWM. For each location there was a negative control

bottle for culturing, which was opened in the field and in a laboratory. A branch from each sampled tree was taken also for microbial community and physical/chemical analyses.

After preparation samples were stored in dark at 4°C. After this the headspace of the bottles was first made anoxic with nitrogen gas and then flushed with gas containing 0.5 ppm of nitrous oxide. First gas samples from bottles were taken one hour after flushing and then the samples were incubated at 28°C for seven days. The next gas samples were collected on the third and on the seventh day of incubation.

After incubation, growth media from each bottle was plated and spread on petri dishes with agar solidified FWM. Plates were incubated in anoxic growing chambers at 28°C, with 0.5 ppm of N₂O as an electron acceptor, from one to three weeks, until single colonies appeared. Plates of negative control bottles were empty after incubation. Between eight and sixteen colonies were collected to pure cultures in incubation bottles. Also, sample for colony-PCR analysis of *nosZ*-gene (both clade I and II) were taken for further analysis of *nosZ* gene structures. These isolates were incubated at 28°C first for one week with anoxic headspace having 0.5 ppm of N₂O as the electron acceptor for denitrifying microbes, then with oxic headspace with 0.5 ppm of N₂O. Gas samples were taken in the beginning and in the end of incubations.

We are going to determine the original microbial population of spruce phyllospheric samples with targeted metagenomic sequencing of nitrogen cycling genes, with 16S rRNA amplicon sequencing. To study the chemical and physical properties on branch surfaces the particle size distribution and anion (e.g. nitrate and phosphate) concentrations will be analysed.

CONCLUSIONS

The contribution of phyllospheric microbes to the N₂O fluxes of trees has not been studied earlier. Our preliminary data suggest that the epiphytic microbes of spruce branches from central and southern parts of Finland have the potential to reduce N₂O although the variation within sites was notable. Isolation of microbial clones containing *nosZ*-gene and consuming N₂O in oxic and/or anoxic circumstances from spruce branches showed that N₂O reduction on phyllosphere has a microbial origin. As a conclusion, phyllospheric N₂O consuming microbes can potentially affect the N₂O sink in trees.

ACKNOWLEDGEMENTS

This work was supported by the European Research Council (ERC) under the European Union's Horizon 2020 research and innovation program (grant agreement number 757695), and the Academy of Finland (grant numbers 290315, 319329 and 2884941).

REFERENCES

- Butterbach-Bahl, K., Baggs, E. M., Dannenmann, M., Kiese, R., Zechmeister-boltenstern, S., 2013. Nitrous oxide emissions from soils: how well do we understand the processes and their controls? *Philosophical Transactions of the Royal Society B* 368: 20130122.
- Desloover, J., Roobroeck, D., Heylen, K., Puig, S., Boeckx, P., Verstraete, W., Boon, N. 2014. Pathway of nitrous oxide consumption in isolated *Pseudomonas stutzeri* strains under anoxic and oxic conditions. *Environmental Microbiology* 16 (10): 3143-3152.
- Machacova K., Maier M., Svobodona K., Lang F., Urban O. 2017. Cryptogamic stem covers may contribute to nitrous oxide consumption by mature beech trees. *Scientific Reports* 7 (1): 13243

- Monier, J & Lindow, S, 2003. Differential survival of solitary and aggregated bacterial cells promotes aggregate formation. *PNAS* 100 (26): 5977-15982.
- Myhre, G., D. Shindell, F.-M. Bréon, W. Collins, J. Fuglestedt, J. Huang, D. Koch, J.-F. Lamarque, D. Lee, B. Mendoza, T. Nakajima, A. Robock, G. Stephens, T. Takemura and H. Zhang, 2013. Anthropogenic and Natural Radiative Forcing. In: *Climate Change 2013: The Physical Science Basis. Report of the IPCC*. Cambridge University Press, Cambridge, United Kingdom and New York, NY, USA, pp. 659–740.
- Wessel A.K., Arshad T.A., Fitzpatrick M., Connell J.L., Bonnecaze R.T., Shear J.B., Whiteley M. 2014. Oxygen limitation within a bacterial aggregate. *mBio* 5(2): e00992-14.

EXTREME WEATHER EVENTS AND CARBON AND WATER FLUXES AT SUBARCTIC SCOTS PINE AND NORWAY SPRUCE SITES IN FINLAND

L.MATKALA¹, P. KOLARI², M.AURELA³, J.BÄCK¹ and L.KULMALA^{1,3}

¹Institute for Atmospheric and Earth System Research / Forest Sciences, University of Helsinki, Helsinki, Finland

²Institute for Atmospheric and Earth System Research / Physics, University of Helsinki, Helsinki, Finland

³Finnish Meteorological Institute, P.O. BOX 503 Helsinki, Finland.

Keywords: PHOTOSYNTHESIS, RESPIRATION, EVAPOTRANSPIRATION, DROUGHT, HEAT

INTRODUCTION

The ongoing climate change is predicted to increase the frequency of extreme weather events around the globe (IPCC 2013). Within the past twenty years, Europe has already experienced a few dramatically dry summers, when the production rates of forests declined (Ciais et al. 2005, Gao et al. 2017). Forests in the northern latitudes are considered to be vulnerable to climate change and the more regularly occurring extreme weather events could cause unforeseen harm to them (Karl et al., 1995; Beniston 2004, IPCC 2013). In general, the northern regions should receive more precipitation in the future. However, recent findings from Finnish subarctic forest sites indicate that also these forests have suffered from reduction of growth due to drought (Aakala 2018). Similarly, cold spells during the growing season have halted leaf development at a subarctic Norway spruce site (Linkosalmi 2016) and caused at least temporary reduction in the carbon dioxide (CO₂) uptake of a subarctic Scots pine site (Kulmala et al. 2019). We wanted to explore the occurrence and possible effects of extreme weather events on the CO₂ and water (H₂O) dynamics of two subarctic forest sites; a Scots pine site in Värriö and Kenttäröva Norway spruce site in Pallas. We formulated three research questions:

- 1) Have extreme weather events occurred frequently at our sites during the measurement periods?
- 2) Have these events affected the CO₂ and H₂O exchange and water use efficiency, or photosynthetic capacity of our sites?
- 3) Do the responses to events differ between Scots pine and Norway spruce stand?

METHODS

Our sites were located in Finnish Lapland; Värriö Scots pine site in eastern Lapland (67° 46' N, 29° 35' E), and Kenttäröva Norway spruce site in western Lapland (67.973°N, 24.116°E). Both sites have towers with eddy covariance based flux measurements above the canopy. The data from these measurements formed the basis of our dataset, which in addition included flux data from the shoot chambers from Värriö. Additionally, we used soil moisture and temperature data as well as meteorological data. We studied years 2003-2013 from Kenttäröva and years 2012-2018 from Värriö. We started by comparing the meteorological data from the study years to the long-term meteorological data in the search for extremely dry/wet/warm years. We used the IPCC definition (IPCC 2001) of an extreme event as the starting point. According to that, a climatological weather extreme is an event, which does not fit between the 10th and 90th percentile of climate events at a certain place at a certain time. To support the meteorological findings in search of droughts, we also calculated soil moisture anomalies (SMA, Orlowsky and Seneviratne 2013) from the sites with the following equation:

$$SMA_{y,m} = \frac{SM_{y,m} - \mu_m}{\sigma_m}$$

where y and m denote year and time period (1 or 2, referring to periods May-June and July-August, respectively), $SM_{y,m}$ the corresponding soil moisture, while μ_m and σ_m denote the mean and standard deviation of the soil moisture of month m calculated over the period from which we have carbon exchange data.

Momentary CO_2 and H_2O fluxes respond to instantaneous weather but here, we were interested in slower changes in the photosynthetic and respiration potential. Thus we calculated photosynthetic capacity, P1200, using the site-specific gapfilling parameters and empirical models for GPP and photosynthetically active radiation (PAR) of $1200 \mu\text{mol m}^{-2} \text{s}^{-1}$. The long-term changes in respiration capability, R_{10} , was calculated with the site-specific gapfilling parameters and empirical models for R and temperature (T) of 10°C .

We calculated water use efficiency (WUE) as a ratio between GPP and ET as it should increase during drought stress. In addition, we analysed the changes in the ratio between ET and sensible heat flux (H), and the ratio between ET and VPD, which both should decrease during dry periods.

The optimal stomatal control model (Hari and Mäkelä 2003, Kolari et al. 2007) was fitted to these measurements daily to achieve parameters describing the saturation and initial slope of the light response curve, the temperature response of respiration, and the cost of transpiration. Especially, we were interested in the photosynthetic capacity β , which is the saturation value of the light response curve. In the further analysis, we used a running mean of these parameters over 3 days. We calculated the water use efficiency for the chamber measurements (WUEshoot) as the ratio of CO_2 flux and transpiration.

PRELIMINARY RESULTS

We found extremely warm summers from both sites during the years of flux measurements. We also found two years with short cold spells during the growing season in Värriö. The effects of warm and dry summers were visible in R_{10} , but not as clearly in P1200. The R_{10} dropped with low soil moisture in Kenttäröva but not in Värriö indicating that spruce sites react to dry periods more than Scots pine. Nevertheless, this is most likely due to decreased soil respiration rates whereas the tree functions were not affected. The cold spells caused temporary reductions in total ecosystem respiration (TER) and in photosynthetic capacity, but the forest and trees recovered from the spell quickly. Overall, we saw a glimpse of what might be the effects of extreme weather events in these ecosystems, although they were still rather mild indicating that the forests are more resistant to extreme events than expected. The subarctic forests may be sensitive to climate change, but they seem to benefit from slightly warming air temperature and are durable towards short cold spells.

ACKNOWLEDGEMENTS

This work was supported by Center of Excellence (grant no 307331).

REFERENCES

- Aakala T., Berninger F. and Starr M., 2018. The roles of competition and climate in tree growth variation in northern boreal old-growth forests. *Journal of Vegetation Science* **29**:1040–1051.
- Beniston M., 2004. The 2003 heat wave in Europe: A shape of things to come? An analysis based on Swiss climatological data and model simulations. *Geophysical Research Letters* **31**.
- Ciais P., Reichstein M., Viovy N., Granier A., Ogee J., Allard V., Aubinet M., Buchmann N., Bernhofer C., Carrara A., Chevallier F., De Noblet N., Friend A. D., Friedlingstein P., Grünwald T., Heinesch B., Keronen P., Knohl A., Krinner G., Loustau D., Manca G., Matteucci G., Miglietta F., Ourcival J. M., D. Papale D., Pilegaard K., Rambal S., Seufert G., Soussana J.

- F., Sanz M. J., Schulze E. D., Vesala T., Valentini R. 2005. Europe-wide reduction in primary productivity caused by the heat and drought in 2003. *Nature Letters* **437**: 529-533.
- Gao, Y., Markkanen, T., Thum, T., Aurela, M., Mammarella I., Thum T., Tsuruta A., Yang H., and Aalto T., 2017. Response of water use efficiency to summer drought in a boreal Scots pine forest in Finland. *Biogeosciences*, **14**:4409–4422.
- Hari, P. and Mäkelä, A. 2003. Annual pattern of photosynthesis in Scots pine in the boreal zone. *Tree Physiology* **23**:145–155.
- Hartmann, D.L., Klein Tank A.M.G., Rusticucci M., Alexander L.V., Brönnimann S., Charabi Y., Dentener F.J., Dlugokencky E.J., Easterling D.R., Kaplan A., Soden B.J., Thorne P.W., Wild M. and Zhai P.M., (IPCC) 2013: Observations: Atmosphere and Surface. In: *Climate Change 2013: The Physical Science Basis. Contribution of Working Group I to the Fifth Assessment Report of the Intergovernmental Panel on Climate Change* [Stocker, T.F., Qin D., Plattner G.-K., Tignor M.,
- IPCC, 2001. *Climate Change 2001: The Scientific Basis. Contribution of Working Group I to the Third Assessment Report of the Intergovernmental Panel on Climate Change*. Cambridge University Press, United Kingdom and New York, NY, USA.
- Karl T.R., Knight R.W., Plummer N., 1995. Trends in high frequency climate variability in the twentieth century. *Nature* **377**, 217-220.
- Kolari P., Lappalainen H. K., Hänninen H., Hari P. 2007. Relationship between temperature and the seasonal course of photosynthesis in Scots pine at northern timberline and in southern boreal zone. *Tellus* **59B**: 542-552.
- Kulmala L., Pumpanen J., Kolari P., Dengel S., Berninger F., Köster K., Matkala L., Vanhatalo A., Vesala T., Bäck J., 2019. Inter- and intra-annual dynamics of photosynthesis differ between forest floor vegetation and tree canopy in a subarctic Scots pine stand. *Agricultural and Forest Meteorology*, **271**: 1-11.
- Linkosalmi M., Aurela M., Tuovinen J-P, Peltoniemi M., Tanis C. M., Arslan A. N., Kolari P., Böttcher K., Aalto T., Rainne J., Hatakka J., Laurila T., 2016. Digital photography for assessing the link between vegetation phenology and CO₂ exchange in two contrasting northern ecosystems, *Geosci. Instrum. Method. Data Syst.* **5**: 417–426.

COMPARISON OF STOMATAL CONDUCTANCE APPROACHES IN JSBACH

A. MAURANEN¹, J. MÄKELÄ², T. HÖLTTÄ³, Y. SALMON^{1,3} and T. VESALA^{1,3}

¹ Institute for Atmospheric and Earth System Research / Physics, Faculty of Science, University of Helsinki, Helsinki, Finland.

² Finnish Meteorological Institute, Helsinki, Finland.

³ Institute for Atmospheric and Earth System Research / Forest Sciences, Faculty of Agriculture and Forestry, University of Helsinki, Helsinki, Finland.

Keywords: photosynthesis modelling, climate modelling, JSBACH, stomatal control.

INTRODUCTION

New stomatal conductance functions are implemented in the JSBACH land surface model and tested on a single site, that is the SMEAR II station in Hyytiälä, Finland. The purpose is to compare the new functions to the previously implemented functions in terms of the predictions they yield, and ultimately to see whether the implementation of the new functions could improve JSBACH on a more general level.

MODELS AND DATA

The JSBACH land surface model is the land component of the Earth system model MPI-ESM. Knauer *et al.* (2015) implemented four alternative stomatal conductance functions into JSBACH, tested them and compared the results to those yielded by the functions initially used in JSBACH.

In this study we compare three stomatal control functions: USO, CAP-V and CAP-L. USO stands for Unified Stomatal Optimisation (Medlyn *et al.* 2011). From Dewar *et al.* (2018) we take the general framework as well as the optimisation hypothesis in which the non-stomatal limitations to photosynthesis affect stomatal conductance directly (the CAP hypothesis). To obtain CAP-V, we combine this with the photosynthesis model proposed by Vico *et al.* (2013) in which the two branches of the Farquhar model are interpolated to produce a single, continuously differentiable function for the photosynthesis rate. CAP-L is the combination of the CAP hypothesis and the light-limited regime of the photosynthesis model by Farquhar *et al.* (1980).

The resulting stomatal control models resemble each other closely, but the CAP-based functions have more detail in terms of sensitivity to tree and soil properties and environmental drivers. Formulated as functions of the optimal photosynthesis rate, the three models yield the following formulae (see Table 1 for meanings of symbols):

The USO model:
$$g_s^U \approx g_0^U + \left(1 + \frac{g_1^U}{\sqrt{D}}\right) \frac{A}{C_a}$$

The CAP-V model:
$$g_s^V \approx g_0^V + \left(1 + g_1^V \sqrt{\frac{K P |\Psi_0|}{1.6 D} \left(\frac{k_m}{V_{cmax}} + \frac{4 \Gamma_*}{J(Q)}\right)}\right) \frac{A}{C_a}$$

The CAP-L model:
$$g_s^L \approx g_0^L + \left(1 + g_1^L \sqrt{\frac{K P |\Psi_0|}{1.6 D} \left(\frac{12 \Gamma_*}{J(Q)}\right)}\right) \frac{A}{C_a}$$

This functions were implemented into the JSBACH photosynthesis module, after which a stand-alone (offline) version of JSBACH with climate forcing data was run on a single grid cell representing the

SMEAR II station in Hyytiälä. The parameters g_0 and g_1 for both models were fitted against the climate forcing data to produce the smallest cumulative error in relation to observations. The observation data used for the run was from the FLUXNET2015 dataset, in between 2001 and 2012.

RESULTS

All of the stomatal conductance functions produce mostly very similar results. In both evapotranspiration (ET) and gross photosynthetic production (GPP) the predictions go closely hand in hand at almost all times, but during dry periods there are more notable differences. The drought of August 2006 (Figure 1) produces a swift drop in ETT in CAP-V and a slower drop in USO, but an inverse reaction in CAP-L. During the drought GPP also drops in all of the models, fastest in CAP-V and slowest in CAP-L.

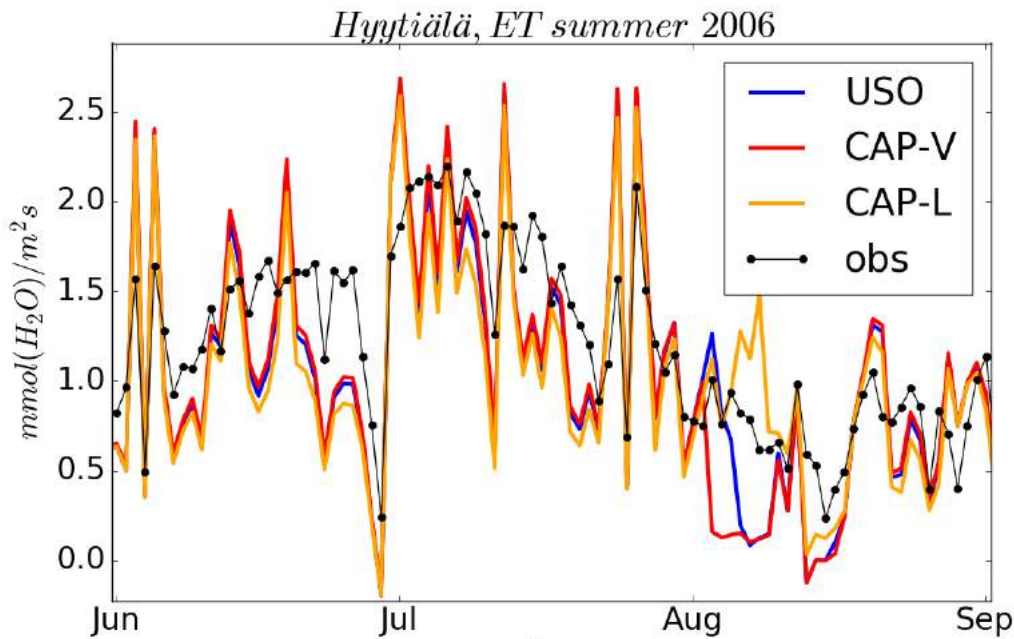


Figure 1. Evapotranspiration predictions for the summer of 2006 at SMEAR II using the USO (blue line), CAP-V (red line) and CAP-L (orange line) stomatal conductance models. Observations in black. The drought in August has a strong effect on the predictions.

Symbol	Meaning
A	photosynthetic rate
C_a	carbon dioxide concentration of ambient air
D	vapour pressure difference between the air inside and outside the leaf
g_0^V, g_0^L, g_0^U	residual conductances for CAP-V, CAP-L and USO respectively
g_1^V, g_1^L, g_1^U	fitted parameters for CAP-V, CAP-L and USO respectively
g_s^V, g_s^L, g_s^U	optimal stomatal conductances for CAP-V, CAP-L and USO respectively
J	electron transport rate
k_m	Michaelis-Menten coefficient related to the Farquhar photosynthesis model
K	hydraulic conductance from soil to leaf
P	ambient air pressure
Q	incident photosynthetically active radiation
V^{cmax}	carboxylation capacity
Γ_*	CO ₂ compensation point
Ψ_0	leaf water potential at which photosynthesis stops due to drought

Table 1. Meanings of symbols.

ACKNOWLEDGEMENTS

This research was funded by the Academy of Finland National Centre of Excellence (307331) and Academy Professor Research project (312571).

REFERENCES

Dewar, R., A. Muraenen, A. Mäkelä, T. Hölttä, B. Medlyn and T. Vesala (2018). New insights into the covariation of stomatal, mesophyll and hydraulic conductances from optimization models incorporating nonstomatal limitations to photosynthesis. *New Phytol.* **217**, 571–585.

Farquhar, G.D., S. von Caemmerer and J.A. Berry (1980). A biochemical model of photosynthetic CO₂ assimilation in leaves of C₃ species. *Planta* **149**, 78.

Knauer, J., C. Werner, and S. Zaehle (2015). Evaluating stomatal models and their atmospheric drought response in a land surface scheme: A multibiome analysis. *J. Geophys. Res. Biogeosci.* **120**, 1894–1911.

Medlyn, B.E., R.A. Duursma, D. Eamus, D.S. Ellsworth, I.C. Prentice, C.V.M. Barton, K.Y. Crous, P. De Angelis, M. Freeman and L. Wingate (2011). Reconciling the optimal and empirical approaches to modelling stomatal conductance. *Glob. Change Biol.* **17**, 2134–2144.

Vico, G., S. Manzoni, S. Palmroth, M. Weith and G. Katul (2013). A perspective on optimal leaf stomatal conductance under CO₂ and light co-limitations. *Agric. For. Meteorol.* **182–183**, 191–199.

CALIBRATING CHEMICAL IONIZATION MASS SPECTROMETERS WITH A DROPLET EVAPORATION BASED METHOD

M. MEDER¹, F. GRAEFFE¹, J. SHEN¹, H. VIRTA¹, Y. ZHANG¹, O. GARMASH¹, O. PERÄKYLÄ¹, L. QUÉLÉVER¹ AND M. EHN¹

¹Institute for Atmospheric and Earth System Research / Physics, Faculty of Science, University of Helsinki, Helsinki, 00140 Finland

Keywords: Chemical Ionization, Mass Spectrometry, HOM, Calibration.

INTRODUCTION

Highly Oxygenated Organic Molecules (HOM) are important precursor gases in the formation of Secondary Organic Aerosol (SOA). HOM are low volatility organic compounds that form from Volatile Organic Compounds (VOCs) through a process called autoxidation (Bianchi *et al.*, 2019). Chemical Ionization Atmospheric Pressure interface Time of Flight mass spectrometers (CI-APi-ToF) utilizing nitrate NO_3^- in the ionization process are used commonly when measuring HOM (Jokinen *et al.*, 2012; Ehn *et al.*, 2014). These instruments are used due to their chemical selectiveness (Hytinen *et al.*, 2018). However, there are still high uncertainties in the quantification of these measurements, as HOM cannot be purchased as easy-to-use standards. Thus, there is a need to develop calibration methods for assessing the sensitivity of the instruments towards different compounds, preferably in a fast and robust way. A particular challenge comes from the fact that the CI-APi-ToF is selective mainly towards very low-volatile species, meaning the compounds of interest need to be added close to the inlet in order to avoid losses in the transfer line. We experimented with droplet evaporation, where a known concentration of the studied compound is generated by heating and evaporating a droplet of a solution of the said compound.

METHODS

The droplet evaporation approach is similar to what is done with the FIGAERO (Filter Inlet for Gases and AEROsols), which is used to study aerosol chemical composition by gathering aerosol on a filter, then heating them and monitoring the compounds being released (Lopez-Hilfiker *et al.*, 2014).

We tested several different iterations of the set-up for the optimal evaporation of the calibration compounds. A schematic of the droplet evaporation calibrator that yielded the most promising results, the “Easy Y-piece” calibrator, is shown in figure 1. The calibrator consists of two main parts: the evaporation surface and the heater. In addition to the calibrator, calibration solutions are required. A single calibration measurement is done in the following way: A known volume of the calibration solution is injected onto the evaporation surface, from which the solution evaporates generating a known concentration in the sample flow. The evaporation process is accelerated by heating the flow directed over the surface and the surface itself. The sample flow is directed to the mass spectrometer and the resulting signals are monitored.

In addition to the heater and the small metal T-piece as the evaporation surface, the “Easy Y-piece” set-up includes a Y-piece to enable combining the calibration flow with a clean air flow to gain the desired 10 lpm sample flow.

The goal of the calibration process is to calculate the calibration coefficient CC as shown by Jokinen *et al.*, (2012)

$$CC = \frac{[sample\ flow,\ true]}{[measured]} [reagent\ ions] \quad (1)$$

The coefficient is the true concentration of the compound in the sample flow $[sample\ flow,\ true]$ divided by the sum of the calibration compound ion concentrations $[measured]$ and multiplied with the total concentration of the reagent ions $[reagent\ ions]$. To calculate the calibration coefficient, only the sample flow rate and injected volume of the calibration solution of a certain concentration have to be known, making the analysis process quite simple. Ehn *et al.* (2014) found that the calibration coefficient should theoretically get values within the range of $(0,4 - 9,5) \cdot 10^{10} \frac{molecules}{cm^3}$.

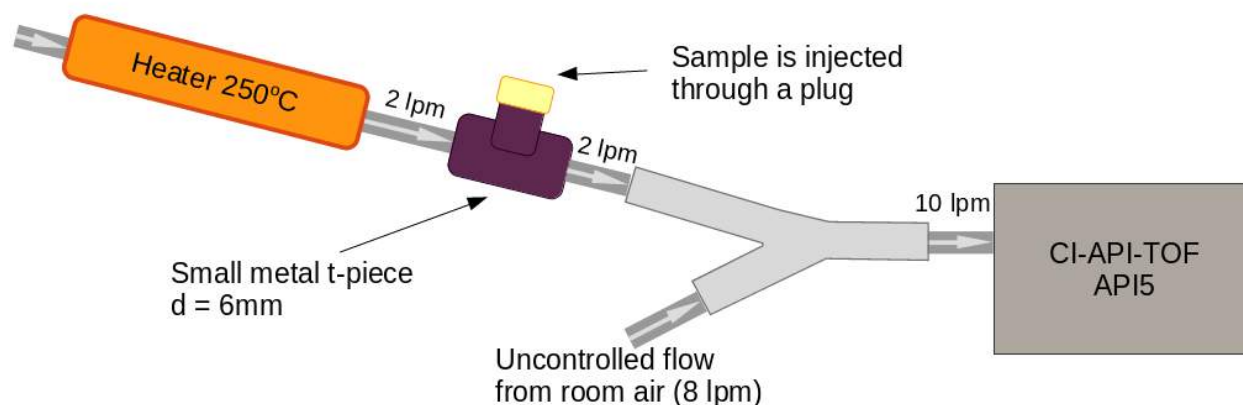


Figure 1. Schematic of the Easy Y-piece calibrator. The calibrator is composed of the heater, the small metal T-piece as the evaporation surface and the Y-piece that enables combining the calibration flow and clean flow to get the desired sample flow rate.

Suitable calibration compounds should optimally have similar properties to HOM, i.e. they should be low volatility organic compounds. The compounds should also be readily available, and easy and safe to use. The CI-API-ToF is very sensitive, with a detection limit of around $10^5 \frac{molec}{cm^3}$, but at higher concentrations around $10^{10} \frac{molec}{cm^3}$, the instrument starts to saturate, i.e. it no longer can measure the concentration but caps off at a maximum. Thus, the concentrations in the sample flow must be low enough, meaning in practice the compounds must be highly diluted in a solvent, even if adding $1\mu l$ of the solution into the heater. Furthermore, optimally the compounds should span from low to high masses in order to calibrate the instrument for all masses relevant to HOM. Low volatility organic compounds studied were malonic acid, citric acid and succinic acid to name a few. Additionally, sulphuric acid was tested as a possible calibration compound, as it is known to be well detected with nitrate CI-API-ToF mass spectrometers. Of these compounds, malonic acid was the most extensively tested.

The calibrators and the droplet evaporation method itself were validated by calibrating Proton Transfer Reaction (PTR) and VOCUS-PTR mass spectrometers using volatile acetone, and comparing the determined calibration coefficients with those found in literature.

CONCLUSIONS

We studied droplet evaporation as a method for calibrating the nitrate Chemical Ionization Atmospheric Pressure interface Time of Flight mass spectrometer for detecting Highly Oxygenated Organic Molecules

using low volatility organic compounds. The low volatility of the tested compounds, their interactions with the surfaces they were injected on (Teflon filters, Teflon tubing, glass, stainless steel), and potential thermal decomposition resulted in a large number of challenges, and ultimately in poor reproducibility of measurements. Furthermore, often the calculated values did not correspond with calibration coefficient values, being multiple orders of magnitude greater, meaning the instrument saw multiple orders of magnitude lower concentrations than expected.

Despite the challenges, the method is still of great interest, as it was successfully validated using PTR and VOCUS mass spectrometers. While using more volatile calibration compounds, the results were reproducible and gave similar values as when using more traditional calibration methods for the PTR instruments. Nothing conclusive can be said about the studied HOM surrogate compounds when calibrating the CI-API-ToF except for malonic acid, which was deemed most likely unfit to be used as a calibration compound with this method, due to the previously mentioned poor reproducibility. What is more, other compounds could be looked into, for example, perfluorinated carboxylic acids, and sulphuric acid should be examined further, as these are more stable and inert than many of the tested compounds, yet still known to be efficiently detected by the CI-API-ToF. More importantly, developing the calibrator hardware will be the main target for future work on this method. Optimizing materials, flow profiles and heating efficiency are all attributes to improve upon.

ACKNOWLEDGEMENTS

The European Research Council (Grant 638703-COALA) supported this research. We thank the tofTools team for providing tools for mass spectrometry data analysis.

REFERENCES

- Bianchi, F., Kurtén, T., Riva, M., Mohr, C., Rissanen, M. P., Roldin, P., Berndt, T., Crouse, J. D., Wennberg, P. O., Mentel, T. F., Wildt, J., Junninen, H., Jokinen, T., Kulmala, M., Worsnop, D. R., Thornton, J. A., Donahue, N., Kjaergaard, H. G., and Ehn, M. (2019). Highly oxygenated organic molecules (HOM) from gas-phase autoxidation involving organic peroxy radicals: A key contributor to atmospheric aerosol. *Chem Rev.*, 119(6):3472-3509. doi:10.1021/acs.chemrev.8b00395.
- Ehn, M., Thornton, J. A., Kleist, E., Sipilä, M., Junninen, H., Pullinen, I., Springer, M., Rubach, F., Tillmann, R., Lee, B., Lopez-Hilfiker, F., Andres, S., Acir, I.-H., Rissanen, M., Jokinen, T., Schobesberger, S., Kangasluoma, J., Kontkanen, J., Nieminen, T., Kurtén, T., Nielsen, L. B., Jørgensen, S., Kjaergaard, H. G., Canagaratna, M., Dal Maso, M., Berndt, T., Petäjä, T., Wahner, A., Kerminen, V.-M., Kulmala, M., Worsnop, D. R., Wildt, J., and Mentel, T. F. (2014). A large source of low-volatility secondary organic aerosol. *Nature*, 506:476–496.
- Hyttinen, N., Otkjær, R. V., Iyer, S., Kjaergaard, H. G., Rissanen, M. P., Wennberg, P. O., and Kürten, A. (2018). Computational comparison of different reagent ions in the chemical ionization of oxidized multifunctional compounds. *Journal of Physical Chemistry*, 122:269–279.
- Jokinen, T., Sipilä, M., Junninen, H., Ehn, M., Lönn, G., Hakala, J., Petäjä, T., Mauldin, R. L. I., Kulmala, M., and Worsnop, D. R. (2012). Atmospheric sulphuric acid and neutral cluster measurements using CI-API-TOF. *Atmospheric Chemistry and Physics*, 12:4117–4125.
- Lopez-Hilfiker, F. D., Mohr, C., Ehn, M., Rubach, F., Kleist, E., Wildt, J., Mentel, T. F., Lutz, A., Hallquist, M., Worsnop, D., and Thornton, J. A. (2014). A novel method for online analysis of gas and particle composition: description and evaluation of a filter inlet for gases and aerosols (figaero). *Atmospheric Measurement Techniques*, 7:983–1001.

ABOUT BLACK CARBON IN THE ARCTIC AND SIGNIFICANCE COMPARED TO HIGH-LATITUDE DUST SOURCES (FINNISH-RUSSIAN WORKSHOP AT THE LOMONOSOV MOSCOW STATE UNIVERSITY, 17-18 SEPTEMBER 2019, IN CO-OPERATION WITH MSU, INAR, PEEEX, MFA/IBA AND FMI)

O. MEINANDER¹, S. CHALOV², H. LAPPALAINEN³, J.EKMAN¹, K. ELEFThERiADiS⁴, D. FROLOV², A. HYVÄRINEN¹, V. IVANOV², N. KARVOSENOJA⁵, K. KUPIAINEN⁶, O. POPOVICHEVA², I. SEMENKOV², L. SOGACHEVA¹, and THE MSU WORKSHOP PARTICIPANTS¹⁻⁶

¹Finnish Meteorological Institute, FMI, Erik Palmenin aukio 1, Helsinki, Finland

² Lomonosov Moscow State University, MSU, Russia

³ University of Helsinki, UHE, Finland

⁴National Centre for Scientific Research Demokritos, Greece

⁵ Finnish Environment Research Institute, SYKE, Finland

⁶ Ministry of the Environment, YM, Finland

Keywords: Black carbon, dust, high latitude dust, atmosphere-cryosphere interactions, effects, Russia.

INTRODUCTION

Black carbon in the atmosphere contributes to Arctic warming by two main mechanisms: the dark particles absorb solar radiation thus warming the surrounding air, and they reduce the albedo of snow and ice covered surfaces thus accelerating the melting of glaciers (Bond et al. 2013; Sand et al. 2016; Boy et al. 2019). High latitude dust (HLD) refers to particles deflated from a surface that travel by suspension in the atmosphere, including mineral particles, soil particles, and volcanic ash but excluding direct volcanic emissions during eruptions, and originating from $\geq 50^\circ\text{N}$ and $\geq 40^\circ\text{S}$ latitudes (Bullard et al. 2016; Fig. 1). These HLD particles are capable of being long-range transported to the Arctic, over the Atlantic and towards Europe. In the latest IPCC Special Report on the Ocean and Cryosphere in a Changing Climate (IPCC 2019), dust has been recognized as an important climate driver causing snow darkening and melting in Polar Regions. Similarly to HLD, Saharan dust can be long-range transported and have impacts at long distances elsewhere (e.g., di Mauro 2019) and affect even the Arctic region. Towards this end the mid latitude free troposphere station (GAW, Global Atmosphere Watch, World Meteorological Organization) of Helmos Mountain, Greece, (2314 m asl) can serve as a comparative reference on the Saharan dust load arriving there from long range transport and contribute towards the understanding of the chemical transformations, impact and radiative transfer, mineral dust and black carbon have in the high latitude in comparison with that experienced in the free troposphere in Mid latitudes based on related work performed in the area (Diapouli et al. 2017, Vasilatou et al. 2017).

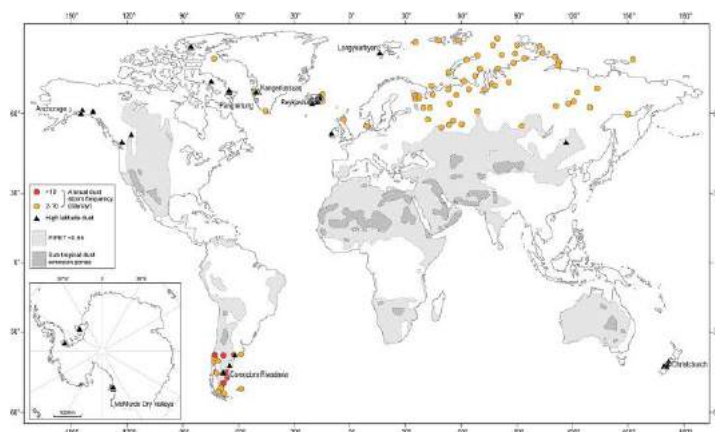


Figure 1. Global observations of high-latitude dust where filled circles indicate dust storm frequency based on visibility data, and black triangles indicate georeferenced published observations of dust storms (see text for details). Areas where the precipitation: potential evapotranspiration ratio < 0.65 (aridity index) [United Nations Environment Programme, 1997] and subtropical dust emission zones are included for reference. Figure 3 of Bullard et al. (2016).

The IBA-project of “Black carbon in the Arctic and significance compared to dust sources” (IBA-BCDUST, <https://en.ilmatieteenlaitos.fi/iba-project>) is part of the Ministry of Foreign Affairs of Finland IBA funding scheme and aims to assess black carbon in the Arctic and significance compared to dust sources for their climate impacts. Special focus is on Finland, Iceland and Russia, including cryospheric impacts, health effects and shipping. The Arctic Council AMAP SLCF (Arctic Monitoring and Assessment Programme, Expert Group of Short-Lived Climate Forcers) serves as a bridge between science and policy. The IBA-BCDUST project is planned to support the activities of the Finnish chairmanship of the Arctic Council (e.g., Ekman 2018) and work in the AMAP EGSLCF working group (e.g., AMAP 2015, Kupiainen 2018), as well as the activities in Iceland and Russia as the next chairs of the Arctic Council after Finland. The project aims at organizing three workshops: one in Iceland (WS was arranged at the Agricultural University of Iceland in February 2019 in collaboration with, e.g., IASC, International Arctic Science Committee; the WS report is available at <https://iasc.info/communications/news-archive/530-workshop-report-iasc-workshop-on-effects-and-extremes-of-high-latitude-dust>), one in Russia (reported here) and one in Finland (will take place 1 November 2019 at FMI, as part of Pyry national snow seminar; see also www.geophysica.fi for “Pyry snow seminar Finland 100” -special issue (Meinander 2018), arranged also as part of the Finnish Chairmanship of the Arctic Council (Ekman 2018).

Here we summarize the Finish-Russian workshop of “Black carbon in the atmosphere and significance compared to dust sources” held at the Lomonosov Moscow State University (MSU), 17-18 September 2019, in co-operation with MSU, INAR (Institute for Atmospheric and Earth System Research, Finland, <https://www.helsinki.fi/en/inar-institute-for-atmospheric-and-earth-system-research>), PEEEX (Pan-Eurasian Experiment, <https://www.atm.helsinki.fi/peex/>), MFA/IBA-project (Ministry for Foreign Affairs of Finland/collaboration between Baltic, Barents and Arctic regions funding scheme of IBA, <https://en.ilmatieteenlaitos.fi/iba-project>) and FMI (Finnish Meteorological Institute, www.fmi.fi) (Figs 2-3). We also provide in the Reference-list some of the most important literature references on BC and HLD with the focus on Russia.

METHODS

The Finnish-Russian workshop (Figs. 1-2) included talks (see Table 1), posters (Fig 3), and discussions, completed with a Webropol-questionnaire documentation and participant replies therein (Fig. 4), as well as participant inputs to the HLD map presented as an interactive poster, where participants could add their observation places of dust sources. This produced new knowledge on new HLD sources (Table 2), not yet included in the map of Bullard et al. (2016). These inputs are aimed at to be included for updating the HLD sources with the participant inputs from the IBA-BCDUST project WSs in Iceland, Russia and Finland (Meinander et al. 2019, in prep.).



Figure 2. The Workshop participants at the Lomonosov Moscow State University 17 September 2019.



Figure 3. Posters presented during the WS at the Lomonosov Moscow State University 17-18 September 2019. Posters included also an interactive map for updating HLD sources map with the participants inputs.

CONCLUSIONS

The WS focused on BC and dust, regarding their emissions, transport, deposition and impacts, as observations and modelling, by Finnish and Russian researchers and their collaborators. The main outcomes can be summarized on the basis of the given talks (Table 1), to include (but not limited to):

Table 1. Summary of the main outcomes of the Workshop (but not limited to) regarding BC and dust by the WS participants, Lomonosov Moscow State University, 17-18 September 2019.

Place / Reference	Conclusions
Tiksi, Russia (Popovicheva et al. 2018)	East Siberian Arctic background and black carbon polluted aerosols at HMO Tiksi have been characterized. Tiksi pollution episodes relate to local and long-transportation emissions of BC and sulfates and pollution BC episodes can be up to 6 times due to long-transportation from GF regions.
Alert, Canada; Barrow, Alaska; Pallas, Finland; Summit, Greenland; Tiksi, Russia; Ny Ålesund, Norway (Backman et al, 2017; Schmeisser et al. 2018)	Aerosol absorption- and scattering coefficients are presented from six different stations in the Arctic analysed with consolidated data handling methods. According to the studies, the seasonal cycles of these properties have ample spatiotemporal variability, and the region cannot be treated as a uniform environment.
Konstantinos Eleftheriadis, NSRC Demokritos Niko Karvosenoja, SYKE Hanna Lappalainen, UHEL Larisa Sogacheva, FMI Vladimir Shevchenko, RAS Tamara Khodzher, Limnology Institute SB RAS Olga Popovicheva, MSU	Lessons learned from extensive source apportionment studies for PM10 and PM2.5 in European urban areas and Megacities Black carbon emissions and tools for climate and health impact assessment Pan-Eurasian Experiment - (PEEX) Program Forest Fires and Aerosol Optical Depth retrieved from Satellites Black carbon and dust over the Russian Arctic seas Environmental impact assessment through an atmospheric channel using the example of certain regions of Eastern Siberia) Microparticles in Moscow atmosphere: physico-chemical characterization for air quality assessment
Nikolay Elansky, Obukhov institute of Atmospheric Physics RAS Murat Nahaev, IPO	Seasonal and weekly cycles of surface concentration of aerosols to PM2.5 in Metropolitan areas (on the example of Moscow) Calculation of fine particle transport to the Arctic region using numerical chemical transport models
Vladimir Kopeikin, Obukhov institute of Atm.Physics RAS Boris Revich, IEF RAS Anna Vinogradova, Obukhov institute of Atm.Phys. RAS	Variations of black carbon concentration in the Arctic in 2016-2018 Particles in atmospheric air - health risks Black carbon in near surface atmosphere on the territory of Pechora-Ilych nature biosphere reserve (the northwest Urals): daily monitoring throughout the year
Dmitry Vlasov, MSU	Metals and metalloids in spring rains in Moscow megacity: first records of concentrations, solubilities, partitioning and depositions
Nikolay Kasimov, MSU	Partition of chemical elements in the river water: connections with hydrometeorological conditions
Natalia Kosheleva, MSU	Road dust in Moscow: chemical composition as indicator of environmental conditions
Sodankylä Finland (Meinander et al. 2013)	BC deposition to Sodankylä snow varied temporally in one place and the detected highest BC concentrations are due to air masses originating from the Kola Peninsula (SILAM modelling)
Various	https://doi.org/10.1016/j.enpol.2019.06.045 ISSN 1024-8560, Atmospheric and Oceanic Optics, 2019, Vol. 32, No. 5, pp. 540–544. © Pleiades Publishing, Ltd., 2019 https://www.atmos-chem-phys-discuss.net/acp-2019-411/ https://doi.org/10.1016/j.atmosenv.2016.06.023 https://doi.org/10.24057/2071-9388-2018-11-1-74-84 ; https://doi.org/10.5194/acp-19-7743-2019 ; https://www.atmos-meas-tech.net/9/313/2016/ ; https://www.researchgate.net/profile/Ivan_Semenkov ;

Global/Sogacheva L. (e.g., Sogacheva et al. 2019)	Satellite remote sensing offers a useful tool for forest fire detection and monitoring. During a fire event, active fires can be detected by detecting the heat, light and smoke plumes emitted from the fires. Smouldering can also be visible through increasing optical depth of the aerosol particles detected with satellites. Satellite remote sensing is well suited to assessing the extent of biomass burning, a prerequisite for estimating emissions at regional and global scales, which, as important input to the climate models, are needed for better understanding the effects of fire on climate change.
Markku Kulmala, UHEL Kaarle Kupiainen, Ministry of Environment, Finland Alexander Baklanov, WMO Olga Popovicheva, MSU Tuukka Petäjä, UHEL Johanna Ekman, FMI Antti-Pekka Hyvärinen, FMI Outi Meinander, FMI	Air quality - climate interactions and feedbacks Short-lived climate forcers and the Arctic WMO GAW observation and modeling of BC in the Arctic and dust storm impacts Source - dependent BC in Russian Arctics Integrative and Comprehensive Understanding on Polar Environments Arctic Council chairmanship - how we did it Measurements of Atmospheric Black Carbon Cryospheric and climate effects of light absorbing soot and dust aerosols in snow

The main outcomes of the Webropol-questionnaire included published literature references of the WS participants, some of which are available in Russian only (see the References), and identified fields of expertise, as presented in Fig 4.)

The main outcome of the updates to the HLD map included (Table 2):

Place	Country	Source
Tiksi	Russia	Local or long-range transported
Kola Peninsula	Russia	Dust from mining
Khibiny	Russia	Natural and man-made river sediments
Mount Helmos	Greece	Natural dust
Marambio	Antarctica	Local or long-range transported

Table 2. The new ongoing dust observations relevant to high latitudes, and new HLD sources identified as additions to map of Bullar et al. (2016).

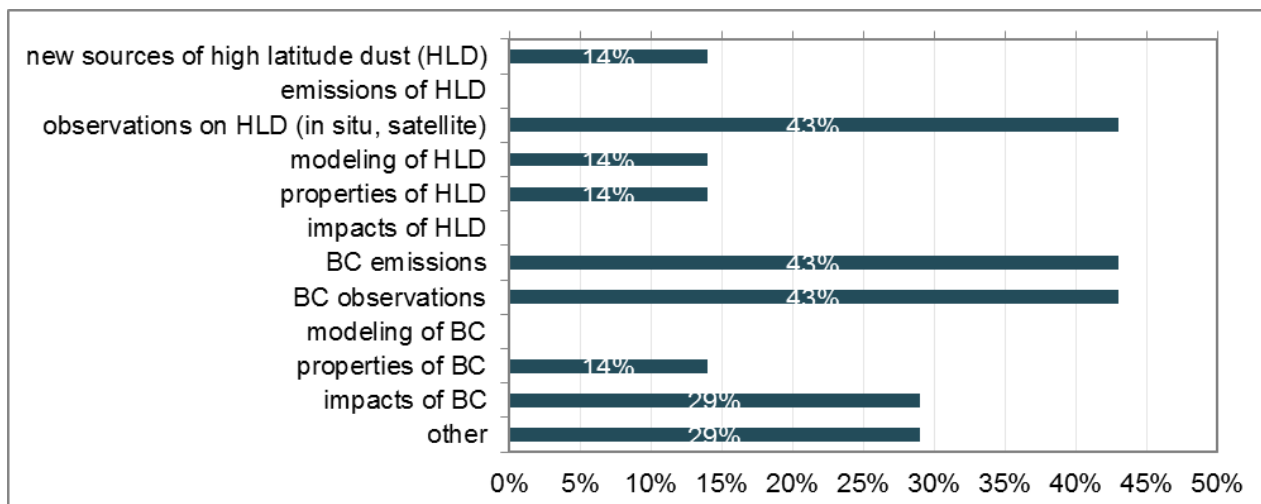


Figure 4. Summary of the Webropol-questionnaire replies of the WS participants, where it was also asked what topics your published papers cover.

A review of HLD is available in Bullard et al. (2016). Evans et al. (2017) reviewed studies on Russia's BC emissions, and reported that Russian policies on flaring and on-road transport appear to have significantly reduced BC emissions recently. They estimate Russia's black carbon emissions at 688 Gg. The study also adds organic carbon and uncertainty estimates. Our WS updated four new dust sources and reported that, e.g., East Siberian Arctic background and black carbon polluted aerosols at HMO Tiksi have been characterized. Tiksi pollution episodes relate to local and long-transportation emissions of BC and sulfates and pollution BC episodes can be up to 6 times due to long-transportation from GF regions. Overall the main findings of the WS can be summarized as: 1. Four new High latitude dust sources as compared to map of Bullard et al. (2016) and one high latitude dust significant GAW station with dust observations outside high latitudes; 2. Temporal and spatial variability in BC and dust in atmosphere and deposited in cryosphere; 3. Some of the technical and scientific gaps in dust and BC research were contributed to, and some gaps were identified where more research input is required.

ACKNOWLEDGEMENTS

We gratefully acknowledge all the workshop participants. This work was supported by the Ministry for Foreign Affairs of Finland (IBA-FIN-BCDUST-project coordinated by the Finnish Meteorological Institute), the Russian Science Foundation (projects 19-77-30004, 17-77-20072), and the PanEurasian Experiment (PEEX) Program coordinated by University of Helsinki INAR. We also gratefully acknowledge COST Action inDust (COST Action CA16202). Tiksi station data were analysed in the framework of RFBR project No. 18-05-60084.

REFERENCES

- AMAP. Black carbon and ozone as Arctic climate forcers, Arctic Monitoring and Assessment Programme (AMAP), Oslo, Norway. vii + 116 pp. ISBN –978-82-7971-092-9, 2015.
- Backman, J., Schmeisser, L., Virkkula, A., Ogren, J. A., Asmi, E., Starkweather, S., Sharma, S., Eleftheriadis, K., Uttal, T., Jefferson, A., Bergin, M., Makshtas, A., Tunved, P., and Fiebig, M.: On Aethalometer measurement uncertainties and an instrument correction factor for the Arctic, *Atmos. Meas. Tech.*, 10, 5039–5062, <https://doi.org/10.5194/amt-10-5039-2017>, 2017
- Bond, T. C., Doherty, S. J., Fahey, D. W., Forster, P. M., Berntsen, T., DeAngelo, B. J., Flanner, M. G., Ghan, S., Kärcher, B., Koch, D., Kinne, S., Kondo, Y., Quinn, P. K., Sarofim, M. C., Schultz, M.

- G., Venkataraman, C., Zhang, H., Zhang, S., Bellouin, N., Guttikunda, S. K., Hopke, P. K., Jacobson, M. Z., Kaiser, J. W., Klimont, Z., Lohmann, U., Schwarz, J. P., Shindell, D., Storelvmo, T., Warren, S. G., and Zender, C. S. 2013. Bounding the role of black carbon in the climate system: A scientific assessment, *J. Geophys. Res.-Atmos.*, 118, 5380–5552, doi:10.1002/jgrd.50171.
- Boy, M., Thomson, E. S., Acosta Navarro, J.-C., Arnalds, O., Batchvarova, E., Bäck, J., Berninger, F., Bilde, M., Brasseur, Z., Dagsson-Waldhauserova, P., Castarède, D., Dalirian, M., de Leeuw, G., Dragosics, M., Duplissy, E.-M., Duplissy, J., Ekman, A. M. L., Fang, K., Gallet, J.-C., Glasius, M., Gryning, S.-E., Grythe, H., Hansson, H.-C., Hansson, M., Isaksson, E., Iversen, T., Jonsdottir, I., Kasurinen, V., Kirkevåg, A., Korhola, A., Krejci, R., Kristjansson, J. E., Lappalainen, H. K., Lauri, A., Leppäranta, M., Lihavainen, H., Makkonen, R., Massling, A., Meinander, O., Nilsson, E. D., Olafsson, H., Pettersson, J. B. C., Prisle, N. L., Riipinen, I., Roldin, P., Ruppel, M., Salter, M., Sand, M., Seland, Ø., Seppä, H., Skov, H., Soares, J., Stohl, A., Ström, J., Svensson, J., Swietlicki, E., Tabakova, K., Thorsteinsson, T., Virkkula, A., Weyhenmeyer, G. A., Wu, Y., Zieger, P., and Kulmala, M.: Interactions between the atmosphere, cryosphere, and ecosystems at northern high latitudes, *Atmos. Chem. Phys.*, 19, 2015–2061, <https://doi.org/10.5194/acp-19-2015-2019>, 2019.
- Bullard, J. E., Baddock, M., Bradwell, T., Crusius, J., Darlington, E., Gaiero, D., Gassó, S., Gisláttir, G., Hodgkins, R., McCulloch, R., McKenna-Neuman, C., Mockford, T., Stewart, H. & Thorsteinsson, T. (2016), High-latitude dust in the Earth system, *Rev. Geophys.*, 54, 447–485, doi:10.1002/2016RG000518.
- Diapouli, E., Manousakas, M. I., Vratolis, S., Vasilatou, V., Pateraki, S., Bairachtari, K. A., Querol, X., Amato, F., Alastuey, A., Karanasiou, A. A., Lucarelli, F., Nava, S., Calzolari, G., Gianelle, V. L., Colombi, C., Alves, C., Custódio, D., Pio, C., Spyrou, C., Kallos, G. B., and Eleftheriadis, K.: AIRUSE-LIFE +: estimation of natural source contributions to urban ambient air PM₁₀ and PM_{2.5} concentrations in southern Europe – implications to compliance with limit values, *Atmos. Chem. Phys.*, 17, 3673–3685, <https://doi.org/10.5194/acp-17-3673-2017>, 2017. <https://www.atmos-chem-phys.net/17/3673/2017/>
- Di Mauro, B., Garzonio, R., Rossini, M., Filippa, G., Pogliotti, P., Galvagno, M. et al. (2019). Saharan dust events in the European Alps: role in snowmelt and geochemical characterization. *Cryosphere* 13, 1147-1165. doi.org/10.5194/tc-13-1147-2019.
- Efimov VA, S R Chalov, L E Efimova, V A Ivanov, J Jarsjö and S Fisher, Impact of mining activities on the surface water quality (case study of Khibiny mountains, Russia), IOP Conference Series: Earth and Environmental Science, Volume 263, conference 1, <https://iopscience.iop.org/article/10.1088/1755-1315/263/1/012008>, 2019
- Ekman J, A Short Comment on Finland's Chairmanship of the Arctic Council 2017–2019, *Geophysica* (2018), 53(1), 7–8, http://www.geophysica.fi/pdf/geophysica_2018_53_ekman.pdf
- Frolov D.M. (2019) Peculiarities of Ice Nucleation on Particles in Atmosphere and Soil. In: Chalov S., Golosov V., Li R., Tsyplenkov A. (eds) *Climate Change Impacts on Hydrological Processes and Sediment Dynamics: Measurement, Modelling and Management*. Springer Proceedings in Earth and Environmental Sciences. Springer, Cham., p.39-42, 2019, https://link.springer.com/chapter/10.1007/978-3-030-03646-1_7, DOI: 10.1007/978-3-030-03646-1_7.
- IPCC, 2019. *Summary for Policymakers. In: IPCC Special Report on the Ocean and Cryosphere in a Changing Climate* [H.-O. Pörtner, D.C. Roberts, V. Masson-Delmotte, P. Zhai, M. Tignor, E. Poloczanska, K. Mintenbeck, M. Nicolai, A. Okem, J. Petzold, B. Rama, N. Weyer (eds.)]. In press.
- Khodzher T. V. , Golobokova L. P. , Osipov E. Y. , Shibaev Yu. A. , Lipenkov V. Y. , Osipova O. P. Petit J.R. Spatial–temporal dynamics of chemical composition of surface snow in East Antarctica along the Progress station–Vostok station transe // *The Cryosphere*. – 2014. – № 8. – С. 931-939, 2014.
- Khodzher T.V., Domyшева V.M., Sorokovikova L.M., Sakirko M.V., Tomberg I.V. Current chemical composition of Lake Baikal water // *Inland Waters*. — 2017. — V. 7. — № 3. — P. 250-258. DOI: 10.1080/20442041.2017.1329982, 2017.

- Khodzher, T.V., G.S. Zhamsueva, A.S. Zayakhanov, A.L. Dementeva, V.V. Tsydyпов, Yu.S. Balin, I.E. Penner, G.P. Kokhanenko, S.V. Nasonov, M.G. Klemasheva, L.P. Golobokova, V.L. Potemkin The results of shipborne studies of the aerosol-gas impurities of the atmosphere over Lake Baikal in summer 2018 [Rezultaty sudovyykh issledovaniy aerazol'no-gazovykh primesey atmosfery nad Baykalom letom 2018 g.], Atmospheric and Oceanic Optics, 2019, N4, P289-295 (in Russian; Ходжер Т.В., Жамсуева Г.С., Заяханов А.С., Деметьева А.Л., Цыдыпов В.В., Балин Ю.С., Пеннер И.Э., Коханенко Г.П., Насонов С.В., Клемашева М.Г., Голобокова Л.П., Потемкин В.Л. Результаты корабельных исследований аэрозольно-газовых примесей над акваторией оз. Байкал летом 2018 г. // Оптика атмосферы и океана. – 2019. – Т. 32. – № 4. DOI: 10.15372/AOO20190406, Available in English, 2019.
- Khuriganova O.I., Obolkin V.A., Golobokova L.P., Bukin Y.S., Khodzher T.V. Passive Sampling as a Low-Cost Method for Monitoring Air Pollutants in the Baikal Region (Eastern Siberia) // Atmosphere. – 2019. – V. 10, art# 470. – P. 1-13. DOI: 10.3390/atmos10080470
- Kupiainen K., Black carbon in the Arctic and mitigation options – emissions and policies, presentation available at https://arctic-council.org/images/PDF_attachments/COP24_2018/2018-11-10-COP24-Kupiainen-slcip-presentation.pdf, 2018 (available at Arctic Council webpages of <https://arctic-council.org/index.php/en/our-work/2/8-news-and-events/501-cop24>).
- Meinander O. (ed). Geophysica Finland100 special issue, dedicated to the 7th National Seminar on Snow on the day of Pyry, in collaboration with the COST ES1404 Action (*Blizzard) and as part of the Finland100 celebration programme, held at the Finnish Meteorological Institute on 1 November, 2017. Geophysica 53 (1), 2018. <http://www.geophysica.fi/index.php?action=openlist&decade=2010>
- Meinander, O., Kontu, A., Virkkula, A., Arola, A., Backman, L., Dagsson-Waldhauserová, P., Järvinen, O., Manninen, T., Svensson, J., de Leeuw, G., and Leppäranta, M. (2014). Brief communication: Light-absorbing impurities can reduce the density of melting snow. *Cryosphere* 8, 991–995. doi.org/10.5194/tc-8-991-2014.
- Meinander, Dagsson-Waldhauserova et al. (including all co-authors with contributions from IBA-FIN-BCDUST WSs in Iceland, Russia and Finland in 2019), An Update to High Latitude Dust Sources, manuscript in preparation., 2019.
- Meredydd Evans, Nazar Kholod, Teresa Kuklinski, Artur Denysenko, Steven J. Smith, Aaron Staniszewski, Wei Min Hao, Liang Liu, Tami C. Bond. Black carbon emissions in Russia: A critical review, Atmospheric Environment 163 (2017) 9-21
- Obolkin Vladimir, Khodzher Tamara, Sorokovikova Larisa, Tomberg Irina, Netsvetaeva Olga & Golobokova Ludmila. Effect of long-range transport of sulphur and nitrogen oxides from large coal power plants on acidification of river waters in the Baikal region, East Siberia // International Journal of Environmental Studies. — 2016. — Т. 73. — № 3. — С. 452-461. <https://link.springer.com/article/10.1134/S1024856019040067>)
- Popovicheva, Olga & Diapouli, Evangelia & Makshatas, A. & Shonija, N. & Manousakas, Manousos-Ioannis & Saraga, Dikaia & Uttal, Taneil & Eleftheriadis, Konstantinos. (2018). East Siberian Arctic background and black carbon polluted aerosols at HMO Tiksi. Science of The Total Environment. 655. 10.1016/j.scitotenv.2018.11.165.
- Sakerin, S.M., L.P. Golobokova, D.M. Kabanov, D.A. Kalashnikova, V.S. Kozlov, I.A. Kruglinsky, V.I. Makarov, A.P. Makshatas, S.A. Popova, V.F. Radionov, G.V. Simonova, Yu.S. Turchinovich, T.V. Khodzher, O.I. Khuriganowa, O.V. Chankina, D.G. Chernov Measurements of physical-chemical characteristics of atmospheric aerosol at “Ice Base Cape Baranov” in 2018 [Izmereniya fiziko-khimicheskikh kharakteristik atmosfernogo aerolya na «ledovoy baze mys Baranov» v 2018 godu] Atmospheric and Oceanic Optics, 2019, N6, P421-429 (in Russian; Сакерин С.М., Голобокова Л.П., Кабанов Д.М., Калашникова Д.А., Козлов В.С., Круглинский И.А., Макаров В.И., Макштас А.П., Попова С.А., Радионов В.Ф., Симонова Г.В., Турчинович Ю.С., Ходжер Т.В., Хуриганова О.И., Нанкина О.В., Чернов Д.Г. Результаты измерений физико-химических характеристик атмосферного аэрозоля на научно-исследовательском стационаре «Ледовая база “Мыс Баранова”» в 2018 г. // Оптика атмосферы и океана. – 2019. – Т. 32. – № 6. – С. 421-429. DOI: 10.15372/AOO20190601)

- Sakerin S.M., Bobrikov A.A., Bukin O.A., Golobokova L.P., Pol'kin Vas.V., Pol'kin Vik.V., Shmirko K.A., Kabanov D.M., Khodzher T.V., Onischuk N.A., Pavlov A.N., Potemkin V. L., Radionov V.F. On measurements of aerosol-gas composition of the atmosphere during two expeditions in 2013 along the Northern Sea Route // *Atmos. Chem. Phys.* – 2015. – № 15. – C. 12413-12443.
- Sand, M., Berntsen, T.K., Von Salzen, K., Flanner, M.G., Langner, J. and Victor, D.G. (2016). Response of Arctic temperature to changes in emissions of short-lived climate forcers. *Nature Climate Change*, 6(3), p.286.
- Schmeisser, L., Backman, J., Ogren, J. A., Andrews, E., Asmi, E., Starkweather, S., Uttal, T., Fiebig, M., Sharma, S., Eleftheriadis, K., Vratolis, S., Bergin, M., Tunved, P., and Jefferson, A.: Seasonality of aerosol optical properties in the Arctic, *Atmos. Chem. Phys.*, 18, 11599–11622, <https://doi.org/10.5194/acp-18-11599-2018>, 2018.
- Sogacheva, L., Popp, T., Sayer, A. M., Dubovik, O., Garay, M. J., Heckel, A., Hsu, N. C., Jethva, H., Kahn, R. A., Kolmonen, P., Kosmale, M., de Leeuw, G., Levy, R. C., Litvinov, P., Lyapustin, A., North, P., and Torres, O.: Merging regional and global AOD records from 15 available satellite products, *Atmos. Chem. Phys. Discuss.*, <https://doi.org/10.5194/acp-2019-446>, in review, 2019.
- Vasilatou V, Manousakas M, Gini M, Diapouli E, Scoullou M and Eleftheriadis K (2017) Long Term Flux of Saharan Dust to the Aegean Sea around the Attica Region, Greece. *Front. Mar. Sci.* 4:42. doi: 10.3389/fmars.2017.00042
- Vet R., Artz R.S., Carou S., Shaw M., Ro C.-U., Aas W., Baker A, Bowersox V.C., Dentener F., Galy-Lacaux C., Hou A., Pienaar J.J., Gillett R., Forti. M.C., Gromov S., Hara H., Khodzher T., Mahowald N.M., Nickovic S., Rao P. S. P., Reid N.W. A global assessment of precipitation chemistry and deposition of sulfur, nitrogen, sea salt, base cations, organic acids, acidity and pH, and phosphorus // *Atmospheric Environment*. - 2014. - V. 93, № Special Issue. - P. 3-100.
- Zhamsueva G., Zayakhanov A., Starikov A., Tsydypov V., Khodzher T., Golobokova L., Marinayte I., Onichyk N., Azzaya D., Oyunchimeg D. Water-soluble inorganic ions and PAHs of summer PM10 samples in Mongolia during 2005-2010. // *Atmospheric Pollution Research*. – 2015. – T. 6. – № 1. – C. 120-128. DOI: 10.5094/APR.2015.014 (12887)

CLIMATIC SIGNIFICANCE OF BIOGENIC AEROSOLS IN WARMING BOREAL FOREST: PART 2. SATELLITE OBSERVATIONS OF AEROSOLS AND CLOUDS

T. MIELONEN¹, T. YLI-JUUTI², A. VIRTANEN², A. HIENOLA³, T. KÜHN², J. MERIKANTO³, A. LIPPONEN¹, A. LAAKSO¹, T. BERGMAN², H. KORHONEN², P. KOLMONEN², L. SOGACHEVA², M.R.A. PITKÄNEN¹, A. AROLA¹, G.F.R DE LEEUW^{2,4}, and H. KOKKOLA¹

¹ Finnish Meteorological Institute, Kuopio, Finland.

² University of Eastern Finland, Applied Physics, Kuopio, Finland.

³ Finnish Meteorological Institute, Helsinki, Finland.

⁴ Department of Physics, University of Helsinki, Finland

Keywords: remote sensing, satellite, aerosol, cloud, temperature.

INTRODUCTION

Aerosols are an important regulator of the Earth's climate. They scatter and absorb incoming solar radiation and thus cool the climate by reducing the amount of energy reaching the atmospheric layers and the surface below (direct effect) (e.g. Charlson et al., 1992). A certain subset of the particles can also act as initial formation sites for cloud droplets and thereby modify the microphysics, dynamics, radiative properties and lifetime of clouds (indirect effects) (Albrecht, 1989; Twomey, 1991; Stevens and Feingold, 2009). The magnitude of aerosol radiative effects remains the single largest uncertainty in current estimates of anthropogenic radiative forcing (IPCC, 2013).

One of the key quantities needed for accurate estimates of anthropogenic radiative forcing is an accurate estimate of the radiative effects from natural unperturbed aerosol. The dominant source of natural aerosols over Earth's vast forested regions are biogenic volatile organic compounds (BVOC) which, following oxidation in the atmosphere, can condense onto aerosol particles to form secondary organic aerosol (SOA) and significantly modify the particles' properties. In accordance with the expected positive temperature dependence of BVOC emissions (Penuelas and Staudt, 2010; Duncan et al., 2009), several previous studies have shown that some aerosol properties, such as mass concentration and ability to act as cloud condensation nuclei (CCN), also correlate positively with temperature at many forested sites (e.g. Tunved et al., 2006; Leaitch et al., 2011; Paasonen et al., 2013, Mielonen et al., 2018). The evidence for an effect of temperature on aerosol radiative effects over boreal forests due to increased BVOC emissions, however, is less clear.

The main objective of this study was to investigate the effect of increasing temperatures on the aerosol-cloud interaction, and estimate the significance of the plausible negative feedback in a warming climate. More specifically, we studied the causes of the positive correlation between aerosol properties, temperature and cloud properties over southern Finland where biogenic emissions are a significant source of atmospheric particles. In the first part of this study we concentrated on the observations from measurements done at the Hyytiälä site and analysed the temperature dependence of organic aerosol (OA) concentration and AOD (Yli-Juuti et al., 2019). In this second part we compared the temperature dependence of OA to satellite-based observations to investigate the influence of changes in OA to cloud properties.

METHODS

The study was done using a combination of satellite and re-analysis data. Key remote sensing data used were the aerosol optical depth (AOD), cloud effective radius (CER) and cloud top height (CTH). These data sets were available from the Moderate Resolution Imaging Spectroradiometer (MODIS) instrument on-board the Aqua satellite. The analysis of the satellite retrievals was done using daily Level 3 products with 1×1 degree resolution for the summers 2004-2018. The study region was southern Finland (between latitudes 60° and 66° , and longitudes 21° and 30°).

In order to estimate the effect of meteorology on cloud properties we analysed several meteorological parameters available from the ECMWF ERA-Interim re-analysis. The analysed parameters were: wind speed and direction, relative humidity, lower tropospheric stability, total column water vapour and surface pressure. We collocated the meteorological data with the satellite product and calculated monthly and summertime (July-August) averages for the analysis. The contributions of aerosols and meteorology on aerosol-cloud interaction were evaluated using statistical methods.

RESULTS AND CONCLUSIONS

In this study we estimated the dependency of AOD and CER on temperature over southern Finland and approximated the climatic significance of aerosol-cloud interaction over this region.

The main conclusions of this study are:

- Over Hyytiälä, both ground-based AOD from AERONET and satellite retrieved AOD from MODIS increase as temperature increases.
- Over southern Finland, the satellite based AOD exhibits temperature dependence which is mainly due to biogenic emissions.
- CER decreases as temperature rises but the decrease is mainly caused by changes in synoptic meteorology and decrease in cloud top height, not aerosols.

ACKNOWLEDGEMENTS

This work was funded by the ESA Living Planet Fellowship (ESA contract No. 4000112802/14/I-SBo), the Academy of Finland Centre of Excellence in Atmospheric Science (272041) and Academy Research Fellowship (250348, 256208) and Academy projects RECIA and RECON (287440, 308292), ERC Consolidator Grant ECLAIR (646857), and the Nordic Center of Excellence eSTICC (sScience Tool for Investigating Climate Change in northern high latitudes) funded by Nordforsk (grant 57001).

REFERENCES

- Albrecht, B.A. (1989). Aerosols, Cloud Microphysics, and Fractional Cloudiness. *Science* 245 (4923): 1227–30.
- Charlson et al. (1992). Climate forcing by anthropogenic aerosols. *Science* 255, 423–430.
- Duncan, B. N., Y. Yoshida, M. R. Damon, A. R. Douglass, and J. C. Witte (2009). Temperature dependence of factors controlling isoprene emissions, *Geophys. Res. Lett.*, 36, L05813.
- International Panel on Climate Change (2013). *Climate Change 2013: The Physical Science Basis. Contribution of Working Group I to the Fifth Assessment Report of the Intergovernmental Panel on Climate Change*, edited by: Stocker, T. F., Qin, D., Plattner, G.-K., Tignor, M., Allen, S. K., Boschung, J., Nauels, A., Xia, Y., Bex, V., and Midgley, P. M., Cambridge University Press, Cambridge, United Kingdom and New York, NY, USA, 1535 pp.
- Mielonen, T., Hienola, A., Kühn, T., Merikanto, J., Lipponen, A., Bergman, T., Korhonen, H., Kolmonen, P., Sogacheva, L., Ghent, D., Pitkänen, M.R.A., Arola, A., de Leeuw, G., Kokkola, H. (2018).

Summertime Aerosol Radiative Effects and Their Dependence on Temperature over the Southeastern USA. *Atmosphere*, 9, 180.

- Paasonen, P., Asmi, A., Petäjä, T., Kajos, M. K., Aijala, M., Junninen, H., Holst, T., Abbatt, J. P. D., Arneth, A., Birmili, W., van der Gon, H. D., Hamed, A., Hoffer, A., Laakso, L., Laaksonen, A., Leaitch, W. R., Plass-Duelmer, C., Pryor, S. C., Raisanen, P., Swietlicki, E., Wiedensohler, A., Worsnop, D. R., Penuelas, J. and Staudt, M. (2010). BVOCs and global change, *Trends in Plant Sci.*, 15, 133-144.
- Penuelas, J. and Staudt, M. (2010). BVOCs and global change, *Trends in Plant Sci.*, 15, 133-144.
- Stevens, B., and G. Feingold (2009). Untangling aerosol effects on clouds and precipitation in a buffered system. *Nature*, 461, doi:10.1038/nature08281
- Tunved, P., Hansson, H. C., Kerminen, V-M., Strom, J., Dal Maso, M., Lihavainen, H., Viisanen, Y., Aalto, P. P., and Komppula, M., Kulmala, M. (2006). High natural aerosol loading over boreal forests. *Science*, 312(5771), 261-263. 10.1126/science.1123052.
- Twomey, S. (1991). Aerosols, clouds, and radiation. *Atmos. Environ.*, 25, 2435–2442.
- Yli-Juuti, T. et al. (2019), Climatic significance of biogenic aerosols in warming boreal forest: Part 1. In situ observations of inorganic aerosol in Proceedings of 'the Center of Excellence in Atmospheric Sciences (CoE ATM) -From Molecular and Biological Processes to the Global Climate' Annual Meeting 2019.

Climatic effects of anthropogenic aerosol emissions originating from Chile and Mexico

T. MIINALAINEN¹, H. KOKKOLA², K.E.J. LEHTINEN^{1,2} and T. KÜHN^{1,2}

¹ Department of Applied Physics, University of Eastern Finland (UEF), Kuopio, Finland.

² Atmospheric Research Centre of Eastern Finland, Finnish Meteorological Institute, Kuopio, Finland.

Keywords: GLOBAL CLIMATE MODELING, SHORT-LIVED CLIMATE FORCERS, CHILE, MEXICO

INTRODUCTION

In this study, we analyzed the climatic effects of black carbon (BC), organic carbon (OC) and sulfur dioxide (SO₂) originating from Chile and Mexico. These aerosol emissions are a subset of short-lived climate forcers (SLCFs), which are classified as compounds that have short atmospheric lifetime, but relatively strong impact on the radiative balance of the atmosphere. SLCFs include both warming agents, such as methane, ozone and BC, and also cooling substances, e.g. OC and SO₂ (AMAP, 2015). Along long-lived greenhouse gases, reducing the SLCFs have been considered as an attractive option for slowing down the global climate warming.

As a part of the multidisciplinary research project ClimaSlow, this study addresses how anthropogenic BC, OC and SO₂ potentially affect the regional climate surrounding Chile and Mexico. Principally, we focus on the changes in the radiative balance and in cloud properties since the aerosols are known to have a significant influence on these features.

The two Latin American countries were chosen for exploration mainly due to their ambitious climate strategies that include BC mitigation, and also due to the characteristics of Chilean climate. As a result of the Pacific ocean located on the western side of the Chile, and the Andes on the eastern side, there exists a semi-persistent stratocumulus cloud deck that covers part of the west coast of Chile (Zheng, Y. *et al.*, 2010). This cloud deck is influenced by the aerosols from Chilean territory, but the total magnitude and contribution of different species remain still unclear.

METHODS

We used the aerosol-climate model ECHAM6.3.0-HAM2.3-MOZ1.0 for simulating the effects of the aerosol species (Kokkola, H. *et al.*, 2018). The horizontal resolution for our setup was T63, corresponding to $1.9^\circ \times 1.9^\circ$. The vertical axis was divided to 47 hybrid sigma-pressure levels. In order to reduce the variability between different cases due to meteorology, the wind and pressure fields were nudged towards prescribed meteorology which was composed with a separate ECHAM-HAMMOZ simulation. For the sea surface temperature and sea ice cover, we used fixed monthly mean values for the years 2000 to 2015 from PCMD's Atmospheric Model Intercomparison Project (Taylor, K. E. *et al.*, 2012).

There were altogether four simulations conducted, each run consisting of ten individual simulation years. The spatial and monthly distributions of the anthropogenic aerosol fields were retrieved from the ECLIPSE V6a emission inventory (ECLIPSE V6a, 2019). For the the reference case (BASE), the aerosol emissions were represented with the current legislation scenario for the year 2015. The

other scenarios were otherwise identical to BASE, but the anthropogenic aerosol emissions from Chile and Mexico for each aerosol type were removed (scenarios named as NO_BC, NO_OC and NO_SO2). The aerosol emissions for aviation and shipping were kept identical for all the scenarios, as were the aerosols from natural sources. Finally, the data was post-processed to mean values for each individual simulation year.

CONCLUSIONS

The total anthropogenic emissions from Chile and Mexico are emitted from a relatively small area, and thereby the impacts are expected to be greatly localized. That is why we chose the region of interest (ROI) based on the differences that we obtain in the mean sulfate (SO_4) burden, presented in Figure 1. The sulfur emissions from Mexico seem to be transported towards west, whereas for

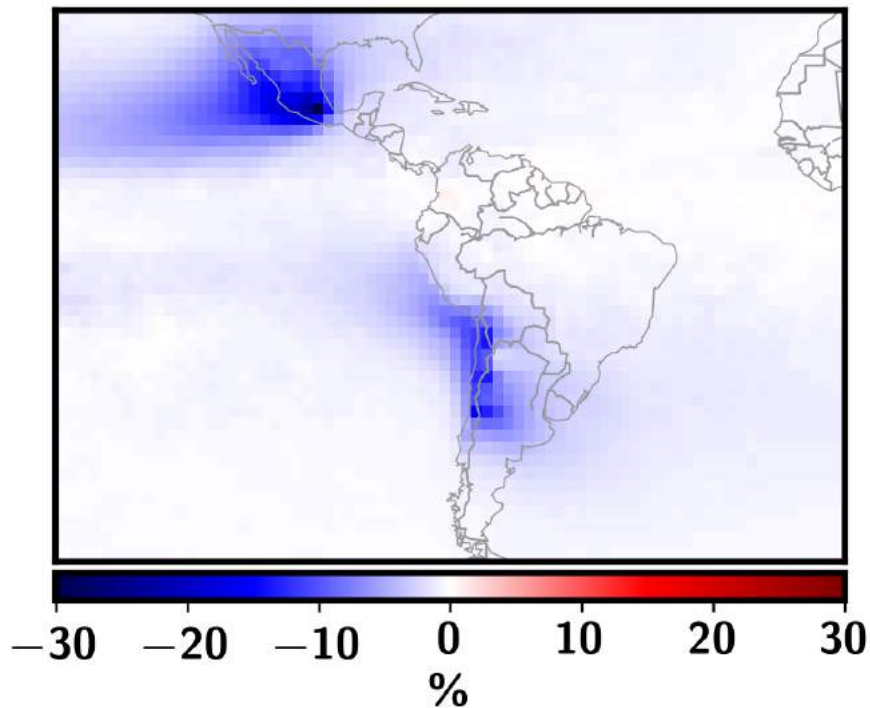


Figure 1: The mean percentage difference of total sulfate (SO_4) burden between NO_SO2 and BASE scenarios.

Chile the direction is more headed for north-west. Based on Figure 1, we chose our ROI to cover the areas where the difference in SO_4 burden is higher than 3 %.

Next, we calculated the mean field values for ROI that we chose for Chile and Mexico, and computed the vertical profiles of aerosol and cloud droplet concentrations. The mean of yearly mean values for vertical differences between scenarios and BASE case are presented in Figure 2.

The N_{100} describes the concentration of aerosol particles that have diameter larger than 100 nm, and PM2.5 refers to the mass concentration of particles that have diameter smaller than $2.5 \mu\text{m}$. As Figure 2 shows, the sulfur emissions seem to contribute the most to both N_{100} and PM2.5. This results was quite expected since the sulfur emission strengths were greater than for BC or OC. Similarly, the cloud droplet number concentration is affected the most by the sulfur emissions. Furthermore, for both Chile and Mexico, the OC emissions show much higher impact on PM2.5 and CDNC than BC. Once again, this result is quite realistic since the OC emissions are almost double the BC emissions.

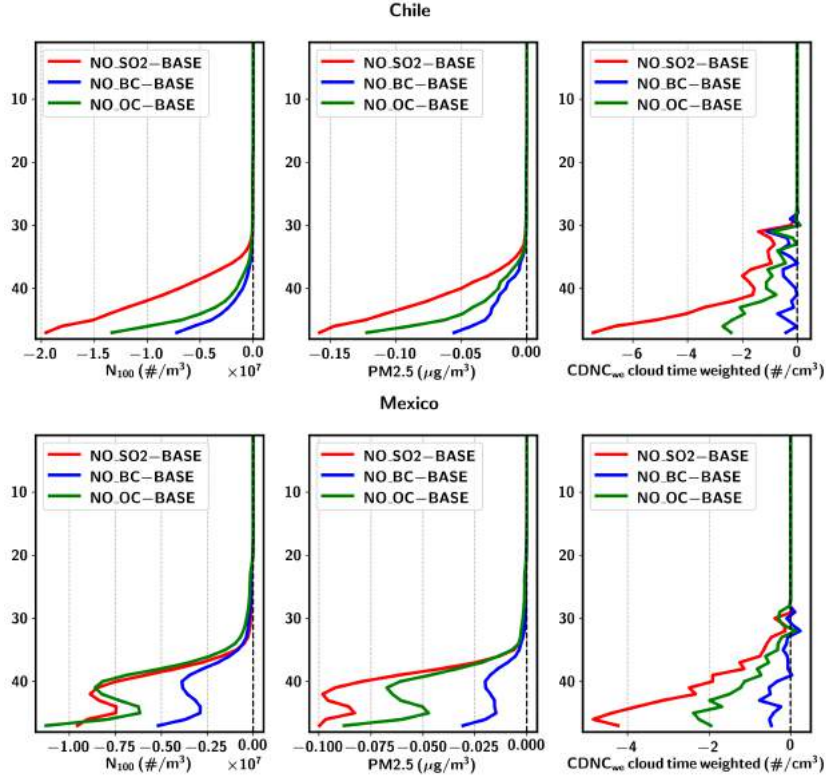


Figure 2: The vertical differences between scenarios and BASE case for N_{100} , $PM_{2.5}$ and cloud time weighted cloud droplet number concentration (CDNC), field mean values for the ROI defined for Chile (upper figure) and Mexico (lower). Here the number on y axis indicates the model height level, surface level corresponding the value of 47.

Similarly, we calculated the aerosol forcing values at the top of atmosphere (TOA) for each of the scenarios, and the results are presented in Table 1.

Chile	
scenario	Aerosol forcing (W/m^2)
NO_SO2	0.033 ± 0.008
NO_BC	-0.055 ± 0.007
NO_OC	-0.000 ± 0.009
Mexico	
scenario	Aerosol forcing (W/m^2)
NO_SO2	0.062 ± 0.015
NO_BC	-0.120 ± 0.012
NO_OC	0.000 ± 0.014

Table 1: The mean direct aerosol forcing at the top of atmosphere for Chile and Mexico.

Although the SO_2 seemed to influence more on cloud properties, the reduction of BC emissions shows a greater effect on the aerosol forcing levels, for both Chile and Mexico ROI. On the other hand, OC emissions seem to have a neutral effect on the forcing caused by anthropogenic aerosols at TOA.

ACKNOWLEDGEMENTS

This work was financially supported by the Academy of Finland Center of Excellence programme (grant no. 307331), European Research Council (ERC Starting Grant 678889) and the University of Eastern Finland Doctoral School Program in Environmental Physics, Health and Biology.

REFERENCES

- AMAP (2015). Summary for Policy-makers: Arctic Climate Issues 2015, *Arctic Monitoring and Assessment Programme (AMAP)*, Oslo, Norway.
- ECLIPSE V6a global emission fields. Personal communication with Z. Klimont, (2019).
- Kokkola, H. *et al.*, (2018). SALSA2.0: The sectional aerosol module of the aerosol-chemistry–climate model ECHAM6.3.0-HAM2.3-MOZ1.0 *Geoscientific Model Development*, **11**, 3833
- Taylor, K. E. *et al.*, (2012). An Overview of CMIP5 and the Experiment Design *Bulletin of the American Meteorological Society*, **93**, 485–498
- Zheng, Y. *et al.* (2010). Upper-Ocean Processes under the Stratus Cloud Deck in the Southeast Pacific Ocean, *J. Phys. Oceanogr.*, **40**, 103-120.

SLOPE AND VALLEY WINDS IN THE HIMALAYAS AS SIMULATED BY THE WEATHER RESEARCH AND FORECAST MODEL (WRF)

J.W. MIKKOLA¹, V. A. SINCLAIR¹, F. BIANCHI¹

¹ Institute for Atmospheric and Earth System Research, University of Helsinki, Helsinki, P.O. Box 64, 00014, Finland

Keywords: Boundary-layer ventilation, Mountain meteorology, Nepal Climate Observatory - Pyramid station, Slope winds, Valley winds, Weather Research and Forecasting Model

INTRODUCTION

Wind systems of mountainous areas are strictly ruled by diurnal cycles of mountain winds. The diurnal cycle of winds are driven by temperature differences caused by an uneven distribution of solar heating between valley center and slopes. Typically the diurnal cycle includes up-slope and up-valley winds during daytime and vice versa. The wind direction is mainly caused by the slopes heating up before valley center during daytime and again cooling down faster at night. The diurnal cycle is strongest on days with clear skies and weak synoptic winds. Valley winds may be dominated by strong synoptic scale winds and flows created by local topography. Our aim is to define valley wind systems characteristics in the area of Himalayas close to Nepal Climate Observatory - Pyramid station (NCO-P). Earlier results from simpler valley simulations give us a good start and the detailed behaviour of valley winds will be determined by analyzing high resolution WRF simulations. NCO-P is located in 27.95°N, 86.82°E at 5079 meters above sea level near Mount Everest base camp.

METHODS

We used the Weather Research and Forecasting (WRF) model (version 3.6.1) in this study. WRF is a state-of-the-art numerical weather prediction model which is a fully compressible, non-hydrostatic model. We performed one continuous simulation with WRF which had a parent domain (referred to as d01) and 3 nested domains (d02, d03 and d04). The parent domain covers an area 3618 km by 2997 km and has a grid spacing of 27 km. The three nested domains have grid spacings of 9, 3 and 1 km respectively. The inner most domain (d04) is centered on the Pyramid station and covers an area of 288 km by 300 km. All nests have 61 vertical levels. The simulation is initialised with Climate Forecast System Reanalysis (CFSR, (Saha et al., 2010)) data which has a horizontal resolution of 0.5 degrees. The surface topography data is from the United States Geological Survey (USGS) at a horizontal resolution of 30 arc seconds (approximately 1 km). During the simulation, the parent domain is nudged towards the reanalysis fields which have a temporal resolution of 6 hours, however, the nudging is only applied above the planetary boundary layer. Performing the nudging allows us to perform one continuous simulation. The simulation is initialized at 00 UTC on 17 December 2014 and runs until 23:59 UTC on 21 December 2014. To ensure that the model did not become numerically unstable, we used an adaptive time step which was calculated based on a target Courant-Friedrichs-Lewy (CFL) criterion of 0.8. Typically, the time step of the inner domain was approximately 1 second. In addition, 6th order numerical diffusion was applied and w-Rayleigh damping was applied over the upper-most 5 km of the model domain. Subgrid-scale physical processes were parameterized: Microphysics was parameterized by the Thompson scheme, long and

short-wave radiation by the RRTMG scheme, but for computational efficiency the radiation scheme was only called every 5 time steps, boundary-layer turbulence was parametrized using the Mellor-Yamada-Janjic (Eta) TKE scheme and surface layer physics with the Monin-Obukhov similarity scheme.

The highest resolution domain covers multiple large valleys. The location of four major valleys was objectively identified using a script that searches for the valley bottom line from a given grid point at the head of the valley. The wind systems in these valleys was studied via various plots. In addition to maps of surface heat flux, 2 meter temperature, 10 meter wind and land use categories we plotted along-valley and slope-to-slope cross sections of wind and potential temperature. Along-valley cross section plotting required the grid points for the valley bottom line, which were available from the objective valley identification code. These grid points were also used for plotting time series from different parts of the valley bottom line and slopes.

CONCLUSIONS

Although four major valleys were considered, the results shown here are for the valley in which the Pyramid station is located. This valley is oriented roughly north-south and is over 100 km in length. Three cross-sections along this valley were analysed and are referred to as the bottom (furthest south, closest to the Indo-Gangetic Plain), the middle, and the head of the valley (furthest north, closest to the Pyramid station and at the highest altitude). Analysis of the slope and valley winds in this valley showed that results from earlier studies apply to this valley on the most part. In the middle and bottom of the valley there is a clear diurnal behaviour that is similar to simulations performed for simpler valleys (Whiteman, 2000) (Figures 1b,c). After sunrise the up-slope wind increases and reaches its peak at noon. During night there is a down-slope wind with a lower velocity.

Slope winds at the head of this valley (Figure 1a) are dominated by effects from synoptic-scale winds and the steep, high topography of the surrounding ridge tops on the first and forth day of simulation. The mountain top to the west (and hence upstream) of the grid points shown in Figure 1a has a huge effect on the slope winds simulated near the head of this valley: on the west slope there are down-slope wind speeds exceeding 9 ms^{-1} on two days. The mountain top acts a barrier to the synoptic-scale, upper-levels winds which are from the west which causes the air to rise rapidly up and over the mountain barrier. This triggers a gravity-wave type response which results in strong vertical motions within the valley on the lee side of the mountain. These vertical motions translate into slope winds which complete dominate over the surface heat flux driven slope wind system. This connection between upper-level wind direction and the slope winds at the head of the valley was identified by comparing Figure 1a and 450 hPa winds (not shown). On days with north or north-west upper-level, synoptic-scale wind the slope winds at the point at the head of the valley were found to behave in a similar manner as in the middle and bottom of the valley.

Along-valley winds in this valley behave as predicted by the surface heat flux driven valley wind. The up-valley wind speed increases from sun rise reaching its peak at 2-3 pm local time each day (Figure 2). During the first day and night of the simulation there was a strong synoptic-scale northerly wind which can also be seen in the valley winds (Figure 2). Future work will include extending the analysis to other major Himalayan valleys in the model domain to quantify variability between valleys, investigating the gravity-wave induced slope-winds further, and determining the relative impact of the slope and valley flows to ventilating particles out of these valleys to the free troposphere.

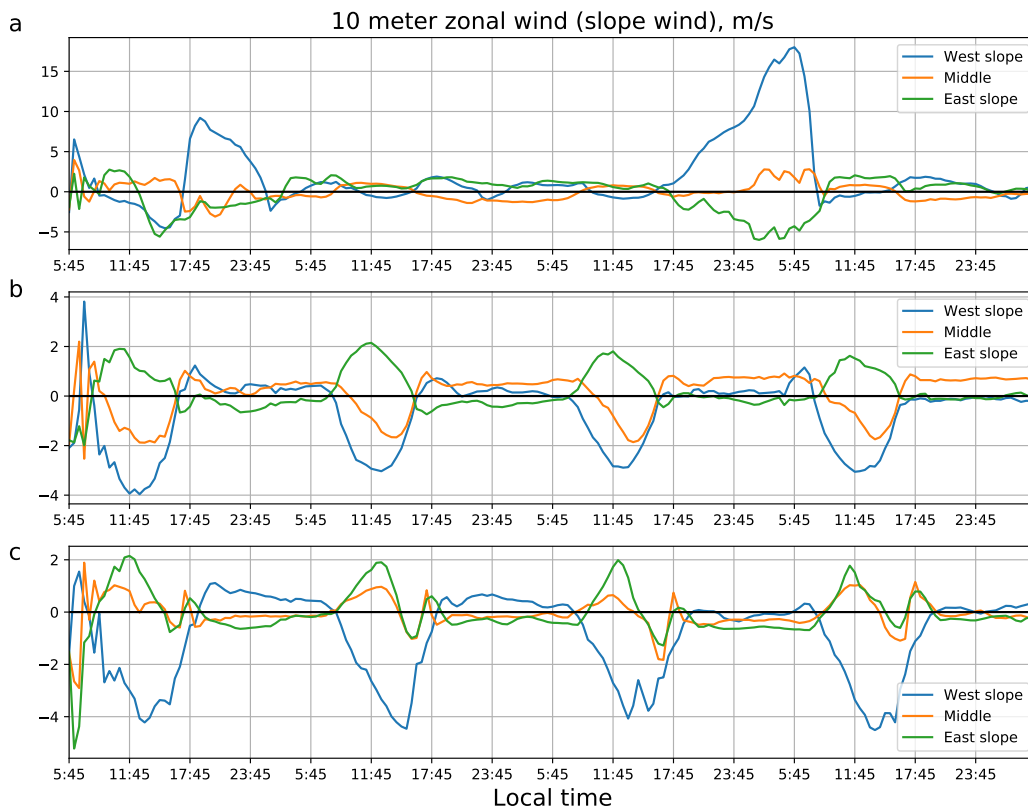


Figure 1: 10 meter zonal wind (slope wind). Panel (a) shows the head of the valley, (b), the middle of the valley and (c) the bottom of the valley. Negative values on west slope (blue lines) and positive values on east slope (green lines) indicates up-slope wind and vice versa.

ACKNOWLEDGEMENTS

We acknowledge CSC –IT Center for Science, Finland, for generous computational resources which enabled the WRF simulations to be conducted.

REFERENCES

C. David Whiteman (2000) *Mountain Meteorology*. Oxford University Press

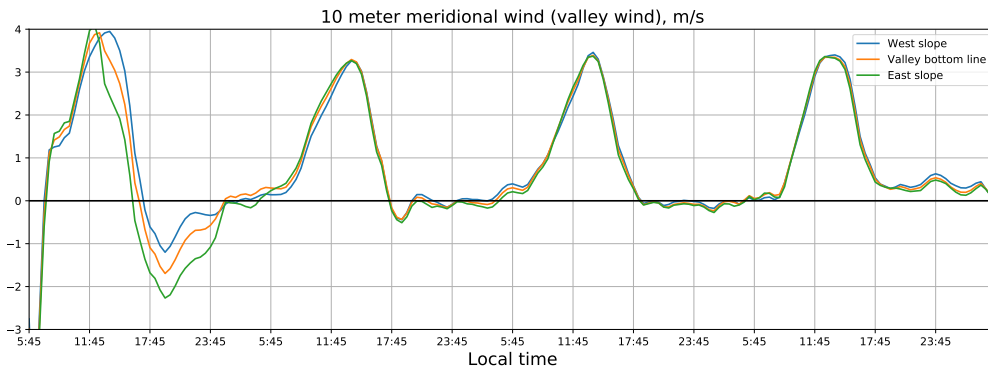


Figure 2: 10 meter meridional wind (along-valley wind). Positive values indicate up-valley wind (approximate southerly wind) and negative values indicated down-valley winds (approximately northerly flow).

TIME TRENDS OF PARTICLE NUMBER CONCENTRATIONS IN BUDAPEST BETWEEN 2008 AND 2018

SANTTU MIKKONEN^{1,2}, ZOLTÁN NÉMETH³, VERONIKA VARGA³, TAMÁS WEIDINGER⁴,
VILLE LEINONEN¹, TAINA YLI-JUUTI¹ and IMRE SALMA³

¹ Department of Applied Physics, University of Eastern Finland, Kuopio, Finland

² Department of Environmental and Biological Sciences, University of Eastern Finland, Kuopio, Finland

³ Institute of Chemistry, Eötvös University, Budapest, Hungary

⁴ Department of Meteorology, Eötvös University, Budapest, Hungary

Keywords: Aerosol Concentration, Trend Analysis, Natural vs. Anthropogenic Emission.

INTRODUCTION

Research activity dedicated to urban new particle formation (NPF) and growth events in Budapest have been going on since November 2008. Measurements for 6 full years were realised in the city centre at a constant and fixed location. Semi-continuous data sets containing particle number concentrations in various size ranges, concentrations of criteria pollutants and meteorological data are available by now and were utilised to determine time trends for particle number concentrations from 2008 to 2018, thus for a decennial interval. The main objectives of this study are to present and discuss the statistical model developed specifically for the time trend analysis of particle number concentrations, to interpret its results for diurnal variability and time trends, and to relate the temporal tendencies to different atmospheric sources, processes and environmental circumstances.

METHODS

The experimental data dealt with in the present study are related to the Budapest platform for Aerosol Research and Training (BpART) facility. The site represents a well-mixed, average atmospheric environment for the city centre due to its geographical, physical and meteorological conditions (Salma et al., 2016). A time interval from 03–11–2008 to 02–11–2018 was considered for the purposes of the present study. The data consists of particle number concentrations measured with differential mobility particle sizer (DMPS), meteorological data and concentrations of key pollutants: SO₂, CO, NO, NO_x, O₃, and PM₁₀ mass.

The data were analysed in two phases. Firstly, the trends for concentrations for particles and main pollutants were estimated with dynamic linear model (DLM), method described in Mikkonen et al. (2015). Secondly, the factors affecting the changes in particle concentration were detected with linear mixed model (LMM) in similar manner as in Mikkonen et al. (2011).

RESULTS

We found that the particle number concentrations have been decreasing within the decennial period covered by our measurements. The deepest decrease in particle number has been in the smallest particle size class of 6-100 nm in diameter. The data suggests that the annual mean relative occurrence frequency of new particle formation events stayed almost constant over the time interval considered and formation rate of new particles has not decreased. Thus the decrease in the number of nucleation mode particles is possibly due to decrease in direct emissions from traffic or industry. This is yet to be confirmed. Fig. 1 shows the diurnal pattern of nucleation mode particle number concentration on event- and non-event days on weekdays and weekends. It shows that traffic is significant contributor on the particle number, as on weekdays a notable peak on morning rush hour can be seen.

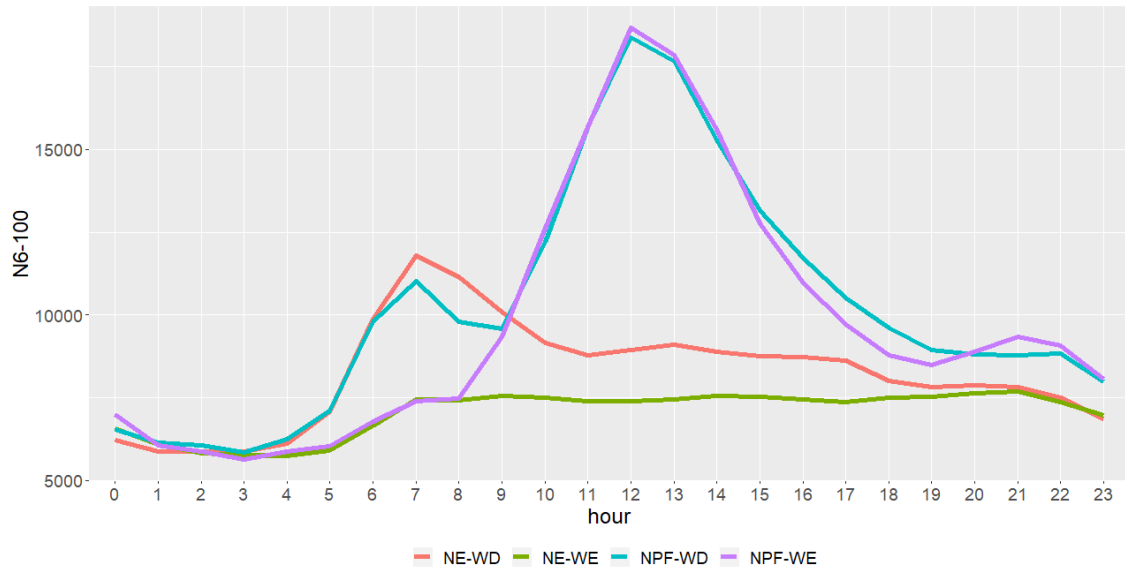


Figure 1. Diurnal pattern of 6-100 nm particle concentration in cm^{-3} units. Red=nonevent on weekday, green=nonevent on weekend, cyan=event on weekday, purple=event on weekend

Figure 2 shows that the effect of NPF on concentration of the larger particles in size group of 100-1000 nm in diameter is not visible in diurnal variation due to moderate growth rates of newly formed particles observed in Budapest. However, morning rush hour peaks are clearly visible in weekdays. In addition, changes in mixing layer height can be seen especially in the evenings in all days.

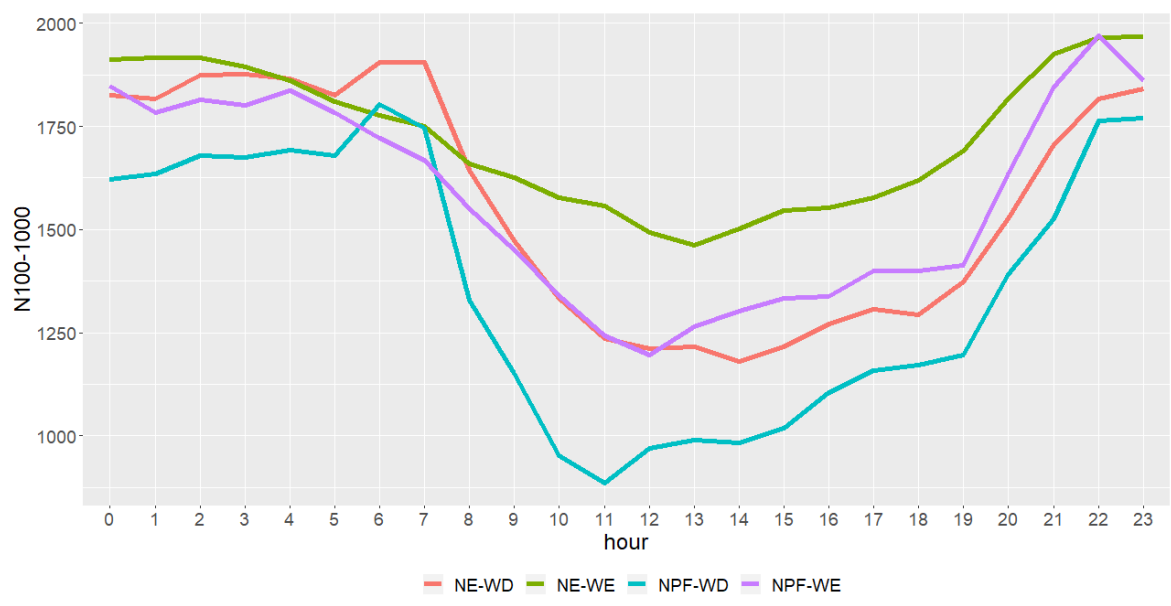


Figure 2. Diurnal pattern of 100-1000 nm particle concentration in cm^{-3} units. Red=nonevent on weekday, green=nonevent on weekend, cyan=event on weekday, purple=event on weekend

ACKNOWLEDGEMENTS

Financial support by The Academy of Finland Centre of Excellence (grant no. 307331), The National Research, Development and Innovation Office, Hungary (contracts K116788 and PD124283) and The Nessling foundation and is gratefully acknowledged.

REFERENCES

- Mikkonen, S. et al. (2011) Meteorological and trace gas factors affecting the number concentration of atmospheric Aitken ($D_p = 50$ nm) particles in the continental boundary layer: parameterization using a multivariate mixed effects model. *Geosci. Model Dev.*, 4, 1-13.
- Mikkonen, S. et al. (2015) Trends in the average temperature in Finland, 1847-2013. *Stoch Environ Res Risk Assess.* 29. 1521-1529.
- Salma, I., et al. (2016) Measurement, growth types and shrinkage of newly formed aerosol particles at an urban research platform. *Atmos. Chem. Phys.*, 16, 7837–7851.

THE ACTIVITY OF ROOTS AND SOIL MICROBES ALONG A LATITUDINAL GRADIENT

M. MÄKI^{1,2}, P. VESTIN³, M. ROLAND⁴, B. TUPEK⁵, K. RYHTI^{1,2}, J. PUMPANEN⁶, J. HEINONSALO^{2,7}, J. BÄCK^{1,2}, and L. KULMALA^{1,2,7}

¹Institute for Atmospheric and Earth System Research / Forest Sciences

²Faculty of Agriculture and Forestry, University of Helsinki, Finland

³Department of Physical Geography and Ecosystem Science, Lund University, Sweden

⁴University of Antwerpen, Belgium

⁵Natural Resources Institute, Finland.

⁶University of Eastern Finland, Finland

⁷Finnish Meteorological Institute, Helsinki, Finland

Keywords: CO₂ FLUX, PINE, SPRUCE, FOREST, CARBON CYCLE.

INTRODUCTION

Tree roots are a major carbon sink in forest ecosystems, but still the dynamics of belowground carbon allocation for growth, maintenance and root symbionts remains poorly understood. For this reason, it is difficult to estimate how the global carbon balance in soils will change, when climate warming proceeds. As heterotrophic activity is mainly driven by temperature, the heterotrophic respiration may overcome ecosystem CO₂ uptake and change soils from carbon sinks and reservoirs to carbon sources. Warming-driven emissions from soil carbon storages were already observed (Bond-Lamberty, 2018). This project aims to assess the following hypotheses by determining the role of heterotrophic (saprotrophic microbial activity) and autotrophic (activity of tree roots, root-associated microbes and forest floor vegetation) respiration in soils along a latitudinal gradient in Northern Europe (Fig. 1). 1) The northern trees allocate more carbon below-ground than the southern ones. 2) Heterotrophic respiration follows more clearly the changes in environmental factors such as soil moisture and temperature than autotrophic respiration which follows also the changes in aboveground physiology. 3) Increased water availability after drought has a different effect on autotrophic and heterotrophic respiration, because drying-wetting cycles accelerate microbial decomposition (Jarvis et al., 2007), when roots release exudates into surrounding soil to balance over uptake of water.



Figure 1. Automatic soil CO₂ flux measurement chambers along a latitudinal gradient in boreal and temperate climates.

METHODS

This experiment was carried out using eight measurement sites: a northern boreal forest covered mainly by Scots pine (*Pinus sylvestris*), three southern boreal forests covered mostly by Scots pine, two southern boreal forests covered mostly by Norway spruce (*Picea abies*), a southern boreal forest covered by a mixture of Scots pine and Norway spruce and a temperate forest covered mainly by Scots pine (Fig. 1). CO₂ fluxes, soil temperature, soil water content and litter decomposition were measured from these sites between 2015 and 2017. In order to separate the contribution of heterotrophic and autotrophic respiration on forest floor CO₂ fluxes, we used the trenching treatment. In this treatment, a volume of soil was dug up to a depth of 40 cm around an intact plot. Roots growing into or out to the plot were cut and the plot was isolated from the surrounding soil using mesh with 1 μm holes. The mesh inhibits the ingrowth of roots and mycorrhizal fungi, but allows the flow of water. Surrounding soil was placed back into the trench and CO₂ fluxes were measured inside these experimental plots to define heterotrophic respiration. Autotrophic respiration was estimated by subtracting heterotrophic respiration from total respiration measured from other intact control plots. CO₂ fluxes were measured using both continuous and campaign based measurements from spring to late autumn. CO₂ fluxes were measured using a dark static chamber technique, where CO₂ concentration of chamber headspace was monitored and the CO₂ efflux was estimated based on linear fitting against time.

PRELIMINARY RESULTS

The total CO₂ emissions of roots, root-associated microbes and forest floor vegetation were highest in the southernmost boreal forest (NORUNDA), in mixed Scots pine and Norway spruce forest stand (Fig. 2d). The forest floor plants, present mostly in Scots pine forest and which abundance could be expected to decrease from north to south, did not affected strongly the north to south increase pattern of forest floor respiration where tree roots were excluded (Fig. 2a). The autotrophic respiration of forest floor plants thus had minor contribution to total forest floor CO₂ emission and the north-south increase can be attributed to the microbial heterotrophic respiration. Microbial activity, defined as heterotrophic respiration, increased from north to south more clearly in the Scots pine than in Norway spruce forests (Figs. 2a and 2c). However, the activity of tree roots, root-associated microbes and forest floor vegetation measured as autotrophic respiration, increased from north to south only in the Norway spruce forests (Fig. 2d).

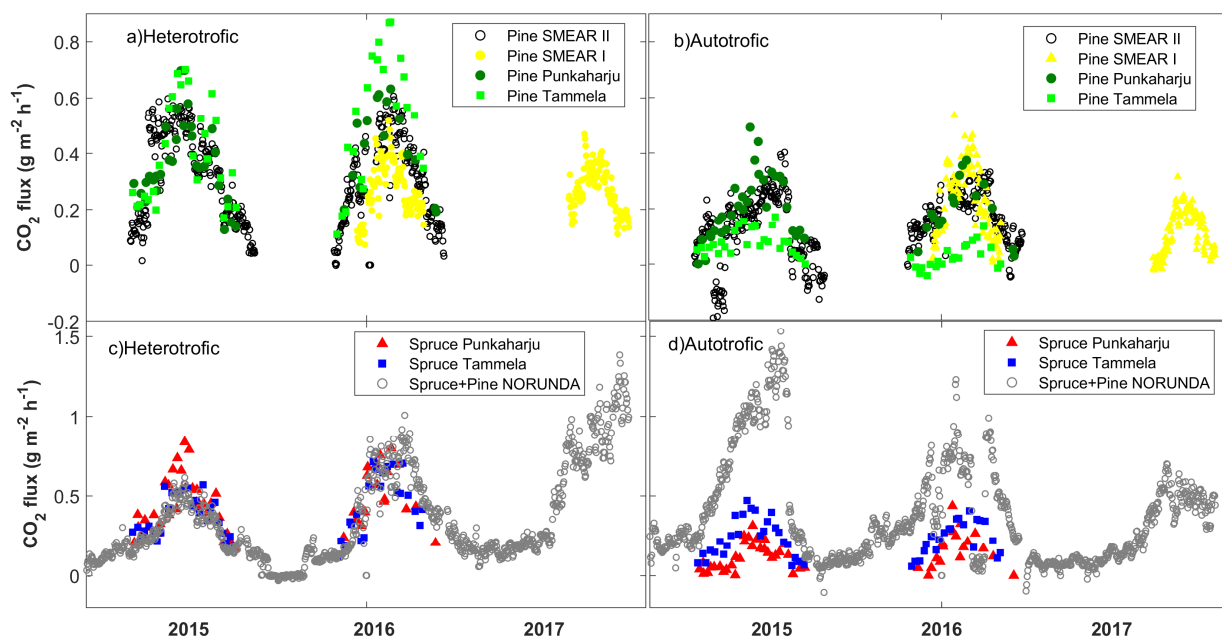


Figure 2. The activity of saprotrophic microbes (heterotrophic) and activity of tree roots, root-associated microbes and forest floor vegetation (autotrophic) in Scots pine and Norway spruce forests along a latitudinal gradient.

ACKNOWLEDGEMENTS

Work was supported by the Helsinki University Funds, Kone Foundation, the Academy of Finland (grant no. 277623) and Academy of Finland Center of Excellence programme (grant no. 307331).

REFERENCES

- Bond-Lamberty, B., V. L. Bailey, M. Chen, C. M. Gough, and R. Vargas (2018) Globally rising soil heterotrophic respiration over recent decades, *Nature*, 560, 80–83. <https://doi.org/10.1038/s41586-018-0358-x>
- Jarvis, P., A. Rey, C. Petsikos, L. Wingate, M. Rayment, J. Pereira, J. Banza, J. David, F. Miglietta, M. Borghetti, G. Manca, V. Riccardo V (2007) Drying and wetting of Mediterranean soils stimulates decomposition and carbon dioxide emission: the “Birch effect”, *Tree Physiology*, 27, 929–940. <https://doi.org/10.1093/treephys/27.7.929>

COMPETITION PROMOTES RELEASE OF VOLATILE ORGANIC COMPOUNDS BY WOOD DECAYING FUNGI ON CONIFEROUS WOOD

M. MÄKI^{1,2}, T. MALI³, H. HELLÉN⁴, J. HEINONSALO^{3,4}, T. LUNDELL³ and J. BÄCK^{1,2}

¹Institute for Atmospheric and Earth System Research / Forest Sciences.

²Faculty of Agriculture and Forestry, University of Helsinki, Finland.

³Department of Microbiology, Faculty of Agriculture and Forestry, University of Helsinki, Finland.

⁴Finnish Meteorological Institute, Helsinki, Finland.

Keywords: VOLATILE ORGANIC COMPOUND, DECOMPOSITION, FUNGAL INTERACTIONS, CARBON CYCLING.

INTRODUCTION

Wood decomposing fungi of Basidiomycota, for instance the brown-rot and white-rot species are a key element in global carbon cycle, because they decompose dead wood effectively (Eastwood et al., 2011; Floudas et al., 2012). Different soil micro-organisms release volatile organic compounds (VOCs) for instance to secure their growing space and resource availability during competition (Müller et al., 2013; El Ariebi et al., 2016; Boddy 2016; Hiscox et al., 2018). Warming climate may alter community structure and shift ecological interactions between species, because temperature increase will likely promote metabolic pathways of microbes (Mancuso et al., 2015). This study aims to determine the role of wood substrate – either Scots pine (*Pinus sylvestris*) or Norway spruce (*Picea abies*) – on hyphal biomass, secreted enzyme activities, wood decomposition and fungal species-species interactions by releasing VOCs.

METHODS

We used a factorial laboratory experiment to study one brown-rot species (*Fomitopsis pinicola*) and two white-rot species (*Phlebia radiata* and *Trichaptum abietinum*) cultivated as single species cultures or in various species-species combinations on coniferous wood sawdust using four biological replicates (Mali et al., 2019). We defined hyphal biomass, secreted enzyme activities, wood decomposition and fungal VOC release in each treatment after 4, 8 and 12 weeks of growth. We sampled VOCs into adsorbent tubes and determined the concentrations of isoprene, monoterpenoids, sesquiterpenes and different oxygenated VOCs using a thermal desorption-gas chromatograph-mass spectrometer (Mäki et al., 2019a).

RESULTS

Wood decomposition by the brown-rot and the white-rot species was a substantial source of VOCs (Fig. 1). Our results show that interaction of different Basidiomycetes, especially between the brown-rot (*Fomitopsis pinicola*) and the white rot (*Trichaptum abietinum*) fungi accelerated VOC release (Fig. 1). Earlier study supports this result by showing that decomposition rates vary between fungal species and competition leads to different metabolic changes depending on species and interaction partners (Hiscox et al., 2015). This study clearly shows that substrate quality affects VOC release of Basidiomycetes, because release of sesquiterpenes and oxygenated VOCs was higher on Scots pine sawdust compared to Norway spruce sawdust. Substrate quality contributes forest floor VOC fluxes as well, because *Pinus sylvestris* dominated floor was discovered to be a stronger VOC source than *Picea abies* forest floor in both boreal and hemiboreal climate (Mäki et al., 2019b).

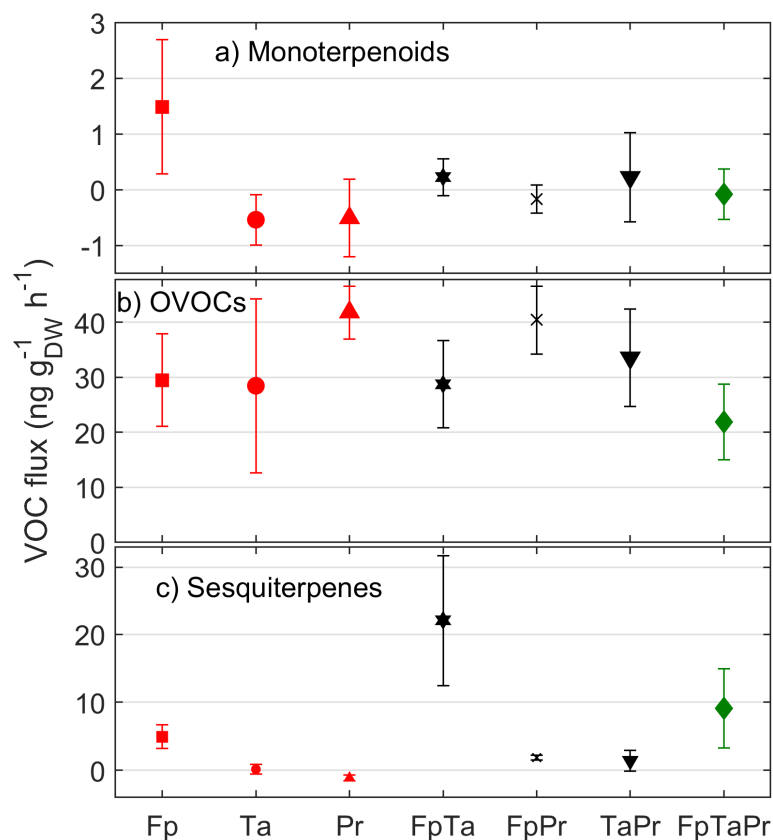


Figure 1. Release of (a) the total monoterpenoids, (b) the total oxygenated VOCs and (c) the total sesquiterpenes by fungal cultures growing on spruce sawdust. Different cultures are fungal species growing individually (Fp=*Fomitopsis pinicola*, Ta=*Trichaptum abietinum* and Pr=*Phlebia radiata*) and in various species-species combinations. The flux rates are means with standard deviation of four biological replicates.

CONCLUSIONS

These results indicate that changing forest cover may also influence VOC release of wood decomposition depending on substrate quality for microbes. Abiotic factors such as temperature may affect the outcome of fungal interaction (Hiscox and Boddy, 2017). For this reason, fungal interactions should be studied in the future using situ measurements, where relative humidity, temperature and soil water content vary in time and space.

ACKNOWLEDGEMENTS

Work was supported by the Academy of Finland Center of Excellence programme (grant no. 307331).

REFERENCES

- Boddy, L. (2016). Interactions between fungi and other microbes. In *The fungi*. (Elsevier, London, UK).
 Eastwood, D. C., D. Floudas, M. Binder, A. Majcherczyk, P. Schneider, A. Aerts, F. O. Asiegbu, S. E. Baker, K. Barry, M. Bendiksby, M. Blumentritt, P. M. Coutinho, D. Cullen, R. P. de Vries, A. Gathman, B. Goodell, B. Henrissat, K. Ihrmark, H. Kauserud, A. Kohler, K. LaButti, A. Lapidus, J. L. Lavin, Y. -H. Lee, E. Lindquist, W. Lilly, S., Lucas, E., Morin, C., Murat, J. A., Oguiza, J., Park,

- A. G., Pisabarro, R., Riley, A. Rosling, A. Salamov, O. Schmidt, J. Schmutz, I. Skrede, J. Stenlid, A. Wiebenga, X. Xie, U. Kües, D. S. Hibbett, D. Hoffmeister, N. Högberg, F. Martin, I. V. Grigoriev, and S. C. Watkinson (2011). The plant cell wall-decomposing machinery underlies the functional diversity of forest fungi, *Science*, 333, 762–765. <https://doi.org/10.1126/science.1205411>
- El Ariebi, N., J. Hiscox, S. A. Scriven, C. T. Müller, L. Boddy (2016). Production and effects of volatile organic compounds during interspecific interactions. *Fungal Ecology*, 20: 144–54. <http://dx.doi.org/10.1016/j.funeco.2015.12.013>
- Floudas, D., M. Binder, R. Riley, K. Berry, R. A. Blanchette, B. Henrissat, ... D. S Hibbett (2012). The Paleozoic origin of enzymatic lignin decomposition reconstructed from 31 fungal genomes, *Science*, 336, 1715-1719. <https://doi.org/10.1126/science.1221748>
- Hiscox, J., M. Savoury, I. P. Vaughan, C. T. Muller, and L. Boddy (2015). Antagonistic fungal interactions influence carbon dioxide evolution from decomposing wood, *Fungal Ecology*, 14, 24-32. <http://dx.doi.org/10.1016/j.funeco.2014.11.001>
- Hiscox, J., and L. Boddy (2017). Armed and dangerous: Chemical warfare in wood decay communities, *Fungal Biology Reviews*, 31, 169e184. <http://dx.doi.org/10.1016/j.fbr.2017.07.001>
- Hiscox, J., J. O'Leary, and L. Boddy (2018). Fungus wars: basidiomycete battles in wood decay, *Studies in Mycology*, 89, 117–124. <https://doi.org/10.1016/j.simyco.2018.02.003>
- Mäki, M., H. Aaltonen, J. Heinonsalo, H. Hellén, J. Pumpanen, and J. Bäck (2019a). Boreal forest soil is a significant and diverse source of volatile organic compounds, *Plant and Soil*, 441, 89–110. <https://doi.org/10.1007/s11104-019-04092-z>
- Mäki, M., D. Krasnov, H. Hellén, S. M. Noe, and J. Bäck (2019b). Stand type affects forest floor fluxes of volatile organic compounds in hemiboreal and boreal climates, *Plant and Soil*, 441, 363–381. <https://doi.org/10.1007/s11104-019-04129-3>
- Mali, T., M. Mäki, H. Hellén, J. Heinonsalo, J. Bäck, and T. Lundell (2019). Decomposition of spruce wood and release of volatile organic compounds depend on decay type, fungal interactions and enzyme production patterns, *FEMS Microbiology Ecology*, fiz135. <https://doi.org/10.1093/femsec/fiz135>
- Mancuso, S., C. Taiti, N. Bazihizina, C. Costa, P. Menesatti, L. Giagnoni, M. Arenella, P. Nannipieri, and G. Renella (2015). Soil volatile analysis by proton transfer reaction-time of flight mass spectrometry (PTR-TOF-MS), *Applied Soil Ecology*, 86, 182–191. <https://doi.org/10.1016/j.apsoil.2014.10.018>
- Müller A, P. Faubert M. Hagen W. zu Castell, A. Polle, J. P. Schnitzler, and M. Rosenkranz (2013). Volatile profiles of fungi - Chemotyping of species and ecological functions, *Fungal Genetical Biology*, 54, 25–33. <http://dx.doi.org/10.1016/j.fgb.2013.02.005>

DO CLIMATE-DRIVEN CHANGES IN TREE HYDRAULICS AFFECT BVOC AND NOX EMISSIONS FROM SILVER BIRCHES?

Mänd, P.¹, T. Hölttä¹, M. Mäki¹, P.Kupper² and J. Bäck¹

¹Department of Forest Sciences, University of Helsinki, Finland

²Institute of Ecology and Earth Sciences, University of Tartu, Estonia

Climate scenarios for next hundred years predict higher atmospheric humidity for northern latitudes. According to previous studies, higher humidity causes significant changes in forest growth and function. Increase in air humidity at FAHM experimental site, Estonia, has shown to affect tree water status and increases the levels of antioxidants and accumulation of carbohydrates in leaves. Such changes suggest potentially higher VOC emissions from trees. Changed nutrient acquisition due to higher humidity on the other hand might affect NO_x emission from forests. However, the effect of higher air humidity and changed water status of trees on reactive volatile compound emissions are rarely studied in field.

The novel results of VOC and NO_x emissions from birch shoots at increased and ambient atmospheric humidity are shown. The effect of tree water status and osmotic potential on VOC emissions is discussed.

FAAR abstract instructions and template

Please read carefully - the text contains instructions for abstract preparation

CROP VEGETATION PARAMETERS FROM SENTINEL-2 FOR MONITORING CARBON UPTAKE BY AGRICULTURAL FIELDS

O. NEVALAINEN¹, L. KULMALA^{1,2}, A. LOHILA^{1,3}, L. HEIMSCH¹, H. VEKURI¹, T. LAURILA¹ and J. LISKI¹

¹Finnish Meteorological Institute (FMI), Climate System Research, Helsinki, Finland.

²Institute for Atmospheric and Earth System Research / Forest Sciences, Faculty of Agriculture and Forestry, University of Helsinki, Finland.

³Institute for Atmospheric and Earth System Research / Physics, Faculty of Science, University of Helsinki, Finland.

Keywords: CO₂, SOC, AGRICULTURE, SENTINEL-2, LAI, FAPAR, NDVI.

INTRODUCTION

Soils are one of the largest carbon stocks on Earth and thus, even small increases in soil carbon stock have the potential to reduce atmospheric carbon considerably and mitigate climate change (Minasny *et al.*, 2017). Since 1970s the amount of soil organic carbon (SOC) in Finnish agricultural lands has decreased due to intensive agricultural management practices (Heikkinen *et al.*, 2013). Changing and developing new agricultural practices that would improve carbon sequestration to soils has large potential to mitigate climate change (Paustian *et al.*, 2016). In order to verify that the agricultural management practices are improving carbon sequestration, a reliable measurement and verification system is required. Satellite-based remote sensing is an essential component of this system, since it provides a measurement approach to extend relevant information to regional scales and areas lacking accurate *in situ* measurement systems, such as eddy covariance towers. SOC can be estimated using remote sensing from bare soil reflectance or indirectly by observing vegetation status and photosynthesis and estimating sequestered carbon through coupled soil-vegetation-atmosphere-transfer models. This study presents our preliminary results of using Sentinel-2 optical satellite data from FMI's two study sites, Qvidja and Ruukki, to produce timeseries of vegetation status through growing season in 2018 and 2019.

METHODS

Sentinel-2 is a constellation of two optical multispectral satellites, S2A (launched in 2015) and S2B (launched in 2017), with temporal resolution of 5 days in the equator and approximately 3 days in Finland. Sentinel-2 satellites have 13 spectral bands ranging from 444 to 2202 nm with spatial resolutions of 10, 20 or 60 m (visible to near infrared (497 – 865 nm), covered with 10 and 20 m resolution (Drusch *et al.*, 2012).

A workflow for downloading and computing vegetation parameters for area of interest (AOI) has been implemented. The AOI is given as a polygon (e.g. shapefile) and the satellite images containing the AOI is downloaded from ESA's SciHub service or FMI's Finhub. Readily atmospherically corrected level 2 (L2A) bottom-of-atmosphere (BOA) reflectance data is downloaded if it is available. If not, then level 1 (L1C) top-of-atmosphere (TOA) reflectance is downloaded and atmospherically corrected to L2A using sen2cor atmospheric correction software. L2A data is then resampled to 10 m resolution and smaller part containing the AOI is cropped from the main image. After that, quality metrics (percentage of shadow and cloud pixels) and multiple vegetation indices, such NDVI (normalized difference vegetation index), are computed for the AOI. In addition, Biophysical processor, available in ESA's SNAP toolbox, is used to retrieve LAI (leaf area index), fapar (fraction of absorbed photosynthetically active radiation (PAR)), canopy chlorophyll content, canopy water content and fractional vegetation cover (FCV). Bad quality data is filtered out using the quality metrics.

FAAR abstract instructions and template

Please read carefully - the text contains instructions for abstract preparation

FMI studies greenhouse gas (GHG) exchange, carbon cycling and other climate impacts at two agricultural study sites in Finland—one in Qvidja, Parainen (60.29550°N, 22°39281°E) and the other in Ruukki, Siikajoki (64.68399°N, 25.10632°E). Qvidja is on a mineral soil whereas Ruukki on a peat soil. Qvidja site has had an operational eddy covariance tower since spring 2018 and Ruukki since June 2019. In addition to the eddy covariance measurements, both sites have had extensive field measurements (e.g. GHG chamber measurements, LAI, chlorophyll, biomass, vegetation height, species composition, soil moisture and temperature) conducted during 2019. At both sites, forage grass was grown on the fields, while at Ruukki also barley was grown in NE direction from the eddy covariance tower. Effect of species mixtures, fertilization and cutting heights to carbon sequestration are investigated at both sites.

RESULTS AND DISCUSSION

Figure 1 presents LAI, fapar and NDVI timeseries for Qvidja site in 2018 and 2019 after filtering out low quality data caused by cloudiness. Summer of 2018 was very dry compared to 2019, which is seen as smaller LAI, fapar and NDVI during midsummer. The start of growing season and the timing of cuttings are visible in both years. In 2018, the yield of the second harvest was left on the field which is visible as no remarkable decrease is observed in LAI, fapar and NDVI. In 2018, the grass growth continued until the end of November, but unfortunately the period from beginning of October to the end of November was cloudy during Sentinel-2 overpasses and therefore no good quality satellite data is available.

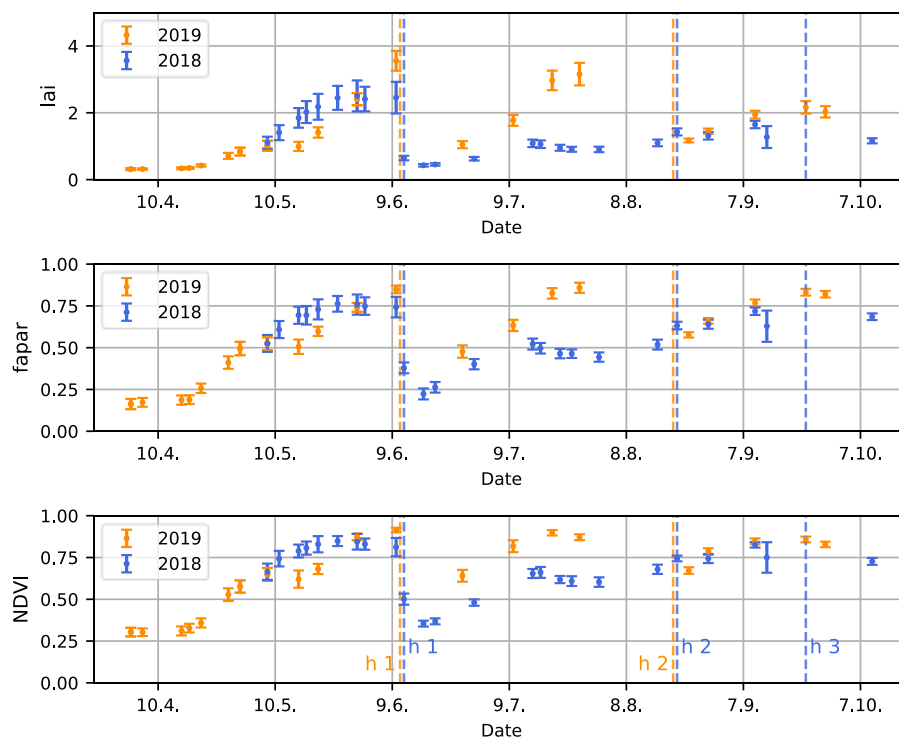


Figure 1. Sentinel-2 LAI, fapar and NDVI timeseries of Qvidja eddy covariance field of 2018 and 2019. Error bars present standard deviation of the pixels within the polygon. The vertical lines mark the timing of the cuttings.

The timeseries of year 2019 for one grass and barley block at Ruukki site is presented in Figure 2. So far, data has been available throughout the whole growing season except for one remarkable gap in the end of August. LAI, fapar, and NDVI all show higher values compared to Qvidja site. NDVI and fapar seem to get saturated and LAI is at the maximum limits of the used algorithm at June and August. These features require further consideration and possible improvements to the retrieval methods.

FAAR abstract instructions and template
Please read carefully - the text contains instructions for abstract preparation

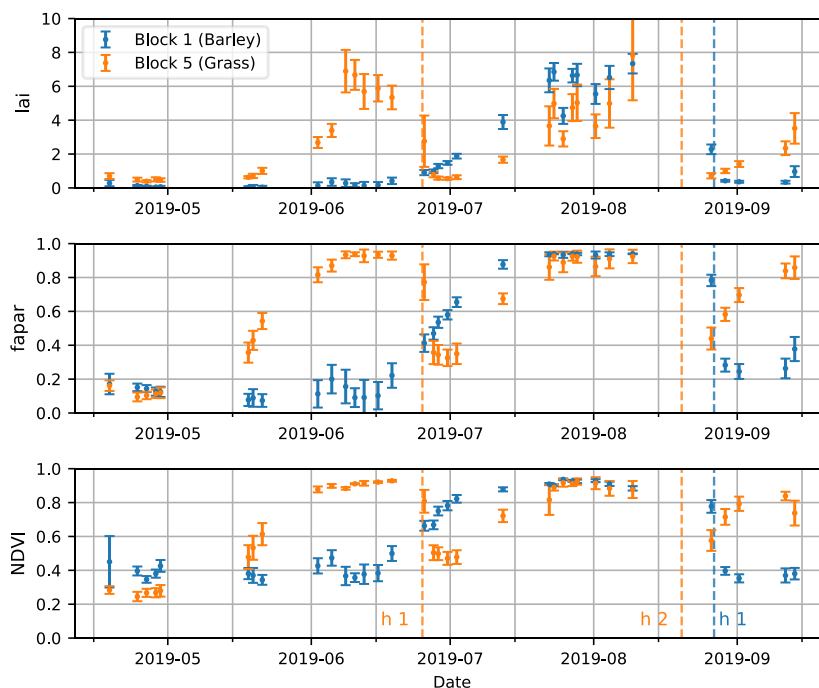


Figure 2. Sentinel-2 LAI, fapar and NDVI timeseries of Ruukki field in 2019. Error bars present standard deviation of the pixels within the polygon. The vertical lines mark the timing of the cuttings.

High revisit time and high spatial resolution of Sentinel-2 enables monitoring of individual fields during the growing season and observing changes in LAI, fapar, greenness and thus potentially photosynthetic activity. Next, the satellite-based measurements will be compared to field measurements and estimates of other approaches and linked to eddy covariance tower measurements and estimates of changes in SOC.

ACKNOWLEDGEMENTS

This work was supported by Business Finland (project CARBO-CREDIT) and the Strategic Research Council at Academy of Finland (project MULTA, decision 327214).

REFERENCES

Drusch, M., Del Bello, U., Carlier, S., Colin, O., Fernandez, V., Gascon, F., Hoersch, B., Isola, C., Laberinti, P., Martimort, P., 2012. Sentinel-2: ESA's optical high-resolution mission for GMES operational services. *Remote Sens. Environ.* 120, 25–36.

Heikkinen, J., Ketoja, E., Nuutinen, V. and Regina, K. (2013). Declining trend of carbon in Finnish cropland soils in 1974–2009. *Global change biology*, 19(5), 1456-1469.

Minasny, B., Malone, B.P., McBratney, A.B., Angers, D.A., Arrouays, D., Chambers, A., Chaplot, V., Chen, Z.-S., Cheng, K. and Das, B.S. (2017). Soil carbon 4 per mille. *Geoderma* 292, 59–86.

Paustian, K., Lehmann, J., Ogle, S., Reay, D., Robertson, G. P. and Smith, P. (2016). Climate-smart soils. *Nature*, 532(7597), 49.

CATEGORIZATION OF GROUND-BASED MEASUREMENT SITES BY AIR MASS SOURCE AREA, LAND-COVER TYPE AND POPULATION DENSITY

T. NIEMINEN¹, J. HEISKANEN¹, V. LEINONEN², O. KURRI²,
S. MIKKONEN², T. YLI-JUUTI², M. KULMALA¹

¹ Institute for Atmospheric and Earth System Research (INAR), University of Helsinki, Helsinki, Finland

² Department of Applied Physics, University of Eastern Finland, Kuopio, Finland

Keywords: airmass back-trajectories, source area, atmospheric boundary layer, land-cover types

INTRODUCTION

Measurements of atmospheric variables such as meteorology, trace gas, and aerosol concentrations are typically performed at ground-based fixed-location stations. The surroundings of these stations are often categorized by subjective criteria using several methods, which can be varying between different studies (e.g. Fleming et al., 2012). Spatial representativeness of an atmospheric measurement site is one important aspect that needs to be understood when interpreting the measurement data obtained from the site, and extending this data to a wider area surrounding the site.

In this study we aim to develop a general framework of analyzing and describing the variability and representativeness of a given measurement location in terms of land-cover types, level of anthropogenic influence, and emission sources of trace gases and aerosols. We apply this framework for more than 30 measurement sites providing long-term observations of aerosol number size-distributions recently analyzed by Nieminen et al. (2018).

MATERIAL AND METHODS

The airmass back-trajectories were calculated using the HYSPLIT Lagrangian transport model developed by NOAA (Stein et al., 2015). The 96-hour transport routes of airmasses arriving at 100 m above ground level to each of the stations were calculated with one hour time intervals over a 14 year period (2005–2018). We concentrated the analyses to airmasses which have resided within the boundary layer, as these airmasses are those that are most influenced by emissions at the ground-level. Frequency maps of airmasses passing over $1^{\circ} \times 1^{\circ}$ grid boxes were calculated by combining the transport routes of all the trajectories arriving to each station over the studied period. An example of the airmass source areas is shown in Figure 1 for the University of Helsinki SMEAR II station in Hyytiälä, Finland. In order to characterize the land-cover in these airmass source areas, we utilized the openly available datasets from the European Space Agency's Climate Change Initiative (CCI; <https://www.esa-landcover-cci.org/>). The CCI database provides detailed information of the land-use based on satellite imagery from European Space Agency. Furthermore, the anthropogenic influence in the airmass source areas was estimated based on the population density data compiled by the NASA Socioeconomic Data and Applications Center (<http://sedac.ciesin.columbia.edu/>).

RESULTS

We categorized the source area types of each station using k-means cluster analysis. For the land-cover data, six was the optimal number of clusters, and in the case of population density five clusters. The land-cover type clusters and population density clusters generally corresponded to each other, i.e. stations with low population densities in their airmass source areas also were surrounded by e.g. forests or water, as

opposed to urban areas or farming land. The categorization of the airmass source areas will be further refined by including information of emission rates of trace gases and particulate matter.

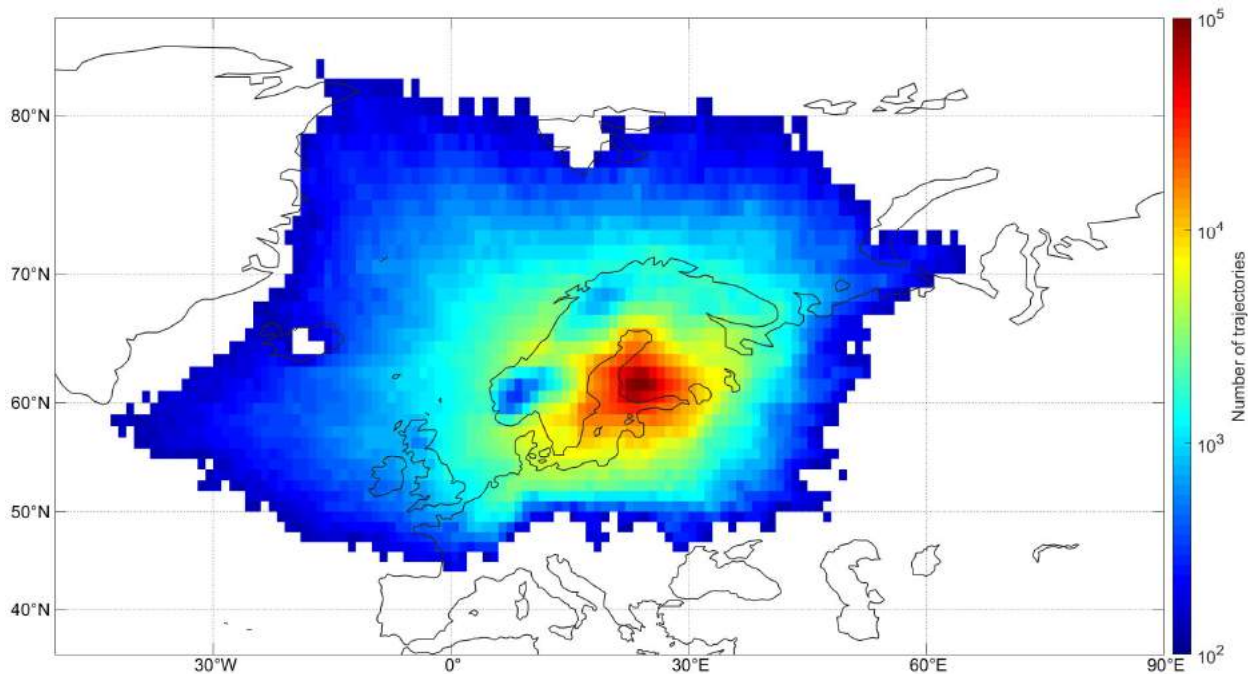


Figure 1. Characterization of the airmass source area for the SMEAR II station in Hyytiälä, Finland. The colorscale represents the number of individual airmass trajectories passing over $1^{\circ}\times 1^{\circ}$ grid cell during years 2005–2006. Only those airmasses staying inside the planetary boundary layer have been taken into account.

ACKNOWLEDGEMENTS

This work was supported by the Academy of Finland Centre of Excellence (project number 307331). We acknowledge the NOAA Air Resources Laboratory (ARL) for the provision of the HYSPLIT transport and dispersion model used in this study, ESA Climate Change Initiative for the land-use data, and NASA for the population density datasets.

REFERENCES

- Fleming, Z. L., Monks, P. S., and Manning, A. J. (2012). Review: Untangling the influence of air-mass history in interpreting observed atmospheric composition, *Atmos. Res.* 104–105, 1–39.
- Nieminen, T., et al. (2018). Global analysis of continental boundary layer new particle formation based on long-term measurements, *Atmos. Chem. Phys.* 18, 14737–14756.
- Stein, A. F., Draxler, R. R., Rolph, G. D., Stunder, B. J. B., Cohen, M. D., and Ngan, F. (2015). NOAA’s HYSPLIT Atmospheric Transport and Dispersion Modeling System, *Bull. Amer. Meteor. Soc.* 96, 2059–2077.

STABLE CARBON ISOTOPIC COMPOSITION TRANSITIONS OF PEAT COLUMNS IN A PARTIALLY FORESTRY-DRAINED BOREAL BOG

H. NYKÄNEN¹, A.J. RISSANEN², J. TURUNEN³, T. TAHVANAINEN⁴ and H. SIMOLA⁴

¹University of Eastern Finland, Department of Environmental Science, Kuopio, Finland

²Tampere University, Bio and Circular Economy Research Group, Faculty of Engineering and Natural Sciences, Tampere, Finland

³Geological Survey of Finland, Espoo, Finland,

⁴University of Eastern Finland, Department of Environmental Science, Joensuu, Finland

Keywords: BIOGEOCHEMISTRY, CARBON CYCLE, ISOTOPE ECOLOGY

INTRODUCTION

Stable isotopic composition ($^{13}\text{C}/^{12}\text{C}$ -ratio, denoted as $\delta^{13}\text{C}$) of peat is the product of $\delta^{13}\text{C}$ of carbon dioxide (CO_2) source, vegetation type (vascular plants vs. bryophytes) and of aerobic and anaerobic degradation. In general, the lighter ^{12}C is preferred over the heavier ^{13}C in aerobic biological processes. Therefore, respired CO_2 tends to be depleted in ^{13}C while remaining peat carbon is enriched in ^{13}C .

Climate change is expected to affect northern peatlands (Gorham, 1991). Drying enables increased aerobic decomposition of formerly anaerobic peat, hence, increase of CO_2 emission, while methane emissions may decrease. Furthermore, water-level drawdown gradually leads to changes in vegetation type, thus, possibly modifying $\delta^{13}\text{C}$ values of peat.

Drainage for forestry involves permanent lowering of the water table, thus leading to somewhat similar situation as expected due to climate change. Prerequisites for changes in hydrology to result in observable changes in $\delta^{13}\text{C}$ values of bulk peat are major changes in processes and concomitant carbon flows. Drainage of peatlands leads to altered carbon dynamics and usually also to increased carbon loss (Simola *et al.* 2012, Pitkänen *et al.*, 2013, Krüger *et al.* 2016). Indeed, the $\delta^{13}\text{C}$ values of bulk peat have been used to study human impact on peatlands (Esmeijer-Liu *et al.*, 2012; Krüger *et al.*, 2014, 2015, 2016, Nykänen *et al.* 2018).

We studied 37 years earlier drained Rahesuo bog in Eastern Finland comparing adjacent drained and undrained parts. This abstract is based on an article under review (Nykänen *et al.*, submitted). In submitted MS, besides $\delta^{13}\text{C}$, also C% and N% were studied, but here only $\delta^{13}\text{C}$ results are discussed. In addition to descriptive comparison of $\delta^{13}\text{C}$ values, also quantitative expression of changes is used.

METHODS

The analyzed samples are from study of Pitkänen *et al.* (2013). Two complete peat profiles from the undrained and from the 1971 drained sites were sampled from the same original *Sphagnum* hollow pattern in 2009. In this nutrient poor bog, the difference in vegetation was clear, as was the subsidence (30 cm) and water table decrease on drained site compared to the undrained site.

Peat samples were analysed with a Vario Pyro Cube coupled with an Isoprime 100 (Elementar, Germany). Stable isotope composition ($\delta^{13}\text{C}$) was expressed in the delta notation as a ‰ deviation of the heavy-to-light isotope abundance ratio in the sample from that of a standard, Vienna PD pelemnite. The results are reported relative to the standard scale. Here, $\delta^{13}\text{C}$ of lost C was calculated based on mass balance change of ^{12}C and ^{13}C of synchronous ash layers in the peat column.

RESULTS AND DISCUSSION

Similarly as in this study, the original study showed that the drained site had lost carbon (Pitkänen *et al.* 2013). In general, drainage increased peat $\delta^{13}\text{C}$ values in the uppermost layers, as a difference to the Lakkasuo bog, where $\delta^{13}\text{C}$ values of the uppermost layers were similar on undrained and drained sites (Nykänen *et al.* 2018). This difference followed from differences in carbon storage: in Rahesuo bog, loss of carbon was clear, while on Lakkasuo bog, effects of drainage on carbon balance were small. Calculation based on ^{12}C and ^{13}C storage change, showed that lost carbon was ^{13}C -depleted compared to peat $\delta^{13}\text{C}$ values on undrained site (Fig. 1). Thus, $\delta^{13}\text{C}$ value integrating carbon loss during 37 years of drainage is in line with straight measurements of respired CO_2 carbon isotopic composition compared to values in source material (Ågren *et al.* 1996). This supports earlier studies showing that respiration increases in drained peatlands (Silvola *et al.* 1996).

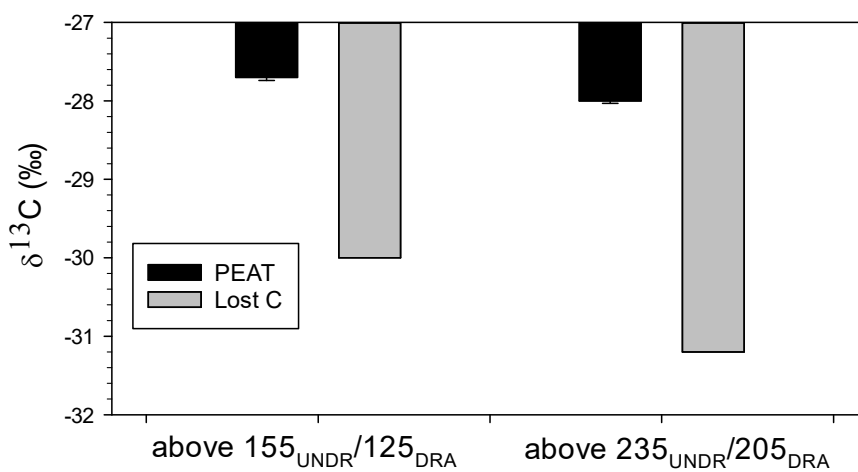


Figure 1. Mass weighted $\delta^{13}\text{C}$ value of lost carbon compared to the original peat $\delta^{13}\text{C}$ values (Average \pm S.E. for peat) over synchronous layers found from undrained and drained sites of Rahesuo.

CONCLUSIONS

Drainage - induced peat loss increased $\delta^{13}\text{C}$ values of the uppermost layers of the drained peatland site. The lost carbon was ^{13}C -depleted compared to original peat. Similarly, as carbon balance can be calculated between undrained and drained pairs of originally similar peat profiles, also $\delta^{13}\text{C}$ values based on measured ^{12}C and ^{13}C mass profiles can be used to track changes in carbon cycle.

ACKNOWLEDGEMENTS

This work was supported by Academy of Finland grants 136455, 140964 and the funding support from The Centre of Excellence in Atmospheric Science - From Molecular and Biological processes to The Global Climate to HN and Academy of Finland grants 286642 to AJR and grant 311655 to TT.

REFERENCES

- Ågren GI, Bosatta E, Balesdent J (1996) Isotope discrimination during decomposition of organic matter: a theoretical analysis. *Soil Sci Soc Am J* 60, 1121.
- Esmeijer-Liu, A. J., W.M. Kürschner, A.F. Lotter *et al.* (2012). Stable Carbon and Nitrogen Isotopes in a Peat Profile Are Influenced by Early Stage Diagenesis and Changes in Atmospheric CO₂ and N Deposition. *Water, Air, and Soil Pollution*, 223(5), 2007.
- Gorham, E. (1991). Role in the Carbon Cycle and Probable Responses to Climatic Warming. *Ecol. Appl.*, 1, 182.
- Krüger, J. P., C. Alewell, K. Minkkinen *et al.* (2016). Calculating carbon changes in peat soils drained for forestry with four different profile-based methods. *For. Ecol. Manag.*, 381, 29.
- Krüger, J. P., J. Leifeld and C. Alewell (2014). Degradation changes stable carbon isotope depth profiles in peatlands. *Biogeosciences*, 11(12), 3369.
- Krüger, J. P., J. Leifeld, S. Glatzel *et al.* (2015). Biogeochemical indicators of peatland degradation - A case study of a temperate bog in northern Germany. *Biogeosciences*, 12, 2861.
- Nykänen, H. K., P. A. Mpamah and A.J. Rissanen (2018). Stable carbon isotopic composition of peat columns, subsoil and vegetation on natural and forestry-drained boreal peatlands. *Isotopes in Environmental and Health Studies*, doi:10.1080/10256016.2018.1523158.
- Pitkänen, A., J. Turunen, T. Tahvanainen and H. Simola (2013). Carbon storage change in a partially forestry-drained boreal mire determined through peat column inventories. *Bor. Env. Res.* 18, 223.
- Silvola J, Alm J, Ahlholm U, et al (1996) CO₂ fluxes from peat in boreal mires under varying temperature and moisture conditions. *J Ecol* 84, 219.
- Simola, H., A. Pitkänen and J. Turunen (2012). Carbon loss in drained forestry peatlands in Finland, estimated by re-sampling peatlands surveyed in the 1980s. *E. J. Soil Science*, 63, 798.

DETECTING POTATO LEAF NUTRIENT CHANGES WITH LEAF LEVEL FLUORESCENCE AND REFLECTANCE MEASUREMENTS

J. OIVUKKAMÄKI¹, J. ATHERTON¹, S. XU¹, A. RIIKONEN¹ and A. PORCAR-CASTELL¹

¹Optics of Photosynthesis Laboratory, Institute for Atmospheric and Earth system research, Department of Forest Sciences, University of Helsinki, Latokartanonkaari 7, PL 27, Helsinki.

Keywords: leaf nutrients, chlorophyll fluorescence, reflectance.

INTRODUCTION

The problems faced by the world's food production are convoluted and complicated. Due to a changing climate, the problems are expected to get worse in the future, even though the growing global population requires the food production to grow as well (Beddington et al 2012). Agricultural production in the world has grown steadily in the last century, partly because of a better availability of micro- and macronutrients for plants, which the plants require for growth. It has been noted that the lack of these nutrients leads to changes in the photochemical apparatus, including the PSII photochemistry in the plant (Larbi et al. 2006, Cigler et al. 2010), as well as causes reduced growth for plants. Plant nutrient availability can be facilitated with fertilization, but using too much fertilizer has the risk of causing eutrophication.

Potato is one of the most important food plants after cereals and it is grown all over the world on different scales (Scott 1985). Due to its naturally high carbohydrate content, potato forms the basis of the diet in many parts of the world (Scott et al 2000, Thiele et al 2010).

Chlorophyll fluorescence is used to monitor stress in plants with non-invasive means. Fluorescence can be used to follow the photosynthetic parameters of a plant and to draw conclusions on those parameters on the well-being of the plant (eg. Maxwell & Johnson, 2000). Fluorescence can be measured from multiple different scales, starting from the molecular scale, to the canopy scale from UAV's, all the way to the landscape scale from satellites. Chlorophyll fluorescence is emitted from the leaf between 640 and 850 nm and it has two peaks, at 680nm and 740nm. In addition to chlorophyll fluorescence, reflectance indices, such as NDVI (Rouse et al 1974) and PRI (Gamon et al 1992) are also used to monitor plant health status by looking at leaf reflectance values, which is affected by changes in leaf pigment content and structure. The objective of this study was to recognize the macro- and micronutrients that can be efficiently and reliably measured with optical signals at leaf level and later on to link those measurements with remote sensing measurements done with drones.

METHODS

The field research was conducted in May – September of 2018 in Helsinki, Finland. The potatoes were planted at the end of May and were irrigated in the following weeks regularly. The plants were fertilized with two fertilizers: YaraMila and YaraBela Suomensalpietari (Yara, Norway). The fertilization was done prior to the plants sprouting, by hand in the beginning of June with four different fertilizer treatments (see Table 1).

Spectral fluorescence of the leaves was measured in laboratory conditions, where the leaves could be measured in standardized conditions. A shoot was first cut from the potato plant and was kept partly under water, from

the shoot a single leaf was taken so that the pedicel was kept under water at all times, until the actual measurement was made. The leaves were illuminated with a white LED-light source MS-602 (Magicshine Technology LLC, China) and measured with a USB-2000 spectrometer (Ocean Optics Inc., United States) connected to a laptop. Between the light source and the leaf, an optical filter was used to block out incoming light from under 650-nanometer wavelength. The leaves were held flat on a dark, opaque surface, under a fiber holder, which held the BIF200-VIS-NIR (Ocean Optics Inc., United States) at a fixed 2 cm distance and 90-degree angle from the leaf. Before the measurement the leaves were dark adapted for 10 minutes, after which a three minute measurement was made to record each leaf's steady state fluorescence. The fluorescence measurement was made with a 30 ms integration time with averaging over five measurements. The reflectance measurements were made with the same setup that the fluorescence measurements were made with, but without the optical filter blocking any incoming light. A Spectralon (Labsphere Inc., United States) white panel was used to gain a reference for the reflectance measurements.

Two or three leaves from each plant were picked during the three measurement points to be stored in plastic tubes, first frozen in liquid nitrogen and later on in a -80°C freezer. 200-300 milligrams from each tube was taken to be analyzed for nutrient content in an iCAP 6000 mass spectrometer (Thermo Fischer Scientific, USA). Extra leaves were picked for pigment analysis, frozen as with the nutrient measurements and later analyzed with a spectrometer (Shimadzu UV-1800, Shimadzu Corporation, Japan).

Nutrient doses kg/ha in treatments				
	N1A1	N2A0	N2A1	N2A2
N	32,5	65,00	65,00	65,00
P	13,59	0	13,59	27,18
K	53,18	2,41	54,39	106,36
Mg	4,73	2,41	5,93	9,45
S	29,55	9,63	34,36	59,09
B	0,15	0,05	0,17	0,30
Cu	0,09	0	0,09	0,18
Fe	0,24	0	0,24	0,47
Mn	0,74	0	0,74	1,48
Mo	0,01	0	0,01	0,01
Zn	0,12	0	0,12	0,24

Table 1. Nutrient contents of different treatments in kg per hectare.

CONCLUSIONS

Fluorescence ratios derived from the two fluorescence peaks at around 680nm and 735nm were found to be a useful tool detect Phosphorus ($R^2 = 0,504$) and Magnesium ($R^2 = 0,637$) changes in potato leaves. Fluorescence emission around the 680nm peak was also useful in detecting plant Magnesium and Sulphur level changes.

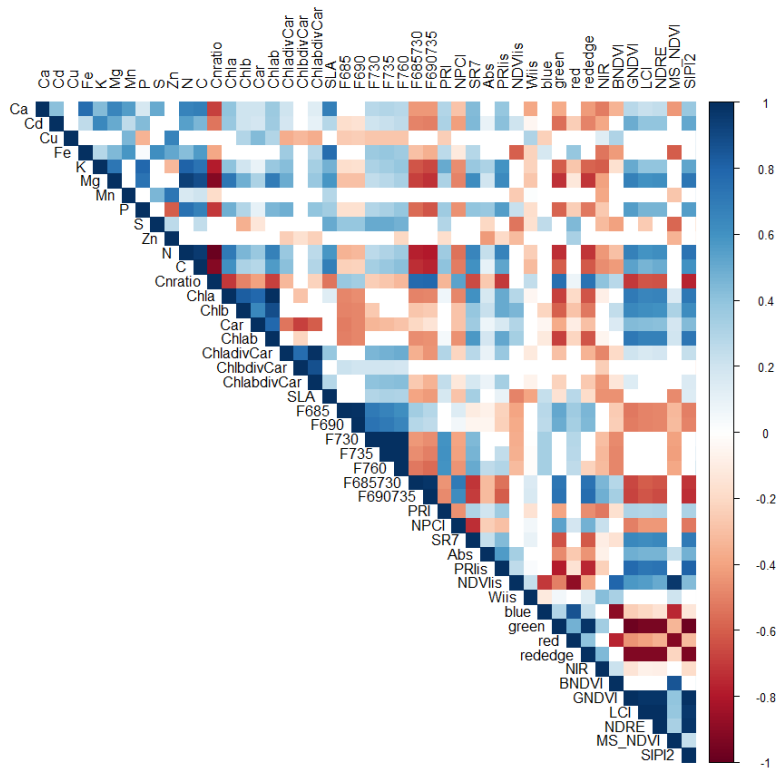


Figure 1. Demonstration of the relationship between measured variables. Blue and red colors indicate high correlation coefficients between two datasets, white squares represent non-significant correlations ($p > 0,01$).

From the reflectance observations NDVI and PRI vegetation indices were unrelated to leaf nutrient changes in this field experiment. However, the green Normalized Difference Vegetation Index, gNDVI (Gitelson et al. 1996), was able to detect changes in the Phosphorus, Magnesium and Nitrogen (Figure 1) content of the leaves. The gNDVI, which is calculated as $R_{780} - R_{550} / R_{780} + R_{550}$ (R being the normalized reflectance at the indicated wavelength), is especially sensitive to changes in the green spectral region. Magnesium has been shown to increase the nitrogen uptake efficiency of a plant (Grzebisz 2013), increase the leaf area and dry matter production of potato plants (Cao & Tibbits, 1992), as well as being an important macronutrient contributing to the overall health of the plant (Huber & Jones 2013). The results seem to indicate that changes in macronutrients linked to the chlorophyll cycle in the leaves, such as Nitrogen and Magnesium, are easier to detect with optical signals.

We are planning on continuing the research by comparing these leaf level results with drone level measurements that were done simultaneously on the same test site. The aim is to recognize those optical signals that can possibly be detected on both the leaf level and on the canopy scale.

ACKNOWLEDGEMENTS

This research was supported by the Academy of Finland under the grant 304097.

REFERENCES

- Beddington, J. R., Asaduzzaman, M., Fernandez, A., Clark, M. E., Guillou, M., Jahn, M. M., ... & Scholes, R. J. (2012). Achieving food security in the face of climate change: Final report from the Commission on Sustainable Agriculture and Climate Change.
- Cao, W. and Tibbitts, T.W. (1992). Growth, carbon dioxide exchange and mineral accumulation in potatoes grown at different magnesium concentrations. *Journal of plant nutrition*, 15(9), pp.1359-1371.
- Gamon, J. A., Penuelas, J., & Field, C. B. (1992). A narrow-waveband spectral index that tracks diurnal changes in photosynthetic efficiency. *Remote Sensing of environment*, 41(1), 35-44.
- Cigler, P., Olejnickova, J., Hruby, M., Csefalvay, L., Peterka, J. and Kuzel, S. (2010). Interactions between iron and titanium metabolism in spinach: a chlorophyll fluorescence study in hydropony. *Journal of plant physiology*, 167(18), pp.1592-1597.
- Gitelson, A.A., Y.J. Kaufman and M.N. Merzlyak (1996). Use of green channel in remote sensing of global vegetation from EOS-MODIS. *Remote Sensing Environ.*, 58: 289–98
- Grzebisz, W. (2013). Crop response to magnesium fertilization as affected by nitrogen supply. *Plant and Soil*, 368(1-2), pp.23-39.
- Huber, D. M., & Jones, J. B. (2013). The role of magnesium in plant disease. *Plant and Soil*, 368(1-2), 73-85.
- Larbi, A., Abadía, A., Abadía, J. and Morales, F. (2006). Down co-regulation of light absorption, photochemistry, and carboxylation in Fe-deficient plants growing in different environments. *Photosynthesis Research*, 89(2-3), pp.113-126.
- Maxwell, K., & Johnson, G. N. (2000). Chlorophyll fluorescence—a practical guide. *Journal of experimental botany*, 51(345), 659-668.
- Scott, G. J. (1985). *Markets, Myths, and Middlemen: A Study of Potato Marketing in Central Peru*. International Potato Center.
- Scott, G. J., Rosegrant, M. W., & Ringler, C. (2000). Global projections for root and tuber crops to the year 2020. *Food policy*, 25(5), 561-597.
- Thiele, G., Theisen, K., Bonierbale, M., & Walker, T. (2010). Targeting the poor and hungry with potato science. *Potato Journal*, 37(3/4), 75-86.
- Tucker, C. J. (1979). Red and photographic infrared linear combinations for monitoring vegetation. *Remote sensing of Environment*, 8(2), 127-150.

PARAMETER ESTIMATION OF THE GENERAL DYNAMIC EQUATION FOR AEROSOLS USING THE EXTENDED KALMAN SMOOTHER: APPROACH TO STEADY STATE CASE

M. OZON¹, A. SEPPÄNEN¹, J.P. KAIPIO^{3,1} and K.E.J. LEHTINEN^{1,2}

¹ Department of Applied Physics, University of Eastern Finland, Kuopio, Finland

² Finnish Meteorological Institute, Kuopio, Finland

³ Department of Mathematics, University of Auckland, Auckland, New Zealand

Keywords: PARAMETER ESTIMATION, EXTENDED KALMAN SMOOTHER, GENERAL DYNAMIC EQUATION, STEADY STATE.

INTRODUCTION

Aerosols play a key role in the global radiative balance of the earth. Their number concentration, size distribution (SD) and chemical composition affect their ability to scatter and absorb solar radiation as well as the formation, properties and lifetimes of clouds (Pachauri et al., 2014; Stocker, 2014, IPCC). The same properties determine how particles enter the human lung and cause various public health problems (Guerreiro et al., 2016). To quantify these effects, we need to be able to determine the rates of the key microphysical processes, aerosol formation and growth, from measurements of aerosol SD evolution.

We propose to apply a method stemming from the Bayesian framework, namely the Extended Kalman Smoother (EKS) (Kaipio and Somersalo, 2006), to estimate parameters such as growth, loss and nucleation rates along with their uncertainties from SD data. In the following, we consider the case of an aerosol system approaching steady state in order to demonstrate that the method works and gives reliable estimates.

METHODS

So far, new particle formation and growth rates have been analyzed with rather simple regression or balance equation approach suffering from potentially crude approximations and permitting no proper estimation of the uncertainties (overview of typical methods in (Kulmala et al., 2012)). As a consequence, it is likely that there are, in the estimated quantities, significant uncertainties which are usually not quantified. It has been shown in (Kürten et al., 2018) that the difference between estimations resulting from a sophisticated aerosol model and a “traditional” simple method can be as large as a factor of ten.

The inverse problem framework —the mathematical framework that allows for estimation of quantities, e.g. particle size density, from convoluted and noisy data, e.g. number concentration from SMPS — have only rarely been used in aerosol settings. Lehtinen et al. (Lehtinen et al., 2004) used a least squares minimization to infer the aerosol microphysical parameters from measured data; this method was later improved by Verheggen et al. (Verheggen and Mozurkewich, 2006) and Kuang et al. (2012) (Kuang et al., 2012). Henze et al. (2004) (Henze et al., 2004) and Sandu et al. (Sandu et al., 2005) used the method of adjoint equations to estimate parameters, such as condensation rates, from particle size distributions. None of the aforementioned studies address the matter of uncertainty quantification.

There are, however, many other studies on closely related problems. Unknown coefficients have been estimated for e.g. Fokker-Planck equations (Banks et al., 1993), age-structured population dynamics (Rundell, 1993) as well as algal and phytoplankton aggregation (Ackleh et al., 2018). The only progress in applying statistical inverse methodology to aerosol size distribution dynamics are, to our knowledge, parameter estimation in aggregation-fragmentation models (Bortz et al., 2015), to better estimate the size distribution

evolution from measurements using Kalman filtering by (Viskari et al., 2012) and estimation of evaporation rates using Markov Chain Monte-Carlo method by Kupiainen-Määttä (Kupiainen-Määttä, 2016).

Our method is designed to estimate the parameters of the General Dynamic Equation (GDE) for aerosols in general. However, for the sake of clarity (and without loss of generality) we consider the GDE without the explicit coagulation terms — the loss by coagulation on the background particles may be interpreted as part of the linear losses. Hence, we consider the following GDE:

$$\frac{\partial n}{\partial t} + \frac{\partial gn}{\partial d} = -\lambda n, \quad t \in [0, \infty), d \in [d^*, d^\infty] \quad (1)$$

$$g(d^*, t)n(d^*, t) = J(t) \quad (2)$$

$$g(d^\infty, t)n(d^\infty, t) = 0 \quad (3)$$

where the Particle Size Density (PSD) is denoted n , the time t and the particle diameter d . The parameters are: the growth rate $g(d, t)$, the linear losses $\lambda(d, t)$ (e.g. wall losses, loss by coagulation on the background particles) and the nucleation rate $J(t)$. The growth rate g and the nucleation rate J are linked by the relation in eq. (2) — boundary condition — which states that the rate of apparition of new particles at size d^* — potentially a critical size — is treated as a flux of particle coming in the size range of the considered particles. Similarly, we consider that the outward flux at size d^∞ (3) — flux a particle lost because they grow bigger than the biggest considered size d^∞ — is set to 0 — this assumption can always be met by putting d^∞ to a numerical value large enough. Our goal is to estimate the aforementioned parameters along with their uncertainties — or at least a reliable estimation — from time series of number concentrations data such as provided by an SMPS. Furthermore, we consider that the linear loss rate is known and its relative uncertainty is about 10% — it may be changed at will. Our method relies on the EKS which requires an evolution model for each quantity to be estimated and a measurement model (i.e. a mapping from the density n to the number concentrations).

To that endeavor, the GDE needs to be discretized, both in time and size, which can be achieved in various ways, but we choose the Finite Difference for its simplicity and somewhat satisfying accuracy — even though it can become an issue when dealing with time step length that reflects the time difference between to consecutive measurements.

The estimation takes advantage of a few known constraints regarding the parameters, i.e. the positivity, the correlation in size of the growth rate and the “slow” time evolution of each parameter. The time-and-size-smoothness are carried by the surrogate evolution models and the positivity is enforced by a parameterizations of the parameters. For instance, g is not directly estimated, but a surrogate variable x is, and the growth rate is formed as, e.g., $g = \log(1 + e^x)$. The discrete evolution model of x — required by the EKS — is not known per se, we use a stochastic process instead. This stochastic process is so designed to account for the a priori of “slow” time evolution and size correlation.

The measurement model for each channel of the device is taken as a simple integration of the density n which is then corrupted by a counting noise, i.e. Poisson distributed. Considering the i^{th} output y^i of the device, we have:

$$y^i = \frac{1}{V} \text{Poisson} \left(\frac{V}{\Delta_t} \int_{t_0}^{t_0 + \Delta_t} \int_{\mathbb{R}} \psi_i(s) n(s, t) ds dt \right) \quad (4)$$

where ψ_i is the efficiency of the i^{th} channel, Δ_t is the measurement time and V the volume of the sample. In the following we consider Gaussian efficiency functions when simulating data and gate function in the estimation method.

RESULTS

In order to prove that our method works, we use simulated data for which the values of the parameters are known — referred to as the Ground Truth (GT). The data are simulated by running the discretized GDE

((1)-(3)) with a very fine resolution in time and size and then applying the measurement model (4), so that we control all the parameters, even the measurement noise — V and Δ_t in (4). Here, we only consider a case with a good signal to noise ratio (SNR), see fig. 1 upper left panel. The results (estimates with their uncertainties) are shown in fig. 1 lower panels and fig. 2, and the simulated density using the estimated parameters is depicted in fig. 1 upper right panel. The two curves shown in each figure are, the filter estimates in blue (knowing only the past data) and the smoother estimates in orange (knowing the whole dataset). The trust region that gives the uncertainties is defined as the highest probability region with a probability of $\simeq 0.7$.

The nucleation rate given by the smoother is fairly well estimated at almost all points in time, except for the final instants because the filter estimates are rather not precise. The effect of the smoother is clearly visible in this case: it forces the estimates to come closer to the GT and reduces the uncertainties because it uses more data than the filter.

The growth rate (GR) estimates show the same trend, the smoother gives better results than the filter. Two features of the EKS come to light in fig. 2. The first is the a priori information given to the algorithm, i.e. the estimated GR is smooth in size because of the size correlation born by the evolution model of the GR. The second (also visible in the lower left panel of fig. 1) is that the algorithm will not produce more than it can. Indeed, upon inspection, it is clear that the estimation of the GR is reliable where there is a significant amount of information (where the PSD values are big enough, and therefore the local SNR is good) and not reliable where the data do not contain information — in which case, the algorithm outputs only the a priori it has been given.

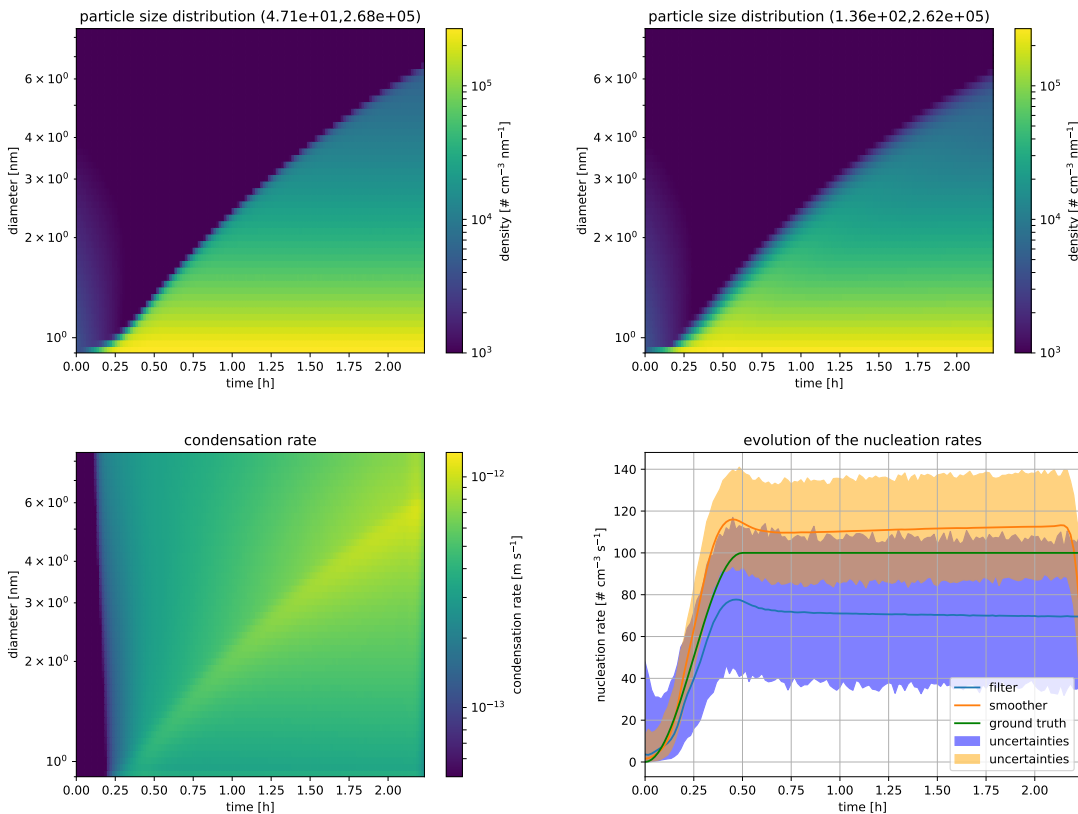


Figure 1: Estimation of the parameters of the GDE for aerosols from a simulated transition to steady state data with good SNR value. The data are shown in the upper left panel, and the reconstruction using the estimated parameters is in the upper right panel. In the lower panels are shown the growth rate (left) and the nucleation rate (right).

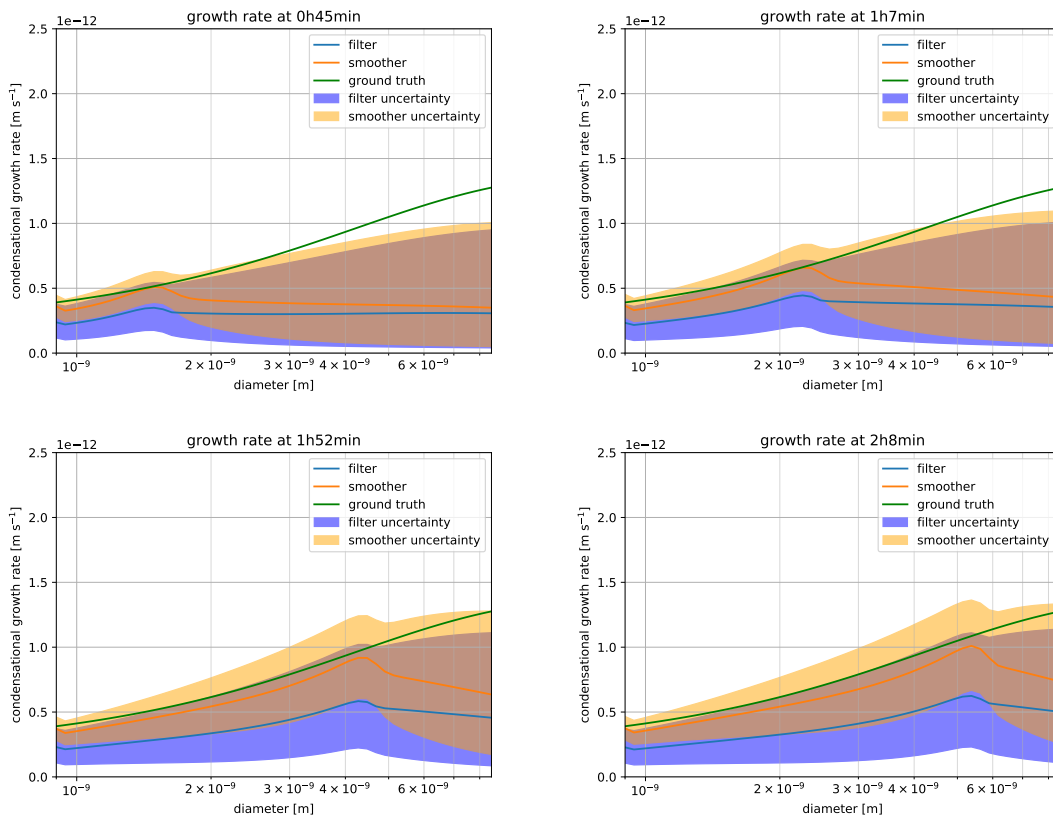


Figure 2: The growth rate estimations at 4 different instants in time: 45 min, 1h7min, 1h52min and 2h8min.

CONCLUSIONS

The foremost conclusion is that we have successfully apply the EKS to the problem of estimating the parameters of the GDE from relevant data for the first time (to the best of our knowledge).

The algorithm depends on a few tuning parameters that haven't been mentioned so far because their choices are almost completely automated. Indeed, the only important parameter to give the algorithm are the characteristic times for the nucleation and growth rate variation — set to 600s in this case — and the rough expected amplitude of the same parameters. Because the results depend on the choice of those parameters, it is a good practice to simulate the density using the estimated parameters and compare to the data for quality control.

In order to fully validate our method, it remains to apply it to measured data — which we are most willing to do. We foresee that a few points could raise concern when applying to measured data:

- 1 The time step used in the simulated data is unrealistically small so that 1) both the discretized model and the dataset have the same, and 2) the model does not diverge. The method is easily modified to accommodate for bigger time steps without modifying the time step of the discretized model. The solution lies in the measurement model used in the EKS — some iterations will use data (therefore a non-null measurement operator) and the rest will not.
- 2 The method assumes that the nucleation happens at the smallest measured size and therefore, in this version, only the apparent nucleation rate is estimated. However, the method can be modified to estimate the nucleation rate at any size. Note that doing so will increase the uncertainties in the

nucleation rate because the estimates relies more on the model than the data contrary to the case introduced here.

- 3 The measurement model used in this paper is a coarse approximation of the measurement device used in the simulation, therefore, it increases the uncertainty in the estimates — a better measurement model would improve results.
- 4 The discretization method is one of the least precise and not really well suited for handling the boundary conditions; using a method such as the Finite Elements Method would most likely benefit the results.
- 5 The evolution models of the parameters are all assumed — based on realistic assumptions. More realistic models would most likely produce better results.

REFERENCES

- Pachauri, R., Allen, M., Barros, V., and others (2014). *Climate change 2014: synthesis report*. IPCC.
- Stocker, T., and others (2014). *Climate change 2013: the physical science basis: Working Group I contribution to the Fifth assessment report of the IPCC*. IPCC.
- Kaipio, J. and Somersalo, E., (2006). *Statistical and computational inverse problems*. (Springer Science & Business Media).
- Guerreiro, C., Ortiz, A. G., de Leeuw, F. and others (2016). *Air Quality in Europe-2016 Report*. Publications Office of the European Union.
- Kulmala, M., Petäjä, T., Nieminen, T., and others (2012). *Nature protocols*, 7:1651–1667.
- Kürten, A., Li, C., Bianchi, F., and others (2018). *Atm. Chem. and Phys.*, 18:845–863.
- Viskari, T., Asmi, E., Kolmonen, P., and others (2012). *Atm. Chem. and Phys.*, 12:11767–11779.
- Lehtinen, K., Rannik, Ü., Petäjä, T., and others (2004). *J. of Geophys. Res.: Atm.*, 109:D21.
- Verheggen, B. and Mozurkewich, M., (2006). *Atm. Chem. and Phys.*, 6:2927–2942.
- Kuang, C., Chen, M., Zhao, J. and others (2012). *Atm. Chem. and Phys.*, 12:3573–3589.
- Henze, D., Seinfeld, J., Liao, W, and others (2004). *J. of Geophys. Res.: Atm.*, 109:D14201.
- Sandu, A., Liao, W., Carmichael, G., and others (2005). *Aero. sci. and tech.*, 39:677–694.
- Banks, H., Tran, H., Woodward, D. (1993). *SIAM J. on Num. Ana.*, 30:1574–1602.
- Rundell, W. (1993). *SIAM J. on Appl. Math.*, 53:1731–1746.
- Ackleh, A. and Miller, R. (2018). *Inv. Prob. in Sci. and Eng.*, 26:152–182.
- Bortz, D., Byrne, E., Mirzaev, I. (2015). *arXiv preprint*, arXiv:1510.01355.
- Kupiainen-Määttä, O. (2016). *Atm. Chem. and Phys.*, 16:14585–14598.

EFFECT OF WATER CONFINEMENT ON ICE NUCLEATION

O. H. PAKARINEN¹, G. ROUDSARI¹, B. REISCHL¹ and H. VEHKAMÄKI¹

¹INAR/Physics, University of Helsinki, Finland.

Keywords: ICE NUCLEATION, SIMULATION, MOLECULAR DYNAMICS.

INTRODUCTION

Understanding the way in which ice forms is of great importance to many fields of science. Pure water droplets in the atmosphere can remain in the liquid phase to nearly -40 C. Crystallization of ice in the atmosphere therefore typically occurs in the presence of aerosol particles, such as mineral dust, soot or organic particles. These ice nucleating particles (INPs) trigger heterogeneous ice nucleation at clearly higher temperatures. Therefore, a better understanding of how the various types of aerosol particles present in the atmosphere affect ice nucleation (IN) in clouds would be an important advance in the field of atmospheric science.

Experiments have shown in great detail what is the IN activity of different types of compounds, and recently also clarified the importance of small surface features such as surface defects. The molecular-scale processes responsible for ice nucleation are still not well known, however, and difficulties in atomic-scale characterization of complex and imperfect surfaces means that a full understanding of these processes from solely experimental evidence is still a distant goal. In recent years, several computational studies have been published on heterogeneous ice nucleation, advancing our understanding of the details of ice nucleation in many materials. The role of defects is starting to become clearer, and recently simulations showed enhanced ice nucleation efficiency in confined geometry such as wedges or pits (Bi, Cao and Li, 2017).

METHODS

We are studying the effect of water confinement on ice nucleation at both low-temperature and high-temperature regimes by utilizing the monatomic water model (Molinero and Moore, 2009) and the TIP4P/Ice (Abascal et al., 2005) all-atom water model for unbiased molecular dynamics (MD) simulations, where a system including a defected surface, such as pyramidal pits, steps or surface cracks in silicon and silver iodide, immersed in water, is cooled continuously below the melting point over tens of nanoseconds of simulation time and crystallization is followed.

To capture the details of the rare stochastic events of ice nucleation, it is necessary to simulate relatively large systems over long time scales, and therefore classical interaction potentials are used. We utilize different types of water – silicon interaction potentials, both to cover different surface treatments and to how strongly ice nucleation activity is dependent on the potentials. Unbiased MD is an ideal method to study physical pathways of ice formation from disordered water requiring collective molecular movement, and we utilize the LAMMPS MD code in NVT ensemble, with periodic boundary conditions, with a few nm thick vacuum layer on top of an open water surface to allow the water density to change during freezing.

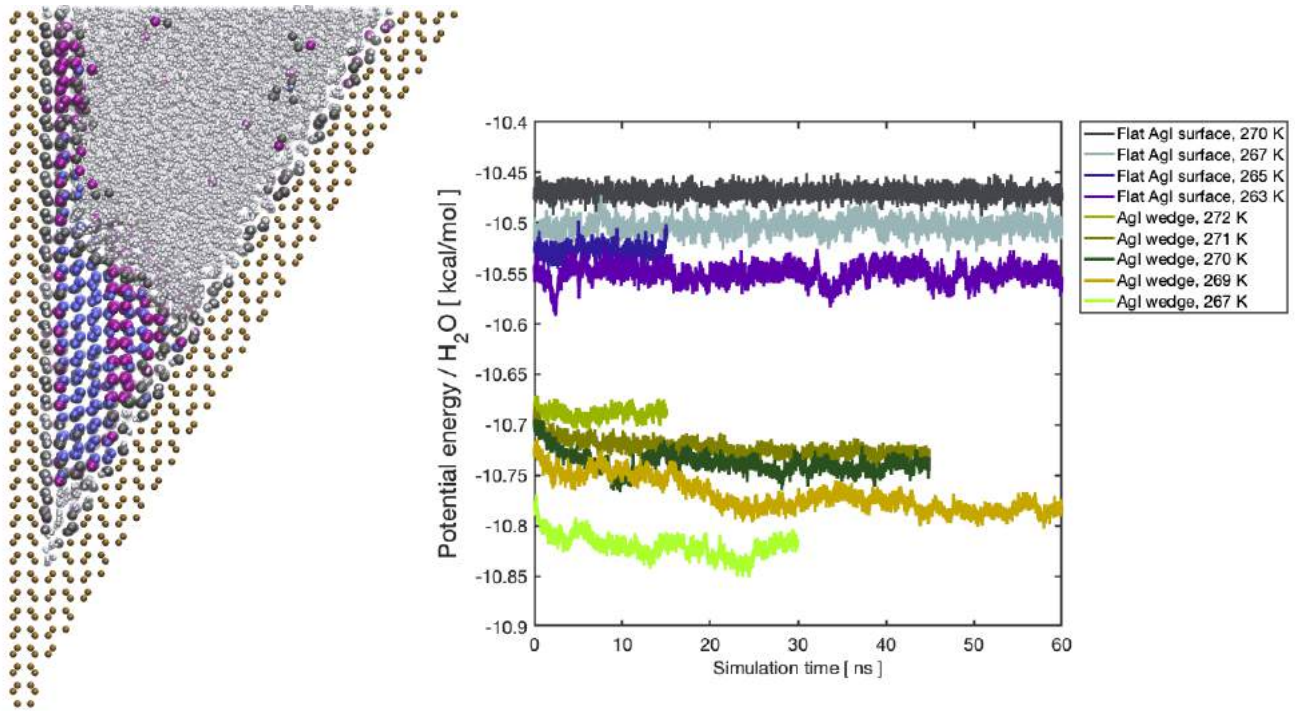


Figure 1. (left) Ice nucleation at the bottom of a wedge-shaped crack in AgI, at an unusually high nucleation temperature of $-4\text{ }^{\circ}\text{C}$. (right) Comparison of ice growth by potential energy shows that ice growth in a wedge-shaped crack progresses similarly to a flat AgI (0001) surface at clearly higher temperatures.

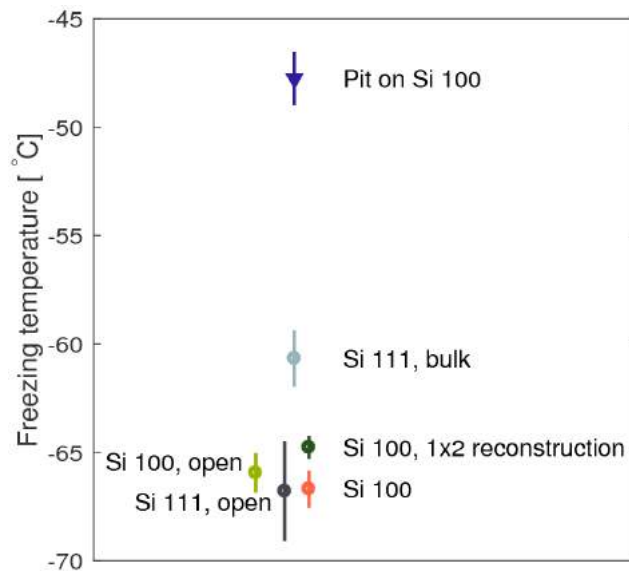


Figure 2. Freezing temperature for different silicon surfaces: a clear $12.9\text{ }^{\circ}\text{C}$ increase in freezing temperature is seen in a pit system, compared to the (111) surface. Enhanced activity in pits is seen in experiments as well.

CONCLUSIONS

Results show that water confinement in nanometer scale defects increases ice nucleation activity of surfaces in both low-temperature and high-temperature regimes. Different crystallographic faces of AgI show differences in ice nucleation activity, with β -AgI (0001) showing the highest activity, causing ice nucleation at high temperatures. By generating wedge-shaped structures with β -AgI (0001) surface as one of the two side walls, we obtained a structure that shows even higher ice nucleation activity than planar β -AgI (0001) surfaces.

Results of simulations on pyramidal pits on Si (100) surfaces (Fig. 2), an experimentally realizable system, show a clear ($\Delta T > 10$ °C) enhancement of ice nucleation compared to flat Si (100) or Si (111) surfaces, in agreement with initial experimental findings of preference of ice to nucleate at these sites. To study the statistical variation of the freezing temperatures in the systems, we calculate as our results the mean and the standard error of mean from three calculations for each system, and results show small variation due to relatively slow cooling rate in simulations. Simulations with truncated pyramidal pits show that the enhancement of ice nucleation is not dependent on atomic sharpness of pits.

Understanding the enhanced activity in these kind of highly IN active surface features may enable characterization of ice nucleation active sites on some atmospheric particles, and lead to designs of new artificial materials optimized for cloud seeding applications, freezing water at temperatures even higher than with the most active natural particles or bacteria.

ACKNOWLEDGEMENTS

This work was supported by the Academy of Finland Center of Excellence programme (grant no. 307331) and ARKTIKO project 285067 ICINA, the National Center for Meteorology and Seismology, Abu Dhabi, UAE, under the UAE Research Program for Rain Enhancement Science, by ERC Grant 692891-DAMOCLES, by University of Helsinki, Faculty of Science ATMATH project, and by supercomputing resources at CSC - IT Center for Science Ltd.

REFERENCES

- Bi, Y., B. Cao and T. Li (2017). *Nat. Commun.* **8**, 15372.
Molinero, V. and E. B. Moore (2009). *J. Phys. Chem. B* **113**, 4008.
Abascal, J. L. F., E. Sanz, R. García Fernández and C. Vega (2005). *J. Chem. Phys.*, **122**(23), 234511

THE DUTCH ELM DISEASE INFECTED FIELD ELMS IN DRY AND MOIST CONDITIONS

T. PALJAKKA^{1,2}, S. KOVACS³, K. BLUMENSTEIN³, R. KASANEN², E. TERHONEN³ and T. HÖLTTÄ^{1,2}

¹Institute for Atmospheric and Earth System Research / Forest Sciences

²Faculty of Agriculture and Forestry, P.O. Box 27, FI-00014 University of Helsinki, Finland

³Forest Pathology Research Group, Büsgen-Institute, Department of Forest Botany and Tree Physiology, Faculty of Forest Sciences and Forest Ecology, University of Göttingen, Büsgenweg 2, 37077 Göttingen

Keywords: DUTCH ELM DISEASE, OPHIOSTOMA NOVO-ULMI, ULMUS MINOR, TREE WATER TRANSPORT

INTRODUCTION

The pathogen Dutch elm disease (DED) has been intensively studied in the past decades because of the tree mortality it has caused in elm trees in Europe and North America (Brasier, 2000). DED causes desiccation in the water transporting tissue (Urban and Dvorak, 2014, Beier *et al.*, 2017) and wilting of elm trees. It is vectored by elm specific bark beetles that bore through the tree bark, and simultaneously introduce the pathogen on the surface of the water transporting sapwood. Connection of tree resistance with the tree water transport under conditions of varying water availability remain under investigation. Our aim was to study the relations behind the declining tree water transport and DED infection, and gain understanding of how varying water availability affect these relations.

METHODS

We conducted an experiment with DED (*Ophiostoma novo-ulmi*) in 3-year old field elm saplings (*Ulmus minor*) to investigate the loss in stem hydraulic conductivity with the tree gas exchange measurements in trees under dry and moist conditions. The study was conducted in a greenhouse in the Göttingen University facilities in Germany during the late spring 2019. Elm saplings were allocated into three treatments: untreated control, wounded control and infected trees in dry and control sites. Trees were watered twice a week during the experiment with 200 ml and 400 ml increment of water to dry and moist sites, respectively, at each watering. The watering treatment was monitored with soil moisture measurements. We measured the stem water transport including the hydraulic conductivity and relative water content from sampled trees, and the leaf gas exchange (Li 6800, Li-Cor, US) with photosynthetic rate and stomatal conductance twice a week during four weeks after the inoculation treatment of DED. In the leaf gas exchange measurements, we used constant 800 $\mu\text{mol m}^{-2} \text{s}^{-1}$ light and controlled CO₂ conditions in the chamber.

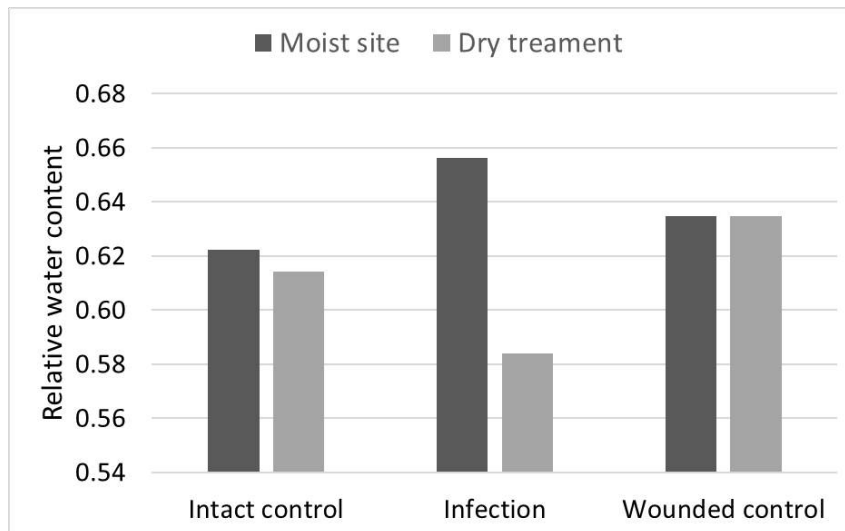


Figure 1. Stem relative water content in *Ophiostoma novo-ulmi* infected and control *Ulmus minor* trees in moist and dry sites.

CONCLUSIONS

The preliminary results indicated decrease in water potential and stem relative water content (Fig. 1) in infected trees compared to the control trees, especially in the dry site. No clear difference in the leaf gas exchange was observed between the treatments. Local wilting symptoms were observed in the canopy of the infected trees. The wilting symptoms in tree canopy may occur rapidly, and therefore, the infection may be observed mainly locally at the site of infection. The lowered stem relative content observed in our study indicates to such local response to the infection. The data analysis is ongoing, and further analyses will be conducted on the xylem sap properties of the treatments and the level of the infection.

ACKNOWLEDGEMENTS

This study was supported by the Faculty of Forest Sciences and Forest Ecology in University of Göttingen, Academy of Finland grant # 324014, and by Wiipurilaisen Osakunnan Stipendisäätiö. We are grateful to Christian Eckert and Ronny Thoms for their assistance with the measurement instruments and study setup.

REFERENCES

- Beier, G.L., B.W. Held, C.P. Giblin, J. Cavender-Bares and R.A. Blanchette (2017). American elm cultivars: Variation in compartmentalization of infection by *Ophiostoma novo-ulmi* and its effects on hydraulic conductivity, *Forest pathology* **47**, e12369.
- Brasier, C. M. (2000). In *Elms: Intercontinental spread and continuing evolution of the Dutch elm disease pathogens*, 61-72, (Springer, Boston, MA).
- Urban, J. and M. Dvořák (2014). Sap flow-based quantitative indication of progression of Dutch elm disease after inoculation with *Ophiostoma novo-ulmi*, *Trees*, **28**, 1599-1605.

AEROBIC METHANE EMISSIONS FROM BOREAL TREES: TEMPORAL VARIATIONS AND THE EFFECTS OF STRESS

M. PATAMA^{1,2}, L. KOHL^{1,2}, M. KOSKINEN^{1,2,3}, S. TENHOVIRTA^{1,2} and M. PIHLATIE^{1,2,4}

¹Department of Agricultural Sciences, Faculty of Agriculture and Forestry, University of Helsinki, Finland

²Institute of Atmospheric and Earth System Research / Forest Sciences, Faculty of Agriculture and Forestry, University of Helsinki, Finland

³Finnish Meteorological Institute, Helsinki, Finland

⁴Viikki Plant Science Centre (ViPS), University of Helsinki, Finland

Keywords: Methane, Boreal Forests, Climate Change

INTRODUCTION

Methane (CH₄) is the second strongest anthropogenic greenhouse gas responsible for ~20 % of the global warming (IPCC, 2013). Recent research has shown that plants can emit CH₄ under aerobic conditions, and may constitute a relevant source of atmospheric CH₄ (Keppler et al., 2006). These non-microbial emissions originate from the foliage, and they have been recorded from plants exposed to e.g. drought and temperature stress (Qaderi & Reid, 2009). In addition, it has been observed that UV-induced generation of reactive oxygen species (ROS) can lead to the production of CH₄ from plant cell wall polysaccharides such as pectins (McLeod et al., 2008). The physiological drivers and controls over aerobic CH₄ emissions, however, remain largely unknown.

Little is known about the contribution of boreal forests to CH₄ emissions, yet trees have also been identified as a possible source of CH₄ (Carmichael et al., 2014). Earlier, CH₄ emissions from trees were thought to be solely of microbial origin, since trees can act as conduits for soil-produced CH₄ (Pangala et al., 2014; Rice et al., 2010; Rusch & Rennenberg, 1998) and CH₄ can be produced within the tree stems by methanogens (Li et al., 2019; Yip et al., 2019). Additionally, different tree species seem to act differently regarding tree canopy CH₄ fluxes: Scots pine (*Pinus sylvestris* L.) shoots emit CH₄ (Halmeenmäki et al., 2017; Machacova et al., 2016), whereas Norway spruce (*Picea abies* (L.) H. Karst.) has been observed consuming CH₄ (Sundqvist et al., 2015). Another conifer, Japanese larch (*Larix kaempferi* (Lamb.) Carr.), has also been shown to emit CH₄ (Itaoka et al., 2007).

So far, no continuous measurements of CH₄ fluxes have been conducted on tree shoots. Information on diurnal and seasonal variations in the fluxes together with environmental variables are critically needed to estimate the contribution of boreal forests to global CH₄ emissions. To fill these knowledge gaps, we will perform high-frequency measurements of shoot CH₄ fluxes focusing on three coniferous tree species: Scots pine, Norway spruce and Siberian larch (*Larix sibirica* Ledeb.), all of which are dominant tree species in boreal forests. Specifically, we address the following research questions: 1) Are the CH₄ fluxes of different boreal tree species subject to temporal variability showing diurnal and seasonal patterns? 2) Do the observed fluxes differ between the studied tree species? 3) How do increasing temperatures affect the fluxes?

METHODS

Our work takes advantage of a recently developed enclosure chamber system placed in a climate controlled growth cabinet (Pihlatie et al., 2019). Environmental parameters, such as light, temperature, and relative humidity, are regulated inside the growth chamber. Typical diurnal cycles are simulated and temperature stress will be applied by altering these factors. The growth cabinet is divided into separate shoot and root compartments, and CH₄, H₂O and CO₂ fluxes from different compartments are measured at high temporal resolution (10 min) by an online gas analyzer. In addition, photosynthetic rate and stomatal conductance are measured to identify possible physiological processes that covary with aerobic CH₄ emissions.

The experiments on diel cycles have already been performed with Scots pine. The seedlings were purchased from a commercial tree nursery where the seedlings were grown in pots containing commercial peat-based soil. The purchased seedlings were 2 years old, and initially, their height ranged from 40 to 60 cm. Three visibly healthy seedlings were chosen as replicates. One seedling was placed in the growth cabinet at a time for 11 days. The experimental period consisted of an adjustment period of 17 h and two different light programs of 5 d with the following conditions: temperature 10 °C and relative humidity of 40 %. The photoperiod of the first light program was 12 h including gradually changing lighting conditions between the day and night to simulate dawn and dusk. During the second 5-d light program, the photoperiod was 12 h with abrupt changes between light and darkness. In addition, similar preliminary experiments have been conducted with Siberian larch.

The seasonality of shoot fluxes will be studied by performing these experiments throughout the year, and some preliminary tests with Scots pine and Siberian larch have already been carried out. The shoot fluxes of Scots pine have been measured during and after the growing season in May, June and September. Siberian larch, instead, has been studied after the growing season in October. In addition, the seedlings will be exposed to increased temperatures to reveal the stress-induced responses in the CH₄ fluxes.

RESULTS

Initial results suggest that the CH₄ emissions from the shoots of Scots pine increase with increasing photosynthetically active radiation (PAR). Respectively, the opposite effect occurred when the PAR value decreased, yet a lag in the emissions was observed after the lights had turned off. Regarding seasonality, positive fluxes have been measured during the growing season with Scots pine. No fluxes were observed in September after the growing season. Additionally, zero fluxes were measured with Siberian larch based on the preliminary tests after the growing season.

CONCLUSIONS

Our results so far suggest that diurnal cycles of CH₄ emissions from Scots Pine shoots are induced by changes in PAR and photosynthesis rates. We also have initial results in support of seasonal changes in the relationship between light and CH₄ emissions.

REFERENCES

- Carmichael, M. J., Bernhardt, E. S., Bräuer, S. L., & Smith, W. K. (2014). The role of vegetation in methane flux to the atmosphere: Should vegetation be included as a distinct category in the global methane budget? *Biogeochemistry*, *119*(1–3), 1–24. <https://doi.org/10.1007/s10533-014-9974-1>
- Halmeenmäki, E., Heinonsalo, J., Putkinen, A., Santalahti, M., Fritze, H., & Pihlatie, M. (2017). Above- and belowground fluxes of methane from boreal dwarf shrubs and *Pinus sylvestris* seedlings. *Plant and Soil*, *420*(1–2), 361–373. <https://doi.org/10.1007/s11104-017-3406-7>
- IPCC. (2013). *Climate Change 2013*. (P. M. Stocker, T.F., Qin, D., Plattner, G.K., Tignor, M., Allen, S.K., Boschung, J., Nauels, A., Xia, Y., Bex, V., Midgey, Ed.), *Climate Change 2013: The Physical Science Basis*. Cambridge, New York: Cambridge University Press.
- Itaoka, S. K., Akata, T. S., Oike, T. K., Obita, H. T., Emura, A. U., Itao, M. K., et al. (2007). Methane Emission from Leaves of Larch, Birch and Oak Saplings Grown at Elevated CO₂ Concentration in Northern Japan – Preliminary Study –. *Nature*, *63*(4), 201–206. <https://doi.org/10.2480/agrmet.63.201>
- Keppler, F., Hamilton, J. T. G., Braß, M., & Röckmann, T. (2006). Methane emissions from terrestrial plants under aerobic conditions. *Nature*, *439*(7073), 187–191. <https://doi.org/10.1038/nature04420>
- Li, H.-L., Zhang, X.-M., Deng, F.-D., Han, X.-G., Xiao, C.-W., Han, S.-J., & Wang, Z.-P. (2019). Microbial methane production is affected by secondary metabolites in the heartwood of living trees in upland forests. *Trees*. <https://doi.org/10.1007/s00468-019-01914-6>
- Machacova, K., Bäck, J., Vanhatalo, A., Halmeenmäki, E., Kolari, P., Mammarella, I., et al. (2016). *Pinus*

- sylvestris as a missing source of nitrous oxide and methane in boreal forest. *Scientific Reports*, 6(March), 1–8. <https://doi.org/10.1038/srep23410>
- McLeod, A. R., Fry, S. C., Loake, G. J., Messenger, D. J., Reay, D. S., Smith, K. A., & Yun, B. W. (2008). Ultraviolet radiation drives methane emissions from terrestrial plant pectins. *New Phytologist*, 180(1), 124–132. <https://doi.org/10.1111/j.1469-8137.2008.02571.x>
- Pangala, S. R., Gowing, D. J., Hornibrook, E. R. C., & Gauci, V. (2014). Controls on methane emissions from *Alnus glutinosa* saplings. *New Phytologist*, 201(3), 887–896. <https://doi.org/10.1111/nph.12561>
- Pihlatie, M., Polvinen, T., Kohl, L., Rissanen, K., Pohja, T., Aalto, J., & Koskinen, M. (2019). Controlled environment chamber system for gas exchange measurements: setup and operating principles. In *European Geosciences Union General Assembly* (p. 4188). Vienna, Austria.
- Qaderi, M. M., & Reid, D. M. (2009). Methane emissions from six crop species exposed to three components of global climate change: Temperature, ultraviolet-B radiation and water stress. *Physiologia Plantarum*, 137(2), 139–147. <https://doi.org/10.1111/j.1399-3054.2009.01268.x>
- Rice, A. L., Butenhoff, C. L., Shearer, M. J., Teama, D., Rosenstiel, T. N., & Khalil, M. A. K. (2010). Emissions of anaerobically produced methane by trees. *Geophysical Research Letters*, 37(3), n/a-n/a. <https://doi.org/10.1029/2009GL041565>
- Rusch, H., & Rennenberg, H. (1998). Black alder (*Alnus glutinosa* (L.) Gaertn.) trees mediate methane and nitrous oxide emission from the soil to the atmosphere. *Plant and Soil*, 201(1), 1–7. <https://doi.org/10.1023/A:1004331521059>
- Sundqvist, E., Persson, A., Kljun, N., Vestin, P., Chasmer, L., Hopkinson, C., & Lindroth, A. (2015). Upscaling of methane exchange in a boreal forest using soil chamber measurements and high-resolution LiDAR elevation data. *Agricultural and Forest Meteorology*, 214–215, 393–401. <https://doi.org/10.1016/j.agrformet.2015.09.003>
- Yip, D. Z., Veach, A. M., Yang, Z. K., Cregger, M. A., & Schadt, C. W. (2019). Methanogenic Archaea dominate mature heartwood habitats of Eastern Cottonwood (*Populus deltoides*). *New Phytologist*, 222(1), 115–121. <https://doi.org/10.1111/nph.15346>

OBSERVING FINE-SCALE SPATIAL DETAILS OF ATMOSPHERIC MIXING WITH DISTRIBUTED TEMPERATURE SENSING

O. PELTOLA¹, P. KOLARI², K. LAPO³, I. MARTINKAUPPI⁴, C.K. THOMAS³ and T. VESALA^{2,5}

¹ Finnish Meteorological Institute, Helsinki, Finland

² Institute for Atmospheric and Earth System Research/Physics, Helsinki, Finland

³ University of Bayreuth, Bayreuth, Germany

⁴ Geological Survey of Finland, Kokkola, Finland

⁵ Institute for Atmospheric and Earth System Research/Forest Sciences, Helsinki, Finland

Keywords: TURBULENCE, ATMOSPHERIC MIXING, SPATIAL ANALYSIS, TEMPERATURE.

INTRODUCTION

Classically atmospheric measurements are done at fixed locations with in-situ sensors (e.g. sonic anemometers, gas analysers, thermometers) or remotely with remote sensing methods (e.g. radars, lidars, sodars). In-situ sensors provide continuous temporal measurements, whereas remote sensing methods can be used to acquire large scale spatial details. However, these two established groups of measurement techniques provide information at clearly different scales and the scales do not fully overlap. Moreover, interesting flow phenomena take place in locations where remote sensing techniques are not possible (e.g. within forest canopies or street canyons). Hence there is a clear need to bridge the scales between these two groups of techniques and to find new ways to study the spatial details of the flow in complicated locations, such as within forests or cities.

Distributed temperature sensing (DTS) measurements provide the possibility to observe spatio-temporal details of the atmospheric flow at temporal scales starting from 1 Hz frequency and spatial scales ranging between 10^{-1} ... 10^3 m. The DTS technique utilises fibre-optic cables as sensing elements and observations of local temperature along the cable are based on Raman scattering of a light pulse travelling in the fibre-optic cable (Selker *et al.*, 2006; Tyler *et al.*, 2009; Thomas *et al.*, 2012). The DTS instrument connected to the cable resolves the temperature along the cable which can be freely distributed in the measurement domain, e.g. up and down a measurement tower, horizontally within forest or as a net above a street canyon. Depending on the configuration, the measurements can then be used to obtain e.g. detailed vertical profiles, two- or three-dimensional structures of the flow.

In this study DTS measurements made within and above boreal forest during summer 2019 are analysed. The measurements are validated against more traditional measurements with 3D sonic anemometers and a first-look on the observed spatial flow patterns is provided.

METHODS

The DTS measurements were conducted at the SMEAR II station located in central Finland (61° 51' N, 24° 17' E, 181 m a.s.l). Forest canopy is located roughly between 10 and 17 m above the ground and below 10 m relative open trunk space exists. During the first part of the campaign

(June-July 2019), fibre-optic cable was attached to the tall tower at the site providing detailed temperature profiles between 2 and 120 m above the ground. During the second part (August-October 2019) the cable was suspended between two towers at several heights providing detailed vertical and horizontal information of temperature variability within the forest.

The DTS instrument (Ultima-S, Silixa ltd., UK) and calibration baths were located in a wooden cabin. The instrument was sampling with 1 Hz and 0.127 m resolution along the cable. Single-core, thin (outer diameter 0.9 mm) aramid reinforced multimode fibre-optic cable (AFL, US) was used. The measurements were run either in double-ended (first part of the campaign) or single-ended (second part) mode and the DTS data were processed following either van de Giesen *et al.* (2012) or Hausner *et al.* (2011), respectively.

RESULTS

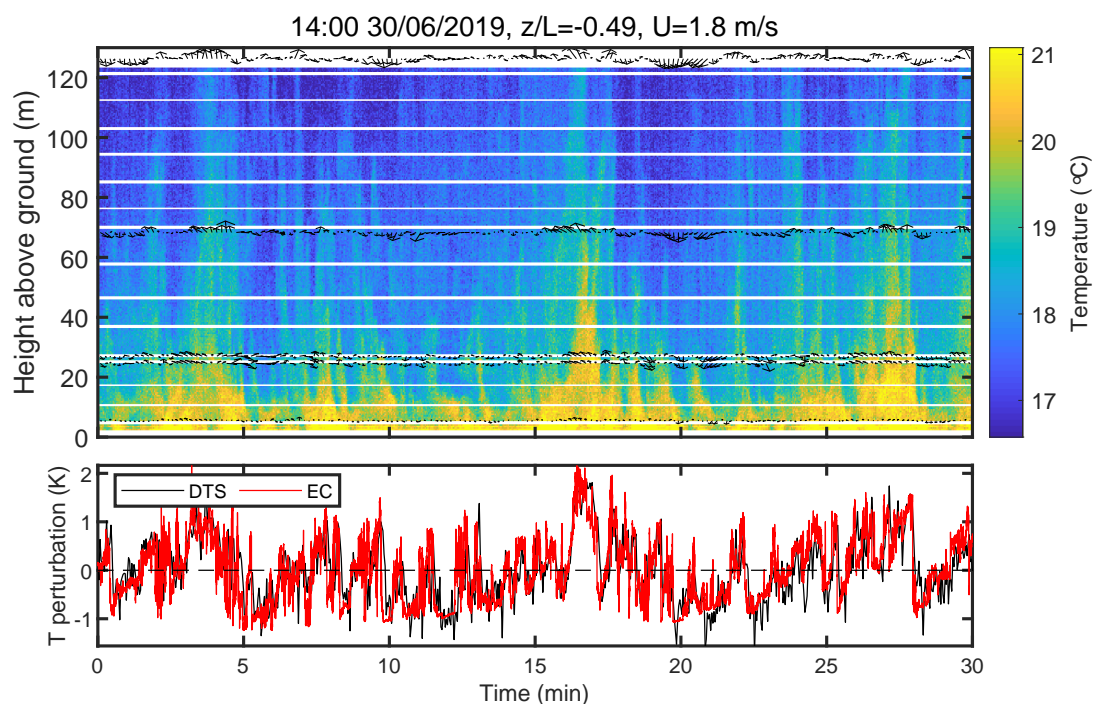


Figure 1: Upper plot: 30-min example time series of the DTS data (shown with color) measured in the tall mast at the SMEAR II site. The arrows show the turbulent fluctuations of wind measured with 3D sonic anemometers. Up and down arrow directions denote positive and negative vertical wind speed fluctuations, respectively, left and right mean positive and negative horizontal wind speed fluctuations, respectively. Bottom plot: Comparison of temperature perturbation ($T - \text{mean}(T)$) time series measured at 27 m height. Values for the stability parameter and mean wind speed measured at 27 m height are shown at the top of the figure.

During the first part of the measurement campaign the fibre-optic cable was attached to the tall mast providing detailed vertical profiles of air temperature and atmospheric mixing between forest floor and 120 m above the ground. Figure 1 shows an example of the data from one 30-min daytime period at the end of June 2019. The air was unstably stratified and wind speed was relatively low during this example period. Large coherent patterns are evident in the top plot. These patterns are the large turbulent eddies that typically dominate the surface layer turbulent transport. The largest eddies span from the forest floor through the canopy up to 120 m height and above, meaning

that the whole 120 m high air column was fully coupled. As expected, the eddy sizes scale with height, meaning the only the largest eddies reach the highest measurement heights.

In fig. 1 the high temperatures (yellow and green colors) match with upward vertical air motions (arrows pointing upwards) and low temperatures with downward motions, as expected since the vertical turbulent heat flux was directed upwards during this 30-min period. The temperature perturbations measured with DTS and EC systems agree well (bottom plot, fig. 1). Both of these findings suggest that the DTS setup was able to resolve the dominant eddies.

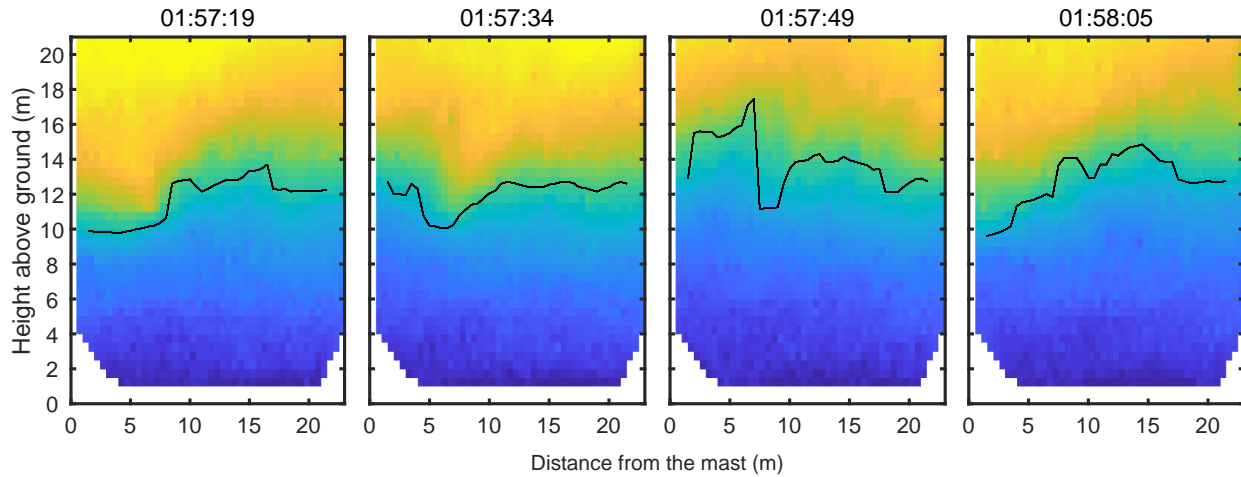


Figure 2: Evolution of two dimensional temperature field within the boreal forest at 27.8.2019 during approximately one minute period (between 01:57:19 and 01:58:05). Color shows the air temperature measured with DTS and interpolated to evenly spaced grid and the lines highlight the maxima in temperature vertical gradient. During the shown period the air was stably stratified due to radiative cooling of the surface.

Figure 2 shows an example of evolution of two-dimensional temperature field within the boreal forest at night during stably stratified situation. The four subplots show a wave passing the measurement domain at 10...15 m above the ground. The strong vertical gradient in temperature decouples the surface from the air above and turbulence is non-existent.

CONCLUSIONS

The vertical and horizontal DTS measurements were able to resolve fine-scale spatial details of the flow within and above the boreal forest in unstable, as well as strongly stable situation. The measurement technique opens up a new view on the spatial details of atmospheric mixing that have typically been unreachable with conventional measurement techniques. The DTS measurements will be combined with EC gas flux measurements in order to get a better understanding on the flow processes controlling ecosystem-atmosphere gas exchange.

ACKNOWLEDGEMENTS

We acknowledge the support from the technical staff at the SMEAR II station. This work was supported by the Postdoctoral Researcher project (decision 315424) funded by the Academy of Finland and Academy of Finland Centre of Excellence program (project number 307331).

REFERENCES

- Hausner *et al.* (2011). Calibrating single-ended fiber-optic Raman spectra distributed temperature sensing data. *Sensors (Basel, Switzerland)*, **11(11)**, 10859-10879.
- Selker *et al.* (2006). Distributed fiber-optic temperature sensing for hydrologic systems. *Water Resources Research*, **42(12)**.
- Thomas *et al.* (2012). High-Resolution Fibre-Optic Temperature Sensing: A New Tool to Study the Two-Dimensional Structure of Atmospheric Surface-Layer Flow. *Boundary-Layer Meteorology*, **142(2)**, 177-192.
- Tyler *et al.* (2009). Environmental temperature sensing using Raman spectra DTS fiber-optic methods. *Water Resources Research*, **45(4)**.
- van de Giesen *et al.* (2012). Double-ended calibration of fiber-optic Raman spectra distributed temperature sensing data. *Sensors (Basel, Switzerland)*, **12(5)**, 5471-5485.

VOLATILITY OF HIGHLY OXYGENATED MOLECULES (HOM) FROM α -PINENE OXIDATION

O. PERÄKYLÄ¹, M. RIVA^{1,2}, L. HEIKKINEN¹, L. QUÉLÉVER¹, P. ROLDIN³ and M. EHN¹

¹ Institute for Atmospheric and Earth System Research / Physics, University of Helsinki, 00014
University of Helsinki, Finland

² Univ Lyon, Université Claude Bernard Lyon 1, CNRS, IRCELYON, F-69626, Villeurbanne,
France

³ Department of Physics, Lund University, Lund, Sweden

Keywords: HOM, SOA, VOLATILITY.

INTRODUCTION

Secondary organic aerosol (SOA) contributes a major fraction of tropospheric aerosol worldwide (Zhang et al., 2007; Jimenez et al., 2009). Still, the detailed formation mechanisms of SOA have remained elusive, despite intensive research efforts (Hallquist et al., 2009). SOA forms from the gas to particle conversion of volatile organic compounds, or their oxidation products (VOC). Recently, a new group of oxidation products of VOC was discovered: this group, highly oxygenated organic compounds (HOM), has been proposed to be efficient in forming SOA, and to contribute to a large fraction of SOA globally (Ehn et al., 2014; Bianchi et al., 2019). These compounds form rapidly in the oxidation of many VOC, and are thought to be of very low volatility. This low volatility enables them to take part in SOA formation, and even in new particle formation (NPF) (Kirkby et al., 2016). However, while we know that HOM are of low volatility, the exact volatilities are still shrouded by mystery, with different estimates disagreeing by up to ten orders of magnitude (Kurtén et al., 2016). Still, to assess the exact role of HOM in aerosol formation, more precise knowledge of their volatilities would be needed (Bianchi et al., 2019). We present a laboratory study, supported by box modelling, to investigate the volatilities of HOM formed in the ozonolysis of α -pinene, the most abundant monoterpene emitted by boreal forests. Our results, in review and expected to be published soon, indicate that HOM volatilities are in between previous estimates, and help to narrow down the uncertainties around them (Peräkylä et al., 2019).

METHODS

We conducted a series of laboratory experiments in the COALA smog chamber at the University of Helsinki. We continuously injected α -pinene and ozone to the two cubic metre teflon chamber to form HOM, while simultaneously sampling the HOM formed using a nitrate chemical ionization mass spectrometer (CI-APi-TOF, Jokinen et al., 2012). In some experiments we also injected nitrogen dioxide, which was photolysed with LED lights to form nitric oxide, to form organic nitrates in addition to the non-nitrate HOM. In addition to the gaseous precursors, we also injected ammonium sulfate seed particles to the chamber. Any compounds of low enough volatility will condense on the seed particles, decreasing their gas phase concentration: in contrast, more volatile products evaporate fast enough back to the gas phase, so that their concentration is unaffected. This allowed us to determine the volatilities of HOM based on their behaviour upon seed injection. The experiments were supported by modelling using the ADCHAM model (Roldin et al., 2014,

2019), allowing us to determine the exact relationship between the volatility of a compound, and its behaviour upon seed injection.

RESULTS

As expected, we found that the volatility of HOM decreases with increasing molecular mass. However, this decrease was not monotonic, and organic nitrates of comparable volatility had a higher mass compared to non-nitrates. This can be explained in terms of the relatively high mass of the nitrate functional group. HOM monomers were found to belong mainly to low volatility organic compounds (LVOC, Donahue et al., 2012), with a minor fraction being semi-volatile. HOM dimers were of low, or more probably of extremely low volatility: however, our method cannot readily distinguish between the two. We were able to parametrize the volatility of a compound based on its elemental composition. We found that HOM formed in the ozonolysis of α -pinene are less volatile compared to the predictions of Kurtén et al. (2016), but more volatile than predicted by Bianchi et al. (2019). The dependence of volatility on the oxygen number in the molecule was similar to Kurtén et al. (2016).

The results may not be directly generalizable to systems other than α -pinene ozonolysis, but the general method should be applicable to a broad range of different conditions. The results can help in future studies to assess the exact role of HOM in particle formation.

ACKNOWLEDGEMENTS

This work was supported by the European Research Council (Grant 638703-COALA), the Academy of Finland Center of Excellence (Grant 307331), and the Vilho, Yrjö and Kalle Väisälä Foundation. We thank the tofTools team for providing tools for mass spectrometry data analysis.

REFERENCES

- Bianchi, F., Kurtén, T., Riva, M., Mohr, C., Rissanen, M. P., Roldin, P., Berndt, T., Crouse, J. D., Wennberg, P. O., Mentel, T. F., Wildt, J., Junninen, H., Jokinen, T., Kulmala, M., Worsnop, D. R., Thornton, J. A., Donahue, N., Kjaergaard, H. G., and Ehn, M. (2019). Highly oxygenated organic molecules (hom) from gas-phase autoxidation involving peroxy radicals: A key contributor to atmospheric aerosol. *Chem. Rev.*
- Donahue, N. M., Kroll, J. H., Pandis, S. N., and Robinson, A. L. (2012). A two-dimensional volatility basis set – part 2: Diagnostics of organic-aerosol evolution. *Atmospheric Chemistry and Physics*, 12(2):615–634.
- Ehn, M., Thornton, J. A., Kleist, E., Sipilä, M., Junninen, H., Pullinen, I., Springer, M., Rubach, F., Tillmann, R., Lee, B., Lopez-Hilfiker, F., Andres, S., Acir, I.-H., Rissanen, M., Jokinen, T., Schobesberger, S., Kangasluoma, J., Kontkanen, J., Nieminen, T., Kurtén, T., Nielsen, L. B., Jørgensen, S., Kjaergaard, H. G., Canagaratna, M., Dal Maso, M., Berndt, T., Petäjä, T., Wahner, A., Kerminen, V.-M., Kulmala, M., Worsnop, D. R., Wildt, J., and Mentel, T. F. (2014). A large source of low-volatility secondary organic aerosol. *Nature*, 506(7489):476–479.
- Hallquist, M., Wenger, J. C., Baltensperger, U., Rudich, Y., Simpson, D., Claeys, M., Dommen, J., Donahue, N. M., George, C., Goldstein, A. H., Hamilton, J. F., Herrmann, H., Hoffmann, T., Iinuma, Y., Jang, M., Jenkin, M. E., Jimenez, J. L., Kiendler-Scharr, A., Maenhaut, W., McFiggans, G., Mentel, T. F., Monod, A., Prévôt, A. S. H., Seinfeld, J. H., Surratt, J. D., Szmigielski, R., and Wildt, J. (2009). The formation, properties and impact of secondary

organic aerosol: current and emerging issues. *Atmospheric Chemistry and Physics*, 9(14):5155–5236.

- Jimenez, J., Canagaratna, M., Donahue, N., Prevot, A., Zhang, Q., Kroll, J., P., D., Allan, J., Coe, H., Ng, N., Aiken, A., Docherty, K., Ulbrich, I., Grieshop, A., Robinson, A., Duplissy, J., Smith, J., Wilson, K., Lanz, V., Hueglin, C., Sun, Y., Tian, J., Laaksonen, A., Raatikainen, T., Rautiainen, J., Vaattovaara, P., Ehn, M., Kulmala, M., Tomlinson, J., Collins, D., Cubison, M., E., E., Dunlea, J., Huffman, J., Onasch, T., Alfarra, M., Williams, P., Bower, K., Kondo, Y., Schneider, J., Drewnick, F., Borrmann, S., Weimer, S., Demerjian, K., Salcedo, D., Cottrell, L., Griffin, R., Takami, A., Miyoshi, T., Hatakeyama, S., Shimono, A., Sun, J., Zhang, Y., Dzepina, K., Kimmel, J., Sueper, D., Jayne, J., Herndon, S., Trimborn, A., Williams, L., Wood, E., Middlebrook, A., Kolb, C., Baltensperger, U., and Worsnop, D. (2009). Evolution of organic aerosols in the atmosphere. *Science*, 326(5959):1525–1529.
- Jokinen, T., Sipilä, M., Junninen, H., Ehn, M., Lönn, G., Hakala, J., Petäjä, T., Mauldin III, R. L., Kulmala, M., and Worsnop, D. R. (2012). Atmospheric sulphuric acid and neutral cluster measurements using CI-API-TOF. *Atmospheric Chemistry and Physics*, 12(9):4117–4125.
- Kirkby, J., Duplissy, J., Sengupta, K., Frege, C., Gordon, H., Williamson, C., Heinritzi, M., Simon, M., Yan, C., Almeida, J., Tröstl, J., Nieminen, T., Ortega, I. K., Wagner, R., Adamov, A., Amorim, A., Bernhammer, A.-K., Bianchi, F., Breitenlechner, M., Brilke, S., Chen, X., Craven, J., Dias, A., Ehrhart, S., Flagan, R. C., Franchin, A., Fuchs, C., Guida, R., Hakala, J., Hoyle, C. R., Jokinen, T., Junninen, H., Kangasluoma, J., Kim, J., Krapf, M., Kürten, A., Laaksonen, A., Lehtipalo, K., Makhmutov, V., Mathot, S., Molteni, U., Onnela, A., Peräkylä, O., Piel, F., Petäjä, T., Praplan, A. P., Pringle, K., Rap, A., Richards, N. A. D., Riipinen, I., Rissanen, M. P., Rondo, L., Sarnela, N., Schobesberger, S., Scott, C. E., Seinfeld, J. H., Sipilä, M., Steiner, G., Stozhkov, Y., Stratmann, F., Tomé, A., Virtanen, A., Vogel, A. L., Wagner, A. C., Wagner, P. E., Weingartner, E., Wimmer, D., Winkler, P. M., Ye, P., Zhang, X., Hansel, A., Dommen, J., Donahue, N. M., Worsnop, D. R., Baltensperger, U., Kulmala, M., Carslaw, K. S., and Curtius, J. (2016). Ion-induced nucleation of pure biogenic particles. *Nature*, 533(7604):521–526. Letter.
- Kurtén, T., Tiusanen, K., Roldin, P., Rissanen, M., Luy, J., Boy, M., Ehn, M., and Donahue, N. (2016). α -Pinene autoxidation products may not have extremely low saturation vapor pressures despite high O:C ratios. *J Phys Chem*, 120(16):2569–2582.
- Peräkylä, O., Riva, M., Heikkinen, L., Quéléver, L., Roldin, P., and Ehn, M. (2019). Experimental investigation into the volatilities of highly oxygenated organic molecules (HOM). *Atmospheric Chemistry and Physics Discussions*, 2019:1–28.
- Roldin, P., Ehn, M., Kurtén, T., Olenius, T., Rissanen, M. P., Sarnela, N., Elm, J., Rantala, P., Hao, L., Hyttinen, N., Heikkinen, L., Worsnop, D. R., Pichelstorfer, L., Xavier, C., Clusius, P., Öström, E., Petäjä, T., Kulmala, M., Vehkamäki, H., Virtanen, A., Riipinen, I., and Boy, M. (2019). The role of highly oxygenated organic molecules in the boreal aerosol-cloud-climate system. *Nature Communications*, 10(1):4370.
- Roldin, P., Eriksson, A. C., Nordin, E. Z., Hermansson, E., Mogensen, D., Rusanen, A., Boy, M., Swietlicki, E., Svenningsson, B., Zelenyuk, A., and Pagels, J. (2014). Modelling non-equilibrium secondary organic aerosol formation and evaporation with the aerosol dynamics, gas- and particle-phase chemistry kinetic multilayer model adcham. *Atmospheric Chemistry and Physics*, 14(15):7953–7993.

Zhang, Q., Jimenez, J. L., Canagaratna, M. R., Allan, J. D., Coe, H., Ulbrich, I., Alfarra, M. R., Takami, A., Middlebrook, A. M., Sun, Y. L., Dzepina, K., Dunlea, E., Docherty, K., DeCarlo, P. F., Salcedo, D., Onasch, T., Jayne, J. T., Miyoshi, T., Shimo, A., Hatakeyama, S., Takegawa, N., Kondo, Y., Schneider, J., Drewnick, F., Borrmann, S., Weimer, S., Demerjian, K., Williams, P., Bower, K., Bahreini, R., Cottrell, L., Griffin, R. J., Rautiainen, J., Sun, J. Y., Zhang, Y. M., and Worsnop, D. R. (2007). Ubiquity and dominance of oxygenated species in organic aerosols in anthropogenically-influenced Northern Hemisphere midlatitudes. *Geophysical Research Letters*, 34(13). L13801.

FORMATION OF HOM FROM AVOCS AND ITS ATMOSPHERIC RELEVANCE

L. PICHELSTORFER¹, M. RISSANEN^{1,2}, P. ROLDIN³, T. KURTEN¹ and M. BOY¹

¹Institute for Atmospheric and Earth System Research/ Physics, University of Helsinki, Helsinki, 00560, Finland

²Aerosol Physics Laboratory, Physics Unit, Tampere University, Tampere, 33101, Finland

³Division of Nuclear Physics, Lund University, SE-221 00, Lund, Sweden

Keywords: HOM, AUTOXIDATION, AROMATIC VOC.

INTRODUCTION

Through natural as well as anthropogenic sources, large amounts of volatile organic compounds are constantly emitted to the atmosphere. Autoxidation, most likely involving intramolecular H abstraction by peroxy radicals and subsequent O₂ addition, can quickly transform VOCs to much less volatile species upon initial oxidation (Ehn et al. 2014). Species formed that way on the one hand impact the particulate matter and CCN number (e.g. by contributing to CCN activation or by increasing new particle formation) or, on the other hand, affect air quality and thus health (e.g.: according to WHO (2016) particulate matter causes millions of premature deaths each year; further, toxic species, such as epoxides from the degradation of alkylbenzenes (Yu and Jeffries, 1996) are formed in the gas phase). Thus investigating the HOM formation is the key in determining its effect on atmospheric processes and assessing its impact on air quality and climate.

METHODS

To approach the complex issue of atmospheric HOM formation and its effects, we develop near explicit gas phase chemistry codes (Type I & II) simulating the peroxy chemistry and couple it to MCMv3.1 (<http://mcm.leeds.ac.uk/MCM>) which describes the tropospheric degradation of VOCs. Unfortunately, experimental data for comparison, produced by means of mass spectrometry, provide only information on the atomic composition of the determined species. However, in order to create a chemical mechanism we aim to close this gap by considering theoretical findings. The huge number of possible reactions does not allow to investigate them one by one. Thus, rate constants determined by means of quantum chemical calculations are available for key reactions only. Structure activity relationships (SAR) allow to determine many of the needed coefficients (Vereecken et al., 2018). As SAR do not cover all types of molecules and reaction classes, a deterministic construction of a peroxy mechanism is not possible yet. In order to use the information available and still come up with codes that predict HOM formation, we decided to construct two different model types.

The first is a near explicit but still lumped code (Type I) aiming to reproduce experimentally determined data (i.e. mass spectra, chemical or mass yields, respectively). Reactions considered are listed in table 1 and described in detail by Roldin et al., (2019). The present set of equations distinguishes between peroxy radicals, alkoxy radicals, closed shell monomers and dimers, respectively. They allow to produce 94 % of the experimentally determined mass peaks for OH oxidation of benzene making up 99 % of the number concentration of detected molecules (experimental data from Molteni et al., 2018). Note that it does not account for species other than HOM (as defined by Bianchi et al., 2019).

While the above described code is very efficient in predicting the atomic composition of the species formed, it does not fully keep track of the molecular structure and functional groups. However, this kind of information determines the species properties. It can be obtained by knowing the reaction path of a given molecule. Thus we are developing a Type II mechanism that aims to consider all known relevant reactions in order to assess the isomeric distribution. Then, we assign rate constants that are obtained from

literature (experiments, quantum chemical calculations for key reactions, SARs). The starting point for the Type II code in the case of benzene is depicted in Fig. 1.

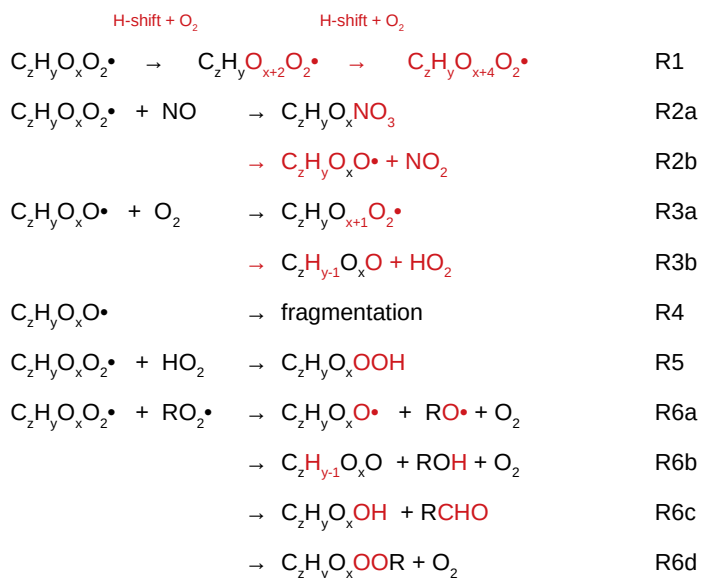


Table 1. List of reactions considered by Type I code. R1, R2, R5 and R6 describe reactions peroxy radicals can undergo. R2 and R3 describe alkoxy reactions. Detailed information can be found elsewhere (Roldin et al., 2019).

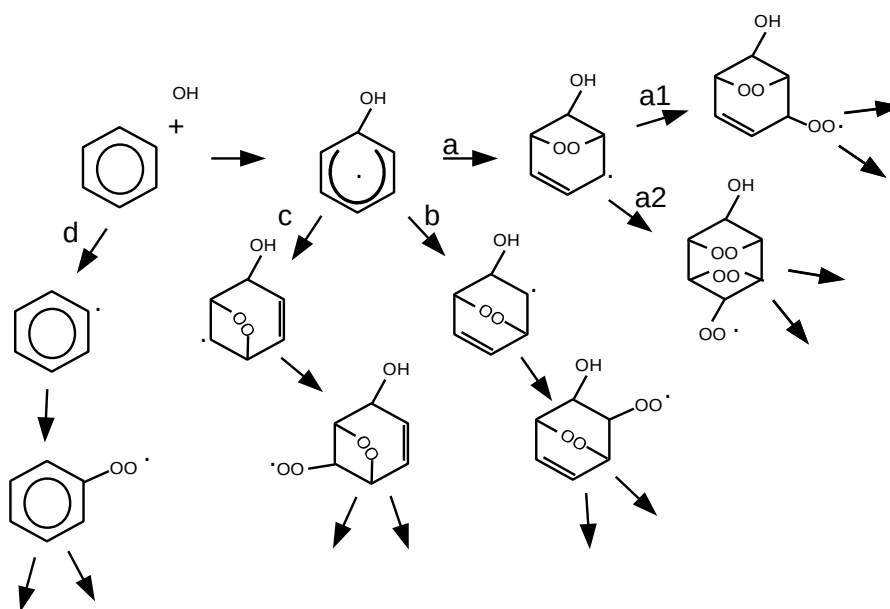


Figure 1. First reactions considered for type II chemistry code.

The next step is to test the two types of the code against experimental data. Type I code can be tested against data obtained from chemical ionization atmospheric pressure time of flight mass spectrometers (CI-api-ToF). However, note that these instruments have limited detection efficiencies that mainly depend on the (typically unknown) chemical structure of all isomers of a given atomic composition and the

clustering ions (Hytinen et al., 2018). Thus, direct comparison of the modeled results to those experimental data has to be done with caution. Type II chemical code can be used to estimate the detection efficiency of the formed species by the CI-api-ToF. Further, its results form the basis to calculate the properties (including estimates on toxicity) of the individual isomers by applying group contribution methods (e.g.: SIMPOL) or quantum chemistry based calculations (e.g.: COSMO-RT). Results are subsequently applied to simulate chamber experiments considering seed particles using chamber model ADCham (Roldin et al., 2014). That way the Type II code can be tested indirectly.

In order to see the effects of HOM formation from precursors related to anthropogenic activity on atmospheric processes, the codes will be integrated in the chemistry transport model SOSAA (Boy et al., 2011) and applied for SORPES station in China and potentially other stations showing anthropogenic influence.

CONCLUSIONS

Understanding the formation of HOM is crucial for the explanation of secondary aerosol loads in the atmosphere. It has been shown very recently that neglecting this process may result in considerable underestimation of organic aerosol mass (Xavier et al., 2019). Further, HOM may play an important role in the understanding of climate change (Roldin et al., 2019). Unfortunately, the scientific basis for fully understanding HOM chemistry is not yet complete. There are unresolved questions on both, the experimental and the theoretical side (e.g.: how to correctly interpret the results from CI-api-ToF; how to determine the isomeric composition or the most relevant reaction paths, respectively).

The present work aims to use the currently available knowledge on HOM for constructing models. That way, potential effects of HOM on climate and air quality can be assessed even though the topic is not fully understood. Simulation results may trigger new experiments or theoretical studies and can help to predict the impact of the findings.

ACKNOWLEDGEMENTS

This work was supported by the Austrian Science Funds (FWF) under grant (J-4241 Schrödinger Programm).

REFERENCES

- Bianchi, F., et al. (2019). Highly Oxygenated Organic Molecules (HOM) from Gas-Phase Autoxidation Involving Peroxy Radicals: A Key Contributor to Atmospheric Aerosol. *Chemical Reviews*, **119**(6), 3472-3509.
- Boy, M., Sogachev, A., Lauros, J., Zhou, L., Guenther, A., & Smolander, S. (2011). SOSAA – a new model to simulate the concentrations of organic vapours and sulphuric acid inside the ABL – Part 1: Model description and initial evaluation. *Atmos. Chem. Phys.*, **11**(1), 43-51.
- Ehn, M., et al. (2014). A large source of low-volatility secondary organic aerosol. [Letter]. *Nature*, **506**(7489), 476-479.
- Hytinen, N., et al. (2018). Computational Comparison of Different Reagent Ions in the Chemical Ionization of Oxidized Multifunctional Compounds. *J. Phys. Chem. A*, **122**, 269–279.
- Molteni, U., Bianchi, F., Klein, F., El Haddad, I., Frege, C., Rossi, M. J., Dommen, J., and Baltensperger, U. (2018). Formation of highly oxygenated organic molecules from aromatic compounds, *Atmos. Chem. Phys.*, **18**, 1909–1921.
- Roldin, P., et al. (2014). Modelling non-equilibrium secondary organic aerosol formation and evaporation with the aerosol dynamics, gas- and particle-phase chemistry kinetic multilayer model ADCHAM. *Atmos. Chem. Phys.*, **14**, 7953-7993.

- Roldin, P., et al. (2019). The role of highly oxygenated organic molecules in the Boreal aerosol-cloud-climate system. *Nature Comm.*, **10**, Article number: 4370.
- Vereecken, L., et al. (2018). Perspective on Mechanism Development and Structure-Activity Relationships for Gas-Phase Atmospheric Chemistry. *Int. J. Chem. Kinet.*, **50**, 435-469.
- WHO. (2016). Ambient air pollution: A global assessment of exposure and burden of disease. Geneva, Switzerland: World Health Organization.
- Xavier, C., Rusanen, A., Zhou, P., Dean, C., Pichelstorfer, L., Roldin, P., and Boy, M. (2019). Aerosol Mass yields of selected Biogenic Volatile Organic Compounds – a theoretical study with near explicit gas-phase chemistry, *Atmos. Chem. Phys. Discuss.*, <https://doi.org/10.5194/acp-2019-424>, in review.
- Yu, J., and Jeffries, H. (1997). Atmospheric photooxidation of alkylbenzenes – II. Evidence of formation of epoxide intermediates. *Atmos. Env.*, **15**, 2281-2287.

HYDROXYL RADICAL (OH) REACTIVITY OF BIRCH AND SPRUCE EMISSIONS FOR *IN SITU* CONDITIONS

A.P. PRAPLAN¹, S. SCHALLHART¹, T. TYKKÄ¹, A. HELIN¹ and H. HELLÉN¹

¹ Finnish Meteorological Institute, P.O. Box 503, 000101 Helsinki, Finland.

Keywords: hydroxyl radical (OH) reactivity, Biogenic Volatile Organic Compounds (BVOCs), biogenic emissions, boreal forest.

INTRODUCTION

The total loss rate the hydroxyl radical (OH) in the atmosphere, also known as *total OH reactivity*, is an important indicator of the oxidation capacity of the atmosphere at a given place and time. High OH reactivity values signify a short OH lifetime due to a large amount of one or several chemical compounds reacting with OH.

Early measurements of total OH reactivity were used to investigate missing OH sinks in photochemical models (Kovacs and Brune, 2001). Since, total OH reactivity measurements have been conducted in various environments (see the review by Yang et al., 2016). By comparing the experimentally measured total OH reactivity with the calculated OH reactivity derived from the known chemical composition, it becomes possible to estimate how well the atmospheric chemistry is understood at the sampling location. Any difference between the total measured OH reactivity and the calculated one corresponds to *missing* reactivity. Di Carlo et al. (2004) first reported high missing reactivity values in a forested environment. The missing reactivity was temperature-dependent, which indicated possible unknown primary biogenic emissions. Sinha et al. (2010) and Nölscher et al. (2012) identified large fractions of missing reactivity in the boreal forest as well (up to 89%).

To our knowledge, only a couple of peer-reviewed studies attempting to assess directly the fraction of missing primary biogenic emissions using total OH reactivity measurements have been published. Kim et al. (2011) found no significant missing reactivity from the emissions of four deciduous tree species over a few summer days only, however. Contrastingly, Nölscher et al. (2013) found that the missing OH reactivity from Norway spruce emissions increased between spring and late summer/autumn from 15–27% to 70–84%.

In the present study, we further investigate the possible contribution of unidentified biogenic primary emissions to OH reactivity. The emissions from two tree species typical of the Finnish boreal forest, birch (*Betula pubescens*) and Norway spruce (*Picea abies*) were investigated *in situ* with gas chromatography coupled to mass spectrometry (GC/MS) to retrieve their chemical composition and with the Comparative Reactivity Method (CRM; Sinha et al., 2008) to measure the total OH reactivity of the emissions.

METHODS

The study took place from May to August 2019 at the SMEAR II station in Hyytiälä, Finland (Hari and Kulmala, 2005). Two branch enclosures were placed around branches of the two studied trees — a birch and a spruce — close to the measurement container containing the instrumentation. The enclosures consist of ca. 6-liter cylinders made of transparent Teflon attached to the branch on one side and to a Teflon frame equipped with inlet and outlet ports on the other side as described

by Hakola et al. (2006). The measurements alternated between the two enclosures. During each measurement periods, one enclosure was flushed by zero air provided by a commercial generator (HPZA-7000, Parker Balston, Lancaster, NY, U.S.A.) at about $4\text{--}6\text{ l min}^{-1}$. The branch enclosures were not entirely tight and operated at a slight overpressure to avoid contamination from ambient air. The relative humidity (RH) and the temperature in the enclosure were monitored and the Photosynthetically Active Radiation (PAR) was measured with a sensor placed on top of the enclosure frame. Total OH reactivity measurements were performed with the instrument described by Praplan et al. (2017) and an online GC/MS method (described in Hellén et al., 2018) was used to identify and quantify isoprene, 2-methyl-3-butenol (MBO), mono-, sesqui- and di-terpenes. Here we present results from two distinct periods: 4–26 June and 8 July – 12 August.

During the June period, the CRM instrument was sampling every 20 minutes for 10 minutes ca. 315 ml min^{-1} from the branch enclosure through a heated Teflon line (ca. 10 m length, i.d. 1/8"). A second heated Teflon line of roughly the same length was used to provide ca. 1.5 l min^{-1} to the CRM instrument to produce its own "internal" zero air by removing reactive compounds from the sampled air using a heated catalyst. The CRM instrument alternated every 10 minutes between direct measurement of air sampled from the enclosure and this same air stripped from reactive species ("internal" zero air) in order to measure the total OH reactivity from the difference in pyrrole signal. Pyrrole is the compound added to the sampled air to monitor the OH reactivity. From this second line, the GC/MS was also sampling about 40 ml min^{-1} every hour for 30 minutes (or 45 minutes after 8 August) and a nitrogen oxide (NO_x) analyzer (Model 42i-TL, Thermo Scientific, Waltham, MA, U.S.A.) was also sampling ca. 0.4 l min^{-1} to monitor NO_x production from the commercial zero air generator.

The correction for the presence of NO is described in Praplan et al. (2017). The change in pyrrole signal is expressed as a function of the concentration of NO in the reactor: $d \cdot [\text{NO}]^2 + e \cdot [\text{NO}]$. The updated values for d and e as average values of regression coefficients for various experimental conditions used in this study are -2.1×10^{-3} and 0.43 respectively.

During the second period, no "internal" zero air was used in the CRM instrument, but instead zero air produced from the commercial generator directly as to remove any need to correct for the NO_x interference. No change was made to the first sampling line from which the CRM sample was taken. During this period, however, the GC/MS subsample (at 40 ml min^{-1}) was taken from another Teflon line (ca. 13.5 m length, 3/8" i.d., unheated) with a main 5 l min^{-1} make-up flow. The NO_x analyzer was no longer used.

CONCLUSIONS

From a technical point-of-view, using the experimentally derived correction for the presence of NO in the sampled air is shown to be satisfactory (June period). Nevertheless, using the same zero air for CRM zero air measurements and flush the branch enclosure simplify the CRM instrumentation setup for total OH reactivity measurement from emissions.

An overview of preliminary results for the measured and calculated OH reactivity from the present study is shown in Fig. 1. Note that these values correspond to the measured and calculated OH reactivity from the branch enclosure and have not been normalized. In addition keep in mind that the GC/MS dataset has not been fully processed yet.

The reactivity from emissions of both birch and spruce had higher reactive emissions in June compared to July and August. The OH reactivity follows a clear diurnal pattern in June with a daily maximum in the afternoon. These maximum peak values are higher than the calculated reactivity when available. Night time values (close to zero) are in better agreement. Earlier studies at the site (Sinha et al., 2010; Nölscher et al., 2012; Praplan et al., 2019) found a large fraction of missing

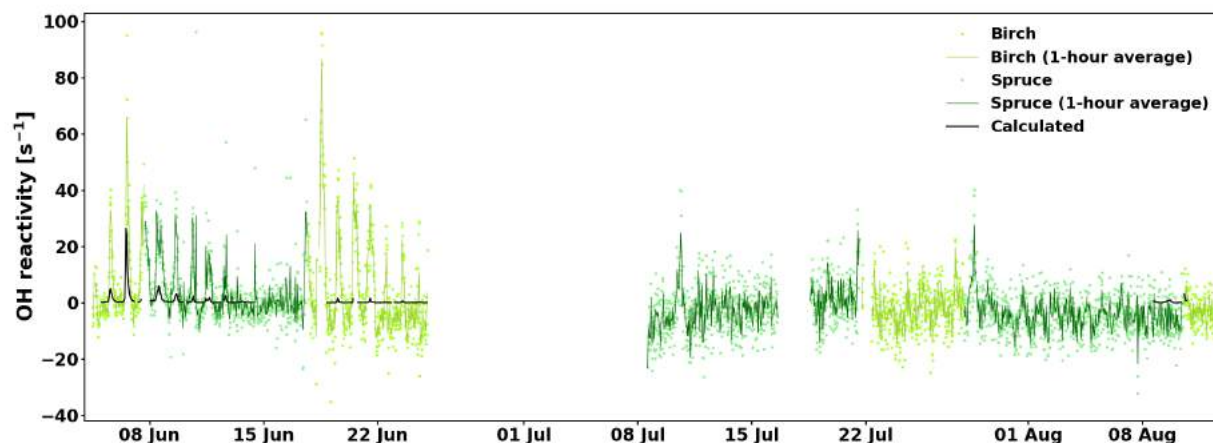


Figure 1: Preliminary results for the OH reactivity measured from birch and spruce in branch enclosures for *in situ* conditions at SMEAR II (Hyytiälä, Finland).

reactivity and the present study seem to indicate that it stems from unknown primary vegetation emissions, at least during the early summer period. Even including reactive sesquiterpenes and diterpenes that were not measured in earlier studies do not reduce the fraction of missing reactivity significantly. In August only a short period of a few days of GC/MS measurements is currently available for comparison, so that it is difficult to generalise but then there is a better agreement with low measured OH reactivity values.

The comparison between the calculated and measured OH reactivity, however, remains a complicated exercise, especially with the inclusion of sesqui- and diterpenes and oxidation products, whose reaction rate coefficients with OH are unknown. Estimation based on structure-activity-relationship were used (US EPA. 2019. Estimation Programs Interface SuiteTM for Microsoft® Windows, v 4.11. United States Environmental Protection Agency, Washington, DC, USA.), which might differ a lot from real experimental values. Therefore, in the future, experimentally derived reaction rate coefficients of sesquiterpenes and diterpenes and their reaction products would benefit this type of study. In addition the presented preliminary measured OH reactivity acquired with the CRM instrument has not been corrected for deviation from the pseudo-first-order kinetics inside the reactor. This correction will also affect the final measured OH reactivity values.

ACKNOWLEDGEMENTS

The presented research has been funded by the Academy of Finland (Academy Research Fellowships, projects nos. 275608 and 307797, and Centre of Excellence in Atmospheric Science, grant no. 272041). The authors thank Hannele Hakola for the continuous support. They also thank the staff at the SMEAR II station for their help and Timo Anttila from FMI's Observation Services for lending them the NO_x analyzer.

REFERENCES

- Di Carlo, P., W. H. Brune, M. Martinez, H. Harder, R. Leshner, X. Ren, T. Thornberry, M. A. Carroll, V. Young, P. B. Shepson, D. Riemer, E. Apel, and C. Campbell (2004). Missing OH Reactivity in a Forest: Evidence for Unknown Reactive Biogenic VOCs. *Science*, 304, 722–725. doi:10.1126/science.1094392.
- Hakola, H., V. Tarvainen, J. Bäck, H. Ranta, B. Bonn, J. Rinne, and M. Kulmala (2006). Seasonal

- variation of mono- and sesquiterpene emission rates of Scots pine. *Biogeosciences*, 3, 93–101. doi:10.5194/bg-3-93-2006.
- Hari, P. and M. Kulmala (2005). Station for Measuring Ecosystem-Atmosphere Relations (SMEAR II). *Boreal Environ. Res.*, 10, 315–322.
- Hellén, H., A. P. Praplan, T. Tykkä, I. Ylivinkka, V. Vakkari, J. Bäck, T. Petäjä, M. Kulmala, and H. Hakola (2018). Long-term measurements of volatile organic compounds highlight the importance of sesquiterpenes for the atmospheric chemistry of a boreal forest. *Atmos. Chem. Phys.*, 18, 13839–13863. doi:10.5194/acp-18-13839-2018.
- Kim, S., A. Guenther, T. Karl, and J. Greenberg (2011). Contributions of primary and secondary biogenic VOC to total OH reactivity during the CABINEX (Community Atmosphere-Biosphere INteractions Experiments)-09 field campaign. *Atmos. Chem. Phys.*, 11, 8613–8623. doi:10.5194/acp-11-8613-2011.
- Kovacs, T. A. and W. H. Brune (2001). Total OH Loss Rate Measurement. *J. Atmos. Chem.*, 39, 105–122. doi:10.1023/A:1010614113786.
- Nölscher, A. C., E. Bourtsoukidis, B. Bonn, J. Kesselmeier, J. Lelieveld, and J. Williams (2013). Seasonal measurements of total OH reactivity emission rates from Norway spruce in 2011. *Biogeosciences*, 10, 4241–4257. doi:10.5194/bg-10-4241-2013.
- Nölscher, A. C., J. Williams, V. Sinha, T. Custer, W. Song, A. M. Johnson, R. Axinte, H. Bozem, H. Fischer, N. Pouvesle, G. Phillips, J. N. Crowley, P. Rantala, J. Rinne, M. Kulmala, D. Gonzalez, J. Valverde-Canossa, A. Vogel, T. Hoffmann, H. G. Ouwersloot, J. Vilà-Guerau de Arellano, and J. Lelieveld (2012). Summertime total OH reactivity measurements from boreal forest during HUMPPA-COPEC 2010. *Atmos. Chem. Phys.*, 12, 8257–8270. doi:10.5194/acp-12-8257-2012.
- Praplan, A. P., E. Y. Pfannerstill, J. Williams, and H. Hellén (2017). OH reactivity of the urban air in Helsinki, Finland, during winter. *Atmos. Environ.*, 169, 150 – 161. doi:10.1016/j.atmosenv.2017.09.013.
- Praplan, A. P., T. Tykkä, D. Chen, M. Boy, D. Taipale, V. Vakkari, P. Zhou, T. Petäjä, and H. Hellén (2019). Long-term total OH reactivity measurements in a boreal forest. *Atmos. Chem. Phys. Discuss.*, pp. 1–31. doi:10.5194/acp-2019-122.
- Sinha, V., J. Williams, J. N. Crowley, and J. Lelieveld (2008). The Comparative Reactivity Method – a new tool to measure total OH Reactivity in ambient air. *Atmos. Chem. Phys.*, 8, 2213–2227. doi:10.5194/acp-8-2213-2008.
- Sinha, V., J. Williams, J. Lelieveld, T. Ruuskanen, M. Kajos, J. Patokoski, H. Hellen, H. Hakola, D. Mogensén, M. Boy, J. Rinne, and M. Kulmala (2010). OH Reactivity Measurements within a Boreal Forest: Evidence for Unknown Reactive Emissions. *Environ. Sci. Technol.*, 44, 6614–6620. doi:10.1021/es101780b.
- Yang, Y., M. Shao, X. Wang, A. C. Nölscher, S. Kessel, A. Guenther, and J. Williams (2016). Towards a quantitative understanding of total OH reactivity: A review. *Atmos. Environ.*, 134, 147–161. doi:10.1016/j.atmosenv.2016.03.010.

SECONDARY ORGANIC AEROSOL FORMATION FROM α -PINENE VERSUS REAL PLANT EMISSIONS

I. PULLINEN¹, A. YLISIRNIÖ¹, O. VÄISÄNEN¹, L. Q. HAO¹, A. BUCHHOLZ¹, S. SCHOBESBERGER¹, Z. LI¹, E.KARI¹, P. MIETTINEN¹, P. YLI-PIRILÄ^{1,2}, and A. VIRTANEN¹

¹Department of Applied Physics, University of Eastern Finland, P.O. Box 1627, 70211 Kuopio, Finland.

²Department of Environmental and Biological Sciences, University of Eastern Finland, P.O. Box 1627, 70211 Kuopio, Finland.

Keywords: SOA, α -PINENE, BVOC, HYGROSCOPICITY.

INTRODUCTION

Atmospheric aerosols (particles and the surrounding gas medium) in general have effect on human health and on climate (Nel, 2005; IPCC, 2013). They can scatter and absorb solar radiation, and act as cloud condensation nuclei (CCN), and regulate cloud properties (Rosenfeld *et al.*, 2008; Clement *et al.*, 2009). Aerosol particles are also counted as pollution deteriorating air quality (Nel, 2005). A large fraction (up to 90%) of atmospheric sub-micrometre particle mass consists of organic compounds (Jimenez *et al.*, 2009).

Due to the complexity of the biogenic volatile organic compound (BVOC) mixtures emitted by trees and other plants, α -pinene has often been used for simplicity as a reference compound for boreal forest emitted BVOCs. The aim of this study was to look at some of the physical and chemical properties of secondary organic aerosol (SOA) formed from α -pinene, and compare them to SOA formed from a BVOC mix taken from real plants, specifically Scots pines. Main focus was on the chemical composition of the particles, and their hygroscopicity.

METHODS

All the experiments were conducted at the labs of University of Eastern Finland. The experiment campaign consisted of two main parts: BVOC collection, and chamber studies. The first phase was conducted by selecting five healthy pines (*Pinus sylvestris*), and bringing them into the lab, where each pine was placed in a separate Teflon bag (dimensions 24" by 39"), which was then sealed around the trunk to stop BVOCs from leaking out. Airflow was introduced to each bag simultaneously, filling them with purified air. Two separate methods of collection were used: continuous and short-term. In short-term method, the bags were filled and then left sealed for 5-8 hours, and then all the air from the bags was filtered through the Tenax tubes. In the continuous method, air was circulating constantly into and out of the bags and through the Tenax tubes, up to several days in total. To analyse the actual sampled BVOC mix, three Tenax tubes were analysed with a gas chromatography mass spectrometer (GC-MS) immediately after collection.

The main part of the experiments was conducted in a 10 m³ Teflon chamber, which was operated as a batch reactor (Figure 1). The chamber was filled with humidified air (45% relative humidity at 22 °C). In the cases of photochemical experiments, H₂O₂ was added as OH precursor, and butanol-D9 was added as a tracer for OH. After target conditions were reached in the chamber, selected VOC (α -pinene or real plant BVOC mix) was added, and ozone injected to begin the reactions. In photochemical experiments UV-lights were turned on to signal the start of the experiments. Experiments lasted on average six hours.

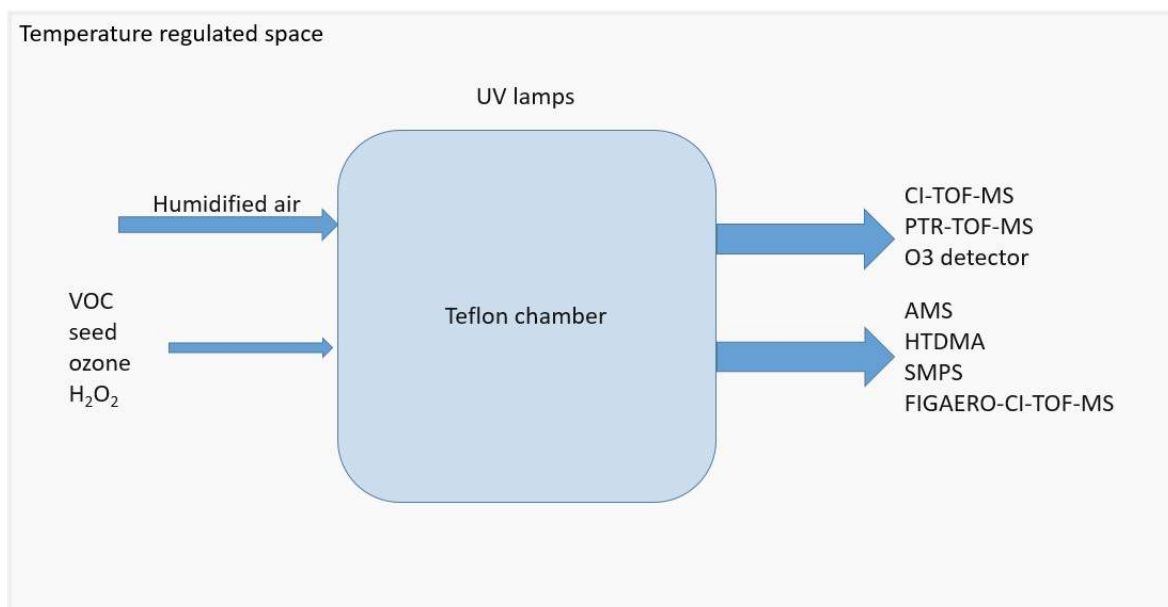


Figure 1. Schematic presentation of the experiment chamber set-up. The chamber was operated in a batch reactor mode. Two inlets were used, one for the main humidified flow, and another for VOCs, ozone, and seed. For sampling, there were two separate sample lines out of the chamber, one for particles and another for gas phase.

Five experiments were conducted in total, four with α -pinene as a precursor, and one real plant reference. With α -pinene both ozonolysis and low NO_x photochemical conditions were probed, while the real plant experiment was in ozone regime only.

The two main instruments used in this study were the Filter Inlet for Gas and Aerosols, (FIGAERO-CIMS, Aerodyne Research Inc., USA and Tofwerk AG, Thun, Switzerland, see Lopez-Hilfiker *et al.*, 2014) for analysing the chemical composition of the particles, and hygroscopic tandem differential mobility analyser (HTDMA, custom made, described in Väisänen *et al.*, 2016) to measure the hygroscopicity of the particles.

Supporting instruments included a high sensitivity proton-transfer-reaction time-of-flight mass spectrometer (PTR-MS, Ionicon) to measure VOC concentrations during chamber experiment, aerosol mass spectrometer (AMS, Aerodyne Research Inc., USA) to get information on particle composition and organic fraction, scanning mobility particle sizer (SMPS, TSI Incorporated, USA) for particle size distribution and number concentration, and ozone monitor (TE49i, Thermo Fischer Scientific).

RESULTS

During real plant BVOC collection, and during early stages of each experiment, Tenax samples were taken to further study the BVOC profile and concentrations reached. These samples were analysed by GC-MS. A set of Tenax samples were analysed immediately after collection, and an identical set was stored and analysed several weeks later. This was done to probe into possible degradation of the BVOCs during storage time. Table 1 shows BVOC profile for a fresh BVOC sample (left), and the equivalent stored sample BVOC profile (on the right). As can be seen, there have been some losses during the storage, but the overall BVOC profile remains quite similar.

BVOC	Fresh concentration/ng	Fresh %	Stored concentration/ng	Stored %
α -Pinene	437,6	51,2	362,2	46,1
Camphene	50,4	5,9	55,4	7,0
Sabinene	6,4	0,8	8,4	1,1
β -Pinene	81,7	9,6	71,6	9,1
β -Myrcene	119,7	14,0	115,9	14,7
3-Carene	113,7	13,3	108,3	13,8
Δ -Limonene	16,4	1,9	17,3	2,2
1,8-Cineole	8,4	1,0	8,7	1,1
γ -Terpinene	1,5	0,2	0,8	0,1
Terpinole	2,7	0,3	1,9	0,2

Table 1. Example on how longer storage times are not degrading the BVOCs in the samples.

Storage time of the real plant BVOC used for the experiments was shorter than the storage time for the comparison samples. For this reason we are confident that as only minimal degradation was observed between the fresh and stored BVOC sample, there was negligible degradation happening in the BVOC samples used in the experiments as well.

Tenax samples were collected from each experiment to study the actual precursor BVOC profile and concentrations of said experiments. Comparing the analysed samples reveals that the BVOC profiles were highly comparable with each other, meaning that it was possible to perform real plant SOA formation experiments with near identical precursor conditions (Table 2). The BVOC profile differs somewhat from those collected during the collection period (see Table 1), but there are several possible reasons for this. The samples used for BVOC profile analysis during collection were taken over very short period (15 minutes or less) and should be considered as point measurements, whereas the samples used to desorb BVOC into the chamber for the experiments were collected over several hours to over several days. It is possible that the BVOC profile emitted by the plants was changing during the total collection period. Another possibility is that the collection efficiency of the Tenax tube is different for different compounds when there is high deposition on the filter. It is also possible that the desorption efficiency is not the same for all compounds, although this seems unlikely, as the Tenax tubes were heated to a 200°C for 15 minutes during desorption into the chamber.

BVOC	Experiment 1	%	Experiment 2	%	Experiment 3	%
	concentration ng		concentration ng		concentration ng	
a-Pinene	23,59	30,7	30,3	29,0	30,0	29,3
Camphene	4,53	5,9	5,5	5,2	6,2	6,1
Sabinene	0,74	1,0	1,0	0,9	1,0	0,9
b-Pinene	2,11	2,7	3,3	3,2	2,8	2,7
b-Myrcene	22,79	29,7	34,5	33,1	31,1	30,4
3-Carene	16,97	22,1	20,4	19,5	22,4	21,9
d-Limonene	4,47	5,8	7,1	6,7	7,0	6,9
1,8-Cineole		0,0		0		0
g-Terpinene		0,0		0		0
Terpinolene	0,51	0,7	0,7	0,6	0,7	0,7

Table 2. Comparison between BVOC concentration and profiles at the beginning of experiments.

CONCLUSIONS

α -pinene was seen to be the major monoterpene compound emitted by the pines, and sampled into the Tenax tubes. Other major VOC observed were 3-carene, and in smaller concentrations limonene and

camphene. The real plant BVOC precursor starting conditions were consistent and comparable over several experiments.

ACKNOWLEDGEMENTS

This work was supported by the Academy of Finland Center of Excellence programme (grant no. 307331), and by the European Research Council (ERC starting grant 335478).

REFERENCES

Clement, A. C., Burgman, R., and Norris, J. R.: Observational and Model Evidence for Positive Low-Level Cloud Feedback, *Science*, 325, 460-464, Science, 2009.

Jimenez, J. L., Canagaratna, M. R., Donahue, N. M., Prevot, A. S., Zhang, Q., Kroll, J. H., DeCarlo, P. F., Allan, J. D., Coe, H., Ng, N. L., Aiken, A. C., Docherty, K. S., Ulbrich, I. M., Grieshop, A. P., Robinson, A. L., Duplissy, J., Smith, J. D., Wilson, K. R., Lanz, V. A., Hueglin, C., Sun, Y. L., Tian, J., Laaksonen, A., Raatikainen, T., Rautiainen, J., Vaattovaara, P., Ehn, M., Kulmala, M., Tomlinson, J. M., Collins, D. R., Cubison, M. J., Dunlea, E. J., Huffman, J. A., Onasch, T. B., Alfarra, M. R., Williams, P. I., Bower, K., Kondo, Y., Schneider, J., Drewnick, F., Borrmann, S., Weimer, S., Demerjian, K., Salcedo, D., Cottrell, L., Griffin, R., Takami, A., Miyoshi, T., Hatakeyama, S., Shimono, A., Sun, J. Y., Zhang, Y. M., Dzepina, K., Kimmel, J. R., Sueper, D., Jayne, J. T., Herndon, S. C., Trimborn, A. M., Williams, L. R., Wood, E. C., Middlebrook, A. M., Kolb, C. E., Baltensperger, U., and Worsnop, D. R.: Evolution of organic aerosols in the atmosphere, *Science*, 326, 1525-1529, 2009.

Lopez-Hilfiker, F. D., Mohr, C., Ehn, M., Rubach, F., Kleist, E., Wildt, J., Mentel, Th. F., Lutz, A., Hallquist, M., Worsnop, D., and Thornton, J. A.: A novel method for online analysis of gas and particle composition: description and evaluation of a Filter Inlet for Gases and AEROSols (FIGAERO), *Atmos. Meas. Tech.*, 7, 983-1001, <https://doi.org/10.5194/amt-7-983-2014>, 2014.

Nel, A.: Air pollution related illness effects of particles, *Science*, 308, 804-806, 2005.

Rosenfeld, D., Lohmann, U., Raga, G. B., O'Dowd, C. D., Kulmala, M., Fuzzi, S., Reissell, A., and Andreae, M. O.: Flood or Drought: How Do Aerosols Affect Precipitation?, *Science*, 321, 1309-1313, 2008.

Väisänen, O., Ruuskanen, A., Ylisirniö, A., Miettinen, P., Portin, H., Hao, L., Leskinen, A., Komppula, M., Romakkaniemi, S., Lehtinen, K. E. J., and Virtanen, A.: In-cloud measurements highlight the role of aerosol hygroscopicity in cloud droplet formation, *Atmos. Chem. Phys.*, 16, 10385-10398, <https://doi.org/10.5194/acp-16-10385-2016>, 2016.

BIOTIC AND ABIOTIC DRIVERS OF SOIL CH₄ PRODUCTION AND OXIDATION PROCESSES IN A NORTHERN BOREAL CATCHMENT

L. KOHL^{1,2}, M. NURMINEN^{1,2}, J.J. HAVISALMI¹, M. KOSKINEN^{1,2,4}, S. GERIN⁴, V. LINDHOLM⁴, K. PELTONIEMI⁵, A. LOHILA^{3,4}, PIHLATIE^{1,2,6} and A. PUTKINEN^{1,2,7}

¹Environmental Soil Sciences, Department of Agriculture, University of Helsinki,

²Institute of atmospheric and Earth system research (INAR) / Forest research, University of Helsinki

³Institute of atmospheric and Earth system research (INAR) / Physics, University of Helsinki

⁴Finnish Meteorological Institute, Helsinki

⁵Natural Resources Institute Finland (Luke), Helsinki

⁶Viikki plant science center (ViPS), University of Helsinki

⁷Department of Microbiology, University of Helsinki

Keywords: METHANE TURNOVER, BOREAL FOREST, MICROBIAL COMMUNITY

INTRODUCTION

While boreal forest soils generally act as consumers of the greenhouse gas methane (CH₄), this may change when the soil gets flooded. During years of high precipitation, catchment-scale upland soil CH₄ emissions can potentially be greater than emissions originating from a more constant source, pristine peatlands (Lohila *et al.*, 2016). This phenomenon may become more common in the northern latitudes, as extreme precipitation events are predicted to increase with the ongoing climate warming, (Lehtonen *et al.*, 2014).

To get a full understanding of the CH₄ dynamics of boreal forest soils, the related processes need to be examined in more detail. In the end, soil net CH₄ emissions are driven by the activity of two microbial groups; methanogenic archaea and methanotrophic bacteria. Methanogens thrive in submerged soils, such as peatlands. Yet, potential CH₄ production has been detected in a wide range of dry upland soils as well (Megonigal, and Guenther, 2008; Angel *et al.*, 2012), which could explain the strong increase in CH₄ emissions during wetter seasons. However, analysis of the actual methanogen populations present in upland soils, and especially in the boreal forests, is still scarce. Aerobic methanotrophs are present both in the upland soils and in the surface layers of submerged areas. Many of them have adapted to use either atmospheric CH₄ concentrations (high-affinity oxidation) or *in situ*-formed high concentrations (low-affinity oxidation), but an increasing number of species are known to utilize CH₄ in a wide range of concentrations (Ho *et al.*, 2019; Tweit *et al.*, 2019). Thus, the methanotrophic community structure could be used as an indicator on how the upland soil is able to adapt to and mitigate the potential increases of *in situ* CH₄ production.

In addition to soil moisture and the directly related variable, gas diffusion, CH₄ cycling organisms are controlled e.g. by soil pH, temperature and organic matter content/quality, but the effects often vary between methanogens and methanotrophs (Nazaries *et al.*, 2013). Also, interactions with other soil biota (Ho *et al.*, 2016; Juottonen *et al.*, 2017) and vegetation (Halmeenmäki *et al.*, 2017) need to be considered when evaluating soil CH₄ processes.

We studied the potential CH₄ turnover and the related microbial communities on a northern boreal catchment, where wet-season induced CH₄ emission increase from the upland soil has been demonstrated (Lohila *et al.*, 2016). Study sites were set along a gradient from an upland forest to drained peatland forests and finally to a pristine peatland, thus enabling the estimation of CH₄ dynamics in sites with varying degrees of upland/peatland properties. As well as the spatial approach (location within the gradient, soil depth), we looked at the temporal variation within the growing season.

METHODS

The studied Pallaslompolo catchment area is located in Pallas in Northern Finland. We sampled seven sites on a gradient starting from a forest hilltop (Kenttäröva, 67° 59.237'N, 24°14.579'E, 347 m asl) and lowering down to the pristine peatland (Lompolojätkä, 67°59.835'N, 24°12.546'E, 269 m asl) (Figure 1). Sampling included three to four soil layers, which were based on horizons (podzolic soils) or taken by 10 cm intervals (peatland sites). Samples were gathered three times during 2019: soon after the snow melt (early June), during the most active growing season (July) and in the end of the growing season (early September), leading to > 300 soil samples in total. Vegetation composition and water table levels were followed throughout the season, as were the soil CH₄ fluxes (measured in the UPFORMET project lead by A. Lohila).

Potential CH₄ production and oxidation were measured from fresh samples with a laboratory incubation setup in either anoxic (N₂ headspace) or aerobic conditions, respectively. Production measurements lasted for 30-43 days with weekly gas samplings. Potential CH₄ oxidation was measured in two different concentrations (10 ppm for the high-affinity and 10 000 ppm for the low-affinity oxidation); both incubations lasted for four days with 1-2 daily gas samplings. Gas samples were analysed with a flame ionization detector (FID)-equipped gas chromatograph and the production/oxidation rates were calculated based on the increase/decrease in the CH₄ concentration. General microbial communities and the methanogenic and methanotrophic community members will be analysed from the most active soil layers by high-throughput sequencing of the 16S rRNA gene and the functional genes *mcrA* and *pmoA*, respectively. Soil chemistry (pH, C/N etc.) is analysed from separate subsamples.

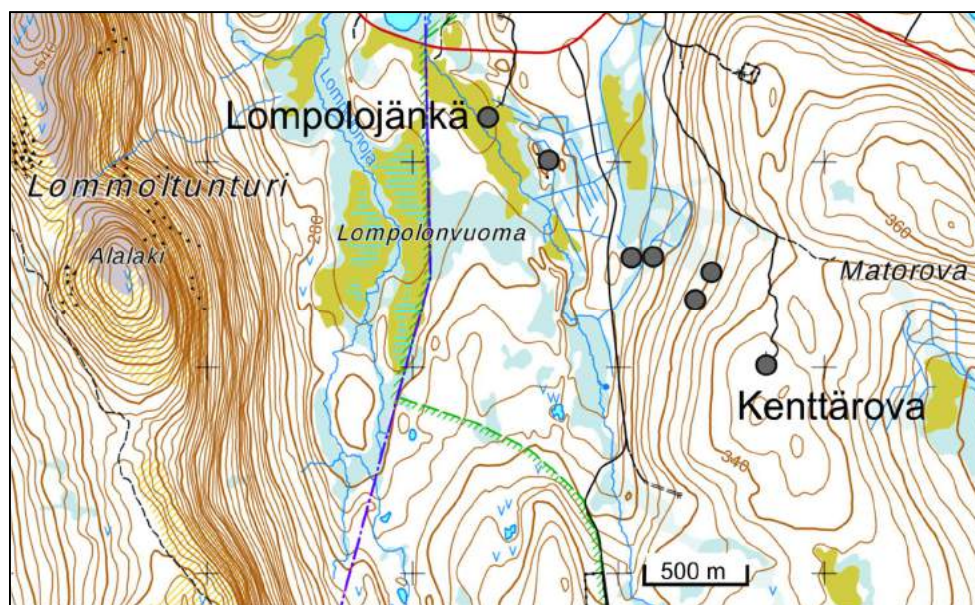


Figure 1. Map of the study sites (dark grey spheres) on the Pallaslompolo catchment.

PRELIMINARY RESULTS AND CONCLUSIONS

Based on the preliminary results from the data analysed thus far, in the upland forest sites, CH₄ production was generally highest in the organic layer. Likewise, within the drained peatland forest sites, highest production occurred in the surface layers with the highest content of fresh organic substrates. Excluding the pristine peatland, oxidation potentials did not change between the sites. Pristine peatland displayed

significantly higher production and low-affinity oxidation potentials than other sites. In general, low-affinity oxidation showed an increase from June to July, possibly reflecting an increase in the *in situ* CH₄ production.

This study enables a detailed view on the biological processes behind the soil CH₄ fluxes. Due to the inclusion of variable forest/peatland types, it will be useful in the modelling of catchment-scale CH₄ dynamics. In addition, our results will be utilized to estimate the role of soil CH₄ production in the CH₄ flux of spruce and birch trees growing on the same sites (also followed during the same season).

ACKNOWLEDGEMENTS

This work was supported by the European Research Council (ERC) under the European Union's Horizon 2020 research and innovation programme (grant agreement number 757695) and the Academy of Finland (grant numbers 319329 and 2884941). Markku Koskinen received a postdoctoral grant from the Maj and Tor Nessling foundation.

REFERENCES

- Angel, R., Claus, P. and Conrad, R. (2012). Methanogenic archaea are globally ubiquitous in aerated soils and become active under wet anoxic conditions. *The ISME journal*, 6(4), 847.
- Halmeenmäki, E., Heinonsalo, J., Putkinen, A., Santalahti, M., Fritze, H. and Pihlatie, M. (2017). Above- and belowground fluxes of methane from boreal dwarf shrubs and *Pinus sylvestris* seedlings. *Plant and Soil*, 420(1-2), 361-373.
- Ho, A., Angel, R., Veraart, A. J., Daebeler, A., Jia, Z., Kim, S. Y., ... and Bodelier, P. L. (2016). Biotic interactions in microbial communities as modulators of biogeochemical processes: methanotrophy as a model system. *Frontiers in microbiology*, 7, 1285.
- Ho, A., Lee, H. J., Reumer, M., Meima-Franke, M., Raaijmakers, C., Zweers, H., ... and Bodelier, P. L. (2019). Unexpected role of canonical aerobic methanotrophs in upland agricultural soils. *Soil Biology and Biochemistry*, 131, 1-8.
- Juottonen, H., Eiler, A., Biasi, C., Tuittila, E. S., Yrjälä, K. and Fritze, H. (2017). Distinct anaerobic bacterial consumers of cellobiose-derived carbon in boreal fens with different CO₂/CH₄ production ratios. *Appl. Environ. Microbiol.*, 83(4), e02533-16.
- Lehtonen, I., Ruosteenoja, K. and Jylhä, K. (2014). Projected changes in European extreme precipitation indices on the basis of global and regional climate model ensembles. *International Journal of Climatology*, 34(4), 1208-1222.
- Lohila, A., Aalto, T., Aurela, M., Hatakka, J., Tuovinen, J. P., Kilkki, J. ... and Viisanen, Y. (2016). Large contribution of boreal upland forest soils to a catchment-scale CH₄ balance in a wet year. *Geophysical Research Letters*, 43(6), 2946-2953.
- Megonigal, J. P. and Guenther, A. B. (2008). Methane emissions from upland forest soils and vegetation. *Tree physiology*, 28(4), 491-498.
- Nazaries, L., Murrell, J. C., Millard, P., Baggs, L. and Singh, B. K. (2013). Methane, microbes and models: fundamental understanding of the soil methane cycle for future predictions. *Environmental microbiology*, 15(9), 2395-2417.
- Tveit, A. T., Hestnes, A. G., Robinson, S. L., Schintlmeister, A., Dedysh, S. N., Jehmlich, N., ... and Svenning, M. M. (2019). Widespread soil bacterium that oxidizes atmospheric methane. *Proceedings of the National Academy of Sciences*, 116(17), 8515-8524.

FROZEN SOIL IN A MODEL OF PEATLAND GAS TRANSPORT

M. RAIVONEN¹, A. LEPPÄNEN¹, T. MARKKANEN², T. AALTO², T. KLEINEN³, X. LI¹, J. MÄKELÄ², M. AURELA², A. LOHILA^{1,2}, K. RAUTIAINEN² and T. VESALA^{1,4}

¹INAR/Physics, University of Helsinki, Finland.

²Finnish Meteorological Institute, Helsinki, Finland.

³MPI for Meteorology, Hamburg, Germany.

⁴INAR/Forest Sciences, University of Helsinki, Finland.

Keywords: peatland, methane, JSBACH, modelling.

INTRODUCTION

Natural wetlands are a significant source of atmospheric methane (CH₄) that is produced in the anoxic conditions prevailing in waterlogged wetland soils. After being produced, CH₄ can escape from the soil, either by diffusion in soil pores or gas-conducting tissue common in wetland plants, or by ebullition. CH₄ can also be oxidized to CO₂ by microbes. In boreal peatlands, CH₄ emissions are typically highest during the growing season e.g. because of input of fresh carbon from growing vegetation and warm temperatures favouring fast decomposition of soil organic matter and methanogenesis. However, nongrowing season emissions have been observed to comprise a significant fraction (up to tens of percent) of annual total on some peatlands (Treat *et al.*, 2018). Especially in the end of winter, during snowmelt and soil thaw, high and highly variable CH₄ fluxes have been observed (Comas *et al.*, 2008; Gazovic *et al.*, 2010). In order to reproduce these patterns in CH₄ emission estimates, realistic descriptions of wintertime processes are necessary in peatland models.

HIMMELI (Helsinki Model of MEthane buiLd-up and emIssion for peatlands) describes a layered peat column, simulates microbial and transport processes that control CH₄ (and CO₂ and O₂) fluxes between peat and the atmosphere, and outputs the fluxes (Raivonen *et al.*, 2017; Peltola *et al.*, 2018; Susiluoto *et al.*, 2018). It needs the source of CH₄, i.e., rate of anoxic soil respiration, as input from outside and is thus driven with e.g. outputs of a biosphere model. We are using HIMMELI with JSBACH, the land surface component of the MPI Earth System Model (Kleinen *et al.*, 2019).

The first version of HIMMELI (v1.0) did not simulate actual effects of ice or possible snow cover on the processes. CH₄ has been observed to get trapped and accumulate in peat when the upper peat layer freezes, and CH₄ emissions to increase after snowmelt (Melloh and Crill, 1996; Comas *et al.*, 2008; Mastepanov *et al.* 2013). Measurements by Tokida *et al.* (2007) indicated that the high release of CH₄ they observed during soil thaw consisted mainly of bubble-form CH₄ (ebullition). They also observed that when snow cover was present, CH₄ emissions were close to zero. The aim of this work is a simple but working implementation of the hindering effect of ice on gas transport in HIMMELI. For the development and testing we utilize observational data from Halssiaapa, a peatland measurement site in northern Finland (Dinsmore *et al.*, 2017).

METHODS

The JSBACH version we use includes peatlands, in particular, implementation of peatland hydrology and YASSO soil carbon model modified for anoxic conditions (Kleinen *et al.*, 2019). JSBACH is forced with meteorological data, and of its output variables we use soil temperature and soil ice content (of all soil layers), snow depth, water table level, leaf area index, and rate of anoxic soil respiration for driving HIMMELI.

In the original HIMMELI, rates of microbial processes already depend on temperature (Raivonen *et al.*, 2017) and so does the rate of anoxic respiration provided by JSBACH. Therefore, so far we have not added specifically ice-related constraints on them but the starting point of model development has been to improve the description of gas transport in winter or whenever the soil is frozen. Utilizing measurements of e.g. ground frost depth, soil temperatures, snow depth and CH₄ fluxes from Halssiaapa, we are searching for a parameterization that describes well in what conditions soil ice and snow hinder gas transport (foremost transport by ebullition and plant transport).

PRELIMINARY RESULTS

The work is still underway. Comparison of the first test model runs and observational data from Halssiaapa indicate that JSBACH can simulate timing of ground frost relatively well but it overestimates frost depth as well as dropping of topsoil temperatures in wintertime. The simulated start of soil thaw seems to coincide well with start of measured CH₄ emissions and our first tentative parameterization of how ice controls gas transport also seems promising, however, so far the simulated spring burst of CH₄ after thaw is too strong. The next step is to analyze what are the reasons for the high spring emissions and continue model development based on that. In addition, we will study also CO₂ fluxes and their relationship between vegetation phenology simulated by JSBACH and observed at the site (Linkosalmi *et al.*, 2016).

ACKNOWLEDGEMENTS

This work is supported by Academy of Finland Center of Excellence (272041), CARB-ARC (285630) and ICOS Finland (281255), the SRC of Academy of Finland project SOMPA (312932), and EU-H2020 projects CRESCENDO (641816) and VERIFY (776810).

REFERENCES

- Comas, X., Slater, L. and Reeve, A. (2008). Seasonal geophysical monitoring of biogenic gases in a northern peatland: Implications for temporal and spatial variability in free phase gas production rates, *Journal of Geophysical Research* **113**, doi: 10.1029/2007JG000575.
- Dinsmore, K.J., Drewer, J., Levy, P.E., George, C., Lohila, A., Aurela, M. and Skiba, U. (2017). Growing season CH₄ and N₂O fluxes from a subarctic landscape in northern Finland; from chamber to landscape scale, *Biogeosciences* **14**, 799-815, doi:10.5194/bg-14-799-2017.
- Gažovič, M., Kutzbach, L., Schreiber, P., Wille, C. and Wilmking, M. (2010). Diurnal dynamics of CH₄ from a boreal peatland during snowmelt, *Tellus* **62B**, 133-139.
- Kleinen, T., Mikolajewicz, U. and Brovkin, V. (2019). Terrestrial methane emissions from Last Glacial Maximum to preindustrial, *Climate of the Past Discussions*, doi: 10.5194/cp-2019-109.
- Linkosalmi, M., Aurela, M., Tuovinen, J-P., Peltoniemi, M., Tanis, C.M., Arslan, A.N., Kolari, P., Böttcher, K., Aalto, T., Rainne, J., Hatakka, J. and Laurila, T. (2016). Digital photography for assessing the link between vegetation phenology and CO₂ exchange in two contrasting northern ecosystems, *Geosci. Instrum. Method. Data Syst.* **5**, 417-426.
- Mastepanov, M., Sigsgaard, C., Tagesson, T., Ström, L., Tamstorf, M. P., Lund, M. and Christensen, T.R. (2013). Revisiting factors controlling methane emissions from high Arctic tundra, *Biogeosciences* **10**, 5139-5158.
- Melloh RA, Crill PM. (1996). Winter methane dynamics in a temperate peatland, *Global Biogeochemical Cycles* **10(2)**, 247-254.
- Peltola, O., Raivonen, M., Li, X., and Vesala, T (2018). Technical note: Comparison of methane ebullition modelling approaches used in terrestrial wetland models, *Biogeosciences* **15**, 937-951, doi: 10.5194/bg-15-937-2018.
- Raivonen, M., S. Smolander, L. Backman, J. Susiluoto, T. Aalto, T. Markkanen, J. Mäkelä, J. Rinne, O. Peltola, M. Aurela, A. Lohila, M. Tomasic, X. Li, T. Larmola, S. Juutinen, E-S. Tuittila, M. Heimann, S. Sevanto, T. Kleinen, V. Brovkin and T. Vesala (2017). HIMMELI v.1.0: Helsinki

Model of MEthane buiLd-up and emISSION for peatlands, *Geoscientific Model Development* **10**, 4665-4691.

Susiluoto, J., Raivonen, M., Backman, L., Laine, M., Mäkelä, J., Peltola, O., Vesala, T., and Aalto, T. (2018). Calibrating a wetland methane emission model with hierarchical modeling and adaptive MCMC, *Geoscientific Model Development* **11**, 1199-1228, doi:10.5194/gmd-11-1199-2018.

Tokida, T., Mizoguchi, M., Miyazaki, T., Kagemoto, A., Nagata, O. and Hatano, R. (2007). Episodic release of methane bubbles from peatland during spring thaw, *Chemosphere* **70(2)**, 165-171.

CORRELATING LEAF-LEVEL SPECTRAL CHLOROPHYLL FLUORESCENCE WITH PHOTOSYNTHESIS-CONTROLLING FACTORS DURING SPRING RECOVERY IN FINNISH BOREAL FOREST

P.A. RAJEWICZ¹, A. RIIKONEN¹, C. ZHANG¹, J. ATHERTON¹, B. FERNANDEZ-MARÍN²,
J.I.G. PLAZAOLA² and A. PORCAR-CASTELL¹

¹Institute for Atmospheric and Earth System Research (INAR)/Forest, Faculty of Agriculture and Forestry, University of Helsinki, Helsinki, Finland.

²Department of Plant Biology and Ecology, University of the Basque Country (UPV/EHU), Bilbao, Spain.

Keywords: BOREAL FOREST, CHLOROPHYLL FLUORESCENCE, LEAF-LEVEL, PHOTOSYNTHESIS, SPRING RECOVERY

INTRODUCTION

Remotely measured Sun-induced fluorescence (SIF) has been shown to reveal strong correlation with gross primary productivity (GPP, gross carbon flux from the atmosphere into the plants) (Sun et al., 2017). This relationship varies, however, among the biomes, canopy structures, temporal scales and presence of stress (Guanter et al., 2012), as well as with retrieval wavelength. The correlation strength can be influenced by environmental conditions and thus by the plants photosynthetic activity (photochemical quenching, PQ) and non-photochemical quenching (NPQ) (Damm et al., 2015; Van der Tol, Verhoef, & Rosema, 2009). Nevertheless, SIF has been successfully used in improving global carbon cycle assessments and in refining dynamic vegetation models (Yang et al., 2015). SIF - remotely measured from towers, aircrafts or satellites - is retrieved within discrete, narrow Fraunhofer or atmospheric absorption bands (Meroni et al., 2009). Fortunately, the continuous fluorescence (F) spectrum (i.e. 650 - 850 nm) can be measured *in vivo* at leaf-level. At leaf-level, steady-state F varies across species, canopy light gradients or in response to various stressors. The sum of leaves-level variations will then determine the top-of-canopy SIF retrieval. Consequently, an accurate definition of factors that might control the F variation at leaf-level, allow a precise interpretation of remotely-acquired SIF (Magney et al., 2019). That, in turn, will potentially improve the accuracy of global carbon cycle assessments and help in refining the dynamic vegetation models via data assimilation schemes.

During winter, photosynthesis is inhibited by freezing stress (Lundmark, Hedén, & Hällgren, 1988) of exposure to potentially high light levels and low temperature. Plants experiencing an imbalance between light absorption and its utilization via photochemistry, develop mechanisms for photo-protection (Merry, Jerrard, Frebault, & Verhoeven, 2017). Then during spring, plants enforce a recovery of photosynthesis. The process of recovery is dependent on increasing amount of light as well as on a (delayed) effect of air temperature rise (Pelkonen & Hari, 1980), with its rate varying among species (Matsubara, Gilmore, Ball, Anderson, & Osmond, 2002).

Boreal forests play a significant role in the global carbon fluxes (Turner et al., 2014) and are predicted to react sharply to global warming (Lenton et al., 2008). A proper understanding of the global carbon cycle - fluorescence relationship is particularly important in mid-to-high latitude ecosystems (Walther et al., 2016). This is, however, unachievable without defining ties between F and environmental factors. Therefore, simultaneous measurements of multiple variables and their spatiotemporal variation are needed to provide a complete picture of photosynthesis within a canopy. Despite many complications, the

seasonal photosynthesis recovery studies in the field – like the one presented here - constitute an essential component in the interpretation of remotely sensed terrestrial vegetation F from space.

METHODS

During “Fluorescence Across Space and Time” (FAST) campaign, carried out at SMEAR-II Hyytiälä Forest Station, Southern Finland, we examined the fluorescence (F) variation at leaf-level for five months of spring recovery period (year 2017). Both pulse-modulated (PAM2500®, Walz, Effeltrich, Germany) and spectral (Optical Chamber, (Rajewicz, Atherton, Alonso, & Porcar-Castell, 2019)) F were measured. For spectral F, we acquired analysis at both ambient and 77 Kelvin temperature. In addition, we measured leaf reflectance (Optical Chamber), absorption (Integrating Sphere), photosynthetic assimilation (GFS3000®) and pigments concentrations. In order to fully illustrate the boreal forest ecosystem, five boreal species were examined: two conifer trees, *Pinus silvestris* and *Picea abies*; one broadleaf tree, *Betula Pendula*; and two shrubs, *Vaccinium vitis-idaea* and *Vaccinium myrtillus*. Samples (of trees) were acquired from two different heights (top and low) to address the variability in F across light regimes present within a forest canopy profile. The light environment (PAR regime) of the sampled canopy positions was estimated using Digital Hemispherical photography (Hemisfer®, WLS, Birmensdorf, Switzerland).

The main aim of FAST campaign was to establish the set of controls that determines the F signal emitted by different species, at different canopy height and during the process of spring recovery of photosynthesis. We examined how the combination of environmental (light, temperature), structural (species-specific leaf morphology), biochemical (pigments composition) and physiological (non-photochemical quenching, photosynthetic activity) factors might reflect the spatiotemporal dynamics in the intensity and shape of F spectra. Here we present the preliminary results of correlating the F observations with accompanying leaf-level measurements.

RESULTS & CONCLUSIONS

The set of fluorescence controls depends on species and, notably, also on the position within the canopy profile. At the same time, different sets of variables showed high correlations with ambient and 77K spectral F (represented by red peak, far-red peak, and ratio between the peaks). The detailed reason why different variables correlate with ambient and 77K spectral F (data not shown) needs further analysis, but surely has to do with the blockage of photosynthesis in frozen leaves.

We performed principal component analysis (PCA), both for separate species (data not shown) and for the whole dataset (results included in *Figure 1*). As predicted, different results were obtained for analyzed species, but in all cases the results were in good correspondence with previous studies (e.g. Magney et al., 2019). First principal component (PC1) explained 99.87% of variance of F spectra across the spring recovery of lingonberry, 99.89% of low canopy pine, 99.85% of top canopy pine, and 99.92% of both position spruce (data not shown). When considering the complete FAST dataset (*Figure 1*), the PC1 (explaining 99.9% of variance on F spectra) revealed strong correlations with: zeaxanthins, both PAM2500® and GFS3000® sustained NPQ and F_vF_m , as well as $V_{c_{max}}$ and A_{1200} and temperature.

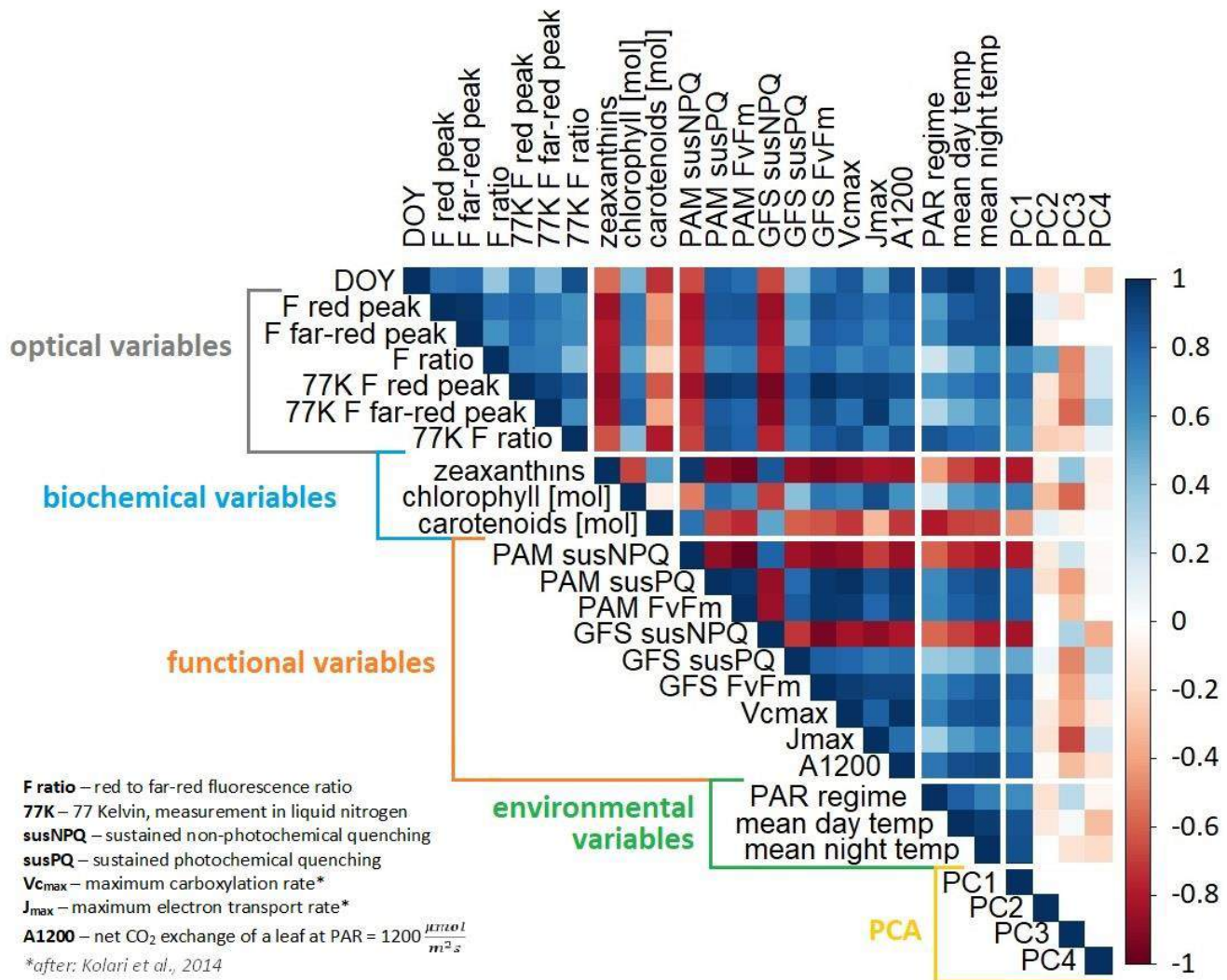


Figure 1. Pearson correlation (r) matrix between key variables measured in FAST campaign for all species, including results of principal component analysis (PC1-4, marked in yellow). The r value is indicated as colour, with positive correlations in blue and negative correlations in red.

We show that the combination of biochemical (pigments composition), physiological/functional (NPQ, photosynthetic activity, gas assimilation) and environmental factors might reflect the spatiotemporal dynamics in the intensity and shape of F spectra. Although further analysis is still needed, we suggest that the set of ecosystem characteristics, which influence the ultimate optical behavior of leaves, is a species-specific feature. Importantly, the light environment (or position within the canopy profile) also plays a crucial role in defining the fluorescence signal of leaves.

ACKNOWLEDGEMENTS

This project was supported by Academy of Finland FLUOSYNTHESIS project #319211 and #288039, as well as Finnish Centre of Excellence project #307331. P.A. Rajewicz acknowledges the Doctoral Programme in Atmospheric Sciences (ATM-DP, University of Helsinki) for financial support. We would like to thank Markus J. Haapala, from the Division of Pharmaceutical Chemistry and Technology, Faculty of Pharmacy, University of Helsinki, Finland for assistance with development of the Optical Chamber method.

REFERENCES

1. Damm, A., Guanter, L., Paul-Limoges, E., Van der Tol, C., Hueni, A., Buchmann, N., . . . Schaepman, M. E. (2015). Far-red sun-induced chlorophyll fluorescence shows ecosystem-specific relationships to gross primary production: An assessment based on observational and modeling approaches. *Remote Sensing of Environment*, *166*, 91-105.
2. Greer, D. H., Berry, J. A., & Björkman, O. (1986). Photoinhibition of photosynthesis in intact bean leaves: Role of light and temperature, and requirement for chloroplast-protein synthesis during recovery. *Planta*, *168*(2), 253-260.
3. Guanter, L., Frankenberg, C., Dudhia, A., Lewis, P. E., Gómez-Dans, J., Kuze, A., . . . Grainger, R. G. (2012). Retrieval and global assessment of terrestrial chlorophyll fluorescence from GOSAT space measurements. *Remote Sensing of Environment*, *121*, 236-251.
4. Lenton, T. M., Held, H., Kriegler, E., Hall, J. W., Lucht, W., Rahmstorf, S., & Schellnhuber, H. J. (2008). Tipping elements in the earth's climate system. *Proceedings of the National Academy of Sciences*, *105*(6), 1786-1793.
5. Lundmark, T., Hedén, J., & Hällgren, J. (1988). Recovery from winter depression of photosynthesis in pine and spruce. *Trees*, *2*(2), 110-114. doi:10.1007/BF00196757
6. Magney, T. S., Frankenberg, C., Köhler, P., North, G., Davis, T. S., Dold, C., . . . Porcar-Castell, A. (2019). Disentangling changes in the spectral shape of chlorophyll fluorescence: Implications for remote sensing of photosynthesis. *Journal of Geophysical Research: Biogeosciences*, *0* doi:10.1029/2019JG005029
7. Matsubara, S., Gilmore, A. M., Ball, M. C., Anderson, J. M., & Osmond, C. B. (2002). Sustained downregulation of photosystem II in mistletoes during winter depression of photosynthesis. *Functional Plant Biology*, *29*(10), 1157-1169.
8. Meroni, M., Rossini, M., Guanter, L., Alonso, L., Rascher, U., Colombo, R., & Moreno, J. (2009). Remote sensing of solar-induced chlorophyll fluorescence: Review of methods and applications. *Remote Sensing of Environment*, *113*(10), 2037-2051.
9. Merry, R., Jerrard, J., Frebault, J., & Verhoeven, A. (2017). A comparison of pine and spruce in recovery from winter stress; changes in recovery kinetics, and the abundance and phosphorylation status of photosynthetic proteins during winter. *Tree Physiology*, *37*(9), 1239-1250.
10. Pelkonen, P., & Hari, P. (1980). The dependence of the springtime recovery of CO₂ uptake in scots pine on temperature and internal factors. *Flora*, *169*(5), 398-404.
11. Rajewicz, P. A., Atherton, J., Alonso, L., & Porcar-Castell, A. (2019). Leaf-level spectral fluorescence measurements: Comparing methodologies for broadleaves and needles. *Remote Sensing*, *11*(5), 532.
12. Sun, Y., Frankenberg, C., Wood, J. D., Schimel, D. S., Jung, M., Guanter, L., . . . Griffis, T. J. (2017). OCO-2 advances photosynthesis observation from space via solar-induced chlorophyll fluorescence. *Science*, *358*(6360), eaam5747.
13. Thurner, M., Beer, C., Santoro, M., Carvalhais, N., Wutzler, T., Schepaschenko, D., . . . Levick, S. R. (2014). Carbon stock and density of northern boreal and temperate forests. *Global Ecology and Biogeography*, *23*(3), 297-310.
14. Van der Tol, C., Verhoef, W., & Rosema, A. (2009). A model for chlorophyll fluorescence and photosynthesis at leaf scale. *Agricultural and Forest Meteorology*, *149*(1), 96-105.
15. Walther, S., Voigt, M., Thum, T., Gonsamo, A., Zhang, Y., Köhler, P., . . . Guanter, L. (2016). Satellite chlorophyll fluorescence measurements reveal large-scale decoupling of photosynthesis and greenness dynamics in boreal evergreen forests. *Global Change Biology*, *22*(9), 2979-2996.
16. Yang, X., Tang, J., Mustard, J. F., Lee, J., Rossini, M., Joiner, J., . . . Richardson, A. D. (2015). Solar-induced chlorophyll fluorescence that correlates with canopy photosynthesis on diurnal and seasonal scales in a temperate deciduous forest. *Geophysical Research Letters*, *42*(8), 2977-2987.
17. Kolari, P., Chan, T., Porcar-Castell, A., Bäck, J., Nikinmaa, E., & Juurola, E. (2014). Field and controlled environment measurements show strong seasonal acclimation in photosynthesis and respiration potential in boreal Scots pine. *Frontiers in Plant Science*, *5*(717)

The extratropical transition of Hurricane Ophelia (2017) as diagnosed with a generalized omega equation and vorticity equation

M. RANTANEN¹, J. RÄISÄNEN¹, V. A. SINCLAIR¹, J. LENTO¹ and H. JÄRVINEN¹

¹ Institute for Atmospheric and Earth System Research / Physics, University of Helsinki, Finland

²CSC - IT Centre of Science, Espoo, Finland

Keywords: OpenIFS model, diabatic heating, extratropical cyclone

INTRODUCTION

Hurricane Ophelia was a category 3 hurricane which underwent extratropical transition and made landfall in Europe as an exceptionally strong post-tropical cyclone in October 2017. Tropical cyclones, such as Hurricane Ophelia, are generally driven by the latent heat release in the deep, moist convection, while extratropical cyclones, in turn, develop primarily from the meridional temperature and moisture gradients at mid-latitudes. Because post-tropical storms hitting Europe are projected to become more frequent (e.g. Haarsma et al., 2013), understanding the relative importance of different forcing mechanisms on transitioning tropical cyclones is of great importance. In this study, the contributions of different forcing terms affecting Ophelia's transformation from a hurricane to a mid-latitude cyclone are analysed, with focus primarily on the transition and extratropical phases of the storm.

METHODS

To diagnose the effects of different atmospheric physical processes on the evolution of Ophelia, we have developed software that uses OpenIFS model output and a system consisting of a generalized omega equation and vorticity equation. By using these two equations, the atmospheric vertical motion and vorticity tendency are separated into the contributions from different physical processes: vorticity advection, thermal advection, friction, diabatic heating, and the imbalance between the temperature and vorticity tendencies. For more information about the decomposition of atmospheric vertical motion, see Rantanen et al. (2017).

Furthermore, the effect of diabatic heating on the cyclone evolution was studied in more detail. This was done by decomposing the total diabatic heating into separate subcomponents which originate from different model parametrization schemes, such as convection scheme, microphysics scheme and radiation scheme. The effect of these model schemes on atmospheric vertical motion and vorticity tendency was studied separately.

RESULTS

Vorticity advection, which is often considered an important forcing for the development of mid-latitude cyclones, was found to play a small role in the re-intensification of Ophelia as an extratropical storm. This was because the low-level convergent circulation transported air with low cyclonic vorticity towards the center of the storm, reducing thus the vorticity maximum associated with Ophelia. Instead, our results show that diabatic heating was the dominant forcing in both the tropical and extratropical phases of Ophelia. Warm air advection from subtropics was found to enhance the cyclone intensity particularly during the transition period, but cold air advection during the extratropical phase had an opposite effect.

We found that the temperature tendency due to the convection scheme was the dominant forcing for the vorticity tendency in the cyclone centre during the tropical phase, but as Ophelia transformed into a mid-latitude cyclone, the microphysics temperature tendency, presumably dominated by large-scale condensation, gradually increased becoming the dominant forcing once the transition was complete. Temperature tendencies caused by other diabatic processes, such as radiation, surface processes, vertical diffusion, and gravity wave drag, were found to be negligible in the development of the storm.

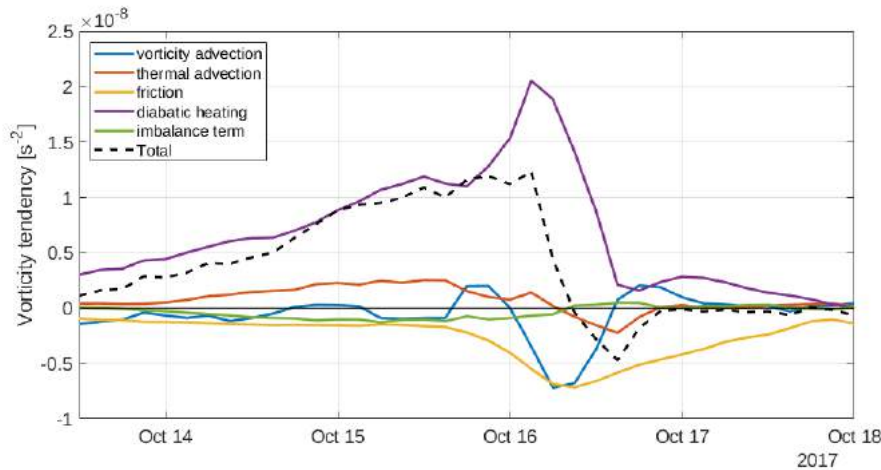


Figure 1: Time series of vorticity tendencies caused by different forcing terms. The values have been averaged over the 900–800-hPa layer and over a circular area with a 1.5° radius centred on the centre of the low-level cyclone. All values are 12-hour moving averages. Figure adapted from Rantanen et al. (2019).

CONCLUSIONS

Our analysis shows that cloud diabatic processes were crucial for the post-tropical intensification of Ophelia when it struck Ireland in October 2017. The leading forcing of diabatic heating aligns well with the earlier research (e.g. Azad and Sorteberg, 2009) regarding on the influence of diabatic processes in the evolution of ex-hurricanes. It is known that the effect of diabatic heating can be sensitive to the model resolution (e.g. Willison et al., 2013), and therefore, our result demonstrates the importance of high-resolution climate model simulations when attempting to estimate the future projections of post-tropical storms.

We also showed that our diagnostic method can be used to assess the effect of various atmospheric forcing terms for the evolution of post-tropical storms. However, several caveats were identified when applying the tool for the tropical phase of Ophelia (see Rantanen et al., 2019). For this reason, we suggest to use the tool only for extratropics and synoptic-scale weather systems in the future studies.

ACKNOWLEDGEMENTS

MR acknowledges the Doctoral Programme in Atmospheric Sciences (ATM-DP, University of Helsinki) for financial support. VAS is funded by the Academy of Finland Center of Excellence programme (project no. 307331). The authors also wish to acknowledge CSC - IT Center for Science, Finland, for computational resources. ECMWF is acknowledged for making the OpenIFS model available.

REFERENCES

- Azad, R. and Sorteberg, A. (2009). A diagnosis of warm-core and cold-core extratropical cyclone development using the Zwack-Okossi equation. *Atmos. Sci. Lett.*, **10**, 220–225.
- Haarsma, R. J., Hazeleger, W., Severijns, C., De Vries, H., Sterl, A., Bintanja, R., Van Oldenborgh, G. J., and van den Brink, H. W. (2013). More hurricanes to hit western Europe due to global warming. *Geophys. Res. Lett.*, **40**, 1783–1788.
- Rantanen, M., Räisänen, J., Lento, J., Stepanyuk, O., Rätty, O., Sinclair, V. A., and Järvinen H. (2017). OZO v.1.0: software for solving a generalized omega equation and the Zwack-Okossi height tendency equation using WRF model output. *Geosci. Model Dev.*, **10**, 827–841.
- Rantanen, M., Räisänen, J., Sinclair, V. A., Lento, J., and Järvinen H. (2019). The extratropical transition of Hurricane Ophelia (2017) as diagnosed with a generalized omega equation and vorticity equation. *Tellus A*, under review.
- Willison, J., Robinson, W. A., and Lackmann, G. M., (2013) The importance of resolving mesoscale latent heating in the North Atlantic storm track. *J. Atmos. Sci.*, **70**, 2234–2250.

TOWARDS UNDERSTANDING HETEROGENEOUS ICE NUCLEATION ON REALISTIC SILVER IODIDE SURFACES FROM ATOMISTIC SIMULATION

B. REISCHL, S. TURTOLA, G. ROUDSARI, O.H. PAKARINEN and H. VEHKAMÄKI

Institute for Atmospheric and Earth System Research / Physics,
Faculty of Science, University of Helsinki, P.O. Box 64, FI-00014, Finland.

Keywords: Heterogeneous ice nucleation, Molecular Dynamics simulation.

INTRODUCTION

While pure water will only freeze homogeneously at temperatures below $-38\text{ }^{\circ}\text{C}$, the presence of seed particles can drastically reduce the supercooling needed to trigger the phase transition. This heterogeneous ice nucleation is ubiquitous in nature and plays an important role in cloud formation, where mineral dust and organic material can serve as ice nucleation particles. Small particles of silver iodide (AgI) are known to have excellent ice nucleating capabilities and have been used in rain seeding applications (Vonnegut, 1947, Marcolli *et al.*, 2016). It is widely believed that the silver terminated (0001) surface of β -AgI acts as a template for the basal plane of hexagonal ice. However, the (0001) surface of ionic crystals with the wurtzite structure is polar and intrinsically unstable. If such a surface is exposed by the crystal, it will therefore exhibit reconstructions and defects. In the present study, we use atomistic molecular dynamics simulations to study how the presence of reconstructions on AgI (0001) surfaces, that cancel the surface dipole, affects the rates and mechanism of heterogeneous ice nucleation at moderate supercooling.

METHODS

Ice nucleation on silver iodide has been studied extensively using atomistic molecular dynamics simulations, due to its importance in rain seeding applications, but also because it is a rare example of a system where induction times, i.e. the average time it takes for a critical nucleus of ice to appear, are short enough that the ice nucleation can be studied directly, even at very moderate undercooling. This excellent ice nucleation ability was only observed on the silver-terminated (0001) surface of silver iodide in the wurtzite structure (Zielke *et al.*, 2014). In fact, this surface has the same hexagonal geometry as the basal plane of ice Ih, with a lattice mismatch of less than 3%, as shown in Figure 1. Not surprisingly, it is commonly believed that patches of Ag-terminated (0001) surfaces on silver iodide particles must be responsible for their ice nucleation activity. However, this is somewhat problematic because the (0001) surface has an intrinsic dipole moment, which makes it unstable and likely to exhibit defects and/or reconstructions, which would certainly reduce its ice nucleating ability. This has been investigated in recent computational studies of AgI (0001) surfaces exhibiting defects such as vacancies, step edges, terraces or pits (Roudsari *et al.*, 2019, Prerna *et al.*, 2019). These simulations found that while point defects had no influence on the nucleation and growth rates, step edges, terraces and pits could reduce the nucleation rate by up to an order of magnitude. The proposed mechanism is that the defect reduces the perfect surface area available for the formation of a critical nucleus, and that the reduction in nucleation rate is proportional to the reduction in perfect surface area available for nucleation. In these studies, the effect of the surface dipole has either been ignored (Prerna *et al.*, 2019), or the dipole field has been canceled by placing a mirror image of the surface slab in the simulation box (Roudsari *et al.*, 2019). In another recent computational study by Sayer and Cox (2019), it was argued that ions present in the liquid could locally compensate the surface charge by forming an electrostatic double layer and alleviate the dipole issue as well. In any case, it is clear that the polar nature of the (0001) surface needs to be addressed properly, and ice nucleation needs to be studied on more realistic surface models.

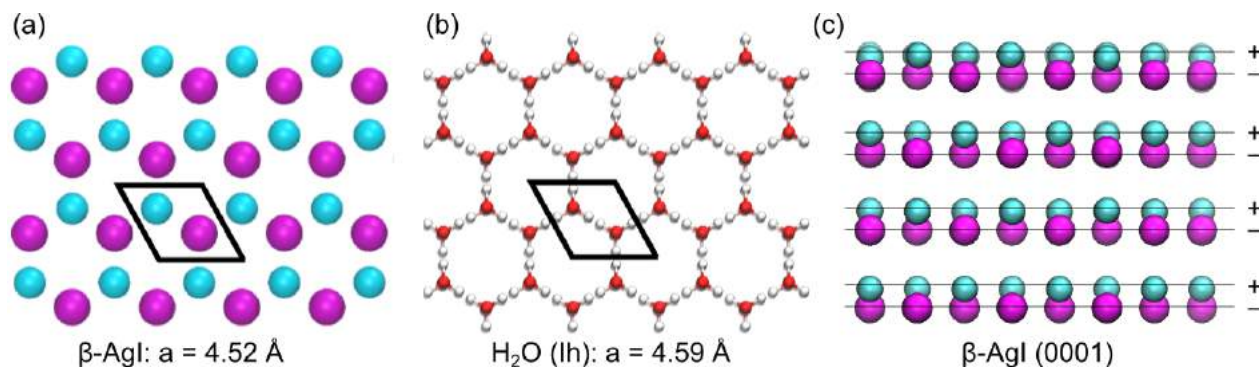


Figure 1. Top view of the (0001) surface of β -AgI (a) and the basal plane of ice Ih (b). Silver, iodine, oxygen and hydrogen atoms are colored in cyan, magenta, red and white, respectively. The hexagonal surface unit cells are indicated by a black line, and the lattice constant a is specified. The β -AgI crystal exposing a (0001) surface seen along the [210] direction (c). Layers of positively charged silver (Ag^+) and negatively charged iodide ions (I^-) alternate along the [001] direction, creating a dipole across the crystal.

The issue of the intrinsic surface dipole is encountered in all surfaces of type 3 according to Tasker's classification (Tasker, 1979), such as ionic crystals with the wurtzite structure, due to the presence of layers of alternating electric charge in the crystal, along the direction perpendicular to the surface (see Figure 1). Not surprisingly, several studies have investigated crystal geometries that will reduce or cancel the dipole and stabilize the crystal structure (Li *et al.*, 2015). In a particularly relevant study by Mora-Fonz *et al.* (2017), surface reconstructions of the (0001) surface of ZnO, which has the same wurtzite structure as AgI, have been shown to greatly reduce the surface dipole. Following a similar approach, we have constructed nine surfaces of AgI exhibiting different reconstruction involving 5×5 surface unit cells, depicted in Figure 2. In these systems, 6 Ag^+ ions have been moved from the surface layer to the bottom of the crystal slab, which effectively cancels the dipole moment across the crystal with a thickness of 8 bilayers. In addition, up to 13 AgI ion pairs have also been moved to the bottom of the crystal slab, to produce nine different surface geometries. In a first step, an energy minimization is performed on a 2×2 supercell of the (5×5) reconstructed surfaces using the LAMMPS code (Plimpton, 1995). Here, the interactions between Ag^+ and I^- ions are described by the potential of Rains *et al.* (1991). Then, water is added to the surface to create a film of approximately 30 Å thickness. The water volume is separated by ~ 60 Å of vacuum from the periodic image of the crystal slab along z , to minimize the effect of spurious interactions. Water molecules are described by the TIP4P/ice potential (Abascal *et al.*, 2005), which reproduces the experimental melting point and the coexistence line between water and ice Ih. Water molecules interact with the AgI crystal using the potential of Hale and Kiefer (1980). To avoid dissolution of the mineral, the positions of Ag^+ and I^- ions are fixed to the relaxed positions in the dry surface. Molecular dynamics simulations are carried out with a velocity Verlet integrator using a time step of 1 fs, and a Nosé-Hoover thermostat of chain length 5 is used to keep a constant temperature of 253 K, corresponding to 20° C undercooling. Lennard-Jones and real-space electrostatic interactions are cut off at 8.5 Å and the PPPM scheme is used to calculate long-range electrostatics.

CONCLUSIONS

We have been able to build models of (5×5) reconstructed AgI (0001) surfaces that greatly reduce the dipole moment. These surfaces are far more realistic than the perfect surfaces, or surfaces with defects, which have been considered in previous atomistic simulations of heterogeneous ice nucleation on silver iodide. The remaining dipole moment is small enough not to cause any spurious alignment of water molecules far away from the interface, which means that the simulation setup does not require any artificial constructs to compensate the surface dipole moment, such as a mirror image geometry or the

placement of additional point charges in the simulation box. Preliminary molecular dynamics simulations at a temperature of 253 K (-20 °C) indicate that the ice nucleation rate on these surfaces is significantly lower compared to simulations using any kind of variation of the perfect (0001) surface, where induction times are easily accessible to unbiased molecular dynamics. Accurate determination of the nucleation rates on the more realistic reconstructed surfaces presented here however will require a more sophisticated approach, such as seeded molecular dynamics (Pedevilla et al., 2018), or advanced sampling techniques such as forward flux sampling (Sosso et al., 2016), which have been successfully used on other atmospherically relevant surfaces.

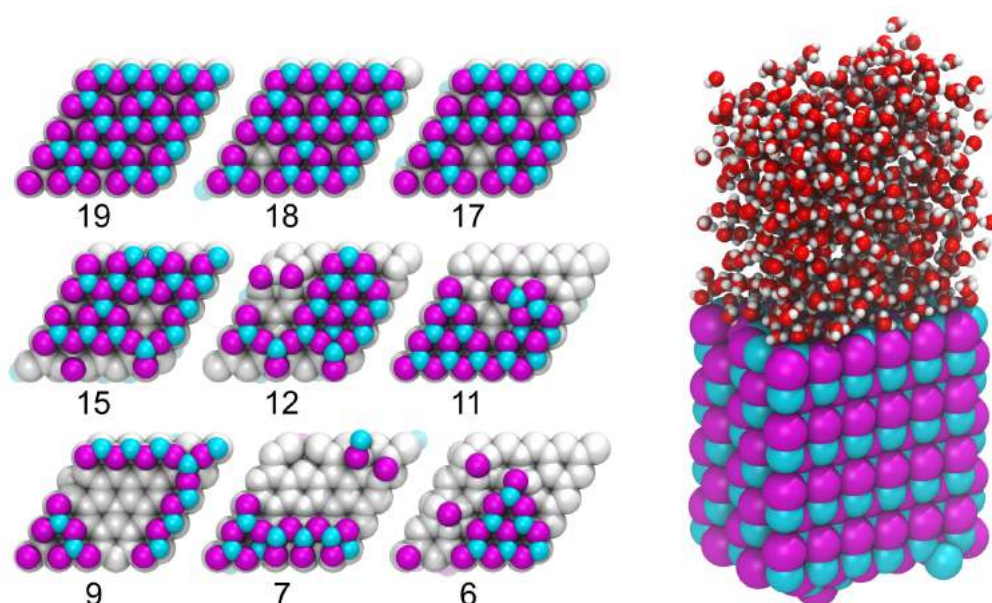


Figure 2. Left: top views of nine (5x5) reconstructed AgI (0001) surfaces. Ag^+ and I^- ions in the top bilayer are colored in cyan and magenta, respectively, the remaining ions in the crystal are shown in light gray. The number of Ag^+ ions remaining in the surface layer is indicated below each image. Right: Snapshot of an ice nucleation simulation, showing the reconstructed AgI surface in contact with a film of liquid water.

ACKNOWLEDGEMENTS

This work was supported by the National Center of Meteorology (NCM), Abu Dhabi, UAE, under the UAE Research Program for Rain Enhancement Science, the Academy of Finland Center of Excellence programme (grant no. 307331) and ARKTIKO project 285067 ICINA, the University of Helsinki, Faculty of Science ATMATH project, and ERC Grant 692891- DAMOCLES. Supercomputing resources were provided by CSC–IT Center for Science, Ltd, Finland. Any opinions, findings and conclusions or recommendations expressed in this material are those of the authors and do not necessarily reflect the views of the National Center of Meteorology, Abu Dhabi, UAE, funder of the research.

REFERENCES

- Abascal, J.L.F., and C. Vega (2005). A General Purpose Model for the Condensed Phases of Water: TIP4P/2005. *J. Chem. Phys.* **123**, 234505.
- Hale, B.N. and J. Kiefer (1980). Studies of H_2O on beta-AgI Surfaces - An Effective Pair Potential Model. *J. Chem. Phys.* **73**, 923–933.
- Li, H., L. Geelhaar, H. Riechert and C. Draxl (2015). Computing Equilibrium Shapes of Wurtzite Crystals: The Example of GaN. *Phys. Rev. Lett.* **115**, 449.

- Marcolli, C., B. Nagare, A. Welti and U. Lohmann (2016). Ice Nucleation Efficiency of AgI: Review and New Insights. *Atmos. Chem. Phys.* **16**, 8915–8937.
- Mora-Fonz, D., T. Lazauskas, M.R. Farrow, C.R.A Catlow, S.M. Woodley and A.A. Sokol (2017). Why Are Polar Surfaces of ZnO Stable? *Chem. Mater.* **29** 5306–5320.
- Pedevilla, P., M. Fitzner, G.C. Sosso and A. Michaelides (2018). Heterogeneous Seeded Molecular Dynamics as a Tool to Probe the Ice Nucleating Ability of Crystalline Surfaces. *J. Chem. Phys.* **149**, 072327.
- Plimpton, S. (1995). Fast Parallel Algorithms for Short-Range Molecular Dynamics. *J. Comput. Phys.* **117**, 1–19.
- Prerna, Rohit Goswami, Atanu K. Metya, S. V. Shevkunov and J.K. Singh (2019). Study of ice nucleation on silver iodide surface with defects. *Mol. Phys.*, DOI: 10.1080/00268976.2019.1657599
- Rains, C.A., R.J. Ray and P. Vashishta (1991) Phase transformations and polytypism in silver iodide: A molecular-dynamics study. *Physical Review B*, **44**(17), 9228–9239.
- Roudsari, G., B. Reischl, O.H. Pakarinen and H. Vehkamäki, Atomistic Simulation of Ice Nucleation on Silver Iodide (0001) Surfaces with Defects, under review in *J. Phys. Chem. C* (2019).
- Sayer, T. and S.J. Cox (2019). Stabilization of AgI's Polar Surfaces by the Aqueous Environment, and its Implications for Ice Formation. *Phys. Chem. Chem. Phys.* **21**, 14546–14555.
- Sosso, G. C., T. Li, D. Donadio, G.A. Tribello, A. Michaelides (2016). Microscopic Mechanism and Kinetics of Ice Formation at Complex Interfaces: Zooming in on Kaolinite. *J. Phys. Chem. Lett.* **7**, 2350–2355.
- Tasker, P.W. (1979). The Stability of Ionic Crystal Surfaces. *J. Phys. C: Solid State Phys.* **12**, 4977–4984.
- Vonnegut, B. (1947). The Nucleation of Ice Formation by Silver Iodide. *J. Appl. Phys.* **18**, 593–595.
- Zielke, S. A., A.K. Bertram and G.N. Patey (2014). A Molecular Mechanism of Ice Nucleation on Model AgI Surfaces. *J. Phys. Chem. B* **119**(29), 9049–9055.

TREE WATER RELATIONS AND CAMBIAL GROWTH AFFECT SCOTS PINE (*PINUS SYLVESTRIS*) STEM VOC EMISSIONS

K. RISSANEN¹, A. VANHATALO¹, Y. SALMON², T. HÖLTTÄ¹ & J. BÄCK¹

¹ Institute for atmospheric and Earth system research / Forest sciences, Faculty of agriculture and forestry, University of Helsinki

¹ Institute for atmospheric and Earth system research / Physics, Faculty of Science, University of Helsinki

Keywords: stem BVOC emissions, monoterpenes, methanol, acetaldehyde, Scots pine

INTRODUCTION

Trees are a major source of volatile organic compounds (VOCs), but the research on tree VOC emissions is strongly concentrated on emissions from foliage whereas tree stems as VOC sources are not well understood. In boreal Scots pine forest, under unstressed conditions, monoterpene emissions from tree stems contribute approximately 2% to the total ecosystem monoterpene emissions (Vanhatalo et al. 2019). While this is a small contribution, left unaccounted it can bias emission sums calculated over long periods and limit our understanding on, for example, tree signalling. Considering the role of stem VOC emissions in the ecosystem functioning and the total emissions requires better understanding on the drivers and dynamics of stem VOC emissions. Here, we studied the environmental variables and physiological processes that could affect the emissions and emission potentials of monoterpenes, methanol and acetaldehyde from Scots pine stem (*Pinus sylvestris*) in a boreal forest.

METHODS

The stem VOC emissions were using steady-state and dynamics stem chambers. The concentrations of methanol, acetaldehyde and monoterpenes in the chamber air were quantified with proton-transfer-reaction mass-spectrometer (IONICON, Innsbruck, Austria), and CO₂ and H₂O concentrations with Li-840 A analyser (Li-Cor, Lincoln, NE, USA). We used data from 2015 and 2017, from June to August. Each year, a different tree stem was measured at the height of 12 or 15 meters.

As the VOC emissions from stem are temperature-dependent (Rissanen et al. 2016, Vanhatalo et al. 2019, Staudt et al. 2019), we used Guenther (1993) temperature normalisation with a semi-flexible temperature impact to acquire emission potentials at 30°C. We calculated the daily mean values of the emission potentials and explanatory variables: ambient relative humidity, soil water content, xylem diameter as a proxy for water potential in tree, stem CO₂ efflux and cambial growth rate, and conducted a lag-analysis (cross-correlation) to capture instant and lagged correlations between the emission potentials and explanatory variables. We also detrended the data by subtracting a 15-day moving mean from the daily mean values, and calculated the cross-correlations also with the detrended variables.

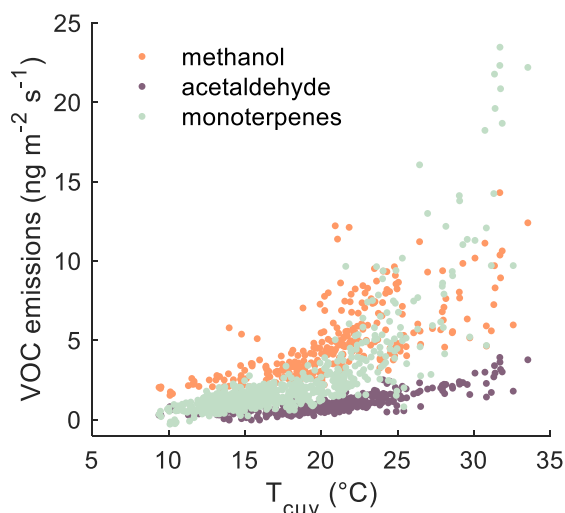


Figure 1: Temperature-dependence of methanol, acetaldehyde and monoterpene emissions from Scots pine stem in July 2015, Hyytiälä, Finland

RESULTS

We found that the daily mean emission potentials of monoterpenes, methanol and acetaldehyde were correlated with soil water content and the rate of cambial growth of stem. Detrended monoterpene emissions correlated with the soil water content without a detectable time lag (Figure 2 a). In the correlations between detrended methanol emission potential and soil water content, there was a lag of two to five days (Figure 2 b), and in the correlation between acetaldehyde emission potential and soil water content, a lag of two to four days (Figure 2 c). These time lags corresponded to the three to five days transport time of water from the tree base to the top stem where the stem chambers were installed. The transport times for the different trees were calculated from the mean transpiration rates and the tree dimensions (not shown). The correspondence between the lag time and the transport time indicates that the emission of acetaldehyde and methanol from the pine stem are affected by their transport in xylem sap.

Longer lags in the range of seven to ten days were found between the cambial growth rates and emission potentials of monoterpenes, and detrended emission potentials of methanol and acetaldehyde (Figure 2 d-f). These lags correspond approximately to the offset between the start of cell elongation phase of cambial growth and the start of cell wall formation phase of cambial growth detected in Norway spruce (*Picea abies*), in corresponding conditions (Jyske et al. 2012). Thus, the cell wall formation or other growth-related metabolism also increased production or release of VOCs from the stem.

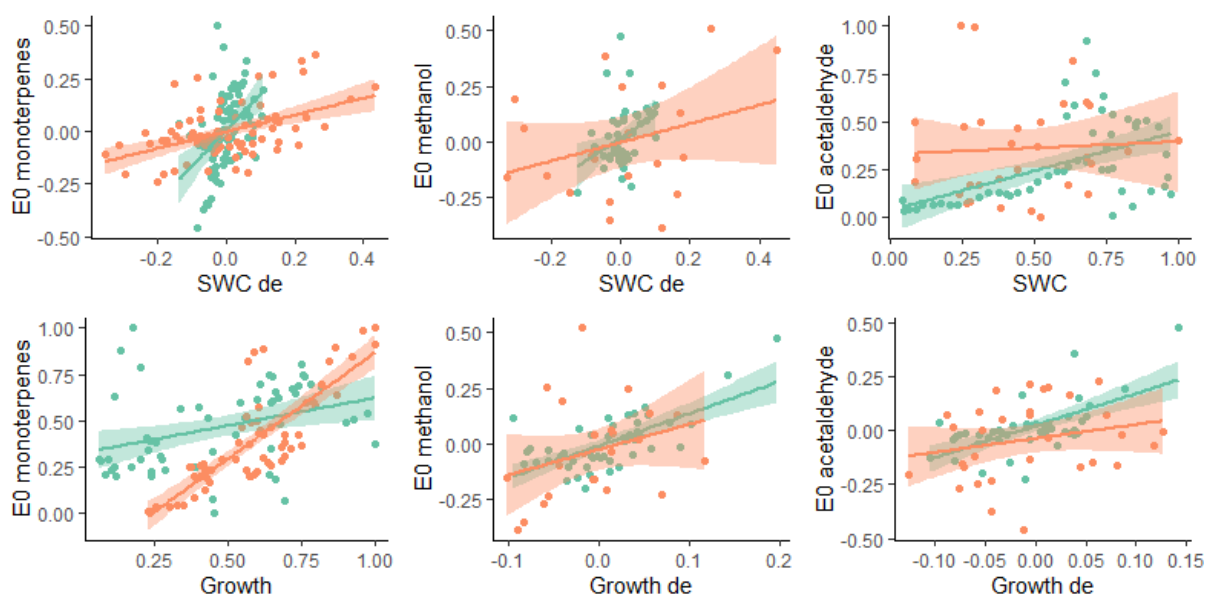


Figure 2: The correlations between daily mean soil water content (SWC) and temperature normalised daily mean a) monoterpene emission potential (E0), b) methanol emission potential with a lag of 3 and 5 days and c) acetaldehyde emission potential with a lag of 4 days; and daily mean cambial growth rate and temperature normalised daily mean d) monoterpene emission potential with a lag of 7–10 days, e) methanol emission potential with a lag of 7 days and f) acetaldehyde emission potential with a lag of 8–10 days. Monoterpene, methanol and acetaldehyde emissions measured from Scots pine stems in June–August 2015 (green) and 2017 (orange). “de” after x-axis label indicates that the data on emission potential and explanatory variable was detrended. For the presentation purposes, data from different years was normalised.

CONCLUSIONS

We found that despite the strong temperature control over the emissions of monoterpenes, methanol and acetaldehyde from Scots pine stem, relatively small changes in water availability and the metabolic activity of the stem could affect their emission potentials. Thus, large changes in water availability could be expected to cause considerable deviations in the stem VOC emission dynamics. In addition, if with dedicated laboratory studies we are able to separate the effects of growth and transport on the emissions of methanol and acetaldehyde, these could be used as non-invasive signals of the processes taking place within the stem.

REFERENCES

- Guenther, A.B., Zimmerman, P.R., Harley, P.C., Monson, R.K. and Fall, R. (1993). Isoprene and monoterpene emission rate variability: model evaluations and sensitivity analyses. *Journal of Geophysical Research* **98**: 12, 609.
- Jyske, T., Manner, M., Mäkinen, H., Nöjd, P., Peltola, H. and Repo, T. (2012). The effects of artificial soil frost on cambial activity and xylem formation in Norway spruce. *Trees* **26**, 405.
- Rissanen, K., Hölttä, T., Vanhatalo, A., Aalto, J., Nikinmaa, E., Rita, H. and Bäck, J. (2016). Diurnal patterns in Scots pine stem oleoresin pressure in a boreal forest. *Plant Cell and Environment* **39**.
- Staudt, M., Byron, J., Piquemal, K. and Williams, J. (2019). Compartment specific chiral pinene emissions identified in a Maritime pine forest. *Science of The Total Environment* **654**: 1158.
- Vanhatalo, A., Aalto, J., Chan, T., Hölttä, T., Kolari, P., Kabiri, K., Hellén, H. and Bäck, J. (2019). Scots pine stems as dynamic sources of isoprenoid and methanol emissions. Manuscript in review.

ATOMISTIC SIMULATIONS OF ICE NUCLEATION ON SILVER IODIDE (0001) SURFACES WITH DEFECTS

G. ROUDSARI, B. REISCHL, O.H. PAKARINEN and H. VEHKAMÄKI

Institute for Atmospheric and Earth System Research / Physics,
University of Helsinki, P.O. Box 64, FI-00014, Finland.

Keywords: heterogeneous ice nucleation, silver iodide, molecular dynamics.

INTRODUCTION

The presence of a seed particle can drastically reduce the supercooling needed for freezing water compared to homogeneous nucleation. This heterogeneous ice nucleation is ubiquitous in nature and plays an important role in cloud formation. (Murray et al, 2012).

Silver iodide (AgI) particles are very effective INPs, used for rain seeding, and they have been studied both experimentally and computationally, focusing on ice nucleation on flat AgI surfaces (Zielke et al., 2014), AgI disks and plates (Zielke et al., 2016), the effect of surface charge distribution (Glatz and Sapna 2016), as well as water adsorption in slit-like AgI pores. In ambient conditions, both AgI crystals with the wurtzite structure (β -AgI) and the zincblende structure (γ -AgI) are stable. Previous simulations have found that ice could nucleate at the silver terminated (001) and (111) surfaces of γ -AgI, and the silver-terminated (0001) surface of β -AgI (Zielke et al., 2014). The ice nucleating ability of AgI has been attributed to the (0001) surface of β -AgI acting as a very good template for the basal plane of hexagonal ice (ice I_h) or the equivalent (111) plane of cubic ice (ice I_c) (Zielke et al., 2016), with a lattice mismatch of approximately 2%.

In this work, we use molecular dynamics (MD) simulations to study the effect of defects, such as vacancies, step edges, terraces and pits, on ice nucleation on AgI (0001) surfaces.

METHODS

Several force fields have been fitted to reproduce bulk crystal structures and the phase diagram of silver iodide (AgI) (Rains et al., 1991, Niu et al., 2018). However, the perfect (0001)-terminated AgI slab has an intrinsic dipole moment and none of these force fields yields a stable surface. In previous ice nucleation simulations, atoms in the AgI surface have therefore either been fixed to bulk positions, or constrained by a spring potential. In the present work, all AgI surfaces considered are bulk-terminated and atoms are completely fixed at the positions of an ideal wurtzite crystal with lattice constants $a = 4.58 \text{ \AA}$ and $c = 7.50 \text{ \AA}$.

The silver and iodide ions only interact with the water molecules, described by the TIP4P/Ice model. It reproduces the properties of bulk liquid water very well, and yields the correct melting point and coexistence curve between water and ice I at low pressures (Abas and Vega, 2005). The interactions between Ag^+ and I^- ions and TIP4P/Ice water molecules are described by the potential of Hale and Kiefer (Hale and Kiefer, 1980). The ions carry a point charge and a Lennard-Jones interaction with the oxygen atom of water, OW. All molecular dynamics (MD) simulations were performed using the GROMACS software version 5 (Berendsen et al., 1995).

To quantify the effectiveness of the different systems for ice nucleation, we calculate nucleation rates at $T = 263 \text{ K}$ following the procedure presented by Cox et al. (Cox et al., 2015). By monitoring

the size of the largest ice cluster in the system using the CHILL+ algorithm (Nguyen et al., 2015), the induction time is found, which is defined as the time when the ice cluster starts growing monotonously. For each system, 10 individual NVT simulations are started with different initial configurations and velocities of the water molecules. The induction times observed are used to calculate the probability $P_{\text{liq}}(t)$ of an ensemble of systems to be still in the liquid state after time t . As the temperature is 10°C below the melting point, we expect the probability to decay exponentially. We fit the data using the equation

$$P_{\text{liq}}(t) = \exp[-(Rt)^\gamma], \quad (1)$$

where R shows the decay rate, equal to the nucleation rate, and the exponent γ is a second fitting parameter, as illustrated in Figure 1.

The nucleation rates obtained for the different surfaces are shown in Table 1. The standard errors were obtained from the least squares error of the fit using Eq. 1. The surface with a double vacancy and the perfect surface exhibit the highest nucleation rates with values of $3.89 \times 10^{23} \text{ m}^{-2}\text{s}^{-1}$ and $3.86 \times 10^{23} \text{ m}^{-2}\text{s}^{-1}$, respectively. Surfaces with a single Ag vacancy show almost the same nucleation rate ($3.75 \times 10^{23} \text{ m}^{-2}\text{s}^{-1}$). The nucleation rates on surfaces with point defects are very similar to the rate on the perfect surface. The two step edges considered affect the nucleation rate with different severity, leading to rates of $0.47 \times 10^{23} \text{ m}^{-2}\text{s}^{-1}$ and $1.06 \times 10^{23} \text{ m}^{-2}\text{s}^{-1}$ for the step edge along $[001]$ and $[210]$ directions, respectively. Finally, nucleation rates of $1.41 \times 10^{23} \text{ m}^{-2}\text{s}^{-1}$ and $1.09 \times 10^{23} \text{ m}^{-2}\text{s}^{-1}$ were observed for the surface with a terrace, or a pit, respectively.

These results are quite surprising, as for many surfaces ice nucleation rates are enhanced by the presence of defects. Here, however, the perfect surface is an excellent template for ice growth, due to the very small lattice mismatch between AgI (0001) and the basal plane, and all extended defects considered in this work reduce the nucleation rate.

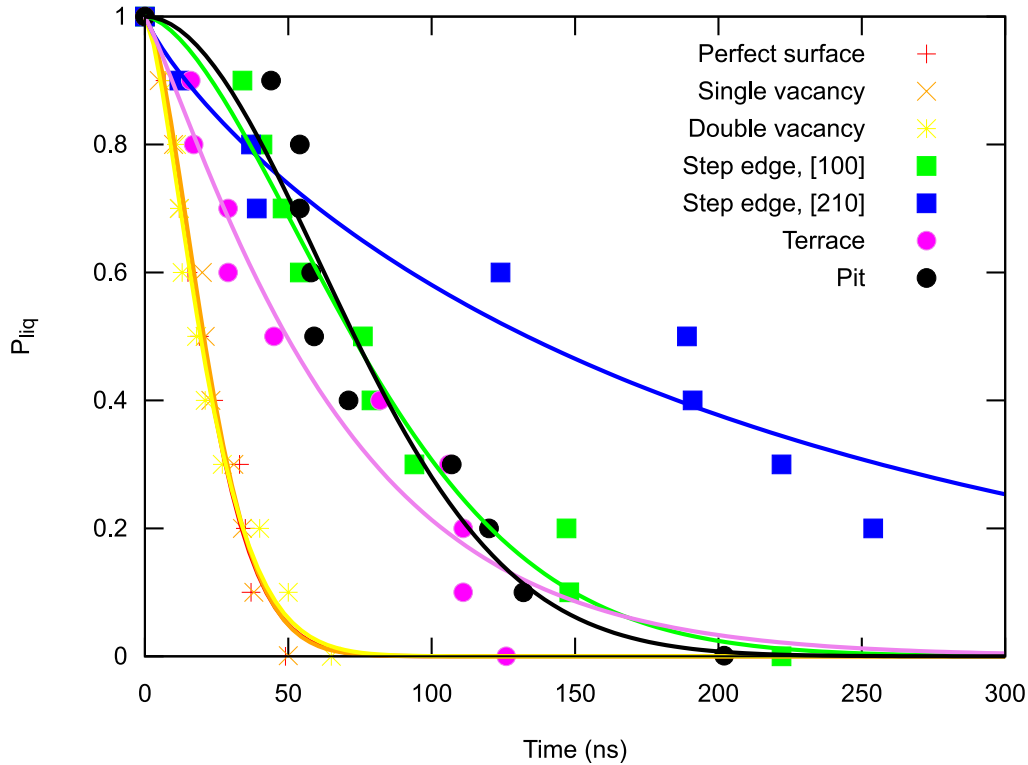


Figure 1: Obtaining ice nucleation rates on different AgI (0001) surfaces from fitting the induction times for ice nucleation in 10 independent molecular dynamics simulations at $T = 263 \text{ K}$.

System	Nucleation rate ($\times 10^{23} \text{ m}^{-2} \text{ s}^{-1}$)
Perfect surface	3.86 ± 0.13
Single vacancy	3.75 ± 0.12
Double vacancy	3.89 ± 0.23
Step edge [100]	1.06 ± 0.04
Step edge [210]	0.47 ± 0.05
Terrace	1.41 ± 0.12
Pit	1.09 ± 0.06

Table 1: Ice nucleation rates and uncertainties on different AgI (0001) surfaces with defects at $T=263 \text{ K}$

To better understand the ice nucleation mechanism at the silver iodide surface and, in particular, how the presence of defects affects the possibility to form a critical nucleus at the interface, we compare the hydration layer structure at the perfect surface and around the step edge along the [210] direction. As can be seen in Figure 2a, the pattern of the first hydration layer is perturbed by the presence of the step edge. In order to quantify the spatial extent of the hydration layer perturbation around the step edge and link it to the observed nucleation rate, we have calculated the average deviation of first hydration layer water molecule oxygen from its ideal position, as a function of the position along x , the direction perpendicular to the step edge (see Figure 2b). Combining the information about the spatial extent of hydration layer perturbation due to the presence of a defect with the average radius of the initial ice clusters at nucleation sites on the surfaces ($r_c \sim 10.3 \text{ \AA}$) allows us to build a very simple model to predict the reduction in nucleation rate compared to the perfect surface, based solely on the surface area excluded for the formation of a critical nucleus around a defect with a certain geometry. As can be seen in Figure 2c, these predicted nucleation rates agree surprisingly well with the nucleation rates obtained from molecular dynamics simulations.

CONCLUSIONS

In this work, we studied the effect of surface defects on the heterogeneous nucleation of ice at the (0001) surface of β -AgI using atomistic molecular dynamics simulations at $T = 263 \text{ K}$. The presence of defects reduces both the nucleation rate and the growth rate, with a clear correlation between the dimensionality of the defects and the severity of the reduction: while single and double vacancies have no significant effect, the presence of step edges, terraces and pits reduces nucleation and growth rates by up to an order of magnitude. However, it is important to note that even surfaces with these last three defect types still exhibit good ice nucleation abilities at very moderate undercooling.

The simulation results show that the β -AgI (0001) surface enhances the formation of a critical nucleus by enforcing its hexagonal structure to the first hydration layer. On the perfect surface, water molecule oxygen atoms in the first hydration layer are hexagonally arranged around the protruding silver ion in the surface. In the proximity of defects such as a step edge, there are significant deviations from these ideal positions, hindering the formation of critical ice nuclei. A very simple model, where the nucleation rate on the perfect surface is scaled by the fraction of surface area available for nucleation, excluding the area around the defects, gives good agreement with the nucleation rates obtained from molecular dynamics simulations of the different surfaces with defects.

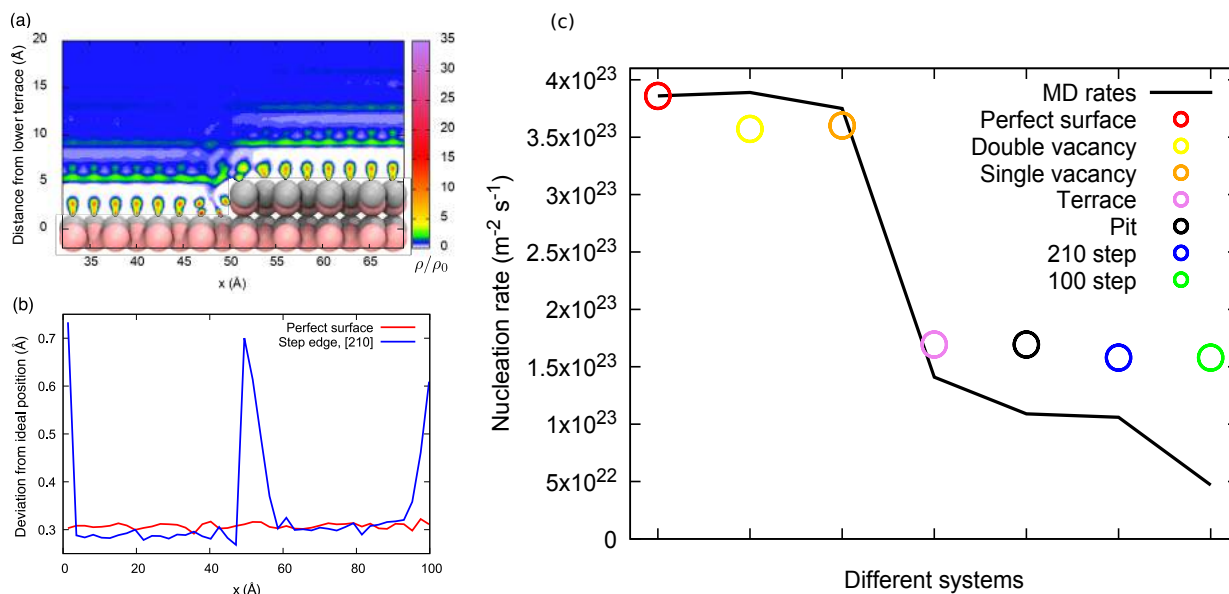


Figure 2: (a) Water oxygen atom density map projection in the xz plane over the AgI (0001) surface with a step edge along [210]. The number density is expressed in units of the equilibrium water density at $T = 263$ K, $\rho_0 \approx 0.032 \text{ \AA}^{-3}$, shown in blue. Surface Ag^+ and I^- ions are colored in silver and pink, respectively. (b) Disturbance of the water patterning in the first hydration layer with respect to the surface lattice, over the perfect surface (red line) and a surface with a step edge along [210] (blue line). (c) Ice nucleation rates obtained by scaling the nucleation rate on the perfect surface by the fraction of surface area exhibiting perfect water patterning (colored circles), compared to nucleation rates obtained from molecular dynamics simulations on the respective non-ideal surface (black line).

ACKNOWLEDGEMENTS

This work was supported by the National Center of Meteorology (NCM), Abu Dhabi, UAE, under the UAE Research Program for Rain Enhancement Science, the Academy of Finland Center of Excellence programme (grant no. 307331) and ARKTIKO project 285067 ICINA, the University of Helsinki, Faculty of Science ATMATH project, and ERC Grant 692891-DAMOCLES. Supercomputing resources were provided by CSC–IT Center for Science, Ltd, Finland. Any opinions, findings and conclusions or recommendations expressed in this material are those of the authors and do not necessarily reflect the views of the National Center of Meteorology, Abu Dhabi, UAE, funder of the research.

REFERENCES

- Abascal, J. L. F. and C. Vega (2005). A General Purpose Model for the Condensed Phases of Water: TIP4P/2005. *J. Chem. Phys.*, **23**, 123.
- Berendsen, H. J. C., D. van der Spoel and R. van Drunen (1995). GROMACS: A Message passing Parallel Molecular Dynamics Implementation. *Comput. Phys. Commun.*, **1**, 91.
- Cox, S. J. , S. M. Kathmann, B. Slater, and A. Michaelides (2015). Molecular Simulations of Heterogeneous Ice Nucleation. I. Controlling Ice Nucleation Through Surface Hydrophilicity. *J. Chem. Phys.*, **18**, 142.

- Glatz, B. and S. Sapna (2016). The Surface Charge Distribution Affects the Ice Nucleating Efficiency of Silver Iodide. *J. Chem. Phys.*, **21**, 145.
- Hale, B. N. and J. Kiefer (1980). Studies of H₂O on beta-AgI Surfaces - An Effective Pair Potential Model. *J. Chem. Phys.*, **2**, 73.
- Murray, B.J. (2017). Cracking the Problem of Ice Nucleation *Science*, **355**, 3456.
- Murray, B. J. , D. O'Sullivan, J. D. Atkinson and M. E. Webb (2012). Ice nucleation by particles immersed in supercooled cloud droplets. *Chem. Soc. Rev.*, **41**, 6519.
- Nguyen, H. Andrew and V. Molinero (2015). Identification of Clathrate Hydrates, Hexagonal Ice, Cubic Ice, and Liquid Water in Simulations: the CHILL+ Algorithm. *J. Phys. Chem. B*, **29**, 119.
- Niu, Hongwei and Jing, Yuhang and Sun, Yi and Aluru, Narayana R (2018). Ab Initio Based Interionic Potential for Silver Iodide. *Solid State Ion.*, **325**, 102.
- Rains, C A ,Ray J R and Vashishta, P (1991). Phase Transformations and Polytypism in Silver Iodide: A Molecular-Dynamics Study. *Phys. Rev. B*, **17**, 44.
- Zielke, S.A., A. Bertram, G. N. Patey (2014). A Molecular Mechanism of Ice Nucleation on Model AgI Surfaces. *J. Phys. Chem. B*, **29**, 119.
- Zielke, S. A., A. Bertram, G. N. Patey (2016). Simulations of Ice Nucleation by Model AgI Disks and Plates. *J. Phys. Chem. B*, **9**, 120.

AERIAL DRONE, A USEFUL AND RELIABLE CARRIER FOR THE DETERMINATION OF CHEMICAL COMPOSITION OF GAS PHASE AND AEROSOLS IN AIR

H. LAN, J. RUIZ-JIMENEZ, N. ZANCA, G. DEMARIA, Y. LELEEV, M. JUSSILA, K. HARTONEN and
M.-L. RIEKKOLA

Department of Chemistry and Institute for Atmospheric and Earth System Research, P.O. Box 55, FI-00014
University of Helsinki, Finland

Keywords: AERIAL DRONE; MINIATURIZED AIR SAMPLING; SAMPLING ACCESSORIES; QUALITY ASSURANCE AND CONTROL

INTRODUCTION

Aerial drones, also called unmanned aerial vehicles, remotely piloted aircraft systems or simply drones, have become very popular over the last decade. Among others, aerial drones can be used as carriers for air sampling systems, analyzers and sensors, replacing or complementing the traditional ways to sample at high altitudes such as airships, aircrafts, tethered balloons and meteorological towers (Ruiz-Jimenez, et al., 2019).

A wide variety of sensors and sampling systems have been attached to aerial drones to provide continuous monitoring of different parameters and concentration values related to individual compounds in the samples. Different miniaturized air sampling (MAS) techniques, including solid phase microextraction (SPME) Arrow and in-tube extraction (ITEX), have been developed to provide reliable sampling for environmental applications.

SPME Arrow, a passive sampling technique, consists of a steel rod coated with a larger volume of extraction sorbent than traditional SPME fibers, improving the detection limits of the method. SPME Arrow design protects the sorbent, minimizing unfavorable influences and analyte losses during desorption step. In addition, SPME Arrow allows the exclusive collection of gas phase compounds.

ITEX system, an active sampling technique designed as a two-part stainless steel needle attached to a pumping system, was developed to provide high sampling performance. However, unlike SPME Arrow, ITEX needs a pump for the collection of the analytes on the sorbent and an external heater to facilitate thermal desorption to the GC system. Using ITEX is possible to collect both gas phase compounds and aerosol particles. Accessories such as, filters and traps attached to ITEX system, allow also the collection of gas phase compounds and/or prevent the samples from undesirable chemical reactions. This kind of approach is not feasible for SPME Arrow using the configuration developed in this research. However, the use of a dynamic air sampling system by SPME Arrow would help to control its sampling variables (Barreira et. al. 2018).

Quality Control (QC)/Quality Assurance (QA) in the laboratory is the crucial step before field sampling by the MAS systems. The laboratory designed sampling conditions should be as close as possible to the real working atmosphere which can reduce the sampling and detection errors and also save the sampling time. For SPME Arrow sampler, selection of the most selective coating towards targeted analytes and optimal sampling time are essential. For ITEX sampler, the key point is to optimize the total sampling volume in advance to ensure its quantitative property (without breakthrough). Since multiple samplers were placed on the aerial drone for simultaneous

sampling, the variations between each sampler should be minimized. When a short/long term storage of samplers is needed before analysis, the storage conditions, e.g. temperature and time length, should be taken into consideration to avoid any analyte losses (Lan et al. 2019 a).

The potential applicability of an aerial drone as a carrier for new miniaturized air sampling systems, such as SPME Arrow and ITEX, was evaluated in this research after assessment of QC/QA. These sampling techniques help to overcome problems encountered in traditional sampling techniques, such as SPME fiber or thermal desorption tube (TDT). Different experimental approaches, based on the use of sampling accessories were developed for the evaluation of the sampler performance. The effect of vertical displacements of the drone during the sampling was also evaluated to allow the almost simultaneous air sampling at different altitudes, making possible the development of low-cost vertical profile studies. Finally, an aerial drone, furnished with both, ITEX and SPME Arrow sampling systems, was used for the simultaneous collection of air samples in difficult access places.

METHODS

Air samples were collected by a sampler, consisting of a remote controlled drone Geodrone X4L, with dimensions 58 x 58 x 37 cm and a total weight of 2 kg, (Videodrone, Finland) furnished with a drone box, which allows the simultaneous sampling on multiple ITEX and SPME Arrow systems. Drone box device involved four SPME Arrow holders with remote controlled opening/closing system and two sampling pumps. The total weight of drone box including the pumps was about 1.4 kg, which allowed a total flight time close to 35 min. Free frequencies of the aerial drone remote controller were used to switch on/off the ITEX pumps and opening/close the SPME holders.

Samples collected by SPME Arrow and ITEX were analyzed by thermal desorption gas chromatography- mass spectrometry (Agilent Technologies). The chromatograph was furnished with a GL Sciences (Eindhoven, The Netherlands) InertCap for Amines (30 m x 0.25 mm i.d., no information was provided for the film thickness) fused silica column coupled with a 3-m deactivated retention gap (i.d. 0.53 mm, Agilent).

Samplers included laboratory made MCM-41-, commercial poly(dimethylsiloxane)/divinylbenzene (PDMS/DVB)-SPME Arrows and laboratory-made polyacrylonitrile-ITEX. For each type of sampler, three devices were prepared in the laboratory or ordered from manufacturer in a batch. They were therefore used for testing reproducibility, equilibrium time, breakthrough volume, and storage time under the same sampling conditions. Nine chemicals representing very, medium, and low volatile organic compounds (VOCs) were placed in a permeation system to form a constant gas flow for dynamic sampling. An extra permeation system for internal standard (ISTD) was also constructed. An independent ISTD addition step before air sampling minimized the variations between each sampling.

The applicability of aerial drone as a carrier for miniaturized air sampling systems was evaluated in three different campaigns. The first one was carried from the 22nd to 26th of October 2018 at the SMEAR II station (Station For Measuring Ecosystem–Atmosphere Relations). The second one took place also at SMEAR II station from the 1st to 12th of July 2019. The last was done at Qvidia site (60°17'42.6"N 22°23'32.3"E) from 24th of July 2019 10th of September 2019.

CONCLUSIONS

Accessories, such as filters and traps for ITEX system, allowed the collection of gas phase compounds and/or to prevent the samples from undesirable chemical reactions.

The use of a trap for aerosol particles decreased the number of detected compounds in comparison with the raw experiments. Similar trend was found for the sum of the relative peak areas (Σ RPA). Filters, used as traps for

aerosol particles, removed gas phase compounds from air samples by adsorption on the filter surface or on the particles retained on the filters.

The use of water traps reveal similar results, in terms of number of compounds and \sum RPA values, than aerosol traps. However, the comparison between them revealed that most of the compounds present in the samples were different. The low number of compounds in the sample can be explained by the design of the water trap, similar to a filter. In addition, differences in the composition of the samples collected with water trap or filter can be explained by the drying capacity of the $\text{Mg}(\text{ClO}_4)_2$, which is able to retain water molecules on its surface and therefore most of the water soluble compounds, such as acids and nitrogen containing compounds.

It was expected that an ozone trap should provide only a relatively small extra effect on the sample composition considering that gas phase and aerosol particles were collected by the ITEX system. However, clear differences were detected in comparison with the samples collected without accessories, most probably due to the fact that ozone trap is able to remove ozone from the air sample, thus protecting compounds from oxidation during sampling. More and different compounds, most of them oxidized, were found in the case of samples collected without ozone trap.

The use of fast vertical drone movements and the remote control of the multiple sampling systems allowed the almost simultaneous air sampling at different altitudes, making the development of low-cost vertical profile studies possible. Similar trend was observed in the case of drone vertical displacement for ITEX and SPME Arrow sampling systems. Namely, the number of compounds detected in the samples and their relative peak area values decreased with the sampling altitude. These results are in good agreement with the values found in the literature for VOCs vertical profile distribution.

A proper quality assurance/quality control (QA/QC), was developed to assure reliable and quantitative (or at least semiquantitative) analytical information. By using the ISTD, the reproducibility of Arrow-to-Arrow and ITEX-to-ITEX can be clearly improved. The SPME Arrow systems were tested with several sampling times to elucidate the extraction kinetic. Laboratory-made MCM-41-SPME Arrow provided faster sampling kinetics than that of commercial PDMS/DVB/SPME Arrow owing to its thinner coating thickness. Laboratory-made MCM-41-SPME Arrow was especially suitable for sampling of basic VOCs while commercial PDMS/DVB-SPME Arrow was excellent for aromatic compounds. Therefore, the combination of these two Arrows in the same flight can provide a more comprehensive view of the VOCs composition in the air. The laboratory-made PAN-ITEX showed a good agreement with our previous publication (Lan et al. 2019b) and no obvious breakthrough occurred for all of the VOCs under testing. The storage time of SPME Arrow and ITEX systems was only tested in a limited time at three different temperatures. For more practical applications (according to our campaigns), a longer storage time test is needed and has been processed in our most recent study.

ACKNOWLEDGEMENTS

Financial support was provided by the Academy of Finland Centre of Excellence program (project no. 307331). H.L is also grateful to China Scholarship Council (grant no. 201508330310).

REFERENCES

- Ruiz-Jimenez, J., Zanca, N., Lan, H., Jussila, M., Hartonen, K. and Riekkola, M.-L. (2019). Aerial drone as a carrier for miniaturized air sampling systems, *J. Chromatogr. A* **1597**, 202.
- Lan, H., Ruiz-Jimenez, J., Demaria, G., Leleev, Y., Jussila, M., Hartonen, K., Riekkola, M.-L. (2019). Aerial drone, a reliable platform for the chemical determination of gas phase and aerosol particles in air, Manuscript will be submitted to *J. Chromatogr. A*.

- Lan, H., Holopainen, J., Hartonen, K., Jussila, M., Ritala, M. and Riekkola, M.-L. (2019). Fully automated online dynamic In-Tube Extraction for continuous sampling of volatile organic compounds in air, *Anal. Chem.* **91**, 8507.
- Barreira, L.M.F., Duporté, G., Rönkkö, T., Parshintsev, J., Hartonen, K., Schulman, L., Heikkinen, E., Jussila, M., Kulmala, M. and Riekkola, M.-L. (2018). Field measurements of biogenic volatile organic compounds in the atmosphere using solid-phase microextraction Arrow, *Atmos. Meas. Tech* **11**, 881.

CHARACTERIZATION OF PRIMARY BIOLOGICAL AEROSOL PARTICLES AT THE BOREAL FOREST BY DIFFERENT METHODS

M. OKULJAR^{1,5}, J. RUIZ-JIMENEZ^{1,5}, O.-M. SIETIÖ^{2,4}, G. DEMARIA¹, E. ZAGATTI¹, T. LIANGSUPREE¹, K. HARTONEN^{1,5}, J. HEINONSALO³, J. BÄCK⁴, T. PETÄJÄ⁵ and M-L RIEKKOLA^{1,5}

¹Department of Chemistry, P.O. Box 55, FI-00014 University of Helsinki, Finland

²Department of Microbiology, P.O. Box 56 University of Helsinki, FI-00014, Finland

³Department of Forest Sciences, P.O. Box 27, FI-00014 University of Helsinki, Finland

⁴Institute for Atmospheric and Earth System Research/Forest Sciences, Faculty of Agriculture and Forestry, P.O. Box 64, FI-00014 University of Helsinki, Finland

⁵Institute for Atmospheric and Earth System Research, Faculty of Science, P.O. Box 64, FI-00014 University of Helsinki, Finland

Keywords: PRIMARY BIOLOGICAL AEROSOL PARTICLES, CHEMICAL TRACERS, DNA-MICROORGANISMS, MACHINE LEARNING

INTRODUCTION

Primary biological aerosol particles (PBAPs) play an important role in the atmosphere by affecting cloud and precipitation formation processes by acting as cloud and ice nuclei. In addition, the contribution of pollen, plant fragments, spores, bacteria, algae and viruses from multiple sources to the composition of PBAPs is well-known (Morris, et al., 2011). The elucidation of PBAPs chemical and microbial composition is nowadays a relevant topic in the atmospheric chemistry field (Okuljar et al., 2019). Chemical tracers, saccharides and amino acids, have been traditionally used for the determination of particles of biological origin. However, this approach fails to identify the different species involved in the aerosol particle composition. In this way, the use molecular genetic analysis techniques, such as quantitative polymerase chain reaction (qPCR) or next-generation sequencing (NGS), is mandatory for the elucidation of these species (Helin et al., 2017).

The expansion of computer methods allows to researchers the use of machine learning (ML) techniques, a branch of artificial intelligence, to clarify environmental issues. According to the datasets used for the development of the models ML techniques can be classified into two broad categories unsupervised ML, input data without labeled responses, and supervised ML, input attributes (independent variables) and a target attribute (dependent variable). The latter can be further classified into two main categories; classification and regression. In regression output variable takes continuous values while in classification output variable takes class labels (Smola et al., 2008).

In this study, 84 size-segregated aerosol samples from four particle size fractions (< 1.0–2.5 µm, 2.5–10 µm and > 10 µm) were collected at SMEAR II station in autumn 2017. Free amino acids (19) and saccharides (8) were analyzed in aerosol samples by liquid chromatography-mass spectrometry (LC-MS). In addition, DNA present in the aerosol samples was extracted and amplified to evaluate the concentration and size distribution variation of bacteria, pseudomonas and fungi. Multiple linear regression, a simple machine learning tool, was used to evaluate: 1) the effect of gas phase VOCs on the microbiological composition of the aerosol particles; and 2), the effect of the microbiological composition, total amount of bacteria, pseudomonas and fungi, on the chemical profile of the

aerosol particles. Seasonal and size influence on primary biological aerosol particles emission was also evaluated by machine learning approaches such as, discriminant analysis and neural network, using as input data the chemical and microbiological composition of the particles.

METHODS

84 aerosol samples were collected at SMEAR II station in autumn 2017 (4.09.2017-22.11.2017) using a Dekati PM10 impactor for the sampling of four particle size fractions (< 1.0 , $1-2.5$ μm , $2.5-10$ μm and > 10 μm). After ultrasound-assisted extraction, using an aqueous solution containing 0.1 % of formic acid as extractant, an Agilent 1260 Infinity HPLC furnished with a SeQuant ZIC-cHILIC column (150 x 2.1 mm, particle size 3 μm , 100 \AA , MERCK, Darmstadt, Germany), coupled to an Agilent 6420 electrospray ionization triple quadrupole mass spectrometer (Agilent Technologies, USA) was employed for the determination of free saccharides (inositol, sucrose, fructose, mannose, D-arabitol, D-mannitol, 1,6-anhydro- β -D-Glucose and D(+)-trehalose dehydrate) and amino acids (L-alanine (Ala), L-aspartic acid (Asp), L-glutamic acid (Glu), L-glutamine (Gln), L-glycine (Gly), L-isoleucine (Iso), L-leucine (Leu), L-lysine (Lys), L-methionine (Met), L-phenylalanine (Phe), L-proline (Pro), L-threonine (Thr), L-tryptophan (Try), L-tyrosine (Tyr), L-valine (Val), L-arginine (Arg), L-histidine (His), L-asparagine (Asn) and L-serine (Ser)). All the compounds were analyzed in MS/MS mode, with the exception of levoglucosan, analyzed by single ion monitoring. Total nucleic acids were extracted from the collection filters with a commercial DNA extraction kit (PowerWater DNA Isolation Kit, MoBio Laboratories, USA), following the procedure developed in our previous paper (Helin et al. 2017). The bacterial and fungal DNA amounts of the filter samples were quantified with qPCR using target-specific primer pairs, Eub338F and Eub518R, and FF390 and FR1. Genus-specific primers, Eub338F and PseudoR, were utilized to detect the bacteria belonging to the genus *Pseudomonas*. In both cases, chemical and microbiological parameters, results were normalized by the total amount of sampled air.

Multiple linear regression, a very simple machine learning tool, was used to elucidate the effect of gas phase VOCs on the microbiological composition of the aerosol particles. The amount of the different microbiological agents, expressed as number of genes copies/ m^3 , were used as dependent variables. 13 VOCs such as methanol ($m/z = 33$), acetonitrile ($m/z = 42$), ethanol ($m/z = 47$), acetone ($m/z = 59$), acetic acid ($m/z = 61$) isoprene ($m/z = 69$), butenal ($m/z = 71$), 2-butanone ($m/z = 73$), benzene ($m/z = 79$), α -pinene fragment ($m/z = 81$), 2-methyl-3-buten-2-ol ($m/z = 87$), toluene ($m/z = 93$) and α -pinene ($m/z = 137$), were used as independent variables. In all the cases the number of samples used for the development of the models were over 19.

The effect of the microbiological species on the chemical composition of the aerosol particles was also evaluated by multiple regression analysis. As response variable (dependent variable) the concentration of bacteria, *pseudomonas* and fungi in the PBAP samples were used. The concentration of the different amino acids (19) and sugars (8) present in the aerosol particles were used as independent variables.

Size influence and seasonal differences on primary biological aerosol particles emission were evaluated by machine learning approaches such as, discriminant analysis and neural network, using the chemical and microbiological composition of the particles as input data. 84 samples were evaluated in this study.

Cluster analysis was used to establish seasonal differences using as reference a database containing 41 meteorological and environmental parameters.

CONCLUSIONS

It was possible to find a correlation between the VOCs gas phase emission and their presence in the aerosol particles of different microorganisms. Individual MLR models were developed for the different particle sizes based on potential variations in the microorganism species present in the samples. Explained variance of the models was over 92.0% in all the cases. The limited number of samples used in the models development could affect their reliability. Additional samples should be included in the models in order to confirm the results.

It was not possible to find a single correlation trend between the aerosol particle size and their microbiological composition. Up to three different trends were found for pseudomonas, fungi–bacteria and total amount of DNA in the samples. Discriminant analysis was able to provide correct classification of 85.0 % of the samples. The use of neural network for the classification of the samples allowed the correct classification of 78.5 % of the samples.

The enormous variety of microorganisms made the elucidation of their contribution to the chemical composition of the aerosol particles difficult. Different MLR models should be developed for the different particle sizes and microorganism. Explained variance of the developed MLR models was over 94.8% in all the cases. Relevant information about the different developed models, including the number of samples used in the model development, the explained variance (EV) and the variables with a statistical influence can be found in Table 1.

Finally, it was found a clear relationship between the environmental and meteorological variables and the microbiological and chemical composition of the aerosol particles. Groups obtained from the cluster analysis of the meteorological and environmental variables were used for the classification of the PBAPs using their chemical and microbiological composition as input data. Discriminant analysis was able to provide correct classification of 85.7 % of the samples. The use of neural network for the classification of the samples allowed the correct classification of 78.6 % of the samples.

Table 1. Multiple linear regression models for the evaluation of the microbiological species contribution to the aerosol particles composition.

PM (µm)	Microorganism	N	EV (%)	Variables (+)*	Variables (-)*
< 1.0	Bacteria	20	96.2	Ala, Manni, Tyr	Glu, Ile, Leu, Thr
	Pseudomonas	20	94.8	Fruct, Arab, Arg, Ala	Glu, Gln, Ser, Phe
	Fungi	19	83.8	Arab, Fruct, Manni, Pro	Ala, Levo, Arg
1–2.5	Bacteria	20	99.7	Thr, Pro, Ala	Suc, Glu, His
	Pseudomonas	20	99.5	Suc, Threh, Fruct, Arg	Manno, Ala, Glu Phe
	Fungi	19	98.3	Suc, Manni, Arg, Pro	Fruct, Arab, Phe
2.5–10	Bacteria	19	95.5	Ser, Manni.	Pro, Suc, Trp
	Pseudomonas	20	99.7	Levog, Asn, Ala, Arg	Thr, Fruct, Val, Manno
	Fungi	20	98.3	Manno, Inno, Arab	Arg
> 10	Bacteria	19	99.1	Ala, Manni, Tyr	Glu, Ile, Leu, Thr
	Pseudomonas	19	99.9	Ala, Manni, Manno, Trp, Ser	Fruct, Ile, Leu, Arg, Suc
	Fungi	19	99.3	Ile, Leu, Pro	Thr, Manno, Lys

* p value < 0.05 for the regression coefficient. Mannitol (Manni), Fructose (Fruct), arabitol (Arab), threhalose (Threh), levoglucosan (Levog), mannose (Manno), inositol (Inno) and sucrose (Suc).

ACKNOWLEDGEMENTS

The financial support of the Academy of Finland Centre of Excellence program (project no. 307331) and research project no. 292699 (O. M. Sietiö, J. Heinonsalo) are gratefully acknowledged. University of Helsinki Doctoral Program in Microbiology and Biotechnology (MBDP) (O.-M. Sietiö) are thanked for support.

REFERENCES

- Helin, A., Sietiö, O.-M., Heinonsalo, J., Bäck, J., Riekkola, M.-L. and Parshintsev, J. (2017). Characterization of free amino acids, bacteria and fungi in size-segregated atmospheric aerosols in boreal forest: seasonal patterns, abundances and size distributions, *Atmos. Chem. Phys.*, **17**, 13089.
- Morris, C.E., Sands, D.C., Bardin, M., Jaenicke, R., Vogel, B., Leyronas, C., Ariya, P.A. and Psenner, R. (2011). Microbiology and atmospheric processes: research challenges concerning the impact of airborne microorganisms on the atmosphere and climate, *Biogeosciences*, **8**, 17.
- Okuljar, M., Ruiz-Jimenez, J., Sietiö, O.-M, Demaria, G., Zagatti, E., Liangsupree, T., Hartonen, K., Heinonsalo, J., Bäck, J., Petäjä, T. and Riekkola, M.-L. (2019). Chemical and microbiological characterization of primary biological aerosol particles at the boreal forest. Manuscript will be submitted to *Atmos. Chem. Phys.*
- Smola, A. and Vishwanathan, S. (2008). *Introduction to Machine Learning*. (Cambridge University Press, Cambridge, UK).

THE EFFECT OF ATMOSPHERIC AEROSOL PARTICLES ON CLOUD ICING RATE

RUUSKANEN¹, A. LESKINEN^{1,2}, H. KOKKOLA¹, M. KOMPPULA¹ AND S. ROMAKKANIEMI¹

¹Finnish Meteorological Institute, P.O.Box 1627, FI-70211, Kuopio, Finland

² University of Eastern Finland, Department of Applied Physics, P.O.Box 1627, FI-70211, Kuopio, Finland

Keywords: CLOUD ICING, MODELLING, AEROSOL-CLOUD INTERACTION

INTRODUCTION

Icing is an atmospheric process where ice accumulates on surfaces of any kind. While couple of different icing processes exists, the most interesting related to atmospheric aerosol studies is in-cloud icing. This icing process can be caused either by liquid rain drops or cloud droplets. The most important differences between the two are droplet concentration and size.

Icing can cause damage to structures or financial losses. For example, wind energy power plants might have unplanned shutdown or flights might get delayed/cancelled. With well-structured forecasting models these kinds of unplanned events could be avoided.

Current forecasting models typically have simplified representation of droplets due to the lack of reliable measurement data for verifying the models (Makkonen et al., 2010). The size distributions with typical droplet size are the most important parameters that are needed for reliable icing forecasts.

METHODS

We have studied cloud droplet properties and icing conditions for several years at the Puijo measurement station (306 m a.s.l. and 224 m above the surrounding lake level) located in Kuopio, Finland (Leskinen et al., 2009). In addition to Puijo measurement station, Finnish Meteorological Institute is running another measurement station, Vehmasmäki, which is focused for mast measurements. At the Vehmasmäki site there is a 318 m high mast equipped with meteorological instrumentation at various heights including icing measurements started in 2016 at two different levels (115 m and 272 m). The icing data (see Figure 1) can be linked to the meteorological conditions as well as the profile measurements of wind, aerosols and water vapour located on the site.

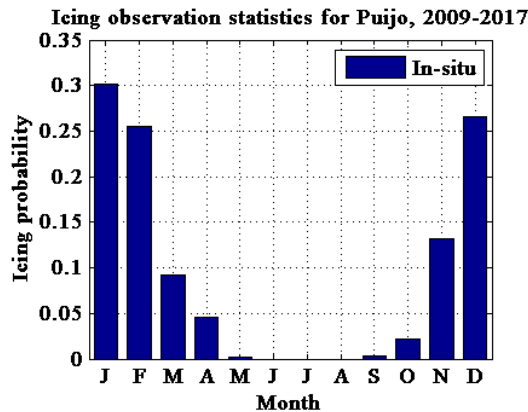


Figure 1: Occurance of icing events at Puijo measurement station, measured with an icing detector

The main focus of the study is to investigate connection between aerosol particles and cloud microphysical properties, meteorology and icing rate. The study includes several icing detectors (on/off and accumulation speed), cloud droplet probe (CDP), aerosol size distributions, and meteorological instruments for air temperature and wind speed/direction. Beyond, cloud modelling tools with explicit description of aerosol and cloud microphysics will be employed to support the data analysis (Tonttila et al., 2017).

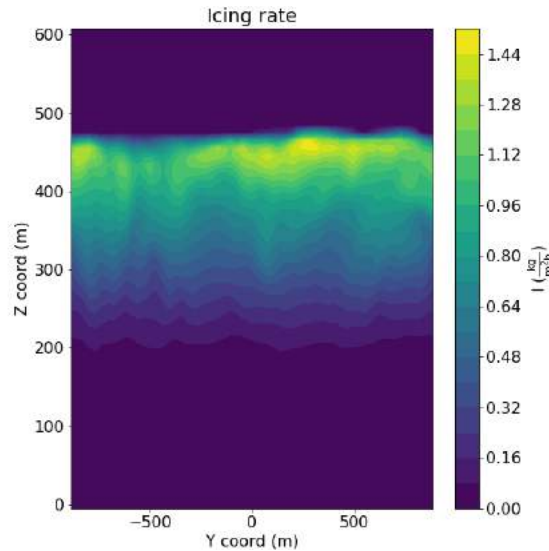


Figure 2. Calculated icing rate by icing model for cylinders in a simulated low level cloud.

RESULTS

Preliminary results show difference between measured and modelled icing rates (figure 3). While the main focus is on qualitative differences caused by aerosol, the comparison of absolute icing rate values show similarities. While the measured icing rate is about 2 to 4 times higher than modelled one, the ratio of measurement altitudes is about the same, 5 to 6. This confirms that relative changes between different altitudes behave similarly in modelled as well as in measured data.

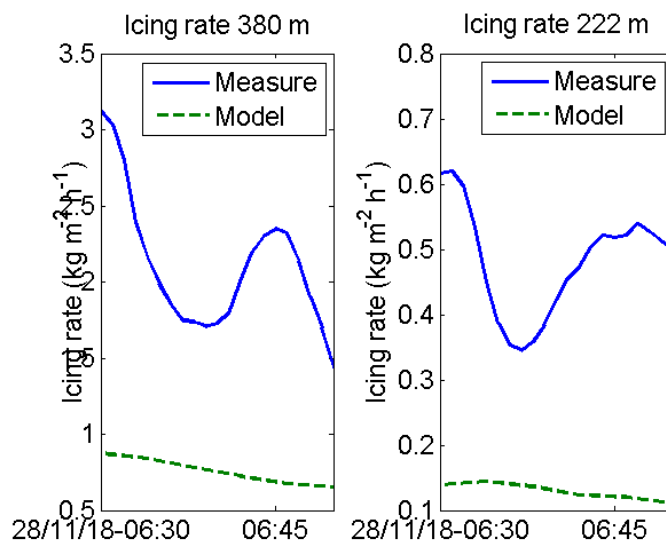


Figure 2. Preliminary comparison of measured and modelled icing rates at Kuopio Vehmasmäki station. The measured icing rate is from 2.2 to 4.5 times higher than modelled one.

ACKNOWLEDGEMENTS

This work has been supported by Fortum Foundation (201800249) for PhD thesis work.

REFERENCES

- Leskinen, A., Portin, H., Komppula, M., Miettinen, P., Arola, A., Lihavainen, H., Hatakka, J., Laaksonen, A., Lehtinen, K. E. J. (2009) *Overview of the research activities and results at Puijo semi-urban measurement station*, *Boreal Env. Res.*, 14, 576–590
- Makkonen, L., Laakso, T., Marjaniemi, M., Finstad, K. J. (2010). *Modelling and prevention of ice accretion on wind turbines*. *Wind Engineering*, 25:3-21.
- Tonttila, J., Maalick, Z., Raatikainen, T., Kokkola, H., Kühn, T., and Romakkaniemi, S. (2017): *UCLALES–SALSA v1.0: a large-eddy model with interactive sectional microphysics for aerosol, clouds and precipitation*, *Geosci. Model Dev.*, 10, 169-188, doi:10.5194/gmd-10-169-2017.
- Chapman, D.H. (1975). Optical scattering from combustion aerosols, *J. Aerosol Science* **36**, 3456.

SEASONAL DYNAMICS OF SCOTS PINE ROOT RESPIRATION IN FINLAND

K. RYHTI¹, S. SALKO¹, J. BÄCK¹ and L. KULMALA^{1,2}

¹ Institute for Atmospheric and Earth System Research / Forest Sciences
Faculty of Agriculture and Forestry, P.O. Box 27, FIN-00014, University of Helsinki, Finland.

² Finnish Meteorological Institute, Helsinki, Finland.

Keywords: Scots pine, root respiration, CO₂, climate change, drought.

INTRODUCTION

Warming of the climate is generally assumed to stimulate the photosynthetic production in the boreal region (Jansson et al. 2008, Briceno-Elizondo et al. 2006), however, drought periods may become prevalent during growing seasons and unpredictably affect belowground carbon processes of plants and soil. Studies have indicated that the most common tree species in Finland, Scots pine (*Pinus sylvestris* L.), would benefit from the changes in the climate (Reich and Oleksyn 2008, Kellomäki et al. 2008). How the warmer climate and drought periods affect to tree growth and their ability to bind atmospheric carbon in future, would require a holistic view on whole tree actions including also understanding in the belowground processes, not only more easily measurable aboveground processes.

Soil respiration (CO₂ efflux) is a sum of maintenance and growth respiration of roots and emissions from root-associated microbes, such as mycorrhizal fungi (i.e. autotrophic root respiration), and from decomposition of soil organic matter by non-symbiotic microbes, such as saprophytic fungi (i.e. heterotrophic respiration). Roots are in direct contact with the soil; consequently, measuring carbon fluxes of roots and soil microbes, such as mycorrhizal fungi, has been challenging. In order to study these processes under field conditions, the emissions from various sources should be separated. However, this far, the measuring respiration of roots might be biased due to the methodological disturbance with the tight interaction these processes have in undisturbed soils.

Our aim was to separate different components of forest floor respiration and to study the seasonal dynamics in mature Scots pine stand in the field. Dynamics were followed in growing seasons of moister and colder year 2017 and warmer and dryer year 2018 (Fig. 1A, B).

METHODS

The experiment was conducted in middle-aged Scots pine stand at SMEARII located near Hyytiälä forestry field station in southern Finland. Trenching plots were established in June 2017. First a trench was dug around the plot and all the roots, mainly of tree and dwarf shrubs, were cut. A mesh fabric with pore size of 1 µm (which enables water and nutrients to flow in) was installed around the plot to prevent new root growth into the plot. After installation the trench around the plot was re-filled. Soil inside the plot was left untouched, but ground vegetation was removed. All roots were left intact on control plots, but ground vegetation was removed.

Soil temperature and moisture were regularly measured at all plots with iButton (Maxim Integrated, San Jose, CA, USA) and moisture content (SWC) profile with HH2 moisture meter and PR2 soil moisture profile probe (Delta-T Devices, Cambridge, UK). Decomposition rate of cut roots in each plot was determined using root litter bags. Soil respiration (CO₂ efflux) from trenched plots and nontrenched controls was measured using dark chamber, where air was circulated with a pump. Chamber was put on permanently installed collar and CO₂ concentration in the chamber was measured with infra-red absorption sensor (GMP343, Vaisala Oyj, Finland) every 5 seconds for 30 minutes. The chamber and the flux calculations are described in Pumpanen et al. (2015). Air temperature was monitored in chamber.

Respiration from excised roots was measured in ambient air temperature in an aluminium bag with air circulation system and a CO₂ sensor (GMP343, Vaisala). Root samples for incubation were dig from soil, cut from coarse roots as a hole with root tips, and cleaned by hands. Samples were put in aluminium bag as soon as possible after cutting to prevent major decrease in CO₂ emissions. Bag was sealed, emptied from air and filled with 500 ml ambient air. CO₂ concentration in the bag was measured every 5 seconds and during 15 minutes in total. The flux ($\mu\text{g s}^{-1}$) was calculated from the increase in CO₂ concentration inside the bag. After incubation, root samples were photographed (in 2018), put into 15 ml Eppendorf tubes and kept in cold for approximately an hour before using microwave (1 minute, 600 W) in order to stop enzymatic activity. The samples were kept in freezer (-18 °C) before freeze-drying (SciQuip Ltd, Merrington, UK) for three days (72 hours) and re-weighting (dry weight). Root respiration from excised roots was upscaled per area using pine root (<5 mm) biomass and growth dynamics studied at SMEARII.

Respiration from trenched plots was assumed to contain only heterotrophic respiration as all autotrophic plants were removed. Autotrophic respiration was calculated as a difference between mean respiration from control (hetero- and autotrophic respiration) and trenched plots (heterotrophic respiration).

PRELIMINARY RESULTS AND DISCUSSION

Temperatures in spring and during the summer were considerably higher in year 2018 compared to 2017 (Fig. 1A). The thermal time (i.e. the effective temperature sum, degree-day, °Cd), calculated as the sum of the daily average temperatures above 5 °C from the days, when the average temperature was more than 5 °C, was 1610 °Cd in 2018, which was also higher compared to 1030 °Cd in 2017.

The year 2017 was evenly moist, while in 2018 SWC in SMEARII station decreased low during the summer (Fig. 1B). Mean SWC in trenched plots was higher in 2018 compared to continuously measured SWC at SMEARII station. Similar difference was not seen in 2017. Mean SWC in control plots (data not shown) was comparable with SWC at SMEARII station in both years. Higher SWC in trenched plots is mostly due to lack of tree roots up taking water from the plots, and this has probably effect on soil respiration rate.

Hetero- and autotrophic respirations were highest when temperature was highest, but lower SWC may have restricted respiration rate in 2018 (Fig. 1C, D). Heterotrophic respiration was slightly higher compared to autotrophic root respiration, however, heterotrophic respiration presented here contains additional CO₂ emissions from decaying residual roots and due to higher soil moisture, which should be taken into account in final results. Autotrophic root respiration from incubated root samples was comparable to autotrophic respiration calculated as a difference between control and trenching, in middle of the growing season, but not in the end or beginning. The differences may be caused by different temperature during the measurements as incubated samples are dug from soil and incubated in air temperature, which was probably higher than soil temperature. Also diffusion of CO₂ from soil may be slower when the soil is frozen or cold.

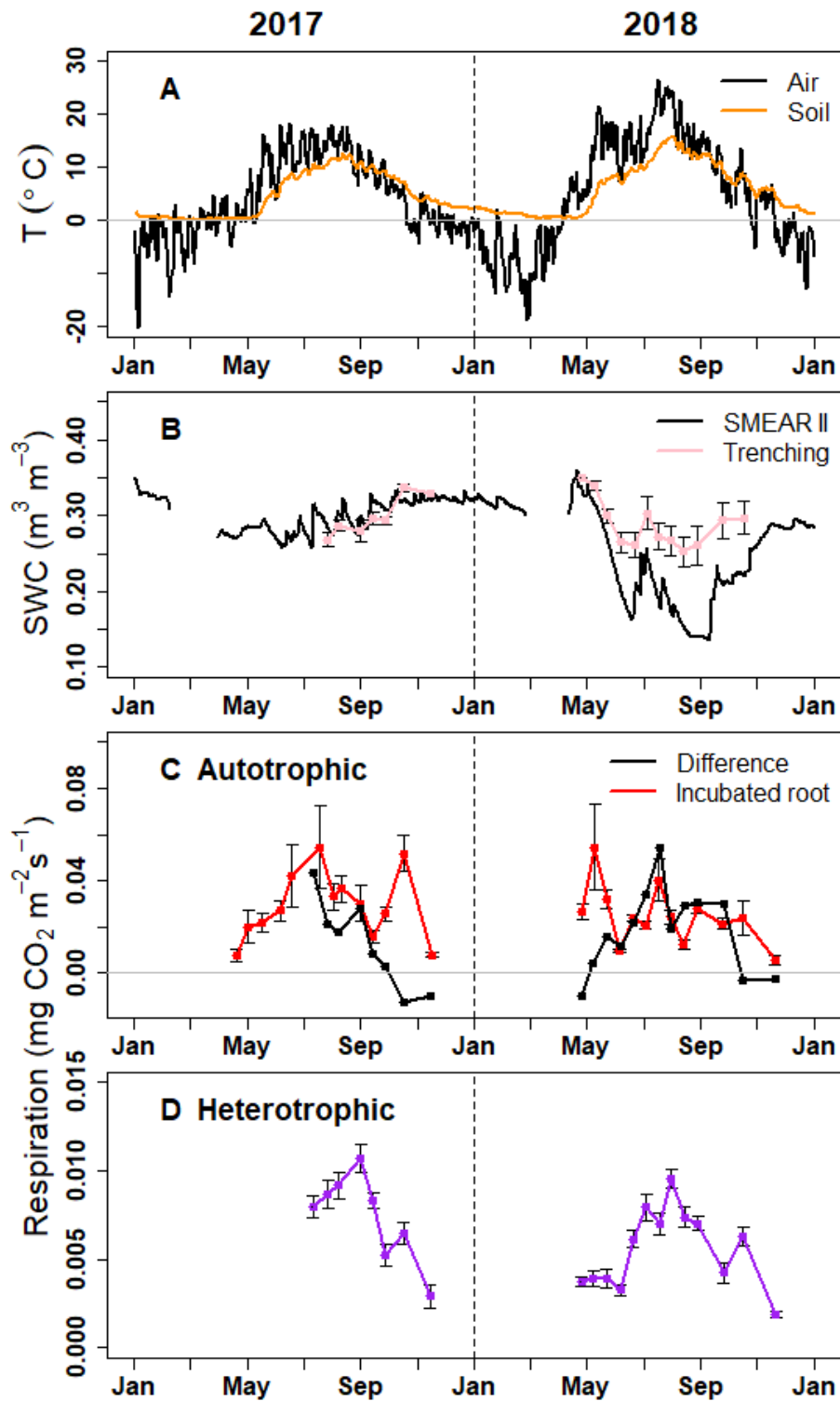


Figure 1. Daily mean temperature (T) in the air (black) and soil A-horizon in orange (A), soil-water content (SWC) in the A-horizon at the SMEARII station and in trenching plots in pink \pm standard error (SE) in black (B), autotrophic respiration calculated as difference (between control and trenching) in black and mean incubated root respiration and red \pm SE in black (C), and mean heterotrophic respiration in purple \pm SE in black (D) at the SMEARII station during the study years 2017 and 2018.

ACKNOWLEDGEMENTS

Kone Foundation, the University of Helsinki Funds and Finnish Centre of Excellence Programme by the Academy of Finland (grant no.307331) are acknowledged for financial support. We thank Henri Jokinen and Anna Tuovinen for help of construction of experimental plots in SMEARII, and Anna Tuovinen with the CO₂ flux and soil moisture measurements.

REFERENCES

- Briceno-Elizondo, E., Garcia-Gonzalo, J., Peltola, H. & Kellomäki, S. Carbon stocks and timber yield in two boreal forest ecosystems under current and changing climatic conditions subjected to varying management regimes. *Environmental Science & Policy* **9**, 237-252 (2006).
- Jansson, P., Svensson, M., Kleja, D. B. & Gustafsson, D. Simulated climate change impacts on fluxes of carbon in Norway spruce ecosystems along a climatic transect in Sweden. *Biogeochemistry* **89**, 81-94 (2008).
- Kellomäki, S., Peltola, H., Nuutinen, T., Korhonen, K. T. & Strandman, H. Sensitivity of managed boreal forests in Finland to climate change, with implications for adaptive management. *Philosophical Transactions of the Royal Society B - Biological Sciences* **363**, 2341-2351 (2008).
- Pumpanen, J., Kulmala L., Linden, A., Kolari, P., Nikinmaa, E. & Hari P. Seasonal dynamics of autotrophic respiration in boreal forest soil estimated by continuous chamber measurements. *Boreal Environment Research* **20**: 637-650 (2015).
- Reich, P. B. & Oleksyn, J. Climate warming will reduce growth and survival of Scots pine except in the far north. *Ecology Letters* **11**, 588-597 (2008).

FAAR abstract instructions and template

Please read carefully - the text contains instructions for abstract preparation

THE EFFECT OF ATMOSPHERIC CIRCULATION ON RECENT TEMPERATURE CHANGES IN FINLAND

J. RÄISÄNEN¹

¹Institute for Atmospheric and Earth System Research / Physics, Faculty of Science, FI-00014 University of Helsinki, Finland

Keywords: climate change, temperature, atmospheric circulation, Finland.

INTRODUCTION

Weather conditions vary substantially from year to year. For example, the summer in one year might be cool and rainy, that in the following year warm and dry. At extratropical latitudes, most of this interannual variability is caused by variations in the atmospheric circulation. This circulation-induced variability is so large that, even though it partly cancels out in longer-term averages, it may also have a non-negligible impact on climate changes observed during a period of several decades (Deser et al. 2012). Thus, isolating the effect of atmospheric circulation may help to better delineate the underlying long-term anthropogenic climate change that would have occurred without the change in circulation (Saffioti et al. 2016). Obviously, changes in circulation might also occur as part of long-term anthropogenic climate change, but climate model simulations suggest that their effect should be secondary for temperature change (e.g., Saffioti et al. 2017). Here, we study the effect of atmospheric circulation change on temperature change in Finland in the years 1979-2018. Expanding on a method presented by Parker (2009), we use an approach that infers the circulation-related temperature variations on the point of origin of 1-to-7-day air parcel back trajectories arriving in Finland. The current research was reported in more depth in Räisänen (2019).

METHODS

Two datasets are used: daily mean surface air (2 m) temperatures from the European Climate Assessment & Dataset gridded E-OBS dataset version 19.0e (Haylock et al. 2008), and horizontal wind components and vertical motion (ω) from the ERA-Interim reanalysis (Dee et al. 2011). The E-OBS data are averaged over two 1° latitude \times 2° longitude boxes: one in southern (61° - 62° N, 23° - 25° E) and the other one in northern Finland (67° - 68° N, 26° - 28° E). The ERA-Interim data have a higher native resolution but were reduced to a 50 hPa vertical and $2.5^\circ \times 2.5^\circ$ horizontal grid to cut down the data volume. This study covers the years 1979-2018.

Back-trajectories ending in the centres of the two study areas (61.5° N, 24° E and 67.5° N, 27° E) are calculated four times per day (00, 06, 12 and 18 UTC), at 10-minute timestep using linear interpolation of wind and vertical motion in latitude, longitude, pressure and time. This is done for trajectories ending at 7 pressure levels (1000, 925, ... 550 hPa) and extending 1 to 7 days back in time. For each day, the coordinates of the four trajectories are averaged before relating them to the daily mean temperature anomaly in the E-OBS data set.

The dependence of temperature on the coordinates of the trajectory origin is estimated using regression analysis. First, the coordinates are transformed to a rotated grid in which the centre of the target area in southern or northern Finland is at (0° N, 0° E). Then the coefficients in the linear regression equation

$$\Delta T_{day} = a_0 + \sum_{i=1}^N a_i f_i + \varepsilon \quad (1)$$

are determined using the least squares method. Here ΔT_{day} is the anomaly in daily mean temperature relative to the 40-year (1979-2018) mean for the same day, and $N = 19$ is the number of predictors. The predictors are first- (x , y , z), second- (x^2 , y^2 , z^2 , xy , xz , yz) and third-order (x^3 , y^3 , z^3 , x^2y , xy^2 , x^2z , y^2z , xz^2 , yz^2 , xyz)

FAAR abstract instructions and template

Please read carefully - the text contains instructions for abstract preparation

functions of x , y and z , which are defined as follows: $x = \sin(\Delta\lambda) \cos(\Delta\varphi)$, $y = \sin(\Delta\varphi)$, and $z = \Delta p$, where $\Delta\lambda$, $\Delta\varphi$ and Δp are the longitude, latitude and pressure difference between the trajectory end and start points in the rotated grid. These formulations ensure that x and y increase nearly linearly with distance for short trajectories while simultaneously avoiding spuriously large far-field values and discontinuities that would result from using λ and φ directly. The coefficients $a_0 \dots a_N$ are estimated separately for each 12 calendar months.

An initial estimate for the monthly circulation-related temperature anomaly (ΔT_1) is obtained by averaging the daily values from (1). However, the resulting monthly mean temperature residuals ($\Delta T - \Delta T_1$) have systematic positive correlation with this initial circulation-related anomaly (Räsänen 2019). In other words, temperature is more sensitive to atmospheric circulation on monthly than daily time scales. To account for this, linear regression

$$\Delta T_2 = b_0 + b_1 \Delta T_1 + \varepsilon \quad (2)$$

is used to rescale the monthly mean temperature anomalies.

The time span of the trajectory (between 24 and 168 hours) and the end level (between 550 and 1000 hPa) are both somewhat arbitrary choices. In general, medium-long (72-96 h) trajectories ending at mid-levels (700-850 hPa) are found to give the smallest regression residuals, but this dependence is not very sharp. Therefore, a final estimate for the circulation-related monthly temperature anomaly is calculated as

$$\Delta T_3 = c_0 + c_1 \langle \Delta T_2 \rangle + \varepsilon \quad (3)$$

where the brackets indicate averaging over all the 49 alternatives (7 time spans, 7 end levels).

In all cases, the regression coefficients were calculated separately for each year, using only the data for the other 39 years. Thus, the predicted temperature anomalies are not affected by the observed temperature anomaly in the same year. Furthermore, the predictor and predictand time series were linearly detrended when deriving the regression coefficients. These procedures serve to minimize both artificial skill in the regression and the aliasing between circulation-related anomalies and non-circulation-related climate change.

RESULTS

As an example, Figure 1 compares the observed and circulation-related anomalies in December mean temperature in northern Finland, chosen for this illustration because of the particularly large observed warming in this case. Interannual variability in December is large and well captured by the trajectory method. The variance of the residual time series (grey line) is only 15% of that of the observed series, and this ratio decreases to 14% when both time series are detrended to eliminate the effect of climate change. Thus, 86% of the detrended variance of December mean temperature in northern Finland is explained by the origin of the trajectories. As averaged over all 12 months, 81% of the detrended variance of monthly mean temperatures is explained by this method in both southern and northern Finland.

FAAR abstract instructions and template
Please read carefully - the text contains instructions for abstract preparation

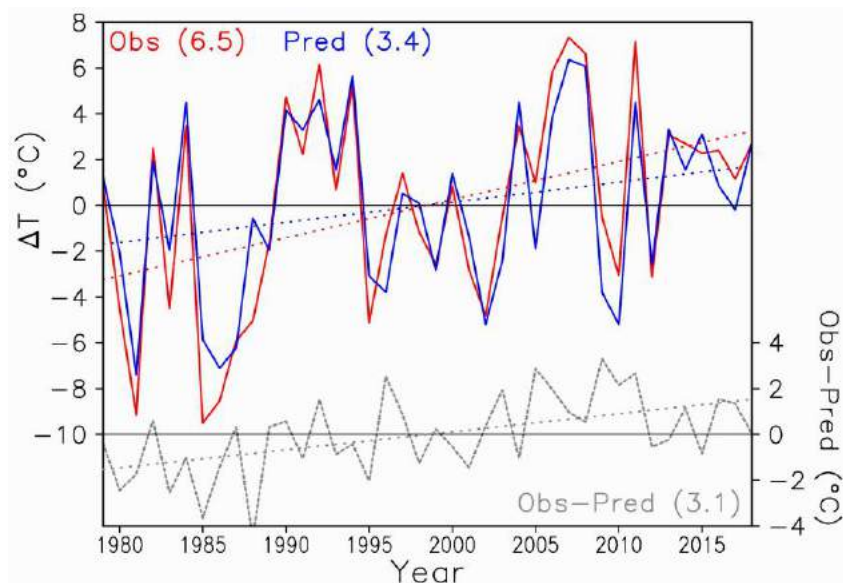


Figure 1. Temperature anomalies in December in northern Finland. The red line shows the observed anomaly, the blue line the anomaly predicted by Eqs. (1)-(3), and the grey line their difference. Linear trend lines and the corresponding 39-year temperature changes (in parentheses) are also included.

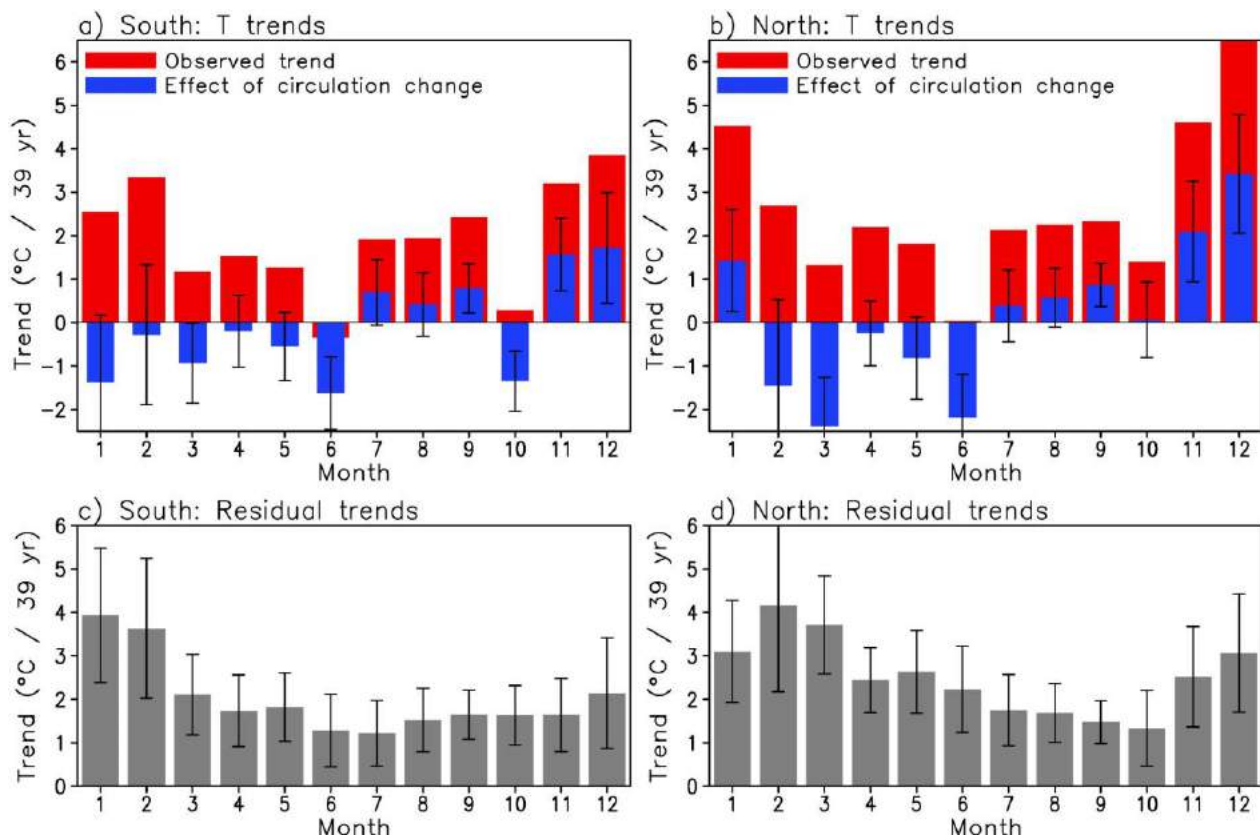


Figure 2. Trends in monthly mean temperature from 1979 to 2018 in (a, c) southern and (b, d) northern Finland. In (a) and (b), the red bars show the observed temperature trends and the blue bars the best-estimate circulation-related trends (Eq. 3). In (c) and (d), the residual trends are given. The 5-95% error bars for the circulation-related trends and the residual trends are derived from interannual variability, as detailed in Räisänen (2019). Reproduced from Räisänen (2019).

FAAR abstract instructions and template

Please read carefully - the text contains instructions for abstract preparation

The observed temperature trends in Finland in 1979-2018 varied from month to month, with generally smaller warming in summer than in winter (red bars in Fig. 2a-b). In particular, June mean temperatures decreased slightly in southern Finland and remained nearly constant in northern Finland. There was also a distinct local minimum in warming in October in southern Finland, between larger warming in September and November. By contrast, a sharp maximum in warming occurred in December particularly in northern Finland.

Many of these apparent irregularities in the seasonal cycle of warming are explained by atmospheric circulation (blue bars in Fig. 2a-b). Most notably, the lack of warming in June is due to a negative contribution of circulation change that, if acting alone, would have cooled the June mean temperature by about 1.6°C in southern and 2.2°C in northern Finland. Circulation changes also distinctly reduced the warming in southern Finland in October, while amplifying the warming in November and December in both of the two study areas.

The lower part of Fig. 2 shows the residual trends not explained by circulation change. In both areas, the annual cycle of the residual warming is much smoother than that of the observed warming. However, there is still a large contrast between larger warming in winter and smaller warming in summer and early fall. The residual trends in southern Finland vary from 1.2°C in July to 3.9°C in January, and those in northern Finland from 1.3°C in October to 4.2°C in February.

Although changes in atmospheric circulation have substantially modified the temperature trends in individual months, their effect largely cancels out in the annual average. The residual trends in the annual mean temperature between 1979 and 2018 (2.0°C and 2.5°C in southern and northern Finland, respectively) are therefore very near the corresponding observed trends (1.9°C and 2.7°C). Thus, climate in Finland has warmed substantially during the past four decades and this is not explained by changes in atmospheric circulation.

ACKNOWLEDGEMENTS

This work was supported by the Academy of Finland Centre of Excellence in Atmospheric Science – From Molecular and Biological processes to the Global Climate (project 307331).

REFERENCES

- Dee, D. P. et al., 2011: The ERA-Interim reanalysis: configuration and performance of the data assimilation system. *Quart. J. Roy. Meteorol. Soc.*, 137, 553–597
- Deser, C., A. Phillips, V. Bourdette and H. Teng, 2012: Uncertainty in climate change projections: the role of internal variability. *Climate Dynamics*, 38, 527-546
- Haylock, M.R., N. Hofstra, A.M.G. Klein Tank, E.J. Klok, P.D. Jones and M. New. 2008: A European daily high-resolution gridded dataset of surface temperature and precipitation. *J. Geophys. Res (Atmospheres)*, 113, D20119
- Parker, D.E., 2009: Anomalies of Central England Temperature classified by air source. *J. Climate*, 22, 1069-1081
- Räisänen, J. 2019: Effect of atmospheric circulation on recent temperature changes in Finland. *Climate Dynamics*, doi: 10.1007/s00382-019-04890-2
- Saffioti, C., E. M. Fischer, S. C. Scherrer, and R. Knutti, 2016: Reconciling observed and modelled temperature and precipitation trends over Europe by adjusting for circulation variability. *Geophys. Res. Lett.*, 43, 8189–8198
- Saffioti, C., E.M. Fischer and R. Knutti, 2017: Improved consistency of climate projections over Europe after accounting for atmospheric circulation variability. *J. Climate*, 30, 7271-7291

THE EFFECT OF BOREAL FOREST ON CLOUDS AND PRECIPITATION BASED ON LONG-TERM ATMOSPHERIC OBSERVATIONS

M. RÄTY¹, P. AALTO¹, K. TABAKOVA¹, H. KESKINEN¹, L. SOGACHEVA², M.
PARAMONOV³, V.-M. KERMINEN¹, E. EZHOVA¹, M. KULMALA¹

¹Institute for Atmospheric and Earth System Research (INAR) / Physics, Faculty of Science,
University of Helsinki, Finland.

²Finnish Meteorological Institute, Helsinki, Finland

³Institute for Atmospheric and Climate Science, ETH Zürich, Zürich, Switzerland

Keywords: BOREAL FOREST, WATER VAPOUR, CLOUD CONDENSATION NUCLEI,
CLOUDS

INTRODUCTION

Clouds can greatly affect local radiation balance at the surface. Any changes in cloud cover and properties due to climate change, could thus cause a considerable climatic feedback (Boucher et al., 2013). As any atmospheric process, cloud formation is deeply intertwined with processes taking place at the surface. The COntinental Biosphere-Aerosol-Clouds-Climate (COBACC) feedback loop (Kulmala et al., 2014) describes the complicated web of responses that CO₂ increase may drive in biosphere productivity, aerosol population and clouds; and ergo, the feedback that will eventually affect the energy balance and temperature at the surface. The boreal forest covers vast areas of the land mass in the northern hemisphere. It is a source of both secondary aerosol (Tunved et al., 2006) and water vapour (Zagirova et al., 2019), which are the essential components in cloud formation; aerosol particles grown large enough act as Cloud Condensation Nuclei (CCN), and thus enable droplet formation from the available water vapour. In our study, the aim is to observe the evolution of the factors related to cloud formation, resulting from an air mass transport over the Fennoscandian boreal forest. Eventually, we examine if an observable response can be detected in clouds as a result, as well as in accumulated precipitation.

METHODS

The analysis utilised 96-hour long HYSPLIT (Stein et al., 2015) back trajectories of air masses arriving to SMEAR II station in Hyytiälä (61°10'N, 24°17'E, 170m a.s.l.), , Finland, between years 2006 and 2016. To minimise anthropogenic contamination, we investigated only air masses that were either westerly, northerly or anything in between. We named this the 'Clean sector', as it is mostly covered by forests and has no large cities or other industrial sites of significant size in this context. Thus, only air masses traversing land areas north from 61°N and west from 30°W, were accepted, whereas trajectories from continental and eastern Europe were disregarded. Furthermore, we only considered the growing season i.e. months from April to September, as we wished to focus on months with active vegetation. For every trajectory, we calculated the Time (of travel) over Land (ToL). As the considered land areas are mostly covered by the boreal forest, we used this quantity as an indicator for the influence the forests had on the air mass. Simultaneous measurements of both in-situ and remote-sensed variables were compared to the ToL, to seek out any emerging trends. The in-situ observations of meteorological quantities and aerosol number concentrations were acquired from continuous measurements in Hyytiälä. Analysed cloud properties on the other hand, were

from open access satellite data products produced by NASA. They were based on measurements with the satellites MODIS Terra and Aqua.

CONCLUSIONS

The analysis presents further evidence of the boreal forest being a source of cloud condensation nuclei. Air masses with short transport times over the boreal forest are on average characterised by an aerosol profile of smaller particles, but the fraction of particles in the CCN size range grows when the exposure to the boreal forest is longer. However, the resulting positive trend between absolute number concentration of CCN and ToL only lasts until 60 hours at most, after which CCN concentration is stable and does not increase with added ToL.

The results also indicate that the boreal forest supplies water into the atmosphere. Specific humidity was higher in air masses with longer ToL. Temperature showed a similar trend and is thus likely to facilitate the increased uptake of water vapour, as relative humidity varied only little with different boreal transport times. The added atmospheric water vapour might also influence precipitation. Although most precipitation falls with relatively low ToL values that are associated with fronts, any rain that does fall at longer ToLs is likely to lead to a higher overall accumulation.

The higher CCN concentration and humidity at the surface might translate into altered cloud properties. A modest response in cloud optical thickness (COT) was observed, as the observed values were on average higher with longer ToLs. In a further examination in an attempt to unveil any potential Twomey effect (Twomey, 1977), we compared COT to simultaneous observations of liquid water path (LWP) and CCN. COT however only showed correlation with LWP, while remained largely unaffected by variation in CCN concentration. Weaker response to CCN is however expected, and it is likely the relatively small variation in the observed number concentrations is not enough to have a clear effect.

ACKNOWLEDGEMENTS

This study is part of the Pan-Eurasian Experiment program. The work was supported by the Academy of Finland Centre of Excellence under grant 307331.

REFERENCES

- Boucher, O., Randall, D., Artaxo, P., Bretherton, C., Feingold, G., Forster, P., and Kerminen, V. M. (2013). *Clouds and Aerosols*. Climate Change 2013: The Physical Science Basis. Intergovernmental Panel on Climate Change.
- Kulmala, M., Nieminen, T., Nikandrova, A., Lehtipalo, K., Manninen, H. E., Kajos, M. K., Kolari, P., Lauri, A., Petäjä, T., Krejci, R., Hansson, H.-C., Swietlicki, E., Lindroth, A., Christensen, T. R., Arneth, A., Hari, P., Bäck, J., Vesala, T., and Kerminen, V.-M. (2014). Co₂-induced terrestrial climate feedback mechanism: From carbon sink to aerosol source and back. *Boreal Environment Research*, 19.
- Stein, A. F., Draxler, R. R., Rolph, G. D., Stunder, B. J. B., Cohen, M. D., and Ngan, F. (2015). NOAA's hysplit atmospheric transport and dispersion modeling system. *Bulletin of the American Meteorological Society*, 96(12).
- Tunved, P., Hansson, H., Kerminen, V., Strom, J., Maso, M. D., Lihavainen, H., Viisanen, Y., Aalto, P., Komppula, M., and Kulmala, M. (2006). High natural aerosol loading over boreal forests. *Science*, 312(5771).

Twomey, S. (1977). Influence of pollution on shortwave albedo of clouds. *Journal of the Atmospheric Sciences*, 34(7).

Zagirova, S. V., Mikhailov, O. A., and Elsakov, V. V. (2019). Carbon dioxide and water exchange between spruce forest and atmosphere in springsummer under different weather conditions. *Contemporary Problems of Ecology*, 12(1).

Effect of particle composition on PSM cut-offs during the CLOUD experiments

B. Rörup¹, L. Dada¹, R. Baalbaki¹, J. Kangasluoma¹, M. Kulmala¹, K. Lehtipalo¹ and the CLOUD Collaboration

¹ Institute for atmospheric and Earth system research, University of Helsinki, Helsinki, Finland.

Keywords: particle size magnifier, cloud experiment, laboratory experiments.

INTRODUCTION

Atmospheric aerosols are liquid or solid particles suspended in the air and affect human life in many ways. They influence the radiative budget indirectly by acting as cloud condensation nuclei (CCN) and affect the microphysical properties of clouds and thereby their lifetime, albedo and precipitation efficiency (Curtius, 2009; Haywood, 2000). Furthermore, aerosol particles can scatter and absorb shortwave and longwave radiation, resulting in a direct radiative forcing (Lohmann, 2005). Even though aerosol particles have been investigated thoroughly, large uncertainties remain in understanding their direct and indirect effect on the climate.

There are many natural and anthropogenic sources of aerosol particles, which can emit particles into the atmosphere. Besides this primary aerosol formation, there is also the secondary aerosol formation, whereby new particle formation (NPF) is a key process. Small clusters and molecules grow in size and form a critical cluster, which subsequently grows to a detectable size (Kulmala, 2004; Kulmala, 2013). These clusters can either be electrically charged or neutral. According to Merikanto et al. 2010, 40 to 70% of cloud condensation nuclei are formed from nucleated particles. Since these newly formed particles are just 1 to 3nm big, it is challenging for many instruments to detect them. The neutral air ion spectrometer (NAIS) is able to detect charged clusters but can't detect neutral particles of that size. The particle size magnifier (PSM) can detect these small particles also in neutral conditions and in very small concentrations (Vanhanen 2011).

METHODS

In the cloud chamber in CERN (Conseil Européen pour la Recherche Nucléaire) experiments are being conducted under controlled atmospheric conditions to better understand the NPF mechanisms and aerosol-cloud interactions. The CLOUD (Cosmics Leaving OUtdoor Droplets) project uses a 26m³ stainless steel chamber which is surrounded by analysing equipment, that continuously extract samples from within the chamber. It is also the first experiment to reach the ultralow contamination levels necessary to qualitatively analyse aerosol nucleation and growth under precisely controlled conditions. Since 2006, when the CLOUD experiments started, 12 series of nucleation experiments have been performed at CERN. These experiments have brought valuable knowledge and important new findings.

The University of Helsinki provides Particle Size Magnifiers to study the NPF and the subsequent growth in the CLOUD chamber. The PSM is an aerosol pre-conditioner that grows aerosol particles as small as 1 nm to a size which can be detected by a CPC. Inside the saturator clean air is heated and exposed to diethylene glycol, which vaporises to the flow. Afterwards the flow is led to the cooled mixing part where it is turbulently mixed with the aerosol flow. Due to the cooling the diethylene glycol reaches supersaturation and starts to condense on the particles. After the mixing part, the sample flow is led through a cooled growth tube, where the condensing diethylene glycol causes the particles to grow. The particles are now big enough to be detected by the CPC

(Vanhanen 2011).

The PSM is the only instrument that can detect neutral concentrations of sub 3nm particles in the CLOUD chamber. Therefore, its data is important for the calculation of the formation rates and needs to be analysed carefully. During the CLOUD campaigns, new particle formation from different precursor vapours was studied under marine, biogenic and anthropogenic conditions. Since the PSM cut-off diameter is dependent on the chemical composition of the particles, the correct cut-off diameter needs to be found for every chemical system (Kangasluoma 2014). This was done by using the neutral air ion spectrometer (NAIS), which can measure the charged clusters and is not dependent on chemical composition. This data will be systematically analysed to determine the cut-off diameter for different chemical compounds, like sulphuric acid, iodic acid and organic particles. Additionally, laboratory experiments are conducted to verify the findings.

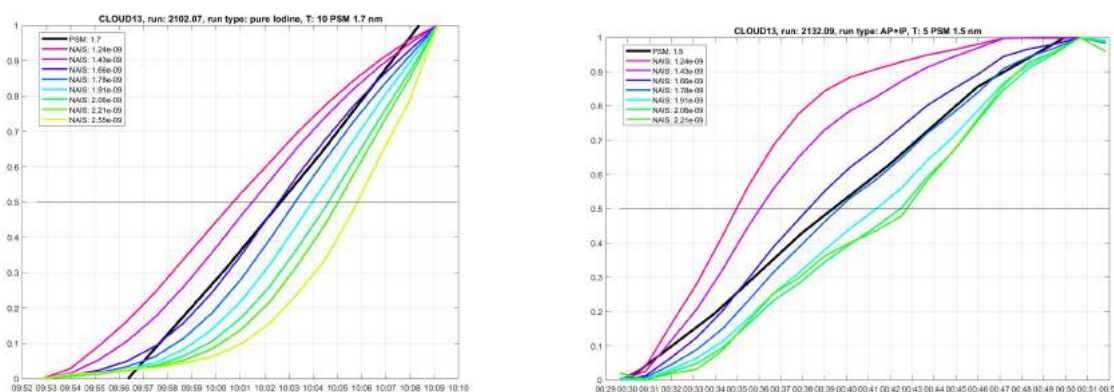


Figure 1: The PSM cut-off was compared to the NAIS cutoff for different chemical systems. On the left an example for an inorganic run with iodine and on the right an organic run with alphapinene and isoprene is shown.

CONCLUSIONS

The preliminary results show, that in the pure inorganic systems, the PSM agrees with the NAIS, whereas in the organic systems, the PSM classifies the particles as smaller as they are. Therefore a cut-off shift of +0.3nm is needed for pure organic systems to adjust the size. systems with organic and inorganic mixtures were also analysed and a cut-off shift of +0.15nm was determined.

Due to dedicated data analysis of past CLOUD campaigns, the cut-off diameter for pure organic samples as well as mixtures of organic and inorganic samples will be determined, which can be used for chamber experiments as well as for field studies.

ACKNOWLEDGEMENTS

This work has received funding from the European Union's Horizon 2020 research and innovation programme under the Marie Skłodowska-Curie grant agreement No 764991 (CLOUD-MOTION).

REFERENCES

Curtius, J. (2009). Nucleation of atmospheric particles *The European Physical Journal Conferences* 1, 199-209.

- Haywood, J. and Boucher, O. (2000). Estimates of the direct and indirect radiative forcing due to tropospheric aerosols: A review. *Reviews of geophysics* 38.4: 513-543.
- Lohmann, U., and Feichter, J. (2005). Global indirect aerosol effects: a review *Atmospheric Chemistry and Physics*, 5 (3), 715-737.
- Kangasluoma J., Franchin A., Duplissy J., Ahonen L., Korhonen F., Attoui M., Mikkilä J., Lehtipalo K., Vanhanen J., Kulmala M. and Petäjä T. (2016) Operation of the Airmodus A11 nano Condensation Nucleus Counter at various inlet pressures and various operation temperatures, and design of a new inlet system. *Atmospheric Measurement Techniques*, vol 9, no. 7, pp. 2977-2988.
- J. Kangasluoma, C. Kuang, D. Wimmer, M. P. Rissanen, K. Lehtipalo, M. Ehn, D. R. Worsnop, J. Wang, M. Kulmala, and T. Petäjä (2016) Sub-3nm particle size and composition dependent response of a nano-CPC battery. *Atmospheric Measurement Techniques*, 7(3), 689-700.
- Kulmala, M., et al. (2004) Formation and growth rates of ultrafine atmospheric particles: a review of observations. *Journal of Aerosol Science* 35.2: 143-176.
- Kulmala M, Kontkanen J, Junninen H, Lehtipalo K, Manninen HE, Nieminen T, et al. (2013) Direct Observations of Atmospheric Aerosol Nucleation. *Science* 2013; 339: 943-946.
- Merikanto J, Spracklen D, Mann G, Pickering S, Carslaw K. (2009) Impact of nucleation on global CCN. *Atmospheric Chemistry and Physics*; 9: 8601-8616.
- Pope III, C.A. and D.W. Dockery, (2012). *Health Effects of Fine Particulate Air Pollution: Lines that Connect*, . (Journal of the Air & Waste Management Association).
- Vanhanen, J., Mikkilä, J., Lehtipalo, K., Sipilä, M., Manninen, H. E., Siivola, E., Petäjä, T., and Kulmala, M.: (2011). *Particle size magnifier for nano-CN detection*. (Aerosol. Sci. Tech., 45, 533-542).

MULTIFRACTAL ANALYSIS OF VELOCITY AND TEMPERATURE FLUCTUATIONS IN THE ATMOSPHERIC SURFACE LAYER OVER THE HYYTIÄLÄ FOREST

Soumak Bhattacharjee¹, Rahul Pandit¹, Timo Vesala², Ivan Mammarella², and Ganapati Sahoo²

¹ Centre for Condensed Matter Theory, Department of Physics, Indian Institute of Science, Bangalore 560012, India

² Institute for Atmospheric and Earth System Research and Department of Mathematics and Statistics, University of Helsinki, Finland.

Keywords: Multiscale Multifractal Analysis; Atmospheric Boundary Layer; Hyytiälä Forest

INTRODUCTION

The characterization of the structure of non-stationary, noisy fluctuations in a time series, e.g., the time series of the velocity components or temperature in turbulent flows, is a problem of central importance in fluid dynamics, nonequilibrium statistical mechanics, atmospheric physics and climate science. Over the past few decades, a variety of statistical techniques, like detrended fluctuation analysis (DFA), have been used to reveal intricate, multiscaling properties of such time series. We present an analysis of velocity and temperature time series, which have been obtained by measurements over the canopy of Hyytiälä Forest in Finland.

In our study we use (a) DFA, (b) multifractal detrended fluctuation analysis (MFDFA) (Kantelhardt *et al.*, 2002), a generalization of DFA, and (c) the recently developed multiscale multifractal analysis (MMA) (Gieraltowski *et al.*, 2012; Zeng *et al.*, 2016), which is an extension of MFDFA. These methods allow us to characterize the rich hierarchy or *multifractality* of the dynamics of the time series of the velocity components and the temperature. In particular, we can clearly distinguish these time series from white noise and the signals that display simple, *monofractal*, scaling with a single exponent (also called the Hurst exponent). It is useful to recall that monofractal scaling is predicted for fluid turbulence at the level of the Kolmogorov's phenomenological approach of 1941 (K41); experiments and direct numerical simulations suggest that three-dimensional (3D) fluid turbulence must be characterised by a hierarchy of exponents for it is truly multifractal.

MEASUREMENTS

The wind-speed and the air temperature time series have been measured in the atmospheric surface layer above Hyytiälä forest, in Southern Finland, at the SMEAR II station (61°51' N, 24°17' E), which is 181m above the mean sea level. This is a boreal coniferous forest that has Scots pine trees, with an average height of 17m. The measurements, which we present here, have been carried out with three-dimensional (3D) sonic anemometers at heights of 23.3m and 33m with sampling frequencies of 10Hz. Our MFDFA and MMA studies have been carried for 30-minute traces that have been obtained in the summers of 2015 and 2016.

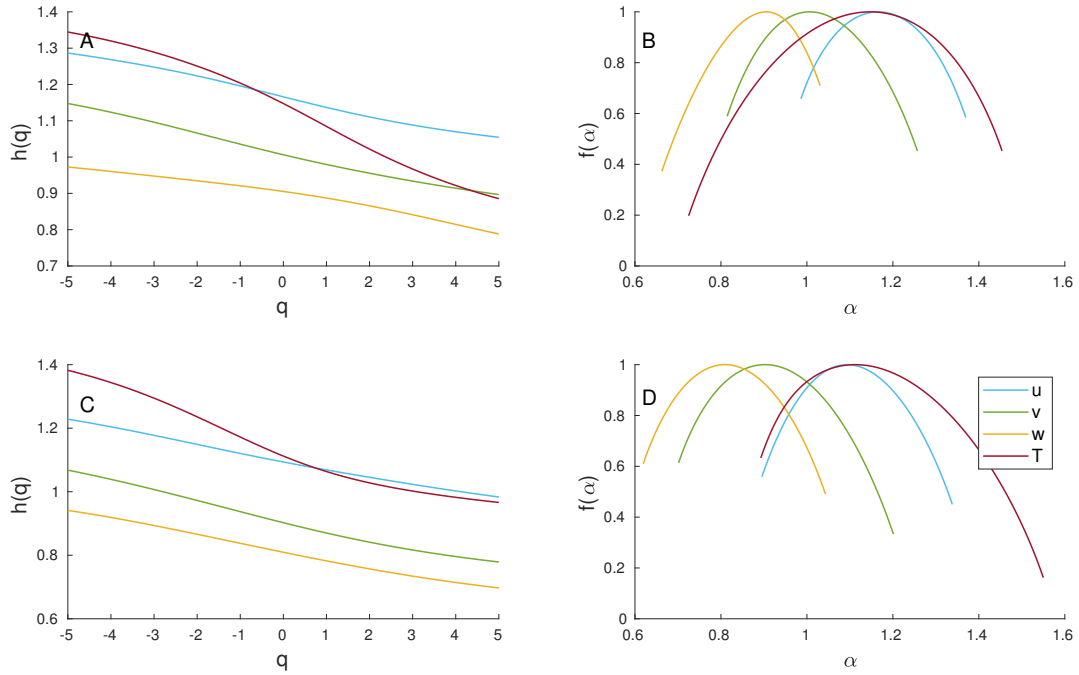


Figure 1: MF DFA results for the Hurst exponents $h(q)$ the singularity spectra $f(\alpha)$ for the temperature and all three components of the velocity for the measurements at heights of 23.3 m (top panel) and 33 m (bottom panel)

METHODS

Multifractal Detrended Fluctuation Analysis (MF DFA):

In the MF DFA (Kantelhardt *et al.*, 2002), the time series is partitioned into intervals of length s and the averaged order- q fluctuation function $F_q(s)$ is calculated (we refer the reader to Ref. (Kantelhardt *et al.*, 2002) for the exact formula for $F_q(s)$). The scaling exponent of $F_q(s)$ is $h(q)$; this is the q -dependent Hurst exponent that measures the degree of multifractality. The singularity spectrum $f(\alpha)$ is the Legendre transform of the classical multifractal scaling exponent $\tau(q) \equiv qh(q) - 1$, i.e., $f(\alpha) = q\alpha - \tau(q)$, where $\alpha = \tau'(q)$.

Multiscale Multifractal Analysis (MMA):

The multiscale multifractal analysis (MMA) consists of calculating the local scaling of $F_q(s)$ to obtain the local Hurst exponent, $h(q, s)$. For a stationary monofractal time series, this does not contain any extra information. But when $F_q(s)$ shows a scale-dependent differential scaling, which is often the case, it contains a much richer structure as it reflects the behaviour of fluctuations of all amplitudes. We obtain the local Hurst exponent $h_q(s)$ and study it especially in the small-, medium-, and large- s ranges $16 \lesssim s \lesssim 50$, $150 \lesssim s \lesssim 200$, and $500 \lesssim s$.

We have built on the routines outlined in Ref. (Ihlen *et al.*, 2012) for our MF DFA and MMA.

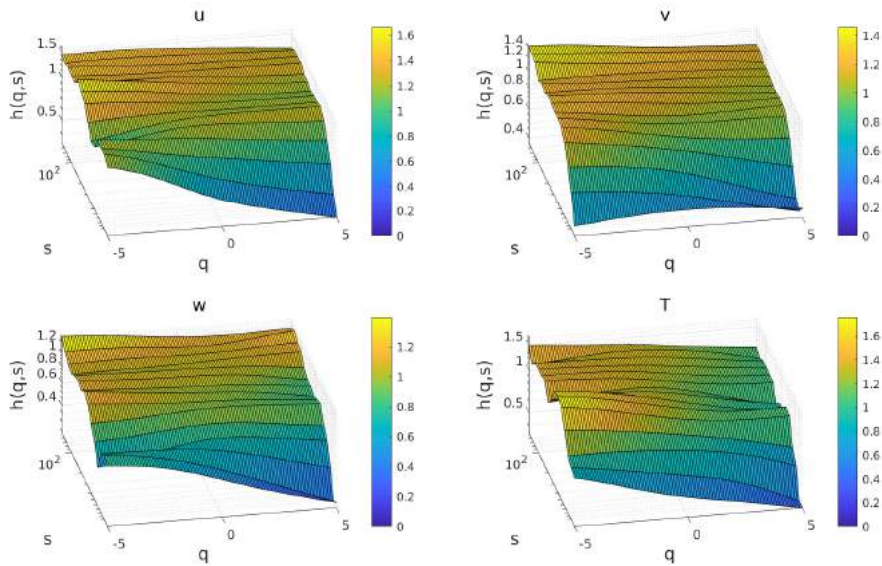


Figure 2: Hurst surface $h(q, s)$ at $z = 23.3m$

RESULTS

Illustrative plots of our MFDFA results for the Hurst exponents $h(q)$ the singularity spectra $f(\alpha)$ for the temperature and all three components of the velocity are given in Fig. 1 for the measurements at heights of 23.3 m (top panel) and 33 m (bottom panel). The widths of the $f(\alpha)$ multifractal spectra is a clear measure of this multifractality; the difference between these spectra, for different components of the velocity, characterises the anisotropy of this flow. By comparing the plots in the top and bottom panels, we see that the multifractality decreases with an increase in the height, at which we measure the velocity and temperature fields.

In Figs. 2 and 3 we show, respectively, for the measurements at heights of 23.3m and 33m, plots of $h(q, s)$ versus q and s . We see that $h(q, s)$ decreases as q and s increase; a section through these plots, with a fixed value of s , yield plots that are similar to those of $h(q)$ in Fig. 1.

CONCLUSIONS

We present an analysis of multifractality of velocity and temperature fields that have been measured, at different heights, over the canopy of Hyytiälä Forest in Finland. In particular, we carry out a detailed study of velocity and temperature time series by using MFDFA and MMA. Results from both these methods are consistent, as they must be; but, of course, the MMA results contain more information because they account for the dependence of the multifractality in the scale s . A detailed examination of our results will be published elsewhere.

ACKNOWLEDGEMENTS

We thank AtMath collaboration at University of Helsinki and the DST and CSIR (India) for support.

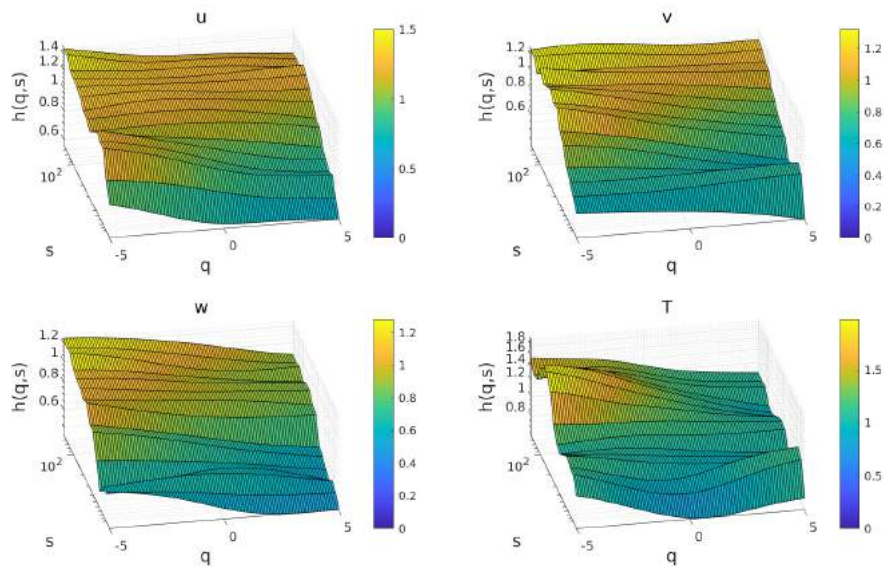


Figure 3: Hurst surface $h(q, s)$ for $z = 33m$

REFERENCES

- J. Gieraltowski, J. J. Zebrowski and R. Baranowski (2012). Multiscale multifractal analysis of heart rate variability recordings with a large number of occurrences of arrhythmia. *Physical Review E* 85, 021915
- Jan W. Kantelhardt, Stephan A. Zschiegner, Eva Koscielny-Bunde, Shlomo Havlin, Armin Bunde, H. Eugene Stanley (2002). Multifractal detrended fluctuation analysis of nonstationary time series. *Physica A* 316
- Ming Zeng, Xiao-Nei Zhang, Jing-Hai Li, Qing-Hao Meng (2016). The Scaling Properties Of high-frequency wind speed records based on Multiscale Multifractal Analysis. *ACTA PHYSICA POLONICA B*
- Espen A. F. Ihlen (2012) Introduction to multifractal detrended fluctuation analysis in Matlab. *Frontiers in Physiology*

THE ROLE OF LIVING BARK IN *BETULA PENDULA* ABILITY TO REFILL EMBOLISED XYLEM

Y. SALMON¹, A. LINTUNEN¹, M. TIAN¹, H. SUHONEN², T. VESALA¹, and T. HÖLTTÄ¹

¹Institute for Atmospheric and Earth System Research, University of Helsinki

²Department of Physics, University of Helsinki, Helsinki, Finland

Keywords: PHLOEM, SILVER BIRCH, SUGAR, STARCH.

INTRODUCTION

Embolism formation and its potential run away spreading through the plant vascular system has received a lot of attention in the recent years, as it appears central to the observed drought-induced mortality of trees. However, the tree ability to recover from such embolism has received less attention. In particular, the tree ability to refill embolism causes by drought or freezing stress is under debate in the last recent years. This debate has been fuelled by the discovery that some earlier method used to assess tree embolism and refilling ability were prone to artefact (e.g., Wheeler et al. 2013). And if or when refilling happens, the mechanisms allowing it remains unknown despite several hypothesis (Nardini et al. 2011).

However, our recent studies have nonetheless shown that silver birch (*Betula pendula*) might be able to refill (Salmon et al. 2018), and hypothesised that it might be related to its ability to pressurised sap in the spring prior to budburst (Hölttä et al. 2018). These earlier studies led to two hypothesis about the mechanisms involved in the refilling process: 1) the phloem in the living bark plays a role in initiating the refilling; 2) the refilling process is an activate process involving energy cost for the tree, which are supplied by the stored starch and non-structural carbohydrates.

We conducted an experiment to test these two hypothesis and further explore the mechanisms underlying birch refilling ability.

METHODS

Branches of silver birch were sampled at the greenhouse of the university of Helsinki, Viikki campus. The sampled branches were longer than 70cm and without divisions. The sample was let to bench dry until fully embolised and not conductive., with a water potential (Ψ) lower than -3 MPa (Choat et al. 2012) as controlled by water potential measurement of a 10 cm subsample with a pressure chamber. The samples were divided in two subsamples of more than 30cm length to avoid open vessels artefacts. One subsample was peeled of its bark, phloem and cambium and wrap with PTFE tap to limit evaporation and avoid leakage during the refilling experiment.

For each subsample, hydraulic recovery was induced with a small hydraulic positive pressure provided by a water column attached to the upper end of the branches held vertically on a stand. The amount of water flowing through each subsample was recorded with balances to measure the restoration of the hydraulic conductivity.

After each measurement, a 5 to 10cm piece was cut from the subsamples and used to measure non-structural carbohydrates and starch concentrations. The cut piece was frozen in liquid nitrogen to stop enzymatic activity, dried and ground to powder and stored until analyses. The procedure continues with

shorten sub-samples until the branches stopped being able to refill or became too short for further measurements (i.e. after a maximum of three refilling attempts).

We also measured the osmolality of the first drop of sap coming out of the refilling branches to assess whether refilling might have happened by loading sugars in the xylem to osmotically draw water from surrounding cells.

CONCLUSIONS

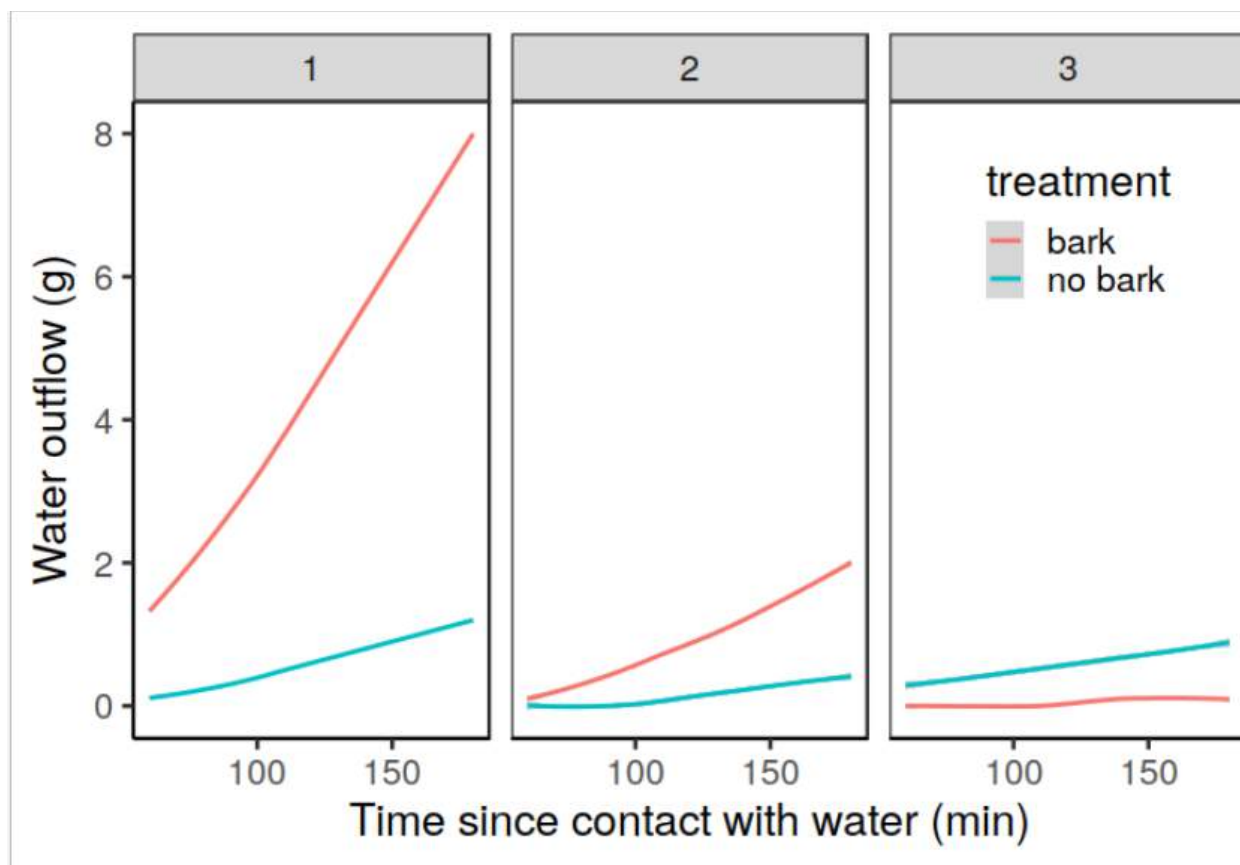


Figure 1: Amount of water conducted through a branch of silver birch as a function of time since the branches was put in contact with water per successive runs of embolism and refilling (1, 2 and 3) for sub-samples with the living bark intact (“bark”, red) or with the living bark removed (“no bark”, blue).

The preliminary results show the presence of living bark originally allows the studied branches to restore conductivity faster than the branches on which living bark has been removed (Fig. 1, panel 1). The refilling ability of branches with living bark clearly declines with the number of refilling events (compare runs 1, 2 and 3), eventually becoming smaller than that of the branches without bark.

The osmolality of the sap after refilling is not sufficient to explain the refilling through sugar loadings in the embolised xylem.

On-going measurements of non-structural carbohydrates and starch are expected to shed further light on the potential mechanisms underlying these differences between treatments as well as improve our understanding of the mechanisms underlying silver birch refilling ability.

ACKNOWLEDGEMENTS

Funding from Academy of Finland: Academy professors project of Timo Vesala (#312571).

REFERENCES

- Choat B., Jansen S., Brodribb T.J., Cochard H., Delzon S., Bhaskar R., Bucci S.J., Field T.S., Gleason S.M., Hacke U.G. et al. (2012). Global convergence in the vulnerability of forests to drought. *Nature* 491: 752–756
- Hölttä, T., Dominguez, M., Salmon, Y., Aalto, J., Vanhatalo, A., Bäck, J. and A. Lintunen (2018). Water relations in silver birch during springtime. How is sap pressurized? *Plant Biology*, 20: 834-847.
- Nardini, A., Lo Gullo, M.A., and Salleo, S. (2011). Refilling embolized xylem conduits: Is it a matter of phloem unloading? *Plant Sciences*. 180, 604-611.
- Salmon, Y., Lintunen, A., Lindfors, L. Suhonen, H., Sevanto, S., Vesala, T. and T. Hölttä (2018). Silver birch ability to refill fully embolised xylem conduits under tension. *Acta Horticulturae*, 1222, 67-73.
- Wheeler JK, Huggett BA, Tofte AN, Rockwell FE, Holbrook NM (2013) Cutting xylem under tension or supersaturated with gas can generate PLC and the appearance of rapid recovery from embolism. *Plant Cell and Environment*, 36, 1938-1949

PARTICIPATORY CLIMATE COMMUNICATION PLATFORM: SERVICE FOR CITIZENS AND RESEARCHERS

M.A. SANTALA¹, R. MAKKONEN^{2,1}

¹Institute for Atmospheric and Earth System Research, University of Helsinki, Finland.

²Finnish Meteorological Institute, Helsinki, Finland.

Keywords: CLIMATE COMMUNICATION, CLIMATE EDUCATION, CITIZEN SCIENCE, SOCIAL MEDIA.

INTRODUCTION

Media coverage of climate change is higher than ever in Finland (Nikkanen, 2017), however the public confidence in climate science is lacking (Harmanen and Mervaala, 2017; Hallamaa, 2018; Ilmastobarometri, 2019; Cook et al., 2013), and the voice of scientists is drowning in public debate (Lehtonen and Cantell, 2015). This Master's thesis (Santala, 2019) is a case study that provides an approach to promote climate science and communication by social media. Interaction supports phenomenon-based learning (Lehtonen ja Cantell, 2015), providing interdisciplinary and user-friendly climate change information that is easily applicable to everyday life. Dialogue enables meeting the citizens needs and motives, which increases the impact of communication (Jylhä, 2016; Sturgis and Allum, 2004; Wilcox, 2012). In particular, personal face-to-face interaction enhances participants' commitment, sense of belonging and stability of results (Broockman and Kalla, 2016; Cook and Overpeck, 2018; Pina et al., 2017).

METHODS

The study provides information on why interactive climate communication and citizen science have good potential to promote climate science and increase the public trust in it. The thesis demonstrates by use cases and communication and education theories, how the social media based approach increases understanding of climate system and climate change, as well as climate science and its research methods. The focus of the study is the interactive climate communication platform (Kysyilmastosta.fi) involving citizens and researchers, and enabling direct and reciprocal online communication between them. In addition to the web service, the package also includes citizen science workshops where citizens participate in the design and planning of research projects.

Online communication principle for the web service is that citizens ask climate related questions and researchers answer to them. The web service and its materials are open to all, so the web site can serve as a data bank for citizens, while researchers can find new research questions from there. The material consisting of citizens' questions also serves research and development of climate education. Students attending climate change courses (e.g. Climate.now) post questions on the web service, and those questions will be used for mapping students' expectations, development points of the course and the impact of climate education.

DISCUSSION

The web service provides researchers an easy channel to present their research and make their voice heard in the public debate. In current network society, presence in social media and public debate are crucial for influencing public perceptions (Castells, 2010). By listening to citizens, researchers are able produce information that benefits the society (Juholin, 2006). This social media based approach supports intersectoral collaboration that is required for climate research as well as climate change mitigation and adaptation (Hilden et al., 2016). The whole service package is scalable to international level and therefore has the potential to promote international cooperation as well.

ACKNOWLEDGEMENTS

This work was supported by the Institute for Atmospheric and Earth System Research (INAR), University of Helsinki.

REFERENCES

- Broockman, D. and Kalla, J. (2016). Durably reducing transphobia: A field experiment on door-to-door canvassing, *Science*, **352**, 6282.
- Castells, M. (2010). *The Rise of the Network Society*, (Blackwell Publishing, Cambridge, U.K.).
- Cook, J., Nuccitelli, D., Green, S., Richardson, M., Winkler, B., Painting, R., Way, R., Jacobs, P. and Skuce, A. (2013). Quantifying the Consensus on Anthropogenic Global Warming in the Scientific Literature, *Environmental Research Letters*, **8**, 2.
- Cook, B. and Overpeck, J. (2018). Relationship-building between climate scientists and publics as an alternative to information transfer, *WIREs Climate Change*, **10**, 2.
- Hallamaa, T. (2018). Ylen kysely: Suomalaisilla on taas varaa olla huolissaan ilmastonmuutoksesta, *Yle.fi*, 2.1.2018. Available at <https://yle.fi/uutiset/3-9998441> (last accessed 6.5.2019).
- Harmanen, S. and Mervaala, E. (2017). Tosi valheita, *Hyvän sään aikana*, (Into Kustannus Oy, Helsinki, Finland).
- Hilden, M., Groundstroem, F., Carter, T., Halonen, M., Perrels, A. and Gregow, H. (2016). Crossborder effects of climate change in Finland, *Publications of the Government's analysis, assessment and research activities*, **46**, (prime Minister's office, Helsinki, Finland).
- Ilmastobarometri (2019). Ilmastobarometri 2019 –tiivistelmä, *Ilmastobarometri 2019*, (Valtionhallinnon ilmastoviestinnän ohjausryhmä). Available at <https://www.ym.fi/download/noname/%7B85477EF4-C481-4BDE-804D-A0D0F2D6A820%7D/144778> (accessed 18.4.2019).
- Juholin, E. (2006). *Communicare! Viestintä strategiasta käytäntöön*, (WS Bookwell, Porvoo, Finland).
- Jylhä, K. (2016). Denial Versus Reality of Climate Change, in DellaSala, D. and Goldstein, M. (edit.) *Encyclopedia of the Anthropocene*, (Elsevier). Available at https://www.researchgate.net/publication/311915469_Denial_Versus_Reality_of_Climate_Change (accessed 8.2.2019).
- Lehtonen, A. and Cantell, H. (2015). Ilmastokasvatus osaamisen ja vastuullisen kansalaisuuden perustana, *Suomen ilmastopaneelin raportteja 1/2015*, (Suomen ilmastopaneeli). Available at <https://www.ilmastopaneeli.fi/wp-content/uploads/2018/10/Ilmastokasvatuksen-raportti-9.6.2015.pdf> (accessed 14.2.2019).
- Nikkanen, H. 2017: Uutisista suurin, *Hyvän sään aikana*, (Into Kustannus Oy, Helsinki, Finland).
- Pina, V., Torres, L. and Royo, S. (2017). Comparing online with offline citizen engagement for climate change: Findings from Austria, Germany and Spain, *Government Information Quarterly*, **34**, 1.
- Santala, M.A. (2019). *Osallistava toimintamalli ilmastoviestintään: verkkopalvelu kansalaisille ja tutkijoille*. Master's thesis, Institute for Atmospheric and Earth System Research, University of

Helsinki, Finland. Available at <https://helda.helsinki.fi/handle/10138/303433> (accessed 24.10.2019).

Sturgis, P. and Allum, N. (2004). Science in society: re-evaluating the deficit model of public attitudes, *Public Understanding of Science*, **13**.

Wilcox, C. (2012). Guest Editorial: It's Time To e-Volve: Taking Responsibility for Science Communication in a Digital Age, *The Biological Bulletin*, **222**, 2.

FIRST RESULTS OF MULTI-SCHEME CHEMICAL IONIZATION INLET MEASUREMENTS IN BOREAL FOREST

N. SARNELA¹, J. HAKALA², O. KAUSIALA², J. MIKKILÄ², T. PETÄJÄ¹, M. SIPILÄ¹ and M. KULMALA¹

¹Institute for Atmospheric and Earth System Research (INAR) / Physics, University of Helsinki, FI-00014 Helsinki, Finland

²Karsa, A. I. Virtasen aukio 1, 00560, Helsinki. Finland

Keywords: chemical ionization, mass spectrometry, ambient ions, low-volatility vapours

INTRODUCTION

In new particle formation molecular clusters form from atmospheric vapours by condensation and/or chemical reactions, thus, the presence of suitable low-volatility vapours is crucial for new particle formation. In favourable conditions the clusters can grow into larger particle sizes and act as cloud condensation nuclei. New measurement techniques have enabled the on-site measurements for low-volatility compounds but due to the expenses and high maintenance of the measurements, despite their importance these low-volatile compounds have not been comprehensively measured.

Atmospheric Pressure interface Time of Flight Mass Spectrometry (APi-TOF-MS) is a versatile tool to study atmospheric ions (Junninen *et al.* 2010) and, when coupled with chemical ionization, also vapours (Jokinen *et al.* 2012). A selective ionization method is needed to separate the compounds of interest from the complex gas mixture and the selectivity of the chemical ionization method can be altered by using different reagent ions. Often it is not possible to measure all the compounds of interest with only one reagent ion chemistry which means that there is a need for measuring with multiple ion chemistries simultaneously, but having several mass spectrometers at a same measurement site may not be feasible due to their high expense. We have developed a new chemical ionization inlet which enables fast switching between several reagent ion chemistries and also allows the measurement of ambient ions without contaminating the inlet with reagent vapours.

METHODS

We have measured ambient ion and low-volatility vapour concentrations using Multi-scheme chemical IONization Inlet (MION, Rissanen *et al.* 2019) combined with APi-TOF-MS at SMEAR II station (Station for Measuring Ecosystem-Atmosphere Relations, Hyytiälä, southern Finland) starting from November 2018. In these measurements we have used a measurement cycle with two reagent ions: nitrate and bromide. In addition we have measured the ambient ions and done regular zero measurements. The measurement cycle consist of 8 minutes chemical ionization with nitrate ion, 8 minutes chemical ionization with bromide ion followed by 10 minutes of ambient ion measurements and 4 minutes zero measurements. Ion filter was used during the chemical ionization modes to ensure measurements of only neutral vapours and molecular clusters. The reagent ion signals during the measurement cycle are shown in Figure 1.

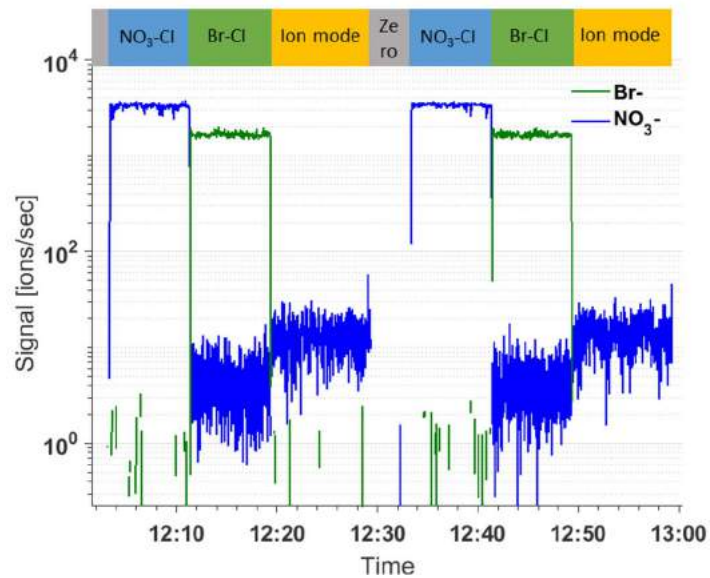


Figure 1. The reagent ion signals during two measurement cycles. We can see that the switching from one mode to another happens very fast and no memory effect from previous mode can be seen.

RESULTS

The new inlet has functioned well in continuous measurements without any sign of reagent (HNO_3 or CH_2Br_2) contamination in other modes. Examples of mass spectra of different modes can be seen in Figure 2.

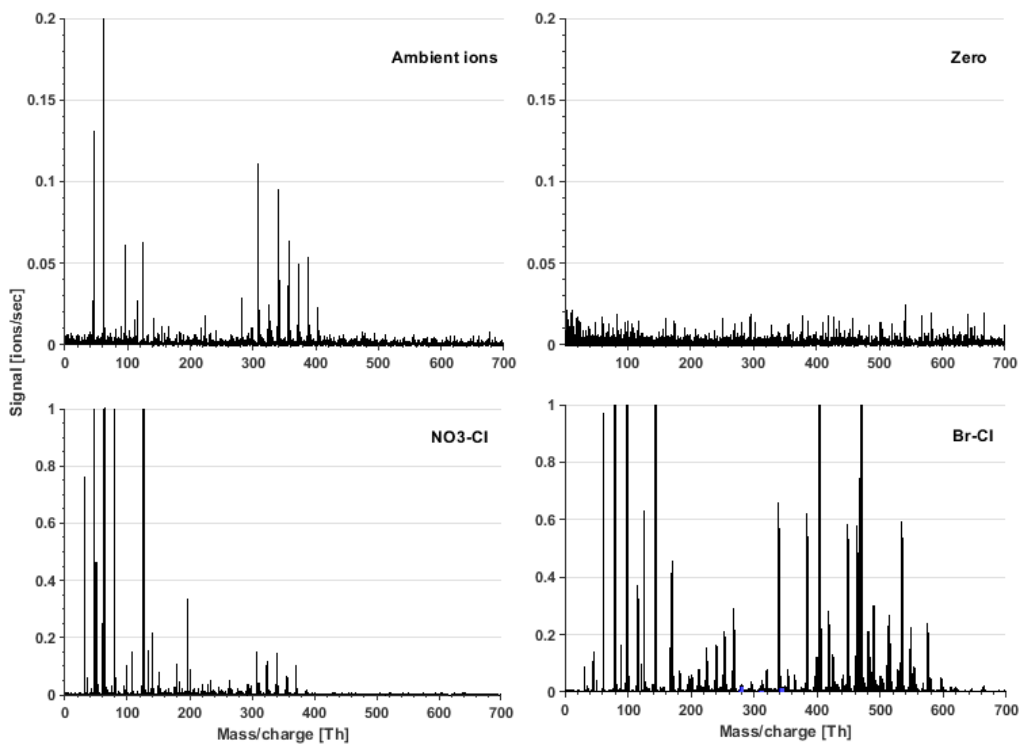


Figure 2. Examples of the mass spectrum of each mode measured at SMEAR II station.

Ambient ion mode is highest in sensitivity and we can detect charged molecular clusters with it. The zero mode shows that the observed ions are not formed in the inlet. With Br-CIMS we can detect HO₂ radical, sulphuric acid and least oxidized organic compounds while with NO₃-CIMS we can detect sulphuric acid, iodic acid, methane sulfonic acid and highest oxidized organic compounds.

We have long term measurements with another NO₃-CI-APi-TOF using inlet that is described by Eisele and Tanner (1993) at SMEAR II station at 35 m altitude. We have compared MION NO₃-mode results with those and found good agreement (example of sulphuric acid concentrations is shown in figure 3.). The MION measurement are done at ground level so some variation in concentrations is due to the altitude difference.

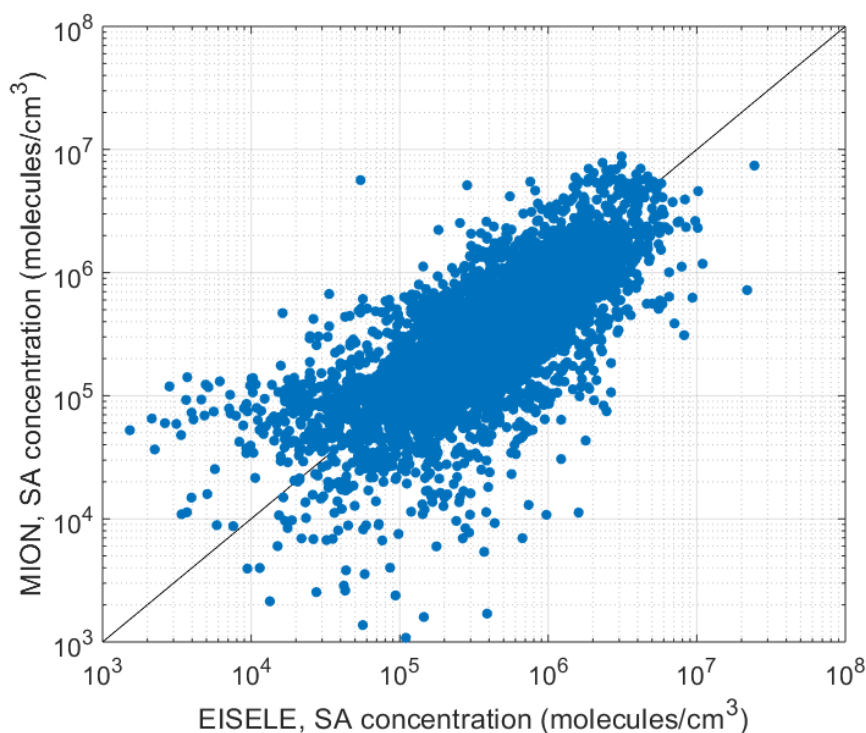


Figure 3. Comparison on sulphuric acid concentrations measured with Eisele-inlet at 35 m altitude and MION inlet at ground level (March –July 2019).

CONCLUSIONS AND OUTLOOK

We have measured ions, vapours and molecular clusters with MION-inlet in Boreal forest for 11 months. We have compared the results with another NO₃-CI-APi-TOF at the site and found good agreement with the concentrations. The instruments are measuring at different altitudes and some intercomparison with them at same altitude would be needed to understand the variation in concentration levels. More data analysis is needed to identify the organic compounds measured with Br-mode.

ACKNOWLEDGEMENTS

All the researchers contributing to the Hyytiälä long term measurements and Hyytiälä personnel are acknowledged for their help in conducting the measurements. We thank the tofTools team for providing tools for mass spectrometry data analysis. This work was supported by the Centre of Excellence program of the Academy of Finland (project 272041) and the Advanced Grant program of the European Research Council (project 227463).

REFERENCES

- Eisele F. and Tanner D. (1993) Measurement of the gas phase concentration of H₂SO₄ and methane sulfonic acid and estimates of H₂SO₄ production and loss in the atmosphere, *J. Geophys Res.* **98**, 9001-9010.
- Jokinen, T., Sipilä, M., Junninen, H., Ehn, M., Lönn, G., Hakala, J., Petäjä, T., Mauldin, R. L., Kulmala, M. and Worsnop, D. R. (2012) Atmospheric sulphuric acid and neutral cluster measurements using CI-API-TOF, *Atmos. Chem. Phys.*, **12**, 4117–4125.
- Junninen, H., Ehn, M., Petäjä, T., Luosujärvi, L., Kotiaho, T., Kostianen, R., Rohner, U., Gonin, M., Fuhrer, K., Kulmala, M. and Worsnop, D. R. (2010) A high-resolution mass spectrometer to measure atmospheric ion composition *Atmos. Meas. Tech.*, **3**, 1039–1053.
- Rissanen, M. P., Mikkilä, J., Iyer, S. and Hakala, J. (2019) Multi-scheme chemical ionization inlet (MION) for fast switching of reagent ion chemistry in atmospheric pressure chemical ionization mass spectrometry (CIMS) applications, *Atmos. Meas. Tech. Discuss.*, *in review*.

VOC FLUXES FROM A BOREAL FOREST MEASURED BY VOCUS PTR-TOF: A FIRST LOOK

S. SCHALLHART¹, H. LI², P. A. RANTALA², F. BIANCHI², M. EHN², H. HELLÉN¹

¹Finnish Meteorological Institute, P.O. Box 503, 00101 Helsinki, Finland

²Institute for Atmospheric and Earth System Research INAR / Physics, Faculty of Science, University of Helsinki, Finland.

Keywords: VOCs, VOCUS PTR-TOF, EDDY COVARIANCE, FLUXE, SMEAR II, SESQUITERPENES.

INTRODUCTION

Volatile organic compounds (VOCs) play important roles in the biosphere and the atmosphere. Plants use them to communicate or as remedy for various kinds of stress. Released to the atmosphere, these VOCs are major participants in atmospheric chemistry and are important for the air quality as well as for aerosol formation and climate. Measuring VOCs can be very challenging, as their number is estimated to be well over 10^6 different molecules (Goldstein and Galbally, 2016), which can be present in very low concentrations. This is caused partly by their reactivity, where one emitted compound can lead to a cascade of oxidation products, which all have their respective properties (e.g. life-time, volatility, ozone formation potential). To understand atmospheric chemistry, it is crucial to know the exchange between the biosphere and the atmosphere.

The SMEAR II station in Hyytiälä, Finland, has a long history of VOC emission and flux measurements. The first flux measurements were conducted in 1998 (Rinne et al., 2000), using the gradient method and offline samples, which were analysed in the laboratory. This method uses two simultaneous measurements of VOCs with a vertical displacement, which need to be analysed exactly the same way, so that there is no difference in treatment of the samples. However, for this method empirical transfer coefficients need to be calculated. Other emission measurements in Hyytiälä used branch chambers (e.g. Tarvainen et al., 2005; Hakola et al., 2006). This method has low instrumental requirements, as the measured concentrations are quite high and the analyser can be slow. It excels in finding emission mechanisms of a branch, however, enclosing a branch can disturb it and alter the emissions. Also, it is unclear how representative one branch is when upscaling the emissions to forest scale (Acton et al., 2017). Another way to measure direct fluxes, i.e. without empirical coefficients, is eddy covariance (EC). The method is used to calculate ecosystem exchange using high frequency measurements. This is very challenging for the instruments, as whole VOC spectra must be measured with 10 Hz time resolution. In Schallhart et al. (2018) EC VOC fluxes were measured using a Proton Transfer Reaction-Time Of Flight (PTR-TOF 8000; Ionicon Analytik GmbH) mass spectrometer. Overall, the exchange of 25 different VOCs was measured, but especially compounds with higher masses, like sesquiterpenes, which were measured in branch chambers, could not be seen. The used instrument seemed not sensitive enough, and the wall losses in the setup too high.

METHODS

We will present the first results of EC flux measurements using a VOCUS PTR-TOF (Tofwerk AG; Krechmer et al., 2018). Compared to the PTR-TOF 8000 in Schallhart et al. (2018) the sensitivity should be approximately 100 times higher. Also the mass resolution ($\frac{\Delta m}{m}$) is three times higher in the VOCUS, which makes the identification of multiple peaks easier. To reduce the losses in the inlet system, the instrument was lifted to a container mounted atop of a tower, which allowed to shorten the inlet tubing drastically (Fig.

1). Also all inlet flows were increased, to shorten the time the air has to interact with the walls inside the inlet tubing. Overall, the inlet in Schallhart et al. (2018) was 20 m long pumped with 20 L min⁻¹, while the new setup has a 3 m inlet, flushed with over 200 L min⁻¹. The measurements were done during a 2 week window and are used as proof of concept for the campaign next year.



Figure 1. 3D-anemometer with part of the 3 m inlet tube. In the background the main source of the emissions (forest) can be seen.

In summer 2020, we plan to have VOC fluxes (VOCUS PTR), speciated VOC concentrations (GC-MS) and OH reactivity (Comparative Reactivity Method; Sinha et al., 2008) measured next to each other, to investigate the sesquiterpene fluxes and their influence to the OH reactivity.

CONCLUSIONS

At the moment the data is still being processed, which is challenging, as the VOCUS PTR records over 45 GB of data per day. Therefore the fitting of the VOC spectra to get time series of the individual compounds is very time intensive. The VOC spectra look very promising, as clear peaks of sesquiterpenes can be seen in the 30 min averaged spectra (Fig. 2) and the first flux results will be soon available.

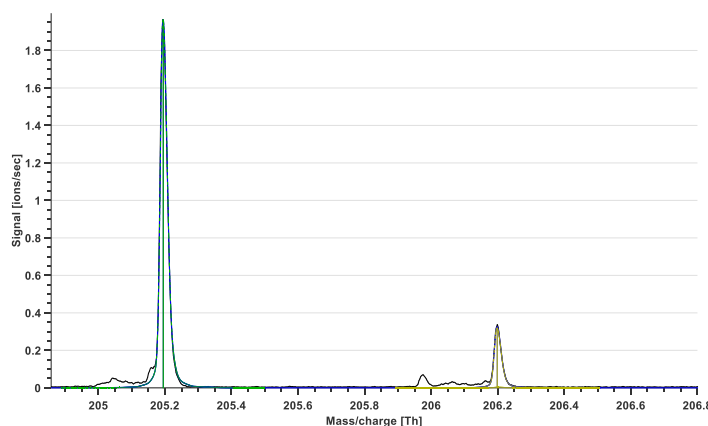


Figure 2. Mass spectrum from the 30.09.2019 at 12:00 (30 min averaged) showing the protonated sesquiterpene peak at 205.195 Th and its isotope at 206.198 Th.

ACKNOWLEDGEMENTS

The research was supported by the Academy of Finland via the Postdoctoral researcher grant (323255) and Academy of Finland via the Center of Excellence in Atmospheric Sciences (grant no. 307331). Many thanks also to the SMEAR II staff for all the logistical help and the ToFTools team for providing tools for mass spectrometry analysis.

REFERENCES

- Acton, W. J. F., Schallhart, S., Langford, B., Valach, A., Rantala, P., Fares, S., Carriero, G., Tillmann, R., Tomlinson, S. J., Dragosits, U., Gianelle, D., Hewitt, C. N., and Nemitz, E (2016). Canopy-scale flux measurements and bottom-up emission estimates of volatile organic compounds from a mixed oak and hornbeam forest in northern Italy, *Atmos. Chem. Phys.*, 16, 7149-7170.
- Goldstein, A. H. and Galbally, I. E (2007). Known and unexplored organic constituents in the Earth's atmosphere, *Environ. Sci. Technol.*, 41, 1514–1521, <https://doi.org/10.1021/es072476p>.
- Hakola, H., Tarvainen, V., Bäck, J., Ranta, H., Bonn, B., Rinne, J., and Kulmala, M (2006). Seasonal variation of mono- and sesquiterpene emission rates of Scots pine, *Biogeosciences*, 3, 93-101, doi:10.5194/bg-3-93-2006.
- Krechmer, J., Lopez-Hilfiker, F., Koss, A., Hutterli, M., Stoermer, C., Deming, B., Kimmel, J., Warneke, C., Holzinger, R., Jayne, J. T., Worsnop, D. R., Fuhrer, K., Gonin, M., and deGouw, J. A. (2018). Evaluation of a New Reagent-Ion Source and Focusing Ion-Molecule Reactor for use in Proton-Transfer-Reaction Mass Spectrometry, *Anal. Chem.*, 90, 12011–12018, <https://doi.org/10.1021/acs.analchem.8b02641>.
- Rinne, J., Hakola, H., Laurila, T. and Rannik, U. (2000). Canopy scale monoterpene emissions of *Pinus sylvestris* dominated forests *Atmospheric Environment*, 34, pp. 1099-1107.
- Schallhart, S., Rantala, P., Kajos, M. K., Aalto, J., Mammarella, I., Ruuskanen, T. M. and Kulmala M.: Temporal variation of VOC fluxes measured with PTR-TOF above a boreal forest, *Atmospheric Chemistry and Physics*. 18, 2, s. 815-832.
- Sinha, V., Williams, J., Crowley, J. N., and Lelieveld, J (2008). The Comparative Reactivity Method – a new tool to measure total OH Reactivity in ambient air, *Atmos. Chem. Phys.*, 8, 2213-2227, <https://doi.org/10.5194/acp-8-2213-2008>.
- Tarvainen, V., Hakola, H., Hellén, H., Bäck, J., Hari, P., and Kulmala, M (2005). Temperature and light dependence of the VOC emissions of Scots pine, *Atmos. Chem. Phys.*, 5, 989-998, doi:10.5194/acp-5-989-2005.

USING A WHOLE TREE CARBON ISOTOPE MODEL TO EVALUATE MESOPHYLL CONDUCTANCE HYPOTHESES AND TO LINK WEATHER TO PHLOEM SUGAR ISOTOPIC COMPOSITION

P. SCHIESTL-AALTO^{1,2}, Z.R. STANGL², L. TARVAINEN³, G. WALLIN³, J. MARSHALL, A. MÄKELÄ¹²

¹Institute for atmospheric and earth system research (INAR) / Forest sciences, Finland

²Department of Forest ecology and management, SLU, Umeå, Sweden

³Department of biological and environmental sciences, University of Gothenburg, Sweden

Keywords: mesophyll conductance stable carbon isotopes, dynamic modelling.

INTRODUCTION

Atmospheric carbon dioxide is the raw material of photosynthesis. The pathway of a carbon dioxide molecule from ambient air to a glucose molecule is most commonly divided into three subprocesses: 1) the flux of CO₂ into the leaf intercellular airspaces through stomata, 2) the flux of CO₂ from intercellular airspaces to chloroplasts and 3) the conversion of CO₂ to glucose in Calvin cycle. There are two stable isotopes of carbon in atmosphere, more abundant ¹²C with a small share of ¹³C. All these three processes discriminate against the heavier ¹³C, i.e. the ratio ¹³C / ¹²C decreases during the pathway. The final ratio of ¹³C and ¹²C in sugars depends on environmental conditions and tree characteristics.

Stomatal resistance, which controls the first subprocess, has been widely studied. Mesophyll resistance that controls the rate of the CO₂ flux from intercellular airspaces into the chloroplasts was for a long time considered negligible and oppositely, its inverse, mesophyll conductance (g_m), was considered infinite. This is, however, not the case: mesophyll resistance may strongly limit carbon flux to chloroplasts (Ogée et al. 2018) and it is denoted as one of the most important missing factors from terrestrial biosphere models (Rogers et al. 2017). Mesophyll conductance cannot be directly measured. However, if we know the rate of stomatal diffusion of carbon as well as the assimilation rate and furthermore, we know the discrimination rates related to all three fluxes, we can infer g_m from the isotopic ratio of assimilates.

From leaves, part of the photosynthates is transported to other tree organs. Thus, the isotopic composition of the carbon ($\delta^{13}\text{C}$) in e.g. phloem theoretically reflects the isotopic composition of newly photosynthesized sugars of the whole canopy with a time delay (Ubierna & Marshall 2011). Therefore, phloem $\delta^{13}\text{C}$ coupled with sapflow data can further be used for estimating photosynthesis.

We formulated a dynamic model that describes the photosynthesis of ¹²C and ¹³C, taking into account isotopic fractionation related to stomatal conductance (g_s), g_m and Rubisco activity as well as mitochondrial respiration and photorespiration. Thereafter the model describes the transportation of the photosynthesized sugars down the phloem. For describing g_m , we formulated seven equations based on factors known to affect the flow rate of carbon inside the leaves. We used gas exchange measurements conducted in Rosinedal experimental forest in northern Sweden in 2017 to parameterize the model and used concurrent carbon isotope measurements from nine days to compare modelled g_m with measurement based g_m . Our specific aims were:

1. To see the effect of our different g_m descriptions on the $\delta^{13}\text{C}$ of photosynthates and furthermore to compare the predicted g_m with measurement driven g_m estimates.

2. To study the within day and within summer variation of the $\delta^{13}\text{C}$ of photosynthates and its responses to variations in weather conditions.
3. To predict $\delta^{13}\text{C}$ measured from phloem extracts with environmental data during summer 2018

METHODS

Half-hourly values of air temperature, PAR radiation, relative humidity and ambient CO_2 concentration were measured during years 2017 and 2018 in the Rodinedalsheden experimental site. The site is a 100 year old Scots pine forest located in northern Sweden. CO_2 and H_2O exchange of one year old shoots was continuously measured with shoot cuvettes during growing season 2017. Furthermore, $\delta^{13}\text{C}$ of net photosynthesis was calculated for nine sunny days during the summer 2017. In addition, we took phloem samples from three trees during growing season 2018 with 2-4 week intervals and analyzed the $\delta^{13}\text{C}$ of the phloem extracts (for further information, see Stangl et al. 2019).

To study our hypotheses, we formulated a dynamic model. The state variables of the model are carbon in leaf intercellular airspaces ($C_{i,l}$), carbon in chloroplasts ($C_{c,l}$) and carbon in needle sugar pool ($C_{s,l}$), (mol m^{-2} (leaf)) (Fig. 1). The rates of the changes of the state variables ($\text{mol m}^{-2} \text{s}^{-1}$), are defined with CO_2 concentrations or concentration differences in the pools and commonly used environmental responses of photosynthesis rate, stomatal conductance and respiration.

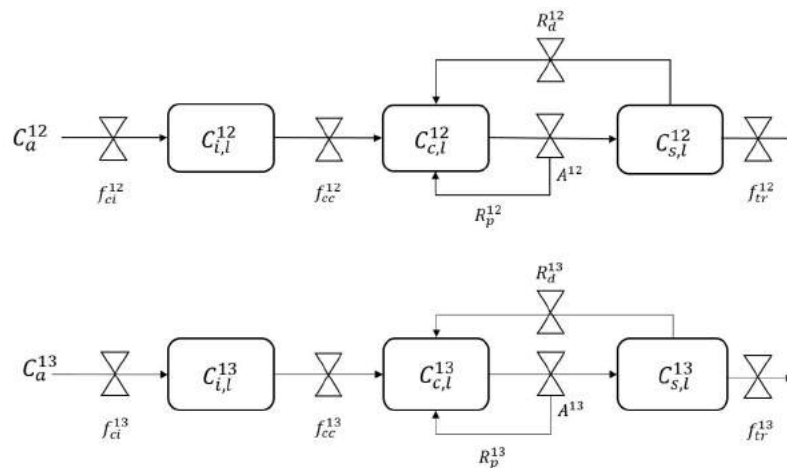


Fig 1. Model structure

Mesophyll conductance is described with seven different equation options (Table 1)

Table 1 mesophyll conductance ($\text{mol m}^{-2} \text{s}^{-1}$) equations.

	<i>Equation</i>	<i>Affecting factors</i>
Option 1*	$g_m(t) = g_m^0 + \frac{a_2 A^{12}(t)}{C_c(t) - \Gamma^*} r_w(t)$	Photosynthesis rate, C_c , water availability
Option 2*	$g_m(t) = g_m^0 + \frac{a_2 A^{12}(t)}{C_c(t) - \Gamma^*(t)}$	Photosynthesis rate, C_c

Option 3⁺	$g_m(t) = g_m^0 + g_m^{25} r_T(t) r_l^l$	Temperature, light environment
Option 4⁺	$g_m(t) = g_m^0 + g_m^{25} r_T(t) r_l^l r_w(t)$	Temperature, light environment, water availability
Option 5^{*+}	$g_m(t) = g_m^0 + \frac{a_2 A^{12}(t)}{C_c(t) - \Gamma^*(t)} r_T(t)$	Photosynthesis rate, C_c , temperature
Option 6	$g_m = g_m^{c,l}$	Constant g_m
Option 7	$g_m = g_m^{c,h}$	Constant g_m

g_m^0 is the residual mesophyll conductance, a_2 is a parameter, A^{12} is photosynthesis rate ($\text{mol m}^{-2} \text{s}^{-1}$), C_c is the g_m^{25} is mesophyll conductance at 25 °C, r_w , r_T and r_l are the effects of water, temperature and light environment (unitless), respectively (eqs x, x and x). The value of r_l varies over canopy layers but is constant over time. $g_m^{c,l}$ is constant with value derived from the measurements by Stangl et al. (2019). $g_m^{c,h}$ is higher constant approximately leading to $C_c = C_i$

*Based on Dewar et al. (2017)

+Based on Sun et al. (2014)

After photosynthesis, the model describes the mixing of the photosynthesized sugars with the sugar pool in needles. From leaves, sugars are transported with a constant rate to stem and roots via phloem where they get mixed with the existing phloem sugar pool.

The model was parameterized with net photosynthesis and g_s measurements in 2017. We analysed the importance of the non-steady-state structure of the model compared with the commonly used steady-state assumption. Furthermore, we analysed the sensitivity of the model results to certain respiration related parameters.

RESULTS

Different g_m descriptions (Table 1) resulted in different kinds of daily patterns of mesophyll conductance (Fig 2a) and furthermore in different $\delta^{13}\text{C}$ of the new photosynthates (Fig 2b). The degree of differences depended on the weather conditions. The relationship between net photosynthesis and g_m / g_s was very different with different g_m options (Fig 2c). The form of the modelled relationship resembled that found in measurements of Stangl et al. (2019) with g_m options 1 and 2 whereas the other options led to an opposite form.

The daily pattern of the modelled $\delta^{13}\text{C}$ of the new photosynthates resembled that of measured except for early morning and late evening (Fig 2d).

The model was able to reproduce the strong drought effect in the isotopic composition of phloem sugars detected during summer 2018 (Fig. 3).

The modelled $\delta^{13}\text{C}$ level was sensitive to used discrimination parameters of mitochondrial and photorespiration. However, the day to day variations in sugar $\delta^{13}\text{C}$ values were similar with different parameter combinations. The non-steady-state-structure seemed to be important at low flux conditions, i.e. in the morning and evening.

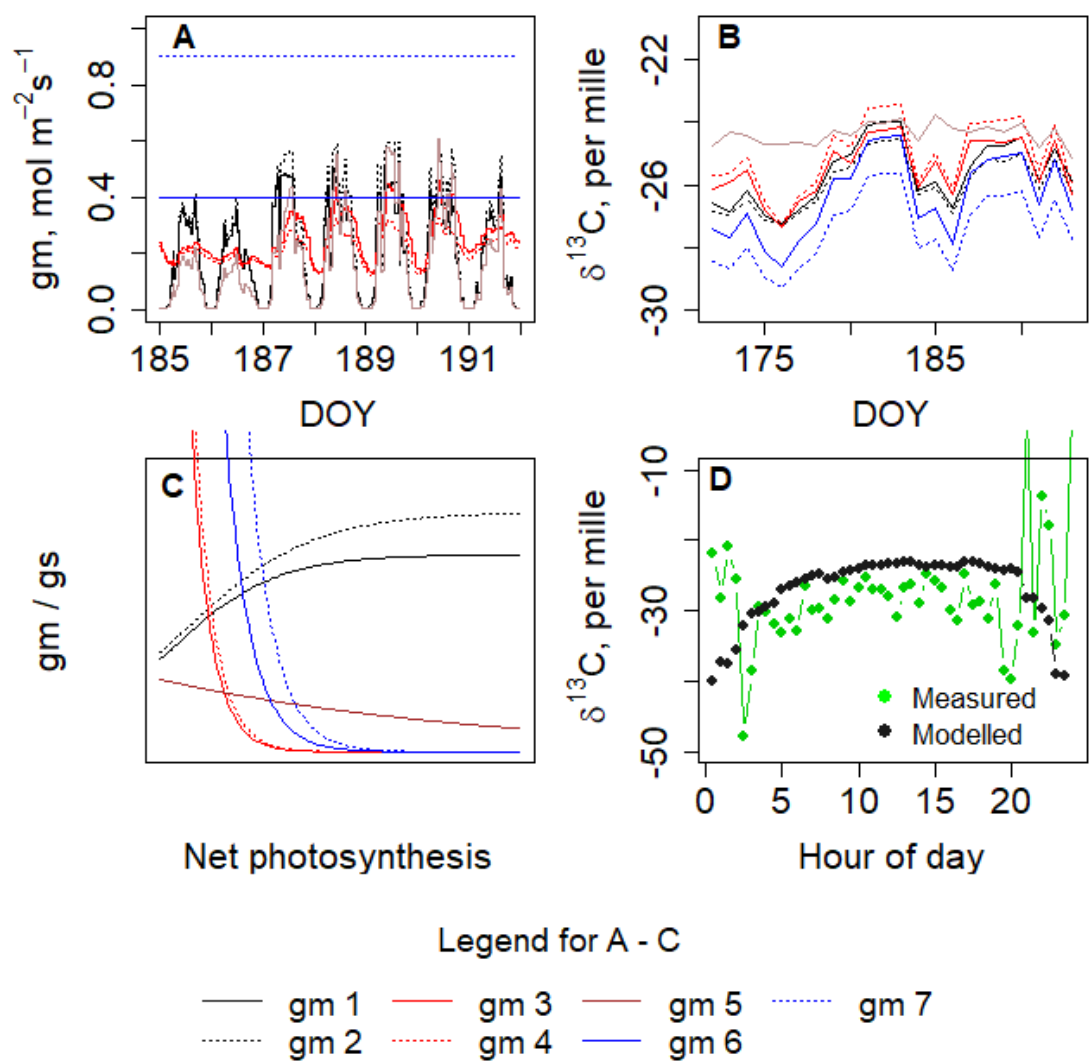


Figure 2. A) Mesophyll conductance during seven days with different descriptions, B) Resulting daily photosynthesis weighted $\delta^{13}\text{C}$ of photosynthates, C) Relationship between net photosynthesis and g_m/g_s . D) Daily pattern of half-hourly $\delta^{13}\text{C}$ of photosynthates.

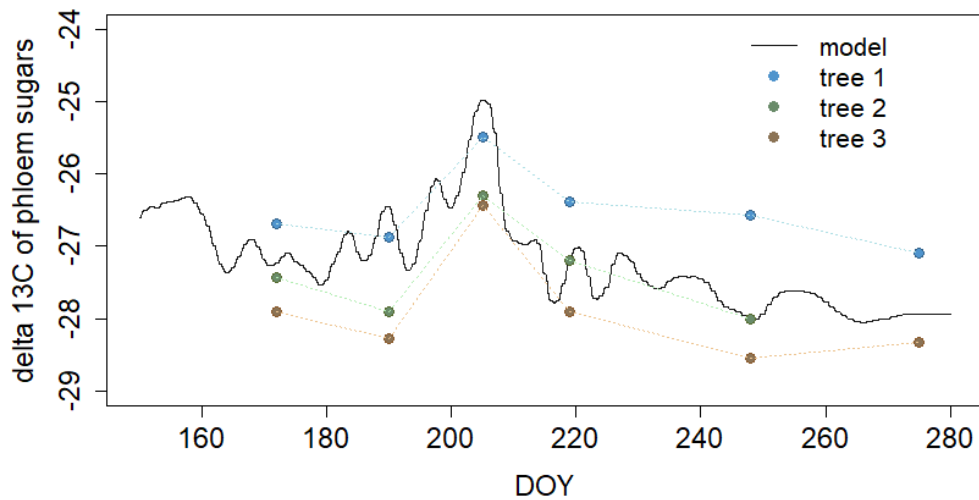


Figure 3. Measured and modelled isotopic composition of phloem soluble sugars from breast height during summer 2018.

CONCLUSIONS

The in-depth understanding of g_m and how it varies daily or seasonally requires knowledge about how environmental factors affect it. As measuring g_m is difficult, especially under field conditions, model inspection provides us with a mean to study different hypotheses related to factors affecting g_m . We found that the options that related g_m to photosynthesis rate and CO_2 concentration in chloroplasts produced patterns that most closely resembled measured ones. There were significant daily variations in the modelled $\delta^{13}\text{C}$ of sugars caused by varying weather conditions. Furthermore, we succeeded in predicting the seasonal variation in phloem $\delta^{13}\text{C}$ in 2018 based on measured weather input data.

ACKNOWLEDGEMENTS

This work was supported by the Knut and Alice Wallenberg Foundation and the Finnish Centre of Excellence Programme by the Academy of Finland (grant No 272041).

REFERENCES

- Ogé J., Wingate, L., Genty, B., (2018). Estimating mesophyll conductance from measurements of C^{18}O photosynthetic discrimination and carbonic anhydrase activity. *Plant Physiol* **178**: 728-752
- Rogers, A., Medlyn, B., Dukes, J.S., Bonan, G., von Caemmerer, S. et al. (2017). A roadmap for improving the representation of photosynthesis in Earth system models. *New Phytol.* **213**: 22-42
- Stangl, Z.R., Tarvainen, L., Röntfors, M., Wallin, G., Marshall, J.D. (2019). Diurnal variation in mesophyll conductance and its influence on modelled water-use efficiency in a mature boreal *Pinus sylvestris* stand. *Photosynth Res* **141**: 53-63
- Ubierna, N., Marshall, J.D. (2011). Estimation of canopy average mesophyll conductance using $\delta^{13}\text{C}$ of phloem contents. *Plant, cell environ* **34**: 1521-1535

EFFECTS OF MARINE FUEL SULPHUR RESTRICTIONS ON PARTICLE PROPERTIES IN ATMOSPHERIC ENVIRONMENT

S.D. SEPPÄLÄ¹, S. SAARIKOSKI¹, H. TIMONEN¹, N. KIVEKÄS¹, J. KESKINEN², A.-P. HYVÄRINEN¹

¹Atmospheric aerosols, Finnish Meteorological Institute, Helsinki, Finland.

²Department of Aerosol Physics, Tampere University, Tampere, Finland.

Keywords: aerosol size distribution, shipping emissions, Baltic Sea.

INTRODUCTION

Ambient concentrations of airborne particulate matter (PM) have been shown in many studies to be large factor in increasing the cardiorespiratory mortality and morbidity (Landis, Norris et al. 2001, Pope 1996, Schwartz, Dockery et al. 1996). Shipping is a large source of PM emissions and other air quality problems including ground-level ozone and Sulphur emission in breathing air while nearly 70 % of all maritime emissions are produced within 400 km from coastlines. Problems are mostly located around heavily trafficked shipping lanes and harbor areas, but ozone and aerosol precursor emissions can be transported even several hundreds of kilometers inland. (Eyring, Isaksen et al. 2010) While shipping emission cause many negative health effects, they also have an impact on climate. Sulphur dioxide (SO₂) from shipping causes cooling effects by particles and altering reflectivity of clouds. This results to emissions produced by shipping to strengthen the negative radiative forcing (RF) of clouds. The cooling effect of negative radiative forcing outweighs climate warming effects of carbon dioxide (CO₂) and other greenhouse gasses produced by shipping. As a result, shipping has overall cooling effect on climate. (Eyring, Isaksen et al. 2010, Fuglestedt, Berntsen et al. 2009)

Shipping emissions have long been mostly unregulated until 2nd November the International Convention for the Prevention of Pollution from Ships (MARPOL) was initiated by the International Maritime Organization (IMO). The convention was modified in 1978. These regulations aiming to reduce nitrous oxides (NO_x), Sulphur oxides (SO_x) and particulate matter from marine engines. These regulations have been effective since May 19th, 2005. Additional restrictions have been presented by some nations and for specific delicate areas. For example, Sulphur Emission Control Areas (SECAs) have been set in Baltic Sea, the North Sea area, the North American region, and the United States Caribbean Sea areas. In SECA areas the fuel Sulphur content is limited to 0,1% in mass from beginning of 2015. (Chu Van, Ramirez et al. 2019) Global maximum Sulphur content in fuel has been limited from 4,5% to 3,5% in 2012 and in 2020 or alternatively in 2025 the amount Sulphur in marine fuels is going to be restricted to 0.5%. In SECAs the limits have been stricter being 1,5% between June 2006 and June 2010, 1.0% between July 2010 and December 2014 and 0.1% from beginning of January 2015. (Antturi, Hänninen et al. 2016).

This work focuses on the effect of Sulphur restrictions implemented in beginning of July 2010 and January 2015 on marine atmospheric air quality. Restrictions effect on particle size number distributions (NSD) as well as total effect on concentrations in the Baltic sea SECA area are discussed. The overall effect of shipping emissions to marine atmospheric air quality and comparability of emission measurements made from atmospheric air to direct emission measurements are also discussed. I didn't take part in any of the measurements used in this work, but only used the data produced by Finnish Metrological Institute in Utö's air quality measurement site.

METHODS

Measurement data used in this thesis was measured at Utö Atmospheric and Marine research Station located on a small island Utö belonging to Finland. Utö is located in the Archipelago Sea in Baltic Sea Utö's coordinates are (59° 46'50N, 21° 22'23E).

Data processing in this study was based on pieces of MATLAB code made earlier by other personnel at Finnish Meteorological Institute for other projects. For producing end results these codes needed modification. Differential Mobility Particle Sizer (DMPS) data together with, weather and Automatic Identification System (AIS) data were analysed.

AIS data was used for estimating shipping routes around Utö and evaluating types of ships passing by the island. Shipping routes around Utö in 400 km² area are presented in following figure.

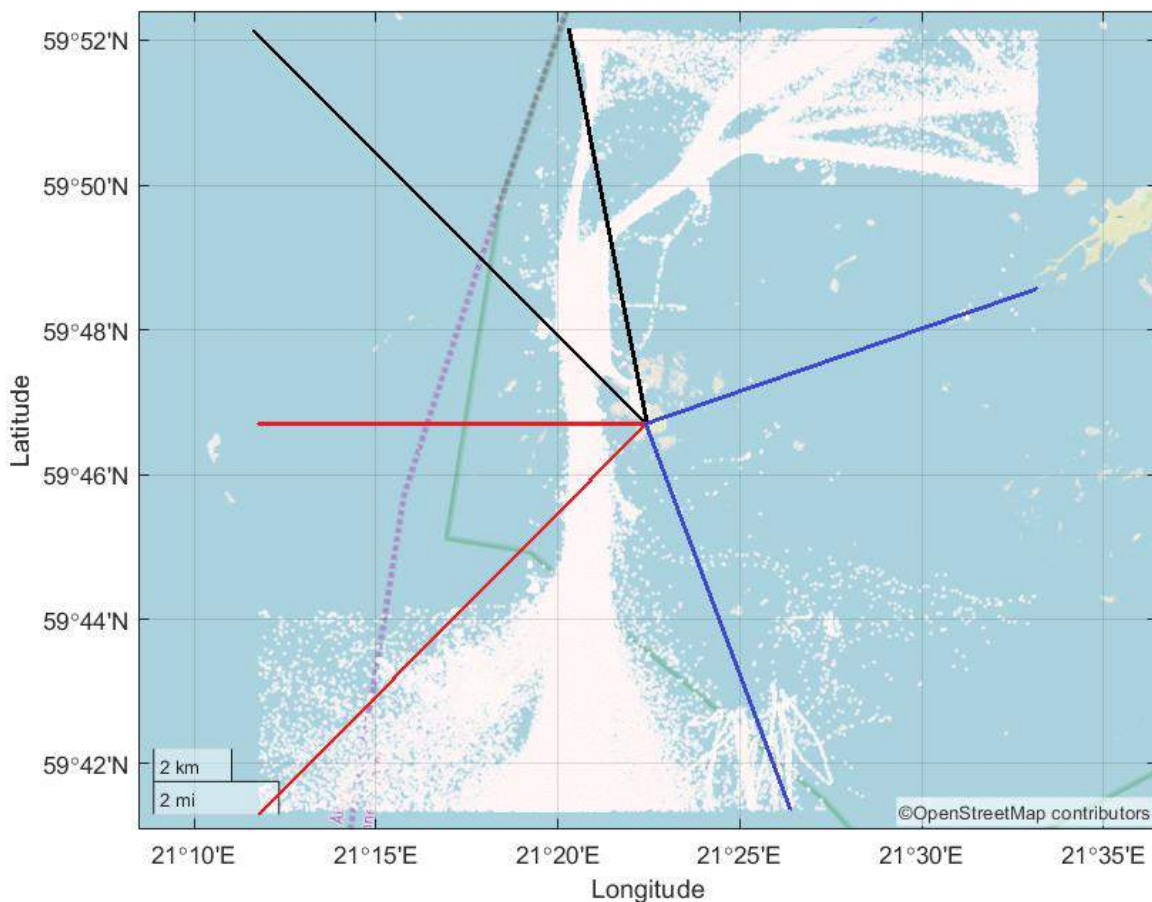


Figure 1. Large vessels with International Maritime Organization (IMO) numbers during time period of 2007-2016 are marked with white dots. Black lines are used for identifying harbor sector, red lines for identifying nearby shipping lines sector and blue lines for identifying distant shipping lines sector. Sector limits are the angle limits for wind during the plume in order to classify the plume to be from the current sector.

It can be seen from the figure that there is a busy shipping line on the western side of the island approximately 1-2 km from the coastline and there is almost no shipping activity on western side of island. Sectors marked in figure were chosen so that they would resemble plumes coming from different distances.

DMPS data was used for identifying plumes arriving to measurement station from different wind directions. Ship plumes were found from the measurement data as in article Kivekäs, Massling et al. (2014). the used criteria for identifying plumes was that the peak particle number concentration (N_p) had to be at least 500 #/cm³ above or peak to background ratio (R_{Np}) 1,5 times the current background concentration. The

background concentration was defined as a 25th percentile values of sliding window of width of 40 consecutive measurements. Total number of valid plumes found using this method in time the period of 11.1.2007-31.12.2016 was 42322. Found plumes were divided into three categories: harbor, nearby shipping lane and distant shipping lanes sectors according to their arrival wind directions. For the plumes their number size distributions (NSD) were calculated and their total effect on atmospheric particle number concentrations were evaluated. These properties were analysed separately for each sector and plume restriction period

In the following figure, the average particle number size distributions (NSD) of plumes arriving from distant shipping lanes sector as well as their geometric standard deviations are presented. The NSDs have been normalized to total concentrations of 1000 #/cm³.

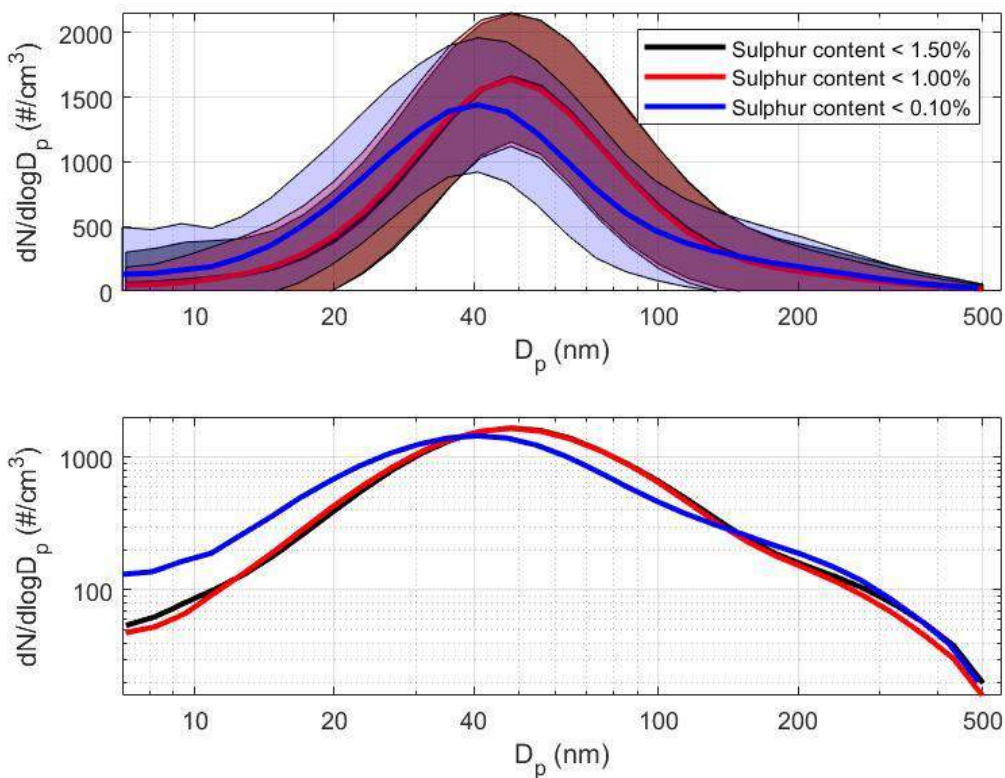


Figure 2. Average normalized particle number size distributions (NSD) and their geometric standard deviations during different sulphur restriction periods from distant shipping lanes sector.

The implementation of first sulphur content restriction in marine fuels from 1.50% to 1.00% has almost no effect on NSD or peak diameter. The second larger restriction from 1.00% to 0.10% in fuel sulphur content has a clear effect on the NSD sifting the of peak size from 48nm to 42 nm, also increasing the relative number of particles smaller than 35 nm in diameter and decreasing relative number of particles in size range 35-150nm.

In next figure the yearly contributions of plumes to total particle number concentrations have been presented. Also average contributions during different sulphur restriction periods and restriction changes have been marked to figure.

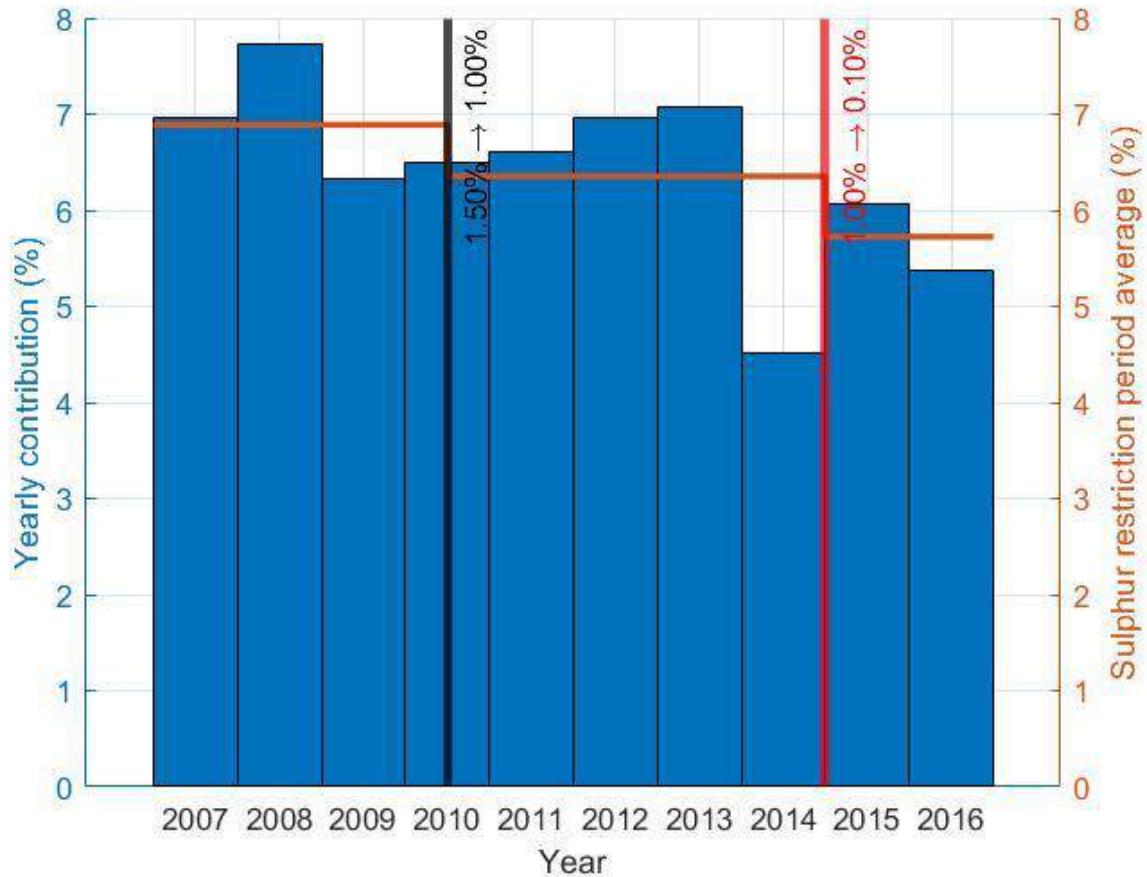


Figure 3. Contributions of plumes to total particle concentrations. Blue bars are yearly contributions and orange lines are the averages for different sulphur restriction periods. Black vertical line is the first sulphur restriction in beginning of July 2010 and the red vertical line is the second sulphur restriction in beginning of January 2015.

Plume contributions to total particle number concentrations have dropped after each of the sulphur restrictions indicating the effectiveness of lowering sulphur content in marine fuels. Similar values for plume contributions to total particle concentrations in areas near shipping lanes have earlier been reported by Kivekäs, Massling et al. (2014).

CONCLUSIONS

Marine fuel sulphur content restrictions have had a clear effect on particle emissions of ships. Reduced amount of sulphur content in fuel especially after the sulphur content restriction from 1.00% to 0.10% has led to lowered average particle size of plumes as well as total concentrations during plumes.

ACKNOWLEDGEMENTS

Academy of Finland Center of Excellence program (project number 272041), European Union's Horizon 2020 research and innovation programmes under grant agreement No 654109 (ACTRIS-2), No 814893 (SCIPPER).

REFERENCES

- Antturi, J., Hänninen, O., Jalkanen, J., Johansson, L., Prank, M., Sofiev, M. and Ollikainen M., 2016. Costs and benefits of low-sulphur fuel standard for Baltic Sea shipping. *Journal of Environmental Management*, 184(Pt 2), pp. 431-440.
- Chu Van, T., Ramirez, J., Rainey, T., Ristovski, Z. and Brown, R.J., 2019. Global impacts of recent IMO regulations on marine fuel oil refining processes and ship emissions. *Transportation Research Part D*, 70, pp. 123-134.
- Eyring, V., Isaksen, I.S.A., Berntsen, T., Collins, W.J., Corbett, J.J., Endresen, O., Grainger, R.G., Moldanova, J., Schlager, H. and Stevenson, D.S., 2010. Transport impacts on atmosphere and climate: Shipping. *Atmospheric Environment*, 44(37), pp. 4735-4771.
- Fuglestedt, J., Berntsen, T., Eyring, V., Isaksen, I., Lee, D.S. and Sausen, R., 2009. Shipping Emissions: From Cooling to Warming of Climate—and Reducing Impacts on Health. *Environmental science & technology*, 43(24), pp. 9057-9062.
- Kivekäs, N., Massling, A., Grythe, H., Lange, R., Rusnak, V., Carreno, S., Skov, H., Swietlicki, E., Nguyen, Q.T., Glasius, M. and Kristensson, A., 2014. Contribution of ship traffic to aerosol particle concentrations downwind of a major shipping lane. *Atmospheric Chemistry and Physics*, 14(16), pp. 8255-8267.
- Landis, M.S., Norris, G.A., Williams, R.W. and Weinstein, J.P., 2001. Personal exposures to PM 2.5 mass and trace elements in Baltimore, MD, USA. *Atmospheric Environment*, 35(36), pp. 6511-6524.
- Pope, C.A., 1996. Adverse health effects of air pollutants in a nonsmoking population. *Toxicology*, 111(1), pp. 149-155.
- Schwartz J., Dockery, D.W. and Neas, L.M., 1996. Is daily mortality associated specifically with fine particles? *Journal of the Air & Waste Management Association* (1995), 46(10), pp. 927.

Identification of molecular cluster evaporation rates, enthalpies and entropies by Monte Carlo method

A. Shcherbacheva¹, T. Balehowsky², T. Olenius³, T. Helin⁴, J. Kubečka¹, M. Laine⁵, H. Haario^{4, 5}, T. Kurtén¹ and H. Vehkamäki¹

¹ Institute for Atmospheric and Earth System Research, University of Helsinki, Helsinki, Finland

² Department of Mathematics and Statistics Subunit, University of Helsinki, Helsinki, Finland ³

Department of Environmental Science and Analytical Chemistry & Bolin Centre for Climate

Research, Stockholm University, Stockholm, Sweden ⁴ LUT School of Engineering Science,

Lappeenranta-Lahti University of Technology, Lappeenranta, Finland ⁵ Finnish Meteorological

Institute, Helsinki, Finland

Keywords: Markov Chain Monte Carlo (MCMC), New Particle formation, birth-death equations, cluster population dynamics, enthalpies, entropies, evaporation rates

INTRODUCTION

Recent advances in instrumentation have enabled detection and quantification of ionic clusters containing between one and some tens of molecules which are formed in the gas phase from precursor vapours with ppt-level concentrations. Although individual cluster concentrations can be measured by modern instruments, the individual rates of molecular-scale processes have not been directly measured. Simulations for cluster populations which incorporate collision and evaporation rates of the clusters (such as Becker-Döring models) have been shown to provide some quantitative agreement with experimental data.

However, different quantum chemistry methods give considerably discrepant values for the evaporation rates, leading to ambiguity for the true evaporation rates of the clusters. In this paper we treat the rates as unknown parameters and explore the following problem: given the measured cluster concentrations, determine the evaporation rates that reproduce the data with sufficient degree of accuracy, assuming that the collision probabilities are known.

We address the problem via Bayesian parameter estimation using a Markov chain Monte Carlo (MCMC) algorithm. In particular, we create synthetic cluster concentration data for a set of neutral sulphuric acid and ammonia clusters. We use two different procedures to determine the evaporation rates. First, evaporation rates are treated as constants which we aim to determine from time-dependent cluster concentrations measured before the system has attained a steady state. We are able to identify a subset of the rates with this information. Second, the evaporation rates are represented as functions of temperature, depending on cluster formation enthalpies and entropies which in this case are the free parameters. This enables us to use multiple data sets at different temperatures. It also reduces the number of unknown parameters, as multiple evaporation rates depend on the same cluster formation enthalpy and entropy parameters. In this setting, we successfully identified the thermodynamic parameters from steady-state cluster concentrations measured at two different temperatures under varying concentrations of sulphuric acid and ammonia monomers.

METHODS

1 SIMULATION METHODS

The kinetics of cluster formation is described by Becker-Döring equations (see (Hingant and Yvinec(2017)), (?)), which model cluster birth and death which arises from collisions of the smaller clusters into larger ones and evaporations from the bigger clusters into smaller ones. Precisely, labelling the clusters by $i \in \{1, 2, \dots, N\}$, the time derivative of the i th cluster concentration C_i is governed by

$$\frac{dC_i}{dt} = \frac{1}{2} \sum_{j < i} \beta_{i,(i-j)} C_i C_{(i-j)} + \sum_j \gamma_{i+j \rightarrow i,j} C_{i+j} - \sum_j \beta_{i,j} C_i C_j - \frac{1}{2} \sum_{j < i} \gamma_{i \rightarrow j,i-j} C_i + Q_i - S_i, \quad (1)$$

where $\beta_{i,j}$ is the collision coefficient of clusters i with j , and $\gamma_{i+j \rightarrow i,j}$ is the evaporation coefficient of cluster $i + j$ into clusters i and j . The loss term S_i represents losses **of different types**, (see (?), (?)), **and Q_i stands for external sources**.

We now specify the quantity and type of sources and sinks included in our studies. We assume that the concentration of ammonia monomers is constant, while sulphuric acid monomers are supplied to the system at a constant rate comprising $6.3 \times 10^4 \text{ cm}^{-3} \text{ s}^{-1}$. This settings are selected to imitate the conditions inside of the CLOUD chamber, (see (Kirkby et al.(2011)), (Kürten et al.(2015))). Further, we include wall losses arising from clusters sticking on the walls of the experimental chamber (see (Kürten et al.(2015))). These wall losses are parametrized by the size of the cluster

$$S_{\text{wall},i} = 10^{-12} / (2r_i + 0.3 \times 10^{-9}) \text{ s}^{-1}, \quad (2)$$

where r_i is the mass radius of the cluster (in cm). From Equation 11, wall loss rates decrease with cluster size; in practise it also varies with respect to cluster position in the chamber and time. We neglect any uncertainties attributed to the wall losses. However, we do account for dilution losses, with size-independent value comprising $S_i = 9.6 \times 10^{-5} \text{ s}^{-1}$, which had previously been determined in the CLOUD chamber, (see (Kirkby et al.(2011)), (Kürten et al.(2015))).

Let T denote the temperature of the system of molecular clusters. Using classical kinetic gas theory, the collision rates $\beta_{i,j}$ in Equation 10 obey

$$\beta_{i,j} = \sqrt{T} \left(\frac{3}{4\pi} \right)^{1/6} \left[6k_B \left(\frac{1}{m_i} + \frac{1}{m_j} \right) \right]^{1/2} \left(V_i^{1/3} + V_j^{1/3} \right)^2, \quad (3)$$

where m_i and V_i are respectively the mass and volume of cluster i , and k_B is Boltzmann's constant. Further we assume that the masses and volumes are temperature-independent.

The cluster evaporation rates $\gamma_{i+j \rightarrow i,j}$ in Equation 10 are given by the expression

$$\gamma_{i+j \rightarrow i,j} = \beta_{i,j} \frac{P_{\text{ref}}}{k_B T} \exp \left(\frac{\Delta G_{i+j} - \Delta G_i - \Delta G_j}{k_B T} \right), \quad (4)$$

where P_{ref} is the reference pressure and ΔG_i is the Gibbs free energy of formation for cluster i . We may further describe the i th Gibbs free energy in terms of the cluster formation enthalpy ΔH_i and entropy ΔS_i :

$$\Delta G_i = \Delta H_i - T \Delta S_i. \quad (5)$$

1.1 Generation of synthetic data

For demonstration purposes, we consider a system of neutral sulphuric acid and ammonia clusters. In this case, the coefficients (such as cluster recombination coefficient, ionization rates, etc.) specifically associated with charged clusters and their interactions are unnecessary, and so in the neutral

case we isolate the problem of determining the evaporation rate coefficients. Below we summarize in Table 5 the 16 cluster types included in our study. To save computational time, we consider only the stable clusters which are detected via mass spectrometric measurements, as they do not evaporate before entering the ToF ¹, (see (Kirkby et al.(2011)), (Schobesberger et al.(2015)), (Elm and Kristensen(2017)), (Yu et al.(2018))). Further, we address varying concentrations of ammonia monomers and the constant source of sulphuric acid monomer, summarized in the Table 6.

Synthetic concentration data for such neutral clusters were generated by the following method.

The evaporation rate coefficients computed in (Olenius et al.(2013b)), the associated collision rates as determined by Equations 12-13, the wall losses calculated by Equation 11, and dilution losses of ($S_i = 9.6 \times 10^{-5} \text{s}^{-1}$), are substituted in to the ACDC algorithm (McGrath et al.(2012)), which computes the first-order non-linear, ordinary differential system of cluster concentrations as given by 10. Similarly to the earlier paper (Kupiainen-Määttä(2016)), we then integrate the system produced by ACDC using the Fortran ordinary differential equation solver VODE ((N. Brown et al.(1989))). A detailed description of this program was published in (McGrath et al.(2012)). We note that unlike in (Kupiainen-Määttä(2016)), the system is considered at various temperatures in this paper.

Two data sets were generated. First, time evolution of the concentrations $C_i(t)$ is computed for time values less than the time at which the system has attained the steady state. The maximum time we run is 60 minutes in the above model configurations. In this case, it is assumed that the concentrations for all the clusters are measured under constant temperature with time resolution comprising 1.5 minutes, which comprises overall 41 transient concentration measurements for each of the cluster types i .

Secondly, we solve for time-independent steady-state concentrations for all the cluster types for two temperatures comprising 278 K and 292 K. In both data configurations, the steady-state cluster concentrations are calculated as the average of the concentrations determined for time instances $t_1 := 50 \text{ min}$ and $t_2 := 60$. The measure of how close the system has reached to the steady state is monitored by a convergence parameter, which is the ratio of the concentrations at times t_2 and t_1 , taken in each case for the cluster for which this ratio deviated most from unity, (Kupiainen-Määttä(2016)).

In both data settings, the simulation outputs are amended with the measurement errors sampled from a multivariate, non-correlated, Gaussian distribution, where the variance of the distribution depends on cluster type i , temperature T and time instance t . While a simplification of noise characteristics of the real data obtained from a mass or ion spectrometer, we impose that the standard deviation of the noise comprises 0.001% of the original concentration.

Note that apart from generation of synthetic data, we apply the ACDC as a kinematic model of cluster population in the MCMC simulations. The ACDC outputs are compared to the synthetic measurements and explained in Section 2.2.

1.2 Markov chain Monte-Carlo simulations

The evaporation rate coefficients $\gamma_{i+j \rightarrow i,j}$ appearing in the ACDC simulation of 10 are treated as unknown parameters. Our purpose is to determine all the parameter sets that reproduce the synthetic data within their noise level (which is known). We do this using Markov Chain Monte Carlo (MCMC) sampling.

The MCMC approach computes a posterior probability density function of the parameters as point-wise likelihood approximations across the parameter space. The algorithm samples the candidate

¹Time-of-flight mass spectrometer

Table 1: Neutral molecular clusters included into model system. The first column indicates the number of sulphuric acid molecules, the second column stands for the number of ammonia in the cluster.

Number of H ₂ SO ₄ molecules	Number of NH ₃ molecules
0	1
1	0-1
2	0-2
3	1-3
4	2-5
5	3-5

Table 2: Monomer concentrations used in simulations

[H ₂ SO ₄] monomers (in cm ⁻³)	[NH ₃] monomers (in ppt)
1e + 7	35
5e + 7	61.875
1e + 8	88.75
-	115.625
-	142.5
-	169.375
-	196.25
-	223.125
-	250

Table 3: Domain limitations for two data settings under consideration imposed to exclude non-physical parameters in parameter identification procedure.

Data settings	Estimated parameters	Minimal value	Maximal value
Data setting 1	Base 10 logarithms of evaporation rates	-12	12
Data setting 2	Cluster formation enthalpies and entropies	-400	0

Table 4: Additional domain limitations for the data setting 2 from Table 7 (identification of cluster formation enthalpies and entropies), where the cluster formation enthalpy of the i -th cluster is denoted by ΔH_i and the symbols A and N stand for ammonia and sulphuric acid, respectively.

$\Delta H_{2A} > \Delta H_{2A1N}$	$\Delta H_{3A2N} > \Delta H_{4A2N}$
$\Delta H_{1A1N} > \Delta H_{2A1N}$	$\Delta H_{4A2N} > \Delta H_{4A3N}$
$\Delta H_{2A1N} > \Delta H_{3A1N}$	$\Delta H_{4A3N} > \Delta H_{4A4N}$
$\Delta H_{2A2N} > \Delta H_{3A2N}$	$\Delta H_{4A4N} > \Delta H_{5A5N}$
$\Delta H_{3A1N} > \Delta H_{3A2N}$	$\Delta H_{4A4N} > \Delta H_{4A5N}$

parameter points from a predefined proposal distribution, and then either accept or reject it, according to how closely the output model fits the data. The fundamental technique is the Metropolis algorithm (Metropolis et al.(1953)). The sets of parameters which produce cluster concentrations within the allotted noise level of the data are kept in the sampled distribution. Finally, the approximation of the posterior distribution is constructed from the retained parameter sets. We remark that to create a reliable sample from the underlying parameter distribution, many different parameter combinations must be tested; that is, the length of the MCMC chain must be large enough (Haario et al.(1999)), (Haario et al.(2001))). In both our studies, the MCMC chain length typically comprised 3 million samples. The MCMC acceptance probabilities (defined below) in each of the cases were about 88.0%, which a typical level of acceptance since the “forward” ACDC model (in which the rate coefficients are known) is deterministic.

In this paper we employ a variant of the Metropolis algorithm which is more efficient at parameter sampling when the parameter space is large (Haario et al.(2006)). This variant is called the Delayed Rejection Adaptive Metropolis (DRAM), introduced in (Haario et al.(2006)). We briefly explain our approach below.

First, an initial prior distribution for the parameter values θ (represented in array form) is chosen and set to be the proposed “true” distribution from which possible parameters are sampled. In our case, we chose the flat prior, but impose some domain restrictions for sampling from this prior to exclude unphysical parameters (see Tables 7-8).

We emphasize that there are currently *no theoretical principles or experimental results which indicate possible restrictions for even the order of magnitude of the evaporation rates*. However, we assume that the evaporation rates with orders of magnitude less than 10^{-10}cm^{-3} are irrelevant in practise, since such an evaporation event is highly improbable, and it is very likely that instead the cluster will grow further by collisions. Similarly, when the evaporation rate is of the order of magnitude more than 10^{+10}cm^{-3} , it is reasonable to expect that the cluster will most certainly evaporate before it has a chance to grow further. With these assumptions, the prior distribution of the evaporation rates spans over several orders of magnitude, and the base 10 logarithm of evaporation rates was sampled from the range of -12 to 12.

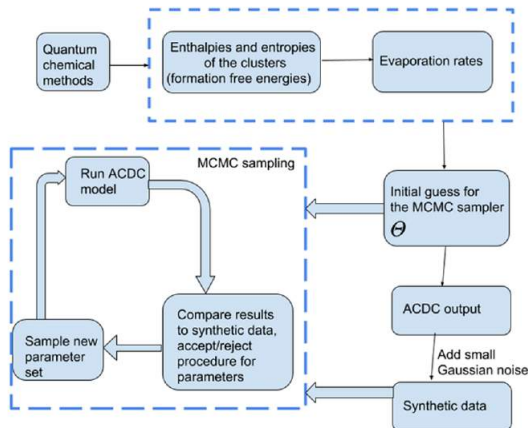


Figure 1: Schematic representation of the study methods.

Further, observe that the sampled parameters of the posterior distribution represent the model evaluations which produce values within the noise level of 0.001% of the data concentrations for each of the respective cluster types.

An outline of the above procedure is illustrated in Figure 2 below.

We next explicitly describe what \mathbf{C}_{exp} and θ (which give the acceptance probability in the expression ?? represent in the two study cases.

In the first study, the free parameters θ represent the evaporation rates. The data \mathbf{C}_{exp} is either the time-independent steady-state or transient cluster concentrations measured at temperature 278 K.

In the second study, we use Equations 13 and 14 to express the evaporation rates as functions of thermodynamic data, parametrized by temperature:

$$\gamma_{i+j \rightarrow i,j} = f(T, \{\Delta H_k, \Delta S_k\}_{k \in \{i+j, i, j\}}). \quad (6)$$

In 15, we set $T = 278$ K or $T = 292$ K. We emphasize that the rates $\gamma_{i+j \rightarrow i,j}$ now depend on temperature and six parameters: the cluster formation enthalpy ΔH_{i+j} and entropy ΔS_{i+j} of the evaporating cluster $i + j$, and the formation enthalpies $\Delta H_i, \Delta H_j$ and entropies $\Delta S_i, \Delta S_j$ of the clusters i and j respectively. In this setting θ represents the array of quantities $\Delta H_{i+j}, \Delta S_{i+j}, \Delta H_i, \Delta H_j, \Delta S_i, \Delta S_j$ with $i + j \in \{1, 2, \dots, 16\}$.

At either temperature $T = 278$ K or $T = 292$ K, the smaller clusters for certain combinations of ammonia and sulphuric acid may arise from the evaporation of several larger clusters. This implies that several of the pairs $\Delta H_i, \Delta S_i$ appear in expression 15 for the evaporation rates of different cluster types. Additionally, the Gibbs formation free energies of monomers are fixed to be zero, and their associated enthalpies and entropies do not vary in our simulations. This imposes additional constraints on possible parameter values. One can calculate that of the 39 evaporations that are involved in the dynamics of the neutral cluster system under consideration, only 28 distinct entropy and enthalpy rates appear. Consequently, in this case the number of free parameters has been reduced from 39 to 28. This information is summarized in Table 7. Moreover, from this table one can see that the entropy and enthalpy values lie within two orders of magnitude. This feature of the entropies and enthalpies has the effect of reducing the *stiffness* of the differential system 10 (computed via ACDC) which allows for easier integration via VODE.

For the setting above, the data \mathbf{C}_{exp} are the time-independent steady-state cluster concentrations measured at temperature 278 K or 292 K.

1.2.1 Likelihood, data and cost function

The likelihood of observing the data \mathbf{C}_{exp} given the parameter values θ is

$$p(\mathbf{C}_{exp}|\theta) = \frac{1}{(2\pi)^{n_{out}/2}} \exp\left(-\frac{1}{2}SS_{sum}(\theta)\right), \quad (7)$$

where n_{out} is the number of measurements and $SS_{sum}(\theta)$ is the cost function. We elucidate the cost function below. In our first study in which simulations are conducted with time-dependent data, the number of measurements is $n_{out} = 27 * (N_c * N_t + 1)$, where $N_c = 16$ is the number of cluster types whose concentrations are measured and $N_t = 41$ is the number of time-step measurements available for each of the cluster types. As explained in Section 2.1, after each VODE integration, a convergence coefficient is computed from the steady-state cluster concentrations to ensure that the system has attained the steady-state.

In our first study, the parameter fit to the data was evaluated by the sum of squared residuals of the model outputs \mathbf{C}_{mod} and the measurements, \mathbf{C}_{exp} . Since concentrations of molecular clusters span a large range (from 10^{-5} to 10^9 particles per cm^3), the sum of squared residuals, (or *cost function*) normalizes the residuals by the measurement error variance. In this manner, we avoid fitting mainly the high values of the concentration. Precisely,

$$SS_{sum} = \sum_{i=1}^{N_c} \sum_{j=1}^{N_t} \frac{(C_{exp,i}(t_j) - C_{mod,i}(t_j))^2}{\sigma_{ji}^2}. \quad (8)$$

Note that the standard deviation σ_{ji} is matched separately for each cluster type and every time instance. Here we assume that the instrument is capable of detecting all the cluster types represented in the system at arbitrary small levels of concentration. This simplification was considered in order to illustrate the proposed approach.

When parameter estimation is conducted with steady-state cluster concentrations (as is considered in our second study), we use the following cost function:

$$SS_{sum} = \sum_{i=1}^{N_c} \sum_{j=1}^{N_T} \frac{(C_{exp,i}(T_j) - C_{mod,i}(T_j))^2}{\sigma_{ji}^2}. \quad (9)$$

Now N_T denotes the number of steady state configurations at different *temperatures* (not times!) and T_j stands for the measured *temperature*. In this study, the number of measurements for the likelihood given by Equation 16 is $n_{out} = 4 * (N_c * N_T + 1)$ (again $N_c = 16$ cluster types).

2 RESULTS

2.1 Identification of the evaporation rate coefficients from steady-state and transient data

First, we generate synthetic steady-state data by the method in Section 3.1, for varying initial ammonia monomer concentrations, previously summarized in Table 6; the sulphuric acid monomer is supplied to the system at a constant rate comprising 6.3335×10^4 at the temperature $T = 278$ K. As an output, we obtain the concentrations for all cluster types considered (listed earlier in Table 5), measured when the system has attained the steady-state. A graphical representation of the data set is given below in Figure 3.

2.2 Estimating enthalpies and entropies from steady-state concentration measurements

In this section we describe another method for regularizing our problem of estimating evaporation rates from steady-state concentration data. We will determine the cluster formation enthalpies and entropies from two sets of synthetic, steady-state cluster concentrations, now measured at two temperatures: 278 and 292 K. This data set is plotted in Figures 3 and ??.

We also write the evaporation rate parameters as functions of the cluster formation enthalpies and entropies, parametrized by the temperature (either 278K or 292 K). By re-expressing our unknown evaporation parameters in this way, the number of free parameters in our problem reduces from 39 to 28, as many evaporation rates are determined by the same sets of thermodynamic data. The cluster formation enthalpy and entropy are our new free parameters, which now take values within same order of magnitude of 10^2 (kcal mol⁻¹ and cal K⁻¹ mol⁻¹ for cluster formation enthalpy and entropy, respectively). We will demonstrate that these changes plus the extended data set transforms our parameter identification problem from an ill-posed problem to a well-posed one. We use synthetic steady-state cluster concentrations generated for two temperatures to recover the thermodynamic parameters. This is done to improve the identification by using the temperature dependence of the Gibbs free energies (and the evaporation rates).

From our MCMC simulations, we see that the formation enthalpies and entropies of the molecular clusters exhibit strong correlations; these correlations are captured in Figures ??, ??-??. Strong correlations are observed between formation enthalpies (enthalpies) of the clusters containing same number of ammonia molecules larger than 2, except the case of (H₂SO₂)₅(NH₃)₅. Since our parameters are strongly correlated, we may alternatively consider just cluster formation enthalpies or the ratios of cluster formation entropies and enthalpies as our free parameters.

Notice that the evaporation rates calculated from a posterior distribution of sampled thermodynamic parameters for the temperature 278 K are close to the baseline values from (Ortega et al.(2012)) used for generation of the synthetic data and their variances are less than one order of magnitude, see Figures ??-??.

3 SIMULATION METHODS

The kinetics of cluster formation is described by Becker-Döring equations (see (Hingant and Yvinec(2017)), (?)), which model cluster birth and death which arises from collisions of the smaller clusters into larger ones and evaporations from the bigger clusters into smaller ones. Precisely, labelling the clusters by $i \in \{1, 2, \dots, N\}$, the time derivative of the i th cluster concentration C_i is governed by

$$\frac{dC_i}{dt} = \frac{1}{2} \sum_{j < i} \beta_{i,(i-j)} C_i C_{(i-j)} + \sum_j \gamma_{i+j \rightarrow i,j} C_{i+j} - \sum_j \beta_{i,j} C_i C_j - \frac{1}{2} \sum_{j < i} \gamma_{i \rightarrow j,i-j} C_i + Q_i - S_i, \quad (10)$$

where $\beta_{i,j}$ is the collision coefficient of clusters i with j , and $\gamma_{i+j \rightarrow i,j}$ is the evaporation coefficient of cluster $i + j$ into clusters i and j . The loss term S_i represents losses **of different types**, (see (?), (?)), **and Q_i stands for external sources**.

We now specify the quantity and type of sources and sinks included in our studies. We assume that the concentration of ammonia monomers is constant, while sulphuric acid monomers are supplied to the system at a constant rate comprising 6.3×10^4 cm⁻³s⁻¹. This settings are selected to imitate the conditions inside of the CLOUD chamber, (see (Kirkby et al.(2011)), (Kürten et al.(2015))). Further, we include wall losses arising from clusters sticking on the walls of the experimental chamber (see (Kürten et al.(2015))). These wall losses are parametrized by the size of the cluster

$$S_{\text{wall},i} = 10^{-12} / (2r_i + 0.3 \times 10^{-9}) \text{ s}^{-1}, \quad (11)$$

where r_i is the mass radius of the cluster (in cm). From Equation 11, wall loss rates decrease with cluster size; in practise it also varies with respect to cluster position in the chamber and time. We neglect any uncertainties attributed to the wall losses. However, we do account for dilution losses, with size-independent value comprising $S_i = 9.6 \times 10^{-5} \text{s}^{-1}$, which had previously been determined in the CLOUD chamber, (see (Kirkby et al.(2011)), (Kürten et al.(2015))).

Let T denote the temperature of the system of molecular clusters. Using classical kinetic gas theory, the collision rates $\beta_{i,j}$ in Equation 10 obey

$$\beta_{i,j} = \sqrt{T} \left(\frac{3}{4\pi} \right)^{1/6} \left[6k_B \left(\frac{1}{m_i} + \frac{1}{m_j} \right) \right]^{1/2} \left(V_i^{1/3} + V_j^{1/3} \right)^2, \quad (12)$$

where m_i and V_i are respectively the mass and volume of cluster i , and k_B is Boltzmann's constant. Further we assume that the masses and volumes are temperature-independent.

The cluster evaporation rates $\gamma_{i+j \rightarrow i,j}$ in Equation 10 are given by the expression

$$\gamma_{i+j \rightarrow i,j} = \beta_{i,j} \frac{P_{\text{ref}}}{k_B T} \exp \left(\frac{\Delta G_{i+j} - \Delta G_i - \Delta G_j}{k_B T} \right), \quad (13)$$

where P_{ref} is the reference pressure and ΔG_i is the Gibbs free energy of formation for cluster i . We may further describe the i th Gibbs free energy in terms of the cluster formation enthalpy ΔH_i and entropy ΔS_i :

$$\Delta G_i = \Delta H_i - T \Delta S_i. \quad (14)$$

3.1 Generation of synthetic data

For demonstration purposes, we consider a system of neutral sulphuric acid and ammonia clusters. In this case, the coefficients (such as cluster recombination coefficient, ionization rates, etc.) specifically associated with charged clusters and their interactions are unnecessary, and so in the neutral case we isolate the problem of determining the evaporation rate coefficients. Below we summarize in Table 5 the 16 cluster types included in our study. To save computational time, we consider only the stable clusters which are detected via mass spectrometric measurements, as they do not evaporate before entering the ToF ², (see (Kirkby et al.(2011)), (Schobesberger et al.(2015)), (Elm and Kristensen(2017)), (Yu et al.(2018))). Further, we address varying concentrations of ammonia monomers and the constant source of sulphuric acid monomer, summarized in the Table 6.

Synthetic concentration data for such neutral clusters were generated by the following method.

The evaporation rate coefficients computed in (Olenius et al.(2013b)), the associated collision rates as determined by Equations 12-13, the wall losses calculated by Equation 11, and dilution losses of ($S_i = 9.6 \times 10^{-5} \text{s}^{-1}$), are substituted in to the ACDC algorithm (McGrath et al.(2012)), which computes the first-order non-linear, ordinary differential system of cluster concentrations as given by 10. Similarly to the earlier paper (Kupiainen-Määttä(2016)), we then integrate the system produced by ACDC using the Fortran ordinary differential equation solver VODE ((N. Brown et al.(1989))). A detailed description of this program was published in (McGrath et al.(2012)). We note that unlike in (Kupiainen-Määttä(2016)), the system is considered at various temperatures in this paper.

Two data sets were generated. First, time evolution of the concentrations $C_i(t)$ is computed for time values less than the time at which the system has attained the steady state. The maximum time we run is 60 minutes in the above model configurations. In this case, it is assumed that the

²Time-of-flight mass spectrometer

Table 5: Neutral molecular clusters included into model system. The first column indicates the number of sulphuric acid molecules, the second column stands for the number of ammonia in the cluster.

Number of H ₂ SO ₄ molecules	Number of NH ₃ molecules
0	1
1	0-1
2	0-2
3	1-3
4	2-5
5	3-5

Table 6: Monomer concentrations used in simulations

[H ₂ SO ₄] monomers (in cm ⁻³)	[NH ₃] monomers (in ppt)
1e + 7	35
5e + 7	61.875
1e + 8	88.75
-	115.625
-	142.5
-	169.375
-	196.25
-	223.125
-	250

concentrations for all the clusters are measured under constant temperature with time resolution comprising 1.5 minutes, which comprises overall 41 transient concentration measurements for each of the cluster types i .

Secondly, we solve for time-independent steady-state concentrations for all the cluster types for two temperatures comprising 278 K and 292 K. In both data configurations, the steady-state cluster concentrations are calculated as the average of the concentrations determined for time instances $t_1 := 50$ min and $t_2 := 60$. The measure of how close the system has reached to the steady state is monitored by a convergence parameter, which is the ratio of the concentrations at times t_2 and t_1 , taken in each case for the cluster for which this ratio deviated most from unity, (Kupiainen-Määttä(2016)).

In both data settings, the simulation outputs are amended with the measurement errors sampled from a multivariate, non-correlated, Gaussian distribution, where the variance of the distribution depends on cluster type i , temperature T and time instance t . While a simplification of noise characteristics of the real data obtained from a mass or ion spectrometer, we impose that the standard deviation of the noise comprises 0.001% of the original concentration.

Note that apart from generation of synthetic data, we apply the ACDC as a kinematic model of cluster population in the MCMC simulations. The ACDC outputs are compared to the synthetic measurements and explained in Section 2.2.

Table 7: Domain limitations for two data settings under consideration imposed to exclude non-physical parameters in parameter identification procedure.

Data settings	Estimated parameters	Minimal value	Maximal value
Data setting 1	Base 10 logarithms of evaporation rates	-12	12
Data setting 2	Cluster formation enthalpies and entropies	-400	0

3.2 Markov chain Monte-Carlo simulations

The evaporation rate coefficients $\gamma_{i+j \rightarrow i,j}$ appearing in the ACDC simulation of 10 are treated as unknown parameters. Our purpose is to determine all the parameter sets that reproduce the synthetic data within their noise level (which is known). We do this using Markov Chain Monte Carlo (MCMC) sampling.

The MCMC approach computes a posterior probability density function of the parameters as point-wise likelihood approximations across the parameter space. The algorithm samples the candidate parameter points from a predefined proposal distribution, and then either accept or reject it, according to how closely the output model fits the data. The fundamental technique is the Metropolis algorithm (Metropolis et al.(1953)). The sets of parameters which produce cluster concentrations within the allotted noise level of the data are kept in the sampled distribution. Finally, the approximation of the posterior distribution is constructed from the retained parameter sets. We remark that to create a reliable sample from the underlying parameter distribution, many different parameter combinations must be tested; that is, the length of the MCMC chain must be large enough (Haario et al.(1999)), (Haario et al.(2001))). In both our studies, the MCMC chain length typically comprised 3 million samples. The MCMC acceptance probabilities (defined below) in each of the cases were about 88.0%, which a typical level of acceptance since the “forward” ACDC model (in which the rate coefficients are known) is deterministic.

In this paper we employ a variant of the Metropolis algorithm which is more efficient at parameter sampling when the parameter space is large (Haario et al.(2006)). This variant is called the Delayed Rejection Adaptive Metropolis (DRAM), introduced in (Haario et al.(2006)). We briefly explain our approach below.

First, an initial prior distribution for the parameter values θ (represented in array form) is chosen and set to be the proposed “true” distribution from which possible parameters are sampled. In our case, we chose the flat prior, but impose some domain restrictions for sampling from this prior to exclude unphysical parameters (see Tables 7-8).

We emphasize that there are currently *no theoretical principles or experimental results which indicate possible restrictions for even the order of magnitude of the evaporation rates*. However, we assume that the evaporation rates with orders of magnitude less than 10^{-10}cm^{-3} are irrelevant in practise, since such an evaporation event is highly improbable, and it is very likely that instead the cluster will grow further by collisions. Similarly, when the evaporation rate is of the order of magnitude more than 10^{+10}cm^{-3} , it is reasonable to expect that the cluster will most certainly evaporate before it has a chance to grow further. With these assumptions, the prior distribution of the evaporation rates spans over several orders of magnitude, and the base 10 logarithm of evaporation rates was sampled from the range of -12 to 12.

An outline of the above procedure is illustrated in Figure 2 below.

We next explicitly describe what \mathbf{C}_{exp} and θ (which give the acceptance probability in the expression ?? represent in the two study cases.

Table 8: Additional domain limitations for the data setting 2 from Table 7 (identification of cluster formation enthalpies and entropies), where the cluster formation enthalpy of the i -th cluster is denoted by ΔH_i and the symbols A and N stand for ammonia and sulphuric acid, respectively.

$\Delta H_{2A} > \Delta H_{2A1N}$	$\Delta H_{3A2N} > \Delta H_{4A2N}$
$\Delta H_{1A1N} > \Delta H_{2A1N}$	$\Delta H_{4A2N} > \Delta H_{4A3N}$
$\Delta H_{2A1N} > \Delta H_{3A1N}$	$\Delta H_{4A3N} > \Delta H_{4A4N}$
$\Delta H_{2A2N} > \Delta H_{3A2N}$	$\Delta H_{4A4N} > \Delta H_{5A5N}$
$\Delta H_{3A1N} > \Delta H_{3A2N}$	$\Delta H_{4A4N} > \Delta H_{4A5N}$

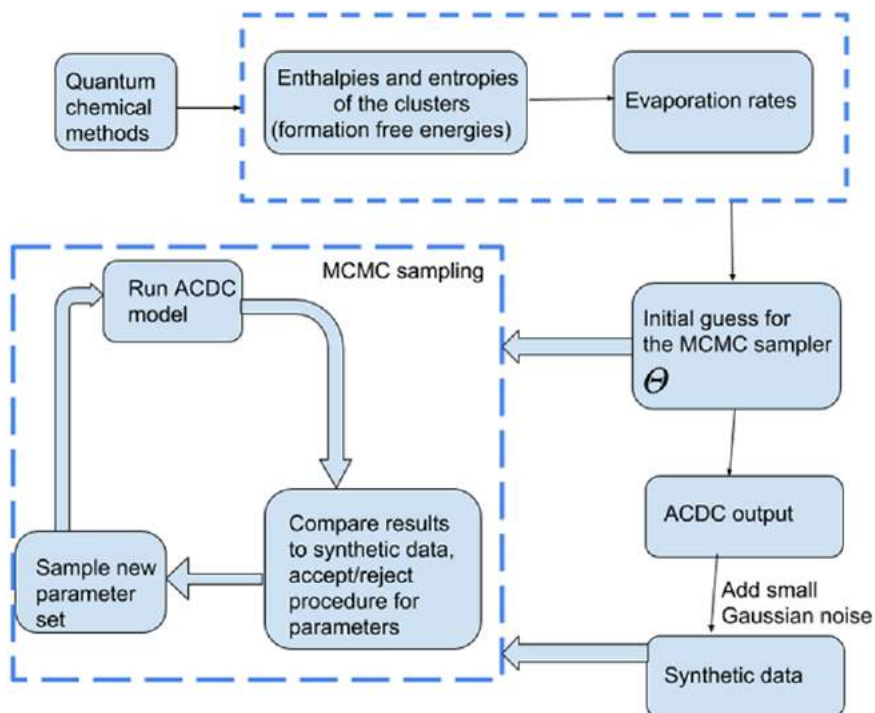


Figure 2: Schematic representation of the study methods.

In the first study, the free parameters θ represent the evaporation rates. The data \mathbf{C}_{exp} is either the time-independent steady-state or transient cluster concentrations measured at temperature 278 K.

In the second study, we use Equations 13 and 14 to express the evaporation rates as functions of thermodynamic data, parametrized by temperature:

$$\gamma_{i+j \rightarrow i,j} = f(T, \{\Delta H_k, \Delta S_k\}_{k \in \{i+j, i, j\}}). \quad (15)$$

In 15, we set $T = 278$ K or $T = 292$ K. We emphasize that the rates $\gamma_{i+j \rightarrow i,j}$ now depend on temperature and six parameters: the cluster formation enthalpy ΔH_{i+j} and entropy ΔS_{i+j} of the evaporating cluster $i + j$, and the formation enthalpies $\Delta H_i, \Delta H_j$ and entropies $\Delta S_i, \Delta S_j$ of the clusters i and j respectively. In this setting θ represents the array of quantities $\Delta H_{i+j}, \Delta S_{i+j}, \Delta H_i, \Delta H_j, \Delta S_i, \Delta S_j$ with $i + j \in \{1, 2, \dots, 16\}$.

At either temperature $T = 278$ K or $T = 292$ K, the smaller clusters for certain combinations of ammonia and sulphuric acid may arise from the evaporation of several larger clusters. This implies that several of the pairs $\Delta H_i, \Delta S_i$ appear in expression 15 for the evaporation rates of different cluster types. Additionally, the Gibbs formation free energies of monomers are fixed to be zero, and their associated enthalpies and entropies do not vary in our simulations. This imposes additional constraints on possible parameter values. One can calculate that of the 39 evaporations that are involved in the dynamics of the neutral cluster system under consideration, only 28 distinct entropy and enthalpy rates appear. Consequently, in this case the number of free parameters has been reduced from 39 to 28. This information is summarized in Table 7. Moreover, from this table one can see that the entropy and enthalpy values lie within two orders of magnitude. This feature of the entropies and enthalpies has the effect of reducing the *stiffness* of the differential system 10 (computed via ACDC) which allows for easier integration via VODE.

For the setting above, the data \mathbf{C}_{exp} are the time-independent steady-state cluster concentrations measured at temperature 278 K or 292 K.

3.2.1 Likelihood, data and cost function

The likelihood of observing the data \mathbf{C}_{exp} given the parameter values θ is

$$p(\mathbf{C}_{exp}|\theta) = \frac{1}{(2\pi)^{n_{out}/2}} \exp\left(-\frac{1}{2}SS_{sum}(\theta)\right), \quad (16)$$

where n_{out} is the number of measurements and $SS_{sum}(\theta)$ is the cost function. We elucidate the cost function below. In our first study in which simulations are conducted with time-dependent data, the number of measurements is $n_{out} = 27 * (N_c * N_t + 1)$, where $N_c = 16$ is the number of cluster types whose concentrations are measured and $N_t = 41$ is the number of time-step measurements available for each of the cluster types. As explained in Section 2.1, after each VODE integration, a convergence coefficient is computed from the steady-state cluster concentrations to ensure that the system has attained the steady-state.

In our first study, the parameter fit to the data was evaluated by the sum of squared residuals of the model outputs \mathbf{C}_{mod} and the measurements, \mathbf{C}_{exp} . Since concentrations of molecular clusters span a large range (from 10^{-5} to 10^9 particles per cm^3), the sum of squared residuals, (or *cost function*) normalizes the residuals by the measurement error variance. In this manner, we avoid fitting mainly the high values of the concentration. Precisely,

$$SS_{sum} = \sum_{i=1}^{N_c} \sum_{j=1}^{N_t} \frac{(C_{exp,i}(t_j) - C_{mod,i}(t_j))^2}{\sigma_{ji}^2}. \quad (17)$$

Note that the standard deviation σ_{ji} is matched separately for each cluster type and every time instance. Here we assume that the instrument is capable of detecting all the cluster types represented in the system at arbitrary small levels of concentration. This simplification was considered in order to illustrate the proposed approach.

When parameter estimation is conducted with steady-state cluster concentrations (as is considered in our second study), we use the following cost function:

$$SS_{\text{sum}} = \sum_{i=1}^{N_c} \sum_{j=1}^{N_T} \frac{(C_{\text{exp},i}(T_j) - C_{\text{mod},i}(T_j))^2}{\sigma_{ji}^2}. \quad (18)$$

Now N_T denotes the number of steady state configurations at different *temperatures* (not times!) and T_j stands for the measured *temperature*. In this study, the number of measurements for the likelihood given by Equation 16 is $n_{\text{out}} = 4 * (N_c * N_T + 1)$ (again $N_c = 16$ cluster types).

4 RESULTS

4.1 Identification of the evaporation rate coefficients from steady-state and transient data

First, we generate synthetic steady-state data by the method in Section 3.1, for varying initial ammonia monomer concentrations, previously summarized in Table 6; the sulphuric acid monomer is supplied to the system at a constant rate comprising 6.3335×10^4 at the temperature $T = 278$ K. As an output, we obtain the concentrations for all cluster types considered (listed earlier in Table 5), measured when the system has attained the steady-state. A graphical representation of the data set is given below in Figure 3.

4.2 Estimating enthalpies and entropies from steady-state concentration measurements

In this section we describe another method for regularizing our problem of estimating evaporation rates from steady-state concentration data. We will determine the cluster formation enthalpies and entropies from two sets of synthetic, steady-state cluster concentrations, now measured at two temperatures: 278 and 292 K. This data set is plotted in Figures 3 and ??.

We also write the evaporation rate parameters as functions of the cluster formation enthalpies and entropies, parametrized by the temperature (either 278K or 292 K). By re-expressing our unknown evaporation parameters in this way, the number of free parameters in our problem reduces from 39 to 28, as many evaporation rates are determined by the same sets of thermodynamic data. The cluster formation enthalpy and entropy are our new free parameters, which now take values within same order of magnitude of 10^2 (kcal mol⁻¹ and cal K⁻¹ mol⁻¹ for cluster formation enthalpy and entropy, respectively). We will demonstrate that these changes plus the extended data set transforms our parameter identification problem from an ill-posed problem to a well-posed one. We use synthetic steady-state cluster concentrations generated for two temperatures to recover the thermodynamic parameters. This is done to improve the identification by using the temperature dependence of the Gibbs free energies (and the evaporation rates).

For each temperature choice, we use the methods described in Section 2 to obtain synthetic steady-state cluster concentration data. We summarize this data in Table 6; the data sets are plotted in Figure 3 for 278 K and ?? for 292 K. Three MCMC runs were conducted to average the bias attributed to random noise added to the data, as discussed in the previous section. An example of

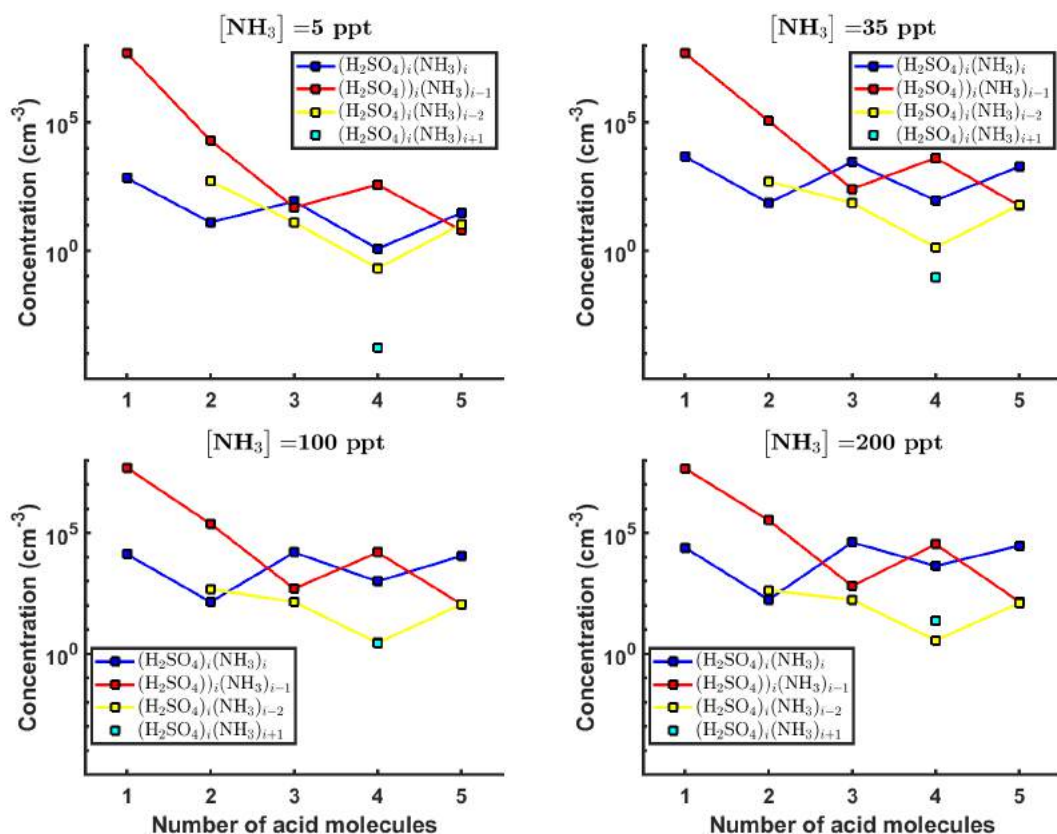


Figure 3: Steady-state cluster concentrations for the clusters containing sulphuric acid and a varying number of ammonia molecules as a function of the number of acid molecules for $[\text{NH}_3]$ concentrations comprising (a) 5 ppt, (b) 35 ppt, (c) 100 ppt and (d) 200 ppt at temperature $T=278$ K. The concentrations have been amended with multivariate non-correlated Gaussian noise with standard deviation comprising 0.001% of the original cluster concentration. The source of sulphuric acid monomers is $[\text{H}_2\text{SO}_4] = 6.3335 \times 10^4 \text{ s}^{-1}$ in each of the simulations.

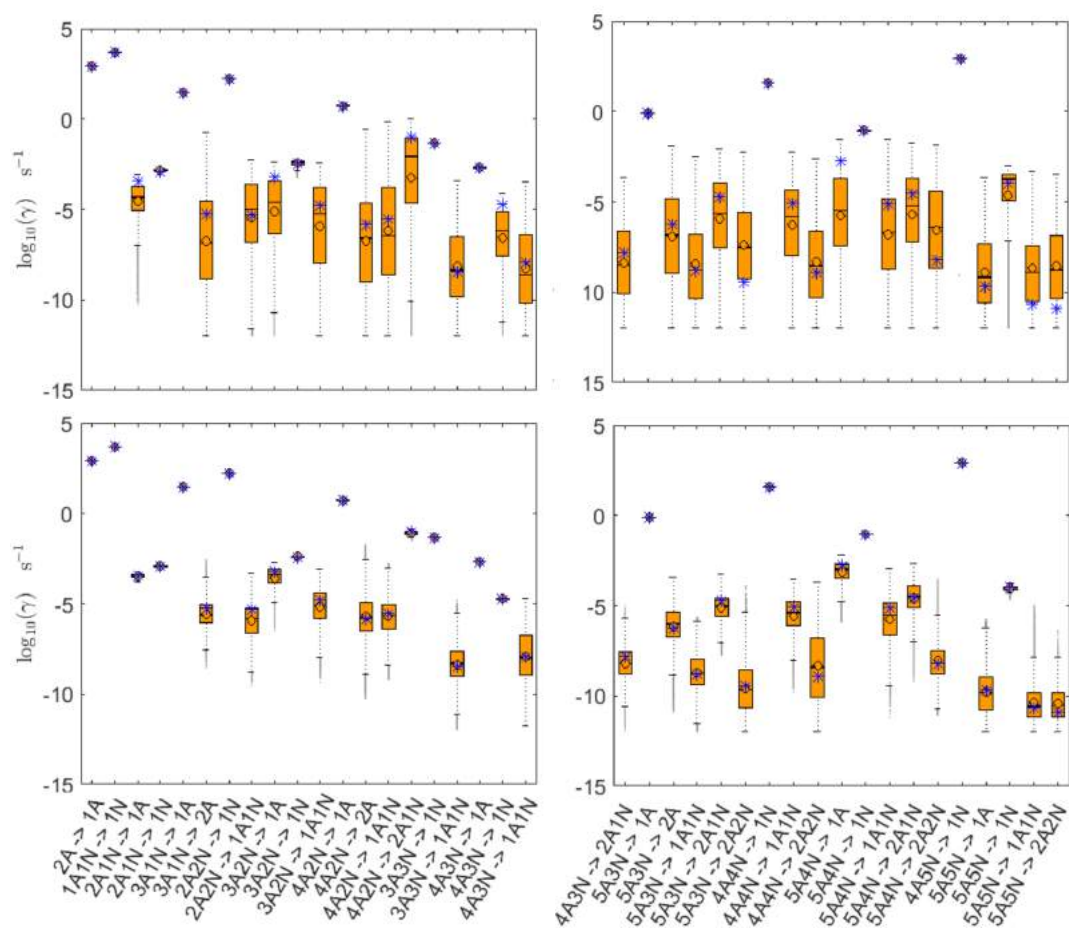


Figure 4: Comparison of 95 % confidence intervals (orange box plots) of base 10 logarithms of the evaporation rates determined from (a)-(b) steady-state and (c)-(d) time-dependent synthetic data measured at temperature 278 K. In reactions "A" stands for H_2SO_4 and "N" for NH_3 . Here blue asterisks denote the baseline values used for creating the synthetic data (borrowed from (Ortega et al.(2012))).

one of the sampled chains is illustrated in Figure ?? . It can be seen that all the chains are bounded, with the exception of the formation enthalpy and entropy of the biggest cluster $((\text{H}_2\text{SO}_2)_5(\text{NH}_3)_5)$.

Next we consider the one-dimensional marginal posterior distributions of free parameters build from the stationary parts of the three sampled chains merged together, see Figure ?? . It can be seen that for all the clusters except $(\text{H}_2\text{SO}_2)_5(\text{NH}_3)_5$ the estimated formation enthalpies vary at most by 1 kcal mol^{-1} , while the variance for the formation entropies is less than $1 \text{ cal K}^{-1} \text{ mol}^{-1}$. The estimated free parameters together with the baseline quantum chemistry-based values from (Ortega et al.(2012)) used for generation of the synthetic data are summarized in Table ?? .

From our MCMC simulations, we see that the formation enthalpies and entropies of the molecular clusters exhibit strong correlations Notice that the evaporation rates calculated from a posterior distribution of sampled thermodynamic parameters for the temperature 278 K are close to the baseline values from (Ortega et al.(2012)) used for generation of the synthetic data and their variances are less than one order of magnitude.

CONCLUSIONS

In this paper we studied two proposed computational scenarios for the determination of evaporation rates of molecular clusters from concentration measurements. We generated several sets of synthetic data for the purpose of parameter identification.

In the first scenario, we sought to determine the cluster evaporation rates from both steady-state and time-dependent cluster concentration data. Due to the mathematical stiffness of the ordinary differential equations describing the time evolution of the cluster concentrations, we were only able to identify a subset of the free parameters (evaporation rates) from the available data. This stiffness originates from the vastly different timescales of some of the key evaporation rates.

In the second scenario, we used steady-state concentration data for two different temperatures. We introduced a reparametrization expressing the evaporation rates in terms of cluster formation enthalpies and entropies, and temperature. This reduced the number of parameters we sought to identify. It also lessened the stiffness of the system, as the cluster formation enthalpies and entropies for our system have comparable orders of magnitude. We demonstrated that steady-state concentration data at two different temperatures could be used to determine all the unknown formation enthalpies and entropies, and thus the evaporation rates, to within acceptable accuracy.

The approach presented here can also be applied to infer evaporation rates from mass spectrometric measurements of molecular cluster concentrations. This naturally requires accounting for the process of charging neutral clusters, with its associated uncertainties. A clear conclusion of our proof-of-concept study is that steady-state data at different temperatures is more useful for determining evaporation rates than time-dependent data at a single temperature. Determining very low (below 10^{-5} s^{-1}) evaporation rates may also require additional measurements at low vapor concentrations, which naturally require longer timescales to reach a steady state.

ACKNOWLEDGEMENTS

This work was supported by the European Research Council project 692891-DAMOCLES, Academy of Finland (project number 307331), and University of Helsinki: Faculty of Science ATMATH project, for funding, and the CSC-IT Centre for Science in Espoo, Finland, for computational resources. We also thank Olli Pakarinen (Institute for Atmospheric and Earth System Research, University of Helsinki, Helsinki, Finland) for advise in plotting the synthetic data used in the present study.

REFERENCES

- Almeida, J., Schobesberger, S., Kürten, A., Ortega, I. K., Kupiainen-Määttä, O., Praplan, A. P., Adamov, A., Amorim, A., Bianchi, F., Breitenlechner, M., David, A., Dommen, J., Donahue, N. M., Downard, A., Dunne, E., Duplissy, J., Ehrhart, S., Flagan, R. C., Franchin, A., Guida, R., Hakala, J., Hansel, A., Heinritzi, M., Henschel, H., Jokinen, T., Junninen, H., Kajos, M., Kangasluoma, J., Keskinen, H., Kupc, A., Kurtén, T., Kvashin, A. N., Laaksonen, A., Lehtipalo, K., Leiminger, M., Leppä, J., Loukonen, V., Makhmutov, V., Mathot, S., McGrath, M. J., Nieminen, T., Olenius, T., Onnela, A., Petäjä, T., Riccobono, F., Riipinen, I., Rissanen, M., Rondo, L., Ruuskanen, T., Santos, F. D., Sarnela, N., Schallhart, S., Schnitzhofer, R., Seinfeld, J. H., Simon, M., Sipilä, M., Stozhkov, Y., Stratmann, F., Tomé, A., Tröstl, J., Tsagkogeorgas, G., Vaattovaara, P., Viisanen, Y., Virtanen, A., Vrtala, A., Wagner, P. E., Weingartner, E., Wex, H., Williamson, C., Wimmer, D., Ye, P., Yli-Juuti, T., Carslaw, K. S., Kulmala, M., Curtius, J., Baltensperger, U., Worsnop, D. R., Vehkamäki, H., and Kirkby, J.: Molecular understanding of sulphuric acid-amine particle nucleation in the atmosphere, *Nature*, 502, 359, URL <https://doi.org/10.1038/nature12663>, 2013.
- Ball, J. M., Carr, J., and Penrose, O.: The Becker-Doring cluster equations: basic properties and asymptotic behaviour of solutions, *Comm. Math. Phys.*, 104, 657–692, URL <https://projecteuclid.org:443/euclid.cmp/1104115173>, 1986.
- Bianchi, F., Tröstl, J., Junninen, H., Frege, C., Henne, S., Hoyle, C. R., Molteni, U., Herrmann, E., Adamov, A., Bukowiecki, N., Chen, X., Duplissy, J., Gysel, M., Hutterli, M., Kangasluoma, J., Kontkanen, J., Kürten, A., Manninen, H. E., Münch, S., Peräkylä, O., Petäjä, T., Rondo, L., Williamson, C., Weingartner, E., Curtius, J., Worsnop, D. R., Kulmala, M., Dommen, J., and Baltensperger, U.: New particle formation in the free troposphere: A question of chemistry and timing, *Science*, 352, 1109, URL <http://science.sciencemag.org/content/352/6289/1109.abstract>, 2016.
- Braak, C. J. F. T.: A Markov Chain Monte Carlo version of the genetic algorithm Differential Evolution: easy Bayesian computing for real parameter spaces, *Statistics and Computing*, 16, 239–249, URL <https://doi.org/10.1007/s11222-006-8769-1>, 2006.
- Ehn, M., Thornton, J. A., Kleist, E., Sipilä, M., Junninen, H., Pullinen, I., Springer, M., Rubach, F., Tillmann, R., Lee, B., Lopez-Hilfiker, F., Andres, S., Acir, I.-H., Rissanen, M., Jokinen, T., Schobesberger, S., Kangasluoma, J., Kontkanen, J., Nieminen, T., Kurtén, T., Nielsen, L. B., Jørgensen, S., Kjaergaard, H. G., Canagaratna, M., Maso, M. D., Berndt, T., Petäjä, T., Wahner, A., Kerminen, V.-M., Kulmala, M., Worsnop, D. R., Wildt, J., and Mentel, T. F.: A large source of low-volatility secondary organic aerosol, *Nature*, 506, 476, URL <https://doi.org/10.1038/nature13032>, 2014.
- Eisele, F. L. and Hanson, D. R.: First Measurement of Prenucleation Molecular Clusters, *J. Phys. Chem. A*, 104, 830–836, <https://doi.org/10.1021/jp9930651>, URL <https://doi.org/10.1021/jp9930651>, 2000.
- Elm, J. and Kristensen, K.: Basis set convergence of the binding energies of strongly hydrogen-bonded atmospheric clusters., *Physical chemistry chemical physics : PCCP*, 19, 1122–1133, 2017.
- Elm, J., Bilde, M., and Mikkelsen, K. V.: Assessment of binding energies of atmospherically relevant clusters., *Physical chemistry chemical physics : PCCP*, 15, 16 442–5, 2013.

- Haario, H., Saksman, E., and Tamminen, J.: Adaptive proposal distribution for random walk Metropolis algorithm, *Computational Statistics*, 14, 375–395, URL <https://doi.org/10.1007/s001800050022>, 1999.
- Haario, H., Saksman, E., and Tamminen, J.: An adaptive Metropolis algorithm, *Bernoulli*, 7, 223–242, URL <https://projecteuclid.org:443/euclid.bj/1080222083>, 2001.
- Haario, H., Laine, M., Mira, A., and Saksman, E.: DRAM: Efficient adaptive MCMC, *Statistics and Computing*, 16, 339–354, URL <https://doi.org/10.1007/s11222-006-9438-0>, 2006.
- Halonen, R., Zapadinsky, E., Kurtén, T., Vehkamäki, H., and Reischl, B.: Rate enhancement in collisions of sulfuric acid molecules due to long-range intermolecular forces, *Atmospheric Chemistry and Physics Discussions*, 2019, 1–17, <https://doi.org/10.5194/acp-2019-400>, URL <https://www.atmos-chem-phys-discuss.net/acp-2019-400/>, 2019.
- Hingant, E. and Yvinec, R.: Deterministic and Stochastic Becker-Döring Equations: Past and Recent Mathematical Developments, pp. 175–204, 2017.
- Hyttinen, N., Otkjær, R. V., Iyer, S., Kjaergaard, H. G., Rissanen, M. P., Wennberg, P. O., and Kurtén, T.: Computational Comparison of Different Reagent Ions in the Chemical Ionization of Oxidized Multifunctional Compounds, *J. Phys. Chem. A*, 122, 269–279, <https://doi.org/10.1021/acs.jpca.7b10015>, URL <https://doi.org/10.1021/acs.jpca.7b10015>, 2018.
- Junninen, H., Ehn, M., Petäjä, T., Luosujärvi, L., Kotiaho, T., Kostianen, R., Rohner, U., Gonin, M., Fuhrer, K., Kulmala, M., and Worsnop, D. R.: A high-resolution mass spectrometer to measure atmospheric ion composition, *Atmospheric Measurement Techniques*, 3, 1039–1053, <https://doi.org/10.5194/amt-3-1039-2010>, URL <https://www.atmos-meas-tech.net/3/1039/2010/>, 2010.
- Kirkby, J., Curtius, J., Almeida, J., Dunne, E., Duplissy, J., Ehrhart, S., Franchin, A., Gagné, S., Ickes, L., Kürten, A., Kupc, A., Metzger, A., Riccobono, F., Rondo, L., Schobesberger, S., Tsagkogeorgas, G., Wimmer, D., Amorim, A., Bianchi, F., Breitenlechner, M., David, A., Dommen, J., Downard, A., Ehn, M., Flagan, R. C., Haider, S., Hansel, A., Hauser, D., Jud, W., Junninen, H., Kreissl, F., Kvashin, A., Laaksonen, A., Lehtipalo, K., Lima, J., Lovejoy, E. R., Makhmutov, V., Mathot, S., Mikkilä, J., Minginette, P., Mogo, S., Nieminen, T., Onnela, A., Pereira, P., Petäjä, T., Schnitzhofer, R., Seinfeld, J. H., Sipilä, M., Stozhkov, Y., Stratmann, F., Tomé, A., Vanhanen, J., Viisanen, Y., Vrtala, A., Wagner, P. E., Walther, H., Weingartner, E., Wex, H., Winkler, P. M., Carslaw, K. S., Worsnop, D. R., Baltensperger, U., and Kulmala, M.: Role of sulphuric acid, ammonia and galactic cosmic rays in atmospheric aerosol nucleation, *Nature*, 476, 429, URL <https://doi.org/10.1038/nature10343>, 2011.
- Kupiainen-Määttä, O.: A Monte Carlo approach for determining cluster evaporation rates from concentration measurements, *Atmospheric Chemistry and Physics*, 16, 14 585–14 598, <https://doi.org/10.5194/acp-16-14585-2016>, URL <https://www.atmos-chem-phys.net/16/14585/2016/>, 2016.
- Kupiainen-Määttä, O., Olenius, T., Kurtén, T., and Vehkamäki, H.: CIMS Sulfuric Acid Detection Efficiency Enhanced by Amines Due to Higher Dipole Moments: A Computational Study, *J. Phys. Chem. A*, 117, 14 109–14 119, <https://doi.org/10.1021/jp4049764>, URL <https://doi.org/10.1021/jp4049764>, 2013.
- Kürten, A.: New particle formation from sulfuric acid and ammonia: nucleation and growth model based on thermodynamics derived from CLOUD measurements for a wide range of conditions, *Atmospheric Chemistry and Physics*, 19, 5033–5050, <https://doi.org/10.5194/acp-19-5033-2019>, URL <https://www.atmos-chem-phys.net/19/5033/2019/>, 2019.

- , URL <https://www.atmos-chem-phys.net/15/10701/2015/>, 2015.
- Kurtén, T., Torpo, L., Ding, C.-G., Vehkamäki, H., Sundberg, M. R., Laasonen, K., and Kulmala, M.: A density functional study on water-sulfuric acid-ammonia clusters and implications for atmospheric cluster formation, *J. Geophys. Res.*, 112, <https://doi.org/10.1029/2006jd007391>, URL <https://doi.org/10.1029/2006JD007391>, 2007.
- Lee, S.-H., Reeves, J. M., Wilson, J. C., Hunton, D. E., Viggiano, A. A., Miller, T. M., Ballenthin, J. O., and Lait, L. R.: Particle Formation by Ion Nucleation in the Upper Troposphere and Lower Stratosphere, *Science*, 301, 1886, URL <http://science.sciencemag.org/content/301/5641/1886.abstract>, 2003.
- Matsugi, A.: Collision Frequency for Energy Transfer in Unimolecular Reactions, *J. Phys. Chem. A*, 122, 1972–1985, <https://doi.org/10.1021/acs.jpca.8b00444>, URL <https://doi.org/10.1021/acs.jpca.8b00444>, 2018.
- McGrath, M. J., Olenius, T., Ortega, I. K., Loukonen, V., Paasonen, P., Kurtén, T., Kulmala, M., and Vehkamäki, H.: Atmospheric Cluster Dynamics Code: a flexible method for solution of the birth-death equations, *Atmospheric Chemistry and Physics*, 12, 2345–2355, <https://doi.org/10.5194/acp-12-2345-2012>, URL <https://www.atmos-chem-phys.net/12/2345/2012/>, 2012.
- Metropolis, N., Rosenbluth, A. W., Rosenbluth, M. N., Teller, A. H., and Teller, E.: Equation of State Calculations by Fast Computing Machines, *J. Chem. Phys.*, 21, 1087–1092, <https://doi.org/10.1063/1.1699114>, URL <https://doi.org/10.1063/1.1699114>, 1953.
- N. Brown, P., D. Byrne, G., and C. Hindmarsh, A.: VODE: a variable-coefficient ODE solver, vol. 10, 1989.
- Nadykto, A. B., Herb, J., Yu, F., and Xu, Y.: Enhancement in the production of nucleating clusters due to dimethylamine and large uncertainties in the thermochemistry of amine-enhanced nucleation, vol. 624, 2014.
- Olenius, T., Kupiainen-Määttä, O., Ortega, I. K., Kurtén, T., and Vehkamäki, H.: Free energy barrier in the growth of sulfuric acid-ammonia and sulfuric acid-dimethylamine clusters, *J. Chem. Phys.*, 139, 084312, <https://doi.org/10.1063/1.4819024>, URL <https://doi.org/10.1063/1.4819024>, 2013a.
- Olenius, T., Schobesberger, S., Kupiainen-Määttä, O., Franchin, A., Junninen, H., Ortega, I. K., Kurtén, T., Loukonen, V., Worsnop, D. R., Kulmala, M., and Vehkamäki, H.: Comparing simulated and experimental molecular cluster distributions, *Faraday Discuss.*, 165, 75–89, <https://doi.org/10.1039/C3FD00031A>, URL <http://dx.doi.org/10.1039/C3FD00031A>, 2013b.
- Ortega, I. K., Kupiainen, O., Kurtén, T., Olenius, T., Wilkman, O., McGrath, M. J., Loukonen, V., and Vehkamäki, H.: From quantum chemical formation free energies to evaporation rates, *Atmospheric Chemistry and Physics*, 12, 225–235, <https://doi.org/10.5194/acp-12-225-2012>, URL <https://www.atmos-chem-phys.net/12/225/2012/>, 2012.
- Schobesberger, S., Franchin, A., Bianchi, F., Rondo, L., Duplissy, J., Kürten, A., Ortega, I. K., Metzger, A., Schnitzhofer, R., Almeida, J., Amorim, A., Dommen, J., Dunne, E. M., Ehn, M., Gagné, S., Ickes, L., Junninen, H., Hansel, A., Kerminen, V.-M., Kirkby, J., Kupc, A., Laaksonen, A., Lehtipalo, K., Mathot, S., Onnela, A., Petäjä, T., Riccobono, F., Santos, F. D., Sipilä, M., Tomé, A., Tsagkogeorgas, G., Viisanen, Y., Wagner, P. E., Wimmer, D., Curtius, J., Donahue, N. M., Baltensperger, U., Kulmala, M., and Worsnop, D. R.: On

- the composition of ammonia-sulfuric-acid ion clusters during aerosol particle formation, *Atmospheric Chemistry and Physics*, 15, 55–78, <https://doi.org/10.5194/acp-15-55-2015>, URL <https://www.atmos-chem-phys.net/15/55/2015/>, 2015.
- Vahteristo, K., Laari, A., Haario, H., and Solonen, A.: Estimation of kinetic parameters in neopentyl glycol esterification with propionic acid, *Chemical Engineering Science*, 63, 587–598, <https://doi.org/10.1016/j.ces.2007.09.023>, 2008.
- Yan, C., Dada, L., Rose, C., Jokinen, T., Nie, W., Schobesberger, S., Junninen, H., Lehtipalo, K., Sarnela, N., Makkonen, U., Garmash, O., Wang, Y., Zha, Q., Paasonen, P., Bianchi, F., Sipilä, M., Ehn, M., Petäjä, T., Kerminen, V.-M., Worsnop, D. R., and Kulmala, M.: The role of $\text{H}_2\text{SO}_4\text{-NH}_3$ anion clusters in ion-induced aerosol nucleation mechanisms in the boreal forest, *Atmospheric Chemistry and Physics*, 18, 13 231–13 243, <https://doi.org/DOI = 10.5194/acp-18-13231-2018>, URL URL = <https://www.atmos-chem-phys.net/18/13231/2018/>, 2018.
- Yang, H., Goudeli, E., and Hogan, C. J. J.: Condensation and dissociation rates for gas phase metal clusters from molecular dynamics trajectory calculations., *The Journal of chemical physics*, 148, 164 304, 2018.
- Yu, F. and Turco, R.: Ultrafine aerosol formation via ion-mediated nucleation, *Geophysical Research Letters*, 27, 2000.
- Yu, F., Nadykto, A. B., Herb, J., Luo, G., Nazarenko, K. M., and Uvarova, L. A.: $\text{H}_2\text{SO}_4\text{-H}_2\text{O-NH}_3$ ternary ion-mediated nucleation (TIMN): kinetic-based model and comparison with CLOUD measurements, *Atmospheric Chemistry and Physics*, 18, 17 451–17 474, <https://doi.org/10.5194/acp-18-17451-2018>, URL <https://www.atmos-chem-phys.net/18/17451/2018/>, 2018.
- Zhao, J., Eisele, F. L., Titcombe, M., Kuang, C., and McMurry, P. H.: Chemical ionization mass spectrometric measurements of atmospheric neutral clusters using the cluster-CIMS, *J. Geophys. Res.*, 115, <https://doi.org/10.1029/2009jd012606>, URL <https://doi.org/10.1029/2009JD012606>, 2010.

The Yield of Methanesulfonic Acid and Sulphuric Acid From the Oxidation of Dimethyl Sulfide

J.Shen¹, X.He¹, W.Scholz², J.Them¹, G.Mario³, M.Sipilä¹, K.Lehtipalo¹, and CLOUD collaboration

1. Institute for Atmospheric and Earth system research, University of Helsinki, Helsinki, Finland.
2. Institute for Ion Physics and Applied Physics, University of Innsbruck, 6020 Innsbruck, Austria
3. Goethe University Frankfurt, Institute for Atmospheric and Environmental Sciences, 60438 Frankfurt am Main, Germany

Keywords: Cloud experiment, flow tube experiment, oxidation, OH radicals

INTRODUCTION

Dimethyl sulphide (DMS) produced by organisms from oceans is the main natural source of the sulphur to Earth's atmosphere. The production of sulphate from the oxidation of dimethyl sulphide (DMS) was proposed as precursor for sulphur-containing aerosols in the marine condition¹. In the gas-phase, the initial oxidation process starts from OH addition and OH abstraction, accompanying with the reaction of the HO₂, RO₂, NO, and isomerization, the final production leads to sulphuric acid (H₂SO₄), methanesulfonic acid (MSA: CH₃SO₃H), dimethyl sulfoxide (DMSO: CH₃S(O)CH₃) and so on². Out of all final products, MSA and especially SA play role in the new particle formation and growth. CLOUD chamber and flow tube experiments were conducted to measure the yields of MSA and SA from the oxidation of DMS, since it is not easy to perform field measurement where the sole source of SO₂ is the atmospheric oxidation of DMS. Once we know the effect of NO_x, temperature and OH radicals to the yields of MSA and SA from the oxidation of DMS, we can explain more for the oxidation process and polish the MCM (Master Chemical Mechanisms) model³.

METHODS

CLOUD chamber is the cleanest chamber in the world, where we can simulate the atmosphere conditions with high precision. In the CLOUD chamber, the gases are mixed well and the reaction time is long enough for the atmospherically relevant oxidation process. The inner diameter of the flow tube is 222 mm and length is 3500 mm and the reaction time around 5 minutes. Therefore, flow tube experiment can provide us more information about initial steps of oxidation process.

CONCLUSIONS

We first focused on the effect of NO_x in SA and MSA yields. Based on the results from the CLOUD chamber, the ratio of MSA and SA changed with changing concentration of NO_x, although the effect was small. The flow tube experiment (Figure 1b) indicate that the increase of NO_x will promote more SA, which imply the relationship between the NO_x concentration and SA yield. Besides, temperature diplococus (keep all the gases constant, only change temperature) also suggest that the importance of isomerization in the initial step of the oxidation process.

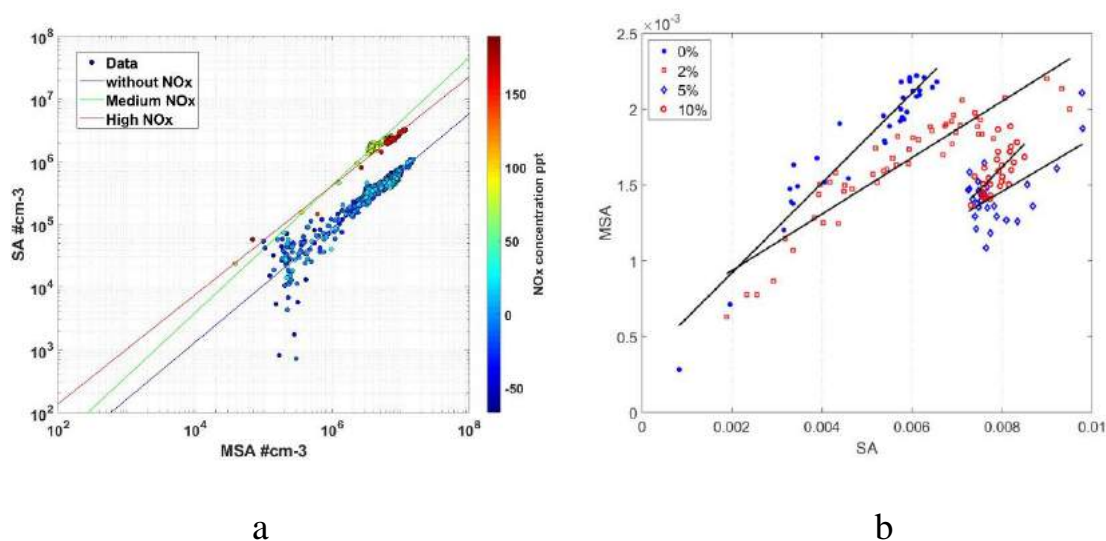


Figure 1 The effect of the NO_x on the yield of MSA and SA (a: CLOUD chamber experiment, there are three conditions with different concentration of NO_x, O₃ and DMS b: flow tube results, in these experiments the concentration of NO_x is the only changed parameter)

ACKNOWLEDGEMENTS

This work has received funding from the European Union's Horizon 2020 research and innovation programme under the Marie Skłodowska-Curie grant agreement No 764991 (CLOUD-MOTION).

REFERENCES

1. Mardyukov, A. and P.R. Schreiner, Atmospherically Relevant Radicals Derived from the Oxidation of Dimethyl Sulfide. *Accounts of Chemical Research*, 2018. 51(2): p. 475-483.
2. Berndt, T., et al., Fast Peroxy Radical Isomerization and OH Recycling in the Reaction of OH Radicals with Dimethyl Sulfide. *The Journal of Physical Chemistry Letters*, 2019: p. 6478-6483.

3. Jenkin et al., *Atmos. Environ.*, 31, 81, 1997; Saunders et al., *Atmos. Chem. Phys.*, 3, 161, 2003

LONG-TERM ASSESMENT OF AIR QUALITY IN HELSINKI, FINLAND

S. SILLANPÄÄ¹, P. L. FUNG¹, M. A. ZAIDAN¹ AND T. HUSSEIN^{1,2}

¹Institute for Atmospheric and Earth System Research/ Physics, Faculty of Science, University of Helsinki, Finland.

²Department of Physics, University of Jordan, Amman 11942, Jordan.

Keywords: AIR QUALITY, AIR QUALITY INDEX

INTRODUCTION

Today's largest environmental threat is air pollution. According to WHO approximately 3 million deaths were caused by exposure to outdoor air pollution in 2012 (WHO, 2016). Air pollution affects human health by increasing both morbidity and mortality cases all around the world. The premature deaths triggered by air pollution are most often related to stroke, lung cancer, heart disease, chronic obstructive pulmonary disease and children's acute respiratory infections.

Air quality index (AQI) describes air quality situation at a specific time and place. It usually takes into account several air pollutants including particulate matter and different gases. AQI is calculated for each of these pollutants separately based on limit values (Hewings, 2001). The air pollutant with the highest index value determines the actual AQI. The pollutants included in the AQI and the limit values vary between countries. In Finland AQI consists of particulate matter (PM_{2.5} and PM₁₀), ozone (O₃), carbon monoxide (CO), nitrogen dioxide (NO₂) and sulphur dioxide (SO₂) (HSY, 2017).

This study aims to evaluate the development of air quality in Helsinki, Finland during the last 23 years. We investigate the variations of several air pollutants and AQI at different monitoring stations. Our aim is to evaluate how the parameters contributing to air quality have changed during the last 23 years and compare the changes between different monitoring stations.

DATA COLLECTION AND METHODS

The measurement data is collected from seven monitoring stations around Helsinki metropolitan area between years 1996 and 2018. Helsinki metropolitan includes the cities of Helsinki, Espoo, Vantaa and Kauniainen. The monitoring stations are operated by Helsinki region Environmental Services Authority. The measurement periods and measured variables vary between the stations. Different types of environments are covered by the monitoring sites including busy traffic sites, areas with active wood burning, background and urban background stations.

Time series and statistical analysis were conducted for each pollutant separately. We calculated hourly, daily, monthly and yearly averaged concentrations and compared them to Finnish national guideline limits and guidelines given by World Health Organisation (WHO).

Air quality index was evaluated in a similar manner at each monitoring stations as the individual parameters. Based on the hourly and monthly averaged values we investigated who the contribution to AQI by air pollutants vary by hour of the day and seasons. The comparison of AQI at the different monitoring stations can be tricky since the measured parameters may vary between stations.

PRELIMINARY RESULTS

Table 1 shows the yearly averaged PM_{2.5} mass concentration at the seven monitoring sites. Based on the slopes the yearly mean values seem to be decreasing at all of the monitoring sites as the slopes vary between -0.327 and -0.136. The red values in table indicate the years when the guideline limit of 10 µg/m³ set by WHO was exceeded. In Kallio, Mannerheimintie and Vallila monitoring stations yearly mean has exceeded the WHO guideline multiple times. All of these stations are located in a proximity of busy road. The number of years when the WHO limit value is exceeded has decreased at all of the stations.

Table 1 Yearly averaged PM_{2.5} mass concentration [µg/m³] at the different monitoring stations. Two last rows represent the slope and 95 % confidence interval for the yearly averaged values. The values in red exceed the WHO guideline limit [10 µg/m³] for the yearly mean. The horizontal line indicates that there is no data available for the specific year.

	Kallio	Leppävaara	Luukki	Mäkelänkatu	Mannerheimintie	Tikkurila	Vallila	Vartiokylä
1996	-	-	-	-	-	-	-	-
1997	-	-	-	-	-	-	11.154	-
1998	-	-	-	-	-	-	12.519	-
1999	11.645	-	-	-	-	-	13.226	-
2000	9.154	-	-	-	-	-	9.866	-
2001	9.406	-	-	-	-	-	10.569	-
2002	10.182	-	-	-	-	-	11.640	-
2003	10.549	-	-	-	-	-	11.351	-
2004	9.246	-	9.340	-	-	-	-	-
2005	10.346	-	11.175	-	12.126	-	-	-
2006	10.285	-	8.542	-	11.125	-	-	-
2007	9.040	-	5.405	-	9.789	-	-	-
2008	8.618	-	7.388	-	9.561	-	-	-
2009	8.267	7.678	7.287	-	9.999	7.854	-	7.364
2010	9.021	8.778	8.790	-	11.231	9.350	-	8.105
2011	7.805	8.902	7.902	-	10.197	8.033	-	7.416
2012	7.499	7.842	7.260	-	8.806	7.123	-	6.597
2013	7.050	7.244	6.604	-	8.736	7.154	-	6.897
2014	8.189	8.068	7.641	-	10.187	8.424	-	9.772
2015	5.658	6.150	6.266	8.102	6.922	5.855	-	7.046
2016	6.100	6.236	5.837	8.485	7.432	7.133	-	5.919
2017	5.159	5.586	4.669	6.234	6.311	5.814	-	5.556
2018	6.805	7.064	5.939	7.840	8.409	7.403	-	7.219
Slope	-0.261	-0.275	-0.268	-0.304	-0.327	-0.217	-0.136	-0.136
95 % CI	0.064	0.173	0.146	0.995	0.135	0.201	0.453	0.256

Figure 1 represents the hourly averaged AQI at Kallio monitoring station. The black line represents official AQI and the coloured lines AQI calculated for the individual air pollutants. Carbon monoxide which is included in the Finnish AQI is not measured in Kallio. Based on the Figure air quality is typically good in Kallio throughout the day. The highest AQI values are attributed to ozone. The AQI calculated for ozone varies between 32 and 41 with lowest values measured during morning peak. PM_{2.5}, PM₁₀ and NO₂ show the opposite pattern as they peak during the morning rush hour. The contribution of SO₂ to AQI is very small during all hours the day.

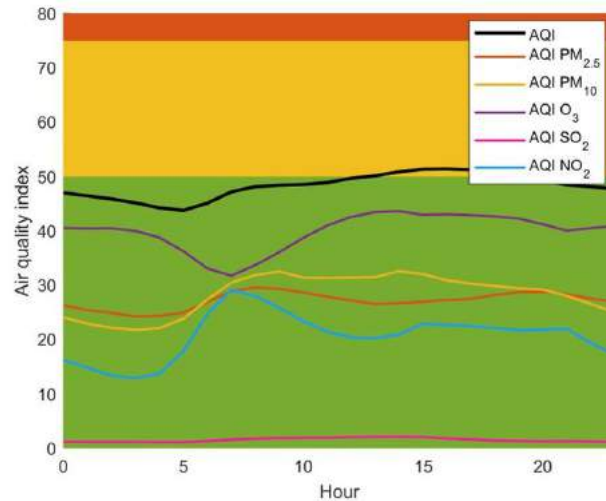


Figure 1 Hourly averaged air quality index at the Kallio monitoring site. The black line represents the actual AQI. The lines with different colours represent the AQI calculated for the individual air pollutants (PM_{2.5}, PM₁₀, O₃, SO₂ and NO₂) based on the Finnish national limit values. The colours on the back represent the index classes. Green is good (below 50), yellow is satisfactory (50-75) and orange is moderate (75-100).

ACKNOWLEDGEMENTS

This work was supported by the EU Urban Innovative Actions via HOPE project (grant number UIA03-240).

REFERENCES

- World Health Organization; 2014. Methods for burden of disease attributable to ambient air pollution for the year 2012. (http://www.who.int/phe/health_topics/outdoorair/databases/AAP_BoD_methods_March2014.pdf?ua=1).
- Hewings, J. Air Quality Indices: A Review; Pollution Probe: Toronto, ON, Canada, 2001; pp. 13–30.
- HSY, 2017. Air quality index. Last modified 20.7. <https://www.hsy.fi/en/experts/air-protection/informing-the-public/Pages/Air-quality-index.aspx>

THE STRUCTURE OF EXTRA-TROPICAL CYCLONES IN THE FUTURE.

V. A. SINCLAIR¹, M. RANTANEN¹, P. HAAPANALA¹, J. RÄISÄNEN¹, H. JÄRVINEN¹

¹ Institute for Atmospheric and Earth System Research, University of Helsinki, Helsinki, P.O. Box 64, 00014, Finland

Keywords: Aqua-planet, extra-tropical cyclones, idealised modelling, OpenIFS, precipitation, vertical motion,

INTRODUCTION

Extra-tropical cyclones (also referred to as mid-latitude cyclones) are a fundamental part of the atmospheric circulation in the mid-latitudes as they are responsible for a major amount of the poleward transport of heat, moisture and momentum. Extra-tropical cyclones are the source of most of the day-to-day weather variability in the mid-latitudes and climatologically they are responsible for over 70% of precipitation in the mid-latitudes (Hawcroft *et al.*, 2012). Intense extra-tropical cyclones can cause heavy rain or snow which can result in floods and travel disruption. Furthermore, extra-tropical cyclones can be associated with strong winds which can fell trees, down power lines and damage other infrastructure. Most insured losses over Europe are related to winter storm events such as extra-tropical cyclones. Thus, it is important to know how the weather associated with these systems will change in the future as the climate warms. The aim of this study is to quantify how the structure of extra-tropical cyclones, in particular precipitation, will change with warming.

METHOD

We adopt an idealising modelling approach as it is anticipated that results from these highly controlled simulations will be easier to understand and explain than results from complex, fully coupled climate model simulations. We use OpenIFS, a state-of-the-art global numerical prediction model, and configure this model as an aqua-planet. Thus in the simulations the Earth's surface is an uniform ocean surface. The sea surface temperatures (SSTs) are fixed in time and are specified to be uniform in the zonal direction. In the meridional direction, the SSTs have a maximum value of 27°C at the equator and decrease to 0°C at 60°N following the QObs function of (Neale and Hoskins, 2000). The aqua-planet configurations has a diurnal cycle but no seasonal cycle; perpetual Spring equinox conditions are prescribed.

We perform two experiments: a control experiment (CNTL) and a warm experiment in which the SSTs are uniformly warmed by 4K (SST4). Both experiments are run for a total of 11 years. The first year is discarded to ensure that the model has spun up into a balanced state. Both aquaplanet simulations are run at T159 resolution (approximate grid spacing of 1.125 degrees / 125 km) and with 60 model levels.

In both numerical experiments, extra-tropical cyclones are tracked using an objective cyclone identification and tracking algorithm, TRACK (Hodges, 1994; Hodges, 1995). Extra-tropical cyclones are identified as localised maxima in the 850-hPa relative vorticity truncated to T42 spectral resolution based on 6 hourly output from OpenIFS. The tracks are filtered to remove any that are short lived (less than 48 hours), are stationary (do not move at least 1000 km) or are tropical cyclones

(remain south of 20°N). From these cyclone tracks we obtain information of the genesis and lysis latitudes, the maximum vorticity and track duration. We then use the cyclone tracks as the basis for creating cyclone composites of the strongest (in terms of the 850-hPa relative vorticity) 200 extra-tropical cyclones in both the CNTL and SST4 experiment. Cyclone composites essentially show the average or typical structure of a pre-selected subgroup of extra-tropical cyclones. This means that results are much more generic compared to results obtained from case studies which examine much fewer cyclones.

CONCLUSIONS

A total of 3581 extra-tropical cyclones are identified in the CNTL simulation whereas in the SST4 simulation there are 3462 – a decrease of 3.3% which is not statistically significant. The median maximum vorticity of extra-tropical cyclones in CNTL is $5.94 \times 10^{-5} \text{ s}^{-1}$ which is slightly larger than that found in the SST4 experiment ($5.75 \times 10^{-5} \text{ s}^{-1}$). A two-sided student t-test shows that these mean values are not statistically significantly different and a Wilcoxon rank sum test shows that the median maximum intensities between the CNTL and SST4 are not statistically significantly different. In contrast, a one tailed F-test applied to the maximum vorticity distributions shows that the maximum vorticity distribution in the SST4 experiment has a larger variance than in the CNTL experiment. Thus, the average intensity of extra-tropical cyclones does not change with warming but there are more stronger, and more weak cyclones in the SST4 experiment than in CNTL.

The median genesis and lysis regions are found to move poleward with warming, which is associated with a poleward shift of the eddy-driven jet (not shown). The median genesis region moves 2 degrees polewards from 44.2°N to 46.2°N and the median lysis region moves poleward by 1.9 degrees from 51.4°N to 53.3°N. These changes are found to be statistically significant at the 95% confidence level in a two-sided student t-test.

Cyclone composites of mean sea level pressure, total column water vapour, relative vorticity, 900–700-hPa layer averaged potential vorticity, total, large-scale and convective precipitation and vertical velocity were created at different offset times relative to the time of maximum vorticity ($t = 0$ h). Composites of the total, large-scale and convective precipitation in the CNTL valid at -48, -24 and 0 hours are shown in Figure 1 as contours and the change due to warming (SST4 - CNTL) is shown by the shading. Large-scale stratiform precipitation is calculated from the cloud scheme whereas the convective precipitation is produced by the convection scheme.

In the CNTL experiment, at all offset times, the maximum in the total precipitation occurs downstream and poleward of the cyclone centre. At $t = -48$ h, the total precipitation has the largest values in the warm sector of the cyclone and near the warm front (Fig. 1a). Twenty-four hours later, at $t = -24$ h, (Fig. 1d) the total precipitation in the CNTL simulation has a more distinct comma shape, covers a larger area, extends south of the cyclone centre along the cold front and is slightly heavier than at $t = -48$ h. At the time of maximum intensity, $t = 0$ h, the total precipitation has rotated cyclonically around the cyclone centre (Fig. 1g) and the maximum values have decreased compared to during the intensification stage. The effect of warming on the total precipitation is a large increase at all offsets times. Nowhere in the cyclone composite is there a decrease in precipitation. The maximum absolute increases are 2.5, 3.5 and 2.0 $\text{mm} (6 \text{ h})^{-1}$ at $t = -48$ hr, $t = -24$ h, and the time of maximum vorticity ($t = 0$ hr) respectively which corresponds to relative increases of up to almost 50%. The maximum increase in the total precipitation is not co-located with the maximum in the CNTL simulation indicating that the spatial structure of the composite cyclone changes with warming.

In CNTL, the large-scale precipitation (Fig. 1b, e, h) contributes more to the total precipitation than the convective precipitation (Fig. 1c, f, i) particularly at $t = -24$ h and the time of maxi-

mum intensity ($t=0$ h). The exception is in the equatorward parts of the warm sector, where the temperature and moisture content are higher, where the convective precipitation is larger and of equal magnitude to the large-scale precipitation. At all offset times, the large-scale precipitation increases with warming in the warm frontal region, poleward of the maximum in the CNTL simulation. This spatial pattern is very similar to that observed for the total precipitation meaning that the resolved precipitation is leading to the poleward shift in the total precipitation with warming. In contrast, the convective precipitation, which increases by almost 50%, has the largest increases co-located with the maximum in the control simulation, meaning that the position of convective precipitation relative to the cyclone centre does not change with warming. Further results can be found in (Sinclair *et al.*, 2019).

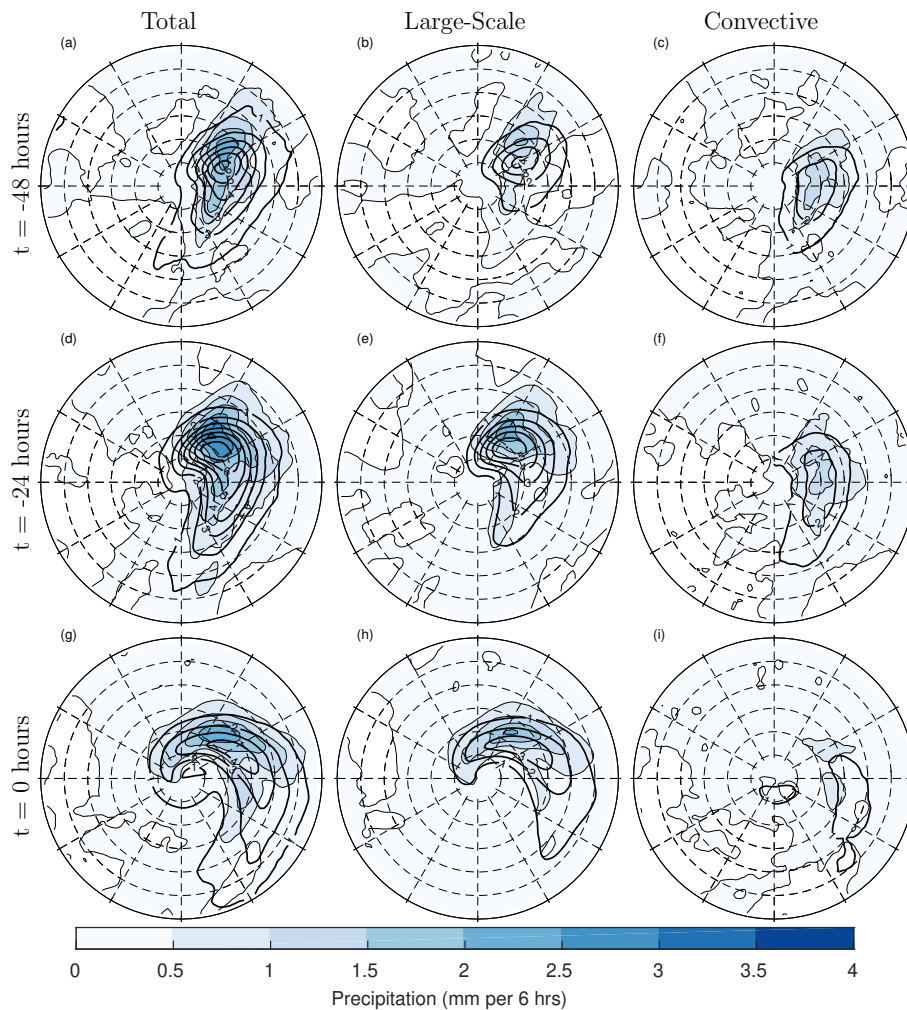


Figure 1: Composites of total precipitation (a,d,g), large-scale precipitation (b,e,h) and convective precipitation (c,f,i) in the CNTL simulation (black contours) and the difference between SST4 and control (shading). Panels a-c are valid 48 hours before the time of maximum intensity, panels d-f are valid 24 hours before the time of maximum intensity and panels g-i are valid at the time of maximum intensity. All composites are of the strongest 200 extra-tropical cyclones in each experiment.

ACKNOWLEDGEMENTS

We acknowledge ECMWF for making the OpenIFS model available and CSC – IT Center for Science Ltd. for the allocation of computational resources. We thank Glenn Carver, Filip Váňa and Gabriela Szépszó for assistance with OpenIFS and for creating the initial conditions for the simulations. We also thank Kevin Hodges for providing the cyclone tracking code, TRACK, and Helen Dacre for providing the cyclone composite code. VAS is funded by the Academy of Finland (project no. 307331).

REFERENCES

- Hawcroft, M. K., Shaffrey, L. C., Hodges, K. I., and Dacre, H. F. (2012). How much northern hemisphere precipitation is associated with extratropical cyclones? *Geophys. Res. Lett.*, **39**(24).
- Hodges, K. I. (1994). A general method for tracking analysis and its application to meteorological data. *Mon. Wea. Rev.*, **122**(11), 2573–2586.
- Hodges, K. I. (1995). Feature tracking on the unit sphere. *Mon. Wea. Rev.*, **123**(12), 3458–3465.
- Neale, R. B. and Hoskins, B. J. (2000). A standard test for AGCMs including their physical parametrizations: I: The proposal. *Atmospheric Science Letters*, **1**(2), 101–107.
- Sinclair, V. A., Rantanen, M., Haapanala, P., Räisänen, J., and Järvinen, H. (2019). The characteristics and structure of extra-tropical cyclones in a warmer climate. *Weather Clim. Dynam. Discuss.* in review.

DMA-MS ANALYSIS OF ALPHA-PINENE OXIDATION PRODUCTS

A. SKYTTÄ¹, L. R. AHONEN¹ and J. KANGASLUOMA¹

¹Institute for Atmospheric and Earth System Research/Physics, Faculty of Science, University of Helsinki, Helsinki, 00140, Finland.

Keywords: Alpha-Pinene, electrical mobility, cluster oxidation, ozone.

INTRODUCTION

Secondary organic aerosols affect the climate and weather of the Earth by scattering solar radiation and acting as cloud condensation nuclei. They can be formed from volatile organic compounds emitted by forests after undergoing chemical reactions in the atmosphere. One example of them is Alpha-Pinene. The aim of this research is to get one step closer to understanding of the behavior of secondary organic aerosols in the atmosphere.

Alpha-Pinene ($C_{10}H_{16}$) is a monoterpene emitted by vegetation and its low volatile oxidation products are important source for secondary organic aerosols (SOA) in the atmosphere (e.g. Ehn et al., 2014). Like all aerosols in the atmosphere, also SOAs have an impact to the formation of clouds and to the scattering of light. These are important reasons to understand better the formation of SOA. Because of the significant amount of Alpha-Pinene in the atmosphere, we investigated the oxidation products of Alpha-Pinene.

Alpha-Pinene was oxidized by ozone and the formed neutral molecules and clusters, were charged via electrospray ionization (ESI). We studied the oxidation products of Alpha-Pinene and electrical mobilities with a combination of Differential Mobility Analyzer and time-of-flight mass spectrometer (DMA-MS). We used several different solutions in the electrospray ionization to compare if the charger ion affects the charging efficiency and mobilities of compounds. Based on the measured mass spectrum, the chemical composition of the oxidation products was determined. MS data combined with the mobility analysis, gives the mobility spectrum for each of the identified compounds.

METHODS

In our setup we used parallel plate DMA (SEADM; Fernández de la Mora et al. (2006)) coupled with APITOF-MS (Tofwerk AG; Junninen et al. (2010)) and a flow tube system. A DMA can be used to measure the electrical mobility of the molecule or cluster and mass spectrometer to measure the mass of those clusters. The DMA had resolving power around 40-50 with the used configuration.

The electrospray solution is sprayed through a thin capillary (40 μ m ID) into the chamber through which neutral sample is passed through. Particles that are charged by reagent ions are led into the DMA via narrow inlet slit. In the DMA, particle-free sheath flow is moving at velocity U and an electric field, in orthogonal direction compared to sheath flow. The electrostatic force on charged particles is causing them to traverse (electrophoresis) across the sheath flow (Figure 1).

By changing the strength of the electric field, we can vary the mean mobility of the compound detected at the sampling slit. Compounds with the largest mobility are detected with smaller voltages. During a specific measurement, sheath flow and the width of the DMA chamber Δ are constant and the voltage is scanned over certain voltage range. Because the strength of the electric field is $E = \frac{V_{DMA}}{\Delta}$ we get at voltage V_{DMA} the mobility $Z = \frac{U \Delta^2}{L V_{DMA}}$. The sample flow is split directly at DMA's outlet into the electrometer and MS. The interface between the two instruments is optimized for high transmission. Mass spectrum is recorded for

every DMA voltage setting. With the mobility and mass spectrum information we can detect the chemical composition of the cluster and the mobility of the cluster with certain mass (J. F. de la Mora 2009).

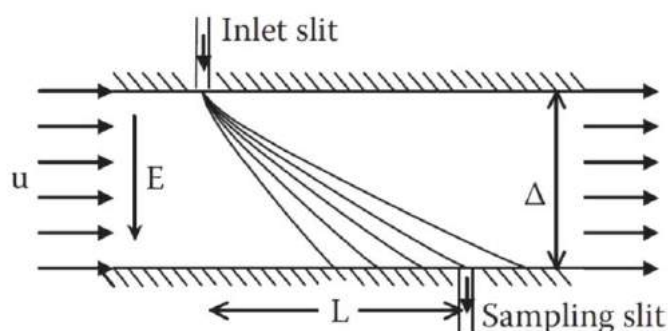


Figure 1. Graph of DMA chamber. Sheath gas flows at velocity U when charged particles come to sheath from inlet slit. Compound are detected at sampling slit (J. F. de la Mora 2009).

Sheath flow is usually used some non-reacting gas. In our measurements we used N_2 . Instruments were calibrated using Tetra-Heptyl-Ammonium-Bromide in positive mode.

We prepared a setup to oxidize Alpha-Pinene in gas phase (Figure 2). Alpha-Pinene was evaporated into a carrier gas flow with known constant rate which was federated with syringe pump. To make sure it evaporates we used warming resistor before Alpha-Pinene was lead to the flow tube. The temperature of the warming resistor was 50 degrees. To oxidize Alpha-Pinene we used ozone produced with UV-light. Synthetic air was lead to ozone generator, where ozone is formed, and then further to the mixing tube. The oxidation products are detected by charging them with ions sprayed from the electrospray solution and then directed into the DMA chamber. Charged clusters drift to an electric field in the sheath flow and after that to the mass spectrometer where their mass is specified based on their flight time.

We produced charger ions from four different salts dissolved in methanol. As a solute we used $NaNO_3$, NaI , $LiCl$ and CH_3CO_2K all charged in positive and negative mode. Therefore, the positive ions we used were Na^+ , K^+ and Li^+ , negative ones were NO_3^- , I^- , Cl^- and $CH_3CO_2^-$.

To make analysis a bit easier we tried to optimize the concentration of the electrospray solution in the way that multiple charging was minimized. Solvent of about 2 mM turned out to be diluted enough to produce mainly singly charged clusters.

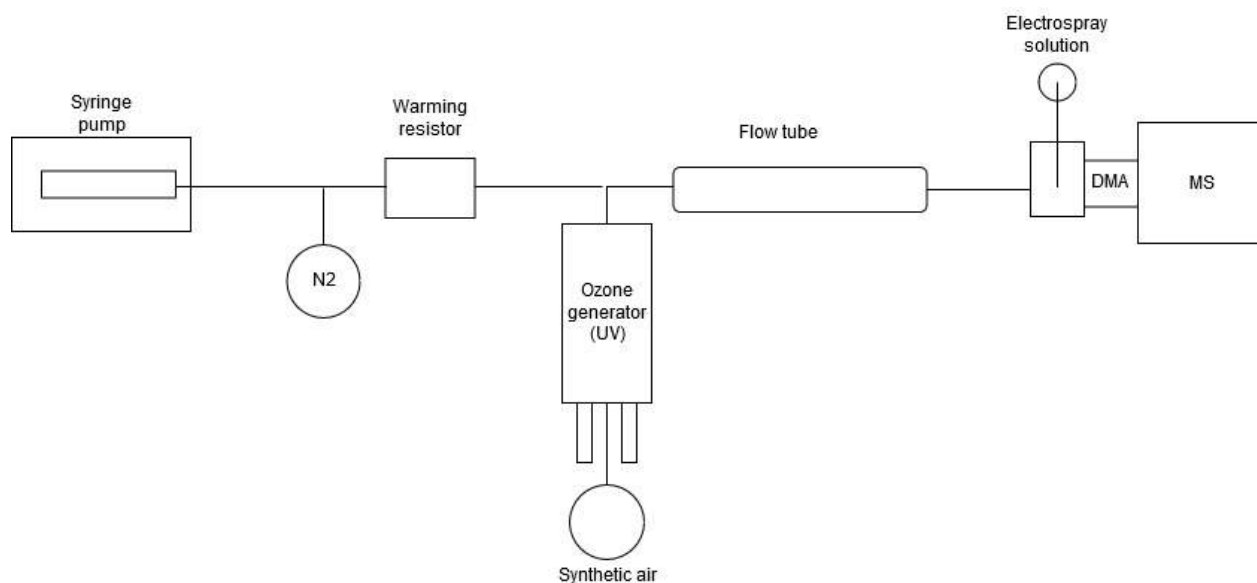


Figure 2. Graph of the setup. Ozone and Alpha-Pinene are led to the flow tube and then charged by ions sprayed from electro spray solution. In the DMA the electrical mobility of the clusters is measured and then the mass is determined in the MS.

RESULTS

Alpha-Pinene oxidation products of oxidation state $C_{10}H_{16}O_{2-7}$ were detected with almost all charger ions. Also, other products were detected, for example $C_{10}H_{18}O_2$ and compositions with odd amount of carbon for instance $C_7H_{12}O_x$ and $C_9H_{16}O_x$. In the positive mode, much more clusters are detected than in the negative mode. Also we were observing a lot of cluster fragmentation in the mass spectrometer after mobility analysis in the measurements in the positive mode. Because of this, the measurements made in the negative mode were easier to analyze so we concentrated to examine them.

The inverse mobility spectrum of the compound $C_{10}H_{16}O_3$ charged by negative reagent ions is depicted in figure 3. As we can see the charger ion affect the mobility of the cluster. The intensities of the peaks are not normalized so the intensities are not comparable. Still we can notice that $C_2H_3O_2^-$ is hardly charged by $C_{10}H_{16}O_3$ but with all other negative ions the signal is strong enough that we can analyze the mobility spectrum.

For the cluster charged with I^- , there is just one mobility peak whereas with NO_3^- there is two and molecule charged by Cl^- has three mobility peaks. One explanation to the multiple peaks is that some bigger cluster is fragmented after the mobility analysis and the latter mobility peaks in the spectrum are actually the signal of this cluster with larger mass. If a larger parent ion fragments, the signal appears in the mass of the fragment, but the mobility corresponds to the parent ion. In our measurements there are many clusters that have multiple peaks in the mobility spectrums. This makes the analysis of the data quite difficult. In the future, we are planning to optimize the measurements to decrease the fragmentations.

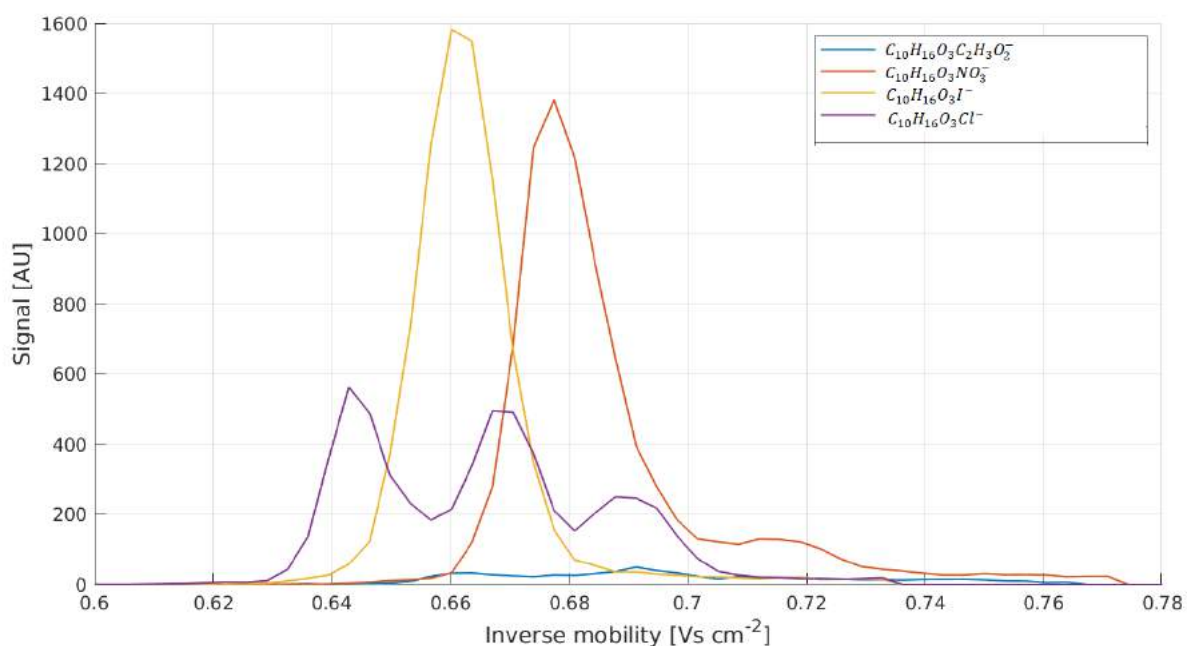


Figure 3. Mobility spectrum of the $C_{10}H_{16}O_3$ charged by negative charger ions.

Mobility also can provide information on the structure of the compound. One cluster can have multiple peaks if it has multiple different structures. In this kind of case, the mobility peaks does not differ from each other as much as in the figure 3 but we have managed to detect them based on the mobility data. In some mobility spectrums the shape of peak seems to have two peaks inside it. These peaks are quite wide and we are able to fit two peaks with the expected resolution of DMA (Figure 4). This supports the theory that there exists multiple structures of the clusters. These initial measurements are not made with the most optimal settings because of instrumental problems related to the sheath flow laminarity. This was reducing the resolving power of the DMA from the maximum value it is capable in the most optimal condition.

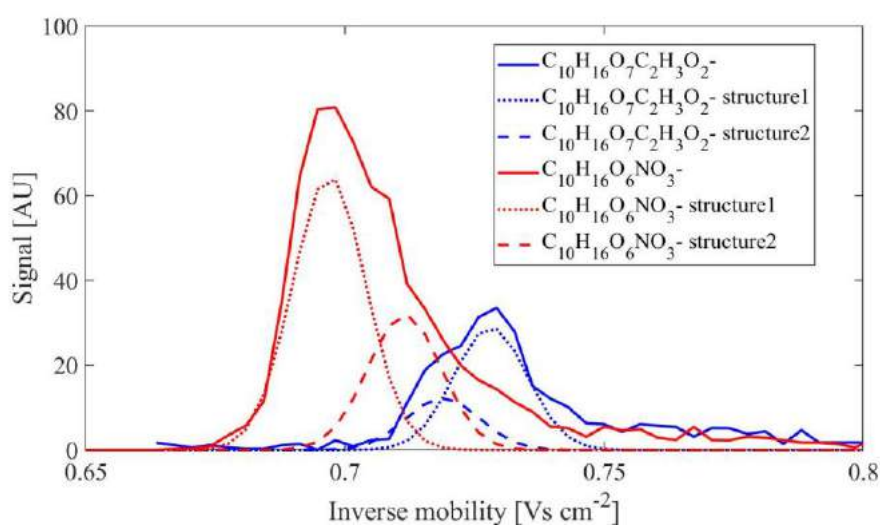


Figure 4. The compounds $C_{10}H_{16}O_7C_2H_3O_2^-$ and $C_{10}H_{16}O_6NO_3^-$ seem to have two different kind of structures based on the mobility spectrum.

CONCLUSIONS

We detected almost the same oxidation products of Alpha-Pinene with every charger ion that we use. We did not detect as high oxidation states as expected based on other studies (e.g. Jordan et al., 2016). We were able to measure the electrical mobilities of the oxidation products. Based on this mobility information, we concluded that some products can form different structures. In this measurement we could not determine these structures but potentially in future they can be clarified by modelling.

REFERENCES

- Ehn, M., Thornton, J. A., Kleist, E., Sipilä, M., Junninen, H., Pullinen, I., Springer, M., Rubach, F., Tillmann, R., Lee, B., Lopez-Hilfiker, F., Andres, S., Acir, I. H., Rissanen, M., Jokinen, T., Schobesberger, S., Kangasluoma, J., Kontkanen, J., Nieminen, T., Kurten, T., Nielsen, L. B., Jorgensen, S., Kjaergaard, H. G., Canagaratna, M., Dal Maso, M., Berndt, T., Petäjä, T., Wahner, A., Kerminen, V. M., Kulmala, M., Worsnop, D. R., Wildt, J., and Mentel, T. F. (2014). A large source of low-volatility secondary organic aerosol. *Nature*, 506(7489), 476-+. doi:10.1038/nature13032
- Fernández de la Mora, J., Ude, S., and Thomson, B. A. (2006). The potential of differential mobility analysis coupled to MS for the study of very large singly and multiply charged proteins and protein complexes in the gas phase. *Biotechnology Journal*, 1(9), 988-997. doi:10.1002/biot.200600070
- Fernández de la Mora (2009). *Ion Mobility Spectroscopy - Mass Spectrometry: Theory and Applications*, C. Wilkins and S. Trimpin editors, Taylor and Francis. Chapter 5: *The Differential Mobility Analyzer (DMA). Adding a True Mobility Dimension to a Preexisting API-MS*
- Jordan E. Krechmer, Michael Groessl, Xuan Zhang, Heikki Junninen, Paola Massoli, Andrew T. Lambe, Joel R. Kimmel, Michael J. Cubison, Stephan Graf, Ying-Hsuan Lin, Sri H. Budisulistiorini, Haofei Zhang, Jason D. Surratt, Richard Knochenmuss, John T. Jayne, Douglas R. Worsnop, Jose-Luis Jimenez, and Manjula R. Canagaratna (2016). *Ion mobility spectrometry–mass spectrometry (IMS–MS) for on- and offline analysis of atmospheric gas and aerosol species*.
- Junninen, H., Ehn, M., Petäjä, T., Luosujärvi, L., Kotiaho, T., Kostianinen, R., Rohner, U., Gonin, M., Fuhrer, K., Kulmala, M., and Worsnop, D. R. (2010). A high-resolution mass spectrometer to measure atmospheric ion composition. *Atmospheric Measurement Techniques*, 3(4), 1039-1053. doi:10.5194/amt-3-1039-2010

SUB-10 NM SIZE-DISTRIBUTION MEASUREMENTS IN HIGHLY CHALLENGING ENVIRONMENTS: AN OUTLOOK

D. STOLZENBURG¹, R. CAI¹, J. KONTKANEN¹ and J. KANGASLUOMA¹

¹Institute for Atmospheric and Earth System Research/Physics, University of Helsinki, 00530 Helsinki, Finland.

Keywords: aerosol size-distribution, new particle formation, data inversion

INTRODUCTION

New particle formation (NPF) by gas-to-particle conversion is a global phenomenon, which has an influence on the global climate (Gordon et al., 2017) and can also affect air pollution (Guo et al., 2014). The decisive step for new particle formation are molecular cluster formation and their subsequent growth, as the small clusters are highly diffusive and therefore vulnerable to scavenging loss by larger pre-existing particles (Pierce and Adams, 2007). The dynamics in the size-range below 10 nm therefore crucially influence the occurrence and importance of NPF in the atmosphere.

However, our abilities to access this size-range with precision measurements of the particle size-distribution are still limited and subject to large uncertainties (Kangasluoma and Kontkanen, 2017). This results in difficulties in disentangling the effects of condensational growth, coagulation and different sources/sinks in the sub-10 nm range. As a consequence, the uncertainties in the size-distribution measurements also accumulate into derived parameters, such as nucleation and cluster growth rates. This, in turn, directly influences the input in global climate models. An improved assessment of sub-10 nm particle size-distributions is thus required to understand NPF in e.g. urban environments, where high cluster and pre-existing aerosol concentrations are measured (Kulmala et al., 2017).

Sub-10 nm size-distributions mostly rely on condensation particle counters (CPCs) either used in a CPC-battery design (Kangasluoma et al., 2014) or within an electrical mobility spectrometer, where particles are first size-classified in a differential mobility analyser (Jiang et al., 2011). The particle concentration measurement uncertainties mainly arise from low particle counting statistics, from chemical composition dependent variation in the lowest threshold diameter of the used CPCs, from unknown charging probabilities in the sub-3 nm size range and data inversion simplifications (Kangasluoma and Kontkanen, 2017).

METHODS

Here we present some of the most recent advances and ideas in reducing the above described uncertainties. The different approaches in measuring sub-10 nm size distributions result in different advantages and disadvantages of different applied instruments. While, e.g. the particle size magnifier in scanning mode (Vanhanen et al., 2011) achieves high counting statistics as it does not rely on particle charging, its size-resolving power as well as its systematic uncertainty in particle sizing are much lower compared to mobility spectrometers. Combining the information of several available instruments within a combined inversion (e.g. Fiebig et al., 2005) should provide a possibility in exploiting the benefits of each applied instrument. Moreover, such an inversion would also reduce the error due to data inversion simplifications as described by Kangasluoma and Kontkanen (2017).

Datasets where sub-10 nm size-distributions are measured by a complementary, array of state-of-the-art sizing instruments are thus key in advancing our understanding of NPF. We explore the potential of such datasets in Figure 1, where size-distribution measurements at the CERN CLOUD experiment are shown. The resulting instrument-by-instrument inverted size-distributions show discrepancies of up to a factor of 10, depending on the conditions of the experiment (iodic acid or anthropogenic vapour driven NPF).

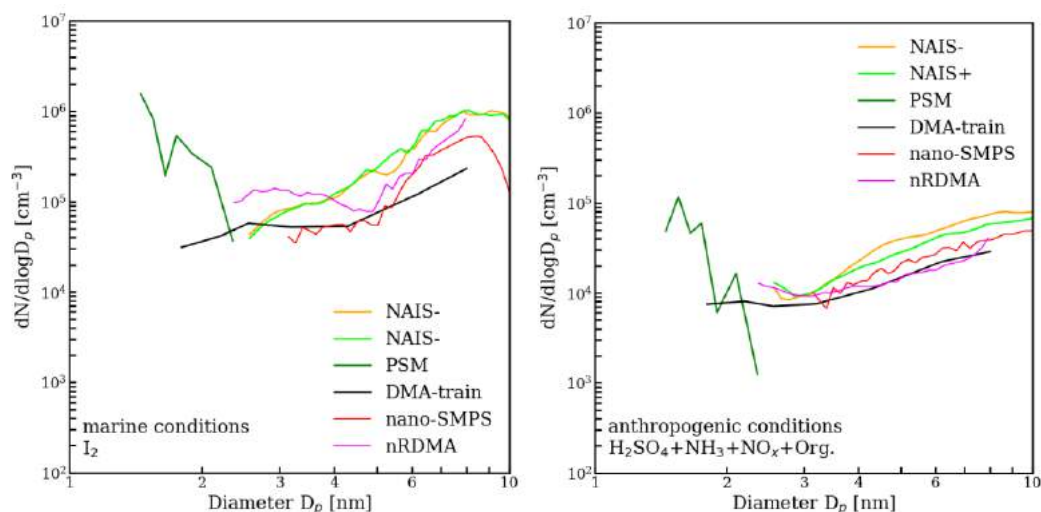


Figure 1. Sub-10 nm particle size-distribution measurements from several instruments at the CERN CLOUD experiment during different type of experiments (i.e. different chemical composition of the measured particles).

Besides from a combining instrument inversion approach, also the uncertainties in CPC counting efficiencies and charging probabilities need to be reduced. The development of CPCs which offer high counting statistics and minimal particle seed composition dependence should be a major focus within the next years. Here results from a tuned butanol CPC (Barmounis et al., 2018) seem to be promising. Moreover, measuring and stabilizing bipolar particle charging efficiencies under challenging ambient conditions could greatly reduce the uncertainties in sub-10 nm size-distribution measurements. The addition of charge carrying vapours to the ion atmosphere inside the used charger (Mäkelä et al., 1996) could be valuable, as the ion mobility distribution inside the charger is stabilized, which should enable the reliable application of laboratory performed charging efficiency measurements to ambient datasets. By modifying the mobility distribution inside the charger also the charging efficiency can be altered and possibly pushed towards higher values, generally increasing the counting statistics of mobility spectrometers (Tigges et al., 2015).

CONCLUSIONS

Altogether, the proposed new methods can yield more reliable insights into sub-10 nm size-distributions compared to previous measurements. Datasets from SMEAR III, Helsinki and Beijing University of Chemical Technology are expected to be analysed and improved by the above methods. First results of simulated datasets and laboratory experiments confirm the method's high potential for improving sub-10 nm size-distribution retrieval. Combined with novel tools for analysing particle growth rates (Pichelstorfer et al., 2018), this could yield unprecedented insights into the dynamics of the sub-10 nm regime, identifying possible drivers of NPF in urban areas (Kulmala et al., 2017).

ACKNOWLEDGEMENTS

The work is supported by Academy of Finland (grant nos. 307331, 316114 and 325656)

REFERENCES

- Barmounis, K., et al.: Enhancing the detection efficiency of condensation particle counters for sub-2nm particles, *J. Aerosol Sci.*, 117, 44–53, doi:10.1016/j.jaerosci.2017.12.005, 2018.
- Fiebig, M. et al.: Inversion of data containing information on the aerosol particle size distribution using multiple instruments, *J. Aerosol Sci.*, 36(11), 1353–1372, doi:https://doi.org/10.1016/j.jaerosci.2005.01.004, 2005.

- Gordon, H. et al.: Causes and importance of new particle formation in the present-day and preindustrial atmospheres, *J. Geophys. Res.-Atmos.*, 122, doi:10.1002/2017JD026844, 2017.
- Guo, S. et al.: Elucidating severe urban haze formation in China, *Proc. Nat. Acad. Sci. USA*, 111(49), 17373 LP – 17378, doi:10.1073/pnas.1419604111, 2014.
- Jiang, J. et al.: Electrical Mobility Spectrometer Using a Diethylene Glycol Condensation Particle Counter for Measurement of Aerosol Size Distributions Down to 1 nm, *Aerosol Sci. Tech.*, 45(4), 510–521, doi:10.1080/02786826.2010.547538, 2011.
- Kangasluoma, J. and Kontkanen, J.: On the sources of uncertainty in the sub-3nm particle concentration measurement, *J. Aerosol Sci.*, 112(Supplement C), 34–51, doi:<https://doi.org/10.1016/j.jaerosci.2017.07.002>, 2017.
- Kangasluoma, J. et al.: Sub-3 nm particle size and composition dependent response of a nano-CPC battery, *Atmos. Meas. Tech.*, 7(3), 689–700, doi:10.5194/amt-7-689-2014, 2014.
- Kulmala, M. et al.: Atmospheric gas-to-particle conversion: why NPF events are observed in megacities?, *Faraday Discuss*, 200(0), 271–288 [online] Available from: <http://dx.doi.org/10.1039/C6FD00257A>, 2017.
- Mäkelä, J. M. et al.: Comparison of mobility equivalent diameter with Kelvin-Thomson diameter using ion mobility data, *J. Chem. Phys.*, 105(4), 1562–1571, doi:10.1063/1.472017, 1996.
- Pichelstorfer, L. et al.: Resolving nanoparticle growth mechanisms from size- and time-dependent growth rate analysis, *Atmos. Chem. Phys.*, 18(2), 1307–1323, doi:10.5194/acp-18-1307-2018, 2018.
- Pierce, J. R. and Adams, P. J.: Efficiency of cloud condensation nuclei formation from ultrafine particles, *Atmos. Chem. Phys.*, 7(5), 1367–1379, doi:10.5194/acp-7-1367-2007, 2007.
- Tigges, L., Jain, A. and Schmid, H.-J.: On the bipolar charge distribution used for mobility particle sizing: Theoretical considerations, *J. Aerosol Sci.*, 88, 119–134, doi:<http://dx.doi.org/10.1016/j.jaerosci.2015.05.010>, 2015.
- Vanhanen, J. et al.: Particle Size Magnifier for Nano-CN Detection, *Aerosol Sci. Tech.*, 45(4), 533–542, doi:10.1080/02786826.2010.547889, 2011.

TIME SERIES ANALYSIS OF LONG-TERM MEASUREMENTS OF 1-3 NM PARTICLE SIZE DISTRIBUTIONS AND AEROSOL PRECURSOR GASES FROM THE SMEAR II STATION

J. SULO¹, J. KONTKANEN¹, P. PAASONEN¹, J. KANGASLUOMA¹, N. SARNELA¹, L. AHONEN¹, T. LAURILA¹, T. JOKINEN¹, M. KULMALA¹ and K. LEHTIPALO^{1,2}

¹Institute for atmospheric and Earth system research (INAR), University of Helsinki, 00014, Finland.

²Finnish Meteorological Institute, Erik Palmenin aukio 1, 00560 Helsinki, Finland.

Keywords: NEW PARTICLE FORMATION, AEROSOL MEASUREMENTS, ATMOSPHERIC AEROSOLS, PARTICLE SIZE MAGNIFIER.

INTRODUCTION

Atmospheric aerosols are the largest source of uncertainty for climate models and in order to diminish these uncertainties it is vital to understand the sources and formation pathways of sub-3nm particles. It is estimated that up to 60% of atmospheric aerosols are formed in the atmosphere from condensing vapors and thus gas-to-particle conversion plays a significant role in the dynamics of aerosol concentrations in the atmosphere (Merikanto et al., 2009). Sulphuric acid plays a significant role in atmospheric new particle formation (Sipilä et al., 2010) and the growth of new particle in the atmosphere. Studies also indicate that when sulphuric acid is stabilized by a base, the formation rate of new particles is enhanced (Kirkby et al., 2011). In addition, biogenic new particle formation has been observed to occur at rural areas in which highly oxygenated organic vapours (Bianchi et al., 2019) act as the condensing vapors needed for particle growth (Rose et al., 2018).

In this study, the longest available time series of sub-3nm particle concentrations measured by the Particle Size Magnifier (Vanhanen et al., 2011) along with measurements of aerosol precursor molecule concentrations were investigated. The available dataset was analyzed for its implications on atmospheric regional new particle formation and concentrations of sub-3nm particles.

METHODS

Four years of data from the Hyytiälä SMEAR II station in Finland was analyzed to investigate potential links between precursor vapors and sub-3nm particles. A time series analysis was performed on the sub-3nm particle size distribution measurements measured by the Particle Size Magnifier (Kontkanen et al., 2017) and aerosol precursor molecule measurements by the CI-APi-ToF (Jokinen et al., 2012) to study seasonal variability, diurnal patterns, data quality and relevant correlations between condensing gases and nanoparticles. The seasons were defined as spring being March-May, summer as June-August, autumn as September-November and winter as December-February. The time series were compared both with all available data points and with only new particle formation event times. The event times were determined by an automatic event classification algorithm described in Dada *et al* (2018).

RESULTS

The diurnal patterns of the concentrations of sub-3nm particles in three size classes during all four seasons are shown in Figure 1. The diurnal patterns show distinct differences, with much higher concentrations of 1.3-1.7 nm particles in spring than during other seasons. Springtime 1.15-1.3 nm particle concentrations show two maxima, one around midday and one in the evening. Summer-time concentrations are higher than during other seasons for 1.15-1.3 nm particle concentrations. Summertime 1.15-1.3 nm particle concentrations also exhibit two maxima similar to spring, with one around midday and one in the evening. The 1.3-1.7 nm and 1.7-2.5 nm particle concentrations remain relatively stable throughout summer, autumn and winter. Autumntime 1.15-1.3 nm particle concentrations rise throughout the day, showing a maximum just after sunset and wintertime 1.15-1.3 nm particle concentrations show only one maximum, centered around midday.

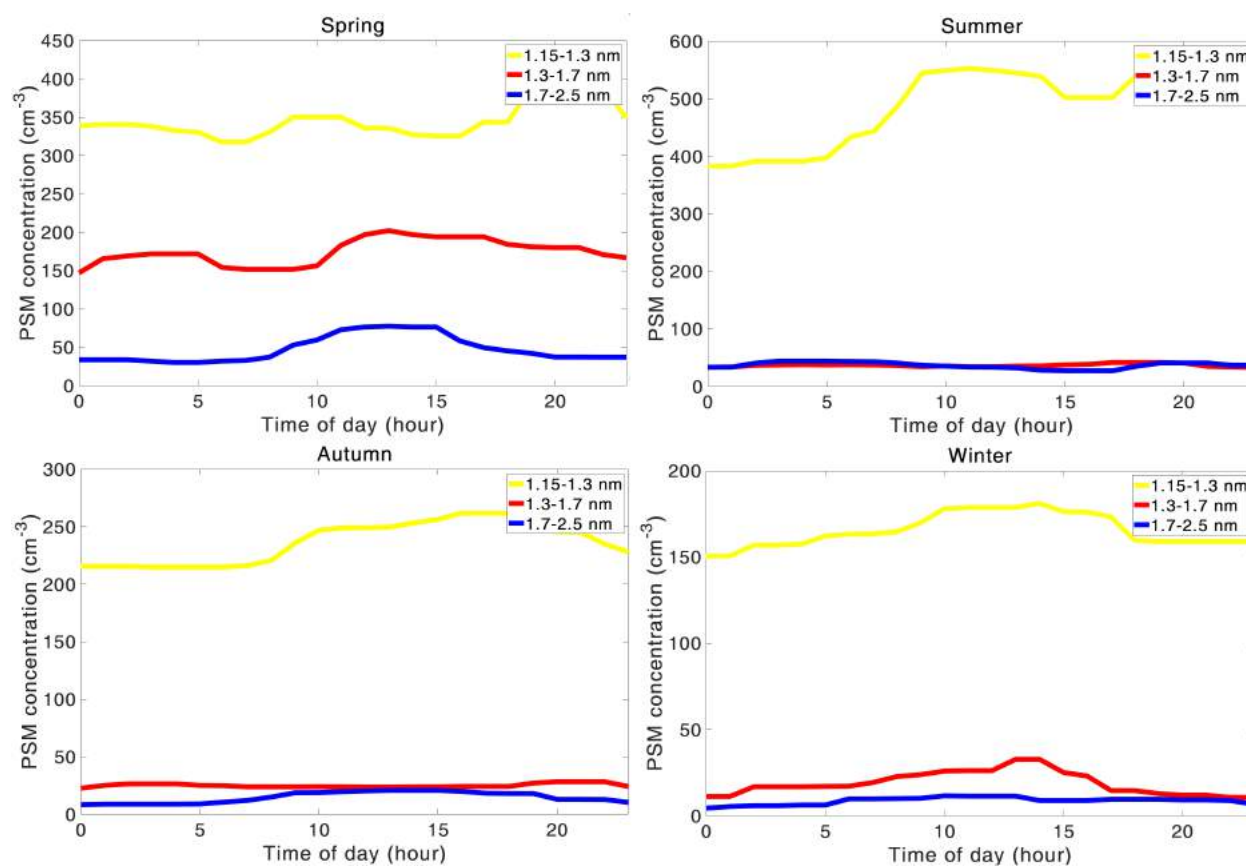


Figure 1: The diurnal cycles of sub-3nm particle concentrations for each season. The yellow lines are 1.15-1.3 nm particle concentrations, red lines are 1.3-1.7 nm particle concentrations and blue lines are 1.7-2.5 nm concentrations.

Sub-3nm particle concentrations were also compared to the measured concentrations of atmospheric aerosol precursor molecules during daytime (10:00-14:00) atmospheric new particle formation events. The best correlations for 1.15-1.3 nm, 1.3-1.7 nm and 1.7-2.5 nm particle concentrations are presented in Figure 2. Highly oxygenated organic molecule (HOM) dimer concentrations correlate well with particle concentrations in all size ranges. Sulphuric acid and HOM dimer concentrations multiplied together correlate the best with the 1.7-2.5 nm particle concentration.

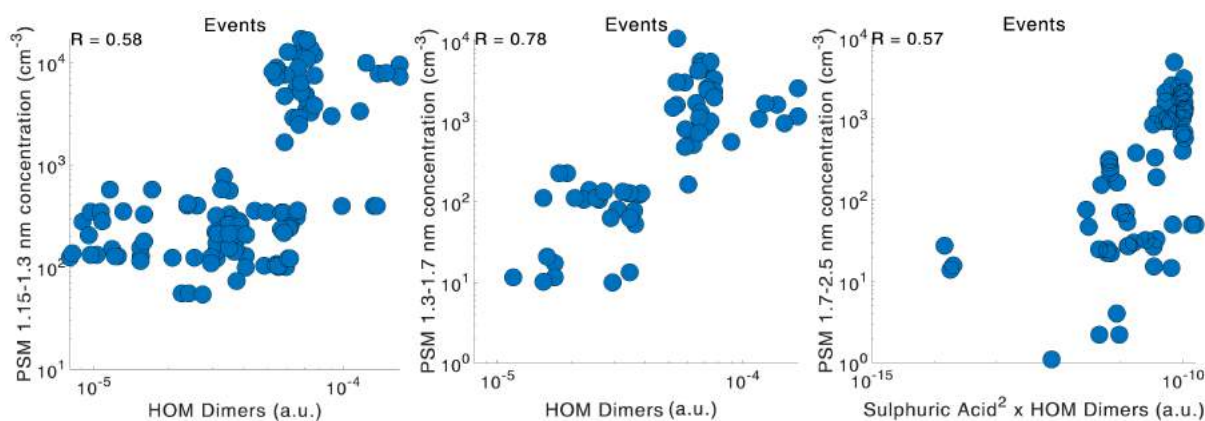


Figure 2: The best correlations between particle concentrations in each size range and aerosol precursor molecule concentrations. The correlations presented are logarithmic. The correlations are shown at the top left of each graph with the symbol R. The data includes all available data points from 2014 to 2018 during daytime (10:00-14:00) regional NPF events when sub-3nm particle concentration and aerosol precursor molecule data are available.

CONCLUSIONS

The analysis of the PSM time series shows clear seasonal differences for sub-3nm particle concentrations. Higher springtime concentrations of 1.3-1.7 nm underline the increased frequency of regional new particle formation events in spring. The correlation analysis with aerosol precursor molecules shows that HOM dimers correlate very well with sub-3nm particle concentrations and appear to play an important role in the formation and growth of the smallest atmospheric aerosol particles.

ACKNOWLEDGEMENTS

This work was supported by the Academy of Finland (grants 307331 and 316114).

REFERENCES

- Bianchi, F., Kurtén, T., Riva, M., Mohr, C., Rissanen, M., Roldin, P., Berndt, T., Crouse, J., Wennberg, P., Mentel, T., Wildt, J., Junninen, H., Jokinen, T., Kulmala, M., Worsnop, D., Thornton, J., Donahue, N., Kjaergaard, H., and Ehn, M. (2019). Highly oxygenated organic molecules (hom) from gas-phase autoxidation involving peroxy radicals: A key contributor to atmospheric aerosol. *Chemical Reviews*, 119(6):3472–3509.
- Dada, L., Chellapermal, R., Buenrostro Mazon, S., Paasonen, P., Lampilahti, J., Manninen, H. E., Junninen, H., Petäjä, T., Kerminen, V.-M., and Kulmala, M. (2018). Refined classification and characterization of atmospheric new-particle formation events using air ions. *Atmospheric Chemistry and Physics*, 18(24):17883–17893.
- Jokinen, T., Sipilä, M., Junninen, H., Ehn, M., Lönn, G., Hakala, J., Petäjä, T., Mauldin III, R. L., Kulmala, M., and Worsnop, D. R. (2012). Atmospheric sulphuric acid and neutral cluster measurements using ci-api-tof. *Atmospheric Chemistry and Physics*, 12(9):4117–4125.
- Kirkby, J., Curtius, J., Almeida, J., Dunne, E., Duplissy, J., Ehrhart, S., Franchin, A., Gagné, S., Ickes, L., Kürten, A., Kupc, A., Metzger, A., Riccobono, F., Rondo, L., Schobesberger, S., Tsagkogeorgas, G., Wimmer, D., Amorim, A., Bianchi, F., Breitenlechner, M., David, A.,

- Dommen, J., Downard, A., Ehn, M., Flagan, R. C., Haider, S., Hansel, A., Hauser, D., Jud, W., Junninen, H., Kreissl, F., Kvashin, A., Laaksonen, A., Lehtipalo, K., Lima, J., Lovejoy, E. R., Makhmutov, V., Mathot, S., Mikkilä, J., Minginette, P., Mogo, S., Nieminen, T., Onnela, A., Pereira, P., Petäjä, T., Schnitzhofer, R., Seinfeld, J. H., Sipilä, M., Stozhkov, Y., Stratmann, F., Tomé, A., Vanhanen, J., Viisanen, Y., Vrtala, A., Wagner, P. E., Walther, H., Weingartner, E., Wex, H., Winkler, P. M., Carslaw, K. S., Worsnop, D. R., Baltensperger, U., and Kulmala, M. (2011). Role of sulphuric acid, ammonia and galactic cosmic rays in atmospheric aerosol nucleation. *Nature*, 476(7361):429–433.
- Kontkanen, J., Lehtipalo, K., Ahonen, L., Kangasluoma, J., Manninen, H. E., Hakala, J., Rose, C., Sellegri, K., Xiao, S., Wang, L., Qi, X., Nie, W., Ding, A., Yu, H., Lee, S., Kerminen, V.-M., Petäjä, T., and Kulmala, M. (2017). Measurements of sub-3 nm particles using a particle size magnifier in different environments: from clean mountain top to polluted megacities. *Atmospheric Chemistry and Physics*, 17(3):2163–2187.
- Merikanto, J., Spracklen, D. V., Mann, G. W., Pickering, S. J., and Carslaw, K. S. (2009). Impact of nucleation on global ccn. *Atmospheric Chemistry and Physics*, 9(21):8601–8616.
- Rose, C., Zha, Q., Dada, L., Yan, C., Lehtipalo, K., Junninen, H., Mazon, S. B., Jokinen, T., Sarnela, N., Sipilä, M., Petäjä, T., Kerminen, V.-M., Bianchi, F., and Kulmala, M. (2018). Observations of biogenic ion-induced cluster formation in the atmosphere. *Science Advances*, 4(4).
- Sipilä, M., Berndt, T., Petäjä, T., Brus, D., Vanhanen, J., Stratmann, F., Patokoski, J., Mauldin, R. L., Hyvärinen, A.-P., Lihavainen, H., and Kulmala, M. (2010). The Role of Sulfuric Acid in Atmospheric Nucleation. *Science*, 327(5970):1243–1246.
- Vanhanen, J., Mikkilä, J., Lehtipalo, K., Sipilä, M., Manninen, H. E., Siivola, E., Petäjä, T., and Kulmala, M. (2011). Particle size magnifier for nano-cn detection. *Aerosol Science and Technology*, 45(4):533–542.

FILTER EXPERIMENTS WITH SOOT: INSIGHTS TO LIGHT-ABSORPTION MEASUREMENTS OF SNOW SAMPLES

J. Svensson^{1*}, J. Ström², and A. Virkkula¹

¹Atmospheric Composition Research, Finnish Meteorological Institute, Helsinki, Finland

²Department of Environmental Science and Analytical Chemistry, Stockholm University, Stockholm, Sweden

*Now at Institute for Geosciences and Environmental Research, University of Grenoble Alpes, Grenoble, France

Keywords: Light-absorbing aerosol, black carbon, snowmelt

INTRODUCTION

Light-absorbing aerosol (LAA), such as black carbon (BC) and mineral dust, are constituents that modulate the Earth's radiative balance. Once deposited onto a snow surface, LAA will alter the reflectance occurring at the surface, and ultimately lead to an accelerated and increased snowmelt. This has been observed in different regions such as the Rockies in the U.S., The European Alps, and most notably High Mountain Asia (HMA; Skiles et al., 2018). HMA contains the most amount of snow and ice outside of the poles, and is especially susceptible due to the close proximity of large emission sources of LAA (Gertler et al., 2016).

Different measurement techniques collect the LAA in a snow sample onto filters through filtration. In this work, we focus on measurements of the filters with the thermal-optical method (TOM), coupled with additional transmittance measurements, in order to examine the LAA species present on the filter. Here specifically, we evaluate micro quartz filters optical behavior when sampling BC particles in an airborne and liquid phase in a set of laboratory experiments.

METHODS

Soot (used as a proxy for BC) aerosol were deposited onto filters by blowing collected soot through a series of tubing into a cylindrical chamber, where a sample inlet fed two PSAPs (Particle Soot Absorption Photometer) for the airborne tests. The same blowing system was utilized for the liquid tests, however, the outlet pipe was submerged into a 20 L contained filled with MQ-water. From this solution, different amounts of liquid were filtered. The filters were thereafter measured with a PSAP and TOM.

CONCLUSIONS

From our experiments we determined the multiple-scattering correction factor (C_{ref}), a commonly used correction factor in absorption measurements, for the quartz filter to be 3.41 ± 0.03 at $\lambda=530$ nm. Moreover, in Fig. 1 it is shown how the filters optically behave differently depending on how the aerosol were deposited onto the filter. In the airborne phase, the slope is half of the slope of the particles mixed in water. When the liquid solution was treated in an ultrasonic bath before filtration the slope was further

elevated. The difference in slope is mostly likely an effect of the penetration depth of the soot particles in the filter and have further implications for ambient field samples (e.g. Svensson et al. 2018).

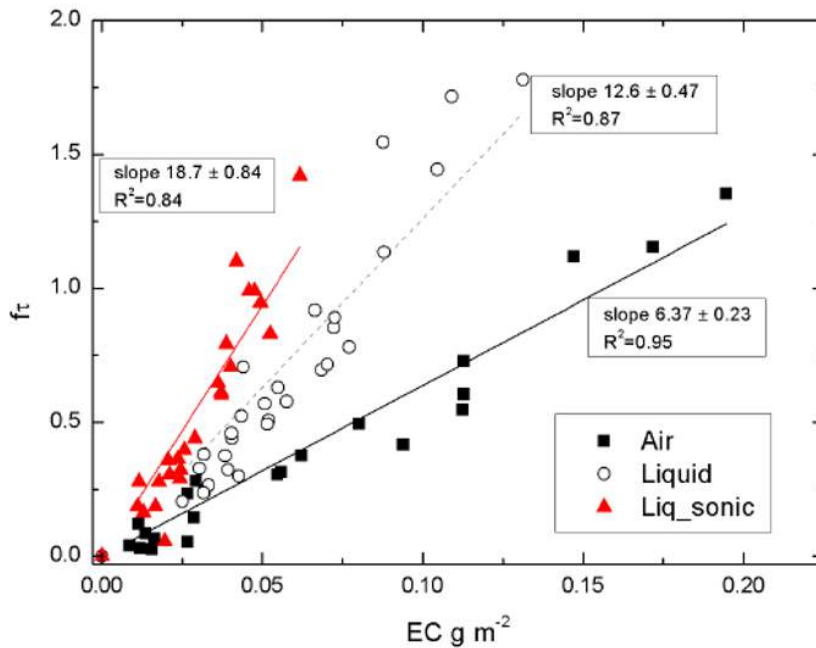


Figure 1. Linear regressions of transmittance-corrected optical depth $f_t(\lambda=530 \text{ nm})$ vs. EC of the soot particles blown into the mixing chamber (Air), into water (Liquid) and blown into water and treated in the ultrasonic bath (Liq_sonic). The regressions were calculated by forcing offset to 0.

ACKNOWLEDGEMENTS

This work has been supported by the consortium: “Novel Assessment of Black Carbon in the Eurasian Arctic: From Historical Concentrations and Sources to Future Climate Impacts” (NABCEA project number 296302); and “Absorbing Aerosols and Fate of Indian Glaciers” (AAFIG; project number 268004). J. Svensson further acknowledges personal support from the Maj and Tor Nessling foundation. J. Ström acknowledges support by the Swedish Research Council (VR 2017-03758) “Black carbon particle size distributions from source to sink.”

REFERENCES

- Gertler, et al.: Black carbon and the Himalayan cryosphere: a review, *Atmos. Environ.*, 125, 404–417, doi.org/10.1016/j.atmosenv.2015.08.078, 2016.
- Skiles, et al.: Radiative forcing by light-absorbing particles in snow, *Nat. Clim. Change*, 8, 964–971, doi.org/10.1038/s41558-018-0296-5, 2018.
- Svensson et al.: Light-absorption of dust and elemental carbon in snow in the Indian Himalayas and the Finnish Arctic, *Atmos. Meas. Tech.*, 11, 1403-1416, doi.org/10.5194/amt-11-1403-2018, 2018.

STAND AGE AND SEASON DEPENDENT IMPORTANCE OF INCLUDING THE EMISSION OF MONOTERPENES FROM NEW SCOTS PINE FOLIAGE IN MODELS

D. TAIPALE^{1,2}, J. AALTO^{1,2}, P. SCHIESTL-AALTO^{1,2}, M. KULMALA¹ and J. BÄCK³

¹Institute for Atmospheric and Earth System Research / Physics, Faculty of Science, University of Helsinki, P.O. Box 64, 00014 Helsinki, Finland.

²Hyytiälä Forestry Field Station, Hyytiäläntie 124, 35500 Korkeakoski, Finland.

³Institute for Atmospheric and Earth System Research / Forestry, Faculty of Science, University of Helsinki, P.O. Box 64, 00014 Helsinki, Finland.

Keywords: SCOTS PINE, MONOTERPENE EMISSION POTENTIAL, FOREST GROWTH.

INTRODUCTION

A significant fraction of assimilated carbon is emitted back to the atmosphere in the form of a variety of biogenic volatile organic compounds (BVOCs). These BVOCs serve many ecological functions (see e.g. Holopainen, 2004) and play important roles in atmospheric processes, including in the formation (Donahue *et al.*, 2013; Kulmala *et al.*, 2014; Riccobono *et al.*, 2014; Schobesberger *et al.*, 2013) and growth (Ehn *et al.*, 2014; Riipinen *et al.*, 2012) of atmospheric aerosol particles. The emissions of BVOCs to the atmosphere are predicted by different biogenic emission models, with MEGAN (Guenther *et al.*, 2006, 2012) being the most popular. Traditionally, these models have utilised emission potentials derived from enclosure measurements of mature foliage. As more and more studies have illustrated that the emissions of VOCs depend on leaf age (e.g. Guenther *et al.*, 1991; Monson *et al.*, 1994; Goldstein *et al.*, 1998; Hakola *et al.*, 2001; Petron *et al.*, 2001; Karl *et al.*, 2003; Räisänen *et al.*, 2009; Aalto *et al.*, 2014), attempts have been made to include this response in models (e.g. Guenther *et al.*, 2006, 2012). However, since by far most measurements have been conducted on deciduous isoprene emitting species, the emission rates of isoprene, methanol, 2-methyl3-buten-2-ol, mono- and sesquiterpenes predicted by MEGAN are only modulated by the leaf developmental stages of deciduous land cover types (Sindelarova *et al.*, 2014). Also, it is assumed that leaf age impacts the emission rates of individual BVOCs differently, but that this dependency is not tree species specific (Guenther *et al.*, 2012). The emission rates do not respond to the developmental stages of conifers needles in models, however, measurements show that growing Scots pine foliage has a much higher potential to emit monoterpenes than mature needles (Räisänen *et al.*, 2009; Aalto *et al.*, 2014). We investigate the importance of including the monoterpene emissions from new foliage as a function of season, stand age, and tree provenance. We calculate how much predictions of the emissions of monoterpenes from Finland would increase if the emissions from new Scots pine foliage would be considered. Finally, we evaluate how our findings impact predictions of new particle formation and growth. Ultimately we try to answer whether it is worth to include emissions of monoterpenes from new Scots pine foliage in biogenic emission models?

METHODS

We utilised several years (2009-2011) of continuously measured emission rates of monoterpenes and chamber temperatures described and published in Aalto *et al.* (2014). The flux of monoterpenes was measured separately from a new and mature shoot on a 50 year old Scots pine tree at SMEAR II, in Hyytiälä, southern Finland. In practice, the flux was measured with an automated chamber and detected by PTR-QMS (proton transfer reaction-quadrupole mass spectrometer). A detailed description of the measurement set-up can be found from Aalto *et al.* (2014). The emission rates were then standardised by equation 5 in Guenther *et al.* (1993).

We used two different Scots pine tree growth models to calculate the seasonal and yearly development of Scot pine needles, respectively. The seasonal needle mass growth of a Scots pine stand growing in the conditions of Hyytiälä was calculated by the CASSIA model (Schiestl-Aalto *et al.*, 2015).

Using 5 years of gross primary production data obtained from SMEAR I and II, the results by CASSIA were further modulated in order to give estimates of the seasonal needle mass development in northern Finland. The yearly development of needle mass was calculated for southern and northern Finland, respectively, by a new simple model that takes total amounts of needle classes present in the stand and maximum stand needle biomass as input. We considered the amount of needle classes reported by Ľupeć *et al.* (2015), and maximum stand needle biomass reported by Ilvesniemi and Liu (2001) and Kulmala *et al.* (2019). The model assumes a typical stocking density, and hence the needle mass development is assumed to follow a sigmoidal form (e.g. Mäkelä, 1995).

CONCLUSIONS

We conclude that (1) it is vital to account for the emissions of monoterpenes from new Scots pine foliage until the needles reach maturity, and especially critical during spring. If new Scots pine foliage is not considered in models, the emissions of monoterpenes from southern Finland is underestimated by ~57% and ~68%, considering the full growing season and mid April-end May, respectively. The corresponding values for northern Finland are ~35% and ~47%. (2) The importance of considering the emissions from growing Scots pine needles decreases with increased stand age, since the fraction of new foliage decreases with stand age. For example, the error of not considering the emissions from new needles on a 10 year old Scots pine stand in southern Finland during mid April-end May is ~81%, whereas it is “only” ~72% in the case of a 50 year old stand in similar environmental conditions. (3) It is more important to account for the emissions from growing needles when simulating southern Finland than northern Finland, as the fraction of new foliage is less in colder environments. For example, the emissions from a 50 year old Scots pine stand in southern Finland are underestimated by ~72% during mid April-end May if the emissions from new foliage are not considered, whereas the underestimation for a 50 year old Scots pine stand in northern Finland is “only” 47%. (4) Predictions of the emissions of monoterpenes from Finland would increase by ~20 Gg monoterpenes / year if the emissions from new Scots pine foliage would be considered. (5) The formation and growth rates of small particles would have the potential to increase by 98-258% and 60-255%, respectively, if the emissions from new Scots pine needles would be included into emission models. (6) It is absolutely vital to include emissions of monoterpenes from new Scots pine foliage in biogenic emission models.

ACKNOWLEDGEMENTS

This work was supported by the Academy of Finland (no. 307331). D. Taipale was additionally supported by the Academy of Finland (no. 307957).

REFERENCES

- Aalto, J., P. Kolari, P. Hari, V.-M. Kerminen, P. Schiestl-Aalto, H. Aaltonen, J. Levula, E. Siivola, M. Kulmala and J. Bäck (2014). New foliage growth is a significant, unaccounted source for volatiles in boreal evergreen forests, *Biogeosciences* **11**, 1331.
- Donahue, N.M., I.K. Ortega, W. Chuang, I. Riipinen, F. Riccobono, S. Schobesberger, J. Dommen, U. Baltensperger, M. Kulmala, D.R. Worsnop, H. Vehkamäki (2013). How do organic vapors contribute to new-particle formation?, *Faraday Discuss* **165**, 91.
- Ehn, M., J.A. Thornton, E. Kleist, M. Sipilä, H. Junninen, I. Pullinen, M. Springer, F. Rubach, R. Tillmann, B. Lee, F. Lopez-Hilfiker, S. Andres, I.-H. Acir, M. Rissanen, T. Jokinen, S. Schobesberger, J. Kangasluoma, J. Kontkanen, T. Nieminen, T. Kurtén, L.B. Nielsen, S. Jørgensen, H.G. Kjaergaard, M. Canagaratna, M.D. Maso, T. Berndt, T. Petäjä, A. Wahner, V.-M. Kerminen, M. Kulmala, D.R. Worsnop, J. Wildt and T.F. Mentel (2014). A large source of low-volatility secondary organic aerosol, *Nature* **506**, 476.
- Goldstein, A., M. Goulden, J.W. Munger, S. Wofsy and C. Geron (1998). Seasonal course of isoprene emissions from a midlatitude forest, *J Geophys Res* **103**, 31045.

- Guenther, A.B., R.K. Monson and R. Fall, R. (1991). Isoprene and monoterpene emission rate variability: Observations with eucalyptus and emission rate algorithm development, *J Geophys Res-Atmos* **96**, 10799.
- Guenther, A.B., P.R. Zimmerman, P.C. Harley, R.K. Monson, and R. Fall (1993). Isoprene and monoterpene emission rate variability: Model evaluations and sensitivity analyses, *J Geophys Res Atmos* **98**, 12609.
- Guenther, A., T. Karl, P. Harley, C. Wiedinmyer, P.I. Palmer and C. Geron (2006). Estimates of global terrestrial isoprene emissions using MEGAN (Model of Emissions of Gases and Aerosols from Nature), *Atmos Chem Phys* **6**, 3181.
- Guenther, A.B., X. Jiang, C.L. Heald, T. Sakulyanontvittaya, T. Duhl, L.K. Emmons and X. Wang (2012). The Model of Emissions of Gases and Aerosols from Nature version 2.1 (MEGAN2.1): an extended and updated framework for modeling biogenic emissions, *Geosci Model Dev* **5**, 1471.
- Hakola, H., T. Laurila, V. Lindfors, H. Hellén, A. Gaman and J. Rinne (2001). Variation of the VOC emission rates of birch species during the growing season, *Boreal Environ Res* **6**, 237.
- Holopainen, J.K. (2004). Multiple functions of inducible plant volatiles, *Trends Plant Sci* **9**, 529.
- Ilvesniemi, H. and C. Liu (2001). Biomass distribution in a young Scots pine stand, *Boreal Env Res* **6**, 3.
- Karl, T., A. Guenther, C. Spirig, A. Hansel and R. Fall (2003). Seasonal variation of biogenic VOC emissions above a mixed hardwood forest in northern Michigan, *Geophys Res Lett* **30**, 2186.
- Kulmala, L., J. Pumpanen, P. Kolari, S. Dengel, F. Berninger, K. Köster, L. Matkala, A. Vanhatalo, T. Vesala and J. Bäck (2019). Inter- and intra-annual dynamics of photosynthesis differ between forest floor vegetation and tree canopy in a subarctic Scots pine stand, *Agric For Meteorol* **271**, 1.
- Kulmala, M., T. Petäjä, M. Ehn, J. Thornton, M. Sipilä, D.R. Worsnop, V.-M. Kerminen (2014). Chemistry of Atmospheric Nucleation: On the Recent Advances on Precursor Characterization and Atmospheric Cluster Composition in Connection with Atmospheric New Particle Formation, *Annu Rev Phys Chem* **65**, 21.
- Mäkelä, A. (1995). A carbon balance model of growth and self-pruning in trees based on structural relationships, *FoR Sci* **43**, 7.
- Monson, R., P. Harley, M. Litvak, M. Wildermuth, A. Guenther, P. Zimmerman and R. Fall (1994). Environmental and developmental controls over the seasonal pattern of isoprene emission from aspen leaves, *Oecologia* **99**, 260.
- Petron, G., P. Harley, J. Greenberg and A. Guenther (2001). Seasonal temperature variations influence isoprene emission, *Geophys Res Lett* **28** 1707.
- Räisänen, T., A. Ryyppö and S. Kellomäki (2009). Monoterpene emission of a boreal Scots pine (*Pinus sylvestris* L.) forest, *Agric For Meteorol* **149** 808.
- Riccobono, F., S. Schobesberger, C.E. Scott, J. Dommen, I.K. Ortega, L. Rondo, J. Almeida, A. Amorim, F. Bianchi, M. Breitenlechner, A. David, A. Downard, E.M. Dunne, J. Duplissy, S. Ehrhart, R.C. Flagan, A. Franchin, A. Hansel, H. Junninen, M. Kajos, H. Keskinen, A. Kupc, A. Kürten, A.N. Kvashin, A. Laaksonen, K. Lehtipalo, V. Makhmutov, S. Mathot, T. Nieminen, A. Onnela, T. Petäjä, A.P. Praplan, F.D. Santos, S. Schallhart, J.H. Seinfeld, M. Sipilä, D.V. Spracklen, Y. Stozhkov, F. Stratmann, A. Tomé, G. Tsagkogeorgas, P. Vaattovaara, Y. Viisanen, A. Vrtala, P.E. Wagner, E. Weingartner, H. Wex, D. Wimmer, K.S. Carslaw, J. Curtius, N.M. Donahue, J. Kirkby, M. Kulmala, D.R. Worsnop and U. Baltensperger (2014). Oxidation Products of Biogenic Emissions Contribute to Nucleation of Atmospheric Particles, *Science* **344**, 717.
- Riipinen, I., T. Yli-Juuti, J.R. Pierce, T. Petäjä, D.R. Worsnop, M. Kulmala and N.M. Donahue (2012). The contribution of organics to atmospheric nanoparticle growth, *Nature Geoscience* **5**, 453.
- Schiestl-Aalto, P., L. Kulmala, H. Mäkinen, E. Nikinmaa and A. Mäkelä (2015). CASSIA - a dynamic model for predicting intra-annual sink demand and interannual growth variation in Scots pine, *New Phytol* **206**, 647.
- Schobesberger, S., H. Junninen, F. Bianchi, G. Lönn, M. Ehn, K. Lehtipalo, J. Dommen, S. Ehrhart, I.K. Ortega, A. Franchin, T. Nieminen, F. Riccobono, M. Hutterli, J. Duplissy, J. Almeida, A. Amorim, M. Breitenlechner, A.J. Downard, E.M. Dunne, R.C. Flagan, M. Kajos, H. Keskinen, J. Kirkby, A. Kupc, A. Kürten, T. Kurtén, A. Laaksonen, S. Mathot, A. Onnela, A.P. Praplan, L. Rondo, F.D. Santos, S. Schallhart, R. Schnitzhofer, M. Sipilä, A. Tomé, G. Tsagkogeorgas, H. Vehkamäki, D.

- Wimmer, U. Baltensperger, K.S. Carslaw, J. Curtius, A. Hansel, T. Petäjä, M. Kulmala, N.M. Donahue and D.R. Worsnop (2013). Molecular understanding of atmospheric particle formation from sulfuric acid and large oxidized organic molecules, *PNAS* **110**, 17223.
- Sindelarova, K., C., Granier, I. Bouarar, A. Guenther, S. Tilmes, T. Stavrou, J.-F. Müller, U. Kuhn, P. Stefani and W. Knorr (2014). Global data set of biogenic VOC emissions calculated by the MEGAN model over the last 30 years, *Atmos Chem Phys* **14**, 9317.
- Župek, B., R. Mäkipää, J. Heikkinen, M. Peltoniemi, L. Ukonmaanaho, T. Hokkanen, P. Nöjd, S. Nevalainen, M. Lindgren and A. Lehtonen (2015). Foliar turnover rates in Finland - comparing estimates from needle-cohort and litterfall-biomass methods, *Boreal Environ Res* **20**, 283.

WHILE ART PERFORATES THE WALLS OF DATA SILOS: CLIMATE WHIRL ARTS PROGRAM 2013-19 AND BEYOND

U.K. TAIPALE¹, T.S. HAAPOJA², A. MEYER-BRANDIS³, V. SUONPÄÄ⁴, P. SÖDERLUND⁴

¹Institute for Atmospheric and Earth System Research (INAR), Climate Whirl, Department of Physics,
University of Helsinki, Finland

² Parsons Fine Arts and NYU New York, US

³ Forschungsfloss für Unterirdische Riffologie u.V. (FFUR), Berlin, Germany

⁴ IC-98, Sampsantie 40 G 18, 00610 Helsinki, Finland

Keywords: ART, CLIMATE WHIRL, HYYTIÄLÄ FORESTRY FIELD STATION

INTRODUCTION

In 2013 Climate Whirl¹ arts program was launched and Art and Science research and activities at University of Helsinki Hyytiälä Forestry Field Station began under its umbrella. The initiative was funded by Kone Foundation until the year 2018 and in 2019, Institute for Atmospheric and Earth System Research (INAR) decided to continue and integrate the program to the activities of the research unit.

EARLY STAGES OF CLIMATE WHIRL

The first cracks on the silo walls were already occasioned by visual artist Terike Haapoja, who in 2008 approached the station in search for sources of knowledge while doing background research for a series of artworks, dealing with the science and scientific grounds behind the mundane processes such as decomposition, photosynthesis and cycles of carbon.



Figure 1-2. Exhale-Inhale, Terike Haapoja, 2008/2013

Three coffin-sized glass cases, filled with soil and dead leaves. Carbon dioxide that is produced by decomposing is measured with CO₂ sensors and the level is sonificated. Ventilation fans on both sides open and close in 20 second intervals. The ventilation fans function as gills, regulating the CO₂ level inside the coffin. As a result the coffin seems to slowly inhale and exhale as the CO₂ level goes up and down. In biology this process is called "soil respiration", as the soil seems to "breath out" carbon dioxide.

¹ www.climaterwhirl.fi/en

Her well-in-advance studied enquiry and punctual visits to the SMEAR II forestry field station opened eyes of some scientists and staff to see the arts as more than a mere diversion and made them eager to integrate arts as part of the research done at Hyytiälä Forestry Field Station. In 2013 Haapoja represented Finland at Venice Biennale and had a solo show at Nordic Pavilion where the durational sculpture *Inhale – Exhale* and the interactive installation *Dialogue* were exhibited. Eija Juurola and Toivo Pohja, among other scientists were named as scientific advisors of these art installations that were seen by tens of thousands of visitors (Haapoja, 2013).

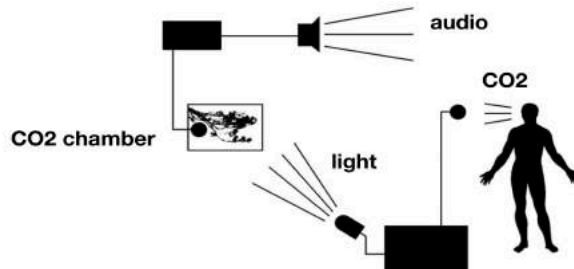


Figure 3-4. Dialogue, Terike Haapoja 2008/2013
The installation enables an audible dialogue between breathing and the plants' photosynthesis process.

IN SEARCH FOR SOCIETAL IMPACT, BEYOND ACADEMIA

At the same time, in other scientific research centers, similar initiatives were occurring. Good examples are CERN at Geneva, where the arts program of the world's largest laboratory of particle physics, Arts at CERN² was founded in 2011. The program welcomes annually 15-20 artists for 1-3 months curated research residencies. The Joint Research Centre (JRC) of the European Commission celebrated in 2015 the first Resonances Festival. The Festival has been biannual since then, presenting the work of selected artists who had a chance to peer into the research happening in the JRC Science Hubs in Europe and enter into a dialogue with scientists in their working environment with very limited access.

CLIMATE WHIRL ART PROGRAM 2013 -> TEA DRINKING, AEROSOLS, VOCs AND THE FOREST GREEN

The first artist-in-residence at Climate Whirl program, Agnes Meyer-Brandis (DE) was shortlisted and later invited to work to Hyytiälä Research Station in 2013. The scientific field station offered a cornucopia of impressions and information for her work. Since the research residence at Hyytiälä station (2013-14) she has been very focused in the forests, trees, atmospheric phenomena and the science around them. To get in contact with other researchers at the forestry field station, she actively looked for communication strategies. Designing and building a special table to invite other visitors of the station for a cup of tea with her and a tree in a forest were the initial steps for creating a reciprocal trust and curiosity, the grounds for any creative interchange of ideas. In 2015, the *Permanent Tealemetree Station*³ was installed in the SMEAR II station in the proximity of measurement equipment.

² <https://arts.cern>

³ Tea: a traditional beverage made from steeping the processed leaves, buds in water.

Telemetry: the word is derived from Greek roots: tele = remote, and metron = measure.

Tree: there is no universally recognized precise definition of what a tree is, neither botanically nor in common language. (Meyer-Brandis, 2015)

Aerosols and their influence on the atmosphere and the phenomena of cloud formation were topics Meyer-Brandis had worked already with before her residence at the SMEAR II station. During 2013-14 she developed a “multifunctional tool for the investigation of tiny micro clouds above tea, for communication and for tea drinking” (Meyer-Brandis, 2014). This kinetic and cybernetic sculpture was named *Teacup Tools*. Resonating with the GlobalSMEAR⁴ vision of the director of the Centre of Excellence for Atmospheric Sciences, academy professor Markku Kulmala, she also aims at expanding the local network of *Teacup Tools* to a global one (GTN). Her network is meant to go global through public exhibitions at cultural venues. By now the *Teacup Tools* were exhibited in Switzerland, Spain, Austria, Germany and Finland. The work was awarded at the Ars Electronica in 2015 with Award of Distinction, in the category of Hybrid Art⁵.

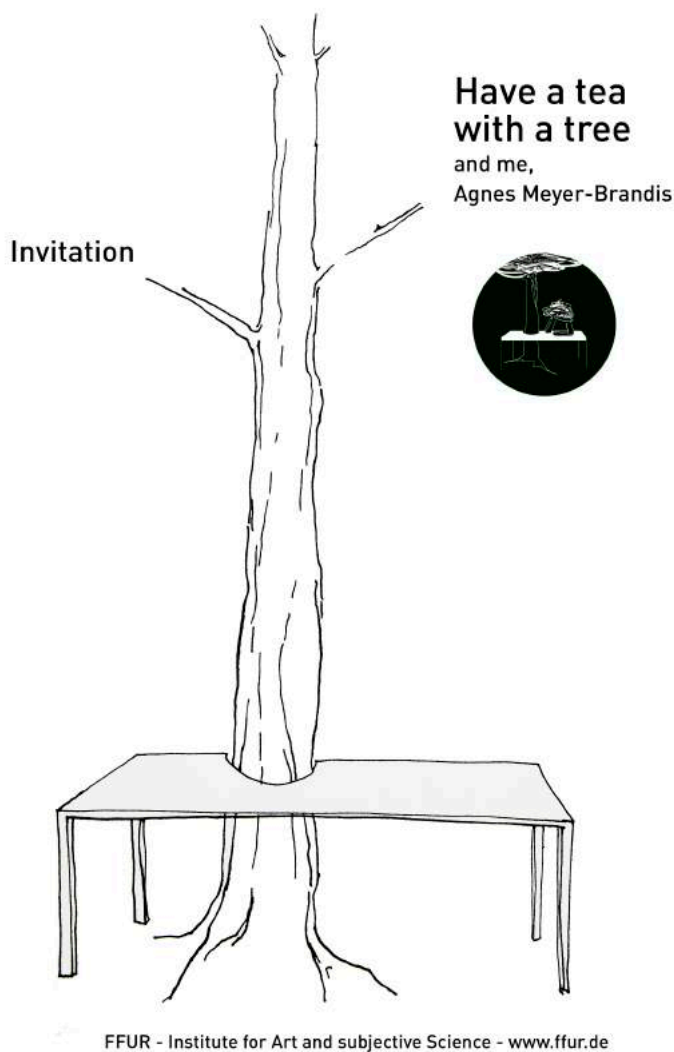


Figure 5. Have a Tea with the Tree and Me, Agnes Meyer-Brandis, 2013. @ Agnes Meyer-Brandis, VG Bildkunst 2019.

⁴ GlobalSMEAR, <https://www.helsinki.fi/en/inar-institute-for-atmospheric-and-earth-system-research/infrastructure/globalsmear>

⁵ Prix Ars Electronica 2015, <http://prix2015.aec.at/prixwinner/16815/>

Continuous tea drinking under trees at Finnish forests might have given inspiration for a series of further works, developed during the recent years, such as *One Tree ID* (2019), which transforms the VOCs (Volatile Organic Compound) of a specific tree to a perfume for human use, enabling persons to communicate with trees at a biochemical level. The work has been developed in dialogue with researchers at Institute for Biosciences at University Rostock and with a senior perfumer Marc von Ende. (Meyer-Brandis, 2019) Another long-term project, *The Office for Tree Migration (OTM)* is a work in progress that observes the slow movement of trees in various areas of the Earth, in search for suitable living conditions in changing climates. (Meyer-Brandis, 2019)

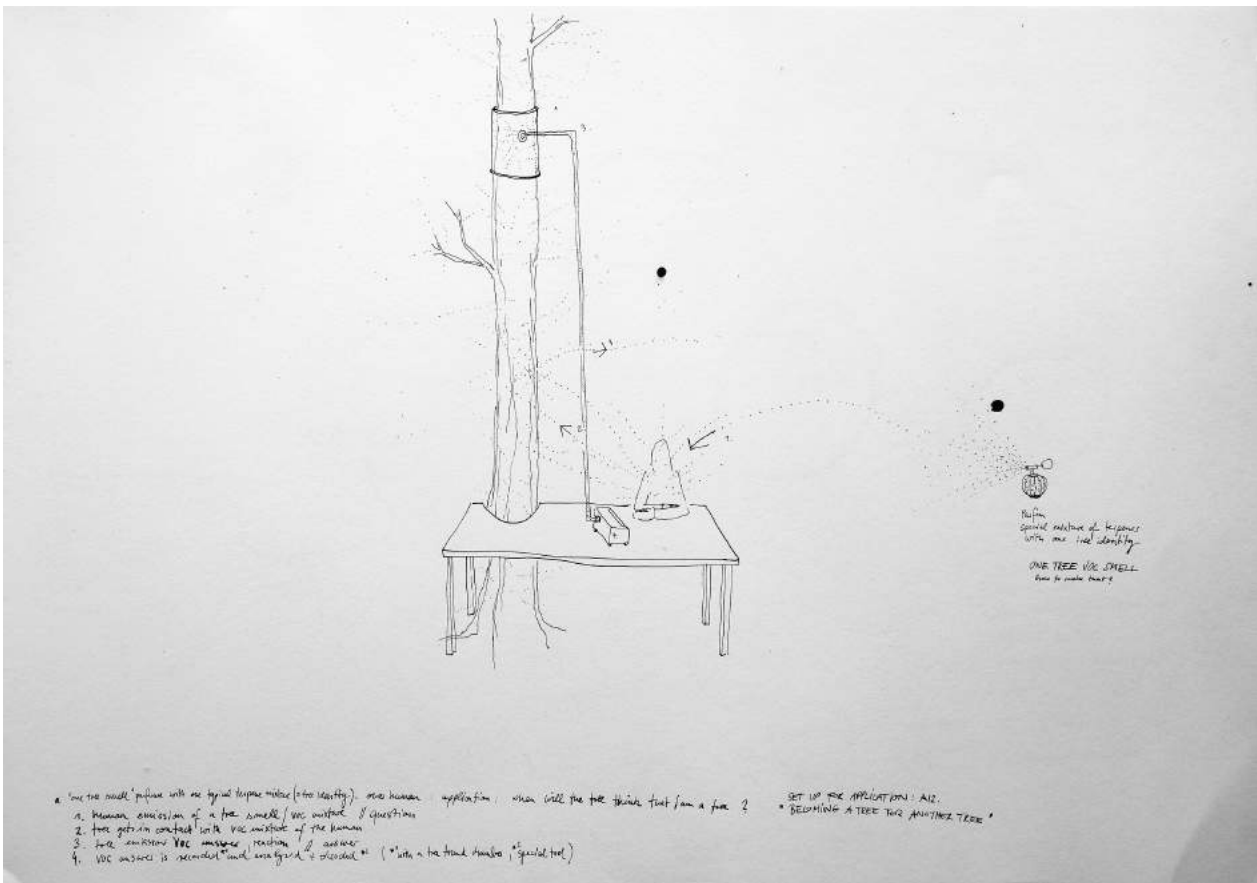


Figure 6. Illustration for One Tree ID, Agnes Meyer-Brandis, 2019. @ Agnes Meyer-Brandis, VG Bildkunst 2019.

POETIC COUNTER-STORY IN AN OLD FOREST 2017-19

Meanwhile the discussion of the boreal forest management policies and their influence to the global climates and economies has been warming up, Finnish artist group IC-98, composed by Patrik Söderlund and Visa Suonpää started working with a new art project related to the realms of the Hyttiälä station. Their work, which is grounded to the cultural history and visionary conceptual thinking, offers an interesting angle to explore the forestry field station – and to wander in a natural forest. The roots of Hyttiälä research complex lay in the education of the traditional forest management. Later the focus has diversified and the station converted to a field station for a Center of Excellence in Atmospheric Sciences, a creative research environment producing data that contributes in understanding the global climate.

The new artwork by IC-98 (2017-19) is called *LÄI*. It is a common effort of a workgroup set by Suonpää and Söderlund, consisting of three Finnish poets, Henriikka Tavi, Mikael Brygger and Olli-Pekka Tennilä, a nature cartographer Jyrki Lehtinen and two crafts persons Andrei Baharev and Kaius Paetau.

The Finnish words and syllables, composed by the poets, are carved in 35 different places in the natural forest located at the station. Three of them are located at Department of Forest Sciences at Viikki Campus. The words can be found on the wooden or stony surfaces of trees, rocks and stones, and their meanings guide the visitor or the reader to the sources of the Finnish language and to the manifold cultural meanings that forest has had and still has for Finnish people. The work is immersed in the natural environment and landscape, in a forest at Hyytiälä.



Figure 5-6. IÄI, Sielu-Jää, IC-98, 2017-19

The work of IC-98 converts the forest to an artwork, huge in size and thought-provoking and sensitising as experience, evoking mental linkages from our past as a forest people to our present as part of a global capitalist system. The work is multi-dimensional, sensorial experience that is constantly changing due to the weather, the time of the day and the season. The visibility ends with the sunset even though the “exhibition space” is open 24/7. In addition to the carved words within the wood and university campus, a booklet designed by the artists forms part of the whole artwork, that will be published in late 2019.

CONCLUSIONS

In most of the cases works of art are shown in museums, galleries and in public sphere where the access of general public is less restricted than in the scientific research centers and publications. Sometimes art is offered generously space in media, that is read or watched by millions of people. Political and economic influencers visit art exhibitions and fairs. Art informed by science can be interpreted without having a specific PhD in the topic, even though having related studies may reveal several extra layers of the artwork. In any case, art needs skillful minds, economic resources and time to become significant and thought-provoking.

Sufficiently informed funding bodies enable new and state-of-the-art phenomena to develop. Brave funders are trailblazers and trendsetters for sciences and for arts. Institutions in both disciplines should seriously estimate the value and impact of the initiatives that have been developed thanks to the external funding. Without long-term vision and support from the institutions the impacts remain short-lived.

Climate Whirl continues in 2019 with an international Open Call for Artists. By the end of the year an artist or an artist group will be selected by a jury, composed by scientists and art experts and can begin their work at the field station in 2020. An international open call outreaches a global art and cultural audience and is a way to communicate about the research done at the Center of Excellence in Atmospheric Science to non-scientific crowd. Each artwork created start living its own life in the minds of audiences once the works are exhibited and showed up.

ACKNOWLEDGEMENTS

Climate Whirl is supported by INAR and by the Kone Foundation 2013-18.

REFERENCES

- Haapoja, T. (2013) . Closed Circuit - Open Duration. Retrieved 26th 2019, from URL: <http://www.terikehaapoja.net/closed-circuit-open-duration-exhibition-venice-biennale-nordic-pavilion/>
- Meyer-Brandis, A. (2014) . Teacup Tools. Retrieved October 25th, 2019 from URL: <http://www.ffur.de/tea>
- Meyer-Brandis, A. (2018) . Forest Green. Retrieved October 25th, 2019 from URL: <http://www.blubblubb.net/forestgreen/>
- Meyer-Brandis, A. (2019) . One Tree ID. Retrieved October 25th, 2019 from URL: <http://www.blubblubb.net/OneTreeID/index.html>
- Meyer-Brandis, A. (2019) . The Office for Tree Migration. Retrieved October 25th, 2019 from URL: <http://www.blubblubb.net/otm/>

LIST OF FIGURES

- Fig 1. Carmeni, U. (2013) . Inhale-Exhale by T. Haapoja, in exhibition.
- Fig 2. Kantanen, S. (2013) . Inhale-Exhale by T. Haapoja, interior of the installation.
- Fig 3. Carmeni, U. (2013) . Dialogue by T. Haapoja, in exhibition at Nordic Pavillon, Venice Biennale.
- Fig 4. Haapoja, T. (2008) . Dialogue by T. Haapoja, chart of the installation.
- Fig 5. Meyer-Brandis, A. (2013) . Have a Tea with the Tree and Me. Poster illustration.
- Fig 6. Meyer-Brandis, A. (2019) One Tree ID, illustrative sketch.
- Fig 7. Taipale, U. (2019) . IÄI - Sielu, Poetic counter-story at Hyytiälä Forestry Field Station, an artwork by IC-98
- Fig 8. Taipale, U. (2019) . IÄI - Jää, Poetic counter-story at Hyytiälä Forestry Field Station, an artwork by IC-98

Abstract for Center of Excellence Seminar in Atmospheric Sciences

CLIMATE SIGNAL IN PINE NEEDLE SUGAR STABLE CARBON ISOTOPE RATIOS FOR TWO SITES IN NORTHERN AND SOUTHERN FINLAND

Y. TANG^{1,2}, P. SCHIESTL-AALTO², E. SAHLSTEDT¹, J. BÄCK², K. RINNE-GARMSTON¹

¹Natural Resources Institute, Helsinki, Finland

²Institute for Atmospheric and Earth System Research (INAR)/ Forest Sciences, Faculty of Science, University of Helsinki, Helsinki, Finland

Keywords: stable carbon isotope, sugars, boreal forest, climate signal

INTRODUCTION

Stable isotopes in tree rings (e.g. $\delta^{13}\text{C}$ and $\delta^{18}\text{O}$) have been proven to be a powerful tool to study the impact of climate change on boreal forests, as they can sensitively respond to the changing environment where the tree lives (Farquhar *et al.*, 1982, McCarroll and Loader, 2004). However, significant gaps exist in our knowledge about how these climatically driven isotopic signals are modified after photosynthesis by metabolic processes and isotopic fractionations prior to tree ring formation (Gessler *et al.*, 2014).

Compound-Specific Isotope Analyses provides us the possibility to examine e.g. reserve effects and post-photosynthetic fractionation processes by comparing compound-specific $\delta^{13}\text{C}$ in leaves and $\delta^{13}\text{C}$ of tree rings (e.g. Rinne *et al.*, 2015a; 2015b). This project on $\delta^{13}\text{C}$ dynamics of individual sugars and starch in needles and phloem in response to climatic factors will enhance our understanding of the tree ring isotope ratio and will help decipher environmental conditions in retrospect more reliably.

METHODS

Scots pine needles were collected 22 times during 2018 from five mature trees in Värriö (SMEAR I, northern Finland) and Hyytiälä (SMEAR II, southern Finland). Sugars were extracted from needle powder in Milli-Q water at 85°C (Wanek *et al.*, 2001) and purified using sample treatment cartridges (Rinne *et al.*, 2012). The $\delta^{13}\text{C}$ values of bulk sugars were determined using a EA-IRMS.

RESULTS

In both sites, $\delta^{13}\text{C}$ values of both current-year-old (0N) and one-year-old (1N) needle sugars are significantly positively correlated with photosynthetically active radiation (PAR) and air temperature (T), and negatively correlated with relative humidity during the growing season. $\delta^{13}\text{C}$ values of needle sugars correlate best with air T in Värriö ($r_{T_0N}=0.85$; $r_{T_1N}=0.66$) but with PAR in Hyytiälä ($r_{PAR_0N}=0.83$; $r_{PAR_1N}=0.72$), probably indicating different limiting factors in photosynthesis in the two sites. Besides, we observed a significant inter-tree difference in absolute $\delta^{13}\text{C}$ values of needle sugars during the growing season for Hyytiälä but not for Värriö, which suggests more heterogeneous and competitive growth conditions in Hyytiälä. Higher needle sugar concentration in winter was observed in Värriö than in Hyytiälä, reflecting higher importance of sugars for frost hardiness in Värriö.

At the beginning of the growing season, $\delta^{13}\text{C}$ values and concentration of 0N sugars were significantly higher than 1N sugars in Hyytiälä, probably indicating use of reserves in 0N. However, no such trends were observed in Värriö. During dry periods, although relatively higher $\delta^{13}\text{C}$ values were observed (at the end of July in Värriö, at the end of August in Hyytiälä), $\delta^{13}\text{C}$ values correlate well with climate signal (i.e. PAR in Hyytiälä, air T in Värriö). There was no clear sign of using of reserves during droughts in 2018.

CONCLUSIONS

Abstract for Center of Excellence Seminar in Atmospheric Sciences

Our results indicate the potential of using tree-ring $\delta^{13}\text{C}$ data for climate reconstruction in these two sites, and provide valuable data for deciphering post-photosynthesis processes prior to tree ring formation, which can contribute to a more reliable climate reconstruction model.

ACKNOWLEDGEMENTS

This work was supported by the ERC 755865 and the Academy of Finland 295319. Thanks are due to E.P. Karvinen, A.J.M. Ovaska, T. Hietajarvi, T. Kylli, J.T. Levula, A. Seppänen, A. Kinnunen, A. Bartosz, M.L. Koskela, and K. Pynnönen for their valuable help in field work and lab work in 2018.

REFERENCES

- Farquhar, G.D., M.H. O'Leary and J.A. Berry (1982). On the relationship between carbon isotope discrimination and the intercellular carbon dioxide concentration in leaves. *Aust. J. Plant Physiol.* **9**, 121.
- Gessler, A., J.P. Ferrio, R. Hommel, K. Treydte, R.A. Werner and R.K. Monson (2014). Stable isotopes in tree rings: towards a mechanistic understanding of isotope fractionation and mixing processes from the leaves to the wood. *Tree physiology* **34**, 796.
- McCarroll, D., and N.J. Loader (2004). Stable isotopes in tree rings. *Quaternary Science Reviews* **23**, 771.
- Rinne, K.T., M. Saurer, A.V. Kirilyanov, M.V. Bryukhanova, A. S. Prokushkin, O.V. Churakova (Sidorova) and R. T.W. Siegwolf (2015a). Examining the response of needle carbohydrates from Siberian larch trees to climate using compound-specific $\delta^{13}\text{C}$ and concentration analyses. *Plant cell Environ* **38**, 2340.
- Rinne, K.T., M. Saurer, A.V. Kirilyanov, N.J. Loader, M.V. Bryukhanova, R.A. Werner and R.T.W. Siegwolf (2015b). The relationship between needle sugar carbon isotope ratios and tree rings of larch in Siberia. *Tree physiology* **35**, 1192.
- Rinne, K.T., M. Saurer, K. Streit and R.T.W. Siegwolf (2012). Evaluation of a liquid chromatography method for compound-specific $\delta^{13}\text{C}$ analysis of plant carbohydrates in alkaline media *Rapid Commun Mass Spectrom* **26**, 2173.
- Wanek, W., S. Heintel and A. Richter (2001). Preparation of starch and other carbon fractions from higher plant leaves for stable carbon isotope analysis. *Rapid Commun Mass Spectrom* **15**, 1136.

A PULSE LABELLING EXPERIMENT TO CONSTRAIN THE BIOCHEMICAL PRECURSORS OF AEROBICALLY PRODUCED METHANE

S. TENHOVIRTA^{1,2}, L. KOHL^{1,2}, T. POLVINEN^{1,2}, M. KOSKINEN^{1,2} and M. PIHLATIE^{1,2,3}

¹Department of Agricultural Sciences, Faculty of Agriculture and Forestry, University of Helsinki, Finland

²Institute of Atmospheric and Earth System Research / Forest Sciences, Faculty of Agriculture and Forestry, University of Helsinki, Finland

³Viikki Plant Science Centre (VIPS), University of Helsinki, Finland

Keywords: Methane, ¹³C pulse-labelling, *Pinus sylvestris*, online chamber measurements.

BACKGROUND

Methane is one of the three most important greenhouse gases alongside water vapor and carbon dioxide, and its atmospheric concentration has notably increased since preindustrial times. Biogenic methane production has previously been thought to occur only in anaerobic conditions by methanogenic Archaea (Conrad, 2009). Recently it was discovered that plants can also produce methane in an unknown aerobic, non-microbial process, deriving from structural or active biochemical compounds within the plant (Althoff et al., 2014; Bruhn et al., 2009; Covey & Megonigal, 2018; Lenhart et al., 2015; Martel & Qaderi, 2019; McLeod et al., 2008). The actual methane precursor(s) in living plant material, however, have not been identified.

In-vitro experiments have shown that methane can be produced from different compounds including pectins (Keppler et al., 2008; McLeod et al., 2008), lignin (Fraser et al., 2015), leaf surface wax (Bruhn et al., 2014), and organosulfur compounds like methionine (Lenhart et al., 2015; Martel & Qaderi, 2019). Methane emissions from plant material have been demonstrated to be increased by UV-radiation, increasing temperatures, wounding of the plant tissues and reactive oxygen species (Bruhn et al., 2009; Keppler et al., 2006; McLeod et al., 2008; Messenger et al., 2009; Vigano et al., 2008; Wang et al., 2009). Although many options have been studied, there are still considerable uncertainties in the precursors and processes involved (Covey & Megonigal, 2018).

Stable isotope pulse-labelling plants with the ¹³C can be used to trace photosynthetically assimilated carbon through plant pools (Olsson & Johnson, 2005). We will utilize this method to investigate the apparent turnover time of the methane precursors, and by doing so shed light to the process of origin of the leaf-level methane emissions from samplings of Scots pine (*Pinus sylvestris*).

METHODS

Our plan is to pulse-label young saplings of Scots pine with ¹³C-carbon dioxide after spring recovery and bud burst, and to measure the emissions and isotopic composition of methane from shoots for the following six to eight weeks. The pulse labelling will be done by enclosing six saplings into a chamber and adding 99% ¹³C-carbon dioxide to replace the carbon dioxide fixed by photosynthesis. The carbon dioxide concentration of the chamber is measured during the pulse-labelling. The ¹³C-carbon dioxide addition is repeated throughout the day, every time the carbon dioxide concentration inside the chamber drops low enough for the photosynthetic rate to slow down. Additional lighting is used to support photosynthesis. Control trees are treated with similar pulses of natural abundance ¹²C-carbon dioxide.

After labelling, the gas exchange of the saplings will be measured online for six to eight weeks. For this purpose, we have constructed an experimental system that enables the continuous measuring of the shoot methane emissions of six individual trees (Fig.1). Needle samples will be collected regularly throughout the measurement period, for quantifying the ¹³C-content in structural, storage and soluble compounds.

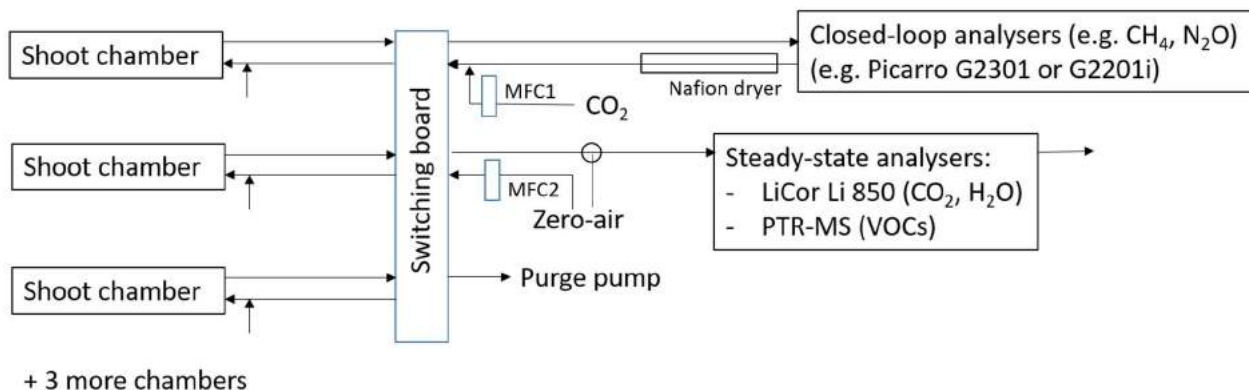


Figure 1. The instrumental setup for automatic continuous measuring of the greenhouse gas exchange, transpiration and volatile organic compounds (VOCs) from shoots.

The setup for continuous measurements consists of a novel shoot chamber system capable of replacing fixed carbon dioxide, removing transpired water, and cooling the shoot chambers to near ambient temperatures. Each sapling has a shoot enclosed into a chamber that is connected to gas analyzers via a switching board. The shoot chambers are alternately placed (a) in closed loop with a Picarro G2201i cavity ring-down spectroscopy (CRDS) isotopic and gas concentration analyzer (to measure carbon dioxide and methane concentrations and their ^{12}C - and ^{13}C -isotopes), (b) in a flow-through set-up with a Li-Cor 850 CO_2 - H_2O analyzer (to measure photosynthesis and transpiration), or (c) flushed with ambient air. Additionally, we will monitor methanol and ^{13}C -methanol emissions by proton transfer reaction mass spectrometer (PTR-MS), also in flow-through mode.

The additions of carbon dioxide into the shoot chambers, and the zero air for the PTR-MS measurements, are controlled by two mass flow controllers. Each chamber is also equipped with temperature sensors, temperature controlled Peltier elements for cooling the chambers, and sensors for measuring photosynthetically active radiation (PAR). The system is controlled by a switching board that can be programmed to switch the mode assigned to each chamber automatically, at regular intervals.

EXPECTED RESULTS AND CONCLUSIONS

The shoot chamber system was constructed during the spring and summer of 2019, and it is currently conducting baseline measurements on non-labelled pine saplings. The pulse-labelling and the follow-up measurements will be carried out in the spring of 2020.

As a result of this experiment, we are expecting to be able to determine the time it takes for the ^{13}C to show up in the methane emissions from the shoots. We hypothesize that the temporal pattern of the ^{13}C content of the emitted methane implicate its precursors: If the ^{13}C content of emitted methane at first increases and then decreases rapidly after pulse-labelling (days to hours), methane is likely derived from active metabolic processes using recently fixed carbon. To support this, we expect to find a higher ^{13}C content in labile carbon compounds such as soluble sugars in the needles sampled within the corresponding time period.

Respectively, if changes in the ^{13}C -content of methane occur more slowly (over weeks) and the corresponding needle samples have a higher ^{13}C content in compounds such as pectins or lignin, we conclude that structural compounds are a source of methane. In addition, we are looking if there is a temporal correlation in the emissions of ^{13}C -methane and ^{13}C -methanol to find out, if methanol could be a tracer gas of methane. Such a finding would also give a hint on the processes involved in the aerobic formation of plant-derived methane.

ACKNOWLEDGEMENTS

This project has received funding from the European Research Council (ERC) under the European Union's horizon 2020 research and innovation program (757695), the Academy of Finland Fellows program (319329 and 2884941), and the Academy of Finland Centers of Excellence program (307331). Markku Koskinen has received a postdoctoral grant from the Maj and Tor Nessling foundation.

REFERENCES

- Althoff, F., Benzing, K., Comba, P., McRoberts, W. C., Boyd, D. R., Greiner, S., & Keppler, F. (2014). Abiotic methanogenesis from organosulphur compounds under ambient conditions. *Nature Communications*, 5(May), 1–9. <https://doi.org/10.1038/ncomms5205>
- Bruhn, D., Mikkelsen, T. N., Øbro, J., Willats, W. G. T., & Ambus, P. (2009). Effects of temperature, ultraviolet radiation and pectin methyl esterase on aerobic methane release from plant material. *Plant Biology*, 11(SUPPL.1), 43–48. <https://doi.org/10.1111/j.1438-8677.2009.00202.x>
- Bruhn, D., Mikkelsen, T. N., Rolsted, M. M. M., Egsgaard, H., & Ambus, P. (2014). Leaf surface wax is a source of plant methane formation under UV radiation and in the presence of oxygen. *Plant Biology*, 16(2), 512–516. <https://doi.org/10.1111/plb.12137>
- Conrad, R. (2009). The global methane cycle: Recent advances in understanding the microbial processes involved. *Environmental Microbiology Reports*. <https://doi.org/10.1111/j.1758-2229.2009.00038.x>
- Covey, K. R., & Megonigal, J. P. (2018). Methane production and emissions in trees and forests. *New Phytologist*. <https://doi.org/10.1111/nph.15624>
- Fraser, W. T., Blei, E., Fry, S. C., Newman, M. F., Reay, D. S., Smith, K. A., & McLeod, A. R. (2015). Emission of methane, carbon monoxide, carbon dioxide and short-chain hydrocarbons from vegetation foliage under ultraviolet irradiation. *Plant, Cell and Environment*, 38(5), 980–989. <https://doi.org/10.1111/pce.12489>
- Keppler, F., Hamilton, J. T. G., Braß, M., & Röckmann, T. (2006). Methane emissions from terrestrial plants under aerobic conditions. *Nature*, 439(7073), 187–191. <https://doi.org/10.1038/nature04420>
- Keppler, F., Hamilton, J. T. G., McRoberts, W. C., Vigano, I., Braß, M., Röckmann, T., & Keppler, F. (2008). Methoxyl groups of plant pectin as a precursor of atmospheric methane: evidence from deuterium labelling studies. *New Phytologist*, 178, 808–814.
- Lenhart, K., Althoff, F., Greule, M., & Keppler, F. (2015). Technical note: Methionine, a precursor of methane in living plants. *Biogeosciences*, 12(6), 1907–1914. <https://doi.org/10.5194/bg-12-1907-2015>
- Martel, A. B., & Qaderi, M. M. (2019). Unravelling the effects of blue light on aerobic methane emissions from canola. *Journal of Plant Physiology*, 233(July 2018), 12–19. <https://doi.org/10.1016/j.jplph.2018.12.006>
- McLeod, A. R., Fry, S. C., Loake, G. J., Messenger, D. J., Reay, D. S., Smith, K. A., & Yun, B. W. (2008). Ultraviolet radiation drives methane emissions from terrestrial plant pectins. *New Phytologist*, 180(1), 124–132. <https://doi.org/10.1111/j.1469-8137.2008.02571.x>
- Messenger, D. J., McLeod, A. R., & Fry, S. C. (2009). Reactive oxygen species in aerobic methane formation from vegetation. *Plant Signaling and Behavior*, 4(July), 629–630. <https://doi.org/10.1111/j.1365-3040.2008.01892.x> Importantly
- Olsson, P. A., & Johnson, N. C. (2005). Tracking carbon from the atmosphere to the rhizosphere. *Ecology Letters*. <https://doi.org/10.1111/j.1461-0248.2005.00831.x>
- Vigano, I., Weelden, H. Van, Holzinger, R., Keppler, F., & McLeod, A. R. (2008). Effect of UV radiation and temperature on the emission of methane from plant biomass and structural components, 937–947.
- Wang, Z. P., Gullede, J., Zheng, J.-Q., Liu, W., Li, L. H., & Han, X. G. (2009). Physical injury stimulates aerobic methane emissions from terrestrial plants. *Biogeosciences*, 6(4), 615–621. <https://doi.org/10.1158/1055-9965.EPI-07-2865>

POTENTIAL SOURCES OF BIOGENIC VOLATILE ORGANIC COMPOUNDS IN ARCTIC- FIRST RESULTS FROM NY-ÅLESUND, SVALBARD

ROSELINE C. THAKUR*¹, MARI MÄKI^{1,2}, HEIDI HELLEN³, LISA BECK¹, MIKKO SIPILÄ¹ and
JAANA BÄCK^{1,2}

¹Institute for Atmospheric and Earth System Research, University of Helsinki, Helsinki, 00014, Finland.

²Faculty of Agriculture and Forestry, University of Helsinki, Helsinki, 00790, Finland.

³Finnish Meteorological Institute, Erik Palménin aukio 1, Helsinki, 00560, Finland.

*roseline.thakur@helsinki.fi

Keywords: BVOCS, CHAMBER, ARCTIC, BIOSPHERE, TUNDRA

INTRODUCTION

The Volatile Organic Compounds (VOCs) emissions in the air-soil, snow or ocean interface plays a major role in the atmospheric oxidation processes, gas to particle conversion and the formation of secondary organic aerosols (SOAs). VOCs are capable of forming secondary organic aerosols which constitutes the largest fraction of organic aerosol (Hallquist *et al.*, 2009). Recent studies indicate that some VOCs produce low volatility vapours through the process of auto-oxidation (Ehn *et al.*, 2014; Crouse *et al.*, 2013; Bianchi *et al.*, 2019). These low volatility vapours under atmospheric conditions may rapidly form highly oxygenated molecules (HOMs). This also includes the release of BVOCs from the Arctic biosphere which can alter the chemical and physical properties of the atmosphere which could lead to either positive or negative climate forcing (Arneth *et al.*, 2010). The most abundant VOCs produced on Earth is Isoprene (2-methyl-1,3-butadiene, C₅H₈). Monoterpenes (various C₁₀-chains) are the second largest group. There are other reactive and less reactive biogenic VOCs which are also taken into account while estimating the net emissions from the vegetation or soil cover. The highly reactive BVOCs account for the largest uncertainties in the estimations. The new particle formation processes may be induced by the BVOC emissions (Kirkby *et al.*, 2016) which may lead to increase in CCN (cloud condensation nuclei) and ultimately increase in cloud cover (Paasonen *et al.*, 2013). BVOC emissions are important to study since they can deplete the hydroxyl radicals via oxidation reactions leading to increase in the lifetime of methane in the atmosphere, which could increase the global warming potential of methane (Peñuelas and Staudt, 2010). This study was motivated by the lack of data to understand the role of VOCs in new particle formation specifically in the Polar Regions is the motivation to carry out this study, which is the first of its kind in the Svalbard region which hosts the world's northernmost terrestrial vegetation.

METHODS

The measurements were carried out in the European high Arctic site, Ny-Ålesund, Svalbard from 25th June 2019 to 12th July 2019. The VOCs fluxes from soil, vegetation, snow and ocean surface were measured using manual steady-state flow-through flux chambers (Mäki *et al.*, 2017) made from glass which were placed on soil collars (Fig.1). Filtered (active carbon trap and MnO₂-coated copper net) ambient air was continuously pumped (1 L min⁻¹) into the chamber, and the chamber air volume was flushed for 0.5 h before sampling to form a steady state chamber. Chamber temperature was measured using a thermometer (Fluke 54II, Fluke, WA, USA) from 20–30 cm aboveground. Incoming and outgoing air was sampled for 1.5–2 h using sampling flow (0.1 L min⁻¹) through two Tenax TA Carbopack B adsorbent tubes, and the flux was calculated from the difference between ingoing and outgoing air. The ambient air VOCs measurements were made through heated air inlet line attached to Tenax tube and automated pump system. The Tenax TA–Carbopack-B adsorbent tubes were analyzed for various VOCs through a thermal desorption-gas chromatography-mass spectrometer (TD-

FAAR abstract

GC-MS). The fluxes were calculated based on the difference of VOC concentration in the ingoing and outgoing air. Hemiterpenes (isoprene and 2-methyl butenol), monoterpenes (α -pinene, camphene, β -pinene, Δ -3-carene, p-cymene, limonene, and terpinolene), monoterpenoids (bornylacetate, 1.8-cineol and linalool), and sesquiterpenes (longicyclene, iso-longifolene, β -farnesene, β -caryophyllene, α -humulene) were quantified from the adsorbent tubes.

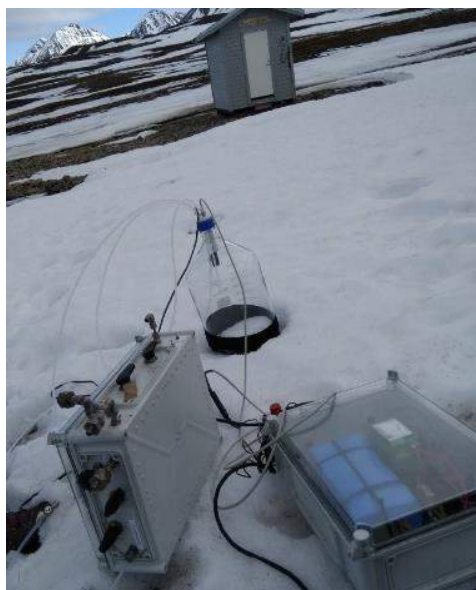


Figure 1: VOCs flux measurements in Ny-Ålesund, Svalbard.

RESULTS AND CONCLUSION

It was observed that Isoprene, α -pinene and linalool were the three most abundant compounds emitted from the Arctic biosphere. Results indicate that vegetation including flowers and grasses emit isoprene ($9.52 \mu\text{g m}^{-2} \text{h}^{-1}$) and tundra (mosses over permafrost soil) emit primarily 2-methyl-3-buten-2-ol ($0.46 \mu\text{g m}^{-2} \text{h}^{-1}$). The ocean surface having the underlying sea weed/algae emit monoterpenoids (linalool flux being the highest, $9.22 \mu\text{g m}^{-2} \text{h}^{-1}$). Interestingly the snow cover did not emit isoprene, however when the snow melted in the second week of July, the patch of soil exposed emitted $4.45 \mu\text{g m}^{-2} \text{h}^{-1}$ of isoprene. Most of the monoterpenes and sesquiterpenes emissions which were not detected in the snow cover, showed measurable fluxes after the snow melt, indicating the potential underlying soil source. Most of the ambient day measurements of monoterpenes and sesquiterpenes showed twice higher concentrations than nighttime except the mean concentration of linalool, which was higher during nighttime. Generally high molecular weight isoprenoids are known to be less volatile than monoterpenes and sesquiterpenes hence not many studies focus on their emissions. Isoprene and MBO fluxes from the soil and grasses correlated well with the chamber temperatures. This observation could possibly indicate that a warming of Arctic could increase BVOC emissions leading to more NPF events and CCN formation.

Although the fluxes and ambient concentrations are small yet the study shows that the ecosystem of pristine Arctic region has potential sources of BVOCs which needs to be taken into account while deciding on the formation pathways of SOA and HOMs in these remote places. Based on this first preliminary study, we will be conducting long term experiments in Ny-Ålesund along with HOMs measurements through Atmospheric pressure interface-time of flight mass spectrometer, to investigate further on the formation pathways of new particles in Arctic atmosphere.

ACKNOWLEDGEMENTS

We acknowledge European Research Council (GASPARCON, grant No. 714621). We greatly acknowledge the logistical support by Kings Bay staff and the researchers of the Arctic Station "Dirigibile Italia" during the field campaigns in Ny-Ålesund. I am very grateful to the Finnish Meteorological Institute for providing facilities for laboratory analysis of the samples through TD-GC-MS.

REFERENCES

- Arneth, A., S.P. Harrison, S. Zaehle, K. Tsigaridis, S. Menon, P.J. Bartlein, J. Feichter, A. Korhola, M. Kulmala, D. O'Donnell, G. Schurgers, S. Sorvari, and T. Vesala (2010). Terrestrial biogeochemical feedbacks in the climate system. *Nature Geosci.*, 3, 525-532, doi:10.1038/ngeo905.
- Bianchi, Federico., Kurtén, Theo., Riva, Matthieu., et al (2019). Highly Oxygenated Organic Molecules (HOM) from Gas-Phase Autoxidation Involving Peroxy Radicals : A Key Contributor to Atmospheric Aerosol. *Chemical Reviews*, vol. 119, no. 6, pp. 3472-3509. <https://doi.org/10.1021/acs.chemrev.8b00395>.
- Crouse J.D., Nielsen L.B., et al (2013). Autoxidation of Organic Compounds in the Atmosphere. *J. Phys. Chem. Lett.* 4: 3513–3520.
- Ehn, M., Thornton, J. A., et al (2014). A large source of low-volatility secondary organic aerosol, *Nature*, 506, 476–479.
- Hallquist, M., Wenger, J. C., et al (2009). The formation, properties and impact of secondary organic aerosol: current and emerging issues, *Atmos. Chem. Phys.*, 9, 5155-5236, <https://doi.org/10.5194/acp-9-5155-2009>.
- Kirkby, J. et al. (2016). Ion-induced nucleation of pure biogenic particles. *Nature*, 533, <http://dx.doi.org/10.1038/nature17953>.
- Mäki M, Heinonsalo J, Hellén H, Bäck J (2017). Contribution of understory vegetation and soil processes to boreal forest isoprenoid exchange. *Biogeosci.*, 14:1055–1073.
- Paasonen, P., Asmi, A., Petäjä, T., et al (2013). Warming-induced increase in aerosol number concentration likely to moderate climate change, *Nat. Geosci.*, 6, 438-442.
- Peñuelas, J. and Staudt, M (2010). BVOCs and Global Change, *Trends in Plant Science*, 15, 133-144. <http://dx.doi.org/10.1016/j.tplants.2009.12.005>.

FIRST AMBIENT OBSERVATION OF HClO₃ AND HClO₄ IN THE ARCTIC ENVIRONMENT

Y.J. THAM¹, N. SARNELA¹, I. SIDDHARTH², L. BECK¹, A. SAIZ-LOPEZ³ and M. SIPILÄ¹

¹ Institute for Atmospheric and Earth System Research/Physics, University of Helsinki, 00014, Helsinki, Finland.

² Department of Chemistry, University of Helsinki, 00014 Finland.

³ Department of Atmospheric Chemistry and Climate, Institute of Physical Chemistry Rocasolano, CSIC, Madrid 28006, Spain.

Keywords: CHLORIC ACID, PERCHLORATE ACID, OZONE DEPLETION, ARCTIC.

INTRODUCTION

The springtime ozone (O₃) destruction in the polar region has been linked to the halogens chemistry like the catalytic reactions of bromine and chlorine radicals with O₃ (e.g. Simpson et al., 2007; Neuman et al., 2010). Despite the important roles of halogen in the ozone destruction, the oxidation processes of halogen are not fully understood. For instance the initial atmospheric oxidation step of chlorine is well understood, but the final oxidation steps leading to the formation of chlorate (ClO₃⁻) and perchlorate (ClO₄⁻) remain unresolved due to the lack of direct evidence of their presence in the atmosphere to date. However, Jaeglé et al. (1996) modeled the existence of HClO₄ in the stratosphere and concluded that this new species could bring to closure the inorganic chlorine budget deficiency made apparent by their in-situ measurements of hydrochloric acid (HCl). Study also showed that elevated levels of chlorate and perchlorate were found in the Arctic snow, representing a sink for the stratospheric chlorine and being removed via precipitation (Furdui and Tomassini, 2010).

In 2015, we conducted an intensive field measurement at Greenland during the springtime, with the major aim of studying the inorganic gas-phase species (i.e. halogen, sulfuric acids, etc.) in the Arctic environment, and also to assess their contribution to nucleation mechanisms as well as ozone depletion. In this study, we present the first high-resolution ambient data set of gas-phase HClO₃ (chloric acid) and HClO₄ (perchlorate acid), and discuss on their potential formation pathway in the Arctic environment. We will further assess their potential roles and fates in the atmosphere.

METHODS

The field measurement was taken place at the Villum Research Station, Station Nord, located on the in high arctic North Greenland (81°36' N, 16°40' W). The sampling period was during the spring time from February to May of 2015. A state-of-the-art chemical ionization atmospheric pressure interface – time-of-flight mass spectrometer (CI-APi-TOF) was used in negative ion mode with nitrate ion (NO₃⁻) as the reagent ion to detect the gas-phase HClO₃ and HClO₄. Quantum chemical calculation showed that these species should be detected efficiently, by clustering with the NO₃⁻ and then deprotonated to ClO₃⁻ during the ionization process in the mass spectrometer. The study was also augmented by other measurements in the facility like the ozone and gaseous elemental mercury. We used high-level quantum-chemical methods (Saiz-Lopez et al., 2018; 2019) to calculate the Ultraviolet-Visible absorption spectra and cross-section of HClO₃ and HClO₄ in the gas-phase to assess their fates in the atmosphere.

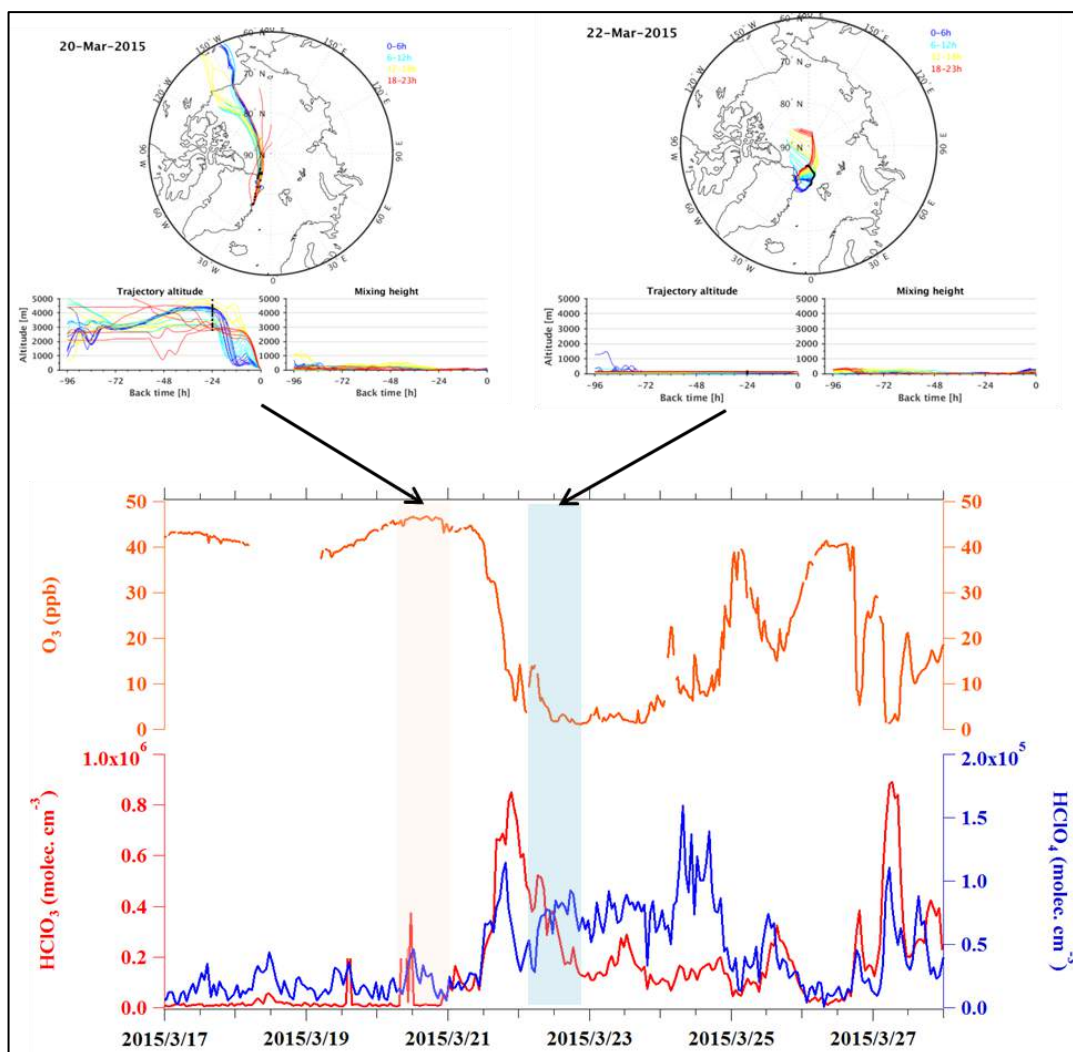


Figure 1. Observation of enhanced-level of HClO_3 and HClO_4 during the ozone depletion events in Greenland. Upper panel shows examples of air mass back-trajectories during non-depletion period on 20 March 2015 and during O_3 depletion event on 22 March 2015.

CONCLUSIONS

Our study presents the first ambient measurement of HClO_3 and HClO_4 in the atmosphere. Enhance level of HClO_3 and HClO_4 were measured during the springtime ozone depletion events in the Greenland (see Figure 1), with concentration up to 9×10^5 molecule cm^{-3} . Air mass trajectory analysis shows that the air during ozone depletion events was confined to near-surface, which is a common phenomenon of Arctic ozone depletion events (e.g. Moore et al., 2014). This result indicates that the O_3 and surface of sea-ice/snowpack may play important roles in the formation of HClO_3 and HClO_4 . In-depth analysis of the data is still on-going.

ACKNOWLEDGEMENTS

This work was supported by the European Research Council (GASPARCON) and Academy of Finland.

REFERENCES

- Furdui, V.I., and Tomassini, F. (2009). Trends and sources of perchlorate in Arctic snow. *Environmental Science & Technology*, **44**, 588-592.
- Jaeglé L., Yung, Y.L., Toon, G.C., Sen, B., Blavier, J.F. (1996). Balloon observations of organic and inorganic chlorine in the stratosphere: The role of HClO₄ production on sulfate aerosols. *Geophysical Research Letters*, **23**, 1749-1752.
- Moore, C.W., Obrist, D., Steffen, A., Staebler, R.M., Douglas, T.A., Richter, A., and Nghiem, S.V. (2014). Convective forcing of mercury and ozone in the Arctic boundary layer induced by leads in sea ice. *Nature*, **506**, 81.
- Neuman, J., Nowak, J., Huey, L.G., Burkholder, J., Dibb, J.E., Holloway, J., Liao, J., Peischl, J., Roberts, J., Ryerson, T.B., Scheuer, E., Stark, H., Stickel R. E. , Tanner, D. J., and Weinheimer, A. (2010). Bromine measurements in ozone depleted air over the Arctic Ocean. *Atmospheric Chemistry and Physics*, **10**, 6503-6514.
- Saiz-Lopez, A., Acuña, A.U., Trabelsi, T., Carmona-García, J., Dávalos, J.Z., Rivero, D., Cuevas, C.A., Kinnison, D.E., Sitkiewicz, S.P., Roca-Sanjuán, D., and Francisco, J.S. (2019). Gas-Phase Photolysis of Hg(I) Radical Species: A New Atmospheric Mercury Reduction Process. *Journal of the American Chemical Society*, **141**, 8698-8702.
- Saiz-Lopez, A., Sitkiewicz, S.P., Roca-Sanjuán, D., Oliva-Enrich, J.M., Dávalos, J.Z., Notario, R., Jiskra, M., Xu, Y., Wang, F., Thackray, C.P., Sunderland, E.M., Jacob, D.J., Travnikov, O., Cuevas, C.A., Acuña, A.U., Rivero, D., Plane, J.M.C., Kinnison, and D.E., Sonke, J.E.. (2018). Photoreduction of gaseous oxidized mercury changes global atmospheric mercury speciation, transport and deposition. *Nature Communications*, **9**, 4796.
- Simpson, W., Glasow, R.v., Riedel, K., Anderson, P., Ariya, P., Bottenheim, J., Burrows, J., Carpenter, L., Frieß U., and Goodsite, M.E. (2007). Halogens and their role in polar boundary-layer ozone depletion. *Atmospheric Chemistry and Physics*, **7**, 4375-4418.

EXTENDING THE RANGE OF APPLICABILITY OF THE SEMI-EMPIRICAL ECOSYSTEM MODEL PRELES FOR VARYING FOREST TYPES AND CLIMATE

X. TIAN^{1,2}, F. MINUNNO², T. CAO¹, M. PELTONIEMI³,

T. KALLIOKOSKI^{2,4} and A. MÄKELÄ²

¹College of Forestry, Northwest A&F University, Yangling, 712100, China

²Department of Forest Sciences, University of Helsinki, P.O. Box 27, Helsinki FI-00014, Finland

³Natural Resources Institute Finland, Latokartanonkaari 9, Helsinki FI-00790, Finland

⁴Department of Physics, University of Helsinki, P.O. Box 64, Helsinki FI-00014, Finland

Keywords: Light-use efficiency, plant functional type, gross primary production, inverse modelling.

INTRODUCTION

PRELES (PREdict Light-use efficiency, Evapotranspiration and Soil water) is a hybrid ecosystem model that predicts daily gross primary production (GPP), evapotranspiration (ET) and soil water (Peltoniemi et al., 2015a). The model requires soil characteristics, daily f_{APAR} and meteorological observations as inputs. The GPP predictions are based on a reformulation of the light-use efficiency (LUE) model of Mäkelä et al. (2008). The reformulated LUE-based model PRELES has been calibrated and validated in the boreal region mainly for coniferous forests (Minunno et al., 2016; Peltoniemi et al., 2012; Peltoniemi et al., 2015b). When national inventory and map data were available, PRELES predicted GPP estimates in Finland similar to those in the model JSBACH and MODIS GPP product, implying its high reliability in extrapolations and regional applications for current boreal forest (Peltoniemi et al., 2015b). Linked with downscaled global circulation model projections, PRELES sufficiently predicted boreal forest productivity under climate change scenarios with marginal proportions of parametric uncertainty (Kalliokoski, Mäkelä, Fronzek, Minunno, & Peltoniemi, 2018). Mäkelä et al. (2008) showed that daily temperature, vapour-pressure deficit (VPD) and absorbed PPFD (photosynthetic photon flux density) accounted for most of the daily variation in GPP in the model, but unexplained variation remained in the site-specific maximum LUE, which correlated linearly with canopy nitrogen (Peltoniemi et al. 2012). When the model was fitted to the data, differences between sites could be explained by potential LUE, leaf area and environmental conditions. If the resulting model is to be utilized, its ability to extrapolate to conditions outside the original modelling sites must be evaluated. Minunno et al. (2016) tested the applicability of PRELES for 10 boreal coniferous forests in Fennoscandia and obtained a generic vector of model parameters by multisite calibration. Based on a comparison between site-specific and multisite calibration, the generic parameter vector from multisite calibration can be reliably used at the regional scale for boreal coniferous forests. Incorporating the processes of light saturation, temperature acclimation, VPD stress, and soil water dynamics, PRELES is theoretically qualified for monitoring and predicting ecosystem productivity of various forest-climate types, but this wide range of applicability has not been tested in warmer climate types, broad-leaved forests or very fertile soils.

The objectives of the study were: 1) to test, with additional modules of seasonality and water dynamics incorporated, whether the LUE approach could sufficiently explain geographical variations of GPP and ET, with respect to contrasting environmental conditions and distinctive forest ecosystems; 2) to propose a generic parameter vector for each PFT and to hierarchically quantify the differences among sites while fitting the model with pooled data and 3) to quantify the uncertainty in extrapolating to conditions outside the original sites.

MATERIAL AND METHODS

we evaluated a semi-empirical ecosystem model, PRELES, for various forest types and climate conditions, based on eddy covariance data from 55 sites. A Bayesian approach was adopted for model calibration and uncertainty quantification. We applied the site-specific calibrations and multisite calibrations to nine plant functional types (PFTs) to respectively obtain the site-specific vectors and regional/global generic vectors of parameters in PRELES.

The meteorological and eddy covariance data were maintained and shared by the FLUXNET community. Daily meteorological and flux records of 399 site-years from 55 sites (Fig. 1) were selected and downloaded from the ‘FLUXNET2015 dataset’, in which half-hourly observations were gap-filled, aggregated and transformed to daily records by a standard methodology (Papale et al., 2006; Reichstein et al., 2005).

Statistical calibration of the PRELES model parameters was accomplished in a Bayesian framework by inferring the joint posterior probability density distribution of parameters conditioned on observations (van Oijen et al., 2005). We implemented two types of calibration: site-specific calibration and multisite calibration. The site-specific calibration included 17 parameters and was applied to each site independently. For each forest-climate cluster, we proposed a generic vector of parameters by multisite calibration within a Bayesian hierarchical modelling approach.

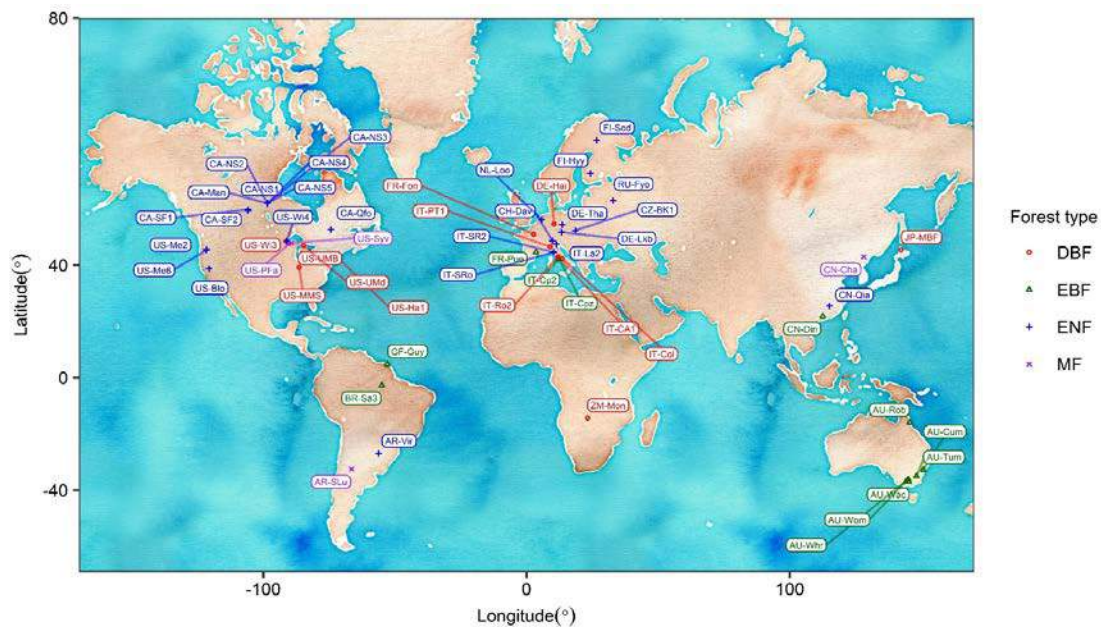


Figure 1. Study sites. DBF = deciduous broad-leaved forest, EBF = evergreen broad-leaved forest, ENF = evergreen needle-leaved forest, MF = mixed forest.

CONCLUSIONS

The multisite calibrations performed as accurately as the site-specific calibrations in predicting gross primary production (GPP) and evapotranspiration (ET). The combination of plant physiological traits and climate patterns generated significant parameter variation across but not within PFTs. Moreover, the variations among sites within one PFT could be effectively simulated by simply adjusting the parameter of potential light-use efficiency (LUE), implying significant convergence of simulated vegetation processes within PFT. The multisite calibrations showed higher reliability than the site-specific calibration in extrapolating to environmental conditions outside the original modelling sites. The hierarchical modelling of PRELES provides a compromise between satellite-driven LUE and physiologically oriented approaches, in both satellite-based monitoring and process-based extrapolating the geographical variation of ecosystem productivity. Although measurement errors of eddy covariance and remotely sensed data propagated a substantial proportion of uncertainty or potential biases, the results illustrated that PRELES could reliably simulate GPP and ET for contrasting forest types on large geographical scales.

PRELES aims at a compromise between predictive accuracy and model complexity. The generalization of ecosystem processes on the one hand makes the model convincing in extrapolating to changing environments, and on the other hand makes it convenient to parameterize and apply on large geographical scales. The model accurately simulated and explained the seasonal and daily GPP variations for most forest-climate types. Thus, PRELES can be a good candidate for mapping forest production and quantifying uncertainty on regional to global scales under the background of climate change. The potential risk in global applications is that we only calibrated parameters, while the optimal model structure should vary as plant traits and environments change. For instance, the modifier of temperature acclimation was crucial for boreal and temperate PFTs, but was impractical for tropical forests. A key developmental need of PRELES for global application is to sufficiently generalize and quantify the eco-physiological distinctions of varying biomes. A more reliable global calibration of PRELES should focus on not only adjusting parameters, but also optimizing the PFT-specific model structures.

ACKNOWLEDGEMENTS

This work was supported by the Academy of Finland project CARB-ARC (No. 286190), the National Natural Science Foundation of China (NSFC 31640646), the Strategic Research Council at the Academy of Finland (IBC-CARBON, decision. #312635), and the Horizon 2020 Research and innovation framework program (Forest Carbon Flux and Storage Mapping Service, proposal #821860).

This work used eddy covariance data acquired and shared by the FLUXNET community, including these networks: AmeriFlux, AfriFlux, AsiaFlux, CarboAfrica, CarboEuropeIP, CarboItaly, CarboMont, ChinaFlux, Fluxnet-Canada, GreenGrass, ICOS, KoFlux, LBA, NECC, OzFlux-TERN, TCOS-Siberia and USCCC. The ERA-Interim reanalysis data were provided by the ECMWF and processed by the LSCE. The FLUXNET eddy covariance data processing and harmonization were carried out by the European Fluxes Database Cluster, AmeriFlux Management Project and Fluxdata project of FLUXNET, with the support of the CDIAC and ICOS Ecosystem Thematic Centre, and the OzFlux, ChinaFlux and AsiaFlux offices.

REFERENCES

- Kalliokoski, T., Mäkelä, A., Fronzek, S., Minunno, F., & Peltoniemi, M. (2018). Decomposing sources of uncertainty in climate change projections of boreal forest primary production. *Agricultural and Forest Meteorology*, 262, 192-205.
- Mäkelä, A., Pulkkinen, M., Kolari, P., Lagergren, F., Berbigier, P., Lindroth, A., ... Hari, P. (2008). Developing an empirical model of stand GPP with the LUE approach: analysis of eddy covariance data at five contrasting conifer sites in Europe. *Global Change Biology*, 14, 92-108.
- Minunno, F., Peltoniemi, M., Launiainen, S., Aurela, M., Lindroth, A., Lohila, A., ... Mäkelä, A. (2016). Calibration and validation of a semi-empirical flux ecosystem model for coniferous forests in the Boreal region. *Ecological Modelling*, 341, 37-52.

- Papale, D., Reichstein, M., Aubinet, M., Canfora, E., Bernhofer, C., Kutsch, W. L., ... Yakir, D. (2006). Towards a standardized processing of net ecosystem exchange measured with eddy covariance technique: Algorithms and uncertainty estimation. *Biogeosciences*, 3, 571-583.
- Peltoniemi, M., Pulkkinen, M., Aurela, M., Pumpanen, J., Kolari, P., & Mäkelä, A. (2015a). A semi-empirical model of boreal-forest gross primary production, evapotranspiration, and soil water — calibration and sensitivity analysis. *Boreal Environment Research*, 20, 151-171.
- Peltoniemi, M., Markkanen, T., Härkönen, S., Muukkonen, P., Thum, T., Aalto, T., & Mäkelä, A. (2015b). Consistent estimates of gross primary production of Finnish forests — comparison of estimates of two process models. *Boreal Environment Research*, 20, 196-212.
- Peltoniemi, M., Pulkkinen, M., Kolari, P., Duursma, R. A., Montagnani, L., Wharton, S., ... Mäkelä, A. (2012). Does canopy mean nitrogen concentration explain variation in canopy light use efficiency across 14 contrasting forest sites? *Tree Physiology*, 32, 200-218.
- Reichstein, M., Falge, E., Baldocchi, D., Papale, D., Aubinet, M., Berbigier, P., ... Valentini, R. (2005). On the separation of net ecosystem exchange into assimilation and ecosystem respiration: Review and improved algorithm. *Global Change Biology*, 11, 1424-1439.
- van Oijen, M., Rougier, J., & Smith, R. (2005). Bayesian calibration of process-based forest models: Bridging the gap between models and data. *Tree Physiology*, 25, 915-927.

MOLECULAR DYNAMICS SIMULATIONS OF HOMOGENEOUS CO₂ NUCLEATION

V. TIKKANEN, R. HALONEN, B. REISCHL, H. VEHKAMÄKI

Institute for Atmospheric and Earth System Research/Physics,
Faculty of Science, University of Helsinki, P.O. Box 64, FI-00014 Finland.

Keywords: Homogeneous nucleation, non-isothermal nucleation, molecular dynamics simulations.

INTRODUCTION

Nucleation is the limiting step in any first-order phase transitions such as droplet condensation, bubble cavitation, crystallisation or cloud formation. During such a transition, a finite amount of latent heat is either released or absorbed due to the emergence of a new phase. The standard theoretical approach to calculate homogeneous nucleation rates is classical nucleation theory (CNT). Despite of all the extensions and adjustments to CNT, the predicted rates differ from the experimental measurements by several orders of magnitude. In addition, the presence of a surface of a different material can lower the free energy for the formation of a new phase considerably. Since impurities are ubiquitous in nature, the pathway of heterogeneous nucleation is often favored in nature.

Here we study the homogenous nucleation of carbon dioxide (CO₂) from the vapour phase by utilizing molecular dynamics (MD) simulations. The MD approach is free from assumptions that are made in nucleation theories concerning the treatment of equilibrium and idealistic bulk liquid nature of the clusters. The condensation of CO₂ is a topic of general interest in view of global decarbonization targets, e.g. in low-temperature CO₂ capture technologies promoting the phase transition of CO₂ gas is the crucial step. Another motivation for the study is the Martian atmosphere, where the clouds are formed mostly of CO₂.

COMPUTATIONAL METHODS

We utilized the LAMMPS simulation software (Plimpton, 1995) to carry out atomistic molecular dynamics (MD) simulations. The Yasuoka-Matsumoto method (Yasuoka and Matsumoto, 1998) was used to calculate nucleation rates by studying the growth of many clusters in a large simulation system (see Figure 1). In MD simulations, temperature is most often controlled with artificial thermostats such as velocity scaling or the Nosé-Hoover method. However, these thermostats are unable to remove the latent heat released to the clusters in a physical manner (Halonen *et al.*, 2018). To properly thermalise the system, we are using an atmosphere of carrier gas as a heat bath for the CO₂ molecules. This approach increases the computational effort substantially, but it also brings the simulated system closer to the experimental set-up where the thermalisation of the clusters can be incomplete.

In order to simulate the required time scales of several nanoseconds, we utilise the rigid TraPPE force field for CO₂ (Potoff and Siepmann, 2001) and a time step of 5 fs to integrate the equations of motion with a Velocity verlet scheme. The carrier gas is modelled as argon interacting via a Lennard-Jones potential with parameters $\epsilon/k_B = 119.8$ K and $\sigma = 3.405$ Å. Interactions between the atoms in the CO₂ molecule and the carrier gas are obtained from Lorentz-Berthelot mixing rules. A Nosé-Hoover chain thermostat of length 3 and a time constant of 0.1 ps was used to keep the temperature of the carrier gas at 75 K. We have considered CO₂ densities between 5×10^{-6} Å⁻³ and 5×10^{-5} Å⁻³, corresponding to pressures between 5.2 kPa and 52 kPa.

CONCLUSIONS

In addition to the nucleation rates calculated directly from the number of clusters exceeding the threshold critical size, the atomistic simulations also enable us to study the structure of the clusters during nucleation, which cannot be determined in nucleation experiments. Our simulations indicate that even the largest clusters observed during the nucleation ($N \approx 90$) have an amorphous structure, even though the bath temperature of $T = 75$ K is substantially lower than the sublimation point of CO_2 ($T_s = 194.64$ K at 1 bar). Indeed, we observe that cluster temperatures are significantly higher than the bath temperature, as latent heat released during nucleation events cannot be removed at the same rate through collisions with the carrier gas, as described in non-isothermal nucleation theory (Feder *et al.*, 1966). A snapshot of a cluster of size $N = 95$ and a plot showing C-C radial distribution functions in different clusters, as well as bulk crystalline and liquid CO_2 is shown in Figure 2.

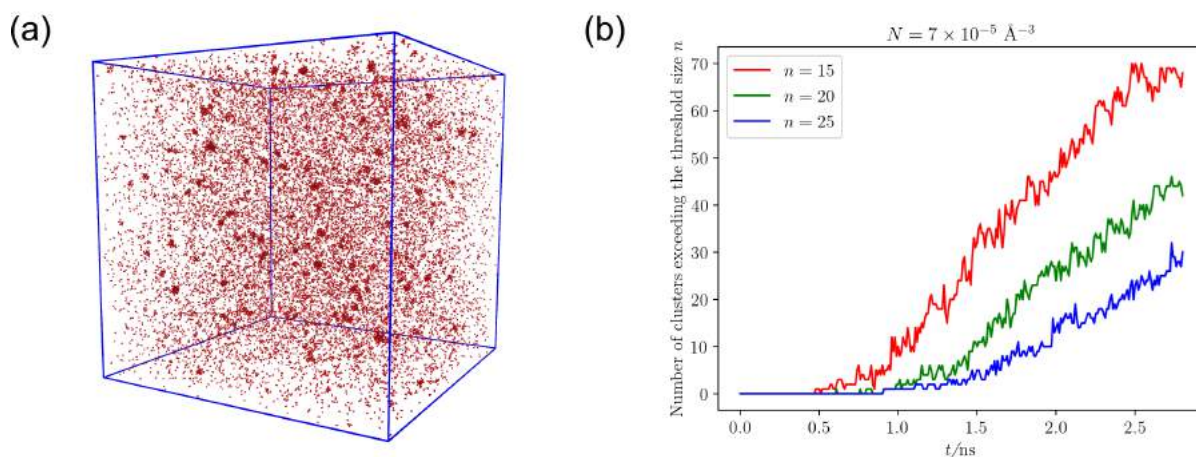


Figure 1: (a) Snapshot of a CO_2 nucleation simulation with 20 000 CO_2 molecules. The Argon carrier gas atoms are not shown for clarity. (b) Example curves of the number of clusters in the simulation box exceeding a certain threshold size n , as a function of time.

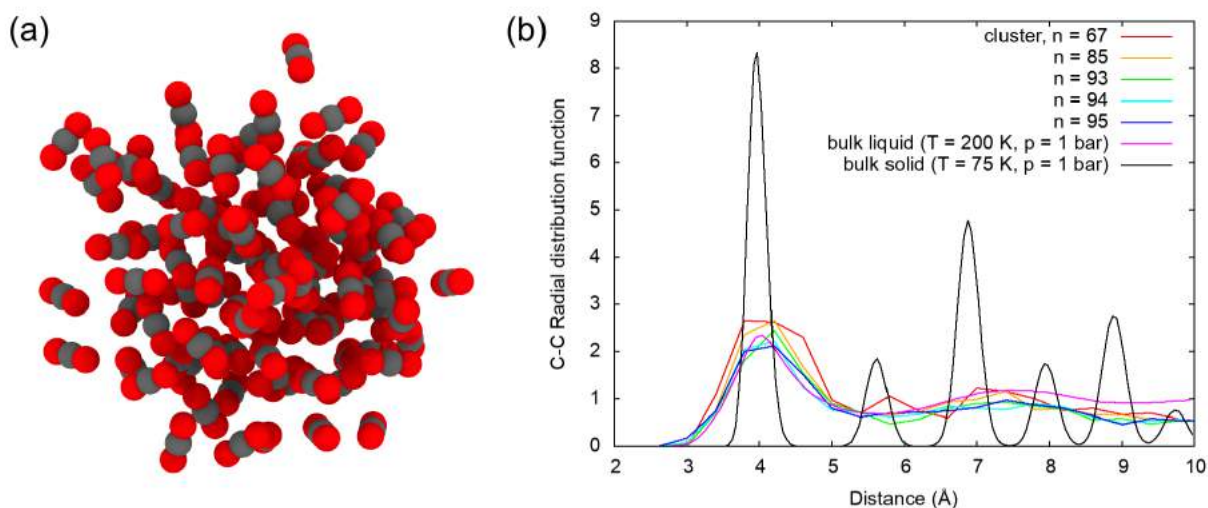


Figure 2: (a) An example of an over-critical cluster consisting of 95 CO_2 molecules. Carbon and oxygen atoms are colored in dark gray and red, respectively. (b) Carbon-carbon radial distribution functions in over-critical clusters and in crystalline CO_2 at 75 K and 1 bar as well as undercooled liquid CO_2 at 200 K and 1 bar, for comparison.

ACKNOWLEDGEMENTS

This work was supported by the European Research Council (Grant No. 692891-DAMOCLES) and University of Helsinki, Faculty of Science ATMATH project.

REFERENCES

- Feder, J., K. Russell, J. Lothe and G. Pound (1966). Homogeneous nucleation and growth of droplets in vapours. *Adv. Phys.* **15**(57):111-178.
- Halonen, R., E. Zapadinsky and H. Vehkamäki (2018). Deviation from equilibrium conditions in molecular dynamic simulations of homogeneous nucleation. *J. Chem. Phys.* **148**, 164508.
- Plimpton, S. (1995). Fast parallel algorithms for short-range molecular dynamics. *J. Comput. Phys.* **117**(1):1-19.
- Potoff, J.J. and J.I. Siepmann (2001). Vapor-liquid equilibria of mixtures containing alkanes, carbon dioxide and nitrogen. *AIChE J.* **47**, 1676-1682.
- Yasuoka, K. and M. Matsumoto (1998). Molecular dynamics of homogeneous nucleation in the vapor phase. I. Lennard-Jones fluid. *J. Chem. Phys.* **109**, 8451-8462.

ARE SOA VOLATILITY DISTRIBUTIONS ESTIMATED FROM ISOTHERMAL EVAPORATION AND FIGAERO-CIMS THERMOGRAM DATA SIMILAR?

O.-P. TIKKANEN, A. BUCHHOLZ, A. YLISIRNIÖ, S. SCHOBESBERGER, A. VIRTANEN and T. YLI-JUUTI

Department of Applied Physics, University of Eastern Finland, Kuopio, Finland

Keywords: α -PINENE, SOA, VOLATILITY

INTRODUCTION

Secondary organic aerosol (SOA) is formed from the oxidation of volatile organic compounds (VOC) and the subsequent gas-particle partitioning (Hallquist et al., 2009). A substantial fraction of the submicrometer particulate mass is from SOA (Jimenez et al., 2009). Due to the multitude of different VOCs and possible reaction pathways there exists thousands of different organic compounds in the SOA (Goldstein and Galbally, 2007). Because of the vast amount of different species, it is difficult to estimate the properties of SOA in the atmosphere and ultimately their impact on climate.

A key quantity in understanding the SOA dynamics in the atmosphere is the volatility of the organic compounds (Glasius and Goldstein, 2016). The volatility of the compounds in the SOA can be described with a volatility distribution (VD) where organic compounds are grouped based on their saturation concentration. The different volatility groups are model compounds in the sense that they do not present any particular compound but rather are surrogates with set properties.

Isothermal evaporation experiments, where the evaporation of SOA particles is monitored over several hours, are useful for directly estimating the VD of SOA (Tikkanen et al., 2019; Yli-Juuti et al., 2017). These kind of measurements are important because the ambient conditions such as relative humidity (RH) and temperature can be controlled during the evaporation. Recently, Buchholz et al., (2019) showed that the VD can also be estimated from measurements performed with Filter Inlet for Gases and AEROSOLS (FIGAERO, (Lopez-Hilfiker et al., 2014) coupled to the Chemical Ionization Mass Spectrometer (CIMS, (Lee et al., 2014). In this work these two VD are compared.

METHODS

SOA was generated by photo-oxidation and ozonolysis of α -pinene in a Potential Aerosol Mass (PAM; Lambe et al., 2011) reactor at constant temperature and RH ($T=295\text{K}$, $\text{RH}=40\%$). SOA particles with electrical mobility diameter of 80 nm were selected with a differential mobility analyzer and the gas phase was diluted which initiated the evaporation of the particles. The monodisperse particles were then directed to a 100 L stainless steel residence time chamber (RTC) where the evaporation was monitored by continuous measurements of the changing (shrinking) particle sizes with a scanning mobility particle sizer (SMPS). The collection of particles onto a FIGAERO filter was performed at two times, directly after the size selection and 3-4 hours after the evaporation was initiated. These two samples are labeled fresh and RTC sample, respectively.

The photo-oxidation conditions resulted in an average oxygen-to-carbon O:C ratio of 0.69 (measured with a High-Resolution Time-of-Flight Aerosol Mass Spectrometer). The temperature in the chamber was 293 K and the relative humidity (RH) was between 82-83%.

A process model optimization method described in Tikkanen et al., (2019) was used to estimate the VD from the particle size change data. The goal in the process model optimization is to find a VD that produces particle shrinkage similar to the measurements, when the VD is used as an input to a process model that describes the evaporation process. A process model (Liquid-like evaporation model, LLEVAP) that assumes the particles are in a liquid-like state was used to model the evaporation at the studied conditions (Tikkanen et al., 2019; Yli-Juuti et al., 2017). The VD was represented with six model compounds with effective saturation mass concentration C^* between $10^{-3} \mu\text{gm}^{-3}$ and $10^2 \mu\text{gm}^{-3}$. A global optimization algorithm was used to search for a set of dry particle

mole fractions of these model compounds at the start of the evaporation. In the optimization, the mean squared error between the measured and simulated evaporation curves was used as a goodness of fit statistic. The resulting VD is referred to as VD_{evap} . The molar mass of each model compound was assumed to be 200 gmol^{-1} and the particle phase density 1200 kgm^{-3} .

The PMF method (Paatero and Tapper, 1994) was applied to estimate the VD from the FIGAERO-CIMS thermogram data. The application of the method is described in detail in Buchholz et al., (2019). In short, PMF groups the mass spectrometer data into predefined number of factors. When applying the method to FIGAERO-CIMS thermogram data, the measurement matrix is explained by the multiplication of two matrices where the first contains the mass loading profile of each factor and the second contains the mass spectra of the factors. In this work, each factor was interpreted to be a model compound in a VD. Each model compound was characterized by the relative amount in the sample calculated from the relative signal strength of the mass loading profile and the C^* calculated from the peak desorption temperature (T_{max}) of each factor using a calibration with compounds with known C^* values. The resulting VD is referred to as VD_{PMF} . For modeling purposes, the other properties of the model compounds were set to be the same as in the process model optimization method.

RESULTS

A direct comparison of the VD is challenging due to the fact that the C^* values of the two studied VD are not the same. However, both of the VD can be used as an input to the LLEVAP model and their evaporation profiles can be compared. Figure 1a shows the measured evaporation at the studied conditions (blue circles) and the best fit simulation from the process model optimization method (calculated with VD_{evap} , black line). The blue and brown lines in Fig. 1a show the simulated evaporation calculated with the LLEVAP model using the VD_{PMF} derived from the fresh and RTC samples as an input.

The simulated evaporation calculated with VD_{evap} fits well to the measured value as is expected since this is the goal of the process model optimization method. The simulated evaporation calculated with VD_{PMF} is slightly faster than the measured evaporation suggesting that the two VD are not similar.

In Fig. 1b the C^* values of each model compound / PMF factor in VD_{PMF} is allowed to contain uncertainty which is constrained by the width of each factor mass loading profile. The C^* values are calculated from the 25th and 75th percentiles of the desorption temperature range of each factor in the mass loading profile. Within that range, the C^* value for each factor was then optimized by minimizing the mean squared error between the measured and simulated evaporation curves similarly to the process model optimization method. The optimized VD is referred to as the $VD_{\text{PMF,opt}}$. The simulated evaporation calculated using $VD_{\text{PMF,opt}}$ matches well the measured values showing that the VD estimated with the two methods are similar when the uncertainty in the C^* values in the FIGAERO-CIMS derived VD are taken into account.

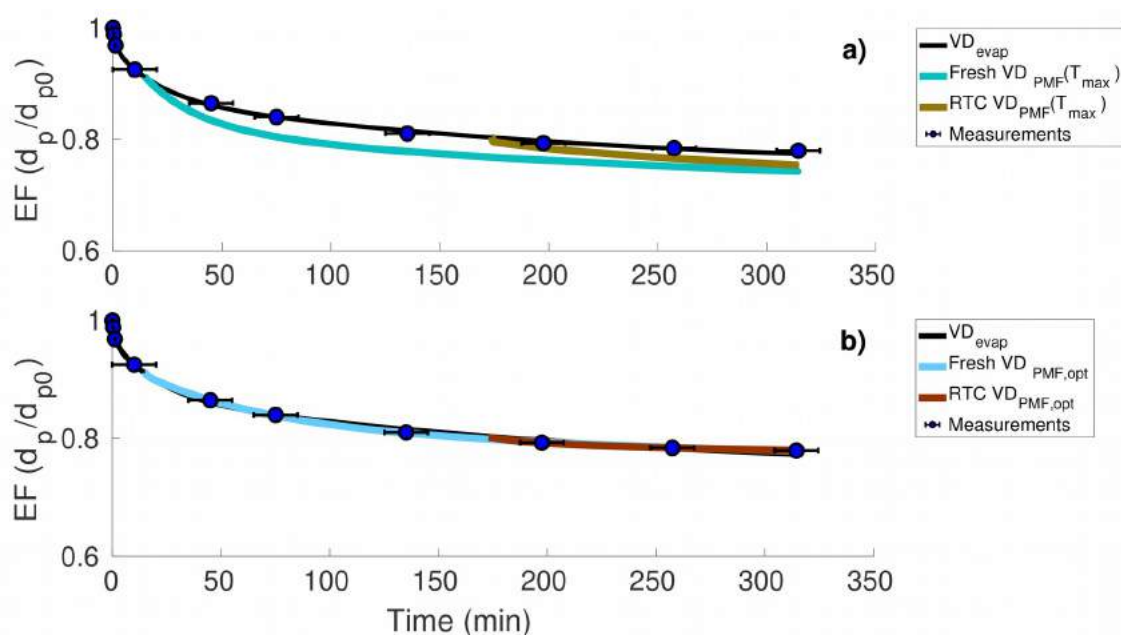


Figure 1: Measured and modelled evaporation. Horizontal axis shows the time in minutes from the start of the evaporation and the vertical axis shows the evaporation factor (EF) defined as the particle diameter at a certain time divided by the initial particle diameter. Blue markers show the measured evaporation and the black lines shows the modelled evaporation using the process model optimization method. a) blue and brown lines show the modelled evaporation calculated using a VD where the C^* of a factor is calculated from T_{\max} b) blue and brown lines show the modelled evaporation calculated using a VD that allowed uncertainty in the C^* value of each factor (see results for details).

CONCLUSIONS

This work compared the VD estimated with two different measurement methods during isothermal SOA particle evaporation. The VD were estimated from isothermal particle size change data and from FIGAERO-CIMS measurements. The two VD were found to be similar if the C^* values of the PMF factors calculated from the FIGAERO-CIMS data were allowed to contain uncertainty.

The results indicate that the VD derived from the FIGAERO-CIMS measurements is consistent with the measured evaporation and that the $VD_{PMF,opt}$ is a good approximation for the volatility of organic compounds in the SOA. Furthermore the results obtained in this study open the possibility to quantify other properties by combining the FIGAERO-CIMS data with the particle size change data and the process model optimization method since the FIGAERO-CIMS data constrain the VD estimation more than using only the VD_{evap} . Including the FIGAERO-CIMS thermogram data to VD estimation effectively decreases the search space that needs to be traversed with the global optimization algorithms.

ACKNOWLEDGMENTS

This work was supported by the Academy of Finland Center of Excellence programme (grant no. 307331), the Academy of Finland (project no. 299544, 310682) and the European Research Council Starting grant 335478.

REFERENCES

Buchholz, A., Ylisirniö, A., Huang, W., Mohr C., Canagaratna M., Worsnop, D.R., Schobesberger, S., Virtanen, A.: Deconvolution of FIGAERO-CIMS thermal desorption profiles using Positive Matrix Factorisation to

- Identify chemical and physical processes during particle evaporation., 2019b, Submitted to Atmospheric Chemistry and Physics.
- Glasius, M. and Goldstein, A. H.: Recent Discoveries and Future Challenges in Atmospheric Organic Chemistry, *Environ. Sci. Technol.*, 50(6), 2754–2764, doi:10.1021/acs.est.5b05105, 2016.
- Goldstein, A. H. and Galbally, I. E.: Known and Unexplored Organic Constituents in the Earth's Atmosphere, *Environ. Sci. Technol.*, 41(5), 1514–1521, doi:10.1021/es072476p, 2007.
- Hallquist, M., Wenger, J. C., Baltensperger, U., Rudich, Y., Simpson, D., Claeys, M., Dommen, J., Donahue, N. M., George, C., Goldstein, A. H., Hamilton, J. F., Herrmann, H., Hoffmann, T., Iinuma, Y., Jang, M., Jenkin, M. E., Jimenez, J. L., Kiendler-Scharr, A., Maenhaut, W., McFiggans, G., Mentel, Th. F., Monod, A., Prévôt, A. S. H., Seinfeld, J. H., Surratt, J. D., Szmigielski, R. and Wildt, J.: The formation, properties and impact of secondary organic aerosol: current and emerging issues, *Atmos Chem Phys*, 9(14), 5155–5236, doi:10.5194/acp-9-5155-2009, 2009.
- Jimenez, J. L., Canagaratna, M. R., Donahue, N. M., Prevot, A. S. H., Zhang, Q., Kroll, J. H., DeCarlo, P. F., Allan, J. D., Coe, H., Ng, N. L., Aiken, A. C., Docherty, K. S., Ulbrich, I. M., Grieshop, A. P., Robinson, A. L., Duplissy, J., Smith, J. D., Wilson, K. R., Lanz, V. A., Hueglin, C., Sun, Y. L., Tian, J., Laaksonen, A., Raatikainen, T., Rautiainen, J., Vaattovaara, P., Ehn, M., Kulmala, M., Tomlinson, J. M., Collins, D. R., Cubison, M. J., Dunlea, E. J., Huffman, J. A., Onasch, T. B., Alfarra, M. R., Williams, P. I., Bower, K., Kondo, Y., Schneider, J., Drewnick, F., Borrmann, S., Weimer, S., Demerjian, K., Salcedo, D., Cottrell, L., Griffin, R., Takami, A., Miyoshi, T., Hatakeyama, S., Shimono, A., Sun, J. Y., Zhang, Y. M., Dzepina, K., Kimmel, J. R., Sueper, D., Jayne, J. T., Herndon, S. C., Trimborn, A. M., Williams, L. R., Wood, E. C., Middlebrook, A. M., Kolb, C. E., Baltensperger, U., Worsnop, D. R. and Worsnop, D. R.: Evolution of organic aerosols in the atmosphere., *Science*, 326(5959), 1525–9, doi:10.1126/science.1180353, 2009.
- Lambe, A. T., Ahern, A. T., Williams, L. R., Slowik, J. G., Wong, J. P. S., Abbatt, J. P. D., Brune, W. H., Ng, N. L., Wright, J. P., Croasdale, D. R., Worsnop, D. R., Davidovits, P. and Onasch, T. B.: Characterization of aerosol photooxidation flow reactors: heterogeneous oxidation, secondary organic aerosol formation and cloud condensation nuclei activity measurements, *Atmospheric Meas. Tech.*, 4(3), 445–461, doi:10.5194/amt-4-445-2011, 2011.
- Lee, B. H., Lopez-Hilfiker, F. D., Mohr, C., Kurtén, T., Worsnop, D. R. and Thornton, J. A.: An Iodide-Adduct High-Resolution Time-of-Flight Chemical-Ionization Mass Spectrometer: Application to Atmospheric Inorganic and Organic Compounds, *Environ. Sci. Technol.*, 48(11), 6309–6317, doi:10.1021/es500362a, 2014.
- Lopez-Hilfiker, F. D., Mohr, C., Ehn, M., Rubach, F., Kleist, E., Wildt, J., Mentel, Th. F., Lutz, A., Hallquist, M., Worsnop, D. and Thornton, J. A.: A novel method for online analysis of gas and particle composition: description and evaluation of a Filter Inlet for Gases and AEROSols (FIGAERO), *Atmospheric Meas. Tech.*, 7(4), 983–1001, doi:10.5194/amt-7-983-2014, 2014.
- Paatero, P. and Tapper, U.: Positive matrix factorization: A non-negative factor model with optimal utilization of error estimates of data values, *Environmetrics*, 5(2), 111–126, doi:10.1002/env.3170050203, 1994.
- Tikkanen, O.-P., Hämäläinen, V., Rovelli, G., Lipponen, A., Shiraiwa, M., Reid, J. P., Lehtinen, K. E. J. and Yli-Juuti, T.: Optimization of process models for determining volatility distribution and viscosity of organic aerosols from isothermal particle evaporation data, *Atmospheric Chem. Phys.*, 19(14), 9333–9350, doi:https://doi.org/10.5194/acp-19-9333-2019, 2019.
- Yli-Juuti, T., Pajunoja, A., Tikkanen, O.-P., Buchholz, A., Faiola, C., Väisänen, O., Hao, L., Kari, E., Peräkylä, O., Garmash, O., Shiraiwa, M., Ehn, M., Lehtinen, K. and Virtanen, A.: Factors controlling the evaporation of secondary organic aerosol from α -pinene ozonolysis, *Geophys. Res. Lett.*, 44(5), 2016GL072364, doi:10.1002/2016GL072364, 2017.

MODELLING PRECIPITATION ENHANCEMENT VIA HYGROSCOPIC SEEDING IN WARM AND MIXED-PHASE CLOUDS USING UCLALES-SALSA

J. TONTTILA¹, H. KOKKOLA¹, A. AFZALIFAR¹, H. KORHONEN², S. ROMAkkANIEMI¹

¹Atmospheric Research Centre of Eastern Finland, Finnish Meteorological Institute, Kuopio, Finland

²Finnish Meteorological Institute, Helsinki, Finland.

Keywords: large-eddy simulation, weather modification, cloud seeding

INTRODUCTION

Weather modification, particularly rain enhancement via cloud seeding by aerosol, is an increasingly active field of research due to the need to improve water security in many regions across the globe. Water shortage is a major challenge in arid regions and the problem in general is expected to get worse, given the present consumption rate and the effects of climate warming. Artificial increase of rainfall by purposely emitting aerosol particles within clouds has been tested in many field experiments (e.g. Ghatte et al., 2007, Jung et al., 2015; Flossmann et al., 2019), but the scientific basis for understanding the factors controlling the seeding efficacy is still rather weak. In experimental studies, this arises from the problem of attribution: it is most often difficult to distinguish the effects of seeding from meteorological variations. Nevertheless, if the seeding proves successful, it is in all likelihood mainly the result of the seeding aerosol boosting the collision growth processes (Rosenfeld et al., 2010). To achieve this, the seeding particles are required to be sufficiently large, on the order of several micrometers.

Modelling with sophisticated microphysical schemes within cloud resolving frameworks has become a viable option to study the cloud seeding effects (e.g. Segal et al., 2004;2007). They provide a method to create multiple realizations of the same meteorological setting and they enable reproducibility of the results. In our work, we use the Sectional Aerosol module for Large-Scale Applications (SALSA) aerosol-cloud model coupled with the UCLA Large-Eddy Simulation code (UCLALES), a.k.a. UCLALES-SALSA (Tonttila et al., 2017) to study the cloud seeding efficacy. Our investigation focuses on the use of hygroscopic seeding particles, which are applied in marine stratocumulus clouds as well as in convective mixed-phase clouds of intermediate intensity.

METHODS

The core of UCLALES-SALSA is the widely used UCLALES code (Stevens et al., 2005) for idealized cloud studies. It holds the typical set of prognostic equations for temperature, moisture variables and wind components. The aerosol and cloud microphysics are represented by SALSA, which describes the evolution of particle size distributions using the bin approach. The size distributions and particle compositions are resolved for up to 4 particle categories: aerosol, two sets of liquid hydrometeors (cloud droplets and a separate regime for small drizzle and precipitation) and ice. Condensation and collision/collection processes are solved in all bins of all categories. Cloud activation is determined directly by modelling the aerosol growth and drizzle formation takes place within the coagulation routines of the model. For ice, we employ the basic methodology from the P3 scheme (Morrison and Milbrandt, 2015), where the growth of ice particles through vapor deposition and riming is tracked by separate mass variables. This enables to simulate the ice particle properties and shape in a physically flexible and computationally efficient way.

UCLALES-SALSA is very well suited to study the effects of cloud seeding, because its design emphasizes the tracking of the features of the aerosol size distribution in both the activated and non-activated particle regimes. This enables a detailed representation of the cloud processing of the aerosol through scavenging effects and the eventual removal mechanisms, which are essential in order to capture the seeding effect.

The model represents the seeding emissions either by emission from a moving point source, or by simply injecting the seeding aerosol to all the grid points instantaneously at a predefined model layer. In our experiments, we use sea salt aerosol as a proxy for the seeding particle composition. The particles are assumed to occupy the diameter space between approximately 1 and 10 μm with different number concentrations depending on the experiment.

In the first part of the current work, we have used our model to investigate the effects of hygroscopic seeding on warm marine stratocumulus clouds. The setup for the model simulations is based on the results from a field experiment reported in Jung et al. (2015). This includes the initial temperature and moisture profiles as well as the ambient aerosol size distribution.

In the second part, we focus on cumulus convection over the United Arab Emirates (UAE), where the clouds exhibit a mixed-phase structure, with occasionally and locally occurring strong rain showers. In this case, the model is initialized using observed aerosol size distributions from the FMI's instruments deployed at the UAE during 2018. This comprises both surface-based in-situ measurements as well as ground-based remote sensing observations. The initial temperature and moisture profiles are created based on the output from the operational mesoscale forecast model HARMONIE for a case that represents a tropospheric structure that is often seen in the UAE area in summer conditions.

CONCLUSIONS

Marine stratocumulus

The model results of the seeding experiments in marine stratocumulus highlight the importance of the total mass of the seeding aerosol released in the cloud layer, both via varying the emission rate as well as the seeding strategy. This essentially means, that the seeding aerosol concentration in the diluted plume should be, according to our results, at least on the order of 0.01 cm^{-3} in order to yield a considerable increase in the precipitation fluxes. Different seeding strategies to obtain this are tested: a moving point emission source with a prescribed trajectory across the model domain (corresponding to an aircraft, denoted Seed1 and Seed2), and directly injecting the seeding aerosol in every grid point in a domain-wide slab at a predefined altitude (Seed3). The latter produces the highest diluted concentration of the seeding aerosol in our experiments, which translates to the highest increase in the domain mean precipitation flux, as compared to the control run (no seeding), as shown in Figure 1.

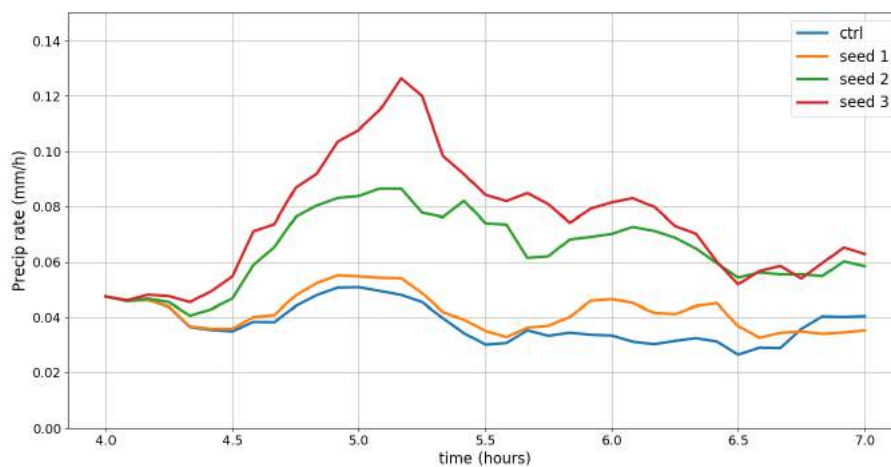


Figure 1: Domain mean precipitation rate as a function of time since the start of the seeding emission (at 4 hours). Seed1 and Seed2 are experiments with a point emissions source, Seed3 uses a domain-wide slab emission. CTRL is the control run with no seeding.

Convective mixed-phase clouds

In the experiments on cumulus convection performed so far we have only employed the domain-wide slab seeding emissions. The model generates an ensemble of clouds with tops reaching a maximum height of about 6-8 km. The lifetime of the convective cells and therefore also the lifetime of an individual precipitation event is rather short, 10-30 minutes. In this case, the most intensive precipitation is formed via the cold precipitation process, where riming is a pivotal factor in the mixed-phase part of the clouds.

Our model experiments suggest, that the effect of hygroscopic seeding via the warm precipitation process is very weak in comparison with the overall precipitation rates produced by the strongest cells. Moreover, this weak precipitation is most often evaporated before it reaches the ground, due to the rather high cloud base heights (3-3.5 km).

Instead, considering the mixed-phase, the cold precipitation process is closely linked with the riming process. Our simulations show, that in suitable conditions, hygroscopic seeding above the melting layer may significantly increase the rime fraction of the total ice mass, as shown for an example case in Figure 2. When this happens, it has the potential to produce at least a transitory increase in the surface precipitation. Work is ongoing to identify the conditions which best support a significant increase in rime fraction in response to the seeding emission, as well as to provide a more robust estimate of the expected increase in the precipitation yield.

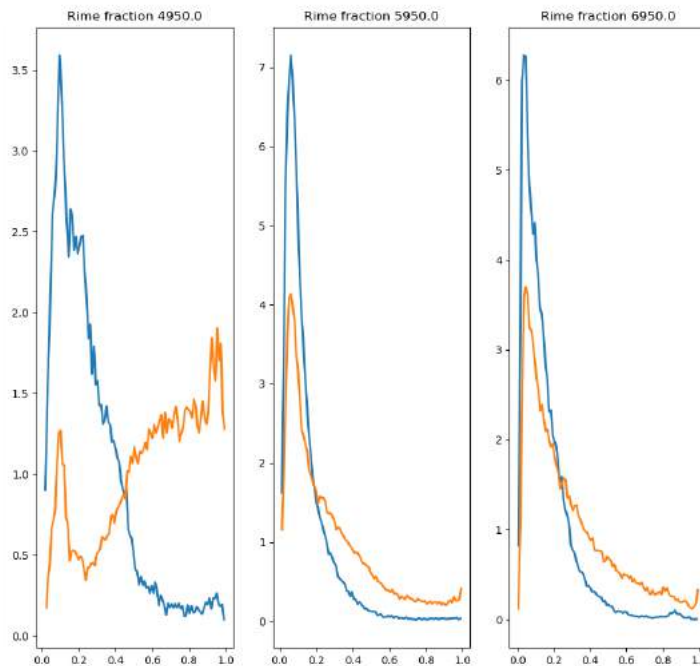


Figure 2: Histograms of rime fraction for then control run (blue) and the seeding experiment (orange) in the mixed phase cumulus case at three altitudes (4950m, 5950m and 6950m). Seeding aerosol is released close to the lowest sampling altitude.

ACKNOWLEDGEMENTS

This material is based on work supported by the National Center of Meteorology, Abu Dhabi, UAE under the UAE Research Program for Rain Enhancement Science. The work is also supported by the Academy of Finland (project numbers 283031, 309127, 285068 and the Centre of Excellence in Atmospheric Science, 272041).

REFERENCES

- Flossmann, A. I., Manton, M., Abshaev, A., Bruintjes, R., Murakami, M., Prabhakaran, T., Yao, Z.: Review of advances in precipitation enhancement research. *BAMS*, DOI: 10.1175/BAMS-D-18-0160.1, 2019.
- Ghate, V. P., Albrecht, B. A., Kollias, P., Jonsson, H. H., Breed, D. W.: Cloud seeding as a technique for studying aerosol-cloud interactions in marine stratocumulus, *Geophys. Res. Lett.*, 34, L14807, doi:10.1029/2007GL029748, 2007.
- Jung, E., Albrecht, B. A., Jonsson, H. H., Chen, Y.-C., Seinfeld, J. H., Sorooshian, A., Metcalf, A. R., Song, S., Fang, M., Russell, L. M.: Precipitation effects of giant cloud condensation nuclei artificially introduced into stratocumulus clouds. *Atmos. Chem. Phys.*, 15, 5645–5658, doi:10.5194/acp-15-5645-2015, 2015.
- Morrison, H., Milbrandt, J. A.: Parameterization of Cloud Microphysics Based on the Prediction of Bulk Ice Particle Properties. Part I: Scheme Description and Idealized Tests. *J. Atmos. Sci.*, 72, DOI: 10.1175/JAS-D-14-0065.1, 2015.
- Rosenfeld, D., Axisa, D., Woodley, W. L., Lahav, R.: A Quest for Effective Hygroscopic Cloud Seeding. *J. Appl. Meteorol. Clim.*, 49, DOI: 10.1175/2010JAMC2307.1, 2010.
- Segal, Y., Khain, A., Pinsky, M., Rosenfeld, D.: Effects of hygroscopic seeding on raindrop formation as seen from simulations using a 2000-bin spectral cloud parcel model. *Atmos. Res.*, 71, 3–34, 2004.
- Segal, Y., Pinsky, M., Khain, A.: The role of competition effect in the raindrop formation. *Atmos. Res.*, 83, 106–118, 2007.
- Stevens, B., Moeng, C.-H., Ackerman, A. S., Bretherton, C. S., Chlond, A., de Roode, S., Edwards, J., Golaz, J.-C., Jiang, H., Khairoutdinov, M., Kirkpatrick, M. P., Lewellen, D. C., Lock, A., Müller, F., Stevens, D. E., Whelan, E., and Zhu, P.: Evaluation of Large-Eddy Simulations via observations of nocturnal marine stratocumulus, *Mon. Weather Rev.*, 133, 1443–1462, 2005.
- Tonttila, J., Maalick, Z., Raatikainen, T., Kokkola, H., Kühn, T., and Romakkaniemi, S.: UCLALES–SALSA v1.0: a large-eddy model with interactive sectional microphysics for aerosol, clouds and precipitation, *Geosci. Model Dev.*, 10, 169–188, <https://doi.org/10.5194/gmd-10-169-2017>, 2017.

EUROPEAN METHANE BUDGETS ESTIMATED FROM CTE-CH₄ ATMOSPHERIC INVERSE MODEL

A. TSURUTA¹, L. BACKMAN¹, J. HAKKARAINEN¹, E. KIVIMÄKI¹, H. LINDQVIST¹, V. KANGASAHO¹, M. TENKANEN¹, T. MARKKANEN¹, M. RAIVONEN¹, A. REPPÄNEN¹ AND T. AALTO¹

¹Finnish Meteorological Institute, Helsinki, Finland.

Keywords: METHANE EMISSIONS, ATMOSPHERIC INVERSION, SATELLITE, EUROPE.

INTRODUCTION

Spatial and temporal variations of methane (CH₄) emissions in Europe are complex due to a mixture and collocation of sources. Anthropogenic sources, such as those from industries and agriculture, are still the main sources of methane in Europe, determining the long-term trend, while emissions from wetlands have high seasonal and year to year variations, which could potentially change due to global warming and mitigation policies. In this study, we examine the European CH₄ budgets estimated from an atmospheric inverse model and their sensitivity prior flux fields and role of new satellite data for quantifying the budgets.

METHODS

We estimated European anthropogenic (e.g. fossil fuels, agriculture and landfills) and biospheric (e.g. wetlands, peatlands, mineral soil) CH₄ emissions for recent decades optimized using Carbon Tracker Europe-CH₄ (CTE-CH₄; Tsuruta *et al.*, 2017) data assimilation system. The emissions for 2000 – 2018 were optimized at 1°x1° (latitude x longitude) horizontal resolution using various sets of observations and prior flux fields. Observations we used are 1) surface atmospheric CH₄ observations from global institutions as in Global Carbon Project (GCP; Saunio *et al.*, 2019), ICOS and other individual collaborators, and 2) dry-air total column-averaged mole CH₄ fraction (XCH₄) data from GOSAT (TANSO-FTS, NIES retrieval v2.80; Yoshida *et al.*, 2013) and 3) XCH₄ data from Sentinel 5P (TROPOMI). Prior flux fields used includes anthropogenic, biospheric, fire, termite, geological and ocean sources. “GCP sets” used estimates from EDGAR v4.3.2 for anthropogenic sources, average from Pouter *et al.*, 2017 as climatology for biospheric sources, and other sources and soil sinks as in Saunio *et al.*, 2019. Another sets used estimates from EDGAR v4.2 FT2010 for anthropogenic sources, LPX-Bern DYPTOP process-model (Stocker *et al.*, 2014) for biospheric sources and soil sinks, and other sources as in Tsuruta *et al.*, 2019.

The inversion estimates were compared to data from the UNFCCC reports and JSBACH-HIMMELI process-based model (Reik *et al.*, 2013; Raivonen *et al.*, 2017), which were not used as prior in the inversions.

CONCLUSIONS

We found that the estimated anthropogenic European CH₄ emissions have a decreasing trend for 2000-2014 in the surface inversion, similarly to those reported to UNFCCC. On the other hand, in the GOSAT inversion, we found insignificant trend in the European emission estimates. Year to year variation of biospheric emissions do not fully agree between inversions and JSBACH-HIMMELI. The discrepancies between inversions are mostly in the seasonal cycle amplitude, where GOSAT inversion show higher summer maximums. Estimates from JSBACH-HIMMELI start to increase much earlier than the inversion estimates, producing higher spring emissions. Those show that temporal variation in the biospheric

emissions are still difficult to constrain by the inversion and therefore, further development is needed from both top-down and bottom-up sides to come to a collective understanding.

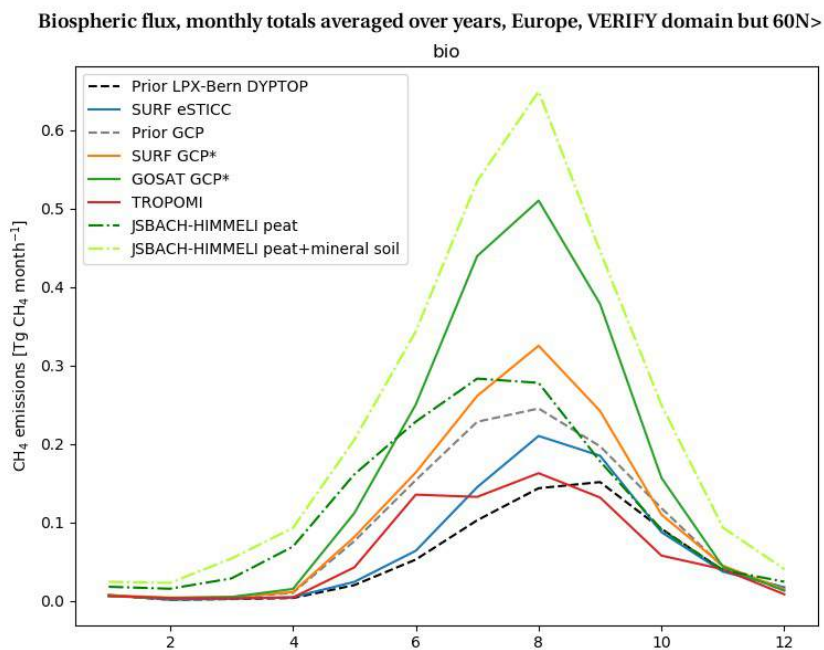


Figure 1. Average monthly European biospheric CH₄ fluxes, estimated from process-based models and inversions using different setups. Dashed lines are those from process-based models, and solid lines are estimates from the inverse model.

ACKNOWLEDGEMENTS

This work was supported financially by the Academy of Finland under grant no. 285630 (CARB-ARC) and grant no. 307331 (UPFORMET), and Grant Agreement number 776810, and the Horizon 2020 Framework Programme the ‘Observation based system for monitoring and verification of greenhouse gases (VERIFY)’ project. This work was also supported by Academy of Finland Centre of Excellence under grant no. 272041, Academy Professor projects (no. 1284701 and 1282842) and ICOS-Finland (project no. 281255). We also thank the contributors and coordinators of Global Carbon Project Methane Budgets.

REFERENCES

- Reick, C. H., Raddatz, T., Brovkin, V. and Gayler, V.: Representation of natural and anthropogenic land cover change in MPI-ESM, *Journal of Advances in Modeling Earth Systems*, 5(3), 459–482, doi:10.1002/jame.20022, 2013.
- Saunois, M., Stavert, A. R., Poulter, B., Bousquet, P., Canadell, J. G., Jackson, R. B., Raymond, P. A., Dlugokencky, E. J., Houweling, S., Patra, P. K., Ciais, P., Arora, V. K., Bastviken, D., Bergamaschi, P., Blake, D. R., Brailsford, G., Bruhwiler, L., Carlson, K. M., Carrol, M., Castaldi, S., Chandra, N., Crevoisier, C., Crill, P. M., Covey, K., Curry, C. L., Etiope, G., Frankenberg, C., Gedney, N., Hegglin, M. I., Höglund-Isakson, L., Hugelius, G., Ishizawa, M., Ito, A., Janssens-Maenhout, G., Jensen, K. M., Joos, F., Kleinen, T., Krummel, P. B., Langenfelds, R. L., Laruelle, G. G., Liu, L., Machida, T., Maksyutov, S., McDonald, K. C., McNorton, J., Miller, P. A., Melton, J. R., Morino, I., Müller, J., Murgía-Flores, F., Naik, V., Niwa, Y., Noce, S., O’Doherty, S., Parker, R. J., Peng, C., Peng, S., Peters, G. P., Prigent, C., Prinn, R., Ramonet, M., Regnier, P., Riley, W. J., Rosentretter, J. A., Segers, A., Simpson, I. J., Shi, H., Smith, S. J., Steele, P. L., Thornton, B. F., Tian, H., Tohjima, Y., Tubiello, F. N., Tsuruta, A., Viovy, N., Voulgarakis, A.,

- Weber, T. S., Weele, M. van, Werf, G. R. van der, Weiss, R. F., Worthy, D., Wunch, D., Yin, Y., Yoshida, Y., Zhang, W., Zhang, Z., Zhao, Y., Zheng, B., Zhu, Q., Zhu, Q. and Zhuang, Q.: The Global Methane Budget 2000-2017, *Earth System Science Data Discussions*, 1–138, doi:<https://doi.org/10.5194/essd-2019-128>, 2019.
- Stocker, B. D., Spahni, R. and Joos, F.: DYPTOP: a cost-efficient TOPMODEL implementation to simulate sub-grid spatio-temporal dynamics of global wetlands and peatlands, *Geosci. Model Dev.*, 7(6), 3089–3110, doi:[10.5194/gmd-7-3089-2014](https://doi.org/10.5194/gmd-7-3089-2014), 2014.
- Tsuruta, A., Aalto, T., Backman, L., Hakkarainen, J., Laan-Luijkx, I. T. van der, Krol, M. C., Spahni, R., Houweling, S., Laine, M., Dlugokencky, E., Gomez-Pelaez, A. J., Schoot, M. van der, Langenfelds, R., Ellul, R., Arduini, J., Apadula, F., Gerbig, C., Feist, D. G., Kivi, R., Yoshida, Y. and Peters, W.: Global methane emission estimates for 2000–2012 from CarbonTracker Europe-CH4 v1.0, *Geoscientific Model Development*, 10(3), 1261–1289, doi:[doi:10.5194/gmd-10-1261-2017](https://doi.org/10.5194/gmd-10-1261-2017), 2017.
- Tsuruta, A., Aalto, T., Backman, L., Krol, M. C., Peters, W., Lienert, S., Joos, F., Miller, P. A., Zhang, W., Laurila, T., Hatakka, J., Leskinen, A., Lehtinen, K. E. J., Peltola, O., Vesala, T., Levula, J., Dlugokencky, E., Heimann, M., Kozlova, E., Aurela, M., Lohila, A., Kauhaniemi, M. and Gomez-Pelaez, A. J.: Methane budget estimates in Finland from the CarbonTracker Europe-CH4 data assimilation system, *Geosci. Model Dev.*, 0(0), 1–20, doi:[10.1080/16000889.2018.1565030](https://doi.org/10.1080/16000889.2018.1565030), 2019.
- Yoshida, Y., Kikuchi, N., Morino, I., Uchino, O., Oshchepkov, S., Bril, A., Saeki, T., Schutgens, N., Toon, G. C., Wunch, D., Roehl, C. M., Wennberg, P. O., Griffith, D. W. T., Deutscher, N. M., Warneke, T., Notholt, J., Robinson, J., Sherlock, V., Connor, B., Rettinger, M., Sussmann, R., Ahonen, P., Heikkinen, P., Kyrö, E., Mendonca, J., Strong, K., Hase, F., Dohe, S. and Yokota, T.: Improvement of the retrieval algorithm for GOSAT SWIR XCO₂ and XCH₄ and their validation using TCCON data, *Atmos. Meas. Tech.*, 6(6), 1533–1547, doi:[10.5194/amt-6-1533-2013](https://doi.org/10.5194/amt-6-1533-2013), 2013.

INVESTIGATING EFFECTIVE CONDENSATION SINK BASED ON HETEROGENEOUS NUCLEATION THEORY

S. TUOVINEN¹, J. KONTKANEN¹, C. YAN^{1,2}, C. DENG³, Y. FU³, K. R. DAELLENBACH¹, W. DU¹, Y. LIU², J. JIANG³, and M. KULMALA^{1,2}

¹Institute for Atmospheric and Earth System Research / Physics, Faculty of Science, University of Helsinki, Helsinki, Finland

²Aerosol and Haze Laboratory, Beijing Advanced Innovation Center for Soft Matter Science and Engineering, Beijing University of Chemical Technology, Beijing, China

³State Key Joint Laboratory of Environment Simulation and Pollution Control, State Environmental Protection Key Laboratory of Sources and Control of Air Pollution Complex, School of Environment, Tsinghua University, Beijing, China

Keywords: CONDENSATION SINK, HETEROGENEOUS NUCLEATION, NEW PARTICLE FORMATION

INTRODUCTION

New particle formation (NPF) is a commonly observed phenomenon in the atmosphere and its occurrence depends on the conditions of the surrounding environment (Kerminen *et al.*, 2018). In theory, NPF events should not occur in heavily polluted environments due to the high condensation sink (CS) caused by pre-existing particles (Kulmala *et al.*, 2017). However, NPF events regularly occur in Chinese megacities despite the high CS (Wu *et al.*, 2007). This can be explained if CS is smaller or the growth rate of particles is larger than assumed (Kulmala *et al.*, 2017). In this study, we explore the possibility of ineffective heterogeneous nucleation resulting in the effective condensation sink being lower than expected.

METHODS

Heterogeneous nucleation was investigated based on classical nucleation theory (Lazaridis, 1991; Fletcher, 1958). We studied how different properties, such as vapour concentration, surface tension or molecular mass, affect heterogeneous nucleation probability. In addition, we studied heterogeneous nucleation probability of compounds with properties corresponding to a vapor composed of sulfuric acid and dimethylamine clusters and to a vapour composed of clusters of low-volatile organic molecules.

We determined contact angles of nucleation that are large enough for heterogeneous nucleation to be ineffective for all the investigated situations. This was done by assuming that nucleation probability of 0.5 corresponds to the onset of heterogeneous nucleation and that no heterogeneous nucleation occurs when nucleation probability is lower than that.

We assumed that CS can be described by heterogeneous nucleation and investigated how large the effective condensation sink (CS_{eff}) caused by an existing aerosol particle population will be if a certain contact angle is assumed. In practice this means that we assumed that particles below a certain diameter, determined by the contact angle and other properties, do not act as a sink because of ineffective heterogeneous nucleation.

To study the impact of ineffective heterogeneous nucleation on CS_{eff} in a Chinese megacity, we used particle size distribution data measured with a PSD (Particle Size Distribution) system at the measurement station of Beijing University of Chemical Technology (39°56'31"N, 116°17'50"E, Beijing) between January 17 and April 1 2018. From this data set, we calculated a median particle number size distribution on NPF event days between 9:00 and 11:00 a.m.

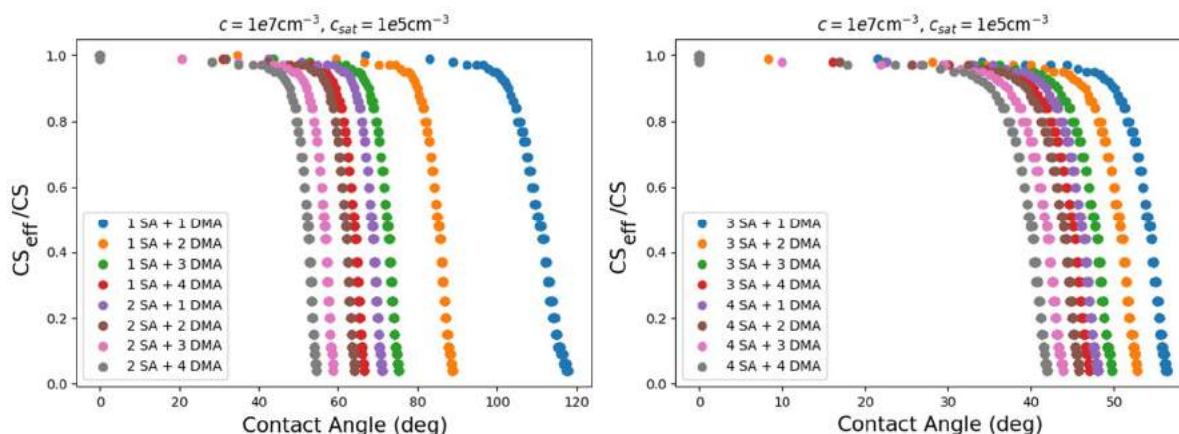


Figure 1: Ratio of effective condensation sink (CS_{eff}) to condensation sink (CS) as a function of contact angle for a vapor composed of different numbers of sulfuric acid (SA) and dimethylamine (DMA) clusters. In left panel there is clusters of one or two sulfuric acid molecules and 1-4 dimethylamine molecules. In right panel there is clusters of three or four sulfuric acid molecules and 1-4 dimethylamine molecules.

RESULTS

We found that heterogeneous nucleation probability depends on the vapour concentration and saturation concentration. Heterogenous nucleation is more likely at high vapor concentrations and at low saturation concentration. In these conditions, the contact angle needs to be large for heterogeneous nucleation to be ineffective and in some cases such a contact angle does not exist at all. Correspondingly, if vapor concentration is low and saturation concentration is high, heterogenous nucleation is less likely and a smaller contact angle is needed for heterogeneous nucleation to be ineffective. In addition, if the vapor molecules have large mass or the vapor has a high surface tension, heterogeneous nucleation probability is low and therefore a rather small contact angle is enough for there to be no heterogeneous nucleation.

Figure 1 shows the ratio of CS_{eff} , calculated for different contact angles of heterogeneous nucleation, to CS for a vapor consisting of sulfuric acid and dimethylamine clusters. For a vapor with larger clusters, a smaller contact angle is enough to clearly reduce CS_{eff} . Therefore, if a significant fraction of vapours present in the atmosphere consists of large molecules or clusters, the effective condensation sink can in theory be considerably lower than the predicted condensation sink.

CONCLUSIONS

In this study, we investigated the possibility of ineffective heterogeneous nucleation resulting in the effective condensation sink being lower than expected. We found that in theory it is possible that a relatively high contact angle of nucleation, caused by chemical properties of the seed particle and the condensing compound, significantly reduces the effective condensation sink. Therefore, ineffective heterogenous nucleation is one possible explanation for the unexpected occurrence of NPF events in polluted environments.

ACKNOWLEDGEMENTS

The work is supported by Academy of Finland (grant nos. 307331 and 316114) and European Research Council (ATM-GTP; grant no. 742206).

REFERENCES

- Fletcher, N. (1958). Size effect in heterogeneous nucleation. *The Journal of chemical physics*, 29(3), 572–576
- Kerminen, V.-M., Chen, X., Vakkari, V., Petäjä, T., Kulmala, M., & Bianchi, F. (2018). Atmospheric new particle formation and growth: review of field observations. *Environmental Research Letters*, 13(10), 103003
- Kulmala, M., Kerminen, V.-M., Petäjä, T., Ding, A., & Wang, L. (2017). Atmospheric gas-to-particle conversion: why npf events are observed in megacities? *Faraday discussions*, 200, 271–288
- Lazaridis, M., Kulmala, M., & Laaksonen, A. (1991). Binary heterogeneous nucleation of a water-sulphuric acid system: The effect of hydrate interaction. *Journal of aerosol science*, 22(7), 823–830
- Wu, Z., Hu, M., Liu, S., Wehner, B., Bauer, S., Maßling, A., ... & Kulmala, M. (2007). New particle formation in Beijing, China: Statistical analysis of a 1-year data set. *Journal of Geophysical Research: Atmospheres*, 112(D9).

ON EXTRACTING INFORMATION FROM CLOSURE PARAMETER CONVERGENCE TESTS USING OPENIFS

L. TUPPI¹, P. OLLINAHO², M. EKBLÖM¹, V. SHEMYAKIN³ and H. JÄRVINEN¹

¹Division of Atmospheric Sciences, Department of Physics, University of Helsinki,
Gustaf Hällströminkatu 2, Helsinki, Finland

²Finnish Meteorological Institute, Erik Palmeninkatu 2, Helsinki, Finland

³School of Engineering Science, Lappeenranta University of Technology, 53851 Lappeenranta, Finland

Keywords: ALGORITHMIC TUNING, ENSEMBLE FORECASTING, BEST PRACTICES

INTRODUCTION

Numerical weather prediction (NWP) models solve non-linear differential equations in finite representation. This usually means that small scale atmospheric processes are not described explicitly by the model. Instead, net effect of these small sub-grid scale processes is taken in account using bulk equations containing constants that are called closure parameters. Unfortunately, exact values of these closure parameters are difficult to infer, and are always somewhat uncertain. Therefore maximizing predictive skill of the model requires some trial-and-error model tuning.

Many do the tuning manually (e.g. Mauritsen et al. 2012) but some have been tuning NWP models using various different algorithms (e.g. Ollinaho et al. 2013, Ollinaho et al. 2014). However, they have not studied how do the parameters converge the best. Aksoy et al. (2006) and Schirber et al. (2014) have studied also the convergence but not as thoroughly as we have done. Here convergence test means tuning of NWP model towards a known truth. This means that instead of analyses or observations, the reference data consists of output of a reference model run with known fixed parameter values. We have concentrated on properties of convergence tests, and based on those convergence tests, we have been thinking about the best practices to do algorithmic tuning. This abstract will loosely follow what has been done in Tuppi et al. (2019) that is to be submitted in November 2019.

METHODS

In order to study properties of convergence tests, we need 1. a NWP model, 2. an ensemble prediction system, 3. a cost function and an optimization algorithm. As a NWP model we use Open Integrated Forecasting System (OpenIFS) cycle 40R1v1 of European Centre for Medium-Range Weather Forecasts (ECMWF). OpenIFS has one stochastic physics scheme that is used in here: Stochastically Perturbed Parametrization Tendencies (SPPT, Palmer et al. 2009). Operational ensemble prediction systems cannot be run outside operational centers so we use OpenEPS ensemble prediction workflow manager (<https://github.com/pirkkao/OpenEPS>) specifically designed for ensemble forecasting experiments in research purposes. We decided to use two optimization algorithms for our convergence tests. The first one is a modified version of the Ensemble Prediction and Parameter Estimation System (EPPES, Järvinen et al. 2012, Laine et al. 2012). We have added an additional constraint on how fast the distribution mean value can move in EPPES. This constraint enables us to shorten the memory, and thus make EPPES more flexible. The other optimization algorithm is Differential Evolution (DE, Shemyakin and Haario 2018). We use two different cost functions here: basic root mean squared error of 850 hPa geopotential (RMSEZ850) and moist total energy norm (ΔE_m , e.g. Ehrendorfer et al. 1999). For evaluation of the convergence tests we use kernel representation of fair Continuous Ranked Probability Score (fCRPS, e.g. Leutbecher 2018). The fact that fCRPS is a fair score is extremely useful since we need to be able to compare convergence tests which use ensembles of different sizes.

Next we present the parameters and different convergence test set-ups we used. We chose five parameters from the convection scheme of OpenIFS. The parameters are entrainment rate for deep convection

(ENTRORG), entrainment rate multiplier for shallow convection (ENTSHALP), detrainment rate for penetrative convection (DETRPEN), cloud water/ice to rain/snow conversion factor (RPRCON) and depth of layer for shallow convection (RDEPTH). In the most convergence tests we use only ENTRORG and ENTSHALP. ENTRORG and ENTSHALP are always initialized so that they have 10% too large values relative to the parameter default values used in the control model. Moreover, ENTRORG and ENTSHALP have large initial uncertainty.

The main focus is on different levels of realism as described in table 1 and level 2 (L2) experiments done with several forecast length – ensemble size combinations. There are four different levels of realism in table 1: L0, L1, L2 and L3. First we show the pros and cons of using these different levels of realism. Then we use one L1 set-up to show why to choose a proper cost function ΔE_m over RMSEZ850. Next different forecast lengths and ensemble sizes are used in L2 level of realism to demonstrate the most efficient way to do a convergence test. From these combinations we select a couple of examples and test how reproducible those tests are. In Tuppi et al. (2019) we discuss quite extensively about the problems that might be encountered during the convergence tests but here it will be discussed very shortly.

	Number of parameters	Different initial conditions	Stochastic physics (SPPT)
Level 0 (L0)	2	No	No
Level 1 (L1)	2	Yes	No
Level 2 (L2)	2	Yes	Yes
Level 3 (L3)	5	Yes	Yes

Table 1. Covnrgence tests with increasing degree of realism; from idealistic experiments step by step towards genuine model tuning.

RESULTS

We begin with discussion about which level of realism to use. Figure 1 shows a comparison of convergence tests done with four different levels of realism as in Table 1. All of the tests converge even though ENTRORG converges slightly different value than expected in L1, L2 and L3 tests. We think that L0 tests are too idealistic to indicate how well the optimization method is going to work in genuine model tuning. L1, L2 and L3 tests lead to relatively similar outcomes. Adding noise to the tests with SPPT and additional parameters does not provide new insights so already L1 tests provide most of the information about the convergence.

Comparison of similar convergence tests with the two cost functions RMSEZ850 and ΔE_m (not shown) shows that selection of cost function does matter. For ENTSHALP, RMSEZ850 does not show convergence at all, and for ENTRORG, ΔE_m leads to twice as fast convergence as RMSEZ850. ΔE_m covers entire atmosphere whereas RMSEZ850 only a single level. Moreover, ΔE_m includes more sensitive variables than RMSEZ850 so it is natural that ΔE_m leads to better convergence.

Figure 2 shows a number of L2 convergence test results for ENTRORG with EPPES as optimizer. Left panel of Figure 2 shows end results from a number of forecast length – ensemble size combinations. As blue color means better convergence, one can easily see that the best forecast length for ENTRORG is 24 hours. As ENTSHALP is less sensitive parameter, there is more noise in those results. However, it seems that also ENTSHALP favors relatively short forecasts of 24 to 48 hours (not shown). In order to see more clearly which ensemble size works best, we look at the right panel of Figure 2. It takes a closer look at the best forecast length of 24 hours. Interpretation of the blocks is the same as in the left panel but now there is number of iterations on the x-axis. The right panel shows how fast the convergence happens with different ensemble sizes. It is also possible to look at the right panel so that how much sample points have been used to reach reasonable convergence. As all but those tests with the smallest ensembles seem to proceed roughly equally fast, it means that using large ensembles is meaningless burning of computational resources. The best way to see this is to compare blocks having the same amount of sample

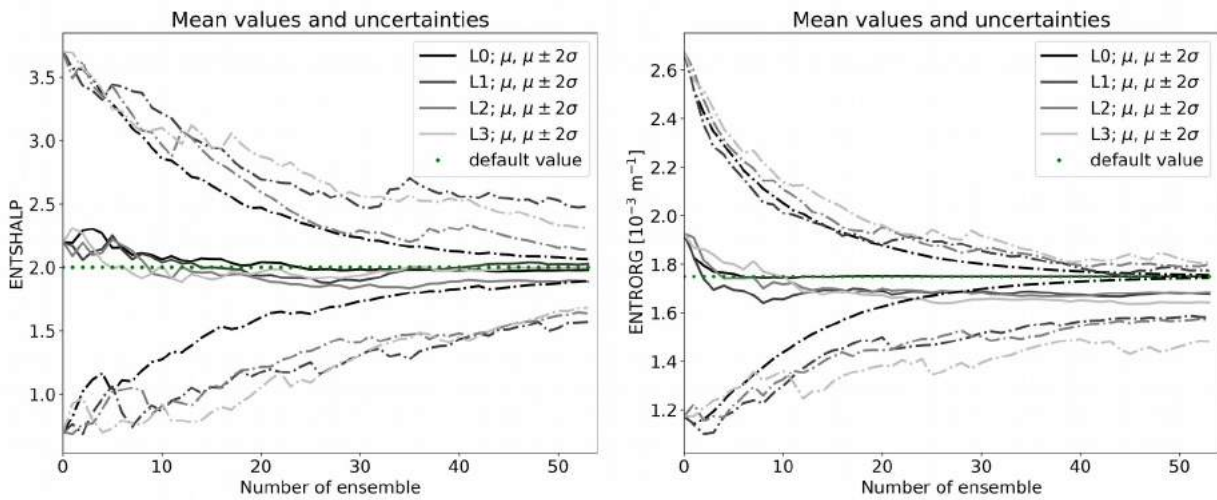


Figure 1. Comparison of convergence tests with different levels of realism. Left panel shows evolution of ENTSHALP and right panel ENTRORG respectively. X-axes show running number of ensembles. Distribution mean values are shown with solid lines and mean \pm two times the standard deviation with dash dotted lines. ΔE_m is used as cost function, and the legends refer to different levels of realism explained in more details in Table 1. Green dots show the parameter default values. All convergence tests have been done with 48 hour forecasts and 50 ensemble members.

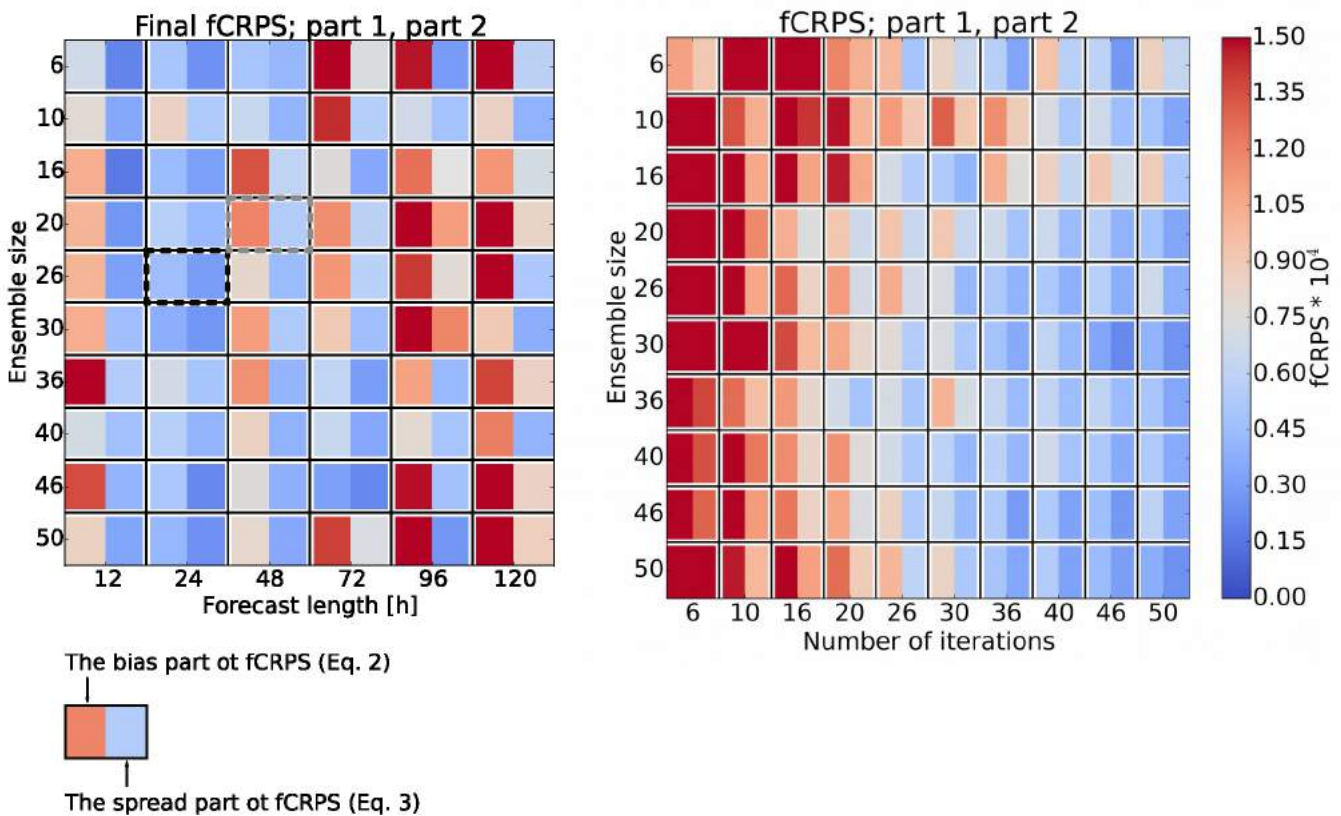


Figure 2. On the left, end results of numerous convergence tests with different forecast lengths and ensemble sizes measured with fair continuous ranked probability score (fCRPS, see e.g. Leutbecher 2018, equation 6). We have broken the equation to two parts to avoid cancellation. On the right, evolution of convergence tests when forecast length of 24 hours is used. Number of iterations tells how many times the optimization algorithm has been called. The parameter used is ENTRORG in convection scheme of OpenIFS, and the optimization algorithm is EPPES (Järvinen et al. 2012, Laine et al. 2012). The colorbar is common for both panels. Blue colors denote better convergence.

points for example 20 iterations and 50 members, and 50 iterations and 20 members. The latter leads to much better convergence. The best ensemble size is a trade-off between use of computer resources and stability of the convergence tests. Medium-sized ensembles of ~ 20 members seem to lead to fast and stable enough convergence with moderate use of resources.

Left panel of Figure 2 shows also two highlighted blocks. We used those example combinations to study reproducibility of L1 and L2 convergence tests. Results with L1 level of realism show that both of the examples are fairly reproducible (not shown). Instead, when SPPT is added for L2 tests, the combination of 48 hour forecasts and 20 member ensembles becomes significantly more unstable, and is not reproducible anymore (not shown). Reproducibility of the better combination of 24 hour forecasts and 26 member ensembles is not affected by the additional noise.

Figure 1 already showed that at least ENTRORG misses convergence to the parameter default value. This is further emphasized in Figure 3. Figure 3 shows parameter values at the end of the L2 convergence tests. White color means convergence to the default values whereas purple and green colors denote convergence above and below the default values. Both panels of Figure 3 seem systematic but especially the right panel, which shows results of ENTRORG. With longer forecasts than 24 hours, ENTRORG tends to converge below the default value, and with shorter forecasts than 24 hours, slightly above. We also tested ENTRORG alone with only initial condition perturbations activated, and it seems to behave in the similar way also alone. We think that this happens because using initial condition perturbations enables minimization of the cost function different way than by minimizing the error in parameter values. It seems that also growth of other perturbations can be minimized with certain parameter values. We are, however, unsure whether this is a real problem or only a feature of convergence test.

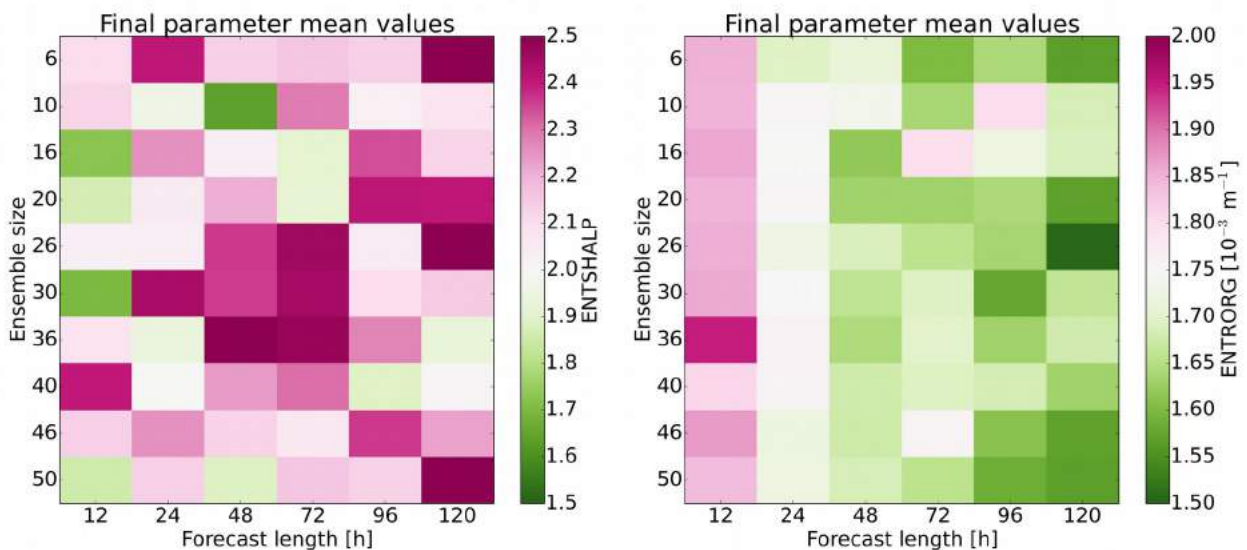


Figure 3. Mean values of the parameter distributions proposed by EPPES at the end of the convergence tests. Mean values of ENTSHALP are on the left and mean values of ENTRORG on the right. Purple (green) colour means that the final mean values are larger (smaller) than the default value.

CONCLUSIONS

Here we have summarized the key results of manuscript Tuppi et al. (2019) to be submitted in November 2019. We began with looking at which levels of realism should be chosen. L0 test is a good way to check that the parameters respond to the chosen cost function. L1 provides information about the behavior when also other perturbations are present. L2 and L3 were not seen to provide additional information. The only value in L2 and L3 tests is that if they work, simpler test will work also. We tested two different cost functions in order to show that the choice really matters. One should choose such a cost function that is comprehensive and sensible to the parameter variations. We searched for such a set-up that 1. converges

well, 2. is relatively cheap to run and 3. is reproducible. Medium-sized ensembles of ~20 members and forecast length of 24 hours meet these criteria the best. We noticed that convergence tests have some intrinsic problems. If other perturbations are applied besides the parameter perturbations, there are several ways to minimize the cost function so the parameters might not converge to the default values.

ACKNOWLEDGMENTS

The authors are grateful to CSC-IT for providing computational resources. We thank Olle Rätty at Finnish Meteorological Institute for assisting in graphical design of Figure 3. We are also thankful to Marko Laine at Finnish Meteorological Institute for the insightful discussions about evaluation of convergence tests and user support for EPPES. The figures have been plotted with help of Python Matplotlib library (Hunter, 2007).

REFERENCES

- Aksoy A., Zhang F., J.W. Nielsen-Gammon (2006). Ensemble-based simultaneous state and parameter estimation in a two-dimensional sea-breeze model. *Monthly Weather Review*, 134(10):2951–2970. doi: 10.1175/MWR3224.1. URL <https://doi.org/10.1175/MWR3224.1>.
- Ehrendorfer M., Errico R.M., and K.D. Raeder (1999). Singular-vector perturbation growth in a primitive equation model with moist physics. *Journal of the Atmospheric Sciences*, 56(11):1627–1648. doi: 10.1175/1520-0469(1999)056<1627:SVPGIA>2.0.CO;2. URL [https://doi.org/10.1175/1520-0469\(1999\)056<1627:SVPGIA>2.0.CO;2](https://doi.org/10.1175/1520-0469(1999)056<1627:SVPGIA>2.0.CO;2).
- Hunter J.D. (2007). Matplotlib: A 2d graphics environment. *Computing In Science & Engineering*, 9(3):90–95. doi: 10.1109/MCSE.2007.55.
- Järvinen H., Laine M., Solonen A., and H. Haario (2012). Ensemble prediction and parameter estimation system: the concept. *Quarterly Journal of the Royal Meteorological Society*, 138(663):281–288. doi: 10.1002/qj.923. URL <https://rmets.onlinelibrary.wiley.com/doi/abs/10.1002/qj.923>.
- Laine M., Solonen A., Haario H., and H. Järvinen (2012). Ensemble prediction and parameter estimation system: the method. *Quarterly Journal of the Royal Meteorological Society*, 138(663):289–297. doi: 10.1002/qj.922. URL <https://rmets.onlinelibrary.wiley.com/doi/abs/10.1002/qj.922>.
- Leutbecher M (2018). Ensemble size: How suboptimal is less than infinity? *Quarterly Journal of the Royal Meteorological Society*, 0(0). doi: 10.1002/qj.3387. URL <https://rmets.onlinelibrary.wiley.com/doi/abs/10.1002/qj.3387>.
- Mauritsen T., Stevens B., Roeckner E., Crueger T., Esch M., Giorgetta M., Haak H., Jungclaus J., Klocke D., Matei D., Mikolajewicz U., Notz D., Pincus R., Schmidt H., and L. Tomassini (2012). Tuning the climate of a global model. *Journal of Advances in Modeling Earth Systems*, 4(3). doi: 10.1029/2012MS000154. URL <https://agupubs.onlinelibrary.wiley.com/doi/abs/10.1029/2012MS000154>.
- Ollinaho P., Bechtold P., Leutbecher M., Laine M., Solonen A., Haario H., and H. Järvinen (2013). Parameter variations in prediction skill optimization at ECMWF. *Nonlinear Processes in Geophysics*, 20(6):1001–1010. doi: 10.5194/npg-20-1001-2013. URL <https://www.nonlin-processes-geophys.net/20/1001/2013/>.
- Ollinaho P., Järvinen H., Bauer P., Laine M., Bechtold P., Susiluoto J., and H. Haario (2014). Optimization of nwp model closure parameters using total energy norm of forecast error as a target. *Geoscientific Model Development*, 7(5):1889–1900. doi: 10.5194/gmd-7-1889-2014. URL <https://www.geosci-model-dev.net/7/1889/2014/>.
- Palmer T.N., Buizza R., Doblas-Reyes F., Jung T., Leutbecher M., Shutts G.J., Steinheimer M., and A. Weisheimer (2009). Stochastic parametrization and model uncertainty. *ECMWF Technical Memoranda*, 598:1–42.
- Schirber S., Klocke D., Pincus R., Quaas J., and J.L. Anderson (2014). Parameter estimation using data assimilation in an atmospheric general circulation model: From a perfect toward the real world. *Journal of Advances in Modeling Earth Systems*, 5(1):58–70, 2013. doi: 10.1029/2012MS000167. URL <https://agupubs.onlinelibrary.wiley.com/doi/abs/10.1029/2012MS000167>.
- Shemyakin V. and H. Haario (2018). Online identification of large-scale chaotic system. *Nonlinear Dynamics*, 93(2):961–975. ISSN 1573-269X. doi: 10.1007/s11071-018-4239-5. URL <https://doi.org/10.1007/s11071-018-4239-5>.

Tuppi L., Ollinaho P., Ekblom M., Shemyakin V. and H. Järvinen. (2019) On extracting information from closure parameter convergence tests using OpenIFS, manuscript, to be submitted.

SIMULATIONS OF NEW PARTICLE FORMATION IN BOREAL FOREST USING CLUSTER DYNAMICS SIMULATION, PARAMETERIZATION AND MEASUREMENT RESULTS

HELMU UUSITALO¹, JENNI KONTKANEN¹, ANASTASIIA DEMAKOVA¹, MIKHAIL ARSHINOV², TUOMO NIEMINEN¹, MARKKU KULMALA¹

¹ Institute for Atmospheric and Earth System Research / Physics, University of Helsinki, Finland

² V.E. Zuev Institute of Atmospheric Optics SB RAS, Tomsk, Russia

INTRODUCTION

Atmospheric new particle formation (NPF) is an important phenomenon which affects climate and human health (Neuberger, 2012; Pöschl, 2005). It has been shown that NPF is affected by many atmospheric conditions, for example concentrations of sulphuric acid and organic vapors and it has been observed to occur in all kinds of environments all over the world (Donahue *et al.*, 2013; Kulmala *et al.*, 2013; Kulmala *et al.*, 2017). Wiedensohler *et al.* (2019) analyzed new particle formation in Zotino Tall Tower Observatory (ZOTTO) in Siberian forest and according to their results, NPF events were significantly less frequent in ZOTTO than for example in Hyytiälä SMEAR II station. In this work, we used Atmospheric Cluster Dynamics Code (ACDC), parametric equations for particle growth and formation rate and measurement data from two measurement stations surrounded by a boreal forest to investigate how concentrations of sulphuric acid and organic vapors influence new particle formation. In addition, we investigated if temperature or saturation vapor pressure and surface tension of organic vapor has an effect on new particle formation.

MATERIAL AND METHODS

In this work, we used measurement data from two measurement stations, Hyytiälä SMEAR II (Hari *et al.*, 2005) and Tomsk Fonovaya station in Siberia (Antonovich *et al.*, 2018). From Hyytiälä, we used particle number size distributions measured by DMPS (differential mobility particle sizer) (Aalto *et al.*, 2001) (2017-2018), particle concentrations measured by PSM (particle size magnifier) (Vanhanen *et al.*, 2011) (2017-2018), number concentrations of sulphuric acid and HOM (highly oxygenated molecule) compounds (2018) measured by CIMS (Jokinen *et al.*, 2012) and concentration of sulphur dioxide, as well as measured temperature and relative humidity (2017-2018). From Tomsk, we used particle number size distributions, sulphur dioxide concentration, radiation (2017-2018) and condensation sink values calculated from particle size distribution data (2017). We used mode fitting method to determine growth rates from number size distribution data. (Hussein *et al.*, 2005) Formation rates were determined from particle size distribution data for both stations. In Tomsk, calculated condensation sink values were also used.

We used parametric equations to simulate particle growth rates with assumed vapor molecule masses, saturation vapor pressure and surface tension of organic vapor and temperature (Nieminen *et al.*, 2010) and we used four different functions to calculate particle formation rate at 1.5 nm with sulphuric acid and organic vapor concentrations (Paasonen *et al.*, 2010). Finally, we used the equation from Kerminen and Kulmala (2002) to calculate formation rates of larger particles (3 nm or 10 nm). With the latter equation, we also calculated particle survival probabilities.

ACDC was used to simulate new particle formation in different conditions. In ACDC, cluster birth-

death equations are solved explicitly. Evaporation rates are calculated with cluster free energies obtained from quantum chemistry calculations and smallest clusters are assumed to include sulphuric acid and ammonium (McGrath *et al.*, 2012). We changed sulphuric acid and organic vapor concentrations, and other conditions like temperature, and saturation vapor pressure and surface tension of organic vapor. For condensation sink, the typical Hyytiälä value 0.001 1/s was used.

RESULTS

In this work, we found that in 2017 and 2018 there were 150 NPF event days in Hyytiälä, during which growth rates (GR) and formation rates could be determined on 70 days (33 in 2017 and 37 in 2018). In Tomsk, in 2017 and 2018 there were 50 event days (21 in 2017 and 29 in 2018) when parameters could be calculated. Growth rates and formation rates were determined for all 21 days in 2017. Average growth rates of nucleation mode particles (GR_{3-25nm}) were 2.3 nm/h in Hyytiälä and 1.7 nm/h in Tomsk, and average formation rates at 3 nm (J_3) were 0.28 1/cm³s in Hyytiälä and 0.24 1/cm³s in Tomsk. We also found that condensation sinks (CS) were around 3 times higher in Tomsk (median 0.0042 1/s) than in Hyytiälä (median 0.0016 1/s). Also sulphur dioxide concentrations were up to ten times higher in Tomsk during the studied period. In Hyytiälä, growth rates and formation rates were also calculated for sub-3 nm particles, $GR_{1-2.5nm}$ (average 1.4 nm/h) and $J_{1.5}$ (average 0.53 1/cm³s).

The simulations were done with both parametric equations and ACDC. With parametric equations, all four equations for $J_{1.5}$ were used and sulphuric acid and organic vapor concentrations along with other conditions were changed to investigate their participation to new particle formation. The comparison between different simulations and conditions and measured values of Hyytiälä and Tomsk are shown in Figure 1. We found that along with sulphuric acid and organic vapor concentrations, temperature is one of the most important factor influencing new particle formation. The higher the temperature, the smaller the formation rate. The saturation vapor pressure of organic compound also has an impact on formation rate: the higher the saturation vapor pressure, the smaller the formation rate.

In ZOTTO, the particle number size distribution measurements start from 10 nm when in Hyytiälä the lowest measured size is around 1.5 nm from PSM and 3 nm from DMPS. We estimated particle survival probabilities in above-mentioned situations and found that larger particle diameter (along with GR and CS) has a significant impact on particle survival probability during an event.

CONCLUSIONS

The goal of the work was to find explanations for the infrequent new particle formation in Zotino Tall Tower Observatory by simulating new particle formation in different conditions and by comparing simulated values to measured parameters in Hyytiälä and Tomsk measuring stations. It is possible that some conditions in ZOTTO cause NPF events to occur rarely. We found that these conditions could be different properties of organic compound, such as a lower saturation vapor pressure which makes formation rates smaller, or higher temperature. In Siberia, day-time temperatures are higher in summer than in Hyytiälä, and most of the events happen during spring and summer. Therefore in summer time, temperature could be a probable reason for events being infrequent in Siberia.

We found that condensation sinks are significantly higher in Tomsk than in Hyytiälä and growth rates are lower in Tomsk. This makes the ratio GR'/CS' remarkably lower in Tomsk, which affects the survival probability and can cause events to leave unnoticed. When we also take in account that in ZOTTO particles are only measured starting from 10 nm, the cluster survival probability measured in ZOTTO becomes very low. If we estimate the survival probability in Hyytiälä and Tomsk with typical CS ja GR values and particle diameter of 3 nm and in ZOTTO with typical

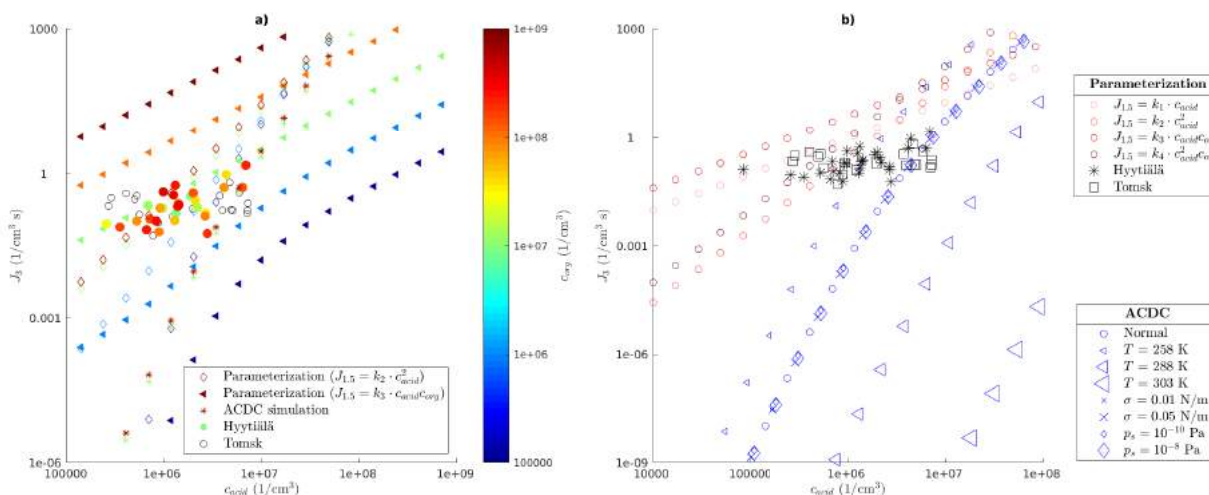


Figure 1: Particle formation rate J_3 as a function of (a) sulphuric acid concentration (c_{acid}) and (b) both sulphuric acid and organic compound concentrations (c_{org}). a) Two simulations with parametric equations, ACDC simulation and data points for Hyytiälä and Tomsk event days. The concentration of organic compound is shown with color. b) Four simulations with parametric equations, ACDC simulations with different temperature, surface tension and saturation vapor pressure, and Hyytiälä and Tomsk event day data points. In normal conditions, $T = 273 \text{ K}$, $\sigma = 0.023 \text{ Pa}$ and $p_s = 10^{-12} \text{ Pa}$.

Tomsk CS and GR values and particle diameter of 10 nm , we get the probability of 62% for Hyytiälä, 20% for Tomsk and only 6.6% for ZOTTO. The small cluster survival probability due to higher CS , lower GR and bigger measured particle diameter can be considered to affect the frequency of NPF events observed in ZOTTO.

ACKNOWLEDGEMENTS

The work is supported by Academy of Finland (grant nos. 307331 and 316114) and European Research Council (ATM-GTP; grant no. 742206).

REFERENCES

- Aalto, P., Hämeri, K., Becker, E., Weber, R., Salm, J., Mäkelä, J. M., Hoell, C., O’ Dowd, C. D., Hansson, H.-C., Väkevä, M., Koponen, I. K., Buzorius, G., Kulmala, M. (2001) Physical characterization of aerosol particles during nucleation events, *Tellus B: Chemical and Physical Meteorology*, 53:4, 344-358
- Antonovich, V. et al.: Station for the comprehensive monitoring of the atmosphere at Fonovaya Observatory, West Siberia: current status and future needs *ResearchGate* 10.1117/12.2504388, 2018
- Donahue, N. M., Ortega, I. K., Chuang, W., Riipinen, I., Riccobono, F., Schobesberger, S., Dommen, J., Baltensperger, U., Kulmala, M., Worsnop D. R., and Vehkamäki, H.: How do organic vapors contribute to new- particle formation? *Faraday Discuss* 2013, 165, 91
- Hari, P., and Kulmala, M.: Station for Measuring Ecosystem–Atmosphere Relations (SMEAR II) *BOREAL ENVIRONMENT RESEARCH* 10: 315–322, 2005

- Hussein, T., Dal Maso, M., Petäjä, T., Koponen, I. K., Paatero, P., Aalto, P., Hämeri, K., and Kulmala, M.: Evaluation of an automatic algorithm for fitting the particle number size distributions *Boreal Env. Res.* 10: 337–355, 2005
- Jokinen, T. , Sipilä, M., Junninen, H., Ehn, M., Lönn, G., Hakala, J., Petäjä, T., Mauldin III, R. L., Kulmala, M., and Worsnop, D. R.: Atmospheric sulphuric acid and neutral cluster measurements using CI-API-TOF *Atmos. Chem. Phys.*, 12, 4117–4125, 2012
- Kerminen, V.-M., Kulmala, M.: Analytical formulae connecting the “real” and the “apparent” nucleation rate and the nuclei number concentration for atmospheric nucleation events *Journal of Aerosol Science* 33, 609-622, 2002
- Kulmala M. et al.: Direct Observations of Atmospheric Aerosol Nucleation *Science* (6122), 943-946, 2013
- Kulmala, M., Kerminen, V.-M., Petäjä, T., Ding, A. J., and Wang, L.: Atmospheric gas-to-particle conversion: why NPF events are observed in megacities? *Faraday Discuss.*, 2017, 200, 271
- McGrath, M. J., Olenius, T., Ortega, I. K., Loukonen, V., Paasonen, P., Kurtén, T., Kulmala, M., and Vehkamäki, H.: Atmospheric Cluster Dynamics Code: a flexible method for solution of the birth-death equations *Atmos. Chem. Phys.*, 12, 2345–2355, 2012
- Neuberger, M.: Human health effects of aerosols. *ResearchGate* 2012
- Nieminen, T., Lehtinen, K. E. J., and Kulmala, M.: Sub-10 nm particle growth by vapor condensation – effects of vapor molecule size and particle thermal speed *Atmos. Chem. Phys.*, 10, 9773-9779, 2010
- Paasonen, P., Nieminen, T., Asmi, E., Manninen, H. E., Petäjä, T., Plass-Dülmer, C., Flentje, H., Birmili, W., Wiedensohler, A., Hörrak, U., Metzger, A., Hamed, A., Laaksonen, A., Facchini, M. C., Kerminen, V.-M., and Kulmala, M.: On the roles of sulphuric acid and low-volatility organic vapours in the initial steps of atmospheric new particle formation *Atmos. Chem. Phys.* 10, 11223-11242, 2010
- Pöschl, U.: Atmospheric Aerosols: Composition, Transformation, Climate and Health Effects *Angew. Chem. Int. Ed.* 2005, 44, 7520-7540
- Vanhanen, J., Mikkilä, J., Lehtipalo, K., Sipilä, M., Manninen, H. E., Siivola, E., Petäjä, T., and Kulmala, M.: Particle Size Magnifier for Nano-CN Detection, *Aerosol Science and Technology*, 45:4, 533-542, 2011
- Wiedensohler, A., Ma, N., Birmili, W., Heintzenberg, J., Ditas, F., Andreae, M. O., Panov, A.: Infrequent new particle formation over the remote boreal forest of Siberia *Atmospheric Environment* 200 (2019) 167–169

MEASUREMENTS OF AEROSOL PARTICLE DEPOLARIZATION RATIO AT WELGEGUND, SOUTH AFRICA

V. VAKKARI^{1,2}, E.J. O'CONNOR³ and P.G. VAN ZYL²

¹Finnish Meteorological Institute, Helsinki, Finland

²North-West University, Unit for Environmental Sciences and Management, Potchefstroom, South Africa.

³Department of Meteorology, University of Reading, Reading, UK.

Keywords: remote sensing, depolarization ratio, lidar, savannah.

INTRODUCTION

Remote sensing measurements provide important information on the vertical structure of the atmosphere, which cannot be extracted from surface measurements alone. In aerosol profiling depolarization ratio is a valuable parameter as it enables differentiation of non-spherical particles such as dust and volcanic ash from spherical droplets. Typically aerosol particle depolarization ratio is measured at wavelengths of 355 nm and/or 532 nm, though recently also 1064 nm wavelength has been utilised in studying the depolarization ratio spectral dependency (e.g. Haarrig *et al.*, 2018). Here, utilising 11-month measurement campaign at Welgegund, South Africa, we show that Halo Doppler lidars can be used to measure aerosol particle depolarization ratio at 1.5 μm wavelength.

METHODS

Measurements with a Halo Photonics Stream Line scanning Doppler lidar were carried out at the Welgegund measurement station (26.57°S, 26.94°E, 1480 m a.s.l.) from August 2016 to June 2017. Halo Photonics Stream Line is an eye-safe 1.5 μm pulsed Doppler lidar with a heterodyne detector (Pearson *et al.*, 2009). The lidar was configured to switch between co- and cross-polar channels in vertically pointing measurement, yielding depolarization ratio measurements from 90 m above ground. We used a recently-developed post-processing method (Vakkari *et al.*, 2019) to reduce the instrument noise level so that we can utilise signals down to -32 dB.

Welgegund measurement station is extensively equipped for aerosol and trace gas measurements. The measurement site is located 100 km west of Johannesburg on a private farm with no local anthropogenic sources, but it is frequently impacted by relatively fresh savannah and grassland fire smoke (Vakkari *et al.*, 2018). We utilised the ground-based in-situ measurements to identify wind-blown dust, biomass burning smoke and industrial aerosols within the mixing layer.

RESULTS

We analysed depolarization ratio at liquid cloud base (Fig. 1) during the measurement campaign to evaluate the performance of the depolarization channel. On average, the liquid cloud depolarization ratio was 1.5 % and we observed no temporal drift. This indicates a constant bleed-through of co-polar radiation through the depolarization filter. For wind-blown dust, we observed depolarization ratio ranging from 30 to 35 % (Fig. 1). Relatively fresh industrial aerosol cases presented depolarization ratio of 7-12 %. A case of aged biomass burning smoke had even lower depolarization ratio of approx. 5%, but in this case also ambient relative humidity was high (>90%) and hygroscopic growth of the aerosol probably contributed to the low depolarization ratio.

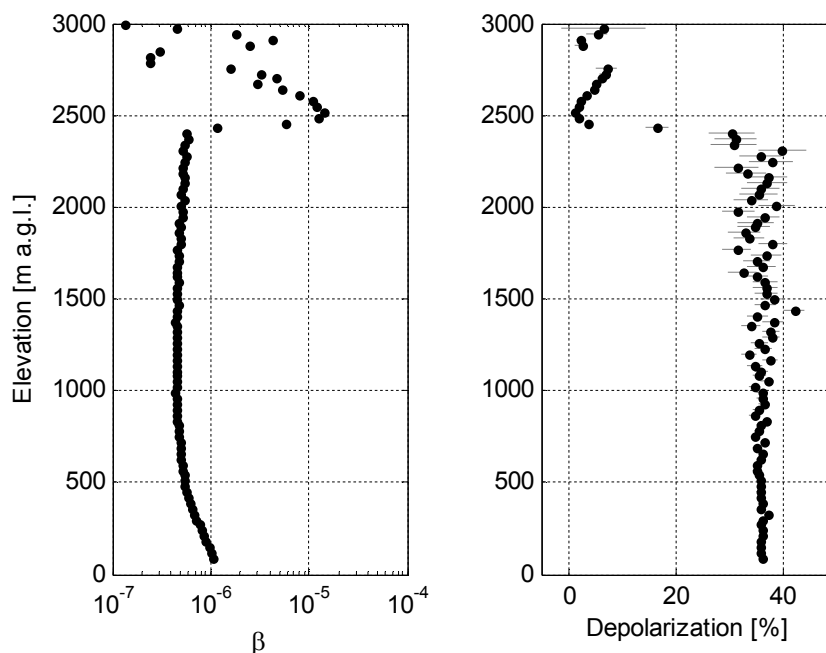


Figure 1. Vertical profiles of attenuated backscatter (β) and depolarization ratio on 17 November 2016 at Welgegund. Cloud base is at 2400 m a.g.l., below that aerosol signal is dominated by wind-blow dust.

CONCLUSIONS

Here, we have used for the first time a Halo Photonics Stream Line Doppler lidar to retrieve aerosol particle depolarization ratio at 1.5 μm wavelength. A combination of in-situ and remote sensing measurements at Welgegund, South Africa, show clear differences in the 1.5 μm depolarization ratio for different aerosol types, including dust, industrial emissions and biomass burning.

ACKNOWLEDGEMENTS

This research was supported by the Academy of Finland Center of Excellence (grant no. 307331), North-West University and Finnish Meteorological Institute.

REFERENCES

- Haarig, M., A. Ansmann, H. Baars, C. Jimenez, I. Veselovskii, R. Engelmann and D. Althausen (2018). Depolarization and lidar ratios at 355, 532, and 1064 nm and microphysical properties of aged tropospheric and stratospheric Canadian wildfire smoke. *Atmos. Chem. Phys.* **18**, 11847–11861.
- Pearson, G., F. Davies and C. Collier (2009). An Analysis of the Performance of the UFAM Pulsed Doppler Lidar for Observing the Boundary Layer. *J. Atmos. Oceanic Technol.* **26**, 240–250.
- Vakkari, V., J.P. Beukes, M. Dal Maso, M. Aurela, M. Josipovic and P.G. van Zyl (2018). Major secondary aerosol formation in southern African open biomass burning plumes, *Nature Geosci.* **11**, 580–583.
- Vakkari, V. A.J. Manninen, E.J. O’Connor, J.H. Schween, P.G. van Zyl and E. Marinou (2019). A novel post-processing algorithm for Halo Doppler lidars. *Atmos. Meas. Tech.* **12**, 839–852.

PHOTOSYNTHETIC ENERGY REGULATION UNDER EXCESSIVE LIGHT: THE QUICK IN VIVO ROLE OF XANTHOPHYLL POOL CONVERSIONS

S. VAN WITTENBERGHE^{1,2}, N. IGNACIO GARCIA³, B. FERNÁNDEZ-MARÍN^{3,4}, A. PORCAR-CASTELL¹ and J. MORENO²

¹Optics of Photosynthesis Laboratory, Institute for Atmospheric and Earth System Research/ Forest Sciences, University of Helsinki, Latokartanonkaari 7, 00014 Helsinki, Finland

²Laboratory of Earth Observation, Image Processing Laboratory, University of Valencia, C/ Catedrático José Beltrán, 2, 46980 Paterna (Valencia), Spain

³Department of Plant Biology and Ecology, University of the Basque Country (UPV/EHU), Barrio Sarriena sn, 48940 Leioa, Spain

⁴Department of Botany, Ecology and Plant Physiology, University of La Laguna (ULL), 38200 S.C. de La Laguna, Canary Islands, Spain

Keywords: LIGHT ABSORPTION, PHOTOSYNTHESIS, CONTROLLED ENERGY DISSIPATION.

INTRODUCTION

The absorbed energy flux by the light-harvesting antenna complexes of vegetation supplies the photosynthetic light reactions with a very high efficiency transfer of quantum energy from one molecule to another, until such absorbed energy is efficiently transferred to the reaction centres of photosynthesis. The energy transfer is hereby highly regulated by the variable aggregation of pigments in the antenna complexes and even actively controlled by the antenna itself (Krüger and van Grondelle 2017). To control and protect themselves and the reaction centres from a potentially harmful solar radiance excess, several regulated photoprotection mechanisms are activated at different time scales at the level of these antenna complexes. The understanding of these processes of energy regulation from remote sensing are essential to monitor plant adaptation strategies to a stressful environment. Under a changing climate, such strategies managing an excess of energy in a controlled way can be considered highly beneficial to withstand drought and heat extremes.

The carotenoids and especially the group of xanthophylls are known for their key role in modifying the energy absorption and dissipation by the antenna. Under excessive light, chemical and enzymatic conversions are triggered, converting the xanthophyll pools, which bind to the antenna and modify the absorbance properties of the complexes. The chemical conversions are prompted by an acidifying lumen and a further built-up of a pH gradient across the thylakoid membrane (ΔpH). The versatile violaxanthin-antheraxanthin-zeaxanthin (VAZ) and Lutein epoxide-Lutein (LxL) cycles are two de-epoxidation processes under excessive light. The VAZ cycle is ubiquitous in the subkingdom *Viridiplantae* (which includes all organisms from green algae to angiosperms), while the LxL cycle taxonomically restricted being present in approximately 60% of plant species analysed thus far (García-Plazaola et al. 2007; Leuenberger et al. 2017). Both cycles are known to act upon sudden illumination, but less is known on their quick dynamics *in vivo* and activity for different light-grown plant material.

METHODS

High-spectral resolution monitoring of vegetation allows for a higher-detailed observation of dynamic absorbance changes, which may occur during the chemical and/or structural changes of the antenna during an imposed energy excess. Simultaneous measurements of both upward and downward leaf radiance ($L_{\text{up}}(\lambda)$, $L_{\text{dw}}(\lambda)$, $\text{W m}^{-2} \text{sr}^{-1} \text{nm}^{-1}$) in a proper set-up with an accuracy of $\pm 1 \text{ nm}$ and a resolution of $< 3 \text{ nm}$ allow to observe the specific absorbance changes at leaf level (Van Wittenberghe et al. 2019). Excessive incoming radiance ($> 1200 \mu\text{mol m}^{-2} \text{s}^{-1}$) given over the full photosynthetic active radiation (PAR, 400-700 nm) range was given for an adaptation time of 3 minutes for several tree species. For one of the species

FAAR abstract

(*Quercus robur*) 2h-dark-adapted shade and sun grown leaves were sampled as two leaf disks of 6 mm diameter and exposed to saturating light of approximately $1,600 \mu\text{mol m}^{-2} \text{s}^{-1}$ during respectively 1, 10, 20, 30, 40, 60, 90, 120, 180, 300 and 400 seconds before freezing them immediately in liquid N_2 for pigment analyses by HPLC.

RESULTS

In parallel to the dynamics of chlorophyll fluorescence (ChlF) upon 1Chl* excitation, the absorbance of vegetation shows a dynamic light-induced activation effect of the biochemical pigment pool changes related to the downregulation of photosynthesis. Upon this excessive light, the absorbance increases with a peak around 531 nm caused by the gradual conversion of photoprotective pigments, which attach to the antenna and redistribute the absorbed energy in the local environment of the antenna (Figure 1). The spectral changes of this absorbance feature show a sigmoidal behaviour saturating around 3 min after light exposure.

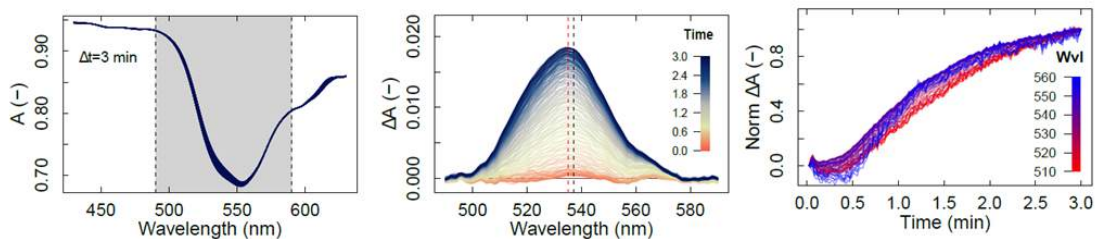


Figure 1. The absorbance (A), absorbance change (ΔA) and normalized ΔA of a *M. alba* leaf during a 3-min transient under excessive light in the 490-590 nm range

Quick xanthophyll pool (VAZ, LxL) conversions were analysed for the same time frame of light exposure in *Q. robur* sun and shade grown leaves showing the difference in light response of these pools (Figure 2).

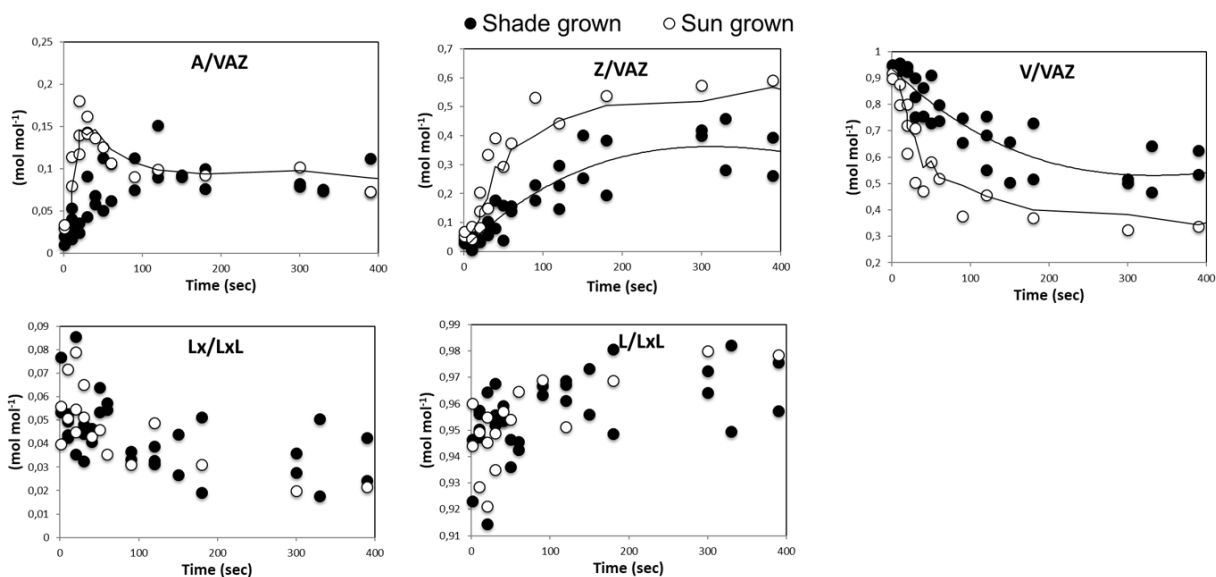


Figure 2. Conversion states of the VAZ and LxL pools during ± 5 min of excessive light exposure

The total LxL pool for sun leaves was slightly higher than for shade leaves (78.3 ± 10.0 vs. $70.2 \pm 11.0 \mu\text{mol m}^{-2}$), while the total VAZ pool was clearly higher for sun grown leaves (46.1 ± 9.4 vs. $23.0 \pm 3.6 \mu\text{mol m}^{-2}$). Both pools showed a quick de-epoxidation upon light excess (Figure 2) but sun grown leaves showed a quicker and stronger de-epoxidation of the VAZ pool. The conversions took place in the same time span as the spectral changes in the 490-590 nm range, as shown by other authors (Gamon et al. 1990; Peguero-Pina

et al. 2013). Interestingly, sun leaves showed a quicker and stronger conversion to antheraxanthin within the first 30 sec compared to the shade leaves. A higher VAZ/Chl a ratio for sun grown compared to shade grown leaves was measured (Figure 3), indicating a stronger relative pool with capacity to quench 1Chl a*.

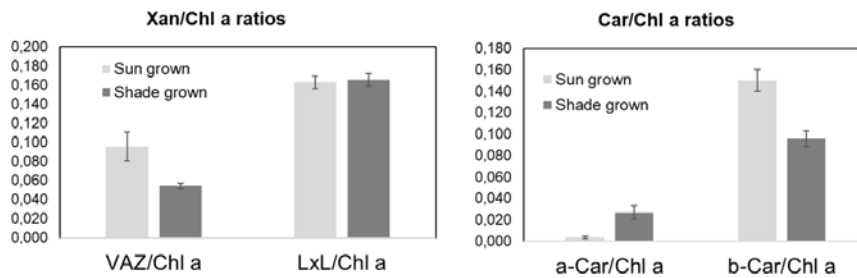


Figure 3. Xanthophyll and carotene vs. Chl a ratios

CONCLUSIONS

Short-term changes in the amount of absorbed sunlight at the leaf level and their link with energy quenching are explored in this research, revealing several biochemical and structural mechanisms related to the energy distribution under excessive light (Van Wittenberghe et al. 2019). The xanthophyll pools hereby play a crucial role in the quenching of 1Chl a*, but their direct role in this energy redistribution has been often disputed. Here, sun leaves of *Q. robur* showed almost a double relative VAZ/Chl a pool ratio compared to shade leaves, and fast reactivity of antheraxanthin within 20-30 sec. This quick in vivo conversion and reactivity of the Xan pools seems further to support their active role in the quick redistribution of excitation energy in the antenna, showing in parallel an absorbance increase in the 490-590 nm region. A good quantitative understanding of such mechanisms of energy regulation in plants is essential to better model the adaptations of vegetation to changing climate and environmental conditions, and to better predict future trends in global vegetation dynamical models.

ACKNOWLEDGEMENTS

The work was funded by the postdoctoral scholarship APOSTD/2018/162 funded by the Generalitat Valenciana and co-funded by the 'Fondo Social Europeo'.

REFERENCES

- Gamon JA, Field CB, W. Bilger, Björkman O, et al (1990) Remote sensing of the xanthophyll cycle and chlorophyll fluorescence in sunflower leaves and canopies. *Oecologia* 85:1–7
- García-Plazaola JI, Matsubara S, Osmond CB (2007) The lutein epoxide cycle in higher plants: Its relationships to other xanthophyll cycles and possible functions. *Funct Plant Biol* 34:759–773 . doi: 10.1071/FP07095
- Krüger TPJ, van Grondelle R (2017) The role of energy losses in photosynthetic light harvesting. *J Phys B At Mol Opt Phys* 50:132001
- Leuenberger M, Morris JM, Chan AM, et al (2017) Dissecting and modeling zeaxanthin- and lutein-dependent nonphotochemical quenching in *Arabidopsis thaliana*. *Proc Natl Acad Sci U S A* 114:E7009–E7017 . doi: 10.1073/pnas.1704502114
- Peguero-Pina JJ, Gil-Pelegrín E, Morales F (2013) Three pools of zeaxanthin in *Quercus coccifera* leaves during light transitions with different roles in rapidly reversible photoprotective energy dissipation and photoprotection. *J Exp Bot* 64:1649–1661 . doi: 10.1093/jxb/ert024
- Van Wittenberghe S, Alonso L, Malenovský Z, Moreno J (2019) In vivo photoprotection mechanisms observed from leaf spectral absorbance changes showing VIS – NIR slow - induced conformational pigment bed changes. *Photosynth Res* 1–23 . doi: 10.1007/s11120-019-00664-3

GREENHOUSE GAS FLUX MEASUREMENTS ON AN AGRICULTURAL GRASSLAND ON PEAT SOIL

H. VEKURI¹, A. LOHILA^{1,2}, L. KULMALA^{1,3}, J-P. TUOVINEN¹, J. RAINNE¹, T. MÄKELÄ¹, J. HATAKKA¹, E. JOKI-TOKOLA⁴, J. LISKI¹ and T. LAURILA¹

¹Finnish Meteorological Institute, Helsinki, Finland.

²Institute for Atmospheric and Earth System Research / Physics, Faculty of Science, University of Helsinki, Finland.

³Institute for Atmospheric and Earth System Research / Forest Sciences, Faculty of Agriculture and Forestry, University of Helsinki, Finland.

⁴Natural Resources Institute Finland, Oulu, Finland.

Keywords: EDDY COVARIANCE, CHAMBER MEASUREMENTS, CLIMATE SOLUTIONS

INTRODUCTION

Mitigation of climate change requires a rapid reduction in greenhouse gas (GHG) emissions but also sequestration of large quantities of carbon already in the atmosphere. Land-based measures, the so-called natural climate solutions, are considered the most efficient ways to remove and keep CO₂ away from the atmosphere (Paustian et al., 2016; Griscom et al., 2017; Smith et al., 2019). Climate-smart agriculture, afforestation, reforestation and peatland restoration are examples of such methods. To make these actions an accredited solution for climate policy, the amount of carbon sequestered must be quantified reliably.

Measuring soil carbon stock directly is slow, laborious and expensive, and has significant uncertainties due to high spatial variability. An alternative is to infer the change in soil carbon stock from greenhouse gas flux measurements between ecosystems and the atmosphere using flux chambers or eddy covariance (EC). EC measurements provide an area-averaged estimate of such fluxes and do not disturb the target surface. On the other hand, flux chambers are in practice the only option for studying spatial variability or different small-scale management options, such as fertilizer use and cover crops.

Finland has a globally high areal proportion of peatlands and as compared to mineral soils, drained peat soils experience greater carbon losses. This is due to accelerated decomposition of carbon-rich peat resulting from oxic conditions, fertilization and ploughing. Drained peat soils in agricultural use are widely considered as hot spots for greenhouse gas emissions but still their climatic impact has been incompletely quantified. Thus, we started studying agricultural grassland on peat soil in Ruukki, Siikajoki (64.68399°N, 25.10632°E) in western Finland in 2019 in order to quantify its climatic impact and to study the possibilities to reduce climate impacts via different agricultural management practices.

MATERIALS AND METHODS

The site consists of two main fields; the southern field growing a mixture of *Phleum pratense* and *Festuca pratensis* sown in 2018 and the northern field, which was sown with the same mixture of grasses and barley as a cover crop in spring 2019. The depth of the peat layer at the site is 30-70cm. Eddy covariance tower located between the fields has provided continuous measurements of the net ecosystem exchange rate of carbon dioxide between the atmosphere and the two fields since June 2019. The eddy covariance instrumentation consists of a three-axis ultrasonic anemometer uSonic-3 (METEK) and a LI-7200 CO₂/H₂O gas analyzer (Li-Cor, Inc) and the measurement height is 2.3m. Supporting meteorological and hydrological variables (temperature, rainfall, radiation, soil temperature and volumetric water content) and vegetation indices (leaf area index, chlorophyll content) are measured and will later be used for upscaling and gap-

filling the flux data. In addition, the effects of fertilizer type and timing of fertilization, cutting height and biodiversity on GHG fluxes (CO₂, CH₄ and N₂O) were studied on separate experiments using manual chambers during the growing season. Light response measurements were conducted using a transparent flux chamber accompanied with a Li840 CO₂/H₂O gas analyzer (Li-Cor, Inc).

RESULTS

The eddy covariance CO₂ exchange measurements started in Ruukki in June 2019 and have been running continuously aside from two relatively short breaks due to technical difficulties. The wind direction has been changing throughout the growing season and therefore the measurements have represented fluxes from both the southern field growing grass, and the northern field growing grass with barley as a cover crop (Fig. 1). The grass has been harvested twice, on 25-27.6.2019 and on 20.8.2019, and the harvests can be clearly seen in the eddy covariance data as more positive net ecosystem exchange (NEE) values. The chamber measurements will continue until November 2019 and the fluxes will be processed during the winter 2019-2020.

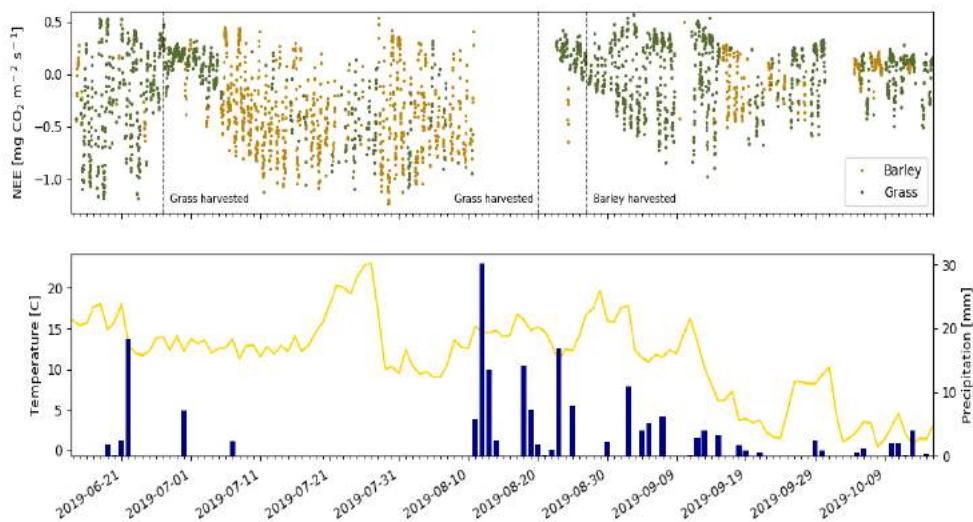


Figure 1. Net ecosystem CO₂ exchange (NEE, top panel) and daily mean air temperature and precipitation (lower panel) over a barley and grass field in Ruukki peat fields, mid-Finland, since June 2019.

ACKNOWLEDGEMENTS

SITRA, Business Finland, Strategic Research Council (SRC) at the Academy of Finland and the Finnish Centre of Excellence Programme by Academy of Finland are acknowledged for financial support. We thank the staff at FMI and Ruukki research station (Luke) for practical help.

REFERENCES

- Griscom, B. W., Adams, J., Ellis, P. W., Houghton, R. A., Lomax, G., Miteva, D. A., ... & Woodbury, P. (2017). Natural climate solutions. *Proceedings of the National Academy of Sciences*, 114(44), 11645-11650.
- Paustian, K., Lehmann, J., Ogle, S., Reay, D., Robertson, G. P., & Smith, P. (2016). Climate-smart soils. *Nature*, 532(7597), 49.

Smith, P., Soussana, J. F., Angers, D., Schipper, L., Chenu, C., Rasse, D. P., ... & Arias-Navarro, C. (2019). How to measure, report and verify soil carbon change to realize the potential of soil carbon sequestration for atmospheric greenhouse gas removal. *Global change biology*.

NOVEL ASSESSMENT OF BLACK CARBON IN THE EURASIAN ARCTIC (NABCEA): A SELECTION OF RESULTS AFTER THREE YEARS OF RESEARCH

A. VIRKKULA¹, J. PAATERO¹, E. ASMI¹, H. LIHAVAINEN¹, J. SVENSSON¹, M. VESTENIUS¹, P. RÄISÄNEN¹, A. HIENOLA¹, O. MEINANDER¹, H.-R. HANNULA¹, S. MANNINEN², M. RUPPEL², A. KORHOLA², J. TISSARI³, O. SIPPULA³, P. TIITTA³, M. IHALAINEN³, H. LAMBERG³, K. KUPIAINEN⁴, M. SAVOLAHTI⁴, V.-V. PAUNU⁴, N. KARVOSENOJA⁴

¹Finnish Meteorological Institute, Helsinki, Finland

²University of Helsinki, Department of Environmental Sciences, Helsinki, Finland

³University of Eastern Finland, Kuopio, Finland

⁴Finnish Environmental Institute, Helsinki, Finland

Keywords: Black carbon, Arctic, Scenarios

INTRODUCTION

Black carbon (BC) has been estimated to be the second most important climate warming pollutant after CO₂. The recently started 4-year project *Novel Assessment of Black Carbon in the Eurasian Arctic: From Historical Concentrations and Sources to Future Climate Impacts (NABCEA)*, 1 September 2016 – 31 August 2020, funded by the Academy of Finland, will produce new research knowledge on BC emitted from increased economic activity in the Arctic, especially flaring associated with oil and gas drilling, shipping, and domestic heating by small-scale wood combustion. These are increasing emission sources but their effects on Arctic climate change are not well known. The objective of NABCEA is to identify the most important BC sources affecting the warming and melting in the Arctic in the recent past, present and the future. The detailed goals of the project are 1) to quantify the contribution of the most important sources, especially flaring related to oil drilling, shipping, and wood combustion to the BC observed in the Arctic atmosphere, snow and ice in the present time and in the recent past, 2) to quantify the climate forcing of BC in the atmosphere and snow, and 3) to estimate how the above-mentioned processes/impacts affect Arctic climate during the next 50 years.

Here we present a selection of published results obtained during the first 3 years (2016-2019) of NABCEA.

METHODS

The project consists of field and laboratory experiments, analyses of existing field samples, and modeling. The five work packages (WP1 – WP5) of the project are depicted schematically in Figure 1.

In WP1, BC analyses will be made for ice core samples collected from glaciers in Svalbard, and lake sediment samples from north western Russia (flaring area), Finnish Lapland, and Svalbard to determine past BC concentrations and deposition in the Arctic. These data will help in the assessment of past and modeling of future climate impacts of BC pollution in the Arctic. The relative contribution of contemporary biomass versus fossil fuel combustion to the BC in the samples will be determined by radiocarbon measurements.

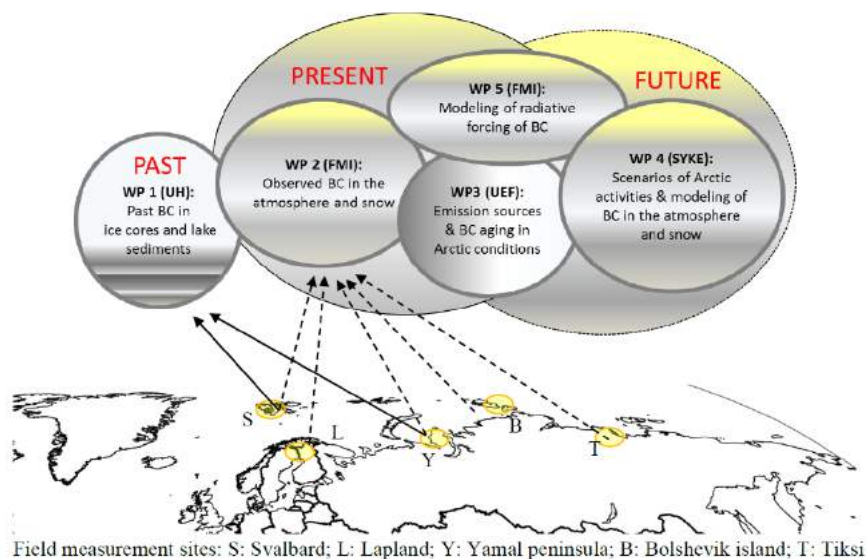


Figure 1. Field measurement sites and work packages of the NABCEA project.

An important goal of WP1 is to decipher whether the increase in BC concentrations observed in 1970-2004 in the Holtedahlfonna ice core (Ruppel et al., 2014) has continued, and whether it is a local signal or can be found in other glaciers and/or lake sediments as well. Ruppel et al. (2017) studied the BC deposition trend during the last 10 years on the previously studied Holtedahlfonna glacier. For this, a new 14.7m deep firn core and a 2.5m thick accumulated winter–spring snow profile were collected from Holtedahlfonna in April 2015. BC was analysed from the samples as elemental carbon (EC) with the same methodology (thermal–optical with the EUSAAR 2 protocol) as in Ruppel et al. (2014). In addition, the source of the BC deposited at the glacier was investigated using the SILAM model of FMI. Ruppel et al. (2017) found that the firn EC concentrations (from 2005 to 2015) are lower than the EC concentrations in the first half of the 1980s in the 300-year ice core. They also found that the modelled BC deposition at Holtedahlfonna is about a magnitude lower than the measured EC deposition in the ice and firn cores (Fig. 2) and that the modelled deposition does not show an increasing trend from ca. 2005 to 2015 as indicated by the firn core measurements (Fig. 2). One of the conclusions of Ruppel et al. (2017) was that precipitation and other meteorological factors (such as temperature and cloud phase (liquid, mixed or ice)) are crucial parameters as they drive the scavenging of BC, both on site and during the transport of BC to the Arctic. Consequently, it seems oversimplified to assume that the BC deposition trend would strictly follow its emission and/or atmospheric concentration trends.

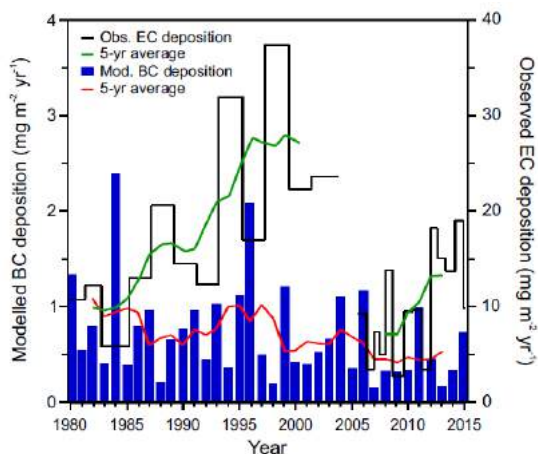


Figure 2. Modelled BC deposition compared to ice and firn core EC deposition at Holtedahlfonna from 1980 to 2015; 5-year running averages are included. Adapted from Ruppel et al. (2017).

In WP 2, the present BC concentrations in air and snow are determined from ground-based measurements at the Pallas-Sodankylä GAW station in Finnish Lapland, and at Tiksi, Yakutsk, in the Russian Siberia in cooperation with the Russian Roshydromet and the US NOAA. Snow samples have already been and will be collected from several sites in the Arctic: northern Scandinavia, Svalbard, and sites in northern Siberia. Samples will be taken in a gradient from near the sources (Yamal Peninsula, in respect of flaring) to the background (Tiksi (Siberia), Svalbard). Schmeisser et al. (2018) presented temporal evolution and seasonal cycles of aerosol optical properties from six Arctic monitoring stations Alert, Barrow, Pallas, Summit, Tiksi, and Zeppelin. Aerosol optical properties were derived from common absorption and scattering instruments. An important conclusion was that aerosol optical properties vary widely with season at any individual site, and they vary widely from station to station throughout the Arctic. An example of this is the seasonal cycle of absorption coefficient at the six stations. This result means that the Arctic cannot be treated as a uniform region.

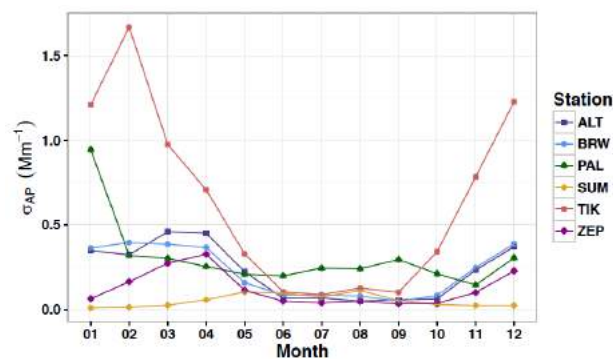


Figure 3. Monthly averages of of aerosol light absorption coefficient at 550 nm at six Arctic sites: Alert, Barrow, Pallas, Summit, Tiksi, and Zeppelin. Adapted from Schmeisser et al. (2018).

Mass absorption coefficients of BC in snow sampled from Finnish Lapland and a Himalayan site were determined first by making light transmittance measurements without any corrections (Svensson et al.,

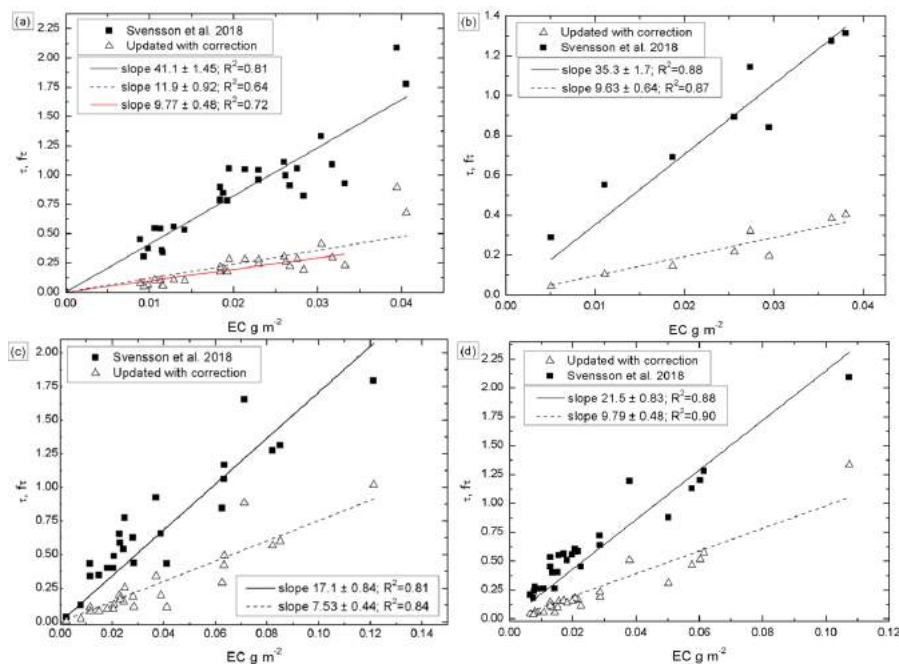


Figure 4. Reanalysis of regressions of Svensson et al. (2018). a) chimney soot, with the red line showing the slope with the two points with the highest EC content are excluded, b) NIST soot, c) field samples from the Indian Himalaya, d) field samples from Finnish Lapland. Adapted from Svensson et al. (2019).

2018) and then by taking nonlinearities of the transmittance measurements into account (Svensson et al., 2019). The MACs of field samples from the Indian Himalaya and from Finnish Lapland decreased from $17.1 \pm 0.8 \text{ m}^2 \text{ g}^{-1}$ and $21.5 \pm 0.8 \text{ m}^2 \text{ g}^{-1}$ to $7.5 \pm 0.4 \text{ m}^2 \text{ g}^{-1}$ and $9.8 \pm 0.5 \text{ m}^2 \text{ g}^{-1}$, respectively (Fig 4c and 4d). All slopes above are in the range of published MAC of BC.

In WP 3, the evolution of physical properties and chemical composition of BC aerosols emitted from burning processes will be studied in laboratory experiments at the University of Eastern Finland (UEF). Two experimental campaigns, one for flaring emissions and another for wood combustion emissions will be performed during the project. As far as wood combustion is concerned, Savolahti et al. (2019) concluded that wood heating is the least climate friendly option of the common heating methods in Finland, when all relevant emissions are taken into account. Kortelainen et al. (2019) showed that BC emissions vary during the burning in small-scale wood combustion and it is different for different types of wood (Fig. 5).

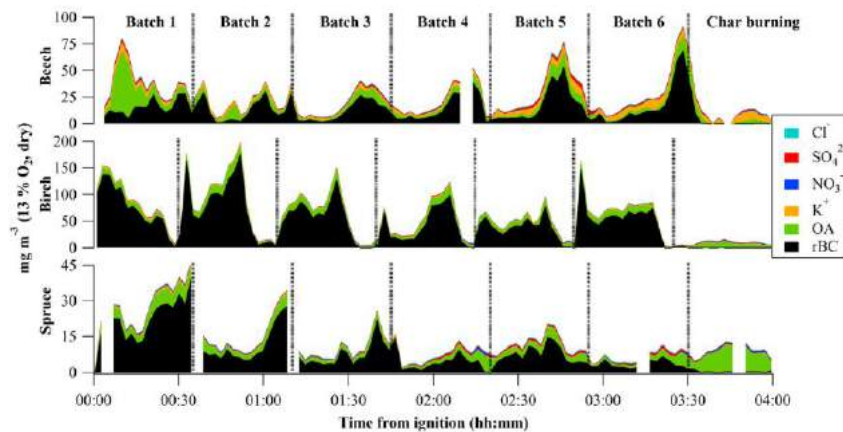


Figure 5. Chemical composition of particulate emissions during small-scale wood combustion, measured by SP-AMS. Adapted from Kortelainen et al. (2018).

In WP 4, Finnish Environment Institute (SYKE), in collaboration with the International Institute for Applied Systems Analysis (IIASA), will study the emissions and the resulting concentrations of BC in air and snow in the current and future Arctic. The scenarios will be done by using the Greenhouse Gas and Air Pollution Interactions and Synergies model (GAINS, gains.iiasa.ac.at). Special attention from the Arctic perspective will be paid to the emission sectors prioritized in this project. One of the tasks was to prepare global BC emission inventories, including emissions from flaring in oil/gas exploration with an explicit spatial allocation (Fig. 6) (Klimont et al., 2018).

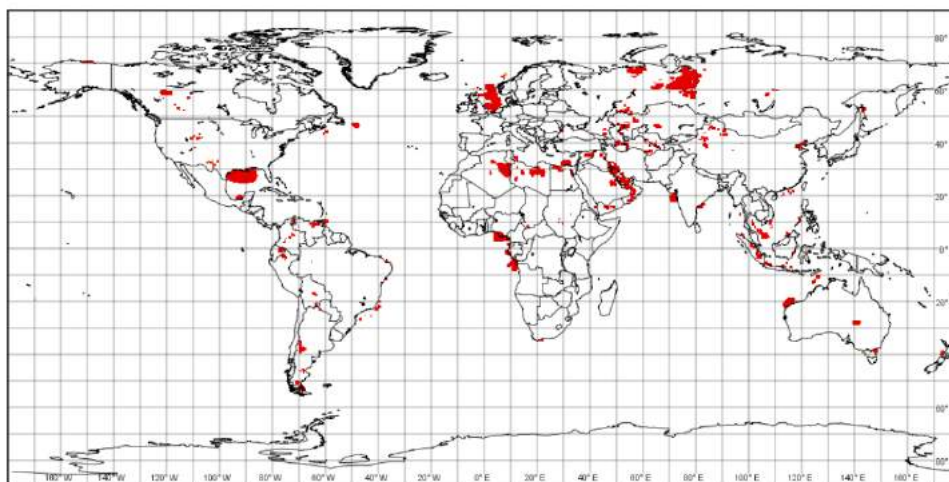


Figure 6. Global distribution of grids ($0.5^\circ \times 0.5^\circ$) for which flaring of associated petroleum gas emissions was calculated. Adapted from Klimont et al. (2017).

In WP 5, the current and future BC radiative forcing in an Arctic-wide scale will be estimated by using the NorESM climate model, which has a relatively sophisticated treatment of snow and aerosols. Emission scenarios developed in WP4 will be employed. This task will be supported by off-line radiation calculations and comparison of NorESM results with in situ observations collected in the projected. Räisänen et al. (2017) studied the sensitivity of simulated climate to the assumed snow grain shape. Two snow grain shape assumptions were considered: spherical snow grains (the default assumption in NorESM) and non-spherical snow grains. The primary conclusion from this work is that, especially at high latitudes, the simulated climate can be quite sensitive to the assumed snow grain shapes (Fig. 7), and most probably, to the parameterization of snow albedo in general.

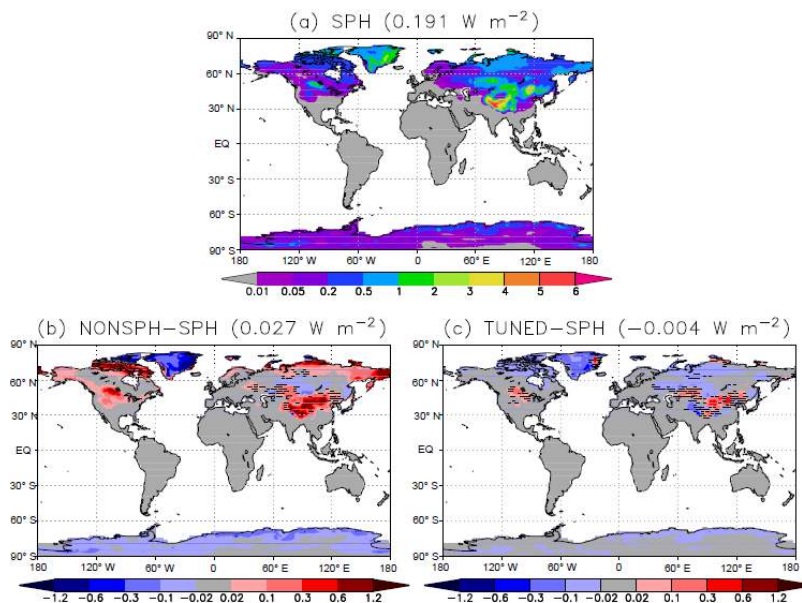


Figure 5. (a) Annual-mean surface radiative effect of absorbing aerosols in snow on land in the SPH experiment (W m^{-2}). (b) The corresponding differences between the NONSPH and SPH experiments, and (c) between the TUNED and SPH experiments. Global land-area mean values are given in the panel titles. Hatching indicates differences that exceed the threshold for colour shading (0.02 W m^{-2}) but are not significant at the 5% level. Adapted from Räisänen et al. (2017).

ACKNOWLEDGEMENTS

This work is supported by the Academy of Finland, decisions nr. 296302 and 307331.

REFERENCES

- Ruppel, M. M., Isaksson, E., Ström, J., Beaudon, E., Svensson, J., Pedersen, C. A., and Korhola, A. (2014) Increase in elemental carbon values between 1970 and 2004 observed in a 300-year ice core from Høltedahlfonna (Svalbard), *Atmos. Chem. Phys.*, **14**, 11447-11460.
- Ruppel, M. M., Soares, J., Gallet, J.-C., Isaksson, E., Martma, T., Svensson, J., Kohler, J., Pedersen, C. A., Manninen, S., Korhola, A., and Ström, J.: Do contemporary (1980–2015) emissions determine the elemental carbon deposition trend at Høltedahlfonna glacier, Svalbard?, *Atmos. Chem. Phys.*, **17**, 12779–12795, <https://doi.org/10.5194/acp-17-12779-2017>, 2017.
- Klimont, Z., Kupiainen, K., Heyes, C., Purohit, P., Cofala, J., Rafaj, P., Borken-Kleefeld, J., and Schöpp, W.: Global anthropogenic emissions of particulate matter including black carbon, *Atmos. Chem. Phys.*, **17**, 8681–8723, <https://doi.org/10.5194/acp-17-8681-2017>, 2017.

- Kortelainen, M., Jokiniemi, J., Tiitta, P., Tissari, J., Lamberg, H., Leskinen, J., et al: Time-resolved chemical composition of smallscale batch combustion emissions from various wood species. *Fuel*, 233, 224–236. <https://doi.org/10.1016/J.FUEL.2018.06.056>, 2018.
- Räisänen, P., Makkonen, R., Kirkevåg, A., and Debernard, J. B.: Effects of snow grain shape on climate simulations: sensitivity tests with the Norwegian Earth System Model, *The Cryosphere*, 11, 2919–2942, <https://doi.org/10.5194/tc-11-2919-2017>, 2017.
- Savolahti, M., Karvosenoja, N., Soimakallio, S., Kupiainen, K., Tissari, J., Paunu, V.-V. Near-term climate impacts of Finnish residential wood combustion. *Energy Policy*, 133, 110837, <https://doi.org/10.1016/j.enpol.2019.06.045>, 2019
- Schmeisser, L., Backman, J., Ogren, J. A., Andrews, E., Asmi, E., Starkweather, S., Uttal, T., Fiebig, M., Sharma, S., Eleftheriadis, K., Vratolis, S., Bergin, M., Tunved, P., and Jefferson, A.: Seasonality of aerosol optical properties in the Arctic, *Atmos. Chem. Phys.*, 18, 11599–11622, <https://doi.org/10.5194/acp-18-11599-2018>, 2018.
- Svensson, J., Ström, J., Kivekäs, N., Dkhar, N. B., Tayal, S., Sharma, V. P., Jutila, A., Backman, J., Virkkula, A., Ruppel, M., Hyvärinen, A., Kontu, A., Hannula, H.-R., Leppäranta, M., Hooda, R. K., Korhola, A., Asmi, E., and Lihavainen, H.: Light-absorption of dust and elemental carbon in snow in the Indian Himalayas and the Finnish Arctic, *Atmos. Meas. Tech.*, 11, 1403–1416, <https://doi.org/10.5194/amt-11-1403-2018>, 2018.
- Svensson, J., Ström, J., and Virkkula, A.: Multiple scattering correction factor of quartz filters and the effect of filtering particles mixed in water: implications to analyses of light-absorption in snow samples, *Atmos. Meas. Tech.*, <https://doi.org/10.5194/amt-2019-142>, in print, 2019.

TEMPERATURE RESPONSE TO EVAPORATION OF STRATIFORM PRECIPITATION IN IDEALIZED WRF SIMULATIONS

M. VIRMAN¹, M. BISTER¹, V.A. SINCLAIR¹, J. RÄISÄNEN¹ and H. JÄRVINEN¹

¹Institute for Atmospheric and Earth System Research, University of Helsinki, Helsinki, Finland.

Keywords: DEEP CONVECTION, HUMIDITY, PRECIPITATION

INTRODUCTION

Atmospheric deep convection is a major source of water vapour in the free-troposphere and a major contributor to large-scale circulations due to significant latent heat release. Any process that causes lower free-tropospheric warm anomalies may inhibit the formation of deep convection. A recent observational study by Virman *et al.* (2018) suggested that mesoscale convective systems (MCSs) are associated with such warming, thus likely being able to regulate the formation of new deep convection. More specifically, they hypothesized that warm anomalies form as result of strong evaporation of stratiform precipitation associated with MCSs and resulting subsidence warming. Here we conduct idealized simulations of falling stratiform precipitation to quantify the temperature structures associated with its evaporation.

METHODS

The idealized simulations are conducted with the Weather Research and Forecasting (WRF) model, and are initialized with a sounding representing moist tropical atmosphere (Dunion, 2011). In the simulations, a large round area (roughly 100 km in radius) of liquid water is added at every timestep at one model level near the zero isotherm, below which the rain is allowed to fall freely. The rain area is at the centre of a 1500x1500 km model domain. A double-moment microphysics scheme of Morrison *et al.* (2009) was used. Time step was 15 seconds, horizontal grid spacing 2.5 km, with 65 vertical levels between the surface and model top at 27 km.

CONCLUSIONS

After roughly two hours of precipitation, evaporative cooling and subsidence warming result in a cold anomaly between roughly 560-750 hPa and a warm anomaly between roughly 750-900 hPa (Figure 1a-c). The cold anomaly and the warm anomaly persist throughout the 10 hour long simulations, propagate to the environment (Figure 1d-f), and persist even after precipitation has stopped (not shown). The cold and the warm anomalies are larger when the initial relative humidity is decreased, due to stronger evaporative cooling and resulting stronger subsidence warming (not shown). The simulated temperature structures qualitatively resemble those observed after precipitation by Virman *et al.* (2018).

The warm anomalies, with magnitudes between 0.7-1.2 K depending on the initial relative humidity, are large enough to potentially inhibit the formation of new convection by increasing convective inhibition (Raymond *et al.*, 2003). As already suggested by Virman *et al.*, evaporation of stratiform precipitation may therefore, at least partly, explain why deep convection is sensitive to the amount of moisture in the lower free-troposphere.

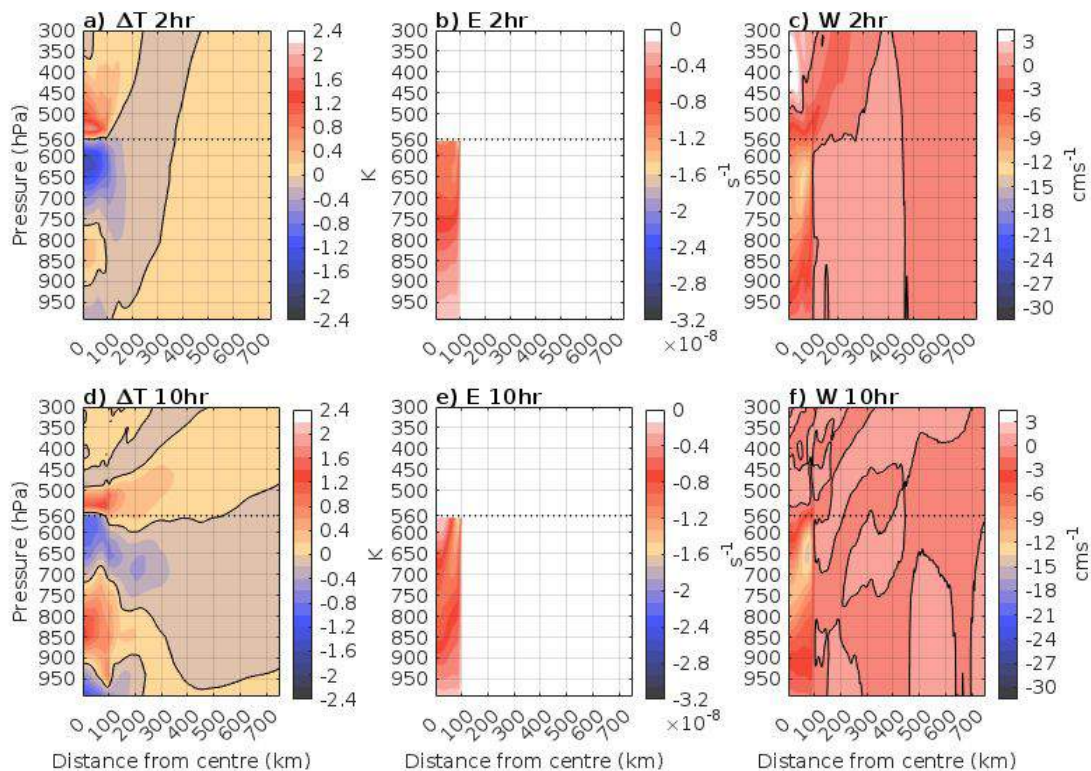


Figure 1. Vertical cross-sections of temperature anomaly, evaporation and vertical velocity at 2 hours (upper panel) and 10 hours (lower panel) into the simulations. Black dotted line indicates the level where rain is added and the black solid line is the zero contour. The edge of the round rain area is at roughly 100 km.

The dependence of deep convection on the amount of lower free-tropospheric moisture has been studied extensively (e.g. Bretherton *et al.*, 2004). However, the underlying mechanisms have not been entirely understood and numerical weather prediction and climate models still struggle to represent the occurrence of deep convection realistically (Kim *et al.*, 2011; Kim *et al.*, 2018; Bechtold, 2019). The results of this study and Virman *et al.* suggest that in order for deep convection to occur correctly in numerical weather prediction and climate models, evaporation of stratiform precipitation and the associated processes should be represented realistically in them.

ACKNOWLEDGEMENTS

This work was funded by the Vilho, Yrjö and Kalle Väisälä Foundation and by the Academy of Finland (project no. 307331). The simulations were conducted using the high performance computing services of CSC - IT Center for Science.

REFERENCES

- Bechtold, P. (2019). Challenges in tropical numerical weather prediction at ECMWF. *Current Trends in the Representation of Physical Processes in Weather and Climate Models*, Springer, 29-50.
- Bretherton, C.S., M.E. Peters, and L.E. Back (2004). Relationships between water vapor path and precipitation over the tropical oceans. *J. Climate* **17** (7), 1517–1528.
- Dunion, J.P. (2011). Rewriting the climatology of the tropical North Atlantic and Caribbean Sea

- atmosphere. *J. Climate* **24** (3), 893–908.
- Kim, D., A.H. Sobel, E.D. Maloney, D.M. Frierson and I.-S. Kang (2011). A systematic relationship between intraseasonal variability and mean state bias in AGCM simulations. *J. Climate* **24** (21), 5506–5520.
- Kim, H., F. Vitart, and D.E. Waliser (2018). Prediction of the Madden-Julian Oscillation: A review. *J. Climate* **31** (23), 9425–9443.
- Morrison, H., G. Thompson, and V. Tatarskii (2009). Impact of cloud microphysics on the development of trailing stratiform precipitation in a simulated squall line: Comparison of one- and two-moment schemes. *Mon. Wea. Rev.* **137** (3), 991–1007.
- Raymond, D.J., G.B. Raga, C.S. Bretherton, J. Molinari, C. López-Carrillo, and Z. Fuchs (2003). Convective forcing in the intertropical convergence zone of the eastern pacific. *J. Atmos. Sci.* **60** (17), 2064–2082.
- Virman, M., M. Bister, V.A. Sinclair, H. Järvinen, and J. Räisänen (2018). A new mechanism for the dependence of tropical convection on free-tropospheric humidity. *Geophys. Res. Lett.* **45** (5), 2516–2523.

CARBON DIOXIDE AND METHANE FLUXES OVER A BOREAL RIVER MEASURED WITH EDDY COVARIANCE

A. VÄHÄ¹, M. AURELA², S. GUSEVA³, K.-M. KOHONEN¹, A. LINDROTH⁴, A. LORKE³, S. MACINTYRE⁵, J. MELACK⁵, A. OJALA^{1,6,7}, T. VESALA^{1,6}, M. WALLIN⁸, I. MAMMARELLA¹

¹Institute for Atmospheric and Earth System Research INAR/Physics, Faculty of Science, University of Helsinki, Helsinki, Finland.

²Finnish Meteorological Institute, Helsinki, Finland.

³Institute for Environmental Sciences, University of Koblenz-Landau, Landau, Germany.

⁴Department of Physical Geography and Ecosystem Science, Lund University, Lund, Sweden.

⁵Department of Ecology, Evolution and Marine Biology, University of California, Santa Barbara, California.

⁶Institute for Atmospheric and Earth System Research INAR/Forest Sciences, Faculty of Agriculture and Forestry, University of Helsinki, Helsinki, Finland.

⁷Faculty of Biological and Environmental Sciences, University of Helsinki, Lahti, Finland.

⁸Department of Earth Sciences, Uppsala University, Uppsala, Sweden.

Keywords: river, greenhouse gas, eddy covariance, flux.

INTRODUCTION

Rivers have a significant role in the lateral transport of carbon from terrestrial ecosystems to the ocean. As rivers are generally supersaturated with CO₂ with respect to the atmospheric concentration (Raymond et al. 2013), their turbulent nature may make them effective emitters of carbon into the atmosphere (Allen and Pavelsky 2018). Rivers cover a varying fraction of the total land area. The largest coverages of up to 2% are found in the boreal zone, Southeast Asia and the Amazon (Allen and Pavelsky 2018). The flux of carbon from boreal rivers into the atmosphere is therefore potentially large.

The eddy covariance (EC) technique enables the direct measurement of turbulent fluxes within the flux source area. EC is a robust and widely used method for measuring trace gas and energy fluxes between land ecosystems and the atmosphere (Baldocchi 2014). More recently, advances have been made in applying EC over lakes but the methodology is not yet as established as on land (Mammarella et al. 2015). For rivers however, there exists only one previous campaign where greenhouse gas fluxes were measured using the EC method (Huotari et al. 2013). In addition, most of the earlier riverine flux studies, mainly conducted with flux chambers, have been carried out in temperate or tropical regions. Consequently, fluxes from the boreal rivers form a considerable knowledge gap.

From June to October 2018, the international KITE campaign on the river Kitinen was arranged. The aim of the campaign was to measure the turbulent greenhouse gas and energy fluxes over a boreal river with an EC system throughout the growing season as well as all the essential supporting variables, so that a comprehensive view of the river–atmosphere greenhouse gas fluxes and their physical rivers could be formed.

METHODS

The boreal river Kitinen is located in northern Finland. It is 235 km long and its catchment area is 7 672 km². The catchment area comprises mostly of coniferous forest, wetlands and a few low fells. An EC

system as well as several other instruments were set up on a floating platform, anchored in the middle of the river next to the Tähtelä research station of the Finnish Meteorological Institute (coordinates: 67.37° N, 26.62° E). The river is 180 m wide at the experiment site and approximately straight for 0.7 km upstream (north-northwest) and 1.1 km downstream (south-southeast).

On the platform, the turbulent carbon dioxide (CO₂) and methane (CH₄) fluxes above the river were measured. The EC system consisted of a METEK uSonic-3 sonic anemometer, a LI-COR LI-7200 gas analyser for measuring the CO₂ and H₂O concentration and a Picarro G-1301f gas analyser for measuring the CH₄ concentration. The system was set up at a height of approximately 2 m above the river surface. Additionally, the carbon dioxide concentration in the river surface water was measured with Los Gatos UGGA and CONTROS HydroC gas analysers, making it possible to calculate the gas exchange coefficient for CO₂. Other measured parameters included flow velocity, river temperature profile, river oxygen concentration, meteorological variables and several others.

The campaign provided with EC flux data from the 15th of June to the 2nd of October of 2018. The data were quality-flagged and wind direction-flagged so that only the good-quality fluxes that originated from the river were included in the data analysis. The accepted wind sectors were determined using flux footprint analysis. The temporal coverage of the quality and wind direction-flagged data was 34% for the CO₂ flux and 26% for the CH₄ flux.

RESULTS

Throughout the campaign, the river was supersaturated with CO₂. The aqueous CO₂ concentration varied between 550 and 1320 ppm. The wind was channeled along the river during approximately half of the campaign, making it possible to measure fluxes from the river with EC.

The mean carbon dioxide flux during the campaign was 0.8 μmol m⁻² s⁻¹. The monthly mean flux was highest in July. The CO₂ flux had a diurnal variation such that the daytime fluxes were smaller than the nighttime fluxes. In June, the CO₂ flux at around the local noon was slightly negative, or from the atmosphere into the river. Apart from that however, the river was a source of carbon dioxide during the campaign.

The mean methane flux during the campaign was 5 nmol m⁻² s⁻¹. The monthly mean CH₄ flux was also highest in July. Unlike the CO₂ flux, the CH₄ showed no diurnal cycle and the river was a constantly a source, although small, of CH₄. Both the CO₂ and CH₄ flux had significant variation, the standard deviation being 2.2 μmol m⁻² s⁻¹ for the CO₂ flux and 15 nmol m⁻² s⁻¹ for the CH₄ flux. The variability of fluxes was higher during nighttime than during daytime.

The mean gas exchange coefficient k_{600} was 19 cm h⁻¹. This value is comparable to the one determined by Huotari et al. (2013) and the ones revised by Lauerwald et al. (2015). Although there was much scatter in the values, the coefficient was slightly and positively correlated with the wind speed except for small wind speeds (< 1 m s⁻¹). The gas exchange between the river and the atmosphere therefore increases with an increasing wind speed.

CONCLUSIONS

The turbulent carbon dioxide and methane fluxes were measured with eddy covariance on the boreal river Kitinen during four months of summer and autumn in 2018. The river emitted both CO₂ and CH₄ throughout the campaign, except during daytime in June when the river was absorbing CO₂. The CO₂ flux had a diurnal pattern of higher nighttime fluxes whereas the CH₄ had no diurnal variation. The gas exchange between the river and the atmosphere was increased by increasing wind speed. The measured

fluxes were generally small and the variability was high, which is a sign of the many challenges in applying the eddy covariance method over water bodies.

ACKNOWLEDGEMENTS

This work was supported by the Academy Professor projects (312571 and 282842) and ICOS-Finland (281255) by the Academy of Finland.

REFERENCES

- Allen, B. H. and T. M. Pavelsky (2018). Global extent of rivers and streams. *Science*, 361(6402), 585–588, doi:10.1126/science.aat0636.
- Baldocchi, D. (2014). Measuring fluxes of trace gases and energy between ecosystems and the atmosphere – the state and future of the eddy covariance method. *Global Change Biology*, 20(12), 3600–3609, doi:10.1111/gcb.12649.
- Huotari, J., S. Haapanala, J. Pumpanen, T. Vesala and A. Ojala (2013). Efficient gas exchange between a boreal river and the atmosphere. *Geophysical Research Letters*, 40(21), 5683–5686, doi:10.1002/2013GL057705.
- Lauerwald, R., G. G. Laruelle, J. Hartmann, P. Ciais and P. A. G. Regnier (2015). Spatial patterns in CO₂ evasion from the global river network. *Global Biogeochemical Cycles*, 29, 534–554, doi:10.1002/2014GB004941.
- Mammarella, I., A. Nordbo, Ü. Rannik, S. Haapanala, J. Levula, H. Laakso, A. Ojala, O. Peltola, J. Heiskanen, J. Pumpanen and T. Vesala (2015). Carbon dioxide and energy fluxes over a small boreal lake in Southern Finland. *Journal of Geophysical Research: Biogeosciences*, 120(7), 1296–1314, doi:10.1002/2014JG002873.
- Raymond, P. A., J. Hartmann, R. Lauerwald, S. Sobek, C. McDonald, M. Hoover, D. Butman, R. Striegl, E. Mayorga, C. Humborg, P. Kortelainen, H. Dürr, M. Meybeck, P. Ciais and P. Guth (2013). Global carbon dioxide emissions from inland waters. *Nature*, 503(7476), 355–359, doi:10.1038/nature12760.

**EXPLORING THE REGIONAL POLLUTION CHARACTERISTICS AND
METEOROLOGICAL FORMATION MECHANISM OF PM_{2.5} AND O₃ IN NORTH CHINA
DURING 2013-2017**

LILI WANG^{1,3}, MINGGE LI^{1,7}, JINGDA LIU^{1,8}, JIA MAO^{1,8}, WENKANG GAO¹, TAO SONG¹, YANG SUN¹, LIANG LI⁴, XINGRU LI⁶, YONGHONG WANG³, LILI LIU⁵, KASPAR R. DAELLENBACH³, PAULI J PAASONEN³, VELI-MATTI KERMINEN³, YUESI WANG^{1,2,7,8}, MARKKU KULMALA^{3,9}

¹State Key Laboratory of Atmospheric Boundary Layer Physics and Atmospheric Chemistry (LAPC),
Institute of Atmospheric Physics, Chinese Academy of Sciences, Beijing, 100029, China

²Centre for Excellence in Atmospheric Urban Environment, Institute of Urban Environment, Chinese
Academy of Science, Xiamen, Fujian 361021, China

³Institute for Atmospheric and Earth System Research / Physics, Faculty of Science, University of
Helsinki, Finland

⁴China National Environmental Monitoring Center, Beijing, 100012

⁵Tianjin Institute of Meteorological Science, Tianjin 300074, China

⁶Department of Chemistry, Analytical and Testing Center, Capital Normal University, Beijing 100048,
China

⁷University of the Chinese Academy of Sciences, Beijing, 100049, China

⁸Department of Atmospheric Physics, Nanjing University of Information Science & Technology, Nanjing,
210044, China

⁹Aerosol and Haze Laboratory, Beijing Advanced Innovation Center for Soft Matter Science and
Engineering, Beijing University of Chemical Technology, Beijing, China

ABSTRACT

In the last decade, North China (NC) has been one of the most populated and polluted regions in the world. The regional air pollution has had a serious impact on people's health; thus, all levels of government have implemented various pollution prevention measures since 2013. Based on multi-city in situ environmental and meteorological data, as well as the meteorological reanalysis dataset from 2013 to 2017, regional pollution characteristics and meteorological formation mechanisms were analyzed to provide a more comprehensive understanding of the evolution of PM_{2.5} and O₃ in NC.

The domain-averaged PM_{2.5} was 79±17 µg m⁻³ from 2013 to 2017, with a decreasing rate of 10 µg m⁻³ yr⁻¹. Two automatic computer algorithms were established to identify 6 daily regional pollution types (DRPTs) and 48 persistent regional pollution events (PRPEs) over NC during 2014-2017. The average PM_{2.5} concentration for the Large-Region-Pollution type (including the Large-Moderate-Region-Pollution and Large-Severe-Region-Pollution types) was 113±40 µg m⁻³, and more than half of Large-Region-Pollution days and PRPEs occurred in winter. The PRPEs in NC mainly developed from the area south of Hebei. The number of Large-Region-Pollution days decreased notably from 2014 to 2017, the annual number of days varying between 194 and 97 days, whereas a slight decline was observed in winter. In addition, the averaged PM_{2.5} concentrations and the numbers and durations of the PRPEs decreased. Lamb-Jenkinson weather typing was used to reveal the impact of synoptic circulations on PM_{2.5} across NC. Generally, the contributions of the variations in circulation to the reduction in PM_{2.5} levels over NC between 2013 and 2017 were 64% and 45% in summer and winter, respectively. The three most highly polluted weather types were types C, S and E, with an average PM_{2.5} concentration of 137±40 µg m⁻³ in winter. Furthermore, three typical circulation dynamics were categorized in the peak stage of the PRPEs, namely, the southerly airflow pattern, the northerly airflow pattern and anticyclone pattern; the averaged relative humidity, recirculation index, wind speed and boundary layer height were 63%, 0.33, 2.0 m s⁻¹ and 493 m, respectively.

The domain-averaged maximum daily 8-h running average O₃ (MDA8 O₃) concentration was 122±11 µg m⁻³, with an increase rate of 7.88 µg m⁻³ year⁻¹, and the three most polluted months were closely related to the variations in the synoptic circulation patterns, which occurred in June (149 µg m⁻³), May (138 µg m⁻³) and July (132 µg m⁻³). Twenty-six weather types (merged into 5 weather categories) were objectively identified using the Lamb-Jenkinson method. The highly-polluted weather categories included S-W-N directions (geostrophic wind direction diverts from south to north), low-pressure related weather types (LP) and cyclone type, which the study area controlled by low-pressure center (C), and the corresponding domain-averaged MDA8 O₃ concentrations were 122, 126 and 128 µg m⁻³, respectively. Based on the frequency and intensity changes of the synoptic circulation patterns, 39.2% of the interannual increase in the domain-averaged O₃ from 2013 to 2017 was attributed to synoptic changes, and the intensity of the synoptic circulation patterns was the dominant factor. Using synoptic classification and local meteorological factors, the segmented synoptic-regression approach was established to evaluate and forecasted daily ozone variability on an urban scale. The results showed that this method is practical in most cities, and the dominant factors are the maximum temperature, southerly winds, relative humidity on the previous day and on the same day, and total cloud cover. Overall, 41-63% of the day-to-day variability in the MDA8 O₃ concentrations was due to local meteorological variations in most cities over North China, except for two cities: QHD (Qinhuangdao) at 34% and ZZ (Zhengzhou) at 20%.

An intensive and persistent regional ozone pollution event occurred over eastern China from 25th June to 5th July in 2017. During the pollution process, 73 out of 96 selected cities, most of which located in Beijing-Tianjin-Hebei and its surroundings (BTHS), suffered severe ozone pollution. A north-south contrast ozone distribution, with higher ozone (199 ± 33 µg/m³) in BTHS and lower ozone (118 ± 25 µg/m³) in Yangtze River Delta (YRD), was found dominated by the position of West Pacific Subtropical High (WPSH) and mid-high-latitudes wave activities. In BTHS, the positive anomalies of geopotential height at 500 hPa and temperature at surface indicated favorable meteorological conditions for local ozone formation. Prevailing northwesterly winds in the mid-high troposphere and warm advection induced by weak southerly winds in the low troposphere resulted in low-moderate relative humidity (RH), less cloud cover (TCC), strong solar radiation and high temperature at surface. On one hand, deep sinking motion and inversion layer can suppress the dispersion of pollutants. On the other hand, O₃-rich air in the upper layer was maintained at night due to temperature inversion, which facilitated O₃ vertical transport to surface in the next day morning

due to elevated convection. Generally, temperature, UV radiation, and RH showed good correlations with O₃ in BHTS, with the rate of 8.51 (μg/m³)/°C within the temperature range of 20-38°C, 59.54 (μg/m³)/(MJ/m²) and -1.93 (μg/m³)/%, respectively. The results can provide a better understanding of regional O₃ pollution and suggestion for air quality control strategies over eastern China.

Our quantitative exploration of the influence of both synoptic and local meteorological factors on PM_{2.5} and ozone variability will provide a scientific basis for evaluating emission reduction measures that have been implemented by the national and local governments to mitigate air pollution in North China, in addition, our results imply that additional emission reduction measures should be implemented under unfavorable meteorological situations to attain ambient air quality standards in the future.

Keywords: North China, PM_{2.5}, Surface O₃, Regional pollution events, Identification of regional pollution type, Meteorological formation mechanism, Synoptic patterns

ACKNOWLEDGEMENTS

This work was partially supported by the grant of National Key R&D Plan (Quantitative Relationship and Regulation Principle between Regional Oxidation Capacity of Atmospheric and Air Quality 2017YFC0210003), the National Natural Science Foundation of China (No. 41505133&41775162), National research program for key issues in air pollution control (DQGG0101) and the program of China Scholarships Council. We thank European Research Council via ATM-GTP 266 (742206), and Academy of Finland Centre of Excellence in Atmospheric Sciences (grant number: 272041).

FORMATION OF HIGHLY OXIDIZED MULTIFUNCTIONAL ORGANIC COMPOUNDS FROM CHLORINE ATOM INITIATED OXIDATION OF ALPHA-PINENE

YONGHONG WANG¹, MATTHIEU RIVA^{2,1}, HONGBIN XIE¹, LIINE HEIKKINEN¹, AND MIKAEL EHN¹

¹Department of Physics, University of Helsinki, Finland

²Univ Lyon, Université Claude Bernard Lyon 1, CNRS, IRCELYON, F-69626, Villeurbanne, France

INTRODUCTION

Highly oxidized multifunctional organic compounds (HOMs) from oxidation of α -pinene in the atmosphere can irreversibly condense to particles and contribute to secondary organic aerosol formation. Recently, the formation of nitryl chloride (ClNO₂) from heterogeneous reactions, and subsequent photolysis of nitryl chloride to produce chlorine atom is suggested to be extensive in the atmosphere. However, the oxidation of monoterpenes such as α -pinene by chlorine radicals has received very little attention, and the ability of this reaction to form HOM is completely unstudied.

METHOD

Here, chamber experiments were conducted with α -pinene and chlorine gas under low NO and high NO conditions, respectively. A NO₃-based CI-APi-L-TOF was used to measure highly oxidized products. Simultaneously, other state-of-the-art instruments were used to measure other parameters in the chamber. Clear distributions of monomers with 9-10 carbon atoms and dimers with 18-20 carbon atoms were observed under low NO conditions. With increased concentration of NO in the chamber, the formation of dimers was suppressed due to the competition reactions of peroxy radicals with NO. We calculated the HOMs yields from chlorine-initiated oxidation of α -pinene under low NO conditions, while the yield at high NO could not be determined because of interference from ozone produced from the NO_x, which subsequently reacted with α -

pinene.

CONCLUSION

Our study demonstrates that chlorine radical initiated oxidation of alpha-pinene will produce low volatility organic compounds, especially these HOMs, which indicates that autoxidation processes in chlorine radical oxidation of a-pinene will be important. Further analysis will provide insights on the expected importance of the studied reactions in the atmosphere.

ACKNOWLEDGEMENTS

This work is supported by Academy of Finland via Center of Excellence in Atmospheric Sciences.

Reference

- Crouse, J. D., Nielsen, L. B., Jørgensen, S., Kjaergaard, H. G. and Wennberg, P. O.: Autoxidation of organic compounds in the atmosphere, *J. Phys. Chem. Lett.*, 4(20), 3513–3520, doi:10.1021/jz4019207, 2013.
- Ehn, M., Thornton, J. A., Kleist, E., Sipilä, M., Junninen, H., Pullinen, I., Springer, M., Rubach, F., Tillmann, R., Lee, B., Lopez-Hilfiker, F., Andres, S., Acir, I.-H., Rissanen, M., Jokinen, T., Schobesberger, S., Kangasluoma, J., Kontkanen, J., Nieminen, T., Kurtén, T., Nielsen, L. B., Jørgensen, S., Kjaergaard, H. G., Canagaratna, M., Maso, M. D., Berndt, T., Petäjä, T., Wahner, A., Kerminen, V.-M., Kulmala, M., Worsnop, D. R., Wildt, J. and Mentel, T. F.: A large source of low-volatility secondary organic aerosol, *Nature*, 506(7489), 476–479, doi:10.1038/nature13032, 2014.
- Thornton, J. A., Kercher, J. P., Riedel, T. P., Wagner, N. L., Cozic, J., Holloway, J. S., Dubé, W. P., Wolfe, G. M., Quinn, P. K., Middlebrook, A. M., Alexander, B. and Brown, S. S.: A large atomic chlorine source inferred from mid-continental reactive nitrogen chemistry, *Nature*, 464(7286), 271–274, doi:10.1038/nature08905, 2010.

DEPOSITION ICE NUCLEATION ON CLOUD SEEDING AGENTS

A. WELTI¹, A.A. PIEDEHIERRO¹, Y.VIISANEN¹, A. VIRTANEN², K. KORHONEN² and A. LAAKSONEN^{1,2}

¹ Finnish Meteorological Institute, Helsinki, Finland

²Department of Applied Physics, University of Eastern Finland, Kuopio, Finland

Keywords: Cloud seeding, ice nucleation, water adsorption.

INTRODUCTION

Seeding cold clouds with the intent of artificially enhancing rain, producing snow or cloud dispersion, is worldwide practice. Since the start of cloud seeding operations, several seeding agents have been experimented on to achieve optimal results. High ice nucleation onset temperature is common to all seeding agents, but little information on their humidity dependent activity is available. To investigate the mechanisms how deposition ice nucleation on seeding agents works at water sub-saturated conditions, we characterize the ice nucleation activity of *AgI*, *PbI₂* and Phloroglucinol experimentally and compare the measurements with current theories.

METHODS

Ice nucleation in the deposition mode is measured using a modified version of SPIN, equipped to perform experiments down to 213K. By scanning the T-RH_i-space above ice saturation up to water saturation in a broad temperature range, a sample specific map of its ice nucleation activity is obtained. The maps of ice nucleation activity are compared to theoretically predicted conditions of ice nucleation from classical nucleation theory of deposition nucleation (Fletcher, 1962), pore condensation freezing (Marcolli, 2014) and adsorption nucleation theory (Laaksonen and Malila, 2016). Necessary input parameters for these theories are obtained experimentally using the same samples as for the ice nucleation experiments.

Adsorption isotherms of *H₂O* and *N₂* on sample powders are measured with a Belsorp-MaxII instrument and are used to determine Brunauer-Emmett-Teller (BET) surface area and the amount of adsorbed water as function of saturation ratio (p/p_0). Water adsorption isotherms are fitted using the Frenkel-Halsey-Hill (FHH) equation.

Contact angles are measured using a Drop Shape Analyzer DSA100. Droplets are placed on a sample covered surface and illuminated from one side. Images of the droplet are recorded on the opposite side to measure the contact angle. It is assumed that the contact angle between a sample and a water droplet is similar to the contact angle of an ice germ and the sample.

Results of adsorption and contact angle measurements are used as input parameters to predict the conditions of ice nucleation. Examples of calculated onset conditions of ice nucleation are shown in Fig. 1.

Classical nucleation theory allows to calculate the fraction of ice forming particles AF by

$$AF = 1 - \exp \left[-\mathcal{K} \cdot \exp \left(-\frac{\Delta G \cdot f_{\text{het}}(\alpha)}{kT} \right) \mathcal{A} \cdot t \right] \quad (1)$$

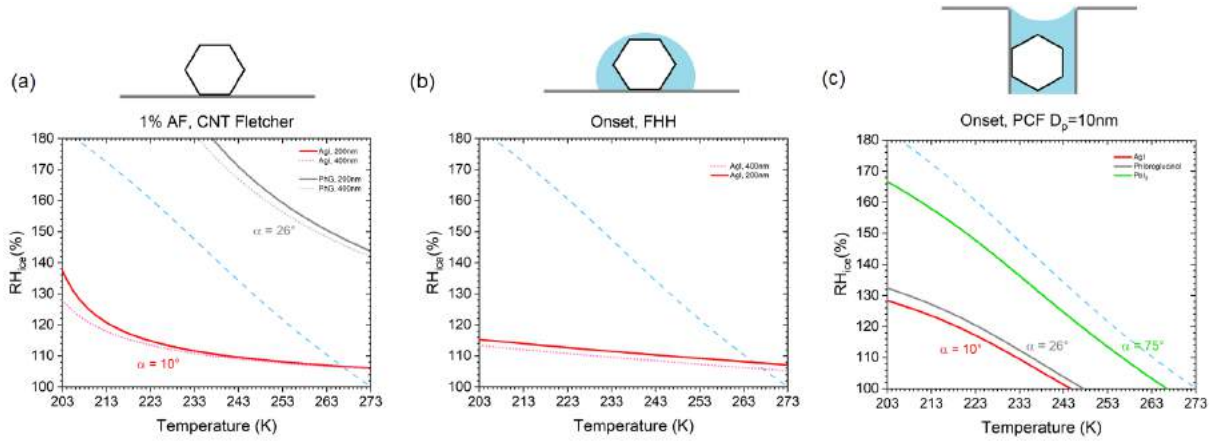


Figure 1: Theoretical predicted conditions of ice nucleation onset for AgI , PbI_2 and Phloroglucinol using (a) classical nucleation theory (Eq.1), (b) adsorption nucleation theory (Eq.2), (c) pore condensation freezing (Eq.3). The concept of ice nucleation described by the theory is illustrated above the corresponding subfigure.

where \mathcal{K} is the pre-exponential factor, ΔG is Gibbs free energy, $f_{het}(\alpha)$ is the contact angle dependent wetting factor, \mathcal{A} is surface area of the particle, k is Boltzmann's constant, T is temperature, and t is time.

The onset saturation of ice nucleation is derived by the FHH adsorption nucleation theory from

$$\ln(S) = -A \cdot N^B + \frac{2\gamma v}{kTr_g} \quad (2)$$

where S denotes onset saturation, A and B are FHH parameters, N the number of adsorbed monolayers, γ is surface tension, v is the volume of a water molecule, and r_g is the radius of the critical ice germ. N and r_g can be related to the contact angle α and the radius of the adsorbent particle.

Saturation conditions where pores or cavities fill up with water and can freeze by immersion or homogeneous freezing are derived from

$$S = \exp \left[\frac{-4\gamma v}{\frac{D}{\cos(\alpha)} \cdot RT} \right] \quad (3)$$

where D is the pore diameter and R the ideal gas constant.

RESULTS

The experiments show that high onset temperature do not coincide with high activity at low humidity in all cases. For ice nucleation on 400nm AgI particles, RH_i well above ice saturation is required (see Fig.2 c). The prediction from pore condensation freezing (Fig.1 c) matches the experimental result. However, AgI is not expected to have a porous surface and measurements of adsorption isotherms confirm the absence of pores. Phloroglucinol and PbI_2 nucleate ice at low RH_i with a characteristic increase at the lowest explored temperatures (see Fig.2 a and b). This increase is consistent with classical nucleation theory (Fig.1 b). However, classical nucleation theory under-predicts the absolute ice activity if contact angles measured in this study are used as input parameter for the calculation.

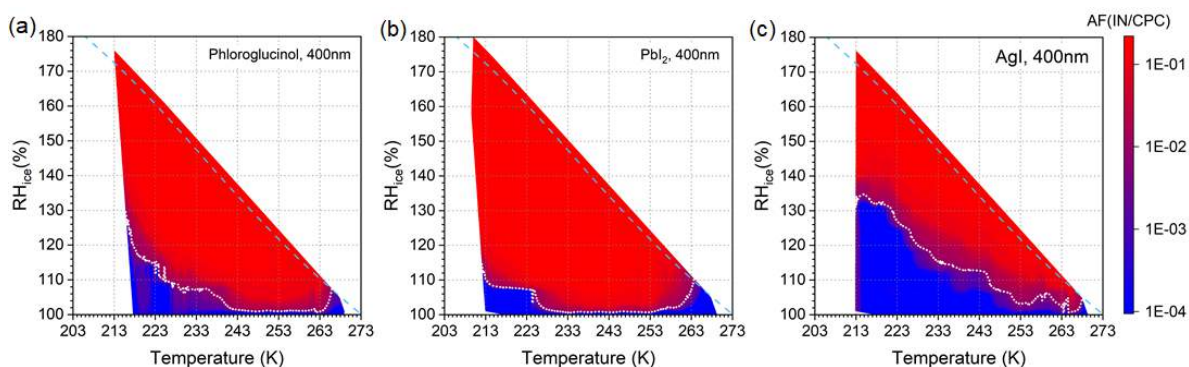


Figure 2: Contour plots of ice active fraction as function of T and RH_i of (a) Phloroglucinol, (b) PbI_2 and (c) AgI. High activity is indicated in red colors and low or no activity in blue. Activated fraction of 1% (indicating ice nucleation onset conditions) are shown as white lines.

CONCLUSIONS

Based on the careful characterization of three cloud seeding agents and the comparison of measured ice nucleation activity with current theories, it remains undecided by which mechanism ice is nucleated below water saturation. While there is some agreement between measurements and theory concerning the dependence of ice nucleation on T , RH_i , a quantitative prediction is not established. Future experiments are directed to determine the substance specific phase state of adsorbed water, to elucidate the onset of ice nucleation in the sub-saturated regime.

ACKNOWLEDGEMENTS

This work was supported by the Academy of Finland, C-Main project (grant no. 309141), and the Center of Excellence programme (grant no. 307331).

REFERENCES

- Fletcher, N. (1962). *The physics of rainclouds*. (Cambridge University Press, Cambridge, U.K.)
- Laaksonen A., and Malila, J. (2016). An adsorption theory of heterogeneous nucleation of water vapour on nanoparticles. *Atmos. Chem. Phys.*, **16**, 135-143.
- Marcolli, C. (2014). Deposition nucleation viewed as homogeneous or immersion freezing in pores and cavities *Atmos. Chem. Phys.*, **14**, 2071-2104.

FAAR abstract instructions and template

Please read carefully - the text contains instructions for abstract preparation

CAN BIOGENIC AEROSOL AFFECT INP CONCENTRATION IN A BOREAL FOREST?

Y. Wu, Z. Brasseur¹, D. Castarède², P. Aalto¹, L. Hao³, L. Heikkinen¹, N. Sarnela¹, P. Heikkilä⁴, M. Kulmala¹, T. Petäjä¹, E.S. Thomson² and J. Duplissy¹

¹Institute for Atmospheric and Earth System Research/Physics, Faculty of Science, University of Helsinki, 00014 Helsinki, Finland

²Department of Chemistry and Molecular Biology, Atmospheric Science, University of Gothenburg, 41296, Gothenburg, Sweden

³University of Eastern Finland, Kuopio, 70211, Finland

⁴Tampere University of Technology, 33101, Tampere, Finland

Keywords: ice nucleation, INP, machine learning.

INTRODUCTION

Aerosol particles emitted from anthropogenic and natural sources can modulate the formation of ice in clouds via heterogeneous ice nucleation (Murray et al., 2012). However, the fundamental understanding of ice nucleation is still poor, and many questions in the field remain unresolved (Kanji et al., 2017).

METHODS

Here, we investigate the potential of aerosol present in the boreal environment to act as Ice Nucleating Particles (INP). The measurements were performed in spring 2018 during the HyIce2018 field campaign, at the SMEAR II research station, located in a boreal environment in Southern Finland. The SMEARII station provides continuous measurements of many atmospheric and ecosystem variables including aerosol particle and gas phase properties. INP concentration was measured using a second-generation Portable Ice Nucleation Chamber (PINCii), designed as an upgrade to the PINC (Stetzer et al., 2008). The working principle of such Continuous Flow Diffusion Chambers (CFDCs) was originally developed and refined at Colorado State University (Rogers et al., 1988).

CONCLUSIONS

During the HyIce2018 field campaign, the PINCii measured successfully for seven weeks (21/4/2018 - 10/6/2018), capturing the later part of the transition period between winter and summer. Machine learning methods have been used to analyze the time series and initial results show that INP is strongly correlated with particle surface area concentration. Other important factors include inorganic aerosols, biogenic particles and Cloud Condensation Nuclei (CCN). Additionally, the travel time that air masses spent over land from different source regions was investigated and results suggest that high INP concentrations correlate with regional-scale transport.

REFERENCES

- Murray, B. J., O'sullivan, D., Atkinson, J. D., & Webb, M. E. (2012). Ice nucleation by particles immersed in supercooled cloud droplets. *Chemical Society Reviews*, 41(19), 6519-6554.
- Kanji, Z. A., Ladino, L. A., Wex, H., Boose, Y., Burkert-Kohn, M., Cziczo, D. J., & Krämer, M. (2017). Overview of ice nucleating particles. *Meteorological Monographs*, 58, 1-1.
- Rogers, D. C. (1988). Development of a continuous flow thermal gradient diffusion chamber for ice nucleation studies. *Atmospheric Research*, 22(2), 149-181.
- Stetzer, O., Baschek, B., Lüönd, F., & Lohmann, U. (2008). The Zurich Ice Nucleation Chamber (ZINC)- A new instrument to investigate atmospheric ice formation. *Aerosol Science and Technology*, 42(1), 64-7

Aerosol Mass yields of selected Biogenic Volatile Organic Compounds – a theoretical study with near explicit gas-phase chemistry

XAVIER. C.¹, RUSANEN. A¹, CHEN. D¹, ZHOU. P¹, PICHELSTOFER. L.¹, ROLDIN P. ², BOY M.¹

¹Institute for Atmospheric and Earth System Research / Physics, University of Helsinki, Finland

²Division of Nuclear Physics, Lund University, Sweden

Keywords: SOA, Mass yields, BVOCs, PRAM

INTRODUCTION

Biogenic Volatile Organic Compounds (BVOCs) are a significant source of Secondary Organic Aerosols (SOA) but quantifying their aerosol forming potential still remains an active and challenging task (Hao et al., 2011). This work presents the results of SOA mass loadings derived from model simulations of BVOCs (isoprene, α -pinene, limonene and β -caryophyllene and β -pinene) with the main atmospheric oxidants (OH, O₃ and NO₃) using the zero-dimensional model MALTE-BOX (Boy et al., 2006). We utilize the most common and widely used Master Chemical Mechanism (MCM), an explicit chemical mechanism detailing the gas phase processes involved in the tropospheric degradation of volatile organic compounds (<http://mcm.leeds.ac.uk/MCM>) along with the newly developed Peroxy radical autoxidation mechanism (PRAM) (Roldin et al., 2019). The aim of this work is to test and compare the efficacy of a coupled MCM+PRAM against a standalone MCM, and parametrize the SOA mass yields (with temperature (258.15 - 313.15 K) and NO_x (2.5 -7.5 ppb) dependence), keeping in mind the larger picture of applicability to large scale models (e.g. EC-EARTH, ECHAM etc.).

METHODS

The process is initiated by extracting the complete mechanism subset for the interested VOC species from the MCM website including the molecular weights and SMILES (Simplified Molecular Input Line Entry System), a chemical notation which facilitates the chemical structure to be read by the computer. The generated SMILES provide the required molecular information which when fed as an input to the normal boiling point method (Nannoolal et al., 2004) can be used to estimate the pure liquid vapour pressures of the organic compounds using the group-contribution method described in Nannoolal et al. (2008). A newly developed Peroxy radical autoxidation mechanism (PRAM) (Roldin et al., 2019) is then combined with the MCM scheme (MCM+PRAM). To simulate SOA formation the PRAM+MCM is coupled to an aerosol module as the compounds partitioning to the condensed phase vary as a function of vapour pressure.

The onset of semi or low volatile organic vapour condensation onto the inorganic seed particles are determined inside the aerosol module, which is described e.g. in Hermansson et al. (2014). The motivation is now to evaluate the efficacy of PRAM+MCM scheme in simulating the SOA mass yields derived from the oxidation of individual precursor BVOCs with the aim to test the temperature and NO_x-level dependence. The aim also extends to identify important compounds that contribute to the increasing SOA yields (i.e. compounds which contribute more than 95 % to SOA mass loadings).

The simulations performed in this study are aimed to closely resemble an idealized smog chamber and flow tube without considering the wall losses of gas phase compounds. For the chamber runs the VOC and oxidants were introduced at the beginning (time, t=0 sec) and allowed to react. The condensation sink (CS) for the chamber and OFR simulations was set to 0.00067 s⁻¹ and 0.067 s⁻¹ respectively. SOA mass yields obtained using an OFR are sensitive to short residence time used, hence the seed particle surface area should be chosen in order to overcome the mass yield underestimation (Ahlberg et al., 2019). CS sensitivity runs were performed for α -pinene-O₃ to determine the CS for which there are no appreciable change in mass yields with increasing particle surface.

The simulation is run for a maximum time of 24 hours and ends when either of the 2 criteria are satisfied (1) the simulation time reaches the 24-hour mark or (2) 90 % of the initial precursor VOC has reacted away. In the latter case the simulation is continued for an additional 2 hours to ensure enough time for the vapors to condense onto the seed particles (ammonium sulfate) and grow. On the contrary the flow tube runs were simulated for 100 seconds ensuring all initial precursor vapors were oxidized. Seed particles were also added in the OFR simulations. The oxidant concentrations for the flow tube simulations were higher in comparison to the simulated chamber runs (~2 orders of magnitude larger). The time step for the chamber and flow tube simulations was set to $t=10$ s and $t=0.1$ s respectively. The oxidant (OH , O_3 or NO_3) concentrations in both the chamber and flow tube simulation was constant for each run. The runs performed were oxidant specific i.e. VOCs would be oxidized by only one specific oxidant at any given time.

CONCLUSIONS

SOA mass yields for ozonolysis of α -pinene, limonene, β -caryophyllene and β -pinene were simulated using the coupled MCM+PRAM and standalone MCM. In Fig. 1 the upper panel indicates the MCM+PRAM contribution to SOA mass from BVOCs ozonolysis of α -pinene and limonene (currently PRAM is only available for ozonolysis of α -pinene and limonene) and the lower panel shows the ratio of yields between MCM and MCM+PRAM. The abscissa depicted on a log scale considers the entire range of SOA mass loading's from 1-8000 $\mu\text{g}/\text{m}^3$. The yields obtained from using only MCM for β -caryophyllene and β -pinene ozonolysis is shown in Fig. 2. The yields derived from using coupled MCM+PRAM are in good agreement with the measured values (Kristensen et al., 2017; Pathak et al., 2007), whereas a standalone MCM scheme under-predicts mass yields (Chen et al., 2012).

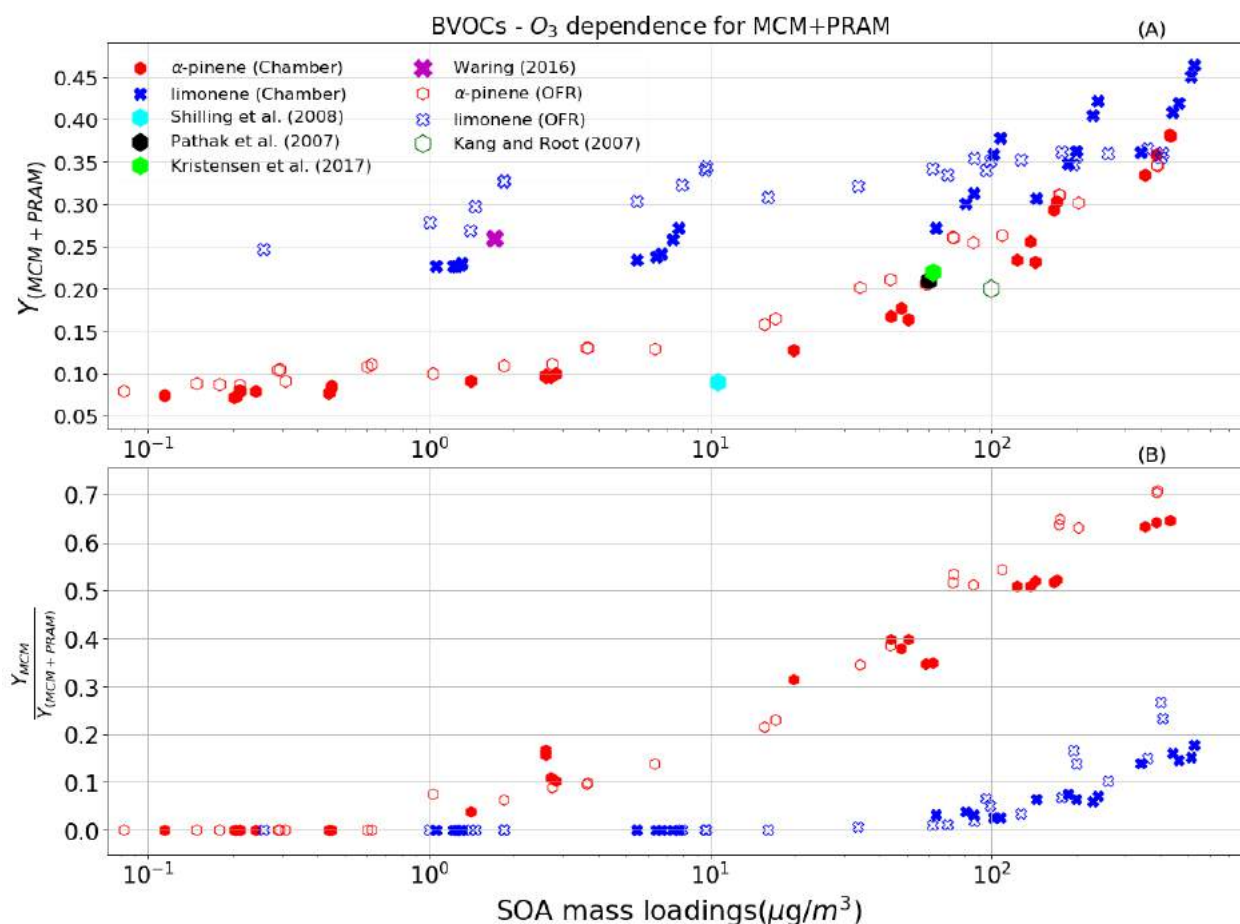


Figure 1. The mass yields from the ozonolysis of BVOCs α -pinene (red heptagon) and limonene (blue crosses) modelled after chamber (filled symbols) and flow-tube settings (open symbols). The figure shows a comparison of

SOA mass yields obtained from simulations with MCM + PRAM (panel A) and ratio of yields from MCM and MCM+PRAM (panel B). Currently PRAM is available for ozonolysis of limonene and α -pinene. The clumps are a result of SOA mass yields for the oxidation of specific oxidant concentration with varying BVOC concentration.

BVOCs - O_3 dependence for MCM

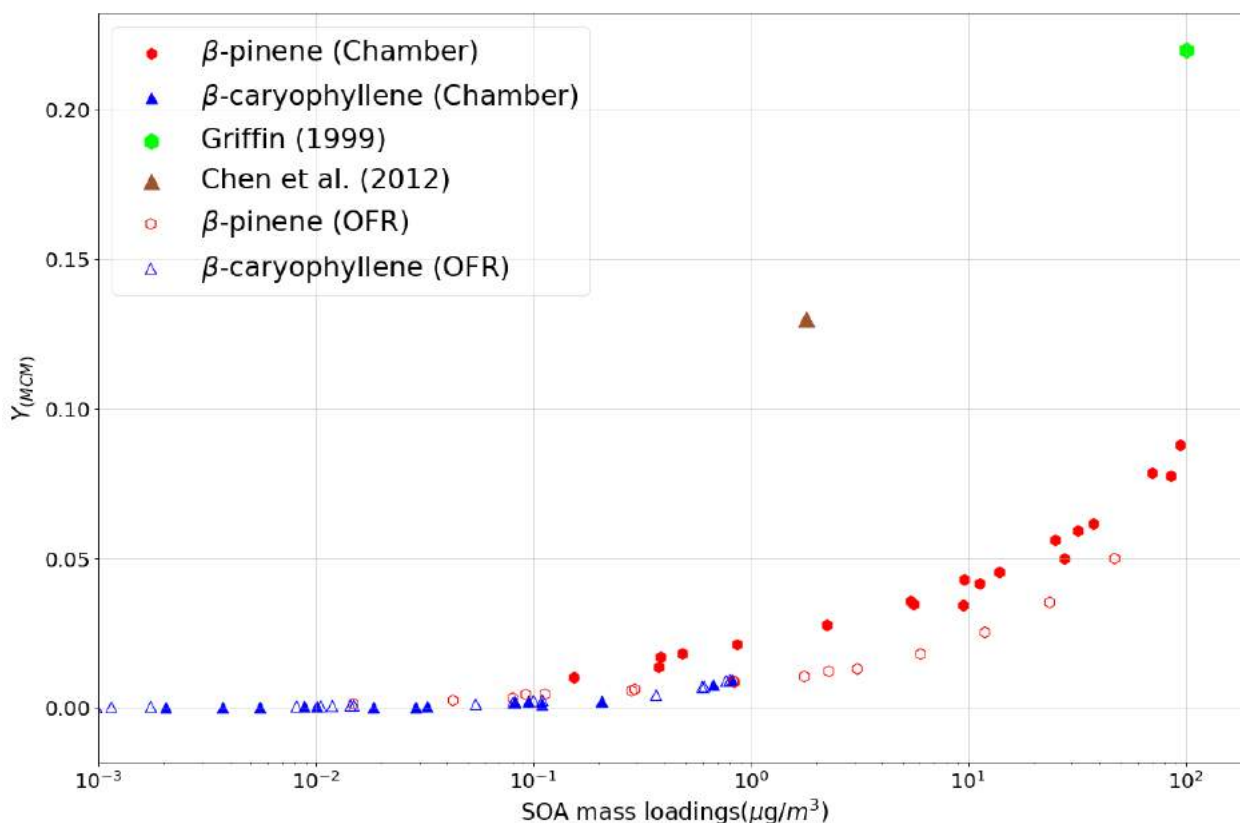


Figure 2. The mass yields from the ozonolysis of BVOCs β -pinene and β -caryophyllene modelled after chamber (filled symbols) and flow-tube (open symbols) settings. The figure shows a comparison of SOA mass yields obtained from simulations with only MCM as currently there is no PRAM available for these compounds. The experimental values are provided for comparison.

ACKNOWLEDGMENTS

The presented research has been funded by the Academy of Finland (Center of Excellence in Atmospheric Sciences) grant no. 4100104 and the Swedish Research Council FORMAS, project no. 2018-01745. We would also like to acknowledge the invaluable contribution of computational resources from CSC – IT Center for Science, Finland.

REFERENCES

Ahlberg, E., Eriksson, A., Brune, W. H., Roldin, P. and Svenningsson, B.: Effect of salt seed particle surface area, composition and phase on secondary organic aerosol mass yields in oxidation flow reactors, *Atmos. Chem. Phys.*, 19(4), 2701–2712, doi:10.5194/acp-19-2701-2019, 2019.

Boy, M., Hellmuth, O., Korhonen, H., Nilsson, E. D., Revelle, D., Turnipseed, A., Arnold, F. and Kulmala, M.: MALTE - Model to predict new aerosol formation in the lower troposphere, *Atmos. Chem. Phys.*, 6(12), 4499–4517, doi:10.5194/acp-6-4499-2006, 2006.

Chen, Q., Li, Y. L., McKinney, K. A., Kuwata, M. and Martin, S. T.: Particle mass yield from β -caryophyllene ozonolysis, *Atmos. Chem. Phys.*, 12(7), 3165–3179, doi:10.5194/acp-12-3165-2012, 2012.

Hao, L. Q., Romakkaniemi, S., Yli-Pirilä, P., Joutsensaari, J., Kortelainen, A., Kroll, J. H., Miettinen, P., Vaattovaara, P., Tiitta, P., Jaatinen, A., Kajos, M. K., Holopainen, J. K., Heijari, J., Rinne, J., Kulmala, M., Worsnop, D. R., Smith, J. N. and Laaksonen, A.: Mass yields of secondary organic aerosols from the oxidation of α -pinene and real plant emissions, *Atmos. Chem. Phys.*, 11(4), 1367–1378, doi:10.5194/acp-11-1367-2011, 2011.

Hermansson, E., Roldin, P., Rusanen, A., Mogensen, D., Kivekäs, N., Väänänen, R., Boy, M. and Swietlicki, E.: Biogenic SOA formation through gas-phase oxidation and gas-to-particle partitioning—a comparison between process models of varying complexity, *Atmos. Chem. Phys.*, 14(21), 11853–11869, doi:10.5194/acp-14-11853-2014, 2014.

Kristensen, K., Jensen, L. N., Glasius, M. and Bilde, M.: The effect of sub-zero temperature on the formation and composition of secondary organic aerosol from ozonolysis of alpha-pinene, *Environ. Sci. Process. Impacts*, 19(10), 1220–1234, doi:10.1039/c7em00231a, 2017.

Nannoolal, Y., Rarey, J., Ramjugernath, D. and Cordes, W.: Estimation of pure component properties Part 1. Estimation of the normal boiling point of non-electrolyte organic compounds via group contributions and group interactions, *Fluid Phase Equilib.*, 226, 45–63, doi:10.1016/j.fluid.2004.09.001, 2004.

Nannoolal, Y., Rarey, J. and Ramjugernath, D.: Estimation of pure component properties part 3. Estimation of the vapor pressure of non-electrolyte organic compounds via group contribution and group interactions, *Fluid Phase Equilib.*, 269(1–2), 117–133, doi:10.1016/j.fluid.2008.04.020, 2008.

Pathak, R. K., Stanier, C. O., Donahue, N. M. and Pandis, S. N.: Ozonolysis of α -pinene at atmospherically relevant concentrations: Temperature dependence of aerosol mass fractions (yields), *J. Geophys. Res. Atmos.*, 112(3), 1–8, doi:10.1029/2006JD007436, 2007.

Roldin, P., Ehn, M., Kurtén, T., Olenius, T., Rissanen, M. P., Sarnela, N., Elm, J., Rantala, P., Hao, L., Hyttinen, N., Heikkinen, L., Worsnop, D. R., Pichelstorfer, L., Xavier, C., Clusius, P., Öström, E., Petäjä, T., Kulmala, M., Vehkamäki, H., Virtanen, A., Riipinen, I. and Boy, M.: The role of highly oxygenated organic molecules in the Boreal aerosol-cloud-climate system, *Nat. Commun.*, 10(1), 4370, doi:10.1038/s41467-019-12338-8, 2019.

THE EFFECT OF CANOPY STRUCTURE AND PHYSIOLOGY ON CANOPY SOLAR-INDUCED CHLOROPHYLL FLUORESCENCE UNDER WATER STRESS IN POTATO

S. XU ^{1,2,3}, J. ATHERTON ¹, A. RIIKONEN ¹, C. ZHANG ¹, J. OIVUKKAMÄKI ¹, A. PORCAR-CASTELL¹

¹ Optics of Photosynthesis Laboratory, Institute for Atmospheric and Earth System Research/Forest Sciences, Faculty of Agriculture and Forestry, University of Helsinki, 00014 Helsinki, Finland;

² State Key Laboratory of Remote Sensing Science, Jointly Sponsored by Beijing Normal University and Institute of Remote Sensing and Digital Earth of Chinese Academy of Sciences, Beijing 100875, China; 100875, China;

³ Beijing Engineering Research Center for Global Land Remote Sensing Products, Institute of Remote Sensing Science and Engineering, Faculty of Geographical Science, Beijing Normal University, Beijing 100875, China.

Keywords Solar-induced Chlorophyll Fluorescence, Canopy structure, Physiology, Water stress.

INTRODUCTION

Solar-induced chlorophyll fluorescence (SIF) carries information on plant photosynthesis and can provide new opportunities for monitoring plant status and function through remote sensing (Porcar-Castell et al., 2014).

Previous studies have reported a decrease in SIF in response to water stress (Ač et al., 2015), which has been interpreted in terms of a reduction in the quantum efficiency of fluorescence emission Φ_{F_PSII} at the level of photosystem II (PSII), mediated by the activation of regulatory non-photochemical quenching (NPQ) of excitation energy. Importantly, in contrast to woody plants, crops present soft stems and smaller water storages, which make them particularly sensitive to turgor loss during water stress. This phenomena can induce visible canopy structural changes (such as leaf angle distribution, LAD) that will also affect the canopy SIF emission alongside the physiological variation in Φ_{F_PSII} . In addition, potato leaves and shoots present also remarkable circadian cycles thereby adapting themselves to the diurnal changes in environmental factors. Since both canopy structural and physiological adjustments can operate simultaneously in response to water stress at canopy scale, it still remains unclear to what extent canopy structure and physiology affect the dynamics of SIF under water stress and its correlation with photosynthesis.

In this study, we aimed to understand how physiology and canopy structure affect canopy SIF in potato. First, we measured diurnal changes in leaf angle distribution (LAD), Φ_{F_PSII} , and canopy SIF. Subsequently, we used a process-based and radiative transfer model to quantify the relative impact of canopy structure and physiology on the SIF diurnal pattern. Lastly, we assess the impact of LAD dynamics on the link between SIF and photosynthesis.

METHODS

A potato experiment was conducted at the Viikki campus of University of Helsinki experimental field, Finland (60°14'N, 25°11'E), in the summer of 2018. And split-plot design with five replicates of potato cultivar under drought or irrigated, in a total of 10 plots, were used for the experiment. Experimental data including canopy SIF, leaf angle, Φ_{F_PSII} and biochemical data, was used to disentangle the effects of LAD and Φ_{F_PSII} on SIF in the diurnal scale in controlled and stressed plants, where Φ_{F_PSII} was estimated from

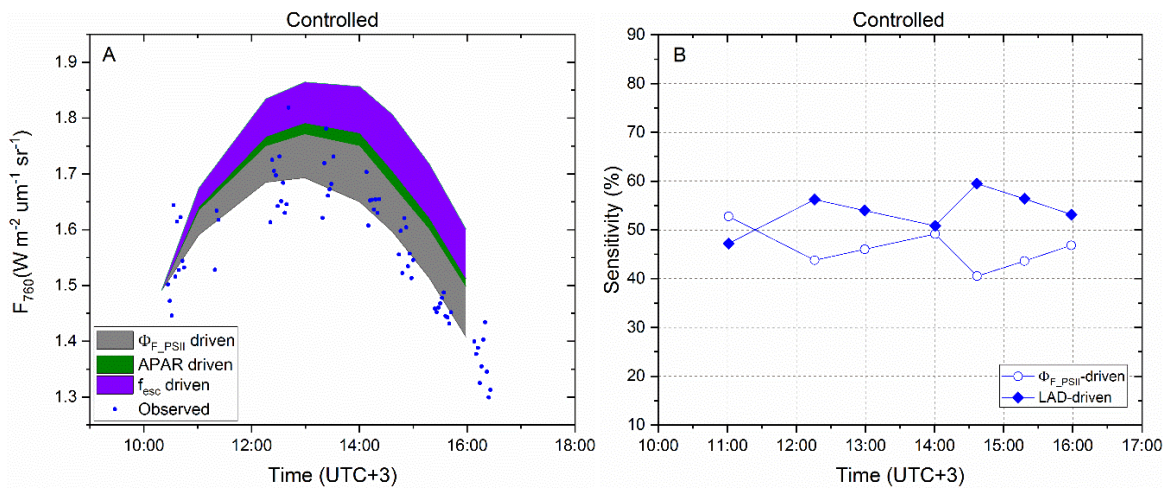
PAM 2500 measurements and LAD obtained from digital photography. The SCOPE (Van der Tol, Verhoef, Timmermans, Verhoef, & Su, 2009) model was used as quantitative framework to assess the relative impact of different factors. We first retrieved leaf structural and biochemical parameters from measured leaf reflectance and transmittance by inverting the Fluspect routine. Afterwards, we produced four types scenarios of diurnal SIF using different combination of Φ_{F_PSII} and LAD using SCOPE (as Table 1). Finally, we analysed the sensitivity of diurnal TOC SIF to LAD and Φ_{F_PSII} , and how LAD affect TOC SIF by comparing four types of simulated SIF.

Variable	Fixed Φ_{F_PSII}	Dynamic Φ_{F_PSII}
Fixed LAD	$\Phi_{F_PSII}(-)$, LAD(-)	$\Phi_{F_PSII}(+)$, LAD(-)
Dynamic LAD	$\Phi_{F_PSII}(-)$, LAD(+)	$\Phi_{F_PSII}(+)$, LAD(+)

Table 1 LAD and Φ_{F_PSII} combinations for different simulation scenarios for simulation.

RESULTS AND CONCLUSIONS

The results (Figure 1) show that: (i) Compared with SIF under fixed LAD and Φ_{F_PSII} during the day, actual canopy SIF have different diurnal sensitivity pattern to LAD and Φ_{F_PSII} between controlled and stressed. LAD and Φ_{F_PSII} for controlled have constant contribution to diurnal SIF change compared with SIF under fixed LAD and Φ_{F_PSII} , accounting for 47%-59% and 41%-53%, respectively. For water stressed, their contribution to diurnal SIF change are dynamic, ranging from 30% increase to 53% for LAD, while the contribution of Φ_{F_PSII} decrease from 70% to 47% from morning to afternoon; (ii) Although not shown here, LAD affects SIF through escape probability of SIF and absorbed photosynthetically active radiation (APAR), but proximately 80% of LAD total influence is caused by escape probability (f_{esc}). In conclusion, we demonstrate that both canopy structure and NPQ play an important role in diurnal SIF variation. Therefore it is critical to consider the effect of canopy structural dynamics on SIF when we use SIF to monitor water stress.



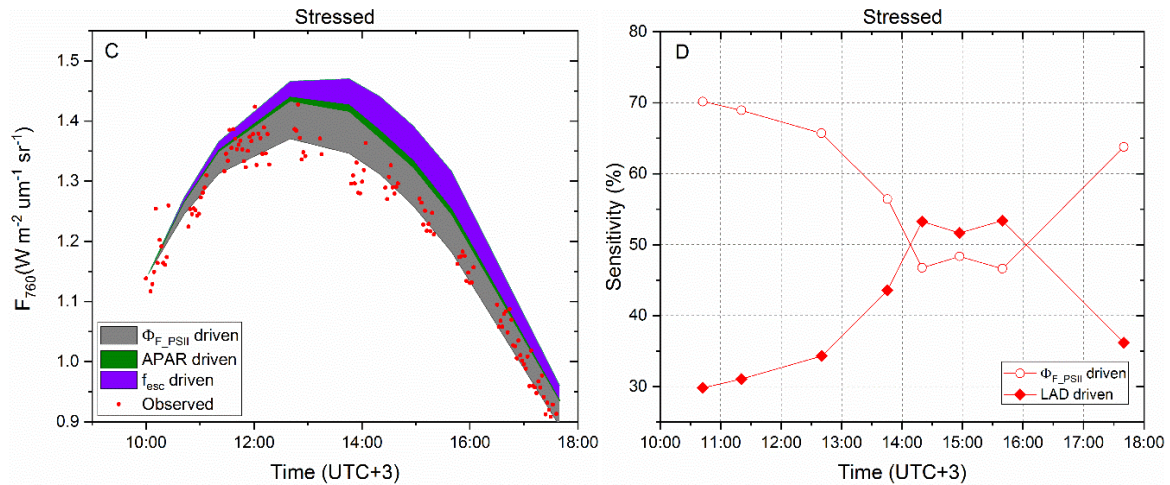


Figure 1 Sensitivity of diurnal F_{760} variation to LAD and Φ_{F_PSII} for controlled and stressed.

ACKNOWLEDGEMENTS

This work was supported by the Academy of Finland (grant numbers 288039, 304097) and the China Scholarship Council for 1 year study at the University of Helsinki.

REFERENCES

- Ač, A., Malenovský, Z., Olejníčková, J., Gallé, A., Rascher, U., & Mohammed, G. J. R. S. o. E. (2015). Meta-analysis assessing potential of steady-state chlorophyll fluorescence for remote sensing detection of plant water, temperature and nitrogen stress. *168*, 420-436.
- Porcar-Castell, A., Tyystjärvi, E., Atherton, J., Van der Tol, C., Flexas, J., Pfündel, E. E., . . . Berry, J. A. J. J. o. e. b. (2014). Linking chlorophyll a fluorescence to photosynthesis for remote sensing applications: mechanisms and challenges. *65*(15), 4065-4095.
- Van der Tol, C., Verhoef, W., Timmermans, J., Verhoef, A., & Su, Z. J. B. (2009). An integrated model of soil-canopy spectral radiances, photosynthesis, fluorescence, temperature and energy balance. *6*(12), 3109-3129.

GAS-PHASE CHEMISTRY OF HSO₅ AND SO₄ IN URBAN BEIJING, CHINA

L. Yao¹, B.W. Chu¹, S.X. Wang², Y.H. Wang¹, X.L. Fan³, Q.Z. Zha¹, J. Cai¹, W. Du¹, Y.C. Liu², H. Li², L. Wang³, M. Ehn¹, T. Petäjä¹, Veli-Matti Kerminen¹, D.R. Worsnop^{1,4}, M. Kulmala^{1,2}, F. Bianchi¹.

¹ Institute for Atmospheric and Earth System Research / Physics, Faculty of Science, University of Helsinki, Finland

² Aerosol and Haze Laboratory, Beijing Advanced Innovation Center for Soft Matter Science and Engineering, Beijing University of Chemical Technology, Beijing, China

³ Department of Environmental Science & Engineering, Fudan University, Shanghai, China

⁴ Aerodyne Research Inc., Billerica, Massachusetts 01821, USA

Keywords: SO₄, HSO₅, OZONOLYSIS, REACTION MECHANISM, URBAN AIR.

INTRODUCTION

Gaseous sulphur-containing compounds (mainly sulphur dioxide, SO₂) are ubiquitous in urban air. Their products (e.g. sulfuric acid) from atmospheric oxidation by OH radicals, ozone and stabilized Criegee intermediates play essential roles in urban atmospheric physico-chemical processes (e.g. urban new particle formation) (Mauldin *et al.*, 2012; Sipila *et al.*, 2010; Yao *et al.*, 2018). In the atmosphere, during the daytime, SO₂ are dominantly oxidized by OH radicals to form sulfuric acid, and their intermediate products and formation mechanisms are well known (Finlayson-Pitts & Pitts, 2000). The HSO₅ molecule is one of the intermediate products from the OH- initiated gas-phase oxidation process and its lifetime is short, whereas hydrolyzation can increase the lifetime of it (Kurten *et al.*, 2009; Laaksonen *et al.*, 2008). However, in ambient air (especially in urban air), the detection of neutral HSO₅ is scarce. According to previous work, the ozonolysis of SO₂ also can lead to sulfuric acid formation. Besides the production of sulfuric acid, other sulphur-compounds from ozonolysis of SO₂ are still not well known. The SO₄ molecule has also been known as an atmospheric intermediate from the reaction of sulphur trioxide (SO₃) with atomic oxygen (Jacob *et al.*, 1972; Mckee *et al.*, 1993). Moreover, SO₄ has been predicted to be a C_{2v} molecule with a very high electron affinity (EA) of 5.28 eV (McKee *et al.*, 1996). Although many laboratory experimental studies have dealt with the formation pathways of HSO₅ and SO₄ and the oxidative capacity of SO₄ in solution (Merga *et al.*, 1994). However, in the ambient air (especially in urban air), due to the limitation of detection methods, their gas-phase concentration, properties (e.g. oxidizing capacity) and atmospheric fates remain almost completely unknown. In this study, using nitrate-Chemical Ionization - Atmospheric Pressure interface - Long Time Of Flight - Mass Spectrometry (CI-APi-LTOF), a long-term ambient observation was carried out in urban Beijing from November 2018 to May 2019. Combined ambient measurements results with the conclusions of our laboratory experiments, atmospheric formation mechanisms of HSO₅ and SO₄ molecules and their roles/fates in atmospheric chemistry processes in polluted urban air were tentatively investigated.

METHODS

From November 2018 to May 2019, a long-term ambient observation was conducted at BUCT (Beijing University of Chemical Technology) monitoring site (N 33.94°, E 116.30°) in urban Beijing. Atmospheric gaseous sulfuric acid (H₂SO₄), HSO₅, SO₄, SO₃ and other sulfur-containing compounds were measured by nitrate- CI-APi-LTOF. The compounds of HSO₅ and SO₄ were quantified utilizing the calibration coefficient of sulfuric acid monomer. Compared with the energy of H₂SO₄, the higher energy of HSO₅ and SO₄ molecules, could lead to underestimated concentrations. Besides, trace gases including SO₂, O₃, NO_x and CO were monitored with a series of Thermo Scientific gas analyzers (model 42i-TL, 43i-TLE, 48i-TLE, and 49i). Meanwhile, meteorological parameters and visibility were measured by a Vaisala weather station. Potential Aerosol Mass Reactor (PAM) chamber was used to conduct laboratory experiments to confirm and reveal the formation pathways and atmospheric roles and fates of HSO₅ and SO₄.

CONCLUSIONS

During the whole campaign periods, the diurnal patterns of HSO₅ and SO₄ are similar with that of sulfuric acid monomer in urban Beijing, and during the daytime, the peaks of median concentrations of HSO₅ and SO₄ are $\sim 2 \times 10^5$ and $\sim 5 \times 10^4$ molecule cm⁻³, respectively (Figure 1). Furthermore, the mixing ratios of HSO₅ and SO₄ are lower than sulfuric acid monomer concentration. From ambient measurements, it shows a positive correlation between HSO₅ and SO₄ which means these two compounds may derive from the same reaction pathway (Figure 2). From laboratory experiments, we can conclude that HSO₅ and SO₄ can be charged by nitrate ions and they can be formed from the ozonolysis of SO₂; HSO₅ can also be produced from the OH-initiated gas-phase oxidation of SO₂; HSO₅ may have two molecular structures. In addition, relative humidity (RH) has no significant effect on HSO₅ and SO₄ formation. Regarding the SO₄ formation pathway, SO₄ molecules are formed from the reaction between SO₃ and O(³P) instead of SO₃ and O(¹D). The oxidative capacity needs further laboratory experiments to reveal.

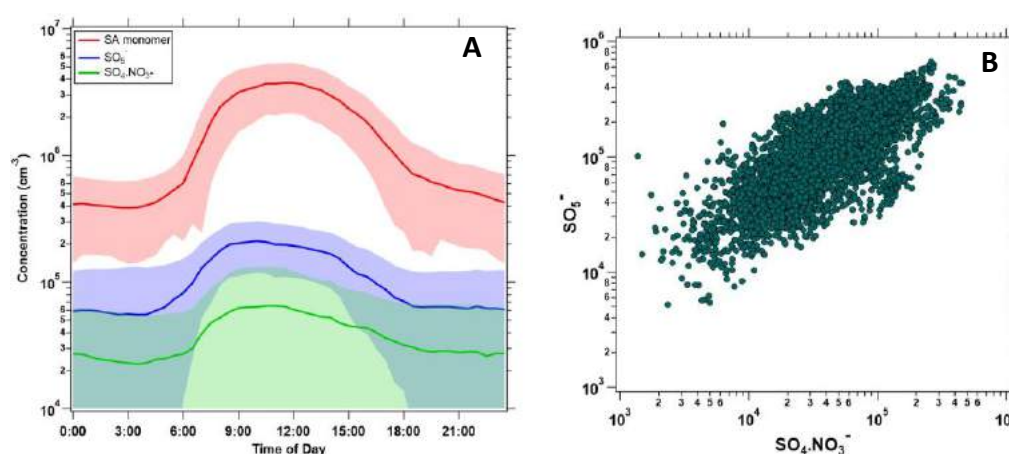


Figure 1. Diurnal pattern of sulfuric acid, HSO₅ and SO₄ (A) and the relationship between HSO₅ and SO₄ (B).

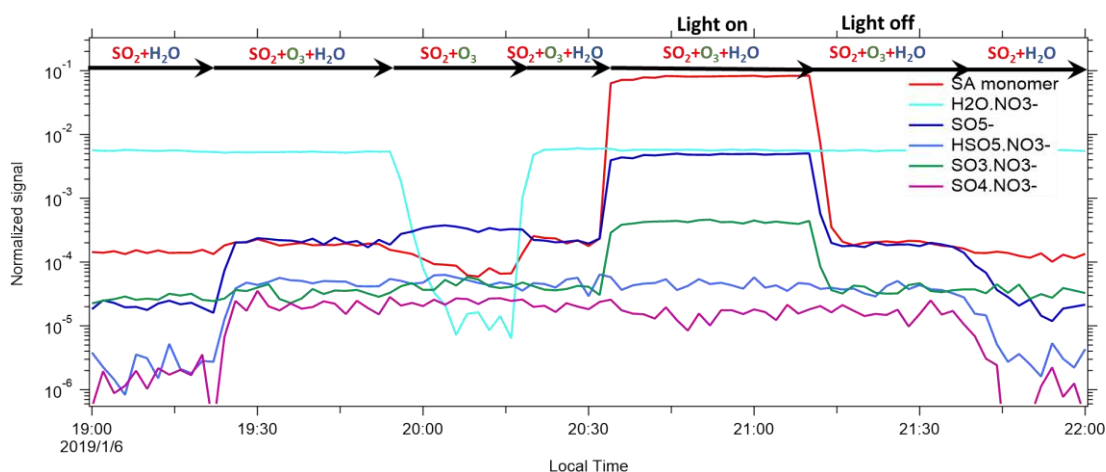


Figure 2. Variation of sulfuric acid monomer, HSO₅, SO₄, SO₃ and H₂O.NO₃⁻ under different reaction conditions. The wavelength of the UV light is 253nm which was used to generate OH radicals from the photolysis of ozone.

ACKNOWLEDGEMENTS

This work was supported by Academy of Finland (1251427, 1139656, 296628, 306853, Finnish center of excellence 1141135), and the EC Seventh Framework Program and European Union's Horizon 2020 program (ERC, project no.742206 "ATM-GTP").

REFERENCES

- Finlayson-Pitts, B.J., & Pitts, J.N. (2000). *Chemistry of the upper and lower atmosphere : theory, experiments, and applications*. Academic Press, San Diego.
- Jacob, A., and Winkler C. A. (1972). Kinetics of the Reactions of Oxygen Atoms and Nitrogen Atoms with Sulphur Trioxide. *J. CHEM. SOC. FARADAY TRANS.*, **68**, 2077.
- Kurten, T., Berndt, T., & Stratmann, F. (2009). Hydration increases the lifetime of HSO₅ and enhances its ability to act as a nucleation precursor - a computational study. *Atmospheric Chemistry and Physics*, **9**, 3357-3369.
- Laaksonen, A., Kulmala, M., Berndt, T., Stratmann, F., Mikkonen, S., Ruuskanen, A., Lehtinen, K.E.J., Dal Maso, M., Aalto, P., Petaja, T., Riipinen, I., Sihto, S.L., Janson, R., Arnold, F., Hanke, M., Ucker, J., Umann, B., Sellegri, K., O'Dowd, C.D., & Viisanen, Y. (2008). SO₂ oxidation products other than H₂SO₄ as a trigger of new particle formation. Part 2: Comparison of ambient and laboratory measurements, and atmospheric implications. *Atmospheric Chemistry and Physics*, **8**, 7255-7264.
- McKee, M.L. (1993). Computational Studies on SO₄ and S₂O₃. *Journal of the American Chemical Society*, **115**, 9136-9142.
- McKee, M.L. (1996). Computational Study of the Mono- and Dianions of SO₂, SO₃, SO₄, S₂O₃, S₂O₄, S₂O₆, and S₂O₈. *J. Phys. Chem.*, **100**, 3473-3481
- Merga, G., Aravindakumar, C. T., and Rao, B. S. M. (1994) Pulse Radiolysis Study of the Reactions of SO₂- with some Substituted Benzenes in Aqueous Solution. *J. CHEM. SOC. FARADAY TRANS.*, **90(4)**, 597-604.
- Mauldin, R.L., Berndt, T., Sipila, M., Paasonen, P., Petaja, T., Kim, S., Kurten, T., Stratmann, F., Kerminen, V.M., & Kulmala, M. (2012). A new atmospherically relevant oxidant of sulphur dioxide. *Nature*, **488**, 193-196.
- Sipila, M., Berndt, T., Petaja, T., Brus, D., Vanhanen, J., Stratmann, F., Patokoski, J., Mauldin, R.L., Hyvarinen, A.P., Lihavainen, H., & Kulmala, M. (2010). The Role of Sulfuric Acid in Atmospheric Nucleation. *Science*, **327**, 1243-1246.
- Yao, L., Garmash, O., Bianchi, F., Zheng, J., Yan, C., Kontkanen, J., Junninen, H., Mazon, S.B., Ehn, M., Paasonen, P., Sipila, M., Wang, M., Wang, X., Xiao, S., Chen, H., Lu, Y., Zhang, B., Wang, D., Fu, Q., Geng, F., Li, L., Wang, H., Qiao, L., Yang, X., Chen, J., Kerminen, V.M., Petaja, T., Worsnop, D.R., Kulmala, M., & Wang, L. (2018). Atmospheric new particle formation from sulfuric acid and amines in a Chinese megacity. *Science*, **361**, 278-281.

CLIMATIC SIGNIFICANCE OF BIOGENIC AEROSOLS IN WARMING BOREAL FOREST: PART 1. IN SITU OBSERVATIONS ON ORGANIC AEROSOL

T. YLI-JUUTI¹, T. MIELONEN², H. KOKKOLA², A. AROLA², A. LIPPONEN², L. HEIKKINEN³, T. NIEMINEN^{1,3}, M. EHN³, T. PETÄJÄ³ and A. VIRTANEN¹

¹Department of Applied Physics, University of Eastern Finland, Kuopio, Finland.

²Finnish Meteorological Institute, Kuopio, Finland.

³Institute for Atmospheric and Earth System Research, University of Helsinki, Helsinki, Finland.

Keywords: AEROSOL, OA, TEMPERATURE, AEROSOL-CLOUD INTERACTION.

INTRODUCTION

Biogenic secondary organic aerosol (SOA) form a major fraction of aerosol above the boreal forest area. Therefore, aerosol radiative forcing can be affected by changes in temperature and consequent changes in emissions of volatile organic compounds (VOC) from vegetation. The increasing VOC emissions with increasing temperature are expected to lead to enhanced formation of biogenic SOA and increasing organic aerosol (OA) mass loadings and aerosol number concentrations. Such changes in aerosol concentrations may lead to strengthening of both the direct and indirect aerosol radiative forcing. The increase in particle number concentrations and total particle mass concentration with temperature has been observed in previous studies (Paasonen *et al.*, 2013; Asmi *et al.*, 2016). However, direct evidence of temperature dependence of OA has been lacking and the effect on radiative forcing requires quantification. In this study we combine in situ data from the boreal forest site Hyytiälä with remote sensing observations in order to investigate the temperature dependence of OA and its effect on aerosol radiative forcing. In this first part we concentrate on the observations from measurements at the Hyytiälä site and analyse the temperature dependence of OA concentration and aerosol optical depth (AOD). In the second part (Mielonen *et al.*, 2019) we compare the temperature dependence of OA to satellite-based observations to investigate the influence of changes in OA to cloud properties.

METHODS

We use long-term aerosol composition data measured with an Aerosol Chemical Speciation Monitor (ACSM) to study the temperature dependence of OA mass loadings. Additionally, we use aerosol size distribution data measured with a Differential Mobility Particle Sizer (DMPS) to study the temperature dependence of number concentration of particles large enough to act as cloud condensation nuclei. By limiting our analyses to two summer months, July and August, each year we aim at isolating the temperature dependence of the organic mass loading from the seasonal effects arising from the vegetation growth season. The analysis is based on measurements over the years 2012-2018 at Hyytiälä, Southern Finland. This period includes two years where the average summer temperature was considerably higher than the current average and we use these warm summers as a future projection.

We use air mass back trajectories calculated with HYSPLIT (Stein *et al.*, 2015) to account for the origin of the air masses and the different source regions in the analyses. We use also various in situ measurements of atmospheric variables, such as SO₂, black carbon and UVB, in order to distinguish the temperature effect from effects of anthropogenic emissions, biomass burning and oxidation.

We accompany the in situ measurements of OA with AERONET sun photometer observations of AOD. We analyse the AOD data on basis on monthly mean values and we utilize the AOD measured at two wavelengths, 340 nm and 550 nm, in order to gain information about the aerosol size distribution.

RESULTS AND CONCLUSIONS

Our results show that summertime OA concentration increases with temperature. The analysis on the air mass source areas as well as SO₂, particle phase sulfate and black carbon concentrations indicate that the temperature trend in OA is not explained by anthropogenic or biomass burning emissions. Therefore, main part of the OA increase with temperature likely originates from enhanced biogenic SOA formation, although quantifying the temperature induced changes in OA requires consideration of these other atmospheric variables.

Consistently with the trend in OA, also clear sky AOD over the measurement station increases with temperature. The difference between the wavelengths in the increase of AOD with temperature suggest that the temperature dependence of AOD comes mainly from smaller particles. Therefore, the temperature dependent increase of AOD is likely related to regional sources, rather than long-range transportation. This is consistent with the temperature dependence of AOD being driven by the changes in OA and biogenic SOA formation. This observation suggests that the enhanced biogenic SOA formation in warmer conditions strengthens the aerosol direct radiative effect.

Number concentration of particles large enough to act as cloud condensation nuclei increases with temperature similarly to OA concentration. However, the consequent changes in cloud properties and aerosol indirect effect are not straightforward or clear (Mielonen *et al.*, 2019).

ACKNOWLEDGEMENTS

This work was supported by the Academy of Finland Centre of Excellence (grant no 307331) and Academy of Finland project no. 299544.

REFERENCES

- Asmi, E. *et al.* (2016), Aerosol size distribution seasonal characteristics measured in Tiksi, Russian Arctic, *Atmos. Chem. Phys.* **16**, 1271.
- Mielonen, T. *et al.* (2019), Climatic significance of biogenic aerosols in warming boreal forest: Part 2. Satellite observations of aerosols and clouds, in Proceedings of 'the Center of Excellence in Atmospheric Sciences (CoE ATM) -From Molecular and Biological Processes to the Global Climate' Annual Meeting 2019.
- Paasonen, P. *et al.* (2013). Warming-induced increase in aerosol number concentration likely to moderate climate change, *Nature Geoscience* **6**, 438.
- Stein, A.F. *et al.* (2015), NOAA's HYSPLIT Atmospheric Transport and Dispersion Modeling System, *Bull. Amer. Meteor. Soc.* **96**, 2059.

SOLVING THE MYSTERY OF WILDLY DIFFERING RESULTS IN CALIBRATING FIGAERO TOF-CIMS DESORPTION TEMPERATURE WITH SATURATION VAPOUR PRESSURE

ARTTU YLISIRNIÖ¹, LUIS BARREIRA^{1,2}, IIDA PULLINEN¹, ANGELA BUCHHOLZ¹, JOHN JAYNE³, JORDAN KRECHMER³, DOUGLAS WORSNOP³, ANNELE VIRTANEN¹, and SIEGFRIED SCHOBESBERGER¹

¹Department of Applied Physics, University of Eastern Finland, FI-70211 Kuopio, Finland.

²Atmospheric Composition Research, Finnish Meteorological Institute, Helsinki, Finland.

³Center for Aerosol and Cloud Chemistry, Aerodyne Research, Inc., Billerica, MA, USA.

Keywords: FIGAERO, ToF-CIMS, calibration

INTRODUCTION

The Filter Inlet for Gases and AEROsols, coupled to a Time-of-Flight Chemical Ionization Mass Spectrometer (FIGAERO-ToF-CIMS, Lopez-Hilfiker et al., 2014) has been employed in numerous studies to investigate the composition and volatility of aerosol particles from both ambient atmosphere and laboratory environments. Earlier studies have used syringes to deposit solutions of organic acids or series of polyethylene glycols (PEG) with known saturation vapour pressures (P_{sat}) onto the FIGAERO filter and related them to the temperature of peak signal (T_{max}) during the FIGAERO heating cycle. (Bannan et al., 2018; Lopez-Hilfiker et al., 2014; Stark et al., 2017). However, some of these studies have suffered from covering a range of only relatively low measured T_{max} values (below 100 °C; for compounds with relatively high P_{sat}); and crucially they have produced rather inconsistent results when compared to each other (Fig. 1), spanning up to 4 orders of magnitude in P_{sat} for a given compound.

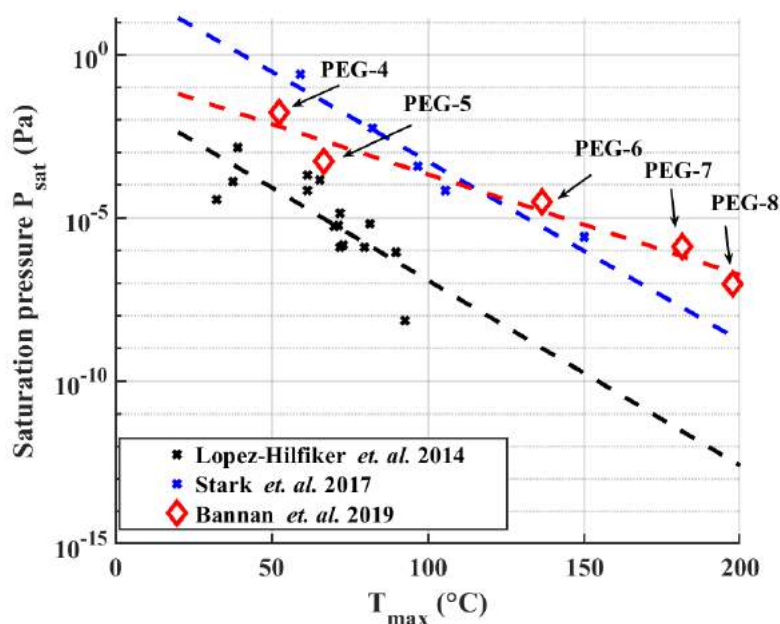


Figure 1. Comparison of calibration lines between different previous studies. They used either varieties of organic acids (crosses) or PEG compounds (diamonds).

In this study we investigate the critical effect of calibration solution concentration on calibration results, i.e. on how the solute compounds' P_{sat} relate to the observed T_{max} , and we propose a new method for obtaining such calibration based on the atomization of calibration compound solutions. We also investigate the effect of different methods on sensitivity calibrations, in which the total measured signal is related to the deposited amount of material.

METHODS

In the syringe method used by earlier studies, a known amount of compounds in solution are deposited onto the FIGAERO filter using a microliter syringe. In the atomizer method, solutions of the same compounds are atomized to create aerosol particles, which are then collected onto FIGAERO filter while the aerosol size and mass distributions are monitored by an Scanning Mobility Particle Sizer (SMPS) system (TSI Inc.). For both methods, compounds are subsequently desorbed from the FIGAERO filter and carried into the ToF-CIMS by a nitrogen flow that is gradually heated from room temperature to 200 °C, i.e. as per the standard instrument operating procedure. We thoroughly tested both methods, using a series of PEG-compounds as well as mixtures of organic acids, and also investigated the effect of varying the heating rates.

CONCLUSIONS

In our study we found a clear correlation of the measured T_{max} values to the calibrant solution concentrations for the syringe method, as well as differences in calibration results when using the different deposition methods. These results explain the wildly differing FIGAERO calibration results reported earlier, and we describe and propose a new and robust calibration procedure.

ACKNOWLEDGEMENTS

This work was supported by the Academy of Finland (259005, 272041, 299544, 310682), the European Research Council (ERC-StQ QAPPA 335478) and the University of Eastern Finland Doctoral Program in Environmental Physics, Health and Biology.

REFERENCES

- Bannan, T. J., Le Breton, M., Priestley, M., Worrall, S. D., Bacak, A., Marsden, N. A., Merha, A., Hammes, J., Hallquist, M., Alfarra, M. R., Krieger, U. K., Reid, J. P., Jayne, J., Robinson, W., Mcfiggans, G., Coe, H., Percival, C. J. and Topping, D.: A method for extracting calibrated volatility information from the FIGAERO-HR-ToF-CIMS and its application to chamber and field studies, , (August), 1–12, doi:10.5194/amt-2018-255, 2018.
- Lopez-Hilfiker, F. D., Mohr, C., Ehn, M., Rubach, F., Kleist, E., Wildt, J., Mentel, T. F., Lutz, A., Hallquist, M., Worsnop, D. and Thornton, J. A.: A novel method for online analysis of gas and particle composition: Description and evaluation of a filter inlet for gases and AEROSOLS (FIGAERO), *Atmos. Meas. Tech.*, 7(4), 983–1001, doi:10.5194/amt-7-983-2014, 2014.
- Stark, H., Yatavelli, R. L. N., Thompson, S. L., Kang, H., Edward, J., Kimmel, J. R., Palm, B. B., Hu, W., Hayes, P. L., Day, D. A., Canagaratna, M. R., Jayne, J. T., Worsnop, D. R., Jimenez, J. L., Krechmer, E., Kimmel, J. R., Palm, B. B., Hu, W., Hayes, P. L., Worsnop, D. R. and Jimenez, J. L.: Impact of thermal decomposition on thermal desorption instruments : advantage of thermogram analysis for quantifying volatility distributions of organic species, , doi:10.1021/acs.est.7b00160, 2017.

SULFURIC ACID PROXY REVISED: THE EFFECT OF CRIEGEE INTERMEDIATES AND DIMERS

I. YLIVINKKA^{1,3}, L. DADA^{1,2}, N. SARNELA¹, C. YAN^{1,2}, L. YAO^{1,2}, R. BAALBAKI¹, T. JOKINEN¹,
T. PETÄJÄ¹, V.-M. KERMINEN¹ and M. KULMALA^{1,2}

¹Institute for Atmospheric and Earth System Research INAR / Physics, Faculty of Science, University of Helsinki, Finland.

²Aerosol and Haze Laboratory, Beijing Advanced Innovation Center for Soft Matter Science and Engineering, Beijing University of Chemical Technology, Beijing, China.

³SMEAR II station, University of Helsinki, 35500 Korkeakoski, Finland

Keywords: SULFURIC ACID, PROXY, NEW PARTICLE FORMATION.

INTRODUCTION

Atmospheric new particle formation is a commonly observed phenomenon almost all around the world (Kulmala et al., 2004). It is a source of large number of nanometer-size particles that are formed from gas phase precursors. The formed particles may be removed by coagulation with pre-existing particles or grow to larger sizes by condensation of low volatile vapors. Sulfuric acid has been confirmed to play an important role both in nucleation and growth of the particles (Kulmala et al., 2013) but also other molecules may participate in the process (Hallquist et al., 2009). In order to get insight into how big contribution different molecules have, information of the atmospheric concentrations of vapors are needed. Unfortunately, despite the importance of sulfuric acid in the atmospheric chemistry and aerosol physics, it is rather rarely measured, especially in continuous basis, and the spatial resolution of the measurements is sparse. Hence, different proxies have been developed to estimate the concentration based on commonly measured variables (Petäjä et al., 2009; Mikkonen et al., 2011).

Here, we introduce a revised proxy for sulfuric acid concentration with strong physical basis. The method is based on the proxy introduced by Petäjä et al. (2009). Their proxy accounted for the formation of sulfuric acid by oxidation of sulfur dioxide by OH radicals and loss of the molecules on the pre-existing particles (condensation sink, CS). However, recent studies have shown the importance of stabilized criegee intermediates in the oxidation of sulfur dioxide (Mauldin et al., 2012). Thus, the revised proxy accounts also for the formation of sulfuric acid due to oxidation by stabilized criegee intermediates but also takes into account the loss of sulfuric acid due to formation of dimers (Jen et al., 2014).

METHODS

Criegee intermediates are formed in the ozonolysis of alkenes (Mauldin et al., 2012). In boreal forests monoterpenes (MT) form a significant share of emitted organic compounds, and are thus used here as a proxy for alkenes (Hellén et al., 2018). When including all the above mentioned processes, the rate of change in sulfuric acid concentration is

$$\frac{d[H_2SO_4]}{dt} = k_0[OH][SO_2] + k_2[O_3][MT][SO_2] - CS[H_2SO_4] - k_3[H_2SO_4]^2. \quad (1)$$

In the equation, k_0 , k_2 and k_3 are empirical scaling coefficients. Because ambient OH concentration is difficult to measure, in this work we use UVB radiation to estimate the concentration since it is mainly formed in the photolysis of ozone by UVB radiation (Petäjä et al., 2009). Therefore, the equation becomes

$$\frac{d[H_2SO_4]}{dt} = k_1 UVB [SO_2] + k_2 [O_3] [MT] [SO_2] - CS [H_2SO_4] - k_3 [H_2SO_4]^2, \quad (2)$$

where k_1 is empirical scaling parameter. Assuming a steady state condition, we finally get a formula for the concentration of sulfuric acid

$$[H_2SO_4] = \frac{-CS}{2k_3} + \sqrt{\left(\frac{CS}{2k_3}\right)^2 + \frac{[SO_2]}{k_3} (k_1 UVB + k_2 [O_3] [MT])} \quad (3)$$

The proxy is developed with measurement data from SMEAR II (Station for Measuring Ecosystem-Atmosphere Relations) in Hyytiälä, Finland from years 2016-2019 (Hari et al., 2013). Condensation sink is obtained from the number size distribution measurements with differential mobility particle sizer (Aalto et al., 2001). Ozone, sulfur dioxide and UVB radiation are measured in continuous basis at the station. Alkenes represented by monoterpenes are measured with proton-transfer-reaction mass spectrometer and sulfuric acid with chemical ionization ambient pressure interface time-of-flight mass spectrometer (Taipale et al., 2008; Jokinen et al., 2012). Sulfuric acid concentration is measured at 35 m high tower, and other gas concentrations at 16.8 m height above the ground level. The scaling factors are obtained by minimising the sum of the squared difference between the proxy values and measured sulfuric acid concentration using a build-in function *fminsearch* of MATLAB, giving the optimal values for the coefficients.

To take into account the diurnal variation in the atmospheric chemistry, we separate day and nighttime values with respect to solar zenith angle (SZA). As daytime, we consider times when SZA is less than 65°, and nighttime when SZA is equal to or larger than 65°. Equation (3) is used in both cases, but the scaling coefficients are calculated independently.

RESULTS

Table 1 lists the scaling coefficients found by minimising the sum of squared difference between modeled and measured sulfuric acid. Applying the coefficients to the Equation (3) we could finally calculate the modeled sulfuric acid concentration. Figure 1 displays a scatter plot between the measured and modeled sulfuric acid concentration. The values correlate well, and the calculated Pearson's correlation coefficient was 0.79. Diurnal variation was also investigated. Figure 2 shows hourly medians of measured sulfuric acid concentration, new proxy and proxy by Petäjä et al. (2009). The plot shows that new proxy follows well the diurnal cycle of measured sulfuric acid concentration. Because the proxy by Petäjä et al. (2009) accounts only for production of sulfuric acid by oxidation of sulfur dioxide by OH radicals, the proxy does not take into the consideration the diurnal variation in atmospheric chemistry. During nighttime, when OH is not present, sulfuric acid is mainly produced by stabilized criegee intermediates, and thus the proxy by Petäjä et al. (2009) underestimates especially the nighttime values (Mauldin et al., 2012).

	$k_1 (\cdot 10^{-6} \text{ m}^2 \text{ W}^{-1} \text{ s}^{-1})$	$k_2 (\cdot 10^{-29} \text{ cm}^6 \text{ s}^{-1})$	$k_3 (\cdot 10^{-9} \text{ cm}^3 \text{ s}^{-1})$
Day	5.84	5.41	2.28
Night	1.37	8.40	1.12

Table 1. Scaling factors for boreal forest determined minimizing the sum of squared difference between measured and modeled sulfuric acid data.

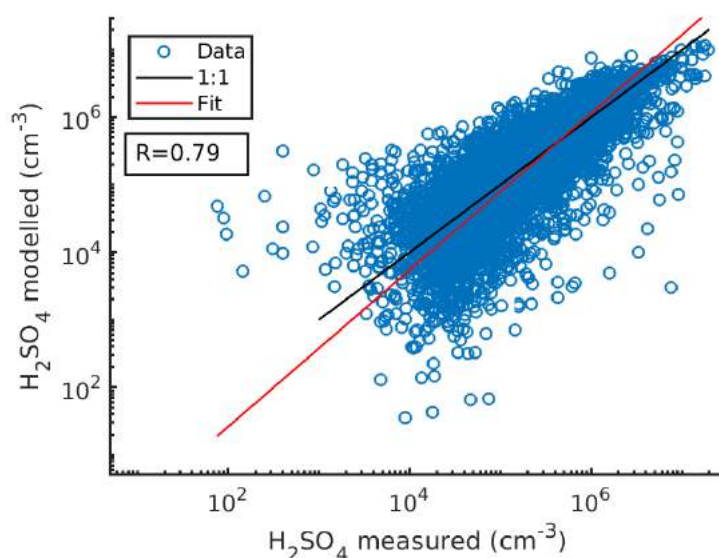


Figure 1. Scatter plot between the measured and modeled sulfuric acid concentration. Black line shows 1:1 line and red line fitted bivariate regression. Calculated Pearson's correlation coefficient was 0.79.

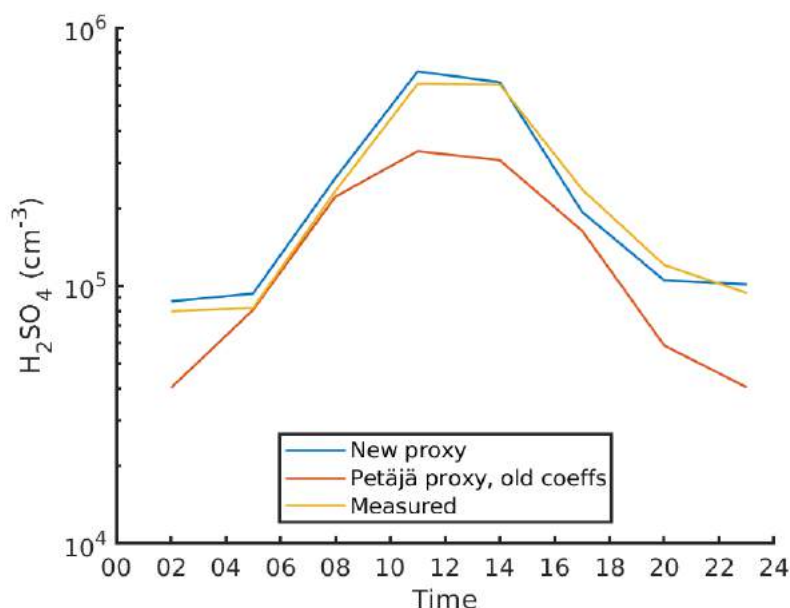


Figure 2. Hourly medians of revised sulphuric acid proxy (blue), proxy introduced by Petäjä et al. (2009; yellow), and measured sulfuric acid concentration at SMEAR II.

CONCLUSIONS

The revised proxy accounts for production of sulfuric acid by oxidation by both stabilized criegee intermediates and OH radicals and loss by condensation on pre-existing particles and dimer formation. Thus, the proxy is able to produce the observed diurnal variation in the sulfuric acid concentration. The obtained equations and coefficients should be used in the modeling of sulfuric acid concentration in boreal forests where the alkene concentration can be estimated with monoterpenes, and where the diurnal and seasonal variation in solar radiation are similar to the conditions in southern Finland.

ACKNOWLEDGEMENTS

This project has received funding from the ERC advanced grant No. 742206, the European Union's Horizon 2020 research and innovation program under grant agreement No. 654109, the Academy of Finland Center of Excellence project No. 27204.

REFERENCES

- Aalto, P., Hämeri, K., Becker, E. D. O., Weber, R., Salm, J., Mäkelä, J. M., ... & Koponen, I. K. (2001). Physical characterization of aerosol particles during nucleation events. *Tellus B: Chemical and Physical Meteorology*, 53(4), 344-358.
- Hallquist, M., Wenger, J. C., Baltensperger, U., Rudich, Y., Simpson, D., Claeys, M., ... & Hamilton, J. F. (2009). The formation, properties and impact of secondary organic aerosol: current and emerging issues. *Atmospheric chemistry and physics*, 9(14), 5155-5236.
- Hari, P., Nikinmaa, E., Pohja, T., Siivola, E., Bäck, J., Vesala, T., & Kulmala, M. (2013). Station for measuring ecosystem-atmosphere relations: SMEAR. In *Physical and physiological forest ecology* (pp. 471-487). Springer, Dordrecht.
- Hellén, H., Praplan, A. P., Tykkä, T., Ylivinkka, I., Vakkari, V., Bäck, J., ... & Hakola, H. (2018). Long-term measurements of volatile organic compounds highlight the importance of sesquiterpenes for the atmospheric chemistry of a boreal forest. *Atmospheric Chemistry and Physics*, 18(19), 13839-13863.
- Jen, C. N., McMurry, P. H., & Hanson, D. R. (2014). Stabilization of sulfuric acid dimers by ammonia, methylamine, dimethylamine, and trimethylamine. *Journal of Geophysical Research: Atmospheres*, 119(12), 7502-7514.
- Jokinen, T., Sipilä, M., Junninen, H., Ehn, M., Lönn, G., Hakala, J., ... & Worsnop, D. R. (2012). Atmospheric sulphuric acid and neutral cluster measurements using CI-API-TOF. *Atmospheric Chemistry and Physics*, 12(9), 4117-4125.
- Kulmala, M., Vehkamäki, H., Petaja, T., Maso, M. D., Lauri, A., Kerminen, V. M., ... & McMurry, P. H. (2004). Formation and growth rates of ultrafine atmospheric particles: a review of observations. *Aerosol Science* 35, 143-176.
- Kulmala, M., Kontkanen, J., Junninen, H., Lehtipalo, K., Manninen, H. E., Nieminen, T., ... & Franchin, A. (2013). Direct observations of atmospheric aerosol nucleation. *Science*, 339(6122), 943-946.
- Mauldin III, R. L., Berndt, T., Sipilä, M., Paasonen, P., Petäjä, T., Kim, S., ... & Kulmala, M. (2012). A new atmospherically relevant oxidant of sulphur dioxide. *Nature*, 488(7410), 193.
- Mikkonen, S., Romakkaniemi, S., Smith, J. N., Korhonen, H., Petäjä, T., Plass-Duelmer, C., ... & Hamed, A. (2011). A statistical proxy for sulphuric acid concentration. *Atmospheric Chemistry and Physics*, 11(21), 11319-11334.
- Petäjä, T., Mauldin III, R. L., Kosciuch, E., McGrath, J., Nieminen, T., Paasonen, P., ... & Kulmala, M. (2009). Sulfuric acid and OH concentrations in a boreal forest site. *Atmospheric Chemistry and Physics*, 9(19), 7435-7448.
- Taipale, R., Ruuskanen, T. M., Rinne, J., Kajos, M. K., Hakola, H., Pohja, T., & Kulmala, M. (2008). Quantitative long-term measurements of VOC concentrations by PTR-MS—measurement, calibration, and volume mixing ratio calculation methods. *Atmospheric Chemistry and Physics*, 8(22), 6681-6698.

MUTUAL INFORMATION INPUT SELECTOR AND PROBABILISTIC MACHINE LEARNING UTILISATION FOR AIR POLLUTION PROXIES

M.A. ZAIDAN¹, L. DADA¹, M.A. ALGHAMDI², H. AL-JEELANI², H. LIHAVAINEN^{3,4},
A. HYVÄRINEN³ AND T. HUSSEIN^{1,5}

¹Institute for Atmospheric & Earth System Research, Helsinki University, 00560 Helsinki, Finland

²Department of Environmental Sciences, Faculty of Meteorology, Environment and Arid Land Agriculture, King Abdulaziz University, P.O. Box 80208, Jeddah 21589, Saudi Arabia

³Finnish Meteorological Institute, Erik Palménin Aukio 1, FI-00101 Helsinki, Finland

⁴Svalbard Integrated Arctic Earth Observing System, PO Box 156, N-9171 Longyearbyen, Norway

⁵Department of Physics, The University of Jordan, Amman 11942, Jordan

Keywords: AIR POLLUTION, OZONE PROXY, PROBABILISTIC MACHINE LEARNING,
MUTUAL INFORMATION

INTRODUCTION

Air pollution describes the presence of harmful substances in the atmosphere, which are detrimental to human health as well as the Earth's climate. Air quality indicators are typically monitored by environmental or government authorities using networks of fixed monitoring stations, equipped with instruments specialised for measuring a number of pollutants, such as carbon monoxide (CO), nitrogen oxides (NO_x), sulphur dioxide (SO₂), ozone (O₃) and particulate matter (PM). In practice, a comprehensive measurement covering a large area may not always be possible as air pollutant analysers are generally complicated, bulky and labour-intensive (Kumar et al., 2015). Furthermore, instrument failure, fault in data acquisition or data corruption often result in missing data during research campaigns or continuous measurements (Junger and De Leon, 2015). If the data gap is relatively large, interpolation methods become ineffective. As a result, these problems pose a significant obstacle for comprehensive air pollution data analysis and time series prediction scheme.

In this work, we propose a solution by developing a pollutant proxy that is also known as a model or an estimator. A pollutant proxy can be defined as a mathematical model that estimates an unobserved air pollutant using other measured variables. Such a proxy acts as a virtual sensor or an expert system to fill missing data or to substitute one or more real measurements, thus the number of operated instruments can be minimised leading to a reduction in operational cost as well as the operators involved. Therefore, the area with pollution information can also be widened.

METHODOLOGY

Figure 1 presents a generic data-driven-based methodology for a pollutant proxy development and deployment. The concept is mainly based on two key approaches. The first is called a mutual information (MI) approach that is used to select the most relevant proxy inputs. The second is a probabilistic machine learning (PML) method that is used to model an air pollutant.

From data exploration, it is known how one measured variable is related to other measured variables. Standard correlation methods, such as Pearson correlation coefficient (PCC), is typically applied. However, as air pollution is a complex process, the relationship between the measured variables

may not always be linear. Therefore, we complement the correlation analysis by an information theory-based technique, named mutual information (MI), to search relevant measured variables correlated linearly and nonlinearly to an air pollutant to be modelled (Zaidan et al., 2018).

There is also a substantial amount of missing data. To solve the problem in practice, an additional guidance method is required for inputs selection. When generating a proxy, we are often limited to the measurement period during which data of all variables exist (i.e., the data with same time index). This leads to fewer data points available as the inputs for training phase of the pollutant proxy. The missing data scenario results in significant data loss for the training purposes. Furthermore, the use of a large number of inputs typically increases the model complexity leading to poor proxy performance. Limiting the number of inputs also allows the proxy to be used flexibly without relying on many other measurements in practice. Therefore, it is vital to consider these effects when determining the number of inputs involved in modelling, shown as the box of performance and data loss monitoring in Figure 1. The selected input data is then used for PML training and validation data. In this case, we select Bayesian neural network (BNN) as PML method due to its nature in providing confidence interval as well as robustness in dealing with over-fitting (Gal and Ghahramani, 2016; Zaidan et al., 2016). Finally the results are validated and analysed.

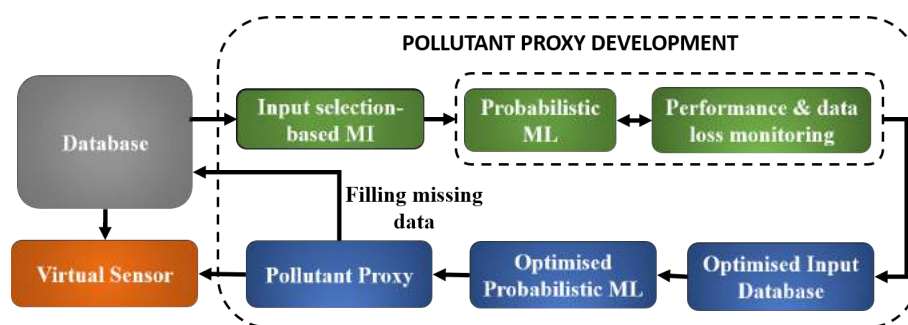


Figure 1: The block diagram of general methodology for pollutant proxy development.

In order to validate our approach, we use an extensive measurement data obtained in Jeddah, Saudi Arabia. The site is located at 21.4869 °N, 39.2517 °E and the altitude is 38.7 m above sea level. The measurement site is about 105 m and 1.7 km to the nearest road and the major highway, respectively. The measurements were performed at the height of 3.5 m and 6.7 m for gaseous air pollutants and meteorological parameters above the ground level, respectively. The sampling originally took place from 31 July 2011 to 28 February 2013. In particular, we choose to develop a proxy of ozone (O₃) concentration, but the proposed method is also generic for other types of air pollutant. The O₃ concentration data is only available for 258 days. Other measured variables include trace gases, such as NO, NO₂, NO_x, volatile organic compound (VOC), particulate matter, such as PM₁₀, PM_{2.5} and PM₁ and particle number concentrations as well as solar radiation and meteorological variables. The detailed explanation of the sampling site, data sets and the instruments used in this research campaign can be found in the previous work (Alghamdi et al., 2014a).

RESULTS AND CONCLUSIONS

The developed proxy was validated using the remaining data that was not used in the proxy training (i.e. test data). The performance metric values of MAE and R² are at 5.595 μg/m³ and 0.83, respectively. The proxy performance is considered to be adequate and the proxy is then tested against long-term measurements in Jeddah city.

It is known that the pollutant O₃ concentration differs between weekend and weekday, as well as day and night, due to the variation of traffic volumes in big cities (Blanchard et al., 2008). An

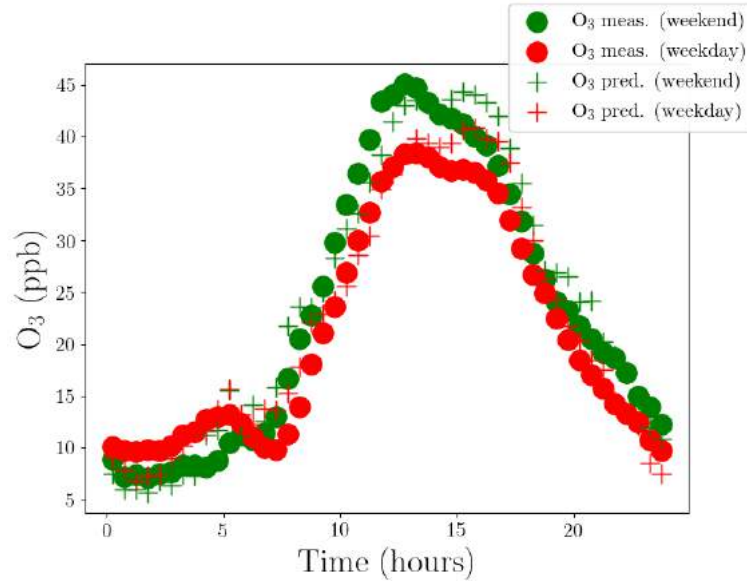


Figure 2: The average of the measurement and estimation of Ozone concentration from two different models on weekday and weekend in Jeddah, Saudi Arabia.

investigation of weekday and weekend differences in O_3 - NO_x levels is an important indicator to understand whether O_3 has its origin in local photochemical production or in transport processes (Alghamdi et al., 2014a). Figure 2 presents the average of the measured and estimated O_3 concentration on weekday and weekend. It can be seen that lower NO_x levels and higher O_3 values at weekends than on weekdays took place in Jeddah. This phenomenon is common to be observed mainly within areas with an influence from urban emissions. This occurs due to weekly changes in emissions from human activities. The relationship of emission-concentration relationship at urban, suburban and rural sites is discussed in Stephens et al. (2008). Considering the significance of having both measurements of O_3 and NO_x concentration, the developed proxy performance on the O_3 is evaluated on the concentration characteristic in the area as shown in Figure 2. It can be seen clearly that our developed estimated O_3 concentration fits very well the average measurement data on weekday and weekend. This suggests that the developed O_3 proxy is reliable and accurate as the substitution of O_3 real measurement. Having the O_3 virtual measurement is then beneficial to study the pollutant sources by reducing the cost and operator involvement.

ACKNOWLEDGEMENTS

This research was part of a close collaboration between King Abdulaziz University (KAU) and the Institute for Atmospheric and Earth System Research (INAR/Physics) University of Helsinki via ERA-PLANET (www.era-planet.eu), transnational project SMURBS (www.smurbs.eu) (Grant Agreement no. 689443), funded under the EU Horizon 2020 Framework Programme and Academy of Finland via the Center of Excellence in Atmospheric sciences (grant no. 272041) and NanoBioMass (project number 1307537). The research campaign was funded by Deanship of Scientific Research (DSR) at KAU, Jeddah (grant no. I-122-30). The first author (M.A.Z.) was supported by the Academy of Finland Centre of Excellence in Atmospheric Sciences (project number 307331) and the EU Urban Innovative Actions via HOPE project (grant number UIA03-240).

REFERENCES

- Junger, W.; De Leon, A.P. Imputation of missing data in time series for air pollutants. *Atmos. Environ.* **2015**, *102*, 96–104.
- Kumar, P.; Morawska, L.; Martani, C.; Biskos, G.; Neophytou, M.; Di Sabatino, S.; Bell, M.; Norford, L.; Britter, R. The rise of low-cost sensing for managing air pollution in cities. *Environ. Int.* **2015**, *75*, 199–205.
- Zaidan, M.A.; Haapasilta, V.; Relan, R.; Paasonen, P.; Kerminen, V.M.; Junninen, H.; Kulmala, M.; Foster, A.S. Exploring nonlinear associations between atmospheric new-particle formation and ambient variables: A mutual information approach. *Atmos. Chem. Phys.* **2018**, *18*, 12699–12714.
- Gal, Y.; Ghahramani, Z. Dropout as a Bayesian approximation: Representing model uncertainty in deep learning. In Proceedings of the International Conference on Machine Learning, New York, NY, USA, 19–24 June 2016; pp. 1050–1059.
- Zaidan, M.A.; Canova, F.F.; Laurson, L.; Foster, A.S. Mixture of clustered Bayesian neural networks for modeling friction processes at the nanoscale. *J. Chem. Theory Comput.* **2016**, *13*, 3–8.
- Alghamdi, M.; Khoder, M.; Harrison, R.M.; Hyvärinen, A.P.; Hussein, T.; Al-Jeelani, H.; Abdelmaksoud, A.; Goknil, M.; Shabbaj, I.; Almehmadi, F.; et al. Temporal variations of O₃ and NO_x in the urban background atmosphere of the coastal city Jeddah, Saudi Arabia. *Atmos. Environ.* **2014**, *94*, 205–214.
- Blanchard, C.L.; Tanenbaum, S.; Lawson, D.R. Differences between weekday and weekend air pollutant levels in Atlanta; Baltimore; Chicago; Dallas–Fort Worth; Denver; Houston; New York; Phoenix; Washington, DC; and surrounding areas. *J. Air Waste Manag. Assoc.* **2008**, *58*, 1598–1615.
- Alghamdi, M.; Khoder, M.; Harrison, R.M.; Hyvärinen, A.P.; Hussein, T.; Al-Jeelani, H.; Abdelmaksoud, A.; Goknil, M.; Shabbaj, I.; Almehmadi, F.; et al. Temporal variations of O₃ and NO_x in the urban background atmosphere of the coastal city Jeddah, Saudi Arabia. *Atmos. Environ.* **2014**, *94*, 205–214.
- Stephens, S.; Madronich, S.; Wu, F.; Olson, J.; Ramos, R.; Retama, A.; Munoz, R. Weekly patterns of México City’s surface concentrations of CO, NO_x, PM₁₀ and O₃ during 1986–2007. *Atmos. Chem. Phys.* **2008**, *8*, 5313–5325.

HOM CLUSTER FRAGMENTATION IN API-TOF MASS SPECTROMETERS

T. ZANCA¹, J. KUBEČKA¹, E. ZAPADINSKY¹, M. PASSANANTI^{1,2}, T. KURTÉN³
and H. VEHKAMÄKI¹

¹ Institute for Atmospheric and Earth System Research / Physics, Faculty of Science, University of Helsinki, P.O. Box 64, 00014 Helsinki, Finland.

² Dipartimento di Chimica, Università di Torino, via Giuria 5, 10125 Torino, Italy

³ Institute for Atmospheric and Earth System Research / Chemistry, Faculty of Science, University of Helsinki, P.O. Box 55, 00014, Helsinki, Finland

Keywords: Fragmentation of clusters, APi-TOF mass spectrometers, HOM.

INTRODUCTION

Recent developments in mass spectrometry have brought huge advancements to the field of atmospheric science. For example, mass spectrometers are now able to detect ppq-level concentrations of both clusters and precursor vapours in atmospheric samples (Junninen et al., 2010; Jokinen et al., 2012), as well as directly explore the chemistry of new particle formation (NPF) in the atmosphere (Kulmala et al., 2014; Bianchi et al., 2016; Ehn et al., 2014). One of the most common mass spectrometers used to measure online cluster composition and concentration in the atmosphere is the Atmospheric Pressure interface Time Of Flight Mass Spectrometer (APi-TOF MS). Unfortunately, the detection process in the APi-TOF involves energetic interactions between the carrier gas and the clusters, possibly leading to their fragmentation, and thus altering the measurement results.

Cluster fragmentation in the APi-TOF is one of the main sources of uncertainty in the measurements. Despite this, its dynamics has not been studied very thoroughly so far, and it still misses fundamental work. Here we use a theoretical model to study in detail the fragmentation of clusters involving so-called Highly-Oxygenated organic Molecules (HOM), which have recently been identified as a key contributor to NPF (Bianchi et al., 2019). Our study involves a specific kind of representative HOM ($C_{10}H_{16}O_8$). This elemental composition corresponds to one of the most common mass peaks observed in experiments on ozone-initiated autoxidation of α -pinene, which also fulfills the “HOM” definition of (Bianchi et al., 2019). The precise molecular structure was adopted from (Kurtén et al., 2016), and corresponds to the lowest-volatility structural isomer of the three $C_{10}H_{16}O_8$ compounds investigated in that study. The structure of the molecule is shown in Fig. 1.

The main scope of this work is to determine to what extent we are able to perform measurements of atmospheric cluster concentrations using APi-TOF mass spectrometers. More specifically, we want to determine whether fragmentation can possibly be responsible for the lack of observations of some HOM-containing clusters in an APi-TOF. Here, we predict both an upper bound for fragmentation energy necessary for fragmentation in the APi-TOF, and a lower bound for new-particle formation in the atmosphere given realistic vapor concentrations. The former can be evaluated using a numerical model initially developed by (Zapadinsky et al., 2018), while the latter is computed using the Atmospheric Cluster Dynamics Code (ACDC) (McGrath et al., 2012).

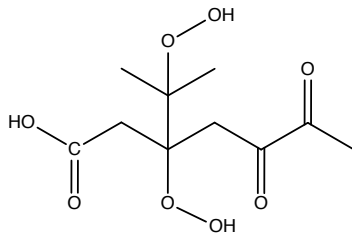


Figure 1: Molecular structure of the model $C_{10}H_{16}O_8$ HOM used in this study.

METHODS

The model computes the probability of fragmentation of a single negatively-charged cluster from a large number ($\approx 10^3$) of independent stochastic realizations of its dynamics in the APi. We give here a brief description. For detailed description see (Zapadinsky et al., 2018).

The dynamics starts with the ionized cluster accelerating in the mass spectrometer under the effect of an electric field generated by the electrodes inside the APi. While moving, a random time interval to the next collision is computed from the cumulative distribution function $\mathcal{P}_{\text{coll}}(t)$, which expresses the probability to encounter a collision after a time t :

$$\mathcal{P}_{\text{coll}}(t) = 1 - e^{-\int_0^t \Upsilon[v(t')] dt'} . \quad (1)$$

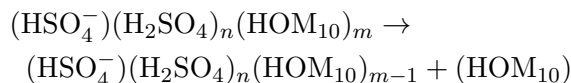
Here, Υ is the collision frequency which depends on the cluster velocity v , while $t = 0$ is the moment when the previous collision occurred. Simultaneously, another random time interval is computed for the fragmentation event from a Poisson distribution, which corresponds to the time-dependent survival probability $\mathcal{P}_{\text{surv}}$ after collision:

$$\mathcal{P}_{\text{surv}}(t) = 1 - \mathcal{P}_{\text{frag}} = e^{-k(\Delta E)t} , \quad (2)$$

where $\mathcal{P}_{\text{frag}}$ is the fragmentation probability and k , the fragmentation rate constant, is the inverse of the statistical average of fragmentation time, which depends on the cluster excess energy ΔE beyond its fragmentation energy threshold. The fragmentation time is interpreted as the time the cluster spends intact before fragmenting. The fragmentation rate constant is derived from equilibrium condition between fragmentation and recombination processes using the detailed balance condition (Zapadinsky et al., 2018). At this point, if the time required by the cluster to escape from the simulated region of the mass spectrometer is less than both the collision and fragmentation times, the single realization is completed and the counting of intact clusters is increased by one. A second possibility is that the fragmentation time is smaller than collision and escape times, in which case the count of fragmented clusters is increased by one. Finally, as third possibility, the collision time may be the smallest, in which case a collision between the cluster and a carrier gas molecule takes place. The dynamics of the collision is described by a stochastic process, where random velocities for the carrier gas molecules are computed from the Maxwell-Boltzmann distribution. In this case, the motion of the gas molecules is considered as solely translational. During the collision, the kinetic energy of the two colliding objects is partially transferred to the internal degrees of freedom of the cluster (vibrational and rotational modes), according to the microcanonical ensemble approach: any equally-energetic configuration of the system is equally-probable. After collision, the energy is then redistributed between rotational and vibrational modes following the same principle, and the dynamics repeats from the acceleration of cluster.

CONCLUSIONS

The simulation region involves only a portion of the total length of the APi-TOF mass spectrometer. Specifically, the simulations take place in the most critical region, between the end of the first chamber and the second one, where the pressure values make fragmentation possible. Before this region the collisions are not energetic enough, while after the carrier gas is so sparse that no collision happens (Zapadinsky et al., 2018). The voltage and pressure configuration in the simulations is the same used in CLOUD10 experiments (Lehtipalo et al., 2018). The clusters studied here are formed by one bisulfate anion, one sulfuric acid molecule and at least one HOM molecule. The clusters are assumed to fragment by losing one HOM, as follows:



with $n = 1, 2$, $m = 1, 2, 3$ and HOM_{10} is the structure shown in Fig. 1. Our specific choice for HOM is not unique: this is one among many potential HOM produced in the α -pinene + O_3 reaction. The compound chosen is broadly representative of autoxidation products as it contains both hydroperoxide, ketone and carboxylic acid groups. The clusters have been constructed by first maximizing H-bonds between the H_2SO_4^- core ion and other molecules, and then maximizing other H-bonds without creating too much strain. The final survival probabilities P_{surv} are shown in Fig. 2.

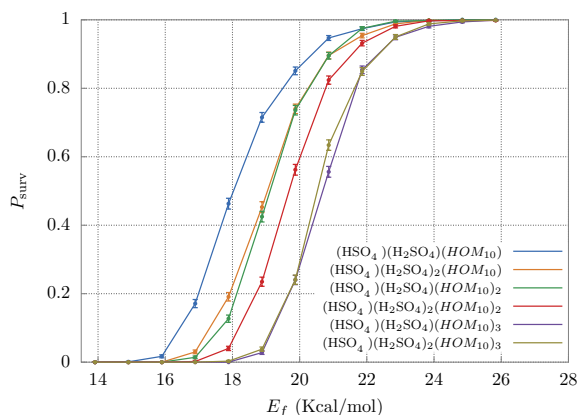


Figure 2: (Color online). Survival probabilities P_{surv} for different HOM clusters as a function of their fragmentation energy E_f . The error bars are relative only to statistical error.

In parallel to the simulations on fragmentation in the APi, we computed with ACDC the concentrations of HOM_{10} needed to provide a reasonable enhancement of new-particle formation rate in the atmosphere. Specifically, at given H_2SO_4 monomer concentration, and for a given value of fragmentation energy E_f , we computed the concentration of HOM_{10} at which the new-particle formation rate is increased by $1 \text{ cm}^{-3}\text{s}^{-1}$ (i.e. $J_{\text{sa+hom}} = J_{\text{sa}} + 1 \text{ cm}^{-3}\text{s}^{-1}$). In the simulation, the formation rate J is relative to clusters growing beyond $(\text{HSO}_4^-)(\text{H}_2\text{SO}_4)_4(\text{HOM}_{10})_{0-3}$ or $(\text{HSO}_4^-)(\text{H}_2\text{SO}_4)_{0-3}(\text{HOM}_{10})_4$. The increment in the formation rate value here is indicative, and it serves as a reference for a reasonable NPF process in the atmosphere (Lehtipalo et al., 2018). In the simulation, we assume a constant concentration of HSO_4^- equal to 700 cm^{-3} , which approximately corresponds to the steady-state anion concentration at a representative total anion pair formation rate due to galactic cosmic rays (GCR) of $J_{\text{ions}} = 4 \text{ cm}^{-3}\text{s}^{-1}$ (Kirkby et al., 2016).

The HOM clusters are subsequently formed by collisions between bisulfate anions, sulfuric acid and HOM molecules. As we can see in Fig. 3, the H_2SO_4 and HOM_{10} concentrations needed to

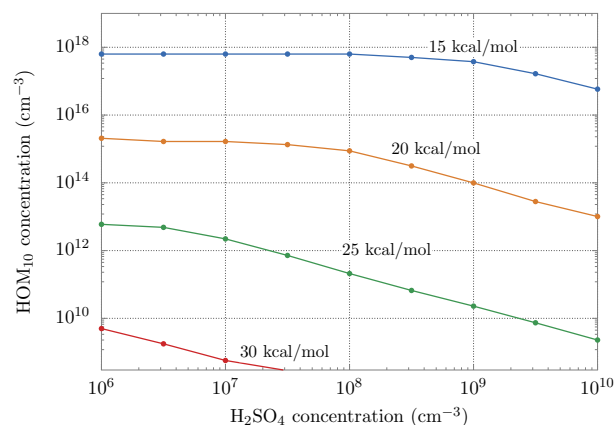


Figure 3: (Color online). Concentrations of HOM₁₀ needed to increment the new-particle formation rate J by $1 \text{ cm}^{-3}\text{s}^{-1}$, for different fragmentation energies.

provide the increment $\Delta J = 1 \text{ cm}^{-3}\text{s}^{-1}$ decrease when the fragmentation energy increases, reaching experimental conditions (e.g. non-nitrate HOM₁₀ and H₂SO₄ concentrations measured in CLOUD experiment (Lehtipalo et al., 2018)) at $E_f > 30 \text{ kcal/mol}$, where HOM₁₀ and H₂SO₄ concentrations do not exceed 10^8 cm^{-3} . At this fragmentation energy, fragmentation in APi is negligible ($P_{\text{surv}} \approx 1$ in Fig. 2). Thus we can conclude that for the case of $(\text{HSO}_4^-)(\text{H}_2\text{SO}_4)_n(\text{HOM}_{10})_m$ clusters, rapid formation in the atmosphere (given typical vapor concentrations) and significant fragmentation in the APi are mutually incompatible situations.

REFERENCES

- Bianchi, F., Kurtén, T., Riva, M., Mohr, C., Rissanen, M. P., Roldin, P., Berndt, T., Crouse, J. D., Wennberg, P. O., Mentel, T. F., Wildt, J., Junninen, H., Jokinen, T., Kulmala, M., Worsnop, D. R., Thornton, J. A., Donahue, N., Kjaergaard, H. G., and Ehn, M. (2019). Highly oxygenated organic molecules (HOM) from gas-phase autoxidation involving peroxy radicals: A key contributor to atmospheric aerosol. *Chemical Reviews*, 119(6):3472–3509.
- Bianchi, F., Trostl, J., Junninen, H., Frege, C., Henne, S., Hoyle, C. R., Molteni, U., Herrmann, E., Adamov, A., Bukowiecki, N., Chen, X., Duplissy, J., Gysel, M., Hutterli, M., Kangasluoma, J., Kontkanen, J., Kurten, A., Manninen, H. E., Munch, S., Perakyla, O., Petaja, T., Rondo, L., Williamson, C., Weingartner, E., Curtius, J., Worsnop, D. R., Kulmala, M., Dommen, J., and Baltensperger, U. (2016). New particle formation in the free troposphere: A question of chemistry and timing. *Science*, 352(6289):1109–1112.
- Ehn, M., Thornton, J. A., Kleist, E., Sipilä, M., Junninen, H., Pullinen, I., Springer, M., Rubach, F., Tillmann, R., Lee, B., Lopez-Hilfiker, F., Andres, S., Acir, I.-H., Rissanen, M., Jokinen, T., Schobesberger, S., Kangasluoma, J., Kontkanen, J., Nieminen, T., Kurtén, T., Nielsen, L. B., Jørgensen, S., Kjaergaard, H. G., Canagaratna, M., Maso, M. D., Berndt, T., Petäjä, T., Wahner, A., Kerminen, V.-M., Kulmala, M., Worsnop, D. R., Wildt, J., and Mentel, T. F. (2014). A large source of low-volatility secondary organic aerosol. *Nature*, 506(7489):476–479.
- Jokinen, T., Sipilä, M., Junninen, H., Ehn, M., Lönn, G., Hakala, J., Petäjä, T., Mauldin, R. L., Kulmala, M., and Worsnop, D. R. (2012). Atmospheric sulphuric acid and neutral cluster measurements using CI-APi-TOF. *Atmospheric Chemistry and Physics*, 12(9):4117–4125.
- Junninen, H., Ehn, M., Petäjä, T., Luosujärvi, L., Kotiaho, T., Kostianen, R., Rohner, U., Gonin,

- M., Fuhrer, K., Kulmala, M., and Worsnop, D. R. (2010). A high-resolution mass spectrometer to measure atmospheric ion composition. *Atmospheric Measurement Techniques*, 3(4):1039–1053.
- Kirkby, J., Duplissy, J., Sengupta, K., Frege, C., Gordon, H., Williamson, C., Heinritzi, M., Simon, M., Yan, C., Almeida, J., Tröstl, J., Nieminen, T., Ortega, I. K., Wagner, R., Adamov, A., Amorim, A., Bernhammer, A.-K., Bianchi, F., Breitenlechner, M., Brilke, S., Chen, X., Craven, J., Dias, A., Ehrhart, S., Flagan, R. C., Franchin, A., Fuchs, C., Guida, R., Hakala, J., Hoyle, C. R., Jokinen, T., Junninen, H., Kangasluoma, J., Kim, J., Krapf, M., Kürten, A., Laaksonen, A., Lehtipalo, K., Makhmutov, V., Mathot, S., Molteni, U., Onnela, A., Peräkylä, O., Piel, F., Petäjä, T., Praplan, A. P., Pringle, K., Rap, A., Richards, N. A. D., Riipinen, I., Rissanen, M. P., Rondo, L., Sarnela, N., Schobesberger, S., Scott, C. E., Seinfeld, J. H., Sipilä, M., Steiner, G., Stozhkov, Y., Stratmann, F., Tomé, A., Virtanen, A., Vogel, A. L., Wagner, A. C., Wagner, P. E., Weingartner, E., Wimmer, D., Winkler, P. M., Ye, P., Zhang, X., Hansel, A., Dommen, J., Donahue, N. M., Worsnop, D. R., Baltensperger, U., Kulmala, M., Carslaw, K. S., and Curtius, J. (2016). Ion-induced nucleation of pure biogenic particles. *Nature*, 533(7604):521–526.
- Kulmala, M., Petäjä, T., Ehn, M., Thornton, J., Sipilä, M., Worsnop, D., and Kerminen, V.-M. (2014). Chemistry of atmospheric nucleation: On the recent advances on precursor characterization and atmospheric cluster composition in connection with atmospheric new particle formation. *Annual Review of Physical Chemistry*, 65(1):21–37.
- Kurtén, T., Tiusanen, K., Roldin, P., Rissanen, M., Luy, J.-N., Boy, M., Ehn, M., and Donahue, N. (2016). α -pinene autoxidation products may not have extremely low saturation vapor pressures despite high O:C ratios. *The Journal of Physical Chemistry A*, 120(16):2569–2582.
- Lehtipalo, K., Yan, C., Dada, L., Bianchi, F., Xiao, M., Wagner, R., Stolzenburg, D., Ahonen, L. R., Amorim, A., Baccarini, A., Bauer, P. S., Baumgartner, B., Bergen, A., Bernhammer, A.-K., Breitenlechner, M., Brilke, S., Buchholz, A., Mazon, S. B., Chen, D., Chen, X., Dias, A., Dommen, J., Draper, D. C., Duplissy, J., Ehn, M., Finkenzeller, H., Fischer, L., Frege, C., Fuchs, C., Garmash, O., Gordon, H., Hakala, J., He, X., Heikkinen, L., Heinritzi, M., Helm, J. C., Hofbauer, V., Hoyle, C. R., Jokinen, T., Kangasluoma, J., Kerminen, V.-M., Kim, C., Kirkby, J., Kontkanen, J., Kürten, A., Lawler, M. J., Mai, H., Mathot, S., Mauldin, R. L., Molteni, U., Nichman, L., Nie, W., Nieminen, T., Ojdanic, A., Onnela, A., Passananti, M., Petäjä, T., Piel, F., Pospisilova, V., Quéléver, L. L. J., Rissanen, M. P., Rose, C., Sarnela, N., Schallhart, S., Schuchmann, S., Sengupta, K., Simon, M., Sipilä, M., Tauber, C., Tomé, A., Tröstl, J., Väisänen, O., Vogel, A. L., Volkamer, R., Wagner, A. C., Wang, M., Weitz, L., Wimmer, D., Ye, P., Ylisirniö, A., Zha, Q., Carslaw, K. S., Curtius, J., Donahue, N. M., Flagan, R. C., Hansel, A., Riipinen, I., Virtanen, A., Winkler, P. M., Baltensperger, U., Kulmala, M., and Worsnop, D. R. (2018). Multicomponent new particle formation from sulfuric acid, ammonia, and biogenic vapors. *Science Advances*, 4(12):eaau5363.
- McGrath, M. J., Olenius, T., Ortega, I. K., Loukonen, V., Paasonen, P., Kurtén, T., Kulmala, M., and Vehkamäki, H. (2012). Atmospheric cluster dynamics code: a flexible method for solution of the birth-death equations. *Atmospheric Chemistry and Physics*, 12(5):2345–2355.
- Zapadinsky, E., Passananti, M., Mylly, N., Kurtén, T., and Vehkamäki, H. (2018). Modeling on fragmentation of clusters inside a mass spectrometer. *The Journal of Physical Chemistry A*, 123(2):611–624.

OBSERVATION OF HIGHLY OXYGENATED ORGANIC MOLECULES (HOM) ON TOP THE BOLIVIAN ANDES AT 5240M A.S.L.

Q. Zha¹, D. Aliaga¹, O. Peräkylä¹, X. Chen¹, J. Enroth¹, L. Heikkinen¹, M. Sipilä¹, T. Petäjä¹, M. Kulmala^{1,2}, C. Mohr³, and F. Bianchi¹

¹ Institute for Atmospheric and Earth System Research, University of Helsinki, 00014 Helsinki, Finland

² Department of Environmental Science and Analytical Chemistry (ACES), Stockholm University, 10691 Stockholm, Sweden

³ Aerosol and Haze Laboratory, Beijing Advanced Innovation Center for Soft Matter Science and Engineering, Beijing University of Chemical Technology, Beijing, 100029, P.R. China

Keywords: NPF, HOM, Amazon, Upper troposphere.

INTRODUCTION

New particle formation (NPF) is a significant contributor to atmospheric aerosol loading and can produce up to 50% of the world's cloud condensation nuclei (CCN). Most of the field observations of aerosol particles carried out up to date, in the terrestrial environments, are inevitably influenced by anthropogenic emissions, which makes it difficult to understand the particle formation process in the pristine condition. The Amazon rainforest is considered one of the few regions where the environment is close to natural conditions, but no NPF event has been observed in the Amazonian planetary boundary layer (PBL). Recently, high concentrations of the small particles (diameter <50 nm) have been observed in the aircraft-based studies over the Amazon basin, suggesting a large source of small aerosol particles is from the upper troposphere (UT) (Wang et al., 2016; Andreae et al., 2018). Studies from the European Center for Nuclear Research (CERN) Cosmics Leaving Outdoor Droplets (CLOUD) chamber have suggested highly oxygenated organic molecules (HOM) from biogenic emissions could play a key role in the nucleation process under pristine condition, due to their low volatilities (Kirkby et al., 2016; Bianchi et al., 2019). While Bianchi et al., (2016) showed that the frequently observed NPF events at the Jungfraujoch (3580m a.s.l.) in Central Europe was majorly driven by the condensation of HOMs, our results indicate that the nucleation process over Amazon basin may be also driven by HOMs and temperature.

METHODS

The Southern hemisphere high ALTitude Experiment on particle NucleAtion and growth (SALTENA) campaign was performed from December 2017 to June 2018 in the Chacaltaya station (5240m, a.s.l.) in Bolivia. During the nighttime, the station is frequently located in the UT (Rose et al., 2017). The station is ~30km away from the city area of La Paz. A set of state-of-the-art instruments were deployed to systematically understand NPF events. Chemical composition information of ion clusters was provided by an Atmospheric Pressure interface Time-Of-Flight (APi-TOF). Atmospheric HOMs and sulfuric acid (SA) concentrations were measured with a Chemical Ionization APi-TOF (CI-APi-TOF) equipped with a nitrate inlet. Concentration and distribution of aerosol particles were measured with a particle size magnifier (PSM), a neutral cluster air ion spectrometer (NAIS, also measuring ion cluster concentrations), and a scanning mobility particle sizer (SMPS). Trace gases, solar radiation, and meteorological parameters were also measured.

CONCLUSIONS

Preliminary results show that organic molecules were dominated by the oxidation products from isoprene (C_5H_8) during nighttime when the site was considered frequently locating in the UT (Fig. 1).

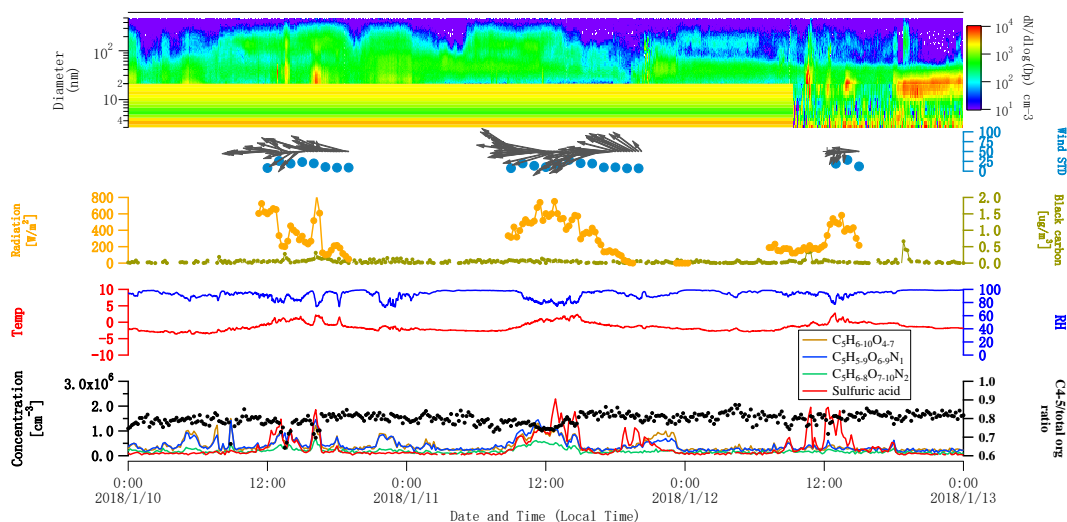


Figure 1. Time series of a selected period when the site was located in the air from Amazon.

ACKNOWLEDGEMENTS

The authors would like to thank all staff at Chacaltaya GAW station for technical support. We also thank the tofTools team for providing tools for mass spectrometry analysis.

REFERENCES

- Andreae, M. O., Afchine, A., Albrecht, R., Amorim Holanda, B., Artaxo, P., Barbosa, H. M. J., Borrmann, S., Cecchini, M. A., Costa, A., Dollner, M., Fütterer, D., Järvinen, E., Jurkat, T., Klimach, T., Konemann, T., Knote, C., Krämer, M., Krisna, T., Machado, L. A. T., Mertes, S., Minikin, A., Pöhlker, C., Pöhlker, M. L., Pöschl, U., Rosenfeld, D., Sauer, D., Schlager, H., Schnaiter, M., Schneider, J., Schulz, C., Spanu, A., Sperling, V. B., Voigt, C., Walser, A., Wang, J., Weinzierl, B., Wendisch, M. and Ziereis, H.: Aerosol characteristics and particle production in the upper troposphere over the Amazon Basin, *Atmos. Chem. Phys.*, 18(2), 921–961, doi:10.5194/acp-18-921-2018, 2018.
- Bianchi, F., Kurtén, T., Riva, M., Mohr, C., Rissanen, M. P., Roldin, P., Berndt, T., Crouse, J. D., Wennberg, P. O., Mentel, T. F., Wildt, J., Junninen, H., Jokinen, T., Kulmala, M., Worsnop, D. R., Thornton, J. A., Donahue, N., Kjaergaard, H. G. and Ehn, M.: Highly Oxygenated Molecules (HOM) from Gas-Phase Autoxidation Involving Organic Peroxy Radicals: A Key Contributor to Atmospheric Aerosol, *Chem. Rev.*, acs.chemrev.8b00395, doi:10.1021/acs.chemrev.8b00395, 2019.

Kirkby, J., Duplissy, J., Sengupta, K., Frege, C., Gordon, H., Williamson, C., Heinritzi, M., Simon, M., Yan, C., Almeida, J., Tröstl, J., Nieminen, T., Ortega, I. K., Wagner, R., Adamov, A., Amorim, A., Bernhammer, A.-K., Bianchi, F., Breitenlechner, M., Brilke, S., Chen, X., Craven, J., Dias, A., Ehrhart, S., Flagan, R. C., Franchin, A., Fuchs, C., Guida, R., Hakala, J., Hoyle, C. R., Jokinen, T., Junninen, H., Kangasluoma, J., Kim, J., Krapf, M., Kürten, A., Laaksonen, A., Lehtipalo, K., Makhmutov, V., Mathot, S., Molteni, U., Onnela, A., Peräkylä, O., Piel, F., Petäjä, T., Praplan, A. P., Pringle, K., Rap, A., Richards, N. A. D., Riipinen, I., Rissanen, M. P., Rondo, L., Sarnela, N., Schobesberger, S., Scott, C. E., Seinfeld, J. H., Sipilä, M., Steiner, G., Stozhkov, Y., Stratmann, F., Tomé, A., Virtanen, A., Vogel, A. L., Wagner, A. C., Wagner, P. E., Weingartner, E., Wimmer, D., Winkler, P. M., Ye, P., Zhang, X., Hansel, A., Dommen, J., Donahue, N. M., Worsnop, D. R., Baltensperger, U., Kulmala, M., Carslaw, K. S. and Curtius, J.: Ion-induced nucleation of pure biogenic particles, *Nature*, 533(7604), 521–526, doi:10.1038/nature17953, 2016.

Rose, C., Sellegri, K., Moreno, I., Velarde, F., Ramonet, M., Weinhold, K., Krejci, R., Andrade, M., Wiedensohler, A., Ginot, P. and Laj, P.: CCN production by new particle formation in the free troposphere, *Atmos. Chem. Phys.*, 17, 1529–1541, doi:10.5194/acp-17-1529-2017, 2017.

Wang, J., Krejci, R., Giangrande, S., Kuang, C., Barbosa, H. M. J., Brito, J., Carbone, S., Chi, X., Comstock, J., Ditas, F., Lavric, J., Manninen, H. E., Mei, F., Moran-Zuloaga, D., Pöhlker, C., Pöhlker, M. L., Saturno, J., Schmid, B., Souza, R. A. F., Springston, S. R., Tomlinson, J. M., Toto, T., Walter, D., Wimmer, D., Smith, J. N., Kulmala, M., Machado, L. A. T., Artaxo, P., Andreae, M. O., Petäjä, T. and Martin, S. T.: Amazon boundary layer aerosol concentration sustained by vertical transport during rainfall, *Nature*, 539(7629), 416–419, doi:10.1038/nature19819, 2016.

A PROTOCOL FOR PROCESSING LONG-TERM FLUORESCENCE DATA OBTAINED FROM MONITORING PAM SYSTEM

C. ZHANG¹, J. ATHERTON¹, A. PORCAR-CASTELL¹

¹Optics of Photosynthesis Laboratory, Institute for Atmospheric and Earth system research (INAR/Forest Sciences), University of Helsinki, PO Box 27, 00014 Helsinki, Finland

Keywords: CHLOROPHYLL A FLUORESCENCE, MONI-PAM, DATA FILTERING, DATA PROCESSING, R PACKAGE

INTRODUCTION

Chlorophyll a fluorescence (ChIF) are re-emitted photons by chlorophyll molecules from absorbed light energy, competing the photosynthetic excitation energy with photochemistry and heat dissipation. The pulse-amplitude-modulated (PAM) technique has been widely used decades to actively measure ChIF and to study leaf photosynthetic properties and partitioning of excitation energy (Baker 2008). The MONITORING-PAM Multi-Channel Chlorophyll Fluorometer (MONI-PAM) provides a continuous and long-term measurement of photosynthetic properties under field conditions (Porcar-Castell et al., 2008, 2011).

The current documentation about the description of MONI-PAM system is not enough to support its utilization. To estimate photosynthetic parameters, absolute ChIF levels measured from MONI-PAM systems are required. However, how to accurately obtain ChIF is challenging because variations of ChIF signal measured from MONI-PAM system are not only dependent on physiological changes but also on other factors (e.g. environmental and physical factors, and instrumental artifacts). In particular, snow, water condensation, or leaf movement could lead to wrong measurement of ChIF, data during which need to be filtered. For long-term measurement, internal MONI-PAM data acquisition system (MONI-DA) clock can suffer from drift or be changed accidentally thus need to be corrected, internal temperature or PAR sensor also need to be calibrated regularly, and ambient temperature can affect performances of LED light and therefore intensities of measuring light and levels of ChIF signal. All aforementioned factors could induce inaccurate measurement of ChIF signals and are necessarily documented. Hence, properly filtering and processing dataset and carefully maintaining the MONI-PAM system are critical for finally estimating ChIF or photosynthetic related parameters and further applying to photosynthetic research.

This protocol aims to detailed describe MONI-PAM system, to introduce how to maintain MONI-PAM, and to provide automatically filtering functions and build an R package for processing data obtained from MONI-PAM system.

RESULTS

Preliminary results from automatically filtering functions are shown in Figure 1. Our results showed that most of strange or bad records (e.g., data measured on May 5th and 6th for

Pine1Top, May 5th for Pine2Top, or May 2nd-6th and May 11th for Pine3) have been successfully selected and flagged. These flagged observations, that had relatively lower values of F' and F'_m compared with normal days (e.g. May 7th-10th for Pine2Mid), were probably resulted from low temperature that induced water condensation in the leaf surface during evening or morning. The next step is to set appropriate thresholds for filtering the dataset to optimize the performance of current filtering functions, and to build an R package to process MONI-PAM dataset.

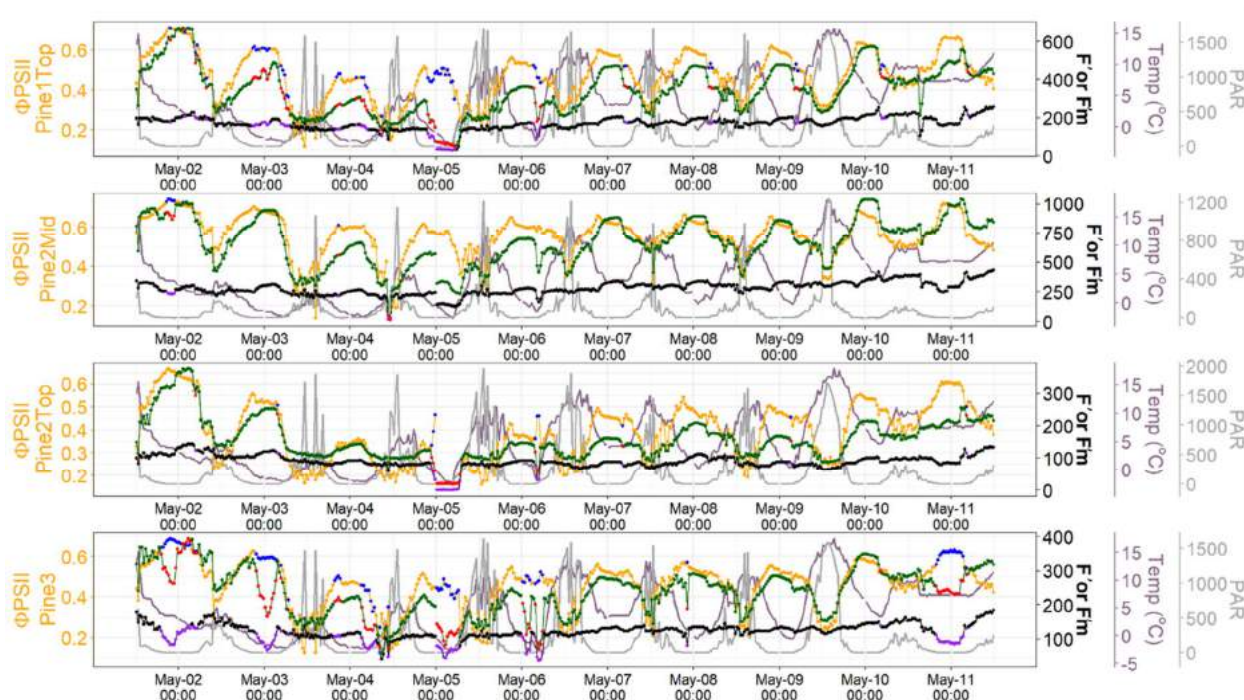


Figure 1. Performance of automatically filtering functions for processing data observed from MONI-PAM system. Measurements were conducted in one-year old needles for mature *Pinus sylvestris* trees for the beginning of May in 2019. Measurements were mainly conducted at the top canopy of three different trees (Pine1Top, Pine2Top and Pine3) respectively, and one more measurement was conducted at the middle canopy of second tree (Pine2Mid). The MONI-PAM system records the instantaneous fluorescence yield (F' , black points), the maximal fluorescence yield (F'_m , green points), the actual quantum yield of PSII (Φ PSII, orange points), incoming PAR (grey line), and temperature (purple line) every 30 min. Blue, red or dark purple points are flagged data or outliers produced from automatically filtering functions for Φ PSII, F'_m , and F' respectively.

ACKNOWLEDGEMENTS

We acknowledge the financial support from the Academy of Finland (Projects 288039, 319211).

REFERENCES

Baker, N.R., 2008. Chlorophyll fluorescence: a probe of photosynthesis in vivo. *Annu. Rev. Plant Biol.*, 59, pp.89-113.

Porcar-Castell, A., Pfündel, E., Korhonen, J.F. and Juurola, E., 2008. A new monitoring PAM fluorometer (MONI-PAM) to study the short-and long-term acclimation of photosystem II in field conditions. *Photosynthesis Research*, 96(2), pp.173-179.

Porcar-Castell, A., 2011. A high-resolution portrait of the annual dynamics of photochemical and non-photochemical quenching in needles of *Pinus sylvestris*. *Physiologia Plantarum*, 143(2), pp.139-153.

THE RESPONSE OF PEATLAND METHANE EMISSIONS TO WARMING

H. ZHANG^{1,2}, A. KORRENSALO³, N. WELTI⁴, A. M. LAINE^{3,5}, E.-S. TUUTTILA³, M. MALJANEN⁶, D. ELLIOTT⁷, T. VESALA¹ and A. LOHILA^{1,8}

¹Institute for Atmospheric and Earth System Research (INAR), Department of Physics, P.O. Box 68 (Pietari Kalmin katu 5), University of Helsinki, Helsinki, Finland

²Helsinki Institute of Sustainability Science (HELSUS), Helsinki, Finland

³Department of Forest Sciences, University of Eastern Finland, Joensuu, Finland

⁴Commonwealth Scientific and Industrial Research Organization, Australia

⁵Department of Ecology and Genetics, University of Oulu, Oulu, Finland

⁶Department of Environmental and Life Sciences, University of Eastern Finland, Joensuu, Finland

⁷College of Life and Natural Sciences, University of Derby, Derby, UK

⁸Climate System Research, Finnish Meteorological Institute, Helsinki, Finland

Keywords: METHANE, PRODUCTION AND OXIDATION, PEATLANDS, TEMPERATURE SENSITIVITY.

Northern peatlands are projected to play a crucial role in future atmospheric methane (CH₄) budget and have a positive feedback to global warming (Zhang *et al.*, 2017). Yet, the mechanistic processes of CH₄ emissions, i.e. CH₄ production and oxidation, especially their sensitivity to global warming are rarely studied, thus large uncertainties still remain for future CH₄ budget projection.

Here we collected peat samples from 14 peatlands in Finland, spanning approximately 10 latitudinal degrees and representing ombrotrophic bogs, and oligotrophic and mesotrophic fens (Figure 1a). We aim to 1) quantify CH₄ production and oxidation potentials in different temperatures (5, 17.5 and 30 °C), and 2) explore the environmental factors that drive CH₄ dynamic patterns.

Our preliminary results showed that CH₄ production and oxidation increased with increasing temperature for all peatland types (Figure 1bc). At the same temperature conditions, CH₄ production potentials showed variable values within different peatland types, while CH₄ oxidation potentials were relatively consistent for different peatland types. In addition, CH₄ production in mesotrophic fens was clearly higher than that in other peatland types, which is likely to explain the generally higher CH₄ flux emissions in fens than bogs (Turetsky *et al.*, 2014). Our next step is to link the CH₄ dynamic patterns to their methanogen and methanotroph communities, substrate properties, and vegetation using ordination analyses and mixed effect models.

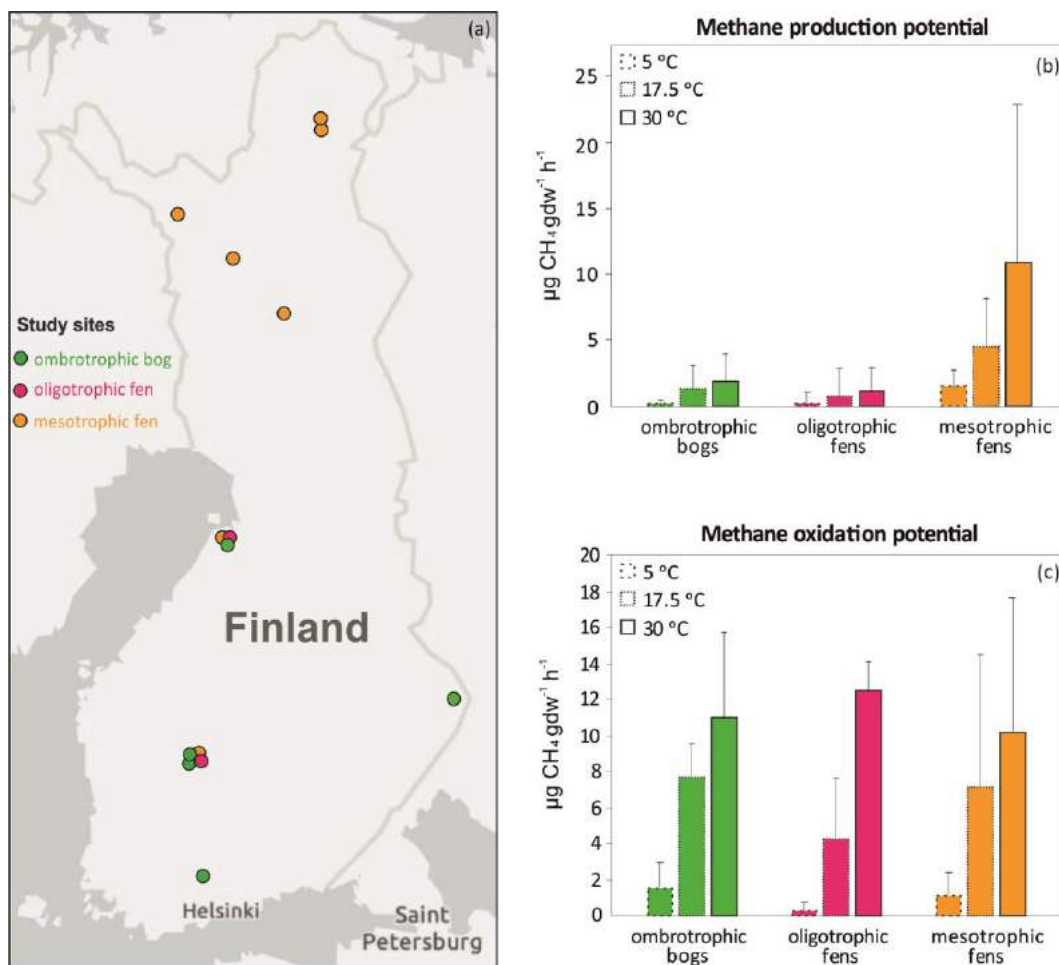


Figure 1. Location of the study sites (a). Basemap source: Esri. The studied peatland types were indicated using green (ombrotrophic bog), red (oligotrophic fen) and orange (mesotrophic fen) colours. Methane (CH_4) production (b) and oxidation (c) potentials (mean and standard deviation) at 5, 17.5 and 30 °C for different peatland types.

REFERENCES

- Zhang, Z., Zimmermann, N. E., Stenke, A., Li, X., Hodson, E. L., Zhu, G. F., Huang, C. L., Poulter, B. (2017). Emerging role of wetland methane emissions in driving 21st century climate change, *Proc. Natl. Acad. Sci. U.S.A* **114**, 9647-9652.
- Turetsky, M. R., Kotowska, A., Bubier, J., Dise, N. B., Crill, P., Hornibrook, E. R., Minkinen, K., Moore, T. R., Myers-Smith, I. H., Nykänen, H., Olefeldt, D., Rinne, J., Saarnio, S., Shurpali, N., Tuittila, E.-S., Waddington, J. M., White, J. R., Wickland, K. P., Wilmking, M. (2014). A synthesis of methane emissions from 71 northern, temperate, and subtropical wetlands, *Glob. Change Biol.* **20**, 2183-2197.

BENEFITS OF FACTOR ANALYSIS ON SUB-RANGES OF MASS SPECTRA

Yanjun Zhang¹, Otso Peräkylä¹, Chao Yan¹, Liine Heikkinen¹, Mikko Äijälä¹, Kaspar Daellenbach¹, Qiaozhi Zha¹, Matthieu Riva^{1,2}, Olga Garmash¹, Heikki Junninen^{1,3}, Pentti Paatero¹, Douglas Worsnop^{1,4}, and Mikael Ehn¹

¹ Institute for Atmospheric and Earth System Research / Physics, Faculty of Science, University of Helsinki, Helsinki, 00140, Finland

² Univ Lyon, Université Claude Bernard Lyon 1, CNRS, IRCELYON, F-69626, Villeurbanne, France

³ Institute of Physics, University of Tartu, Tartu, 50090, Estonia

⁴ Aerodyne Research, Inc., Billerica, MA 01821, USA

Keywords. Mass spectrometry, binned positive matrix factorization (binPMF), high-resolution

INTRODUCTION

Thanks to the advancement in mass spectrometric applications, our capability to detect the oxidized products of volatile organic compounds (VOC) which can contribute to the formation and growth of secondary organic aerosols (Kulmala et al., 2013;Ehn et al., 2014;Kirkby et al., 2016;Troestl et al., 2016), affecting air quality, human health, and climate radiative forcing (Stocker et al., 2013;Zhang et al., 2016;Pope III et al., 2009;Shiraiwa et al., 2017), has been greatly enhanced, as well as our understanding of the complicated atmospheric oxidation pathways in which they take part.

Factor analytical techniques have often been applied to reduce the complexity of the mass spectrometric data by finding co-varying signals that can be grouped into common factors (Huang et al., 1999). The typical approach for using techniques like positive matrix factorization (PMF) is to input all measured data for the factorization in order to separate contributions from different sources and/or processes to the total measured signal. However, an inherent requirement of factorization approaches is that the factor profiles, in this case the relative abundancies of ions in the mass spectra, of each factor stay nearly constant. Due to the complexity and number of atmospheric processes affecting the formation, transformation, and loss of VOC, Oxygenated VOC (OVOC) and aerosol, this is often one of the main limitations of factorization approaches. Given the different volatilities of OVOC, it may even be expected that molecules from the same source may have very different loss time scales, which may affect the factor analysis (Huffman et al., 2009;Crippa et al., 2014;Paciga et al., 2016;Äijälä et al., 2017).

Recently, we proposed a new PMF approach, binPMF, to simplify the analysis of mass spectral data (Zhang et al., 2019a). This method divides the mass spectrum into narrow bins, typically some tens of bins per integer mass, depending on the mass resolving power of the instrument, before performing PMF analyses. In this way, binPMF does not require any time-consuming, and potentially user-sensitive high resolution peak fitting, and can thus be utilized for data exploration at a very early stage of data analysis. The binning greatly increases the number of input variables, which has the advantage that factor analysis with smaller mass ranges becomes more feasible.

METHODS

We designed this study to explore the benefits of separate analysis of different mass ranges from mass spectra. We used a previously published ambient dataset measured by a CI-APi-TOF in Hyytiälä in September of 2016, and conducted binPMF analysis with three different mass ranges of the mass spectra, roughly corresponding to different volatility ranges. We compared the results from the sub-range analyses with each other and with results from binPMF run on the combined ranges, as shown in Figure 1.

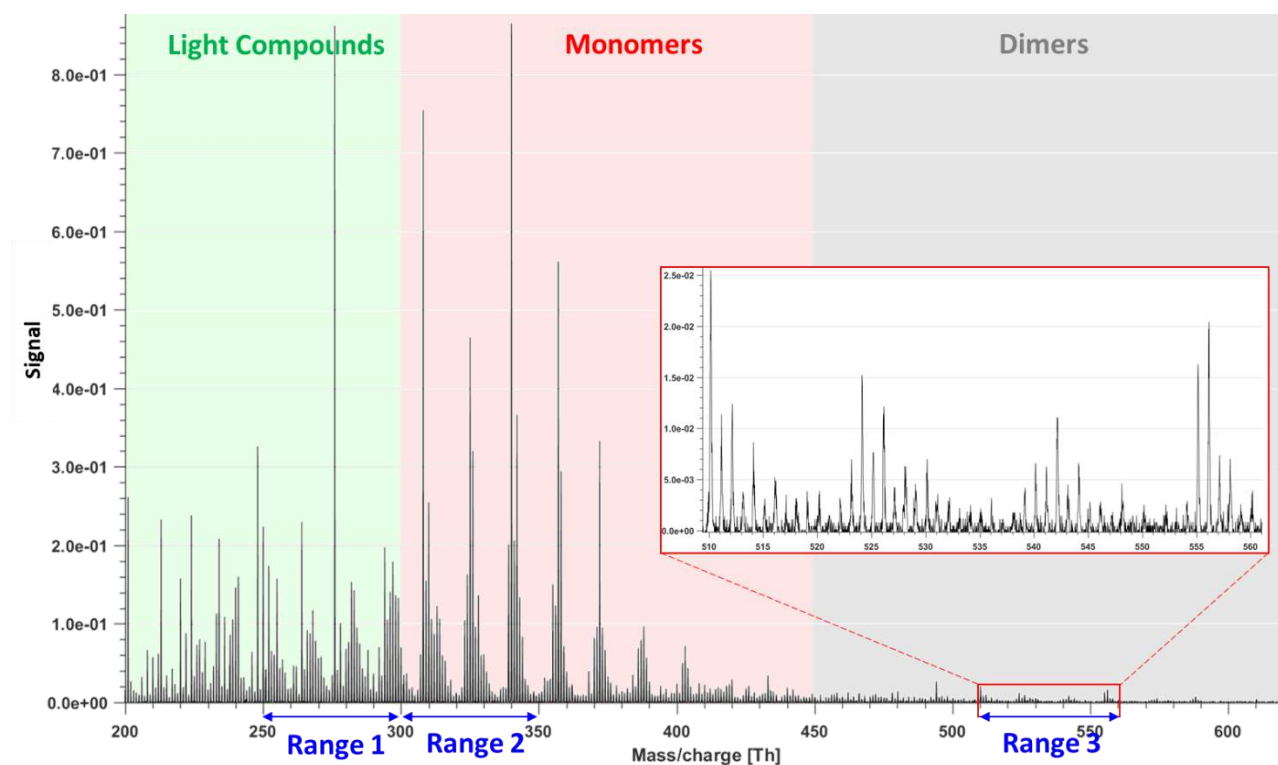


Figure 1. Example of mass spectrum with 1-h time resolution measured from a boreal forest environment during the campaign (at 18:00, Finnish local time, UTC+2). The mass spectrum was divided into three parts and three sub-ranges were chosen from different parts for further analysis in our study.

CONCLUSIONS

The results from these three different ranges, each corresponding to molecules of different volatilities, were compared with binPMF results from the combined range. Separate analysis showed clear benefits in dividing factors for molecules of different volatilities more accurately, in resolving different chemical processes from different ranges, and in giving a chance for high-molecular-weight molecules with low signal intensities to be used to distinguish dimeric species with different formation pathways. In summary, we recommend PMF users to try running their analyses on selected sub-ranges in order to further explore their datasets. And this work has been submitted to ACPD (Zhang et al., 2019b).

ACKNOWLEDGEMENTS

This research was supported by the European Research Council (Grant 638703-COALA), the Academy of Finland (grants 317380 and 320094), and the Vilho, Yrjö and Kalle Väisälä Foundation. K.R.D. acknowledges support by the Swiss National Science postdoc mobility grant P2EZP2_181599. We thank the tofTools team for providing tools for mass spectrometry data analysis. The personnel of the Hyytiälä forestry field station are acknowledged for help during field measurements.

REFERENCES

Äijälä, M., Heikkinen, L., Fröhlich, R., Canonaco, F., Prévôt, A. S. H., Junninen, H., Petäjä, T., Kulmala, M., Worsnop, D., and Ehn, M.: Resolving anthropogenic aerosol pollution types – deconvolution and exploratory classification of pollution events, *Atmos. Chem. Phys.*, 17, 3165-3197, 10.5194/acp-17-3165-2017, 2017.

- Crippa, M., Canonaco, F., Lanz, V. A., Äijälä, M., Allan, J. D., Carbone, S., Capes, G., Ceburnis, D., Dall'Osto, M., Day, D. A., DeCarlo, P. F., Ehn, M., Eriksson, A., Freney, E., Hildebrandt Ruiz, L., Hillamo, R., Jimenez, J. L., Junninen, H., Kiendler-Scharr, A., Kortelainen, A. M., Kulmala, M., Laaksonen, A., Mensah, A. A., Mohr, C., Nemitz, E., O'Dowd, C., Ovadnevaite, J., Pandis, S. N., Petäjä, T., Poulain, L., Saarikoski, S., Sellegri, K., Swietlicki, E., Tiitta, P., Worsnop, D. R., Baltensperger, U., and Prévôt, A. S. H.: Organic aerosol components derived from 25 AMS data sets across Europe using a consistent ME-2 based source apportionment approach, *Atmos. Chem. Phys.*, 14, 6159-6176, 10.5194/acp-14-6159-2014, 2014.
- Huang, S., Rahn, K. A., and Arimoto, R.: Testing and optimizing two factor-analysis techniques on aerosol at Narragansett, Rhode Island, *Atmospheric Environment*, 33, 2169-2185, [https://doi.org/10.1016/S1352-2310\(98\)00324-0](https://doi.org/10.1016/S1352-2310(98)00324-0), 1999.
- Huffman, J. A., Docherty, K. S., Aiken, A. C., Cubison, M. J., Ulbrich, I. M., DeCarlo, P. F., Sueper, D., Jayne, J. T., Worsnop, D. R., Ziemann, P. J., and Jimenez, J. L.: Chemically-resolved aerosol volatility measurements from two megacity field studies, *Atmos. Chem. Phys.*, 9, 7161-7182, 10.5194/acp-9-7161-2009, 2009.
- Paciga, A., Karnezi, E., Kostenidou, E., Hildebrandt, L., Psichoudaki, M., Engelhart, G. J., Lee, B. H., Crippa, M., Prévôt, A. S. H., Baltensperger, U., and Pandis, S. N.: Volatility of organic aerosol and its components in the megacity of Paris, *Atmos. Chem. Phys.*, 16, 2013-2023, 10.5194/acp-16-2013-2016, 2016.
- Pope III, C. A., Ezzati, M., and Dockery, D. W.: Fine-particulate air pollution and life expectancy in the United States, *New England Journal of Medicine*, 360, 376-386, 2009.
- Shiraiwa, M., Ueda, K., Pozzer, A., Lammel, G., Kampf, C. J., Fushimi, A., Enami, S., Arangio, A. M., Fröhlich-Nowoisky, J., Fujitani, Y., Furuyama, A., Lakey, P. S. J., Lelieveld, J., Lucas, K., Morino, Y., Pöschl, U., Takahama, S., Takami, A., Tong, H., Weber, B., Yoshino, A., and Sato, K.: Aerosol Health Effects from Molecular to Global Scales, *Environmental Science & Technology*, 51, 13545-13567, 10.1021/acs.est.7b04417, 2017.
- Stocker, T., Qin, D., Plattner, G., Tignor, M., Allen, S., Boschung, J., Nauels, A., Xia, Y., Bex, V., and Midgley, P.: IPCC, 2013: Climate Change 2013: The Physical Science Basis. Contribution of Working Group I to the Fifth Assessment Report of the Intergovernmental Panel on Climate Change, 1535 pp, in, Cambridge Univ. Press, Cambridge, UK, and New York, 2013.
- Zhang, Y., Cai, J., Wang, S., He, K., and Zheng, M.: Review of receptor-based source apportionment research of fine particulate matter and its challenges in China, *Science of the Total Environment*, 586, 917-929, 2017.
- Zhang, Y., Lin, Y., Cai, J., Liu, Y., Hong, L., Qin, M., Zhao, Y., Ma, J., Wang, X., and Zhu, T.: Atmospheric PAHs in North China: spatial distribution and sources, *Science of the Total Environment*, 565, 994-1000, 2016.
- Zhang, Y., Peräkylä, O., Yan, C., Heikkinen, L., Äijälä, M., Daellenbach, K. R., Zha, Q., Riva, M., Garmash, O., Junninen, H., Paatero, P., Worsnop, D., and Ehn, M.: A novel approach for simple statistical analysis of high-resolution mass spectra, *Atmos. Meas. Tech.*, 12, 3761-3776, 10.5194/amt-12-3761-2019, 2019a.
- Zhang, Y., Peräkylä, O., Yan, C., Heikkinen, L., Äijälä, M., Daellenbach, K. R., Zha, Q., Riva, M., Garmash, O., Junninen, H., Paatero, P., Worsnop, D., and Ehn, M.: Benefits of Performing Factor Analyses on Sub-ranges of Mass Spectra, *Atmos. Chem. Phys. Discuss.*, submitted, 2019b.

WILDFIRE EFFECTS ON BVOC EMISSIONS FROM BOREAL FOREST FLOOR ON PERMAFROST SOIL IN SIBERIA

H. ZHANG-TURPEINEN¹, M. KIVIMÄENPÄÄ¹, H. AALTONEN², F. BERNINGER³, E. KÖSTER^{2,4}, K. KÖSTER^{2,4}, O. MENYAILO⁵, A. PROKUSHKIN⁵ and J. PUMPANEN¹

¹ Department of Environmental and Biological Sciences, P.O.Box 1627, FI-70211 Kuopio, University of Eastern Finland, Finland.

² Department of Forest Sciences, P.O. Box 27, FI-00014 Helsinki, University of Helsinki, Finland.

³ Department of Environmental and Biological Sciences, P.O.Box 111, FI-80101 Joensuu, University of Eastern Finland, Finland.

⁴ Institute for Atmospheric and Earth System Research/ Forest sciences, Faculty of Agriculture and Forestry, University of Helsinki, Helsinki, Finland.

⁵ V.N.Sukachev Institute of forest SB RAS, Russia.

Keywords: BVOC emissions; forest floor; wildfire; permafrost soil.

INTRODUCTION

Common consensus is that global warming will be most pronounced in the Arctic increasing the annual temperature in these regions by 4 – 9 °C by year 2100 (IPCC, 2014). One of the effects of climate change on boreal forest will be more frequent forest wildfires, longer fire seasons (Pechony and Shindell, 2010). Forest wildfire can drastically reduce the vegetation communities in boreal forest floor, where will be covered by revival vegetation as the forest succession proceeds (Köster et al., 2015, 2016). Vegetation is likely the dominant source of BVOCs in terrestrial ecosystems (Monson and Holland, 2001). The quantity and composition of BVOCs released from plants depend on the amount and type of vegetation, and abiotic factors, such as temperature, light availability, CO₂ concentration in the atmosphere and soil moisture (Grote and Niinemets, 2008; Laothawornkitkul et al., 2009). In boreal forest, the forest floor can act as a source or a sink of BVOCs (Aaltonen et al., 2011; Faubert et al., 2012; Hellén et al., 2006; Mäki et al., 2017; Wang et al., 2018). BVOC emission rates from forest floor correlate positively with photosynthetically active radiation (PAR) (Aaltonen et al., 2011) which suggests that the photosynthesis of forest floor vegetation is an important precursor for BVOC emissions (Aaltonen et al., 2013; Laothawornkitkul et al., 2009). In northern boreal or sub-arctic forests, the tree canopy is relatively open which could increase the role of forest floor on BVOCs compared to forests with denser canopy. Thus, the changing of vegetation in boreal forest floor since wildfires might affect the BVOC emission rates (Fehsenfeld et al., 1992).

More frequent forest wildfires will expose larger areas of permafrost to thawing (Johnstone et al., 2010; Taş et al., 2014) which will increase the decomposition of soil organic matter (SOM) (Jorgenson et al., 2010). Soil matrix, decomposing material and belowground plant tissues such as roots and rhizomes can be potential sources of BVOCs (Peñuelas et al., 2014), and the emission profiles vary considerably across soil and litter types (Gray et al., 2014). The changes in SOM caused by wildfire and permafrost thawing could be associated with exchanging distinct types and quantities of BVOCs, but the direction and magnitude of these effects are nearly unknown.

BVOC emissions from boreal forest floor have been little characterized in southern boreal region, and even less so in permafrost soil, which underlies most of the northern boreal region. Here, we report the long-term effects of wildfire on forest floor BVOC emission rates along a wildfire chronosequence in a *Larix gmelinii* forest in central Siberia. The aim of this study was to qualify and quantify BVOC emissions from the northern boreal forest floor at different stages during the forest succession. We studied how forest wildfires and the consequent succession of vegetation influence BVOC emission rates. In addition, we also studied

how permafrost thawing affected SOM availability and its decomposability and consequently BVOC emission rates. We hypothesized that the amount of ground vegetation will decrease as a result of forest wildfires, and this causes also a decrease in BVOC emissions, while the thawing of permafrost soil will increase BVOC emissions because of a greater availability and decomposability of soil organic matter.

METHODS

The study was executed in July of 2016 in larch dominated forest areas (64°20' - 64°33' N, 100°23' - 100°44' E) near Evenkian Field Station in the settlement of Tura of Krasnoyarsky region in Central Siberia, the Russia Federation. Permafrost extends throughout the study area. We determined forest floor BVOC emissions from forests exposed to wildfire in (i) year 2015, (ii) 1993 and (iii) the area with no wildfire for at least 100 years. From each age area, we carried out the measurements of BVOC emissions by enclosed chamber with pre-cleaned transparent polyethylene terephthalate film bag (Stewart-Jones and Poppy, 2006) to form a dome shape and with a conventional push-pull system (Faubert et al., 2012, 2011; Tholl et al., 2006; Tiiva et al., 2009). The headspace air sample through an adsorbent tube (Tenax TA, 100mg and Carbopack B, 100mg, mesh 60/80; Markes International Ltd, Llantrisant, UK). The adsorbent tubes were subjected to analysis for detailed characterization of volatile organic compounds with a thermodesorption instrument (ATD400; Perkin Elmer, Wellesley, MA, USA) and connected to a gas chromatograph-mass spectrometer (Hewlett – Packard 6890, MSD 5973; Hewlett – Packard, Palo Alto, CA, USA). The BVOC concentrations in the adsorbent tube were calculated using the equations from Faubert et al. (2012). The BVOC emission of every compound was calculated using the typical equation for measuring open (push-pull) chamber measurements. BVOC emission rates were also calculated as emission potentials by standardizing to the temperature of 30 °C and the PAR of 1000 $\mu\text{mol m}^{-2} \text{s}^{-1}$ according to Guenther et al. (1993) to reduce the effects of environmental variation.

Photosynthetically active radiation (PAR) was measured under the sampling conditions. Soil temperature and volumetric water content (VWC) were measured manually in situ after the BVOC measurements in all collars. Forest floor vegetation species coverages (%) in the collars were determined using the eye estimation method (Mäki et al., 2017) and the coverage was classified into five groups: vascular plants, mosses, lichen, litter and bare soil. Additionally, we measured plot characteristics such as tree species composition, living tree biomass and dead wood biomass. We also took soil samples for determining soil pH and soil carbon (C) and nitrogen (N) concentrations and for soil texture analyses and soil incubation.

The data of actual emission rates of BVOC groups, vegetation groups, and environmental variables were subjected to principle component analysis (PCA) in order to assess how forest age affected the BVOC emissions, vegetation and soil and microclimatic characteristics in concert.

CONCLUSIONS

The forest floor was a source of a large number of different BVOCs to the atmosphere in the different stages of forest succession after wildfire disturbance, although the emission rates of most of the compounds were quite low on average. Monoterpenes were the most abundant BVOC group in all age classes. Our observations showed that there was an age-related trend in the BVOC emissions with the lowest emissions observed in the recently burnt forest and ca. 2.6 times increase in the older forest areas. The BVOC emissions were lowest in the 1-year-old area which supports our hypothesis that the decrease in BVOC emissions were resulted from the wildfire induced decrease in the amount of ground vegetation. Given the close proximity of the sites and similar driving climatic variables, this suggests that the succession of vegetation was the dominant factor determining the forest floor BVOC emissions and their composition in these northern boreal forests. Fire-induced permafrost thaw resulting in increased availability of SOM for decomposing microorganisms did not increase BVOC emissions. However, the soil and decomposing litter may be significant sources of BVOCs in the future if the soil organic matter microbial decomposition increases as a result of climate warming. Our results showed that forest wildfires play an important indirect role in regulating the amount and composition of BVOC emissions from post-fire originated boreal forest floor. This could have a substantial effect on BVOC emissions if the frequency of forest wildfires increases in the

future as a result of climate warming. However, the net impacts of BVOCs on climate and radiation budget are uncertain, but they might depend on the forest age and ground vegetation cover changes. To better understand the potential dependencies of forest floor BVOC emissions on vegetation succession and changes in environmental factors post fire, it is necessary to carry out measurements over longer period taking into account the seasonal variability.

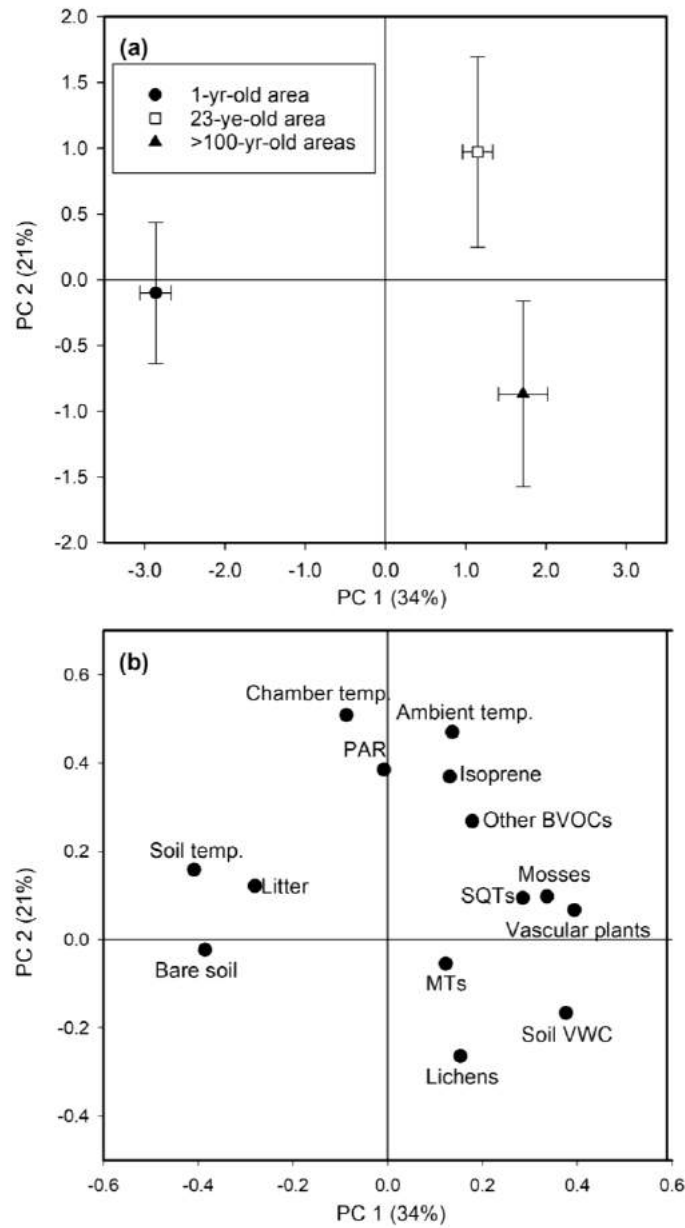


Figure 1. Principle component analysis (PCA) on BVOC emissions, environmental factors and ground coverage. The actual emissions of BVOCs were divided into isoprene, monoterpenes (MTs), sesquiterpenes (SQTs), and other volatile organic compounds (other BVOCs). Environmental factors included ambient, chamber and soil temperatures, soil volumetric water content (VWC) and photosynthetically active radiation (PAR), and ground vegetation coverage sorted into vascular plants, mosses, lichens, litter and bare soil surface. (a) The mean scores (\pm SE; $n=6$) for different aged forest areas (1-, 23- and >100-year-old areas) and (b) the corresponding loading variables. The variation explained by each PC is in parentheses.

ACKNOWLEDGEMENTS

This study is financially supported by strategic funding of the University of Eastern Finland (project number: 931675), project funding of the Academy of Finland (project number: 286685, 294600 and 278424). The authors would also like to thank the Academy of Finland Centre of Excellence (project No. 307331).

REFERENCES

- Aaltonen, H., Aalto, J., Kolari, P., Pihlatie, M., Pumpanen, J., Kulmala, M., Nikinmaa, E., Vesala, T., Bäck, J., 2013. Continuous VOC flux measurements on boreal forest floor. *Plant Soil* 369, 241–256. <https://doi.org/10.1007/s11104-012-1553-4>
- Aaltonen, H., Pumpanen, J., Pihlatie, M., Hakola, H., Hellén, H., Kulmala, L., Vesala, T., Bäck, J., 2011. Boreal pine forest floor biogenic volatile organic compound emissions peak in early summer and autumn. *Agric. For. Meteorol.* 151, 682–691. <https://doi.org/10.1016/j.agrformet.2010.12.010>
- Faubert, P., Tiiva, P., Michelsen, A., Rinnan, Å., Ro-Poulsen, H., Rinnan, R., 2012. The shift in plant species composition in a subarctic mountain birch forest floor due to climate change would modify the biogenic volatile organic compound emission profile. *Plant Soil* 352, 199–215. <https://doi.org/10.1007/s11104-011-0989-2>
- Faubert, P., Tiiva, P., Nakam, T.A., Holopainen, J.K., Holopainen, T., Rinnan, R., 2011. Non-methane biogenic volatile organic compound emissions from boreal peatland microcosms under warming and water table drawdown. *Biogeochemistry* 106, 503–516. <https://doi.org/10.1007/s10533-011-9578-y>
- Fehsenfeld, F., Calvert, J., Fall, R., Goldan, P., Guenther, A.B., Hewitt, C.N., Lamb, B., Liu, S., Trainer, M., Westberg, H., Zimmerman, P., 1992. Emissions of volatile organic compounds from vegetation and the implications for atmospheric chemistry. *Global Biogeochem. Cycles* 6, 389–430. <https://doi.org/10.1029/92GB02125>
- Gray, C.M., Monson, R.K., Fierer, N., 2014. Biotic and abiotic controls on biogenic volatile organic compound fluxes from a subalpine forest floor. *J. Geophys. Res. Biogeosciences* 119, 547–556. <https://doi.org/10.1002/2013JG002575>
- Grote, R., Niinemets, Ü., 2008. Modeling volatile isoprenoid emissions - a story with split ends. *Plant Biol.* 10, 8–28. <https://doi.org/10.1055/s-2007-964975>
- Guenther, A.B., Zimmerman, P.R., Harley, P.C., Monson, R.K., Fall, R., 1993. Isoprene and monoterpene emission rate variability: Model evaluations and sensitivity analyses. *J. Geophys. Res.* 98, 12609. <https://doi.org/10.1029/93JD00527>
- Hellén, H., Hakola, H., Pystynen, K., Rinne, J., Haapanala, S., 2006. C2-C10 hydrocarbon emissions from a boreal wetland and forest floor. *Biogeosciences* 3, 167–174. <https://doi.org/10.5194/bg-3-167-2006>
- IPCC, 2014. Clouds and Aerosols. *Clim. Chang.* 2013 - Phys. Sci. Basis 571–658. <https://doi.org/10.1017/CBO9781107415324.016>
- Johnstone, J.F., Chapin, F.S., Hollingsworth, T.N., Mack, M.C., Romanovsky, V., Turetsky, M., 2010. Fire, climate change, and forest resilience in interior Alaska This article is one of a selection of papers from The Dynamics of Change in Alaska's Boreal Forests: Resilience and Vulnerability in Response to Climate Warming. *Can. J. For. Res.* 40, 1302–1312. <https://doi.org/10.1139/X10-061>
- Jorgenson, M.T., Romanovsky, V., Harden, J., Shur, Y., O'Donnell, J., Schuur, E.A.G., Kanevskiy, M., Marchenko, S., 2010. Resilience and vulnerability of permafrost to climate change This article is one of a selection of papers from The Dynamics of Change in Alaska's Boreal Forests: Resilience and Vulnerability in Response to Climate Warming. *Can. J. For. Res.* 40, 1219–1236. <https://doi.org/10.1139/X10-060>
- Köster, E., Köster, K., Berninger, F., Pumpanen, J., 2015. Carbon dioxide, methane and nitrous oxide fluxes from podzols of a fire chronosequence in the boreal forests in Väriö, Finnish Lapland. *Geoderma Reg.* 5, 181–187. <https://doi.org/10.1016/j.geodrs.2015.07.001>
- Köster, K., Köster, E., Orumaa, A., Parro, K., Jögiste, K., Berninger, F., Pumpanen, J., Metslaid, M., 2016. How Time since Forest Fire Affects Stand Structure, Soil Physical-Chemical Properties and Soil CO₂ Efflux in Hemiboreal Scots Pine Forest Fire Chronosequence? *Forests* 7, 201. <https://doi.org/10.3390/f7090201>
- Laothawornkitkul, J., Taylor, J.E., Paul, N.D., Hewitt, C.N., 2009. Biogenic volatile organic compounds

CoE 2019 abstract

- in the Earth system: Tansley review. *New Phytol.* <https://doi.org/10.1111/j.1469-8137.2009.02859.x>
- Mäki, M., Heinonsalo, J., Hellén, H., Bäck, J., 2017. Contribution of understorey vegetation and soil processes to boreal forest isoprenoid exchange. *Biogeosciences* 14, 1055–1073. <https://doi.org/10.5194/bg-14-1055-2017>
- Monson, R.K., Holland, E.A., 2001. Biospheric Trace Gas Fluxes and Their Control Over Tropospheric Chemistry. *Annu. Rev. Ecol. Syst.* 32, 547–576. <https://doi.org/10.1146/annurev.ecolsys.32.081501.114136>
- Pechony, O., Shindell, D.T., 2010. Driving forces of global wildfires over the past millennium and the forthcoming century. *Proc. Natl. Acad. Sci. U. S. A.* 107, 19167–70. <https://doi.org/10.1073/pnas.1003669107>
- Peñuelas, J., Asensio, D., Tholl, D., Wenke, K., Rosenkranz, M., Piechulla, B., Schnitzler, J.P., 2014. Biogenic volatile emissions from the soil. *Plant, Cell Environ.* <https://doi.org/10.1111/pce.12340>
- Stewart-Jones, A., Poppy, G.M., 2006. Comparison of glass vessels and plastic bags for enclosing living plant parts for headspace analysis. *J. Chem. Ecol.* 32, 845–864. <https://doi.org/10.1007/s10886-006-9039-6>
- Taş, N., Prestat, E., McFarland, J.W., Wickland, K.P., Knight, R., Berhe, A.A., Jorgenson, T., Waldrop, M.P., Jansson, J.K., 2014. Impact of fire on active layer and permafrost microbial communities and metagenomes in an upland Alaskan boreal forest. *ISME J.* 8, 1904–1919. <https://doi.org/10.1038/ismej.2014.36>
- Tholl, D., Boland, W., Hansel, A., Loreto, F., Röse, U.S.R., Schnitzler, J.-P., 2006. Practical approaches to plant volatile analysis. *Plant J.* 45, 540–560. <https://doi.org/10.1111/j.1365-313X.2005.02612.x>
- Tiiva, P., Faubert, P., Rätty, S., Holopainen, J.K., Holopainen, T., Rinnan, R., 2009. Contribution of vegetation and water table on isoprene emission from boreal peatland microcosms. *Atmos. Environ.* 43, 5469–5475. <https://doi.org/10.1016/j.atmosenv.2009.07.026>
- Wang, M., Schurgers, G., Hellén, H., Lagergren, F., Holst, T., 2018. Biogenic volatile organic compound emissions from a boreal forest floor. *Boreal Environ. Res.* 2469, 249–265.

A simulation of SOA over Green Sahara in Mid-Holocene period with prescribed isoprene and monoterpene emissions

P. ZHOU¹, J.-P. KESKINEN^{1,2}, J. Bian¹ and R. MAKKONEN^{1,2}

¹ Institute for Atmospheric and Earth System Research/Physics, Faculty of Science, University of Helsinki, Finland

² Finnish Meteorological Institute, Finland

Keywords: soa, Green Sahara, Mid-Holocene.

INTRODUCTION

A Green Sahara, instead of present desert Sahara, existed in the North-Africa during the early-to mid-Holocene (11,000 to 5,000 years before present) as suggested by comprehensive paleoproxy data and studies (Hoelzmann et al., 1998; Hély et al., 2014).

Several factors are considered to play a role in establishing such a Green Sahara in a cause-effect or a coupled way. For example, the summer insolation in the Northern Hemisphere was larger than today due to the orbital shifting, which resulted in a stronger West African Monsoon (WAM) and a northward West African rain belt. As a consequence, more vegetation were able to grow and more lakes appeared, which induce more precipitation and could further enhance WAM.

These coupled and complex processes have already been simulated by different models (e.g. Egerer et al., 2018). On the basis of previous model works we aim to provide a more comprehensive simulation of the Mid-Holocene period with focus on the Green Sahara area, which can provide a reliable paleoclimate to help further studies, e.g. how human migrates during the Holocene.

In this preliminary study the Earth system model EC-Earth will be used to simulate how the interactions between climate and vegetation can affect the SOA in the air. EC-Earth is developed jointly by 28 European research institutes (Hazeleger et al., 2012). EC-Earth comprises of the atmosphere model IFS (Integrated Forecasting Model), ocean model NEMO with the coupled ice model LIM, and vegetation model LPJ-GUESS, coupled with OASIS coupler. Aerosols and chemistry are included through the global chemistry-transport model TM5.

The EC-Earth model will be applied to early-to-mid-Holocene climate in several different configurations, including forcings from orbital changes, vegetation cover and aerosol components. The forcings will be applied either individually or together to analyze synergistic interactions and feedbacks.

As a start, we simulated the global dust load concentrations and the formation of secondary organic aerosols (SOAs) with different vegetation covers, as well as isoprene and monoterpene emissions according to Lu et al. (2018), representing pre-industrial vegetation (pio), Mid-Holocene vegetation forced by insolation and greenhouse gas concentration of 6000 years before present (BP) with prescribed Green Sahara vegetation and reduced dust concentration (mh2).

METHODS

The TM5-MP model was run for half year from July 2009 to December 2009 as a spinup for each case. And the simulations were forced by different vegetation covers, and corresponding isoprene

and monoterpene emissions (Figs. 1 and 2). The BVOC emissions from north Africa is much larger in the MH period. The results shown here are the average of the data within this half-year period.

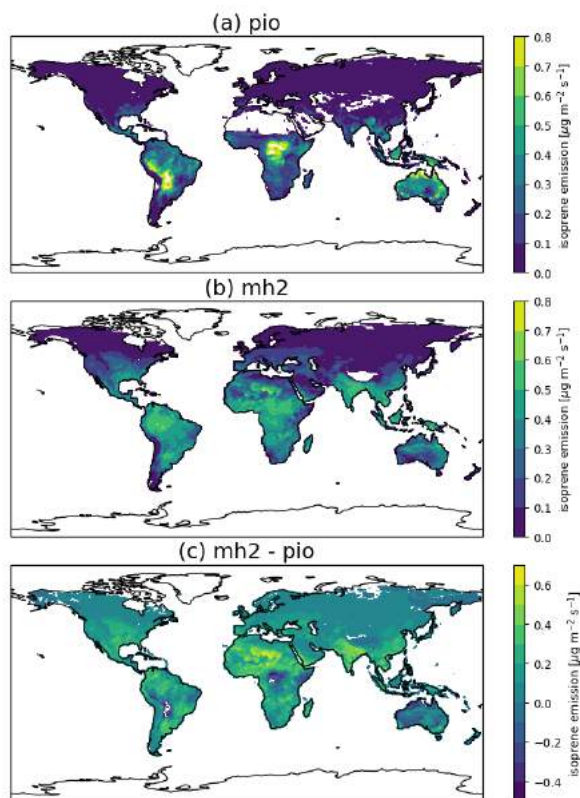


Figure 1: The prescribed isoprene emission rates for the case (a) pio, (b) mh2, and (c) their difference.

RESULTS

Figure 3 shows that SOA load is highly correlated to the emissions of its gas precursors, e.g., isoprene and monoterpene. For example, the SOA load are $1.2 \text{ [mg m}^{-2}\text{]}$ larger in mh2 than pio over the western African coast, while it is lower in mh2 over the middle Africa, Amazon and northwest of Australia. This also results in the corresponding changes of 550 nm AOD due to ambient aerosols over these regions, showing lower AOD with positive SOA change and vice versa. However, the major change of 500 nm AOD is due to the difference of dust load instead of SOA between mh2 and pio (not shown here).

ACKNOWLEDGEMENTS

This work was supported by the AGES (University of Helsinki research grant), eSTICC (272041), the Academy of FCoE (307331), and CSC – IT Center for Science in Finland.

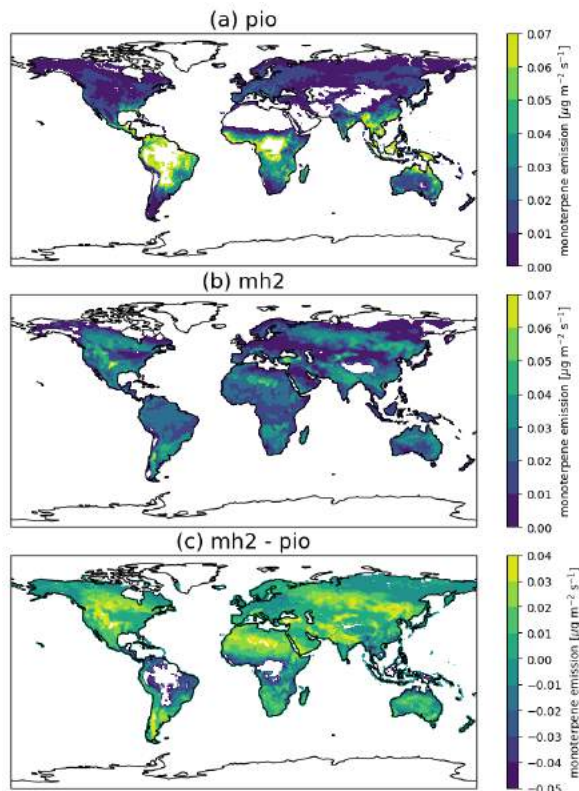


Figure 2: The prescribed monoterpene emission rates for the case (a) pio, (b) mh2, and (c) their difference.

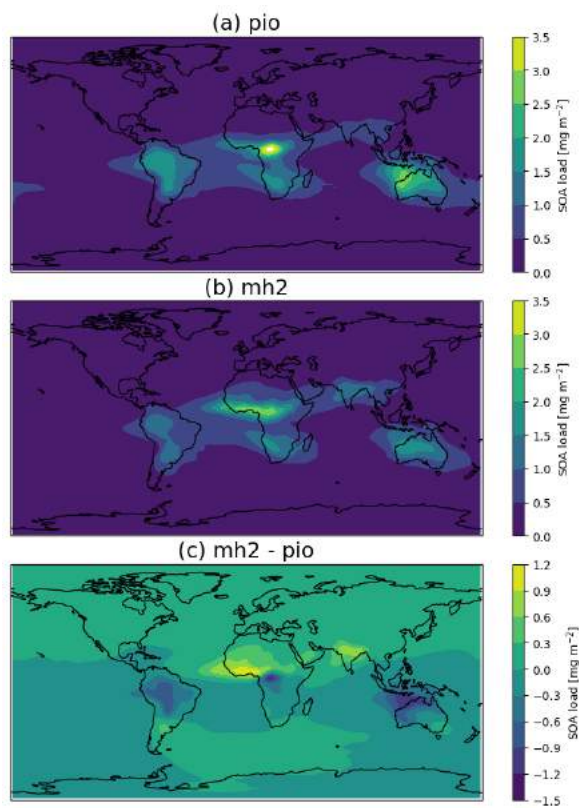


Figure 3: The simulated SOA load for the case (a) pio, (b) mh2, and (c) their difference.

REFERENCES

- Egerer, S., Claussen, M., and Reick, C. (2018). Rapid increase in simulated North Atlantic dust deposition due to fast change of northwest African landscape during the Holocene. *Climate of the Past*, 14(7):1051–1066.
- Hazeleger, W., Wang, X., Severijns, C., Ștefănescu, S., Bintanja, R., Sterl, A., Wyser, K., Semmler, T., Yang, S., van den Hurk, B., van Noije, T., van der Linden, E., and van der Wiel, K. (2012). EC-Earth V2.2: description and validation of a new seamless earth system prediction model. *Climate Dynamics*, 39(11):2611–2629.
- Hély, C., Lézine, A.-M., and contributors, A. (2014). Holocene changes in african vegetation: tradeoff between climate and water availability. *Climate of the Past*, 10(2):681–686.
- Hoelzmann, P., Jolly, D., Harrison, S. P., Laarif, F., Bonnefille, R., and Pachur, H.-J. (1998). Mid-holocene land-surface conditions in northern africa and the arabian peninsula: A data set for the analysis of biogeophysical feedbacks in the climate system. *Global Biogeochemical Cycles*, 12(1):35–51.
- Lu, Z., Miller, P. A., Zhang, Q., Zhang, Q., Wårlind, D., Nieradzik, L., Sjolte, J., and Smith, B. (2018). Dynamic vegetation simulations of the mid-holocene green sahara. *Geophysical Research Letters*, 45(16):8294–8303.

ATMOSPHERIC AEROSOL CHEMISTRY: CLIMATE AND AIR QUALITY

D.R. WORSNOP^{1,2}

¹Institute for Atmospheric Research, Physics, University of Helsinki, 00014 Finland.

²Aerodyne Research, Billerica, MA 01821, U.S.

Keywords: mass spectroscopy, aerosol, HOM

INTRODUCTION

Despite much effort in the past decades, uncertainties in both climate impacts and health effects of atmospheric aerosols remain large. Aerosol mass spectrometry (AMS) has shown that sub-micron aerosol chemical composition is roughly 50:50 inorganic and organic worldwide, with secondary highly oxidized organics dominating the latter. Parallel application of chemical ionization mass spectrometry (CIMS) has provided the first observation of molecular cluster ions involved in atmospheric nucleation, including detection of highly oxidized multifunctional (HOM) organics in the gas phase.

METHODS

The AMS consists of an aerodynamic lens (Liu et al, 1995) coupled to a differentially pumped mass spectrometer. Sub-micron particles are injected by the lens into vacuum and transported about 35 cm to a heated tungsten impactor (600C) placed in an electron impact (EI) ionizer. The original quadrupole MS (Jayne et al, 2000) was replaced by a time-of-flight (ToF) MS with sufficient resolution (4000) for elemental identification of ions (DeCarlo et al, 2006). The AMS provides continuous measurement of sub-micron aerosol chemical composition. EI detection directly separates inorganic and organic components. Positive matrix factorisation (PMF) of the carbon containing fragment ion distribution further resolves primary and secondary components of organic aerosol composition (Canagaratna et al, 2007).

The atmospheric pressure interface (API) ToFMS was first deployed at SMEAR II in Hyytiälä (Junninen et al, 2010). The API-ToF directly samples ambient ions from atmospheric pressure through two differentially quadrupole ion guides that inject the ions into a ToFMS. After identification of ambient organic ions clustered with the nitrate anion (NO_3^-), a NO_3^- source (Eisele and Tanner, 1993) was added to the API-ToF, enabling CIMS detection of sub ppt levels of highly oxidized neutral molecules (Jokinen et al, 2012).

CONCLUSIONS

Results from worldwide AMS measurements can be summarized with two statements (Jimenez et al, 2009): (1) Aerosol chemical composition is roughly 50:50 inorganic (e.g. sulphate, nitrate and ammonia) and organic (carbon containing); (2) The organic fraction is highly oxygenated, corresponding to global average oxygen to carbon ratio (O/C) of about 0.7. The high O/C content is indicative of dominant secondary composition (oxidized organic aerosol, OOA) produced from condensation of photochemically oxidised volatile organic carbon. Primary aerosol, detected as hydrocarbon organic aerosol (HOA), is significant in polluted urban environments, primarily due to combustion emissions; e.g. diesel soot particles coated with lubricating oil. PMF analysis of organic components further separates both primary and secondary components into multiple source and photochemical contributions. For example, in Pittsburgh (eastern United States) three organic factors were clearly resolved: HOA, which correlates with vehicle markers (NO_x and CO); SV-OOA, semivolatile (SV) OOA correlated with SV ammonium nitrate; and LV-OOA, correlated with ammonium sulphate, both irreversibly condensed (Canagaratna et al, 2007).

API-ToF deployment in Hyytiälä immediately identified clusters of sulphuric acid, some containing ammonia, which correlated directly with nano-particle nucleation on sunny mornings in the spring (Junninen et al, 2010). In contrast, during the nights when H_2SO_4 is not photochemically produced, API-ToF mass spectra were dominated by groups of organic containing ions at 300-400 and 500-600 Th. Identification of those species as NO_3^- clusters with highly oxygenated organic molecules (HOM), led to CIMS detection of a range of HOM species (Bianchi et al, 2019). Ehn et al (2014) showed that auto-oxidation of alpha-pinene

with ozone as the major source of night-time HOM in Hyytiälä. Subsequent experiments at the CLOUD chamber in CERN showed that a range of inorganic and HOM molecules and clusters can contribute to new particle formation (NPF) nucleation and growth (Schobesberger et al, 2013).

These results are summarized in Fig. 1. Atmospheric NPF is typically initiated by nucleation of H₂SO₄ and base (ammonia or amines) followed by nanoparticle growth dominated by condensation of extreme low volatile organics (ELVOC, highly oxygenated organic). Ultrafine growth is dominated by the somewhat less oxidized low volatility organic (LVOC) species. Finally, for larger particles and CCN formation, SVOC becomes important. Another key point is that NO_x significantly affects this photochemistry, with the production of organonitrates (Yan et al, 2016). Production of ELVOC and LVOC largely explains the high O/C observed by the AMS, especially in remote regions with little primary aerosol emissions. These results have many implications for aerosol, air quality and climate.

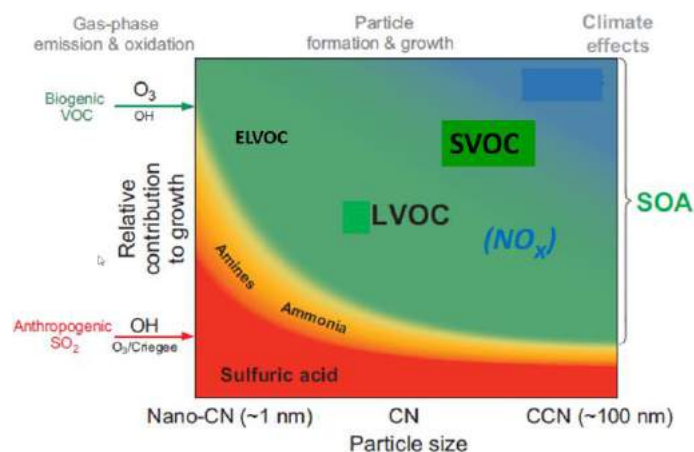


Figure 1. Schematic of atmospheric particle formation and growth (adapted from Ehn et al, 2014).

ACKNOWLEDGEMENTS

This his work was partially funded by Academy of Finland (1251427, 1139656), Finnish Centre of Excellence (1141135).

REFERENCES

- Bianchi, F. E et al. (2019). Highly Oxygenated Organic Molecules (HOM) from Gas-Phase Autoxidation Involving Peroxy Radicals: A Key Contributor to Atmospheric Aerosol. *Chem. Rev.* **119**, 3472.
- Canagaratna M.R. et al. (2007). Chemical and Microphysical Characterization of Ambient Aerosols with the Aerodyne Aerosol Mass Spectrometer, *Mass Spectrometry Reviews* **26**, 185.
- DeCarlo, P. F et al. (2006). Field-deployable, high-resolution, time-of-flight aerosol mass spectrometer. *Anal. Chem.* **78**, 8281.
- Ehn, M. et al (2014). A large source of low-volatility secondary organic aerosol, *Nature* **476**, 506.
- Eisele, F. L. and Tanner, D. J. (1993) Measurement of the gas phase concentration of H₂SO₄ and estimates of H₂SO₄ production and loss in the atmosphere, *J. Geophys. Res.* **98**, 9001.
- Jayne, J. T., et al (2000). Development of an aerosol mass spectrometer for size and composition analysis of submicron particles. *Aer. Sci. Tech.* **33** 49.
- Jimenez, J.L. et al (2009). Evolution of organic aerosols in the atmosphere, *Science* **326**, 1525.
- Jokinen, T. et al (2012). Atmospheric sulphuric acid and neutral cluster measurements using CI-API-TOF. *Atmos. Chem. and Phys.* **12**, 4117.
- Junninen, H. et al (2010). A high-resolution mass spectrometer to measure atmospheric ion composition. *Atmos. Measure. Techniq* **3**, 1039.
- Liu, P., et al (1995). Generating Particle Beams of Controlled Divergence: II. Experimental Evaluation of Particle Motion in Aerodynamic Lenses and Nozzle Expansions, *Aerosol Sci. Technol* **22**, 314.
- Schobesberger, S. et al (2013). Molecular understanding of atmospheric particle formation from sulfuric acid and large oxidized organic molecules. *Proc. Nat. Acad. of Sci. U.S. Amer.* **110**, 17223.
- Yan, C. et al (2016). Source characterization of highly oxidized multifunctional compounds in a boreal forest environment using positive matrix factorization. *Atmos. Chem. Phys.* **16**, 12715.